NBSIR 83-2742 (R)

Photonuclear Data - Abstract Sheets 1955 - 1982 Volume IV (Nitrogen - Oxygen)

U.S. DEPARTMENT OF COMMERCE
National Bureu of Standards
National Measurement Laboratory
Center for Radiation Research
Washington, DC 20234

April 1983

Issued November 1983

U.S. DEPARTMENT OF COMMERCE
NATIONAL BUREAU OF STANDARDS

NBSIR 83-2742

PHOTONUCLEAR DATA - ABSTRACT SHEETS
1955 - 1982
Volume IV (Nitrogen - Oxygen)

E. G. Fuller, Henry Gerstenberg

U.S. DEPARTMENT OF COMMERCE
National Bureau of Standards
National Measurement Laboratory
Center for Radiation Research
Washington, DC 20234

April 1983

Issued November 1983

U.S. DEPARTMENT OF COMMERCE, Malcolm Baldrige, *Secretary*
NATIONAL BUREAU OF STANDARDS, Ernest Ambler, *Director*

TABLE OF CONTENTS

Table of Contents i

Introduction. 1

Nitrogen (A=13) 3

Nitrogen (A=14) 27

Nitrogen (A=15) 117

Nitrogen (A=16) 189

Nitrogen (A=18) 193

Oxygen (A=15) 197

Oxygen (A=16) 215

Oxygen (A=17) 573

Oxygen (A=18) 591

Definition of Abbreviations and Symbols 625

Photonuclear Data-Abstract Sheets
1955-1982

I. Introduction

As used in connection with this collection of data-abstract sheets, the term photonuclear data is taken to mean any data leading to information on the electromagnetic matrix element between the ground state and excited states of a given nuclide. The most common types of reactions included in this compilation are: (e,e'), (γ,γ), (γ,γ'), (γ,n), (γ,p), etc. as well as ground-state particle capture reactions, e.g. (α,γ_0). Two reactions which fit the matrix element criterion are not included in the compilation because of their rather special nature. These are heavy particle Coulomb excitation and the thermal neutron capture reaction (n,γ_0). While the energy region of particular interest extends from 0 to 150 MeV, papers are indexed which report measurements in the region from 150 MeV to 4 GeV. Most of the experiments listed are concerned with the excitation energy range from 8 to 30 MeV, the region of the photonuclear giant resonance.

The hierarchical grouping of the photonuclear data-abstract sheets within the file is by: 1. Target Element, 2. Target Isotope, and 3. by the Bibliographic Reference Code assigned to the paper from which the data on the sheet were abstracted. In this file, colored pages are used to mark the beginning and end of the sheets for each chemical element. A brief historical sketch of the element is given on the divider sheet marking the start of each section; the information for this sketch was derived from references such as the Encyclopaedia Britannica. In those cases where the sheets for a given element make up a major part of a volume, colored pages are also used to delineate sections pertaining to the individual isotopes of the element. Each of the sections of the file, as delineated by two colored divider sheets, represents a 27 year history of the study of electromagnetic interactions in either a specific nuclide or a specifc element.

The data-abstract sheets are filed under the element and/or isotope in which the ground-state electromagnetic transition takes place. For example, the abstract sheet for a total neutron yield measurement for a naturally occurring copper sample would appear in the elemental section of the copper file. On the other hand, a measurement of the ^{62}Cu 9.73 minute positron activity produced in the same sample by photons with energies below the three-neutron separation energy for ^{65}Cu (28.68 MeV) would be filed with the sheets for ^{63}Cu. Similarly a measurement of the ground-state neutron capture cross section in ^{12}C would be filed under ^{13}C while the corresponding ground-state alpha-particle capture cross section would be filed under ^{16}O.

At the end of this volume there is a master list of the abbreviations that have been used in the index section of the abstract sheets. The listings are those used in the final published index, Photonuclear Data Index, 1973-1981, NBSIR 82-2543, issued in August 1982 by the U. S. Department of Commerce, National Bureau of Standards, Washington, DC 20234. In some cases two notations are entered for the same quantity. The second entry is the abbreviation that was used in one or more of the earlier published editions of the index.

NITROGEN
Z=7

Nitrogen was first recognized by C. W. Scheele (1742-1786), a Swedish chemist of great importance. It was discovered independently by Joseph Priestley and Daniel Rutherford, but there is little doubt that Scheele's discovery precludes them by two years. Antoine Lavoisier named the gas "azote" (from the Greek *azotos* "ungirt" taken to mean lifeless) because of its inability to support life; he recognized it as an element. The name nitrogen was introduced in 1790 by J. A. Chaptal to indicate that the element is a constituent of niter (potassium nitrate).

N
A=13

Scheele was a proprietor of a small pharmacy. Pharmacies were then considered quiet centers of original research. He was offered many academic positions, including the chair of chemistry at Berlin, but never exchanged the practice of pharmacy for an academic career. Scheele performed an extraordinary amount of original research and published many papers, most of which contain some major discovery or important observation. His work touched on every area in chemistry of his time. It is said that his unremitting work, particularly at night, in a poorly ventilated laboratory, and his handling of the most toxic materials (with the habit of tasting and smelling them indiscriminately) induced the illness which caused his death at the age of 43 in 1786.

N
A=13

Ref. D.F. Hebbard, J.L. Vogl
Nuclear Phys. 21, 652 (1960)

Elem. Sym.	A	Z
N	13	7

Method 600 kev electrostatic generator; NaI

Ref. No. 60 He 2 JHH

Reaction	E or ΔE	E_o	Γ	∫σdE	Jπ	Notes
$C^{12}(p,\gamma)N^{13}$	140-750 kev	462 kev	$\omega\Gamma_\gamma$=1.52ev			$E_{\gamma o}$ = 2.31 MeV

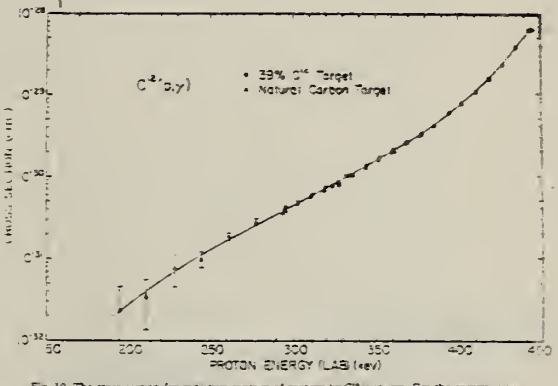

Fig. 10. The cross section for radiative capture of protons by C^{12} is shown. For the energy range from 296 keV to 444 keV a target of 39 %, C^{13} with a thickness of 8.9 keV for 448-keV protons was used. For the energy range from 194 keV to 378 keV, a natural carbon target, approximately 20 keV thick was used. The results from the latter target were normalized in the overlapping range to agree with the results from the target of known thickness, taken at higher energies. The experimental points have been corrected for the effect of the carbon contamination on the surface of the 39 % C^{13} target. Typical errors are shown at intervals in the energy range, and the origin of the solid curve is described in fig. 11.

TABLE 6

Resonance parameters for $C^{12}(p,\gamma)N^{13}$

Resonance energy (defined by $E_\lambda+\Delta_\lambda-\Sigma=0$)	462 keV
Reduced proton width γ_p^2	1.266 keV
Radiative width $\omega\Gamma_\gamma$	1.52 eV
Number ratios (for calculation of Δ_λ and $2\gamma/(F_c^2+G_c^2)$)	4.64×10^{-10} cm

*) A single-level Breit-Wigner formula is used, with all energy dependences included. The energies quoted are in the laboratory system. These parameters lead to a peak cross section of 137 μb at an energy of 440.5 keV.

FORM NBS-418
(8-1-63)
USCOMM-DC 18656-P63

U.S. DEPARTMENT OF COMMERCE
NATIONAL BUREAU OF STANDARDS

REF.
A.W. Parker, G.G. Shute
Australian J. Phys. 15, 443 (1962)

ELEM. SYM.		
N	13	7

METHOD
Inverse; NaI spectrometer

REF. NO.
62 Pa 2 NVB

REACTION	RESULT	EXCITATION ENERGY	SOURCE		DETECTOR		ANGLE
			TYPE	RANGE	TYPE	RANGE	
P,G	ABX	8-11	D	6-9	NAI-D		90
				(6.6, 7.53,			
				8.17, 9.14)			

TABLE 1

LEVEL PARAMETERS OF ^{13}N AND UPPER LIMITS TO $^{12}C(p,\gamma)^{13}N$ CROSS SECTIONS

E_p (MeV)	$E_{^{13}N}$ (MeV)	J^π	$W(\theta)$	$\sigma(p,p')$ (mbn/st)	$\sigma(p,\gamma_0)$ (μbn/st)	$\sigma(p,\gamma_1)$ (μbn/st)
6·6	8·0	3/2+	5—3 $\cos^2(\theta)$	4	<2	<4
7·53	8·89	1/2−	isotropic	16	<2	<10
8·17	9·48	3/2−	5—3 $\cos^2(0)$	19	<2	<2
9·14	10·38	7/2−	complex	24	<2	<2

Ref. E. K. Warburton, H. D. Funsten

Phys. Rev. 128, 1810 (1962)

Elem. Sym.	A	Z
N	13	7

Method

Synchrocyclotron - NaI(Tl)

Ref. No.	
62Wal	BG

Reaction	E or ΔE	E_o	Γ_{keV}	$\int \sigma dE$	$J\pi$	Notes
$(p,p'\gamma)$	E_p=16-20	E_p=17.5	420±30			Resonances in $(p,p'\gamma)$ correspond to N^{13} states at: 18.1 (for E_p=17.5) 18.65 (for E_p=18.05) and 19.8 (for E_p=19.3).
	E_γ=15.1	18.05	230±30			Excitation energy of N^{13}=1.941+0.924E_p
		19.3	250±40			Ground state capture shows little structure.

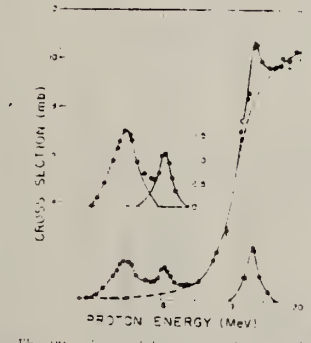

FIG. 4. The 90° differential cross section for the 15.1 MeV gamma rays from $C^{12}(p,\gamma_0)N^{13}$ obtained using a 5-in.×4-in. NaI(Tl) crystal. The ordinate scale gives the total cross section (±20°) if the gamma rays have an isotropic distribution relative to the proton beam. The resonances at 17.5, 18.05, and 19.3 MeV have been enhanced by plotting the difference between the actual data and the smoothed dashed curve.

FIG. 7. The 90° differential cross section for $C^{12}(p,\gamma_0)N^{13}$ obtained using a 5-in.×4-in. NaI(Tl) crystal at 90° to the proton beam. The ordinate scale gives the total cross section (±20°), if the gamma rays have an isotropic distribution relative to the proton beam

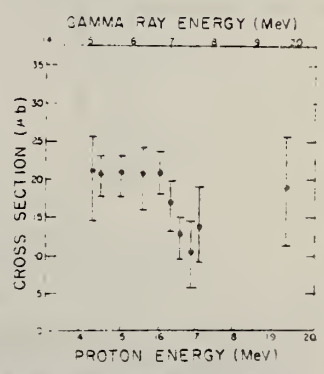

Ref. P.S.Fisher, D. F.Measday, F.A.Nikolaev, A.Kalmykov, A.B.Clegg	Elem. Sym.	A	Z
Nuclear Phys. 45, 113 (1963)	N	13	7

Method	Ref. No.	
50 MeV proton linac - NaI	63Fi1	BG

Reaction	E or ΔE	E_o	Γ	$\int \sigma dE$	Jπ	Notes 266+
$^{12}C(p,\gamma)^{13}N$	10-48.5	$E_{excitation}$				T = 3/2 part of giant electric dipole resonance concentrated largely above 22 MeV.
(p,γ_o)		13				
		20				T = 1/2 resonance found about 13MeV.
		(24)				
		32.5				γ_o, transition to graund state
(p,γ_2)		25				γ_2, transition to 3.5 doublet
						25 MeV resonance probably EI.
						Detector at 90°

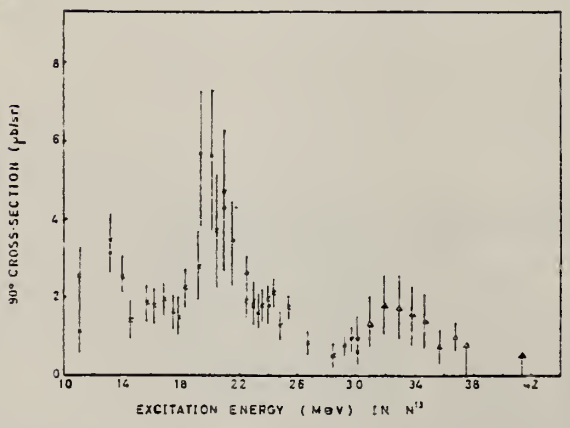

Fig. 4. The excitation function for the reaction $^{12}C(p,\gamma_0)^{13}N$. Run 1 — ×, run 2 — ○, run 3 — △.

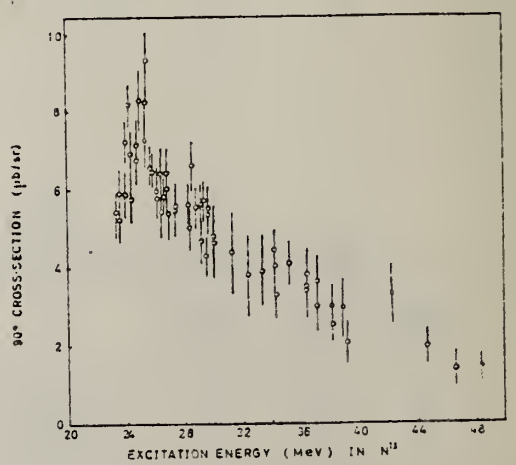

Fig. 5. The excitation function for the reaction $^{12}C(p,\gamma_2)^{13}N$.

Ref. F. C. Young, J.C. Armstrong, J.B. Marion
Nuclear Phys. 44, 486 (1963)
Erratum: Nuclear Phys. 49, 695 (1963)

Elem. Sym.	A	Z
N	13	7

Method: (source not given); γ-ray yield; NaI

Ref. No.: 63 Yo 2 | JHH

Reaction	E or ΔE	E_o	Γ	∫σdE	Jπ	Notes
$C^{12}(p,\gamma)$	1.5-2.0		$\omega\Gamma_\gamma$:			$\sigma(p,\gamma)_{3.51=E_\gamma}$ = 37 μb
	0.46	2.37	1.06 eV			$\sigma(p,\gamma)_{3.56=E_\gamma}$ < 0.16 μb
	1.70	3.51	< 0.006 eV			Parameters in Figure 4a,b,c are for angular distribution: $W(\theta) = A_o P_o(\cos\theta)+A_1 P_1(\cos\theta)+A_2 P_2(\cos\theta)$
		(3.56)				

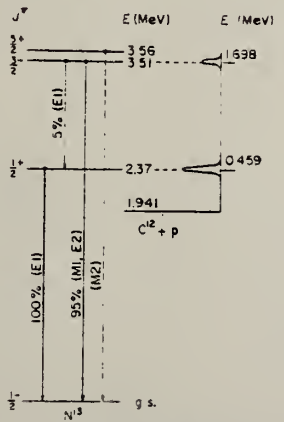

Fig. 1. Energy level diagram for N^{13}.

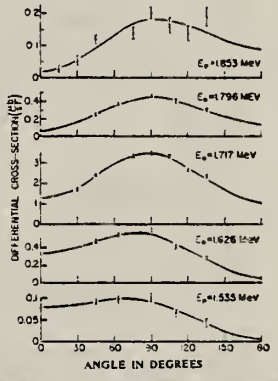

Fig. 2. Typical angular distributions for the ground-state γ rays from the $C^{12}(p,\gamma)N^{13}$ reaction.

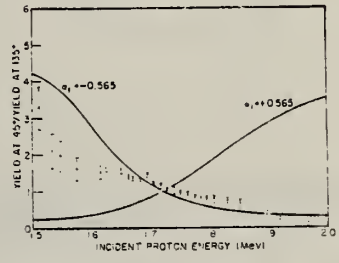

Fig. 3. The ratio of the yield of ground-state γ rays from the $C^{13}(p,\gamma)N^{13}$ reaction at 45° to that a 135°. The solid curves are theoretical calculations of the effect of the interference between the 2.3 and 3.51 MeV levels in N^{13} and are based on the known properties of these levels. The two values o a_1 result from the uncertainty in the sign of the inter-level phase difference.

Elem. Sym.	A	Z
N	13	7

Method

Ref. No.	
63 Yo 2	JHH

Reaction	E or ΔE	E_o	Γ	$\int \sigma dE$	Jπ	Notes

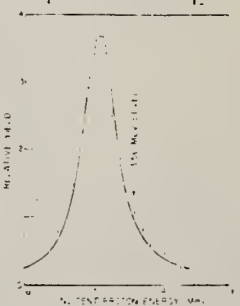

Fig. 5. Measured relative yield for the ground-state γ rays from the $C^{13}(p,\gamma)N^{13}$ reaction at 90°. The maximum yield corresponds to a differential cross section of 3.71 μb sr. The yield curve has not been corrected for the energy dependence of the stopping cross section of the target.

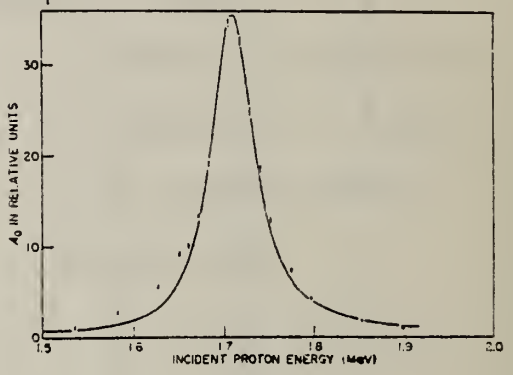

Fig. 4a.

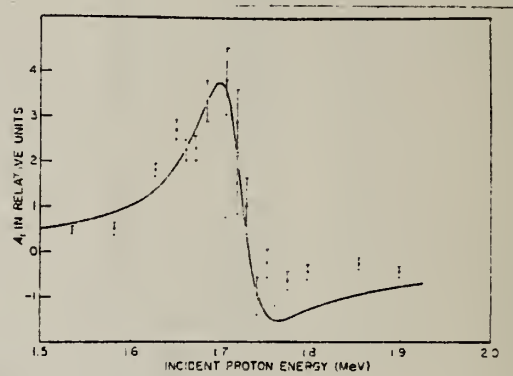

Fig. 4b.

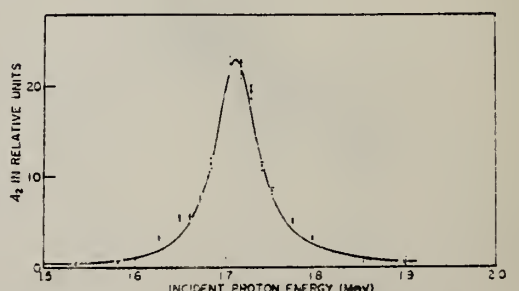

Fig. 4c. Comparison of the theoretically calculated angular distribution coefficients with the values extracted from the measured angular distributions.

REF. F. S. Dietrich, M. Suffert, A. V. Nero and S. S. Hanna
Phys. Rev. 168, 1169 (1968)

ELEM. SYM.	A	Z
N	13	7

METHOD

REF. NO. 68 Di 1 HMG

REACTION	RESULT	EXCITATION ENERGY	SOURCE		DETECTOR		ANGLE
			TYPE	RANGE	TYPE	RANGE	
P,G	LFT	15-16	D	14-15	NAI-D	11-15	DST
		(15.07)		(14.2)			

TABLE I. Parameters of γ transitions from the $T=\frac{3}{2}$, $J^\pi=\frac{1}{2}^-$ state in ^{13}N to lower $T=\frac{1}{2}$ levels.

Final state E_x(MeV)	J^π	Γ_γ(eV) Theor.[a]	Theor.[d]	Expt.	Expt.[e]	A_2[a] Theor.	Expt.	δ[b] Theor.[f]	Expt.
0	$\frac{1}{2}^-$	39	27	>4.7	27±5	−0.75	−0.66±0.09	−0.167	−0.095±0.07
2.365	$\frac{1}{2}^+$	...	...	...	<4.5	0.50[g]			
3.51	$\frac{3}{2}^-$	48	10	>4.0	23±5	0.51	0.30±0.10	+0.074	
3.56	$\frac{3}{2}^+$	...	...			0.10[g]			

[a] Coefficient in $P_0+A_2P_2$.
[b] Amplitude ratio of $E2$ and $M1$ radiation.
[c] J. G. Ginocchio, quoted in Ref. 4.
[d] Reference 13.
[e] Present result combined with Ref. 11.
[f] For $\langle r^2\rangle = 7fm^2$, Ref. 14.
[g] For pure $E1$ radiation.

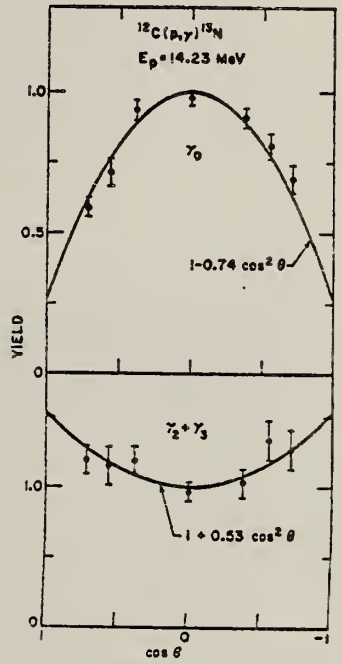

FIG. 3. Angular distributions of the γ's to the ground state of ^{13}N, and to the unresolved second and third excited states. The nonresonant yield has been subtracted.

REF. F. Riess, P. Paul, J. B. Thomas and S. S. Hanna
Phys. Rev. 176, 1140 (1968)

ELEM. SYM.	A	Z
N	13	7

METHOD

REF. NO. 68 Ri 2 HMG

REACTION	RESULT	EXCITATION ENERGY	SOURCE		DETECTOR		ANGLE
			TYPE	RANGE	TYPE	RANGE	
P,G_0	LFT	2	D	1	NAI-D		4PI
		(2.37)		(.459)			

$\Gamma_\gamma = 0.45 \pm 0.05$ eV.

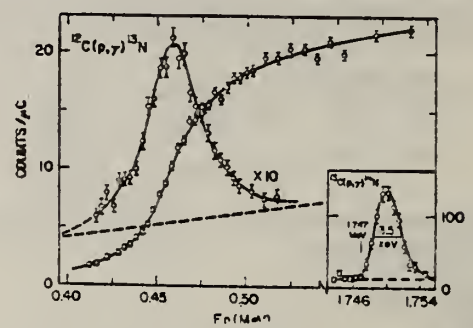

FIG. 6. Thin and thick target yield curves at the 0.459-MeV resonance of the reaction $^{12}C(p,\gamma)^{13}N$. The γ rays were detected with a 3×3-in. NaI(Tl) crystal. The insert shows the thin target yield for the 1.747-MeV resonance of $^{12}C(p,\gamma)^{13}N$.

REF.

R.A.I. Bell, I.G. Graham and J.V. Thompson
Nucl. Phys. A179, 408 (1972)

ELEM. SYM.	A	Z
N	13	7

METHOD

REF. NO.	
72 Be 1	egf

REACTION	RESULT	EXCITATION ENERGY	SOURCE		DETECTOR		ANGLE
			TYPE	RANGE	TYPE	RANGE	
HE,G	ABX	25-33	D	5-15	NAI-I		90

HE=HE3

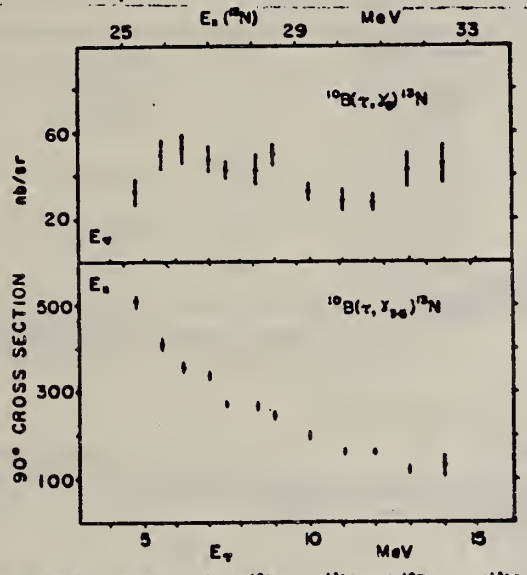

Fig. 4. Differential cross sections at 90° of the ^{10}B(τ, γ_0)^{13}N and ^{10}B(τ, $\gamma_{3.5}$)^{13}N reactions. The absolute cross section scale accuracy is ±20%.

REF.

M. Hasinoff, D. Johnson, and D. F. Measday
Phys. Letters 39B, 506 (1972)

ELEM. SYM.	A	Z
N	13	7

METHOD

REF. NO. 72 Ha 1 egf

REACTION	RESULT	EXCITATION ENERGY	SOURCE TYPE	SOURCE RANGE	DETECTOR TYPE	DETECTOR RANGE	ANGLE
P,G	ABX	10-17	D	8-17	NAI-D		90

546

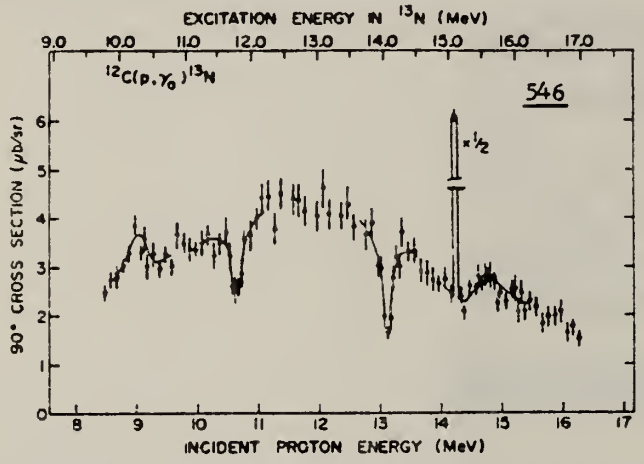

Fig. 1. The 90° differential cross section for the reaction $^{12}C(p,\gamma_0)^{13}N$. The lines represent best fits to the various structures assuming two interfering Breit-Wigner resonances except that the lines at the $T = \frac{1}{2}$ level (E_p = 14.231 MeV) are merely to guide the eye.

Table 1
Resonance parameters for states seen in $^{12}C(p,\gamma_0)^{13}N$ for $J = \frac{1}{2}$, and no non-interfering background. The errors listed are fitting errors only. The values of Γ_{p_0} Γ_{γ_0} and Γ_{γ_0} may be too small by as much as a factor of three if there is a non-interfering background

E_p (MeV)	E_x (MeV)	$\Gamma_{p_0}\Gamma_{\gamma_0}$ (keV)^2	Γ (keV)	Γ_{γ_0} (eV)
9.01	10.25	0.17 ± 0.09	280 ± 100	
10.62	11.74	0.28 ± 0.10	220 ± 50	2.3 ± 1.1 a)
13.12	14.04	0.47 ± 0.12	170 ± 20	3.7 ± 1.0 b)
14.50	15.31	0.21 ± 0.08	380 ± 150	

a) A value of 0.55 ± 0.25 is assumed for Γ_{p_0}/Γ based on the values of 0.26 and 0.82 for the levels at E_p = = 9.132 MeV [13].
b) A value of 126 keV is taken for Γ_{p_0} [2].

REF. D. F. Measday, M. Hasinoff, and D. L. Johnson
Can. J. Phys. 51, 1227 (1973)

ELEM. SYM.	A	Z
N	13	7

METHOD

REF. NO. 73 Me 3 hmg

REACTION	RESULT	EXCITATION ENERGY	SOURCE TYPE	SOURCE RANGE	DETECTOR TYPE	DETECTOR RANGE	ANGLE
P,G	ABX	9- 24	D	9- 24	NAI-D		90

TABLE I. Resonance parameters for states seen in $^{12}C(p, \gamma_0)^{13}N$ assuming no noninterfering background. The errors listed are fitting errors only. The values of $\Gamma_{p_0}\Gamma_{\gamma_0}$ and Γ_{γ_0} may be in error by as much as a factor of three due to a possible noninterfering background. Of the two solutions given for each resonance, the smaller value for Γ_{γ_0} is thought to be the physical one

E_p (MeV)	E_x (MeV)	J^π	$\Gamma_{p_0}\Gamma_{\gamma_0}$ (keV)[a]	Γ (keV)	Γ_{γ_0} (eV)
12.5 ± 0.2	13.0 ± 0.2	3/2+	7500 ± 1000	7000	≥1100
9.01 ± 0.15	10.25 ± 0.15	3/2+	0.17 ± 0.09	280 ± 100	≥0.6
			19 ± 16	330 ± 100	≥58
		or 1/2+	1.7 ± 0.5	300 ± 100	≥6[a]
10.62 ± 0.12	11.74 ± 0.12	3/2+	0.28 ± 0.10	220 ± 50	~4.2[b]
			17.5 ± 4.3	230 ± 60	~254[b]
13.12 ± 0.09	14.04 ± 0.09	3/2+	0.47 ± 0.12	170 ± 20	3.7 ± 1.0[c]
			9.6 ± 3.5	170 ± 30	76 ± 28[c]
14.5 ± 0.2	15.3 ± 0.2	3/2+ (?)	0.21 ± 0.08	380 ± 150	≥0.5
			33 ± 13	310 ± 110	≥100

[a] Assuming no interfering background.
[b] A value of 0.30 ± 0.05 is assumed for Γ_{p_0}/Γ (Meyer and Plattner 1973).
[c] A value of 126 keV is taken for Γ_{p_0} (LeVine and Parker 1969).

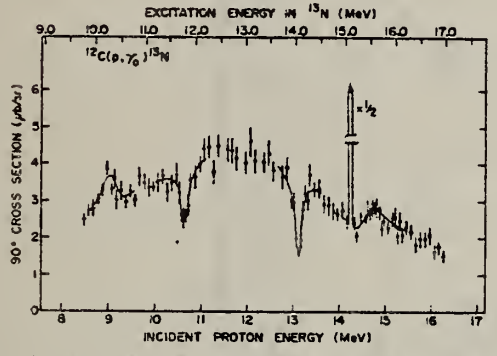

FIG. 4. The 90° yield curve for the reaction $^{12}C(p, \gamma_0)^{13}N$. The solid lines are fits to the data as described in the text. The narrow peak at $E_x = 15.1$ MeV is due to the first $T = 3/2$ level in ^{13}N. The errors shown are purely statistical and do not include a ±25% uncertainty in the absolute normalization.

(a) The Capture Reaction

The yield curve for the reaction $^{12}C(p, \gamma_0)^{13}N$ is presented in Fig. 4. The errors shown are purely statistical and do not include the error on the absolute normalization (±25%) nor the error for the energy dependence of the window efficiency (≃10% between the extremes of the yield curve). The yield for the γ rays leaving ^{13}N in excited states cannot be extracted from the data in a reliable way, although one can state that the cross section for γ_1 is always less than a half that for γ_0, whilst γ_2 and γ_3 have a summed cross section which is typically twice that for γ_0.

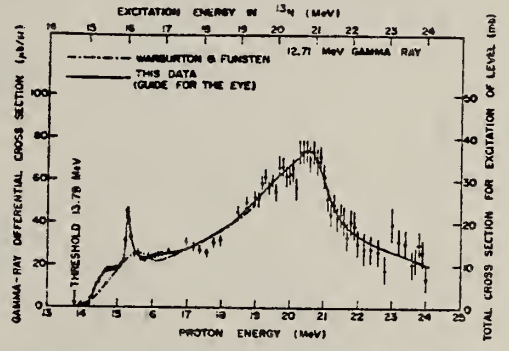

FIG. 5. The 90° yield curve for the 12.71 MeV γ ray in proton–carbon collisions. The errors shown are statistical and do not include a ±25% uncertainty in the absolute normalization.

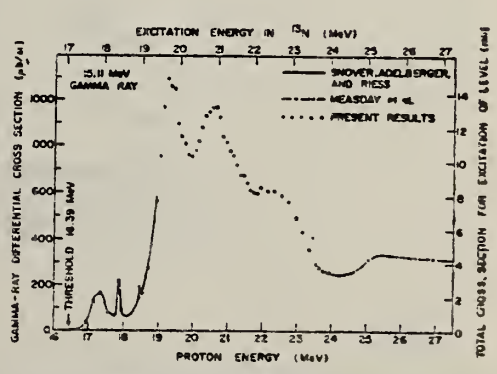

FIG. 6. The 90° yield curve for the 15.11 MeV γ ray in proton–carbon collisions. The errors shown are purely statistical and do not include a ±25% uncertainty in the absolute normalization.

	9/73	✓
	"	✓

REF.

C. Rolfs and R. E. Azuma
Nucl. Phys. A227, 291 (1974)

N	13	7

METHOD

REF. NO. 74 Ro 2 egf

REACTION	RESULT	EXCITATION ENERGY	SOURCE TYPE	SOURCE RANGE	DETECTOR TYPE	DETECTOR RANGE	ANGLE
P,G	ABX	2- 4	D	0- 3	SCD-D		DST

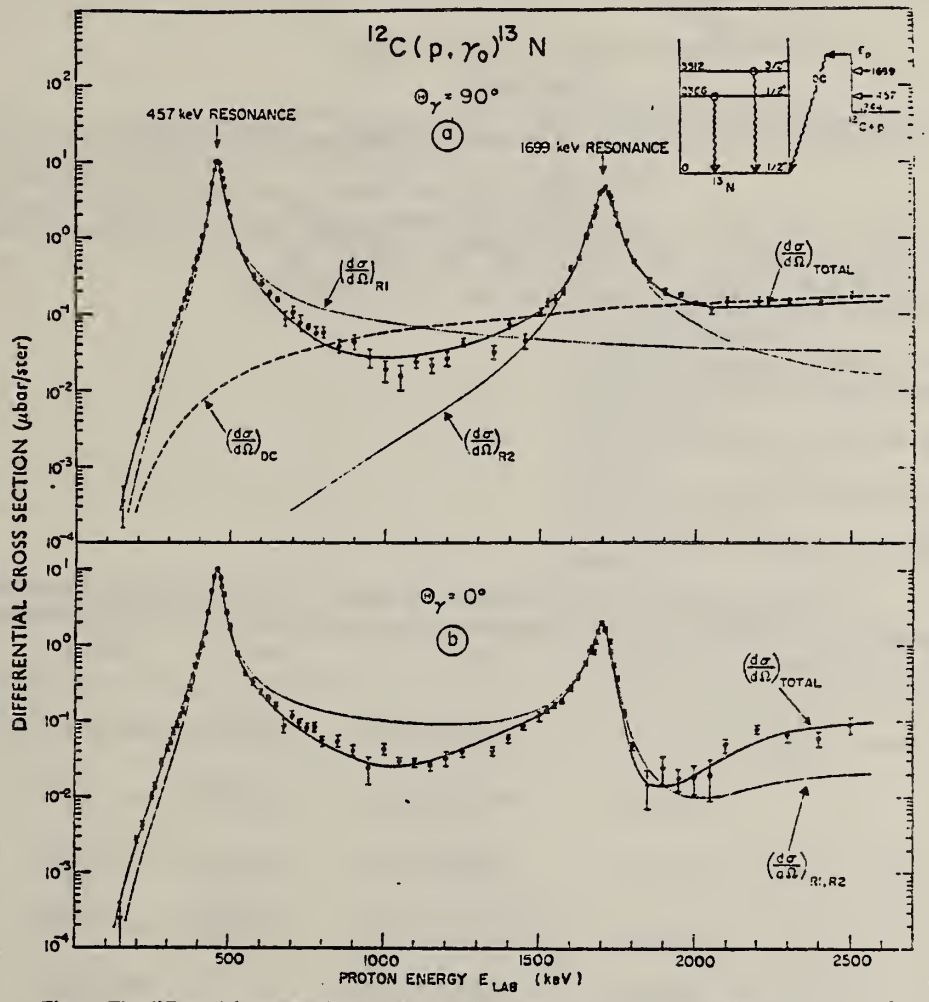

Fig. 4. The differential cross sections at 0° and 90° for the γ-ray transition to the ground state in ^{13}N are shown as a function of beam energy (E_p = 150–2500 keV). The solid lines through the data points represent the optimal theoretical fit (see text). The inset shows the γ-ray decay schemes involved in the yield curves.

(over)

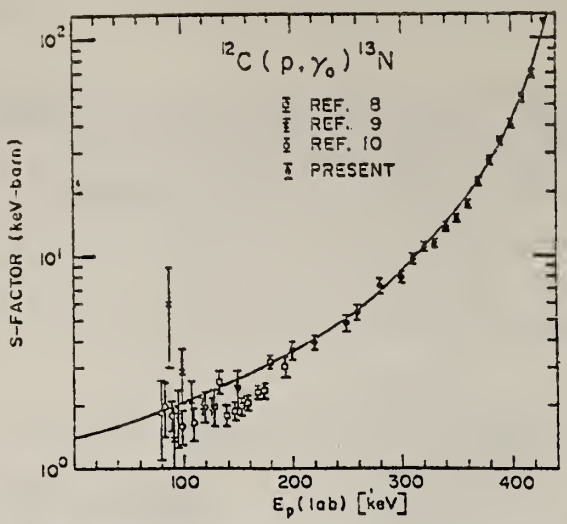

Fig. 5. Astrophysical *S*-factor for the reaction $^{12}C(p,\gamma_0)^{13}N$ from previous [8-10] and present work. The solid line through the data points represents the model calculations.

8) C.L. Bailey et al., Phys. Rev. 77 (1950) 194
9) R.N. Hall et al., Phys. Rev. 77 (1950) 197
10) W.A.S. Lamb et al., Phys. Rev. 107 (1957) 550

REF.	R. E. Marrs, E. G. Adelberger, K. A. Snover, and M. D. Cooper Phys. Rev. Lett. 35, 202 (1975)	ELEM. SYM.	A	Z
		N	13	7

METHOD	REF. NO.
	75 Ma 6 hmg

REACTION	RESULT	EXCITATION ENERGY	SOURCE		DETECTOR		ANGLE
			TYPE	RANGE	TYPE	RANGE	
P,G	LFT	15	D	14- 15	NAI-D		125
		(15.07)					

$\Gamma_{\gamma o}$ = 24.5 ± 1.5 eV

LEVEL AT 15.07 MEV

We have measured the γ-ray branching ratios of the lowest $T = \frac{3}{2}$ levels in ^{13}C and ^{13}N, and the absolute strength of the γ_0 transition in ^{13}N. The mirror electromagnetic selection rule is obeyed by the $M1$ (γ_0 and γ_2) transitions. However the $E1$ (γ_1) transitions exhibit a surprisingly large charge asymmetry. Charge-dependent differences in the radial wave functions do not account for a similar asymmetry in strong $T = \frac{1}{2} \rightarrow T = \frac{1}{2}$ $E1$ transitions in mass 13.

[11]G. Wittwer, H. G. Clerc, and G. A. Beer, Phys. Lett. 30B, 634 (1969).
[12]S. W. Robinson, C. P. Swann, and V. K. Rasmussen, Phys. Lett. 26B, 298 (1968); F. Metzger, private communication.
[13]C. Rolfs and R. E. Azuma, Nucl. Phys. A227, 291 (1974).
[14]M. Chemtob and S. Furui, Nucl. Phys. A233, 435 (1974).
[15]H. Sato and S. Yoshida, Nucl. Phys. A211, 509 (1973).

TABLE I. γ-transition strengths in ^{13}C and ^{13}N. Reduced transition strengths are in Weisskopf units.

	$E_i(J^\pi,T)$	$E_f(J^\pi,T)$	Γ_γ(eV)	B(W.u.)	δ(exp.)	δ(theory)	$\lvert A_2/A_1 \rvert$
^{13}C ^{13}N	15.11 15.07 (3/2⁻,3/2)	0.0 0.0 (1/2⁻,1/2)	22.7 ± 2.6[a] (M1) 24.2 ± 1.5 (M1)	0.318 ± 0.036 (M1) 0.342 ± 0.021 (M1)	-0.07 ± 0.13	0.01[e] -0.049[f]	< 0.065
^{13}C ^{13}N	15.11 15.07 (3/2⁻,3/2)	0.0 0.0 (1/2⁻,1/2)	0.59 ± 0.11[a] (E2) 0.32 ± 0.12 (E2)	0.51 ± 0.10 0.28 ± 0.11 (E2)	$0.82^{+1.2}_{-0.6}$		
^{13}C ^{13}N	15.11 15.07 (3/2⁻,3/2)	3.68 (3/2⁻,1/2) 3.51 (3/2⁻,1/2)	18.2 ± 2.4[b] 19.6 ± 1.4[b] (M1)	0.587 ± 0.077 (M1) 0.613 ± 0.044 (M1)	-0.04 ± 0.14	0.003[e]	< 0.058
^{13}C ^{13}N	15.11 15.07 (3/2⁻,3/2)	3.09 (1/2⁺,1/2) 2.37 (1/2⁺,1/2)	4.12 ± 0.74 ≤2.82 ± 0.30 (E1)	(6.4 ± 1.1) × 10^{-3} ≤(3.69 ± 0.39) × 10^{-3} (E1)	≥0.83 ± 0.29		
^{13}C ^{13}N	3.09 (1/2⁺,1/2) 2.37 (1/2⁺,1/2)	0.0 0.0 (1/2⁻,1/2)		0.040 ± 0.005[c] 0.13 ± 0.01[d] (E1)	-0.69 ± 0.05		
					Δ = 0.03 ± 0.07[g]	-0.007[e]	$\bar{A}$ < 0.016[g]

[a]Ref. 11.
[b]This may contain a small unresolved component (see text).
[c]Ref. 12.
[d]Weighted average from Ref. 13 and references therein.
[e]Isotensor, Ref. 14.
[f]Charge dependent, shell model, Ref. 15.
[g]See text.

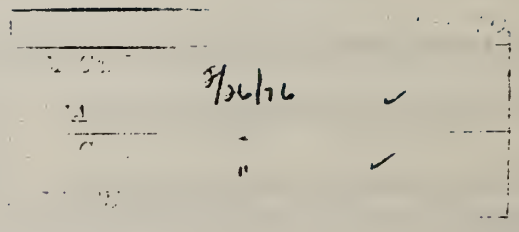
8/26/76

REF.

D. Berghofer, M.D. Hasinoff, R. Helmer, S.T. Lim,
D.F. Measday, K. Ebisawa
Nucl. Phys. A263, 109 (1976)

ELEM. SYM.	A	Z
N	13	7

METHOD

REF. NO.: 76 Be 8 egf

REACTION	RESULT	EXCITATION ENERGY	SOURCE		DETECTOR		ANGLE
			TYPE	RANGE	TYPE	RANGE	
P,G	ABX	10- 24	D	9- 14	NAI-D		DST

Abstract: The reaction $^{12}C(p,\gamma)^{13}N$ has been studied over the energy range $9 < E_p < 14$ MeV. New structure is established around $E_x = 20$ MeV in the giant dipole resonance of ^{13}N. The interference dips at $E_x = 11.74$ MeV and at 14.04 MeV are confirmed as $\frac{3}{2}^+$ levels interfering with a pygmy resonance which has a predominantly $\frac{1}{2}^+$ strength. Total cross-section yield curves for the 12.71 and 15.11 MeV inelastic γ-rays have been obtained up to $E_p = 24$ MeV, and new structure is observed.

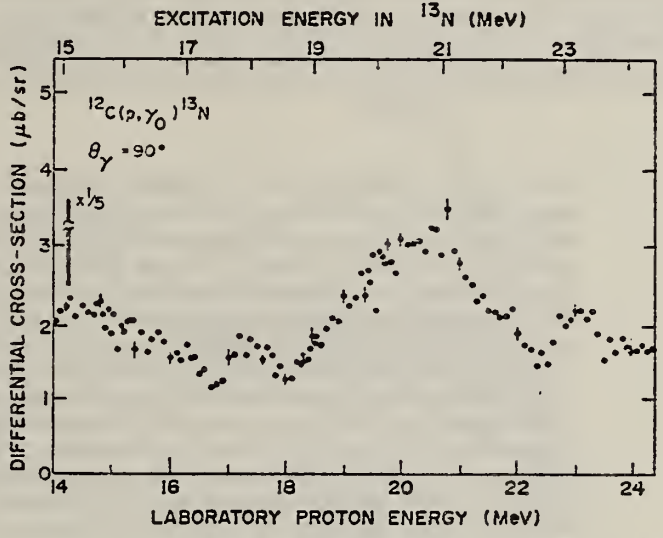

Fig. 3. Differential cross section for the 90° yield of capture γ-rays leading to the ground state of ^{13}N. In addition to the relative errors shown, there is an uncertainty in the absolute normalization of ±20%.

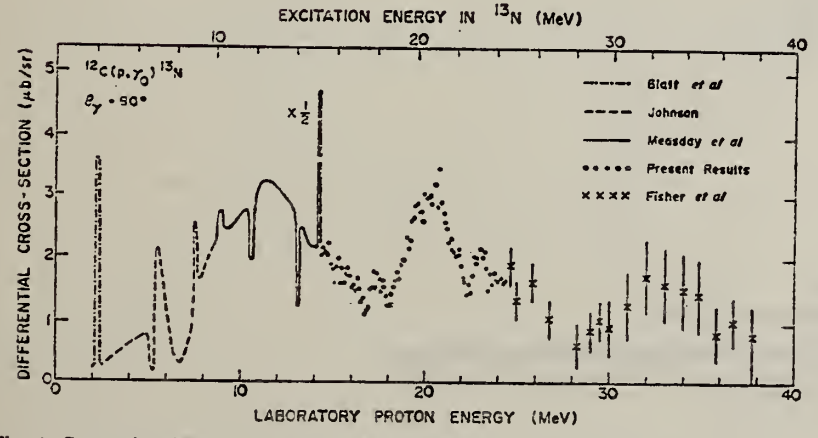

Fig. 4. Composite yield curve for capture γ-rays leading to the ground state of ^{13}N. There has been some slight adjustment of absolute normalizations between the various data (there were always overlapping regions which are not illustrated).

[8] S.L. Blatt et al., Phys. Rev. C10, 1319 (1974).
[15] D.L. Johnson, Ph.D. Thesis, U. of Wash., unpublished.
[3] D.F. Measday et al., Can. J. Phys. 51, 1227 (1973).
[13] P.S. Fisher et al., Nucl. Phys. 45, 113 (1963).

(over)

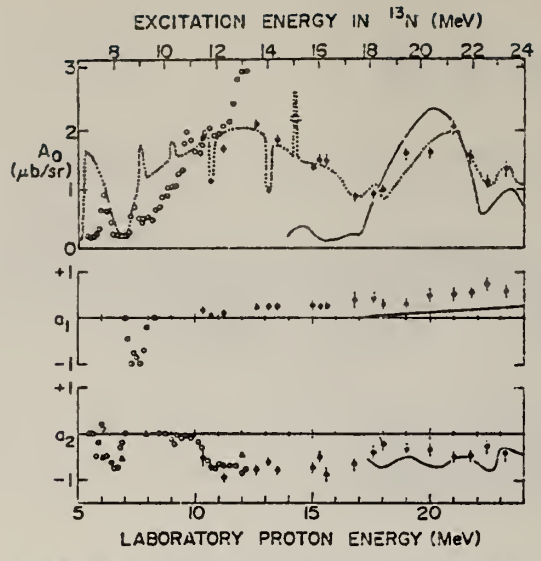

Fig. 6. Legendre coefficients for capture γ-rays leading to the ground state of ^{13}N (solid circles). The open circles represent the ^{12}C(n, γ) reaction, derived from the (γ, n) data of Bertozzi *et al.* [17]). The open triangles represent the ^{12}C(n, γ)^{13}C reaction and were derived from the (γ, n) data of Fukuda [18]). The dotted line represents the 90° yield curve for the ^{12}C(p, γ_0) reaction. The full lines are the data of Allas *et al.* [16]) on the reaction ^{11}B(p, γ_0)^{12}C but shifted down in excitation energy by 2 MeV.

[16] R.G. Allas et al., Nucl. Phys. 58, 122 (1964).

[17] W. Bertozzi et al., Nucl. Instr. 33, 199 (1965).

[18] K. Fukuda, Nucl. Phys. A156, 10 (1970.

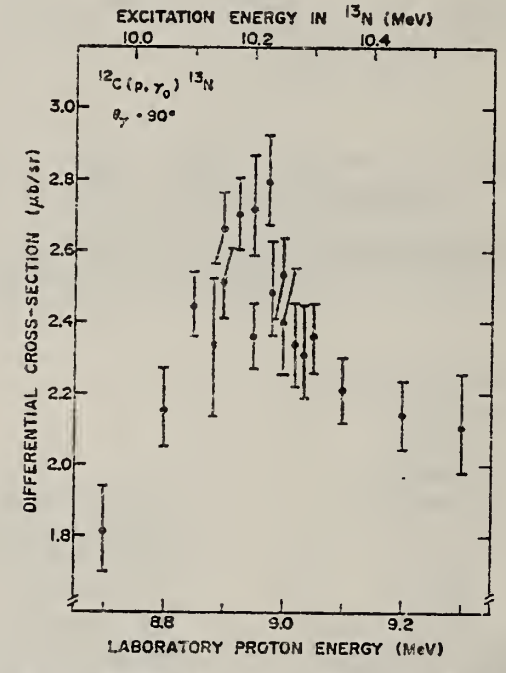

Fig. 7. Differential cross section for the 90° yield of capture γ-rays leading to the ground state over the energy region $8.7 \leqq E_p \leqq 9.3$ MeV. This structure is probably a $\frac{1}{2}^+$ resonance at $E_x \approx 10.25$ MeV with $\Gamma_T \approx 300$ keV.

REF. S. Ferroni, G. Ricco, G.A. Rottigni, M. Sanzone, and G.Lo Bianco
Il Nuovo Cimento 35, 15 (1976)

ELEM. SYM.	A	Z
N	13	7

METHOD

REF. NO. 76 Fe 7 egf

REACTION	RESULT	EXCITATION ENERGY	SOURCE		DETECTOR		ANGLE
			TYPE	RANGE	TYPE	RANGE	
P,G	ABX	15- 37	D	16- 40	NAI-D		90

Summary. — Excitation functions for the reactions $^{12}C(p, \gamma_0)$ and $^{12}C(p, \gamma_{3+2})$ at proton energies in the range 16 to 40 MeV have been measured by means of a scintillation pair spectrometer. In the course of the same experiment, the yields of 4.43, 12.7 and 15.1 MeV γ-rays following inelastic proton scattering have been determined as a function of the incident-proton energy. Resonances are observed at proton energies of 20 and ~32 MeV; the former appears in all reaction channels except (p, γ_{3+2}), while the latter shows up in the capture cross-sections and in the yield of the 4.43 MeV γ-ray. The information collected in the present experiment, complemented by data on proton elastic and inelastic scatterings obtained by other authors, has been interpreted in the framework of the doorway-state-picture. The intermediate state in ^{13}N at an excitation energy of 20.4 MeV has been identified with the giant-dipole resonance, while the presence of *E*1 and *E*2 strength is suggested around 32 MeV.

over

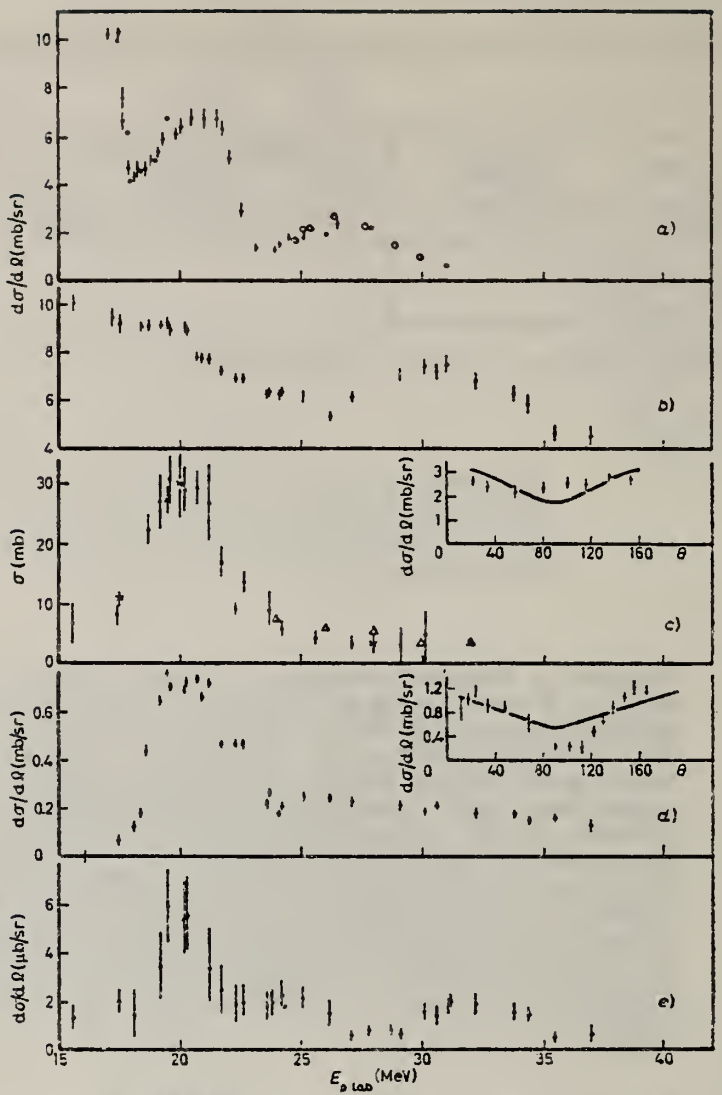

Fig. 4. – Excitation energy in ^{12}N. *a*) Differential cross-section for elastic proton scattering on ^{12}C at 135° (solid points) and 145° (open points); *b*) yield of 4.43 MeV γ-ray following inelastic proton scattering on ^{12}C; *c*) excitation function for the ^{12}C(pp′)^{12}C* (12.7 MeV): the solid points are relative γ-ray data from this experiment, triangles ([11]) and crosses ([12]) are integrated proton data.

[11] H.V. Geramb, K. Amos, H. Spuckmann, K.T. Knopfle, M. Rogge, D. Ingham and C. Mayer-Boricke: Phys. Rev. C, 12, 1697 (1975)

[12] J.K. Dickens, D.A. Haner and C.N. Waddell: Phys. Rev., 132, 2159 (1963)

REF.

R.E. Marrs, E.G. Adelberger, and K.A. Snover
Phys. Rev. C 16, 61 (1977)

EL EM. SYM.	A	Z
N	13	7

METHOD

REF. NO. 77 Ma 7 hmg

REACTION	RESULT	EXCITATION ENERGY	SOURCE TYPE	SOURCE RANGE	DETECTOR TYPE	DETECTOR RANGE	ANGLE
(P,G)	ABY	15	D	14	NAI-D		DST
				(14.2-14.3)			

[NUCLEAR REACTIONS $^{12}C(p,\gamma_0)$, $E=14.23$ MeV resonance; $^{11}B(^3He, p\gamma)$, $^{11}B(^3He, n\gamma)$, particle-γ coincidence; measured Γ_{γ_i}/Γ and deduced Γ_{γ_i} and Γ for ^{13}C ($T=\frac{3}{2}$) and ^{13}N ($T=\frac{3}{2}$); symmetry of mirror transitions.]

15=15.066

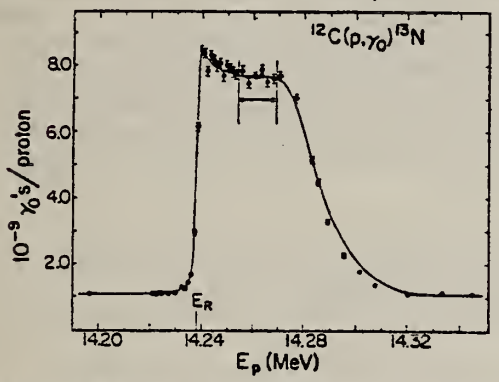

FIG. 4. Resonance yield per incident proton (multiplied by 4π) for the $^{12}C(p,\gamma_0)^{13}N$ reaction at $\theta_\gamma=125°$. Only statistical errors are shown. There is an additional overall systematic error of ±3% due to the NaI efficiency calibration. The solid curve is a Monte Carlo calculation (see text). The plateau region used to obtain the thick-target yield is delineated by the vertical lines. Only the $I_p=35$ nA data are shown here. The energy scale comes from the nominal accelerator calibration.

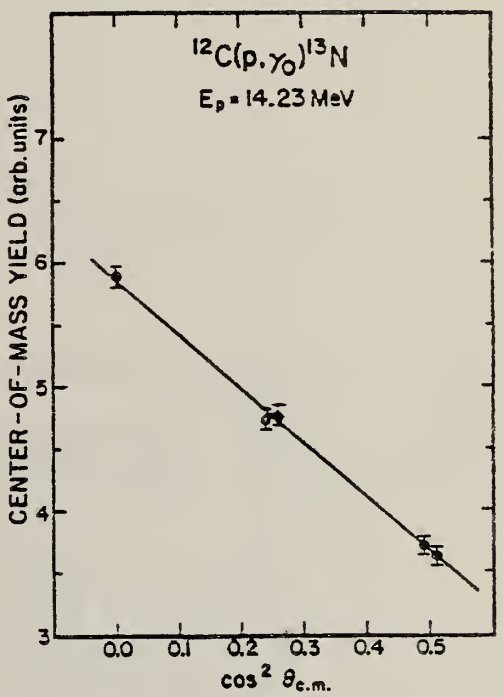

FIG. 5. Angular distribution of the $^{12}C(p,\gamma_0)^{13}N$ resonant yield for the ^{13}N ($T=\frac{3}{2}$) resonance at $E_p=14.23$ MeV. Yields and angles are with respect to the $^{13}N^*$ reference frame. The nonresonant background has been subtracted. The straight line is a least-squares fit to $A_0P_0(\cos\theta)+A_2P_2(\cos\theta)$.

TABLE I. Summary of γ widths (in eV) and branching ratios for the $^{13}C(\frac{3}{2}^-, T=\frac{3}{2})$ and ^{13}N-$(\frac{3}{2}^-, T=\frac{3}{2})$ levels at $E_x=15.1$ MeV. The state labeled $\frac{5}{2}^-$ refers to the level at 7.55 MeV in ^{13}C.

J^π of final state	Γ_γ (eV) ^{13}C	^{13}N	Theory (^{13}N)[a]
$\frac{1}{2}^-$(g.s.)	$22.7\pm2.6(M1)$[b]	$24.2\pm1.5(M1)$	26.24($M1$)
	$0.59\pm0.11(E2)$[b]	$0.32\pm0.12(E2)$	0.74($E2$)
$\frac{1}{2}^+$	4.12 ± 0.74	$\leq2.82\pm0.30$	
$\frac{3}{2}^-+\frac{5}{2}^+$	18.2 ± 2.4	19.6 ± 1.4	10.44 (to $\frac{3}{2}^-$)
$\frac{5}{2}^-$	<0.9		7.0×10^{-3}

Decay properties of the $T=\frac{3}{2}$ levels

^{13}C	^{13}N
$\Gamma_{\gamma_0}/\Gamma=(0.396\pm0.030)\%$	$\Gamma_{p_0}\Gamma_{\gamma_0}/\Gamma=(5.79\pm0.20)$ eV
$\Gamma=(5.88\pm0.81)$ keV	$\Gamma_{\gamma_0}/\Gamma_{p_0}=(12.1\pm1.1)\%$
	$\Gamma=(0.86\pm0.12)$ keV

[a] Reference 32.
[b] Reference 18.

[32] D. Kurath (private communication)

[18] G. Wittwer, H.G. Clerc, and G.A. Beer, Phys. Lett. 30B, 634 (1969)

REF. R.L. Helmer, M.D. Hasinoff, J.E. Bussoletti, K.A. Snover, T.A. Trainor
Nucl. Phys. A336, 219 (1980)

ELEM. SYM.	A	Z
N	13	7

METHOD

REF. NO. 80 He 4 hg

REACTION	RESULT	EXCITATION ENERGY	SOURCE		DETECTOR		ANGLE
			TYPE	RANGE	TYPE	RANGE	
$ P,G	ABX	11-18	D	10-17	NAI-D		DST

Abstract: Cross sections for the $^{12}C(\vec{p},\gamma_0)^{13}N$ reaction have been measured from $E_{\vec{p}}$ = 10 MeV to 17 MeV in the laboratory system by bombarding an enriched carbon-12 target with a beam of polarized protons. A 25 cm diameter × 25 cm NaI(Tl) detector with a plastic anti-coincidence shield was used to detect the gamma rays. The total E2 capture cross sections were of the order of 0.2 μb and no resonance effects were observed. The amount of the E2 energy-weighted sum rule depleted in this energy range is $(8.5 \pm 3.3)\%$. Calculations based on a direct semi-direct capture model provide a good description of the experimental results by including only direct E2 capture and direct plus collective E1 capture.

POLARIZED PROTONS

E NUCLEAR REACTIONS $^{12}C(\vec{p},\gamma_0)^{13}N$, E = 10-17 MeV; measured differential cross-section $\sigma_-(E_{\vec{p}};\theta_\gamma)$, and differential asymmetry $\sigma_-(E_{\vec{p}},\theta_\gamma)$. ^{13}N deduced E1 and E2 cross sections. Enriched target.

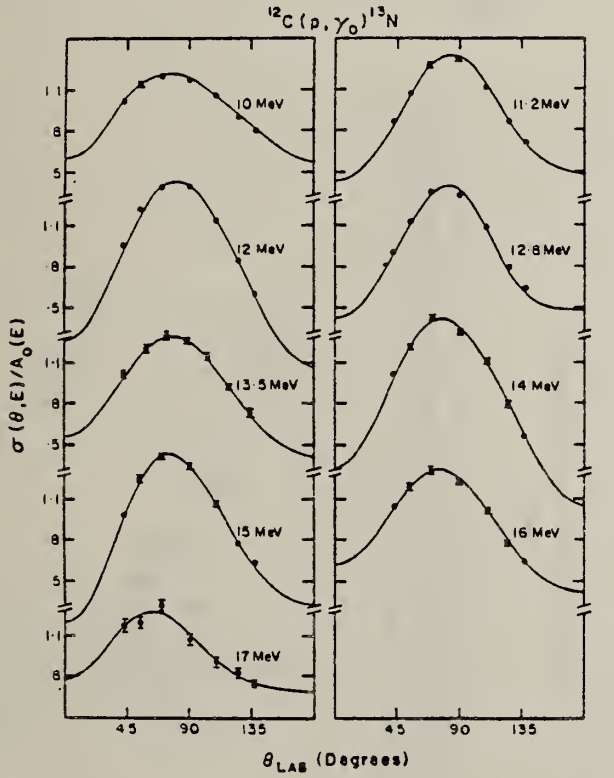

Fig. 4. $^{12}C(\vec{p},\gamma_0)^{13}N$ fractional differential cross sections $\sigma(\theta, E)/A_0(E)$. The solid lines are from a least squares fit to the data (see text). Statistical errors are shown where they are larger than the spot size.

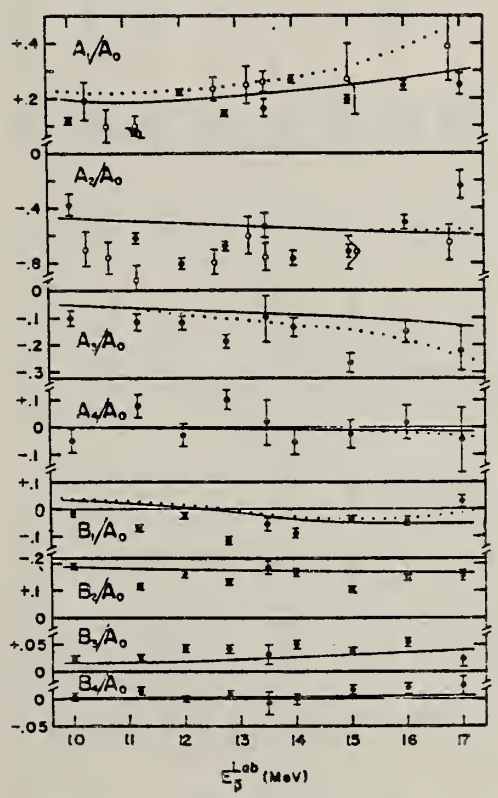

Fig. 6. $^{12}C(\vec{p},\gamma_0)^{13}N$ normalized angular distribution coefficients. The solid points refer to the present data; the open circles refer to the data of ref. [16]. The solid curves are from a calculation which includes direct and collective E1 capture; the dotted curves include, in addition, a compact isoscalar E2 resonance (sect. 4).

(OVER)

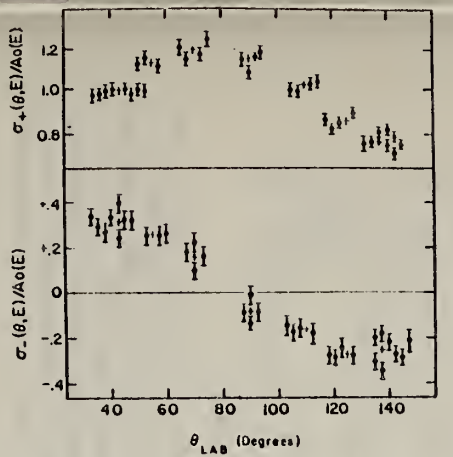

Fig. 3. The complete angular distribution measurements at $E_{\vec{p}} = 10$ MeV. The ordinate of the upper plot is the sum of the spin up and spin down yields. The ordinate of the lower plot is the difference of these yields divided by $2PA_0$ (see text). The plus signs are the averages of the measurements at a given angle; the surrounding points with error bars are the actual measurements at the angle indicated by the + sign.

TABLE I

$^{12}C(\vec{p}, \gamma_0)^{13}N$ angular distribution coefficients

$E_{\vec{p}}$ (MeV)	$4\pi A_0$ [c] (μb)	a_1	a_2	a_3	a_4	b_1	b_2	b_3	b_4	χ^2_ν [a]	χ^2_ν [b]
10.0	22.0	0.120 ±0.012	−0.384 ±0.039	−0.100 ±0.028	−0.017 ±0.045	0.0118 ±0.0088	0.1916 ±0.0055	0.0248 ±0.0053	0.0018 ±0.0064	1.02	1.54
11.2	21.0	0.086 ±0.012	−0.620 ±0.041	−0.114 ±0.029	0.081 ±0.045	−0.0711 ±0.0097	0.1125 ±0.0053	0.0267 ±0.0058	0.0124 ±0.0066	1.02	0.49
12.0	24.9	0.218 ±0.011	−0.804 ±0.038	−0.118 ±0.024	−0.032 ±0.041	−0.0265 ±0.0082	0.1602 ±0.0047	0.0426 ±0.0050	−0.0009 ±0.0056	0.66	0.90
12.8	26.4	0.147 ±0.010	−0.641 ±0.034	−0.186 ±0.024	0.100 ±0.036	−0.1140 ±0.0078	0.1358 ±0.0044	0.0418 ±0.0047	0.0096 ±0.0054	3.58	1.15
13.5	22.7	0.167 ±0.030	−0.525 ±0.092	−0.106 ±0.085	0.104 ±0.085	−0.0571 ±0.0224	0.1860 ±0.0179	0.0334 ±0.0165	−0.0077 ±0.0190	1.04	1.87
14.0	20.8	0.270 ±0.014	−0.766 ±0.050	−0.134 ±0.034	−0.052 ±0.055	−0.0871 ±0.0117	0.1713 ±0.0064	0.0498 ±0.0069	0.0011 ±0.0079	4.24	0.51
15.0	17.8	0.197 ±0.014	−0.713 ±0.048	−0.269 ±0.033	−0.023 ±0.052	−0.0341 ±0.0109	0.1023 ±0.0059	0.0394 ±0.0064	0.0182 ±0.0074	1.15	0.49
16.0	15.7	0.245 ±0.017	−0.497 ±0.055	−0.148 ±0.033	0.018 ±0.062	−0.0359 ±0.0132	0.1522 ±0.0076	0.0538 ±0.0080	0.0186 ±0.0092	0.93	0.13
17.0	10.7	0.253 ±0.037	−0.230 ±0.107	−0.212 ±0.077	−0.045 ±0.121	0.0275 ±0.0241	0.1551 ±0.0157	0.0251 ±0.0157	0.0272 ±0.0177	2.89	0.24

[a]) Reduced chi-squared for fit to yield angular distribution.
[b]) Reduced chi-squared for fit to asymmetry angular distribution.
[c]) A_0 taken from fig. 6 of ref. [10])

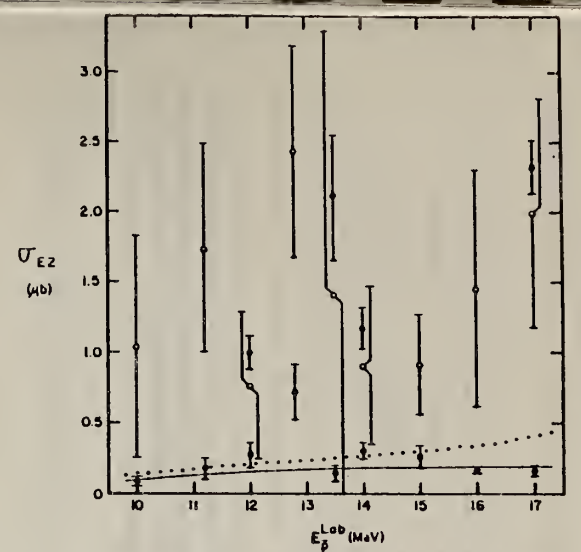

Fig. 11. The E2 cross sections. The solid points are from solution I (or II) and additional solutions which satisfy a 1.0 % confidence limit (see text). The open circles are from solutions obtained with A_1 and B excluded from the T-matrix element fit. The solid and dotted curves are from DSD capture mode calculations (sect. 4).

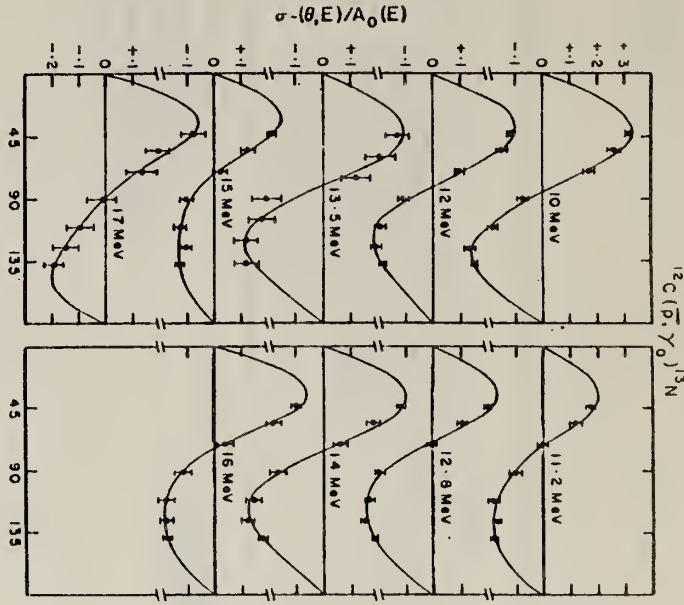

Fig. 5. $^{12}C(\vec{p}, \gamma_0)^{13}N$ fractional cross section asymmetries $\sigma_-(\theta, E)/A_0(E)$. The solid lines are least squares fits to the data (see text). Statistical errors only are shown.

REF. K.A. Snover, P.G. Ikossi, E.G. Adelberger, K.T. Lesko
Phys. Rev. Lett 44, 927 (1980)

ELEM. SYM.	A	Z
N	13	7

METHOD

REF. NO. 80 Sn 1 hg

REACTION	RESULT	EXCITATION ENERGY	SOURCE TYPE	SOURCE RANGE	DETECTOR TYPE	DETECTOR RANGE	ANGLE
$ P,G	RLY	15	D	14-15	NAI-D		DST
		(15.1)		(14.2-14.3)			

POL PROTONS

The interference between the E_p = 14.23 MeV $M1(E2)$ $T = \frac{3}{2}$ resonance and the $E1$ giant-dipole-resonance "background" in the reaction $^{12}C(p_{pol},\gamma_0)^{13}N$ is used to determine uniquely the $E1$ reaction amplitudes. The $E1$ capture is found to be predominantly d wave, in agreement with the basic shell-model description of the nuclear giant dipole resonance.

PACS numbers: 24.30.Cz, 25.40.Lw, 27.20.+n

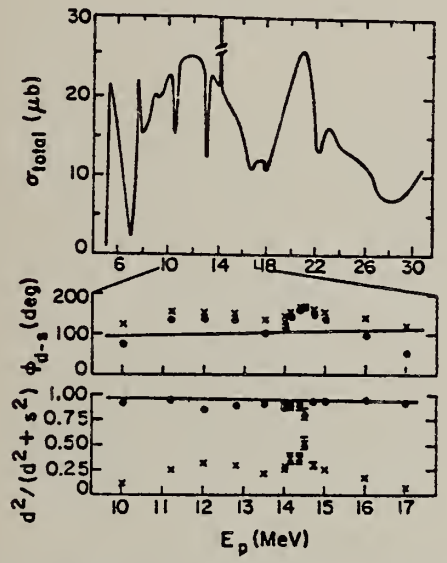

FIG. 1. Upper part: σ_{total} for $^{12}C(p_{pol},\gamma_0)$ for E_p = 5–30 MeV (Refs. 4 and 5). Lower part: The d–s phase difference and the relative d-wave intensity for E_p = 10–17 MeV (Ref. 5 plus the present work for 14 < E_p < 15 MeV). The points and crosses correspond to the two different solutions. The solid lines are DSD calculations described in Ref. 5.

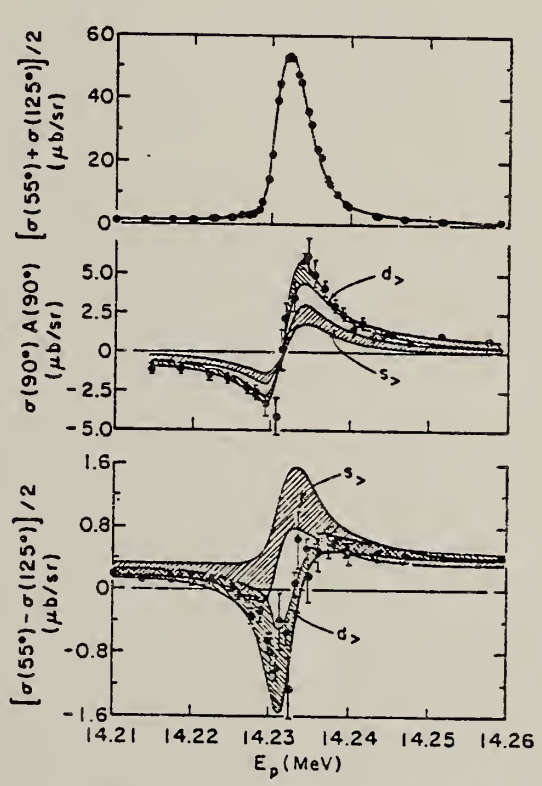

FIG. 3. Excitation curves taken near the lowest $T = \frac{3}{2}$ resonance in $^{12}C(p,\gamma_0)^{13}N$. The solid curve in the top part is a calculated fit. The bands in the lower two parts represent the spread of calculated curves for the $d_>$ and $s_>$ solutions, consistent with the off-resonance angular distributions.

N
A=14

N
A=14

N
A=14

REF. G. Ferguson, J. Halpern, R. Nathans, and P.F. Yergin
Phys. Rev. 95, 776 (1954)

ELEM. SYM.	A	Z
N	14	7

METHOD

REF. NO. 54 Fe 1 rs

REACTION	RESULT	EXCITATION ENERGY	SOURCE		DETECTOR		ANGLE
			TYPE	RANGE	TYPE	RANGE	
G,SN	ABX	10- 25	C	12- 25	BF3-I		4PI

The direct detection of neutrons from (γ,n) reactions induced by betatron bremsstrahlung has been applied to cross-section determinations using gaseous targets at approximately 100 atmospheres pressure. Results from oxygen are consistent with other determinations. The remaining elements represent new results and show the familiar giant dipole resonance for the photoneutron process. Parameters of the resonances are determined and related to the systematic behavior previously reported for other elements.

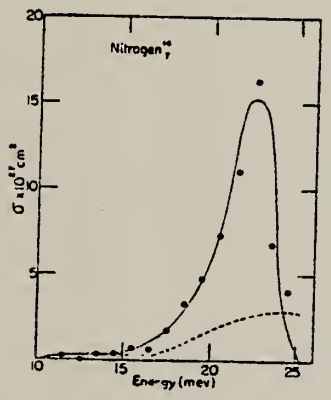

FIG. 5. Photoneutron excitation function for nitrogen.

[4] Johns, Horsley, Haslam, and Quinton, Phys. Rev. 84, 856 (1951).

Ref. D.L. Livesey
Can. J. Phys. 34, 216 (1956)

Elem. Sym.	A	Z
N	14	7

Method: Synchrotron; p + α cross section; nuclear emulsion

Ref. No.: 56 Li 1 NVB

Reaction	E or ΔE	E_o	Γ	$\int \sigma dE$	Jπ	Notes
$N^{14}(\gamma, p+\alpha)$	Bremss. 70			$\int_{25}^{35}$ = 1.3 MeV-mb		

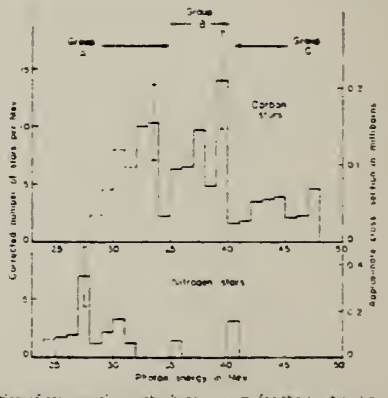

FIG. 1. Variation of cross-section with photon energy for the (γ, p+α) reactions in carbon and nitrogen, based on 82 stars and 23 stars respectively.

Ref. I.F. Wright, D.R.O. Morrison, J.M. Ried, J.R. Atkinson
Proc. Phys. Soc. A 69, 77 (1956)

Elem. Sym.	A	Z
N	14	7

Method 23 MeV synchrotron; x-ray; Wilson cloud chamber; r chamber

Ref. No. 56 Wr 1 EGF

Reaction	E or ΔE	E_o	Γ	$\int \sigma dE$	Jπ	Notes
$N^{14}(\gamma,p)$	23			$\int_{}^{23}$ = ~ 0.02 MeV-b		Statistics are not very good - only about 10 events. Made measurements at 19, 21 and 23 MeV. Lucite at E_p = 0.51, 1.63, 2.92 MeV checks detailed balancing from (p,γ). (γ,p and (γ,pn) seem to follow roughly shape of (γ,n) [Horsely et al, Can. J. Phys. 30, 159 (1952)]. Lower levels are known to p dipole.
$N^{14}(\gamma,pn)$				$\int_{}^{23}$ = ~ 0.02 MeV-b		
$N^{14}(\gamma,\alpha)$				$\int_{}^{23}$ = 0.1 MeV-mb		
$N^{14}(\gamma,\alpha\alpha)$						
$N^{14}(\gamma,\alpha p)$						

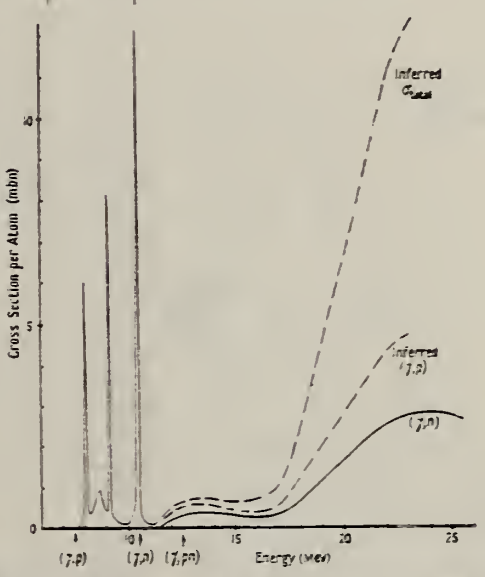

Figure 9. Measured and inferred photonuclear cross sections in ^{14}N. For fuller description see text (§ 5). For clarity the width of the narrow resonances below 10·5 MeV has been increased, but the integrated cross section remains correct.

N.B. The techniques used to obtain the cross sections above 10·5 MeV were incapable of resolving levels such as those observed below this energy.

REF.

D. L. Livesey
Can. J. of Physics 35, 987 (1957)

ELEM. SYM.	A	-
N	14	7

METHOD

REF. NO. 57 L1 1 EGF

REACTION	RESULT	EXCITATION ENERGY	SOURCE		DETECTOR		ANGLE
			TYPE	RANGE	TYPE	RANGE	
G,XP	SPC	THR - 70	C	30,70	EMU-D	5-15	DST

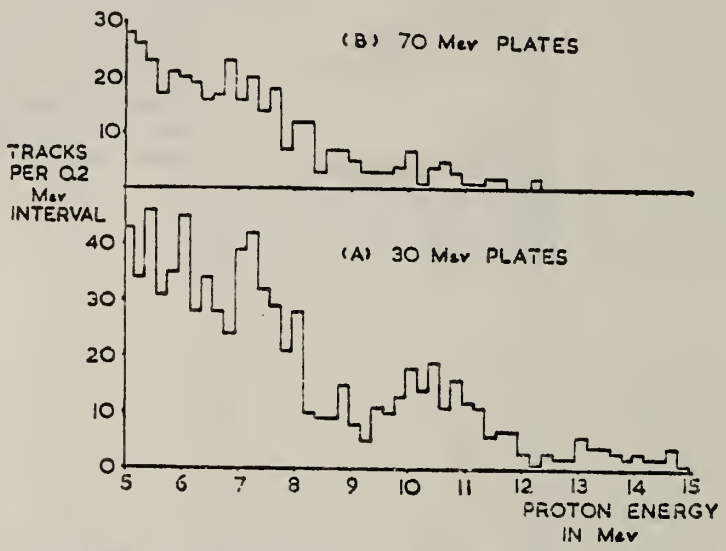

FIG. 4. (A) Energy distribution of 860 proton tracks from nitrogen exposed to 30 Mev. bremsstrahlung. (B) Distribution of 384 tracks in 70 Mev. nitrogen plates.

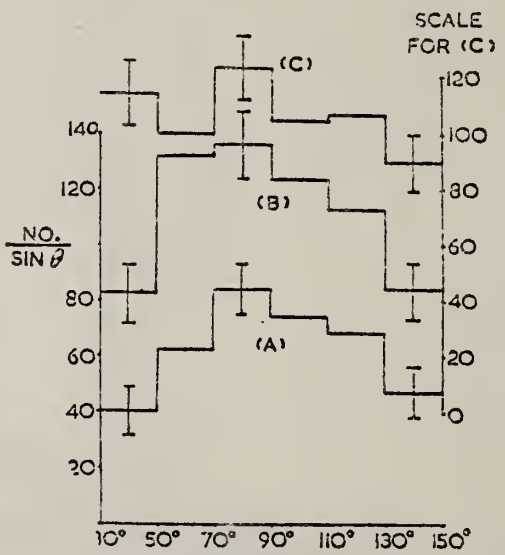

FIG. 5. Angular distributions of photoprotons from nitrogen. (A) Protons above 8.5 Mev. in 30 Mev. plates. (B) Protons between 5.0 and 8.5 Mev. in 30 Mev. plates. (C) Protons between 2.0 and 8.5 Mev. in 70 Mev. plates.

Ref. G. Cortini, C. Milone, R. Rinzivillo, C. Tribuno
Nuovo Cimento 9, 188 (1958)

Elem. Sym.	A	Z
N	14	7

Method Emulsions

Ref. No.	
58 Co 2	EH

Reaction	E or ΔE	E_o	Γ	$\int \sigma dE$	Jπ	Notes
$N^{14}(\gamma,p)$	Bremss					
	18					E_{th} = 7.54 MeV
$N^{14}(\gamma,np)$	23					E_{th} = 12.49 MeV
	30					90° spectrum.

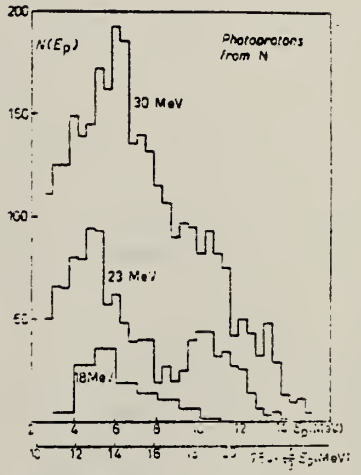

Fig. 1. – Energy spectrum of the photoprotons from N, at 18 MeV, 23 MeV and 30 MeV maximum energy irradiations. $N(E_p)$ (arbitrary units) = number of protons per unit energy interval normalized to the same dose and other experimental conditions. The scale (14/13) E_p +7.54 is also reported.

REF.

G. M. Griffiths
Proc. Phys. Soc. (London) 72, 337 (1958)

ELEM. SYM.	A	Z
N	14	7

METHOD

REF. NO. 58 Gr 1 EGF

REACTION	RESULT	EXCITATION ENERGY	SOURCE		DETECTOR		ANGLE
			TYPE	RANGE	TYPE	RANGE	
G,P	LFT	8	D	8	ION-D	0-2	4PI

Used $^{13}C(p,\gamma)^{14}N$ at 554 keV resonance as source.

Ground state radiation width 10.5±0.6 ev.

Ref. N. Mutsuro, Y. Ohnuki, K. Sato, K. Kageyama, M. Kimura
J. Phys. Soc. Japan 14, 1457 (1959)

Elem. Sym.	A	Z
N	14	7

Method: Betatron; neutron yield; radioactivity; r-chamber

Ref. No.: 59 Mu 1 | NVB

Reaction	E or ΔE	E_o	Γ	$\int \sigma dE$	Jπ	Notes
$N^{14}(\gamma,n)$	Bremss.	11.49±0.05				
	11-17	11.61±0.05				
		12.39±0.05				
		12.92±0.05				
		13.28±0.05				
		13.87±0.05				
		14.62±0.05				
		15.80±0.05				

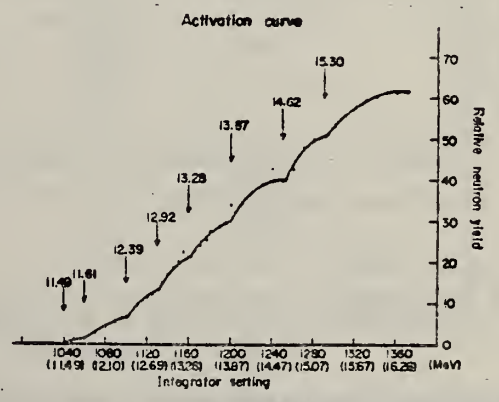

REF.

J. O'Connell, P. Dyal, J. Goldemberg
Phys. Rev. 116, 173 (1959)

ELEM. SYM.	A	-
N	14	7

METHOD: Betatron

REF. NO.: 59 Oc 1 | NVB

REACTION	RESULT	EXCITATION ENERGY	SOURCE TYPE	SOURCE RANGE	DETECTOR TYPE	DETECTOR RANGE	ANGLE
G,2N	RLI	THR-100	C	THR-100	ACT-I		4PI

REL TØ G,N

TABLE II. Relative integrated cross sections.

Element	(γ,n)	Position of the peak for (γ,n)	$(\gamma,2n)$	Position of the peak for $(\gamma,2n)$
C^{12}	1	23 Mev	0.003	42 Mev
N^{14}	1	24 Mev	0.007[a]	
O^{16}	1	22 Mev	0.002	40 Mev
F^{19}	1	20 Mev	0.14	32 Mev
Na^{23}	1	20 Mev	0.05	32 Mev
P^{31}	1	20 Mev	0.06 $(\gamma,2p)$	45 Mev $(\gamma,2p)$
			0.08 $(\gamma,2pn)$	50 Mev $(\gamma,2pn)$

[a] The (γ,n) integrated cross section was taken from reference 4.

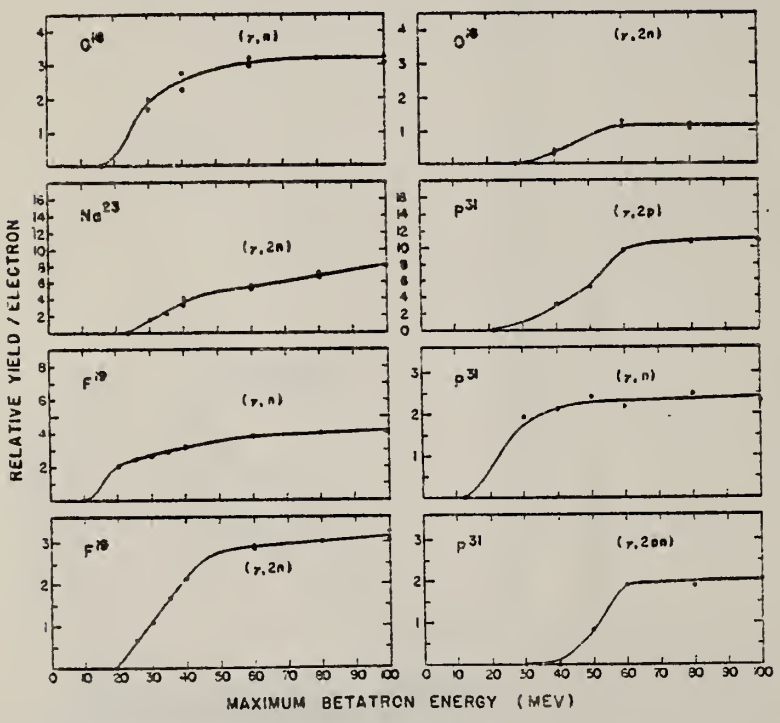

FIG. 1. The energy dependence of several photonuclear reactions. The relative yield scales of different graphs are independent.

N	14	7

METHOD
Synchrotron; proton, neutron relative cross section, spectra, angular distribution; cloud chamber

REF. NO. 60 Ba 7 NVB

REACTION	RESULT	EXCITATION ENERGY	SOURCE		DETECTOR		ANGLE
			TYPE	RANGE	TYPE	RANGE	
G,P	RLX	0-200	C	200	CCH-D		DST
G,XN	RLX	0-200	C	200	CCH-D		DST
G,PN	RLI	0-200	C	200	CCH-D		DST

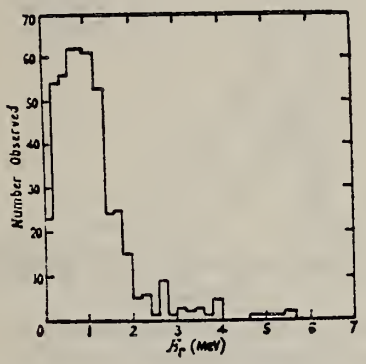

Figure 2. The energy distribution of the recoil nuclei from the reaction $^{14}N(\gamma, p)^{13}C$.

§ 6. Conclusion

From the experimental results, we conclude that:

(i) The cross sections for the reactions $^{14}N(\gamma, p)^{13}C$ and $^{14}N(\gamma, n)^{13}N$ are comparable, the relative values at any energy being shown in figure 13.

(ii) In the giant resonance, the emission of a single nucleon proceeds partly by a direct channel, and partly by the statistical evaporation of a nucleon. At energies greater than 30 Mev the emission proceeds mainly by a direct channel, and at all energies the results are consistent with the ratio of the two processes predicted by Wilkinson (1956).

(iii) The integrated cross section for the reaction $^{14}N(\gamma, pn)^{12}C$ is about 50% greater than that for the emission of either a single neutron or a single proton, for a spectrum of peak energy 200 Mev.

(iv) The (γ, pn) reaction appears to proceed either by a statistical or a knock-on process. The results for protons stopping within the sensitive volume of the chamber favour the statistical model and suggest that most of the observed events result from the absorption of a low energy ($\sim$20 Mev) photon.

(v) No evidence was found to suggest that many of the observed events could be satisfactorily explained by the quasi-deuteron model.

Relative Integrated Cross Section

Group	Reaction	Number	Relative number
(ii)	$^{14}N(\gamma, n)^{13}N$	627	1·18
(iii) (*a*)	$^{14}N(\gamma, p)^{13}C$	528	1·00
(iii) (*b*)	$^{14}N(\gamma, pn)^{12}C$	786	1·49
(iii) (*c*)	$^{14}N(\gamma, \alpha)^{10}B$ $(\gamma, \alpha n)$ etc.	28	0·05

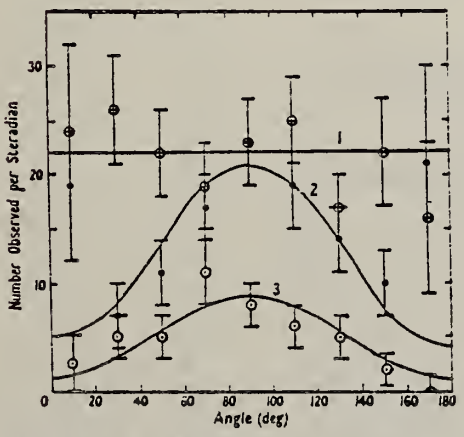

Figure 5. Angular distributions of protons from the (γ, p) reaction: 1, protons of energy less than 12 Mev—the distribution is fitted with the line $f(\theta) = 22$, and the experimental points are plotted as a cross within a circle; 2, protons of energy between 12 Mev and 20 Mev—the distribution is fitted with the curve $4 + 17 \sin^2\theta$, and the experimental points are plotted with a large spot; 3, protons of energy greater than 20 Mev—the distribution is fitted with the curve $1{\cdot}25 + 7{\cdot}4 \sin^2\theta$ and the experimental points are plotted with a small point within a circle.

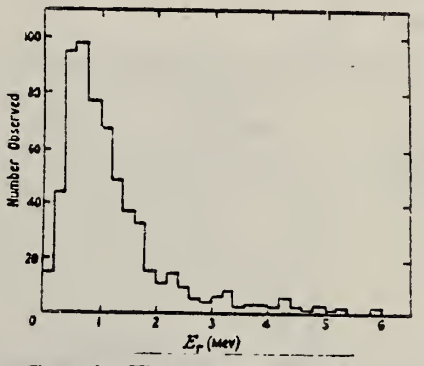

Figure 6. The energy distribution of the recoil nuclei from the reaction $^{14}N(\gamma, n)^{13}N$.

N	14	7

METHOD

REF. NO. 60 Ba 7

REACTION	RESULT	EXCITATION ENERGY	SOURCE TYPE	SOURCE RANGE	DETECTOR TYPE	DETECTOR RANGE	ANGLE

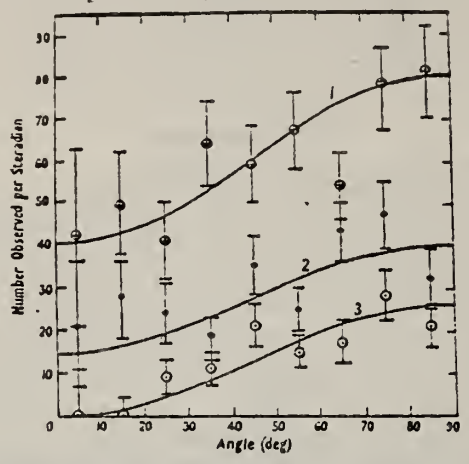

Figure 8. Angular distributions of recoils from the (γ, n) reaction: 1, recoils of energy less than 1 MeV—the distribution is fitted with the curve $40(1+\sin^2\theta)$ and the experimental points are plotted with a cross within a circle; 2, recoils of energy between 1 MeV and 2 MeV—the distribution is fitted with the curve $15+25\sin^2\theta$, and the experimental points are plotted with a large spot; 3, recoils of energy greater than 2 MeV—the distribution is fitted with the curve $26\sin^2\theta$, and the experimental points are plotted with a spot within a circle.

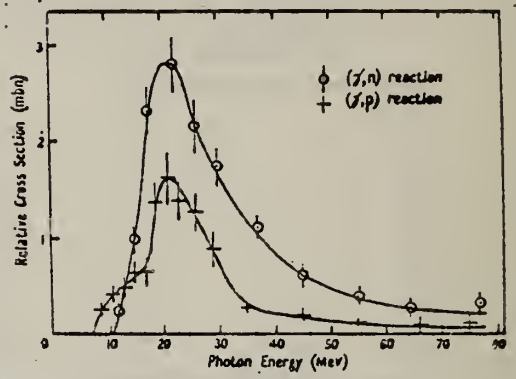

Figure 13. The relative cross sections for the reactions $^{14}N(\gamma, p)^{13}C$ and $^{14}N(\gamma, n)^{13}N$.

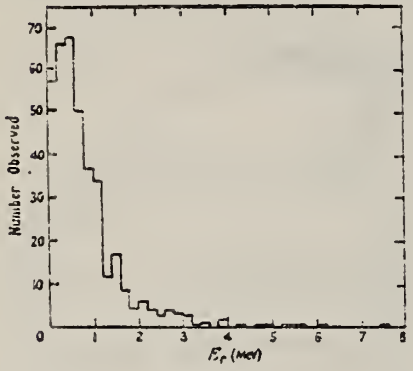

Figure 9.

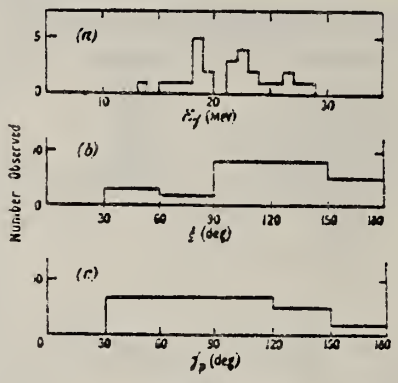

Figure 10.

Figure 9. The energy distribution of the recoil nuclei from the reaction $^{14}N(\gamma, pn)^{12}C$.

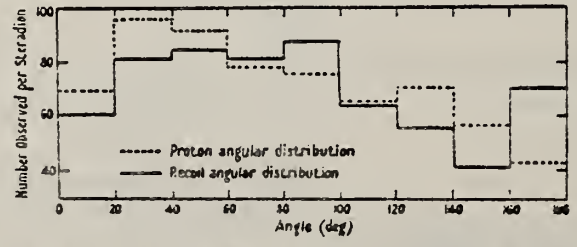

Figure 12. The angular distributions of recoils and protons from (γ, pn) events, with respect to the direction of the photon beam.

Ref.	Elem. Sym.	A	Z
E.E. Carroll, Jr., W.E. Stephens Phys. Rev. 118, 1256 (1960)	N	14	7

Method	Ref. No.	
Monochr. γ's from $H^3(p,\gamma)He^4$ reaction, total abs.; NaI	60 Ca 1	JK

Reaction	E or ΔE	E_o	Γ	$\int \sigma dE$	Jπ	Notes
μ_t	20.0-20.5					No resolved structure; small positive slope of 6 mb/MeV. $\sigma_{av.}$(nuclear) = 10.5 ± 4 mb. Calculated atomic cross-sections substracted, using Borsellino for triplet.

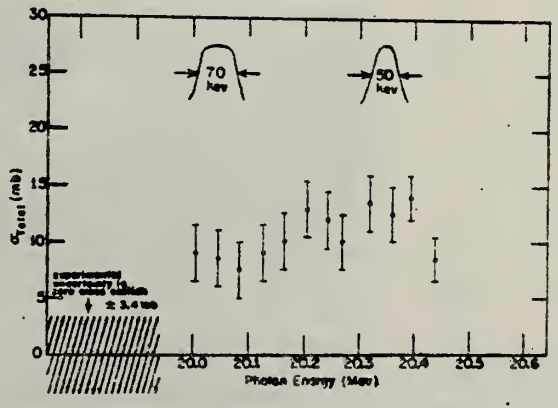

FIG. 4. Total nuclear absorption in nitrogen-14.

Ref.	R.W. Fast, P.A. Flournoy, R.S. Tickle, W.D. Whitehead Phys. Rev. 118, 535 (1960)	Elem. Sym.	A	Z
		N	14	7

Method	Ref. No.	
70 MeV Synchrotron; BF_3 ctrs.	60 Fa 1	JH

Reaction	E or ΔE	E_o	Γ	$\int \sigma dE$	Jπ	Notes
(γ,n)	13.5-60.5	22.5	3.8	0.60 $\int_{13.5}^{25}$ MeV-barns 0.116 $\int_{13.5}^{50}$ MeV-barns		σ_{max}(22.5 MeV) = 14.5 mb

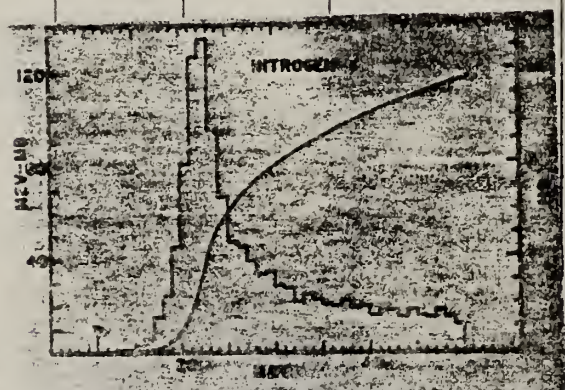

FIG. 6. Cross section and integrated cross section for the nitrogen reaction as function of energy.

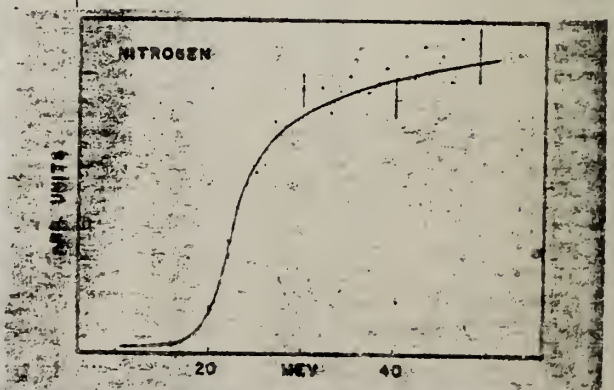

FIG. 5. Integrated reduced cross section for the reaction $N^{14}(\gamma,n)$ as a function of energy.

Ref. K.N. Geller
Phys. Rev. 120, 2147 (1960)

Elem. Sym.	A	Z
N	14	7

Method: Bremss; second-difference analysis; radioactivity

Ref. No.: 60 Ge 1 JHH

Reaction	E or ΔE	E_o	Γ	$\int \sigma dE$	Jπ	Notes
$N^{14}(\gamma,n)$	E_t - 1Γ.2	10.58 10.81 11.07				Mostly an application of analysis method. Data (10.58 and 10.07 MeV resonances) in agreement with known levels. Abscissa in Figure 2 should be labeled E(MeV) instead of E(kev).

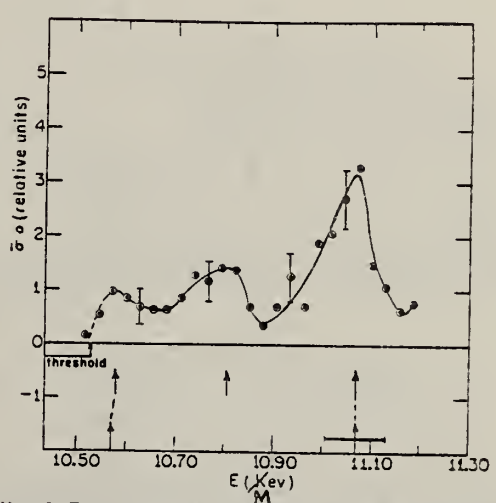

FIG. 2. Zero-order cross section for the reaction $N^{14}(\gamma,n)N^{13}$ near threshold. Baseline arrows indicate energy assignments of known levels and horizontal bars the level widths, where known. Correspondence between levels observed in the present experiment with known levels indicated by dashed line.

Ref.	Elem. Sym.	A	Z
K.H. Geller, J. Halpern, E.G. Muirhead Phys. Rev. 119, 716 (1960)	N	14	7

Method	Ref. No.	
25 MeV betatron; activation of Nitrogen; NaI counters for annih. rad. of positions from residual nuclei	60 Ge 2	JHH

Reaction	E or ΔE	E_o	Γ	$\int \sigma dE$	Jπ	Notes
(γ,n)	10.35-11.22					E_γ (threshold) = 10.53 ± 0.04 MeV to be compared with Everling's neutron separation energy 10.553 ± 0.005 MeV from mass data. Observed break(s) in yield curve (Figure 2) at: 11.07 MeV

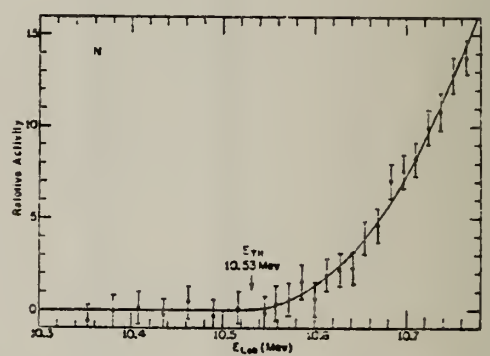

(a)

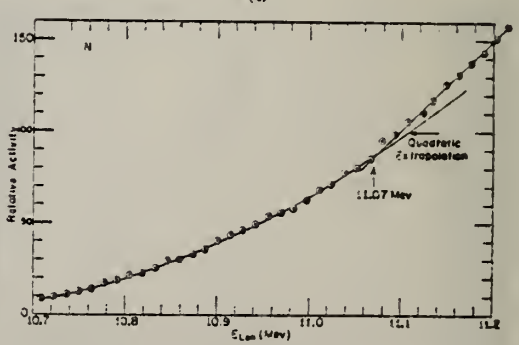

(b)

FIG. 2. Activation curve for the reaction $N^{14}(\gamma,n)N^{13}$.

Ref. D.F. Hebbard, J.L. Vogl
Nuclear Phys. 21, 652 (1960)

Elem. Sym.	A	Z
N	14	7

Method: 600 kev electrostatic generator; NaI

Ref. No.: 60 He 2 JHH

Reaction	E or ΔE	E_o	Γ	∫σdE	Jπ	Notes
$C^{13}(p,\gamma)N^{14}$	130-450 kev	448.5±.5 kev	< 400 ev		2^-	E_γ (level in N^{14}) = 7.966 MeV Resonant γ ray yield, width and angular distribution data in Tables 1 and 2.

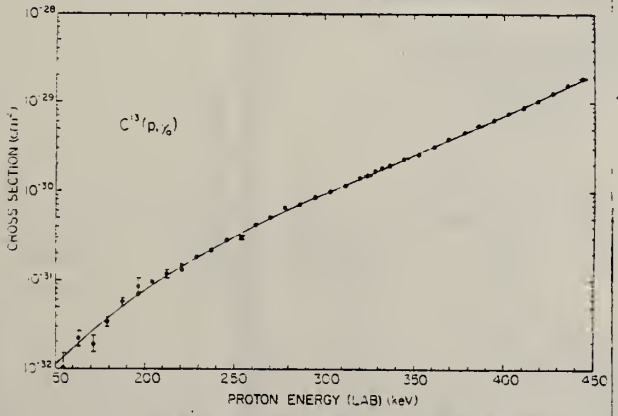

Fig. 8. The cross section for radiative capture of protons by C^{13}, with emission of the ground-state gamma ray, is shown. The target was 9.0 keV thick for 448-keV protons, and was enriched to 61 % C^{13}. Typical errors, due to counting statistics, are shown at intervals along the curve. The solid curve of this figure is derived from the solid curve in fig. 9 where an explanation will be found

TABLE 1
Resonant gamma ray yields and widths

	Transition from the 7.97-MeV level to the		
	ground state	3.95-MeV state	other states [a]
Yield 10^{-13} γ/p (61 % C^{13})	9.7 ±0.5	7.9 ±0.5	≲ 0.5
$\frac{\omega\Gamma_p\Gamma_\gamma}{\Gamma}$ (eV)	0.012	0.010	≲ 0.0005

[a] The cascades to the 2.31-MeV state, 5.10-MeV state and 5.68-MeV state may all be weakly resonant at 448-keV proton energy. Only an upper limit to the strength of this cascade radiation can be given.

TABLE 2
Resonant gamma-ray angular distributions [a]

7.97-MeV level to	Angular distribution
ground state	$P_0 - (0.570 \pm 0.020) P_2 - (0.004 \pm 0.03) P_4$
3.95-MeV state [b]	$P_0 - (0.33 \pm 0.03) P_2$

[a] The non-resonant distributions from the close neighbourhood of the 448-keV resonance were found to be isotropic, within experimental errors. Neither for resonant nor for non-resonant radiations were any odd-order Legendre polynomial coefficients observed. The tabulated distributions have been corrected for the finite solid angle of the detector.

[b] The angular distribution of gamma rays to the 3.95-MeV state was analyzed only for P_0 and P_2 terms. The subtractions necessary to eliminate the ground state radiation make the calculation of a $P_4(\cos\theta)$ term of doubtful value

Ref. J.D. King, R.N.H. Haslam, R.W. Parsons
Can. J. Phys. 38, 231 (1960)

Elem. Sym.	A	Z
N	14	7

Method 25 MeV betatron; radioactivity; ionization chamber

Ref. No. 60 Ki 2 EH

Reaction	E or ΔE	E_o	Γ	$\int \sigma dE$	$J\pi$	Notes
$N^{14}(\gamma,n)$	Bremss. 10.5-25	11.7 13.2 15.2 19.5 22.8		$\int_{th}^{\sim 15.2} = 1.8$ MeV-mb		$\sigma(E_o = 22.8) = 2.9$ mb At 22 MeV, neutron yield is 3.81×10^6 n/mol/100r 1/2 life of N^{13} = 9.93±0.05 m. Cross sections using Danos [Nuclear Phys. 5, 23 (1958)] interpretation, $Q_o = \sim 0.8$b.

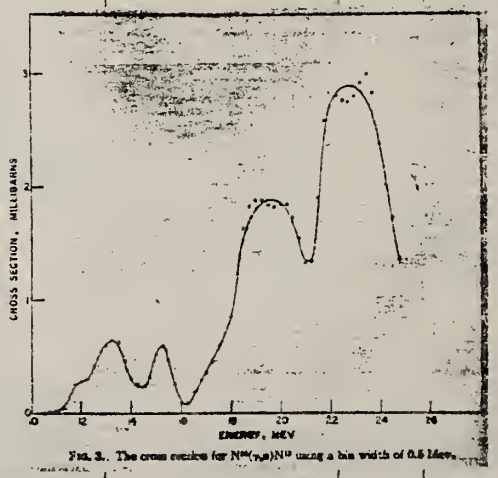

Fig. 3. The cross section for $N^{14}(\gamma,n)N^{13}$ using a bin width of 0.5 Mev.

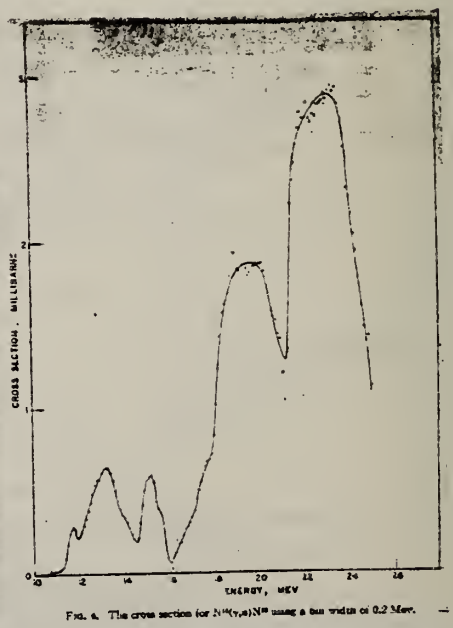

Fig. 4. The cross section for $N^{14}(\gamma,n)N^{13}$ using a bin width of 0.2 Mev.

A.P. Komar, Ya. Krzhemenek, I.P. Iavor
Dokl. Akad. Nauk SSSR 131, 283 (1960); Soviet Phys. Doklady 5, 295 (1961)

N	14	7

METHOD: Synchrotron; proton, n-p spectra, cross section; cloud chamber; angular distribution; He(γ,p) monitor

REF. NO.: 60 Ko 1 | NVB

REACTION	RESULT	EXCITATION ENERGY	SOURCE TYPE	SOURCE RANGE	DETECTOR TYPE	DETECTOR RANGE	ANGLE
G,P	ABI	0 - 90	C	90	CCH-D	2-40	DST
G,NP	SPC	0 - 90	C	90	CCH-D	2-17	DST

PROTON SPECTRUM

σ_{max} (γ,p) at E_γ = 23 MeV, assumes C^{13} left in 3.6 MeV state.

$$\int_0^{90} \sigma_{(\gamma,p)} dE = 0.07 \text{ MeV-b}$$

$$\int_0^{90} \sigma_t dE = 0.3 \text{ MeV-b}$$

In Figure 2, for (γ,p):

$$0.4 \leq E_p \leq 50 \text{ MeV}, \quad W(\theta) = 1 + 1.3 \sin^2\theta + 0.16 \cos\theta$$

$$E_p > 10 \text{ MeV}, \quad W(\theta) = 1 + 2 \sin^2\theta + 0.25 \cos\theta$$

for (γ,np):

$$E_n \gg E_p, \quad W(\theta) = 1 + 2.2 \sin^2\theta$$

Reaction	Yield %	Threshold (Mev)
γp	28	7,55
γn	15	10,55
γα	2	11,62
γnp	33	12,50
γ3αnp	11	19,75
γαp	4	17,21
Other stars	7	--

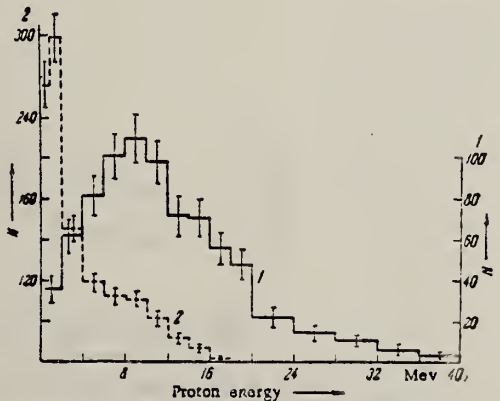

Fig. 1. Photoproton energy spectra: A) proton energy; 1) $N^{14}(\gamma p)C^{13}$ reactions; 2) $N^{14}(\gamma np)C^{12}$ reactions.

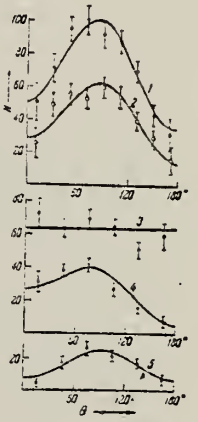

Fig. 2. Angular distributions: 1) protons (p) with energies from 0.4-50 Mev; 2) protons (γp) with energies higher than 10 Mev; 3) protons (γnp) with energies $E_p < E_n$; 4) protons (γnp) with energies $E_p > E_n$; 5) neutrons (γnp) with $E_n \gg E_p$.

REF.

N. Mutsuro, K. Sato, M. Mishina
J. Phys. Soc. Japan 15, 358 (1960)

ELEM. SYM.	A	L
N	14	7

METHOD

Betatron; neutron yield; radioactivity

REF. NO. 60 Mu 1 | NVB

REACTION	RESULT	EXCITATION ENERGY	SOURCE TYPE	SOURCE RANGE	DETECTOR TYPE	DETECTOR RANGE	ANGLE
G,N.	RLY	THR-20	C	15-20	ACT-I		4PI
				(14.7-19.5)			

In Figure 2, cross section is based on previous work (Mutsuro et al, J. Phys. Soc. Japan 14, 1457 (1959)] plus assumption that all resonances have same width.

BREAKS

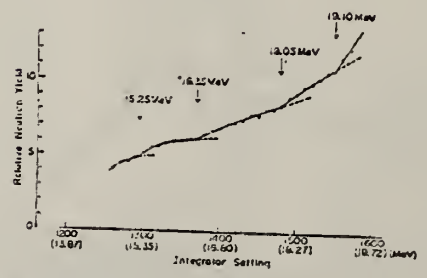

Fig. 1. Activation Curve of $N^{14}(\gamma, n)N^{13}$ above 14.70 MeV.

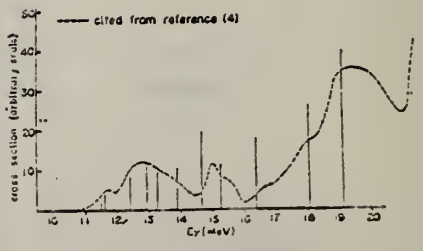

Fig. 2. Cross Section of $N^{14}(\gamma, n)N^{13}$.

REF.

J. M. Reid and B. Lalovic
Proc. Phys. Soc. (London) 76, 65 (1960)

ELEM. SYM.	A	Z
N	14	7

METHOD

REF. NO. 60 Re 2 EGF

REACTION	RESULT	EXCITATION ENERGY	SOURCE		DETECTOR		ANGLE
			TYPE	RANGE	TYPE	RANGE	
G,XP			C	330	CCH		4PI

166 events (γ,p) (γ,pn). Recorded only events where proton with $20 \leq E \leq 120$ MeV was emitted.

Ref. H.J. Rose
Nuclear Phys. 19, 113 (1960)

Elem. Sym.	A	Z
N	14	7

Method Van de Graaff; 3 crystal NaI spectrometer

Ref. No. 60 Ro 1 JHH

Reaction	E or ΔE	E_o	Γ	$\int \sigma dE$	Jπ	Notes
(p,γ)	~ 1.75	1.75			2^+	E_{γ_0} = 9.17 MeV: $\omega(\theta_\gamma) = 1 - (0.55 \pm 0.02)\cos^2\theta$

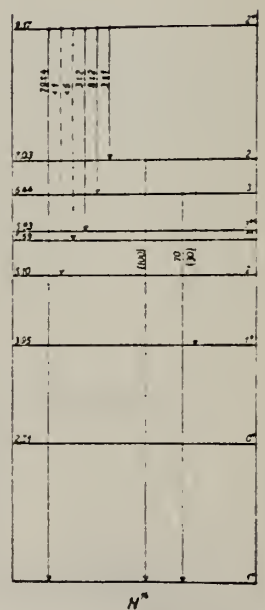

Fig. 13. The decay scheme of the N^{14} 9.17-MeV level as determined in the present work. Only the levels involved in the decay of the 9.17-MeV level are shown. The spin and parity assignments are discussed in the text. Broken arrows denote uncertain transitions.

Ref. H.J. Rose, R. Riess, W. Trost
Nuclear Phys. 21, 367 (1960)

Elem. Sym.	A	Z
N	14	7

Method 5.5 MeV Van de Graaff; NaI.

Ref. No. 60 Ro 2 JHH

Reaction	E or ΔE	E_o	Γ	$\int \sigma dE$	Jπ	Notes
(p,γ)	1.75-3.25	3.11	17 ev		2^+	$E_{\gamma o}$ = 10.43 MeV: $\omega(\theta_\gamma) = 1 + a_1 \cos\theta + a_2 \cos\theta$ where a_1 and a_2 are given in Table 2 and Figure 2. Γ_{tot} = 36 kev.
		1.75			2^+	$E_{\gamma o}$ = 9.17 MeV: $\omega(\theta_\gamma) = 1 - (0.55 \pm 0.02) \cos^2\theta$

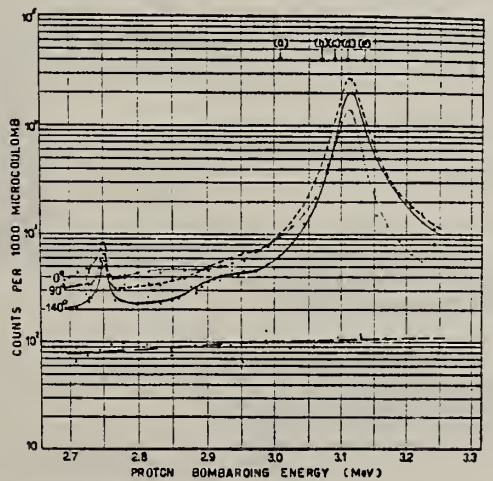

Fig. 1. The $C^{13}(p,\gamma)$ excitation functions as obtained with a 5 keV thick, 60 % enriched C^{13} target. A detailed explanation of this figure is given in sect. 3.

TABLE 2

The coefficients a_1 and a_2 of the angular distribution $W(\theta) = 1 + a_1 \cos\theta + a_2 \cos^2\theta$ of the 10.43-MeV gamma rays at different proton bombarding energies.

Measurement [a])	Bombarding energy (MeV)	a_1	a_2
(a)	3.01	$+(0.32 \pm 0.10)$	$-(0.29 \pm 0.10)$
(b)	3.07	$+(0.15 \pm 0.03)$	$-(0.41 \pm 0.03)$
(c)	3.09	$+(0.08 \pm 0.06)$	$-(0.40 \pm 0.10)$
(d)	3.11	$+(0.03 \pm 0.03)$ [b])	$-(0.50 \pm 0.03)$ [b])
		$+(0.02 \pm 0.02)$ [c])	$-(0.47 \pm 0.03)$ [c])
		$+(0.03 \pm 0.03)$ [d])	$-(0.47 \pm 0.03)$ [d])
(e)	3.135	$-(0.10 \pm 0.04)$	$-(0.46 \pm 0.08)$

With the exception of measurement (d) the errors quoted are due mainly to counting statistics and were evaluated using three standard deviations as uncertainty in a single determination. In measurement (d) the errors are least squares errors.

[a]) Compare fig. 1.
[b]) The values have been re-evaluated from the data displayed in ref. [4]) in order to check on a possible cos θ term.
[c]) Obtained with 45 keV thick target.
[d]) Obtained with a 5 keV thick target from measurements at 0° 90° and 140°.

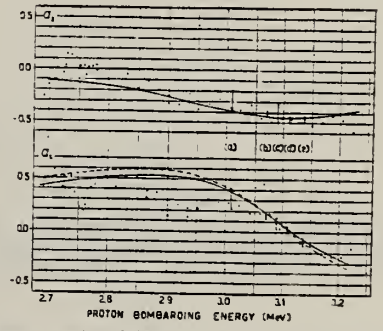

Fig. 2. The coefficients a_1 and a_2 of the angular distribution $W(\theta) = 1 + a_1 \cos\theta + a_2 \cos^2\theta$ as determined from the experiments described in sect. 3. The solid line gives the theoretical fit assuming interference between the 10.43-MeV state and background due to the 8.00-MeV level. The curve was calculated using the formulae of the appendix. The values of the parameters chosen for this calculation are given in the text. The broken line is obtained using a s-wave phase shift 18° larger than the one calculated with $R = 4.7 \times 10^{-13}$ cm from the hard sphere scattering condition. This slight increase of the s-wave phase shift is suggested by comparison of the hard sphere phases with the phases used by Zipoy *et al.* to fit the $C^{12}(p,p)C^{12}$ data.

D. Sadeh
Compt. Rend. 250, 1632 (1960)

ELEM. SYM.	A	Z
N	14	7

METHOD
Betatron; neutron yield; activity; ion chamber

REF. NO.
60 Sa 2

NVB

REACTION	RESULT	EXCITATION ENERGY	SOURCE		DETECTOR		ANGLE
			TYPE	RANGE	TYPE	RANGE	
G,N	RLY	10 - 13	C	10 - 13	ACT-I		4PI

Breaks in activation curve:

10.77 MeV
11.01 MeV
11.32 MeV
11.47 MeV
12.04 MeV
12.22 MeV
12.36 MeV
12.80 MeV

I. Wahlstrom, B. Forkman
Arkiv Fysik 18, 83 (1960)

ELEM. SYM.	A	Z
N	14	7

METHOD: Synchrotron; proton spectrum; cross section; angular distribution; nuclear emulsion

REF. NO.: 60 Wa 1 | NVB

REACTION	RESULT	EXCITATION ENERGY	SOURCE		DETECTOR		ANGLE
			TYPE	RANGE	TYPE	RANGE	
G,P	SPC	8-16	C	12,16	EMU-D		DST
				(11,5,15.5)			

In figure 4, levels at 11.8, 13.0, 15.2.

In figure 5, $W(\theta) = 1 - (0.6 \pm 1) \cos^2\theta$

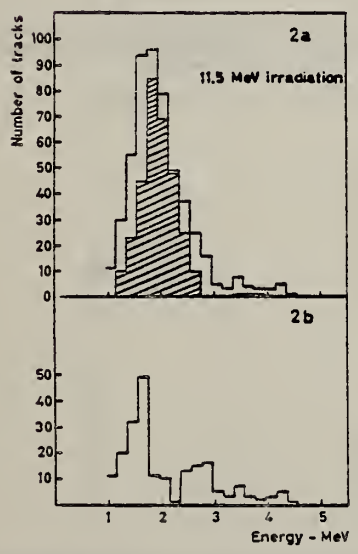

Fig. 2. The proton distribution from the 11.5 Mev irradiation. The energy scale gives the sum of the proton energy and the recoil energy of C^{13}. In Fig. 2*a* the background is shaded and in Fig. 2*b* the background is subtracted.

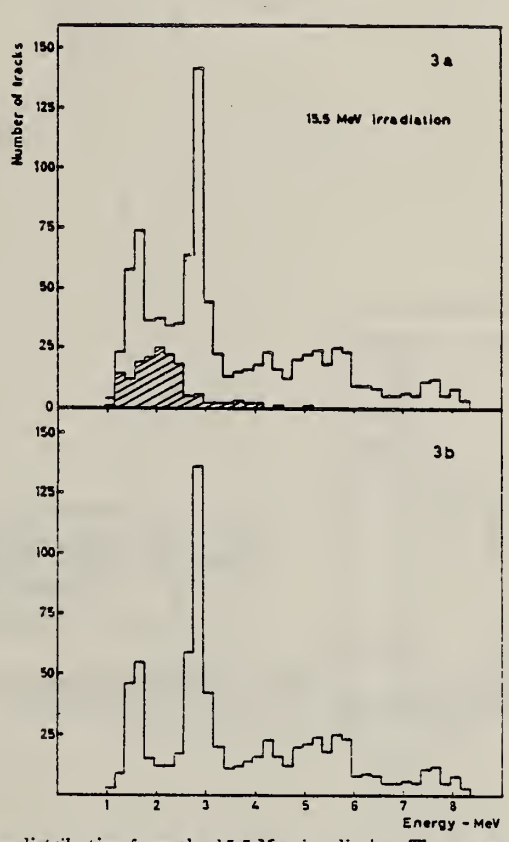

Fig. 3. The proton distribution from the 15.5 Mev irradiation. The energy-scale gives the sum of the proton energy and the recoil energy of C^{13}. In Fig. 3*a* the background is shaded and in Fig. 3*b* the background is subtracted.

METHOD

REF. NO. 60 Wa 1 NVB

REACTION	RESULT	EXCITATION ENERGY	SOURCE		DETECTOR		ANGLE
			TYPE	RANGE	TYPE	RANGE	

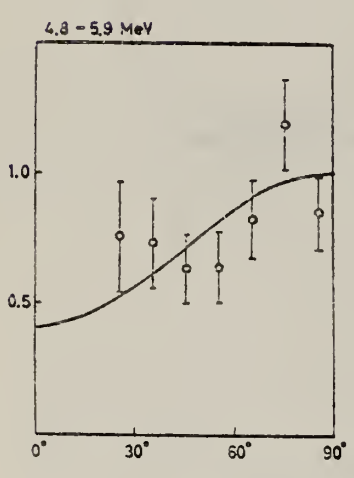

Fig. 5. The angular distribution of the protons from the energy interval 4.8–5.9 Mev.

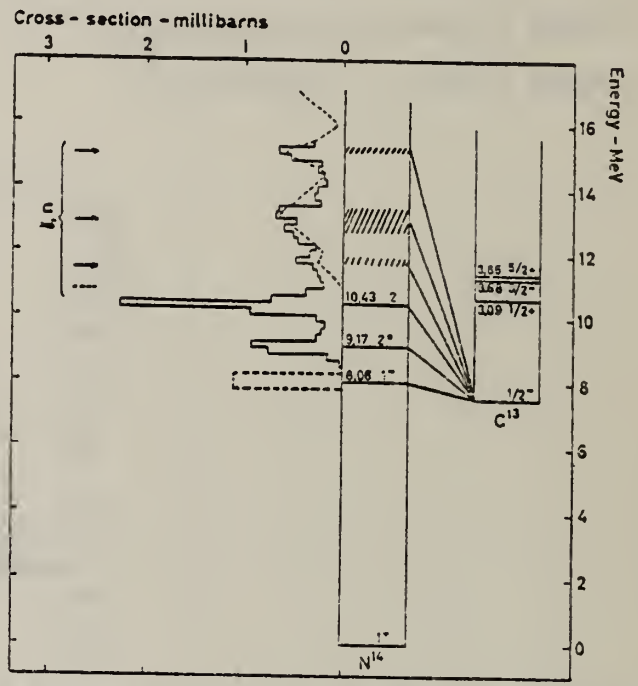

Fig. 4. The level scheme for the photo-disintegration of N^{14}. The cross-section curve is plotted to the left. The energies of the observed resonances from the (γ, n) measurements are indicated. The dotted curve shows the (γ, n) cross-section from [29].

29. J. D. King, R. N. H. Haslam and R. W. Parsons, Can. J. Phys. *38*, 231 (1960).

Ref. R.E. Hester, W.A.S. Lamb
Phys. Rev. 121, 584 (1961)

Elem. Sym.	A	Z
N	14	7

Method Protons from high-current ion injector; reaction with 1.1% natural abundance of C^{13} in graphite target; NaI

Ref. No. 61 He 1 JHH

Reaction	E or ΔE	E_o	Γ	$\int \sigma dE$	Jπ	Notes
(p,γ)	100-140 kev					Photon Energy = 7.65 MeV.

E_p (kev)	$\sigma(p,\gamma)$
100	$(7.7\pm1.8)\times 10^{-34}$ cm^2
129	$(5.8\pm1)\times 10^{-33}$ cm^2
140	$(9.8\pm1.2)\times 10^{-33}$ cm^2

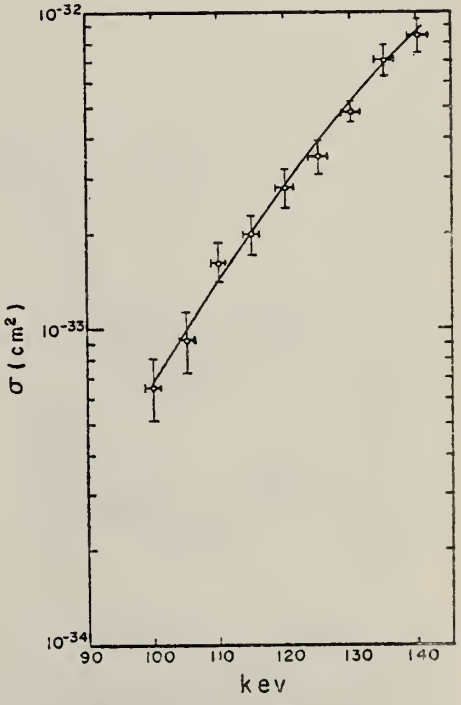

FIG. 5. Excitation curve for the 7.65-Mev gamma ray, calculated from Eq. (3).

REF.

H. H. Knitter and H. Wäffler
Proc. Ruth. Int. Conf. Manchester 823 (1961)

ELEM. SYM.	A	—
N	14	7

METHOD

REF. NO.	
61 Kn 1	JDM

REACTION	RESULT	EXCITATION ENERGY	SOURCE		DETECTOR		ANGLE
			TYPE	RANGE	TYPE	RANGE	
D,G	ABX	10-12	D	0-2	THR-1		4PI

$\sigma \approx 0.6 \pm 0.2$ μb for 1 MeV deuterons.

Ref. R.E. Segel, J. W. Daughtry, J.W. Olness
Phys. Rev. 123, 194 (1961)

Elem. Sym.	A	Z
N	14	7

Method: VandeGraaff; 3-crystal pair spectrometer

Ref. No.: 61 Se 1 | JHH

Reaction	E or ΔE	E_o	Γ	$\int \sigma dE$	Jπ	Notes
$C^{13}(p,\gamma_o)$	1.75	9.17			2+	$W(\theta_\gamma)=1-(0.59\pm0.03)\cos^2\theta+(0.03\pm0.03)\cos^4\theta$.
		6.44			3	$W(\theta_\gamma) = 1+(1.6\pm0.4)\cos^2\theta - (1.1\pm0.4)\cos^4\theta$.

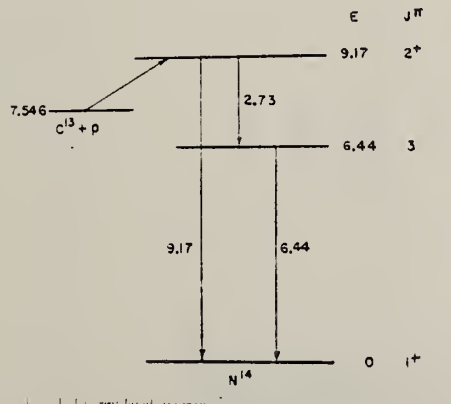

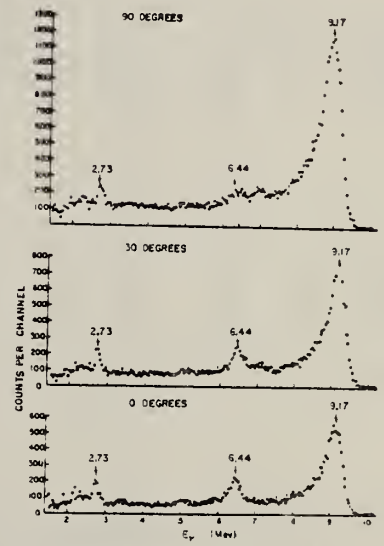

FIG. 2. Spectra taken at the 1.75-Mev $C^{13}(p,\gamma)N^{14}$ resonance with a three-crystal pair spectrometer. The weak peak above the 6.44-Mev line is apparently the same as the 7.05-Mev line seen in reference 2.

FORM NBS-418
(8-1-63)
USCOMM-DC 18556-P63

U.S. DEPARTMENT OF COMMERCE
NATIONAL BUREAU OF STANDARDS

C.P. Swann, V.K. Rasmussen, F.R. Metzger
Phys. Rev. 121, 242 (1961)

ELEM. SYM.	A	Z
N	14	7

METHOD
Van de Graaf; photon scattering; NaI spectrometer

REF. NO.
61 Sw 1 NVB

REACTION	RESULT	EXCITATION ENERGY	SOURCE		DETECTOR		ANGLE
			TYPE	RANGE	TYPE	RANGE	
G,G		2	D	2	NAI-D		DST
		(2.31)		(2.31)			

LIFETIME

Mean life of first excited state:

$\tau = (7.3 \pm 1.8)\ 10^{-14}$ sec.

Ref. R.D. Edge, G.A. Peterson
Phys. Rev. 128, 2750 (1962)

Elem. Sym.	A	Z
N	14	7

Method: Linac; counter telescope

Ref. No.: 62 Ed 1 BG

Reaction	E or ΔE	E_o	Γ_γ(eV)	$\int \sigma dE$(MeV-mb)	$J\pi$	Notes
$N^{14}(e,e')$	41.5	9.2		0.65±0.2		Nuclear states excited by 180° electron scattering; M1 transitions assumed.
		10.5		1.2±0.36		Inelastic electron scattering cross sections obtained by comparing inelastic peaks to e-p elastic scattering peak.
						Γ_γ from virtual photon theory.
						Limits not given for cross sections.

TABLE I. Parameters of nuclear states excited by 180° electron scattering, assuming transitions are $M1$.

Isotope	Excitation energy, k (MeV)	Spin and parity: Ground state I_g	Excited state I_e	Inelastic cross section $d\sigma_i/d\Omega$ (10^{-28} cm^2 sr^{-1})	$\int \sigma_i dk$ (MeV-mb)	Percentage experimental error	Ground-state radiation widths, Γ_{γ_0}(eV): This experiment	Weisskopf units	Other experiments
Be[a]	2.4	3/2−	5/2−	1.3	0.12	15	0.12	0.30	0.13[e]
	14.7	3/2−	1/2−	0.042	0.3	50	36	67	
			3/2−				18		
			5/2−				12		
B[a]	7.9	3−	2+	1.9	0.75	20	17	10	9.5[e]
			3+				12		
			4+				10		
	11.8	3−	2+	1.2	0.75	50	39	34	
			3+				28		
			4+				22		
	14.0	3−	2+	0.6	0.5	50	34	58	
			3+				24		
			4+				15		
B[a]	2.1	3/2−	1/2−	0.72	0.72	20	0.17	0.21	0.15[e]
	4.4	3/2−	5/2−	1.5	0.34	40	1.1	1.8	0.602[e]
	4.9	3/2−	3/2−	2.4	0.59	40	3.7	2.5	
	7.3	3/2−	5/2−	0.4	0.12	50	1.0	8.1	
	9.14	3/2−	7/2+	1.9	0.0097	20	0.10	4×10^{-3}	0.1[e]
	12.9	3/2−	1/2−	1.4	1.0	30	70	45	
			3/2−				36		
			5/2−				24		
C[a]	15.1	0+	1+	1.82	1.95	10	39	73	40[e], 54.5[f], 59.2[g]
N[a]	9.2	1+	0+	1.3	0.65	30	43	17	
			1+				14		
			2+				9		
	10.5	1+	0+	1.9	1.2	30	100	24	
			1+				34		
			2+				20		
O[a]	No resonances detected below 16 MeV.								
Si[a]	11.6	0+	1+	3.5	2.8	40	33	33	47[e], 63[h]

[a] W. C. Barber, F. Berthold, G. Fricke, and F. E. Gudden, Phys. Rev. 120, 2081 (1960).
[b] G. Fricke (private communications).
[c] F. R. Metzger, C. P. Swann, and V. K. Rasmussen, Phys. Rev. 110, 906 (1958).
[d] This transition is assumed to be $M2$.
[e] L. Meyer-Schützmeister and S. S. Hanna, Bull. Am. Phys. Soc. 3, 188 (1958).
[f] G. Hayward and R. Fuller, Phys. Rev. 106, 991 (1957).
[g] E. L. Garwin, Phys. Rev. 114, 143 (1959).
[h] A. B. De Nercy, thesis, University of Paris, Orsay Center, 1962 (unpublished).

Ref. A.N.Gorbunov, V.A.Dubrovina, V.A.Osipova, V.S.Silaeva, P.A.Cerenkov
Zhur.Eksptl. i Teoret.Fiz. 42, 747 (1962);
Soviet Phys. JETP 15, 520 (1962)

Elem. Sym.	A	Z
N	14	7

Method: synchrotron - cloud chamber

Ref. No. 62Dol

BG

Reaction	E or ΔE	E_o	Γ	∫σdE	Jπ	Notes
(γ,p)	$E_{\gamma max}$= 170		$38)^{170}_{0}$			$\sigma_{-1} = \int \sigma(E)E^{-1}dE$ (Table IV)
(γ,n)			$31)^{170}_{\bullet}$			$\sigma_{-2} = \int \sigma(E)E^{-2}dE$ (Table IV)
(γ,pn)			$128)^{170}_{\bullet}$			Absolute value of yields given in the article.
(γ,α)			$8)^{170}_{\bullet}$			(γ,n) and $(\gamma,2n)$ could not be distinguished - all were taken to be (γ,n); similarly (γ,p) and (γ,d) were all taken to be (γ,p).
$(\gamma,\alpha n)$			$5)^{170}_{0}$			Charge distribution parameters were determined.
(γ,μ_T)			$347)^{170}_{0}$ MeV-mb			

Table I

Reaction	Reaction Threshold, MeV N	O	Ne	Reaction	Reaction Threshold, MeV N	O	Ne
(γ, n)	10.54	15.60	16.79	$(\gamma, 2\alpha)$	16.08	—	11.32
(γ, p)	7.54	12.11	12.79	$(\gamma, p\alpha n)$	19.86	34.56	27.61
(γ, d)	10.26	20.72	20.99	$(\gamma, 2pn)$	25.44	30.48	29.81
(γ, t)	11.61	7.15	4.67	$(\gamma, 2\alpha n)$	—	—	30.53
(γ, pn)	12.49	22.94	23.22	$(\gamma, 4\alpha)$	—	14.43	
$(\gamma, 3n)$	20.05	25.86	20.28	$(\gamma, 3\alpha pn)$	19.77	—	
(γ, pt)	18.20	23.10	16.78	$(\gamma, 2p2n3\alpha)$	—	42.71	
$(\gamma, 2p)$	25.08	22.32	20.76				

Table IV

Reaction type	σ_0, MeV-mb He⁴	N¹⁴	O¹⁶	Ne	σ_{-1}, mb He⁴	N¹⁴	O¹⁶	Ne	σ_{-2}, mb-MeV⁻¹ He⁴	N¹⁴	O¹⁶	Ne
γ, p)	38	38	129	165	1.09	12.5	5.3	6.5	0.035	0.13	0.22	0.25
(γ, n)	44	31	165	115	1.09	1.5	5.3	1.5	0.035	0.06	0.11	0.10
(γ, pn)	12	128	59	86	0.18	5.1	1.3	1.1	0.005	0.18	0.05	0.05
(γ, α)	—	8	2	10	—	0.3	0.3	0.3	—	0.01	0.02	0.02
$(\gamma, \alpha n)$	—	5	15	38	—	0.1	0.3	1.0	—	0.01	0.05	0.02
Stars:												
3-prong	—	53	74	151	—	1.2	3.4	4.2	—	0.05	0.03	0.12
4-prong	—	71	37	73	—	1.6	0.3	0.51	—	0.06	0.01	0.01
5-prong	—	11	2	15	—	0.2	0.1	0.2	—	0.01	0.01	0.005
6-prong	—	—	3	10	—	—	0.03	0.1	—	—	0.01	0.01
σ_{exp}*	35±7	317	438	800	1.10±0.15	12.5	12.8	18.0	0.07±0.015	0.36	0.45	0.60
σ_{theor}**	60	210	240	300	2.3	12.1	13.1	19.3	0.023	0.15	0.23	0.33
$\sigma_{exp}/\sigma_{theor}$	1.6	1.65	1.8	2.0	1.04	1.03	0.98	0.9	3.0	2.5	1.8	1.8

* σ_{exp} — experimental value of the integrated absorption cross sections σ_0, σ_{-1} and σ_{-2}.
** The theoretical values σ_{theor} have been calculated by means of the expressions: $\sigma_0 = 60(NZ/A)$MeV-mb; $\sigma_{-1} = 0.36\ A^{4/3}$ mb; $\sigma_{-2} = 2.25\ A^{4/3}$ mb-MeV⁻¹.

Ref. A.P. Komar, Ya. Krzhemenek, I.P. Yavor
Nuclear Phys. 34, 551 (1962)

Elem. Sym.	A	Z
N	14	7

Method: 90 MeV synchrotron; cloud chamber with magnetic field; also use of recoil nuclei ranges

Ref. No.: 62 KO 2 JHH

Reaction	E or ΔE	E_o	Γ	$\int \sigma dE$	Jπ	Notes
(γ,p)	Bremss. 90	23	>12 MeV	76 MeV-mb		$W(\theta_p)$ = isotropic, E_p = 0.5-6 MeV $W(\theta_p) = 1+1.9 \sin^2\theta_p$, E_p = 6-16 MeV $W(\theta_p) = 1+1.1 \sin^2\theta_p + 0.5 \cos\theta_p$, E_p = > 16 MeV
(γ,n)				49±5 MeV-mb		$W(\theta_n)$ = isotropic, $E_n \leq 12$ MeV $W(\theta_n) = 1+1.5 \sin^2\theta_n$, $E_n > 12$ MeV
(γ,np)				110±7 MeV-mb		
(γ,3αpn)						"large yield"
			TOTAL:	330±20 MeV-mb		

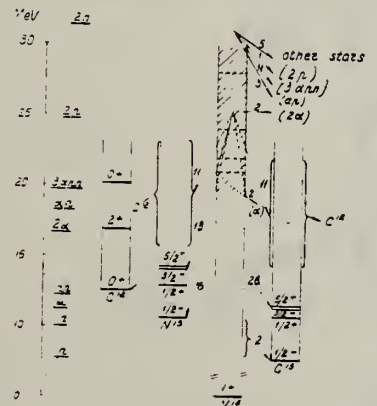

Fig. 5. Scheme of principal channels and probabilities of nitrogen photodisintegration. The dot-and-dash levels are calculated according to the Nilsson scheme ($\hbar\omega_0$ = 23 MeV, δ = 0)

Ref.24: S.G. Nilsson, Mat. Fys. Medd. Dan. Vid. Selsk. 29, No. 1 (1955)

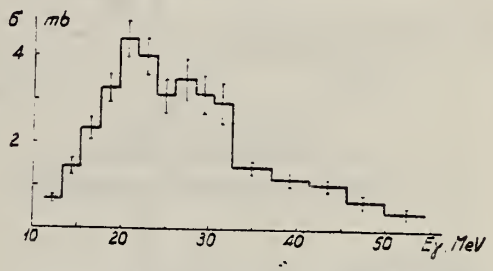

Fig. 2. Excitation function of (γ, p) reaction.

TABLE 1
Relative yields and energy thresholds of the photonuclear reactions on nitrogen

Reaction	Threshold (MeV)	Yield (%)
(γ, p)	7.6	28
(γ, n)	10.6	16
(γ, α)	11.6	2
(γ, pn)	12.5	35
(γ, αp)	18.2	3
(γ, 3αpn)	19.8	11
(γ, 2p)	25.1	2
(γ, 2α)	16.1	2
Others		1

[Figures continued on Sheet 2]

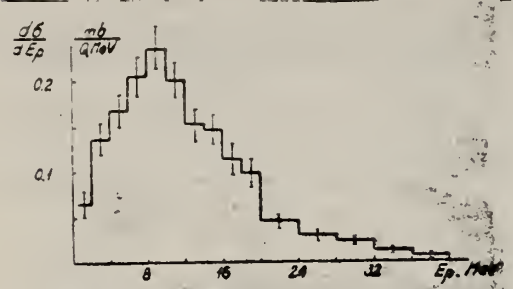

Fig. 3. Energy spectrum of (γ, p) protons.

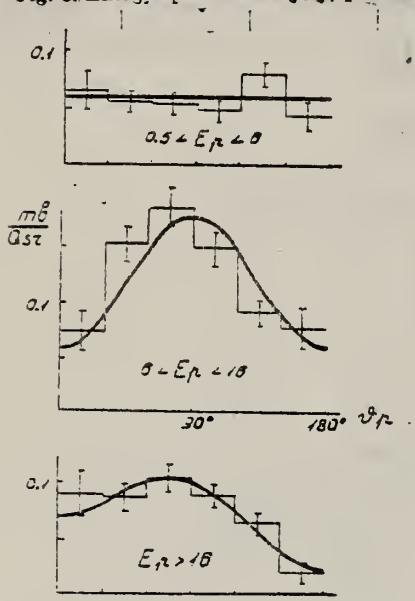

Fig. 4. Angular distributions of (γ, p) protons.

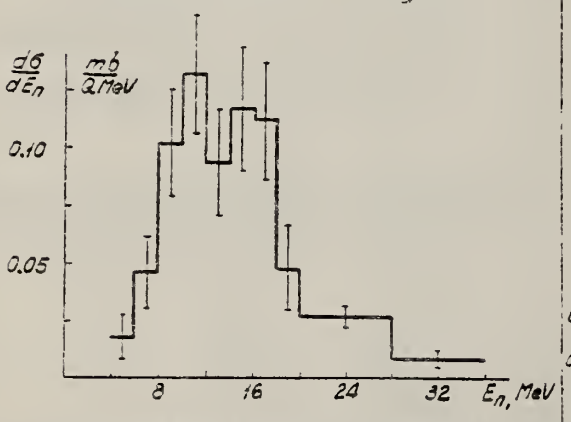

Fig. 6. Energy spectrum of (γ, n) neutrons.

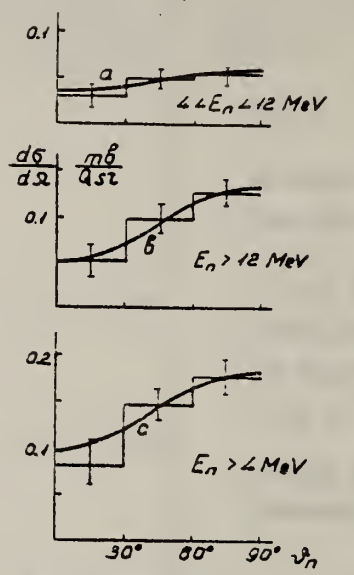

Fig. 7. Angular distributions of (γ, n) neutrons.

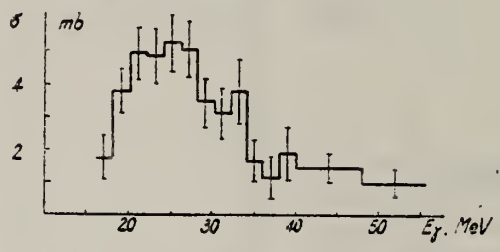

Fig. 8. Excitation function of (γ, np) reaction.

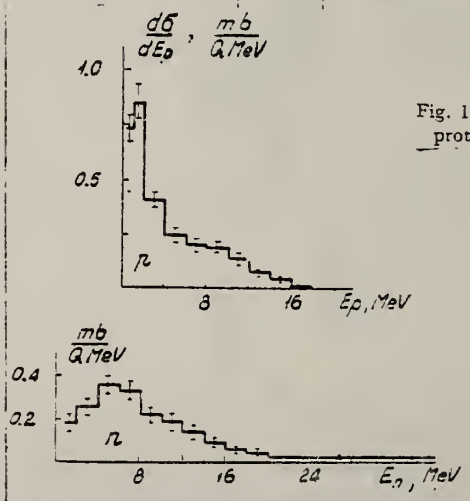

Fig. 9. Energy spectrum of neutrons and protons of (γ, np) reaction.

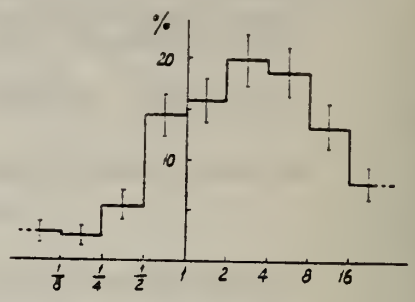

Fig. 10. Probability for different values of E_n/E_p for (γ, np) reaction.

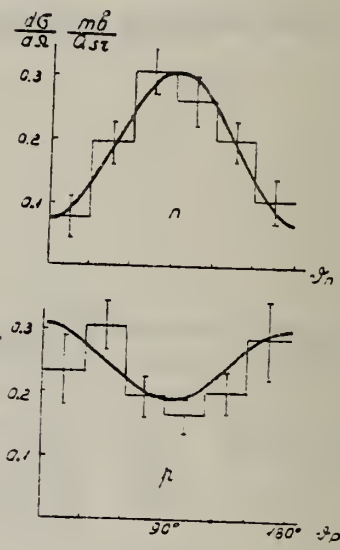

Fig. 11. Angular distributions of neutrons and protons of (γ, np) reaction with $E_n > E_p$.

W.T. Morton, T.G. Walker
Phil. Mag. I, 741 (1962)

ELEM. SYM.		
N	14	7

METHOD

Synchrotron; p and α cross section; nuclear emulsion

REF. NO.	
62 Mo 2	NVB

REACTION	RESULT	EXCITATION ENERGY	SOURCE		DETECTOR		ANGLE
			TYPE	RANGE	TYPE	RANGE	
G,PA	ABI	18-120	C	120	EMU-D		4PI

$$\int_0^{120} \sigma dE = 2.5 \pm 0.5 \text{ MeV-mb}$$

Fig. 2

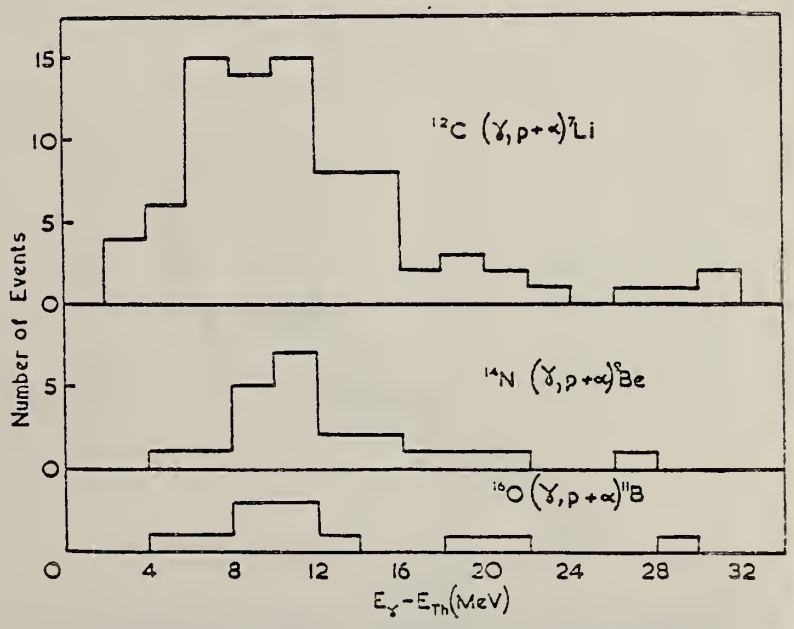

Energy dependence of (γ, p+α) reactions in ^{12}C, ^{14}N and ^{16}O.

Ref.	Elem. Sym.	A	Z
W.C.Barber, J.Goldemberg, G.A.Peterson, Y.Torizuka Nuclear Phys. 41, 461 (1963); erratum to be published (as of 9/9/63)	N	14	7

Method	Ref. No.	
Linac (Stanford Mark II) - counter telescope	63Bal	BG

Reaction	E or ΔE	E_o	Γ	$\int \sigma dE$	Jπ	Notes
(e,e')	41.5		determined see Table II		see Table II	inelastic scattering cross section $(cm^2/sr) \times 10^{-32}$ at 180°
		9.3		0.30		0.92±30%
		10.6		0.25		0.65±30%

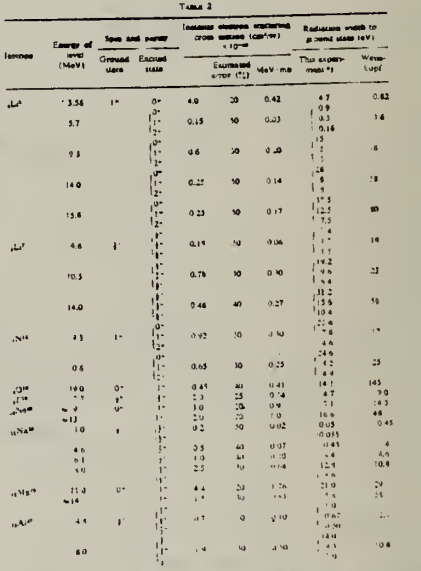

Fig. 5. Spectrum of 41.5 MeV electrons scattered from Li^7 at 180°.

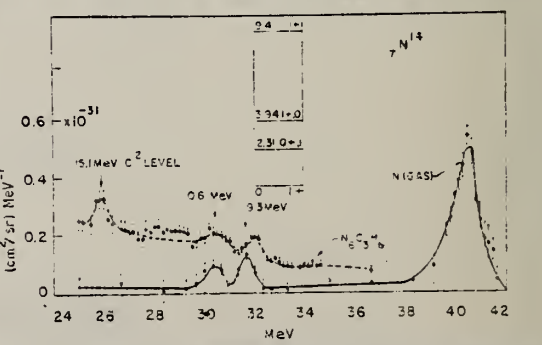

E. Finckh, R. Kosiek, K.H. Lindenberger, K. Maier,
U. Meyer-Berkhout, M. Schechter, J. Zimmerer
Z. Physik 174, 337 (1963)

ELEM. SYM.	A	Z
N	14	7

METHOD: Betatron; proton spectrum, cross section; CsI spectrometer

REF. NO.: 63 Fi 4 NVB

REACTION	RESULT	EXCITATION ENERGY	SOURCE		DETECTOR		ANGLE
			TYPE	RANGE	TYPE	RANGE	
G,XP	SPC	0-31	C	31	SCI-D	2-20	90

Maxima: E_p = 2.7±0.15 MeV
= 7.1 MeV
= 10.2 MeV
= 13.2 MeV

$\int \sigma dE$ = 1.6±0.8 MeV-mb, assuming ground state transition only.

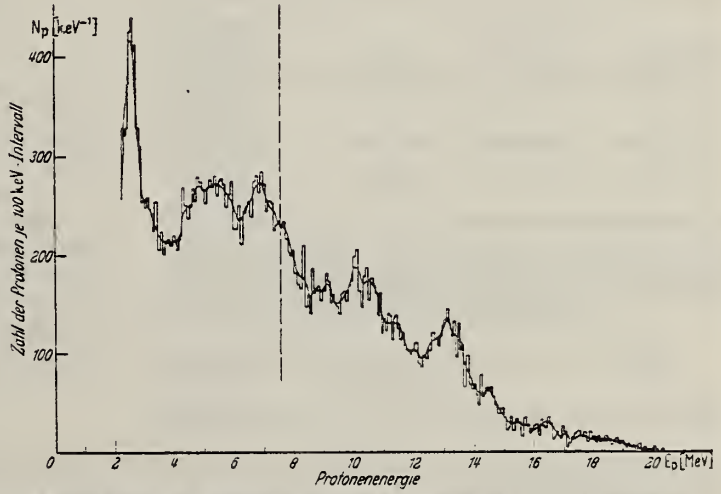

Fig. 4. Energieverteilung der Photoprotonen aus N^{14}, aus zwei Messungen bei E_p=7,6 MeV zusammengesetzt. (Das Histogramm stellt die auf Energieverlust korrigierten Meßwerte dar, die ausgezogene Kurve wurde nach einem Mittelungsverfahren gewonnen.) Nähere Erläuterungen im Text

H. Fuchs
Z. Physik 171, 416 (1963)

N	14	7

METHOD: Betatron; neutron spectrum, cross section; Stilbene scintillator; ion chamber

REF. NO.: 63 Fu 2 | NVB

REACTION	RESULT	EXCITATION ENERGY	SOURCE TYPE	SOURCE RANGE	DETECTOR TYPE	DETECTOR RANGE	ANGLE
G,XN	SPC	10-30 (E_γ)	C	31	SCI-D	3-20 (2.5-20)	90

In spectrum, maxima at:

E_n = 3.9 MeV
= 6.5 MeV
= 11 MeV

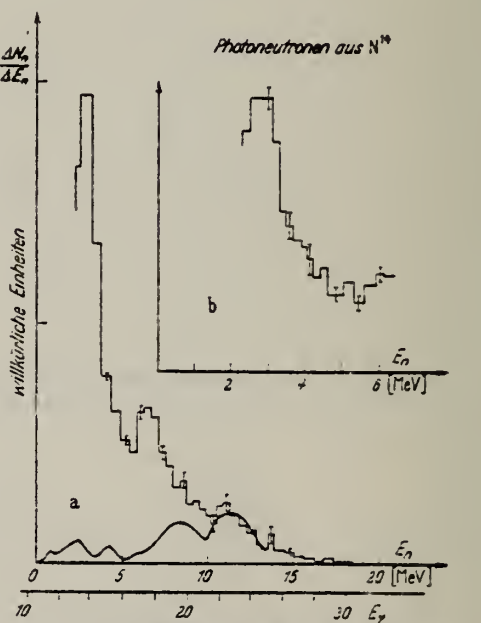

Fig. 2 a u. b. Energieverteilung der Photoneutronen aus N^{14} unter 90° bei E_γ = 30,5 MeV. a Histogramm: Ergebnis dieser Arbeit. Ausgezogene Kurve: Aus dem Wirkungsquerschnitt für $N^{14}(\gamma, n_0)N^{13}$ berechnetes Neutronenspektrum. Nähere Erläuterung im Text. b Spektrum von 2,5 bis 6,5 MeV in feinerer Kanaleinteilung

Ref. F.W. Prosser, Jr., R.W. Krone, J.J. Singh
Phys. Rev. 129, 1716 (1963)

Elem. Sym.	A	Z
N	14	7

Method: Van de Graaff; NaI

Ref. No.: 63 Pr 1 JHH

Reaction	E or ΔE	E_o	Γ	$\int \sigma dE$	Jπ	Notes
(p,γ)	1.75	9.17	8.7 ev (Γ_γ)			$W(\theta) = 1+(-0.44\pm0.01)P_2(\cos\theta)$

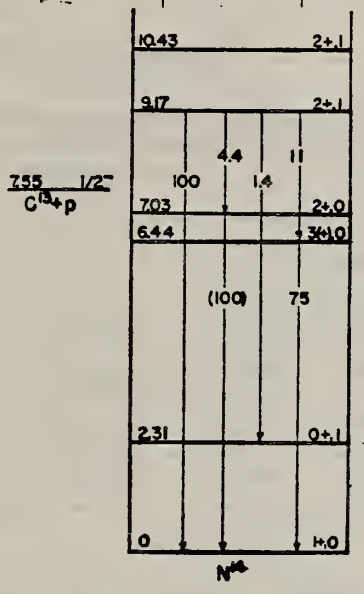

Figure 3: Energy level diagram of N^{14}. Only those levels relevant to the present discussion are included. Intensities of the γ rays from the 9.17 MeV state are normalized to 100 for the transition to the ground state; those from 6.44 and 7.03 MeV states are based on a total of 100. Tentative assignments are given in parentheses. Transitions to other states, discussed by Rose [Nuclear Phys. 19, 113 (1960) and references given there], have not been shown.

TABLE III. Best values of amplitude ratios. Set *A* was calculated with the angular correlation data included; set *B* was not. Values obtained by others have been included for comparison.

Transition and mixing considered	Amplitude ratio Set *A*	Set *B*	Previous work
Formation of compound state, *f*/*p*	−0.43 ±0.18	−0.70 ±0.26	+0.3 < δ < +0.8[a]
9.17 to ground state, *E*2/*M*1	+0.01 ±0.02	−0.005 ±0.020	−0.02 < δ < 0[a]
7.03 to ground state, *E*2/*M*1	−0.65 ±0.15	−0.60 ±0.10	+0.13 < δ < +3.5

[a] See reference 10.
[b] See reference 5. While neither Rose nor Segel *et al.* state the phase convention used in deducing the relative signs of the amplitudes, the agreement of the data and the magnitude of the amplitude ratios suggests that their computations were made without the Huby correction.

Ref 10: Segel et al, Phys. Rev. 123, 194 (1961)
Ref 5: Rose, Nuclear Phys. 19, 113(1960

C.C.M. SYM.		
N	14	7

METHOD	REF. NO.	
Linac, Faraday cup or SEM	64 B1 1	JOC

REACTION	RESULT	EXCITATION ENERGY	SOURCE		DETECTOR		ANGLE
			TYPE	RANGE	TYPE	RANGE	
E,E	ABX	0	D	120,180	MAG-D		DST
E,E/	ABX	0-8	D	120,180	MAG-D		DST

FORM FACTORS

TABLE 1

Experimental elastic and inelastic cross sections in units of 10^{-28} cm²/sr

Incident energy (MeV)	Scattering angle (deg)	Elastic	2.31 MeV	3.95 MeV	5.10 MeV	5.83 MeV	7.03 MeV	8.0 MeV
180.5	50	5480 ±220	3^{+3}_{-1}	24 ±1.4	10 ±2	11 ±2	18 ±6	
180.3	60	1500 ±110	2 ±1	17 ±1.7	7.2 ±0.7	11.3 ±1.2	12 ±1.6	4.0 ±1.0
179.7	70	401 ± 25	1.45±0.6	8.3 ±1.0	5.9 ±0.6	7.4 ±0.8	8.3 ±1.1	
181.1	80	98 ± 10	0.45±0.25	3.7 ±0.9	4.2 ±0.8	4.9 ±0.5	3.3 ±1.0	0.90±0.15
180.5	90	25.3 ± 2.3	0.31±0.20	$1.9^{+0.3}_{-0.6}$	$2.3^{+0.3}_{-0.4}$	$3.1^{+0.2}_{-0.4}$		
179.7	100	6.8 ± 0.5	0.39±0.14	1.3 ±0.2	1.3 ±0.2	2.2 ±0.25	1.2 ±0.2	0.38±0.08
179.0	110	1.88± 0.11	0.21±0.08	0.61±0.07	0.59±0.07	1.22±0.24	0.60±0.20	0.20±0.03
181.1	120	0.42± 0.04	0.14±0.08	0.38±0.04	0.34±0.04	0.71±0.08	0.34±0.04	0.13±0.03
120.7	120	55 ± 5	0.73±0.15	1.4 ±0.16	0.85±0.10	1.2 ±0.2		

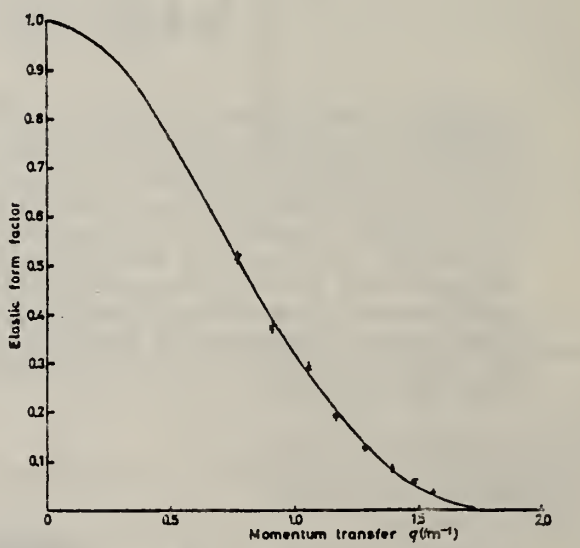

Fig. 1. The elastic form factor derived from the data of table 1, plotted as a function of momentum transfer. For comparison the full curve corresponds to the expression $F(q) = (1-0.3308\,q^4)\exp(-0.7518\,q^8)$.

REACTION	RESULT	EXCITATION ENERGY	SOURCE TYPE	SOURCE RANGE	DETECTOR TYPE	DETECTOR RANGE	ANGLE

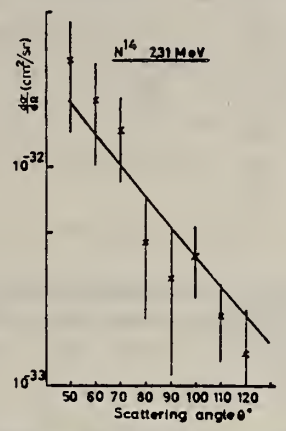

Fig. 2. The cross section for inelastic electron scattering with excitation of the level at 2.312 MeV, ($J = 0^+$, $T = 1$). The full line corresponds to the calculated cross section using the wave function described in the text.

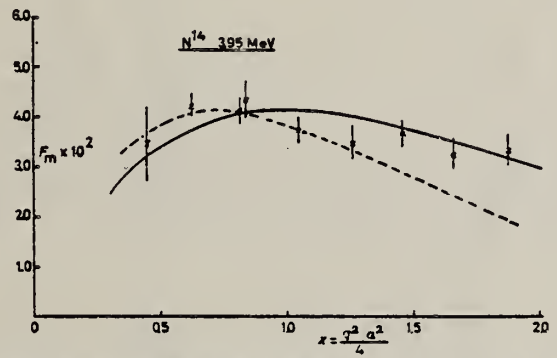

Fig. 3. The inelastic form factor for excitation of the level at 3.945 MeV. The full curve corresponds to the radial integral $\langle 1p|j_3(qr)|1p\rangle$ and the dashed curve to the radial integral $\langle 1p|j_3(qr)|1f\rangle$.

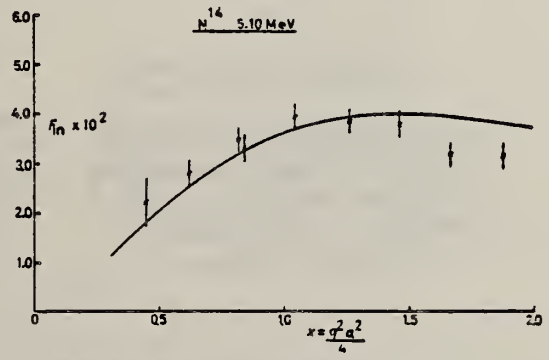

Fig. 4. The inelastic form factor for excitation of the level at 5.10 MeV. The full curve corresponds to the radial integral $\langle 1p|j_3(qr)|1d\rangle$.

REACTION	RESULT	EXCITATION ENERGY	SOURCE TYPE	SOURCE RANGE	DETECTOR TYPE	DETECTOR RANGE	ANGLE

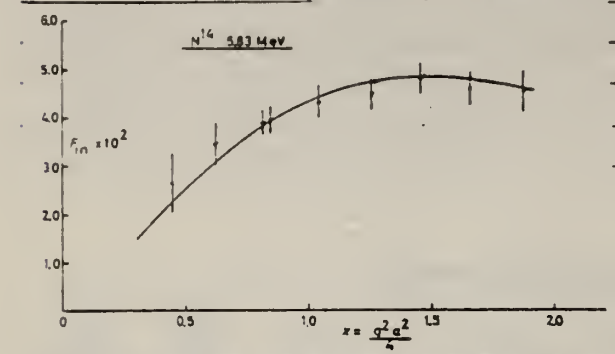

Fig. 5. The inelastic form factor for excitation of the level at 5.83 MeV. The full curve corresponds to the radial integral $\langle 1p|j_1(qr)|1d\rangle$.

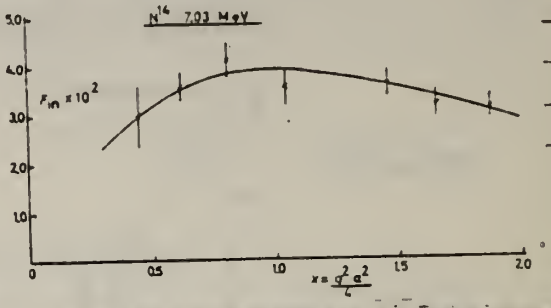

Fig. 6. The inelastic form factor for excitation of the level at 7.03 MeV. The full curve corresponds to the radial integral $\langle 1p|j_1(qr)|1p\rangle$.

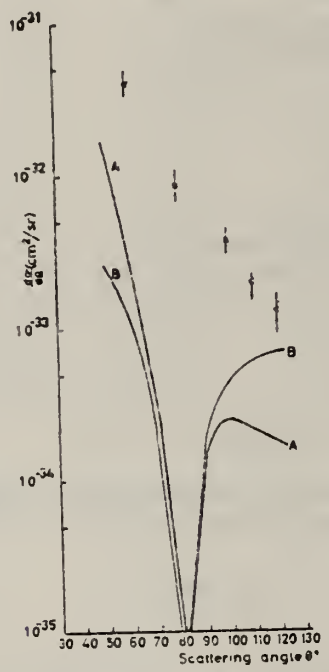

Fig. 7. The cross section for inelastic scattering with excitation of the level at 8.0 MeV. The curve marked A corresponds to the longitudinal E1 component, whilst the curve marked B corresponds to the transverse E1 component, each evaluated for the configuration $(1p_{\frac{1}{2}}2s_{\frac{1}{2}})_{J=1} \rightarrow (1p_{\frac{1}{2}})^2_{J=1}$.

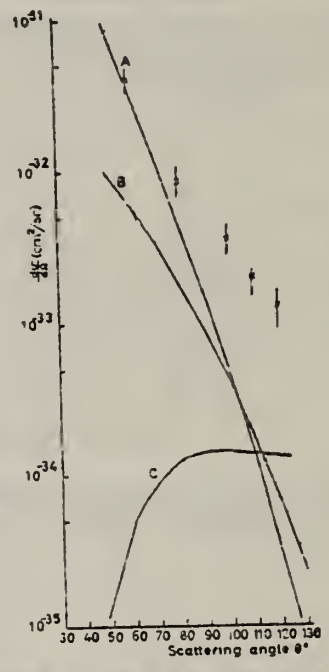

Fig. 8. The cross section for inelastic scattering with excitation of the level at 8.0 MeV. Curve A corresponds to the longitudinal E1 component, curve B to the transverse E1 component, and curve C to the M2 component each for the configuration $(1p_{\frac{1}{2}}1d_{\frac{3}{2}})_{J=1} \rightarrow (1p_{\frac{1}{2}})^2_{J=1}$.

REF. E. C. Booth, B. Chasan and K. A. Wright
Nucl. Phys. 57, 403-420 (1964)

ELEM. SYM.	A	Z
N	14	7

METHOD
Van de Graaff; resonance fluorescence

REF. NO.	
64 Bo 1	NVB

REACTION	RESULT	EXCITATION ENERGY	SOURCE		DETECTOR		ANGLE
			TYPE	RANGE	TYPE	RANGE	
G,G	LFT	1-3	C	1 - 3	NAI-D		100
		(0.5 - 3.0)		(0.5 - 3.0)			

ABI

TABLE 1
Cases of observed resonance fluorescence

Nucleus multipol.	State (MeV)	Spin	Γ_0/Γ	$T(g w \Gamma_0^2/\Gamma^2)^{-1}$ (sec).	Mean lifetime T BCW (sec)	Mean lifetime T other (sec)	Ref.	Γ_0/Γ_W BCW
N^{14}	0.00	0^+						
M1 [a])	2.31	1^+	1	$22 \pm 8 \times 10^{-14}$	$9.7 \pm 3 \times 10^{-14}$	$7.3 \pm 1.8 \times 10^{-14}$	[9])	2.8×10^{-3}

REF.

R. Kosiek, K. Maier und K. Schlüpmann
Phys. Letters 9, 260 (1964)

COMP.		
N	14	7

METHOD

Betatron ; CsI scintillator; ion chamber monitor

REF. NO. 64 Ko 1 JOC

REACTION	RESULT	EXCITATION ENERGY	SOURCE		DETECTOR		ANGLE
			TYPE	RANGE	TYPE	RANGE	
G,XP	SPC	THR - 31	C	15-31	SCI-D	2-22	90

ABX

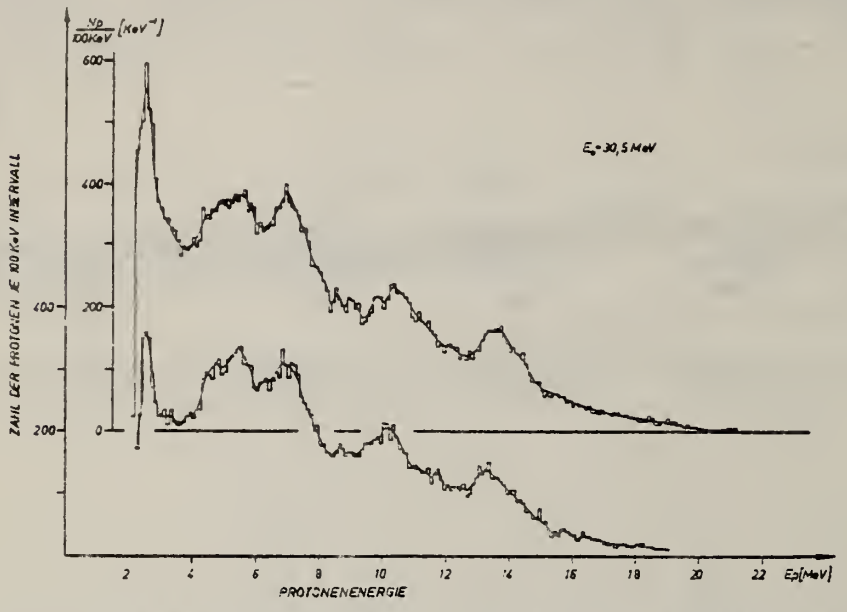

Fig. 1a-f. Energieverteilung der Photoprotonen aus N^{14} bei verschiedenen Endenergien E_0 des Bremsspektrums. Die Histogramme stellen die auf Energieverlust korrigierten Messwerte dar, die ausgezogenen Kurven wurden nach einem Mittelungsverfahren [4] gewonnen Fig. 1f zeigt zwei unabhängige Messungen.

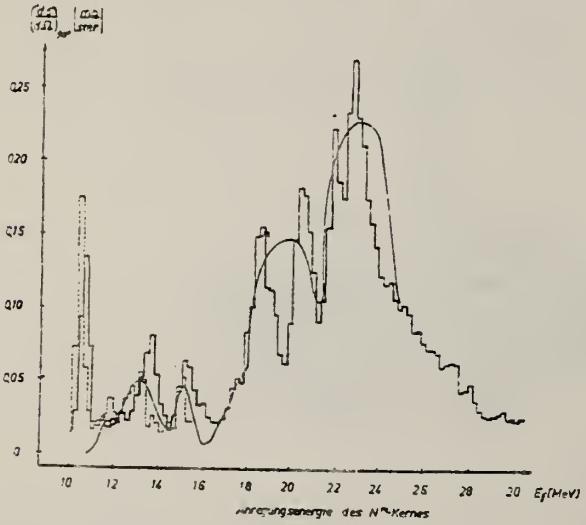

Fig. 2a. Histogramm: (——) Wirkungsquerschnitt für Grundzustandsübergänge beim Prozess $N^{14}(\gamma,p)C^{13}$. Der Fehler in den Absolutwerten wurde auf ± 20% abgeschätzt. b. Histogram (– – –) Ergebnis der Messungen von Wahlström und Forkman [6]. c. Kurve: Wirkungsquerschnitt für Grundzustandsübergänge beim (γ,n)-Prozess am N^{14} nach King et al. [7]. Nähere Erläuterungen im Text.

REF.

M. Elaine Toms
Nucl. Phys. 54, 625-640 (1964)

N	14	7

METHOD
Betatron

REF. NO.
64 To 2 JOC

REACTION	RESULT	EXCITATION ENERGY	SOURCE		DETECTOR		ANGLE
			TYPE	RANGE	TYPE	RANGE	
G,A	ABX	THR - 22	C	22	EMU-D		DST

59 events 0.74 ± 0.11 MeV-mb

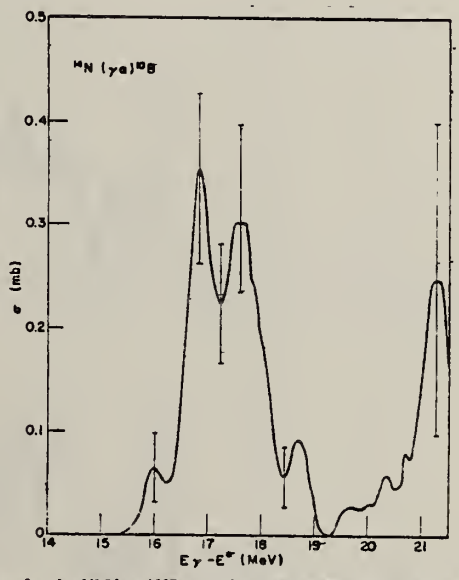

Fig. 2. The cross-section for the $^{14}N(\gamma,\alpha)^{10}B$ reaction versus $E_\gamma - E^*$ where E_γ is the photon energy if E^* equals zero and E^* is the ^{10}B excitation energy.

REF.

R.W. Detenbeck, J.C. Armstrong, A.S. Figuera and J.B. Marion
Nuclear Phys. 72, 552 (1965)

ELEM. SYM.	A	Z
N	14	7

METHOD

$^{13}C(p,\gamma)^{14}N$

REF. NO. 65 De 2 JOC

REACTION	RESULT	EXCITATION ENERGY	SOURCE		DETECTOR		ANGLE
			TYPE	RANGE	TYPE	RANGE	
P,G	LFT	9	D	2	NAI-D		DST

$J^{\pi} = 2^{-}$, T = 0 9.129 MeV → 9.2 $\omega\Gamma_{\gamma} \cong 0.03$ eV

$W(\theta) = 1 + (0.22 \pm 0.09)\ P_2(\cos\theta)$

REF.

P. Kossanyi-Demay and G. J. Vanpraet
Nucl. Phys. 81, 529 (1966)

ELEM. SYM.	A	Z
N	14	7

METHOD

Stanford Mark II; Linac

REF. NO.	
66 Ko 1	JDM

REACTION	RESULT	EXCITATION ENERGY	SOURCE		DETECTOR		ANGLE
			TYPE	RANGE	TYPE	RANGE	
E,E/	ABX	8 - 14	D	50,60	MAG-D	30-60	180

TABLE 4

Excited states observed in $^{14}N(1^+)$ by inelastic scattering at 180° of electrons of primary energy 50 MeV and 60 MeV

ex	J^π	Transition	Γ_w	50 MeV results			60 MeV results			Other measurements
				$d\sigma/d\Omega$ (nb·sr^{-1})	Γ_γ^0 (eV)	M^2	$d\sigma/d\Omega$ (nb·sr^{-1})	Γ_γ^0 (eV)	M^2	
8.7	0^+ $T=1$	M1	13.22	8 ±2	39	3	5 ±1.5	42	3.18	1.3±0.4 eV ref. [45])
	3^- $T=1$	M2	0.006		0.016	2.6				ref. [44])
9.2	2^+ $T=1$	M1	16	10 ±2.5	12	0.75	6.5±1.8	13.8	0.86	8.7±1.5 eV ref. [48])
										9±3 eV ref. [2])
10.4	2^+ $T=1$	M1	23.6	10 ±2.5	17.5	0.74	5 ±1	15.2	0.64	17 eV ref. [49])
										20±6 eV ref. [2])
11.7	3^+	E2	53	4.5±1	4	0.075	2.5±1			
	3^-	M2	0.029		0.07	2.4				
12.7	3^+	E2	67	7.5±2	8.5	0.12	4 ±1			
	3^-	M2	0.04		0.17	4				

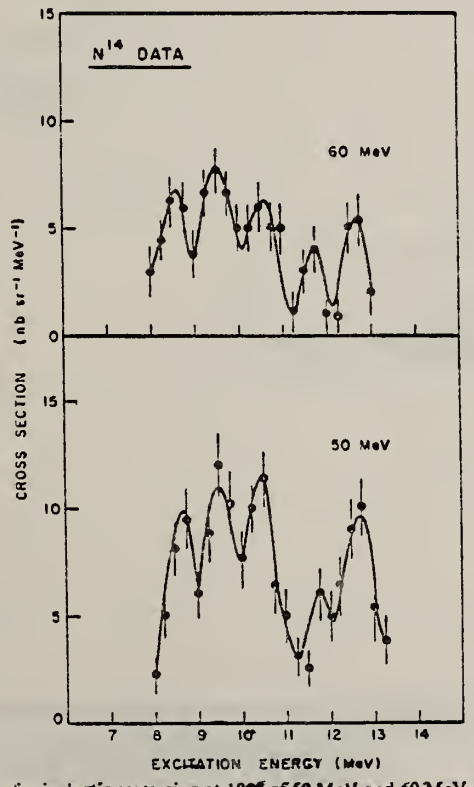

Fig. 6. Cross section for inelastic scattering at 180° of 50 MeV and 60 MeV electrons from ^{14}N target.

REF.

C. P. Swann
Phys. Rev. 148, B1119 (1966)

ELEM. SYM.	A	Z
N	14	7

METHOD

Resonance scattering of Doppler-broadened 7.115 MeV gamma ray from $^{19}F(p,\alpha\gamma)^{16}O$.

REF. NO. 66 Sw 1 JDM

REACTION	RESULT	EXCITATION ENERGY	SOURCE		DETECTOR		ANGLE
			TYPE	RANGE	TYPE	RANGE	
G,G	LFT	7.1	D	7.1	NAI		DST

$W(\theta) = 1 + (1.25 \pm 0.16)\ P_2 + (0.29 \pm 0.26)\ P_4$.

Excited state of N^{14} $E_n = (7.029 \pm -006)$ MeV

$\tau = (5.4 \pm 0.5) \times 10^{-15}$ sec assuming all transitions go to ground state.

$W(\theta)$ consistent with I = 2

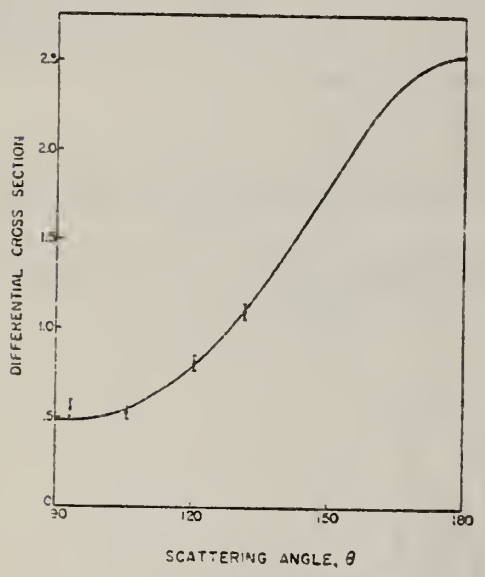

FIG. 4. Angular distribution of the resonantly scattered radiation. The solid curve gives the least-square fit, i.e., $W(\theta) = 1 + (1.25 \pm 0.16) P_2 + (0.29 \pm 0.26) P_4$.

REF.

J. M. Loiseaux, J. M. Maison, and M. Langevin
J. de Physique 28, 11 (1967)

ELEM. SYM.	A	Z
N	14	7

METHOD

REF. NO. 67 Lo 1 JOC

REACTION	RESULT	EXCITATION ENERGY	SOURCE		DETECTOR		ANGLE
			TYPE	RANGE	TYPE	RANGE	
G,G/	ABX	18-32	C	34	NAI-D		DST

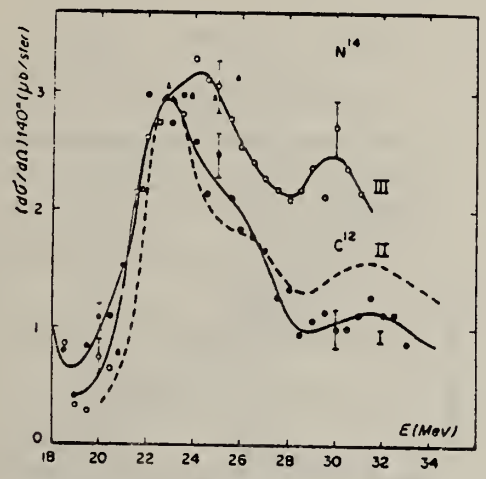

FIG. 4.

I : ^{13}C Section efficace différentielle de diffusion ($E_m = 34$ MeV).

II : ^{13}C Section efficace prévue pour la relation de dispersion et multipliée par 0,55.

III : ^{14}N Section efficace différentielle de diffusion à 140° ($E_m = 27$ MeV), (O $E_m = 32$ MeV).

REF. H. G. Clerc and E. Kuphal
Z. Physik 211, 452 (1968)

ELEM. SYM.	A	Z
N	14	7

METHOD

REF. NO. 68 C1 1 egf

REACTION	RESULT	EXCITATION ENERGY	SOURCE		DETECTOR		ANGLE
			TYPE	RANGE	TYPE	RANGE	
E,E/	LFT	8-12	D	35-58	MAG-D	20-60	DST

9.17, 10.43 MEV

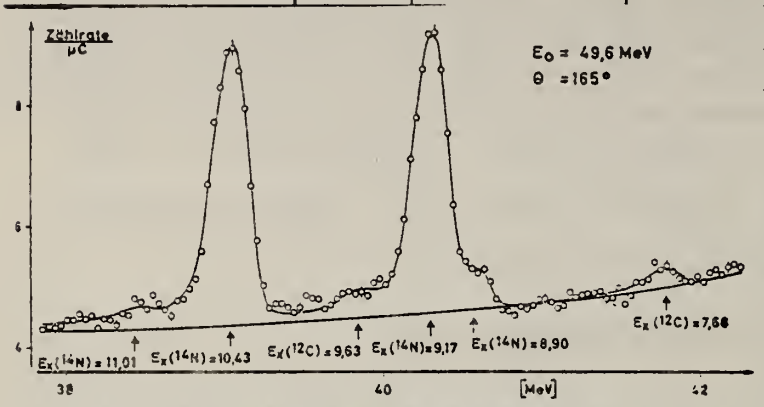

Fig. 2. Spektrum der von einem $N_6C_3H_6$-Target gestreuten Elektronen bei 49,6 MeV Primärenergie und einem Streuwinkel von 165°

Tabelle 4. *Grundzustandsbreiten beim Zerfall des 9,17 und 10,43 MeV-Niveaus im Vergleich mit Literaturwerten*

Γ_γ^0·(eV)		Autoren
9,17 MeV	10,43 MeV	
8,7 ± 1,5		3
	17 ± 5	4
9 ± 3	20 ± 6	5
4,5 ± 1,4	4,9 ± 1,5	6
13 ± 3	16,4 ± 3,0	7
7,7 ± 0,9	12,1 ± 1,5	diese Arbeit

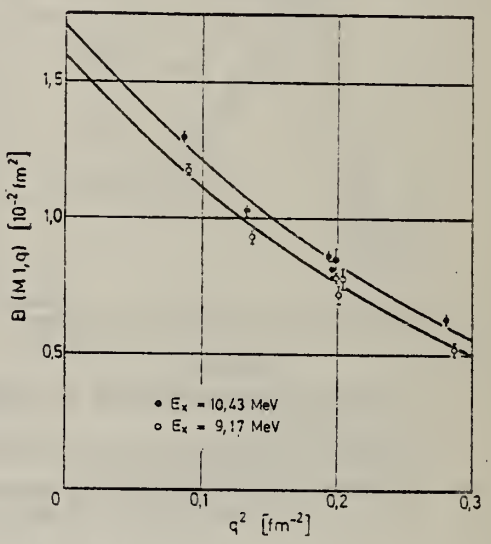

Fig. 4. Reduzierte Übergangswahrscheinlichkeiten $B(M1, q)$ nach der Partialwellenmethode als Funktion von q^2 für das 9,17 und 10,43 MeV-Niveau. Die Figur illustriert, wie zuverlässig der Quotient der $B(k)$ und damit der Γ_γ^0 ausgewertet werden kann

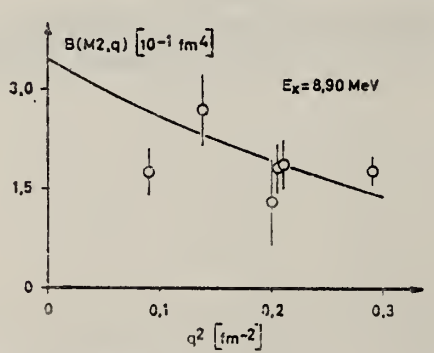

Fig. 6. Reduzierte Übergangswahrscheinlichkeit $B(M2, q)$ in Bornscher Näherung als Funktion von q^2 für das 8,90 MeV-Niveau. Die eingezeichnete Kurve erhält man durch eine Anpassung an die Meßpunkte unter Benutzung eines fest vorgegebenen Übergangsradius von 3,4 fm

REF. N. N. Kaushal, E. J. Winhold, P. F. Yergin, H. A. Medicus and R. H. Augustson
Phys. Rev. 175, 1330 (1968)

ELEM. SYM.	A	Z
N	14	7

METHOD

REF. NO. 68 Ka 1 HMG

REACTION	RESULT	EXCITATION ENERGY	SOURCE		DETECTOR		ANGLE
			TYPE	RANGE	TYPE	RANGE	
G,N	ABX	50-85	C	55,85	TOF-D	10-85	67
							(67.5)

NEUT ENGY SPEC

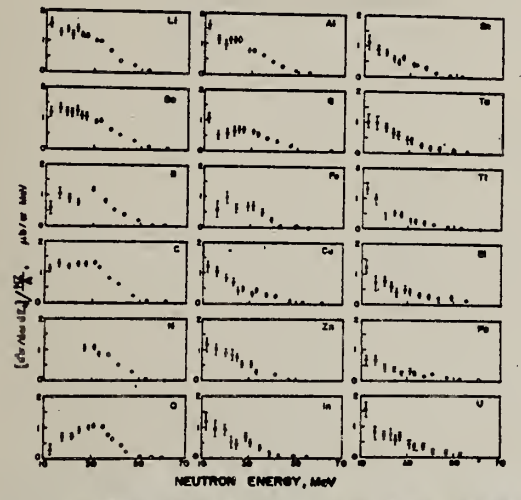

FIG. 6. Observed neutron spectra due to 55–85-MeV difference photon spectra. The effective cross sections have been divided by NZ/A.

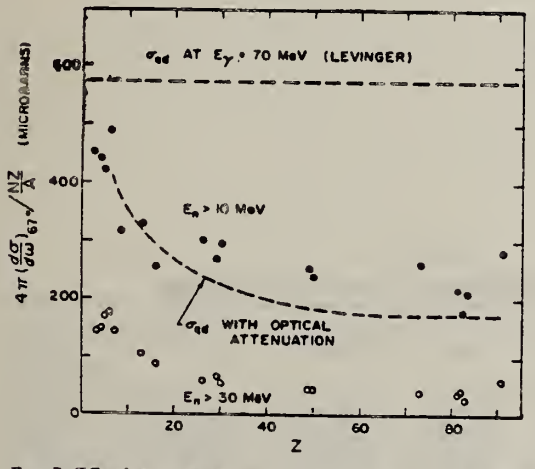

FIG. 7. Effective cross sections for production of fast neutrons with energies greater than 10 MeV (solid circles) and 30 MeV (open circles) by the 55–85-MeV photon difference spectrum. The dashed curves are modified quasideuteron model predictions as discussed in the text.

TABLE I. Comparison of present cross-section values in mb for production of high-energy photoneutrons by 55–85-MeV photons with measured cross sections $\sigma(\gamma,Tn)$, also in mb, for total photoneutron production. The present cross-section values are uncertain by 8 to 10% because of counting statistics and normalization errors; in addition all values depend on an absolute normalization in terms of the deuteron photodisintegration cross section, which is known to about 10% at these energies.

Target	$4\pi(d\sigma/d\omega)_{\pi/2}$ (E_n > 10 MeV) [Present experiment]	$\sigma(\gamma,Tn)$ Jones and Terwilliger[a]	Costa *et al.*[b]	Other results
Li	0.75		1.0	
Be	1.0	2.7	2.3	2.3[c]
B	1.0		1.4	
C	1.5	1.3	1.4	2.4[d]
O	1.3		1.6	
Al	2.8	5.5	4.6	8[d]
S	2.1		4.4	6.5[d]
Fe	4.2	16	12	
Cu	4.3	20	19	
Zn	4.4		15	
In	7.4			
Sn	7.0			
Ta	10.7	95		
Tl	10.7			
Pb	8.3	100		
Bi	13			
U	16	65		

[a] Average cross sections between 55 and 85 MeV, as read from Figs. 4 and 5 of Ref. 4.
[b] $\int_0^{E_m}\sigma dE - \int_0^{E_n}\sigma dE/50$, as taken from Fig. 4 of Ref. 5 and Table I of Ref. 6.
[c] S. Costa, L. Pasqualini, G. Piragino, and L. Roasio, Nuovo Cimento 42, 306 (1966).
[d] G. Bishop, S. Costa, S. Ferroni, R. Malvano, and G. Ricco, Nuovo Cimento 42, 348 (1966).

REF. N. Bezić, D. Brajnik, D. Jamnik and G. Kernel
Nucl. Phys. A128, 426 (1969)

ELEM. SYM.	A	Z
N	14	7

METHOD

REF. NO. 69 Be 2 egf

REACTION	RESULT	EXCITATION ENERGY	SOURCE		DETECTOR		ANGLE
			TYPE	RANGE	TYPE	RANGE	
G,MU-T	ABX	10-30	C	35	MGC-D	10-30	4PI

106+

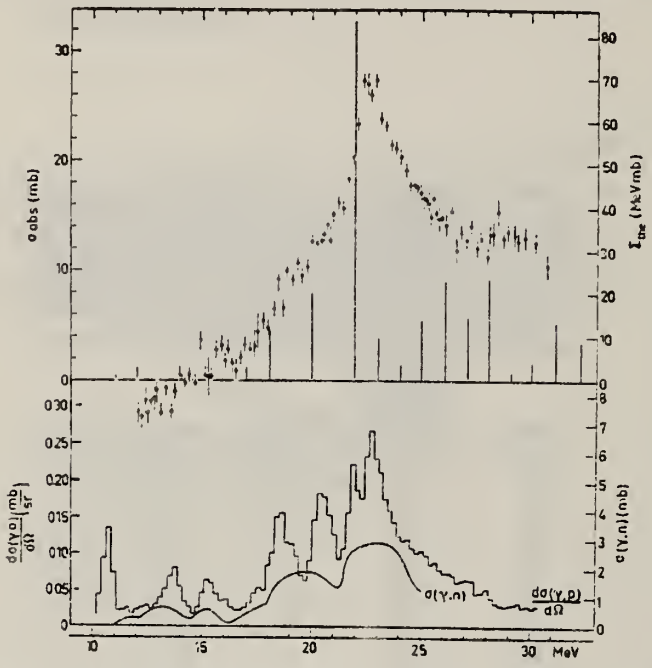

Fig. 2. The nuclear part of the photo-absorption cross section for ^{14}N. The error of the zero line is estimated to be ±2.5 mb. For comparison $\sigma(\gamma, p_0)$ and $\sigma(\gamma, n)$ from refs. [20,19]) are also plotted. Theoretical lines are from fig. 11 of Cooper and Eisenberg [21]).

[19] J. D. King, R. N. H. Haslam and R. W. Parsons, Can. J. Phys. 38, (1960) 231.
[20] R. Kosiek, K. Maier and K. Schlüpmann, Phys. Lett. 9 (1964) 260.
[21] B.S. Cooper and J. M. Eisenberg, Nucl. Phys. A114 (1968) 184.

TABLE 1
Weighted energy-integrated total photonuclear cross sections

	σ_{int} (mb · MeV)	$\frac{\sigma_{int}}{60(NZ/A)}$ (mb · MeV)	σ_{-1} (mb)	$\frac{\sigma_{-1}}{0.30A^{\frac{1}{3}}\ mb}$	σ_{-2} (mb · MeV^{-1})	$\frac{\sigma_{-2}}{3.5\ A^{\frac{1}{3}}}$ (μb · MeV^{-1})
^{12}C	135±13	0.74±0.07	5.4±0.6	0.65±0.07	0.23±0.03	1.04±0.15
^{14}N	195±37	0.93±0.08	8.4±1.7	0.83±0.20	0.36±0.08	1.28±0.29
^{16}O	171±17	0.71±0.07	7.2±0.8	0.60±0.07	0.31±0.04	0.87±0.11
^{19}F	271±50	0.94±0.17	14.1±2.7	0.82±0.19	0.74±0.17	1.60±0.35
^{28}Si	360±30	0.86±0.07	17.5±1.7	0.68±0.07	0.83±0.10	0.93±0.11
^{40}Ca	580±60	0.96±0.10	29 ±3	0.71±0.08	1.5 ±0.2	0.92±0.12

The interval of integration is 10-30 MeV.

REF. B.L. Berman, S.C. Fultz, J.T. Caldwell, M.A. Kelly, S.S. Dietrich
Phys. Rev. C2, 2318 (1970)

ELEM. SYM.	A	Z
N	14	7

METHOD

REF. NO. 70 Be 8 hmg

REACTION	RESULT	EXCITATION ENERGY	SOURCE TYPE	SOURCE RANGE	DETECTOR TYPE	DETECTOR RANGE	ANGLE
G,XN	ABX	10 - 30	D	10 - 30	BF3 -I		4PI
		(10.5 - 29.5)		(10.5 - 29.5)			

513+

$\int_{Thr}^{29.5} \sigma dE$ = 97.6 MeV mb

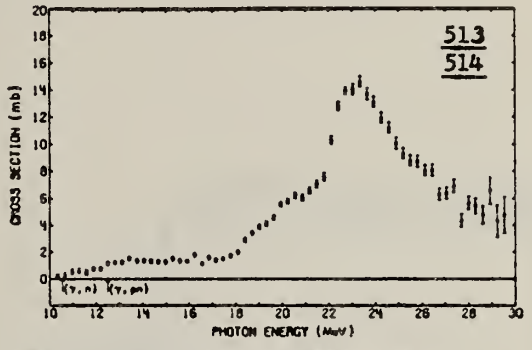

FIG. 2. Total photoneutron cross section for N^{14}, $\sigma[(\gamma,n)+(\gamma,pn)]$. The $(\gamma,2n)$ threshold is above the range of the present measurement.

	Punched	Checked w/PO
IBM Card DATA	6/10/71	✓
IBM Card REFERENCE	"	✓

REF. J. L. Black, W. J. Caelli, W. F. Davidson, R. B. Watson
Nucl. Phys. A153, 233 (1970)

ELEM. SYM.	A	Z
N	14	7

METHOD

REF. NO. 70 B1 1 egf

REACTION	RESULT	EXCITATION ENERGY	SOURCE TYPE	SOURCE RANGE	DETECTOR TYPE	DETECTOR RANGE	ANGLE
HE,G	ABX	21-24	D	1-3	NAI-D		DST
				(.9 - 2.6)			

HE = HE3

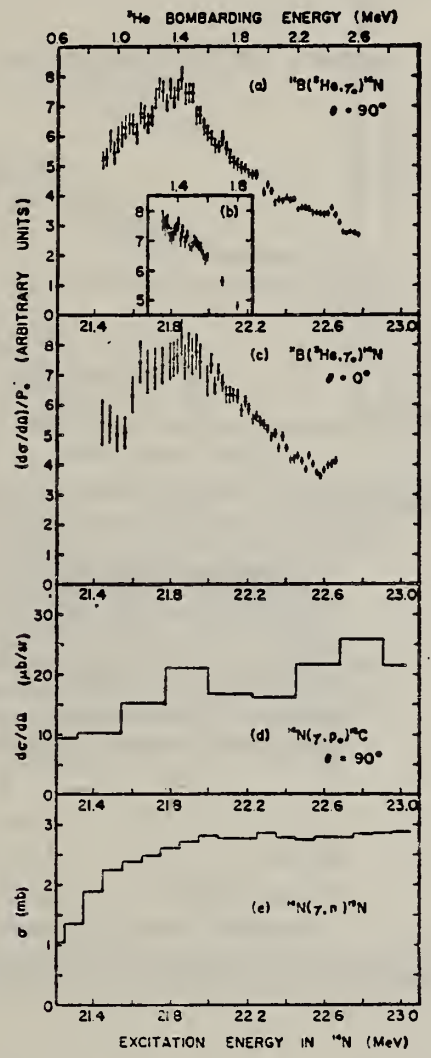

Fig. 3. a) The differential cross section divided by the s-wave penetration factor for the $^{11}B(^3He,\gamma_0)^{14}N$ reaction, measured at $\theta = 90°$. b) A repeat of portion of the data shown in fig. 3a, measured with 15 keV resolution. c) The differential cross section divided by the s-wave penetration factor, measured at $\theta = 0°$. d) A portion of the excitation function [8]) for the reaction $^{14}N(\gamma, p_0)^{13}C$. e) A portion of the excitation function [9]) for the reaction $^{14}N(\gamma, n)^{13}N$.

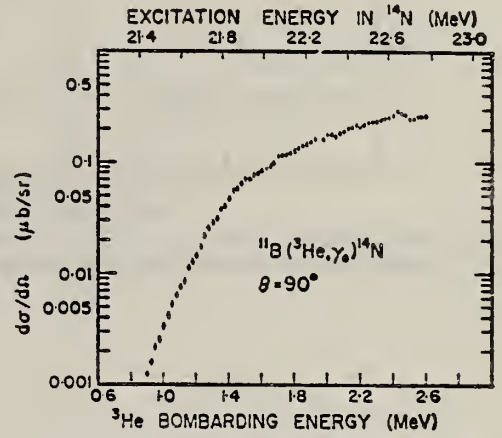

Fig. 2. The measured $^{11}B(^3He,\gamma_0)^{14}N$ excitation function, taken at $\theta = 90°$.

[over]

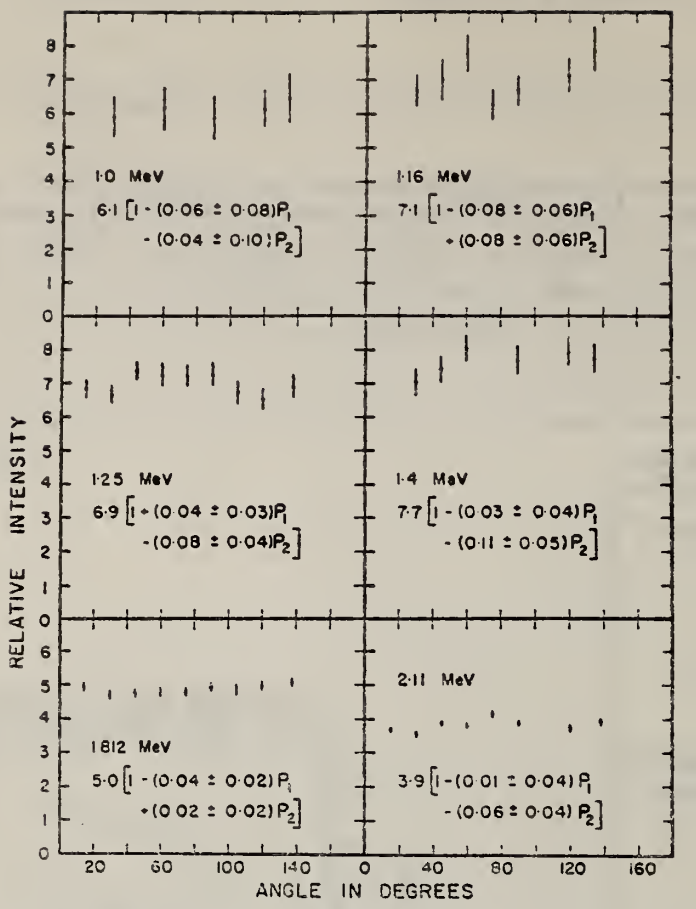

Fig. 4. Gamma-ray angular distributions from the reaction $^{11}B(^3He,\gamma_0)^{14}N$ measured at six energies. Included are least-squares fits to the data in the form $W(\theta) = \Sigma_{l=0}^{2} A_l P_l(\cos\theta)$.

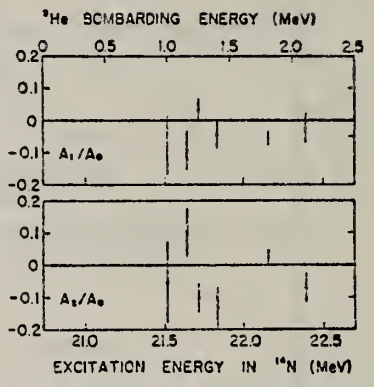

Fig. 5. The coefficients obtained from least-squares fits to the angular distributions. The coefficients have been corrected for the finite size of the detector and for lab-c.m. conversion.

REF. N. K. Sherman, R. W. Gellie, K. H. Lokan and R. G. Johnson
Phys. Rev. Letters 25, 114 (1970)

ELEM. SYM.	A	Z
N	14	7

METHOD

REF. NO. 70 Sh 1 hmg

REACTION	RESULT	EXCITATION ENERGY	SOURCE		DETECTOR		ANGLE
			TYPE	RANGE	TYPE	RANGE	
G,PN	SPC	15-30	C	15-30	TOF-D	0-20	90
		(15.5-29.5)		(15.5-29.5)			

DE-EXCIT. NEUTS.

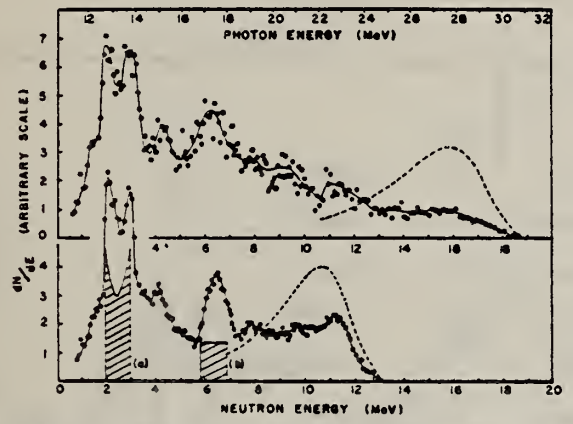

FIG. 2. Measured differences between (i) the 23.5- and 21.5-MeV neutron energy spectra of ^{14}N (lower curve) and (ii) the 29.5- and 27.5-MeV spectra (upper curve). The photon energies k are obtained from ground-state neutron energies T_n by the relation $k \simeq T_n A/(A-1) + B_n{}^A$. The photon differences are shown dotted. The hatched regions are calculated line shapes for de-excitation neutrons, Doppler broadened by photoproton emission. Their vertical scale has no significance. Region (a) is for the 7.55-MeV state of ^{13}C; region (b) is for the 11.8-MeV state.

REF.

M. N. Thompson, R. J. J. Stewart and J. E. M. Thompson
Phys. Letters 31B, 211 (1970)

N	14	7

METHOD

REF. NO. 70 Th 1 egf

REACTION	RESULT	EXCITATION ENERGY	SOURCE		DETECTOR		ANGLE
			TYPE	RANGE	TYPE	RANGE	
G,XG	ABX	THR-29	C	29	SCD-D	1-4	125

^{13}C states: 3.68 7 ± 2 MeV-mb
3.85 1.7 ± 0.7 MeV-mb

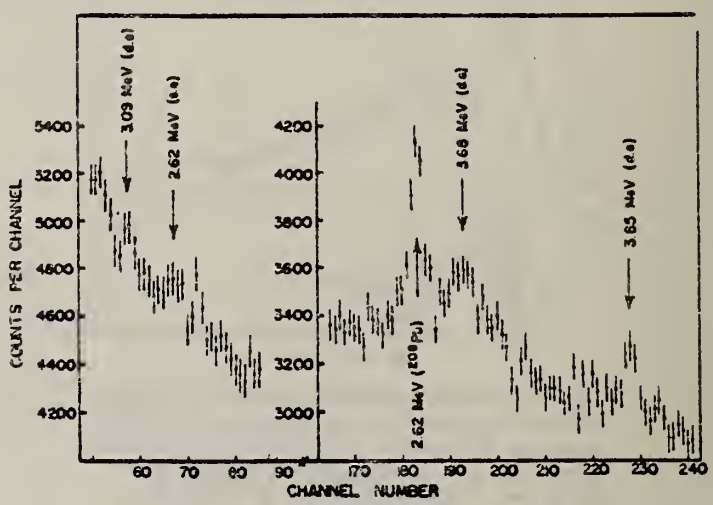

Fig. 1. Spectrum of de-excitation γ-rays following photodisintegration of ^{14}N.

REF.

B. Friberg, G. Andersson and B. Forkman
Nucl. Phys. A171, 551 (1971)

ELEM. SYM.	A	Z
N	14	7

METHOD

REF. NO. 71 Fr 1 egf

REACTION	RESULT	EXCITATION ENERGY	SOURCE		DETECTOR		ANGLE
			TYPE	RANGE	TYPE	RANGE	
G,N	ABY	10-800	C	100-800	ACT-I		4PI

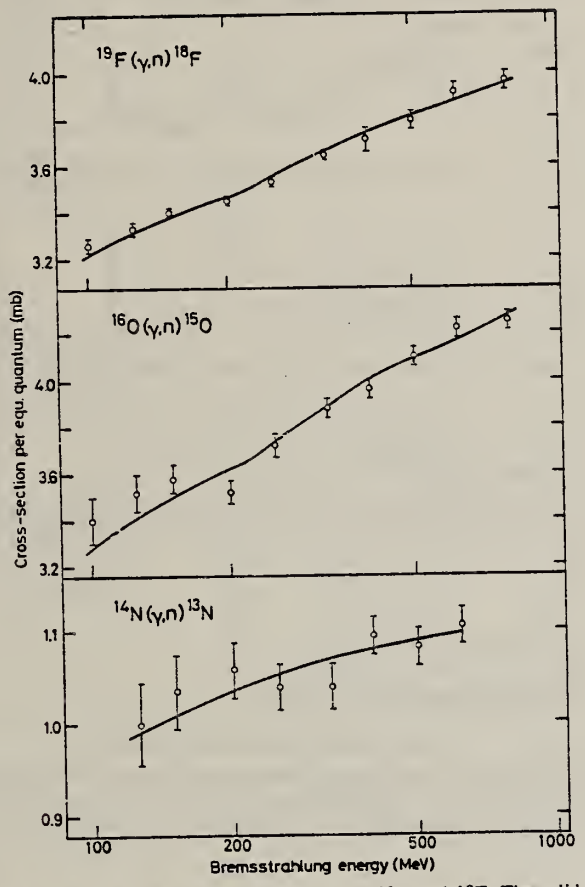

Fig. 1. Absolute yields for the (γ, n) reactions in ^{14}N, ^{16}O and ^{19}F. The solid lines are the least-squares fits of the yields from low-energy processes and photomeson yield.

REF.

F. Riess, W. J. O'Connell and P. Paul
Nucl. Phys. A175, 462 (1971)

ELEM. SYM.	A	Z
N	14	7

METHOD

REF. NO. 71 Ri 1

egf

REACTION	RESULT	EXCITATION ENERGY	SOURCE		DETECTOR		ANGLE
			TYPE	RANGE	TYPE	RANGE	
P,G	ABX	10-24		3-18	NAI-D		DST

6 11+ J-PI

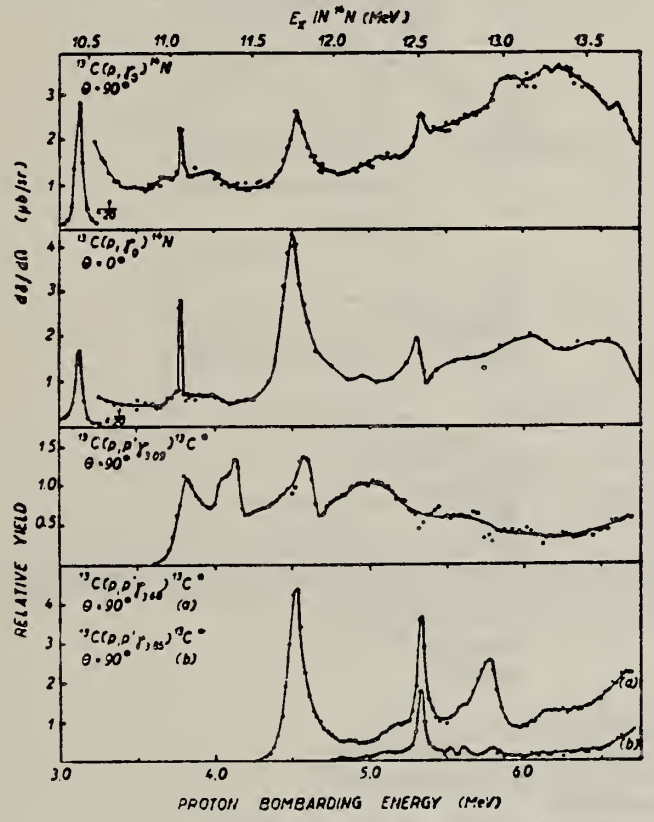

Fig. 4. Excitation function for the capture reaction and inelastic scattering of 3 to 7 MeV protons on ^{13}C, showing from top to bottom: the γ_0 capture yield at 90° and 0°; the yields of 3.09 MeV 3.68 MeV (a) and 3.85 MeV (b) radiation from inelastic scattering, all at 90°.

TABLE 4

Legendre polynomial coefficients obtained from the ^{13}C(p,γ)^{14}N angular distributions in the giant resonance region

E_p (MeV)	a_1 (γ_0)	a_2 (γ_0)	a_1 (γ_1)	a_2 (γ_1)
6.3	0.08±0.02	−0.39±0.02		
8.0	0.07±0.30	−0.45±0.54	0.14±0.24	0.10±0.40
10.5	0.28±0.20	−0.13±0.33	0.29±0.03	−0.10±0.04
12.5	0.15±0.08	−0.63±0.14	0.40±0.24	0.09±0.47
14.0	0.22±0.07	−0.46±0.14	−0.05±0.48	−0.34±0.95
16.6	0.21±0.09	−0.48±0.19		

(ove

D

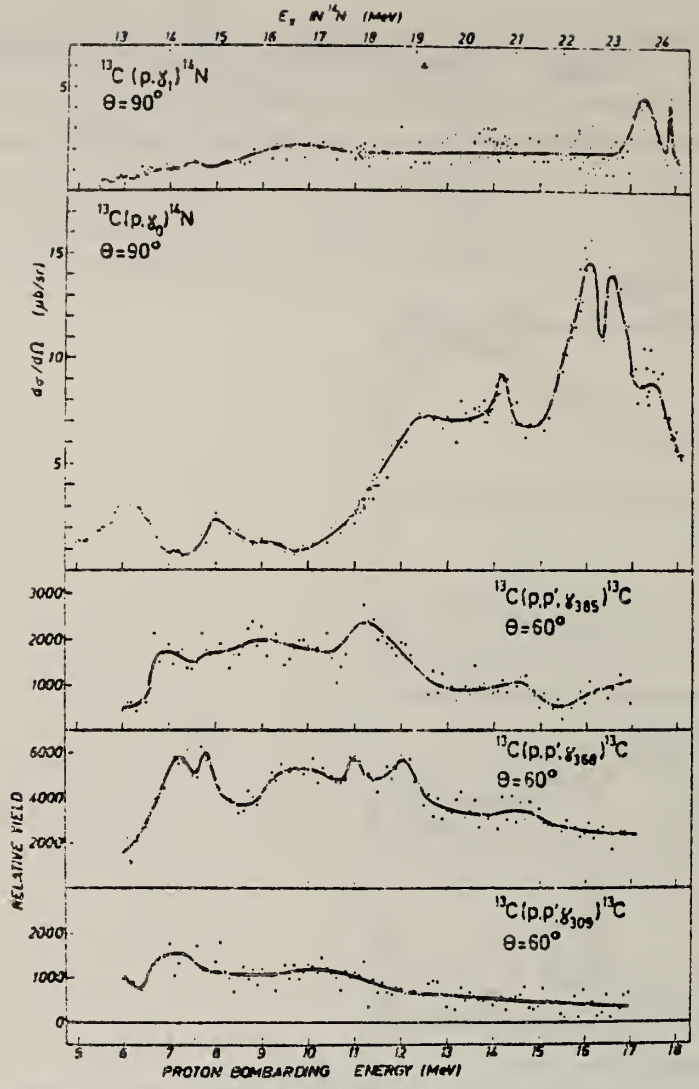

Fig. 9. Excitation function of the γ_0 and γ_1 capture radiation, and of γ-rays from inelastic scattering over the giant-resonance region of ^{14}N. The lines are to guide the eye.

DETECTOR		ANGLE
TYPE	RANGE	

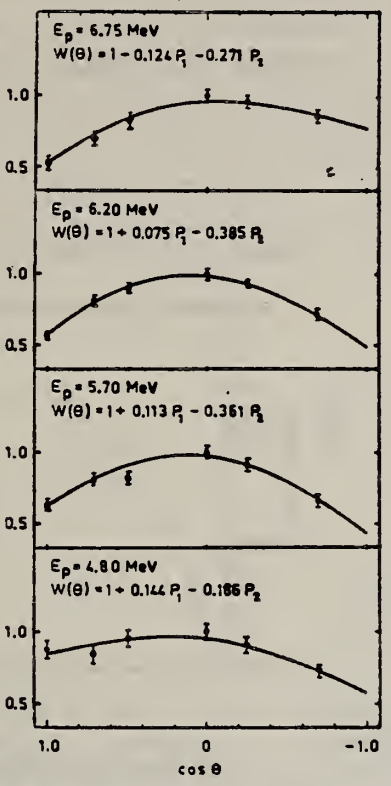

Fig. 8. Angular distributions for γ_0 rays from the $^{13}C(p,\gamma_0)^{14}N$ reaction at various bombarding energies. Best fits with Legendre polynomials are drawn through the data points.

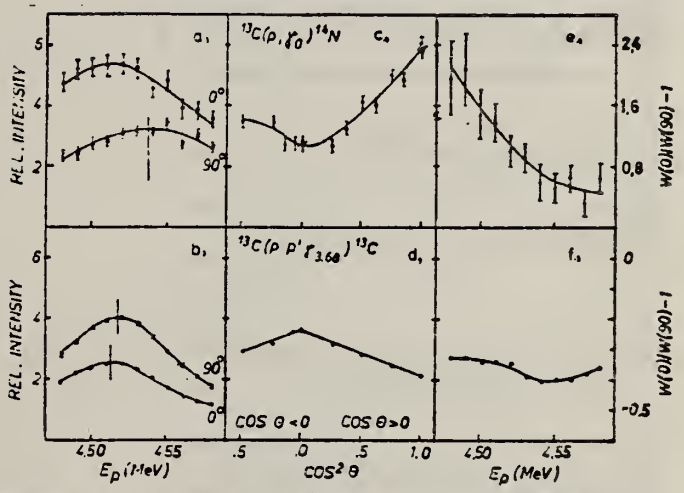

Fig. 7. Experimental data for the $E_p = 4.53$ MeV resonance. (a) and (b) give the 0° and 90° excitation functions for the $^{13}C(p,\gamma_0)^{14}N$ (a) and the $^{13}C(p, p', \gamma\ (3.68))^{13}C$ (b) reactions. (c) and (d) show the angular distribution of the capture γ-ray and the 3.68 MeV γ-ray at $E_p = 4.535$ MeV. The capture γ-ray distribution has been corrected for off-resonance contributions. The solid curves are fits with Legendre polynomials. (e) and (f) give: the anisotropy $A = W(0)/W(90) - 1$ as a function of energy for the capture γ-ray (e) and the 3.68 MeV γ-ray from ^{13}C (f).

REF.

Tatsuya Saito
Nippon Kagaku Zasshi 92, 164 (1971)

ELEM. SYM.	A	-
N	14	7

METHOD

REF. NO.	
71 Sa 1	egf

REACTION	RESULT	EXCITATION ENERGY	SOURCE		DETECTOR		ANGLE
			TYPE	RANGE	TYPE	RANGE	
G,N	ABY	10-68	C	10-68	ACT-I		4PI

Nippon Kagaku Zasshi, 92, 164~168(1971)

The Yields of Radioactivities Induced by (γ, n) Reactions with Bremsstrahlung up to 68 MeV

by Tatsuya SAITO

The (γ, n) yields of 12 target nuclides have been measured at 10, 13, 16, 30, 45 and 68 MeV bremsstrahlung by observing the induced activities.

The energy dependence of the yields has been investigated extensively in the same way as in the previous work at 20 MeV bremsstrahlung.

In the case of heavy nuclides, the yields rise greatly as a function of maximum bombarding energy up to 20 MeV, and rise gradually from 20 MeV up to 68 MeV. However, in the case of light nuclides, the yields rise greatly up to 30 MeV, because the neutron separation energies of light ones are larger than those of heavy ones, and the bremsstrahlung spectrum covers the giant resonance and so the yields rise gradually from 30 MeV up to 68 MeV.

The yields have approximately been estimated from the parameter of the giant resonance, that is the peak cross section and the half width, in order to compare with the experimental data. As a result, the experimental data of light nuclides and heavy ones are nearly in agreement with the estimated data of Nathans et al., Johns et al. and Montalbetti et al., but those of medium weight ones are relatively lower values.

Department of Chemistry, Faculty of Science, Tohoku University; Katahira-cho, Sendai-shi, Japan

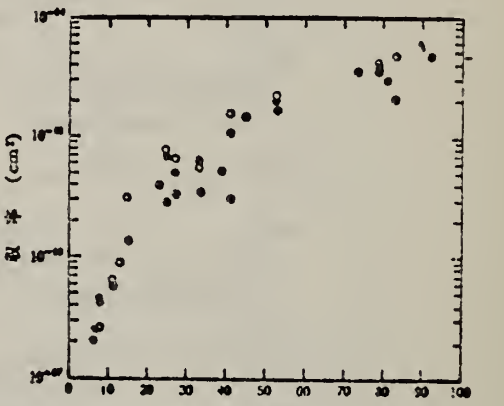

図 4 (γ, n)反応の収率の比較

REF.

R.W. Carr, J.E.E. Baglin, and E.J. Bentz,Jr.
Phys. Rev. C6, 2032 (1972)

EL.EM. SYM.	A	Z
N	14	7

METHOD

REF. NO. 72 Ca 4 hmg

REACTION	RESULT	EXCITATION ENERGY	SOURCE TYPE	SOURCE RANGE	DETECTOR TYPE	DETECTOR RANGE	ANGLE
G,P	ABX	17- 25	C	20- 25	SCD-D		DST
				(20.5-25)			

$$\sigma(\theta) = A_0 + A_1P_1(\cos\theta) + A_2P_2(\cos\theta) + A_3P_3(\cos\theta) + A_4P_4(\cos\theta).$$

586

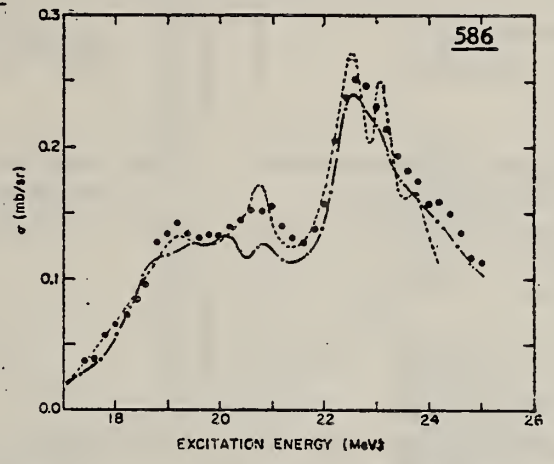

FIG. 7. $^{14}N(\gamma,p_0)$ differential cross section at 90°. Solid dots: present experiment. Dotted line: (p,γ_0) data (Ref. 6). Dashed line: (γ,n_0) data (Ref. 10).

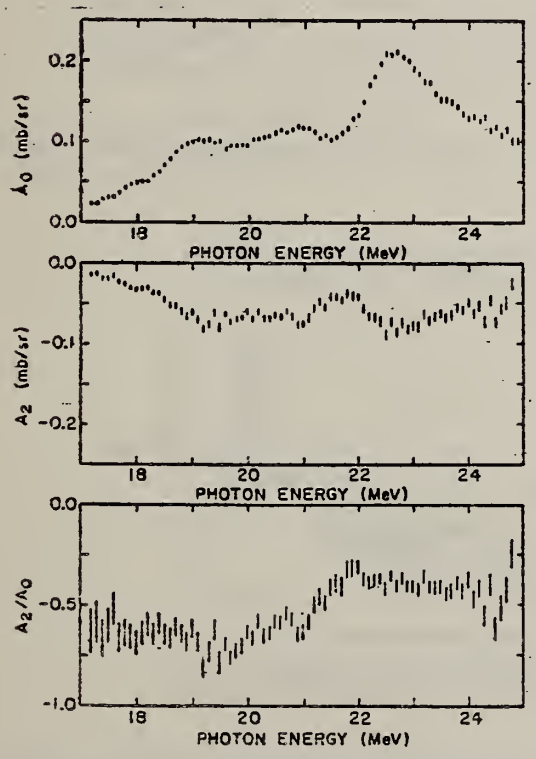

FIG. 4. $^{14}N(\gamma,p_0)$. Angular-distribution coefficients $A_0(=\sigma/4\pi)$, A_2, and the ratio A_2/A_0, plotted as functions of excitation energy in ^{14}N.

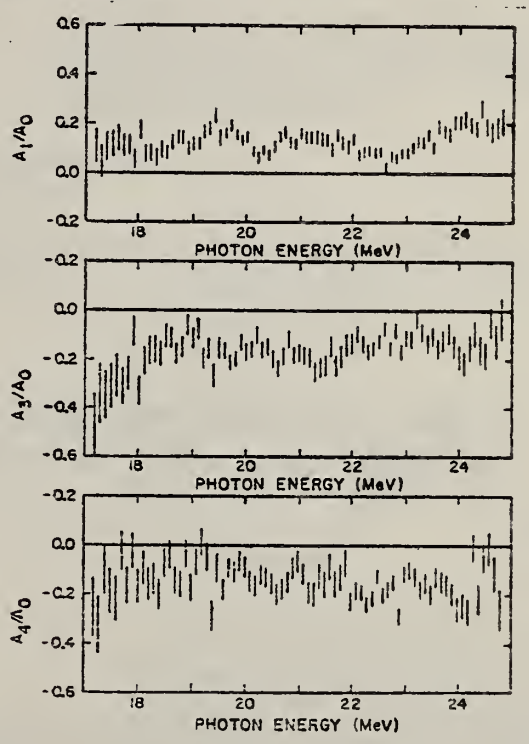

FIG. 6. $^{14}N(\gamma,p_0)$. Ratios of angular-distribution coefficients to A_0: A_1/A_0, A_3/A_0, and A_4/A_0, plotted as functions of excitation energy in ^{14}N.

(over)

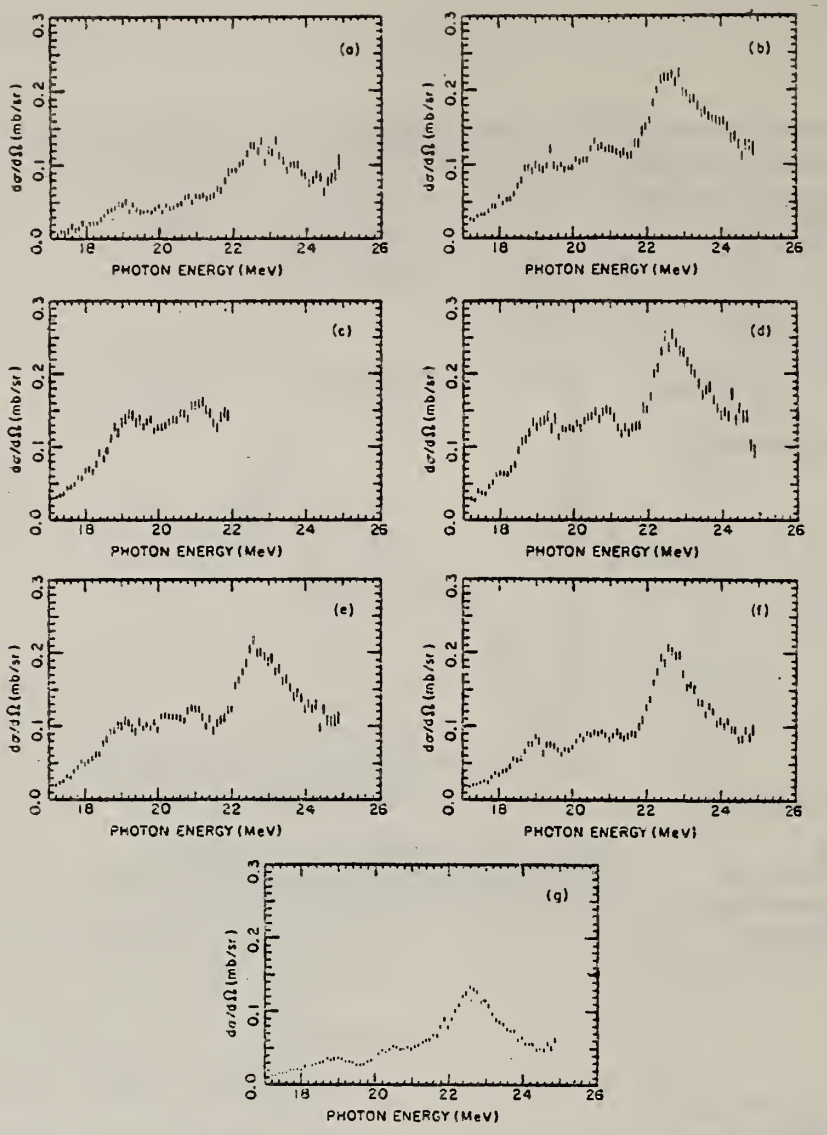

FIG. 3. $^{14}N(\gamma, p_0)$ differential cross section: (a) $\theta = 20°$; (b) $\theta = 45°$; (c) $\theta = 65°$; (d) $\theta = 90°$; (e) $\theta = 115°$; (f) $\theta = 135°$; (g) $\theta = 160°$.

[6]F. Reiss et al., Nucl. Phys. A175, 462 (1971).

[10]N. K. Sherman et al., Phys. Rev. Letters 25, 114 (1970).

REF.

R.W. Gellie, K.H. Lokan, N.K. Sherman, R.G. Johnson, J.I. Lodge
Can. J. Phys. 50, 1689 (1972)

ELEM. SYM.	A	Z
N	14	7

METHOD

REF. NO. 72 Ge 3 hmg

REACTION	RESULT	EXCITATION ENERGY	SOURCE		DETECTOR		ANGLE
			TYPE	RANGE	TYPE	RANGE	
G,N	ABX	10-30	C	15-30	TOF-D		90

Integrated cross section (29 MeV) for all neutron producing interactions is 88±5 MeV mb.

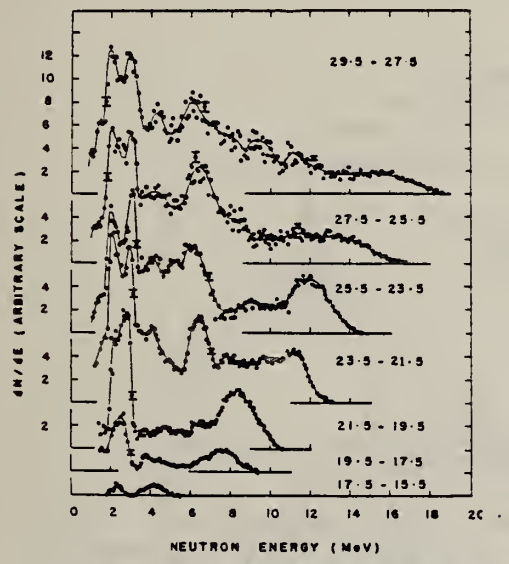

FIG. 6. Photoneutron difference distributions, derived from the data of Fig. 2.

TABLE 1. Integrated partial cross sections in the decay of ^{14}N

Level in $A = 13$ nucleus	Dominant configuration[a]	Integrated cross section to 29 MeV (MeV mb) (γ,n)	(γ,p)
Ground state	$(p_{3/2})^8(p_{1/2})^1$	20[b]	20[c,e,f]
3.51, 3.68	$(p_{3/2})^7(p_{1/2})^2$	6[b]	7[d], 6[e]
7.39, 7.55	$(p_{3/2})^7(p_{1/2})^2$	—	17[b]
8.92, 8.86	$(p_{3/2})^7(p_{1/2})^2$	—	Visible, but not separate from othe reactions
9.48, 9.52			
11.88, 11.80	$(p_{3/2})^7(p_{1/2})^2$	—	5[b,g]

[a] Ball and Cerny (1969).
[b] This experiment.
[c] Kosiek *et al.* (1964).
[d] Thompson *et al.* (1970).
[e] Benz (1971).
[f] By detailed balance from $^{13}C(p,\gamma_0)^{14}N$ (Riess *et al.* 1971).
[g] Includes only that component which yields neutrons to th ground state of ^{12}C.

"Total integrated cross sections were obtained from the 90° differential cross sections by assuming an isotropic angular distribution."

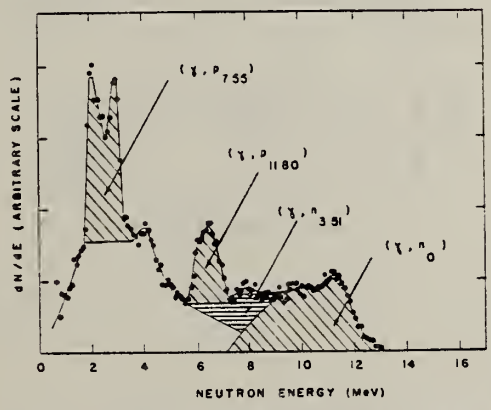

FIG. 7. Breakdown of the (23.5–21.5 MeV) difference spectrum into its major components (see text).

1036

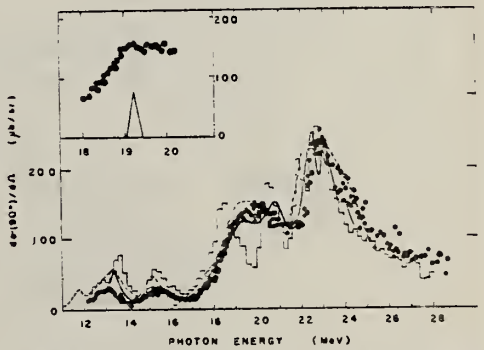

FIG. 4. Cross sections for ground-state photonucleon emission. (●) (γ,n_0): present experiment. (--) (γ,n): King *et al.* (1960). Histogram (γ,p_0): Kosiek *et al.* (1964). (—) (γ,p_0): by detailed balance from the inverse proton capture reaction (Riess *et al.* 1971). The inset shows the (γ,n_0) cross section in the region around 19 MeV, together with the resolution function, and indicates that there is no strong structure evident in this region, at least in the neutron channel.

REF. J.E.E. Baglin and E.J. Bentz, Jr.
PICNS-73, Vol.I, p.161 Asilomar

ELEM. SYM.	A	Z
N	14	7

METHOD

REF. NO. 73 Ba 8 hmg

REACTION	RESULT	EXCITATION ENERGY	SOURCE		DETECTOR		ANGLE
			TYPE	RANGE	TYPE	RANGE	
G,P	ABX	16- 25	C	7- 25	SCD-D		DST

(G,P0),(G,P2)
849

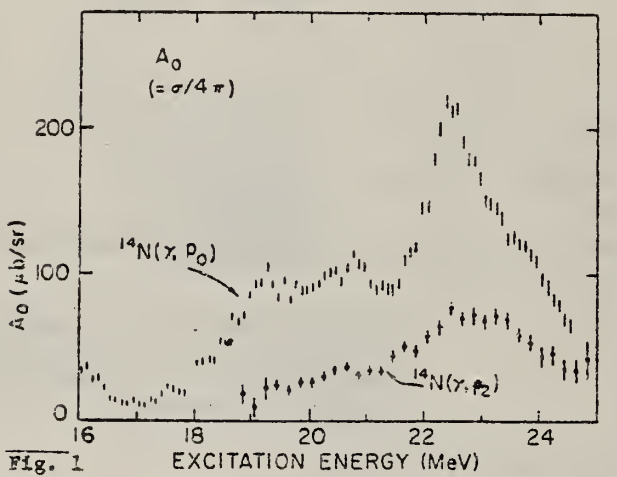

Fig. 1

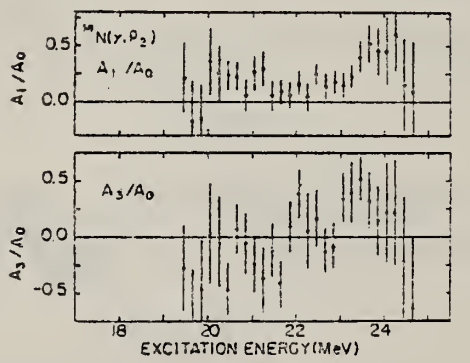

Fig. 3

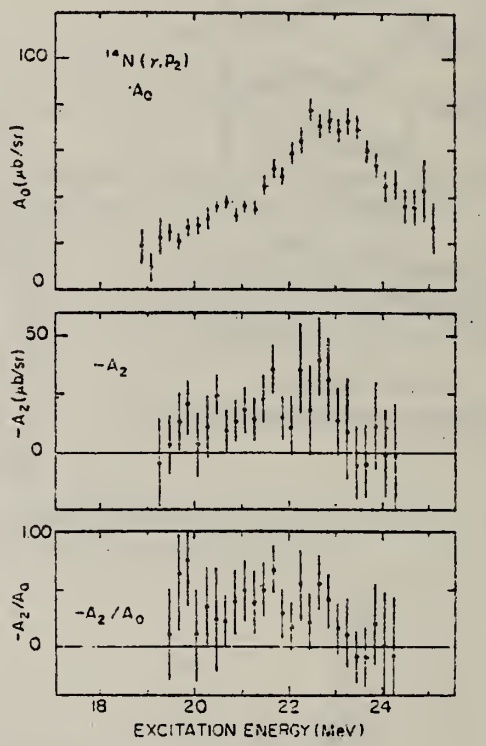

Fig. 2

REF. E.W. Maute, S.L. Blatt, and D.P. D'Amato
PICNS-73, Vol.II, p.933 (1973) Asilomar

ELEM. SYM.	A	Z
N	14	7

METHOD

REF. NO. 73 Ma 5 egf

REACTION	RESULT	EXCITATION ENERGY	SOURCE		DETECTOR		ANGLE
			TYPE	RANGE	TYPE	RANGE	
HE,G	ABX	22- 26	D	1- 6	NAI-D		90

HE=HE-3

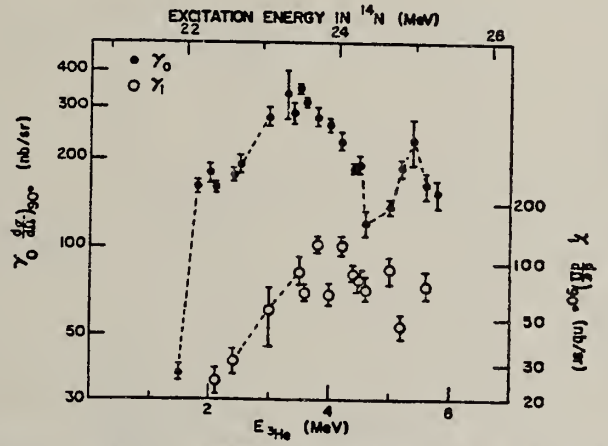

Fig. 2. Excitation functions for the ^{3}He capture gamma radiations to the ground and first excited states at ^{14}N.

REF. J. E. E. Baglin, E.J. Bentz, and R. W. Carr
Phys. Rev. C10, 24 (1974)

EL EM. SYM.	A	Z
N	14	7

METHOD

REF. NO. 74 Ba 4 hmg

REACTION	RESULT	EXCITATION ENERGY	SOURCE TYPE	SOURCE RANGE	DETECTOR TYPE	DETECTOR RANGE	ANGLE
G,P	ABX	16- 25	C	20- 26	SCD-D		DST

Ground state cross section agrees very well with $^{13}C(p,\gamma_0)$ results of O'Connell (71Ri1) -Stanford data.

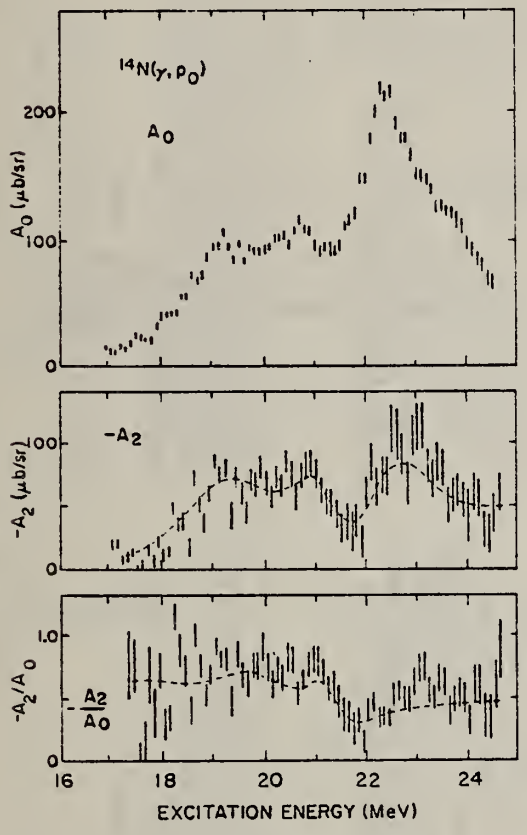

FIG. 4. $^{14}N(\gamma,p_0)$. Angular-distribution coefficients $A_0(=\sigma/4\pi)$, A_2, and the ratio A_2/A_0, plotted as functions of excitation energy in ^{14}N. Dashed lines indicate values obtained previously (Ref. 5).

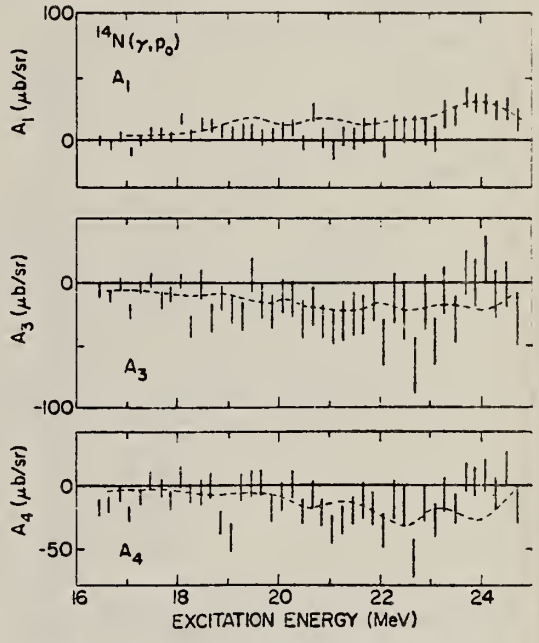

FIG. 5. $^{14}N(\gamma,p_0)$. Angular-distribution coefficients A_1, A_3, and A_4. Dashed lines indicate values obtained previously (Ref. 5).

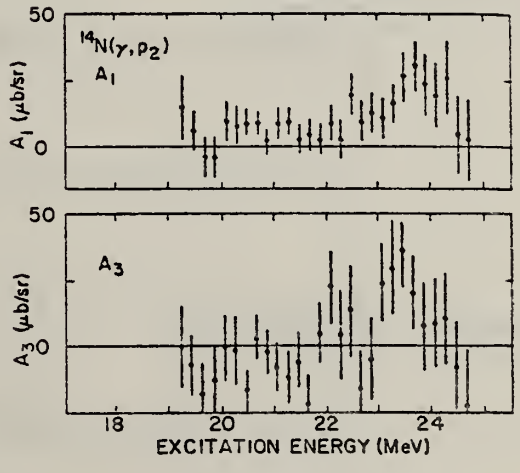

FIG. 7. $^{14}N(\gamma,p_2)$. Angular-distribution coefficients A_1 and A_3. A_4 values obtained were not statistically different from zero.

(over)

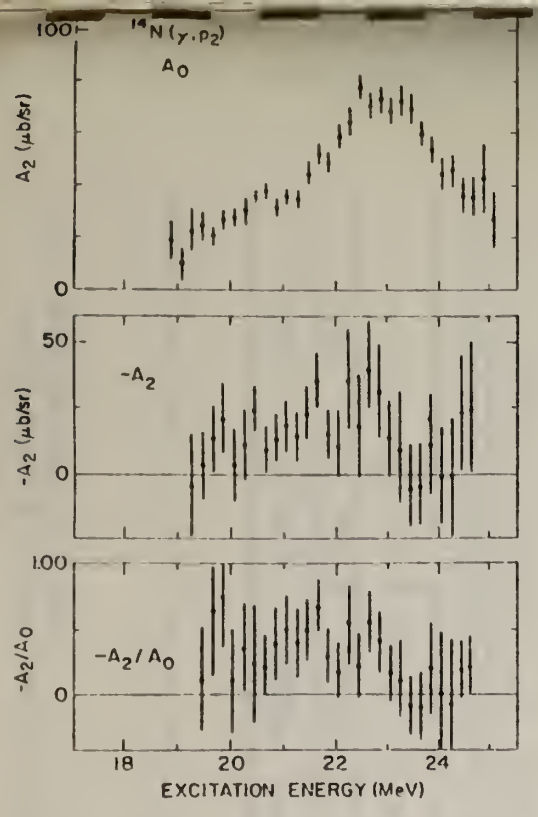

FIG. 6. $^{14}N(\gamma,p_2)$. Angular-distribution coefficients $A_0(=\sigma/4\pi)$, A_2, and the ratio A_2/A_0, plotted as functions of excitation energy in ^{14}N.

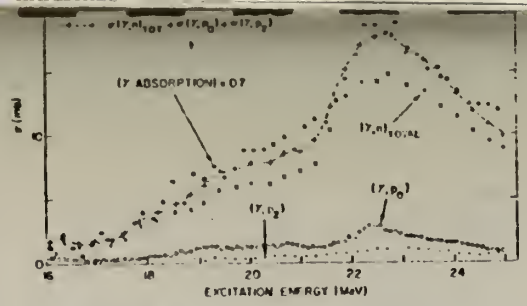

FIG. 9. Total photon absorption cross section in ^{14}N. Displayed are the partial cross sections $\sigma(\gamma,p_0)$ and $\sigma(\gamma,p_2)$ (present work) and $[\sigma(\gamma,n)+\sigma(\gamma,np)+\sigma(\gamma,pn)]$ (Ref. 15, energy scale lowered by 0.5 MeV). Their sum is compared with observed absorption data (Ref. 18, multiplied by 0.70).

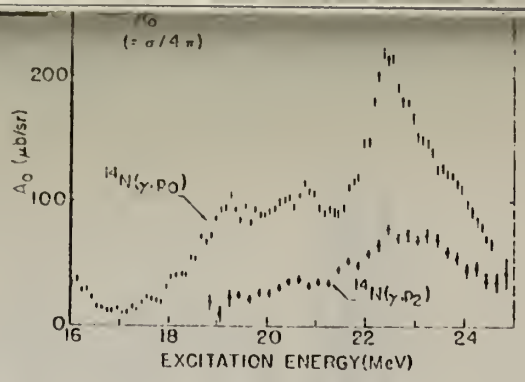

FIG. 10. Comparison of the energy dependence of cross sections for $^{14}N(\gamma,p_0)$ and $^{14}N(\gamma,p_2)$.

TABLE I. Angular-distribution coefficients describing the $E1$ components of the $^{14}N(\gamma,p_0)$ reaction. The notation used is that of Eq. (2) of Ref. 17, from which this table is derived.

$(ljs)_a$	$(ljs)_b$	C_0	C_2
000	000	1.00	···
000	220	···	3.16
011	011	3.00	···
011	211	···	−2.12
011	221	···	−4.74
211	211	3.00	0.75
211	221	···	−3.35
220	220	5.00	−2.50
221	221	5.00	−1.25

TABLE II. Angular-distribution coefficients describing the $E1$ components of the $^{14}N(\gamma,p_2)$ reaction. The notation used is that of Eq. (2) of Ref. 17, from which this table is derived.

$(ljs)_a$	$(ljs)_b$	C_0	C_2
202	202	1.00	···
202	022	···	1.41
202	222	···	−1.69
202	422	···	2.27
011	011	3.00	···
011	211	···	−2.12
011	221	···	−4.74
211	211	3.00	0.75
211	221	···	−2.35
212	212	3.00	−0.75
212	022	···	3.67
212	222	···	−2.20
212	422	···	−3.93
221	221	5.00	−1.25
022	022	5.00	···
022	222	···	4.18
222	222	5.00	0.54
222	422	···	1.92
422	422	5.00	−1.79

REF.

N. Ensslin, W. Bertozzi, S. Kowalski, C.P. Sargent, W. Turchinetz, C.F. Williamson, S.P. Fivozinsky, J.W. Lightbody,Jr., and S. Penner Phys. Rev. C9, 1705 (1974)

N	14	7

METHOD

REF. NO. 74 En 1 hmg

REACTION	RESULT	EXCITATION ENERGY	SOURCE TYPE	SOURCE RANGE	DETECTOR TYPE	DETECTOR RANGE	ANGLE
E,E/	FMF	2- 6	C	60-120	MAG-D		DST

6 LEVELS

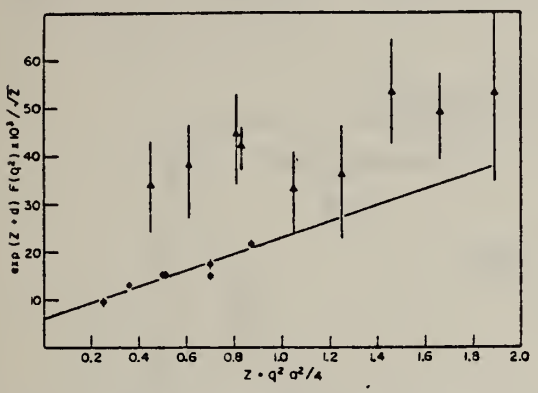

FIG. 5. Transverse magnetic form factors for the 2.313-MeV (0⁺) level. The data of Ref. 9 are denoted by ▲, the present data by ●. The solid line is the fit to Eq. (16b).

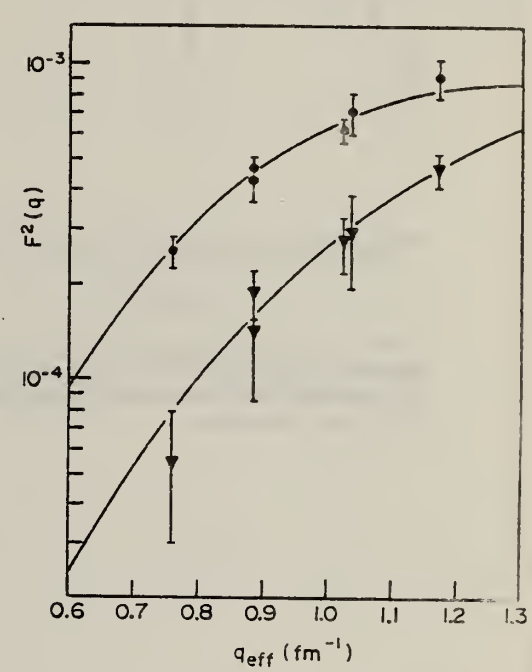

FIG. 8. Form factors squared of the 5.69-MeV (1⁻) (triangles) and 5.83-MeV (3⁻) (circles) states in ^{14}N. The fitted shape is that of Eq. (24) with $a = 1.37$ and 1.93 fm, respectively.

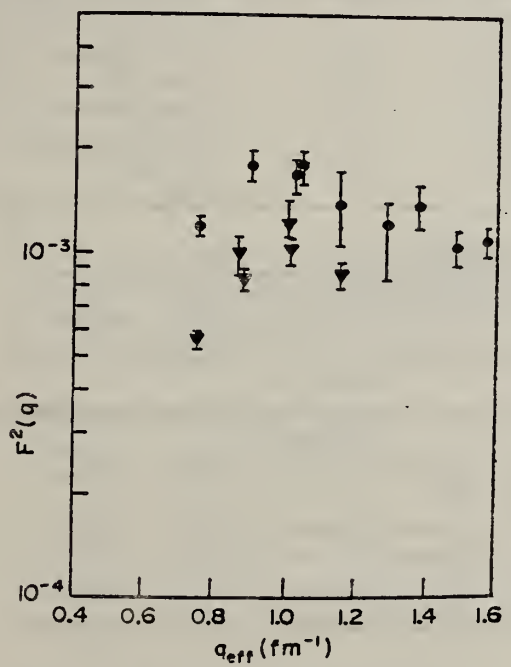

FIG. 6. A comparison of the present data (▼) and the data of Ref. 9 (●) for the 3.945-MeV (1⁺) state in ^{14}N.

[9] G.R. Bishop, M. Bernheim, P. Kossanyi-Demay, Nucl. Phys. 54, 353 (1964).

(over)

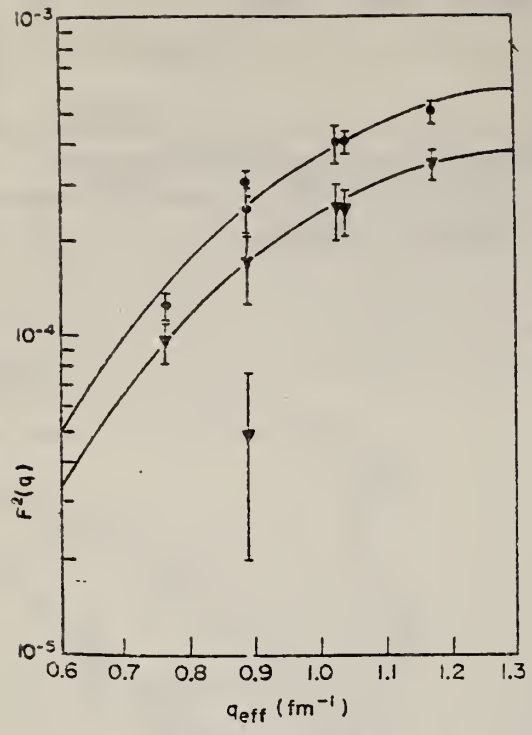

FIG. 7. Form factors squared of the 4.913-MeV (0^-) (triangles) and 5.106-MeV (2^-) (circles) states in ^{14}N. In both cases the fitted shape is that of Eq. (24) with $a = 1.82$ and 1.81 fm, respectively.

TABLE II. Measured reduced transition probabilities.

Transition from ground state	Multipolarity L	$B(L,\omega)\uparrow$ (e^2 fm^{2L})	B/B_{sp}
2.313(0^+)^{14}N	$M1$	$(4.3 \pm 1.3)\times 10^{-30}$	0.065 ± 0.020
3.945(1^+)^{14}N	$C2$	3.40 ± 0.29	1.70 ± 0.14
4.913(0^-)^{14}N	$C1$	$(1.35 \pm 0.65)\times 10^{-8}$	$(1.1 \pm 0.5)\times 10^{-7}$
5.106(2^-)^{14}N	$C3$	80 ± 19	4.1 ± 1.0
5.69(1^-)^{14}N	$C1$	$(1.81 \pm 1.01)\times 10^{-8}$	$(3.8 \pm 2.1)\times 10^{-8}$
5.83(3^-)^{14}N	$C3$	166 ± 35	6.1 ± 1.3

TABLE I. Elastic and inelastic form factors for ^{14}N.

Energy (MeV)	Angle (deg)	q [a] (fm^{-1})	$F^2(q)$ elastic (calculated)	$F^2(q)$ inelastic (measured)$\times 10^3$ 2.313 MeV	3.945 MeV	4.913 MeV	5.106 MeV	5.69 MeV	5.83 MeV
60.65	163.7	0.606	0.468	0.014 ± 0.002					
73.06	163.4	0.729	0.317	0.029 ± 0.003					
89.82	110.8	0.746	0.298		0.56 ± 0.02	0.10 ± 0.02	0.12 ± 0.01	0.06 ± 0.02	0.26 ± 0.03
86.31	163.4	0.860	0.191	0.037 ± 0.004					
90.08	145.9	0.868	0.185	0.038 ± 0.004	1.01 ± 0.13	0.17 ± 0.04	0.25 ± 0.05	0.14 ± 0.06	0.44 ± 0.07
104.95	110.8	0.871	0.184		0.85 ± 0.06	0.05 ± 0.3	0.30 ± 0.03	0.19 ± 0.04	0.47 ± 0.04
100.90	163.7	1.005	0.0970	0.044 ± 0.006					
104.62	145.7	1.006	0.0964	0.031 ± 0.004	$1.22^{+0.24}_{-0.12}$	0.25 ± 0.05	0.40 ± 0.05	0.29 ± 0.10	0.71 ± 0.11
122.00	110.5	1.010	0.0959		1.03 ± 0.10	0.25 ± 0.04	0.40 ± 0.04	0.28 ± 0.06	0.63 ± 0.06
117.62	145.7	1.130	0.0479	0.035 ± 0.004					
120.01	146.0	1.154	0.0412		0.37 ± 0.08	0.35 ± 0.04	0.50 ± 0.04	0.47 ± 0.06	0.92 ± 0.13

[a] Calculated for elastic scattering.

REF.	ELEM. SYM.	A	Z
P. Paul, H. S. Kuan, and E. K. Warburton Nucl. Phys. A254, 1 (1975)	N	14	7

METHOD	REF. NO.	
	75 Pa 1	egf

REACTION	RESULT	EXCITATION ENERGY	SOURCE		DETECTOR		ANGLE
			TYPE	RANGE	TYPE	RANGE	
P,G	ABX	22- 34	D	16- 28	NAI-D		90

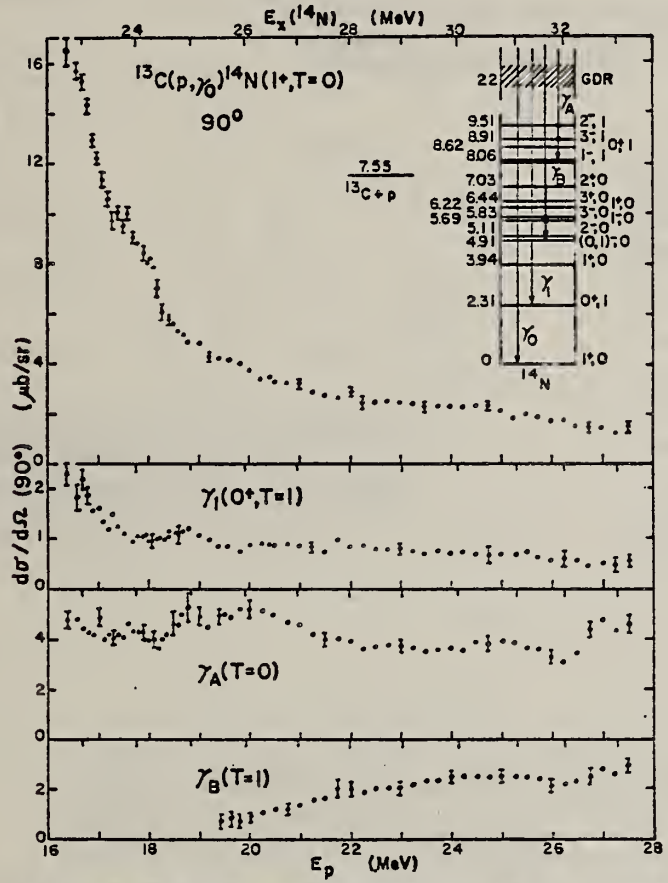

Fig. 2. Excitation functions of γ-decay yield to various final states in ^{14}N indicated in the level scheme insert.

REF. V. K. Rasmussen, F. R. Metzger
Phys. Rev. C12, 706 (1975)

ELEM. SYM.	A	Z
N	14	7

METHOD

REF. NO. 75 Ra 1 hmg

REACTION	RESULT	EXCITATION ENERGY	SOURCE		DETECTOR		ANGLE
			TYPE	RANGE	TYPE	RANGE	
G,G	LFT	2	C	UKN	SCD-D		DST
		(2.31)					

LEVEL AT 2.31 MEV

By observation of the resonant scattering of bremsstrahlung, the width of the 2.31-MeV level of ^{14}N has been measured as 6.2 ± 0.6 meV. This is somewhat smaller than previous values and in disagreement with inelastic electron scattering results and the prediction of the conserved vector current theory from the shape of the $^{14}O \rightarrow {}^{14}N$ β^+ spectrum.

REF.	ELEM. SYM.	A	Z
W.L. Sievers, J.A. Pintar, R.L. Boudrie, F.W. Prosser, Jr., and Paul Goldhammer Phys. Rev. C13, 2546 (1976)	N	14	7

METHOD	REF. NO.	
	76 Si 6	hmg

REACTION	RESULT	EXCITATION ENERGY	SOURCE		DETECTOR		ANGLE
			TYPE	RANGE	TYPE	RANGE	
P,G	LFT	9	D	1	SCD-D		DST
				(1.76)			

9=9.17

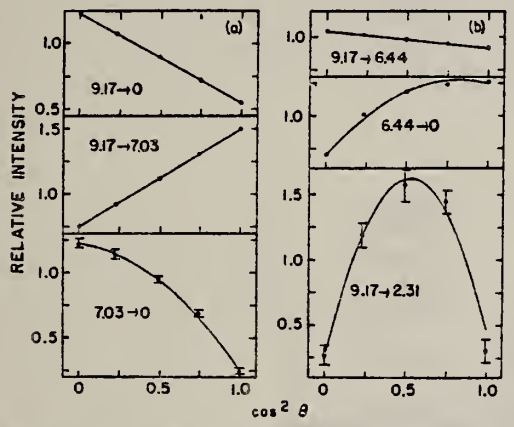

FIG. 3. Experimental angular distributions for the six transitions used in the least squares analysis. The curves are the best fits to each distribution from the simultaneous nonlinear least squares fit, as described in the text. Where error bars are not shown, the error is less than or equal to the size of the point.

TABLE III. Measured values of $\langle||E2||\rangle/\langle||M1||\rangle$ for the 7.03-MeV→0-MeV transition in ^{14}N. The symbol $\langle||XL||\rangle$ represents the reduced matrix element for XL multipole radiation. The mean is the weighted mean of the five values and its error is the weighted internal error. The external error is 0.050.

Reference	Value	Method
Gorodetsky *et al.*, Ref. 4	0.6 ±0.2	^{12}C(^{3}He, $p\gamma$)
Gallmann *et al.*, Ref. 5	0.7 ±0.1	^{12}C(^{2}He, $p\gamma$)
Prosser *et al.*, Ref. 6	0.6 ±0.1	^{13}C(p,γ)
Swann, Ref. 7	0.6 ±0.15	^{14}N(γ,γ)
Present work	0.74 ±0.09	^{13}C(p,γ)
Mean	0.669 ± 0.031	

TABLE I. Mixing ratios and partial γ-ray decay widths for transitions in ^{14}N. The partial widths for each transition were calculated from the branching ratios determined in the present work for the 9.17- and 6.44-MeV states and from Ref. 3 for the 7.03-MeV state. The partial widths for each multipole are given in Weisskopf units.

Transition	Mixing ratio	Multipoles	Γ_γ [a] (eV)	$\Gamma_\gamma(L)$ (W.u.) [b]	$\Gamma_\gamma(L+1)$ (W.u.) [b]
9.17→0	−0.003 ± 0.003	(*E*2/*M*1)	7.7 ±0.9	0.47 ±0.06	<0.003
9.17→2.31	0	(*E*2)	0.077 ± 0.011	3.1 ±0.4	
9.17→6.44	0.031 ± 0.006	(*E*2/*M*1)	0.80 ±0.12	1.9 ±0.3	3.1 ± 1.3
9.17→7.03	−0.037 ± 0.015	(*E*2/*M*1)	0.29 ±0.04	1.4 ±0.2	$5.4^{+6.8}_{-3.8}$
7.03→0	0.74 ±0.09	(*E*2/*M*1)	0.124 ± 0.012	0.0109 ± 0.0014	1.6 ± 0.3
6.44→0	−0.004 ± 0.010	(*M*3/*E*2)	(7.4 ±0.7) × 10^{-4}	0.041 ±0.004	<1.4

[a] Reference 3, corrected for the branching ratio of the 7.03-MeV state.
[b] Reference 9.

(over)

TABLE II. Branching ratios for the decays of the 9.17-, 7.03-, and 6.44-MeV states in ^{14}N.

E_i (MeV)	$J_i^\pi; T_i$ [a]	E_f (MeV)	$J_f^\pi; T_f$	Branching ratio Present (%)	Branching ratio Previous [a] (%)
9.17	$2^+;1$	0.0	$1^+;0$	85.1 ± 1.0	79 ± 4
		2.31	$0^+;1$	0.85 ± 0.08	1.1 ± 0.4
		3.95	$1^+;0$	<0.2	
		4.91	$(0,1)^-;0$	<0.2	
		5.11	$2^-;0$	<0.2	<1
		5.69	$1^-;0$	0.49 ± 0.10	<6
		5.83	$3^-;0$	0.61 ± 0.08	3 ± 2
		6.20	$1^+;0$	<0.2	
		6.44	$3^+;0$	8.8 ± 0.8	8 ± 2 6.3 ± 0.5
		7.03	$2^+;0$	3.2 ± 0.3	3 ± 1 3.5 ± 0.5
		7.97	$2^-;0$	<0.03	
		8.06	$1^-;1$	<0.03	
		8.49	$4^-;0$	<0.03	
		8.62	$0^+;1$	<0.03	
7.03	$2^+;0$	0.0	$1^+;0$	96 ± 4	98.6 ± 0.3
		2.31	$0^+;1$	<3	0.5 ± 0.1
		3.95	$1^+;0$	<3 [b]	0.9 ± 0.25
6.44	$3^+;0$	0.0	$1^+;0$	69.6 ± 1.5	73.1 ± 1.5
		3.95	$1^+;0$	19.6 ± 1.0	18.9 ± 0.9
		4.91	$(0,1)^-;0$	<0.4	
		5.11	$2^-;0$	6.4 ± 0.6	6.8 ± 0.6
		5.69	$1^-;0$	<0.3	
		5.83	$3^-;0$	3.7 ± 0.6	<3, <2, <1

[a] Reference 3.
[b] Present, but observable only at some angles.

[3] F. Ajzenberg-Selove, Nucl. Phys. A152, 1 (1970).

[4] S. Goredtsky et al., Phys. Rev. 149, 801 (1966).

[5] A. Gallmann et al., Phys. Rev. 164, 1257 (1967).

[6] F.W. Prosser et al., Phys. Rev. 129, 1716 (1963).

[7] C.P. Swann, Phys. Rev. 148, 1119 (1966).

[9] D.H. Wilkinson, in Nuclear Spectroscopy, ed. by F. Ajzenberg-Selove (Academic, New York, 1960), Part B, Chap. V.

REF. M. Turk
Fizika 8, 173 (1976)

ELEM. SYM.	A	Z
N	14	7

Remarks: Bremsstrahlung filtered by 40cm of aluminum. Cross section obtained by normalizing to Toms (γ,3α)

REF. NO. 76 Tu 3 egf

REACTION	RESULT	EXCITATION ENERGY	SOURCE		DETECTOR		ANGLE
			TYPE	RANGE	TYPE	RANGE	
G,2A	ABX	16- 42	C	42	EMU-D		4PI
G,He3A	ABX	29- 42	C	42	EMU-D		4PI

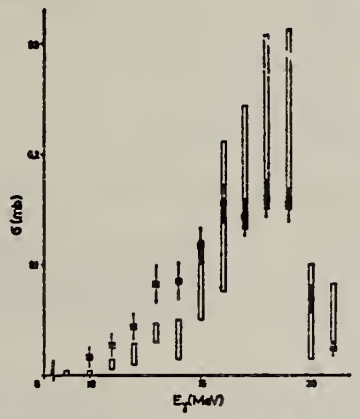

Fig. 3. Cross section for the reaction ^{12}C (γ, 3α) as function of gamma ray energy after normalizing the data (full points) to Toms results. Squares represent the spread of earlier measurements by various authors referenced in Ref.[3].

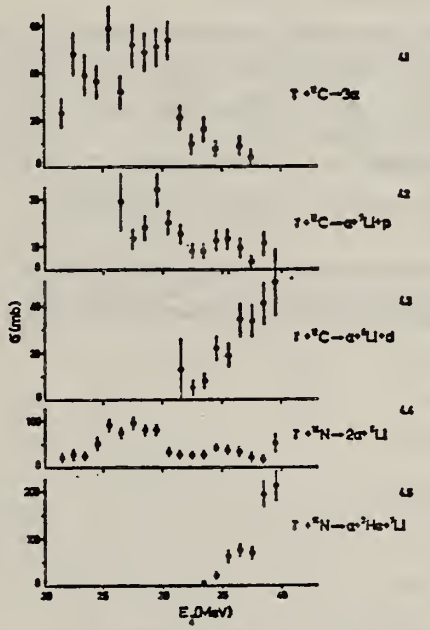

Fig. 4. Measured cross sections for reactions (1-5) as functions of incident gamma ray energy.

[3] M.E. Toms, Nucl. Phys. 50, 561 (1964)

REF. S. V. Dementii, V. I. Ogurtsov, N. G. Afanas'ev
Yad. Fiz. 28, 865 (1978)
Sov. J. Nucl. Phys. 28, 443 (1978)

ELEM. SYM.	A	Z
N	14	7

METHOD

REF. NO. 78De11 hg

REACTION	RESULT	EXCITATION ENERGY	SOURCE		DETECTOR		ANGLE
			TYPE	RANGE	TYPE	RANGE	
E,E/	ABX	30-150	D	1*2	MAG-D		DST
				(799-1178)			

Measurements were made of quasielastic scattering of electrons in the (e, e') reaction by the nuclei ^{9}Be, ^{12}C, ^{14}N, ^{16}O, and ^{27}Al. An experimental estimate is obtained of the effective mass of an intranuclear nucleon. At excitation energies up to 80 MeV, a ratio $M^*/M = 0.6$ is obtained, corresponding to a linear potential $V(E) = V_0 + 0.4E$ and in good agreement with the data on proton scattering by nuclei [C. M. and F. G. Perey, Atomic Data and Nuclear Tables 13, 294 (1974)]. At excitation energies above 120 MeV the nucleon effective mass turned out to be close to that of the free nucleon, $M^*/M = 0.9$.

*GEV, QUASIELASTIC

PACS numbers: 25.30.Cg, 27.20. + n, 27.30. + t

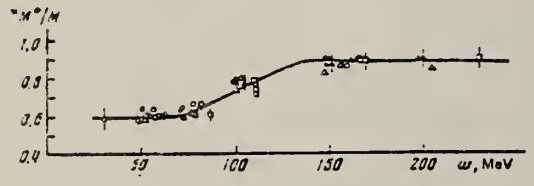

FIG. 4. Reduction coefficient M^*/M as a function of energy transfer: ●—^{9}Be, ▲—^{12}C, ○—^{14}N, △—^{16}O, □—^{27}Al. The curve has been drawn through the experimental points by hand.

REF. V. Di Napoli, J. B. Martins, G. Rosa, F. Salvetti, O. A. P. Tavares, M. L. Terranova and H. G. De Carvalho
J. Inorg. Nucl. Chem. 40, 1619 (1978)

ELEM. SYM.	A	Z
N	14	7

METHOD

REF. NO. 78 Di 10 | hg

REACTION	RESULT	EXCITATION ENERGY	SOURCE		DETECTOR		ANGLE
			TYPE	RANGE	TYPE	RANGE	
G,C11	ABY	22 (22.7)-999	C	300-999	ACT-I		4PI

Abstract—Mean cross sections for the photoproduction of ^{7}Be and ^{11}C from ^{19}F, ^{27}Al, ^{28}Si and ^{32}S targets, ^{7}Be from ^{10,11}B, and ^{11}C from ^{14}N and ^{16}O targets have been measured using bremsstrahlung beams in the energy range 0.3–1.0 GeV. The results have been compared with previous measurements and an excellent agreement has been found. In most cases, the values obtained turned out to be much larger than those expected from a simple spallation mechanism. A fragmentation and/or a fission-like process has been suggested in explaining the mechanism of such reactions.

999=1 GEV

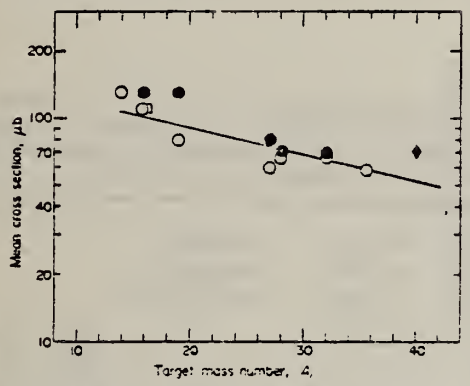

Fig. 1. Mean cross sections per photon, $\bar{\sigma}_A$, of ^{11}C photoproduction vs the target mass number A_t. Experimental data are taken from: ●, Ref. [9]; □, Ref. [13]; ◆, Ref. [2]; ○, present work. The straight line is a least squares fit of the experimental points.

Table 1. Cross sections per equivalent quantum of ^{11}C photoproduction

E_0 (GeV)	Cross Section, σ_Q (μb) ^{14}N	^{16}O	^{19}F	^{27}Al	^{28}Si	^{32}S	^{35,37}Cl
0.30	520±30	200±20	110±20	28±10	35±10	45±10	30±10
0.32	520±30	210±20	120±20	30±10	42±10	50±10	30±10
0.35	530±30	230±20	125±20	38±10	45±10	60±10	40±10
0.40	530±30	230±20	130±20	42±10	52±10	65±10	50±10
0.48	550±30	255±20	150±20	60±10	70±10	80±10	60±10
0.55	570±30	260±20	160±20	60±10	78±10	85±10	60±10
0.65	600±30	290±20	180±20	70±10	85±10	98±10	75±10
0.75	620±30	300±20	180±20	79±10	95±10	110±10	85±10
0.90	650±30	320±20	190±20	90±10	110±10	120±10	95±10
1.00	680±30	330±20	210±20	100±10	115±10	125±10	100±10

Table 3. Comparison between experimentally determined and calculated cross sections of ^{7}Be and ^{11}C photoproduction and indication of the dominant reaction channels

Target Nucleus	Product Nucleus	Nominal Nucleon Loss, ΔA	$\Delta A/A_t$ (x10^3)	$\bar{\sigma}_{exp}$ (*) (μb)	$\bar{\sigma}_{CDMD}$ (**) (μb)	$\frac{\bar{\sigma}_{exp}}{\bar{\sigma}_{CDMD}}$	Apparent Threshold (Exp.) E_{th} (MeV)	Possible Mechanism of Production
^{10,11}B	^{7}Be	(3)	(30).36	67	28	2	≤ 50	Spallation
^{12}C	^{7}Be	5	42	110	20	5	≤ 50	Spallation
^{14}N	^{7}Be	7	50	108	12	9	≤ 50	Fission Spallation
^{14}N	^{11}C	3	21	130	60	2	≤ 50	Spallation
^{16}O	^{7}Be	9	56	107	8	13	50<E_{th}<200	Fission Fragmentation
^{16}O	^{11}C	5	31	117	33	3	≤ 50	Spallation
^{19}F	^{7}Be	12	63	106	5	21	50<E_{th}<200	Fission Fragmentation
^{19}F	^{11}C	8	42	105	16	7	50<E_{th}<200	Fission Fragmentation Spallation
^{27}Al	^{7}Be	20	74	142	2	71	> 200	Fragmentation
^{27}Al	^{11}C	16	59	70	5	14	50<E_{th}<200	Fission Fragmentation
^{28}Si	^{7}Be	21	75	56	2	28	> 200	Fragmentation
^{28}Si	^{11}C	17	61	68	4	17	50<E_{th}<200	Fission Fragmentation
^{32}S	^{7}Be	25	78	114	2	57	> 200	Fragmentation
^{32}S	^{11}C	21	56	68	3	23	50<E_{th}<200	Fission Fragmentation
^{35,37}Cl	^{11}C	24,(26)	69,(70)	59	3	20	50<E_{th}<200	Fission Fragmentation
^{40}Ca	^{7}Be	33	83	70	1	70	> 200	Fragmentation
^{40}Ca	^{11}C	29	73	70	2	35	> 200	Fragmentation

(*) Mean values of the different measurements (see Figs. 1 and 2).

(**) Calculated values according to Ref. [8].

REF. J. Keinonen, A. Anttila, and R. Hentela
Phys. Rev. C 17, 414 (1978)

ELEM. SYM.	A	Z
N	14	7

METHOD

REF. NO. 78 Ke 1 hmg

REACTION	RESULT	EXCITATION ENERGY	SOURCE TYPE	SOURCE RANGE	DETECTOR TYPE	DETECTOR RANGE	ANGLE
P,G	LFT	9	D	1	SCD-D		DST
		(9.130)		(1.701)			

The structure of the midget $E_p = 1701$ keV resonance in the $^{13}C(p,\gamma)^{14}N$ reaction was restudied with a high-volume Ge(Li) detector. The $(82 \pm 3)\%$ ground state ($J^\pi = 1^+$, $T = 0$) transition with the angular distribution $W(\theta) = 1 + (0.48 \pm 0.03) P_2(\cos\theta) - (0.16 \pm 0.03) P_4(\cos\theta)$ and the new $(9 \pm 3)\%$ branches to the 6.444-($J^\pi = 3^+$, $T = 0$) and 5.832-MeV ($J^\pi = 3^-$, $T = 0$) levels along with the deduced transition strengths lead to the new assignment of $J^\pi = 3^+$, $T = 0$ for the 9.130-MeV state.

9.13

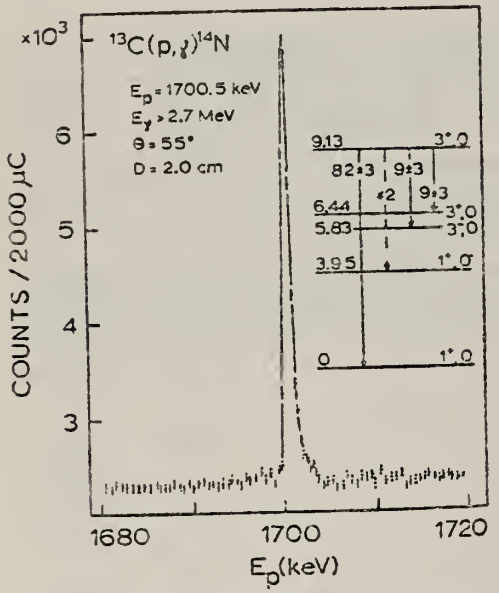

FIG. 1. The excitation function measured in the vicinity of the 1701 keV resonance in $^{13}C(p,\gamma)^{14}N$. The insert shows the γ-decay scheme of the resonance.

TABLE I. Summary of the angular distribution analysis performed for the different spin and parity alternatives for the (9.130→0) MeV transition. The experimental a_2 and a_4 values are 0.48 ± 0.03 and −0.16 ± 0.03, respectively. In the cases where the χ^2 value exceeded the 0.1% confidence limit, the error limits of the mixing ratio δ are not given.

J^π	Orbital momentum l_p	Amplitude-mixing ratio of orbital momenta $b = \frac{l_{p+2}}{l_p}$	Channel spin ratio $\tau = \lvert\frac{s=1}{s=0}\rvert^2$	Amplitude-mixing ratio of γ-ray multipoles δ	a_2	a_4	χ^2
1^+	1	...			0.507	...	45.9[a]
1^-	0,2		∞		0.507	...	45.9[b]
2^+	1,3	0.40	∞	$E2/M1 = -0.70$	0.478	−0.160	1.9
2^-	2	...	54	$M2/E1 = -0.70 \pm 0.05$	0.475	−0.161	1.9
3^+	3	...	43	$M3/E2 = -0.03 \pm 0.02$	0.478	−0.153	1.9
3^-	2,4	0.35	∞	$E3/M2 = -0.03 \pm 0.02$	0.478	−0.152	1.9
4^+	3,5	0	∞	$E4/M3 = 2.0$	0.625	−0.291	600
4^-	4	...	∞	$M4/E3 = 1.1$	0.519	−0.314	148

[a] δ and τ combinations yielding this value are unacceptable.
[b] δ and b combinations yielding this value are unacceptable.

REF. J. Keinonen, A. Anttila and M. Bister
Nucl. Phys. A294, 1 (1978)

ELEM. SYM.	A	Z
N	14	7

METHOD

REF. NO. 78 Ke 2 rs

REACTION	RESULT	EXCITATION ENERGY	SOURCE		DETECTOR		ANGLE
			TYPE	RANGE	TYPE	RANGE	
P,G	LFT	8- 9	D	1- 2	SCD-D		DST

Levels 8.49,8.96,9.13

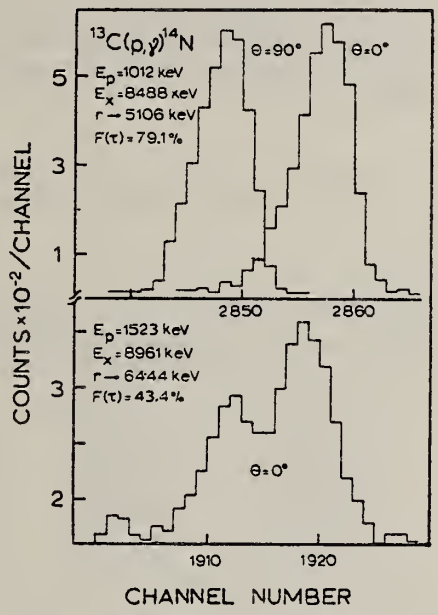

Fig. 1. Portions of γ-ray spectra recorded in the Doppler-shift measurements of the 3382 keV (8.49 → 5.11 MeV) and 2517 keV (8.96 → 6.44 MeV) γ-rays. The photopeaks obtained at the angles 0° and 90° to the beam direction are shown in the same picture. The dispersion is 1.2 keV/ch.

TABLE I

Mean lifetimes observed for the 8.49, 8.96 and 9.13 MeV unbound levels in ^{14}N

E_x (keV)	E_p (keV)	E_γ (keV)	$F(\tau)$ (%)	τ_m (fs)
8488	1012	2656	81.1±2.6	18.8±1.1
		3382	79.1±1.2	
8961	1523	2517	43.4±1.4	105 ±5
9130	1701	2686	89 ±4	13 ±5

REF. N. Ensslin, L.W. Fagg, R.A. Lindgren, W.L. Bendel, E.C. Jones, Jr. Phys. Rev. C19, 569 (1979)

ELEM. SYM.	A	Z
N	14	7

METHOD

REF. NO. 79 En 1 hg

REACTION	RESULT	EXCITATION ENERGY	SOURCE		DETECTOR		ANGLE
			TYPE	RANGE	TYPE	RANGE	
E,E/	ABX	2-17	D	40-61	MAG-D		180

7 LEVELS, J-PI, LFT

Inelastic electron scattering from ^{14}N at 180° has been studied at incident energies of 40.6, 50.6, and 60.2 MeV. Transitions to levels at 2.31, 9.17, and 10.43 MeV excitation energy were observed to be predominantly $M1$. The transition to the level at 16.11 MeV probably contains some $M2$ strength, and transitions to levels at 12.54, 13.27, and 13.76 appear to exhibit some $M1$ strength. Data on the 2.313 MeV transition, combined with earlier experiments, bring the observed reduced transition width into agreement with resonance fluorescence techniques. Transition widths for the other levels with reasonably certain multipolarities are also given.

[NUCLEAR REACTIONS $^{14}N(e,e')$, $\theta=180°$, $E=40.6$, 50.6, 60.2 MeV; measured $\sigma(E)$; deduced Γ_0, multipolarities for transitions excited.]

TABLE I. Values of cross sections for excitation of the nuclear transitions studied at the three incident energies of 40.6, 50.6, and 60.17 MeV.

Excitation energy (MeV)	Cross section (10^{-32} cm^2/sr) 40.6 MeV	50.6 MeV	60.17 MeV
2.31	0.064 ± 0.026	0.064 ± 0.020	0.062 ± 0.010
9.17	1.319 ± 0.077	1.167 ± 0.050	0.932 ± 0.035
10.43	1.317 ± 0.107	1.148 ± 0.079	0.850 ± 0.059
12.54	0.344 ± 0.078	0.354 ± 0.034	0.370 ± 0.040
13.27	0.114 ± 0.081	0.098 ± 0.030	0.133 ± 0.037
13.76	0.114 ± 0.090	0.087 ± 0.029	0.078 ± 0.036
16.11	0.101 ± 0.073	0.150 ± 0.038	0.168 ± 0.036

TABLE II. Multipolarities and ground-state transition widths for states in ^{14}N electroexcited at 180°.

Excitation energy (MeV)	J^π, T[a]	Multipolarity	Γ_0 (eV) This work	Other work
2.31	0⁺, 1	$M1$	$(6.1 \pm 2.0) \times 10^{-3}$	$(6.2 \pm 0.6) \times 10^{-3}$[b] $(7.6 \pm 1.1) \times 10^{-3}$[c]
9.17	2⁺, 1	$M1$	6.6 ± 1.3	7.7 ± 0.9
10.43	2⁺, 1	$M1$	9.6 ± 1.9	12.1 ± 1.5
12.54	d	$(M1, E2)$	$[(14.7 \pm 3.2)/s]$[f]	
13.27	d	$(M1, M2, E2)$		
13.76	e	$(M1, E1)$		
16.11	d	$(M2)$		

[a] Spins and parities from Ref. 19.
[b] Reference 8 and Ref. 15 but with uncertainty, $\pm 0.9 \times 10^{-3}$.
[c] Reference 14.
[d] $J=0,1,2,3$.
[e] $J=0,1,2$.
[f] Where $s=2J+1$.

(over)

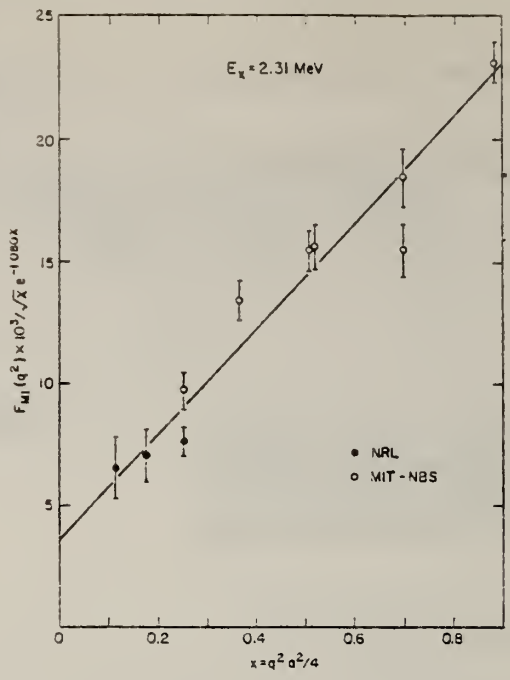

FIG. 2. Plot of $F_{M1}(q^2) \times 10^3/\sqrt{x}\, e^{-1.080x}$ vs $x = q^2a^2/4$ for the 2.31-MeV level, where $e^{-1.080x}$ is the analytical approximation to the hydrogen form factor given in the denominator of the left-hand side Eq. (2). The combination of NRL and MIT-NBS points gives an accurate extrapolation to $x = 0$.

REF. J. W. Jury, C. K. Ross, N. K. Sherman
Nucl. Phys. A337, 503 (1980)

ELEM. SYM.	A	Z
N	14	7

METHOD

REF. NO. 80Jul egf

REACTION	RESULT	EXCITATION ENERGY	SOURCE		DETECTOR		ANGLE
			TYPE	RANGE	TYPE	RANGE	
G,NØ	ABX	17-26	C	20-26	TOF	D	DST

Abstract: Photoneutron angular distributions were measured for the reaction $^{14}N(\gamma, n_0)^{13}N$ using neutron time-of-flight techniques over the region of excitation energy from 17 to 26 MeV. Coefficients of a Legendre polynomial fitted to the data are interpreted in terms of a simple single-particle nuclear model. For reactions to the ground state in ^{13}N, it appears that most of the photon absorption in the giant resonance region studied forms $J^\pi = 2^-$ states in ^{14}N which decay by d-wave neutron emission. Some evidence was found for the existence of $J^\pi = 0^-$ strength at about 22.5 MeV (the peak of the cross section). The results are in general consistent with an identification of the (γ, n_0) process with the promotion of a $p_{1/2}$ neutron to the s-d shell. Little or no E2 or M1 absorption was observed. Comparison with photoproton measurements shows some evidence for a small amount of isospin $T = 0$ mixing also near 22.5 MeV. Comparison with calculations of the ground-state cross section shows reasonable agreement if the theoretical results are displaced upwards in energy by about 1 MeV.

E NUCLEAR REACTIONS $^{14}N(\gamma, n_0)$, $E = 17$–26 MeV; measured $\sigma(\theta_n)$ with time-of-flight; deduced $\sigma(E_\gamma)$, $T = 1$ purity.

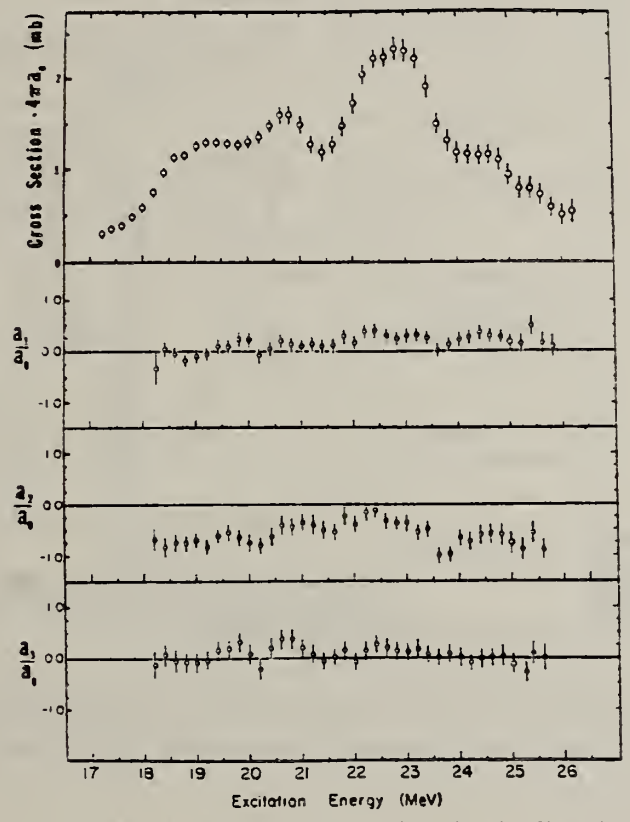

Fig. 5. The energy dependence of the angular distribution coefficients of a series of Legendre polynomials fitted to the eight neutron spectra for each end-point measurement. The a_n coefficient has been corrected by division by the photon distribution shape and has been plotted as the total ground-state cross section, $4\pi a_0$.

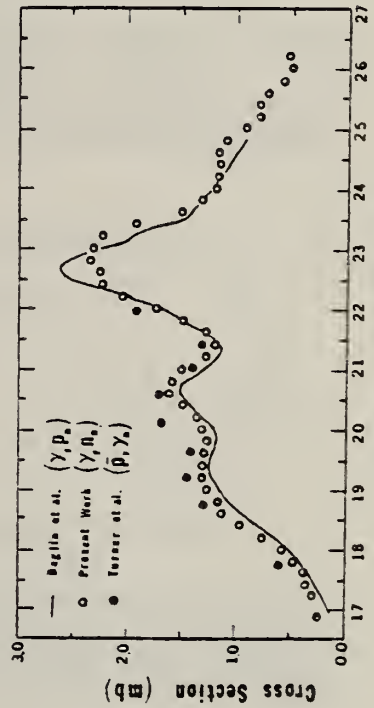

Fig. 7. A comparison of the present cross section data (open circles) with the $^{13}C(p, \gamma_0)$ data of Turner *et al.* [11] (solid circles) and the $^{14}N(\gamma, p_0)$ data of Baglin *et al.* [7] (line).

REF. C. Rangacharyulu, C. St.-Pierre
Can. J. Phys. 58, 150 (1980)

ELEM. SYM.	A	Z
N	14	7

METHOD

REF. NO. 80 Ra 2 hg

REACTION	RESULT	EXCITATION ENERGY	SOURCE		DETECTOR		ANGLE
			TYPE	RANGE	TYPE	RANGE	
P,G	LFT	11	D	4	SCD-D		DST
		(11.05)		(3.77)			

The gamma decay of E_p = 3.77 MeV resonance in $^{13}C(p,\gamma)^{14}N$ has been measured. From the measured excitation functions, the natural width of the resonance was deduced to be 1.2 ± 0.4 keV. The resonance is found to strongly populate the 3.945 MeV level, in addition to the gs transition. Gamma angular distribution measurements determined the resonance spin as 3^+. The reduced proton width is found to be 0.5% of the single particle unit. The transition strengths are measured to be $B(E2)$ = 0.45 ± 0.07 and 3.0 ± 0.8 Wu for transitions to ground state and the level at 3.945 MeV, respectively.

BEL, J-PI

TABLE I. Gamma widths and $B(E2)$ values for the decay of 11.05 MeV state (R) in ^{14}N

Transition	Γ_γ (eV)*	$B(E2)$* This work	$B(E2)$* Ref. 3
$R \rightarrow$ gs	0.12±0.02	0.45±0.07	0.5
$R \rightarrow$ 3.945	0.09±0.02	3.0 ±0.8	—

*Assuming $\Gamma_{tot} \simeq \Gamma_\gamma$ (see text for details).
†In Weisskopf units.

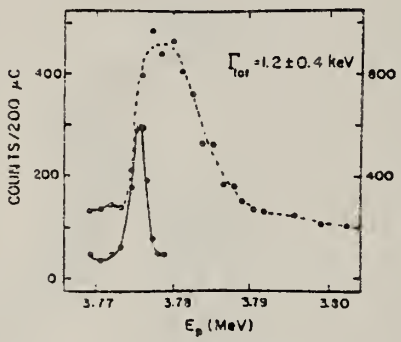

FIG. 1. The $^{13}C(p,\gamma_0)$ yield curves taken with a Ge(Li) detector. The filled circles and scale on the left-hand side are for 10 μg/cm² target. The open circles and scale on the right-hand side are for 100 μg/cm² target. Each point was measured for an integrated charge of 200 μC. The lines are drawn only as a guide to the eye.

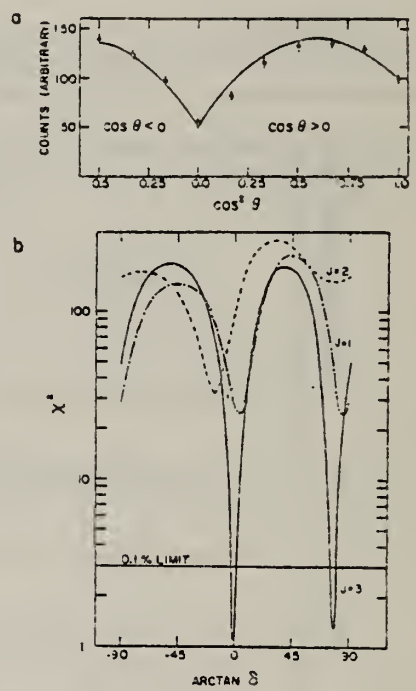

FIG. 3. (*a*) Measured angular distribution and theoretical fit (J = 3) for the ground state transition. (*b*) The χ^2 plot vs. mixing ratio for J = 1, 2, and 3.

REF. H. Taneichi, H. Ueno, K. Shoda, Y. Kawazoe, T. Tsukamoto
Nucl. Phys. A350, 157 (1980)

ELEM. SYM.	A	Z
N	14	7

METHOD

REF. NO. 80 Ta 3 hg

REACTION	RESULT	EXCITATION ENERGY	SOURCE		DETECTOR		ANGLE
			TYPE	RANGE	TYPE	RANGE	
E,D	ABX	15-29	D	18-29	MAG-D		DST

Abstract: Cross sections have been measured for the reaction $^{14}N(e, d_0)^{12}C$ over the incident electron energy range of 18 to 29 MeV together with the angular distributions of emitted deuterons. Analysis of these data has been performed by using a cluster model. The giant quadrupole resonance is deduced around 20 MeV. The dipole strength has two peaks which correspond to the pigmy and the giant resonances of the (γ, p_0) reaction, respectively. A monopole component is found to be necessary to reproduce the experimental results.

E NUCLEAR REACTIONS $^{14}N(e, d)$, $E = 18$–29 MeV; measured $\sigma(E_d, \theta_d)$. ^{14}N deduced resonances. Cluster model analysis. Natural BN target.

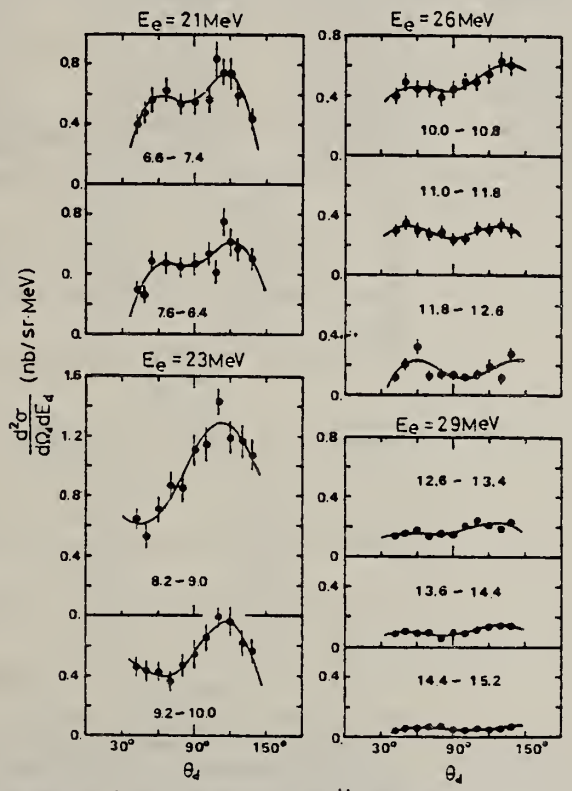

Fig. 3. Angular distributions of deuterons emitted by the $^{14}N(e, d_n)$ reaction. Solid curves are the best-fitted results with a Legendre polynomial series. The deuteron energy ranges (in MeV) used to get the average values of the cross sections under each experimental condition are shown in the figure.

(OVER)

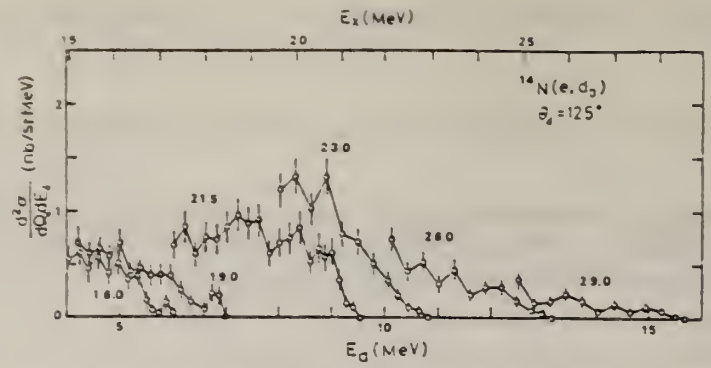

Fig. 2. Deuteron cross sections in the ^{14}N(e, d_0) reaction. The incident electron energies are shown in the figure (in MeV). The upper scale is the excitation energy of emitted deuterons in the laboratory frame. Vertical bars show statistical errors only.

TABLE 1

The values of the coefficients A_n which give the best fitted curves in fig. 3 with the Legendre polynomial series eq. (2).

E_e (MeV)	E_d (MeV)	A_0	A_1	A_2 (nb/sr · MeV)	A_3	A_4
21.0	6.6 ~ 7.4	0.429 ± 0.042	0.011 ± 0.069	−0.665 ± 0.157	0.176 ± 0.108	−0.519 ± 0.153
	7.6 ~ 8.4	0.388 ± 0.054	−0.165 ± 0.088	−0.420 ± 0.201	−0.014 ± 0.138	−0 353 ± 0.196
23.0	8 2 ~ 9.0	0.939 ± 0.054	−0.250 ± 0.089	−0.306 ± 0.210	0.396 ± 0.144	0.011 ± 0.205
	9 2 ~ 10.0	0.513 ± 0.034	0.007 ± 0.056	−0.186 ± 0.132	0.424 ± 0.091	−0.143 ± 0.129
	10.0 ~ 10.8	0.476 ± 0.021	−0.130 ± 0.035	−0.025 ± 0.082	−0.024 ± 0.056	−0.138 ± 0.079
26.0	11.0 ~ 11.8	0.281 ± 0.012	0.004 ± 0.020	−0.048 ± 0.047	0.008 ± 0.032	−0.143 ± 0.046
	11.8 ~ 12.6	0.158 ± 0.040	−0.079 ± 0.065	−0.055 ± 0.153	−0.165 ± 0.105	−0.147 ± 0.149
	12.6 ~ 13.4	0.172 ± 0.018	−0.038 ± 0.029	−0.040 ± 0.068	0.037 ± 0.047	−0.066 ± 0.067
29.0	13.6 ~ 14.4	0.103 ± 0.007	−0.030 ± 0.012	−0.012 ± 0.029	0.013 ± 0.020	−0.063 ± 0.028
	14.4 ~ 15.2	0.055 ± 0.007	−0.025 ± 0.011	−0.015 ± 0.026	−0.044 ± 0.017	−0.023 ± 0.025

REF. J. D. Turner, N. R. Roberson, S. A. Wender, H. R. Weller, D. R. Tilley
Phys. Rev. C21, 525 (1980)

ELEM. SYM.	A	Z
N	14	7

METHOD

REF. NO. 80Tul egf

REACTION	RESULT	EXCITATION ENERGY	SOURCE		DETECTOR		ANGLE
			TYPE	RANGE	TYPE	RANGE	
$ P,G	ABX	13-23	D	6-14	NAI	D	DST

The 90° yield curves for the $^{13}C(\vec{p},\gamma_0)^{14}N$ and $^{13}C(\vec{p},\gamma_1)^{14}N$ reactions have been measured in 200 keV steps for $E_p = 6.25$ to 13.6 MeV and in 100 keV steps for $E_p = 13.6$ to 17.0 MeV. In addition, 50 keV step data were obtained for E_p of 12.6 to 14.55 MeV. Angular distributions of both the cross section and the analyzing power were also obtained for these two reactions at twelve energies which span the giant dipole energy region. The cross section was measured at nine angles between 30° and 154° while the analyzing power was measured at seven angles between 42° and 142°. These data were used to obtain the complex $E1$ and $E2$ transition matrix elements in the case of $^{13}C(\vec{p},\gamma_1)^{14}N$. The results are compared to a direct-semidirect calculation. It is found that there is little justification in introducing $E2$ amplitudes other than a pure direct $E2$ term.

POLARIZED PROTONS

[NUCLEAR REACTIONS $^{13}C(\vec{p},\gamma_0)$, $^{13}C(\vec{p},\gamma_1)$ measured $\sigma(\theta)$ and $A(\theta)$, E_p=8.05–15.5 MeV. $^{13}C(p,\gamma_0)$, $^{13}C(p,\gamma_1)$ measured $\sigma(90°)$, E_p=6.24–17.0 MeV. Deduced $E1$ and $E2$ T-matrix amplitudes and phases. Compared to model calculations.]

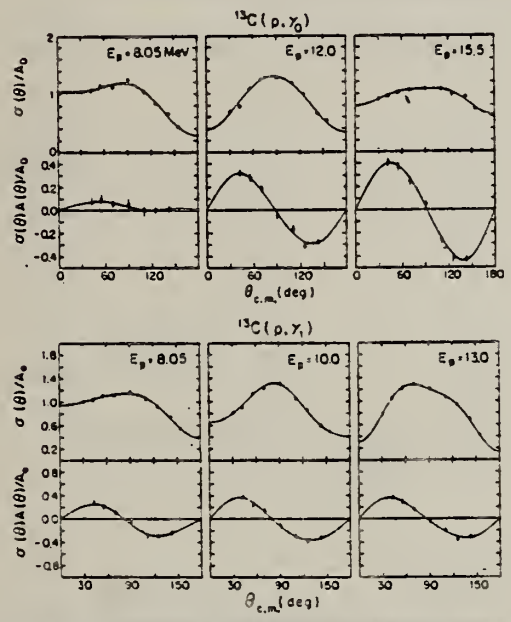

FIG. 5. (a) Typical cross section and analyzing power data for the $^{13}C(p,\gamma_0)^{14}N$ reaction. The error bars represent the statistical errors associated with the data points. The solid curves were generated by fitting the data through fourth order in the Legendre and associated Legendre polynomials as described in the text. (b) Same as for Fig. 5(a), but for $^{13}C(p,\gamma_1)^{14}N$.

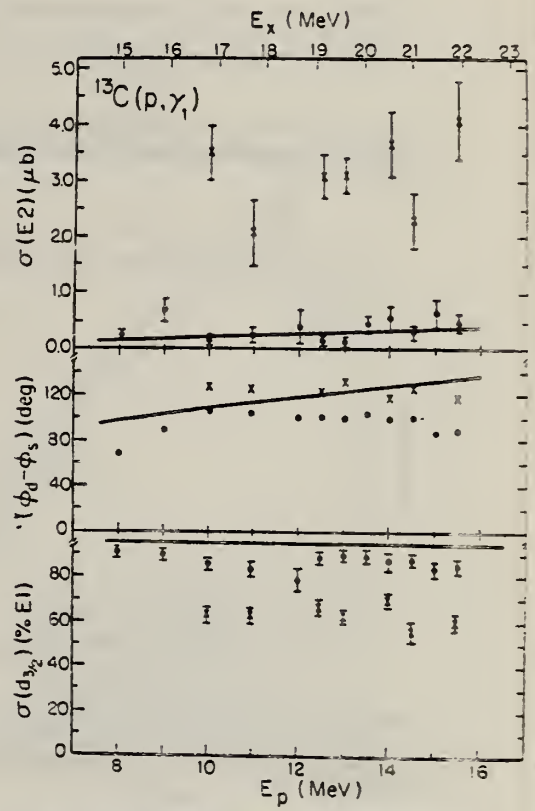

FIG. 8. The results of the $E1$-$E2$ analysis for the $^{13}C(p,\gamma_1)^{14}N$ reaction for dominant $d_{3/2}(E1)$ capture. The bottom plot shows the percentage of the $E1$ cross section due to the $d_{3/2}(E1)$ term. The middle plot shows the relative phase between the two $E1$ terms. The upper plot gives the angle integrated $E2$ cross section. The error bars represent the statistical uncertainties associated with these quantities (the errors associated with the relative phases are ≤4°). The ●'s and ×'s correspond to the two solutions corresponding to "small" and "large" $E2$, respectively. The curves are the result of the calculation described in the text.

(OVER)

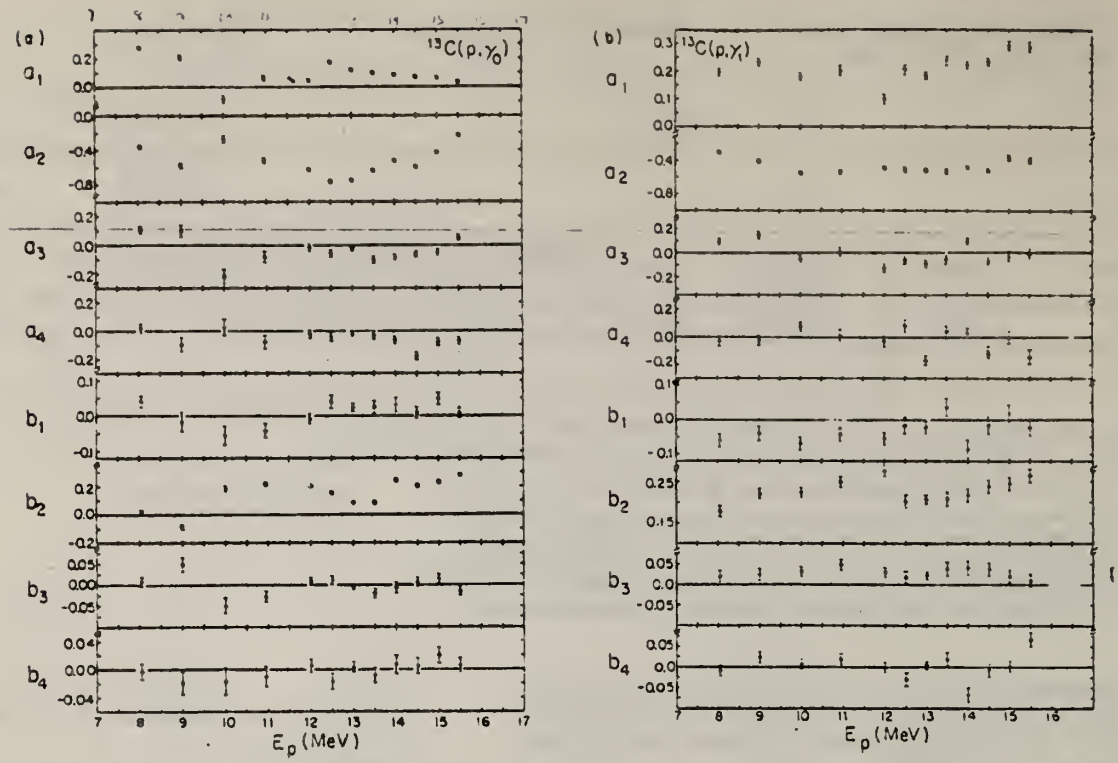

FIG. 6. (a) The a_k and b_k coefficients for the $^{13}C(p,\gamma_0)^{14}N$ reaction obtained from the fits through fourth order. The error bars represent the statistical errors associated with these coefficients. (b) Same as Fig. 6(a), but for $^{13}C(p,\gamma_1)^{14}N$.

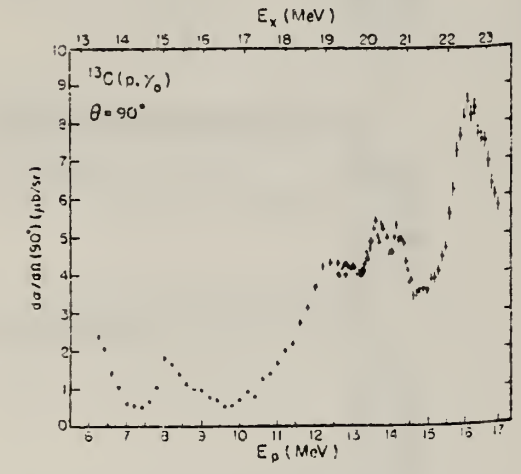

FIG. 2. The differential cross section measured at $\theta_{lab} = 90°$ for the $^{13}C(p,\gamma_0)^{14}N$ reaction. The error bars represent the statistical errors associated with the data points.

TABLE I. Summary of the percent of the $E2$ isoscalar EWSR obtained from experiment and from the direct calculation. The integrated energy weighted strengths are also given. Note: The value of $\langle r_3^2 \rangle$ required to evaluate the sum rule was taken both from electron data (Ref. 23) $\langle r_0^2 \rangle_1$ and from a uniform charged sphere model $\langle r_0^2 \rangle_2$.

	$\int \frac{\sigma dE}{E^2}$ (μb/MeV)	% $(\langle r_3^2 \rangle_1)$	% $(\langle r_0^2 \rangle_2)$
Small solution	1.75	29	35
Large solution	8.0	133	159
Direct calculation	1.0	17	20

REF. W. Biesiot, Ph.B. Smith
Phys. Rev. C24, 2443 (1981)

ELEM. SYM.	A	Z
N	14	7

METHOD

REF. NO. 81 Bi 13 hg

REACTION	RESULT	EXCITATION ENERGY	SOURCE TYPE	SOURCE RANGE	DETECTOR TYPE	DETECTOR RANGE	ANGLE
$ G,MU-T	LFT	9	D	9	NAI-D		DST
		(9.17)		(9.17)			

Mutually consistent measurements of elastic proton scattering and resonance absorption show that the width of the 9.17 MeV level in ^{14}N ($\Gamma = 135 \pm 8$ eV) is almost twice as large as the accepted literature value. The positive parity is unambiguously confirmed. The excitation energy is determined to be 9172.5±0.3 keV, based upon a cascade-crossover technique with a ^{56}Co source for calibration. The expected azimuthal asymmetry of the resonance fluorescence of the plane-polarized photons at this resonance is demonstrated quantitatively.

POL G, AZMUTH ANG DST

[NUCLEAR REACTIONS ^{13}C(p,γ)^{14}N, ^{13}C (p,p)^{13}C, ^{14}N res. abs., ^{14}N res. fluor., $E = 1.75$ MeV; measured $\sigma(E, E_\gamma, \theta)$, ^{14}N deduced levels J, π, Γ, levels. Enriched target.]

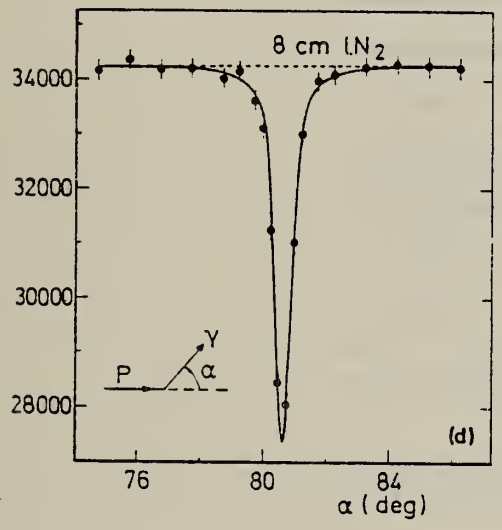

FIG. 6. Transmission curves resulting from the five experiments with absorbers of 64, 32, 16, 8, and 4 cm LN_2 for parts (a)–(e), respectively. The transmissions are not normalized to unity but represent the total number of true counts in the spectrum gate indicated in Fig. 6. The solid lines are best fits to the data.

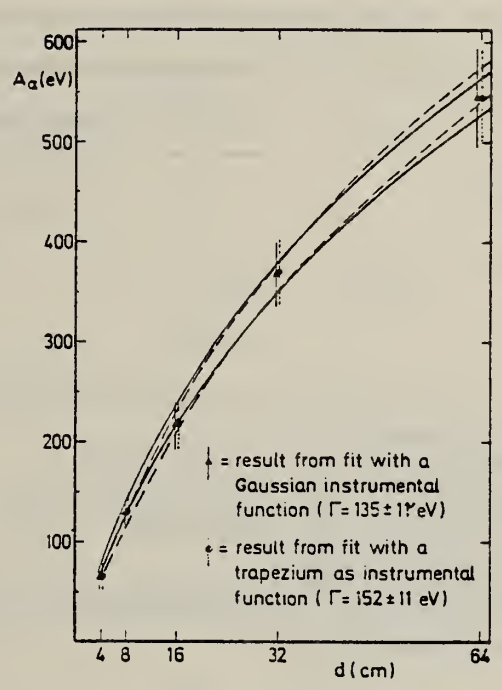

FIG. 9. The absorption integral A_α as a function of absorber length d. The data points represent values obtained from separate fits to the data. The dotted and solid lines mark bands of A_α values resulting from several simultaneous fits to the data, resulting in the best set of parameters for a given fit option. The solid lines arise from the fit option with a Gaussian instrumental function, while the dotted lines result from a fit with a trapezium for $h(\alpha - \alpha')$.

(OVER)

TABLE IV. Results of the analysis of the resonance absorption experiments with the $E_p = 1.75$ MeV resonance in $^{13}C(p,\gamma)^{14}N$ and a N_2 absorber for two options in the fitting procedure.

Absorber length (cm)	Separate fits Γ(eV)	Γ_γ (eV)	$n\sigma_0$	A_a (eV)	χ^2/df	Simultaneous fits Γ (eV)	Γ_{γ_0} (eV)	$n\sigma_0$	A_a (eV)	χ^2/df
Gaussian instrumental function										
64	147±19	6.7±0.8	4.9±0.9	545±53	0.69			5.8 ±0.4	547±19	
32	133±15	7.5±0.6	3.0±0.4	370±33	0.72			2.9 ±0.2	363±14	
16	135±19	6.9±0.6	1.4±0.2	216±26	0.85	135±11[a]	7.2±0.4[a]	1.4 ±0.10	225±11	0.58
8	145±19	7.1±0.5	0.7±0.1	129±16	0.15			0.72±0.05	129± 7	
4	120±22	6.5±0.5	0.4±0.1	63 ±12	0.55			0.36±0.02	70 ± 4	
trapezoidal instrumental function										
64	161±18	6.3±0.6	4.2±0.6	547±47	0.70			4.8 ±0.3	558±18	
32	148±16	7.1±0.6	2.6±0.3	370±32	0.74			2.4 ±0.2	365±15	
16	151±19	6.7±0.6	1.2±0.2	220±25	0.94	152±11	6.8±0.4	1.2 ±0.1	222±10	0.57
8	162±22	7.1±0.6	0.6±0.1	131±17	0.18			0.61±0.03	126± 7	
4	123±23	6.7±0.6	0.4±0.1	65±13	0.53			0.30±0.02	66 ± 3	

[a]Adopted as the best values from this analysis.

TABLE V. Comparison of the results of this work with the Ajzenberg-Selove compilation (Ref. 1).

	This work (p,p)[a]	(γ,γ)[b]	cascade/crossover	Ref. 1
E_p (keV)				1746.6± 0.9[d]
E_x (keV)			9172.5±0.3	9172.5± 0.9[d]
				9170.8± 1.6[e]
$\Gamma_{\gamma_0}/\Gamma_\gamma$ (%)				79 ± 4
Γ (eV)	135±8	135 ±11		74 ± 8[e]
				70 ±50[f]
Γ_{γ_0} (eV)		7.2±0.4		6.1± 0.8[g]
J^π	2^+			2^+ [d,e,h]

[a]The $^{13}C(p,p)$ studies in Sec. II.
[b]The resonance absorption experiments described in Sec. IV.
[c]The cascade/crossover method described in Sec. III.
[d]Cited from Table 14.20 of Ref. 1. The error is inferred from the uncertainty stated for E_p, and does not include the error in the Q value of the (p,γ) reaction.
[e]Cited from Table 14.11 of Ref. 1.
[f]Cited from Table 14.20 of Ref. 1, and based upon (p,γ) measurements only.
[g]Product of multiplication of $\Gamma_{\gamma_0}/\Gamma = 0.79\pm0.04$ eV and $\Gamma_\gamma = 7.7\pm0.9$ eV as quoted in Ref. 1.
[h]Cited from Table 14.12 of Ref. 1.

N
A=15

N
A=15

N
A=15

Ref. J.L. Rhodes, W.E. Stephens
Phys. Rev. 110, 1415 (1958)

Elem. Sym.	A	Z
N	15	7

Method: Betatron; nuclear emulsions

Ref. No.: 58 Rh 1 EH

Reaction	E or ΔE	E_0	Γ	$\int \sigma dE$	Jπ	Notes
$N^{15}(\gamma,p)$	Bremss. 18.7					First excited state in C^{14} is at 6.09 MeV.
	24.6			38±5 MeV-mb		

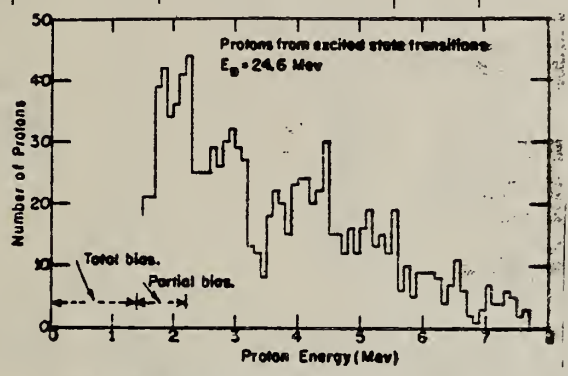

FIG. 4. Energy distribution of protons from excited-state transitions.

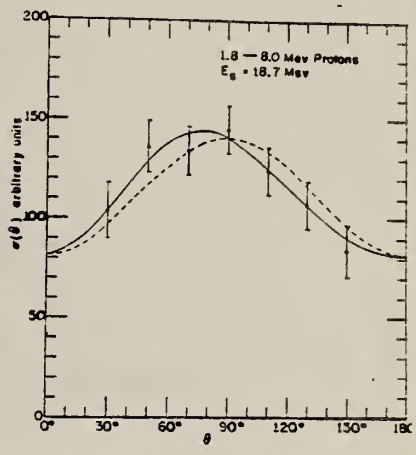

FIG. 5. Angular distribution of protons with 1.8- to 8.0-M energy in the 18.7-Mev run.

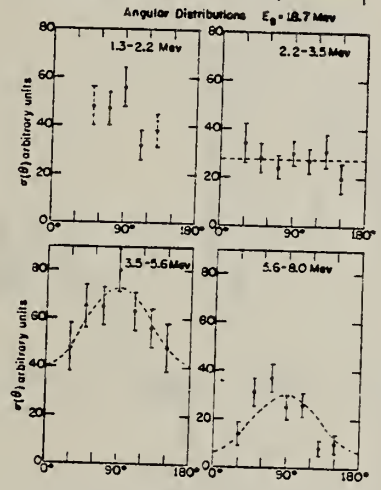

FIG. 6. Angular distributions from 18.7-Mev run for protons of energy: (a) 1.3 to 2.2 Mev, (b) 2.2 to 3.5 Mev, (c) 3.5 to 5.6 Mev, and (d) 5.6 to 8.0 Mev.

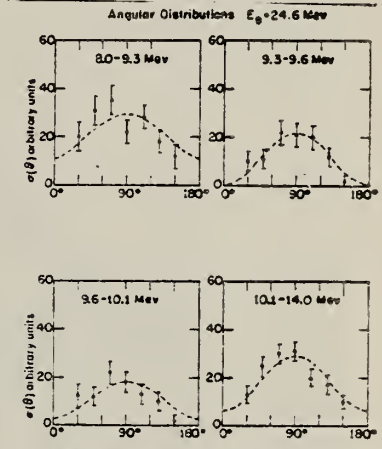

FIG. 7. Angular distributions from 24.6-Mev run for proto energy: (a) 8.0 to 9.3 Mev, (b) 9.3 to 9.6 Mev, (c) 9.6 to 10.1 and (d) 10.1 to 14.0 Mev.

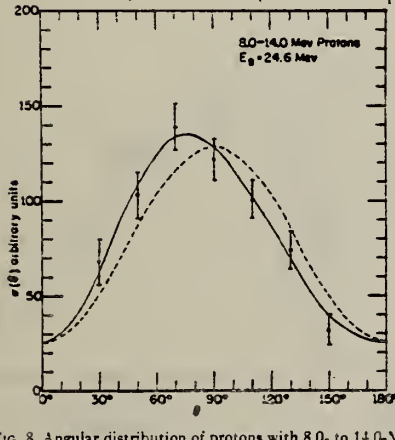

FIG. 8. Angular distribution of protons with 8.0- to 14.0-Mev energy in the 24.6-Mev run.

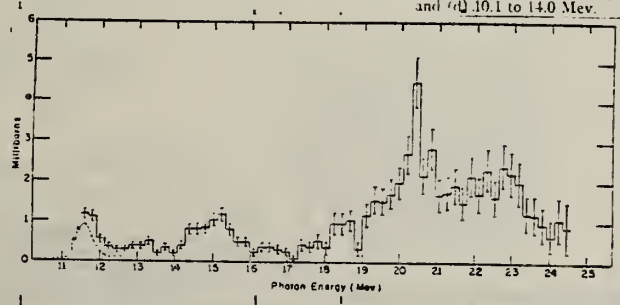

FIG. 9. Variation w energy of the cross s tion for ground-st transitions in $N^{15}(\gamma,$ C^{14}. Dotted curve is rived from the inve reaction $C^{14}(p,\gamma)N^{16}$ detailed balancing.

Ref. E. Finckh, R. Kosiek, K. Schlupmann
Naturwiss. 50, 326 (1963)

Elem. Sym.	A	Z
N	15	7

Method: Betatron; proton spectrum; CsI(Tℓ) spectrometer

Ref. No.: 63 Fi 3 | NVB

Reaction	E or ΔE	E_o	Γ	$\int \sigma dE$	Jπ	Notes
$N^{15}(\gamma,xp)$	Bremss.			$\int_{12.7}^{31}$ = 43±25% MeV-mb		Detector at 90°.
	24.5	3.2				$\int\sigma$ based on assumption that residual C^{14} is left in ground state; angular distribution from Rhodes and Stephens [Phys. Rev. 110, 1415 (1958)].
		4.5				
		8.7				
		9.5				
	31					Target 99.1% pure N^{15} gas.

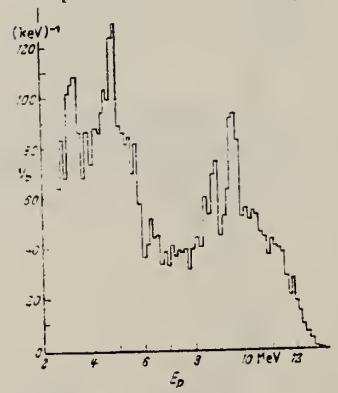

a

Fig. 1 a u. b. Energieverteilung der Photoprotonen aus N^{15}, gemessen unter 90° zum γ-Strahl. Endenergie der Bremsstrahlung a 24,5 MeV, b 31 MeV. — Abszisse: Protonenenergie E_p. Ordinate: Zahl N_p der Protonen je 100 keV-Intervall

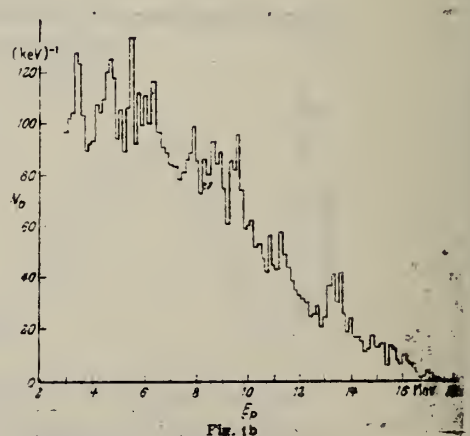

Fig. 1b

R. Kosiek
Z. Physik 179, 544-55 (1964)

N	15	7

METHOD

Betatron; ion chamber

[Page 1 of 3]

REF. NO. 64 Ko 3 NVB

REACTION	RESULT	EXCITATION ENERGY	SOURCE		DETECTOR		ANGLE
			TYPE	RANGE	TYPE	RANGE	
G,P	SPC	12-31	C	19-31	SCI-D		90

Enriched target

ABX

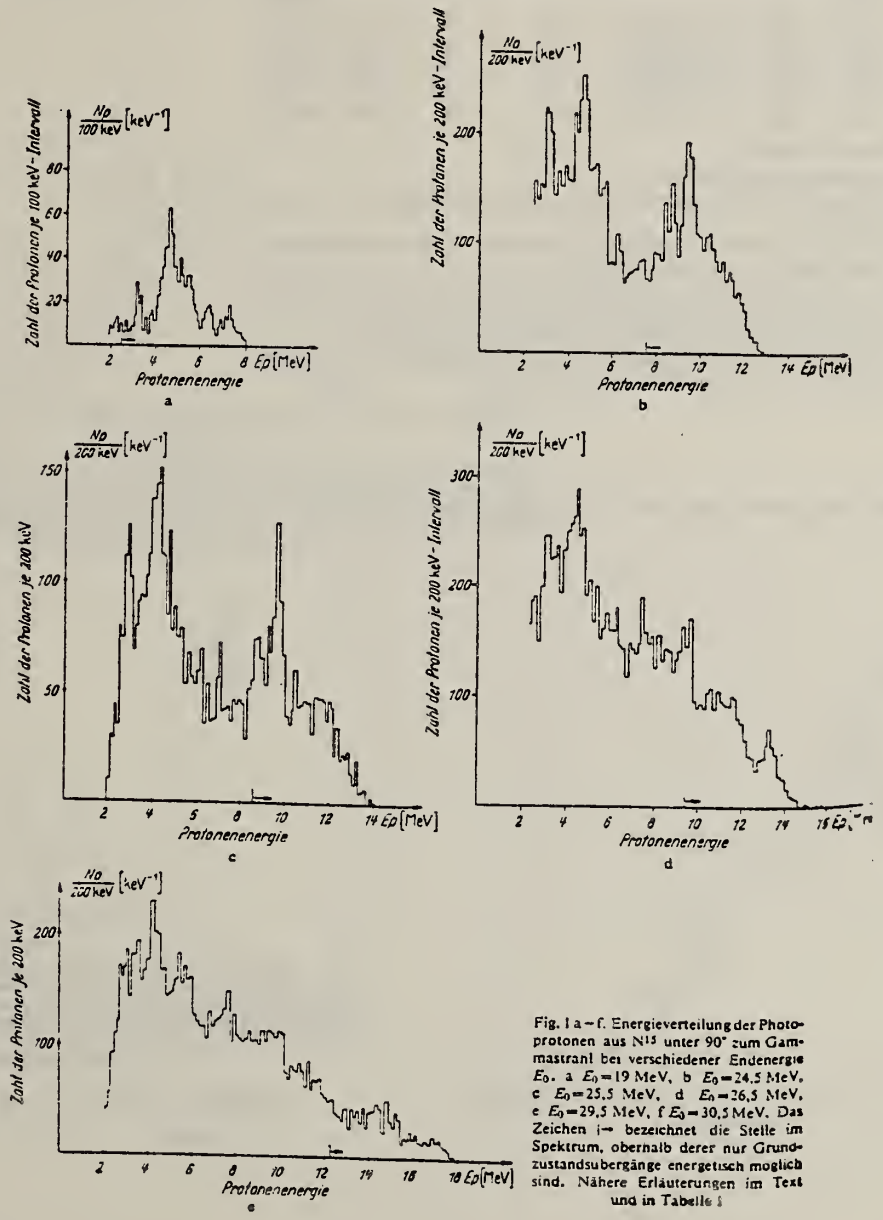

Fig. 1 a–f. Energieverteilung der Photoprotonen aus N^{13} unter 90° zum Gammastrahl bei verschiedener Endenergie E_0. a E_0 = 19 MeV, b E_0 = 24,5 MeV, c E_0 = 25,5 MeV, d E_0 = 26,5 MeV, e E_0 = 29,5 MeV, f E_0 = 30,5 MeV. Das Zeichen |→ bezeichnet die Stelle im Spektrum, oberhalb derer nur Grundzustandsübergänge energetisch möglich sind. Nähere Erläuterungen im Text und in Tabelle 1

REACTION	RESULT	EXCITATION ENERGY	SOURCE TYPE	SOURCE RANGE	DETECTOR TYPE	DETECTOR RANGE	ANGLE

Tabelle 2

Ref.	1 E_0 MeV	2 $\int_{12,5}^{E_0} \sigma(\gamma p_0)\,dE_\gamma$ MeVmb	3 $\frac{Y^+}{Y^-}$	4 $\left(\int_{12,5}^{E_0} \sigma^+ dE_\gamma\right)_{min}$ MeVmb	5 $\left(\int_{12,5}^{E_0} \sigma^+ dE_\gamma\right)_{max}$ MeVmb	6 E_m MeV	7 $\int_{12,5}^{E_0} \sigma(\gamma p)\,dE$ MeVmb
RHODES[8]	24,6	13,5*					37±5*
diese Arbeit	24,5	16±2	0,45±0,15	14	23	23,5	34±6
diese Arbeit	25,5	19±3	0,52±0,15	21	37	24,5	48±8
diese Arbeit	26,5	20±3	0,55±0,15	26	42	25,5	54±15
diese Arbeit	29,5	22±3	0,65±0,15	50	73	27,0	84±15
diese Arbeit	30,5	22±3	0,70±0,15	50	84	28,0	90±20

Erläuterungen zu Tabelle 2:

Spalte 1 E_0 = Endenergie des Betatrons.
Spalte 2 Integrierter Wirkungsquerschnitt für Grundzustandsübergänge beim (γ, p)-Prozeß am N^{15}.
Spalte 3 Verhältnis der Ausbeute aller Protonen aus Nichtgrundzustandsübergängen zur Gesamtzahl der gemessenen Teilchen.
Spalte 4 bzw. 5 Untere bzw. obere Grenze für den integrierten Wirkungsquerschnitt aus Nichtgrundzustandsübergängen (nähere Erläuterungen im Text).
Spalte 6 Gammaenergie, die zur Abschätzung von Spalte 5 benutzt wurde.
Spalte 7 Abgeschätzer Wert für den integrierten Wirkungsquerschnitt für Protonenemission aus N^{15} (nähere Erläuterungen im Text).

*Assumed isotropic angular distribution.

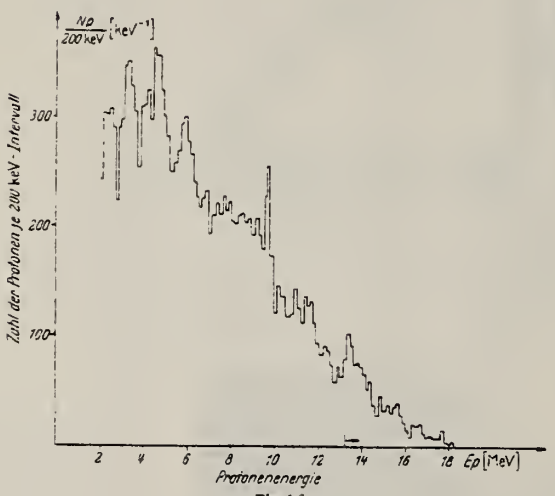

Fig. 1f

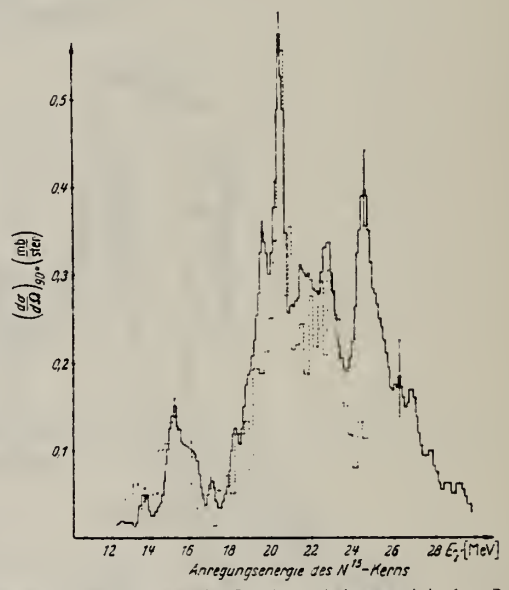

Fig. 3. Differentieller Wirkungsquerschnitt für Grundzustandsübergänge beim (γ, p)-Prozeß am N^{15}. a (———) Ergebnis dieser Arbeit unter 90° zum Gammastrahl. Die eingetragenen Fehlerbalken geben vorzugsweise die statistischen Fehler der Meßergebnisse wieder. Der Wirkungsquerschnitt wurde auf die im Text beschriebene Weise aus den in Fig. 1 a–f dargestellten Spektren berechnet. Jeder Teilbereich ist für sich normiert, die Genauigkeit dieser Normierung wird auf 15% abgeschätzt. b (– – –) Ergebnis der Messungen von RHODES und STEPHENS[8]

*Maxima at 19.5, 20.4, 22.7, 24.5, 15.2, 13.6, 17.0 MeV.

R. Kosiek
Z. Physik 179, 544-55 (1964)

N	15	7

METHOD

· Betatron; ion chamber [Page 3 of 3]

REF. NO. 64 Ko 3 NVB

REACTION	RESULT	EXCITATION ENERGY	SOURCE TYPE	SOURCE RANGE	DETECTOR TYPE	DETECTOR RANGE	ANGLE

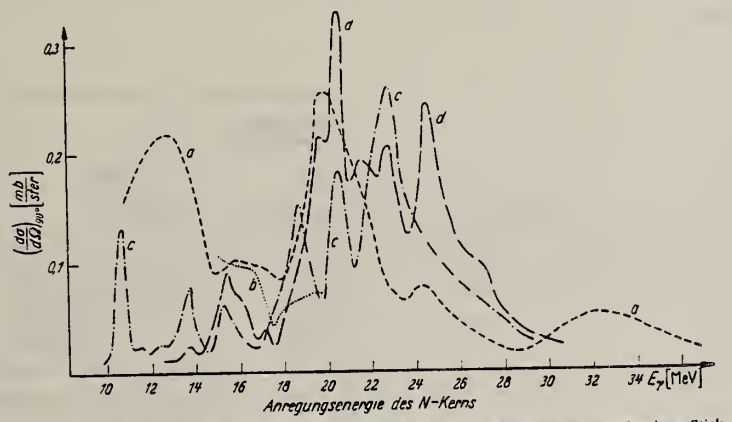

Fig. 4. Wirkungsquerschnitt für Grundzustandsübergänge der (γ, p)-Reaktion an den einzelnen Stickstoffisotopen. *a* N^{13} (γ, p_0) C^{12}, berechnet unter der Annahme der Gültigkeit des detaillierten Gleichgewichtes aus den Ergebnissen der Reaktion $C^{12}(p, \gamma_0)$ N^{13} nach FISHER et al.[14] (Mittlere Kurve durch angegebene Meßpunkte). *b* Desgleichen nach WARBURTON und FUNSTEN[15]; *c* $N^{14}(\gamma, p_0)$ C^{13} nach KOSIEK et al.[13]; *d* $N^{15}(\gamma, p_0)$ C^{14} diese Arbeit

REF. G. A. Beer, P. Brix, H. G. Clerc and B. Laube
Phys. Letters 26B, 506 (1968)

ELEM. SYM.	A	Z
N	15	7

METHOD

REF. NO.	
68 Be 1	EGF

REACTION	RESULT	EXCITATION ENERGY	SOURCE		DETECTOR		ANGLE
			TYPE	RANGE	TYPE	RANGE	
E,E/	LFT	6	D	50-57	MAG-D	43-57	DST

Table 1.
Experimental results for the 6.32 MeV level in ^{15}N. Transition strenghts are expressed in Weisskopf units as defined by Wilkinson [5].

	M1	E2
Γ_γ^0(eV)	3.4 ± 0.7	0.06 ± 0.02
Transition strength	0.64 ± 0.14	3 ± 1
$\lvert\delta(E2/M1)\rvert$	0.13 ± 0.03	

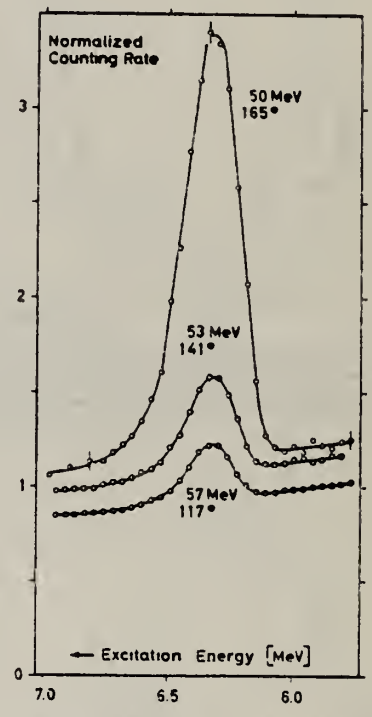

Fig. 1. Spectra of electrons scattered inelastically from a melamine ($C_3N_6H_6$) target enriched to 99% in ^{15}N. The scattering angles and primary energies, shown on the figure, were chosen to give a constant inelastic momentum transfer of 0.47 fm^{-1}. The peak results from the excitation of the 6.32 MeV level in ^{15}N. For convenience the three spectra are normalized to a constant elastic peak area. In such a plot, a pure longitudinal excitation would show a peak area independent of scattering angle. The strong enhancement of the observed peak area at backward angles demonstrates the predominantly transverse (magnetic) character of this transition. Only statistical errors are given: for the 117° spectrum they are smaller than the points.

H. E. Siefken, P. M. Cockburn and R. W. Krone
Nucl. Phys. A128, 162 (1969)

N	15	7

METHOD

REF. NO. 69 Si 1 egf

REACTION	RESULT	EXCITATION ENERGY	SOURCE		DETECTOR		ANGLE
			TYPE	RANGE	TYPE	RANGE	
P,G	ABX	10	D	0-1	NAI-D	0-12	DST
				(.250-670)			

Also used Ge(Li) detector
Levels seen at E_p = 261, 352, 527, 634 keV

SOURCE 250-670 KEV

TABLE 1

Strengths $\omega\gamma$ (in eV) for three $^{14}C(p,\gamma)^{15}N$ resonances

E_p	352 keV	527 keV	634 keV
present experiment †	0.034	1.78	0.23
Hebbard and Dunbar [21])	0.021	0.54	0.11
Hebbard [22])	0.042		

† All errors are estimated to be ≦ 17 %.

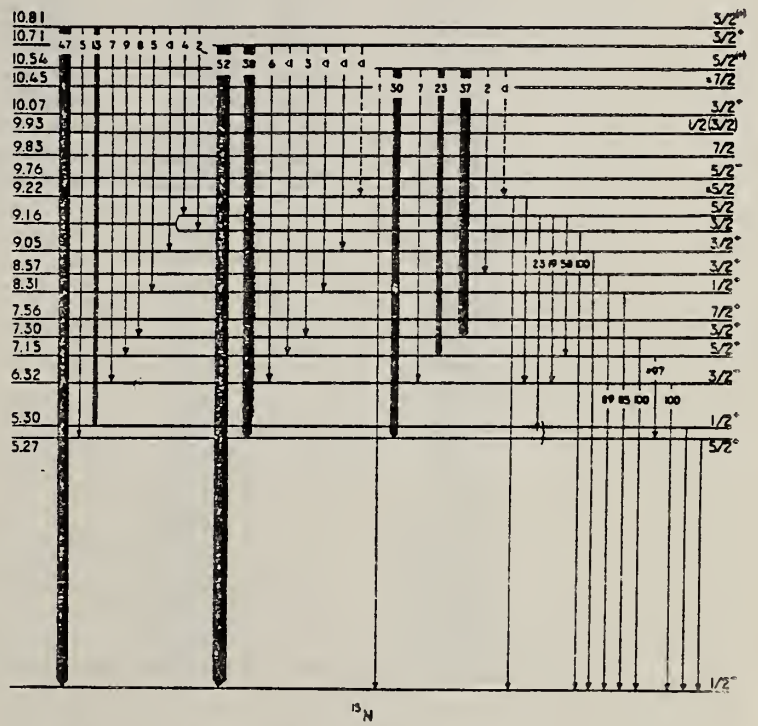

Fig. 7. Energy level diagram and γ-ray decay schemes for ^{15}N. Measured branching ratios are shown

[over]

TABLE 4

Angular distribution coefficients corrected for finite detector size for γ-rays at $E_p = 527$ keV

Transition (MeV)	A_2	Transition (MeV)	A_2
10.71 → 0	−0.73±0.01	9.22 → 6.32	0.07±0.18
10.71 → 9.05	0.38±0.08	9.1 → 0 [a]	0.05±0.06
10.71 → 8.31	−0.11±0.18	8.31 → 0	−0.06±0.06
10.71 → 7.30	0.52±0.05	7.30 → 0	−0.20±0.04
10.71 → 6.32	0.35±0.02	7.15 → 5.27	0.23±0.05
10.71 → 5.27	−0.04±0.02	6.32 → 0	−0.11±0.02
		5.27 → 0	0.39±0.02

[a]) A combination of the 9.05 → 0 and 9.22 → 0 transitions.

TABLE 6

Angular distribution coefficients corrected for finite detector size for γ-rays at $E_p = 634$ keV

Transition (MeV)	A_2	Transition (MeV)	A_2
10.81 → 0	−0.47±0.01	9.16 → 7.15	0.45±0.07
10.81 → 5.27	−0.70±0.07	9.16 → 6.32	−0.64±0.11
10.81 → 5.30	0.47±0.03	9.16 → 5.27	0.50±0.13
10.81 → 6.32	0.49±0.02	7.15 → 5.27	0.24±0.02
10.81 → 7.15	0.06±0.02	8.31 → 0	0.00±0.02
10.81 → 7.30	0.58±0.04	7.30 → 0	−0.07±0.01
10.81 → 8.31	−0.70±0.04	6.32 → 0	−0.13±0.01
10.81 → 9.16 [a])	0.14±0.03	5.30 → 0	−0.04±0.04
9.16 → 0 [b])	−0.10±0.03	5.27 → 0	0.20±0.03

[a]) This is the angular distribution of two 1.65 MeV γ-rays.
[b]) This is the angular distribution of the 9.05 and 9.16 MeV γ-rays.

REF. E. B. Dally, M. G. Croissiaux, and B. Schweitz
Phys. Rev. C2, 2057 (1970)

EL.EM. SYM.	A	Z
N	15	7

METHOD

[Page 1 of 4]

REF. NO. 70 Da 1 hmg

REACTION	RESULT	EXCITATION ENERGY	SOURCE		DETECTOR		ANGLE
			TYPE	RANGE	TYPE	RANGE	
E,E/	ABX	5-8	D	250,400	MAG-D		DST

Elastic data also given for both N^{14} and N^{15}.

LEVELS 5.3-7.56 FMF

TABLE III. Inelastic electron scattering cross sections from N^{15} at 250 and 400 MeV for the doublet level at 5.3 MeV, the 6.3-MeV level, and the triplet level at 7.3 MeV.

E_0 (MeV)	θ (deg)	$10^{33} \times d\sigma/d\Omega$ 5.3-MeV levels	6.3-MeV levels	7.3-MeV levels
250	45	311±31	451±39	296±38
	50	221±32	271±43	200±44
	55	149±24	160±17	140±24
	60	76±11	98±13	83±12
	65	57±9	65±9	48±6.7
	70	39±6	35.4±5	37.4±5
	75	28.5±4	26.6±4	31.7±5
	80	19.8±3	15.4±2	21.6±3
	82	16.6±2	10.5±1.5	19.1±2
	84	13.2±2	7.5±1.3	18.7±3
	85	12.7±2.4	6.5±2.0	16.0±3
	86	9.95±1.4	8.7±1.3	13.9±2
	90	8.28±1.3	4.8±0.7	10.4±1.5
	95	4.80±0.7	4.01±0.6	5.3±0.8
	100	3.19±0.54	2.16±0.3	3.9±0.6
	105	2.20±0.35	0.99±0.2	2.78±0.5
	110	1.78±0.4	0.41±0.13	1.64±0.4
400	32	613±95	475±11	458±103
	35	262±34	385±52	291±41
	38	220±20	266±30	247±27
	40	173±22	189±22	231±25
	42	140±10	122±15	154±21
	45	88.4±9	76±6	103±9
	48	56.8±4	41±4	67±7
	50	43.3±5	26±3	49±6
	53	25.8±3	15.0±2	33±4
	55	18.3±3	12.6±2	21±2.5
	58	10.5±1	5.19±0.9	13.3±2
	60	6.30±1	3.33±0.8	9.04±1.3
	65	3.04±0.7	1.36±0.4	3.76±0.5
	70	0.85±0.2	0.30±0.08	1.38±0.2
	75	0.33±0.08	0.14±0.04	0.36±0.09
	80	0.19±0.05	0.04±0.01	0.18±0.05

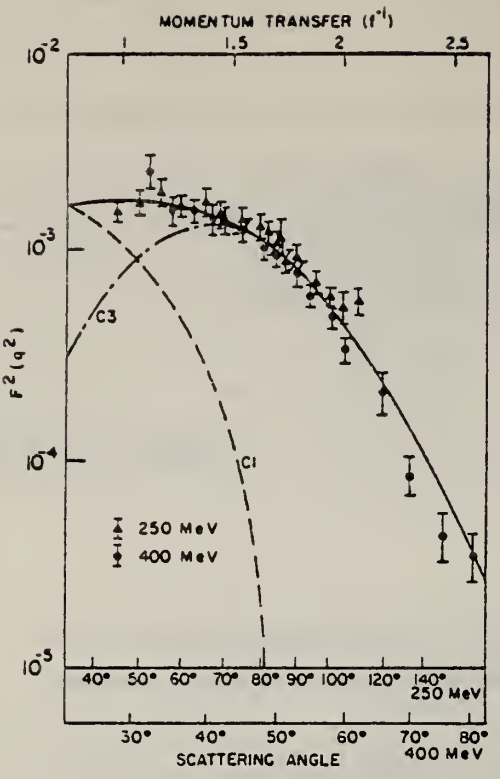

FIG. 6. The form factor versus momentum transfer for the inelastic electron scattering to the 5.3-MeV doulet in N^{15}. The curves labeled $C1$ and $C3$ are the separate contributions to the form factor of these transitions. The magnitude of each is found from a fit to the data as described in the text. The solid curve is the sum of the two transitions.

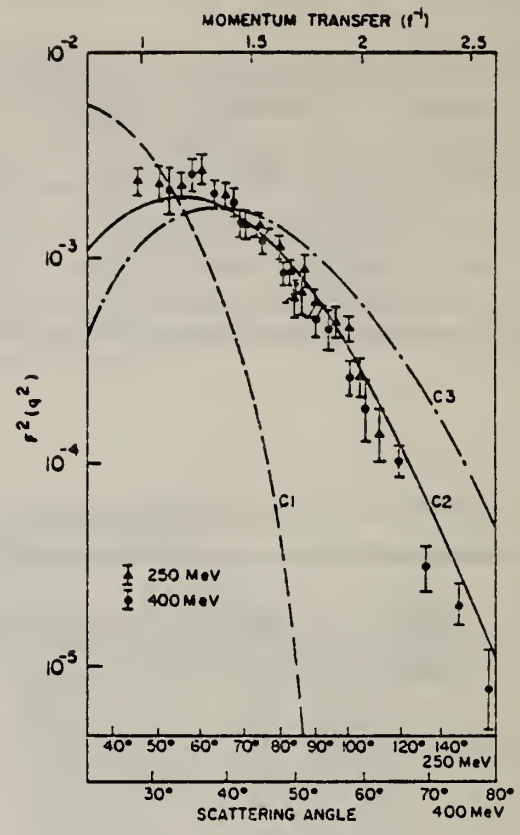

FIG. 7. The same as Fig. 5, for the excitation to the 6.3-MeV level in N^{15}. The curves $C1$, $C2$, and $C3$ are fitted to the data to find which multipole transition is involved in the excitation.

REACTION	RESULT	EXCITATION ENERGY	SOURCE		DETECTOR		ANGLE
			TYPE	RANGE	TYPE	RANGE	

TABLE VII. Summary of the experimental results on the inelastic scattering from N^{15}. Column 1 is the level energy. The 250- and 400-MeV data were separately fitted to the 6.3-MeV transition when $M1$ was included in the fit. The 250- and 400-MeV data were combined for the fits to the other levels and for the fit to the 6.3-MeV level when $C2$ was used alone. Column 2 gives the possible transitions. These transitions in parentheses were not considered for the fits. Column 3 identifies the fitting parameters defined in the text, and column 4 gives their values. Column 5 is the χ^2/degree of freedom for the fits. Column 6 contains the values of $B(M\lambda, J_i, J_f)\downarrow$ found in this experiment. Column 7 has values of $B\downarrow$ found from other experiments, and lifetimes found in this experiment in column 8 can be compared with other experimental values in column 9 and the values obtained using an independent particle model (column 10). The errors are standard deviations weighted by the χ^2 of the fit.

Level	Mode of excitation	Fitted parameters: Parameter	Value	χ^2/degree of freedom	$B(M\lambda)\downarrow$ This expt.	$B(M\lambda)\downarrow$ Other expts.	Lifetimes τ (sec) This expt.	Other values	Weisskopf
5.27	$C3$ ($M2+E3$)	β	$(0.104\pm0.005)\times10^{-1}$	42.8/31	$(62.5\pm2.1)e^2$	$60e^2$ [a]	$(2.46\pm0.1)\times10^{-10}$	2.7×10^{-12} [b]; $>10^{-12}$ [c]; $>5\times10^{-12}$ [d]	11×10^{-10}
5.30	$C1$ ($E1$)	α	$(0.124\pm0.02)\times10^{-1}$		$(0.362\pm0.07)e^2$		$(1.16\pm0.2)\times10^{-17}$	4.3×10^{-14} [e]; $<3\times10^{-13}$ [d]	1.1×10^{-17}
6.3	$C2$ ($M1+E2$)	α	$(0.369\pm0.02)\times10^{-1}$	66/33	$(4.03\pm0.14)e^2$	$4.9e^2$ [a]	$(1.97\pm0.2)\times10^{-14}$		2.23×10^{-14}
6.3 (250)	$C2+M1$ ($E2$)	α	$(0.325\pm0.04)\times10^{-1}$	11.7/14	$(3.49\pm0.3)e^2$	$4.9e^2$ [a]	$(2.18\pm0.3)\times10^{-14}$	1.1×10^{-14} [e]; 1.65×10^{-14} [f]; $<4.5\times10^{-14}$ [g]	2.23×10^{-14}
		β	(0.114 ± 0.06)		$(0.0853\pm0.04)e^2$		$(2.89\pm1.4)\times10^{-17}$	1.94×10^{-16} [e]; 2.43×10^{-16} [f]	1.3×10^{-16}
		γ	(0.072 ± 0.04)						
6.3 (400)	$C2+M1$ ($E2$)	α	$(0.207\pm0.02)\times10^{-1}$	6.1/13	$(2.26\pm0.2)e^2$	$4.9e^2$ [a]	$(3.53\pm0.3)\times10^{-14}$		2.23×10^{-14}
		β	(0.168 ± 0.06)		$(0.182\pm0.06)e^2$		$(1.35\pm0.6)\times10^{-17}$		1.3×10^{-16}
		γ	(0.124 ± 0.06)						
7.30	$C1$ ($E1+M2$)	α	$(0.846\pm0.2)\times10^{-2}$	33/31	$(0.123\pm0.03)e^2$		$(1.30\pm0.3)\times10^{-17}$	$<2.5\times10^{-14}$ [g]	0.41×10^{-17}
7.56	$C3$ ($E3$)	β	$(0.124\pm0.004)\times10^{-1}$		$(56.0\pm1.6)e^2$	$60e^2$ [a]	$(2.19\pm0.07)\times10^{-11}$		9.2×10^{-11}

[a] B. G. Harvey, J. R. Meriwether, J. Mahoney, A. Bussiere de Nercy, and D. J. Horen, Phys. Rev. 146, 712 (1966).
[b] P. G. Bizzeti, A. M. Bizzeti-Sona, S. Kalbitzer, and B. Povh, Nucl. Phys. A104, 577 (1967).
[c] T. K. Alexander, A. E. Litherland, and C. Broude, Can. J. Phys. 43, 2310 (1965).
[d] E. K. Warburton, K. W. Jones, D. E. Alburger, C. Chasman, and R. A. Ristinen, Phys. Rev. Letters 14, 146 (1965).
[e] G. A. Beer, P. Brix, H.-G. Clerc, and B. Laube, Phys. Letters 26B, 506 (1968).
[f] A. R. Poletti, E. K. Warburton, and D. Kurath, Phys. Rev. 155, 1096 (1967).
[g] R. D. Gill, J. S. Lopes, O. Haussen, and H. J. Rose, Lifetime Measurements in Mass 15, Internal Report, Nuclear Physics Laboratory, University of Oxford, Oxford, England, 1968 (unpublished), Ref. 27/68.

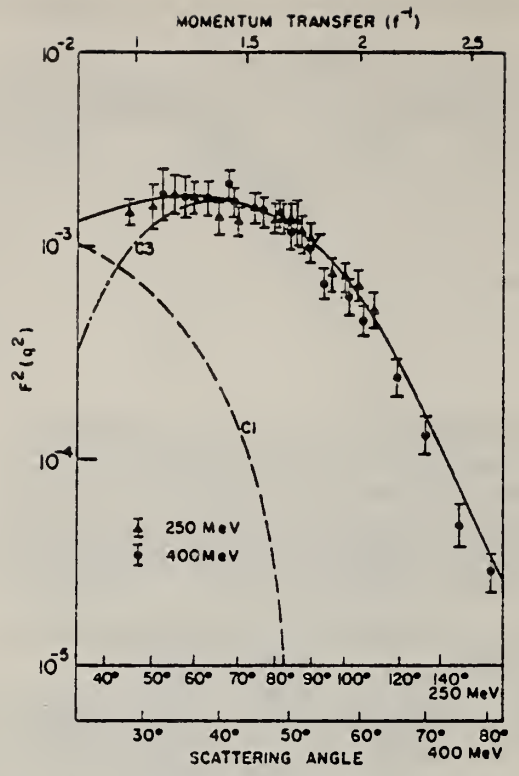

FIG. 8. The same as Fig. 5 for the excitation to the triplet of levels at 7.3 MeV in N^{15}. The curves have the same significance as in Fig. 5. Only two levels are excited strongly.

REF.

V. P. Denisov, L. A. Kul chitskii and I. Ya. Chubukov
Yad. Fiz. 14, 889 (1971)
Sov. J. Nucl. Phys. 14, 497 (1972)

ELEM. SYM.	A	Z
N	15	7

METHOD

REF. NO.	
71 De 2	hmg

REACTION	RESULT	EXCITATION ENERGY	SOURCE		DETECTOR		ANGLE
			TYPE	RANGE	TYPE	RANGE	
G,P	ABX	19-39	C	19-39	TEL-D		90
		(19.6-38.3)		(19.6-38.3)			

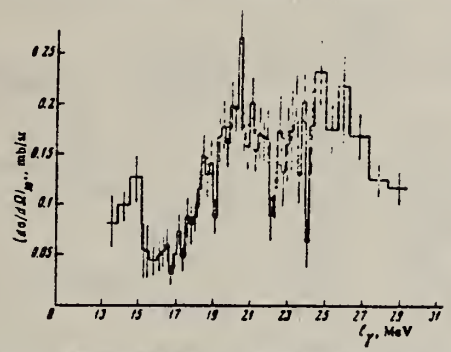

FIG. 3. Cross section $d\sigma/d\Omega$ for the reaction $N^{15}(\gamma, p_0)C^{14}$ with formation of the final nucleus in the ground state for protons emitted at an angle 90° with respect to the γ-ray beam direction.

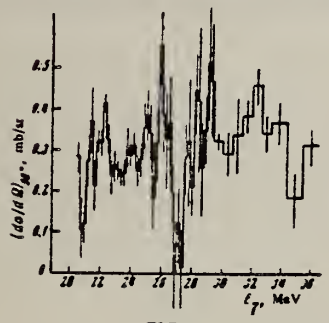

FIG. 4

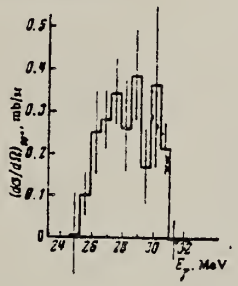

FIG. 5

FIG. 4. Cross section $d\sigma/d\Omega$ for the reaction $N^{15}(\gamma, p)C^{14}$ with formation of the final nucleus in a state with energy 7.01 MeV ($J^\pi = 2^+$) for protons emitted at an angle 90° with respect to the γ-ray beam direction.

FIG. 5. Cross section $d\sigma/d\Omega$ for the reaction $N^{15}(\gamma, p)C^{14}$ with formation of the final nucleus in a state with energy 10.74 MeV for protons emitted at an angle 90° with respect to the γ-ray beam direction.

Table I. Integrated cross sections for the different branches of the (γ, p) reaction in N^{15} and O^{16}

Integration limits, MeV	$N^{15}(\gamma, p)C^{14}$ reaction		$O^{16}(\gamma, p)N^{15}$ reaction, ref. 9	
	State of final nucleus C^{14}	Integrated cross section, MeV-mb	State of final nucleus N^{15}	Integrated cross section, MeV-mb
12.5 — 30.0	Ground, $J^\pi = 0^+$	21±3	Ground, $J^\pi = 1/2^-$	40.5±4.0
20.5 — 32.0	7.01 MeV, $J^\pi = 2^+$	32±5 *	6.33 MeV, $J^\pi = 3/2^-$	27±3
12.5 — 30.5	Sum over all states	72±10 *	Sum over all states	84±8

*The errors take into account the uncertainty in the angular distributions.

Table II. Theoretical and experimental integrated cross sections for the different channels of the reaction $N^{15}(\gamma, p)C^{14}$

Integration limits, MeV	State of the final nucleus C^{14}	Integrated cross section, MeV-mb	
		Theory [7]	Experiment
0—30.5	Ground	22.4	22±3
0—36.4	7.01 MeV	67.8	52±7 *
0—36.4	10.7 MeV	26.5	15±3 *
0—30.5	Sum over all states	107.3	73±10 *

*The errors take into account the uncertainty in the angular distributions.

REF. H. M. Kuan, C. J. Umbarger and D. G. Shirk
Nucl. Phys. A160, 211 (1971)

ELEM. SYM.	A	Z
N	15	7

METHOD

REF. NO. 71 Ku 1 egf

REACTION	RESULT	EXCITATION ENERGY	SOURCE		DETECTOR		ANGLE
			TYPE	RANGE	TYPE	RANGE	
P,G	ABX	11-13	D	1-3	SCD-D	0-12	DST

TABLE 1

Gamma transitions of the first two $T = \frac{1}{2}$ states of ^{15}N

Initial state			Final state					Theory [a]	
E_x (MeV)	J^π	$\Gamma_{c.m.}$ (keV)	E_x (MeV)	J^π	Branching ratio (%)	Γ_γ (meV)	Mixing ratio	Mode	Γ_γ (meV)
11.61	$\frac{1}{2}^+$	450±50	0	$\frac{1}{2}^-$	90.7±3.0	3900±1600		E1	76000
			5.270	$\frac{1}{2}^+$	< 1	< 40		E2	12
			5.299	$\frac{3}{2}^+$	7.4±1.5	320± 150		M1	2130
			6.328	$\frac{3}{2}^-$	1.9±1.5	80± 60			
12.523±008	$\frac{1}{2}^+$	60±10	0	$\frac{1}{2}^-$	< 1	< 4		M2	47
			5.270	$\frac{1}{2}^+$	92 ±2	310± 130	−0.02±0.04 (E2/M1)	M1	5300
								E2	9
			5.299	$\frac{3}{2}^+$	< 1	< 4		E2	5
			6.328	$\frac{3}{2}^-$	8 ±2	30± 15	−0.02±0.04 (M2/E1)		

[a]) Calculated from Zuker-Buck-McGrory [5]) wave functions.

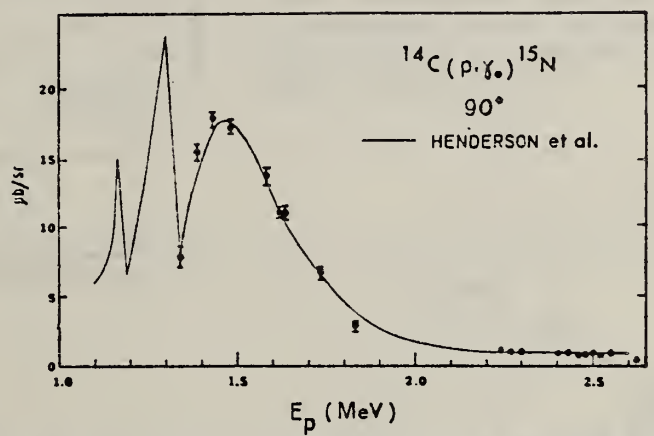

Fig. 4. The 90° excitation function of $^{14}C(p,\gamma_0)^{15}N$, showing the presence of the broad first $T = \frac{1}{2}$ resonance near $E_p = 1.5$ MeV and the absence of structure near $E_p = 2.482$ MeV for the second $T = \frac{1}{2}$ state of ^{15}N. The solid line is from Henderson *et al.* [3]) normalized to the present data.

[3] J.D. Henderson, E.L. Hudspeth, W.R. Smith, Phys. Rev. 172 (1968) 1058.

[5] A.P. Zuker, B. Buck, J.B. McGrory, BNL-14085.

[over]

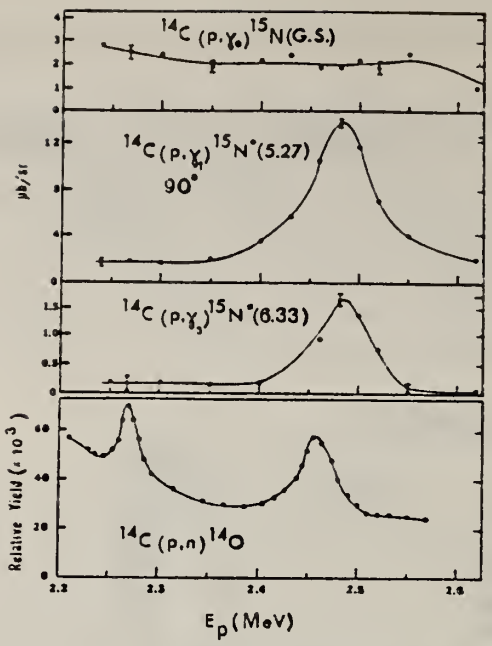

Fig. 5. The 90° excitation functions, in the region of the second $T = \frac{1}{2}$ state of ^{15}N, of three capture reactions: $^{14}C(p,\gamma_0)$, (p,γ_1), and (p,γ_3). The 90° yield curve of $^{14}C(p,n)^{14}O$ is shown at the bottom.

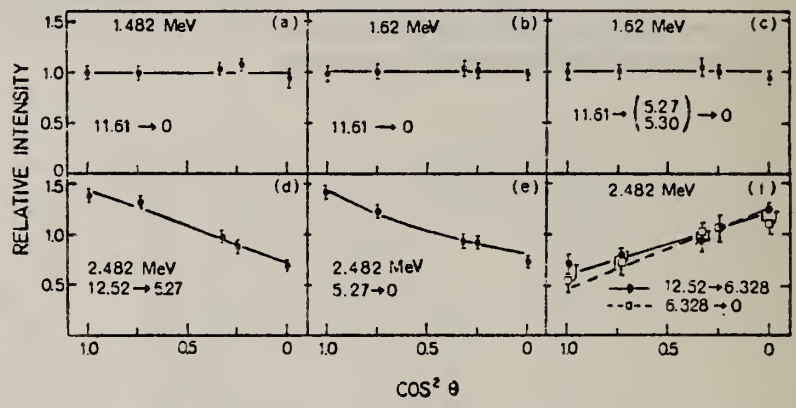

Fig. 6. The angular distributions of the indicated $^{14}C(p,\gamma)$ transitions. The solid lines in (a), (b) and (c) are isotropic, those in (d), (e) and (f) are from the mixing ratio calculations.

REF.

R.W. Gellie, K.H. Lokan, N.K. Sherman, R.G. Johnson, J.I. Lodge
Can. J. Phys. 50, 1689 (1972)

ELEM. SYM.	A	Z
N	14	7

METHOD

REF. NO.	
72 Ge 3	hmg

REACTION	RESULT	EXCITATION ENERGY	SOURCE		DETECTOR		ANGLE
			TYPE	RANGE	TYPE	RANGE	
G,N	ABX	10-30	C	15-30	TOF-D		90

Integrated cross section (29 MeV) for all neutron producing interactions is 88±5 MeV mb.

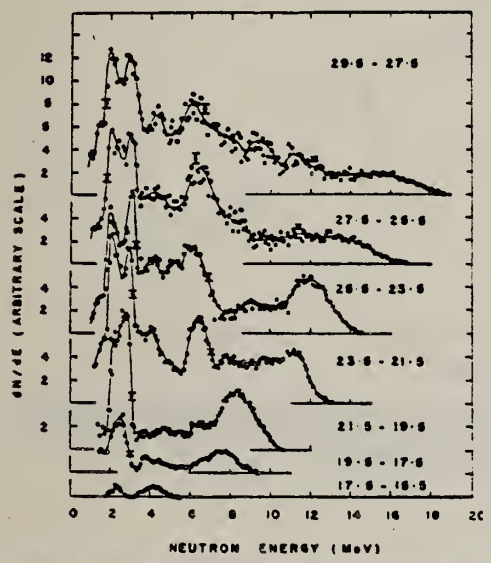

FIG. 6. Photoneutron difference distributions, derived from the data of Fig. 2.

TABLE I. Integrated partial cross sections in the decay of ^{14}N

Level in $A = 13$ nucleus	Dominant configuration[a]	Integrated cross section to 29 MeV (MeV mb) (γ,n)	(γ,p)
Ground state	$(p_{3/2})^8(p_{1/2})^1$	20[b]	20[c,d,f]
3.51, 3.68	$(p_{3/2})^7(p_{1/2})^2$	6[b]	7[d], 6[e]
7.39, 7.55	$(p_{3/2})^7(p_{1/2})^2$	—	17[e]
8.92, 8.86	$(p_{3/2})^7(p_{1/2})^2$	—	Visible, but not separate from other reactions
9.48, 9.52			
11.88, 11.80	$(p_{3/2})^7(p_{1/2})^2$	—	5[e,g]

[a] Ball and Cerny (1969).
[b] This experiment.
[c] Kosiek *et al.* (1964).
[d] Thompson *et al.* (1970).
[e] Benz (1971).
[f] By detailed balance from ^{13}C(p,γ$_0$)^{14}N (Riess *et al.* 1971).
[g] Includes only that component which yields neutrons to the ground state of ^{12}C.

"Total integrated cross sections were obtained from the 90° differential cross sections by assuming an isotropic angular distribution."

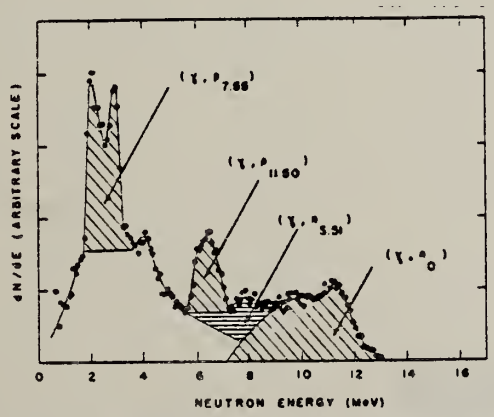

FIG. 7. Breakdown of the (23.5–21.5 MeV) difference spectrum into its major components (see text).

1086

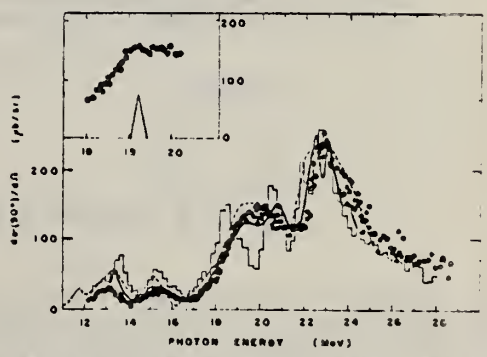

FIG. 4. Cross sections for ground-state photonucleon emission. (●) (γ,n$_0$): present experiment. (--) (γ,n): King *et al.* (1960). Histogram (γ,p$_0$): Kosiek *et al.* (1964). (—) (γ,p$_0$): by detailed balance from the inverse proton capture reaction (Riess *et al.* 1971). The inset shows the (γ,n$_0$) cross section in the region around 19 MeV, together with the resolution function, and indicates that there is no strong structure evident in this region, at least in the neutron channel.

REF.

J. J. Ramirez, R. A. Blue and H. R. Weller
Phys. Rev. C5, 17 (1972)

ELEM. SYM.	A	Z
N	15	7

METHOD

REF. NO.: 72 Ra 2 | hmg

REACTION	RESULT	EXCITATION ENERGY	SOURCE TYPE	SOURCE RANGE	DETECTOR TYPE	DETECTOR RANGE	ANGLE
P,G	RLY	14	D	4	NAI-D		60
		(13.42)		(3.44)			

$\frac{3}{2}^+$ assignment to the 13.42 MeV level.

J-PI, 13.42 MEV LEVEL

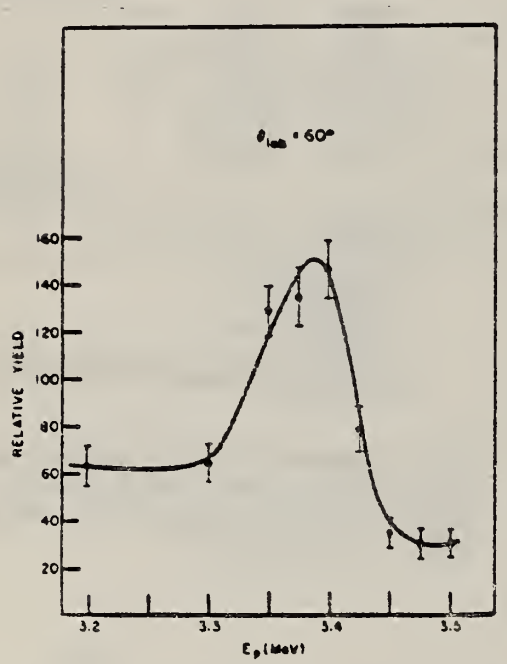

FIG. 15. The measured excitation curve for the reaction $^{14}C(p,\gamma_0)^{15}N$ in the vicinity of the 13.42-MeV level.

REF.

H. R. Weller, R. A. Blue, E. M. Bernstein & J. J. Ramirez
Nucl. Phys. A185, 284 (1972)

ELEM. SYM.	A	Z
N	15	7

METHOD

REF. NO. 72 We 2 egf

REACTION	RESULT	EXCITATION ENERGY	SOURCE		DETECTOR		ANGLE
			TYPE	RANGE	TYPE	RANGE	
P,G	ABX	13-17	D	3-8	NAI-D		DST

J-PI 547

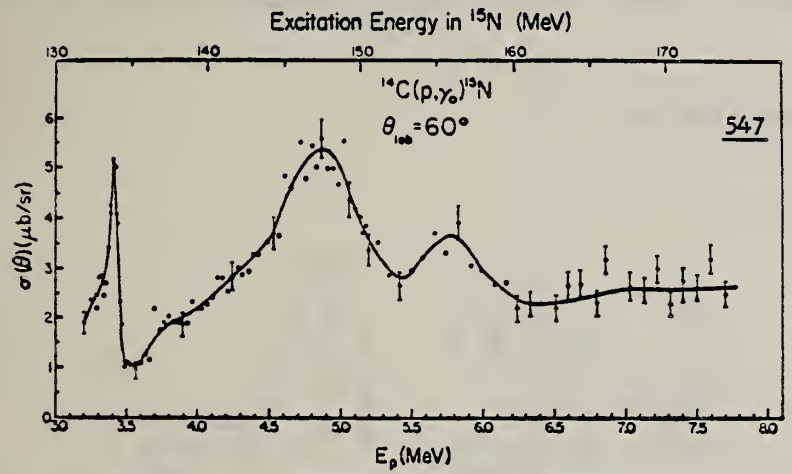

Fig. 2. The measured excitation function for the $^{14}C(p,\gamma_0)^{15}N$ reaction. The error bars shown represent typical statistical errors associated with the data points. The solid line is a smooth curve drawn through the data points.

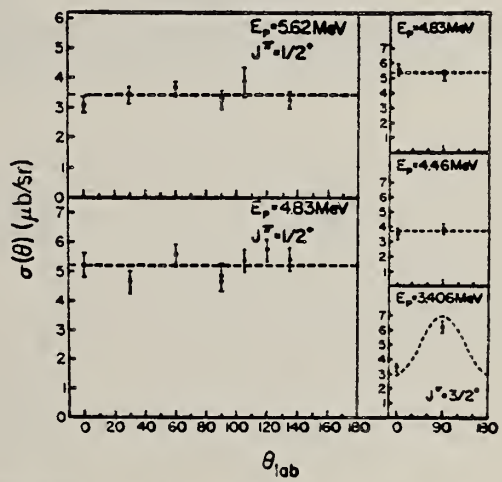

Fig. 3. The measured angular distributions in the region of the pygmy resonance. The two-point angular distribution measured at E_p = 3.406 MeV, on the $\frac{3}{2}^+(\frac{3}{2})$ level, is also shown. The dashed lines indicate the apparent isotropy in all cases except at E_p = 3.406 MeV, where the curve is the angular distribution calculated for a $j^\pi = \frac{3}{2}^+$ resonance. Two independent measurements are shown for E_p = 4.83 MeV.

REF. V.P. Denisov and I.Ya. Chubukov
Yad. Fiz. 17, 682 (1973)
Sov. J. Nucl. Phys. 17, 354 (1973)

EL.EM. SYM.	A	Z
N	15	7

METHOD

REF. NO. 73 De 13 hmg

REACTION	RESULT	EXCITATION ENERGY	SOURCE		DETECTOR		ANGLE
			TYPE	RANGE	TYPE	RANGE	
G,D	ABX	19- 25	C	19- 30	TEL-D		90

$$\int_{19.5}^{25} \sigma d\sigma = 1.0 \pm 0.3 \text{ mb-MeV}$$

for assumed isotropic angular distribution.

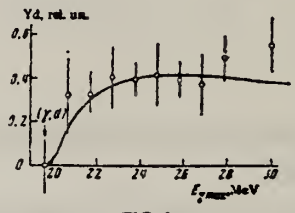

FIG. 2

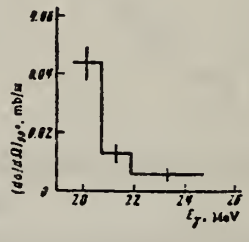

FIG. 3

FIG. 2. Yield of deuterons with energy 3–5 MeV as a function of $E_{\gamma\,max}$. The curve is the isochromat corresponding to the (γ, d) reaction with formation of the C^{13} nucleus in the ground state. The arrow indicates the kinematic threshold of this reaction.

FIG. 3. Cross section $d\sigma/d\Omega$ for deuterons emitted at 90° to the γ-ray direction in the reaction $N^{15}(\gamma, d)C^{13}$ with formation of the final nucleus in the ground state.

REF. H. R. Weller, R. A. Blue, J. J. Ramirez, E. M. Bernstein
Nucl. Phys. A207, 177 (1973)

ELEM. SYM.	A	Z
N	15	7

METHOD

REF. NO. 73 We 2 egf

REACTION	RESULT	EXCITATION ENERGY	SOURCE		DETECTOR		ANGLE
			TYPE	RANGE	TYPE	RANGE	
P,G	ABX	13- 22	D	3- 12	NAI-D		DST

345

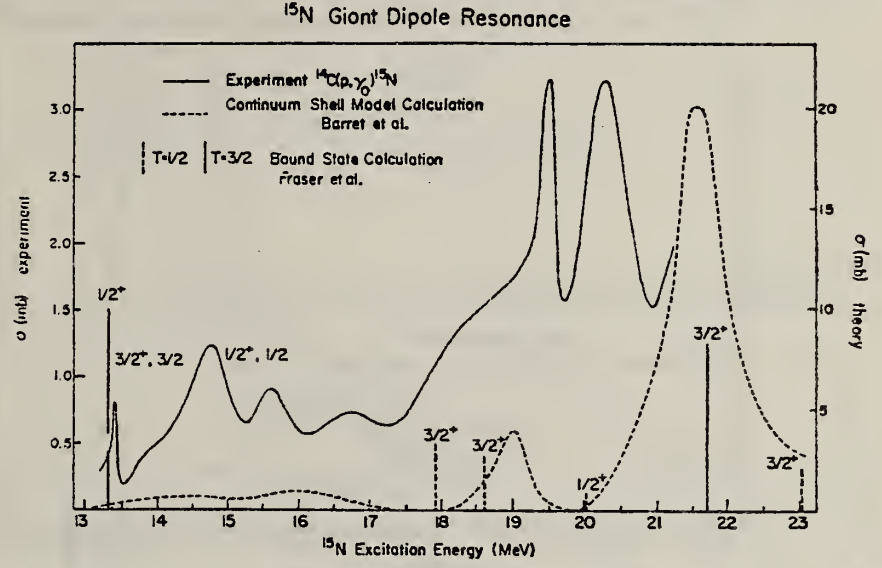

Fig. 4. The solid curve is the transformed integrated cross section obtained in the present work. The bound and continuum calculations are also shown.

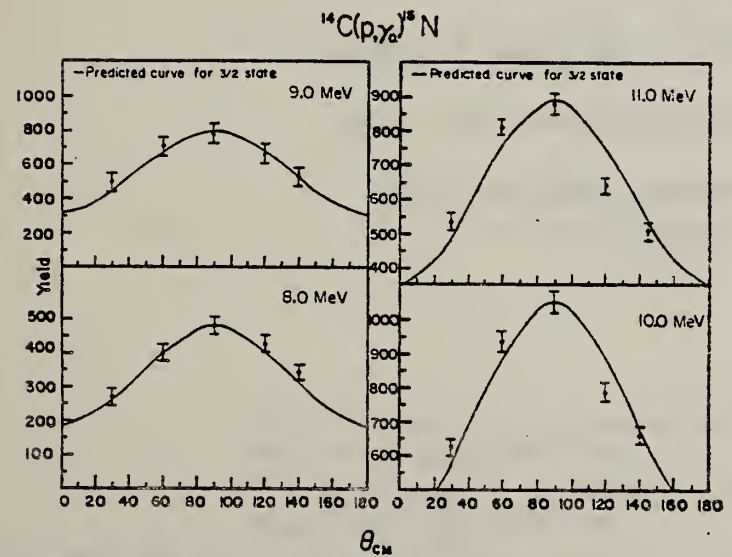

Fig. 3. Measured angular distributions for the $^{14}C(p,\gamma_0)^{15}N$ reaction with the calculated curves for a pure $\frac{3}{2}^+$ level decaying via E1 radiation to ground.

(over)

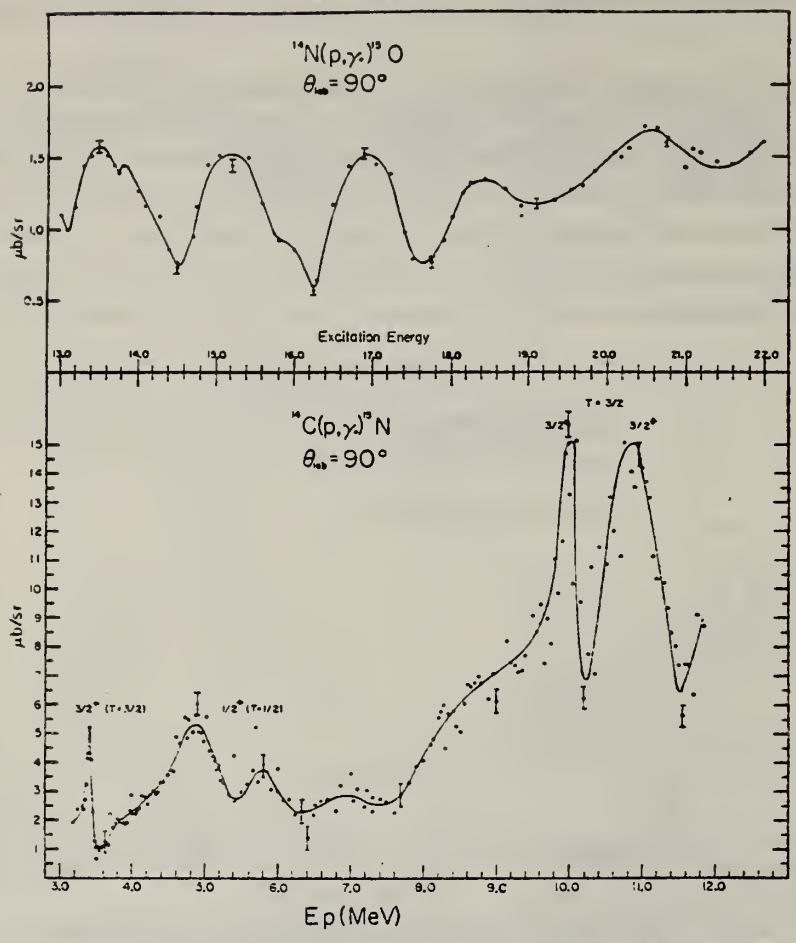

Fig. 2. Excitation curves for the $^{14}C(p,\gamma_0)^{15}N$ and $^{14}N(p,\gamma_0)^{15}O$ reactions. Both are plotted on the same excitation energy scale. The $^{14}N(p,\gamma_0)^{15}O$ data were taken from ref. [3]).

[3] H.M. Kuan, N. Hasinoff, W.J. O'Connell, S.S. Hanna, Nucl. Phys. A151 (1970) 129.

[5] R.F. Fraser, R.K. Garnsworthy, B.M. Spicer, Nucl. Phys. A156, (1970) 489.

[6] R.F. Barrett, R.F. Fraser, P.P. Delsanto, Phys. Letts. 40B (1972) 326.

REF. H. R. Weller and R. A. Blue
Nucl. Phys. A211, 221 (1973)

ELEM. SYM.	A	Z
N	15	7

METHOD

REF. NO. 73 We 3 egf

REACTION	RESULT	EXCITATION ENERGY	SOURCE TYPE	SOURCE RANGE	DETECTOR TYPE	DETECTOR RANGE	ANGLE
D,G	ABX	17- 20	D	1- 4	NAI-D		DST

847

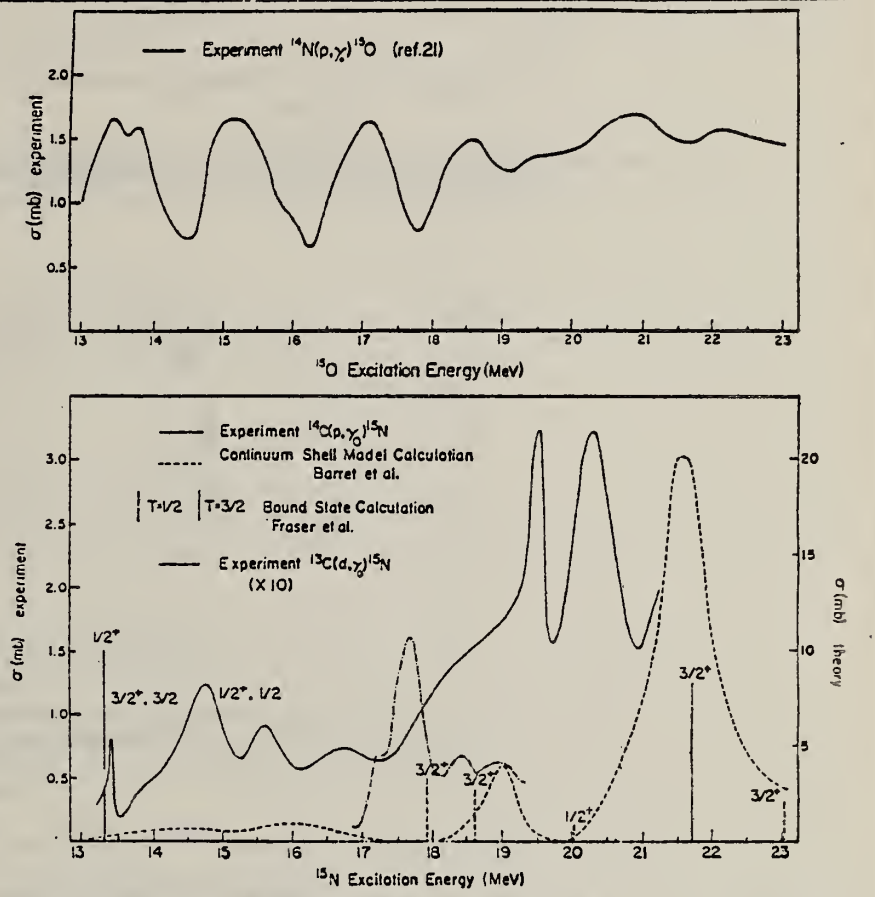

Fig. 9. Comparison of the present experiment with the $^{14}C(p,\gamma_0)^{15}N$ and the $^{14}N(p,\gamma_0)^{15}O$ experiments. All data are shown as integrated, detailed-balanced cross sections. The bound state calculations of ref. [19]) and the continuum calculations of ref. [20]) are also shown.

[19] R. F. Fraser, R. K. Garnsworthy, B.M. Spicer, Nucl. Phys. A156 (1970) 489.

[20] R. F. Barrett, R. F. Fraser, P. P. Delsanto, Phys. Lett. 40B (1972) 326.

(over)

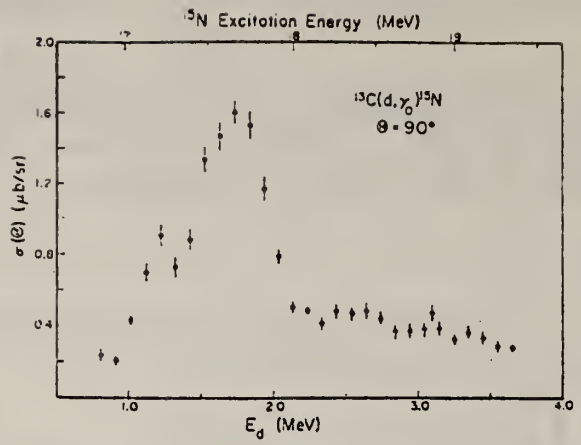

Fig. 7. The measured excitation function for the $^{13}C(d,\gamma_0)^{15}N$ reaction at 90°. The error bars represent the statistical errors associated with the data points.

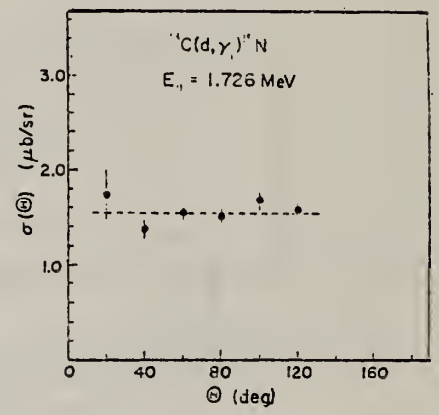

Fig. 8. The measured $^{13}C(d,\gamma_0)^{15}N$ angular distribution at 1.726 MeV. The error bars represent the statistical errors associated with the data points.

REF. H.R. Weller, R.A. Blue, and T. Mo
PICNS-73, Vol.II, p.935 (1973) Asilomar

ELEM. SYM.	A	Z
N	15	7

METHOD

REF. NO. 73 We 4 egf

REACTION	RESULT	EXCITATION ENERGY	SOURCE		DETECTOR		ANGLE
			TYPE	RANGE	TYPE	RANGE	
D,G	RLX	17- 20	D	1- 4	NAI-D		90

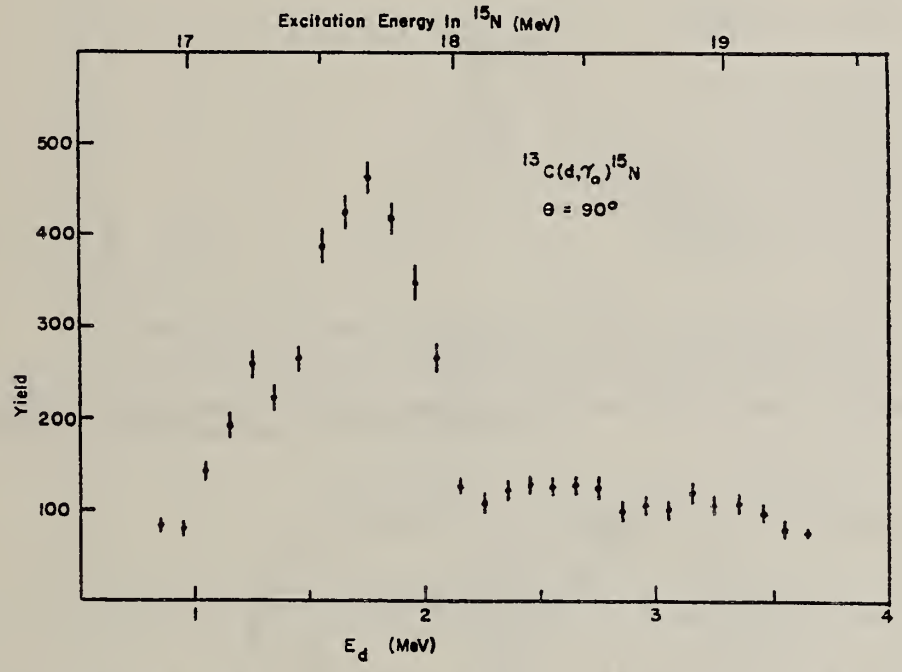

FIG. 1. The 90° excitation curve for the $^{13}C(d,\gamma_0)^{15}N$ reaction. The error bars indicate the statistical error associated with the data points.

REF.

H.R. Weller, N.R. Roberson, D. Rickel, C.P. Cameron, R.D. Ledford, and T.B. Clegg
Phys. Rev. Letters 32, 177 (1974)

EL EM. SYM.	A	Z
N	15	7

METHOD

REF. NO.: 74 We 1 | hmg

REACTION	RESULT	EXCITATION ENERGY	SOURCE		DETECTOR		ANGLE
			TYPE	RANGE	TYPE	RANGE	
$ P,G	ABX	19- 26	D	9- 17	NAI-D		UKN

POLARIZED PROTONS

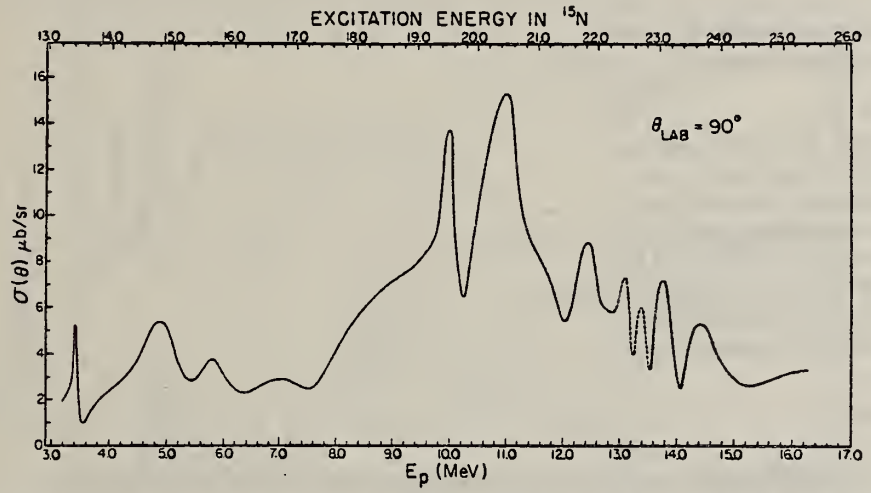

FIG. 1. Yield curve for the reaction $C^{14}(p,\gamma)^{15}N$. Data below 9.0 MeV are taken from Ref. 5. The dashed portion of the curve reflects the poor experimental statistics in this region.

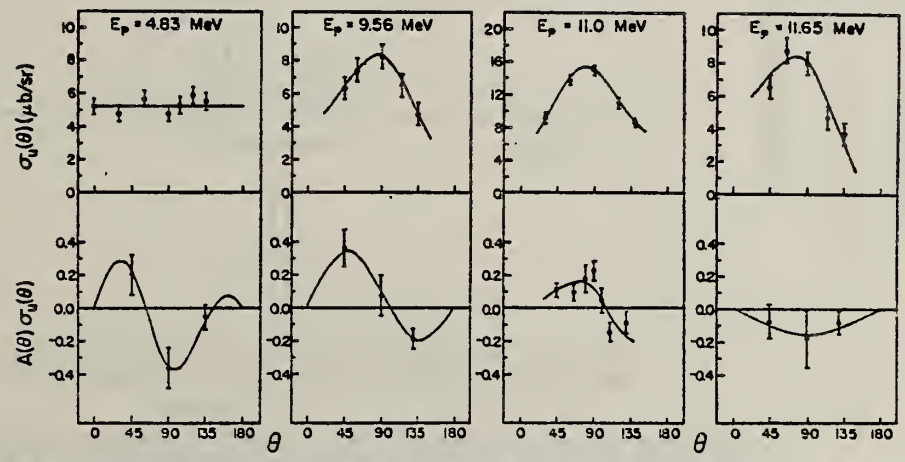

FIG. 2. Angular distributions and analyzing power for the reaction $^{14}C(p,\gamma)$. The error bars represent the statistical errors associated with the data points. The solid lines are fits discussed in the text.

[5] H.R. Weller, R.A. Blue, J.J. Ramirez, and E.M. Bernstein, Nucl. Phys. A207, 177 (1973).

(over)

TABLE I. The coefficients a_k and b_k. The parentheses indicate that the enclosed terms were not required to obtain satisfactory χ^2 for these cases.

Energy	a_1/a_0	a_2/a_0	a_3/a_0	b_1	b_2	b_3
4.83	−0.08±0.08	0.03±0.09		−0.18±0.09	0.10±0.06	0.17±0.08
8.5	0.02±0.2	−0.75±0.43		0.08±0.09	0.14±0.07	(−0.01±0.07)
9.56	0.19±0.10	−0.59±0.22		0.11±0.08	0.22±0.05	(0.02±0.07)
10.0	0.06±0.02	−0.47±0.04		0.04±0.09	0.08±0.06	0.12±0.07
10.3	0.38±0.11	−0.43±0.23		−0.15±0.13	(0.05±0.09	(0.04±0.11)
11.0	0.12±0.03	−0.48±0.06	−0.13±0.07	0.05±0.03	0.12±0.03	−0.07±0.03
11.65	0.50±0.12	−0.54±0.25		−0.16±0.12	(−0.01±0.08)	(0.03±0.10)
12.45	0.26±0.12	−0.55±0.24		−0.07±0.09	0.20±0.07	0.09±0.07

The analyzing power $A(\theta)$ was obtained at a given energy and angle from the expression[2]

$$A(\theta) = -1(N_u - N_d)/P(N_u + N_d), \quad (1)$$

where N_u and N_d are the γ-ray yields for spin up and spin down, respectively. In addition to the analyzing power, data were taken with an unpolarized beam to extend previous cross-section measurements[5,6] from $E_p = 12$ to 16.2 MeV and to obtain angular distributions needed for the present analysis. The angular distributions of cross section were expanded in terms of Legendre polynomials as

$$\sigma_u(\theta) = a_0[1 + \sum_{k=1} a_k P_k(\cos\theta)] \quad (2)$$

and the analyzing power was expanded as

$$A(\theta)\sigma_u(\theta) = \sum_{k=1} b_k P_k^1(\theta), \quad (3)$$

where a_0 in $\sigma_u(\theta)$ of Eq. (3) was set equal to 1.0.

REACTION	RESULT	EXCITATION ENERGY	SOURCE		DETECTOR		ANGLE
			TYPE	RANGE	TYPE	RANGE	
P,G	ABX	13- 38	D	2- 30	NAI-D		DST

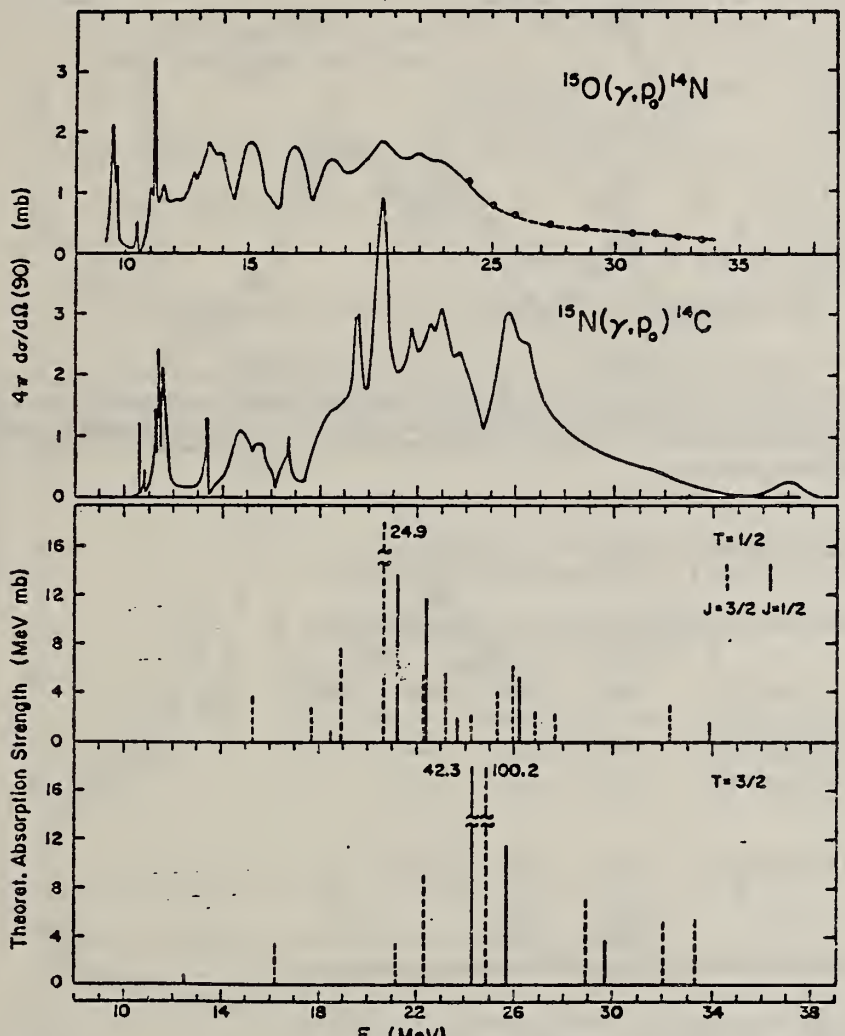

FIG. 6. Comparison of the experimental results from the $^{15}O(\gamma,p_0)^{14}N$ and $^{15}N(\gamma,p_0)^{14}C$ reactions and the theoretical predictions from the 2h-1p model (case B). The data below 25 MeV in the top curve are from Ref. 4, the data points at higher energies stem from the present work. The theoretical plots give the $T=\frac{1}{2}$ and $\frac{3}{2}$ components of the computed integrated photoabsorption cross section proportional to $E_\gamma[B(E1\uparrow)]$. Dashed and solid lines indicate $J=\frac{3}{2}$ and $\frac{1}{2}$, respectively. The top experimental curve should relate to the $T=\frac{1}{2}$ part while the $^{15}N(\gamma,p_0)^{14}C$ curve contains both T components.

Comment on "E1 excitations in $A = 15$ nuclei"

H. R. Weller
University of Florida and Triangle Universities Nuclear Laboratory,† Durham, North Carolina 27706*

N. R. Roberson, D. G. Rickel, C. P. Cameron, and R. D. Ledford
Duke University and Triangle Universities Nuclear Laboratory, Duke Station, Durham, North Carolina 27706

(Received 8 December 1975)

It is shown that the recent $J^\pi = \frac{1}{2}^+$ assignment for the level observed in the $^{14}C(p,\gamma_0)^{15}N$ reaction at $E_p = 6.925$ MeV is not unique.

Phys. Rev. C13, 2062 (1976)

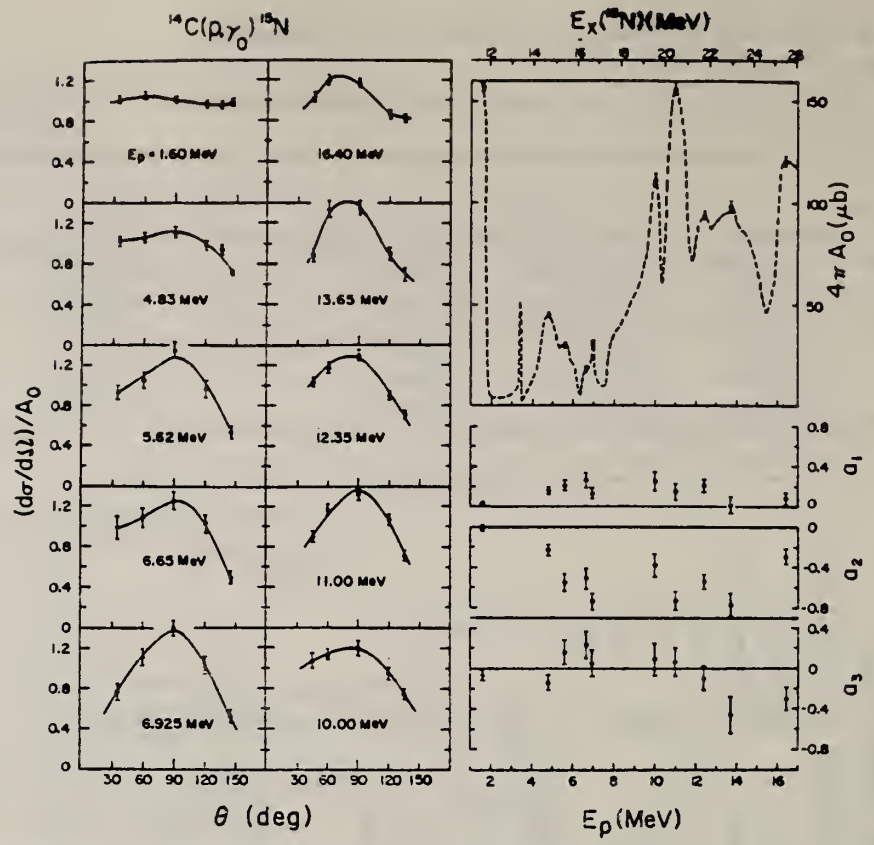

FIG. 4. Normalized angular distributions of the γ_0 yield at several bombarding energies corresponding to peaks in the excitation function. The curve at $E_p = 1.6$ MeV should be isotropic. Solid curves are fits with Legendre polynomials up to P_3. The total cross section $4\pi A_0$ and the normalized Legendre coefficients a_1, a_2, a_3 obtained from the fits are plotted on the right hand side of the figure.

TABLE II. Experimental and calculated reduced $E1$ transition rates, in units of $e^2\,\mathrm{fm}^2$, from the lowest $T=\frac{1}{2}$ states with $J^\pi = \frac{1}{2}^+$, $\frac{5}{2}^+$, and $\frac{3}{2}^+$, to the ground state ($\frac{1}{2}^-$) and the third excited state ($\frac{3}{2}^-$) of ^{15}N.

Initial state J^π, T	Final state E_x (MeV)	Final state J^π	Reduced transition rates Exp.[a]	Theory Case A	Theory Case B	Theory Soga	Theory ZBM[a]
$\frac{1}{2}^+$, $\frac{1}{2}$	0	$\frac{1}{2}^-$	0.030 ± 0.012 (0.010 ± 0.003)[b]	0.009	0.013	0.056	0.0683
	6.33	$\frac{3}{2}^-$	0.0065 ± 0.0052	0.003	0.005	0.010	···
$\frac{5}{2}^+$, $\frac{1}{2}$	0	$\frac{1}{2}^-$		0	0	0	0
	6.33	$\frac{3}{2}^-$	0.0015 ± 0.0008	0.001	0.004	0.015	···
$\frac{3}{2}^+$, $\frac{3}{2}$	0	$\frac{1}{2}^-$		0.011	0.026		
	6.33	$\frac{3}{2}^-$		0.0003	0.0001		

[a] See Ref. 4.
[b] See Ref. 23.

[4] H.M. Kuan et al., Nucl. Phys. A160, 211 (1971); A196, 634 (1972).
[23] G.W. Phillips et al., Phys. Rev. C5, 297 (1972).

REACTION	RESULT	EXCITATION ENERGY	SOURCE TYPE	SOURCE RANGE	DETECTOR TYPE	DETECTOR RANGE	ANGLE

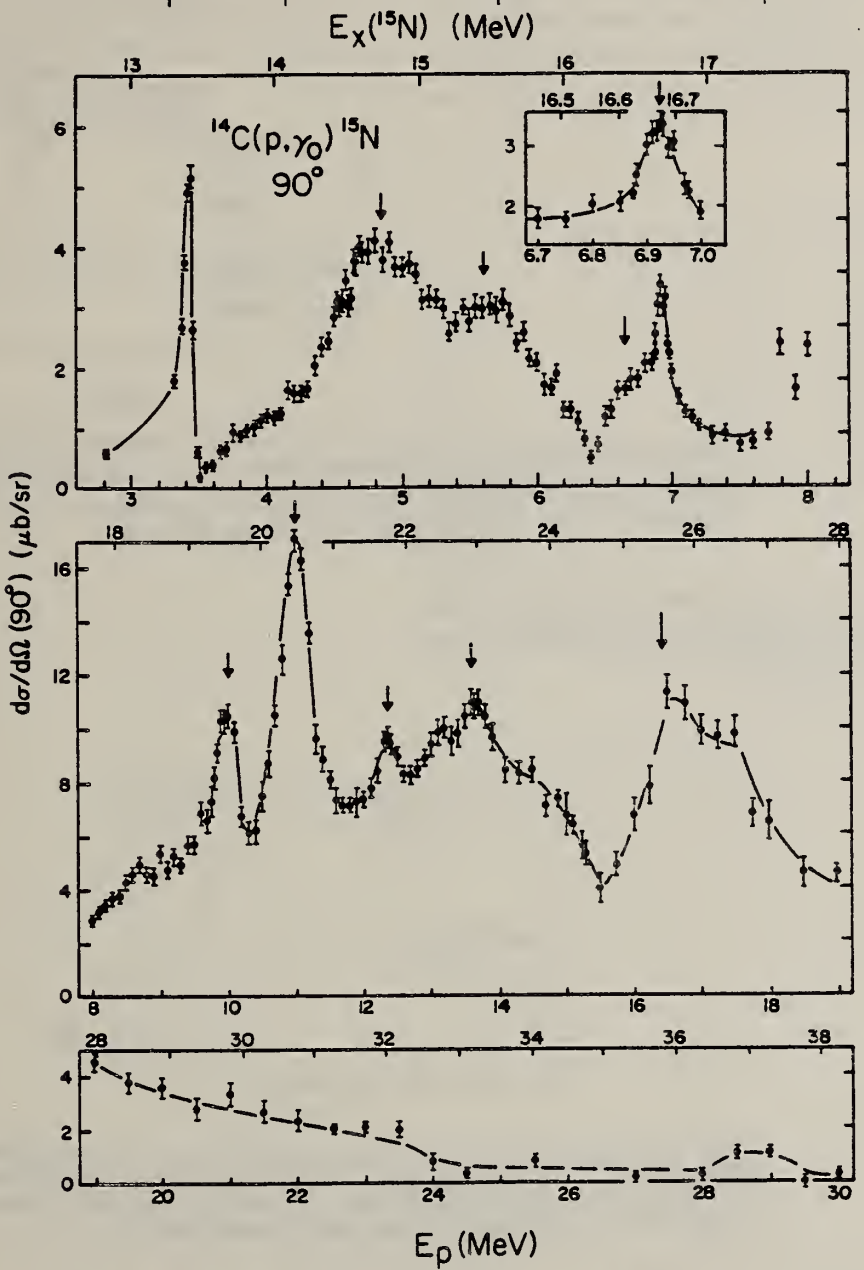

FIG. 3. Excitation function of the $^{14}C(p,\gamma_0)^{15}N$ γ yield at 90°. The top part shows the region where narrow $T=\frac{3}{2}$ resonances may be expected. The insert gives the details of a new resonance at $E_p=6.925$ MeV. The center part shows the region of the GDR and the bottom part the high-energy region up to 30 MeV. Solid lines are drawn to guide the eye. Arrows indicate energies where complete angular distributions were taken.

REF. J. C. Kim, H. S. Caplan, J. C. Bergstrom
Nucl. Phys. A246, 282 (1975)

ELEM. SYM.	A	Z
N	15	7

METHOD

REF. NO. 75 Ki 2 egf

REACTION	RESULT	EXCITATION ENERGY	SOURCE TYPE	SOURCE RANGE	DETECTOR TYPE	DETECTOR RANGE	ANGLE
E,E/	LFT	5- 8	D	84-122	MAG-D		DST

4 LEVELS 5.27-7.56

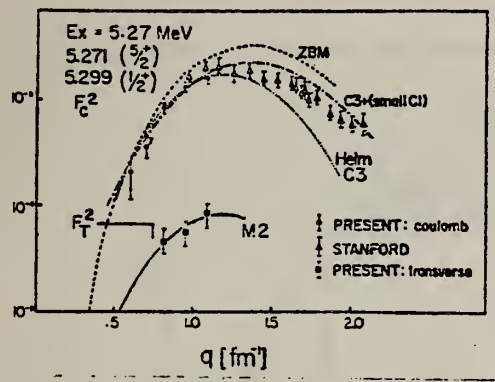

Fig. 2. Coulomb and transverse form factors of the 5.27 MeV doublet: solid circles and squares are the present experimental results, open triangles are taken from ref. [5]). The dash curve represents the theoretical C3 form factor calculated from Zuker, Buck and McGrory wave functions, the dash-dot curve shows a single-particle shell model (C3+C1) fit and the dot and solid curves are a Helm C3 fit and a Helm M2 fit respectively.

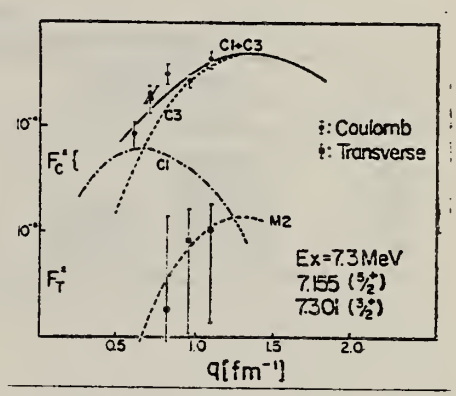

Fig. 3. The present experimental Coulomb and transverse form factors of the 7.3 MeV doublet: The solid curve shows the sum of a single-particle shell model C3 and C1 fit. The C3 contribution and the C1 contribution are shown in the dot and the dash-dot curves respectively. The dash curve represents a Helm M2 fit.

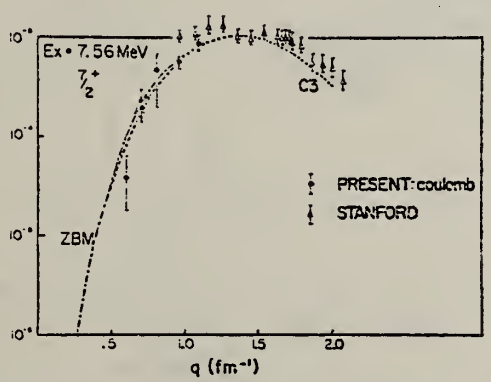

Fig. 4. Coulomb form factors of the 7.56 MeV level; solid circles are the present experimental results, open triangles are taken from ref. [5]) and explained in the text. The dash-dot curve represents the theoretical C3 form factors calculated from Zuker, Buck and McGrory wave functions and the dot curve shows a single-particle shell model C3 fit.

(over)

TABLE 3

The ^{15}N ground state radiative widths Γ_γ^0 (eV)

Level (MeV)	J^π	Transition	Present	Stanford [a])	Darmstadt [a])	Lifetime measurements
5.27	$\frac{5}{2}^+$	C3	$(4.19\pm0.30)\times10^{-6}$	$(2.68\pm0.1)\times10^{-6}$		
		M2	$(1.2\ \pm0.73)\times10^{-4}$		$(2.4\pm2.1)\times10^{-4}$	$(2.3\pm0.4)\times10^{-4}$ [b])
5.29	$\frac{1}{2}^+$	C1	2.17 ± 2.27	56.88 ± 9.8		$0.03\ \pm0.01$ [c]), 0.015 ± 0.005 [d])
7.15	$\frac{3}{2}^+$	C3	$(0.86\pm0.10)\times10^{-5}$			
7.30	$\frac{3}{2}^+$	C1	2.64 ± 1.02	50.73 ± 12	≈ 1.8	<0.066 [e]), <0.026 [f])
		M2	$(0.3\ \pm0.2)\times10^{-5}$			
7.56	$\frac{7}{2}^+$	C3	$(1.84\pm0.16)\times10^{-5}$	$\approx 3.01\times10^{-5}$ [g])		

[a]) See text. [b]) Ref. [16]). [c]) Ref. [12]). [d]) Ref. [13]).
[e]) Cockburn *et al.*, Bull. Am. Phys. Soc. 13 (1968) 1423.
[f]) R. Gill *et al.*, Nucl. Phys. A121 (1968) 209.
[g]) This value should be understood as the sum of Γ_γ^0 (7.15) and Γ_γ^0 (7.56 MeV).

TABLE 2

Inelastic form factors squared (in units of 10^{-4})

q (fm^{-1})	5.27 MeV doublet		7.2 MeV doublet		7.56 MeV
	F^2_C	F^2_T	F^2_C	F^2_T	F^2_C
0.60	2.03 ± 0.90		0.84 ± 0.25		0.39 ± 0.25
0.69	4.01 ± 1.40		1.95 ± 0.45		2.10 ± 0.55
0.81	8.30 ± 0.80	0.46 ± 0.15	3.15 ± 0.65	$0.02\ \pm0.09$	4.70 ± 2.00
0.95	13.40 ± 1.00	0.56 ± 0.14	2.70 ± 0.35	0.082 ± 0.08	5.60 ± 0.60
1.1	$15.9\ \pm1.30$	0.83 ± 0.20	4.30 ± 0.65	$0.11\ \pm0.07$	8.80 ± 0.93

[8] E.B. Daly et al., Phys. Rev. C2 (1970) 2057

[12] K.J. Wetzel, Phys. Rev. 181 (1969) 1465

[13] T.K. Alexander et al., Can. J. Phys. 43 (1965) 2310

[16] P.G. Bizzeti et al., Nucl. Phys. A104 (1967) 577

REF. J. C. Kim, H. S. Caplan, I. P. Auer
Phys. Lett. 56B, 442 (1975)

ELEM. SYM.	A	Z
N	15	7

METHOD

REF. NO. 75 Ki 10 egf

REACTION	RESULT	EXCITATION ENERGY	SOURCE		DETECTOR		ANGLE
			TYPE	RANGE	TYPE	RANGE	
E,E/	FMF	6, 9	D	O* 1	MAG-D		UKN

*Q = 0.5-1.1 FM-1

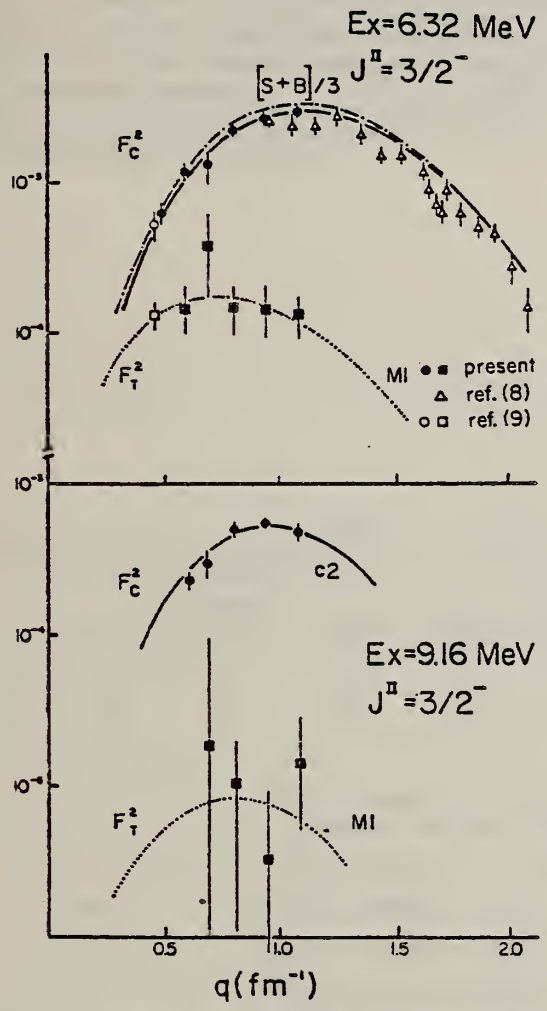

Fig. 1. Coulomb (C2) and transverse (M1) form factors. Solid circles and squares are the present experimental results, open circles and squares are taken from ref. [9], and triangle points are taken from ref. [8]. The solid curve shows a single-particle shell model C2 fit, the dash-dot curve represents the theoretical form factor calculated using Shukla and Brown wave functions divided by a factor 3, and the dotted curve shows a Heim model M1 fit.

(over)

Table 1
The present results of widths and E2/M1 mixing ratios in ^{15}N.

Transition (MeV)	Present Γ_γ^0 (eV)	|δ| present	|δ| others	Remarks	Ref.
			$0.09^{+0.06}_{-0.03}$	$^{18}O(p,\alpha)^{15}N$	[14]
6.32 → 0	0.050 ± 0.004 (E2)	0.16 ± 0.03	0.13 ± 0.03	(e, e')	[9]
	1.9 ± 0.4 (M1)		0.13 ± 0.02	$^{18}O(p,\alpha)^{15}N$	[1]
9.16 → 0	0.095 ± 0.005 (E2)	> 0.3	$0.37^{+0.3}_{-0.09}$	(e, e')	[11]
	0.2 ± 0.8 (M1)		0.09 ± 0.03	$^{14}C(p,\gamma)^{15}N$	[10]

[1] J.S. Lopes et al., Nucl. Phys. 76 (1966) 223.
[8] E.B. Dally, M.G. Croissiaux and B. Schwartz, Phys. Rev. C2 (1970) 2057.
[9] G.A. Beer, P. Brix, H.G. Clerc and B. Laube, Phys. Lett. 26B (1968) 506.
[10] H.E. Siefken, P.M. Cockburn and R.W. Krone, Nucl. Phys. A128 (1969) 162.
[11] H.G. Clerc, Habilitations-Schrift. Technische Hochschule Darmstadt (1968), unpublished.
[12] D. Evers et al., Phys. Lett. 27B (1968) 423.
[13] M. Stroetzel, Phys. Lett. 26B (1968) 376.
[14] E.K. Warburton et al., Phys. Rev. 138 (1965) B104.

REF.

R. Moreh and O. Shahal
Nucl. Phys. A252, 429 (1975)

ELEM. SYM.	A	Z
N	15	7

METHOD

REF. NO.: 75 Mo 8 | egf

REACTION	RESULT	EXCITATION ENERGY	SOURCE		DETECTOR		ANGLE
			TYPE	RANGE	TYPE	RANGE	
$ G,G	LFT	6	D	6	SCD-D		DST

6=6.324,POL SCAT G

Abstract: The 6.324 MeV level of ^{15}N was photoexcited by a chance energy overlap with a γ-line obtained from the Cr(n, γ) reaction using thermal neutrons. By measuring the angular distribution of the scattered radiation and its polarization, the spin and parity of the level was determined to be $J^{\pi} = \frac{3}{2}^-$. The E2/M1 mixing ratio of the $\frac{3}{2}^- \rightarrow \frac{1}{2}^-$ ground-state transition was unambiguously determined to be x(E2/M1) = 0.137±0.005. An upper limit to the branching ratio of the decay of the level to lower lying levels in ^{15}N was obtained. The radiative width of the level was also measured and found to be $\Gamma = 3.1 \pm 0.3$ eV. The result is compared with theoretical predictions.

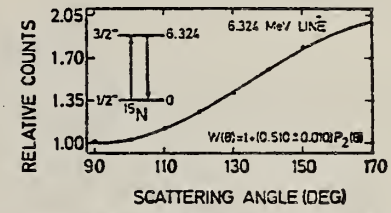

Fig. 3. Angular distribution of the 6.324 MeV scattered line from ^{15}N as measured using a 40 cm^3 Ge(Li) detector. The solid line has the form $W(\theta) = 1 + A_2 P_2(\cos\theta)$ and is a least square fit to the experimental distribution.

TABLE 1

Width and E2/M1 mixing amplitude of the $\frac{3}{2}^- \rightarrow \frac{1}{2}^-$, 6.324 MeV transition in ^{15}N

	Calculated			Experimental		
	ref. [18])	ref. [20])	ref. [19])	ref. [10])	ref. [11])	present work
Γ (eV)	3.7	4	4.9	3.4±0.7		3.1 ±0.3
x(E2/M1)	−0.17	0.13	0.122	0.13	0.13±0.02	0.137±0.005

[10] J.S. Lopes et al., Nucl. Phys. 76, 223 (1966); O. Hausser et al., Phys. Lett. 22, 604 (1966).
[11] G.A. Beer et al., Phys. Lett. 26B, 506 (1968).
[18] A.P. Shukla et al., Nucl. Phys. A112, 296 (1968).
[19] A.R. Poletti et al., Phys. Rev. 155, 1096 (1967).
[20] S. Lie et al., Nucl. Phys. A169, 617 (1971).

REF. J. J. Murphy II, Y. M. Shin, D. M. Skopik
Nucl. Phys. A246, 221 (1975)

ELEM. SYM.	A	Z
N	15	7

METHOD

REF. NO.	
75 Mu 3	egf

REACTION	RESULT	EXCITATION ENERGY	SOURCE		DETECTOR		ANGLE
			TYPE	RANGE	TYPE	RANGE	
E,P	ABX	14- 28	D	19- 30	MAG-D		DST
							1040

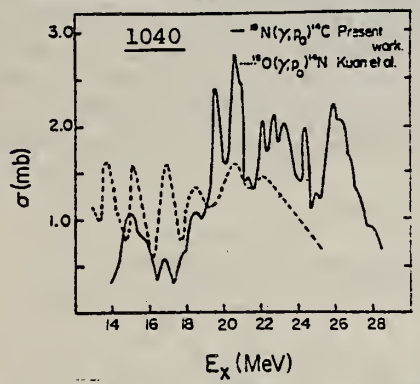

Fig. 4. The ^{15}N(γ, p$_0$)^{14}C cross section compared with the ^{15}O(γ, p$_0$)^{14}N cross section. If isospin is a good quantum number, the fact that the ^{15}N cross section is greater than the ^{15}O cross section above 18 MeV indicates $T = \frac{3}{2}$ strength at these higher energies.

GROUND STATE

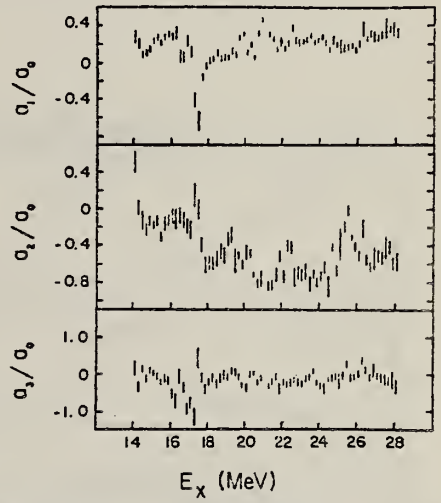

Fig. 3. Coefficients of Legendre polynomial fits at 200 keV intervals. The coefficient, a_0, is shown in fig. 4 multiplied by 4π. Errors are the statistical errors propagated through the fitting procedure.

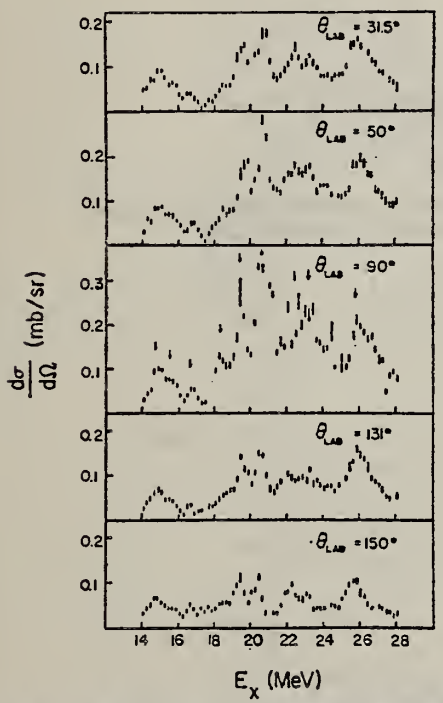

Fig. 2. The ^{15}N(γ, p$_0$)^{14}C differential cross section at the five laboratory angles measured. Typical counting errors are shown. The cross sections were obtained from electrodisintegration data using virtual photon formalism.

(over)

TABLE 2

Coefficients obtained from weighted least squares fits of the angular distributions to Legendre polynomials

E_x (MeV)	J^π	a_0 (μb/sr)	a_1/a_0	a_2/a_0	a_3/a_0
14.8	$\frac{1}{2}^+$	87± 4	0.20±0.07		
15.6	$\frac{3}{2}^+$	63± 3	0.23±0.06	−0.32±0.09	
16.7	$\frac{1}{2}^+$	44± 4			
18.4	$\frac{3}{2}^+$	78± 4	0.13±0.06	−0.66±0.13	
19.5	$\frac{3}{2}^+$	201± 6	0.22±0.03	−0.55±0.07	−0.18±0.09
20.7	$\frac{3}{2}^+$	255± 9	0.15±0.02	−0.73±0.07	
22.5	$\frac{3}{2}^+$	157±10	0.19±0.05	−0.48±0.13	
23.3	$\frac{3}{2}^+$	162± 7	0.24±0.04	−0.70±0.10	−0.27±0.10
25.9	$\frac{3}{2}^+$	177± 7	0.18±0.04	−0.35±0.08	

Also included are the spin and parity assignments indicated by our data. These are the dominant E1 states; at all energies except 16.7 MeV there is also interference from E2 or M1 states.

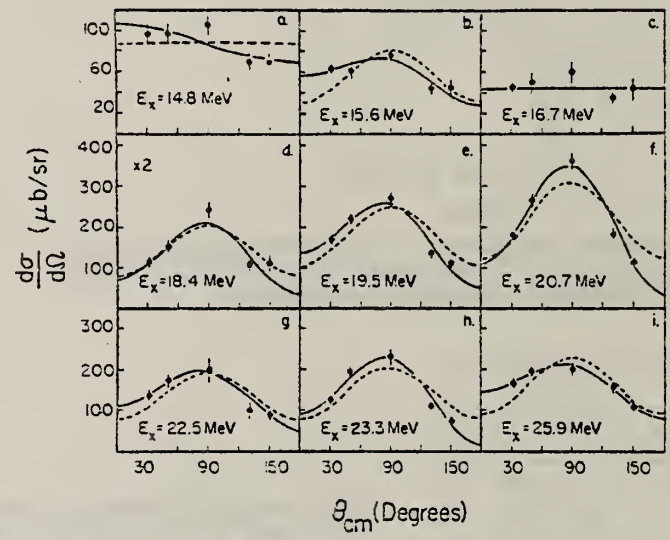

Fig. 6. Experimental angular distribution and fitted Legendre polynomial (solid curve). Dashed curve is distribution for pure $\frac{1}{2}^+$ state (isotropic) or $\frac{3}{2}^+$ state ($4P_0 - 2P_2$).

REF.

W. Del Bianco, S. Kundu, J. Kim
Nucl. Phys. A270, 45 (1976)

ELEM. SYM.	A	Z
N	15	7

METHOD

REF. NO.	
76 De 3	egf

REACTION	RESULT	EXCITATION ENERGY	SOURCE		DETECTOR		ANGLE
			TYPE	RANGE	TYPE	RANGE	
D,G	ABX	19- 23	D	3- 10	NAI-D		DST

Abstract: The 90 differential cross section of the $^{13}C(d, \gamma_0)^{15}N$ reaction has been measured at deuteron energies from E_d = 2.90 to 9.95 MeV in steps of 200 keV. Angular distributions have been obtained at E_d = 3.28, 3.96, 4.30, 4.76, 5.32, 5.92, 6.23, 6.63 and 7.94 MeV. The γ-rays have been detected with a 23 cm long by 23 cm diameter NaI(Tl) crystal spectrometer enclosed in a plastic scintillator anticoincidence shield. The γ-ray yield curve decreases monotonically with energy and shows a resonant behaviour at E_d = 6.65 MeV (E_x = 21.9 MeV) and a wide structure at E_d = 8.8 MeV ($E_x \approx$ 23.8 MeV). The angular distributions are consistent with the hypothesis that states with quantum numbers $J^\pi = \frac{1}{2}^+$ and $\frac{3}{2}^+$ are excited in the capture process followed by emission of E1 radiation. There is also evidence of M1/E2 transitions over the whole energy region investigated.

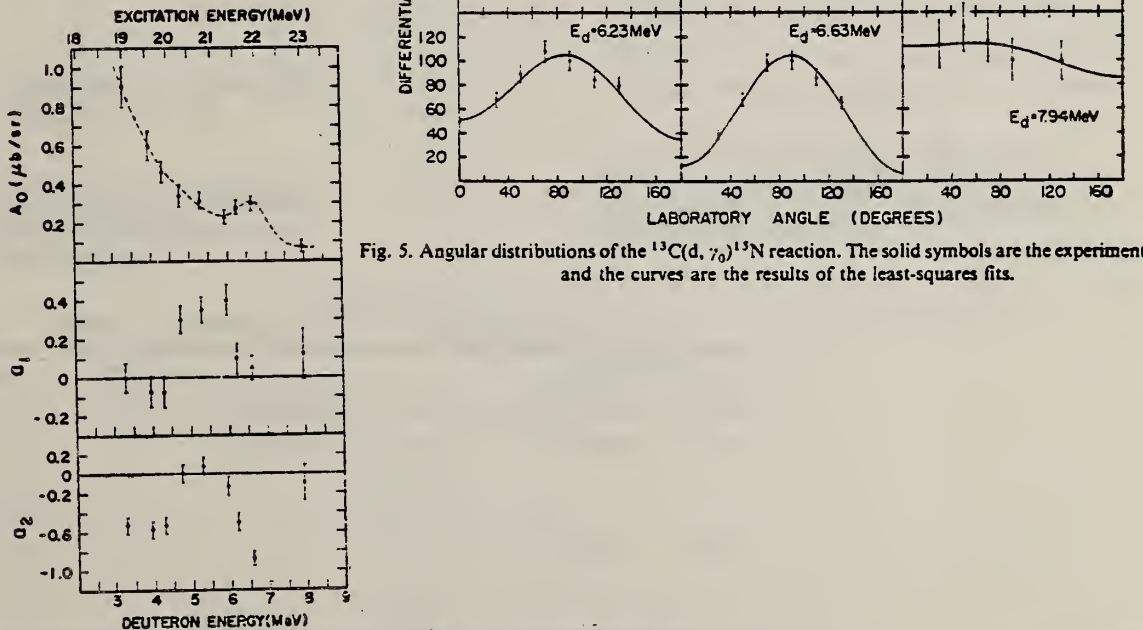

Fig. 5. Angular distributions of the $^{13}C(d, \gamma_0)^{15}N$ reaction. The solid symbols are the experimental points and the curves are the results of the least-squares fits.

Fig. 6. Plot of the coefficients A_0, a_1 and a_2 of eq. (2) versus deuteron energy for the $^{13}C(d, \gamma_0)^{15}N$ reaction.

(over)

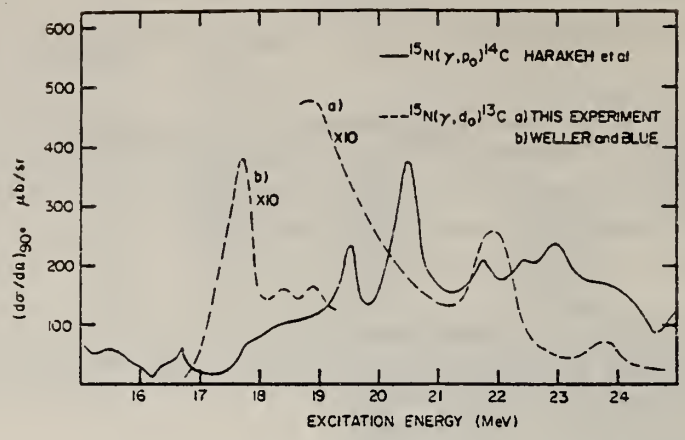

Fig. 8. Comparison of the $^{15}N(\gamma, p_0)^{14}C$ and $^{15}N(\gamma, d_0)^{13}C$ differential cross sections at $\theta_L = 90°$ obtained from the cross sections for the inverse processes by means of the principle of detailed balance.

REF. H. M. Kuan and D. G. Shirk
Phys. Rev. C13, 883 (1976)

ELEM. SYM.	A	Z
N	15	7

METHOD

REF. NO. 76 Ku 2 hmg

REACTION	RESULT	EXCITATION ENERGY	SOURCE TYPE	SOURCE RANGE	DETECTOR TYPE	DETECTOR RANGE	ANGLE
P,G	LFT	13	D	2- 4	SCD-D		DST
		(13.42)					

LEVEL 13.42 MEV

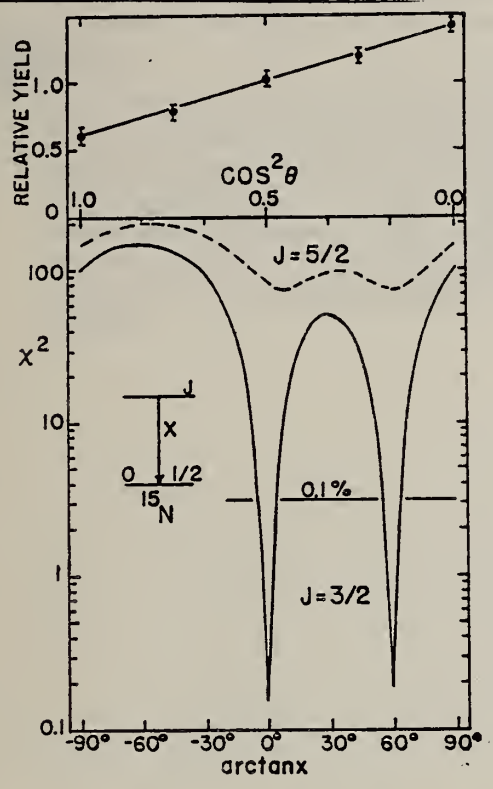

FIG. 3. Top: angular distribution of $^{14}C(p,\gamma_0)$ at E_p =3.405 MeV with the solid line being the theoretical fit for the $J=\frac{3}{2}$ case. Bottom: the χ^2 vs arctan$x$ calculations with assumed J values of $\frac{3}{2}$ and $\frac{5}{2}$.

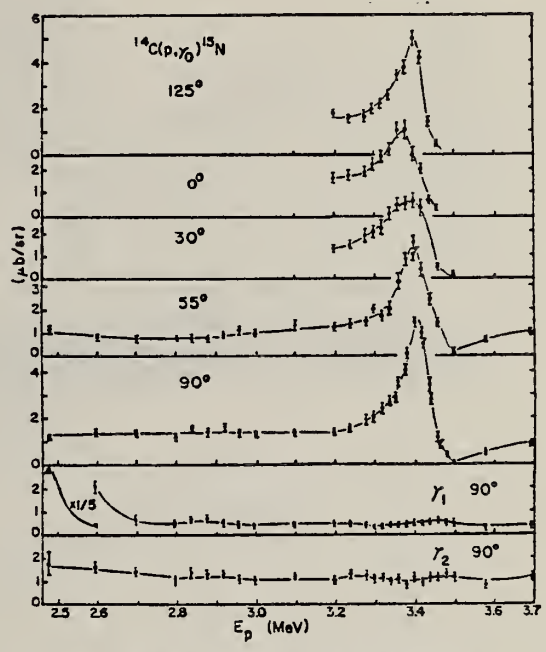

FIG. 2. The yield curves of the capture reaction $^{14}C(p,\gamma)^{15}N$ at 125°, 0°, 30°, 55°, and 90° for γ_0 and at 90° for γ_1(5.270) and γ_2(5.299). The solid lines are drawn through the data points.

TABLE I. γ transitions of the $\frac{1}{2}^+$, 13.42-MeV state of ^{15}N.

Final state E_x (MeV)	J^π	Branching (%)	Mixing ratio	Γ_γ (eV)	$B(E1)$ (e^2fm^2) Experiment	Theory [a]
0	$\frac{1}{2}^-$	100	0.00 ± 0.04	3.0 ± 0.9	0.0012 ± 0.0004	0.0009
5.270	$\frac{5}{2}^+$	<8		<0.25		
5.299	$\frac{1}{2}^+$	<8		<0.25		
6.324	$\frac{3}{2}^-$	<5		<0.15	<0.0005	0.0006
7.16	$\frac{5}{2}^+$	<5		<0.15		
7.30	$\frac{3}{2}^+$	<5		<0.15		

[a] Reference 6.

[6] M.N. Harakeh et al., Phys. Rev. C12, 1410 (1975).

REF.	M.W.S. Macauley, R. P. Singhal, R. G. Arthur, S. W. Brain, W. A. Gillespie, A. Johnston, E. W. Lees, A. G. Slight J. Phys. (London) G2, L35 (1976)	EL EM. SYM.	A	Z
		N	15	7

METHOD	REF. NO.	
	76 Ma 1	egf

REACTION	RESULT	EXCITATION ENERGY	SOURCE		DETECTOR		ANGLE
			TYPE	RANGE	TYPE	RANGE	
E,E/	FMF	6	D	60-120	MAG-D		DST

6=6.32 MEV

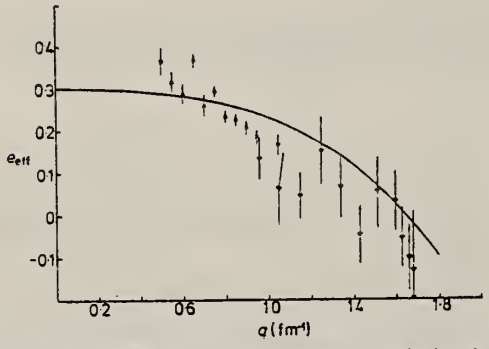

Figure 1. Momentum transfer dependence of effective charge for the 1p → 1p Coulomb transition in ^{15}N. ×, Kelvin; ▽, Stanford. b = 1·69 fm, R = 3·50 fm.

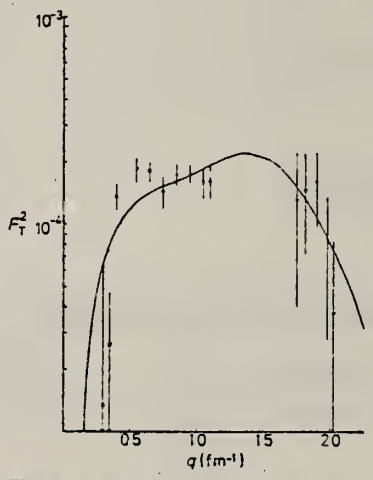

Figure 2. Effective magnetic moment fit to the 6·32 MeV level transverse form factor, $F_T^2 = F_{M1}^2 + F_{E2}^2$. ×, Kelvin; ▽, Stanford.

REF. R. Moreh, O Shahal, and V. Volterra
Nucl. Phys. A262, 221 (1976)

ELEM. SYM.	A	Z
N	15	7

METHOD

REF. NO. 76 Mo 9 egf

REACTION	RESULT	EXCITATION ENERGY	SOURCE		DETECTOR		ANGLE
			TYPE	RANGE	TYPE	RANGE	
G,G	LFT	6	D	6	NAI-D		90

6=6.324 MEV

Abstract: The temperature effect of nuclear resonance scattering from the 6.324 MeV level in ^{15}N was studied as a function of temperature using a gaseous $^{15}N_2$ target and a solid $Li^{15}NO_3$ target. The γ-source was produced by the Cr(n, γ) reaction using thermal neutrons. In order to reproduce the experimental variation of the scattering cross section versus temperature, the Lamb treatment for metallic elements was generalised to the case of diatomic and more complicated molecules. In $^{15}N_2$ an effective temperature was defined in which the zero-point energy of vibration of the diatomic molecule was included. In $LiNO_3$, an effective temperature was also defined by introducing a modified Debye temperature and accounting for the normal modes of vibration of ^{15}N in the $^{15}NO_3^-$ molecule. An excellent agreement between measured and calculated values was obtained. In a way, the present measurement may be viewed as detecting the zero-point vibrations in molecules.

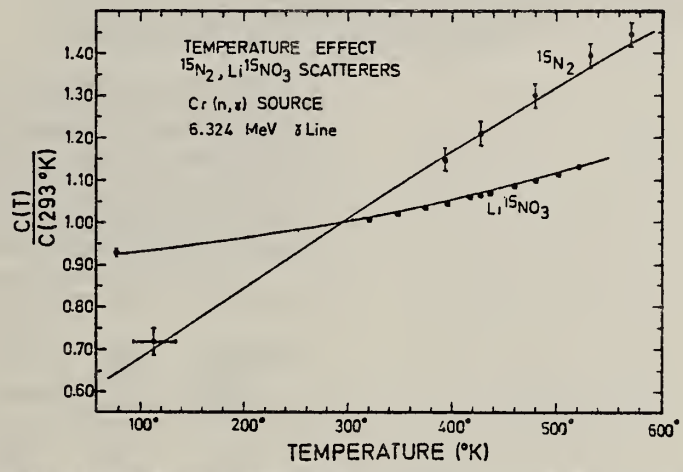

Fig. 2. Relative scattering yield (normalised to $T = 293°$ K) from gaseous $^{15}N_2$ and solid $Li^{15}NO_3$ targets as a function of temperature. The solid lines are the theoretical curves obtained using eq. (1) with $\Gamma_0 = \Gamma = 2.9$ eV and $\delta = 29.5$ eV. For $Li^{15}NO_3$, the value of θ was 160° K.

REF. B.H. Patrick, E.M. Bowey, E.G. Muirhead
J. Phys. G: Nucl. Phys. 2, 751 (1976)

ELEM. SYM.	A	Z
N	15	7

METHOD

REF. NO. 76 Pa 1 egf

REACTION	RESULT	EXCITATION ENERGY	SOURCE		DETECTOR		ANGLE
			TYPE	RANGE	TYPE	RANGE	
G,PG	ABI	16- 35	C	15- 35	SCD-D		112
G,NG	ABI	13- 35	C	15- 35	SCD-D		112
G,TG	ABI	19- 35	C	15- 35	SCD-D		112

Absolute yields based on normalization to $^{59}Co(\gamma,n)$ cross section of Fultz (62Ful). If newer $^{59}Co(\gamma,1n)$ data from Alvarez (73Al7) is used, yields should be increased by a factor of 1.41.

Abstract. The photodisintegration of ^{15}N through excited states of the residual nuclei has been studied by measuring the yields of de-excitation γ rays in a Ge(Li) detector. Cross sections for all observed transitions were deduced from measurements with bremsstrahlung end-point energies ranging from 15 to 35 MeV and account for an integrated cross section of 44 MeV mb. Bound states in ^{14}N and ^{14}C with a dominant $(1p_{1/2})^{-1}$ or $(1p_{3/2})^{-1}$ configuration are found to be strongly populated. On the whole the results do not agree well with the meagre existing experimental information or with published theoretical calculations, with the possible exception of those of Zhusupov and Eramzhyan. The nature of the states in the ^{15}N giant resonance is discussed. The $^{15}N(\gamma,t)^{12}C^*$ (4·44 MeV) reaction was also observed and its integrated cross section is ~5% of the expected value of the E1 sum rule. Integrated cross sections for $^{16}O(\gamma,n_{p_{1/2}})$ transitions measured at the same time are given. Resonance fluorescence is observed from the ^{15}N 10·07 MeV level, for which $\Gamma_{\gamma_0} = 4{\cdot}2 \pm 1{\cdot}5$ eV is deduced.

Table 1. Cross sections, integrated up to 35 MeV, for neutron, proton and triton transitions to specific states of the residual nuclei. In the ^{15}N (γ, n) and (γ, p) cases, all final states lying below particle break-up energies are included. The dominant configurations for ^{14}N were taken from table V in True (1963) and those for ^{14}C from the work of Kaschl *et al* (1971). For the states with configurations given in square brackets, pick-up studies find no evidence for direct transitions and the configurations have been taken from ^{14}N states with the same J^π, T. The last two columns compare the measured integrated cross sections, divided by 150 MeV mb, with the theoretical predictions of Goncharova (1972). Errors on the integrated cross-sections are ~ ±30%.

Reaction	Final state (MeV)	J^π, T	Dominant configuration of final state	$\int_0^{35\,\mathrm{MeV}} \sigma\,dE$ (MeV mb)	$\frac{\int \sigma\,dE}{150}$ (%)	Goncharova (1972) (%)
^{15}N (γ, n) ^{14}N	GS	1^+, 0	$(1p_{1/2})^2$	NM†	—	6·1
	2·31	0^+, 1	$(1p_{1/2})^2$	8·6	5·7	18·4
	3·95	1^+, 0	$(1p_{3/2})^{-1}(1p_{1/2})^3$	8·3	5·5	9·1
	4·91	0^-, 0	$(1p_{1/2})^1(2s_{1/2})^1$	NO‡	—	—
	5·11	2^-, 0	$(1p_{1/2})^1(1d_{5/2})^1$	0·9	0·6	—
	5·83	3^-, 0	$(1p_{1/2})^1(1d_{5/2})^1$			
	5.69	1^-, 0	$(1p_{1/2})^1(2s_{1/2})^1$	NO	—	—
	6·20	1^+, 0	$(2s_{1/2})^2$	NO	—	—
	6·44	3^+, 0	$(2s_{1/2})^1(1d_{5/2})^1$	NO	—	—
	7·03	2^+, 0	$(1p_{3/2})^{-1}(1p_{1/2})^3$	7·9	5·3	4·0
^{15}N (γ, p) ^{14}C	GS	0^+, 1	$(1p_{1/2})^2$	22·0§	14·7	12·1
	6·09	1^-, 1	$(1p_{1/2})^1(2s_{1/2})^1$			
	6·59	0^+, 1	$(2s_{1/2}; 1d_{5/2})^2$	3·4	2·3	—
	6·90	0^-, 1	$(1p_{1/2})^1(2s_{1/2})^1$			
	6·73	3^-, 1	$(1p_{1/2})^1(1d_{5/2})^1$	NO	—	—
	7·01	2^+, 1	$(1p_{3/2})^{-1}(1p_{1/2})^3$	7·9	5·3	17·6
^{15}N (γ, t) ^{12}C	4·44	2^+, 0	—	7·0	4·7	—

† NM: not measured in present experiment.
‡ NO: not observed in present experiment.
§ Value taken from Kosiek (1964); integrated up to 30·5 MeV.

(over)

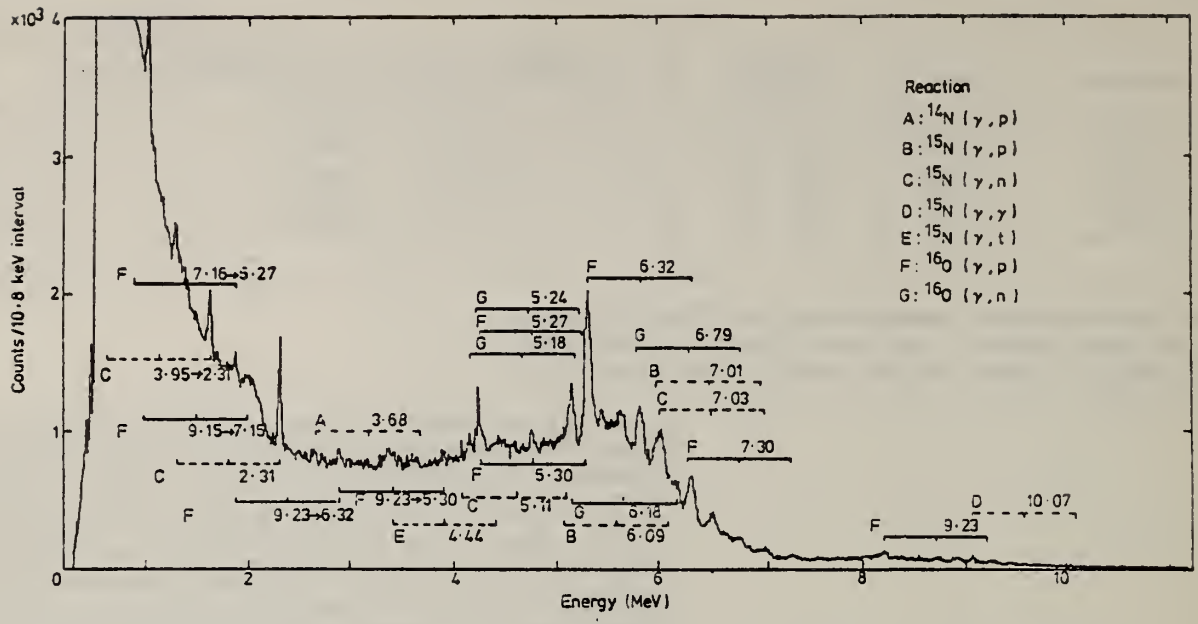

Figure 1. The γ ray spectrum, measured in the Ge(Li) detector, from the $^{15}NH_4{}^{15}NO_3$ target irradiated with bremsstrahlung end-point energy 31 MeV. The positions of the peaks for various transitions, and the reactions producing them, are marked.

REF.		ELEM. SYM.	A	Z
	K.A. Snover, J.E. Bussoletti, K. Ebisawa, T.A. Trainor and A.B. McDonald Phys. Rev. Lett. 37, 273 (1976)	N	15	7

METHOD	REF. NO.	
	76 Sn 8	hmg

REACTION	RESULT	EXCITATION ENERGY	SOURCE		DETECTOR		ANGLE
			TYPE	RANGE	TYPE	RANGE	
$ P,G	ABX	20- 28	D	10- 18	NAI-D		DST

POLARIZED PROTONS

Direct-semidirect radiative-capture calculations are compared to new detailed $^{14}C(p_{pol},\gamma_0)^{15}N$ measurements in the giant-dipole-resonance region. The calculations provide a good description of the data by including only direct $E2$ and direct plus collective $E1$. The experimentally determined $E2$ cross section exhausts (6.8±1.4)% of the isoscalar sum rule and shows no sign of a resonance.

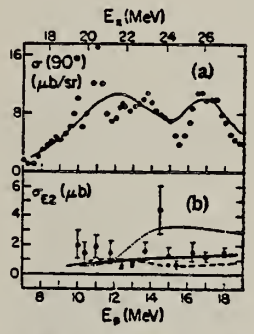

FIG. 2. (a) The 90° cross section (Ref. 6). (b) σ_{E2} derived from the data of Fig. 1 and (a) (see Fig. 1 caption).

[6] M.H. Harakeh et al., Phys. Rev. C12, 1410 (1975).

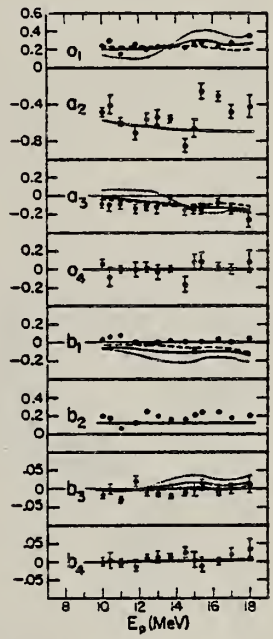

FIG. 1. Measured and calculated angular distribution coefficients for $^{14}C(p_{pol},\gamma)^{15}N$. Solid curve, $E1$ plus direct $E2$; dashed curve, $E1$, direct $E2$ plus an $E2$ IS resonance; dotted curve, $E1$, direct $E2$ plus an $E2$ IV resonance.

REF.

H. R. Weller, R. A. Blue, N. R. Roberson, D. G. Rickel, S. Maripuu, C. P. Cameron, R. D. Ledford, D. R. Tilley
Phys. Rev. C13, 922 (1976)

ELEM. SYM.	A	Z
N	15	7

METHOD

REF. NO.: 76 We 1 hmg

REACTION	RESULT	EXCITATION ENERGY	SOURCE		DETECTOR		ANGLE
			TYPE	RANGE	TYPE	RANGE	
$ P,G	ABX	.13- 26	D	4- 17	NAI-D		DST

POL PROTONS

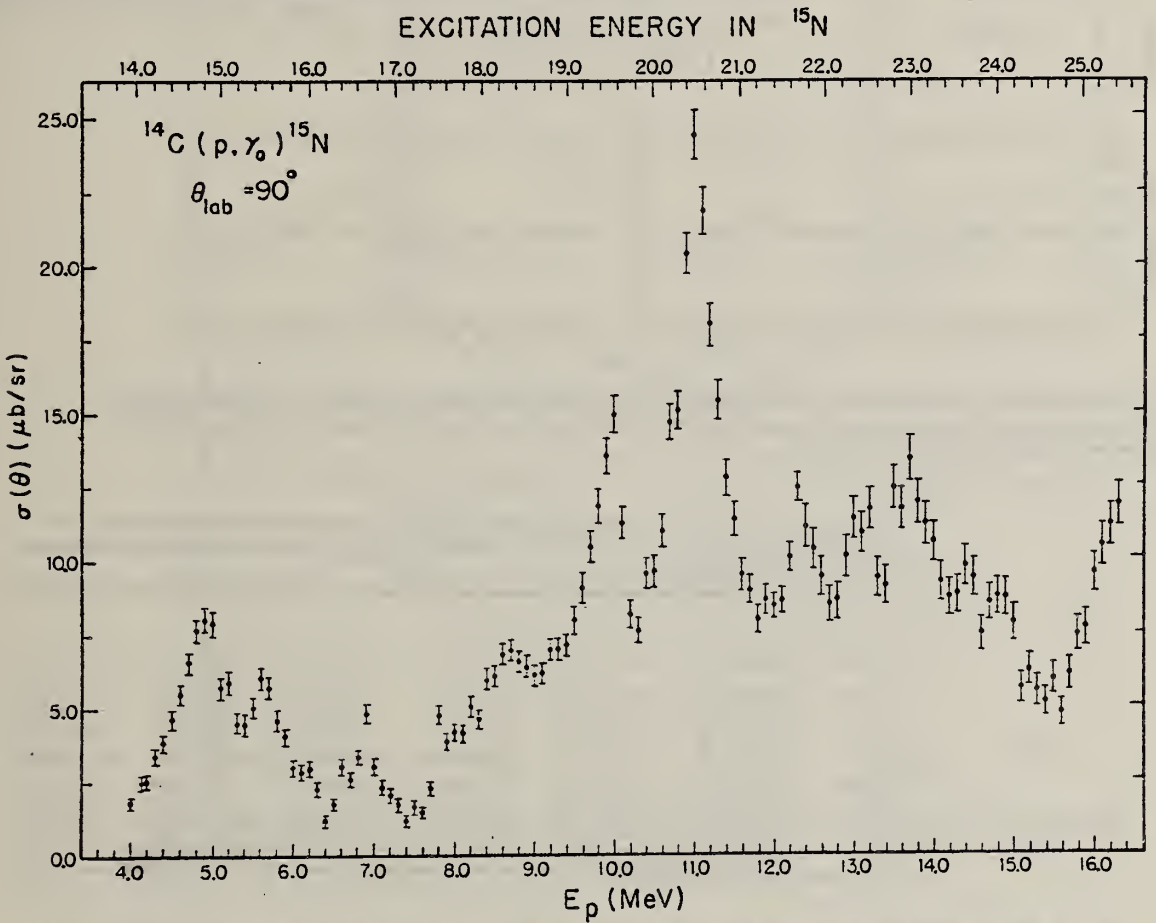

FIG. 4. The excitation curve for the $^{14}C(p,\gamma_0)^{15}N$ reaction at $\theta_{lab} = 90°$. The error bars represent the statistical errors associated with the data points.

(over)

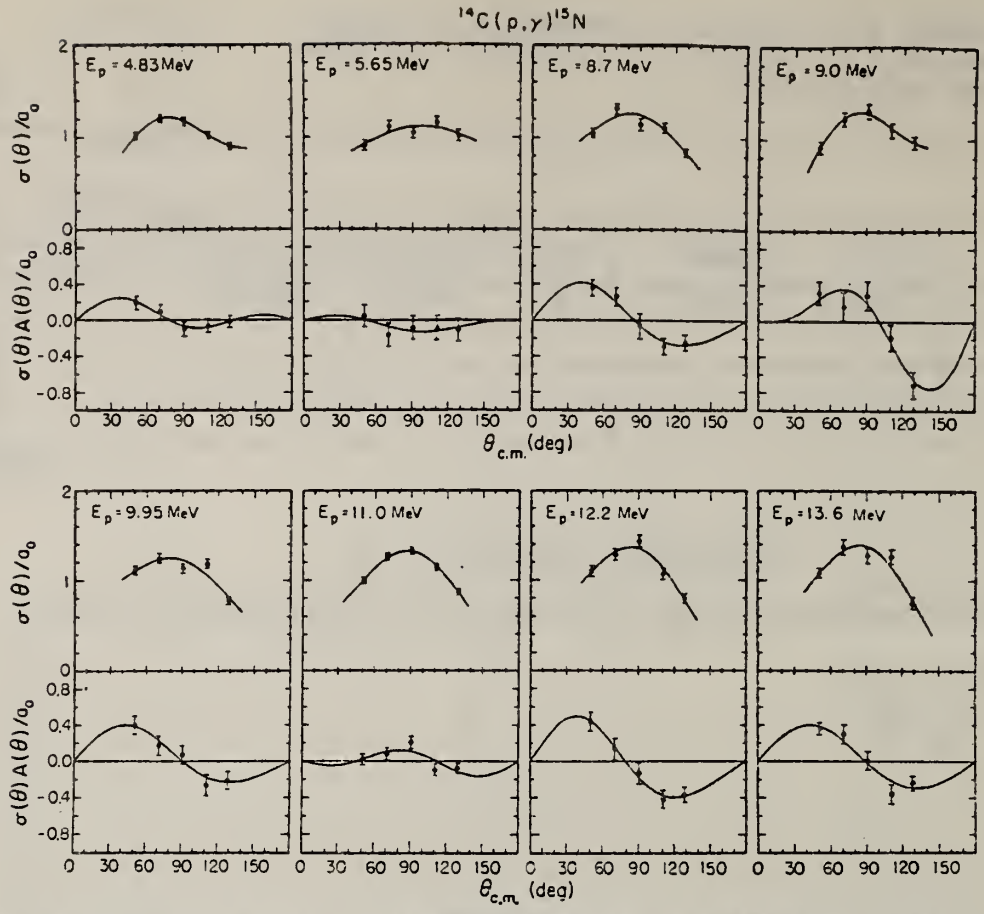

FIG. 5. The normalized cross section and cross section times analyzing power data as a function of energy and angle. The error bars represent the statistical errors associated with the data points. The solid lines are a result of the fits discussed in the text and summarized in Table I.

TABLE I. The a and b coefficients obtained by least squares fitting the data of Fig. 5 as discussed in the text. Entries of 0.0 ± 0.0 indicate that the χ^2 values implied that these terms were not required to fit the data.

E (MeV)	a_1/a_0	a_2/a_0	a_3/a_0	b_1	b_2	b_3
4.83	−0.03 ± 0.10	−0.36 ± 0.08	−0.25 ± 0.14	0.03 ± 0.04	0.07 ± 0.03	0.07 ± 0.03
5.65	−0.08 ± 0.06	−0.24 ± 0.11	0.0 ± 0.0	−0.09 ± 0.07	0.03 ± 0.05	0.03 ± 0.06
8.7	0.21 ± 0.05	−0.50 ± 0.11	0.0 ± 0.0	0.01 ± 0.05	0.23 ± 0.04	0.04 ± 0.05
9.0	−0.18 ± 0.17	−0.57 ± 0.15	−0.30 ± 0.25	−0.02 ± 0.08	0.31 ± 0.06	−0.16 ± 0.06
9.95	0.25 ± 0.05	−0.47 ± 0.10	0.0 ± 0.18	0.05 ± 0.05	0.22 ± 0.04	0.03 ± 0.05
11.0	0.11 ± 0.03	−0.65 ± 0.07	0.0 ± 0.12	0.02 ± 0.03	0.05 ± 0.02	−0.06 ± 0.03
12.2	0.27 ± 0.06	−0.71 ± 0.13	0.0 ± 0.07	−0.07 ± 0.05	0.26 ± 0.04	0.07 ± 0.05
13.6	0.26 ± 0.06	−0.77 ± 0.15	0.0 ± 0.0	0.02 ± 0.05	0.23 ± 0.03	0.03 ± 0.04

REF.

E. J. Ansaldo, J. C. Bergstrom, H. S. Caplan, and R. Yen
Can. J. Phys. 55, 2129 (1977)

ELEM. SYM.	A	Z
N	15	7

METHOD

REF. NO.	
77 An 6	hmg

REACTION	RESULT	EXCITATION ENERGY	SOURCE		DETECTOR		ANGLE
			TYPE	RANGE	TYPE	RANGE	
E,E/	LFT	9- 15	D	60-194	MAG-D		DST

5 LEVELS,9-15 MeV

The electromagnetic form factors of five transitions in ^{15}N have been measured for momentum transfers between 0.48 and 1.27 fm^{-1}. The transitions observed were identified with levels at 9.76, 10.80, 11.88, 12.50, and 14.7 MeV excitation energy. Ground state radiative widths have been extracted by a Helm model analysis.

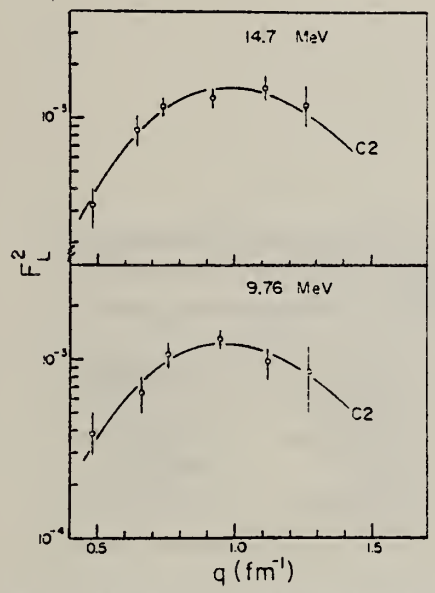

FIG. 2. Form factors for the 9.76 and 14.7 MeV transitions. The solid curves are Helm model fits to the longitudinal electric quadrupole case.

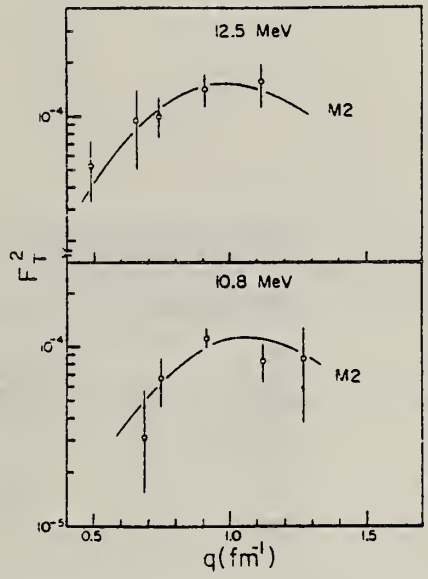

FIG. 3. Form factors for the 10.8 and 12.5 MeV transitions. The solid curves are the Helm model fits for a pure M2 case.

over

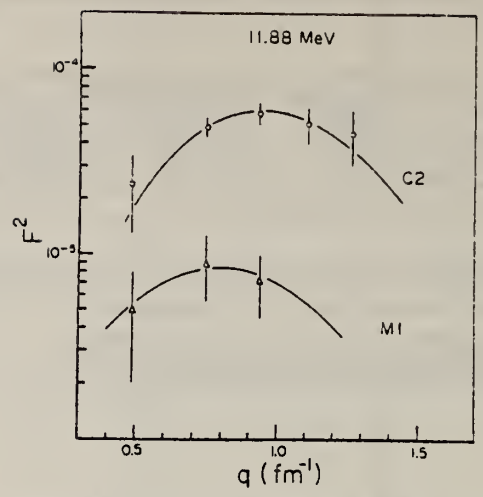

FIG. 4. Form factor for the peak at 11.88 MeV excitation. The curves shown are C2 and M1 Helm model fits using parameters from the 9.76 and 10.8 MeV transitions, respectively.

TABLE 1. Ground state radiative widths obtained from the Helm model analysis of the transitions observed in this work and by Clerc (1968) (low q-model independent technique)

Level (MeV)	J^π	Transition	Γ_{γ_0} (eV)	
			Present	Clerc (1968)
9.76	$5/2^-$	C2	0.20 ± 0.05	0.19 ± 0.08
10.8	$3/2^+$	M2	$(1.8 \pm 0.8) \times 10^{-2}$	$(1.4 \pm 0.4) \times 10^{-2}$
11.88	$3/2^-$	C2	0.44 ± 0.10	0.48 ± 0.22
		M1	4.4 ± 3.8	1.1 ± 0.7
12.5	$5/2^+$	M2	$(5.2 \pm 2.0) \times 10^{-2}$	$(5.0 \pm 1.5) \times 10^{-2}$
14.7	$5/2^-$	C2	1.3 ± 0.2	—

REF. W. Del Bianco, S. Kundu, and J. Kim
Can. J. Phys. 55, 302 (1977)

EL EM. SYM.	A	Z
N	15	7

METHOD

REF. NO. 77 De 1 hmg

REACTION	RESULT	EXCITATION ENERGY	SOURCE		DETECTOR		ANGLE
			TYPE	RANGE	TYPE	RANGE	
A,G	ABX	15- 25	D	5- 18	NAI-D		90

The 90° differential cross section of the $^{11}B(\alpha,\gamma_0)^{15}N$ reaction has been measured at α-particle energies from 5.74 to 17.80 MeV. The γ rays have been detected by a 23 cm long × 23 cm diameter NaI(Tl) crystal spectrometer enclosed in a plastic scintillator anticoincidence shield. The yield curve shows three well separated resonances at E_{exc} = 16.29 ± 0.15, 18.88 ± 0.20, and 21.26 ± 0.20 MeV.

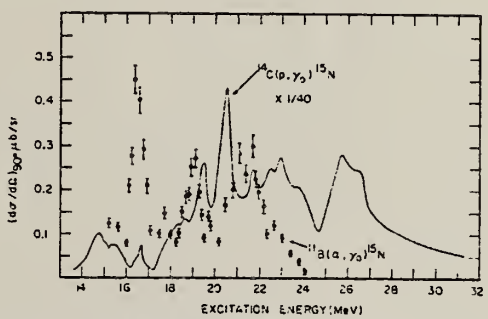

FIG. 1. Experimental differential cross sections at $\theta_L = 90°$ of the $^{14}C(p,\gamma_0)^{15}N$ and $^{11}B(\alpha,\gamma_0)^{15}N$ reactions. The solid line represents the results of Harakeh *et al.* (1975); the solid symbols are the results of this experiment. In the latter instance only statistical errors are shown in the figure.

Harakeh, M., Paul, P., Kuan, H., and Warburton, E. 1975. Phys. Rev. C12, 1410.

REF. M.W.S. Macauley, R.P. Singhal, R.G. Arthur, S.W. Brain, W.A. Gillespie, A. Johnston, E.W. Lees and A.G. Slight
J. Phys. G 3, 1717 (1977)

ELEM. SYM.	A	Z
N	15	7

METHOD

REF. NO. 77 Ma 9 egf

REACTION	RESULT	EXCITATION ENERGY	SOURCE		DETECTOR		ANGLE
			TYPE	RANGE	TYPE	RANGE	
E,E/	FMF	5, 6	D	60-120	MAG-D		DST

5.3,6.32 MeV

Abstract. Form factors for the inelastic scattering of electrons from ^{15}N were measured for the excitation of the 6·32 MeV $\frac{3}{2}^-$ state and of the 5·3 MeV $\frac{5}{2}^+$ $\frac{1}{2}^+$ doublet. The experimental data obtained resolve apparent discrepancies between the results deduced from the previous studies of ^{15}N by electron scattering, and demonstrate that even large-basis shell-model calculations using the Kuo interaction do not produce realistic wave-functions for these states.

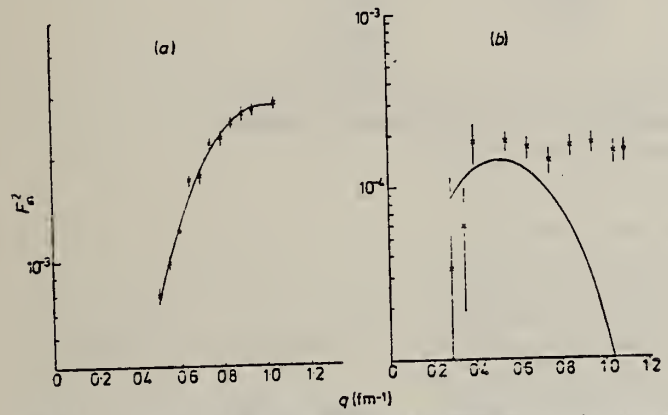

Figure 5. Full curve, DWBA form factors squared calculated from the parameters given in columns 1 and 2 of table 3. (*a*) 6·324 MeV longitudinal form factor; (*b*) 6·324 MeV transverse form factor.

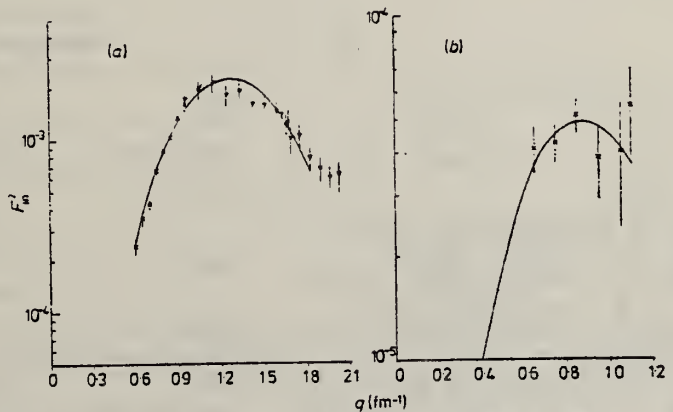

Figure 7. Full curve, DWBA form factors squared calculated from the parameters given in columns 3 and 4 of table 3. (*a*) 5·270 MeV longitudinal form factor: ×, Kelvin; ▽ Stanford. (*b*) 5·270 MeV transverse form factor.

over

Table 1. The experimental data for ^{15}N.

Run no	Incident electron energy (MeV)	Scattering angle (deg)	Momentum transfer q_{in} (fm^{-1})	$F_{el}^2 \times 10$	A_{in}/A_{el} (E_x = 5·3 MeV) $\times 10^4$	A_{in}/A_{el} (E_x = 6·3 MeV) $\times 10^4$
1	120·07	126·1	1·05	0·541	407·2 (4·1)†	654·5 (4·0)†
2	113·99	140·0	1·05	0·535	478·0 (4·5)	782·3 (4·4)
3	111·55	148·0	1·05	0·530	478·2 (4·0)	916·8 (3·7)
4	114·91	114·7	0·95	0·973	179·9 (3·4)	335·5 (3·0)
5	103·35	140·0	0·95	0·949	196·0 (4·8)	423·5 (3·3)
6	101·11	148·0	0·95	0·944	225·7 (3·3)	530·5 (2·8)
7	114·91	97·6	0·85	1·613	71·9 (3·4)	174·6 (2·5)
8	92·73	140·0	0·85	1·555	87·4 (5·5)	241·2 (3·3)
9	90·72	148·0	0·85	1·550	111·9 (3·2)	305·6 (2·1)
10	114·91	83·1	0·75	2·484	30·0 (3·5)	95·2 (2·2)
11	82·12	140·0	0·75	2·388	35·8 (7·1)	129·5 (3·1)
12	80·35	148·0	0·75	2·382	55·8 (4·9)	170·7 (2·0)
13	114·91	70·1	0·65	3·584	11·4 (5·8)	47·8 (2·4)
14	71·53	140·0	0·65	3·454	—	94·6 (4·0)
15	69·99	148·0	0·65	3·448	25·7 (8·1)	106·8 (3·2)
16	111·69	60·0	0·55	4·867	2·3 (27)	23·4 (3·6)
17	92·73	74·6	0·55	4·832	—	22·4 (7·7)
18	59·65	148·0	0·55	4·730	—	69·8 (4·1)
19	116·71	148·0	1·10	0·386	748·7 (4·8)	1239·0 (4·4)
20	114·91	105·7	0·90	1·266	115·3 (3·0)	242·0 (2·4)
21	114·91	90·1	0·80	2·020	47·5 (3·3)	124·4 (2·4)
22	114·91	76·4	0·70	3·011	16·2 (9·1)	64·2 (4·1)
23	114·91	64·0	0·60	4·209	6·77 (11·0)	32·8 (3·4)
24	114·91	60·0	0·50	5·544	2·1 (50)	17·2 (4·7)
25	90·72	53·5	0·40	6·945	1·03 (L9)	7·08 (3·1)
26	86·62	49·0	0·35	7·605	—	3·54 (6·5)
27	86·65	40·0	0·29	8·377	—	1·61 (30)

† The figures given inside the brackets are the percentage errors in F_{in}^2. F_{in}^2 can be obtained by multiplying F_{el}^2 by A_{in}/A_{el}. All form factors are defined with respect to σ_M, i.e. $F^2 = \sigma/\sigma_M$.

Table 2. ^{15}N transverse form factors.

q(fm^{-1})	0·29†	0·35†	0·40†	0·55	0·65	0·75	0·85	0·95	1·05	1·10†
$10^4 \times F_T^2(E_x = 6·3$ MeV)	0·355 ±0·5	0·596 ±0·2	1·82 ±0·19	1·84 ±0·25	1·80 ±0·20	1·44 ±0·25	1·74 ±0·22	1·76 ±0·17	1 60 ±0·28	1·65 ±0·25
$10^5 \times F_T^2(E_x = 5·3$ MeV)	—	—	—	—	4·09 ±0·65	4·24 ±0·55	5·10 ±0·60	3·83 ±0·94	4·01 ±1 60	5·45 ±1·00

The errors in these transverse form factors take into account the variation, at constant q, of the Coulomb form factor with change in energy.
† F_T^2 obtained by subtracting F_L^2 as calculated in DUELS from the parameters given in columns 1 and 3 of table 3.

Table 3. ^{15}N spectroscopic parameters deduced from the DWBA analysis of the electron-scattering data of the present experiment.

State	6·324 MeV $\frac{1}{2}^-$		5·270 MeV $\frac{5}{2}^+$		5·299 MeV $\frac{1}{2}^-$
Transition type	C2	M1†	C3‡	M2	CIE1
$B(XL)$ (e^2 fm^{2L})	17·1 ± 1·3	(2·29 ± 0·23) $\times 10^{-3}$	440 ± 40	0·30 ± 0·07	
c(fm)	1·91	3·4	2·55	2·79	Not
t(fm)	2·25	2·1§	1·82	2·1§	observed
R_{tr}(fm)	3·80 ± 0·4	2·9	4·1 ± 0·4	2·97 ± 0·22	

† B(M1↑) fixed at value of Moreh and Shahal (1975a.b); R_{tr}(M1) fixed at the value for the 10·43 MeV state in ^{14}N (Fagg 1975).
‡ Stanford data (Dally *et al* 1970) included.
§ t fixed at elastic scattering value (§3 of text).
The errors in the transition probabilities and in the transition radii were calculated using the criterion of Cline and Lesser (1970), as amended by Lesser *et al* (1972).

Fagg, L.W. 1975 Rev. Mod. Phys. 47, 683-711
Moreh, R. and Shahal, O. 1975a Nucl. Phys. A252, 429-36
1975b Nucl. Phys. A262, 221-30
Dally, E.B. Croissiaux, M.G., Schwartz, B. 1970 Phys. Rev. C 2, 2057-68
Cline, D. and Lesser P.M.S. 1970 Nucl. Instrum. Meth. 82, 291-3

REF.

M. Schaeffer, A. Degre, M. Suffert, G. Bonneaud, I. Linck
Nucl. Phys. A275, 1 (1977)

ELEM. SYM.	A	Z
N	15	7

METHOD

REF. NO.: 77 Sc 1 egf

REACTION	RESULT	EXCITATION ENERGY	SOURCE		DETECTOR		ANGLE
			TYPE	RANGE	TYPE	RANGE	
T,G	ABX	15- 18	D	1- 4	NAI-D		DST

Abstract: The reaction $^{12}C(t, \gamma_0)^{15}N$ was studied for E_t = 1–3.4 MeV (E_x = 15.7–17.6 MeV). The excitation curve displays a strong resonance with a peak cross section of 4.4±0.5 μb/sr at E_t = 2.3 MeV (E_x = 16.60 MeV, Γ = 0.13 MeV) and evidence for additional structure. The excitation curve and the angular distributions were analysed using the complex eigenvalue theory. The parameters of three $J^\pi = \frac{1}{2}^+$ states and two $J^\pi = \frac{1}{2}^-$ states resulting from this analysis are given. Our results show the importance of complex configurations in this energy region of the ^{15}N giant resonance.

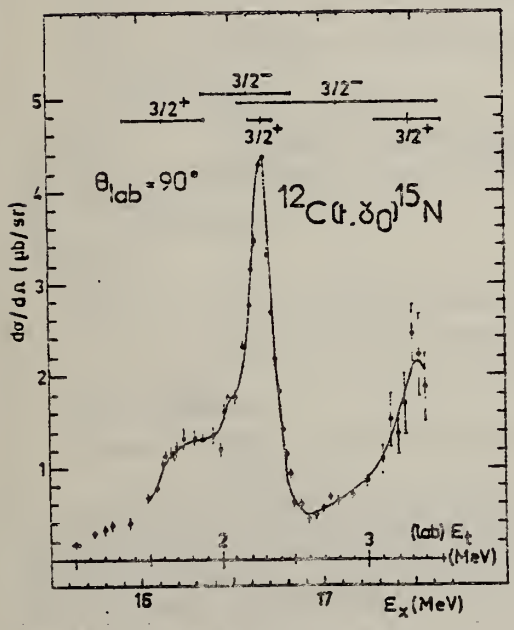

Fig. 3. Excitation function at 90° for the $^{12}C(t, \gamma_0)^{15}N$ reaction. The vertical error bars represent only errors of statistical origin. The solid line corresponds to the *S*-matrix fit. The horizontal bars at the top of the figure indicate the positions and the widths of the levels used in this fit (see also table 1).

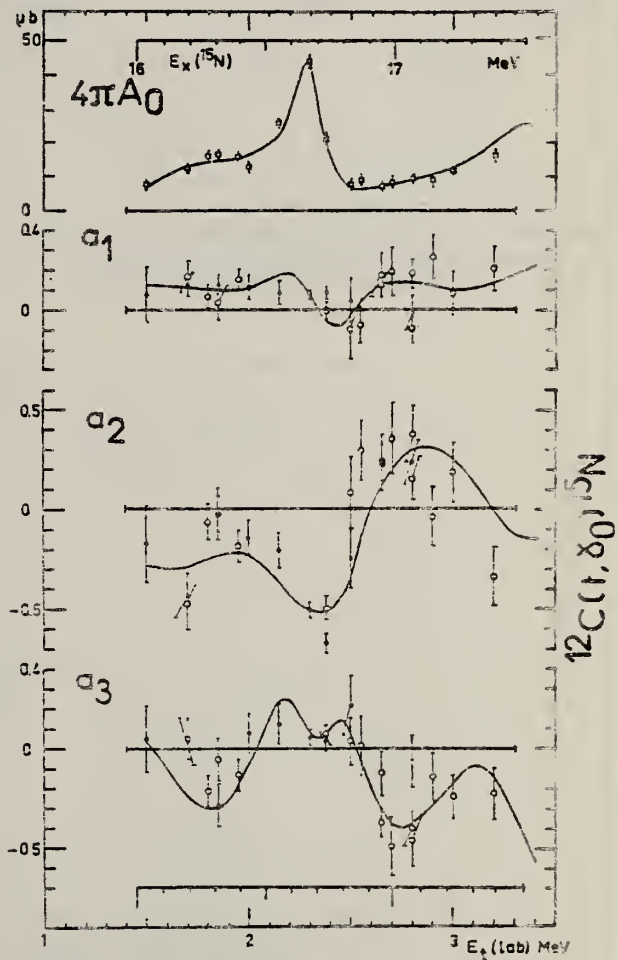

Fig. 5. Total cross section and coefficients of the expansion $d\sigma/d\Omega = A_0[1 + \sum_{n=1}^{3} a_n P_n(\cos\theta)]$ for the $^{12}C(t, \gamma_0)^{15}N$ reaction as a function of energy. The solid lines correspond to the *S*-matrix fit, involving the same parameters as those given in fig. 3 (see also table 1).

(over)

TABLE I

Level parameters obtained in the *S*-matrix analysis of the $^{12}C(t, \gamma_0)^{15}N$ data

E_{res}(c.m.) [a] (MeV)	Γ(c.m.) [a] (keV)	l_t	Transition	$\Gamma_t\Gamma_\gamma$ [b] (keV^2)	J^π	$E_x(^{15}N)$ [a] (MeV)
1.30±0.05	450±100	2	E1	0.8 (1.1)	$\frac{1}{2}^+$	16.15±0.05
1.75	490	1	M1/E2	0.6/2.8	$\frac{1}{2}^-$	16.60
1.84±0.01	130± 15	2	E1	0.32(0.38)	$\frac{1}{2}^+$	16.69±0.01
2.24	1160	1	M1/E2	0.04/20	$\frac{1}{2}^-$	17.09
2.64±0.09	450±120	2	E2	1.8 (3.6)	$\frac{1}{2}^+$	17.49±0.09

[a]) The limits indicate the variation range of the $J^\pi = \frac{1}{2}^+$ states depending on the analysis conditions.

[b]) The $J^\pi = \frac{1}{2}^-$ states were introduced to obtain a better fit (see subsect. 2.4). If these states are omitted one obtains the $\Gamma_t\Gamma_\gamma$ values between parentheses.

REF. E.J. Ansaldo, J.C. Bergstrom and R. Yen
Phys. Rev. C 18, 597 (1978)

EL EM. SYM.	A	Z
N	15	7

METHOD

REF. NO. 78 An 3 hg

REACTION	RESULT	EXCITATION ENERGY	SOURCE TYPE	SOURCE RANGE	DETECTOR TYPE	DETECTOR RANGE	ANGLE
E,E/	FMF	13- 40	D	52-194	MAG-D		DST

The giant resonance region of ^{15}N has been investigated by means of inelastic electron scattering in a momentum transfer range 0.36–1.25 fm^{-1}. The data show a splitting of the dipole resonance into two main peaks at 22 and 25.5 MeV, with some structure around 20 MeV and strength extending down to 13 MeV. The structure from 19 to 30 MeV correlates well with radiative capture and photodisintegration data and is in qualitative agreement with shell model predictions of the isospin splitting of the giant dipole resonance. The data show considerable spin-flip $E1$ strength, which agrees well with the predictions of the generalized Goldhaber-Teller model. Additional structure found in the energy region from ~ 14 to ~ 19 MeV has been analyzed as a $C2$-$C1$ superposition. The $C2$ strength in the 14–18.5 MeV region exhausts up to 22% of the isoscalar energy-weighted sum rule (Helm model, $J = 3/2$ assumed). The amount of $C2$ strength in the region from 18.5 to 30 MeV is negligible.

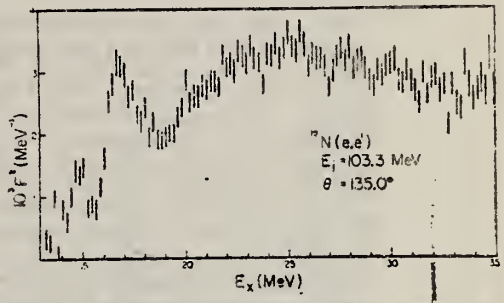

FIG. 3. Differential form factor at 135°. Other backward angle data were obtained at 141° and also show no evidence for strong transverse peaks.

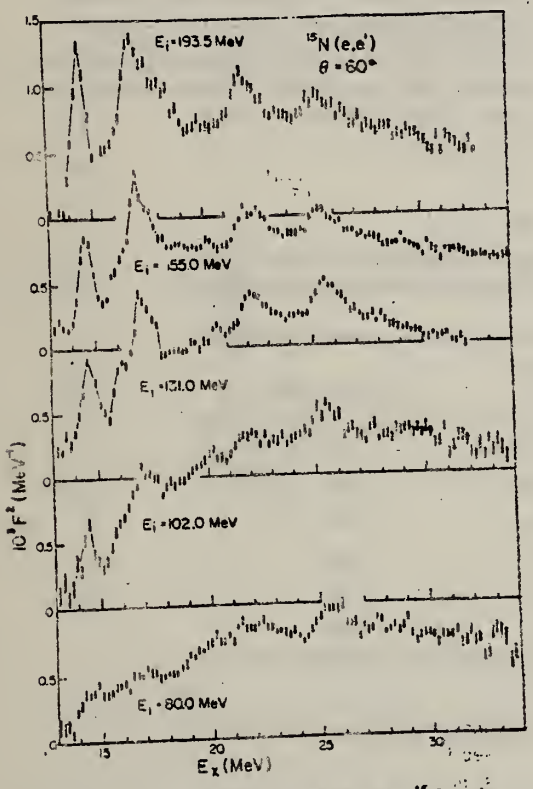

FIG. 2. Electron scattering spectra from ^{15}N in the giant resonance region, presented as differential form factors. All the data taken at 60° are presented here to show qualitatively the evolution of the structure in the GR with increasing momentum transfer.

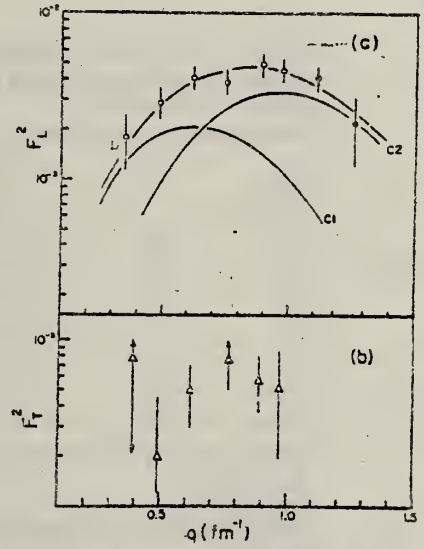

FIG. 4. Integrated longitudinal (a) and transverse (b) form factors for Region I (14–18.5 MeV) as a function of momentum transfer. The solid lines show the average fit and the Helm model $C1$-$C2$ components that yielded the radiative widths quoted in the text. The two points at higher q (dark circles) were obtained from fixed angle spectra by assuming a transverse component extrapolated from Fig. (b). They were not used in the $C1$-$C2$ analysis. The transverse form factor (b) is assigned to the spin-flip $E1$ transitions and as such is considered part of the GDR form factor.

over

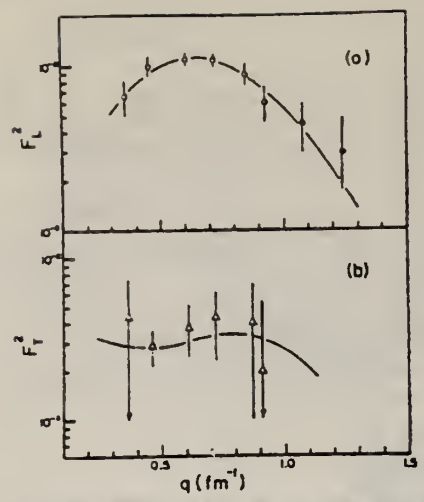

FIG. 5. Integrated form factors for region II plus region III (18.5–30 MeV) as a function of momentum transfer. (a) Longitudinal component. The solid line shows the Helm model fit for a $C1$–$C2$ multipolarity mixture. As discussed in the text, the $C2$ component is negligibly small. Only the data in open circles were used in the fitting. The two points at higher q (dark circles) were obtained from fixed angle spectra by assuming a transverse component extrapolated from (b). They are shown in the plot to demonstrate the consistency of the data at high q with the assumptions made in the analysis. (b) Transverse component. The solid line is the result of using Uberall's generalization of the Goldhaber-Teller model. This calculation is based on the elastic form factor, not a fit to the data points.

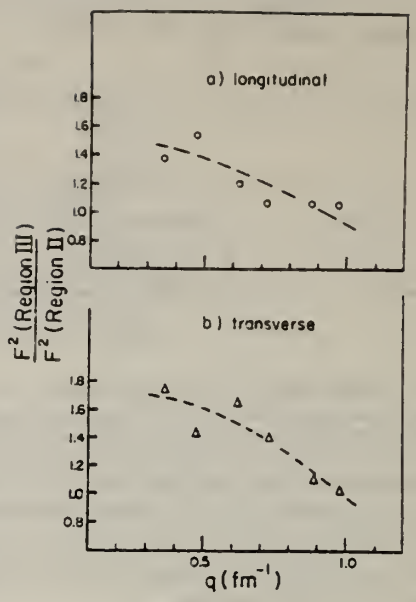

FIG. 6. Ratio of intergrated form factors for region III (24–30 MeV) to region II (18.5–24 MeV) as a function of momentum transfer. The dashed lines were drawn only to guide the eye. The errors were not drawn for the sake of clarity. Statistical errors are about the size of the points, but relative errors due to background subtraction and to longitudinal-transverse decomposition procedure amount typically to 20–25%.

TABLE I. Ground state $C2$ radiative widths, and fractions of the energy-weighted sum rule (isoscalar) from this and previous (e,e') work. The $J^\pi = \frac{1}{2}^-$ values in parentheses were assigned arbitrarily to evaluate Γ_{γ_0}.

E_x (MeV)	J^π	Γ_{γ_0} (eV)	$B(C2)$ (e^2 fm^4)	$E_x B(C2)/\text{EWSR}^c$
6.32	$\frac{1}{2}^-$	0.06 ± 0.004[a]	14.80 ± 1.0	0.05
9.16	$\frac{1}{2}^-$	0.10 ± 0.005[a]	3.85 ± 0.2	0.02
9.76	$\frac{5}{2}^-$	0.20 ± 0.05[b]	8.40 ± 2.1	0.05
11.38	$\frac{1}{2}^-$	0.44 ± 0.10[b]	4.60 ± 1	0.03
14–18.5	$(\frac{1}{2}^-)$	12.5 ± 2.0	24.2 ± 4.0	0.22
18.5–30	$(\frac{1}{2}^-)$	<0.10	<0.04	<0.001

[a] Reference 17.
[b] Reference 18.
[c] See A. Bohr and B. R. Mottelson, *Nuclear Structure*, (Benjamin, New York, 1975), Vol. 2, Chap. 6.

17
J.C. Kim, H.S. Caplan, and I.P. Auer, Phys. Lett. 56B, 442 (1975)
18
E.J. Ansaldo, J.C. Bergstrom, H.S. Caplan, and R. Yen, Can. J. Phys. 55, 2129 (1977)

REF. A. Degre, M. Schaeffer, G. Bonneaud and I. Linck
Nucl. Phys. A306, 77 (1978)

ELEM. SYM.	A	Z
N	15	7

METHOD

REF. NO. 78 De 2 rs

REACTION	RESULT	EXCITATION ENERGY	SOURCE		DETECTOR		ANGLE
			TYPE	RANGE	TYPE	RANGE	
A,G	ABX	16- 20	D	6- 12	NAI-D		DST

J-PI FOR 4 LEVELS

Abstract: The reaction $^{11}B(\alpha, \gamma_0)^{15}N$ is studied for $6 \leqq E_\alpha \leqq 11.5$ MeV ($15.5 \leqq E_x \leqq 19.5$ MeV). The excitation function measured at $\theta_{lab} = 90°$ displays four strongly excited resonances at $E_x = 16.35 \pm 0.02$, 16.73 ± 0.02, 17.67 ± 0.05, and 19.05 ± 0.05 MeV, and a probable one at $E_x = 17.15 \pm 0.05$ MeV. These data and 14 angular distributions ($0 \leqq \theta_{lab} \leqq 135°$ for $16 \leqq E_x \leqq 18$ MeV) have been fitted with the *S*-matrix "many-levels" formalism. We propose J^π assignments for the first four resonances. The cross section is about four times smaller than in $^{12}C(t, \gamma_0)^{15}N$. We will discuss possible correlations with resonances observed in other reactions leading to ^{15}N.

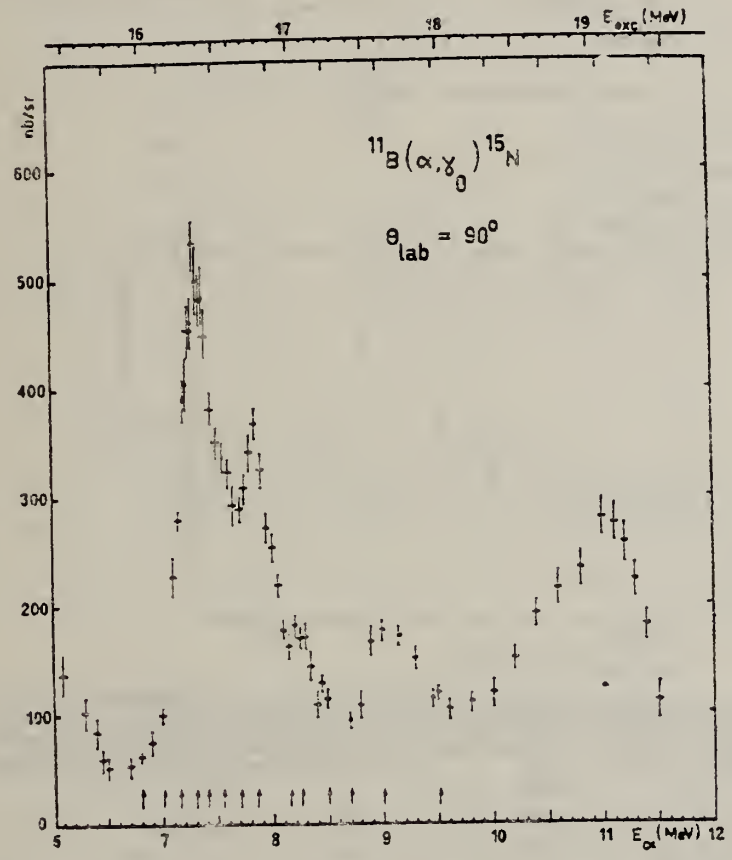

Fig. 2. Differential cross section of $^{11}B(\alpha, \gamma_0)^{15}N$ as a function of ^4He energy. Vertical bars represent only statistical errors and horizontal bars represent energy spread. Fourteen arrows locate energies at which angular distributions have been measured.

TABLE 2

Level parameters obtained in our analysis of the $^{11}B(\alpha, \gamma_0)^{15}N$ reaction for $7 \leq E_\alpha \leq 9.5$ MeV by assuming four positive-parity levels

E_{res} (c.m.) (MeV)	Γ (c.m.) (keV)	l_α	Transition	Γ_γ (eV)	Γ_γ/Γ_w	J^π	E_{exc} (MeV)	E_x (MeV)
5.36 ± 0.02	270 ± 30	1, (3)	E1	≥ 11	$\geq 6 \times 10^{-3}$	$\frac{3}{2}^-$	16.35 ± 0.020	7.32
5.74 ± 0.02	270 ± 30	(1, 3)	(E1)	≥ 11	$\geq 6 \times 10^{-3}$	$(\frac{1}{2}^-, \frac{3}{2}^-)$	16.73 ± 0.020	7.83
6.14 ± 0.05	250 ± 60	(1, 3)	(E1)	2	$\geq 10^{-3}$	$(\frac{1}{2}^-, \frac{3}{2}^-)$	17.15 ± 0.050	8.38 ± 0.1
6.65 ± 0.05	600 ± 80	(1), 3	E1	≥ 7	$\geq 3 \times 10^{-3}$	$\frac{1}{2}^-$	17.67 ± 0.05	9.07 ± 0.1

over

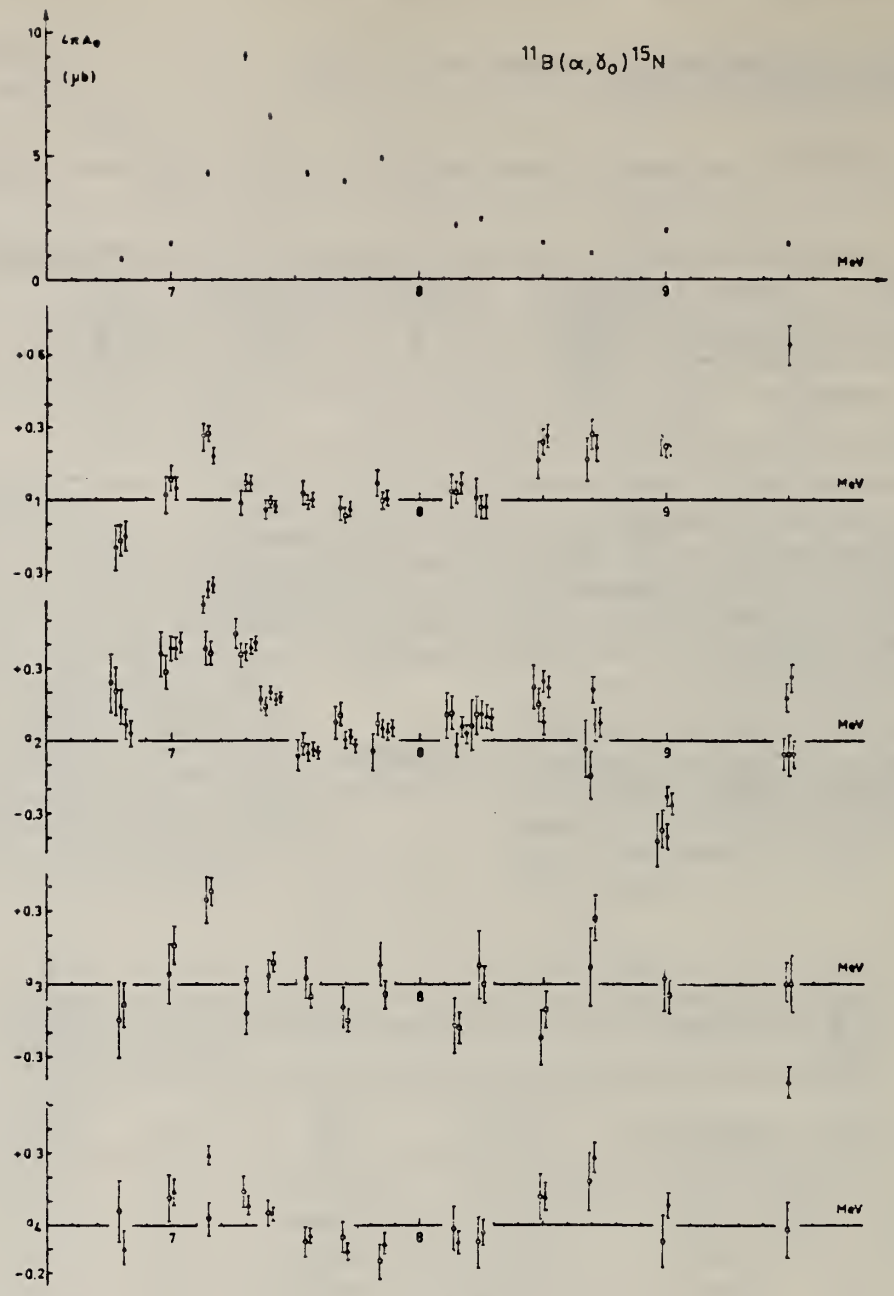

Fig. 4a.

	P_0	1.58	–	–	–	–	1.22	–	1.81	1.71	1.36	–	–	–	–	0
▽	P_{0+2}	1.81	1.7	–	1.73	–	.73	–	1.59	1.95	.90	–	–	–	–	0+2
△	P_{0+2+4}	1.83	.49	5.6	.89	1.83	.49	.47	1.27	1.89	.95	–	1.77	–	–	0+2+4
	P_{0+1}	1.45	–	–	–	–	1.17	–	–	1.50	1.50	1.85	–	–	.78	0+1
◇	P_{0+1+2}	.66	1.9	–	1.13	–	.92	–	–	1.83	.92	1.79	–	1.33	.73	0+1+2
□	$P_{0+1+2+3}$	.88	1.05	.12	1.67	1.33	.89	.43	–	.02	1.23	1.71	1.14	1.67	.37	0+1+2+3
○	$P_{0+1+2+3+4}$	1.21	.91	.08	.07	1.49	.79	.35	–	.03	–	1.81	.64	2.31	1.44	0+1+2+3+4

Fig. 4b.

Fig. 4. Summary of values of Legendre coefficients (a_n) obtained for possible expansion in Legendre polynomials $d\sigma/d\Omega = \sum_{n=0}^{N} A_n P_n(\cos\theta)$ with $0 \leqq N \leqq 4$ and n = odd + even or n = even. Each symbol refers to one combination as indicated. Values are χ^2 minimum obtained for each combination. No value means a bad fit.

REF. W. DelBianco, N. Marquardt, K. Farzine & H.V. Buttlar
Can. J. Phys. 56, 3 (1978)

ELEM. SYM.	A	Z
N	15	7

METHOD

REF. NO. 78 De 8

11/20/80 hmg

REACTION	RESULT	EXCITATION ENERGY	SOURCE		DETECTOR		ANGLE
			TYPE	RANGE	TYPE	RANGE	
D,G	ABX	11-15	D	1-5	NAI-D	---	95
		(11.3-14.4)		(1.1-4.2)			

The 95° differential cross section of the $^{13}C(d,\gamma_0)^{15}N$ reaction has been measured at deuteron energies from 1.1 to 4.2 MeV. The γ rays have been detected by a 25.4 cm long by 25.4 cm diameter NaI(Tl) crystal spectrometer. The yield curve reveals a single resonance structure at E_d = 1.74 ± 0.04 MeV (E_{exc} = 17.7 MeV).

La section efficace différentielle à 95° de la réaction $^{13}C(d,\gamma_0)^{15}N$ a été mesurée pour des énergies des deuterons allant de 1.1 à 4.2 MeV. Les rayons gamma ont été détectés par un crystal de NaI(Tl). La courbe d'excitation montre une résonance à E_d = 1.74 ± 0.04 MeV (E_{exc} = 17.7 MeV).

Can. J. Phys., 56, 3 (1978)

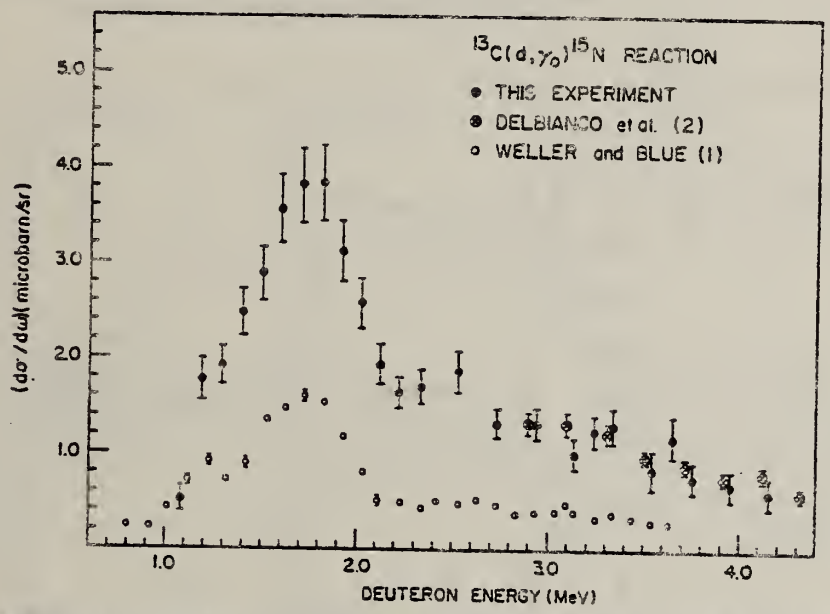

FIG. 1. Differential cross section of the $^{13}C(d,\gamma_0)^{15}N$ reaction as a function of deuteron energy at θ_L = 90°: ●, the results of this experiment; ○, the data of Weller and Blue (1); ⊗, the results of Del Bianco *et al.* (2). The error bars of Weller and Blue represent the statistical errors, whereas the errors of the other two experiments contain also the uncertainties resulting from unfolding the γ-ray spectra.

REF. H.R. Weller, N.R. Roberson & S.R. Cotanch
Phys. Rev. C18, 65 (1978)

ELEM. SYM.	A	Z
N	15	7

METHOD

REF. NO. 78 We 4

hmg

REACTION	RESULT	EXCITATION ENERGY	SOURCE		DETECTOR		ANGLE
			TYPE	RANGE	TYPE	RANGE	
$ P,G	RLX	14-24	D	4-14	UKN-D		DST

Analysis of data in the following references:

Reference 2, 11

POLARIZED PROTONS

Measurements of cross sections and analyzing powers are examined for polarized proton capture on ^{14}C, ^{28}Si, ^{54}Fe, ^{56}Fe, ^{58}Fe, ^{59}Co, and ^{88}Sr at energies which cover the giant dipole resonance region. These data are used to extract the relative amplitudes and phases of the contributing $E1$ T-matrix elements. A typical result exhibits two solutions. Calculations using the direct (or a direct-semidirect) capture model appear to provide a means for choosing the physical solution.

[NUCLEAR REACTIONS: $^{14}C(\vec{p},\gamma_0)$, $^{30}Si(\vec{p},\gamma_0)$, $^{54}Fe(\vec{p},\gamma_0)$, $^{56}Fe(\vec{p},\gamma_0)$, $^{58}Fe(\vec{p},\gamma_0)$, $^{59}Co(\vec{p},\gamma_0)$, $^{88}Sr(\vec{p},\gamma_0)$; measured $\sigma(\theta)$ and $A(\theta)$ over energy region of the giant dipole resonance. Deduced T-matrix amplitudes and phases. Compare results to direct-semidirect model calculations.]

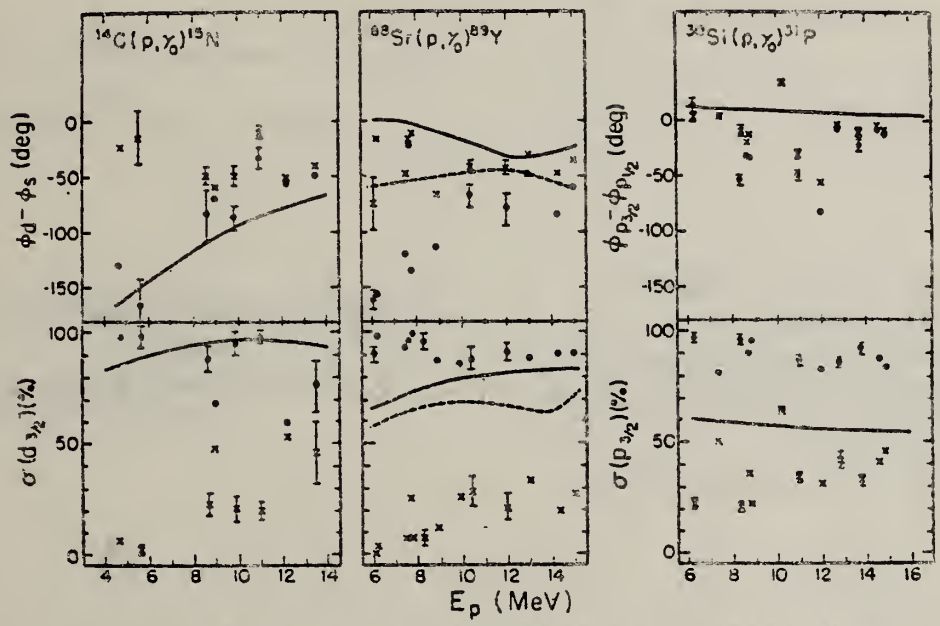

FIG. 1. The two solutions (dots and x's) resulting from a pure $E1$ analysis of the data are shown along with the results of the calculation for target nuclei of ^{14}C, ^{88}Sr, and ^{30}Si. The remaining cross section in the case of ^{14}C and ^{88}Sr is due to the $s_{1/2}$ matrix element. In the case of ^{30}Si it arises from the $p_{1/2}$ matrix element. The error bars represent typical statistical errors associated with the data points. The amplitudes are presented in terms of the percentage of the total cross section for which they are responsible. The curves represent DSD calculations as described in the text. The dashed curves in the case of ^{88}Sr were obtained using the optical model parameters of Ref. 16 while the solid lines were obtained from the parameters of Ref. 18.

(OVER)

[2]H. R. Weller, R. A. Blue, N. R. Roberson, D. G. Rickel, S. Maripuu, C. P. Cameron, R. D. Ledford, and D. R. Tilley, Phys. Rev. C 13, 922 (1976). (Note: an error exists in the sign of the phase in this paper. The quantity $\phi_s - \phi_d$ should be $\phi_d - \phi_s$ wherever it appears.)
[3]C. P. Cameron, N. R. Roberson, D. G. Rickel, R. D. Ledford, H. R. Weller, R. A. Blue, and D. R. Tilley, Phys. Rev. C 14, 553 (1976).
[4]C. P. Cameron, Ph.D. thesis, Duke University, 1976 (unpublished).
[5]R. D. Ledford, Ph.D. thesis, Duke University, 1976 (unpublished).
[6]J. D. Turner, C. P. Cameron, N. R. Roberson, H. R. Weller, and D. R. Tilley, Phys. Rev. C 17, 1853 (1978).

REF. D. M. Skopik, J. J. Murphy II, H. R. Weller, R. A. Blue, N. R. Roberson, S. A. Wender, D. R. Tilley
Phys. Rev. C20, 409 (1979)

ELEM. SYM.	A	Z
N	15	7

METHOD

REF. NO. 79Sk6 hg

REACTION	RESULT	EXCITATION ENERGY	SOURCE		DETECTOR		ANGLE
			TYPE	RANGE	TYPE	RANGE	
E,D	ABX	20-29	D	UKN	MAG-D		DST
$ D,GØ	ABX	20-24	D	5-8	NAI-D		DST
		(20.5-23.3)		(5.08-8.39)			

The cross sections of $^{13}N(\gamma,d_0)^{13}C$ and $^{13}C(d,\gamma_0)^{15}N$ have been measured. A resonance was observed at $E_x \simeq 21.9$ MeV in the (γ,d_0) channel. Vector polarized deuterons were used to measure the angular distribution of gamma rays at this resonance and the results were analyzed assuming the two $S = 1/2$ $E1$ transition matrix elements are dominant.

POL D

[NUCLEAR REACTIONS $^{15}N(\gamma,d_0)^{13}C$, $^{13}C(d,\gamma_0)^{15}N$; measured $\sigma(\theta)$, $A(\theta)$ and σ(tot). Deduced $E1$ T-matrix elements and phases at $E_x \approx 21.9$ MeV.]

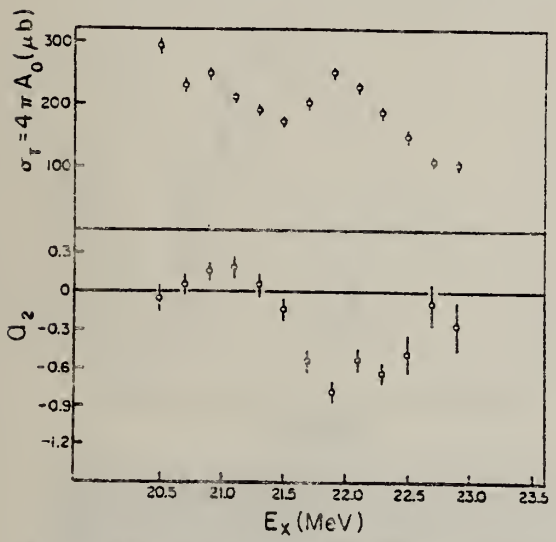

FIG. 2. Results from least squares fitting the (γ,d_0) data to Eq. (1). Shown are $4\pi A_0$ and a_2.

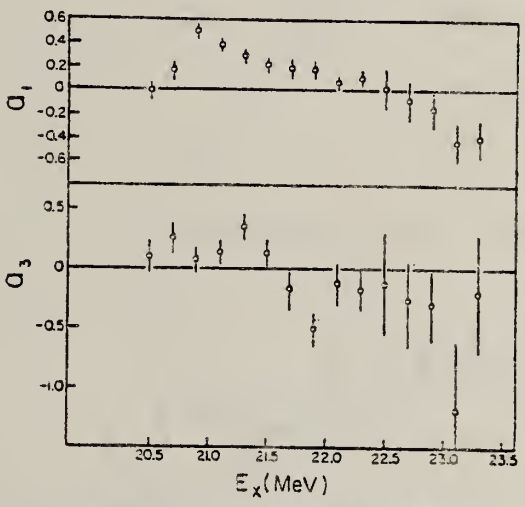

FIG. 3. Results from least squares fitting the (γ,d_0) data to Eq. (1). Shown are the coefficients a_1 and a_3 which reflect interference between different multipoles.

$$\sigma(\theta) = A_0\left[1 + \sum_{k=1} a_k P_k(\cos\theta)\right]. \qquad (1)$$

(OVER)

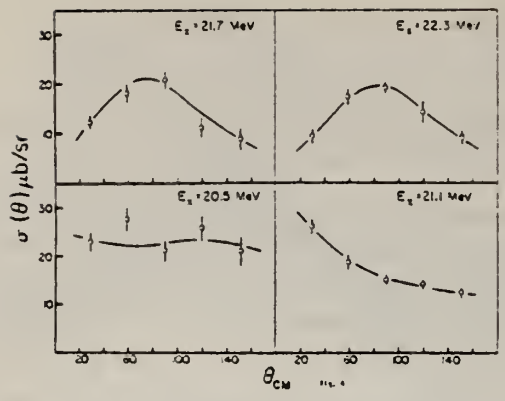

FIG. 4. Representative angular distribution data. The solid lines are the results of least squares fitting the data to Eq. (1).

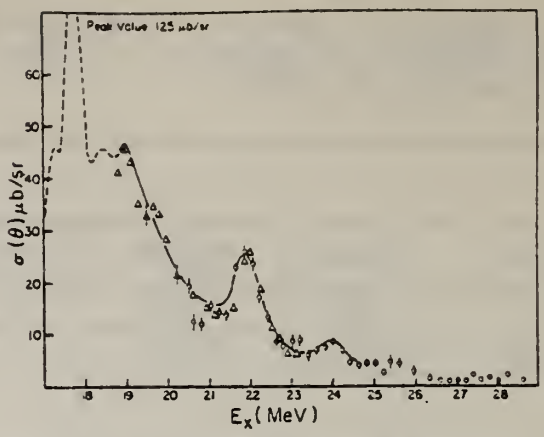

FIG. 5. The 90° cross section for the reaction $^{15}N(\gamma, d_0)$. The dashed line is from Ref. 2 normalized upward by 2.5; the solid line is from Ref. 5; o—$^{15}N(\gamma, d_0)$, this experiment and Δ—$^{13}C(d, \gamma_0)^{15}N$, this experiment.

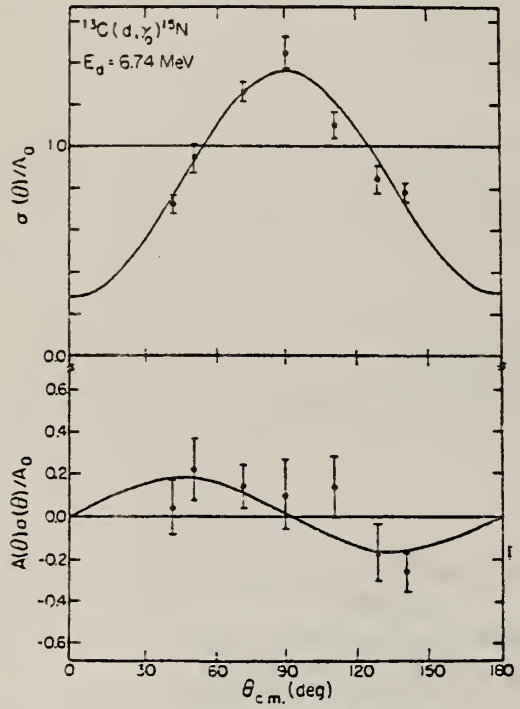

FIG. 6. Asymmetry and cross section data at E_d = 6.74 MeV(E_γ = 21.9 MeV). The solid lines are from least squares fitting the data to Eqs. (2) and (3) as explained in the text.

REF. J. Uegaki, J. Asai, M. K. Leung, J. J. Murphy, II, Y. M. Shin, D. M. Skopik
Can. J. Phys. 57, 1059 (1979)

ELEM. SYM.	A	Z
N	15	7

METHOD

REF. NO. 79Ue1 hg

REACTION	RESULT	EXCITATION ENERGY	SOURCE		DETECTOR		ANGLE
			TYPE	RANGE	TYPE	RANGE	
E,T	ABX	20-25	D	22-26	MAG-D		90

The differential cross section for the reaction $^{15}N(\gamma,t_0)$ at $\theta_{lab} = 90°$ has been obtained for excitation energies between 20 and 25 MeV by the measurement of a triton energy spectrum from the reaction $^{15}N(e,t_0)e'^{12}C$. A virtual photon analysis was used to extract the photodisintegration cross section from the electrodisintegration data. Comparison of this cross section to the cross section at lower excitation energies shows that the $^{15}N(\gamma,t_0)$ strength is concentrated in the region between 16 and 21 MeV. Comparison of the (γ,t_0) cross section with those of other photodisintegration channels suggests an isospin separation energy of 6 MeV.

VIRTUAL PHOTON ANAL.

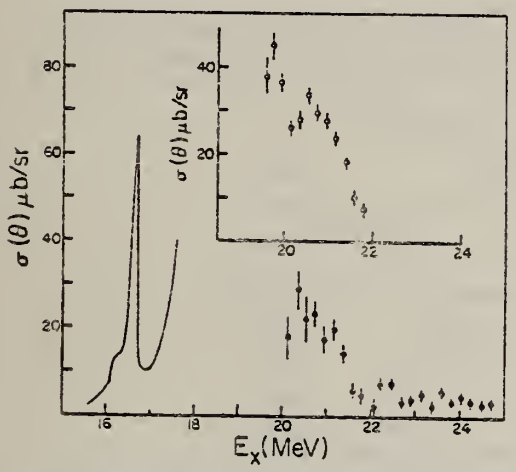

FIG. 2. The 90° cross section for the reaction $^{15}N(\gamma,t_0)^{12}C$. The solid curve is obtained from ref. 11 using detailed balance. The ground state cross section is given by the closed circles. The inset shows the non-ground state cross section in which transitions to the first two excited states in ^{12}C are kinematically allowed.

REF. O. Shahal, R. Moreh, M. Pazi
Nucl. Phys. A339, 157 (1980)

ELEM. SYM.	A	Z
N	15	7

METHOD

REF. NO. 80 Sh 2 hg

REACTION	RESULT	EXCITATION ENERGY	SOURCE		DETECTOR		ANGLE
			TYPE	RANGE	TYPE	RANGE	
G,G	ABX	6	D	6	NAI-D		UKN
		(6.324)		(6.324)			

Abstract: The temperature dependence of the resonance scattering cross section σ_s of the 6.324 MeV photons from ^{15}N in the form of BN and NH_4Cl was measured in the range 78K–640K. Using these data the effective temperatures T_e of the *N-atom* in the two compounds as a function of the temperature T was deduced. At T = 293K we obtained $T_e = 561 \pm 28$K, and 521 ± 57K for BN and NH_4Cl respectively. The values of T_e and the variation versus T were reproduced theoretically by considering the Doppler broadening of the nuclear level, caused by the motion of the N-atom, and described by the frequency distribution function of the lattice in the two compounds. The effect of the values of T_e on the determination of the radiative width of nuclear levels is discussed.

FUNCT. OF TEMP., 6.324

E NUCLEAR REACTION $^{15}N(\gamma, \gamma)$, E = 6.324 MeV; measured temperature dependence of σ. Deduced effective temperatures. Natural BN, enriched NH_4Cl targets.

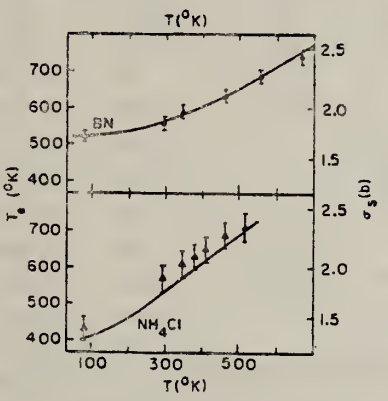

Fig. 3. Absolute scattering cross sections σ_s of the 6.324 MeV photons from ^{15}N in the form of BN and NH_4Cl. The scale of T_e is also given. The solid lines represent theoretical values of T_e (and hence of σ_s) obtained using the function $q(\nu)$ given in figs. 1 and 2 respectively.

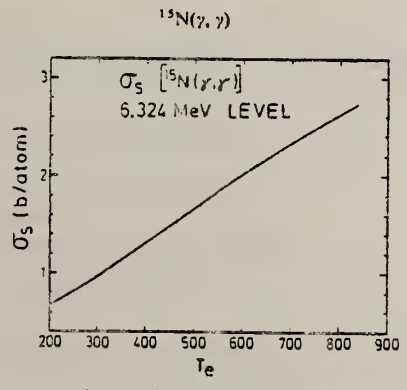

Fig. 4. Calculated scattering cross section σ_s of the 6.324 MeV photons from ^{15}N as a function of T_e as obtained using eq. (2) with the parameters: δ = 29.5 eV, $\Gamma = \Gamma_0$ = 2.9 eV, Δ_i = 9.6 eV, taken from ref. [7]).

(OVER)

TABLE 2

Measured relative scattering intensities I_T/I_{293} of the 6.324 MeV photons from ^{13}N at various temperatures

NH_4Cl			BN		
T(K)	I_T/I_{293}	$T_e(\mp 10\,\%)$	T(K)	I_T/I_{293}	$T_e(\mp 5\,\%)$
78	0.754	433	78	0.928	522
293	1.000	571	293	1.000	561
343	1.059	605	348	1.047	589
364	1.096	627	460	1.123	633
374	1.104	632	558	1.202	682
407	1.140	654	663	1.295	740
461	1.193	687			
513	1.226	708			

The experimental value of T_e was deduced using fig. 4.

REF. R. Moreh, W.C. Sellyey, R. Vodhanel
Phys. Rev. C23, 988 (1981)

EL EM. SYM.	A	Z
N	15	7

METHOD

REF. NO. 81 Mo 1 hg

REACTION	RESULT	EXCITATION ENERGY	SOURCE TYPE	SOURCE RANGE	DETECTOR TYPE	DETECTOR RANGE	ANGLE
G,G	LFT	6-10	C	10,11 (10.3,11.4)	SCD-D		UKN

The ground-state radiative widths of nine levels below 10.2 MeV in ^{15}N were measured using resonance fluorescence. The results are compared with various theoretical predictions and are found to best agree with very recent unpublished calculations in which the full $1\hbar\omega$ configurational basis is included in constructing the wave functions of the ^{15}N levels.

9 LEVELS

[NUCLEAR REACTIONS $^{15}N(\gamma,\gamma')$, E=10.3, 11.4 MeV bremsstrahlung. Deduced E_γ, Γ_0. $LiNO_3$ enriched target.]

TABLE I. Measured widths and excitation energies in ^{15}N. The values of J^π and Γ_0/Γ were taken from Refs. 1 and 17.

E_x (keV)	J^π	Present Γ_0 (eV)	Γ_0/Γ [a] (%)	Others Γ_0 (eV)	Theory Γ_0 [e] (eV)	Theory Γ_0 [f] (eV)	Theory Γ_0 [g] (eV)
6323±1	$\frac{1}{2}^-$	3.12±0.18	100	3.2 ±0.3 [b]	2.8		
7301±1	$\frac{3}{2}^+$	1.08±0.08	99.3±0.7	2.4 ±0.9 [c]	0.2	1.1	1.02
8310±4	$\frac{1}{2}^+$	0.3 ±0.2	79 ±2		0.005	0.006	0.26
8575±4	$\frac{3}{2}^+$	0.3 ±0.3	33 ±2		0.32	0.07	0.41
9048±1	$\frac{1}{2}^+$	1.2 ±0.2	92 ±2		2.6		0.78
9150±1	$\frac{3}{2}^-$	0.47±0.12	100	0.3 ±0.8			
9760±1	$\frac{5}{2}^-$	0.21±0.07	81.5±3	0.20±0.5 [d]	0.004		
9924±1	$\frac{3}{2}^-$	1.6±0.2 [h]	77.6±2		1.12		
10064±1	$\frac{3}{2}^+$	6.3 ±0.4	96.0±0.7		0.11	2.6	5.5

[a] Reference 1.
[b] References 6 and 8.
[c] Reference 7.
[d] Reference 9.
[e] Reference 4.
[f] Reference 14.
[g] Reference 12.
[h] The measured width was obtained by assuming that $J=\frac{3}{2}$ and identification with the theoretical $(\frac{3}{2}^-)_2$ model state.

[1] F. Ajzenberg-Selove, Nucl. Phys. A268, 1 (1976).

[6] G. A. Beer, P. Brix, H. G. Clerc, and B. Laube, Phys. Lett. 26B, 506 (1968).
[7] J. C. Kim, H. S. Caplan, and L. P. Auer, Phys. Lett. 56B, 442 (1975); J. C. Kim, H. S. Caplan, and J. C. Bergstrom, Nucl. Phys. A246, 282 (1975).

[8] R. Moreh and O. Shahal, Nucl. Phys. A252, 429 (1975).
[9] E. J. Ansaldo *et al.*, Can. J. Phys. 55, 2129 (1977).

REF. J.W. Jury, B.L. Berman, J.G. Woodworth, M.N. Thompson, R.E. Pywell, K.G. McNeill
Phys. Rev. C26, 777 (1982)

EL.EM. SYM.	A	Z
N	15	7

METHOD

REF. NO.: 82 Ju 2 | egf

REACTION	RESULT	EXCITATION ENERGY	SOURCE		DETECTOR		ANGLE
			TYPE	RANGE	TYPE	RANGE	
G,1N	ABX	11-38	D	11-38	BF3-I		4PJ
G,2N	ABX	21-38	D	11-38	BF3-I		4PJ
G,SN	ABX	11-38	D	11-38	BF3-I		4PJ

Photoneutron cross sections involving the emission of one and two neutrons from ^{15}N have been measured over the excitation energy interval from threshold (10.8 MeV) to 38 MeV using monoenergetic photons from the annihilation in flight of fast positrons. A very broad giant dipole resonance extending from about 16 to 30 MeV was observed, with a maximum (γ,n_{tot}) cross section of about 11 mb at 23.5 MeV. The magnitude of the measured average photoneutron energies shows that most of the strength below 15 MeV decays to the ground state of ^{14}N, whereas most of the strength in the giant resonance decays to excited states. Comparison with particle-capture cross-section data indicates that multiparticle-multihole interference effects probably account for some of the pronounced intermediate structure observed above 16 MeV in the (γ,n) cross section. Comparison with a recent shell-model calculation favors the use of a Tabakin potential over a δ-function force with a Soper exchange mixture, in marked contrast with recent corresponding results for ^{13}C and ^{17}O. Features of recently measured photoreaction cross sections for the ^{12}C, ^{13}C, ^{14}N, ^{15}N, ^{16}O, ^{17}O, and ^{18}O nuclei are compared as well.

[NUCLEAR REACTIONS $^{15}N(\gamma,n)$, E_γ=10.8–38.0 MeV; measured 4π neutron yield for monoenergetic photons; $(E_\gamma,1n)$, $(E_\gamma,2n)$, integrated cross sections; comparisons of results with other reaction channels and with cross sections for neighboring nuclei; comparison with shell-model theory.]

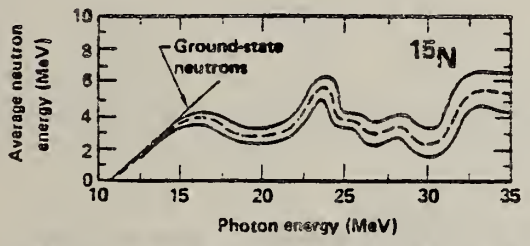

FIG. 2. The average energy of the emitted photoneutrons is plotted as a function of excitation energy in ^{15}N. These average energies were determined from the ring ratios. The light solid lines represent the statistical uncertainty associated with the ring-ratio measurement. The dark line represents the neutron energies expected if all transitions were to the ground state of ^{14}N.

TABLE II. Integrated cross sections for ^{15}N.[a]

Reaction	$\sigma_{int}=\int\sigma dE_\gamma$ (MeV mb)	$\sigma_{-1}=\int\sigma E_\gamma^{-1}dE_\gamma$ (mb)	$\sigma_{-2}=\int\sigma E_\gamma^{-2}dE_\gamma$ (mb MeV^{-1})
$(\gamma,1n)$	98.4	4.38	0.208
$(\gamma,2n)$	7.6	0.26	0.009
(γ,n_{tot})	105.9	4.63	0.216

[a]From threshold to 38.0 MeV.

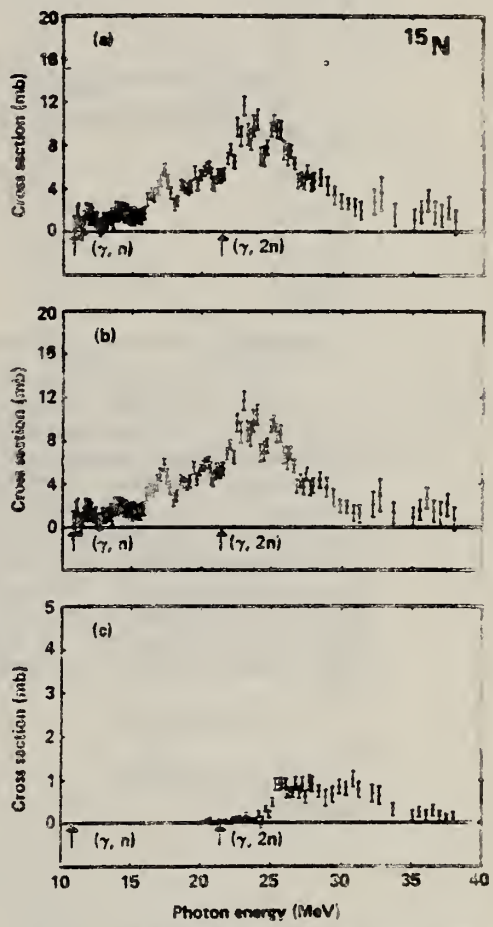

FIG. 1. Photoneutron cross sections for ^{15}N. Part (a) shows the total photoneutron cross section

$$\sigma(\gamma,n_{tot})=\sigma[(\gamma,n)+(\gamma,pn)+(\gamma,\alpha n)+(\gamma,2n)];$$

part (b) shows the single photoneutron cross section

$$\sigma(\gamma,1n)=\sigma[(\gamma,n)+(\gamma,pn)+(\gamma,\alpha n)];$$

part (c) shows $\sigma(\gamma,2n)$. The plotted error flags indicate the statistical uncertainties only. The threshold energies for the (γ,n) and $(\gamma,2n)$ reactions are indicated by arrows. Other photoreaction threshold energies are given in Table I.

(OVER)

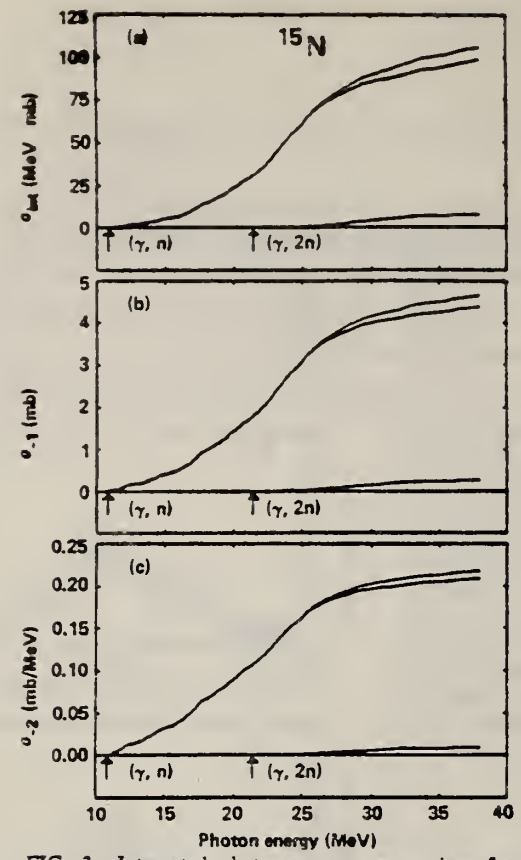

FIG. 3. Integrated photoneutron cross sections for ^{15}N are plotted as functions of the upper limit of integration. Part (a) shows the integrated cross sections $\sigma_{int} = \int \sigma(E_\gamma) dE_\gamma$ for the $(\gamma,2n)$ reaction (bottom curve), the $(\gamma,1n)$ reaction (middle curve), and their sum, the (γ,n_{tot}) reaction (top curve). Integrated cross sections over any desired limits can be obtained from these curves by subtraction. Parts (b) and (c) show the energy-weighted moments of the integrated cross sections

$$\sigma_{-1} = \int \sigma(E_\gamma) E_\gamma^{-1} dE_\gamma$$

and

$$\sigma_{-2} = \int \sigma(E_\gamma) E_\gamma^{-2} dE_\gamma ,$$

respectively.

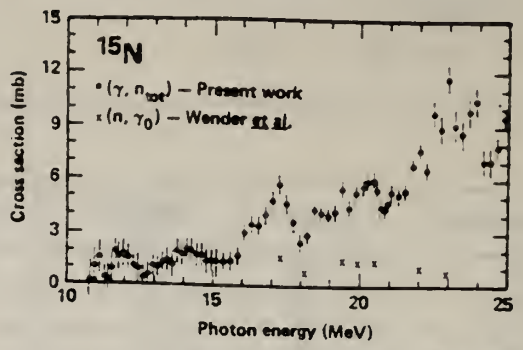

FIG. 4. The present total photoneutron cross section of Fig. 1(a) is shown with expanded scales and compared with the recent ground-state data of Wender *et al.*[12] This shows that $\sigma(\gamma,n_0)$ constitutes only a small part of $\sigma(\gamma,n_{tot})$ above ~17 MeV. [Only those points from Ref. 12 for which angular distributions were measured are plotted here; their 90° excitation function shows more detailed structure (see Table III).]

[12]S. A. Wender, H. R. Weller, N. R. Roberson, D. R. Tilley, and R. G. Seyler, Phys. Rev. C 25, 89 (1982).

82 We 3

REF. S.A. Wender, H.R. Weller, N.R. Roberson, D.R. Tilley, R.G. Seyler
Phys. Rev. C25, 89 (1982)

ELEM. SYM.	A	Z
N	15	7

METHOD

REF. NO.	
82 We 1	hg

REACTION	RESULT	EXCITATION ENERGY	SOURCE		DETECTOR		ANGLE
			TYPE	RANGE	TYPE	RANGE	
N,G	ABX	16-24	C	5-13	NAI-D		DST
				(5.6-13)			

The $^{14}N(n,\gamma_0)^{15}N$ reaction has been studied over a neutron energy range of 5.6 MeV to 13 MeV. Data include a 90° excitation function measured in 200 keV steps, and seven angular distributions. The angular distributions data show good agreement with the results of a phenomenological direct semidirect model calculation. No non-$E1$ radiation is required to account for these data. The cross section as a function of energy is similar to the $^{14}N(p,\gamma_0)^{15}O$ reaction and different from the $^{14}C(p,\gamma_0)^{15}N$ reaction. These differences can be understood in terms of the different isospin states allowed in each reaction.

[NUCLEAR REACTIONS $^{14}N(n,\gamma_0)^{15}N$, measured $\sigma(E,\theta)$ from $E_n=5.6-13.0$ MeV, DSD model calculations, results compared to $^{14}C(p,\gamma_0)^{15}N$ and $^{14}N(p,\gamma_0)^{15}O$.]

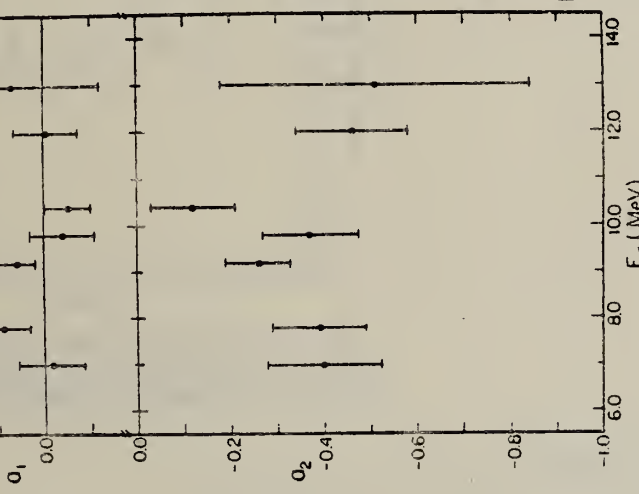

FIG. 6. Coefficients resulting from the Legendre polynomial fits to the angular distributions plotted as a function of γ-ray energy. The error bars represent the statistical errors associated with these coefficients.

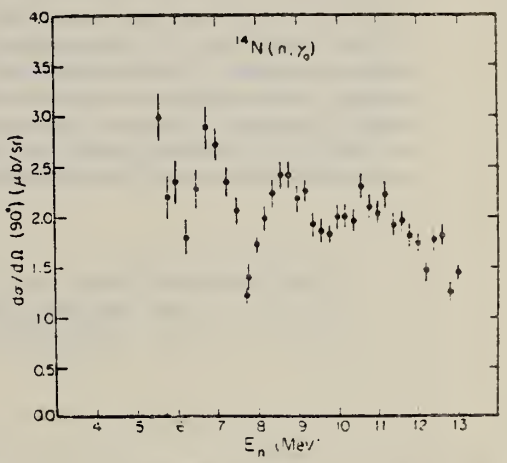

FIG. 4. Cross section at 90 deg for the $^{14}N(n,\gamma_0)^{15}N$ reaction as a function of incident neutron energy. The error bars shown represent only statistical errors.

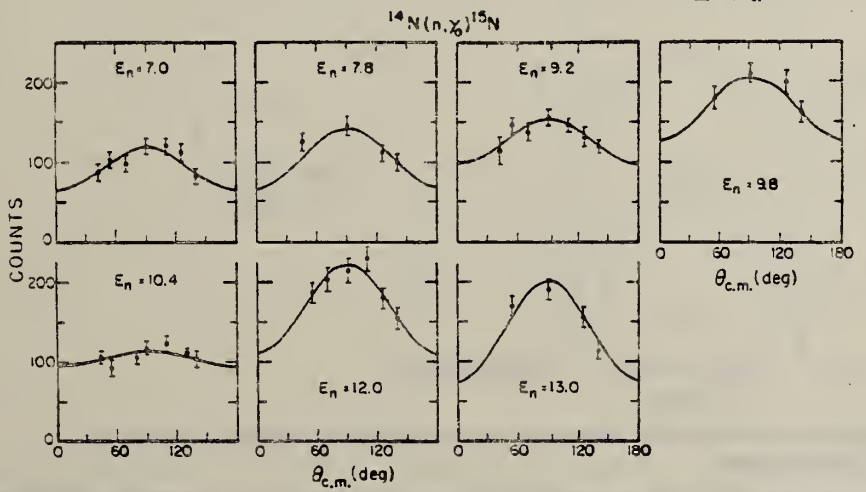

FIG. 5. γ-ray angular distributions for the $^{14}N(n,\gamma_0)^{15}N$ reaction. Curves are the results of Legendre polynomial fits to the data. Error bars represent statistical errors.

REF. S.A. Wender, H.R. Weller, N.R. Roberson, D.R. Tilley, R.G. Seyler
Phys. Rev. C25, 89 (1982)

ELEM. SYM.	A	Z
N	15	7

METHOD

REF. NO. 82 We 3 egf

REACTION	RESULT	EXCITATION ENERGY	SOURCE TYPE	SOURCE RANGE	DETECTOR TYPE	DETECTOR RANGE	ANGLE
N,GØ	ABX	16-23	D	6-13	NAI-D		DST

The $^{14}N(n,\gamma_0)^{15}N$ reaction has been studied over a neutron energy range of 5.6 MeV to 13 MeV. Data include a 90° excitation function measured in 200 keV steps, and seven angular distributions. The angular distribution data show good agreement with the results of a phenomenological direct semidirect model calculation. No non-$E1$ radiation is required to account for these data. The cross section as a function of energy is similar to the $^{14}N(p,\gamma_0)^{15}O$ reaction and different from the $^{14}C(p,\gamma_0)^{15}N$ reaction. These differences can be understood in terms of the different isospin states allowed in each reaction.

[NUCLEAR REACTIONS $^{14}N(n,\gamma_0)^{15}N$, measured $\sigma(E,\theta)$ from $E_n=5.6-13.0$ MeV, DSD model calculations, results compared to $^{14}C(p,\gamma_0)^{15}N$ and $^{14}N(p,\gamma_0)^{15}O$.]

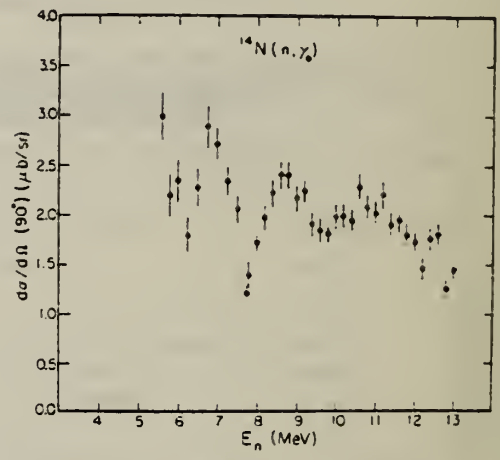

FIG. 4. Cross section at 90 deg for the $^{14}N(n,\gamma_0)^{15}N$ reaction as a function of incident neutron energy. The error bars shown represent only statistical errors.

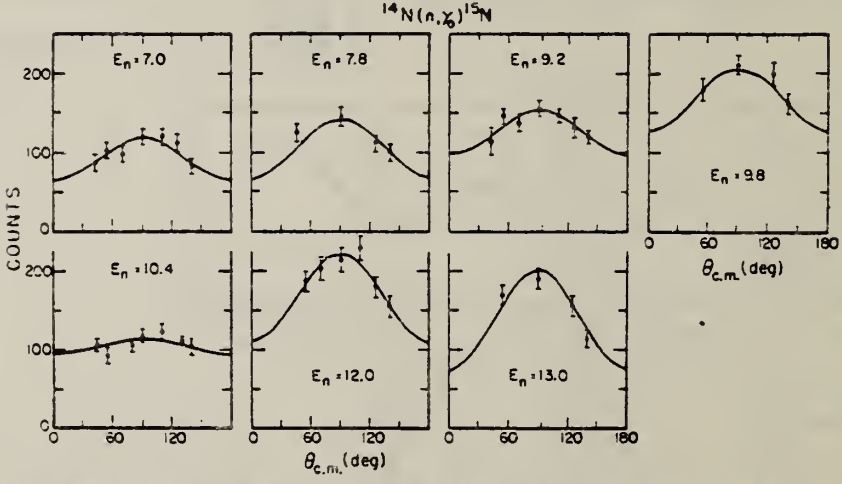

FIG. 5. γ-ray angular distributions for the $^{14}N(n,\gamma_0)^{15}N$ reaction. Curves are the results of Legendre polynomial fits to the data. Error bars represent statistical errors.

N
A=16

N
A=16

N
A=16

REF. G. Strassner, P. Truöl, J.C. Alder, B. Gabioud, C. Joseph, J.F. Loude, N. Morel, A. Perrenoud, J.P. Perroud, M.T. Tran, E. Winkelmann, W. Dahme, H. Panke, D. Renker, H.A. Medicus
Phys. Rev. C20, 248 (1979)

EL EM. SYM.	A	Z
N	16.	7

METHOD

REF. NO. 79 St 8 hg

REACTION	RESULT	EXCITATION ENERGY	SOURCE		DETECTOR		ANGLE
			TYPE	RANGE	TYPE	RANGE	
PI,G	SPC	128	D	*200	MGP-D		90

The photon spectra from the reaction $^{16}O(\pi^-,\gamma)^{16}N$ and $^{18}O(\pi^-,\gamma)^{18}N$ were measured with a high-resolution pair spectrometer. Transitions to 2^- states having $T = 1$ in ^{16}N and $T = 2$ in ^{18}N appear to dominate. Excitation of 1^- states in the giant dipole resonance region, which are the analogs of the levels excited in photoabsorption and inelastic electron scattering on ^{16}O and ^{18}O, respectively, were also observed. The total and partial branching ratios for bound states and giant-resonance transitions are compared with shell-model predictions. Higher admixtures to the predominantly 1p-1h wave functions are found to be necessary to obtain agreement with the measured branching ratios. A new treatment of the continuum and resonance excitation, based on calculations of Ohtsubo *et al.*, is compared with the data.

*MEV/C, PI=PI-

[NUCLEAR REACTIONS Radiative pion capture; measured photon spectra for $^{16}O(\pi^-,\gamma)^{16}N$ and $^{18}O(\pi^-,\gamma)^{18}N$; deduced transitions and transition strength with $J^\pi = 1^-$, 2^- and $T = 1$ and $T = 2$ respectively; comparison with shell-model calculations.]

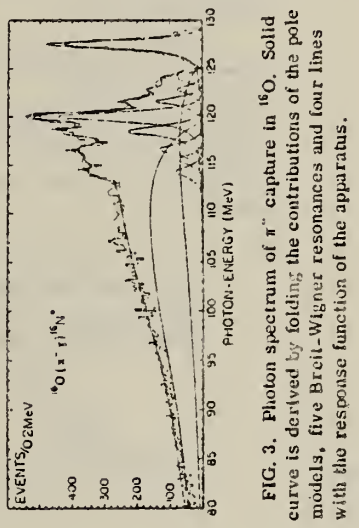

FIG. 3. Photon spectrum of π^- capture in ^{16}O. Solid curve is derived by folding the contributions of the pole models, five Breit-Wigner resonances and four lines with the response function of the apparatus.

TABLE I. Experimental parameters for radiative pion capture $^{16}O(\pi^-,\gamma)^{16}N$. Comparison of deduced excitation energies with levels seen in other reactions and assigned spins. [$T = 1$; all energies in MeV.]

$^{16}O(\pi^-,\gamma)^{16}N$			$^{16}O(e,e')^{16}O^{*}$ [a]		$^{16}O(\gamma,n)^{15}N$ [b]		$^{16}O(\gamma,p)^{15}N$ [c]		$^{15}N(p,\gamma_0)^{16}O$ [d]		$^{15}N(p,\gamma_{3^-,6.13})^{16}O^{*}$ [e]	
E_γ	$E_x(^{16}N)$	$E_x(^{16}O)$	$E_x(^{16}O)$	J^π	$E_x(^{16}O)$	J^π	$E_x(^{16}O)$	J^π	$E_x(^{16}O)$	J^π	$E_x(^{16}O)$	J^π
128.0	0	12.98	12.93	2^-								
123.9	4.1 ± 0.2	17.1 ± 0.2	17.14	1^-	17.3	1^-	17.3	1^-	17.13 17.28	1^- 1^-		
123.2	4.8 ± 0.2	17.7 ± 0.2	17.60	2^-								
121.7	6.1 ± 0.2	19.0 ± 0.2	19.04 19.50	2^- 1^-	19.3	1^-	19.0 19.5	1^- 1^-	19.02 19.52	1^- 1^-	18.38	≥2,3,4
120.5	7.5 ± 0.2	20.4 ± 0.2	20.36	2^-	20.9	1^-	20.85	1^-	20.945	1^-	20.40	2^-
118.8	9.1 ± 0.2	22.2 ± 0.2	22.30	1^-	22.2	1^-	22.16	1^-	22.146	1^-		
116.9	11.1 ± 0.2	24.0 ± 0.2	24.20	1^-	24.05	1^-	24.04	1^-	24.065	1^-		
115.8	12.2 ± 0.2	25.2 ± 0.2			25.20	1^-	25.0 25.5	1^- 1^-	25.117	1^-		
114.5	13.5 ± 0.2	26.4 ± 0.2					26.3	1^-				

[a] Reference 16.
[b] Reference 10-13.
[c] References 10, 14, 15.
[d] Reference 17.
[e] Reference 18.

(over)

TABLE II. The experimental partial branching ratios.

E_γ [a]	N_γ [b]	$R_\gamma \times 10^{-4}$ [c]	$R_\gamma \times 10^{-4}$ [d]	Remarks [e]
Resonance contribution				
128	3642 ± 62	14.5 ± 1.6	15.0 ± 3.0	No separation of 2^-, 0^-, 1^-, 3^-
123.9	583 ± 52	2.3 ± 0.4		Line, $J^\pi = 1^-$
123.2	605 ± 59	2.4 ± 0.4		Line, $J^\pi = 2^-$
121.7	1110 ± 64	4.4 ± 0.6		Line, $J^\pi = 2^-$
120.5	3773 ± 92	15.1 ± 1.6	25 ± 6	BW, Γ = 85 keV, $J^\pi = 2^-$
118.8	2336 ± 81	9.3 ± 1.2		BW, Γ = 220 keV, $J^\pi = 1^-$
116.9	1446 ± 96	5.8 ± 0.8		BW, Γ = 330 keV, $J^\pi = 1^-$
115.8	731 ± 92	2.9 ± 0.6		BW, Γ = 280 keV, $J^\pi = 1^-$
114.5	894 ± 91	3.6 ± 0.6		BW, Γ = 350 keV, $J^\pi = 1^-$, 2^-, (2^+)
Continuum contribution [f]				
125.5	11731 ± 232	46.8 ± 5.2	184 ± 39	Pole model, $^{15}N(E_x = 0)$, $J^\pi \frac{1}{2}^-$
119.2	30070 ± 252	120.0 ± 13.0		Pole model, $^{15}N^*(E_x = 6.3$ MeV), $J^\pi = \frac{1}{2}^-$
Total branching ratio				
	56921 ± 481	227 ± 24	224 ± 48	

[a] Photon energy in MeV.
[b] Number of events in spectrum.
[c] Branching ratio measured in this experiment.
[d] Reference 1.
[e] BW corresponds to Breit-Wigner level shape.
[f] See text.

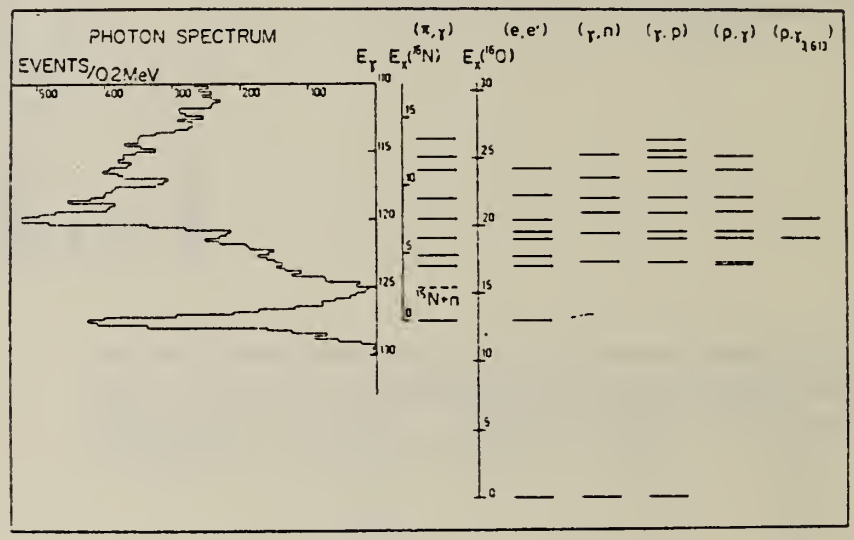

FIG. 2. The photon spectrum for the reaction $^{16}O(\pi^-, \gamma)^{15}N$ in the bound-state and the giant-dipole excitation region. Comparison of observed transitions with levels seen in ^{15}N and ^{16}O.

N
A=18

N
A=18

N
A

REF. G. Strassner, P. Truöl, J.C. Alder, B. Gabioud, C. Joseph, J.F. Loude, N. Morel, A. Perrenoud, J.P. Perroud, M.T. Tran, E. Winkelmann, W. Dahme, H. Panke, D. Renker, H.A. Medicus
Phys. Rev. C20, 248 (1979)

EL, EM. SYM.	A	Z
N	18	7

METHOD

REF. NO. 79 St 8 | hg

REACTION	RESULT	EXCITATION ENERGY	SOURCE		DETECTOR		ANGLE
			TYPE	RANGE	TYPE	RANGE	
PI,G	SPC	128	D	*200	MGP-D		90

*MEV/C, PI=PI-

The photon spectra from the reaction $^{16}O(\pi^-,\gamma)^{16}N$ and $^{18}O(\pi^-,\gamma)^{18}N$ were measured with a high-resolution pair spectrometer. Transitions to 2^- states having $T = 1$ in ^{16}N and $T = 2$ in ^{18}N appear to dominate. Excitation of 1^- states in the giant dipole resonance region, which are the analogs of the levels excited in photoabsorption and inelastic electron scattering on ^{16}O and ^{18}O, respectively, were also observed. The total and partial branching ratios for bound states and giant-resonance transitions are compared with shell-model predictions. Higher admixtures to the predominantly 1p-1h wave functions are found to be necessary to obtain agreement with the measured branching ratios. A new treatment of the continuum and resonance excitation, based on calculations of Ohtsubo *et al.*, is compared with the data.

[NUCLEAR REACTIONS Radiative pion capture; measured photon spectra for $^{16}O(\pi^-,\gamma)^{16}N$ and $^{18}O(\pi^-,\gamma)^{18}N$; deduced transitions and transition strength with $J^\pi = 1^-$, 2^- and $T=1$ and $T=2$ respectively; comparison with shell-model calculations.]

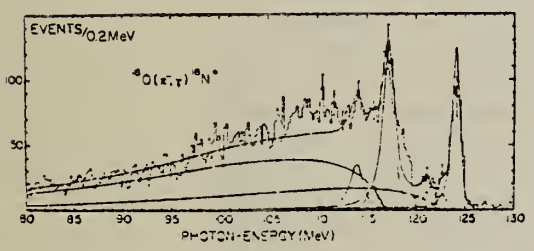

FIG. 4. Photon spectrum of π^- capture in ^{18}O. Solid curve is derived by folding the contributions of the pole models, four Breit-Wigner resonances and two lines with the response function of the apparatus.

TABLE III. Experimental parameters for radiative pion capture $^{18}O(\pi^-,\gamma)^{18}N$; all energies in MeV. The first column gives the photon energy, the second and the third columns give the excitation energies in ^{18}N and for the analog levels in ^{18}O. The third and the fourth columns list the transitions seen in other experiments, while the last column gives the radiative capture branching ratios.

$^{18}O(\pi^-,\gamma)^{18}N$			$^{18}O(e,e')^{18}O$ [a]	$^{18}O(\gamma,n)^{17}N$ [b]	$R_\gamma \times 10^{-4}$	
E_γ	$E_x(^{18}N)$	$E_x(^{18}O)$	$E_x(^{18}O)$	$E_x(^{18}O)$		
124.4	0	16.2	16.6	17.3	12.3 ± 1.6	
123.1	1.3 ± 0.2	17.6 ± 0.2	18.4		1.2 ± 0.4	
121.5	2.9 ± 0.2	19.2 ± 0.2		19.2	1.4 ± 0.3	
			20.2	22.3		
117.5	6.9 ± 0.2	23.2 ± 0.2	21.9	23.4	18.1 ± 2.2	
			23.7			
116.0	8.5 ± 0.2	24.8 ± 0.2	25.2	24.2	2.3 ± 0.8	
				25.2	6.7 ± 0.7	
114.3	10.1 ± 0.2	26.4 ± 0.2	26.9	27.5		
					Pole I 43.6 ± 5.3	
					Pole II 110.2 ± 12.6	
					Total 196 ± 22	

[a] Reference 25.
[b] References 23 and 24.

OXYGEN
Z=8

Oxygen eluded early investigators although it is the most abundant of the elements. A reference to oxygen (*ȳne*), is found in a Chinese book written by Mao-Kho'a in the eighth century A.D. The topics of combustion and the release of oxygen by heating saltpeter is discussed. The authenticity of the manuscript, however, is in question.

O
A=15

The first European to recognize that air contains at least two constituents was Leonardo da Vinci (1452-1519) who noticed that air is consumed, but not completely, in respiration and combustion. The discovery of oxygen is generally attributed to C. W. Scheele who, in 1772, obtained it by heating metal oxides. It was discovered independently in 1774 by Joseph Priestly (1733-1804) in England. Priestly's results were published before those of Scheele because Scheele's publisher had been inexcusably negligent. Antoine-Laurent Lavoisier (1743-1774) was the first to recognize oxygen as a chemical element. He called it oxygène from the Greek (*oxýs+gen*) "for acid maker."

O
A=15

Ref. S.G. Cohen, P.S. Fischer, E.K. Warburton
Phys. Rev. Letters 3, 433 (1959)

Elem. Sym.	A	Z
O	15	8

Method: Princeton FM cyclotron; NaI

Ref. No.: 59 Co 2 JOC

Reaction	E or ΔE	E_o	Γ	$\int \sigma dE$	Jπ	Notes
$N^{14}(p,\gamma_o)$	E_x= 19-25					$4\pi \left(\frac{d\sigma}{dr}\right)\Big\|_{90^\circ} \simeq 30\mu b$

Ref. S.G. Cohen, P.S. Fisher, E.K. Warburton
Phys. Rev. 121, 858 (1961)

Elem. Sym.	A	Z
O	15	8

Method
Synchrocyclotron; NaI

Ref. No. 61 Co 1 JH

Reaction	E or ΔE	E_o	Γ	$\int \sigma dE$	Jπ	Notes
(p,γ_o)	12-19.5			$7.7 \int_{18.7}^{24.6}$ MeV-mb		This proton energy range corresponds to γ exception range 18-25 MeV. Little indication of giant resonance structure. Integral cross section value for (γ,p_o) was obtained from data in Figure 6a.

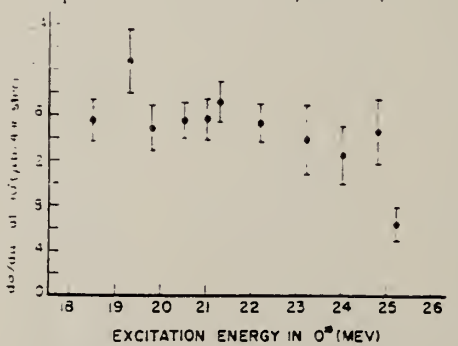

The differential cross section at 90° for the γ rays leading to the ground state of O^{15} from the $N^{14}(p,\gamma_0)O^{15}$ reaction. If the γ rays have an isotropic distribution relative to the proton beam, the scale gives the total cross section.

Ref. G.M. Bailey, D.F. Hebbard
Nuclear Phys. 46, 529 (1963)

Elem. Sym.	A	Z
O	15	8

Method Cockraft-Walton; γ-ray angular distribution; NaI

Ref. No. 63 Ba 2 JHE

Reaction	E or ΔE	E_o	Γ	$\int \sigma dE$	$J\pi$	Notes
$N^{14}(p,\gamma)$	0.800	8.02				$w(\theta_\gamma) = P_o(\cos\theta)-(0.01\pm0.07)P_2(\cos\theta)$ Ground state transition is 19±3%.

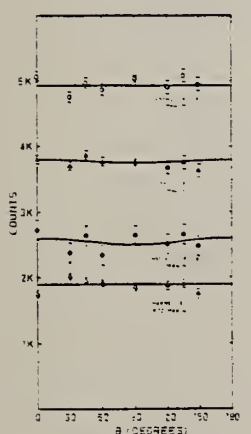

Fig. 3. The experimental points and the least squares fits for the angular distributions (at $E_p = 800$ keV) in the four energy regions defined in fig. 2 are shown in this diagram. A time-dependent background has been subtracted, and correction made for radiation from a beam-defining aperture (by a separate run with a blank target).

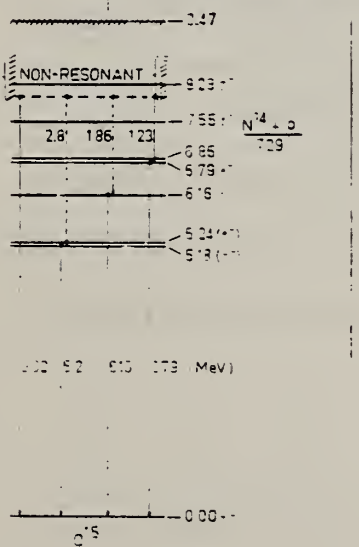

Fig. 4. The full lines on this energy level diagram of O^{15} indicate the non-resonant γ-ray transitions whose angular distributions are measured.

TABLE I

$N^{14}(p,\gamma)$ angular distributions and relative intensities

Gamma ray energy (MeV)	Angular distribution a)	Relative intensity b) mean value
8.02	$P_o + (0.01 \pm 0.07)P_2$	19 ± 3
6.79	$P_o + (0.00 \pm 0.03)P_2$	55 ± 3
6.16	$P_o + (0.02 \pm 0.15)P_2$	17 ± 3
5.2	$P_o + (0.03 \pm 0.30)P_2$	9 ± 5

a) Correction has been made for the smoothing effect of the non-zero solid angle of the de
b) The relative intensities were measured at E_p = 800 keV in the region of non-resonant
and have been corrected for the $N^{15}(p,p\gamma)$ radiation identified. A mean value is taken for
intensities obtained from spectrum peeling of fig. 2 and from the P_2 coefficients extracted dur
angular distribution analysis. The errors quoted reflect the agreement of the two methods.

TABLE III. Decay properties of the 8.28-MeV level of O^{15}.

Energy (MeV)	Interpretation	% yield[a]	Angular distribution	Γ_γ (eV)[b]	Assumed multipolarity	Strength (Weisskopf units)
8.29	8.28 → 0	53.8 ±0.25	$1-(0.035\pm0.02)P_2$	0.531	$E1$	0.0017
3.04	8.28 → 5.24	42.7 ±0.5	Isotropic ±1%	0.405	$M1$	0.37
2.11	8.28 → 6.18	2.2 ±0.6		0.021	$E1$	0.04
1.43	8.28 → 6.86	1.16±0.3		0.011	$E1$, $M1$	0.0055, 0.055
1.61	6.86 → 5.24	1.37±0.3			$E1$, $M1$	
5.25	5.24 → 0	44.8 ±0.5	Isotropic ±2%		$M2$	
6.18	6.18 → 0	2.2 ±0.23			$M1$	
			Nonresonant components			
1.50	to 6.79	1.8 ±1.0[c]	$\sin^2\theta(d)$		$M1$	
6.79	6.79 → 0	0.8 ±0.35			$E1$	
1.09	$O^{16}(p,\gamma)F^{17}$		$\sim\sin^2\theta$			

[a] % of decay of 8.28-MeV level.
[b] Based on the absolute measurements of Duncan and Perry (Ref. 5).
[c] At 45°.
[d] Reference 26.

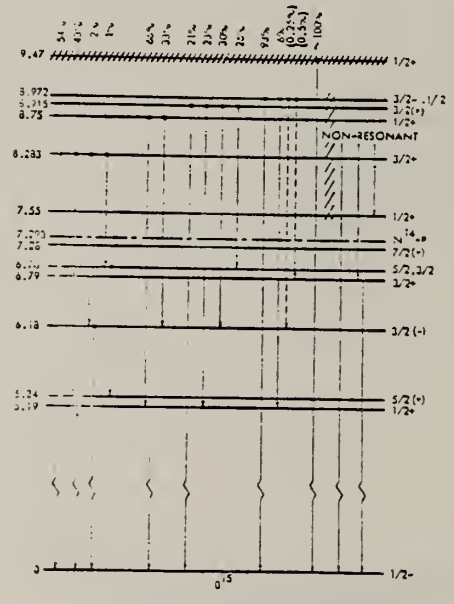

FIG. 13. Decay of excited states of O^{15}.

REACTION	RESULT	EXCITATION ENERGY	SOURCE		DETECTOR		ANGLE
			TYPE	RANGE	TYPE	RANGE	

TABLE IV. Decay of the 8.915-MeV level of O^{16}.

Energy (MeV)	Interpretation	Relative yield (%)	Angular distribution	Γ_γ (eV)[b]	Assumed multipolarity	Strength (Weisskopf units)
8.92	8.92 → 0	21±2	$1+(0.31\pm0.08)P_2$	0.056	$E1$	0.0022
3.73	8.92 → 5.19	23±6		0.094	$M1$	0.038
2.74	8.92 → 6.18	30±3		0.094	$E1$	0.009
2.11	8.92 → 6.79–6.86	26±3		0.069	$E1$, $M1$	0.014, 0.14
1.61	6.86 → 5.24	23±1				
5.19	5.19 → 0	55±4	Isotropic			
	5.24 → 0					
6.18	6.18 → 0	23±4	$1-(0.26+0.2)P_2+(0.1\pm0.2)P_4$			
6.79[a]	6.79 → 0	6±4				

[a] Nonresonant.
[b] Based on the absolute total width given in Ref. 5.

TABLE V. Decay of the 8.972-MeV level of O^{15}.

Energy (MeV)	Interpretation	% yield	Angular distribution	Γ_γ (eV)	Assumed multipolarity	Strength (Weisskopf units)
8.97	8.97 → 0	93.4	$1+(0.053\pm0.03)P_2$ $+(0.0034\pm0.03)P_4$	0.74	$M1$	0.025
3.79	8.97 → 5.19	5.9		0.046	$E1$	0.0018
5.19	5.19 → 0	5.9			$E1$	
6.79	6.79 → 0	(0.50)				
6.18	6.18 → 0	(0.25)				
	(8.97 → 6.79)			(0.004)	$E1$	(0.0008)
	(8.97 → 6.18)			(0.002)	$M1$	(0.0022)

REF.

A. E. Evans
Phys. Rev. 155, 1047 (1967)

ELEM. SYM.	A	Z
O	15	8

METHOD

REF. NO.	
67 Ev 1	JOC

REACTION	RESULT	EXCITATION ENERGY	SOURCE		DETECTOR		ANGLE
			TYPE	RANGE	TYPE	RANGE	
P,G	LFT	9-10	D	1-3	NAI-D		DST

TABLE I. Comparison of measured energies and widths of the 9.49- and 9.60-MeV levels of O^{15}.

Reference	Reaction	9.49-MeV level E_x (MeV)	9.49-MeV level Γ (keV)	9.60-MeV level E_x (MeV)	9.60-MeV level Γ (keV)
9	$N^{14}(p,\gamma)O^{15}$	2.356±0.008	14 ±4	2.489±0.007	11±3
10	$N^{14}(p,p)N^{14}$	2.36		2.49	
11	$N^{14}(p,p)N^{14}$	2.349±0.003	8.5±1.5	2.478±0.004	11±2
12	$N^{14}(p,p)N^{14}$	2.350±0.027	11.3	2.478±002	9.7
This work	$N^{14}(p,\gamma)O^{15}$	2.352±0.005[a]	10 ±2	2.480±0.005[a]	13±2

[a] Based upon $C^{13}(p,\gamma)N^{14}$ 1.7476 MeV (Ref. 8).

TABLE II. Decay of the 9.49-MeV level of O^{15}.

E_γ (MeV)	Interpretation	% yield	Γ_γ (eV)[a]	Assumed multi-polarity	Strength[a] (Weisskopf units)
9.49	9.49 → 0	86	2.1	$E2$	14
4.27	9.49 → 5.24	6.5	0.15	$E1$	0.11
3.31	9.49 → 6.18	0.7	0.02	$M1$	0.03
2.75	9.49 → 6.86	3.4	0.08	$E1$	0.02
2.24	9.49 → 7.28	5.1	0.11	$E1$	0.06
6.18	6.18 → 0	Obscured			
5.24	5.24 → 0	13.4			
2.04	7.28 → 5.24	3.7			
1.62	6.86 → 5.24	3.1			

[a] Assuming $J^\pi = \frac{1}{2}^-$ and $\omega\Gamma_\gamma = 2.4$ eV (Ref. 9) for the 9.49-MeV level.

TABLE III. Decay of the 9.60-MeV level of O^{15}.

E_γ (MeV)	Interpretation	% yield	Γ_γ (eV)[a]	Assumed multi-polarity	Strength[a] (Weisskopf units)
9.60	9.60 → 0	79	4.0	$M1$, $E2$	0.25
4.38	9.60 → 5.24	19	1.0	$E1$	0.07
3.424	9.60 → 6.18	2	0.1	$M1$	0.14
6.18	6.18 → 0	Obscured			
5.24	5.24 → 0	19			

[a] Assuming $\omega\Gamma_\gamma = 3.3$ MeV (Ref. 9) and $J^\pi = 3/2^+$ for the 9.60-MeV level.

REF. H. M. Kuan, M. Hasinoff, W. J. O'Connell, S. S. Hanna
Nucl. Phys. A151, 129 (1970)

ELEM. SYM	A	Z
O	15	8

METHOD

REF. NO. 70 Ku 1

egf

REACTION	RESULT	EXCITATION ENERGY	SOURCE		DETECTOR		ANGLE
			TYPE	RANGE	TYPE	RANGE	
P,G	ABX	11-24	D	2-19	NAI-D	8-24	DST
				(2.2-19.)			

)46

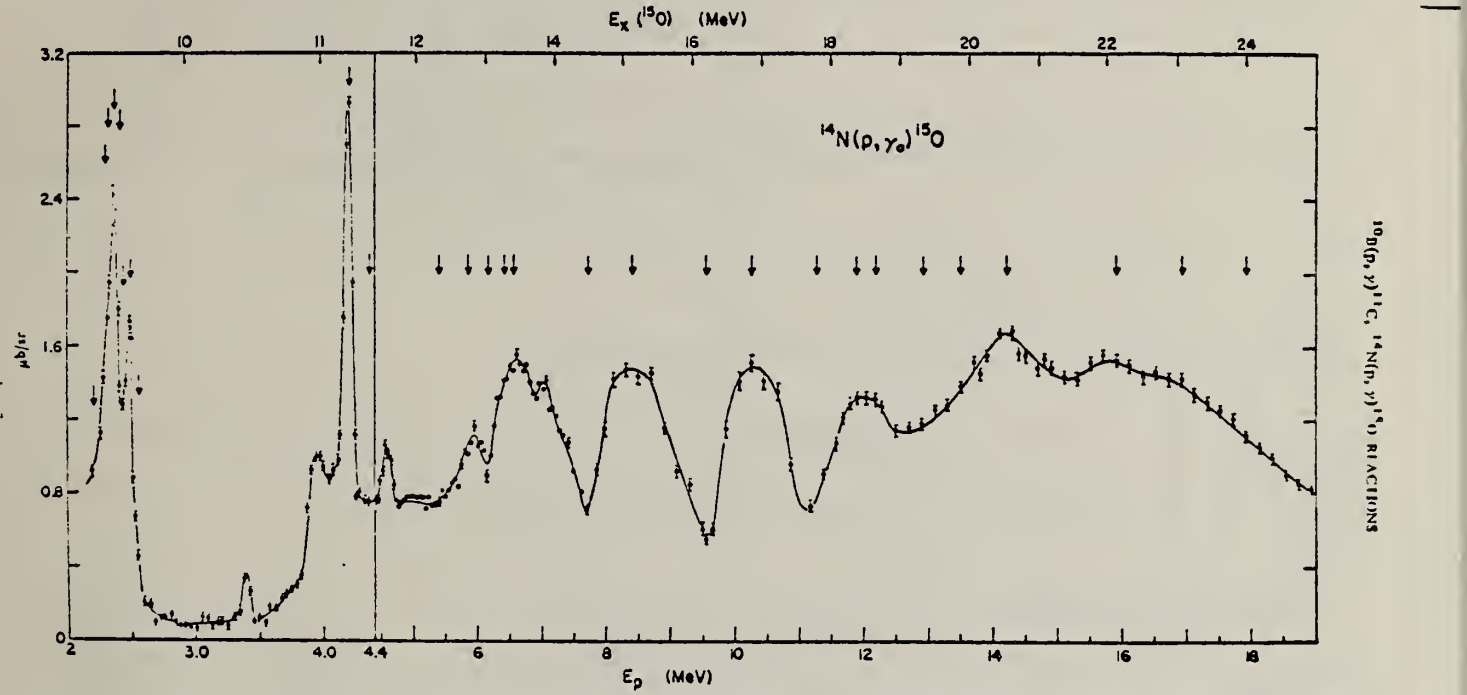

Fig. 7. The 90° yield curve of ^{14}N(p, γ_0)^{15}O. The energy scale below E_p = 4.4 MeV is doubled in order to display the fine structure. The arrows mark energies at which angular distributions were measured.

TABLE 1

Resonances and prominent structure observed in ^{14}N(p, γ_0)^{15}O

E_p (MeV)	E_x(^{15}O) (MeV)	Γ (keV)	J^π	E_p (MeV)	E_x(^{15}O) (MeV)	Γ (keV)	J^π
2.352	9.49	10	$\frac{1}{2}^-$	5.9	12.79	≈ 250	
2.36	9.50	300	$\frac{1}{2}^+$	6.6	13.45	≈ 1000	$(\frac{1}{2}^+, \frac{3}{2}^+)$
2.480	9.60	13	$\frac{3}{2}^-$	7.05	13.87	≈ 150	
3.39	10.45	50		8.4	15.1	≈ 1000	$(\frac{1}{2}^+, \frac{3}{2}^+)$
3.95	10.98	100		10.3	16.8	≈ 1000	$(\frac{1}{2}^+, \frac{3}{2}^+)$
4.20	11.20	40	$\frac{3}{2}^+$	11.9	18.4	≈ 1000	$(\frac{1}{2}^+, \frac{3}{2}^+)$
4.58	11.56	150		14.2	20.5	≈ 2000	$(\frac{1}{2}^+, \frac{3}{2}^+)$
				15.8	21.9	≈ 2000	$(\frac{1}{2}^+, \frac{3}{2}^+)$

[over]

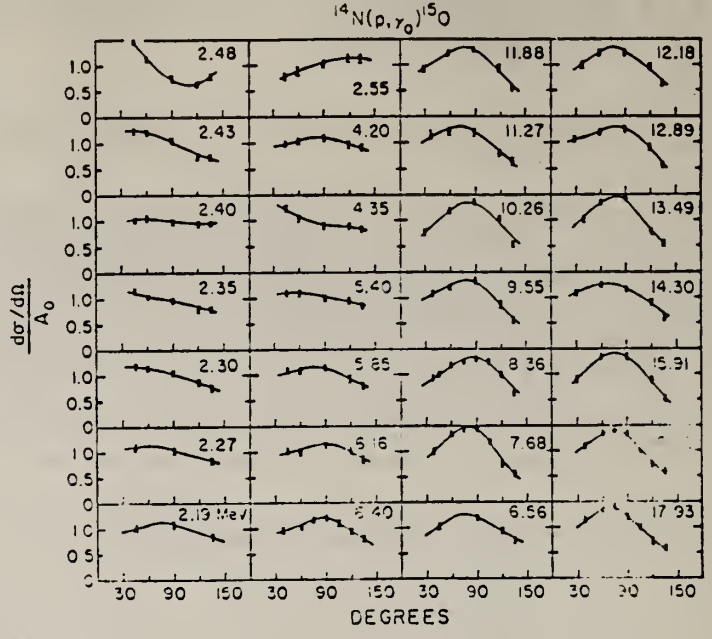

Fig. 8. Angular distributions of $^{14}N(p,\gamma_0)^{15}O$ plotted in units of $1/A_0$, where A_0 is obtained from the least-squares fits to $W(\theta) = A_0(1 + \Sigma a_n P_n)$.

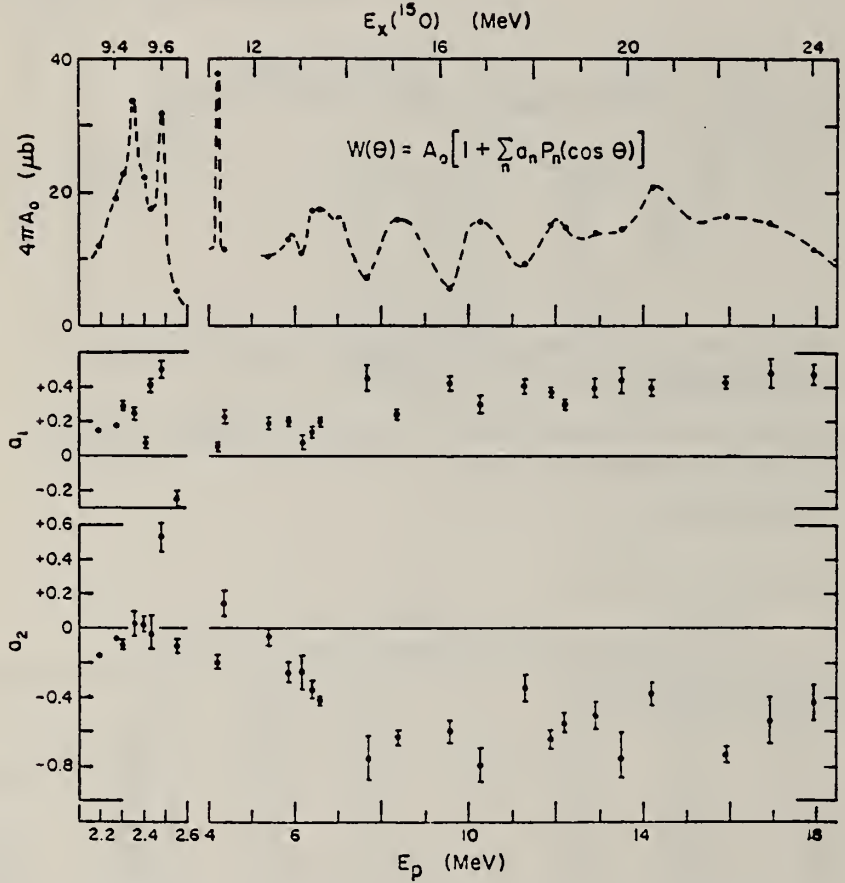

Fig. 9. The coefficients A_0, a_1 and a_2 for $^{14}N(p,\gamma_0)^{15}O$ obtained from least-squares fits to $W(\theta) = A_0(1 + \Sigma a_n P_n)$ with terms up to and including P_2. The solid angle subtended by the detector attenuates a_2 by about 3 %.

ELEM. SYM.	A	Z
O	15	8

METHOD

REF. NO.	
70 Ku 1	egf

REACTION	RESULT	EXCITATION ENERGY	SOURCE		DETECTOR		ANGLE
			TYPE	RANGE	TYPE	RANGE	

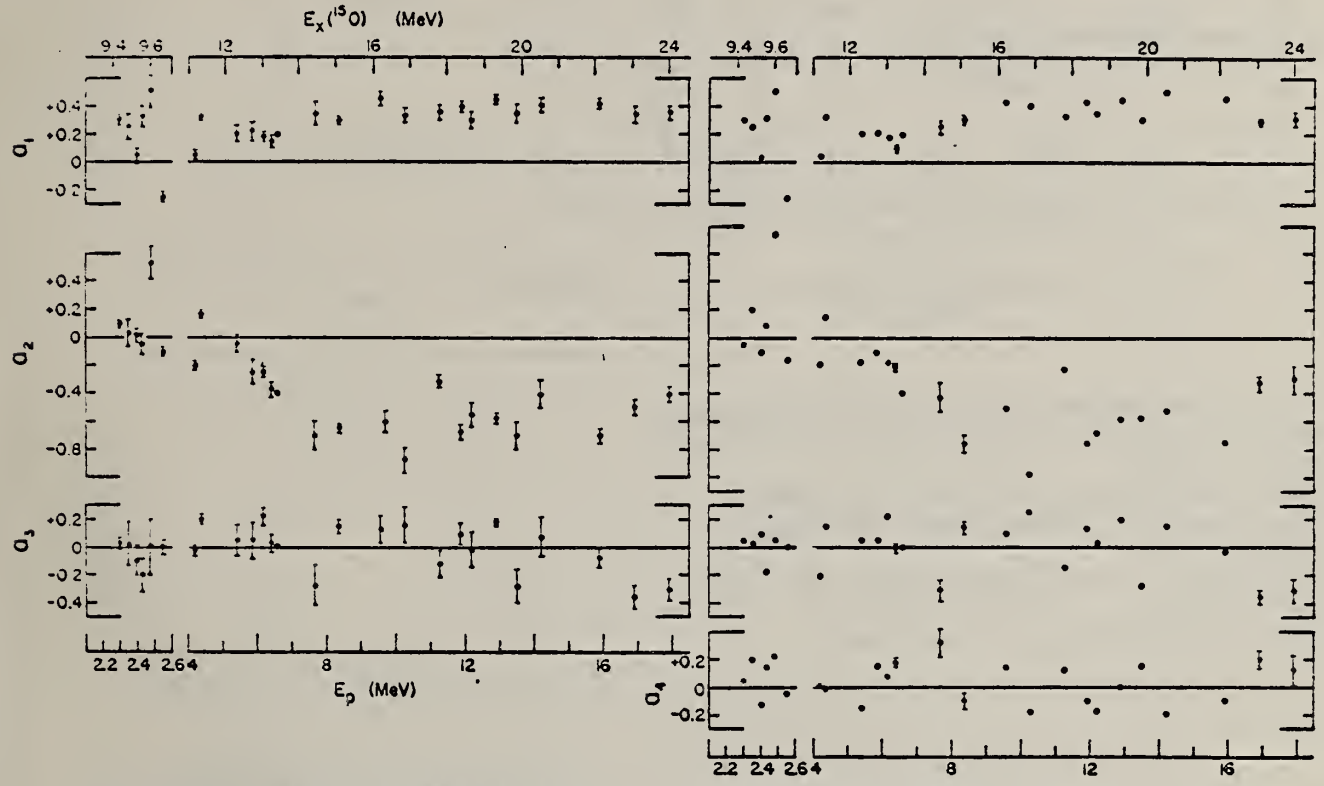

Fig. 10. The coefficients a_n for $^{14}N(p,\gamma_0)^{15}O$ with terms up to and including P_3 and P_4.

[over]

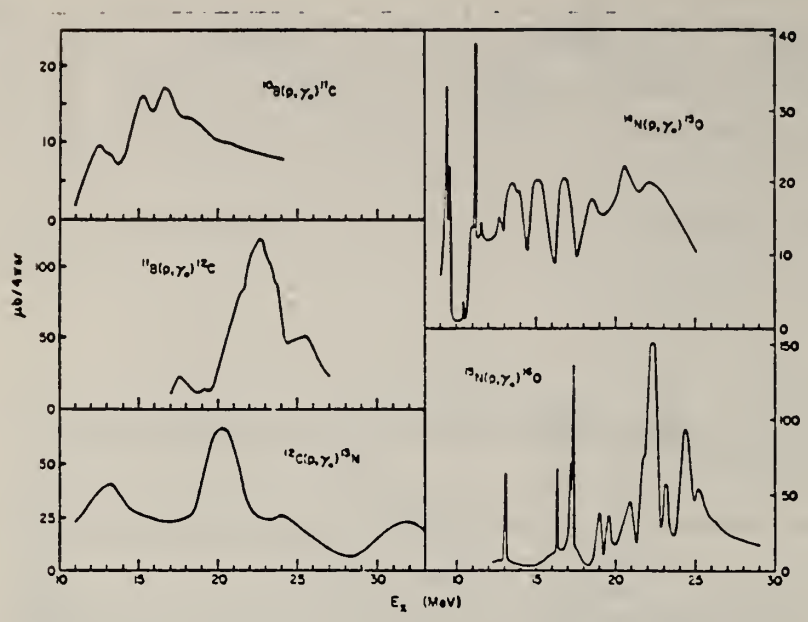

Fig. 11. Comparison of (p,γ₀) reactions on ^{10}B, ^{11}B [ref. [12]], ^{12}C [ref. [23]], ^{14}N and ^{15}N [refs. [13, 15]].

[12] J.F. Eichelberger, G.R. Grove and L.V. Jones, Mound Lab. progress report MLM 1160 (1963), Miamisburg, Ohio.
[13] C.J. Christensen, A. Nielson, A. Bahnsen, W.K. Brown, B.M. Rustad, Phys. Lett. 26B, 11 (1967).
[15] F.E. Emery and T.A. Rabson, Phys. Rev. 140, A2089 (1965).
[23] R.J. Blin-Stoyle, to be published.

REF.

G.W. Phillips, P. Richard, D.O. Elliott, F.F. Hopkins, A. C. Porter
Phys. Rev. C5, 297 (1972)

ELEM. SYM. | 0 | 15 | 8

METHOD

REF. NO. 72 Ph 1 hmg

REACTION	RESULT	EXCITATION ENERGY	SOURCE TYPE	SOURCE RANGE	DETECTOR TYPE	DETECTOR RANGE	ANGLE
P,G	ABX	10-13	D	3-6	NAI-D		90
		(10.91-13.02)		(3.7-5.3)			

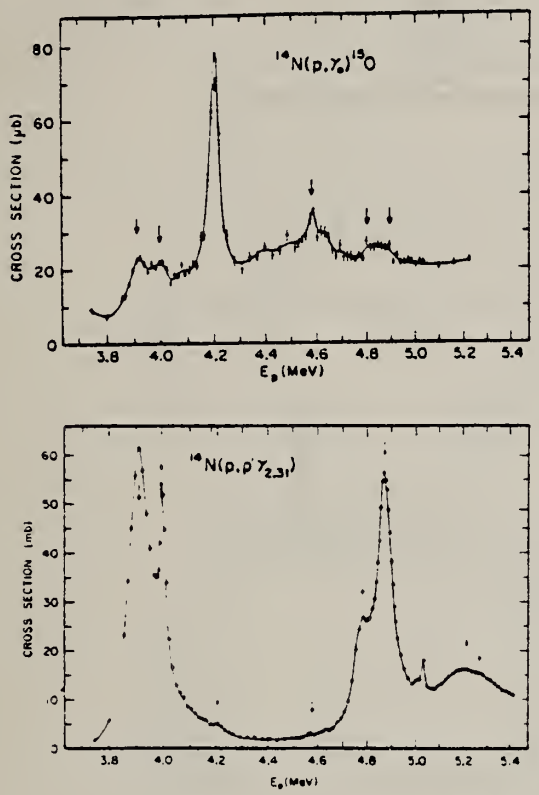

FIG. 1. Excitations for $^{14}N + p$ for $E_p = 3.7$ to 5.5 MeV. The γ_0 resonance decay (to the ^{15}O ground state) is given in the top figure and the $(p, p'\gamma_{2.31})$ resonance decay (through the ^{14}N 2.31-MeV level) is given in the lower figure.

(over)

TABLE I. ^{15}O levels from $^{14}N(p, p'\gamma)$ and $^{14}N(p, \gamma)$.

E_p [a] (MeV)	E_x [a] (MeV)	Γ [b] (keV)	Γ_0 [b] (keV)	Γ_1 [c] (keV)	Γ_2 [c] (keV)	Γ_γ (eV)
3.903	10.936	99	39	60		14 ± 3
3.996	11.023	25	21	4		1.4 ± 0.4
4.203	11.216	40 ± 4	40 ± 4			5.2 ± 0.4
4.58	11.57	20 ± 15	20 ± 15			0.7 ± 0.2
4.63	11.61	80 ± 50	80 ± 50			
4.773	11.747	99	95	4		
4.877	11.845	65	60	5		
5.03	11.99	20 ± 5	20 ± 5	0.2 ± 0.1		
5.18	12.12	200 ± 50	200 ± 50	3 ± 1		
5.28	12.22	100 ± 50		wk.		
5.547	12.467	77		1.3 ± 0.4	0.4 ± 0.1	
5.937	12.831	16			str.	
6.123	13.004	215 ± 30			str.	
6.141	13.022	40 ± 30			str.	

[a] Uncertainty of 3 keV (20 keV) in energies given to 1 (10) keV.
[b] Uncertainty of <5% unless given otherwise.
[c] wk., observed weakly; str., observed strongly.

REF. M. H. Harakeh, P. Paul, H. M. Kuan, E. K. Warburton
Phys. Rev. C12, 1410 (1975)

ELEM. SYM.	A	Z
O	15	8

METHOD

REF. NO. 75 Ha 6 hmg

REACTION	RESULT	EXCITATION ENERGY	SOURCE		DETECTOR		ANGLE
			TYPE	RANGE	TYPE	RANGE	
P,G	ABX	24- 34	D	17- 29	NAI-D		90

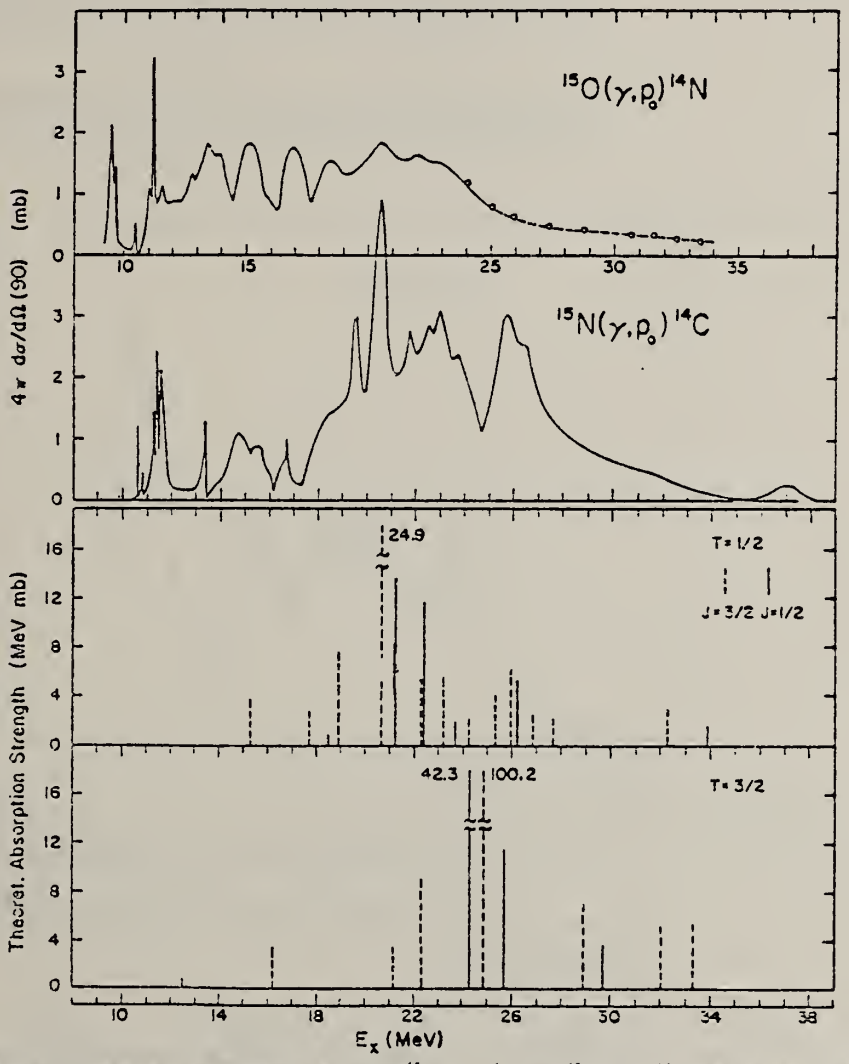

FIG. 6. Comparison of the experimental results from the $^{15}O(\gamma,p_0)^{14}N$ and $^{15}N(\gamma,p_0)^{14}C$ reactions and the theoretical predictions from the 2h-1p model (case B). The data below 25 MeV in the top curve are from Ref. 4, the data points at higher energies stem from the present work. The theoretical plots give the $T=\frac{1}{2}$ and $\frac{3}{2}$ components of the computed integrated photoabsorption cross section proportional to $E_\gamma[B(E1\uparrow)]$. Dashed and solid lines indicate $J=\frac{3}{2}$ and $\frac{1}{2}$, respectively. The top experimental curve should relate to the $T=\frac{1}{2}$ part while the $^{15}N(\gamma,p_0)^{14}C$ curve contains both T components.

Comment on "E1 excitations in A = 15 nuclei"

H. R. Weller
University of Florida and Triangle Universities Nuclear Laboratory, Durham, North Carolina 27706*

N. R. Roberson, D. G. Rickel, C. P. Cameron, and R. D. Ledford
Duke University and Triangle Universities Nuclear Laboratory, Duke Station, Durham, North Carolina 27706

(Received 8 December 1975)

Phys. Rev. C13, 2062 (1976)

It is shown that the recent $J^\pi = \frac{3}{2}^+$ assignment for the level observed in the $^{14}C(p,\gamma_0)^{15}N$ reaction at E_p 6.925 MeV is not unique.

REF. W. Del Bianco, J.C. Kim, G. Kajrys
Can. J. Phys. 56, 1054 (1978)

ELEM. SYM.	A	Z
0	15	8

METHOD

REF. NO. 78 De 14 hg

REACTION	RESULT	EXCITATION ENERGY	SOURCE TYPE	SOURCE RANGE	DETECTOR TYPE	DETECTOR RANGE	ANGLE
HE,G	ABX	16-23	D	5-14	NAI-D		90
				(5.24-13.95)			

HE=HE3, 5 LEVELS

The 90° differential cross section of the $^{12}C(^3He,\gamma_0)^{15}O$ reaction has been measured at ^{3}He-particle energies from 5.24 to 13.95 MeV in steps varying from 100 to 300 keV. The γ rays have been detected by a 23 cm long × 23 cm diameter NaI(Tl) crystal spectrometer enclosed in an anticoincidence shield. The yield curve shows a resonant structure at the energies E_{exc} = 17.04 ± 0.06, 18.65 ± 0.06, 19.55 ± 0.08, 20.40 ± 0.07, and 21.61 ± 0.07 MeV.

La section efficace différentielle de la réaction $^{12}C(^3He,\gamma_0)^{15}O$ a été mesurée pour des énergies des particules-^{3}He allant de 5.24 à 13.95 MeV. Les rayons gamma ont été détectés par un crystal de NaI(Tl) entouré d'un scintillateur plastique en anticoincidence. La courbe d'excitation montre de la structure aux énergies E_{exc} = 17.04 ± 0.06, 18.65 ± 0.06, 19.55 ± 0.08, 20.40 ± 0.07 et 21.61 ± 0.07 MeV.

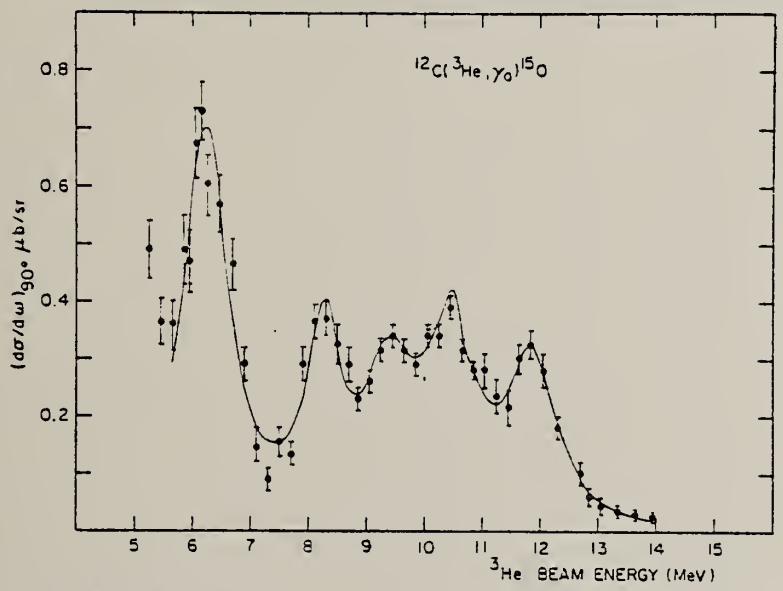

FIG. 1. Experimental differential cross section at $\theta_L = 90°$ of $^{12}C(^3He,\gamma_0)^{15}O$ reaction. The solid symbols are the experimental points; the solid line represents a least-squares-fit to the data with five Breit–Wigner lines. Only the statistical errors are shown in the figure. The ^{3}He beam energies are the average energies in the carbon target.

TABLE 1. Fit of $^{12}C(^3He,\gamma_0)^{15}O$ yield curve with five Breit–Wigner lines*

E_R(lab) (MeV)	E_{exc} (MeV)	Γ_{CM} (MeV)	$\omega_\gamma = \frac{2J+1}{(2I+1)(2S+1)}\frac{\Gamma_r\Gamma_\gamma}{\Gamma_{CM}}$ (eV) $J = 1/2$	$J = 3/2$
6.23±0.07	17.04±0.06	0.70±0.07	22.0± 4.6	27.05± 5.8
8.25±0.07	18.65±0.06	0.52±0.11	9.9± 4.5	12.4 ± 5.7
9.38±0.10	19.55±0.08	0.78±0.27	11.7 ±9.4	14.6 ±11.7
10.45±0.09	20.40±0.07	0.97±0.24	22.6±12.4	28.2 ±15.5
11.87±0.08	21.61±0.07	0.73±0.12	17.7± 6.5	22.1 ± 8.2

*In the expression for ω_γ, the quantities J, I, and S represent the angular momentum of the resonance, the target nucleus, and the projectile, respectively.

(over)

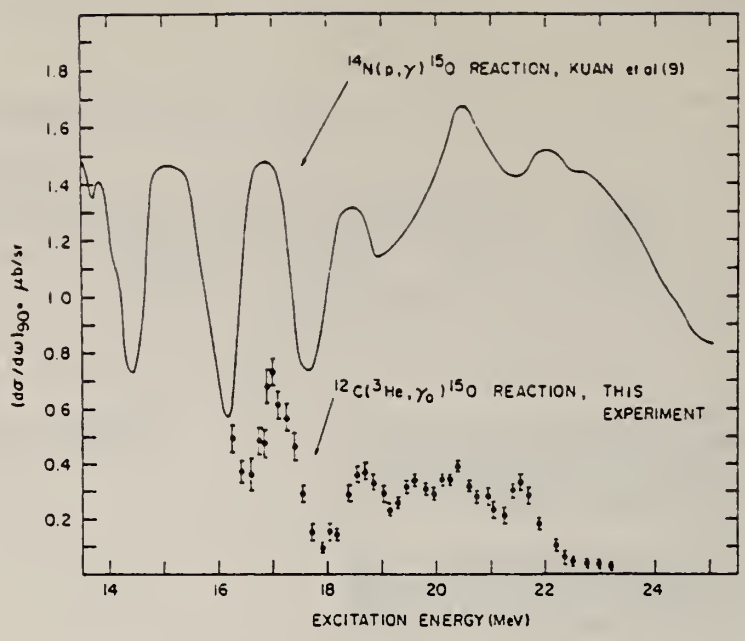

FIG. 2. Experimental differential cross sections at $\theta_L = 90°$ of the $^{14}N(p,\gamma_0)^{15}O$ and $^{12}C(^3He,\gamma_0)^{15}O$ reactions. The solid line represents the results of Kuan *et al.* (9); the solid symbols are the results of this experiment.

0
A=16

0
A=16

0
A=16

REF. G. Ferguson, J. Halpern, R. Nathans, and P.F. Yergin
Phys. Rev. 95, 776 (1954

ELEM. SYM.	A	Z
O	16	8

METHOD

REF. NO. 54 Fe 1 rs

REACTION	RESULT	EXCITATION ENERGY	SOURCE		DETECTOR		ANGLE
			TYPE	RANGE	TYPE	RANGE	
G,SN	ABX	15-25	C	16-25	BF3-I		4PI

The direct detection of neutrons from (γ,n) reactions induced by betatron bremsstrahlung has been applied to cross-section determinations using gaseous targets at approximately 100 atmospheres pressure. Results from oxygen are consistent with other determinations. The remaining elements represent new results and show the familiar giant dipole resonance for the photoneutron process. Parameters of the resonances are determined and related to the systematic behavior previously reported for other elements.

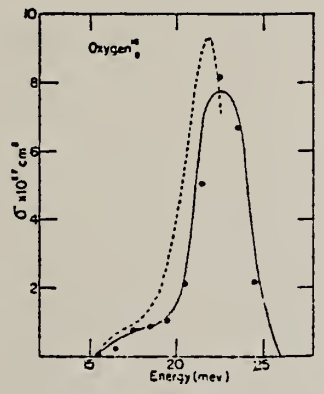

FIG. 6. Photoneutron excitation function for oxygen.

Ref. J.G. Campbell
Australian J. Phys. 8, 445 (1955)

Elem. Sym.	A	Z
O	16	8

Method $Li^7(p,\gamma)$ reaction; 700 keV electrostatic generator; radioactivity

Ref. No. 55 Ca 1 | EGF

Reaction	E or ΔE	E_o	Γ	$\int \sigma dE$	Jπ	Notes
$O^{16}(\gamma,n)$	400 - ~ 700 MeV	17.6-17.9				σ = 0.54±0.14 mb

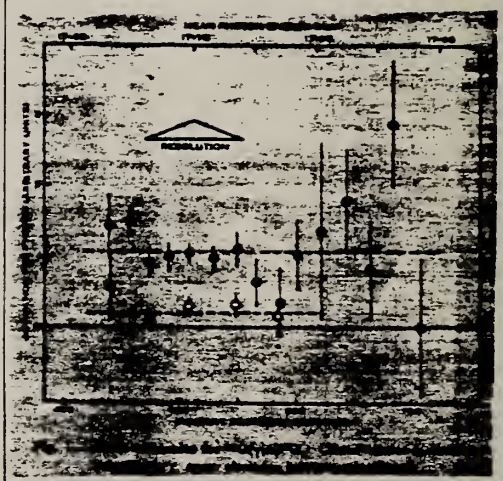

Ref. F.I. Havliček, B. Dobovišek
Phys. Rev. 100, 1355 (1955)

Elem. Sym.	A	Z
O	16	8

Method: plates; bremsstrahlung

Ref. No.: 55 Ha 1

EGF

Reaction	E or ΔE	E_o	Γ	$\int \sigma dE$	Jπ	Notes
(γ,4α)	27 33					E_{th} = 14.5 MeV. Data for two (also[18]) bremsstrhalung energies not separated.

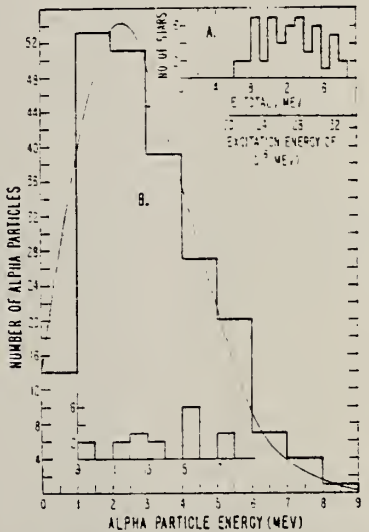

FIG. 5. (A) Distribution of the O^{16} stars according to E_{tot} (top abscissa scale). The lower abscissa scale indicates the corresponding O^{16} excitation energies. (B) Energy distribution of all the alpha particles from the 54 O^{16} stars.

Ref. A.S. Penfold, B.M. Spicer
Phys. Rev. 100, 1377 (1955)

Elem. Sym.	A	Z
O	16	8

Method
Activation; Victoreen chamber behind 4 cm of Lucite at the photoprotons of samples; Betatron

Ref. No. 55 Pe 1 EGF

Reaction	E or ΔE	E_o	Γ	$\int \sigma dE$	Jπ	Notes
(γ,n)	15.6-23.2					Samples 58 and 97 cm from target. $\left(\int \sigma dE\right)_n$ - good to 15% relative and 25% absolute. Figure 8: Shaded areas indicate yield not measured carefully or not measured at all.

TABLE I. Summary of properties for observed levels of O^{16}.

Energy of break (Mev)	$\int \sigma dE$ Mev-mb	σ_{max} (mb)	Radiation width (ev) $J=2^+$	$J=1^-$
15.85	0.0046	0.12	0.81	0.41
16.03	0.040	1.02	4.19	2.57
16.47	0.027	0.69	1.63	1.73
16.75	0.041	1.04	2.09	2.65
16.95	0.084	2.14	4.05	5.30
17.02	0.111	2.83	5.36	7.29
17.13	0.262	6.67	12.2	17.2
17.18	0.404	10.3	18.8	26.6
17.55	0.202	5.14	9.04	13.5
17.68	0.182	4.63	8.15	12.2
17.84	0.254	6.47	11.37	17.2
18.04	0.059	1.50	2.66	4.02
18.70	0.094	2.39	4.47	6.76
19.01	0.130	3.31	6.42	9.89
19.18	0.396	10.1	19.2	29.5
20.33	0.495	12.6	30.8	42.7
20.58	0.603	15.4	39.1	54.3
20.79	0.617	15.7	41.9	58.2
20.93	0.857	21.8	58.8	83.4
21.21	1.36	34.6	98.5	142.9
21.52	0.853	21.7	64.1	98.3
22.37	2.21	56.3	...	322
22.54	3.14	80.0	...	480
22.76	3.47	88.4	...	549
23.02	3.06	77.9	...	501

* σ_{max} was calculated using $\Gamma = 25$ kev for all levels.

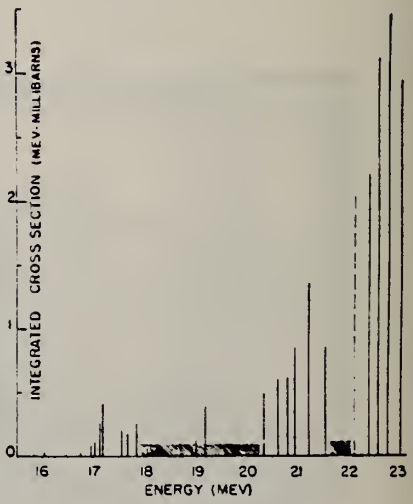

FIG. 8. Integrated cross sections of all levels found in this work.

REF.

J. Schmouker, P. Erdos, P. Jordan and P. Stoll
J. Phys. Radium 16, 169 (1955)

ELEM. SYM.	A	C
0	16	8

METHOD

REF. NO. 55 Sc 2 EGF

REACTION	RESULT	EXCITATION ENERGY	SOURCE		DETECTOR		ANGLE
			TYPE	RANGE	TYPE	RANGE	
G,NA	ABY	THR - 32	C	32	ACT-I		4PI
G,T	ABY	THR - 32	C	32	ACT-I		4PI

Betatron run at 31.5 MeV. Yields measured relative to $^{65}Cu(\gamma,n)^{64}Cu$ = 1.4 barn-MeV
$^{63}Cu(\gamma,n)^{62}Cu$ = 0.7 barn-MeV

$\bar{\sigma}$ $^{16}O(\gamma,n\alpha)^{11}C$ = 0.019±0.005 MeV-mb

$^{16}O(\gamma,t)^{13}N$ = 0.06±0.03 MeV-mb

Ref. B.M. Spicer
Phys. Rev. 99, 33 (1955)

Elem. Sym.	A	Z
O	16	8

Method plates; gas target Bremss.

Ref. No. 55 Sp 1 | EGF

Reaction	E or ΔE	E_o	Γ	$\int \sigma dE$	Jπ	Notes
(γ,p)	18.7	~ 14.8	~ 2			Proton yeild at 18.7 MeV Bremss. was 4×10^4 p/mole r. Angular distribution of protons is $1 + \cos^2\theta$.

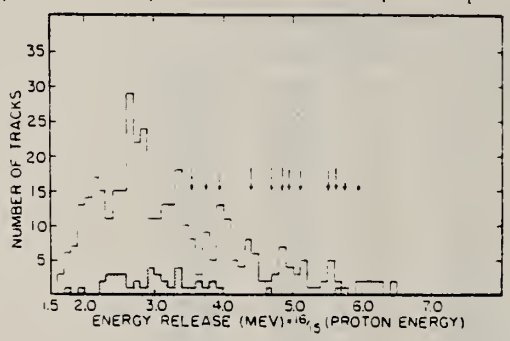

Fig. 1. Energy distribution of photoprotons (100-kev bins). Arrows indicate the energies of breaks found in the (γ,n) reaction (reference 4). The background which was subtracted is indicated by the shaded histogram.

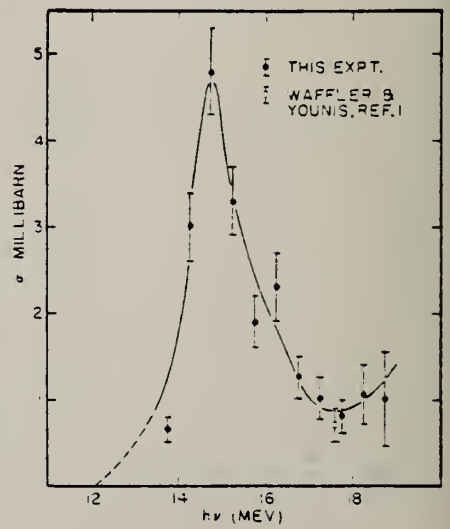

Fig. 4. Cross section for $O^{16}(\gamma,n)O^{15}$

Reference 4: Penfold and Spicer (to be published)

Ref. W.E. Stephens, A. K. Mann, B.J. Patton, E.J. Winhold
Phys. Rev. 98, 839 (1955)

Elem. Sym.	A	Z
O	16	8

Method: Plates; gas target bombarded with 25 MeV Bremss.

Ref. No.: 55 St 1 | EGF

Reaction	E or ΔE	E_o	Γ	$\int \sigma dE$	Jπ	Notes
(γ,p)						Figure 1: 40-50 tracks / 304 MeV peak ⟶ transition to 5,326.3 MeV levels in N^{15}. Figure 2: Peak at 14.5 MeV from work of Spicer. Group between 2 and 6 MeV in Figure 1 results from transition to 5.3 and 6.3 MeV states in N^{15}.

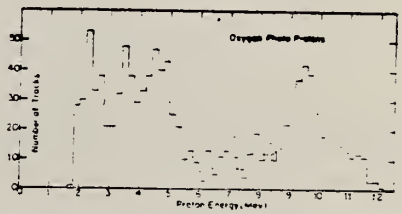

FIG. 1. The energy spectrum of 1123 photoprotons from oxygen. The dashed curve shows the results of a shift of 0.1 Mev in the grouping of the tracks and indicates that the structure is largely independent of such grouping.

FIG. 2. Cross section as a function of energy for transitions to the ground state of N^{13}. The cross represents the value reported by H. Wäffler and S. Younis, Helv. Phys. Acta 22, 614 (1949).

Ref. L. Cohen, A.K. Mann, B.J. Patton, K. Reibel, W.E. Stephens, E.J. Winhold
Phys. Rev. 104, 108 (1956)

Elem. Sym.	A	Z
O	16	8

Method: 90^{o} plates; 25 MeV Bremss.

Ref. No.: 56 Co 1 — EGF

Reaction	E or ΔE	E_o	Γ	$\int \sigma dE$	Jπ	Notes
(γ,p)	Bremss. 25			~ 60 MeV-mb		Proton yield at 25 MeV Bremss. was $11 \pm 3 \times 10^{4}$ p/mole r (corrected for angular distribution).
		19.6		2 MeV-mb		Target at 2 mg/cm^2.
		20.6		2 MeV-mb		Only ground state transition possible.
		22.4		20 MeV-mb		

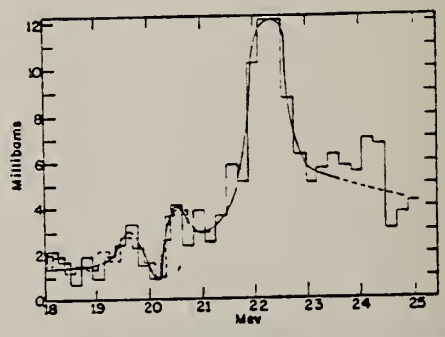

FIG. 10. Photon absorption cross-section curve for the ejection of photoprotons from oxygen obtained from Fig. 6 on the assumption that the resultant N^{15} nucleus is left in its ground state.

Ref. W.K. Dawson, D.L. Livesey
Can. J. Phys. 34, 241 (1956)

Elem. Sym.	A	Z
O	16	8

Method 70 MeV electron snychrotron; 4 prong stars; nuclear emulsions; Baldwin-Farmer BD-2 ionization chamber

Ref. No. 56 Da 1 EGF

Reaction	E or ΔE	E_o	Γ	$\int \sigma dE$	Jπ	Notes
$O^{16}(\gamma,4\alpha)$	Bremss. 70	22.5 32.5 26.0(?) 27.5(?) 29.5(?) 35.2(?)		$\int_{}^{35.5} = \sim 2.8$ MeV-mb		E_o - "(?)" refers to possible peaks. Figure 1: "Δ" - momentum balance error in photon units (energy γ momentum had the same numerical value

TABLE I

ENERGY GROUPS AND INTEGRATED CROSS SECTIONS

Group	Energy range in Mev.	Integrated cross section in Mev-millibarns
A	Up to 25.0	1.0
B	25.0–26.5	0.3
C	26.5–28.0	0.2
D	28.0–30.5	0.5
E	30.5–33.5	0.6
F	33.5–35.5	0.2

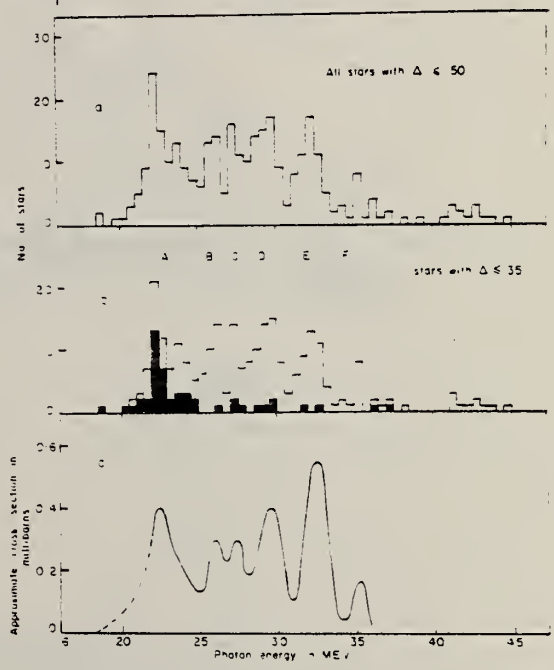

Ref. D.L. Livesey
Can. J. Phys. 34, 1022 (1956)

Elem. Sym.	A	Z
O	16	8

Method Synchrotron; proton spectra, angular distribution; nuclear emulsion; ion chamber

Ref. No. 56 Li 2 NVB

Reaction	E or ΔE	E_0	Γ	$\int \sigma dE$	Jπ	Notes
$O^{16}(\gamma,p)$	Bremss.					
	30	20.7±0.2				
	35	21.9±0.2				
	70	24.0±0.2				

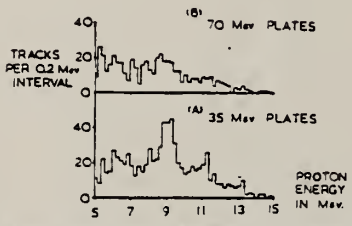

FIG. 3. A. Lower. Energy distribution of 768 proton tracks in plates exposed at 35 Mev. with full beam.
B. Upper. Energy distribution of 487 proton tracks in plates exposed at 70 Mev. with full beam.

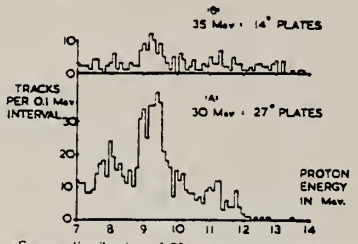

FIG. 2. A. Lower. Energy distribution of 724 proton tracks in plates exposed at 30 Mev. with full beam.
B. Upper. Energy distribution for 205 tracks in a 200 μ plate exposed at 35 Mev. with narrow beam.

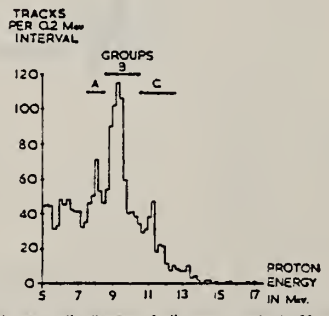

FIG. 4. Combined energy distribution of all proton tracks in 30 and 35 Mev. plates.

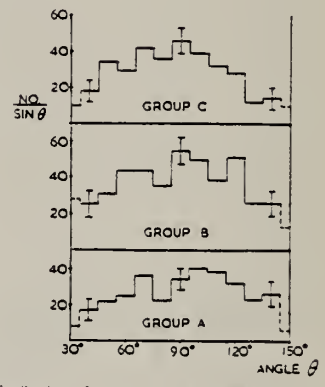

FIG. 5. Angular distributions of protons in energy groups A, B, and C, the ordinates being proportional to yield per unit solid angle of collection.

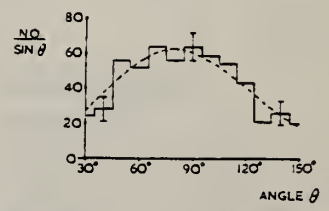

FIG. 7. Angular distribution of all proton tracks observed with energies greater than 10.5 Mev. The dashed curve represents the function:

$$f(\theta) = A + B(\sin\theta - p\sin\theta\cos\theta)^2$$

with A B = 0.2 and p = 0.2.

A.C. Odian, P.C. Stein, A. Wattenberg, B.T. Feld, and R. Weinstein
Phys. Rev. 102, 837 (1956)

METHOD
Synchrotron; plastic scintillator proton telescope, liquid scintillator neutron detector, also integrating neutron detector [Page 1 of 2]

REF. NO. 56 0d 1 NVB

REACTION	RESULT	EXCITATION ENERGY	SOURCE TYPE	SOURCE RANGE	DETECTOR TYPE	DETECTOR RANGE	ANGLE
G,NP	RLX	140-260	C	340	TEL-D	70-125	DST

NP COINCIDENCE

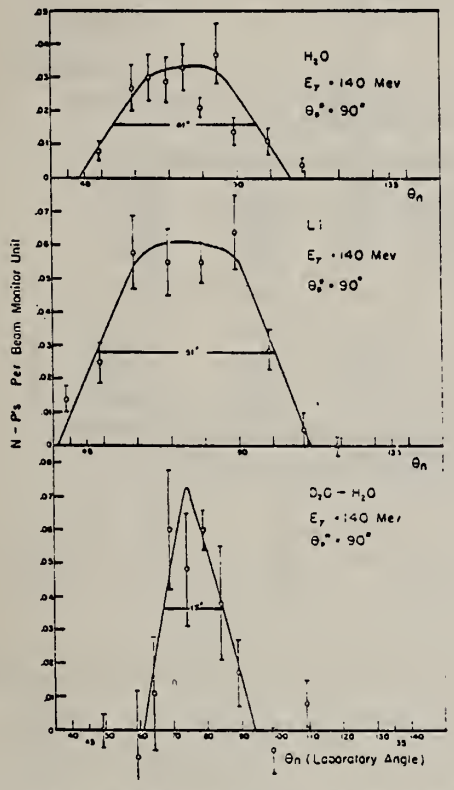

FIG. 2. Variation of neutron-proton coincidences with neutron angle. Gamma-ray energy is 140 Mev.

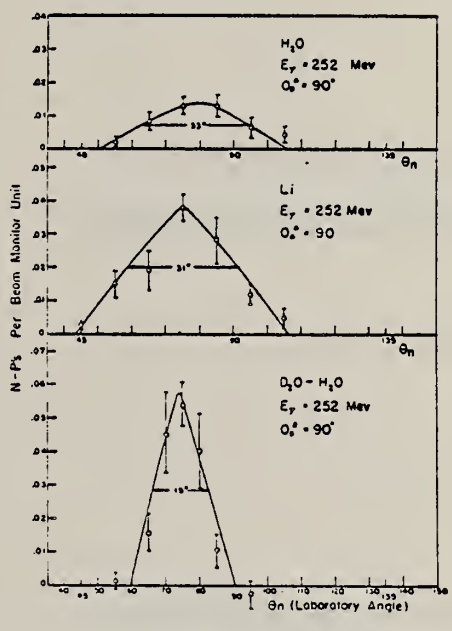

FIG. 3. Variation of neutron-proton coincidences with neutron angle. Gamma-ray energy is 252 Mev.

REACTION	RESULT	EXCITATION ENERGY	SOURCE TYPE	SOURCE RANGE	DETECTOR TYPE	DETECTOR RANGE	ANGLE

NP COINCIDENCE

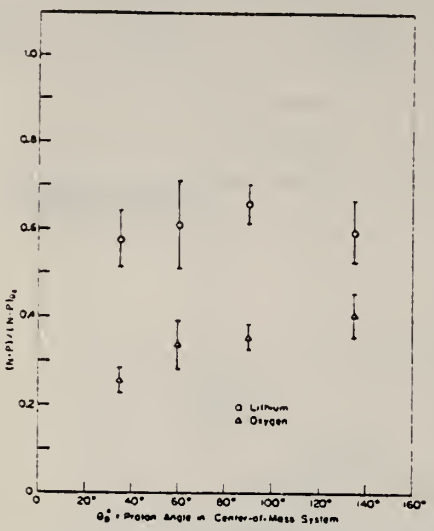

FIG. 6. Angular distribution of photoneutron proton pairs from lithium and oxygen relative to deuterium. $E_\gamma = 260$ Mev.

$$\frac{(N+P)_O}{(N+P)_{Dt}} = 0.57 \pm 0.07$$

TABLE II. Summary of data[a] for lithium and oxygen. $E_\gamma = 260$ Mev; $\theta_P^* = 90°$; $\theta_P = \theta_N = \theta_{lab} = 76°$; $E_P = 129$ Mev; $E_N = 129$ Mev.[b]

Substance	Run[b]	P/M	$(N-P)/M$	$(N-P)/P$
Li	1	5.42	0.244	0.0450
	2	5.42	0.244	0.0450
	3	6.07	0.257	0.0423
	Av	5.64	0.248	0.0441
O_2	1	7.00	0.142	0.0203
	2	7.00	0.142	0.0203
	3	7.55	0.150	0.0198
	Av	7.18	0.145	0.0201

[a] Large counter up close (10 in.).
[b] Each run corresponds to about 2000 monitor units.

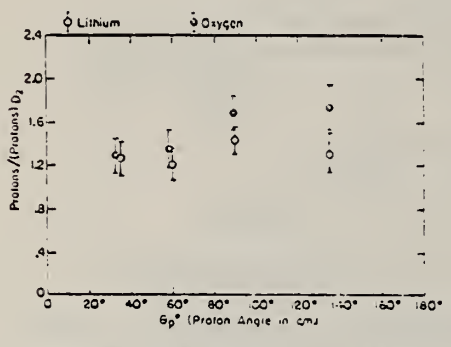

FIG. 7. Proton rates for oxygen and lithium relative to deuterium for various laboratory angles.

TABLE I. Summary of data[a] for H_2O and D_2O. $E_\gamma = 260$ Mev; $\theta_P^* = 90°$; $\theta_P = \theta_N = \theta_{lab} = 76°$; $E_P = 129$ Mev; $E_N = 129$ Mev.

Run[b]	Prot/MH_2O	Prot/MD_2O	$\Delta P/M$	$(N-P)/MH_2O$	$(N-P)/MD_2O$	$\Delta(N-P)/M$	$\Delta(N-P)/P$	$(N-P)/PH_2O$	$(N-P)/PD_2O$
1	7.112	7.964	0.852	0.042	0.140	0.098	0.115	0.0060	0.0176
2	7.553	8.521	0.968	0.048	0.143	0.095	0.098	0.0064	0.0168
3	7.021	8.078	1.057	0.049	0.157	0.108	0.102	0.0070	0.0194
4	7.753	8.520	0.767	0.048	0.148	0.100	0.130	0.0061	0.0174
Av	7.360	8.271	0.91	0.047	0.147	0.100	0.110	0.0064	0.0178
Correction of 0.02 H_2O[c]			0.15			0.001			
Corrected av value:			Prot/M_{D_2} = 1.06			$(N-P)/M_{D_2}$ = 0.101			

[a] Large conuter far away (51 in.).
[b] Each run corresponds to about 2000 monitor units.
[c] The correction of 0.02 H_2O is to correct for the H_2O cell having a thickness that is 0.98 of the thickness of the D_2O cell.

REF. R. Basile
Ann. Phys. (Paris) 2, 267 (1957)

ELEM. SYM.	A	Z
O	16	8

METHOD

REF. NO. 57 Ba 3 JOC

REACTION	RESULT	EXCITATION ENERGY	SOURCE		DETECTOR		ANGLE
			TYPE	RANGE	TYPE	RANGE	
G,N	ABY	15-18	C	15-18	ACT-I		4PI

BREAKS

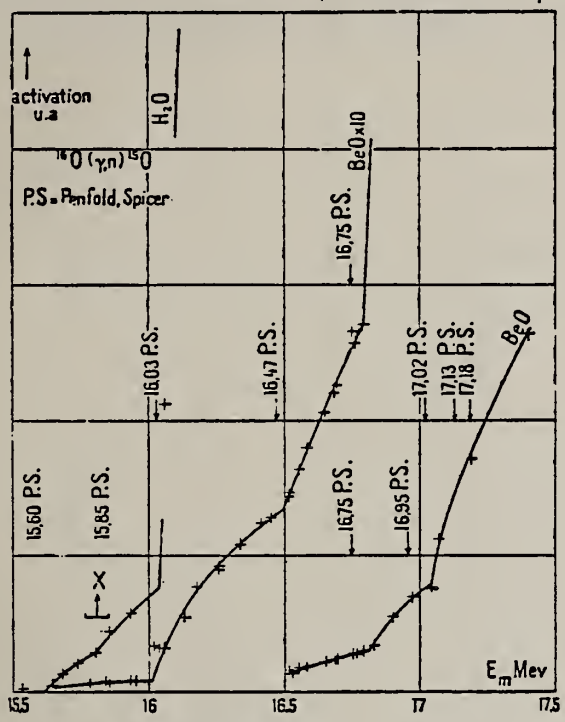

Fig. 5. — Courbe d'activation de ^{16}O.

POSITION DES DISCONTINUITÉS DANS LA COURBE D'ACTIVATION DE ^{16}O

Seuil (MeV) *Energie des discontinuités (MeV)*

15,60 (±0,05) (15,8) 16,03 16,50 (16,7) 16,82 17,04

Ecart entre les discontinuités (keV)

200 230 470 200 120 220

Énergie des discontinuités en MeV	Sections efficaces intégrées des raies en keV.barns			
	Basile et Schuhl norm. sur Katz et al.	Katz et al.	Basile et Schuhl norm. sur P. S.	Penfold et Spicer
15,6			0,0022	
15,8			0,0021	0,0046
16,03	0,06	0,06	0,04	0,04
16,5	0,048	0,05	0,032	0,027
16,7	0,035	0,18	0,023	0,041
16,82	0,36	0,84	0,24	0,084

P. Brix, E.K. Maschke
Z. Naturforsch. 12, 1013 (1957)

0	16	8

METHOD
Betatron; proton cross section; nuclear emulsion; $C^{12}(\gamma,n)C^{11}$ monitor

REF. NO. 57 Br 1 | NVB

REACTION	RESULT	EXCITATION ENERGY	SOURCE TYPE	SOURCE RANGE	DETECTOR TYPE	DETECTOR RANGE	ANGLE
G,XP	SPC	10-19	C	28	EMU-D	10 - +	
		(10-18.5)					

$\sigma_{(28\ MeV)} = 2.3$ mb

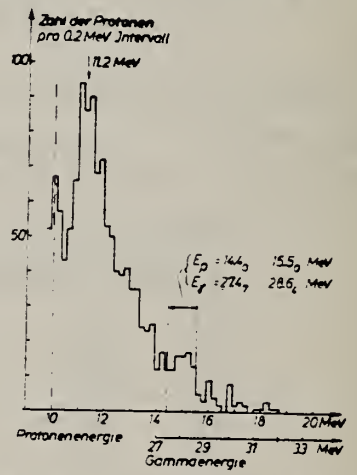

Abb. 1. Spektrum von 1306 Protonen aus vier Photoplatten. Das Spektrum wurde bei 10 MeV abgeschnitten. Für die letzten 5,3 MeV des Spektrums, für die eine Skala der γ-Energie angegeben ist, ist eine eindeutige Zuordnung von Protonen- zu γ-Energie möglich. Im angegebenen Intervall um 28 MeV γ-Energie wurde der mittlere Wirkungsquerschnitt bestimmt.

Ref. J.H. Carver, K.H. Lokan
Australian J. Phys. 10, 312 (1957)

Elem. Sym.	A	Z
O	16	8

Method 33 MeV electron synchrotron; neutron yield; radioactivity;
$Cu^{63}(\gamma,n)$ reaction. (Berman and Brown)

Ref. No. 57 Ca 2 EH

Reaction	E or ΔE	E_o	Γ	$\int \sigma dE$	Jπ	Notes
$O^{16}(\gamma,n)$	Bremss. 15-30	24	$\Gamma_{1/2}$: 3.4 MeV	$\int^{31}$ = 46±7 MeV-mb		

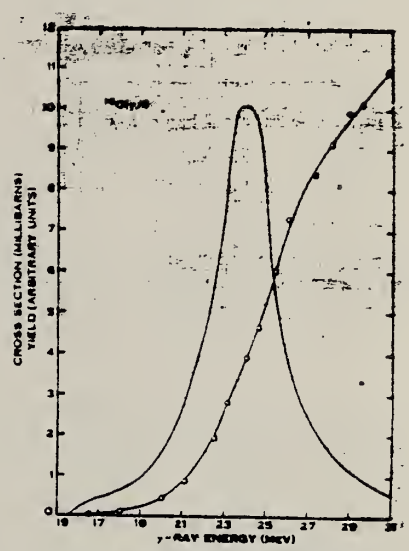

Fig. 3.—The measured yield curve and the derived cross-section curve for the reaction $^{16}O(\gamma,n)^{15}O$.

TABLE 3
PARAMETERS OF THE MEASURED (γ,n) CROSS SECTIONS

Reaction	Peak Energy (MeV)	Width at Half Maximum (MeV)	Integrated Cross Section to 31 MeV (MeV mb)
$^{12}C(\gamma,n)$	23	4·2	42±7
$^{16}O(\gamma,n)$	24	3·4	46±7
$^{56}Fe(\gamma,n)$	19	6·9	290±60

Ref. P. Erdos, P. Scherrer, P. Stoll
Helva. Phys. Acta 30, 639 (1957)

Elem. Sym.	A	Z
O	16	8

Method: Betatron; α yield; radioactivity; $Cu^{65}(\gamma,n)$ reaction

Ref. No.: 57 Er 1 | EGF

Reaction	E or ΔE	E_o	Γ	$\int \sigma dE$	Jπ	Notes
$O^{16}(\gamma,n)$	Bremss. 16-32					Peak used to fix mezy scale.

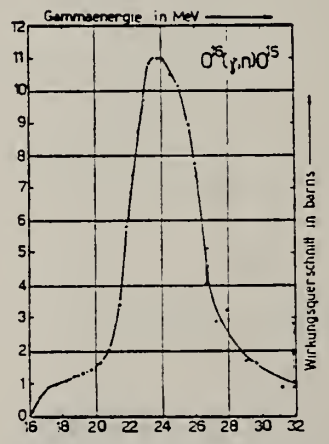

Fig. 4.
Wirkungsquerschnittsverlauf der Reaktion $O^{16}(\gamma,n)O^{15}$, ermittelt am Zürcher Betatron zwecks Eichung der Grenzenergie.

S.A.E. Johansson, B. Forkman
Arkiv Fysik 12, 359 (1957)

ELEM. SYM.	A	Z
O	16	8

METHOD: Synchrotron; proton, alpha spectra, proton cross section; nuclear emulsion; r chamber

REF. NO.: 57 Jo 1 NVB

REACTION	RESULT	EXCITATION ENERGY	SOURCE TYPE	SOURCE RANGE	DETECTOR TYPE	DETECTOR RANGE	ANGLE
G,P	ABX	12-26	C	20-26	EMU-D	1-13	DST
				(20.5,23,26)			
G,A	SPC	7-19	C	19	EMU-D	2-11	DST

$$\int_{THR}^{25.5} \sigma_{(\gamma,p)} dE = 76 \text{ MeV-mb}$$

In figure 7, σ scale based on Stephens, et al., Phys. Rev. 98, 839 (1955), work on ground state transitions.

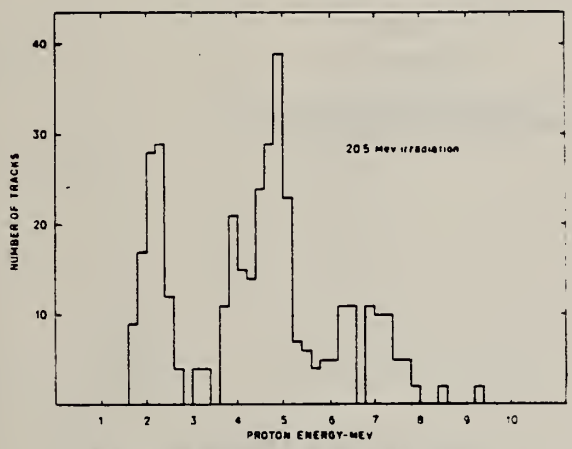

Fig. 1. Proton spectrum for the 20.5 Mev irradiation.

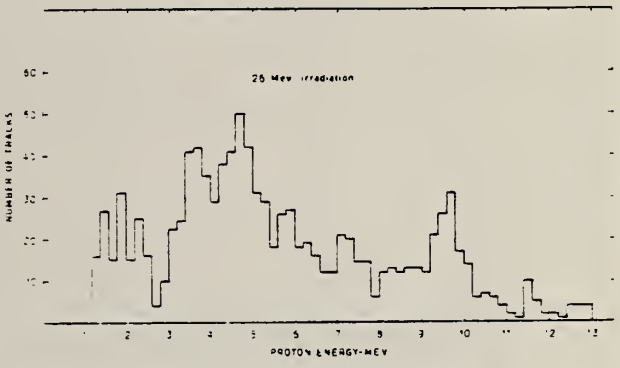

Fig. 3. Proton spectrum for the 26 Mev irradiation.

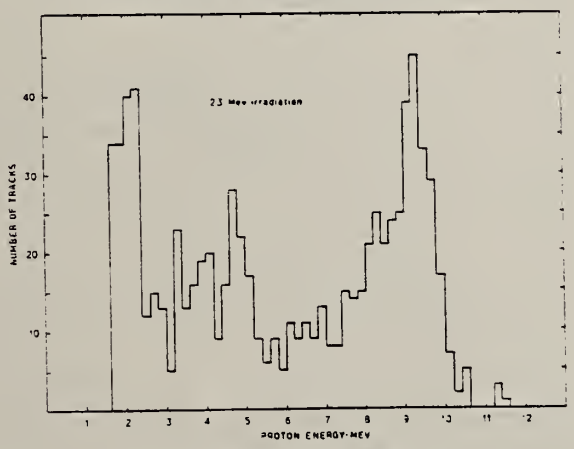

Fig. 2. Proton spectrum for the 23 Mev irradiation.

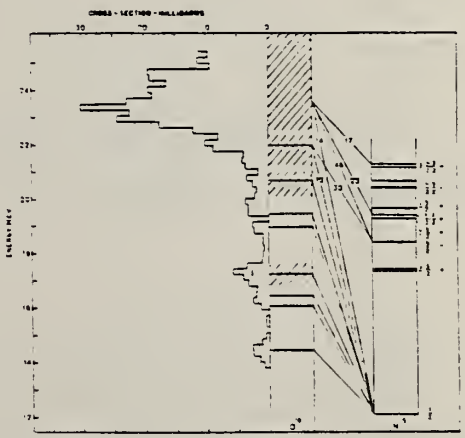

Fig. 7. Level scheme for the photodisintegration of O16. The cross-section curve is plotted to the left. The numbers inserted for some of the transitions denote the relative branching ratios in per cent.

METHOD

REF. NO. 57 Jo 1

REACTION	RESULT	EXCITATION ENERGY	SOURCE TYPE	SOURCE RANGE	DETECTOR TYPE	DETECTOR RANGE	ANGLE

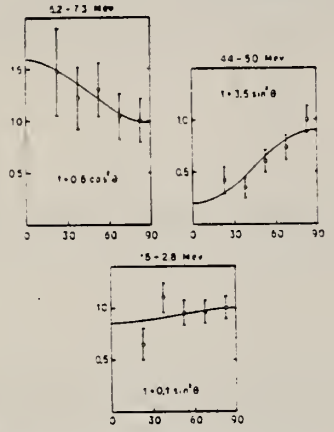

Fig. 8. Angular distributions for the proton groups in the 20.5 Mev irradiation.

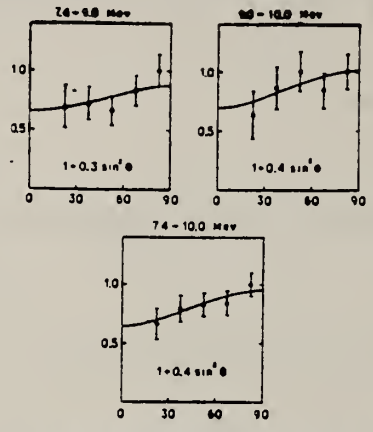

Fig. 9. Angular distribution for the proton groups in the 23 Mev irradiation.

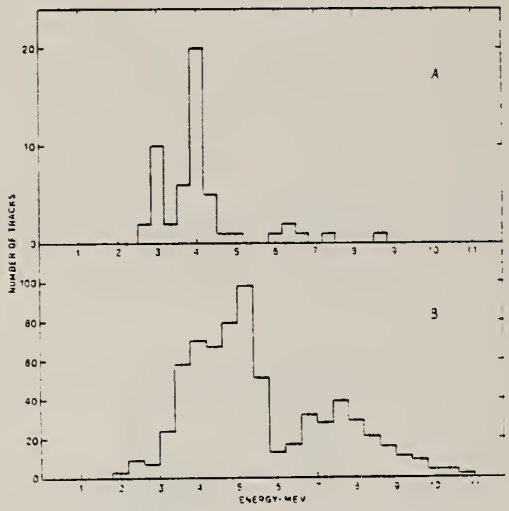

Fig. 11. Energy distribution for the α-particles from the (γ,α) reaction in (a) O^{16}, (b) bromine and silver.

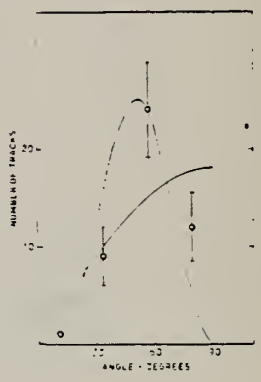

Fig. 12. Angular distribution of the α-particles from the (γ,α) reaction in O^{16}. The two curves correspond to (a) isotropic distribution, (b) a distribution of the form $\sin^2 2\theta$.

Table 1. Comparison between the cross-sections for the (γ,n) and (γ,p) reactions in O^{16}

Energy range, Mev	Integrated cross-section Mev-mb		Ratio between the (γ,p) and (γ,n) integrated cross-sections			
			Experimental	Theoretical		
	γ,p	γ,n		l = 1	l = 1	l = 2
16.5–17.5	3.5	1.6	2.2	1.1	1.9	10
18.0	1.1	0.66	1.6	1.9	1.2	2.5
20.5–21.5	3.3	3.4	1.0	1.0	1.0	1.5
23.0–24.0	13	10	1.3	1.1	1.4	3.2

Ref. C. Milone, R. Ricamo
Nuovo Cimento 5, 1338 (1957)

Elem. Sym.	A	Z
O	16	8

Method: Betatron; proton angular distribution; nuclear emulsion

Ref. No.: 57 Mi 1 NVB

Reaction	E or ΔE	E_0	Γ	$\int \sigma dE$	Jπ	Notes
O(γ,xp)	Bremss. 30					$4 < E_p < 8$ MeV

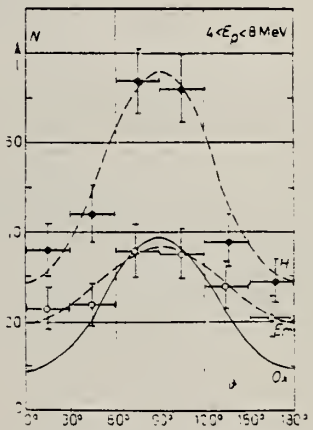

Fig. 1. – Angular distribution of photoprotons in water loaded emulsion = *H*, dry emulsion = *Em* and Oxygen Ox = *H* – *Em*. *N* = number of observed photoprotons in the energy interval 4 to 8 MeV, for constant solid angle.

Ref. B.M. Spicer
Australian J. Phys. 10, 326 (1957)

Elem. Sym.	A	Z
O	16	8

Method: Betatron; radioactivity

Ref. No.: 57 Sp 2 | EGF

Reaction	E or ΔE	E_o	Γ	$\int \sigma dE$	Jπ	Notes
O^{16} (γ,n)	Bremss. 14-25					Yield curve better than 1% above 16.5 MeV. Data ~ 0.2 MeV on yield curve.

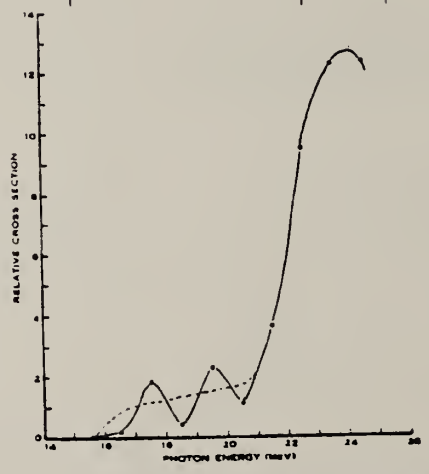

Fig. 2.—The cross section for the $^{16}O(\gamma,n)$ reaction, calculated in 1 MeV steps. A calculation using the smoothing procedure of Katz and Cameron (1951) gives the dashed curve.

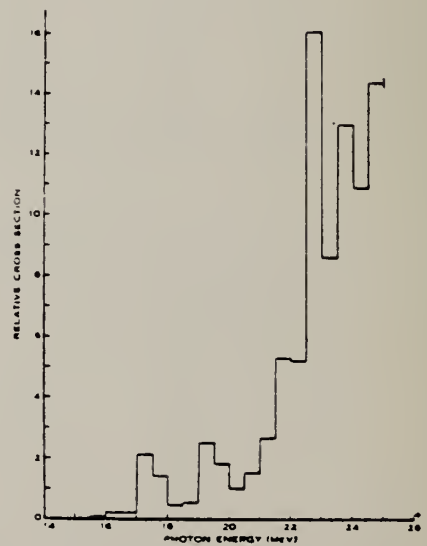

Fig. 3. –The cross section for the $^{16}O(\gamma,n)$ reaction, calculated in 0·5 MeV steps.

Ref. N.L. Svantesson
Nuclear Phys. 3, 273 (1957)

Elem. Sym.	A	Z
O	16	8

Method: Betatron; γ spectrum measurement; NaI spectrometer; ion chamber

Ref. No.: 57 Sv 1 | NVB

Reaction	E or ΔE	E_0	Γ	$\int \sigma dE$	Jπ	Notes
$O^{16}(\gamma,n\gamma)$ $O^{16}(\gamma,p\gamma)$	Bremss. 16-30					Detector at 120°.

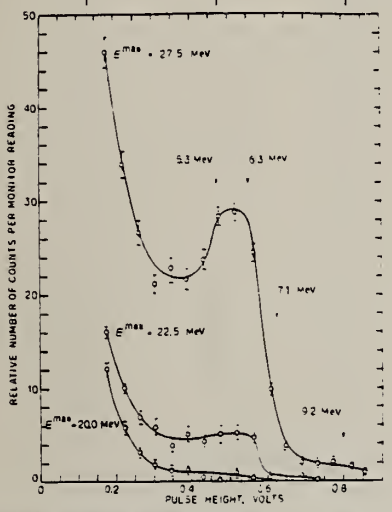

Fig. 3. Pulse height distributions measured when irradiating a 2" water target with 20.0, 22.6, and 27.5 MeV bremsstrahlung spectra. The background distributions are subtracted.

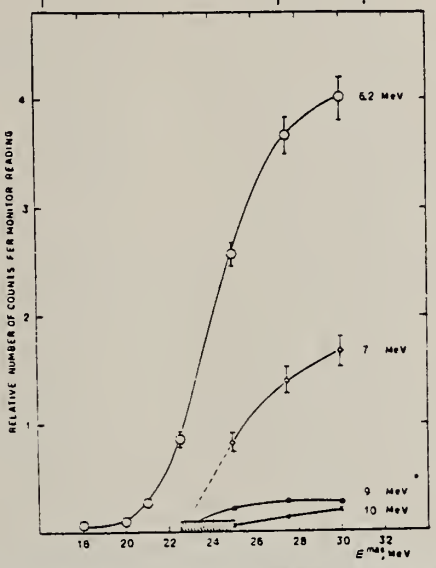

Fig. 9. The yield curves observed for the different daughter photon energies. The shaded area shows the energy interval in which the 7, 9 and 10 MeV photons are predominantly produced. When the statistical errors are not shown, they are within the symbols.

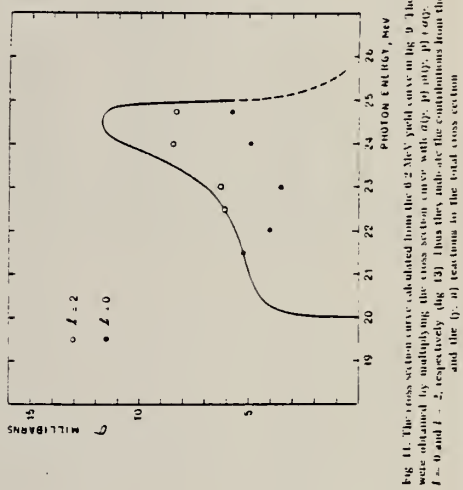

Fig. 11. The cross section curve calculated from the 6.2 MeV yield curve in fig. 9. The points were obtained by multiplying the cross section curve with $d(p,p_0)/d(p,p_0+p_1)$ for $I = 0$ and $I = 2$, respectively (fig. 13). Thus they indicate the contributions from the (γ,p_0) and the (γ,n_0) reactions to the total cross section.

TABLE 2

The integrated cross section (MeV·mb), together with the relative numbers, for the $O^{16}(\gamma,p)N^{15}$ and $O^{16}(\gamma,n)O^{15}$ reactions. The cross section for ground state transitions in the (γ,p) reactions was taken from Stephens *et al.*[3]. The same cross section was also used for ground state transitions in the (γ,n) reaction. In splitting the cross section for 6.2 MeV and 7 MeV photons into cross section for the two different reactions the photonucleons were assumed to have $I = 0$ and $I = 1$, respectively.

Excitation energy in O^{16} (MeV)	Reaction	Photodisintegration to ground state		excited state (MeV) 6.2		7		9		10		Total σ_{int}
		(MeV·mb)	%	(MeV·mb)	%	(MeV·mb)	%	(MeV·mb)	%	(MeV·mb)	%	(MeV·mb)
20.0–21.0	γ, p	3	43	4	57							7
	γ, n	3	100									3
	γ, p–γ, n	6	60	4	40							10
21.0–22.5	γ, p	11	61	7	39							18
	γ, n	11	92	1	8							12
	γ, p–γ, n	22	73	8	27							30
22.5–25.0	γ, p	14	32	11	26	12	28	4	9	2	5	43
	γ, n	14	45	10	32	7	23					31
	γ, p–γ, n	28	38	21	28	19	26	4	5	2	3	74
20.0–25.0	γ, p	28	41	22	32	12	18	4	6	2	3	68
	γ, n	28	61	11	24	7	15					46
	γ, p–γ, n	56	49	33	29	19	17	4	3	2	2	114

FORM NBS-418
(8-1-63)
USCOMM-OC 18556-P63

Ref. C.P. Swann, F.R. Metzger
Phys. Rev. 108, 982 (1957)

Elem. Sym.	A	Z
O	16	8

Method: Van de Graaff; photon scattering; absorption; NaI spectrometer

Ref. No.: 57 Sw 1 NVB

Reaction	E or ΔE	E_o	Γ	$\int \sigma dE$	Jπ	Notes
$O^{16}(\gamma,\gamma)$	6.91 7.12	6.91 7.12				Mean life: $\tau_{6.91} = (1.2 \pm 0.3)\ 10^{-14}$ sec. $\tau_{7.12} = (1.0 \pm 0.3)\ 10^{-14}$ sec.

Ref. W.L. Bendel, J. McElhinney, R.A. Tobin
Phys. Rev. 111, 1297 (1958)

Elem. Sym.	A	Z
O	16	8

Method: Activation

Ref. No.: 58 Be 1 EH

Reaction	E or ΔE	E_o	Γ	$\int \sigma dE$	Jπ	Notes
(γ,n)						First large break observed at 16.17±0.05 MeV based on (γ,n) thresholds in F^{19}, N^{14} and C^{12}.

REF.
V. N. Maikov
J. Exptl. Theoret. Phys. (USSR) 34, 1406 (1958)
Soviet Phys. JETP 34(7), 973 (1958)

ELEM. SYM.	A	Z
0	16	8

METHOD

REF. NO. 58 Ma 1

EGF

REACTION	RESULT	EXCITATION ENERGY	SOURCE		DETECTOR		ANGLE
			TYPE	RANGE	TYPE	RANGE	
G,4A	ABX	20 - 40	C	150,250	EMU-D		4PI
G,PA	ABY	27 - 80	C	150,250	EMU-D		4PI

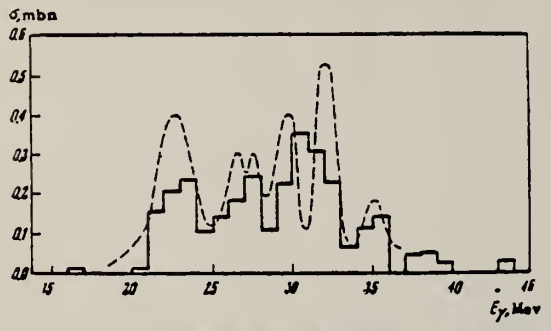

FIG. 2. Dependence of the cross section for reaction (II) on the γ-ray energy. The solid curve gives our data, the dashed one the data of reference 4.

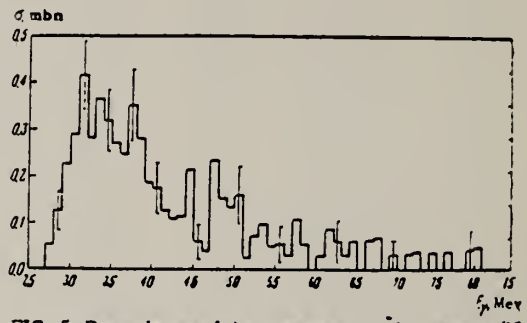

FIG. 5. Dependence of the cross section for reaction (V) on γ-ray energy.

σ(G,4A)

TABLE I. Integral cross sections for reactions (III) and (V) in mbn-Mev

E_γ · Mev	25—40	40—55	55—70	70—85
(III)	3.85±0.20	1.78±0.17	0.82±0.13	0.38±0.11
(V)	3.11±0.21	1.64±0.18	0.64±0.14	0.16±0.08

Reaction III $^{12}C \rightarrow H + {}^4He + {}^7Li$
Reaction V $^{16}O \rightarrow H + {}^4He + {}^{11}B$

Ref. C. Milone, S. Milone-Tamburino, R. Rinzivillo, A. Rubbino, C. Tribuno
Il Nuovo Cimento 7, 729 (1958)

Elem. Sym.	A	Z
O	16	8

Method: Emulsions; Bremss.

Ref. No.: 58 Mi 1 — EH

Reaction	E or ΔE	E_o	Γ	$\int \sigma dE$	Jπ	Notes
(γ,p)	23 26 30					Proton energy distribution measured at 23, 26 and 30 MeV.

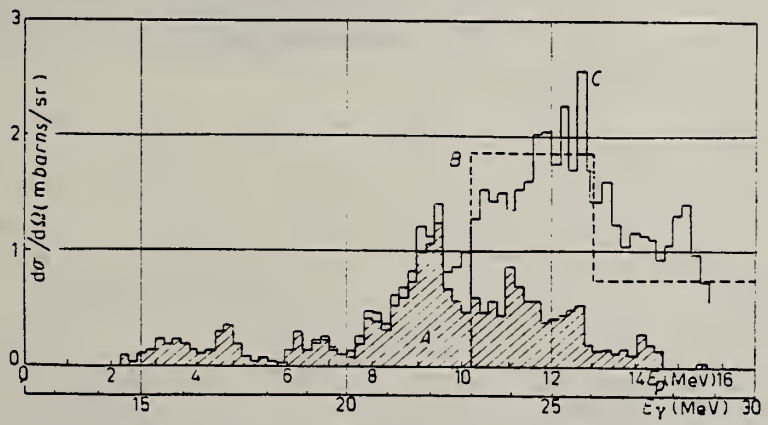

Fig. 7. – Sezione d'urto del processo O(γ, p): *A*) verso lo stato fondamentale del ^{15}N; *B*) sezione d'urto media negli intervalli 23÷26 e 26÷30 MeV; *C*) andamento della sezione d'urto nelle ipotesi della Sez. 4·4.1 del resto.

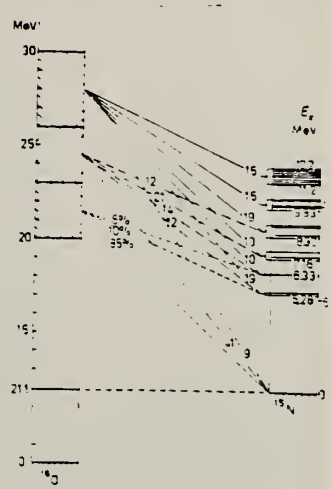

Fig. 10. – Livelli del ^{15}N e percentuale di fotoprotoni che lasciano ^{15}N nello stato fondamentale o in livelli eccitati.

Ref. A.K. M. Siddiq, R.N.H. Haslam
Can. J. Phys. 36, 963 (1958).

Elem. Sym.	A	Z
O	16	8

Method: 25 MeV betatron; nuclear absorption; Zn, C, S, O activity detectors

Ref. No.: 58 Si 3 EH

Reaction	E or ΔE	E_o	Γ	$\int \sigma dE$	Jπ	Notes
$O^{16}(\mu_t)$	Bremss. 15-25					The measured attenuations agree with those predicted on the basis of smooth absorption corss sections.

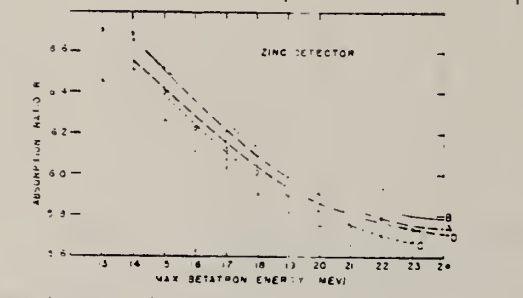

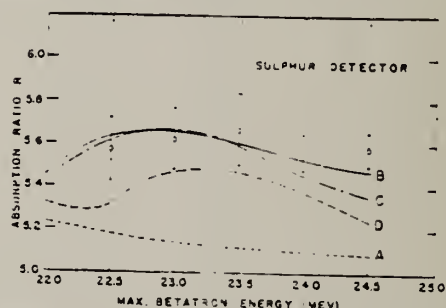

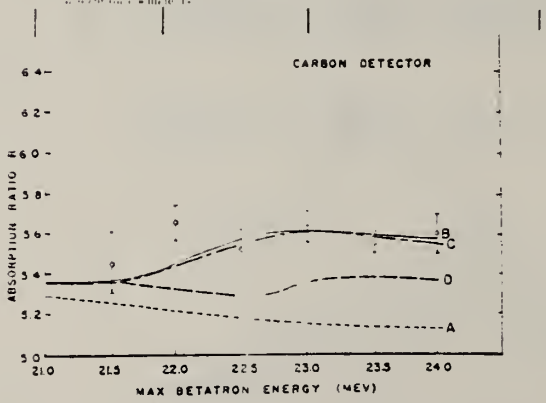

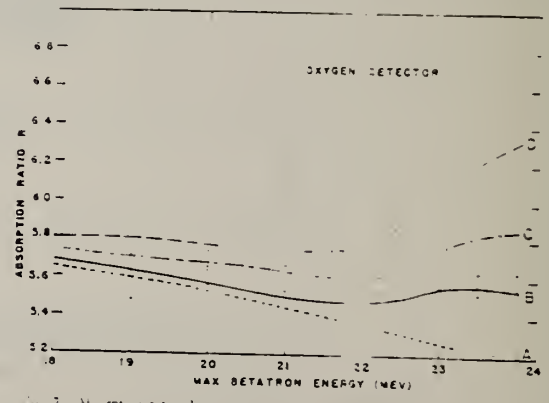

Ref. P. Brix, E.K. Maschke
Z. Physik 155, 109 (1959)

Elem. Sym.	A	Z
O	16	8

Method: 32 MeV betatron; angular distribution; nuclear emulsions; ionization chamber.

Ref. No.: 59 Br 2 EH

Reaction	E or ΔE	E_o	Γ	$\int \sigma dE$	J π	Notes
$O^{16}(\gamma,p)$	Bremss. 32					Angular distribution is peaked near 90° but now slightly forward for higher energies. For E_γ = 28 MeV, $\sigma_{(\gamma,p)gs}$ = 2.1 mb ± 2.5%

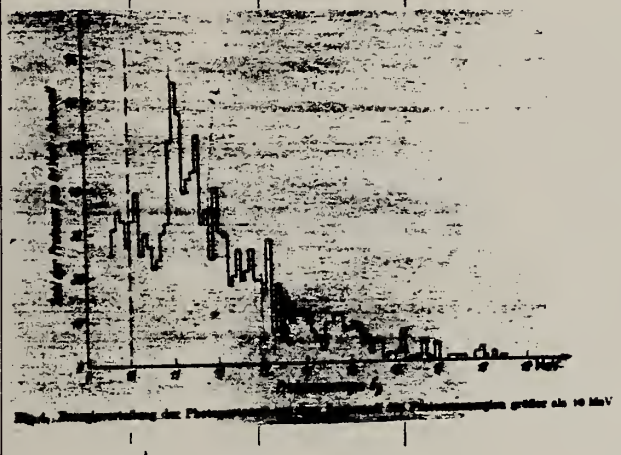

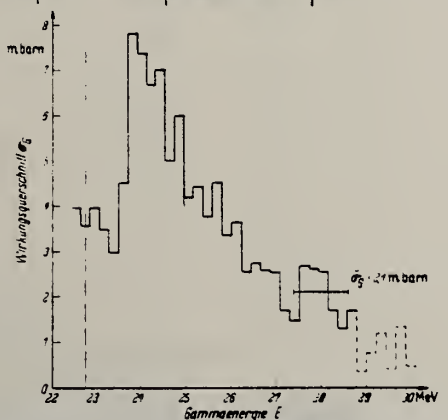

Fig. 6. Wirkungsquerschnitt σ_g des (γ, p)-Prozesses am O^{16} für Übergänge zum Grundzustand des N^{15}, normiert durch $\bar{\sigma}_g$ (28 MeV) = 2,1 mb. Für $E_\gamma \gtrsim 27$ MeV gibt das Histogramm eine obere Grenze für σ_g

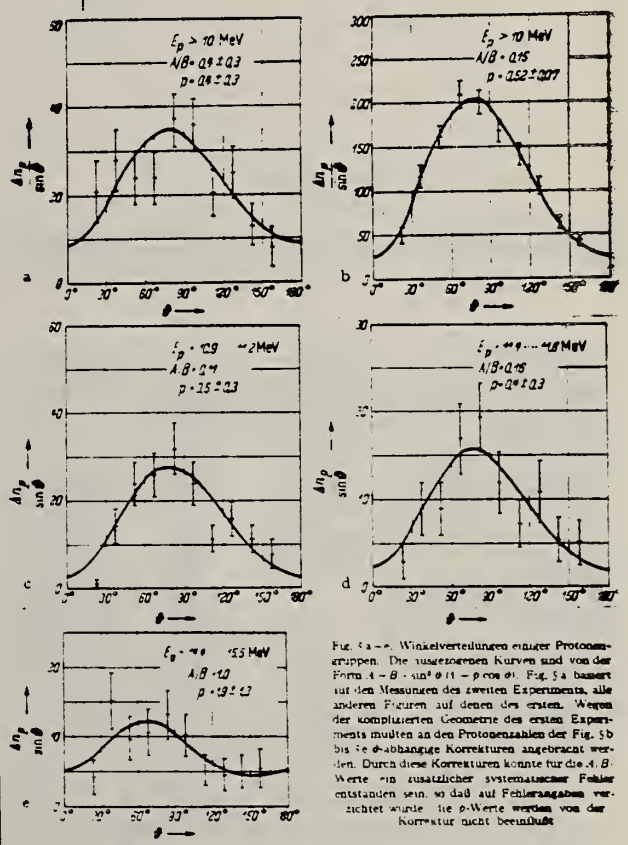

Fig. 5 a–e. Winkelverteilungen einiger Protonengruppen. Die ausgezogenen Kurven sind von der Form $A + B \cdot \sin^2\vartheta\,(1 - p\cos\vartheta)$. Fig. 5 a basiert auf den Messungen des zweiten Experiments, alle anderen Figuren auf denen des ersten. Wegen der komplizierten Geometrie des ersten Experiments mußten an den Protonenzahlen der Fig. 5 b bis 5 e ϑ-abhängige Korrekturen angebracht werden. Durch diese Korrekturen konnte für die A/B-Werte ein zusätzlicher systematischer Fehler entstanden sein, so daß auf Fehlerangaben verzichtet wurde. Die p-Werte werden von der Korrektur nicht beeinflußt

Ref. S.G. Cohen, P.S. Fischer, E.K. Warburton
Phys. Rev. Letters 3, 433 (1959)

Elem. Sym.	A	Z
O	16	8

Method: Princeton FM cyclotron; NaI.

Ref. No.: 59 Co 2 EH

Reaction	E or ΔE	E_o	Γ	$\int \sigma dE$	Jπ	Notes
$N^{15}(p,\gamma_o)$	14.5-19.5	22				
	E_x = 21.8					In agreement with Elliot and Flowers' [Proc. Roy. Soc. (London) A 242, 57 (1957)] calculations.
	= 24.7					

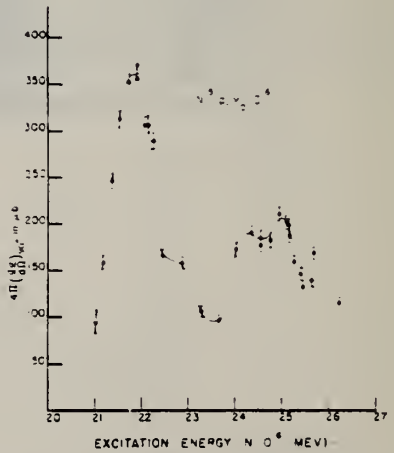

FIG. 1. The 90° yield of γ rays leading to the ground state of O^{16} from the $N^{15}(p,\gamma)O^{16}$ reaction. If the γ rays have an isotropic distribution relative to the proton beam, the ordinate scale gives the total cross section.

Ref. H. King, L. Katz
Can. J. Phys. 37, 1357 (1959)

Elem. Sym.	A	Z
O	16	8

Method Betatron; activation; scintillator

Ref. No. 59 Ki 1 EH

Reaction	E or ΔE	E_0	Γ	$\int \sigma dE$	Jπ	Notes
$O^{16}(\gamma,n)$	Bremss. 17.18			$\int_0^{17.3} = 0.5 \pm 0.1$ MeV- mb		$\int \sigma dE$ arrived at by photon difference method.

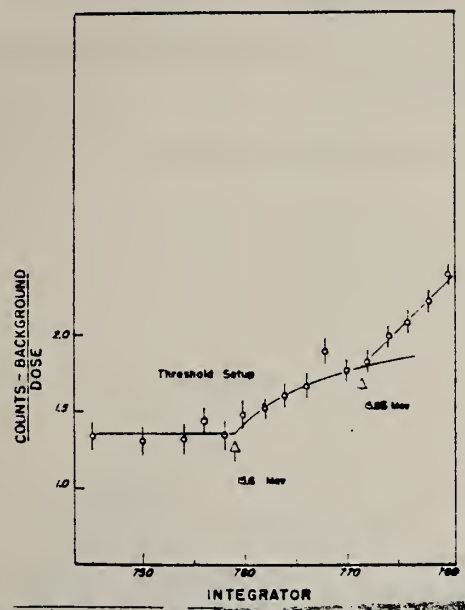

Fig. 2. Yield of O^{16} near threshold measured in recorded counts less the background and irradiation dose. The energy scale has been shifted 0.09 Mev as explained in the text.

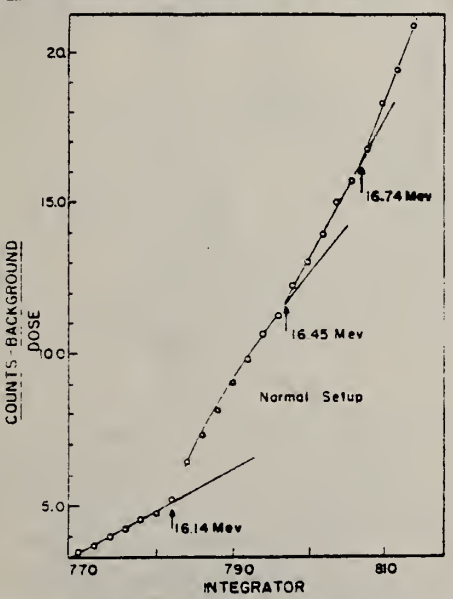

Fig. 4. Breaks in the $O^{16}(\gamma,n)O^{15}$ yield curve between 15.6 and [illegible]

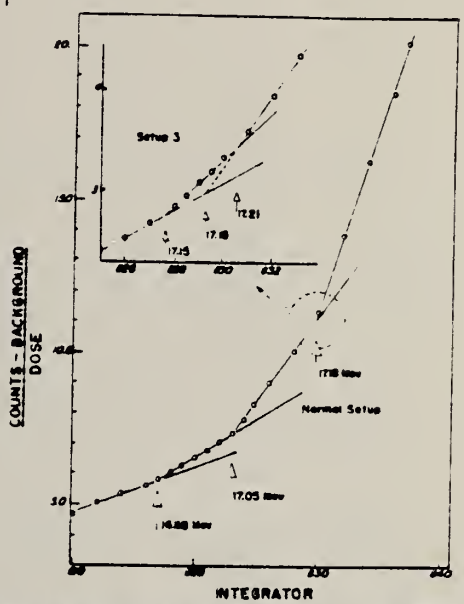

Fig. 3. Breaks in the $O^{16}(\gamma,n)O^{15}$ yield curve between 16.75 and 17.5 Mev. The curve was taken with the setup (a) illustrated in Fig. 2. Insert shows how the 17.18 Mev is resolved into two breaks when setup (c) is used.

TABLE 1

Position of the breaks in the oxygen (γ,n) yield curve, their relative strengths, and comparison with other measurements

Present work: Break position, Mev	Present work: $G\int\sigma dE$, Mev-mb	Bendel *et al.* (1958), $O^{16}(\gamma,n)O^{15}$	Geller and Muirhead (1958), $O^{16}(\gamma,n)O^{15}$	Jones *et al.* (1958), $N^{14}(p,\gamma)O^{15}$
[illegible]			15.79±0.02	
[illegible]	0.001	15.94±0.05	16.08	
16.14±0.04	0.022	16.18±0.02	16.28	16.21(?)
[illegible]	[illegible]			[illegible]
16.45±0.04	0.006		Not explained	
16.74±0.04	0.081		16.97	
15.02±0.04	0.054		17.08	~15.5
17.26±0.04	0.120		17.19	17.18
17.13±0.04 } *	0.195		} 17.33	
17.51±0.04 }	0.138			17.50
$\sum G\int\sigma dE$ = 0.57±0.11				

*Our 17.13-Mev break is the average of these two breaks.

Bendel, L. B., McElhinney, J., and Toren, R. A. 1958. Phys. Rev. 111, 1297.
Cohen, L. and McElhinney, J. 1956. Rev. Sci. Instr. 27, 7731.
Geller, K. N. and Muirhead, E. G. 1958. Precision energy measurements with a 25-Mev betatron (University of Penn. Report).
——— 1959. Bull. Am. Phys. Soc. Ser. II, 4, 32.
Jones, K. W., Lindsey, L. J., and Weil, J. L. 1958. Phys. Rev. 112, 1252.

Ref. C. Milone
Phys. Rev. Letters 3, 43 (1959)

Elem. Sym.	A	Z
O	16	8

Method
Emulsions; Bremss.

Ref. No.
59 Mi 2
EH

Reaction	E or ΔE	E_o	Γ	$\int \sigma dE$	Jπ	Notes
O (γ,n)						Figure 1: "b" - calcaulated from Carver and Loken (γ,n) assuming ground state transitions. "c" - calculated from Spicers' (γ,n). Spectrum measured at 90°

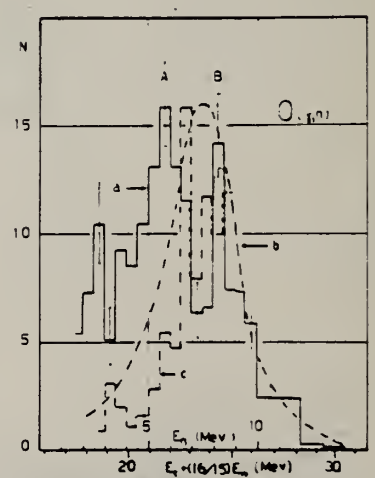

FIG. 1. (a) Experimental photoneutron spectrum. N = neutrons per ΔE_n = 0.5 Mev (arbitrary units). (b) and (c) Spectra calculated from the O(γ,n) cross sec-

Ref. C. Milone, A. Rubbino
Il Nuovo Cimento 13, 1035 (1959)

Elem. Sym.	A	Z
O	16	8

Method: Emulsions; Bremss.

Ref. No.: 59 Mi 3 | EH

Reaction	E or ΔE	E_o	Γ	$\int \sigma dE$	Jπ	Notes
(γ,n)	31					

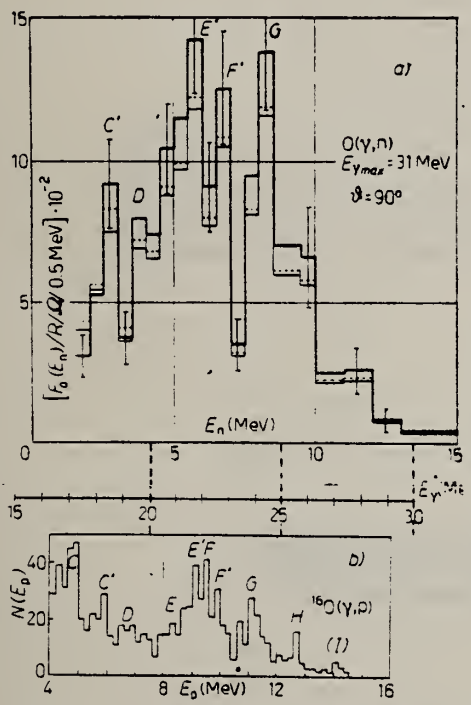

Fig. 2. – *a*) Energy spectrum of the photoneutrons from oxygen at $\theta = 90°$, $E_{\gamma\,max} = 31$ MeV. —— « primary » flux; —— « observed » flux; – – – flux corrected for the absorption in oxygen only. *b*) Energy spectrum of the photoprotons from oxygen at $\theta = 90°$, $E_{\gamma\,max} = 30$ MeV [13].

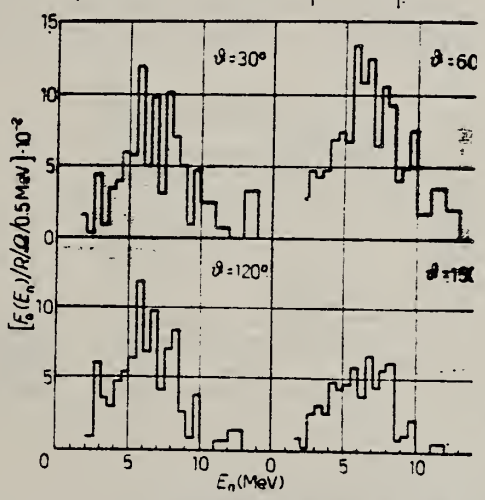

Fig. 3. – Energy spectra of the photoneutrons from oxygen at angles $\theta = 30°$, 60° 120° and 150°.

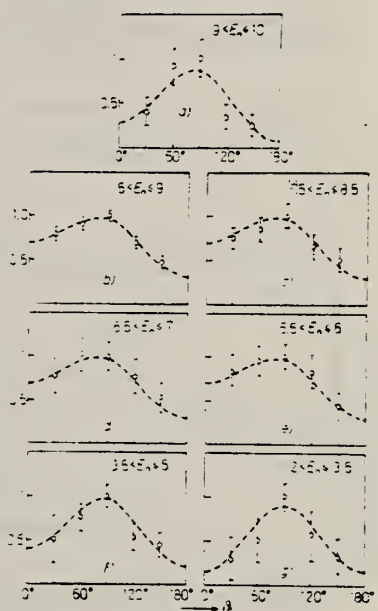

Figure 5: Angular distribution of photoneutrons from oxygen for the various neutron groups.

Ref. 13: Milone, Milone-Tamburino, Rinqivillo, Rubbino, Tribuno, Il Nuovo Cimento 7, 729 (1958)

J. O'Connell, P. Dyal, J. Goldemberg
Phys. Rev. 116, 173 (1959)

0	16	8

METHOD: Betatron

REF. NO.: 59 Oc 1 NVB

REACTION	RESULT	EXCITATION ENERGY	SOURCE TYPE	SOURCE RANGE	DETECTOR TYPE	DETECTOR RANGE	ANGLE
G,2N	RLI	THR-100	C	THR-100	ACT-I		4PI

REL TØ G,N

TABLE II. Relative integrated cross sections.

Element	(γ,n)	Position of the peak for (γ,n)	$(\gamma,2n)$	Position of the peak for $(\gamma,2n)$
C^{12}	1	23 Mev	0.003	42 Mev
N^{14}	1	24 Mev	0.007[a]	
O^{16}	1	22 Mev	0.002	40 Mev
F^{19}	1	20 Mev	0.14	32 Mev
Na^{23}	1	20 Mev	0.05	32 Mev
P^{31}	1	20 Mev	0.06 $(\gamma,2p)$	45 Mev $(\gamma,2p)$
			0.08 $(\gamma,2pn)$	50 Mev $(\gamma,2pn)$

[a] The (γ,n) integrated cross section was taken from reference 4.

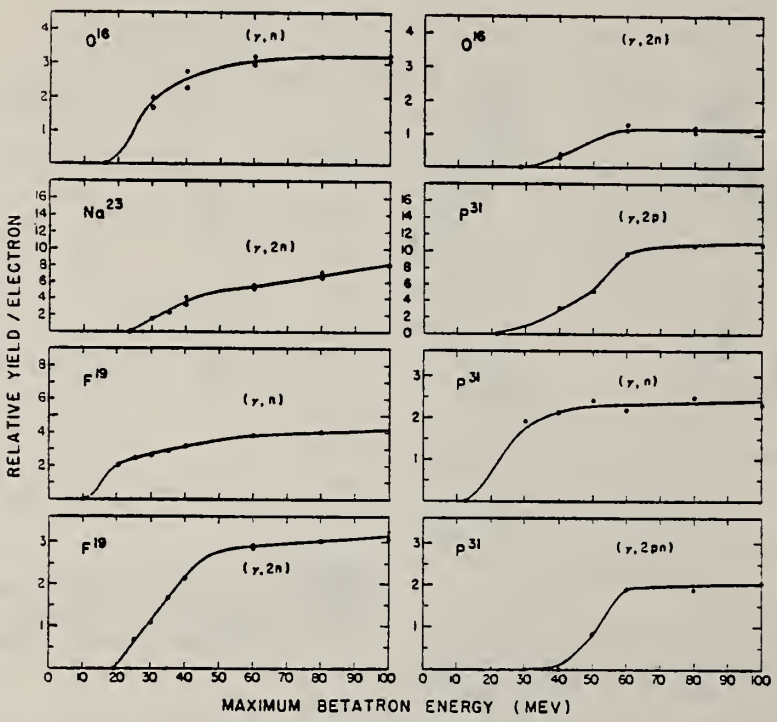

FIG. 1. The energy dependence of several photonuclear reactions. The relative yield scales of different graphs are independent.

REF.

P. Paul and U. Stierlin
Nucl. Physics 13, 576 (1959)

ELEM. SYM.	A	Z
O	16	8

METHOD

REF. NO.	
59 Pa 3	EGF

REACTION	RESULT	EXCITATION ENERGY	SOURCE		DETECTOR		ANGLE
			TYPE	RANGE	TYPE	RANGE	
G, G	ABX	17	D	15,18	NAI-D	17	90

Source Li(p,γ) with E_p = 500 keV.

Tabelle 1

Die gemessenen totalen Streuquerschnitte in cm² unter Annahme von E1- und E2-Streuung

Element	eigene Werte	Fuller und Hayward [12])	Stearns [8])
Pb	$(5.6\pm1)\times10^{-27}$	$(4-8)\times10^{-27}$	$(5-9)\times10^{-27}$
Al	$(2\ \pm1)\times10^{-28}$	$(2-6)\times10^{-29}$	
O	$(1\ -5)\times10^{-30}$		
C	$(5.8\pm2)\times10^{-30}$		

Durch die Wahl der Meßgeometrie ergibt sich für eine E1- wie eine E2-Winkelverteilung innerhalb der Fehlergrenzen der numerischen Rechnung der gleiche Wert für den totalen Streuquerschnitt. Die angegebenen Fehler enthalten nur den Fehler in der Bestimmung des primären γ-Flusses und die statistischen Fehler der Streuraten. Zum Vergleich sind die entsprechenden Ergebnisse von Fuller und Hayward [12]) und Stearns [8]) gegenübergestellt. Die angegebenen Werte gehören jeweils zu den Fehlergrenzen.

Ref. A.S. Penfold, E.L. Garwin
Phys. Rev. 114, 1324 (1959)

Elem. Sym.	A	Z
O	16	8

Method: activation; self absorption measurement

Ref. No.: 59 Pe 2 — EH

Reaction	E or ΔE	E_o	Γ	$\int \sigma dE$	Jπ	Notes
(μ_t)	Bremss. 30.7					Both Carbon and Oxygen detectors were used. σ_{tot} for Oxygen averaged over the giant resonance in 26.7±3.5 mb, 16±4 mb higher than expected for a smooth giant resonance. The resonances near 22 MeV have these properities: $\sigma_{max} = 106 \pm 14$ mb; $\frac{\Gamma_{\gamma gs}}{\Gamma_{tot}} = (6.6 \pm 0.9)10^{-3}$; $\Gamma_{tot} = 30$ KeV

Ref. A. S. Penfold, E.L. Garwin
Phys. Rev. 115, 420 (1959)

Elem. Sym.	A	Z
O	16	8

Method: 100 MeV Betatron

Ref. No.: 59 Pe 3 EH

Reaction	E or ΔE	E_o	Γ	$\int \sigma dE$	Jπ	Notes
(γ,n)						Breaks: 16.19 ± 0.04 17.25 ± 0.04

A. S. Penfold and E. L. Garwin
Phys. Rev. 116, 120 (1959)

0	16	8

METHOD

REF. NO. 59 Pe 5 JOC

REACTION	RESULT	EXCITATION ENERGY	SOURCE		DETECTOR		ANGLE
			TYPE	RANGE	TYPE	RANGE	
G,G	ABX	19 - 61	C	19 - 61	NAI-D		135
G,G/	ABX	19 - 61	C	19 - 61	NAI-D		135

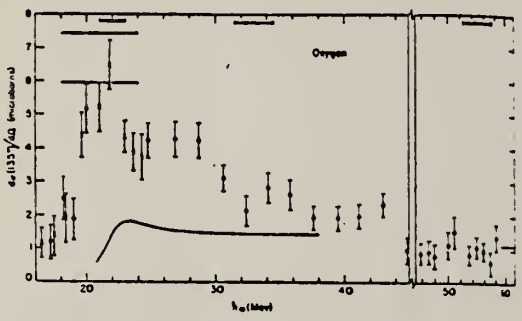

FIG. 6. The scattering corss section for O at 135°. The cross designate points which can only be due to elastic scattering, wh. the dots designate points for mixed elastic and inelastic scatterin: The mixing is defined by Eq. (15) in the text. The data we obtained from irradiations with bremsstrahlung energies of 22.5 26.4, and 61 Mev. The solid curve and the light horizontal line (upper right) are predicted values for the cross section (see tex for details).

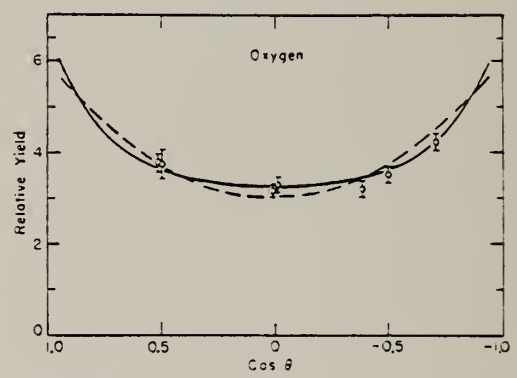

FIG. 8. The angular dependence of the elastically scattered gamma rays from O which lie in the range 19 to 25 Mev. See text for explanation of the dashed and solid lines.

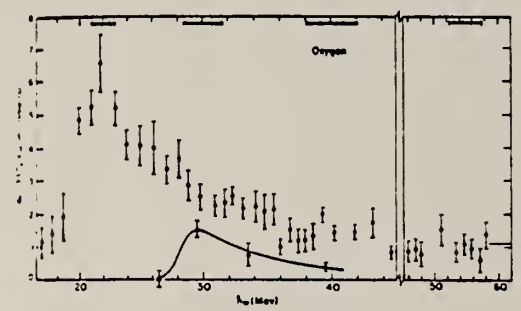

FIG. 7. The elastic scattering cross section for O at 135° (dots) and an inelastic cross section due to transitions to a state near 6 Mev (triangles).

Dror Saden
Compt. Rend. 249, 2313 (1959)

0	16	8

METHOD

REF. NO. 59 Sa 2 EGF

REACTION	RESULT	EXCITATION ENERGY	SOURCE TYPE	SOURCE RANGE	DETECTOR TYPE	DETECTOR RANGE	ANGLE
G,N	NØX	THR-22	C	15-22	ACT-I		4PI

BREAKS

Nos résultats comparés à ceux de Katz (4) *et de Penfold* (3).

Nos résultats (± 0,02 MeV).	Katz (± 0,05 MeV).	Penfold (± 0,05 MeV).
15,65	15,60	15,60
15,74	-	-
15,92	15,82	15,85
16,12	16,11	16,03
16,41	-	-
16,52	16,42	16,47
16,63	-	-
16,70	-	-
16,84	16,71	16,75
16,97	16,85	16,95
17,15	17,02	17,02
17,33	17,18	17,18
17,55	-	17,55
17,68	-	17,68
18,07	-	18,04
18,72	-	18,7
18,89	-	19,01
19,18	-	19,18
20,25	-	20,33
20,58	-	20,58
21,59	21,51	21,52

Ref. N.W. Tanner, G.C. Thomas, W.E. Meyerhof
Il Nuovo Cimento 14, 257 (1959)

Elem. Sym.	A	Z
O	16	8

Method
Proton-capture; NaI spectrometer

Ref. No.
59 Ta 1

EH

Reaction	E or ΔE	E_o	Γ	$\int \sigma dE$	Jπ	Notes
$N^{15}(p,\gamma)$	4.0-9.0					Ground state transitions measured at 90°.

Fig. 1. Excitation function for $^{15}N(p,\gamma)^{16}O$. The points are the experimental results for this reaction. The histogram is the excitation function for $^{15}N(p,\gamma)^{16}O$ considered by detailed balance from the excitation function for $^{16}O(\gamma,p)^{15}N$. The dotted lines indicate the position of resonances that might be expected in $^{15}N(p,\gamma)^{16}O$ from the fine structure in $^{16}O(\gamma,p)^{15}N$.

Ref. E.E. Carroll, Jr., W.E. Stephens
Phys. Rev. 118, 1256 (1960)

Elem. Sym.	A	Z
O	16	8

Method: Monoenr. γ's from $B^{3}(p,\gamma)Be^{4}$ reaction, total abs.; NaI

Ref. No.: 60 Ca 1 JR

Reaction	E or ΔE	E_o	Γ	$\int \sigma dE$	Jπ	Notes
μ_t	20.0-20.5	20.33 or higher				max (20.33 MeV) = 22.5 ± 4 mb. av. (nuclear) = 13.5 ± 4 mb. Calculated atomic cross-sections subtracted, using Borsellino for triplet. Steelply rising cross-sections associated with (γ,p) peak in this region.

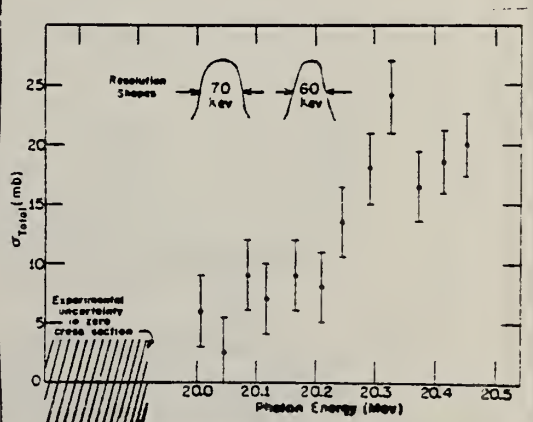

FIG. 5. Total nuclear absorption in oxygen-16.

Ref. K.N. Geller
Phys. Rev. 120, 2147 (1960)

Elem. Sym.	A	Z
O	16	8

Method Bremss; second-difference analysis

Ref. No. 60 Ge 1 JHH

Reaction	E or ΔE	E_0	Γ	$\int \sigma dE$	Jπ	Notes
(γ,n)	E_t -17.6	(See Table I, col. 1)				Mostly an application of the analysis method.

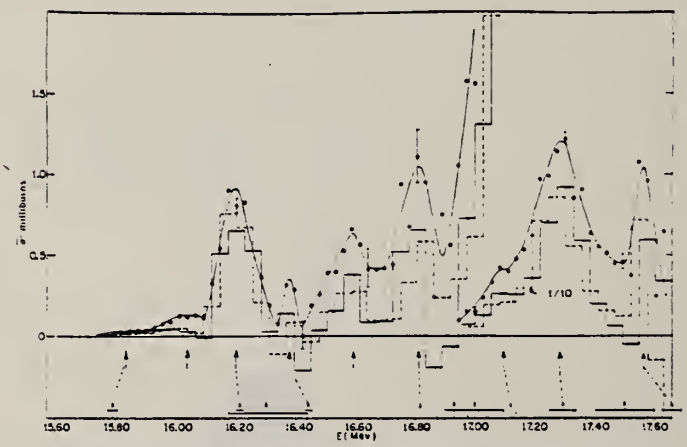

FIG. 3. Zero-order (bars) and final cross section (solid curve) for the $O^{16}(\gamma,n)O^{15}$ reaction from threshold to 17.6 Mev. Baseline arrows indicate energy assignments of known levels and horizontal bars the level widths, where known. Correspondence between levels observed in the present experiment with known levels indicated by dashed line.

TABLE I. Summary of levels observed in the present experiment and in other type reactions

$(\gamma,n)^{15a}$ (Mev)	$(\gamma,n)^{15b}$ (Mev)	Γ[b] (kev)	Reaction
15.83	15.79	30	(γ,α)
16.04			
16.20	16.21	23	(γ,n)
16.38[c]	16.44	24	(γ,α')
16.59			
16.81	16.75		(γ,α)
	16.82		(γ,α)
17.10	17.12	41	(p,n)
	17.24[c]	280	(p,γ)
17.28	17.29	84	(p,n)
	17.30		$\gamma,\alpha)$

[a] Present experiment.
[b] F. Ajzenberg-Selove and T. Lauritsen, Nuclear Phys. 11, 1 (1959).
[c] N. W. Tanner, G. C. Thomas, and W. E. Meyerhof, Nuovo cimento 14, [illegible] (1959).

FORM NBS-418
(8-1-63)
USCOMM-DC 18556-P63

U.S. DEPARTMENT OF COMMERCE
NATIONAL BUREAU OF STANDARDS

Ref. K.H. Beckel, S. Halpern, E.G. Muirhead
Phys. Rev. 119, 716 (1960)

Elem. Sym.	A	Z
O	16	8

Method 25 MeV Betatron; activation of oxygen; NaI counters for annih. rad. of positions from residual nuclei

Ref. No. 60 Ge 2 JHH

Reaction	E or ΔE	E_o	Γ	$\int \sigma dE$	Jπ	Notes
(γ, n)	15.42 → 17.27					E_γ (threshold) = 15.64 ± 0.04 MeV to be compared with Everling's neutron separation energy 15.669 ± 0.006 MeV from mass data. Observed breaks in yeild curve (Figure 3) at: 15.86 MeV 15.99 MeV 16.22 ± 0.02 MeV 17.27 ± 0.03 MeV

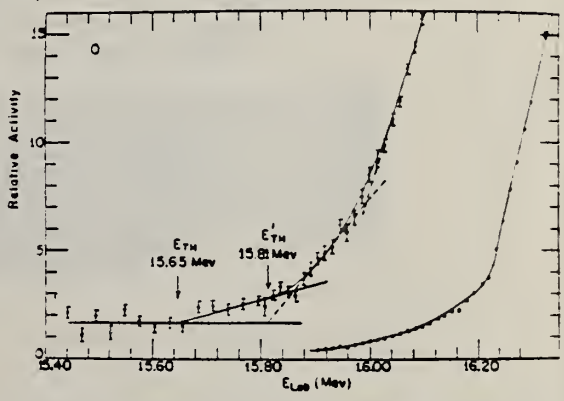

FIG. 3. Activation curve for the reaction $O^{16}(\gamma,n)O^{15}$.

Ref. D.F. Hebbard
Nuclear Phys. 15, 289 (1960)

Elem. Sym.	A	Z
O	16	8

Method: 600 kev electrostatic generator; NaI

Ref. No.: 60 He 1 JHH

Reaction	E or ΔE	E_o	Γ	$\int \sigma dE$	Jπ	Notes
$N^{15}(p,\gamma_0)O^{16}$	200-627 kev	338 kev				This resonance observed for 12 MeV γ's corresponding to the 12.43 MeV level in O^{16}.

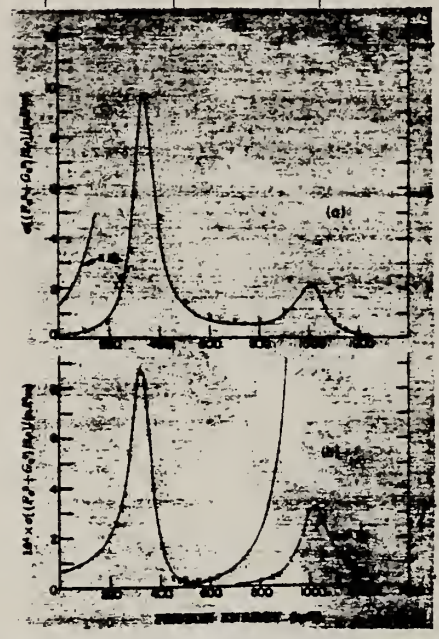

Fig. 6.

(a). The $N^{15}(p,\alpha_0)$ integrated cross section, with the calculated energy dependence included. The full curve represents the calculated cross section for constructive interference between two 1^- resonances at 338 kev and 1010 kev. The points are either experimental, (open circles) or are selected at intervals from the smooth curve of fig. 1. The ordinates at the resonance have been suppressed. The ordinate at high energies is directly proportional to the correction being allowed by multiplication of this ordinate by 4.57×10⁻³ to give S in kev-barns.

(b). The $N^{15}(p,\gamma_0)$ integrated cross section, with the calculated energy dependence included. The full curve represents the calculated cross section for constructive interference between two 1^- resonances at 338 kev and 1010 kev. The points are experimental, the ordinates at the 1010-kev resonance being obtained from the smooth curve of fig. 1, by multiplication by 0.142.

Ref 9: Hagedorn - Phys. Rev. 108, 735 (1957)

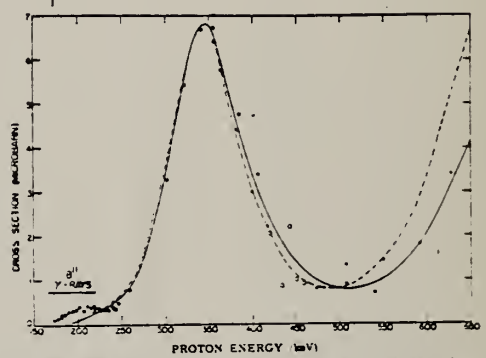

Fig. 4. The cross section for the $N^{15}(p,\gamma_0)O^{16}$ reaction, as a function of proton energy. The open circles are measurements that required correction for the simultaneous detection of both members of a cascade from the 429-keV resonance through the 6 and 7-MeV states in O^{16}. The dashed curve is the theoretical curve for destructive interference between two 1^- resonances at 338 kev and 1010 keV with the 1010-keV resonance having a peak cross section of 1000 μb. The full curve shows the improved agreement when the 1010-keV resonance peak cross section is reduced by the factor 1.42. Both theoretical curves are normalized to match the peak height of the 338-keV resonance. More weight should be attached to the points at 393 keV and 627 keV than to the scattered points between 425 keV and 560 keV.

TABLE 3

Single-level parameters for the 338 and 429 keV resonances

O^{16*} (MeV)	E_R (keV)	Γ_p (keV)	Γ_{α_0} (keV)	Γ_{α_1} (keV)	Γ_{γ_0} (eV)	$\Gamma_{\gamma\text{cascade}}$ (eV)
12.43	338	1.1	93	0.025	8	0.4
12.52	429	0.020	forbidden	0.90	—	0.006

TABLE 4

Two-level parameters for the 338 and 1010-keV resonances

E_R (keV)	γ_p^2 (keV)	$\gamma^2_{\alpha_0}$ (keV)	$\gamma^2_{\alpha_1}$ (keV)	Γ_{γ_0} (eV)
338	354	19.8	76	12.8
1010	450	4.27	20.7	88

D. Isabelle, G. Bishop
Compt. Rend. 251, 693 (1960)

0	16	8

METHOD

Linac; inelastic electron scattering; magnetic spectrometer, Cerenkov counter

REF. NO. 60 Is 1 NVI

REACTION	RESULT	EXCITATION ENERGY	SOURCE TYPE	SOURCE RANGE	DETECTOR TYPE	DETECTOR RANGE	ANGLE
E,E/	RLX	20 - 30	D	60 - 150	MAG - D		DST

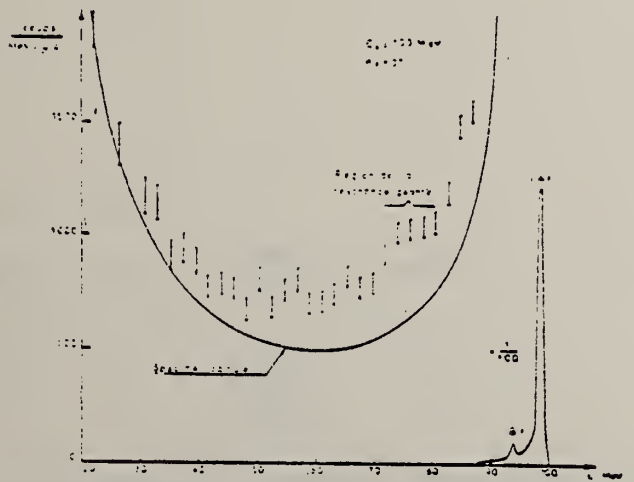

Fig. 1.

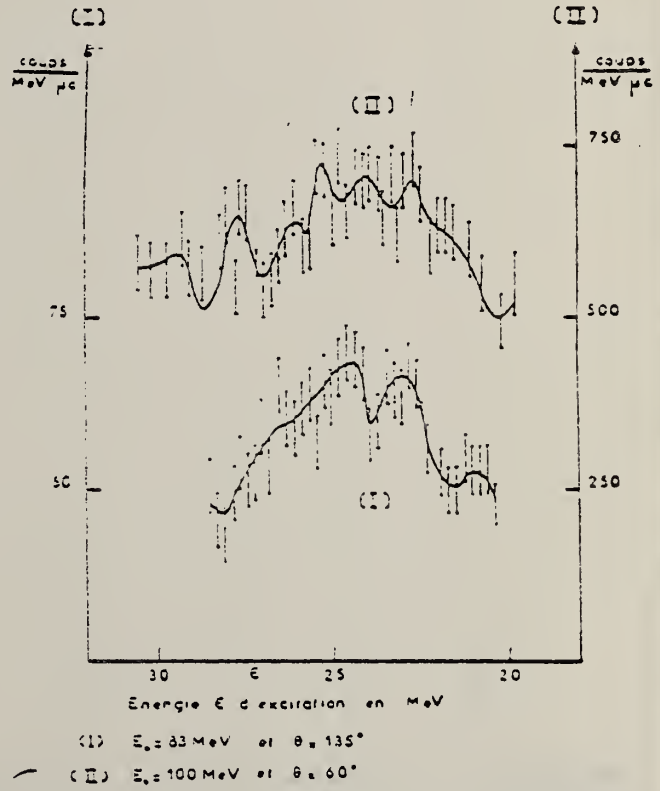

Fig. 2.

Ref. L.A. Kul'chitskii, V. Presperin
Zhur. Eksp. i Teoret. Fiz. 39, 1001 (1960);
Soviet Phys. JETP 12, 696 (1961)

Elem. Sym.	A	Z
O	16	8

Method
90 MeV Synchr.; proton recoil counter telescopes

Ref. No. 60, Ku 2 JH

Reaction	E or ΔE	E_o	Γ	$\int \sigma dE$	Jπ	Notes
(γ,n)	Bremss.; $E_{\gamma max}$=90MeV					Relative yields in table are per nuclear neutron.

Element	Relative neutron yield	Element	Relative neutron yield
Li	1.00±0.05	Cu	0.37±0.02
Be	1.22±0.09	Cd	0.35±0.02
O	0.74±0.05	I	0.39±0.02
Al	0.49±0.03	Bi	0.41±0.03
Ca	0.33±0.02		

Ref. K. Reibel, A.K. Mann
Phys. Rev. 118, 701 (1960)

Elem. Sym.	A	Z
O	16	8

Method: γ's from $F^{19}(\gamma,\alpha\gamma)$ reaction; protons from Van de Graaff; NaI

Ref. No.: 60 Re 1 JHH

Reaction	E or ΔE	E_o	Γ	$\int \sigma dE$	Jπ	Notes
O (γ,γ)	~ 7					$\langle \bar{\sigma} \rangle$ (E_p = 2.05 MeV) = 0.16±0.04 mb $\langle \bar{\sigma} \rangle$ (E_p = 2.40 MeV) = 0.19±0.05 mb Measured at 90° and 120°.

Ref. D. Sadeh
Phys. Rev. Letters 4, 75 (1960)

Elem. Sym.	A	Z
O	16	8

Method: 31 MeV Betatron; NaI(Tℓ), Cu^{62} monitor

Ref. No.: 60 Sa 1 EH

Reaction	E or ΔE	E_o	Γ	$\int \sigma dE$	Jπ	Notes
$O^{16}(\gamma,n)$	Bremss. ~15-16 MeV					"Breaks" at 15.65 and 15.76 MeV. The 15.65 MeV threshold is in agreement with the suggested correction of Penfold and Garwin [Phys. Rev. 115, 420 (1959)].

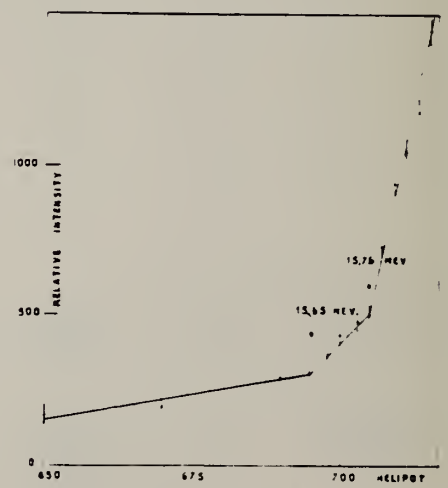

FIG. 1. The threshold and the first "break" of the reaction $O^{16}(\gamma,n)O^{15}$.

Ref. P.C. Stein, A.C. Odian, A. Wattenberg, R. Weinstein
Phys. Rev. 119, 348 (1960)

Elem. Sym.	A	Z
O	16	8

Method: 320 MeV synchrotron; proton telescope; neutron counter

Ref. No.: 60 St 1 JHH

Reaction	E or ΔE	E_o	Γ	$\int \sigma dE$	Jπ	Notes
$O^{16}(\gamma, np)$	Bremss. 320					$(\sigma/\sigma_{H^2}) = 3.1 \pm 0.4$ $[\sigma_{H^2} = 63\ \mu b]$ Mean photon energy - 262 MeV Proton counter at 76°

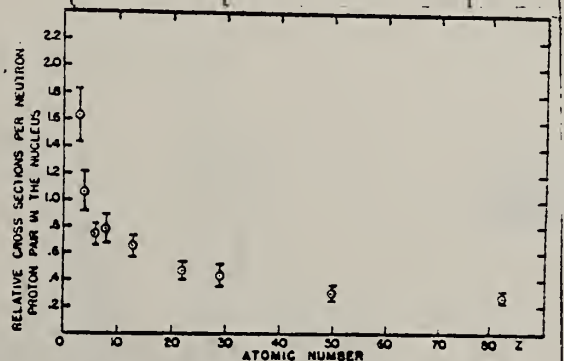

FIG. 2. Relative cross sections per neutron-proton pair in the nucleus versus atomic number. The cross section of the element of interest is divided by the cross section for deuterium and by the factor NZ/A.

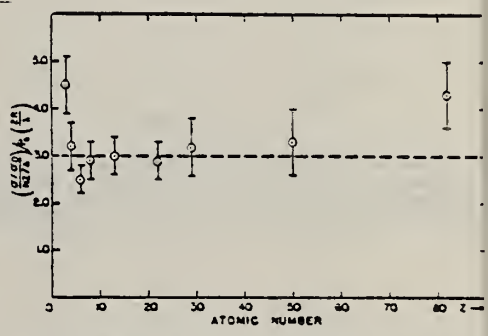

FIG. 3. The relative cross sections per neutron-proton pa corrected for the probability of escape is plotted against atom number. The probability of escape factor is calculated usi $r_0 = 1.30 \times 10^{-13}$ cm and $\lambda = 3.6 \times 10^{-13}$ cm. The probability escape factor is given in expression (1). The data shown are the of Fig. 2 divided by $P(2R/\lambda)$.

Ref.	Elem. Sym.	A	Z
J.M. Wyckoff, H.W. Koch Phys. Rev. 117, 1261 (1960)	O	16	8

Method	Ref. No.	
180 MeV Synchrotron; total absorption; NaI.	60 Wy 1	JMB

Reaction	E or ΔE	E_o	Γ	$\int \sigma dE$	Jπ	Notes
σ_{total}	Increm.: 35-90			0.191 ±15% (γ, meson threshold) ~ 16		Subtraction of electronic as baseline. Just assumed electronic was known for the O. No nuclear σ in H.

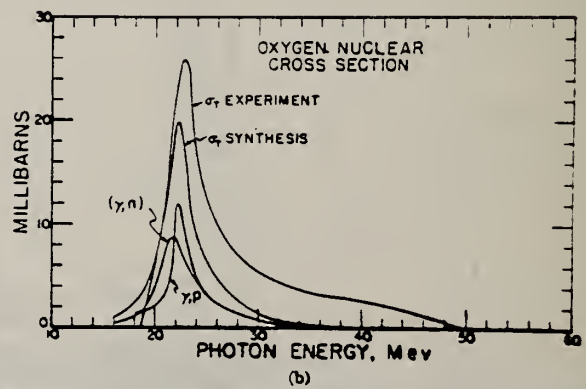

(b)

Ref. B. Ziegler
Nuclear Phys. 17, 238 (1960)

Elem. Sym.	A	Z
O	16	8

Method 32 MeV betatron; magnetic pair spectrometer

Ref. No. 60 Zi 1 JHH

Reaction	E or ΔE	E_o	Γ	$\int \sigma dE$	Jπ	Notes
(μ_t)	Bremss. 10-30					

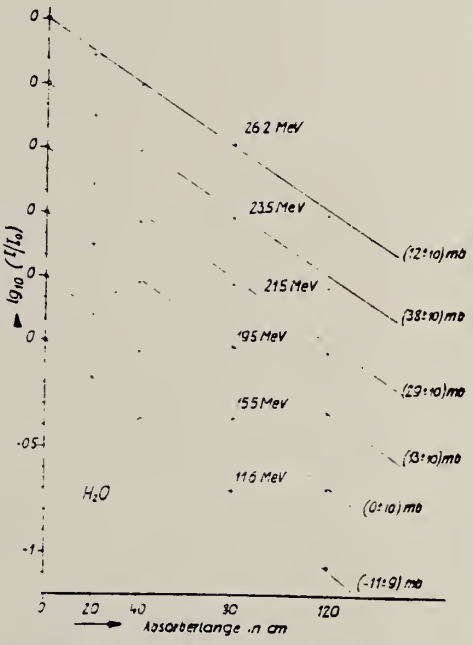

Fig. 8. Schwächung in H_2O bei den angegebenen γ-Energien. Die ausgezogenen Kurven wurden mit theoretischen Werten für $(\sigma_p + \sigma_s)$ berechnet, mit. Comptonfaktor $f(l)$. Die angegebenen Wirkungsquerschnitte wurden mittels Ausgleichrechnung als Differenz zwischen den Neigungen der experimentellen und theoretischen Kurven ermittelt; einfacher mittlerer [illegible]

REF.

P. Brix, H. Fuchs, K.H. Lindenberger, C. Salander
Z. Physik 165, 485 (1961)

ELEM. SYM.	A	Z
O	16	8

METHOD: Betatron; neutron cross section; NaI spectrometer; $C^{12}(\gamma,n)C^{11}$

REF. NO.: 61 Br 1 NVB

REACTION	RESULT	EXCITATION ENERGY	SOURCE		DETECTOR		ANGLE
			TYPE	RANGE	TYPE	RANGE	
G,N	ABI	0-34	C	34	ACT-I		4PI

Weighted average:

$$\int_0^{32} \sigma dE = 64 \pm 8 \text{ MeV- mb}$$

Tabelle 1. *Meßergebnisse für die D-Werte bei der Endenergie* $E_0 = 34$ MeV*

Reaktion	D	$\bar{E}$
$C^{12}(\gamma, n)$ . .	$0{,}2569 \pm 0{,}0015$	$24{,}1 \pm 1$ MeV
$O^{16}(\gamma, n)$ . .	$0{,}2594 \pm 0{,}0015$	$23{,}6 \pm 1$ MeV
$Cu^{63}(\gamma, n)$ . .	$0{,}2974 \pm 0{,}0017$	$15{,}6 \pm 1$ MeV

Tabelle 2. *Ausbeuten und integrierte Wirkungsquerschnitte von* $O^{16}(\gamma, n)$

Vergleichsreaktion	$C^{12}(\gamma, n)C^{11}$	$Cu^{63}(\gamma, n)Cu^{62}$
(1) Y_O/Y_V	$1{,}250 \pm 1{,}2\%$	$0{,}0700 \pm 3{,}4\%$
(2) $\int_{33\,MeV} \sigma_O\, dE \Big/ \int_{33\,MeV} \sigma_V\, dE$	$1{,}215 \pm 2{,}8\%$	$0{,}126 \pm 5{,}3\%$
(3) $\int_{33\,MeV} \sigma_O\, dE$	61 ± 7 MeVmb	71 ± 10 MeVmb

Alle angegebenen Fehler setzen sich aus dem dreifachen statistischen und systematischen Fehlern zusammen.

Zeile (1): Y_V = Ausbeute der Vergleichsreaktion. Zeile (2): Die Verhältnisse der integrierten Wirkungsquerschnitte folgen aus den Zahlen in Zeile (1) und Tabelle 1 durch Anwendung von Formel (1). Zeile (3): Die integrierten Wirkungsquerschnitte ergeben sich aus den in Zeile (2) angegebenen Verhältnissen, wenn man den Messungen von BARBER et al.[2] entnimmt, daß der bis 33 MeV integrierte Wirkungsquerschnitt von $C^{12}(\gamma, n)C^{11}$ 50,3 MeVmb $\pm$ 10% ist, und den Messungen von BERMAN und BROWN[12], daß das Integral bis 33 MeV von $Cu^{63}(\gamma, n)Cu^{62}$ 550 MeVmb $\pm$ 10% ist, und dabei berücksichtigt, daß das Verhältnis EC/β^+ beim Zerfall des Cu^{62} nicht 0 ist, wie BERMAN und BROWN annahmen, sondern 0,021[21].

[21] BUTLER, J.W., and C.R. GOSSETT: Phys. Rev. 112, 1257 (1958).

Ref.	Elem. Sym.	A	Z
S.G. Cohen, P.S. Fisher, E.K. Warburton Phys. Rev. 121, 858 (1961)	O	16	8

Method	Ref. No.	
Synchrocyclotron; NaI	61 Co 1	JH

Reaction	E or ΔE	E_o	Γ	$\int \sigma dE$	Jπ	Notes
(p,γ_0)	10-15	21.8		$0.27\Big|_{21}^{23.5}$ MeV-mb		Γ_γ(21.8 MeV) ≃ 2.2 kev.
		24.7		$0.27\Big|_{23}^{26.5}$ MeV-mb		Γ_γ(24.7 MeV) ≃ 5 - 14 kev.
						(calculated assuming compound nucleus formation).
						Integral cross sections are for excitation curve. For the 21.8 MeV resonsance, the $O^{16}(\gamma,p_0)N^{15}$ intergr cross is estimated as 20.5 Mev-mb

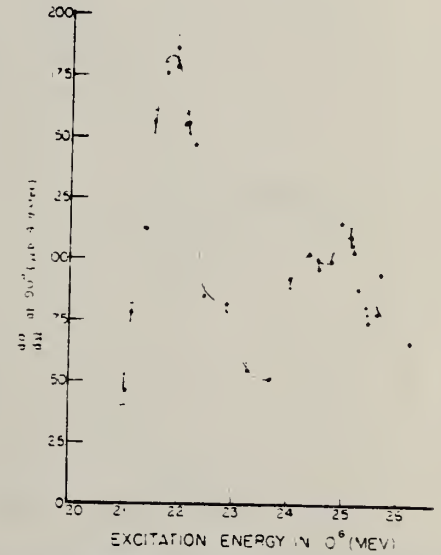

FIG. 5. The differential cross section at 90° for the γ rays leading to the ground state of O^{15} from the $N^{14}(p,\gamma_0)O^{15}$ reaction. If the γ rays have an isotropic distribution relative to the proton beam, then the ordinate scale gives the total cross section.

E. Finckh, U. Hegel
Z. Physik 162, 154 (1961)

CLCM. SYM.	A	Z
0	16	8

METHOD: Betatron; proton cross section; CsI; $C^{12}(\gamma,n)C^{11}$ monitor

REF. NO.: 61 Fi 1 | NVB

REACTION	RESULT	EXCITATION ENERGY	SOURCE TYPE	SOURCE RANGE	DETECTOR TYPE	DETECTOR RANGE	ANGLE
G,P	ABI	0 - 35	C	35	CSI-D	2 - 6	90
		(0 - 34.5)		(34.5)		(2 - 5.5)	

$$\frac{\text{Yield of } O(\gamma,p)}{\text{Yield of } C^{12}(\gamma,n)C^{11}} = 2.06 \pm 14\%$$

$$\int_0^{35} \sigma_{(\gamma,n)+(\gamma,p)} dE \lesssim (1 + 1.68) \int_0^{35} \sigma_{(\gamma,n)} dE = 175 \text{ MeV- mb}$$

U. Hegel, E. Finckh
Z. Physik 162, 142 (1961)

0	16	8

METHOD: Betatron; proton cross section, spectrum; NaI spectrometer; $C^{12}(\gamma,n)C^{11}$ monitor

REF. NO.: 61 He 2 | NVB

REACTION	RESULT	EXCITATION ENERGY	SOURCE TYPE	SOURCE RANGE	DETECTOR TYPE	DETECTOR RANGE	ANGLE
G,XP	SPC	0-35	C	35	SCI-D	6-22	90
		(0-34.5)					

$\frac{d\sigma}{d\Omega}$ = 0.13 mb/sr ± 13% for 30 MeV and 90°

assumes $\frac{d\sigma}{d\Omega} = a + b \sin^2\theta$ for total σ in Figure 7.

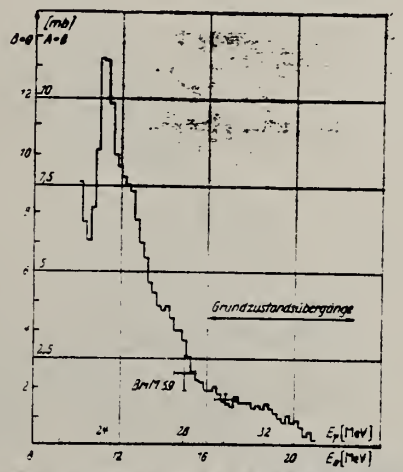

Fig. 7. Das Spektrum der Fig. 6 dividiert durch die Spektralfunktion S^* (34,5 MeV). Oberhalb 29,2 MeV stellt das Histogramm den Verlauf des Wirkungsquerschnittes für Grundzustandsübergänge dar, unterhalb dieser Energie gibt es eine obere Grenze dafür an. Die Ordinate ist normiert durch den bei 30 MeV bestimmten Wirkungsquerschnitt $d\sigma_0$, wobei für die linke Skala isotrope Winkelverteilung, für die rechte $A/B = 4$ angenommen wurde. Der von Brix und Maschke[13] angegebene Wert bei 28 MeV ist auf die rechte Skala herum eingezeichnet

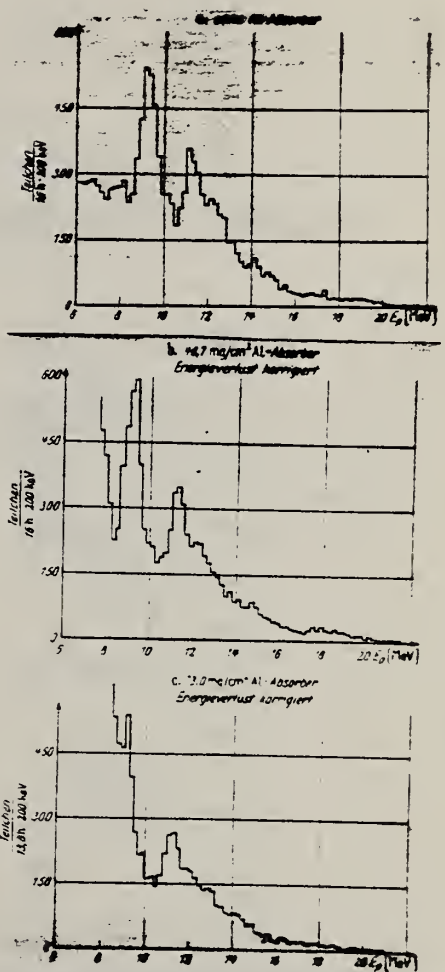

Fig. 8a–c. Protonenspektren mit und ohne Aluminium-Absorber. Abszisse: $E_p = \frac{1}{2}(E_\gamma - 17{,}33$ MeV); Ordinate: Protonenzahlen bezogen auf eingestrahlte Strahlungsenergie im 200 keV-Intervall. Auf dem Energieverlust der Protonen im Szintillator, Lichtopfen und bei b und c im Aluminium ist korrigiert. Der bei eingezeichneter Tangente gemessene Untergrund ist abgezogen

[13] Brix, P., u. E.K. Maschke: Z. Physik 155, 109 (1959).

REF.

D. B. Isabelle, G. R. Bishop
J. Phys. et Radium 22, 548-51 (1961)

ELEM. SYM.	A	Z
O	16	8

METHOD

Linac

REF. NO. 61 Is 1 NVB

REACTION	RESULT	EXCITATION ENERGY	SOURCE		DETECTOR		ANGLE
			TYPE	RANGE	TYPE	RANGE	
E,E/	FMF	0 - 115	D	90-215	MAG-D		DST

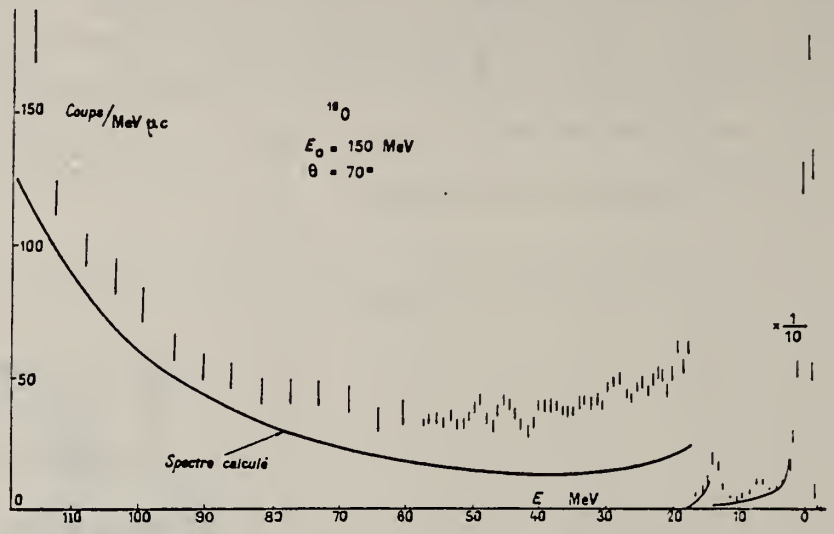

FIG. 1. — Spectre des électrons diffusés sous un angle de 70° et ayant une énergie incidente de 150 MeV. La courbe en bruit plein représente le spectre élastique calculé.

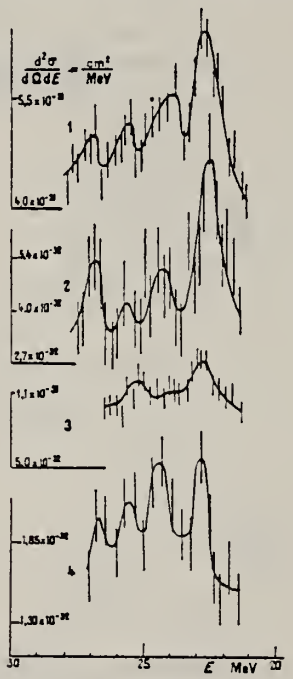

FIG. 2. — Spectres montrant la structure fine de la résonance géante pour quatre valeurs différentes du transfert de quantité de mouvement, pour ^{16}O.

1. E_i = 100 MeV, θ = 60°, q = 0,443 f^{-1}.
2. E_i = 90 MeV, θ = 100°, q = 0,600 f^{-1}.
3. E_i = 150 MeV, θ = 70°, q = 0,803 f^{-1}.
4. E_i = 215 MeV, θ = 80°, q = 1,325 f^{-1}.

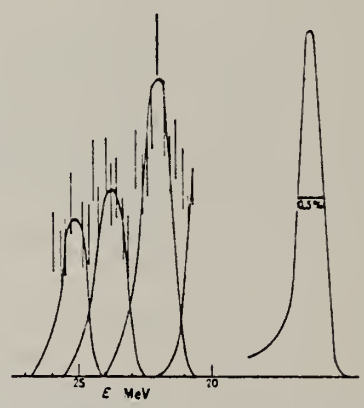

FIG. 3. — Exemple de décomposition d'un spectre détaillé. ^{16}O. Décomposition de la résonance géante.
E_0 = 90 MeV θ = 100°.

REACTION	RESULT	EXCITATION ENERGY	SOURCE TYPE	SOURCE RANGE	DETECTOR TYPE	DETECTOR RANGE	ANGLE

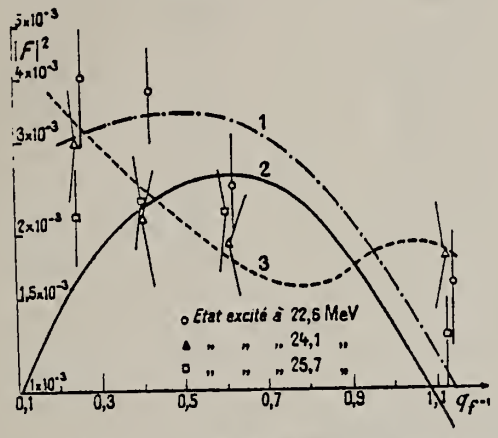

FIG. 4. — Variation du carré du facteur de forme en fonction du transfert de quantité de mouvement, pour ^{16}O.
Courbes :
1) $1{,}65 \times 10^{-2}\, J_1^2[1{,}05\, A^{1/3}\, q] + 1{,}5 \times 10^{-3}\, J_0^2[1{,}05\, A^{1/3} q]$
2) $1{,}38 \times 10^{-2}\, J_1^2[1{,}05\, A^{1/3}\, q]$
3) $5{,}17 \times 10^{-3}\, J_0^2[1{,}05\, A^{1/3}\, q] + 2{,}01 \times 10^{-2}\, J1[1{,}06\, A^{1/3}\, q]$.

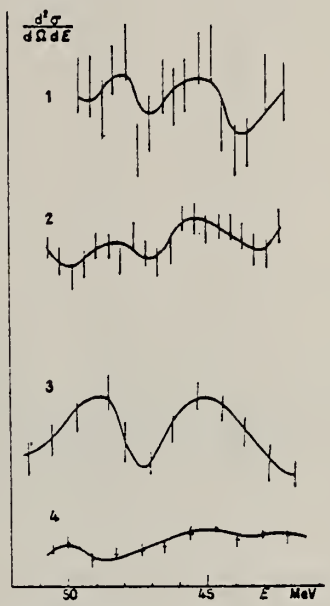

FIG. 6. — Spectres montrant l'existence de deux résonances entre 40 et 50 MeV, pour ^{16}O.
Courbes : 1) $E_0 = 150$ MeV, $\theta = 15°$, $q = 1{,}00$ f^{-1}.
2) $E_0 = 150$ MeV, $\theta = 90°$, $q = 0{,}83$ f^{-1}.
3) $E_0 = 150$ MeV, $\theta = 70°$, $q = 0{,}68$ f^{-1}.
4) $E_0 = 100$ MeV, $\theta = 60°$, $q = 0{,}4$ f^{-1}.

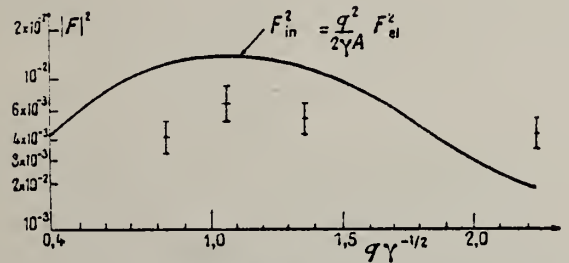

FIG. 5. — Comparaison des résultats expérimentaux avec les calculs théoriques de Fallieros et al., pour ^{16}O. Pour q donné, $|F_{in}|^2 = |F|_{el}\, \sigma_{inel}/\sigma_{el}$.

BIBLIOGRAPHIE

[1] DALITZ (R. H.) et YENNIE (D. H.), *Phys. Rev.*, 1957, **107**, 1598.
[2] ISABELLE (D.) et BISHOP (G.), *C. R. Acad. Sc.*, 1960, **521**, 697.
[3] BOUNIN (P.) et BISHOP (G.), Contribution au Congrès de Strasbourg, donnent les formules détaillées nécessaires pour ce calcul.
[4] SCHIFF (L. I.), *Physical Rev.*, 1956, **96**, 765.
[5] FALLIEROS (S.), FERRELL (R. A.) et PAL (M. K.), *Nuclear Physics*, 1960, **15**, 363.

Ref. L. Keszthelyi, I. Berkes, I. Demeter, I. Fodor
Nuclear Phys. 23, 513 (1961)

Elem. Sym.	A	Z
O	16	8

Method $Li^7(p,\gamma)$ source; activation; NaI coinc. for β^+ from O^{15}

Ref. No. 61 Ke 1 JHH

Reaction	E or ΔE	E_o	Γ	$\int \sigma dE$	Jπ	Notes
(γ,n)	17.5-17.68					Resonances at 17.55 MeV and 17.68 MeV; if they exist, have $\Gamma \gtrsim 150$ kev.

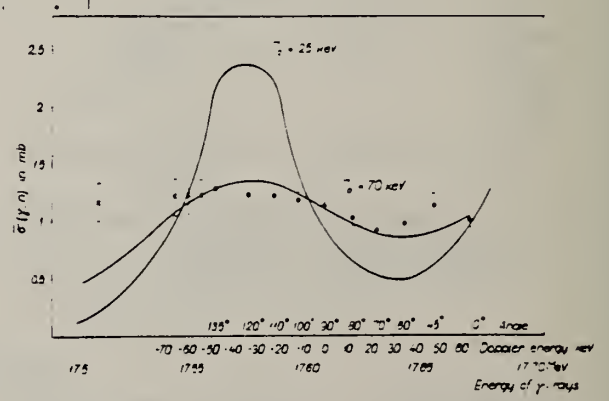

Fig. 1. Dependence of the cross section of the $O^{16}(\gamma,n)O^{15}$ reaction on γ-energy. The data • represent the case of varying the γ-energy via the variation of the angle between the protons and the γ-radiation, the data ○ refer to the variation of the proton energies. The solid curves give the values calculated with the experimental data of Penfold and Spicer.

Ref. F. Lacoste, G.R. Bishop
Nuclear Phys. 26, 511 (1961)

Elem. Sym.	A	Z
O	16	8

Method: Electron Elastic Scattering and unelastic scattering

Ref. No.: 61 La 1 JOC

Reaction	E or ΔE	E_0	Γ	$\int \sigma dE$	Jπ	Notes
$O^{16}(e,e)$	150					

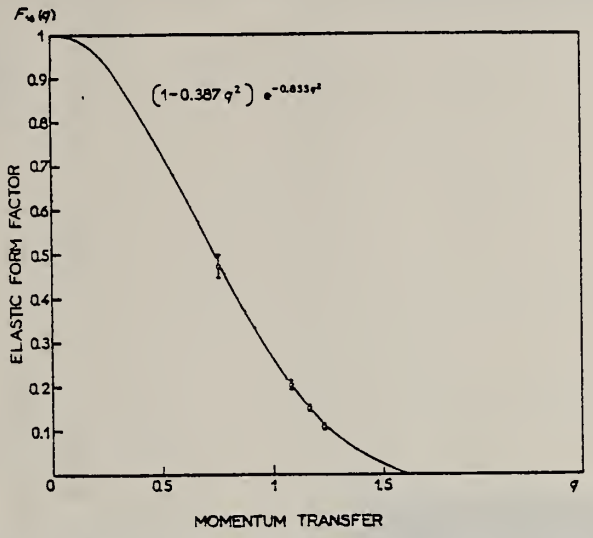

Fig. 6. Experimental values of $F_{16}(q_{16})$ determined by this experiment. The solid curve is the expression $(1-0.387\,q^2)\,e^{-0.633\,q^2}$, which gives the best fit to the data of ref.[9]).

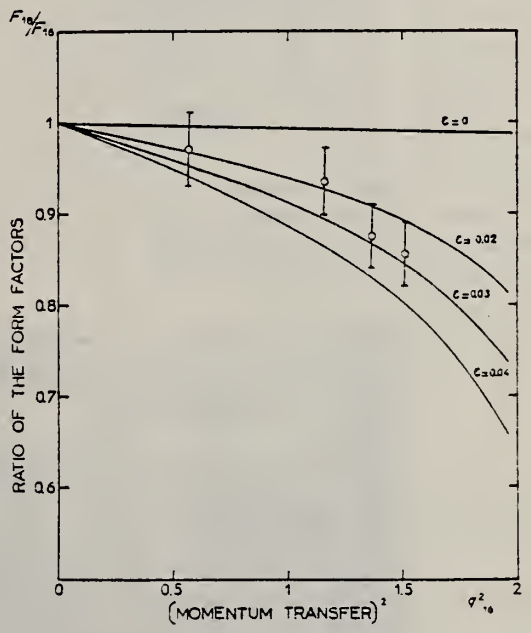

Fig. 7. Experimental ratios of the O^{18} and O^{16} elastic form factors versus q_{16}^2 (defined in sect. 3). The curves labelled $\varepsilon = 0$, $\varepsilon = 0.02$, $\varepsilon = 0.03$ and $\varepsilon = 0.04$ give the shell model predictions assuming a parabolic well potential with a_{cm} $(O^{18}) = (1+\varepsilon)$ a_{cm} (O^{16}).
For $\varepsilon = 0$ the predicted ratio is different from unity because the mass of the two nuclei are different and therefore the recoil corrections are not identical.

Ref. J.P. Roalsvig, I.C. Gupta, R.N.H. Haslam
Can. J. Phys. 39, 643 (1961)

Elem. Sym.	A	Z
O	16	8

Method 24 MeV betatron; radioactivity; neutron yield; proportional counter; r chamber

Ref. No. 61 Ro 2 EH

Reaction	E or ΔE	E_0	Γ	$\int \sigma dE$	Jπ	Notes
$O^{16}(\gamma,n)$	Bremss. 22					Relative yield curve normalized by standard $Cu^{63}(\gamma,n)$ reaction [Roalsvig, Haslam and McKenzie, Can. J. Phys. 37, 607 (1959)].

TABLE I

Absolute yields of $O^{16}(\gamma,n)O^{15}$ and $C^{12}(\gamma,n)C^{11}$ at 22 Mev

References	Absolute yield of $O^{16}(\gamma,n)O^{15}$ (n/g-atom 100 r)	Absolute yield of $C^{12}(\gamma,n)C^{11}$ (n/g-atom 100 r)
Price and Kerst (1950)	0.67×10^{5}	0.67×10^{5}
Haslam, Johns, and Horsley (1951)	—	0.78×10^{5}
Johns, Horsley, Haslam, and Quinton (1951)	1.68×10^{5}	—
Montalbetti et al. (1953)	2.7×10^{5}	3.2×10^{5}
Nathans and Halpern (1954)	—	2.8×10^{5}
Barton et al. (1955)	—	2.3×10^{5}
Cook (1957)	—	1.5×10^{5}
Thomas (1957)	—	0.78×10^{5}
Present work	2.37×10^{5}	1.13×10^{5}

[a] According to the note added in proof the author mentions that this value should be reduced by 10%.
[b] A recalculation of the absolute yield gave results in close agreement with this value.

TABLE II

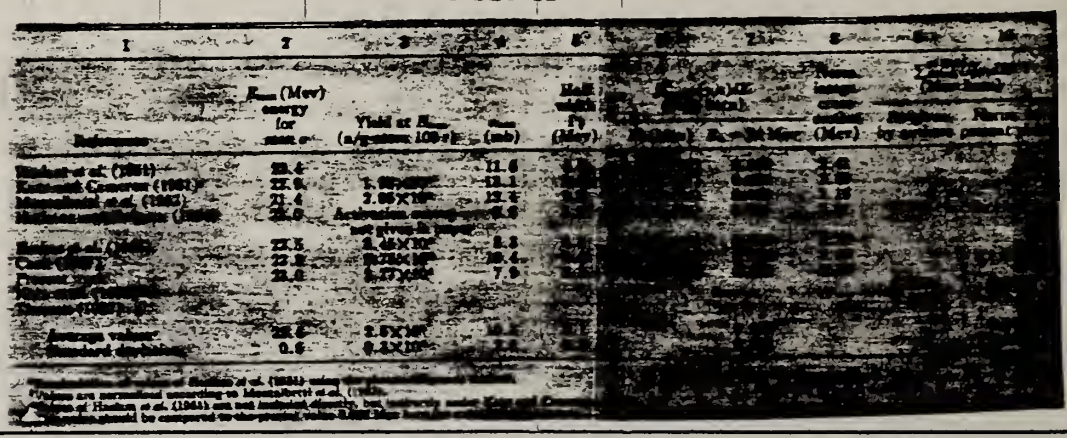

Ref. K. Shoda
J. Phys. Soc. Japan 16, 1841 (1961)

Elem. Sym.	A	Z
O	16	8

Method 24 MeV betatron; proton spectrum; angular distribution; nuclear emulsion; r chamber

Ref. No. 61 Sh 3 NVB

Reaction	E or ΔE	E_0	Γ	$\int \sigma dE$	Jπ	Notes
O(γ,p)	Bremss. 20.5	17.3			1^-	γ's were polarized.

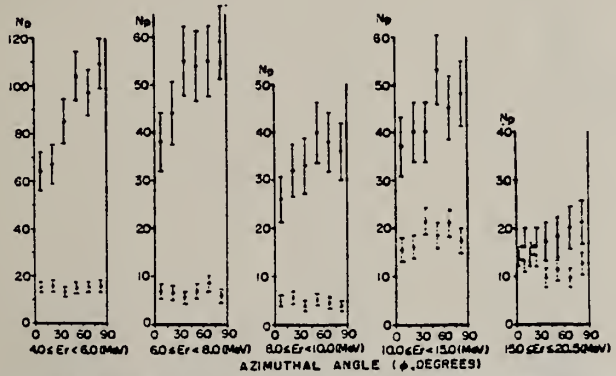

Fig. 4. Azimuthal angular distributions in D_2O and H_2O soaked plates. The proton number from the H_2O plate is normalized to the same number of oxigen atoms as in the D_2O soaked plate. Open and closed circles are the results by D_2O and H_2O soaked plates respectively.

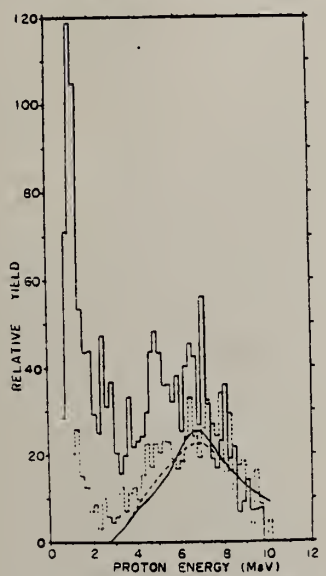

Fig. 7. The proton energy spectra corrected for the emulsion thickness and the back ground spectrum to be subtracted. Full line hystogram: for the H_2O soaked plate; broaken line hystogram: for the unsoaked plate; full curve: spectra of back ground to be subtracted ($F.N_0$); broaken curve: spectra of back ground (N_0).

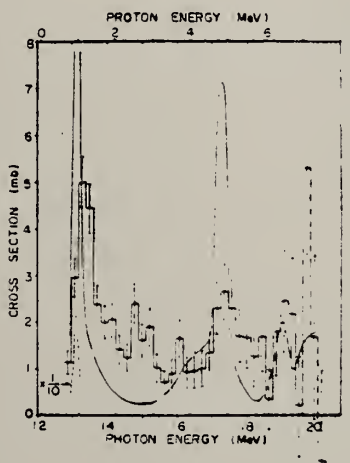

Fig. 8. Cross section of $O^{16}(\gamma, p_1)N^{15}$ assuming that all proton transitions are those to the ground state of N^{15}. The hystogram is the present result and the curves are the calculated cross sections from the experimental p_1 cross section using the detailed balance theorem.

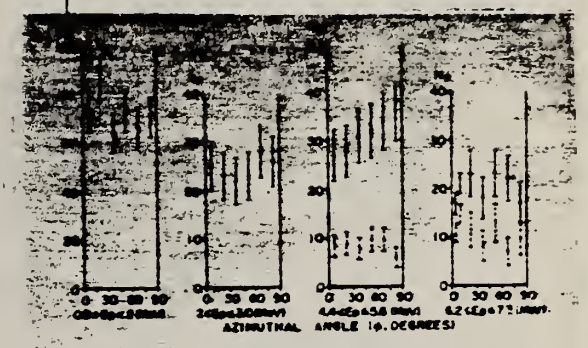

Fig. 9. Azimuthal angular distributions of protons in several energy regions. Open circles show the results in H_2O soaked plate. Closed circles are for the back ground plate.

Table II. Results of the azimuthal angular distributions of photoprotons from O^{16}.

E_γ (MeV)		0.8–2.0	2.0–3.0	4.4–5.6	6.2–7
	$\alpha_0 = a_0/a_1$*	0	−0.091	−0.78	0.6
	E_γ (MeV)	−13.3	−14.8	−17.3	−19.1
	P (%)†	16	12	6	1
Calculation data	$E1$	0	1.1	4.7	−0.6
	$M1$	0	−1.1	−4.7	0.6
$P_{90} \times 10^2$	$E2$	0	0.2	0.9	0.02
	$M2$	0	−0.2	−0.9	−0.02
Experimental results	$P_{90} \times 10^2$	−6.4±6.0	6.5±9.0	21±11	14±8

* Obtained by ref. 7.
† Present data of polarization.
The polar and azimuthal angular distributions are represented as follows:
$I(\theta) = N_0 a_0 + a_1 \cos^2\theta$, $F(\phi) = N_0(1 + P_{90} \cos 2\phi)$.

7) S. A. E. Johansson and B. Forkman: Ark. f. Fys. 12 (1957) 369.

(8-1-63)
USCOMM-DC 18886-P63

U.S. DEPARTMENT OF COMMERCE
NATIONAL BUREAU OF STANDARDS

REF.

N. W. Tanner, G. C. Thomas and E. D. Earle
Proc. Int. Conf. Man. 295 (1961)

ELEM. SYM.	A	Z
O	16	8

METHOD
Tandem; Van de Graaf

REF. NO.
61 Ta 3 JDM

REACTION	RESULT	EXCITATION ENERGY	SOURCE		DETECTOR		ANGLE
			TYPE	RANGE	TYPE	RANGE	
P,G	ABX	12-26	D	0-14	NAI-D		90

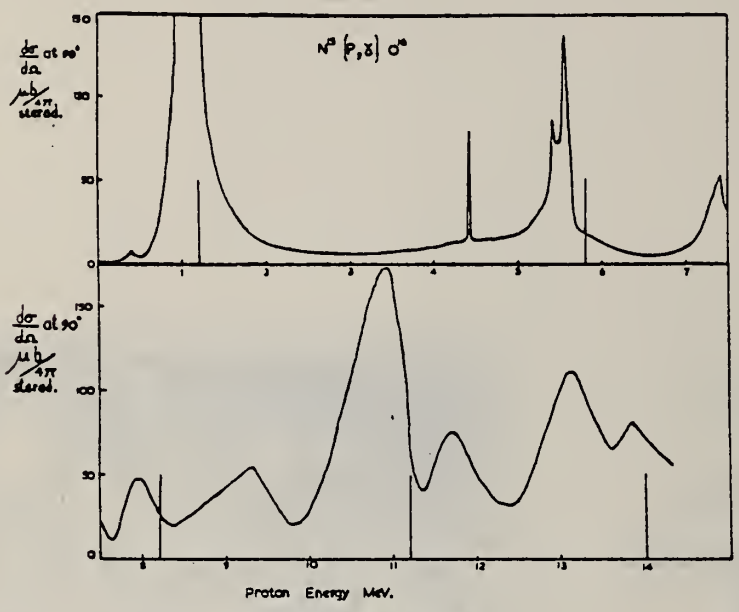

Excitation function of $N^{15}(p,\gamma)O^{16}$

Ref. G.R. Bishop, D.B. Isabelle
Phys. Letters 1, 323 (1962)

Elem. Sym.	A	Z
O	16	8

Method
Linac; electron scattering, magnetic spectrometer

Ref. No. 62 Bi 2 JHH

Reaction	E or ΔE	E_o	Γ	$\int \sigma dE$	Jπ	Notes
$O^{16}(e,e')$	140.6 - 214.8	19.2±0.3			2^+	Electric quadrupole transition.

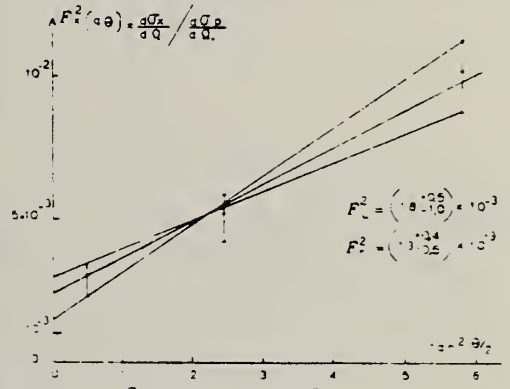

Fig. 1. Plot of $F_x^2(q,\theta)$ versus $\tan^2\theta/2$ for q = 1.2 fermi^{-1}

Table 1
Experimental cross sections and the square of the inelastic form factor defined as $(d\sigma_x/d\Omega)/(d\sigma_p/d\Omega)$.

E_o (MeV)	θ (°)	q_i (f^{-1})	$\frac{d\sigma_x}{d\Omega}$ (cm^2)	$\frac{d\sigma_p}{d\Omega}$ (cm^2)	F_x^2
147.4	70	0.667	2.32 × 10^{-31}	1.97 × 10^{-28}	0.90 × 10^{-3}
141.8	60	0.805	1.30 × 10^{-31}	9.34 × 10^{-29}	1.39 × 10^{-3}
146.8	115	1.183	5.38 × 10^{-32}	8.54 × 10^{-30}	6.3 × 10^{-3}
214.8	70	1.200	1.35 × 10^{-31}	4.45 × 10^{-29}	3.04 × 10^{-3}
140.6	135	1.237	3.48 × 10^{-32}	3.38 × 10^{-30}	10.3 × 10^{-3}
157.5	120	1.311	2.91 × 10^{-32}	5.76 × 10^{-30}	5.05 × 10^{-3}
214	80	1.346	7.13 × 10^{-32}	2.42 × 10^{-29}	2.94 × 10^{-3}

Ref. G.R. Bishop, D.B. Isabelle
Phys. Letters 3, 74 (1962)

Elem. Sym.	A	Z
O	16	8

Method: Linac; electron scattering; magnetic spectrometer

Ref. No.: 62 Bi 3 | JHH

Reaction	E or ΔE	E_o	Γ	$\int \sigma dE$	Jπ	Notes
$O^{16}(e,e')$		44.5 49.0				

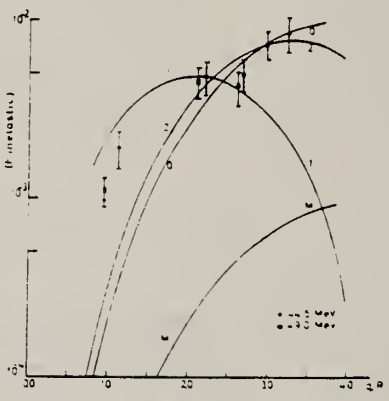

Fig. 1. Comparison of the inelastic form factors, defined as $(\text{exp. points})\cdot$ with the form factors for E0, E1 and E2 transitions. A least squares fit to the data for the 44.5 MeV transition gives $F_{in}^2 = (3.7 \cdot 10^{-3}) F_1^2 + 7.6 \cdot 10^{-2} F_2^2$, and for the 49 MeV transition $F_{in}^2 = (1 \cdot 10^{-2}) F_1^2 + 6 \cdot 10^{-2} F_2^2$. The calculated 7) E0 form factor fits to $6.5 \cdot 10^{-4}(1 - \theta)^2$ (curve M), whereas the experimental points (curve 0) fit on the average to $9 \cdot 10^{-3}(1 - \theta)^2$.

Table 1
The observed radiative widths as found from the normalising factors S_0, S_1 and S_2 of fig. 1, and the formulae in the text. In parentheses the radiative widths calculated for a single particle transition, or the monopole matrix element for a liquid drop.

Energy of transition (MeV)	Observed width (MeV)	Radiative widths $\Gamma(E1)$ (keV)	Radiative widths $\Gamma(E2)$ (keV)	Integrated cross section for E1 (MeV-mb)	Monopole matrix element (cm^2)
44.5	2-3	5.3 (37)	0.35 (0.33)	20	6.8×10^{-26} (5.2×10^{-26})
49.0	2-3	19 (50)	0.45 (0.53)	35	6.4×10^{-26} (5.2×10^{-26})

G.R. Bishop, B. Grossetete, J.C. Risset
J. Phys. Radium 23, 31 (1962)

0	16	8

METHOD: Linac; neutron yield; radioactivity; Faraday cup and SEM

REF. NO.: 62 Bi 4 NVB

REACTION	RESULT	EXCITATION ENERGY	SOURCE		DETECTOR		ANGLE
			TYPE	RANGE	TYPE	RANGE	
G,N	ABI	60-150	C	60-150	ACT-I		4PI
E,N	ABY	60-150	D	60-150	ACT-I		4PI
G,T	ABY	60-150	C	60-150	ACT-I		4PI
G,2P3N	ABY	60-150	C	60-150	ACT-I		4PI

$$\int_{16}^{35} \sigma_{(\gamma,n)} dE = 63.5 \pm 9 \text{ MeV-mb}$$

95% E1, 5% E2 in giant resonance region

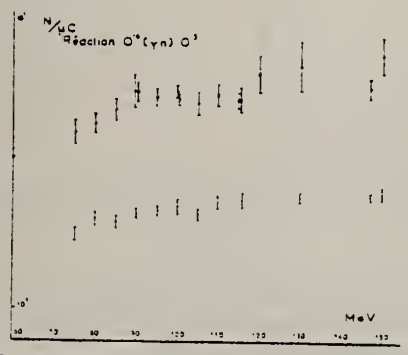

FIG. 5. — Courbes d'excitation avec production de ^{15}O en fonction de l'énergie des électrons incidents. Les cercles pleins correspondent à l'activité dans le compartiment avant et les cercles vides au compartiment arrière.

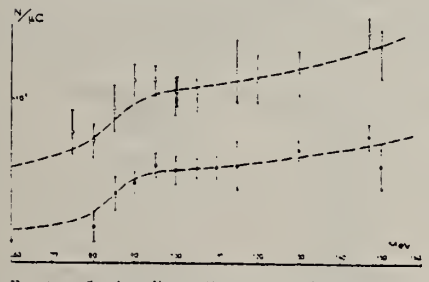

FIG. 6. — Courbes d'excitation avec production de ^{13}N.

L'activité à l'origine d'un isotope donne étant déterminée à partir de n coups dus à cet isotope, il faudra donc tenir compte de l'écart $\sqrt{n}$, mais aussi de l'incertitude sur n qu'introduit le fait de retrancher de l'activité totale l'activité due aux autres isotopes. Ainsi l'incertitude relative sur ^{13}N

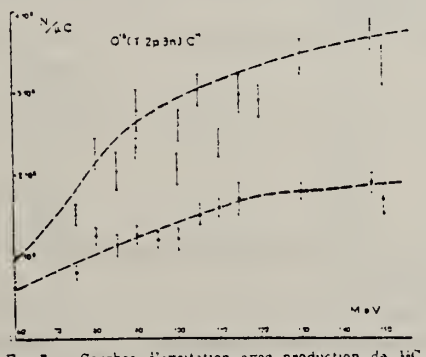

FIG. 7. — Courbes d'excitation avec production de ^{11}C

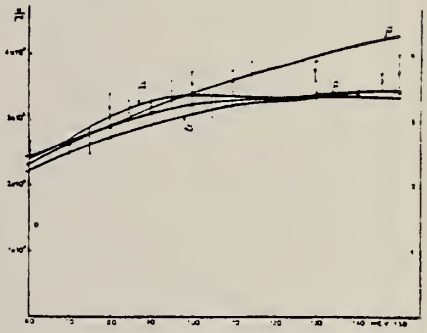

FIG. 9. — Courbe d'excitation de l'électroproduction de ^{15}O. Les courbes calculées correspondent à une isochromate de 24 MeV du spectre de photons virtuels pour les hypothèses suivantes :
a) Transition E_1 pure, noyau ponctuel.
b) Transition E_1 pure, noyau distribué $\langle r^2 \rangle = (2.65 \text{ fermis})^2$.
c) Transition mélangée 95 % E_1, 5 % E_2, noyau distribué.
d) Transition mélangée 90 % E_1, 10 % E_2, noyau distribué.

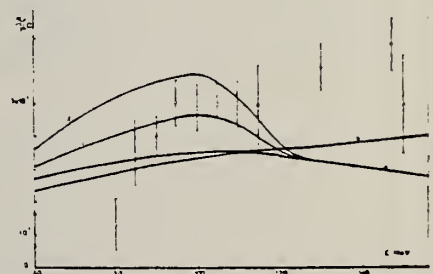

FIG. 10. — Courbe d'excitation de l'électroproduction de ^{13}N. Les courbes calculées correspondent à une isochromate de 30 MeV, noyau distribué :
a) Transition M_1 pure.
b) Transition E_1 pure.
c) Transition mélangée 50 % E_1, 50 % M_1.
d) Transition E_2 pure.

Ref. L.N.Bolen, W.D.Whitehead

Phys.Rev.Letters 9, 458 (1962)

Elem. Sym.	A	Z
O	16	8

Method
70 MeV synchrotron - BF_3

Ref. No. 62Bo2

BG

Reaction	E or ΔE	E_o	Γ	$\int \sigma dE$	Jπ	Notes
(γ,xn)	15-30	17.3 19.3 22.3 24.1	see Table1			The integrated cross section over the two strongest transitions is 30.1 MeV-mb.

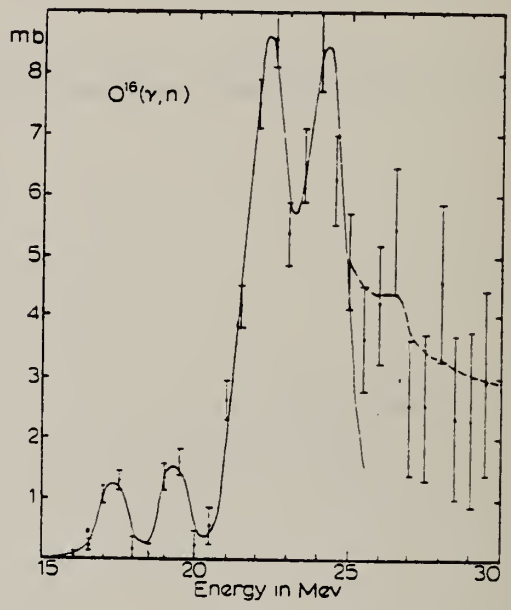

FIG. 1. $O^{16}(\gamma,n)O^{15}$ cross section. Data points are the result of this experimental determination. The solid line is the resultant of the four Gaussian curves used to synthesize the cross section.

215

Table I. The values of the parameters of the Gaussian curves used to synthesize the O^{16} cross section in Fig. 1. E_m is the energy at which the maximum cross section occurs, σ_m is the maximum cross section, and Γ is the width at half maximum of the Gaussian curve. The theoretical values of E_m, of the dipole absorption strength, and of Γ are also given.

E_m (MeV)	σ_m (mb)	Γ (MeV)	$\int\sigma(E)dE$ (MeV-mb)	E_m (theor)[a] (MeV)	% Dipole[a] strength	Γ_{theor}[b] (MeV)
17.3	1.3	1	1.5	18.1	1.0	
19.3	1.6	1	1.8	19.7	2.1	
22.3	8.4	1.7	15.2	22.6	67.9	0.64
24.1	8.3	1.7	14.9	25.4	26.0	1.12

[a] See reference 16.
[b] See reference 18.

Ref. H. Breuer, W. Pohlit
Nuclear Phys. 30, 417 (1962)

Elem. Sym.	A	Z
O	16	8

Method Bremss.; betatron; NaI counter; radioactivity.

Ref. No. 62 Br 1 EGF

Reaction	E or ΔE	E_o	Γ	$\int \sigma dE$	Jπ	Notes
$O^{16}(\gamma,n)$	32.5			53.3±4.7 MeV-mb		Integrals are to 32.5 MeV.
$O^{16}(\gamma,2n)$				0.090±0.020 MeV-mb		

Ref. N.A.Burgov, G.V.Danilyan, B.S.Dolbilkin, L.E.Lazareva, F.A.Nikolaev

Zhur.Eksptl. i Teoret.Fiz. 43, 70 (1962);
Soviet Phys.JETP 16, 50 (1963)

Elem. Sym.	A	Z
O	16	8

Method

250 MeV Synchrotron, μ_T in H_2O - magnetic spectrometer

Ref. No. 62Bul BG

Reaction	E or ΔE	E_o	Γ	$\int \sigma dE$	Jπ	Notes
(γ,μ_T)	18.9-26.6	(18.4)		150^{+30}_{-10} MeV-mb		E_o peak positions corrected for spectrum resolution.
		(21.2)				
		22.3				
		23.05				μ_T result shows cross section for reactions other than (γ,n) and (γ,p) small in giant resonance region.
		24.3				
		25.15				

GAMMA-RAY ABSORPTION BY O^{16} 53

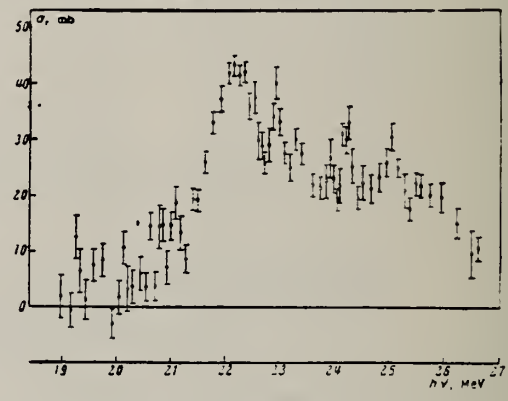

Energy levels of O^{16} in the range 21–25 MeV

Experimental						Theoretical	
	Photoproton spectrum [1]	Photoneutron spectrum [1]			Cross section for reaction with charged particles [2]		
						Oratovskaya forces	Soper forces
20.11							
21.17						21.5	
21.9 ± 0.2**	21.9 ± 0.2**						
22.1	22.1 ± 0.2**			22.25	22.15 ± 0.1		22.2
22.58							
22.9 ± 0.3				23.08	22.9 ± 0.2		
23.1					23.1 ± 0.2		
23.15	23.0 ± 0.2**	23.1 ± 0.1		23.43	23.12 ± 0.1		
				23.61		23.2	25.0
	23.7 ± 0.2	23.8 ± 0.1			^{1}He^4		
					^{1}He^3	25.4	
	25.3 ± 0.2	25.3 ± 0.1			^{2}He^4		

*The data of [1] were recalculated following improvement of the $O^{16}(\gamma,n)$ and $C^{12}(\gamma,n)$ thresholds used here to calibrate the betatron energy scale (private communication from B. Spicer).

**Corresponding peaks in the proton spectrum from O^{16} photodisintegration have also been observed elsewhere: for hν = 21.9 MeV in [3,4], for 22.2 MeV in [3], and for 24.0 MeV in [3,4].

***The same resonances, but not well resolved, have apparently been observed in [4].

Ref. W.E. Del Bianco, W.E. Stephens
Phys. Rev. 126, 709 (1962)

Elem. Sym.	A	Z
O	16	8

Method Electrostatic generator, $H^3(p,\gamma)He^4$ reaction; activation of positron emitter; 2 NaI in coincidence.

Ref. No. 62 De 1 JHH

Reaction	E or ΔE	E_o	Γ	$\int \sigma dE$	Jπ	Notes
(γ,n)	20.48					$\sigma(\gamma,n) = 0.60 \pm 0.12$ mb

Ref. W. R. Dodge, W. C. BArber
Phys. Rev. 127, 1746 (1962)

Elem. Sym.	A	Z
O	16	8

Method: Magnetic analysis of proton spectron produced by electron bombardment

Ref. No. 62 Do 1 | BG

Reaction	E or ΔE	E_o	Γ	$\int \sigma dE$	Jπ	Notes 243 r
(e,p)	30	E_p = 4.85				For ground state transition Eγ= 17.27
		5.60				18.07
		6.45				18.99
		7.00				19.57
		8.30				20.65
		9.53	0.70	14.4		22.30
		10.25	0.32	1.7		23.10
		11.50	0.87	10.9		24.35
		(also see notes)		(see Table IV)		
				27 *		* Calculated assuming $O^{16}(\gamma,p)$ transitions which have N^{15} in its ground state occur.
				56±11)		
				16.6		

Correspondence between (e,pe') reaction and (γ,p) reaction. Assumed electron has associated with it a virtual photon spectrum. Electron production yields analyzed by use of E1 virtual photon spectrum to obtain (γ,p).

Angular distributions measured.

Angular distribution for photon assumed to be given by A' + B'cosθ + C'sin²θ + ...

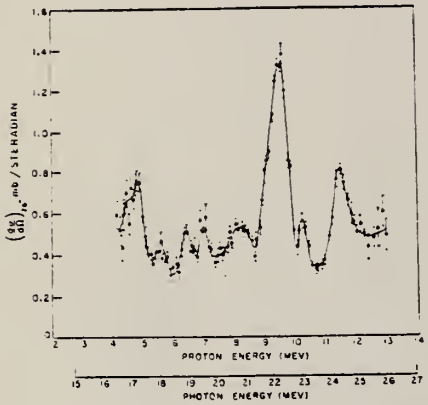

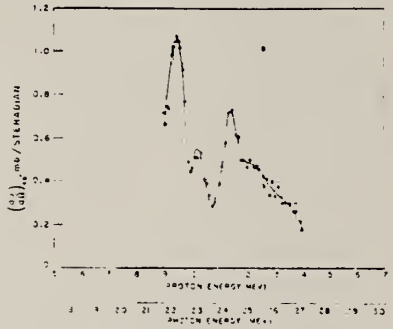

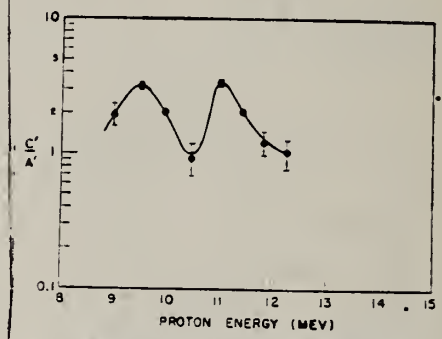

FIG. 27. Ratio of the even-parity terms in the angular distributions of protons from oxygen.

TABLE III. Summary of the excitation characteristics of the O protons for E_p>9.53 MeV.

Proton energy (MeV)	Ground state transition energy (MeV)	Electron energy at which a deviation from an E1 isochromat occurs (MeV)	Branching ratio (%)	Energy of excited state (MeV)
9.58	22.31	31.8±0.5	8±8	9.5±0.5
10.55	23.30	30.0±0 5	25±10	6.7±0.5
11.49	24.35	...	...	...
12.33	25.29	34.0	...	...

TABLE IV. Parameters of an approximate resonance curve fit to the O cross section for $22<E_\gamma<25$ MeV.

Proton energy of peak (MeV)	Photon energy of peak (MeV)	Peak height at 76° (mb/sr)	Photon width at half-height (MeV)	$\int\sigma(\gamma,p)dE_\gamma$ under resonance curve (MeV-mb)	$\%\int_{18.7}^{27}\sigma(\gamma,p)dE_\gamma$
9.53	22.3	1.29	0.70	14.4	26.2
10.25	23.1	0.27	0.32	1.7	3.1
11.50	24.35	0.78	0.87	10.9	19.7
				Total 27.1	49.0

refer p. 2 for figure 28 & 29

Elem. Sym.	A	Z

Method

Ref. No.

Reaction	E or ΔE	E_o	Γ	$\int \sigma dE$	Jπ	Notes

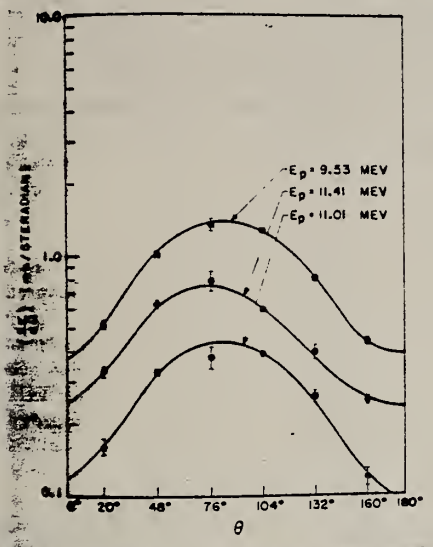

Fig. 28. Oxygen (e,pe') proton peak and valley angular distributions at E_0=30 MeV.

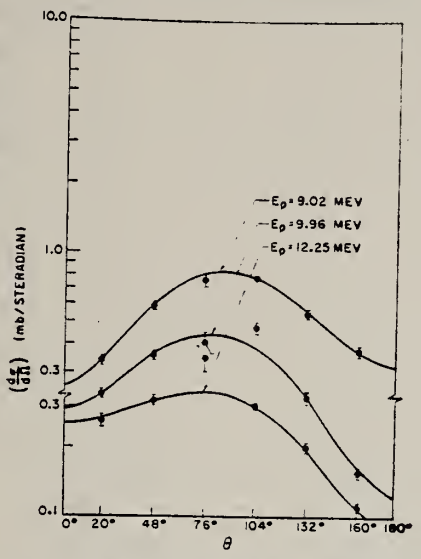

FIG. 29. Oxygen (e,pe') proton angular distributions at E_0=30 MeV.

Ref. R. D. Edge, G. A. Peterson

Phys. Rev. 128, 2750 (1962)

Elem. Sym.	A	Z
O	16	8

Method

Linac - counter telescope

Ref. No. 62Ed1 BG

Reaction	E or ΔE	E_o	Γ	$\int \sigma dE$	Jπ	Notes
		E_e=scattered electron energy E_x=excitation energy				Nuclear states excited by 180° electron ecattering. M1 transitions assumed.
(e,e')	41.5	no resonances detected below E_x=16				

Ref. F.W.K. Firk, K.H. Lokan Phys. Rev. Letters 8, 321 (1962)	Elem. Sym.	A	Z
	O	16	8

Method	Ref. No.	
31 MeV Linac - 20 meter flight tube, liquid scintillator	62F11	BG

Reaction	E or ΔE	E_γ	E_n	∫σdE	Jπ	Notes
		E_γ =	E_n			
$O^{11}(\gamma_0,n)O^{15}$		19.1	3.23			H_2O target
		19.6	3.70			
		20.7	4.70			
		21.0	5.0			
		21.7	5.7			
		22.2	6.1			
		23.0	6.9			
		24.3	8.1			
		25.0	8.8			
		(25.4)	9.1			
			E_n			
$O^{16}(\gamma,n)O^{*15}$		2.43				
		2.76				
		3.96				
		4.27				

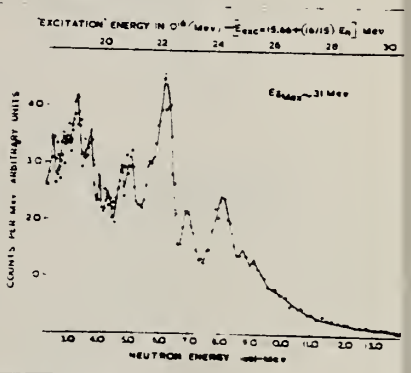

FIG. 1. The observed spectrum of photoneutrons from the reaction $O^{16}(\gamma,n)O^{15}$ uncorrected with [illegible] maximum energy 31 MeV.

Table I. Energy levels in O^{16}.[a]

E_n (Mev)	E_{exc} (Mev)	E_{exc}' (Mev)
1.54	17.3	17.3
2.43	18.25	
2.76	18.70	
3.23	19.1	19.1
3.70	19.6	19.6
3.96	19.9	
4.27	20.2	
4.7	20.7	21.0
5.0	21.0	
5.7	21.7	21.8(?)
6.1	22.2	22.2
6.9	23.0	23.1
8.1	24.3	24.3
8.8	25.0	25.2
9.1	25.4	

[a] E_n = observed neutron energy (Mev) from $O^{16}(\gamma,n)O^{15}$; E_{exc} = "excitation" in O^{16} (Mev) $|E_{exc} = 15.86 + (16/15)E_n|$; E_{exc}' = excitation in O^{16} (Mev) (reference 7) from $N^{15}(p,\gamma_0)O^{16}$.

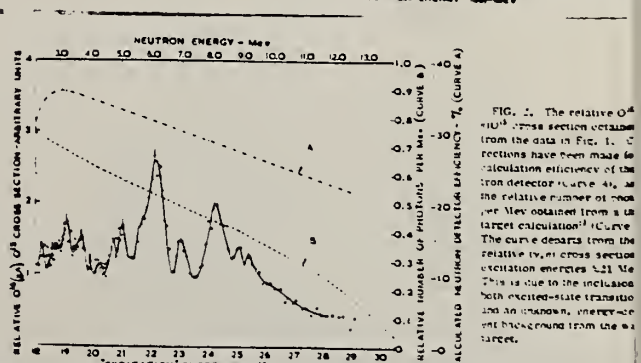

FIG. 2. The relative $O^{16}(\gamma,n)O^{15}$ cross section obtained from the data in Fig. 1. C[illegible] rections have been made for calculation efficiency of the iron detector (curve 4), a the relative number of neut[illegible] per Mev obtained from a th[illegible] target calculation[3] (curve The curve departs from the relative (γ,n) cross section excitation energies 5.21 Me This is due to the inclusion both excited-state transitio and an unknown, energy-de[illegible] background from the ta[illegible] target.

REF.

F. W. K. Firk, K. H. Lokan and E. M. Bowey
Proc. Padua Conf. 804 (1962)

ELEM. SYM.	A	Z
O	16	8

METHOD

REF. NO.: 62 Fi 2 | JDM

REACTION	RESULT	EXCITATION ENERGY	SOURCE		DETECTOR		ANGLE
			TYPE	RANGE	TYPE	RANGE	
G,N	RLX	18-29	C	26-32	TØF-D	2-15	UKN

201

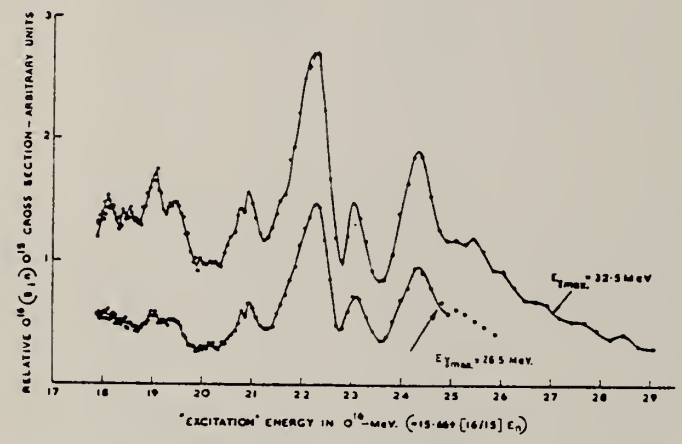

Fig. 1. The relative $C^{12}(\gamma, n)$ cross-section for $E_{\gamma max} = 32.5$ and 25.2 MeV.

H. Fuchs, D. Haag, K.H. Lindenberger, U. Meyer-Berkhout
Z. Naturforsch. 17a, 439 (1962)

0	16	8

METHOD: Neutron spectrum; Stilbene scintillator

REF. NO.: 62 Fu 5 NVB

REACTION	RESULT	EXCITATION ENERGY	SOURCE TYPE	SOURCE RANGE	DETECTOR TYPE	DETECTOR RANGE	ANGLE
G,N	ABX	21 - 31	C	31	SCI-D		90
							(90 ± 15)

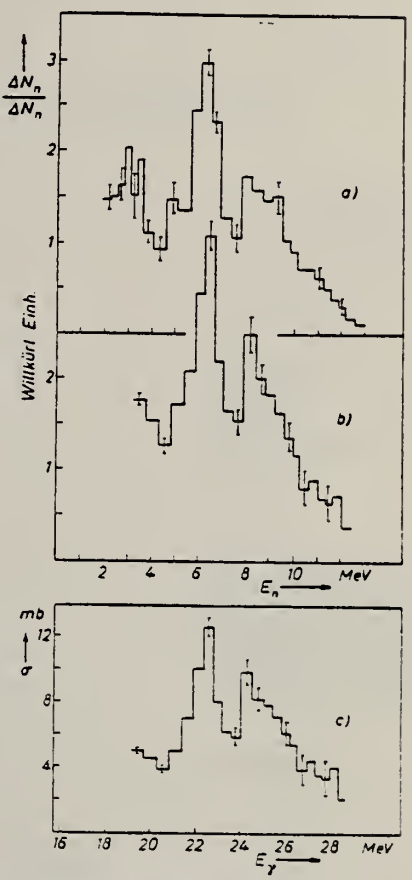

Abb. 2. Ergebnisse für den O^{16}-Kern. 2 a und 2 b: O^{16}-Photoneutronenspektren, gemessen bei zwei voneinander abweichenden Einstellungen der Impulsformdiskrimination. Endenergie des Bremsspektrums E_0=31 MeV. Beobachtungsrichtung gegenüber dem γ-Strahl Θ=90° ± 15°. 2 c: Wirkungsquerschnitt für die $O^{16}(\gamma,n_0)O^{15}$-Reaktion, berechnet aus dem Spektrum 2 b unter der Annahme, daß der O^{16}-Kern stets im Grundzustand zurückbleibt. Die Fehlerbalken geben den statistischen Meßfehler an. Die Unsicherheit der angegebenen Absolutwerte beträgt etwa 25%.

Ref.
A.N.Gorbunov, V.A.Dubrovina, V.A.Osipova, V.S.Silaeva, P.A.Cerenkov

Zhur.Eksptl. i Teoret.Fiz. 42, 747 (1962);
Soviet Phys. JETP 15, 520 (1962)

Elem. Sym.	A	Z
O	16	8

Method

synchrotron - cloud chamber

Ref. No.

62Gol

BG

Reaction	E or ΔE	E_o	Γ	∫σdE	Jπ	Notes
(γ,p)	$E_{\gamma max}$=		$129)_0^{170}$	MeV·mb		$\sigma_{-1} = \int \sigma(E)E^{-1}dE$ (Table IV)
(γ,n)	170		$105)_0^{170}$			$\sigma_{-2} = \int \sigma(E)E^{-2}dE$ (Table IV)
(γ,pn)			$59)_0^{170}$			Absolute value of yields given in the article.
(γ,α)			$4)_0^{170}$			(γ,n) and (γ,2n) could not be distinguished - all were taken to be (γ,n); similarly (γ,p) and (γ,d) were all taken to be (γ,p).
(γ,αn)			$15)_0^{170}$			
(γ,μ_T)			$438)_0^{170}$			Charge distribution parameters were determined.

Table I

Reaction	Reaction Threshold, MeV			Reaction	Reaction Threshold, MeV		
	N	O	Ne		N	O	Ne
(γ, α)	[illegible]	15 [illegible]	[illegible]	[illegible]	[illegible]	—	[illegible]
(γ, 2p)	[illegible]	[illegible]	[illegible]	[illegible]	[illegible]	[illegible]	[illegible]
(γ, pα)	[illegible]	[illegible]	[illegible]	[illegible]	[illegible]	[illegible]	[illegible]
(γ, 3p)	[illegible]	[illegible]	[illegible]	[illegible]	—	—	[illegible]
(γ, 2pα)	[illegible]	[illegible]	[illegible]	[illegible]	—	[illegible]	
(γ, 3pα)	[illegible]	[illegible]	[illegible]	[illegible]	[illegible]	—	
(γ, 2α)	[illegible]	[illegible]	[illegible]	[illegible]	—	[illegible]	
(γ, 4p)	[illegible]	[illegible]	[illegible]				

Table IV

Reaction type	σ_{-1}, MeV-mb				σ_{-2}, mb				σ_{-1}, mb-MeV^{-1}			
	He⁴	N¹⁴	O¹⁶	Ne	He⁴	N¹⁴	O¹⁶	Ne	He⁴	N¹⁴	O¹⁶	Ne
(γ, p)	38	38	129	165	1.09	2.5	5.3	6.5	0.035	0.14	0.22	0.25
(γ, n)	44	41	105	115	1.09	1.5	3.4	3.5	0.031	0.08	0.11	0.10
(γ, pn)	12	128	59	69	0.13	5.1	1.3	1.4	0.003	0.18	0.03	0.03
(γ, α)	—	8	[illegible]	6	—	0.3	0.3	0.8	—	0.01	0.02	0.07
(γ, 2n)	—	5	15	38	—	0.1	0.3	1.0	—	0.003	0.005	0.02
Stars:												
3-prong	—	53	71	151	—	1.2	1.5	3.2	—	0.03	0.03	0.12
4-prong	—	73	27	34	—	1.5	0.5	0.5	—	0.04	0.01	0.01
5-prong	—	14	20	15	—	0.2	0.3	0.2	—	0.002	0.003	0.003
6-prong	—	—	5	10	—	—	0.03	0.1	—	—	0.001	0.001
σ_{exp}*	95±7	347	438	600	2.40±0.15	12.5	12.8	18.0	0.07±0.005	0.46	0.43	0.60
σ_{theor}**	60	210	240	300	2.3	12.1	13.1	19.5	0.023	0.18	0.23	0.33
σ_{exp} / σ_{theor}	1.6	1.65	1.8	2.0	1.04	1.03	0.98	0.9	3.0	2.6	1.9	1.8

* σ_{exp}—experimental value of the integrated absorption cross sections σ_{-1}, σ_{-2} and σ_{-1}.
** The theoretical values σ_{theor} have been calculated by means of the expressions: σ_{-1}=60(N-Z/A)MeV-mb; σ_{-2} = 0.36 $A^{2/3}$ mb; σ_{-1} = 2.25 $A^{5/3}$ mb-MeV^{-1}.

Ref. A. N. Gorbunov, V. A. Osipova

Zhur. Eksptl. i Teoret. Fiz. 43, 40 (1962);
Soviet Phys. JETP 16, 27 (1963)

Elem. Sym.	A	Z
O	16	8

Method: synchrotron - cloud chamber

Ref. No.: 62Go2 BC

Reaction	E or ΔE	E_0	Γ	$\int \sigma dE$	Jπ	Notes
$O^{16}(\gamma,p)N^{15}$	0-170	16.5	117±5			$Y(\gamma,n)/Y(\gamma,p) = 0.60\pm0.024$
		20	see Tables 3 and 4			Angular distribution fitted to $f(\theta) = A + B\sin^2\theta + C\sin^2\theta\cos\theta + D\cos$ (includes interference between E1, E2 and M1 - see Table II)
		23				
$O^{16}(\gamma,n)O^{15}$		21.5	86±3			
		24.5	see Tables 3 and 4			

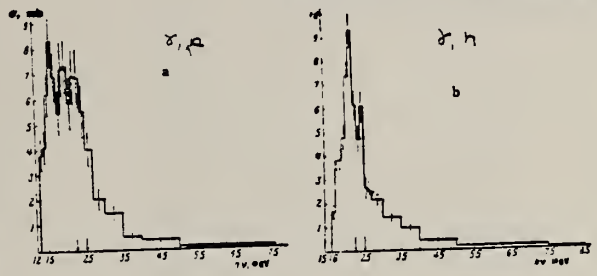

Table I. Yields for various photonuclear reactions in oxygen

Type of Reaction	No. of observed events	Yield relative to (γ, p) yield	Yield relative to total yield from all photonuclear reactions, %
(γ, p)	4996	1	44.0
(γ, n)	3004	0.60 ±0.024	26.4
(γ, pn)	1105	0.220 ± 0.007	9.7
(γ, α)	291	0.058 ± 0.004	2.6
(γ, αn)	204	0.041 ± 0.003	1.8
3-prong stars: total	1147	0.230 ± 0.005	10.1
(γ, pα)	388	0.087 ± 0.004	—
(γ, pαn)	98	0.020 + 0.002	—
(γ, 2p)	370	0.074 ± 0.004	—
(γ, 2pn)	218	0.044 ± 0.003	—
(γ, 2αn)	11	0.002 ± 0.001	—
4-prong stars: total	402	0.080 ± 0.004	3.5
γ, 4α	173	0.035 ± 0.003	
γ, 2αpn	136	0.027 ± 0.003	
5-prong stars: total	189	0.038 ± 0.003	1.7
γ, 2p 3α 2n	160	0.032 ± 0.003	
6-prong stars: total	23	0.005 ± 0.001	0.2

Table II

Energy	A, $\frac{\mu b}{sr \cdot MeV \cdot Q}$	B/A	C/A	D/A
E_p	Protons from $O^{16}(\gamma,p)N^{15}$ reaction			
0.5 — 3	30 ±3	0.6 ±0.1		
3 — 6	90 ±5	1.2 ±0.2	0.6 ±0.6	0.1 ±0.3
6 — 9	18 ±1	1.0 ±0.2	0.1 ±0.6	0.4 ±0.3
9 — 15	12 ±1	1.0 ±0.2	0.7 ±1.1	0.4 ±0.4
15 — 50	0.9 ±0.25	1.2 ±0.7		
E_n	Neutrons from $O^{16}(\gamma,n)O^{15}$ reaction			
5 — 11	15 ±2.5	0.6 ±0.1	—	—
11 — 50	0.9 ±0.2	1.1 ±0.6	1.1 ±0.7	0.1 ±0.3

Table III. Integral cross sections for the (γ, p) and (γ, n) reactions in oxygen (in MeV-mb)

Reaction	1			2			3
	$E_\gamma \leq 30$	$E_\gamma > 30$	$E_\gamma \leq 170$	$E_\gamma \leq 30$	$E_\gamma > 30$	$E_\gamma \leq 170$	$E_\gamma \leq 170$
(γ, p)	90	17	107	100	17	117	129
(γ, n)	60	21	81	65	21	86	105
Total	150	38	188	165	38	203	234

Note: 1 — calculated under the assumption that the final N^{15} and O^{15} nuclei are produced in the ground state; 2 — a correction has been introduced to take into account (qualitatively) transitions to excited states of N^{15} and O^{15}; 3 — estimated in [21] from the absolute yields of the (γ, p) and (γ, n) reactions (E_γ is given in MeV).

Table IV

Reaction	Integral cross section, MeV-mb	
	$E_\gamma \leq 30$ MeV	$E_\gamma \leq 170$ MeV
(γ, p)	100 ± 10***	117 ± 5
(γ, n)	65 ± 2	86 ± 3
(γ, pn)*	9 ± 1	9 ± 3
(γ, 2)	4	4
(γ, 4α)	3	3
Remaining reactions	(15)	13^{+10}_{-6}
Integral cross section for photon absorption $\int_0^{30} \sigma_{abs} dE$	153 (201)**	205^{+10}_{-20}
$\int_0^{170} \sigma_{abs} dE$, %	75 (100)	(100)

*The integral cross section for the (γ, pn) reaction was calculated directly from the cross section for this reaction.
**Shown in the parenthesis is the upper limit for the cross section in which the approximate cross sections for the remaining photonuclear reactions were taken into account.
***The errors connected with the determination of the absolute irradiation intensity are not shown in the table; they are ~8%.

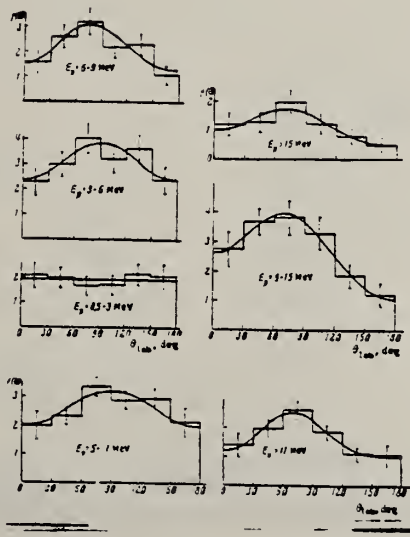

FIG. 3. Angular distributions of protons of different energies emitted in (γ, p) reactions.

FIG. 4. Angular distributions of neutrons emitted in the (γ, n) reactions.

Ref. A.P.Komar, A.V.Kulikov, V.P.Chizhov, I.P.Yavor, Yu.M.Volkov Zhur.Eksptl. i Teoret.Fiz. 43, 1657 (1962); Soviet Phys.JETP 16, 1168 (1963)	Elem. Sym.	A	Z
	O	16	8

Method γ bremsstrahlung - cloud chamber, scintillation counter telescope	Ref. No. 62Kol	BG

Reaction	E or ΔE	E_o	Γ	$\int \sigma dE$	Jπ	Notes
(γ, dn) (γ, dp)	$E_{\gamma max}$= 90 MeV					Emission of photodeuterons accompanied in most cases by emission of protons or neutrons. There is a pronounced correlation between directions of emission of deuterons and accompanying protons and neutrons.

Reaction	Yield, per cent	Threshold, MeV
(γ, dp)	41	28.25
(γ, dn)	41	31.2
Multiprong disintegrations	18	—

Ref. J. Miller, G. Schuhl, G. Tamas, C. Tzara
Phys. Letters 2, 76 (1962)

Elem. Sym.	A	Z
O	16	8

Method
Positron annihilation; neutron yield; 4π neutron; positron current

Ref. No. 62 Mi 2 | JHH

Reaction	E or ΔE	E_o	Γ	$\int \sigma dE$	Jπ	Notes
$O^{16}(\gamma,n)$	15-25	(See Table I below)		(See Table I below)		
$O^{16}(\gamma,np)$						Measurements not extended over any peaks in this reaction.

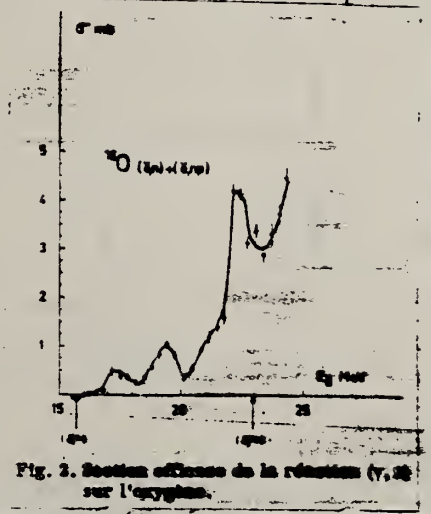

Fig. 2. Section efficace de la réaction (γ,n) sur l'oxygène.

Tableau 1

Noyau	$\int_{\cdot}^{E_{max}} (\gamma n + \ldots) dE$ (MeV - mb)	Energie des niveaux (MeV)	Largeur des niveaux (MeV)	Sections efficaces intégrées des niveaux discrets (MeV-mb)
C^{12}	24	22.2 23.3		
O^{16}	13	17.5 19.4 21.1 22.2 (23) ≥24.2	≃ 1	0.6 1.6 1.4 (4.8) (2.4)
Ca^{40}	83.5	(19.1) 19.9 (21.4)		

REF.

W.T. Morton, T.G. Walker
Phil. Mag. 7, 741 (1962)

ELEM. SYM.	A	Z
O	16	8

METHOD: Synchrotron; p and α cross section; nuclear emulsion

REF. NO.: 62 Mo 2 — NVB

REACTION	RESULT	EXCITATION ENERGY	SOURCE		DETECTOR		ANGLE
			TYPE	RANGE	TYPE	RANGE	
G,PA	ABI	23-120	C	120	EMU-D		4PI

$$\int_0^{120} \sigma dE = 0.3 \pm 0.2 \text{ MeV-mb}$$

Fig. 2

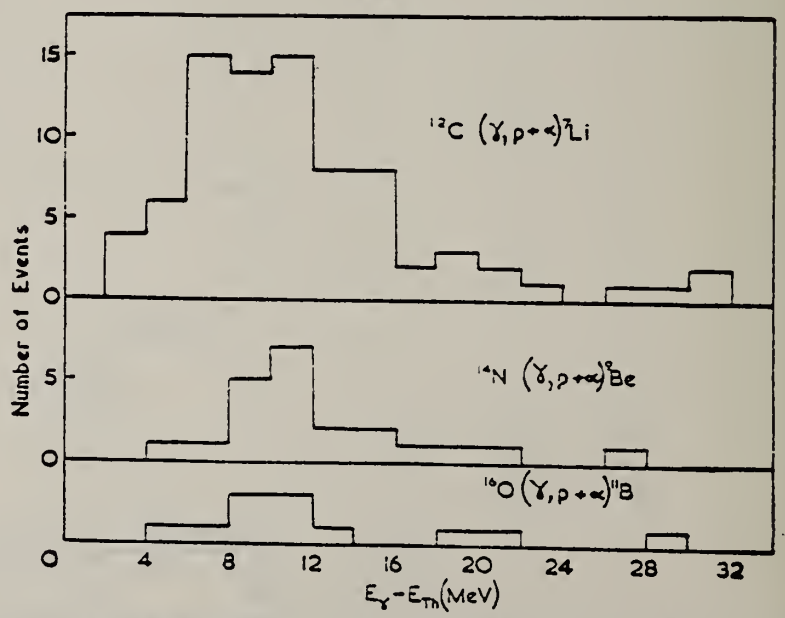

Energy dependence of $(\gamma, p+\alpha)$ reactions in ^{12}C, ^{14}N and ^{16}O.

Ref. T.D. Seward
Phys. Rev. 125, 335 (1962)

Elem. Sym.	A	Z
O	16	8

Method
Linac; NaI; detector at 90°.

Ref. No
62-3e [redacted] JHH

Reaction	E or ΔE	E_0	Γ	$\int \sigma dE$	Jπ	Notes
$O^{16}(\gamma,\gamma)$	Bremss.; ~ 16	6.9±0.1				7.12 MeV level not evident, but data does not exclude its presence.

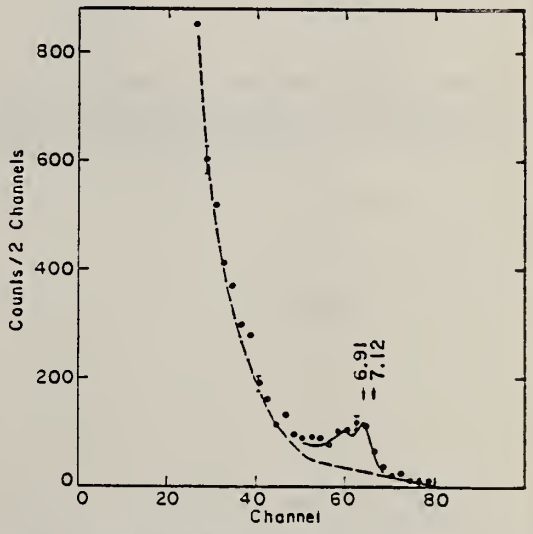

FIG. 6. Pulse-height spectrum for γ rays scattered from a H_2O sample. Sample-out background has been subtracted. The solid line is a KS response function for a 6.9-Mev γ ray. The dashed line is an estimate of the sample-associated background.

REF.

M. Suffert, G. Costa and D. Magnac-Valette
Proc. Padua Conf. 342 (1962)

ELEM. SYM.	A	-
O	16	8

METHOD

REF. NO.	
62 Su 2	JDM

REACTION	RESULT	EXCITATION ENERGY	SOURCE		DETECTOR		ANGLE
			TYPE	RANGE	TYPE	RANGE	
D,G	RLX	21-25	D	1-5	NAI-D		90

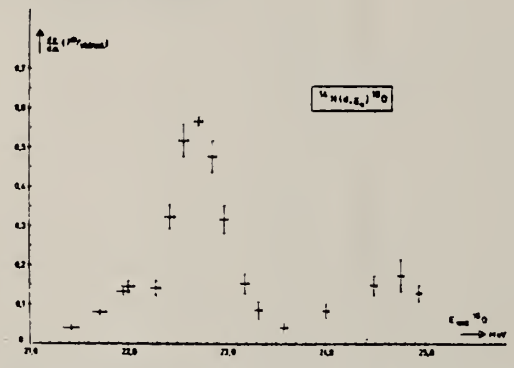

Fig. 2. The differential cross-section at 90° for the ground state γ-transition from the reaction $N^{14}(d, \gamma_0)O^{16}$ versus excitation energy in O^{16}.

The horizontal bars represent the energy loss of the deuterons in the gas-target. The indicated errors on the differential cross-section are only statistical and do not include a possible systematic error on the absolute calibration or background subtraction.

Ref. D.W. Anderson, A.J. Bureau, B.C. Cook, J.E. Griffin, J.R. MCConnell, K.H. Nybo
Phys. Rev. Letters 10, 250 (1963)

Elem. Sym.	A	Z
O	16	8

Method
(γ,n) activity measured

Ref. No.
63 An 1 EGF

Reaction	E or ΔE	E_o	Γ	$\int \sigma dE$	Jπ	Notes
$O^{16}(\gamma,n)O^{15}$	15-60	(see table)				Least structure method of Cook used for analysis. O^{15} activity counted with 3 X 3 in NaI crystal.

Table I. Measured properties of resonances above the giant resonance.

Resonance energy[a] (MeV)	Percent of cross section integrated to 30 MeV
33.0 ±0.5	18.1 %
39.7 ±0.5	7.9 %
45.9 ±0.8	4.9 %
51.6 ±0.8	2.4 %
58.4 ±1.4	4.7 %

[a]Errors on energies are standard deviations of six individual cross-section measurements. Systematic errors have not been taken into account.

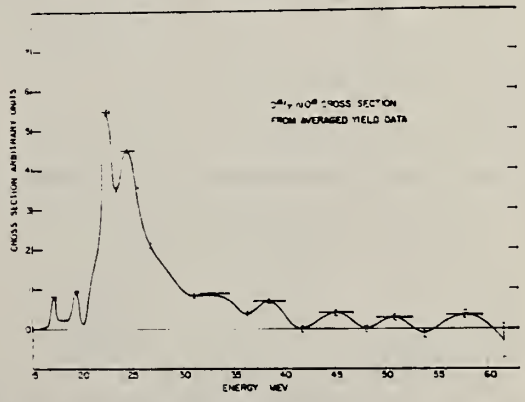

. Relative cross section for the reaction $O^{16}(\gamma,n)O^{15}$ calculated from the average of three radio ves by the least-structure method.

Ref. R.H. Augustson, N.N. Kaushal, H.A. Medicus, W.R. Moyer, E.J. Winhold, P.F. Yergin
Helv. Phys. Acta 36, 816 (1963)

Elem. Sym.	A	Z
O	16	8

Method Linear accelerator; neutron spectrum; time-of-flight.

Ref. No. 63 Au 1 NVB

Reaction	E or ΔE	E_o	Γ	$\int \sigma dE$	Jπ	Notes
$O^{16}(\gamma,xn)$	Bremss.					Neutrons measured at 90°.
	56	27.7				30.4 MeV peak doubtful (HAM)
	46	30.4				

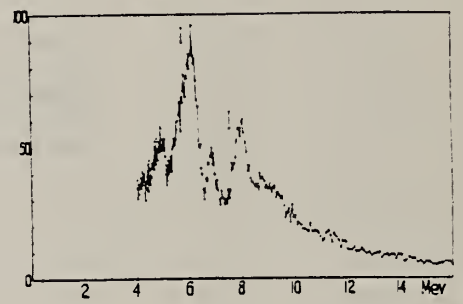

Fig. 1

Photoneutronenspektrum des O^{16}, erzeugt durch Bremsstrahlung von 46 MeV Energie. Das Spektrum ist nicht korrigiert in bezug auf Form des Bremsstrahlungsspektrums und Zähleransprechwahrscheinlichkeit. Aufgetragen ist die Stosszahl in willkürlichen Einheiten als Funktion der Neutronenenergie

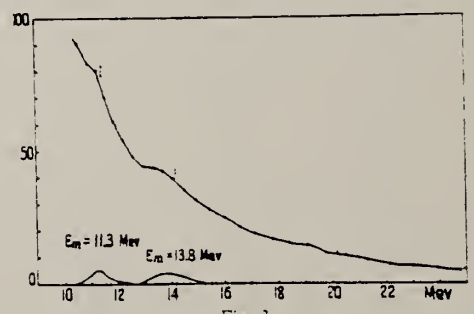

Fig. 2

Energiereicher Teil des Photoneutronenspektrums, erzeugt durch Bremsstrahlung von 56 MeV Energie. Benachbarte Messpunkte wurden in Gruppen von vier zusammengefasst, um die Statistik zu verbessern

Ref. W.C.Barber, J.Goldemberg, G.A.Peterson, Y.Torizuka

Nuclear Phys. 41, 461 (1963); erratum to be published (as of 9/5/63)

Elem. Sym.	A	Z
O	16	8

Method: Linac (Stanford Mark II) - counter telescope

Ref. No.: 63Bal

BG

Reaction	E or ΔE	E_o	Γ	$\int \sigma dE$	Jπ	Notes
(e,e')	41.5	19	14.1	0.41		Inelastic scattering cross section at 180° = .45±40%x10^{-32} cm^2/sr Rad. width corresponds to transition from 0^+ ground state to 1^+ excited state.

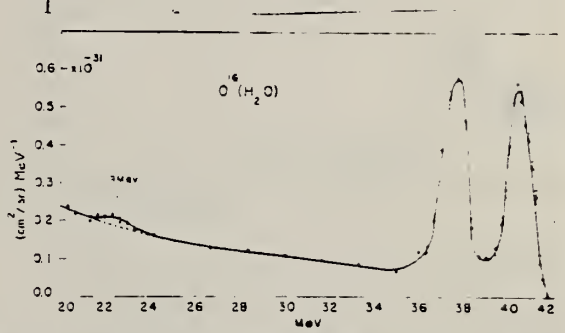

Fig. 7. Spectrum of 41.5 MeV electrons scattered from an H_2O target at 180°.

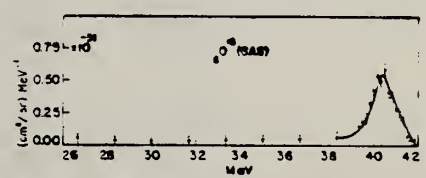

Fig. 8. Spectrum of 41.5 MeV electrons scattered from an oxygen gas target at 180°.

G.R. Bishop, C. Betourne, D.B. Isabelle
J. de Physique 24, 973 (1963)

ELEM. SYM.	A	Z
O	16	8

METHOD: Linac; electron scattering; magnetic spectrometer

REF. NO.: 63 Bi 2 | NVB

REACTION	RESULT	EXCITATION ENERGY	SOURCE		DETECTOR		ANGLE
			TYPE	RANGE	TYPE	RANGE	
E,E/	FMF	11 - 14	D		MAG - D		

TABLEAU 1

Énergie d'excitation MeV	Spin, Parité, Isospin	Largeur totale keV	Probabilité de transition réduite	Configuration	$B(\lambda)$ Single Particle
11,51	2^+ ; 0	80 α	$(25{,}8 \pm 5) \times 10^{-52}$ cm^4	$< 1p\|J_2\|1f >^2$	illegible
12,02	2^+ ; 1	—	$(12{,}0 \pm 2) \times 10^{-52}$ cm^4	$< 1p\|J_2\|1f >^2$	illegible
12,96	2^- ; 1	2 p, α	$(7{,}9 \pm 1{,}5) \times 10^{-53}$ cm^4	$< 1p\|J_1\|1d >^2$	8 × illegible cm^4
13,09	1^- ; 1	130 p, α	$(2{,}1 \pm 0{,}2) \times 10^{-27}$ cm^2	$< 1p\|J_1\|1d >^2$	3,75 × illegible cm^2
13,25	3^- ; 1	21 p, α	$(2{,}84 \pm 0{,}4) \times 10^{-76}$ cm^6	$< 1p\|J_2\|1d >^2$	48 × 10^{-52} cm^6
13,65	1^+ ; 0	64 p, α	$(1{,}47 \pm 0{,}3) \times 10^{-27}$ cm^2	$< 1S\|J_1\|1d >^2$	2,6 × 10^{-25} cm^2

Ref.

N.A. Burgov, G.V. Danilyan, B.S. Dolbilkin, L.E. Lazareva, F.A. Nikolaev
Izv. Akad. Nauk SSR 27, 866 (1963)

Elem. Sym.	A	Z
O	16	8

Method

250 MeV Synchrotron; pair spectrometer

Ref. No. 63 Bu 1 JH

Reaction	E or ΔE	E_o	Γ	$\int \sigma dE$	Jπ	Notes
μ_t	12.5-26.5	(17.3) (19.4) (21.2) 22.3 23.05 24.3 25.15 25.8				Acq. No. 763 For relative intensities, see second column, Table 4, below.

Таблица 3

Энергии уровней O^{16} (MeV) в интервале 17÷27 MeV

По αполному	По кривой выхода O^{16} (γ, n) [9]	По спектру фотонейтронов [14]	По спектру фотопротонов [21]	По сечению реакции (p,γ) [3]	Согласно обзорной статье [5]
1	2	3	4	5	6
—	17,05	—	—	—	—
—	17,12	—	—	—	—
—	17,23	—	—	—	—
(17,3)	17,27	17,3	17,3	17,3	17,28 (p,n)
—	17,62	—	—	—	17,5 (p,n)
—	17,74	—	—	—	17,63 (p,n)
—	17,89	—	—	—	17,85
—	18,08	18,25	18,07	—	17,96 (p,n)
—	18,69	18,70	—	—	18,05 (p,n)
—	18,97	—	—	—	
—	19,12	19,1	18,99	19,1	—
(19,4)	20,14	19,6	19,57	19,6	—
—	—	19,9	—	—	—
—	20,36	20,2	—	—	—
—	20,55	—	—	—	—
—	20,67	20,7	20,65	—	—
—	20,91	—	—	—	—
(21,2)	21,17	21,0	—	21,0	—
—	21,87	21,7	—	—	—
—	22,01	—	—	—	—
—	22,19	—	—	—	—
22,3	22,41	22,3	22,20 (Γ=0,62)	22,35	22,05 (d,n)
23,05	—	23,05	23,1 (Γ=0,17)	23,08	23,05 (d,n)
24,3	—	24,3	24,35 (Γ=0,79)	24,43	23,54 (γ,γ') 24,38 (d,n)
25,15	—	25,0	—	25,11	—
—	—	25,4	—	—	—
25,8	—	—	—	—	25,7 (He^3, α)
—	—	—	—	—	25,4 (He^3, p)

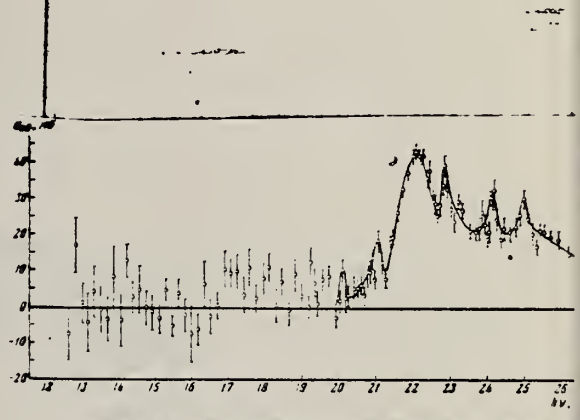

Рис. 1. Аппаратурная кривая ядерного сечения поглощения γ-квантов O

Таблица

Сравнение экспериментальных данных по O^{16} с результатами теоретических расч

Данная работа		[15]		[16]				[17]	
				обычные силы		смеси Сигнера			
E, MeV	I, %	E, MeV	I, %	E, MeV	I, %	E, MeV	I, %	E, MeV	I,
—	—	13,1	1	13,9	1	13,7	1	11,4	0
(17,3)	2	17,3	1	17,7	2	17,6	1	15,6	0
(19,4)	1	20,4	1	19,9	1	20,0	1	18,0	:
(21,2)	4	—	—	21,5	81	—	—	—	—
22,3	33	22,6	67	—	—	22,2	68	21,5	20
23,05	10	—	—	—	—	—	—	23,0	13
24,3	15	—	—	—	—	—	—	23,3	6
25,15	13	25,2	32	25,6	15	25,0	20	23,7	10
25,8	9	—	—	—	—	—	—	24,8	16
								—	—
								27,2	0

FORM NBS-418
(8-1-63)
USCOMM-OC 18556-P63

U.S. DEPARTMENT OF COMMERCE
NATIONAL BUREAU OF STANDARDS

Ref. J.T. Caldwell, R.R. Harvey, R.L. Bramblett, S.C. Fultz
Phys. Letters 6, 213 (1963)

Elem. Sym.	A	Z
O	16	8

Method: Monochromatic photons (annihilation-in-flight)

Ref. No.: 63 Ca 1 | EGF

Reaction	E or ΔE	E_o	Γ	$\int \sigma dE$	Jπ	Notes
(γ,n)	15-30			$\int_0^{24}$ 23 ± 2 $\int_0^{28}$ 44 ± 11 MeV-mb		No sign of (γ,2n); max value <0.1mb

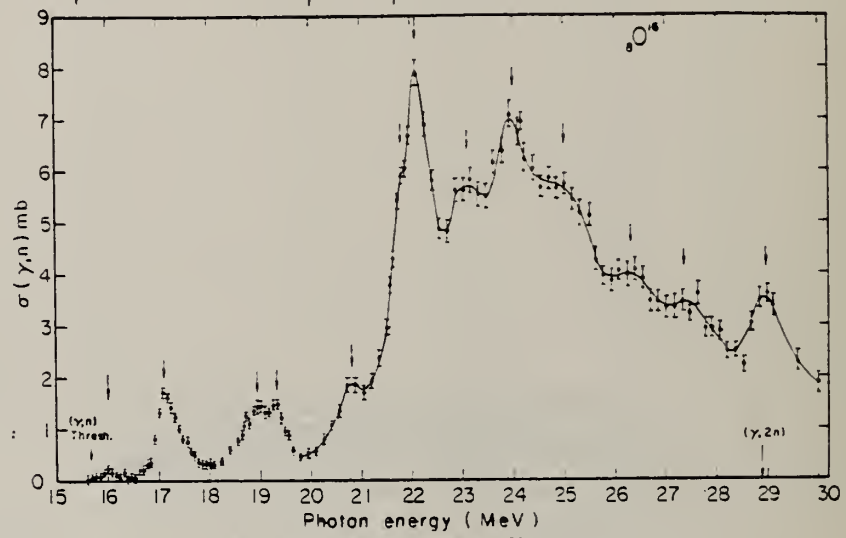

Fig. 2. Photoneutron cross section for Si^{28} versus energy.

Table 1
Energy levels observed for O^{16}

$O^{16}(\gamma,n)4\pi$ (MeV) Present work	$O^{16}(\gamma,n)7^0$ (MeV) Ref. 5)	$N^{15}(p,\gamma)$ (MeV) Ref. 6)	$O^{16}(\gamma,p)7^6$ (MeV) Ref. 7)
16.0		16.2 (1+)	
		17.2 (1-)	
17.1		17.3 (1-)	17.3
19.0	19.1	19.0	19.0
19.3	19.6	19.5	19.6
20.8	20.7	20.8	20.6
	21.0		
21.8	21.7		
22.1	22.2	22.3	22.3
23.1	23.0	23.1	23.1
24.0	24.3	24.4	24.4
25.0	25.0	25.0	
	~25.4		
26.2	26.3		
27.3			
28.9			

Table 2
Experimental and theoretical dipole strengths for O^{16}.

Experimental Levels (MeV)	Particle-hole Levels * (MeV)	Fractional Dipole Strength (Experimental)	Fractional Dipole Strength * (Theoretical)
16.0		0.002 ± 0.001	
17.2	17.3	0.006 ± 0.002	0.08
17.3			
19.0		0.016 ± 0.003	
19.3			
20.7	20.4	0.014 ± 0.005	0.001
21.0			
21.8	22.6	0.19 ± 0.07	0.67
22.1			
23.1			
24.0			
25.0	25.2		0.32
25.4			

* Ref. 3)

Ref.	Elem. Sym.	A	Z
S. Costa, F. Ferrero, S. Ferroni, B. Minetti, C. Molina, R. Malvano Phys. Letters 6, 325 (1963)	O	16	8

Method	Ref. No.	
100 MeV Synchrotron; 4π neutron detector; calculated integrated cross sections - fitted with polynomial of degree 7	63 Co 3	EGP

Reaction	E or ΔE	E_o	Γ	$\int \sigma dE$	$J\pi$	Notes
(γ, xn)						$\sigma_b = \int \frac{\sigma(k)}{k} dk$ gets $\langle \bar{\nu}_p ; \bar{\nu}_n - \bar{\nu}_n \cdot \bar{\nu}_{n-1} \rangle$ $= (k_c^2 - k_p^2 - \frac{3}{\pi} \frac{xrs}{c^2} \sigma_b \frac{A-1}{A^2}) x \frac{2}{A-2}$ See "Boron" for plots of this and $\int \sigma dk/60$ NZ/A

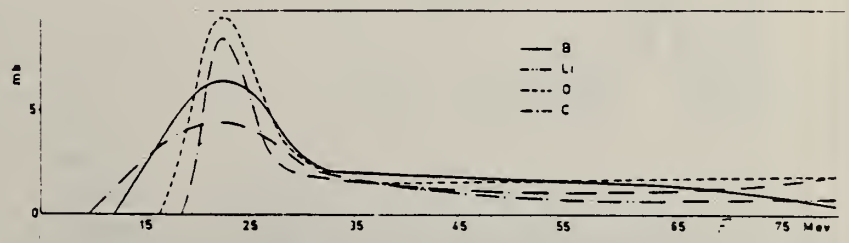

Fig. 1. Photoneutron cross sections for several light elements versus γ-ray energy.

E. Finckh, R. Kosiek, K.H. Lindenberger, K. Maier,
U. Meyer-Berkhout, M. Schechter, J. Zimmerer
Z. Physik 174, 337 (1963)

ELEM. SYM.	A	Z
O	16	8

METHOD
Betatron; proton spectrum, cross section; CsI spectrometer

REF. NO.
63 Fi 4 NVB

REACTION	RESULT	EXCITATION ENERGY	SOURCE		DETECTOR		ANGLE
			TYPE	RANGE	TYPE	RANGE	
G,XP	SPC	14-30	C	31	SCI-D	2-15	90
				(30.5)			

$\int_{14.1}^{30.5} \sigma dE$ = 72 MeV-mb ±15%, assuming ground state transition only and $W(\theta) = 1 + (4\pm2)\sin^2\theta$

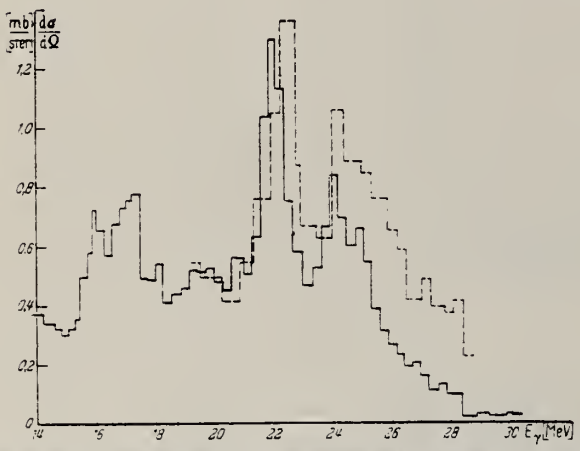

Fig. 6. Differentieller Wirkungsquerschnitt für Photoprotonenemission aus O^{16} unter 90° zum γ-Strahl unter der Annahme, daß nur Grundzustandsübergänge vorliegen (———). Differentieller Wirkungsquerschnitt für Photoneutronenemission aus O^{16} unter 90° nach Fuchs und Haag[6] (– – –)

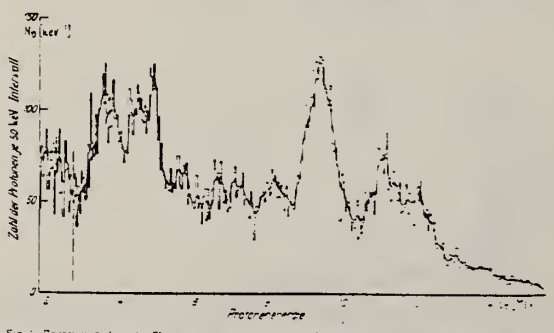

Fig. 7. Energieverteilung der Photoprotonen aus O^{16} aus zwei Messungen bei $E_{\gamma_{max}} = 28$ MeV. Das Histogramm stellt die auf Energieverlust korrigierten Meßwerte dar, die ausgezogene Kurve wurde nach einem Mittelungsverfahren gewonnen. Nähere Erläuterungen im Text

	(16.2)			16.25	16.2*		16.22		16.28
	16.85								16.79
							17.33		
	17.30	17.27		17.35	17.3		17.36		17.34
							17.63		
	18.10	18.07			18.25		18.06	18.2	18.06
	(18.5)				18.7				18.58
	19.10	18.99		19.05	19.1	19.4		19.3	19.19
	19.7	19.57		19.6	19.6				
					19.9			(20.0)	
					20.2				
					20.7				20.45
	20.75	20.98		20.9	21.0	20.9		20.9	21.02
					21.7				21.54
	22.05	22.3	21.8	22.35	22.25	22.2			22.32
		23.05	(22.8)	23.15	23.0	22.9			
	24.05	24.4	24.4	24.5	24.5	24.2			
	(24.3)								
	25.0		25.0	25.15	25.0	25.0			
					25.4	(25.5)			

* Angegeben bei [illegible].

[1] Cohen, S.G., P.S. Fisher and E.K. Warburton: Phys. Rev. 121, 358 (1961).
[2] Tanner, N.W., G.C. Thomas and E.D. Earle: Proc. Rutherford Jubilee Int. Conf. Manchester/London 1961.
[3] Tanner, N.W.: Private Mitteilung.
[4] Lazarewa, L.E.: Private Mitteilung.
[5] Firk, F.W.K., and K.H. Lokan: Phys. Rev. Letters 8, 321 (1962).
[6] Fuchs, H., u. D. Haag: Z. Physik 171, 403 (1963).
[12] Dodge, W.R., and W.C. Barber: Phys. Rev. 127, 1746 (1962).
[30] Jones, K.W., L.J. Lidofsky and J.L. Weil: Phys. Rev. 112, 1252 (1958).
[31] Wong, C., J.D. Anderson, S.D. Bloom, J.W. McClure and B.D. Walker: Phys. Rev. 123, 598 (1961).
[32] Dearnaley, G., D.S. Gemmel, B.W. Hooton and G.A. Jones: Phys. Let. 1, No. 7, 269 (1962).

H. Fuchs, D. Haag
Z. Physik 171, 403 (1963)

0	16	8

METHOD
Betatron; neutron spectrum, cross section; stilbene scintillator ion chamber

REF. NO. 63 Fu 1 NVB

REACTION	RESULT	EXCITATION ENERGY	SOURCE		DETECTOR		ANGLE
			TYPE	RANGE	TYPE	RANGE	
G,XN	SPC.	THR-31	C	31	SCI-D	2-13	90

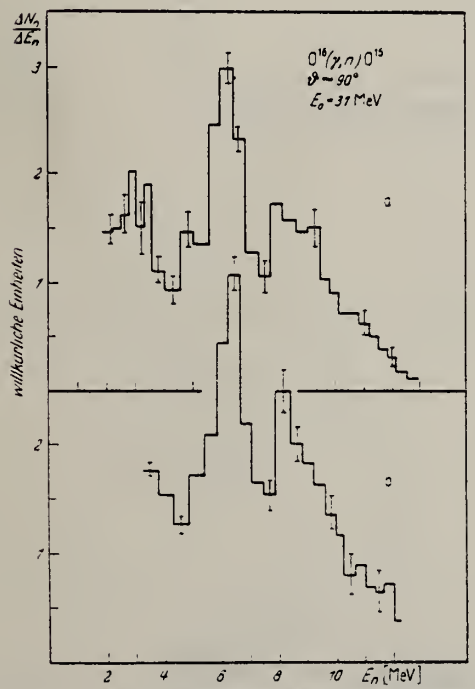

Fig. 5a u. b. Spektren der Photoneutronen aus Sauerstoff, unter 90° bei $E_0 = (30{,}5 \pm 1)$ MeV. a und b Ergebnisse zweier unabhängiger Messungen mit verschiedener Einstellung der Impulsformdiskrimination

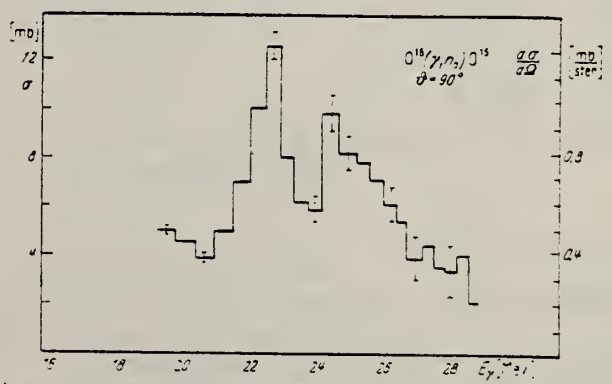

Fig. 6. Wirkungsquerschnitt für $O^{16}(\gamma, n_0)O^{15}$, berechnet aus dem Neutronenspektrum in Fig. 5b unter der Annahme, daß 100% Übergänge zum Grundzustand von O^{15} vorliegen. Die rechte Skala gibt $d\sigma/d\Omega$ (90°) und weist in ihren Absolutangaben einen Fehler von 20% auf, während die linke Skala σ angibt, berechnet aus $d\sigma/d\Omega$ (90°) unter der Annahme, daß die Winkelverteilung die Form $A - B \cdot \sin^2 \vartheta$ habe mit $B/A = 2 = 1$ für alle Neutronenenergien (vgl. Ref. [1]). Der Fehler in den Absolutwerten ist dort etwa 30%. Die Fehlerbalken geben den statistischen Fehler an

[1] Milone, C., and A. Rubbino: Nuovo Cim. 13, 1035 (1951).

Ref. K.N. Geller, E.G. Muirhead
Phys. Rev. Letters 11, 371 (1963)

Elem. Sym.	A	Z
O	16	8

Method
Betatron; radioactivity

Ref. No. 63 Ge 2 JHH

Reaction	E or ΔE	E_o	Γ	$\int \sigma dE$	Jπ	Notes
O^{16}: (γ,n)	Bremss. 15.6-23					For E_o, Γ, and $\int \sigma dE$ data see Table I.

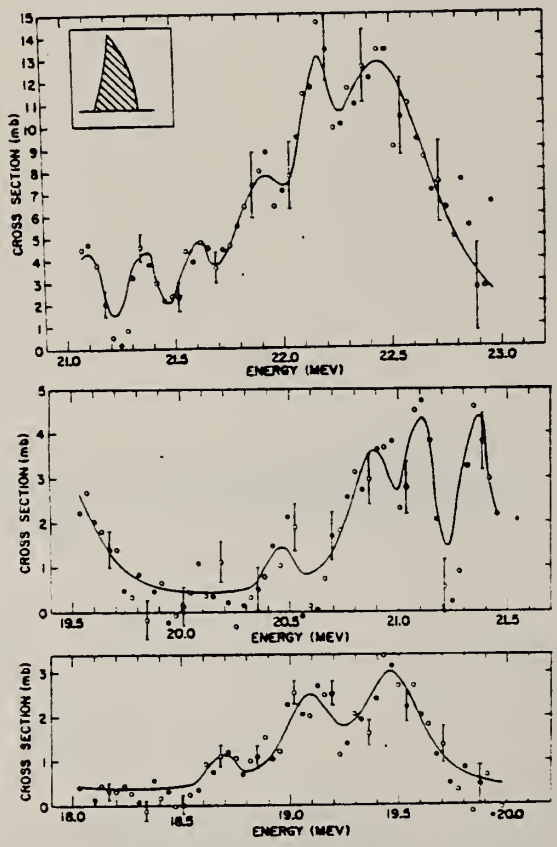

FIG. 2. Cross section for the $O^{16}(\gamma,n)O^{15}$ reaction from 18 to 23 MeV. Analysis bin width, $\Delta E = 68$ keV. Resolution (see inset) $FWHM = 136$ keV.

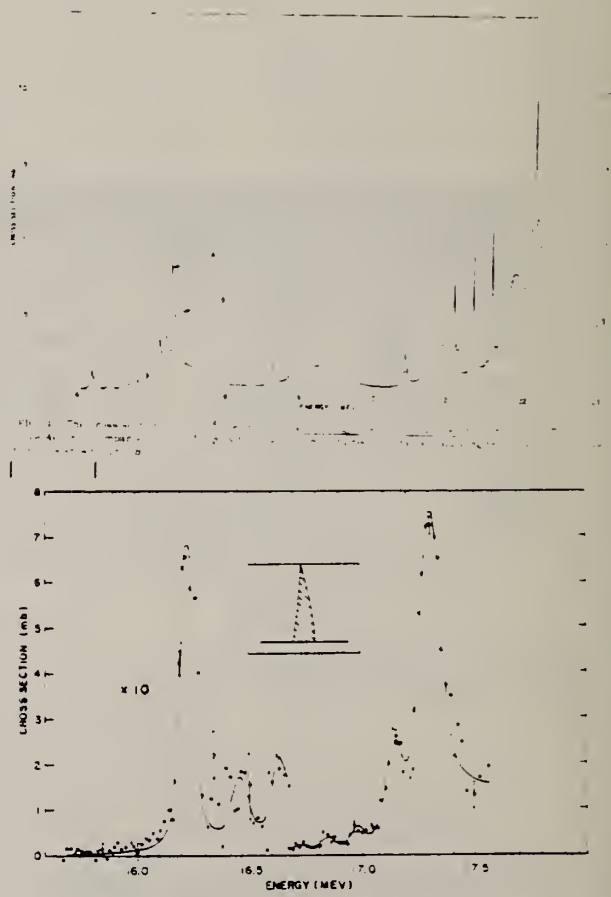

FIG. Cross section for the $O^{16}(\gamma,n)O^{15}$ reaction obtained from the second difference method with analytical smoothing. Analysis bin width, $\Delta E = 14$ keV. Resolution (see inset) $FWHM = 68$ keV.

Reaction	E or ΔE	E_0	Γ	$\int \sigma dE$	Jπ	Notes

Table I. $O^{16}(\gamma,n)$ level structure.

Level energy (MeV) ±Δb	Level width (MeV)	Peak cross section (mb)	Neutron width (MeV)	Proton width (MeV)	Radiative width (dipole) (keV)	Integrated cross section (MeV-mb)
16.23	0.032	1.277	0.004	0.028	0.014	0.064
16.46	0.050	0.196	0.007	0.043	0.0025	0.015
16.91	0.030	0.294	0.005	0.025	0.0013	0.013
17.21	0.020	0.193	0.004	0.016	0.0015	0.012
18.45	0.025	0.549	0.006	0.019	0.0025	0.023
18.87	0.015	1.229	0.004	0.011	0.0029	0.029
19.14	0.045	2.703	0.014	0.031	0.016	0.190
19.70	0.09	9.355	0.033	0.057	0.086	1.140
20.23	0.40	1.228	0.174	0.226	0.344	0.771
20.69	0.05	1.474	0.021	0.029	0.009	0.115
19.09	0.20	2.211	0.071	0.129	0.063	0.634
19.47	0.10	2.949	0.095	0.205	0.146	1.384
20.45	0.04	2.454	0.012	0.029	0.014	0.146
20.84	0.20	3.563	0.062	0.138	0.134	1.114
21.10	0.025	11.796	0.008	0.017	0.056	0.462
21.45	0.025	11.304	0.009	0.016	0.052	0.443
21.84	0.025	4.547	0.009	0.016	0.029	0.247
21.99	0.15	4.315	0.097	0.153	0.210	1.929
22.15	0.04	13.762	0.016	0.024	0.095	0.864
22.47	0.50	12.779	0.221	0.279	1.457	12.037

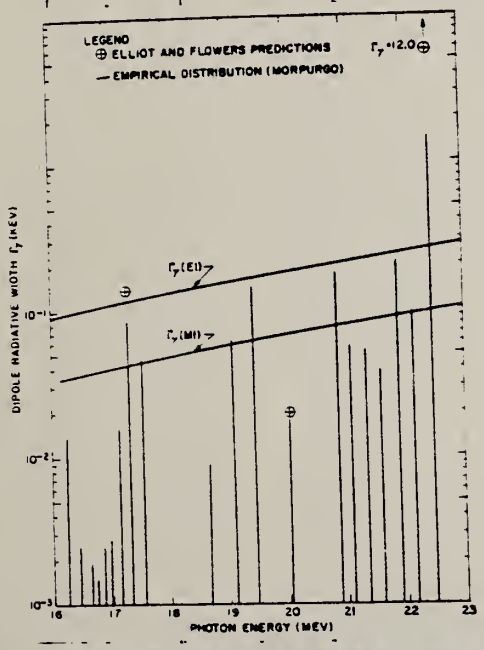

FIG. 3. Distribution of radiative widths from threshold to 23 MeV for the levels of O^{16}. For comparison the predictions of Elliott and Flowers and the systematic *E*1 and *M*1 variations of Morpurgo are included.

Table II. Comparison of resonance parameters of calculations of Elliott and Flowers[a] with this experiment.

Level configuration	Theoretical Energy (MeV)	Theoretical Radiative Width (Γ_γ) (keV)	Experimental Energy (MeV)	Experimental Radiative Width (Γ_γ) (keV)
$p_{1/2}^{-1}d_{3/2}$	17.3	0.140	17.3	0.060
$p_{3/2}^{-1}s_{1/2}$	20.4	0.02	20.45	0.018
$p_{3/2}^{-1}d_{5/2}$	22.8	12.0	22.47	1.46

[a]See reference 3.

[3]J. P. Elliott and B. H. Flowers, Proc. Roy. Soc. (London) A242, 57 (1957).

[4]G. E. Brown, L. Castillejo, and J. A. Evans, Nucl. Phys. 22, 1 (1961).

[5]Evans Hayward, Rev. Mod. Phys. 35, 324 (1963).

[6]N. W. Tanner, G. C. Thomas, and E. D. Earle, Proceedings of the Rutherford Jubilee International Conference, Manchester, 1961, edited by J. B. Birks (Heywood and Co., London, 1962).

Ref. S. Gorodetzky, W. Brenenson, P. Chevallier, D. Disdier, F. Scheibling
Phys. Letters 6, 269 (1963)

Elem. Sym.	A	Z
O	16	8

Method
NaI; plastic scintillators

Ref. No.
63 Go 5 JHH

Reaction	E or ΔE	E_o	Γ	$\int \sigma dE$	Jπ	Notes
$N^{15}(p,\gamma)$						Ratios of $\sigma_{(\text{to 6.06 level})}$ to σ_{γ_o}:
	1.010	13.10			1^-	$(8\pm2)\ 10^{-3}$
	4.4	16.22			1^+	$(1.6\pm0.5)\ 10^{-1}$
	5.4	17.13			1^-	$(1.6\pm0.5)\ 10^{-1}$
	5.55	17.30			1^-	$\leq 1.3 \times 10^{-2}$

Ref. D. F. Hebbard, G.M. Bailey
Nuclear Phys. 49, 666 (1963)

Elem. Sym.	A	Z
O	15	8

Method: Cockcraft-Walton; γ-ray yield; NaI

Ref. No.: 63 He 1 JHH

Reaction	E or ΔE	E_o	Γ	$\int \sigma dE$	Jπ	Notes
$N^{14}(p,\gamma)$	0.21-1.07					
	0.278	7.55	$\omega\Gamma_\gamma$: 0.51×10^{-3} eV			
	1.060	8.28	0.210 eV			

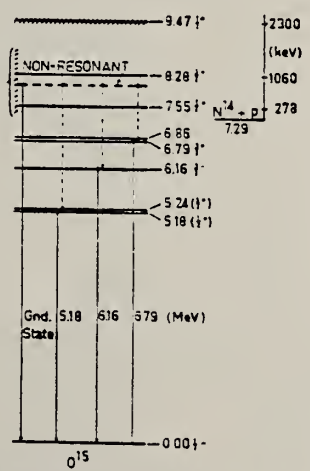

Fig. 1. The non-resonant gamma-ray transition observed experimentally are shown by full lines on this energy level diagram of O^{15}. Several levels, of no importance for non-resonant capture, are omitted from the diagram.

Ref. D.B. Isabelle, G.R. Bishop

Nuclear Phys. 45, 209 (1963)

Elem. Sym.	A	Z
O	16	8

Method

Ref. No.	
63Isl	BG

Reaction	E or ΔE	E_o	Γ	$\int \sigma dE$	Jπ	Notes
(e,e')	$E_e(\theta^\circ)$	22.6				
	90(100)				(1^-)	E1 - some indication that it could be unresolved pair of levels. More important E1, other E2.
	100(60)					
	150(70)				(2^+)	E2
	215(80)				(1^-)	E1

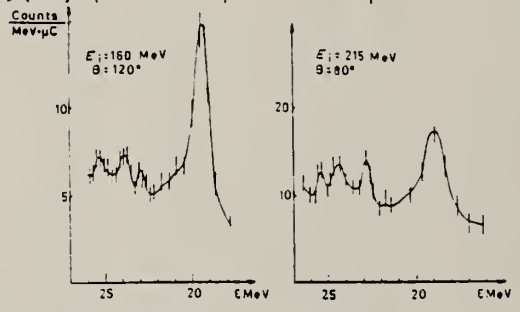

Fig. 5. Spectra of scattered electrons obtained with high resolution in the region of the giant resonance. The momentum transfer is the same, $q = 1.33$ fm^{-1}, but incident energy and scattering angle are varied. It is clear that the three peaks near $\varepsilon = 25$ MeV are independent of scattering angle, whilst the peak at 19.3 MeV shows a strong angular dependence.

Electric character established by performing experiment at constant momentum transfer and various scattering angles.

Details given on radiative tail calculations and corrections to data.

Data given for $\frac{d\sigma}{d\Omega}_{exp}$ and $F^2(q)$, the inelastic form factor (ratio of experimental cross section to Mott cross section)

TABLE 7

Comparison between the experimental values of the radiative transition probability calculated using the folded charge distribution model (F.C.D.) and the independent particle model (I.P.M.) with the theoretical value for the single particle model (S.P.M.)

Level	$B(E1)_{exp}$ F.C.D.	$B(E1)_{exp}$ I.P.M.	$B(E1)_{th}$ S.P.M.
22.6 MeV	9.7×10^{-27} cm^4	8.7×10^{-27} cm^4	8.6×10^{-27} cm^4
25.7 MeV	6.4×10^{-27} cm^4	5.8×10^{-27} cm^4	8.6×10^{-27} cm^4

TABLE 8

List of the different levels observed in oxygen 16 in the energy range 17 to 26 MeV with various type of reactions

Types of reactions	Ref.	Energy of excited levels														
$O^{16}(\gamma, p_1)N^{15}$	a)			18.8		19.3			20.6		22.2			24		25.5
$O^{16}(\gamma, p_1)N^{15}$	b)			(18.7)		(19.5)			(20.5)		22.2			24.2		(25.3)
$N^{15}(p, \gamma_0)O^{16}$	c)				18.97	19.5			21		22.2	23.1		24.3		25.2
$O^{16}(e, pe_1)N^{15}$	d)				18.99	19.57			20.65		22.30	23.10		24.35		25.2
$O^{16}(\gamma, n_0)O^{15}$	e)	17.3	18.25	18.70	19.1	19.6	19.9	20.2	20.7	21.7	22.2	23		24.3	25	25.4
$O^{16}(\gamma, n_1)O^{15}$	f)										22.3	23.06	23.45	24.4	25.15	25.9
$O^{16}(\gamma, n_0)O^{15}$	g)	17.3				19.3					22.5			24		
$O^{16}(\gamma, n_0)O^{15}$	h)	17.5				19.4			21.1		22.2	(23)		(24.2)		
$N^{15}(p, p_1)N^{15}$	i)	17.34	18.06	18.51	19.19			20.45	21.02	21.54	22.32					
$N^{15}(d, \gamma_0)O^{16}$	i)										22.0	22.7			24.8	
$O^{16}(e, e')$	k)	(17.4)			19.1				21		22.6			24.1		25.7

a) C. Milone, S. Milone Tamburino, R. Rinzivillo, A. Rubbino and C. Tribuno, Nuovo Cim. 7 (1958) 729; see also P. Brix and E. K. Maschke, Z. f. Phys. 155 (1959) 109

b) H. G. Dosch, E. Finckh, K. H. Lindenberger, K. Maier and U. Meyer-Berkhout, private communication

c) See ref. a).

d) W. R. Dodge and W. C. Barber, Phys. Rev. 127 (1962) 1746

e) I. W. K. Firk and K. H. Lokan, Phys. Rev. Lett. 8 (1962) 321

f) N. A. Burgov, G. V. Danilyan, B. S. Dolbilkin, L. Lazareva and F. A. Nikolayev, JETP 43 (1962) 70 (English Translation Soviet Physics JETP 16 (1963) 50)

g) L. N. Bolen and W. D. Whitehead, Phys. Rev. Lett. 9 (1962) 458

h) J. Miller, C. Schuhl, G. Tamas and C. Tzara, Phys. Lett. 2 (1962) 76

i) G. Dearnaley, D. S. Gemmell, B. W. Hooton and G. A. Jones, Phys. Lett. 1 (1962) 269

j) M. Suffert, G. Costa and D. Magnac-Valette, Proc. of the International Symposium on Direct Interactions and Nuclear Reactions Mechanisms, Padova (Sept. 1962), ed. by E. Clementel and C. Villi (Gordon and Breach Science Publishers Inc. N.-Y. 1963)

k) This experiment

Ref. J.A. Scheer, K. Schlüpmann, F. Triantafyllidis
Phys. Letters 7, 269 (1963)

Elem. Sym.	A	Z
O	16	8

Method: Betatron; Si solid-state detector

Ref. No.: 63 Sc 1 JHH

Reaction	E or ΔE	E_o	Γ	$\int \sigma dE$	Jπ	Notes
$O^{16}(\gamma,p)$	Bremss. 31					

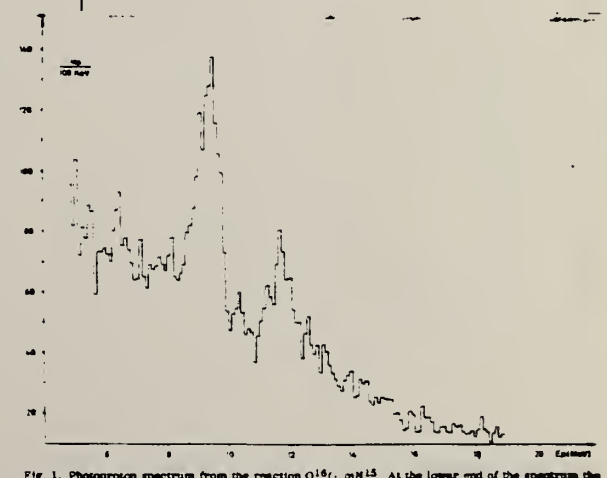

Fig. 1. Photoproton spectrum from the reaction $O^{16}(\gamma,p)N^{15}$. At the lower end of the spectrum the uncertainty in height increases to about 20% due to large energy loss corrections.

M. Suffert, G. Costa, D. Magnac-Valette
J. J. de Physique 24, 1029 (1963)

0	16	3

METHOD: Van de Graaff; inverse; NaI spectrometer

REF. NO.: 63 Su 2 | NVB

REACTION	RESULT	EXCITATION ENERGY	SOURCE TYPE	SOURCE RANGE	DETECTOR TYPE	DETECTOR RANGE	ANGLE
D,G	ABX	21-25	D	1- 5	NAI-D		DST

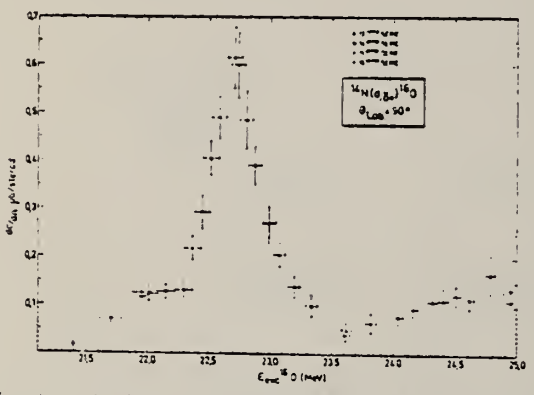

FIG. 8. — Section efficace différentielle à 90° de la réaction $^{14}N(d, \gamma_0)^{16}O$ en fonction de l'énergie d'excitation dans ^{16}O au centre de la cible gazeuse. Les barres horizontales indiquent la dispersion d'énergie due à l'épaisseur de la cible. L'erreur indiquée pour la section efficace ne comprend pas une erreur possible sur le calibrage absolu de l'ensemble.

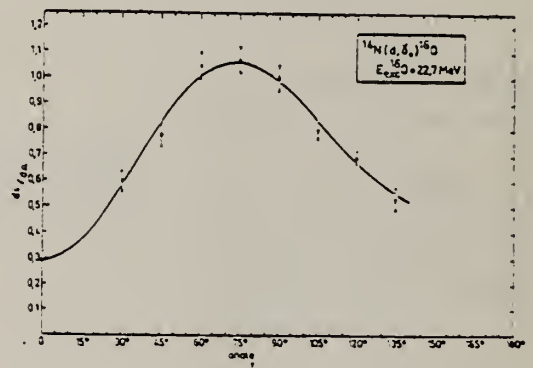

FIG. 9. — Distribution angulaire de la réaction $^{14}N(d, \gamma_0)^{16}O$ à $\overline{E_{exc}} = 22,7$ MeV ($E_{dinc} = 2,56$ MeV). La courbe en trait plein représente la courbe ajustée d'après la méthode des moindres carrés. Elle est de la forme :

$$W(0) = 1 + (0,18 \pm 0,07)\, P_1 - (0,52 \pm 0,09)\, P_2 - (0,27 \pm 0,09)\, P_3 - (0,01 \pm 0,07)\, P_4.$$

REF. G. Baciu
Rev. Roum. Phys. 9, 783 (1964)

ELEM. SYM.	A	Z
O	16	8

METHOD

REF. NO. 64 Ba 3 egf

REACTION	RESULT	EXCITATION ENERGY	SOURCE		DETECTOR		ANGLE
			TYPE	RANGE	TYPE	RANGE	
G,XN	ABX	15-28	C	15-28	BF3-I		4PI

3.2 O/C YLD=1.7(22 MEV)

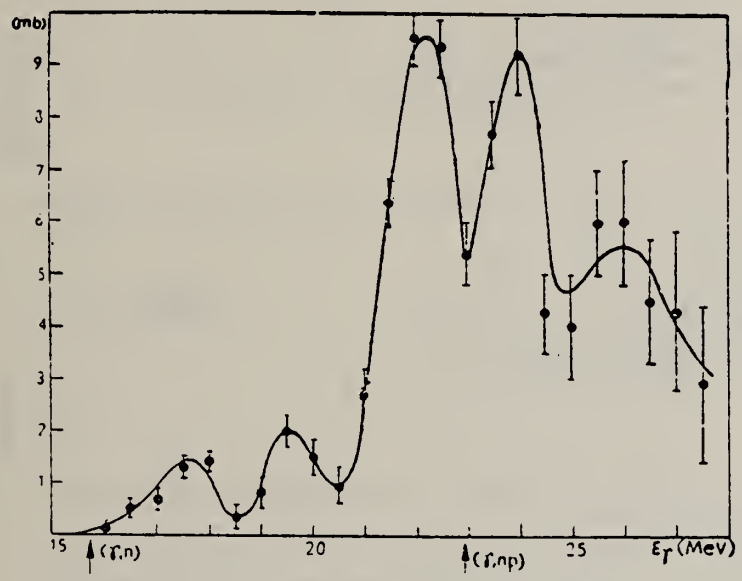

Fig. 5. — Cross-section for the O^{16} (γ, Tn) reaction.

G. Baciu, C. Molino, B. Minetti, L. Pasqualini, G. Piragino
Stud. Cercetari Fiz. 16, 903 (1964)

0	16	8

METHOD

REF. NO. 64 Ba 5 egf

REACTION	RESULT	EXCITATION ENERGY	SOURCE		DETECTOR		ANGLE
			TYPE	RANGE	TYPE	RANGE	
G,XN	ABX	15-28	C	15-28	BF3-I		4PI

Tabela 1

O^{18} (γ, Tn)

Autorii	σ_{max} (mb)	E_0 (Mev)	σ_1/E_1	σ_2/E_2	σ_3/E_3	σ_4/E_4	$Y^0_{(22)}/Y_{(22)}$
Maslam 1951	11,6	22,4					
Katz 1951	13,1	22,9					
Montalbetti 1953	11,0	24,2					0,85
Halpern 1954	8,6	22,0					
Barber 1955	8,3	22,5					
Cook 1957	10,4	22,8					
Roalsving 1961	7,9	23,0					
Valoare medie	10,0	22,4					2,06
Geller 1963	12,78	22,47		2,95/19,47	13,76/22,15		
Lucrarea de			1,23/17,55				
față 1964	9,50	22,45	1,30/17,50	1,95/19,50	9,50/22,45	9,20/24,10	1,70
Bolen 1962	—	—	1,3/17,3	1,6/19,3	8,4/22,3	8,3/24,1	

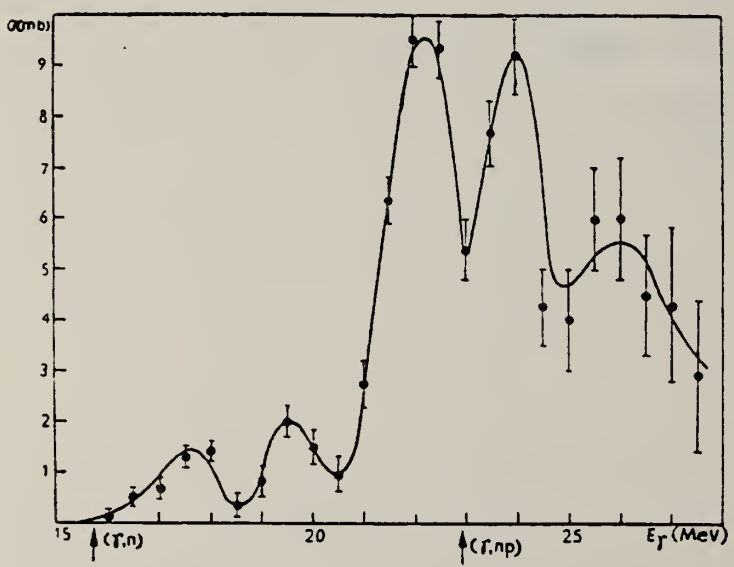

Fig. 1

W. Bertozzi, P. Demos, F. Hanser, S. Kowalski, C. Sargent,
W. Turchinetz, R. Fullwood and J. Russell
Proc. Paris Conf. 1026 (1964)

ELEM. SYM.	A	Z
O	16	8

METHOD
Polarization Data

REF. NO.
64 Be 8

JDM

REACTION	RESULT	EXCITATION ENERGY	SOURCE		DETECTOR		ANGLE
			TYPE	RANGE	TYPE	RANGE	
$G,N	NOX	17-32	C	32	SCI-D	2-14	DST

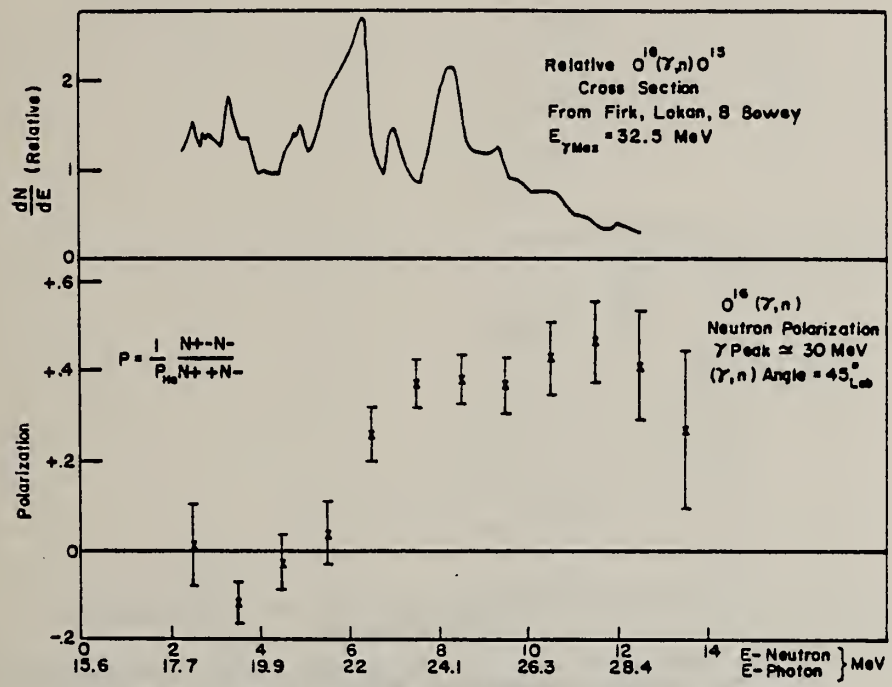

FIG. 1. — Polarization of photoneutrons from $O^{16}(\gamma, n)O^{15}$.

0	16	8

METHOD	REF. NO.	
Linac	64 Bi 2	JOC

REACTION	RESULT	EXCITATION ENERGY	SOURCE		DETECTOR		ANGLE
			TYPE	RANGE	TYPE	RANGE	
E,E/	ABX	0-150	D	90-215	MAG-D		DST

3 sum rules calculated and measured

SUM RULES

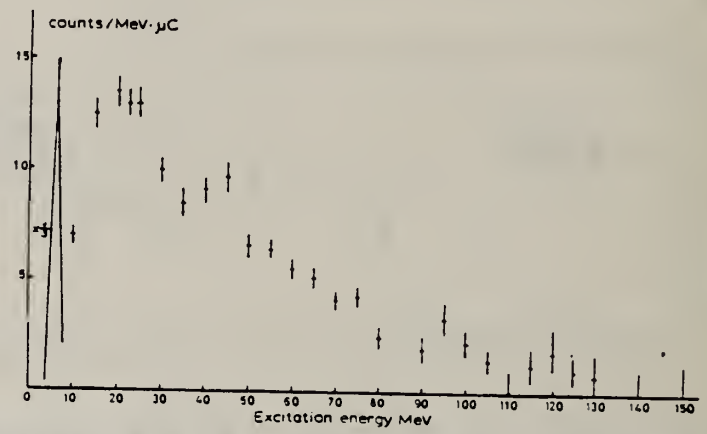

Fig. 4. The inelastic spectrum obtained for a scattering angle of 90° and a momentum transfer of 190 MeV/c, by variation of both incident and final electron energies as the excitation energy ε increases.

TABLE 1

The cross section for electron scattering obtained for fixed incident energy and fixed scattering angle

E_0 (MeV)	$\theta°$	σ_0 (μb/sr)	$\sigma_{\theta.5}$ (μb/sr)	σ_{13} (μb/sr)	$\sigma_{19.5}$ (μb/sr)	σ_{tail} (μb/sr)	$\frac{d\sigma_{tot}}{d\Omega_t}$ exp. (μb/sr)	$\frac{d\sigma_{tot}}{d\Omega_t}$ theor. (μb/sr)
100	60	238	a)	a)	a)	17.2	255	221
90	100	16.2	a)	a)	a)	5.15	21.5	17.7
150	70	10	30.5×10^{-3}	6.04×10^{-3}	10.6×10^{-3}	2.01	12.5	20.6
150	90	1.0	9.00×10^{-3}	13.9×10^{-3}	a)	2.64	5.09	5.02
150	115	6.6×10^{-3}	7.8×10^{-3}	5.78×10^{-3}	7.26×10^{-3}	0.958	1.33	1.68
160	120	1.26×10^{-3}	3.5×10^{-3}	2.68×10^{-3}	4.08×10^{-3}	1.28	1.39	1.35
215	80	5.42×10^{-3}	1.6×10^{-3}	10.7×10^{-3}	9.26×10^{-3}	2.76	3.19	3.06

Contribution of the elastic peak and various regions of inelastic excitation are indicated separately so that their relative importance can be seen. The theoretical integrated cross section is calculated from eq. (7) of the text.

a) Included in σ_{tail}.

METHOD

REF. NO. 64 Bi 2

REACTION	RESULT	EXCITATION ENERGY	SOURCE TYPE	SOURCE RANGE	DETECTOR TYPE	DETECTOR RANGE	ANGLE

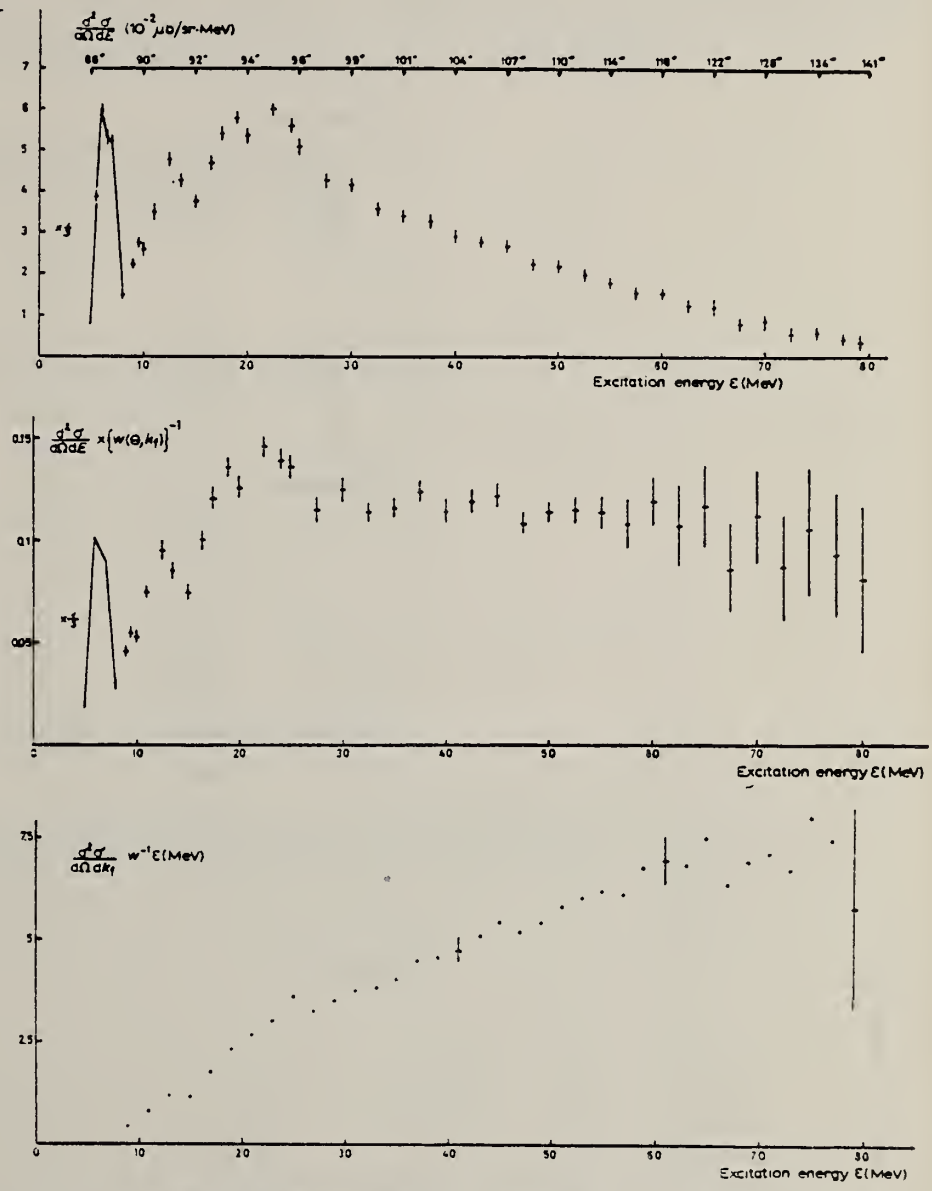

Fig. 2(a). The inelastic cross section for electron scattering by O^{16} as a function of excitation energy ε, for a fixed incident energy of 140 MeV. The scattering angles corresponding to different values of ε are indicated in the upper scale (taken to the nearest degree). (b) The inelastic cross section divided by the weighting factor. (c) The inelastic cross section divided by the weighting factor followed by weighting with the excitation energy ε MeV.

0	16	8

METHOD

REF. NO. 64 Bi 2

REACTION	RESULT	EXCITATION ENERGY	SOURCE		DETECTOR		ANGLE
			TYPE	RANGE	TYPE	RANGE	

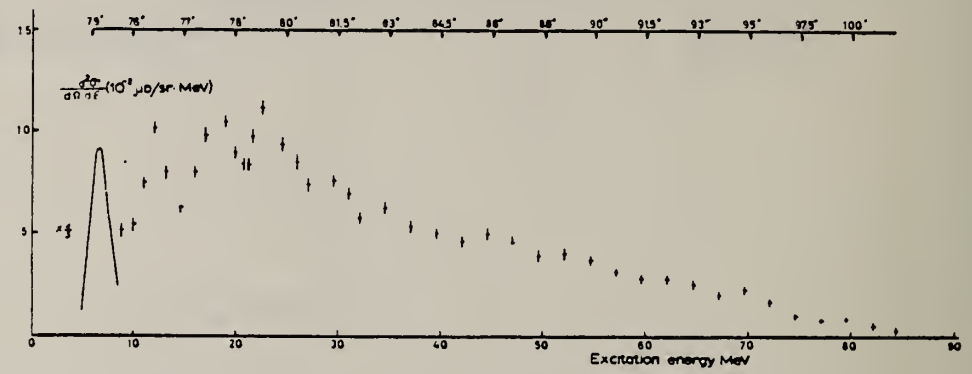

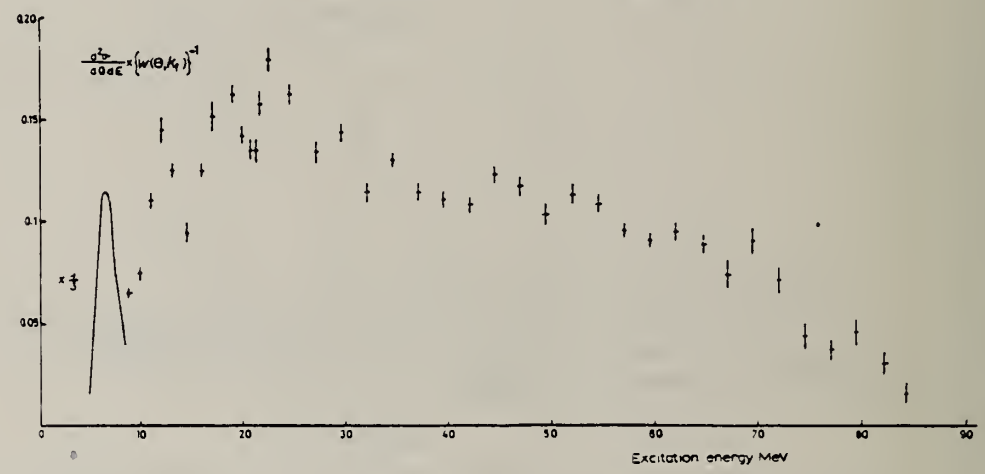

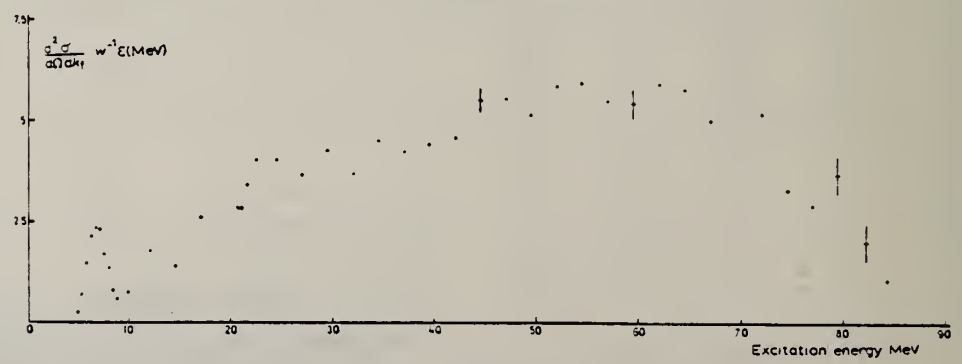

Fig. 3. Similar data to those of fig. 2 but obtained for a fixed incident energy of 160 MeV.

REF.

G. R. Bishop, C. Betourne and D. B. Isabelle
Nucl. Phys. 53, 366-374 (1964)

0	16	8

METHOD

Linac

[Page 1 of 4]

REF. NO. 64 Bi 3 JOC

REACTION	RESULT	EXCITATION ENERGY	SOURCE TYPE	SOURCE RANGE	DETECTOR TYPE	DETECTOR RANGE	ANGLE
E,E/	ABX	6 - 14	D	100-218	MAG-D		DST

400 keV resolution

FORM FACTORS

TABLE 1

The inelastic cross sections and form factors to the level doublets at 6.1 MeV and 6.9 MeV

Energy (MeV)	Angle	σ(6.1 MeV) ($10^{-2}\mu$b/sr)	F_{in}^2(6.1) ($\times 10^3$)	σ(6.9 MeV) ($10^{-2}\mu$b/sr)	F_{in}^2(6.9) ($\times 10^2$)
143.2	60°	47 ±9	2.42	47 ±9	2.42
120.3	90°	14.4 ±2.1	3.14		
148.5	70°	20.5 ±4.7	2.26	24.3 ±5.1	2.60
120.7	120°	5.58±0.84	5.51	5.3 ±1.8	5.11
148.4	90°	15.1 ±3	5.00	8.74±2.0	2.90
157.3	90°	16.7 ±2.5	6.24	9.7 ±1.6	3.60
160.5	100°	10.4 ±1.5	6.74	5.13±0.8	3.30
148.[illegible]	115°	5.41±0.8	6.20	3.3 ±0.7	3.82
15[illegible]	115°	4.86±0.8	6.10	2.9 ±0.5	3.61
15[illegible]	120°	4.50±0.6	7.8	2.25±0.42	3.90
160.1	120°	4.13±0.7	7.3		
16[illegible]	120°	3.86±0.7	6.8	2.22±0.4	3.90
217.5	80°	13.3 ±2.5	5.5	6.27±0.82	2.60
218.5	80°	17.0 ±2.5	7.2	6.61±0.85	2.80

The inelastic form factors are obtained by dividing the cross section by $\sigma_M = (Ze^2/2E)^2 \cos^2 \frac{1}{2}\theta / \sin^4 \frac{1}{2}\theta$.

TABLE 2

The inelastic cross sections and form factors of the peaks observed at 11.5 MeV, 12.0 MeV, 12.5 MeV, 13.2 MeV and 13.65 MeV

Energy (MeV)	Angle	σ(11.5 MeV) ($10^{-2}\mu$b/sr)	F_{in}^2(11.5) ($\times 10^3$)	σ(12.0 MeV) ($10^{-2}\mu$b/sr)	F_{in}^2(12.0) ($\times 10^3$)	σ(12.5 MeV) ($10^{-2}\mu$b/sr)	F_M^2(1.25) ($\times 10^4$)	σ(13.2 MeV) ($10^{-2}\mu$b/sr)	F_{in}^2(13.2) ($\times 10^2$)	σ(13.65 MeV) ($10^{-2}\mu$b/sr)	F_M^2(13.65) ($\times 10^4$)
101.6	60°	44 ±6	1.14	36 ±6	0.94	9.5 ±1.8	2.94	42.5 ±5	1.1	19.4 ±5	6.05
143.2	60°	30.6±4.6	1.58	24 ±3.5	1.23	5.2 ±1.2	3.21	19.5 ±3	1.0	15.0 ±3	9.30
160.6	80°	8.95±1.3	2.03	5.0 ±0.6	1.14	2.2 ±0.4	4.15	12.9 ±1.2	2.92	1.0 ±0.2	1.85
153.0	115°	1.22±0.2	1.52	0.54±0.06	0.67	0.35±0.07	1.47	2.31±0.3	2.90	0.34±0.06	1.44
144.4	135°	0.41±0.06	1.29	0.20±0.03	0.65	0.29±0.06	1.44	2.36±0.3	7.50	0.36±0.07	1.83
160.1	120°	0.48±0.07	0.85	0.23±0.03	0.41	0.24±0.05	1.23	1.99 0.30	3.5	0.31±0.06	1.57
218.5	80°	2.98±0.5	1.27	1.26±0.25	0.54	0.45±0.15	1.59	4.5 ±0.8	1.9	0.40±0.15	1.40

For electric transitions the form factors F_{in}^2 are obtained by dividing the experiment cross section by $\sigma_M = (Ze^2/2E)^2 \cos^2 \frac{1}{2}\theta / \sin^4 \frac{1}{2}\theta$. For magnetic transitions the form factors F_M^2 are obtained by dividing the experimental cross section by $\sigma_{point} = (Ze^2/2E)^2 (1+\sin^2 \frac{1}{2}\theta)/2 \sin^4 \frac{1}{2}\theta$.

EXCITATION LEVELS OF O^{16}

TABLE 3

The inelastic form factor of the peak at 13.2 MeV is compared with the form factors calculated by Willey from the wave functions of Gillet

Energy (MeV)	Angle	F_{in}^2(13.25 MeV) ($\times 10^3$)	F_x^2 (Willey) ($\times 10^3$)
101.6	60°	1.10±0.13	0.43
143.2	60	1.00±0.16	0.67
160.6	80°	2.92±0.27	
153.0	115°	2.90±0.38	3.92
144.4	135°	7.50±1.0	8.83
160.1	120°	3.5 ±0.55	5.01
218.5	80°	1.9 ±0.35	2.37

These calculated values correspond to the sum of transitions to $T = 1$ states with spins and parities 1^-, 2^- and 3^-. For the separate components see ref. [6]).

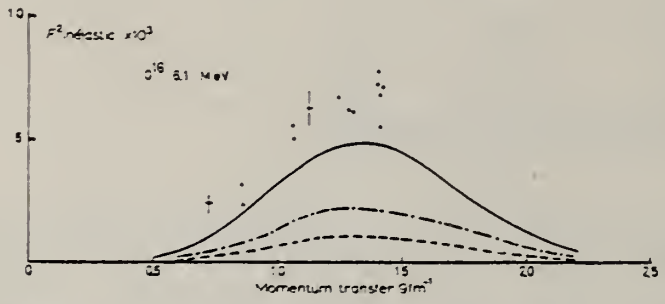

Fig. 1(a). The inelastic form factor of the 6.1 MeV peak taken from table 1. The full line is calculated for approximation II, the dot-dash line for approximation I and the dashed line for the I.P.M.

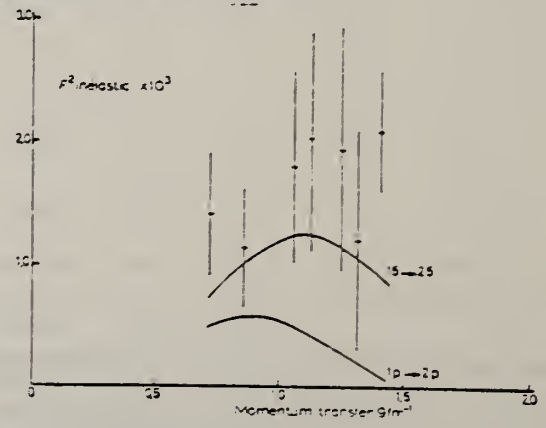

Fig. 1(b). The inelastic form factor which remains after subtraction of the full line curve of fig. 1(a) from the experimental points. For comparison the monopole form factor curves obtained as described in the text are also plotted.

REACTION	RESULT	EXCITATION ENERGY	SOURCE TYPE	SOURCE RANGE	DETECTOR TYPE	DETECTOR RANGE	ANGLE

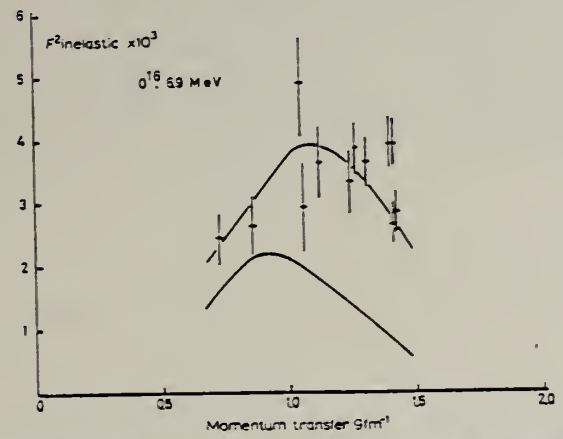

Fig. 2. The inelastic form factor of the 6.9 MeV peak. The upper curve represents the form factor $\langle 1s|j_3(qr)|1d\rangle^2$ and the lower curve the form factor $\langle 1p|j_3(qr)|1f\rangle^2$ each normalized to the radiative width as described in the text.

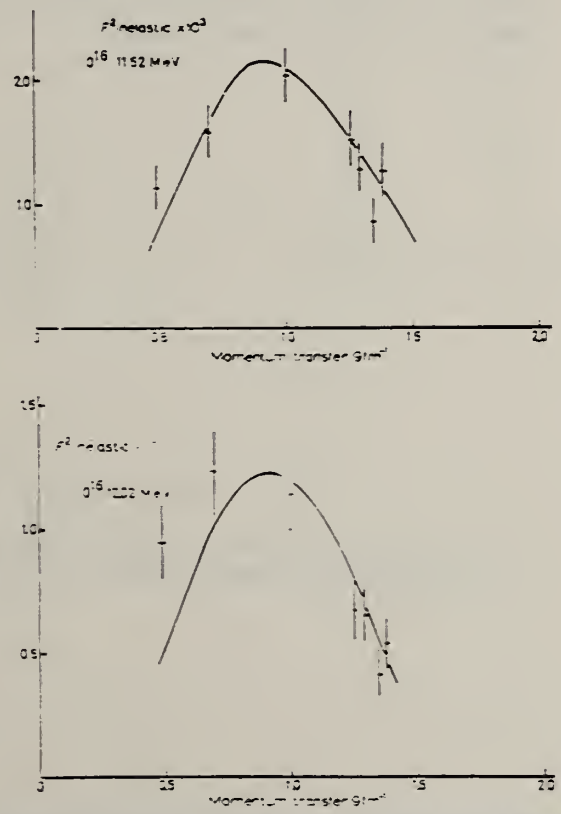

Fig. 3. The inelastic form factors of the 11.5 MeV and 12.0 MeV peaks. The fitted curve corresponds to the expression $F_{in}^2 = \langle p|j_3(qr)|1f\rangle^2$ normalized to give the radiative widths reported in the text.

REACTION	RESULT	EXCITATION ENERGY	SOURCE		DETECTOR		ANGLE
			TYPE	RANGE	TYPE	RANGE	

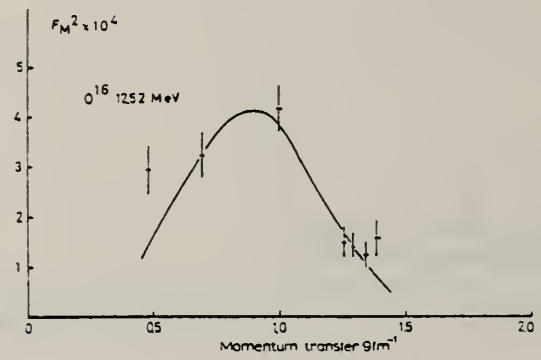

Fig. 4. The inelastic form factor of the 12.5 MeV peak. For this magnetic transition the form factor is obtained by dividing the experimental cross section by $\sigma_{point} = (Ze^2/2E)^2(1+\sin^2\frac{1}{2}\theta)/2\sin^4\frac{1}{2}\theta$. The full curve corresponds to the form factor discussed in the text.

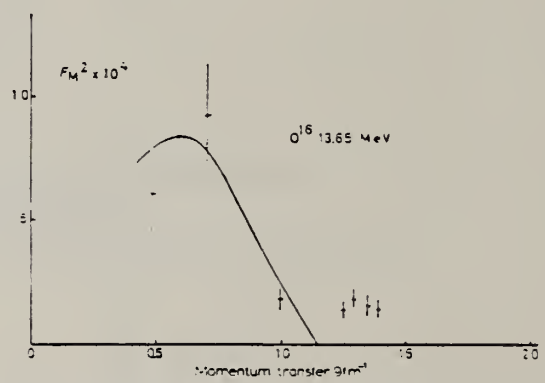

Fig. 5. The inelastic form factor of the 13.65 MeV peak considered as entirely transverse. The full line is the form factor calculated as described in the text. It has a zero value for $q = 1.35$ fm^{-1}.

REF.
R.L. Bramblett, J.T. Caldwell, R.R. Harvey, S.C. Fultz
Phys. Rev. 133, B869-73 (1964)

ELEM. SYM.	A	Z
O	16	8

METHOD
Positron annihilation; linac; ion chamber

REF. NO. 64 Br 1 NVB

REACTION	RESULT	EXCITATION ENERGY	SOURCE TYPE	SOURCE RANGE	DETECTOR TYPE	DETECTOR RANGE	ANGLE
G,N	ABX	15-30	D	15-30	BF3-I		4PI

PØS ANNIHIL.

$$\int_{15}^{24} \sigma(\gamma,n)dE = 23 \pm 2 \text{ MeV-mb}$$

$$\int_{15}^{30} \sigma(\gamma,n)dE = 46 \pm 5 \text{ MeV-mb}$$

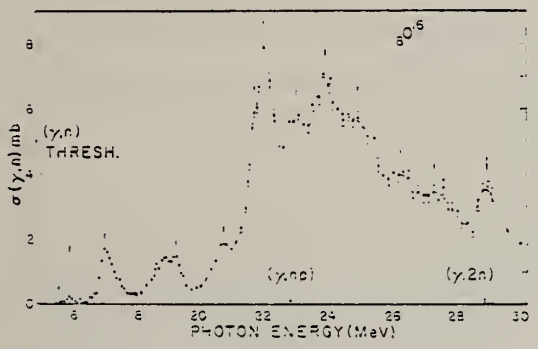

FIG. 3. Photoneutron cross section of O^{16} up to 30 MeV, showing resonances due to levels in O^{16}. The shell model predicts four electric dipole transitions in this energy range.

TABLE I. Energy levels observed for O^{16}.

$O^{16}(\gamma,n)4\pi$ (MeV) Present work	$O^{16}(\gamma,n)70°$ (MeV)[a]	$N^{15}(p,\gamma)$ (MeV)[b]	$O^{16}(e,p)76°$ (MeV)[c]
16.0		16.2(1+)	
		17.2(1−)	
17.1		17.3(1−)	17.3
19.0	19.1	19.0	19.0
19.3	19.6	19.5	19.6
20.8	20.7	20.8	20.6
	21.0		
21.8	21.7		
22.1	22.2	22.3	22.3
23.1	23.0	23.1	23.1
24.0	24.3	24.4	24.4
25.0	25.0	25.0	
	~25.4		
26.2	26.3		
27.3			
28.9			

[a] See Ref. 19.
[b] See Ref. 20.
[c] See Ref. 16.

W. Del Bianco, W.E. Stephens, J. Wiza
Phys. Rev. 136, B418 (1964)

0	16	8

METHOD

Van de Graaff; $Li^7(p,\gamma)$

REF. NO. 64 De 3 NVB

REACTION	RESULT	EXCITATION ENERGY	SOURCE TYPE	SOURCE RANGE	DETECTOR TYPE	DETECTOR RANGE	ANGLE
G,N	ABX	17 - 18	D	17-18	ACT-I		4PI

Obtained three γ energies by placing targets at three angles from proton beam:

45° $E\gamma$ = 17.666 MeV

90° $E\gamma$ = 17.618 MeV

135° $E\gamma$ = 17.571 MeV

Absolute cross section measured only at E_γ = 17.618 MeV; σ = 0.55 ± 0.08 mb.

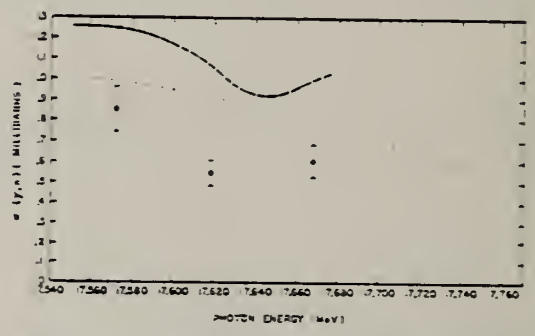

FIG. 2. Oxygen photoneutron cross section in millibarns as a function of photon energy in MeV. The points are the present results. The dashed curve represents the results of Keszthelyi *et al.* The dotted curve gives the corrected trend of Geller and Muirhead measurements.

REF.

E.D. Earle, N.W. Tanner and G.C. Thomas
Proc. Paris Conf. 385 (1964)

ELEM. SYM.	-	-
0	16	8

METHOD

Tandem

REF. NO.	
64 Ea 1	JDM

REACTION	RESULT	EXCITATION ENERGY	SOURCE		DETECTOR		ANGLE
			TYPE	RANGE	TYPE	RANGE	
P,G	NOX	13-25	D	1-13	NAI-D		DST

$W(\Theta) = \Sigma_l A_l P_l(\cos\Theta)$. The angular distribution curve is fitted by Least-Squares method.

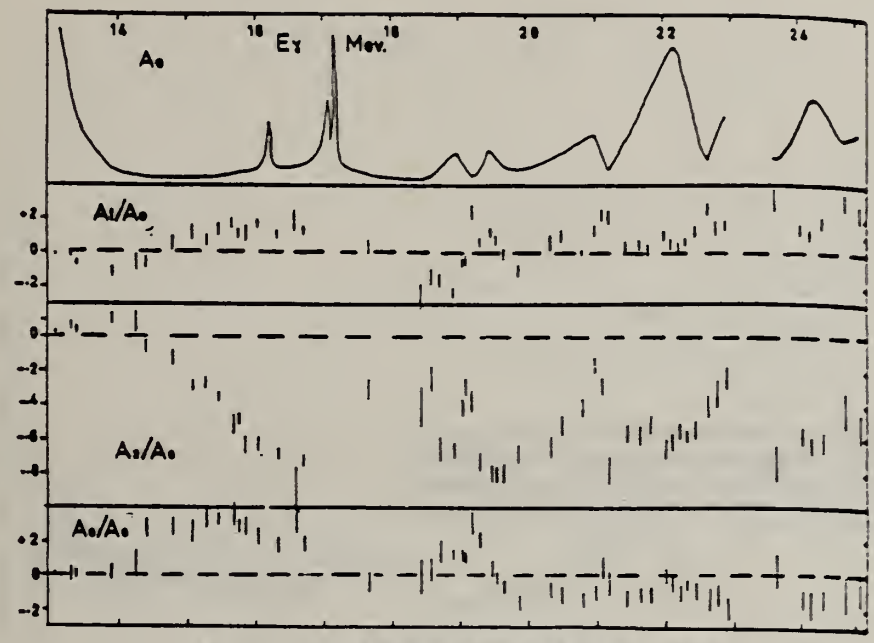

FIG. 1. — The Legendre polynomial coefficients for the $N^{15}(p,\gamma_0)O^{16}$ angular distributions

F. W. K. Firk
Nucl. Phys. 52, 437-48 (1964)

0	16	8

METHOD: Linac

REF. NO.: 64 Fi 1

JOC

REACTION	RESULT	EXCITATION ENERGY	SOURCE TYPE	SOURCE RANGE	DETECTOR TYPE	DETECTOR RANGE	ANGLE
G,XN	SPC	THR-32	C	25-32	TØF-D		70

213

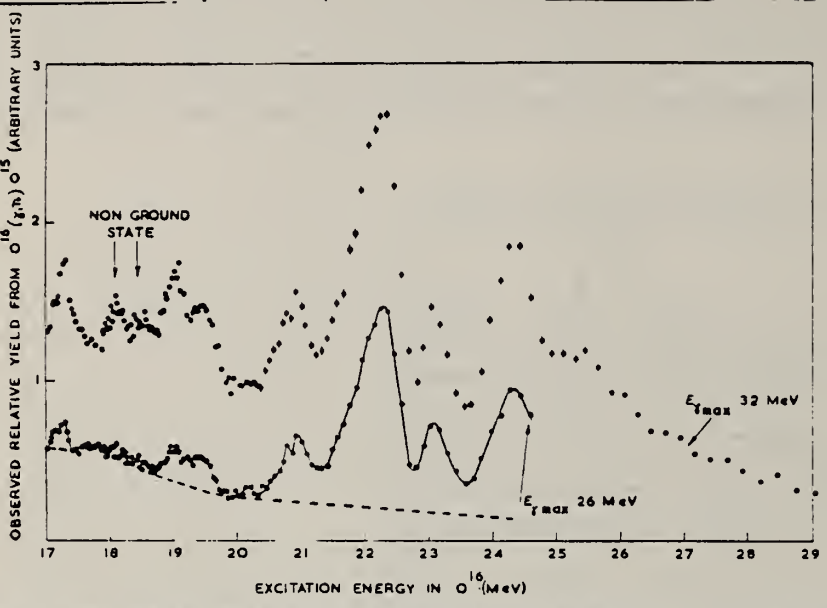

Fig. 1(a). The observed relative yields of photoneutrons from the reaction $O^{16}(\gamma, n)O^{15}$ assuming ground state transitions only. The bremsstrahlung energies are 26 and 32 MeV. No corrections have been made for background effects. The broken curve shown in the 26 MeV measurement indicates the background assumed in obtaining the relative intensities given in table 1. The time-of-flight resolution is 0.5 nsec · m^{-1}.

TABLE 1

A comparison between the present (γ, n_0) yields, the total (γ, n) yields [21] and the theoretical predictions of refs. [29, 30])

This experiment (ground state yield) E(MeV)	Rel. Int. %	Ref. [21]) (total neutron yield) E(MeV)	Rel. Int. %	Ref. [29]) E(MeV)	Rel. Int. %	Ref. [29]) E(MeV)	Rel. Int. %
17.10	0.5						
17.25	2.0	17.3	3	17.6	1	17.3	1
19.0	4.0	19.0	3				
19.4	4.0	19.3	3				
20.1	1.5			20.0	1	20.4	0
20.9	8.5	20.8	6				
21.6	2.5	21.7	1				
22.1 / 22.3	40	22.1	38	22.2	68	22.6	67
23.1	11	23.1	16				
24.1 / 24.3	26	24.1	30	25.0	29	25.2	32

Only the relative yields up to 25 MeV are considered.

REF.

F. W. K. Firk
Nucl. Phys. 52, 437-48 (1964)

ELEM. SYM.	A	Z
O	16	8

METHOD

Linac

REF. NO.

64 Fi 1

JOC

REACTION	RESULT	EXCITATION ENERGY	SOURCE		DETECTOR		ANGLE
			TYPE	RANGE	TYPE	RANGE	

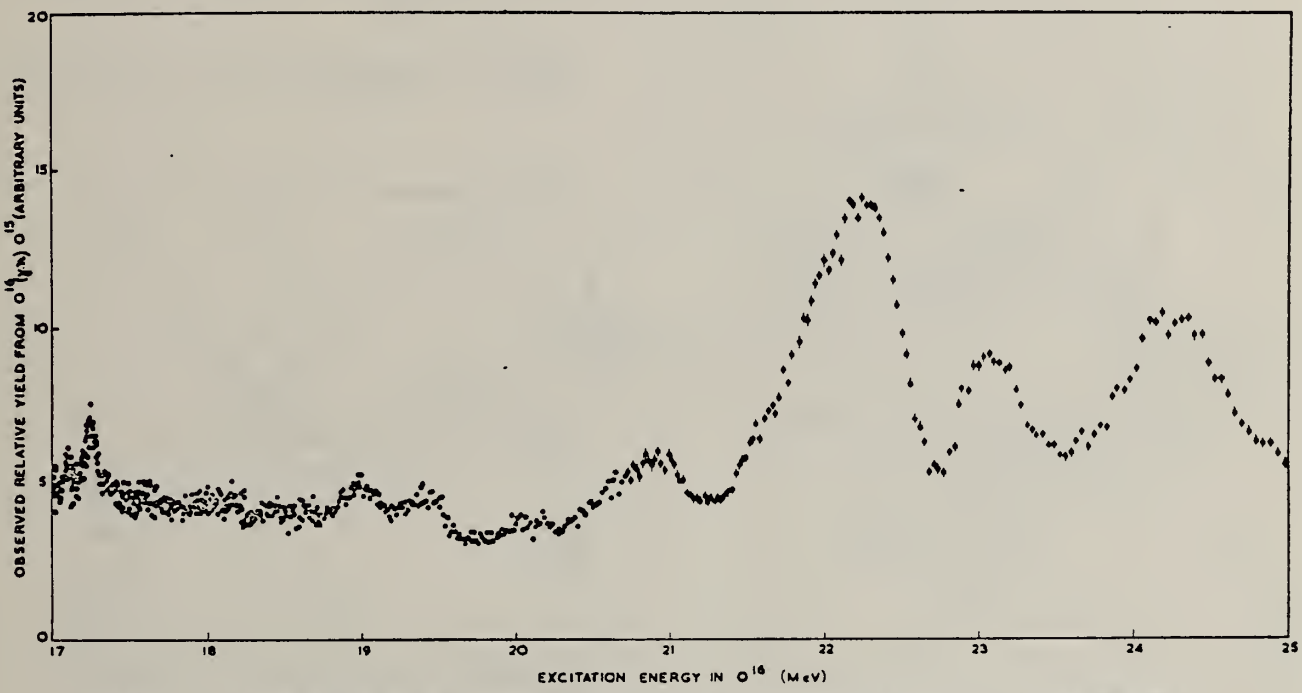

Fig. 1(b). The observed relative yield of photoneutrons from $^{16}O(\gamma, n)^{15}O$ when irradiated with 25 MeV bremsstrahlung. The resolution is 0.16 nsec · m^{-1}.

J. Goldemberg, W. C. Barber
Phys. Rev. 134, B963-71 (1964)

0	16	8

METHOD	REF. NO.	
Linac	64 Go 2	NVB

REACTION	RESULT	EXCITATION ENERGY	SOURCE		DETECTOR		ANGLE
			TYPE	RANGE	TYPE	RANGE	
E,E/	ABX	17-32	D	40-70	MAG-D		180

FMF

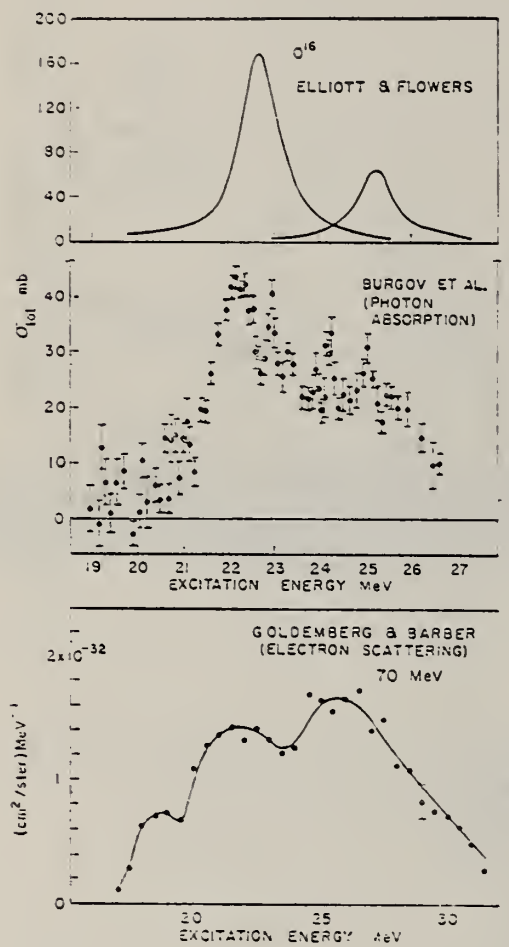

FIG. 10. The lower curve shows the cross section for inelastic scattering from oxygen derived from the spectrum shown in Fig. 9. The middle curve shows for comparison the total cross section for photon absorption by the oxygen nucleus. The upper curve shows the cross section for photon absorption in the region of the giant resonance as calculated by Elliott and Flowers.

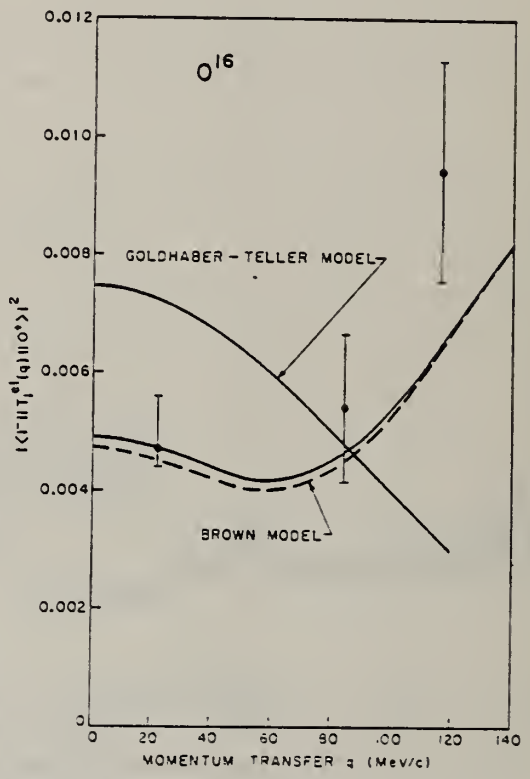

FIG. 13. The square of the form factor for the main part of the O^{16} giant resonance plotted as a function of momentum transfer. The experimental point at 23 MeV is from work with photons. The other three experimental points are from 180° electron scattering experiments. The curves are calculated on the basis of different theories as explained in the text.

REF.

L.H. Greenberg, J.P. Roalsvig, R.N. H. Haslam
Can. J. Phys. 42, 731-61 (1964)

ELEM. SYM.	A	Z
O	16	8

METHOD

Betatron; r-chamber

[Page 1 of 2]

REF. NO. 64 Gr 1 NVB

	REACTION	RESULT	EXCITATION ENERGY	SOURCE TYPE	SOURCE RANGE	DETECTOR TYPE	DETECTOR RANGE	ANGLE
1)	G,A	ABY	7-14	C	17,24	EMU-D		4PI
	G,4A	ABY	14-24	C	24	EMU-I		4PI

γ,4α Yield = 1470 ± 100 $\frac{\text{events}}{\text{mole-r}}$ at 24 MeV.

γ,α Yield = 10,500 ± 1300 $\frac{\text{events}}{\text{mole-r}}$ at 24 MeV.

γ,α Yield = 3,575 ± 40 $\frac{\text{events}}{\text{mole-r}}$ at 17 MeV.

1) SPC

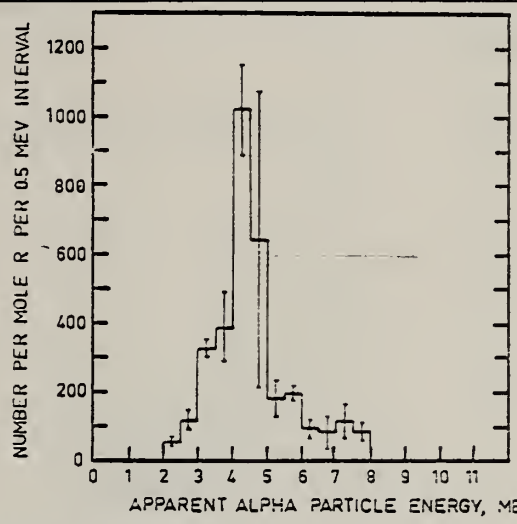

FIG. 8. The yield of alpha particles from oxygen as a function of apparent energy for 17-Mev bremsstrahlung.

True energy = 3/4 of apparent energy.

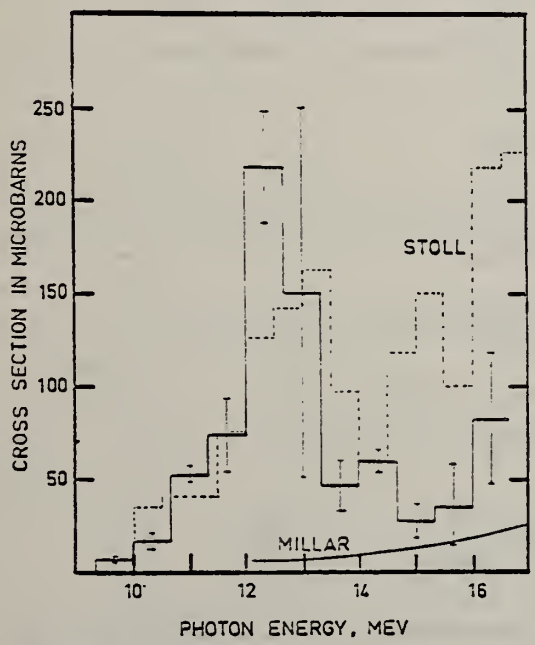

FIG. 9. The cross section for the reaction $O^{16}(\gamma, \alpha)C^{12}$ with C^{12} in the ground state.

Assumed ground-state transitions.

REACTION	RESULT	EXCITATION ENERGY	SOURCE TYPE	SOURCE RANGE	DETECTOR TYPE	DETECTOR RANGE	ANGLE

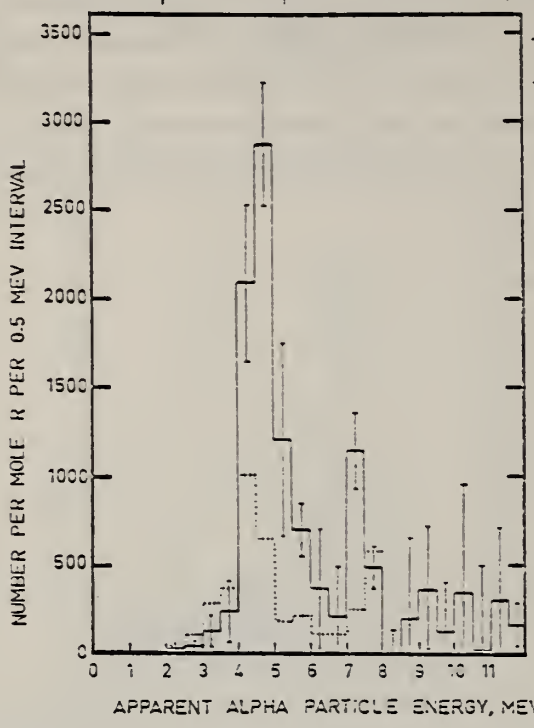

FIG. 10. The yield of alpha particles from oxygen as a function of apparent energy for 24-Mev bremsstrahlung. The dotted curve is the yield expected from $O^{16}(\gamma, \alpha)$ events with C^{12} in the ground state.

Excited states of O^{16} suggested:

E	J^{π}	T
12.5	2^+	0
possibly 14.3	2^+	0
20.8-21.0	2^+	0

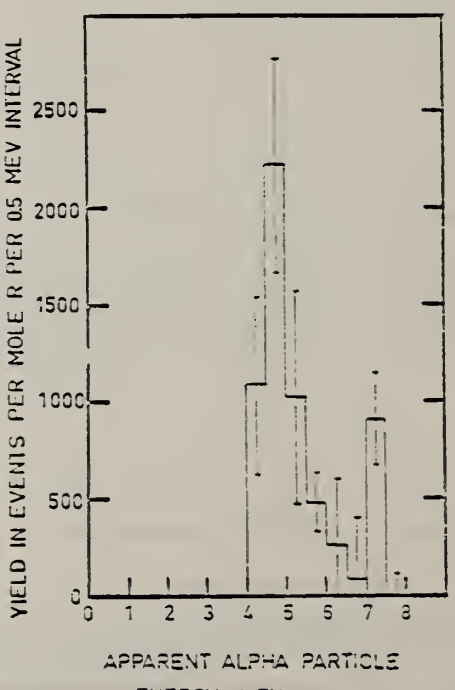

FIG. 11. The yield of alpha particles from the reaction $O^{16}(\gamma, \alpha)C^{12}$ from 24-Mev bremsstrahlung and for which the C^{12} is left in either the 4.43-Mev or the 7.70-Mev state.

REF.

J. D. Larson and R. H. Spear
Nucl. Phys. 56, 497-511 (1964)

[Page 1 of 2]

ELEM. SYM.	A	Z
0	16	8

METHOD

$C^{12}(\alpha,\gamma)$; Tandem

REF. NO. 64 La 2 JOC

REACTION	RESULT	EXCITATION ENERGY	SOURCE		DETECTOR		ANGLE
			TYPE	RANGE	TYPE	RANGE	
A,G	ABX	10-13	D	3-8	NAI-D		DST

J-PI, WIDTHS

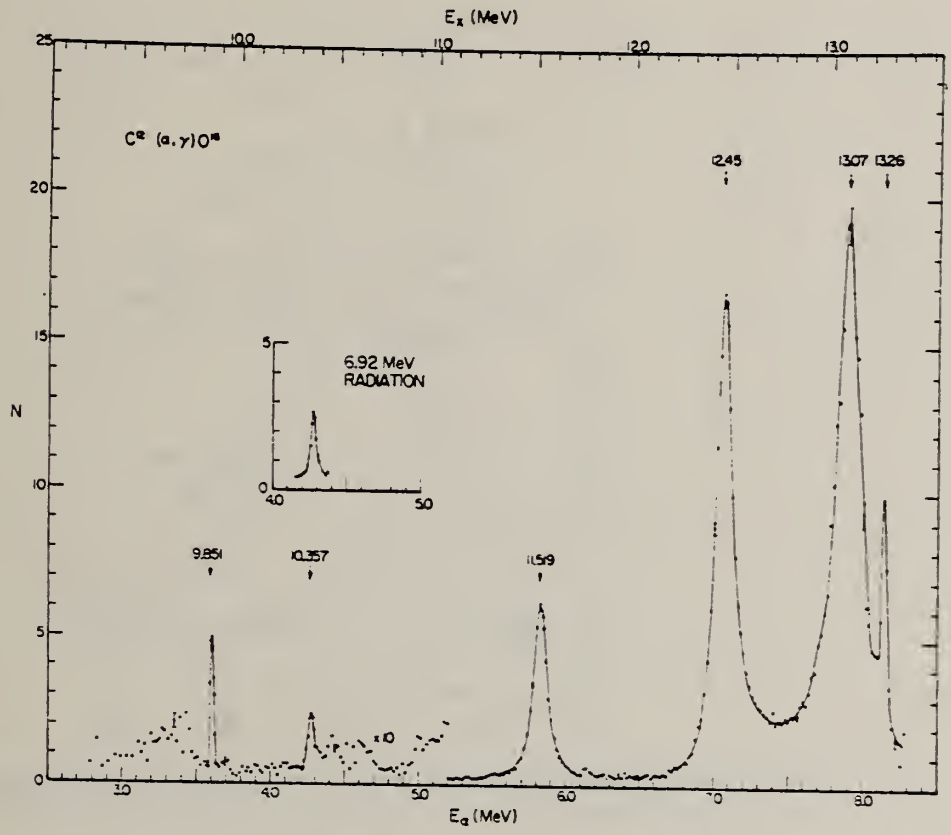

Fig. 2. Excitation function at 45° for the reaction $C^{12}(\alpha,\gamma)O^{16}$ using enriched C^{12} targets. The inset shows 6.92 MeV cascade radiation from the 10.36 MeV state.

TABLE I
Legendre polynomial coefficients for experimental angular distributions of ground state gamma rays from $C^{12}(\alpha,\gamma)O^{16}$

E_x (MeV)	a_0 (μb/sr)	a_1/a_0	a_2/a_0	a_3/a_0	a_4/a_0
7.06	2.8±0.3	0.02±0.04	−1.04±0.07	0.03±0.12	0.01±0.12
7.42	0.3±0.1	−0.04±0.24	−0.58±0.37	−0.16±0.59	0.15±0.62
7.88	2.5±0.3	0.47±0.05	−0.88±0.07	−0.36±0.12	−0.30±0.13
8.00	1.1±0.1	0.28±0.09	−0.70±0.13	−0.37±0.22	−0.12±0.23

Corrections for anisotropic absorption in the target backing and finite solid angle subtended by the detector have been made.

REACTION	RESULT	EXCITATION ENERGY	SOURCE TYPE	SOURCE RANGE	DETECTOR TYPE	DETECTOR RANGE	ANGLE

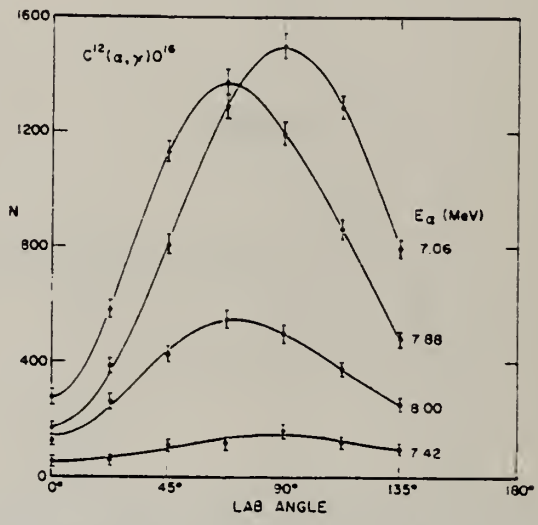

Fig. 4. Angular distributions for the reaction $C^{12}(\alpha, \gamma)O^{16}$ using an enriched C^{12} target. Solid curves represent a least-squares fit to the data by Legendre polynomials to fourth order.

TABLE 3

Radiative widths for some transitions observed in $C^{12}(\alpha, \gamma)O^{16}$

Initial state E_x (MeV)	Final state E (MeV)	Measured radiative width Γ_γ (eV)	Multipolarity of transition	$\lvert M\rvert^2$
9.59 (1^-)	0 (0^+)	0.022 $\pm$0.005	E1	5.8×10^{-4}
9.85 (2^+)	0 (0^+)	0.0059 $\pm$0.0006	E2	0.032
9.85 (2^+)	7	0.0012 $\pm$0.0004		
10.36 (4^+)	6.92 (2^+)	0.046 $\pm$0.006	E2	49
11.52 (2^+)	0 (0^+)	0.66 $\pm$0.09	E2	1.6
12.45 (1^-)	0 (0^+)	7 $\pm$1	E1	0.008

Spins and parities are taken from previous work; $\lvert M\rvert^2$ represents the ratio of the measured radiative width to the width calculated from an extreme single-particle model assuming a nuclear radius, $r = 1.2\,A^{\frac{1}{3}}$ fm.

REF.
M. Langevin, J. M. Loiseaux and J. M. Maison
Proc. Paris Conference 1045 (1964)

ELEM. SYM.	A	Z
O	16	8

METHOD

REF. NO.	
64 La 5	JDM

REACTION	RESULT	EXCITATION ENERGY	SOURCE		DETECTOR		ANGLE
			TYPE	RANGE	TYPE	RANGE	
G,G	RLX	THR-32	C	24,32	NAI-D	2-27	DST

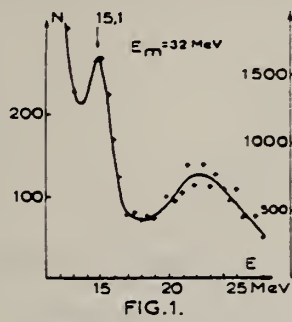

FIG.1.

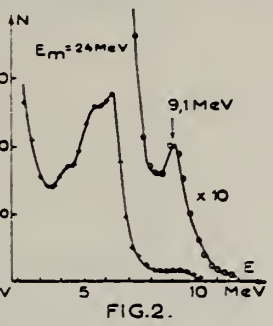

FIG.2.

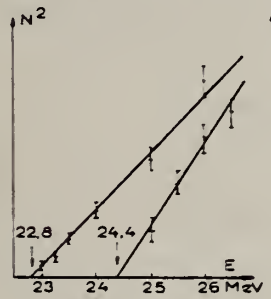

FIG.3.

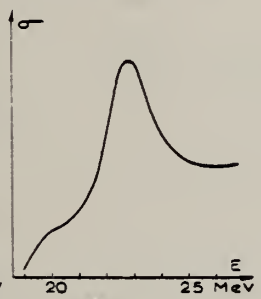

FIG.4.

J. M. Loiseaux, M. Langevin and J. M. Maison
Proc. Paris Conf. 1048 (1964)

0	16	8

METHOD: Betatron

REF. NO.: 64 Lo 3

JDM

REACTION	RESULT	EXCITATION ENERGY	SOURCE		DETECTOR		ANGLE
			TYPE	RANGE	TYPE	RANGE	
G,G	ABX	10-30	C	10-30	NAI-D		140

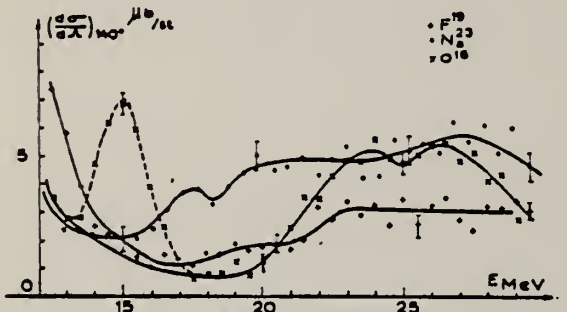

FIG. 2

The effective differential scattering cross section remains quite constant from 20-30 MeV.

REF.

I. V. Mitchell and T. R. Ophel
Nucl. Phys. 58, 529-43 (1964)

ELEM. SYM.	A	Z
O	16	8

METHOD

$C^{12}(\alpha,\gamma_0)O^{16}$; Van de Graaff

REF. NO. 64 M1 1 JOC

REACTION	RESULT	EXCITATION ENERGY	SOURCE TYPE	SOURCE RANGE	DETECTOR TYPE	DETECTOR RANGE	ANGLE
A,G	RLX	13	D	7-8	NAI-D		DST
				(6.9-8.2)			

Level at E_α = 7.90 MeV, $\Gamma_\gamma(2^+) \approx 0.6 \pm 0.3$ eV $\approx 5\%$ of E2 sum rule limit.

J-PI, WIDTH

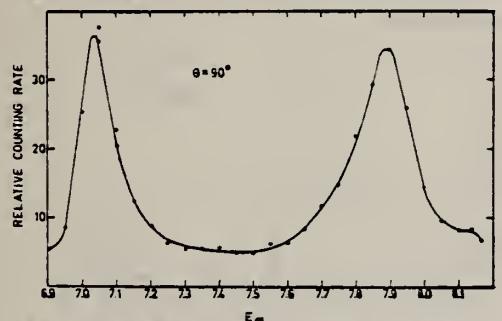

Fig. 3. Excitation function of the $C^{12}(\alpha,\gamma_0)$ reaction at 90°. Statistical errors are ±3% or less.

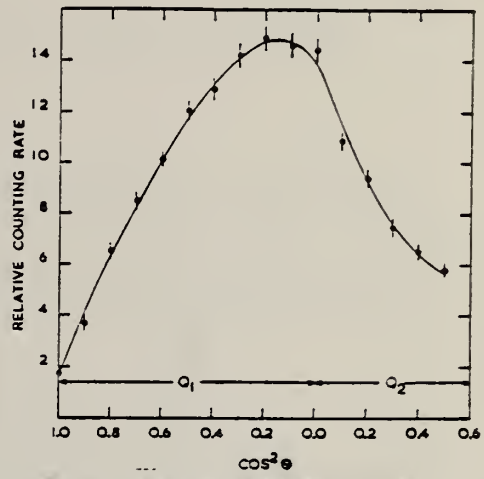

Fig. 6. Angular distribution of the $C^{12}(\alpha,\gamma_0)$ reaction at E_α = 7.90 MeV.

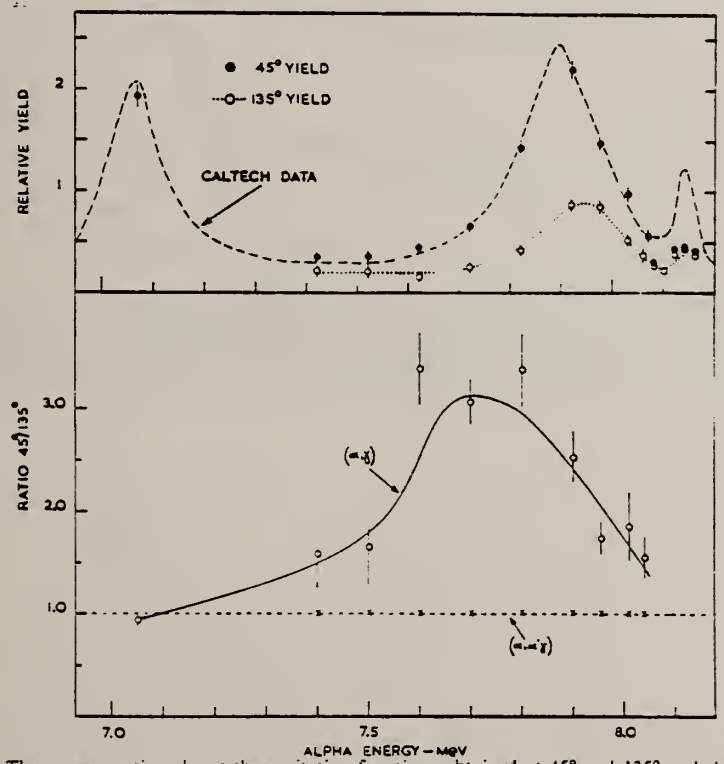

Fig. 5. The upper portion shows the excitation functions obtained at 45° and 135° and the lower portion of the diagram illustrates the ratio of the yields at 45° and 135° as a function of energy. The data in the upper diagram are displaced upwards by 20 keV for comparison with the data of Larson and Spear[15]). (J.D. Larson and R.H.Spear Bull.Am.Phys. Soc. 6(1961)505 and private communication)

M. Suffert, G. Costa and D. Magnac-Valette
Proc. Paris Conf. 1054 (1964)

0	16	8

METHOD

REF. NO. 64 Su 1 JDM

REACTION	RESULT	EXCITATION ENERGY	SOURCE		DETECTOR		ANGLE
			TYPE	RANGE	TYPE	RANGE	
D,G	ABX	21- 25	D	1-5	NAI-D		DST

At 22.7 MeV

$$W(\theta) = 1 + 0.11\ P_1 - 0.47\ P_2 - 0.28\ P_3$$

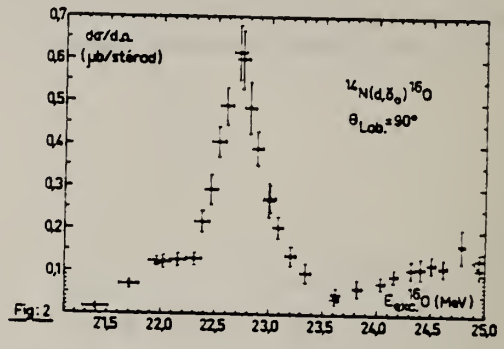

Fig: 2

REACTION	RESULT	EXCITATION ENERGY	SOURCE		DETECTOR		ANGLE
			TYPE	RANGE	TYPE	RANGE	
P,G	ABX	16-26	D	4-14	NAI-D		DST

3o

At E_p = 5.52 MeV $\frac{d\sigma\gamma_o}{dr}$ = 145±35 μb/4πsr

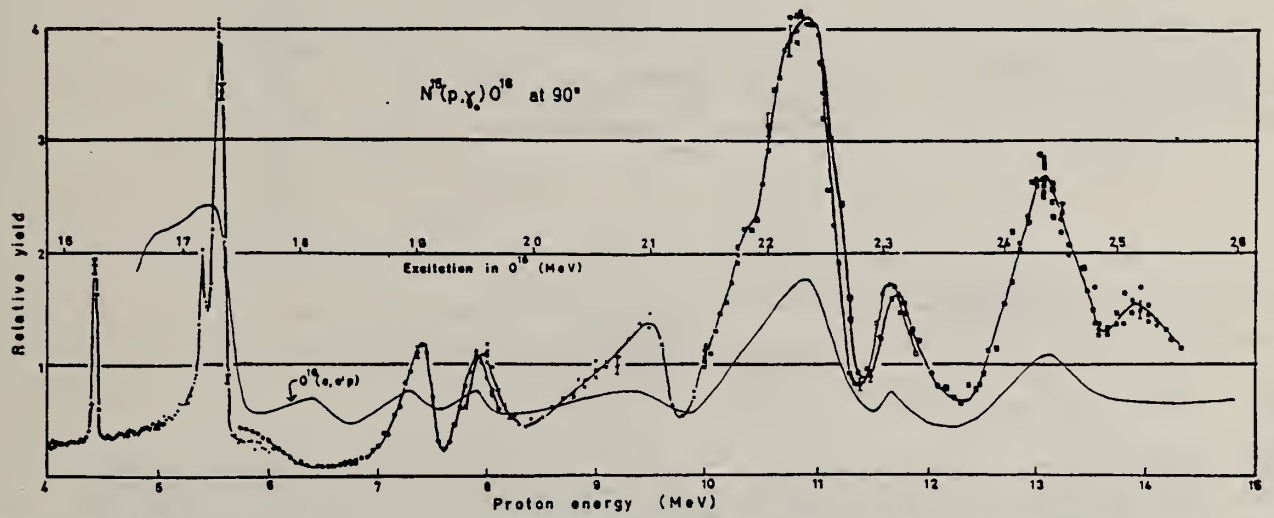

Fig. 2. The experimental excitation function of $N^{15}(p, \gamma_0)O^{16}$ at 90° to the beam. The normalization of the various runs is described in the text. For more detail, see figs. 3, 5, 9 and 10. + – Run A. 4.0 to 5.07 MeV. Target thickness 25 keV. ● – Run B. 5.0 to 6.0 MeV and one point at 9 MeV. 25 keV target ○ – Run. C. 5.75 to 8.10 MeV. 50 keV target × – Run D. 7.8 to 10 MeV and two points at 10.8 MeV. 58 keV target. □ – Run E. 10 to 11.9 MeV. 30 keV target. ■ – Run F. 10.75 to 14.3 MeV. 63 keV target. The $O^{16}(e, e'p)$ results of ref. [18]) are also shown. They have been converted by detailed balance to $N^{15}(p, \gamma)$, but are not normalized to our scale.

REACTION	RESULT	EXCITATION ENERGY	SOURCE		DETECTOR		ANGLE
			TYPE	RANGE	TYPE	RANGE	

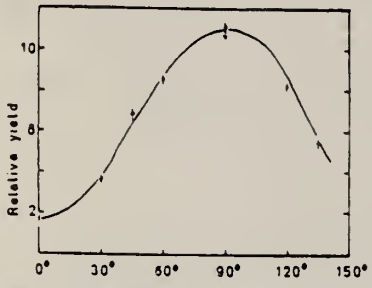

Fig. 4. The angular distribution of γ-rays on the top of the 4.372 MeV resonance. Target thickness, 11 keV. The curve drawn is $1+10\sin^2\theta+0.7\cos\theta$.

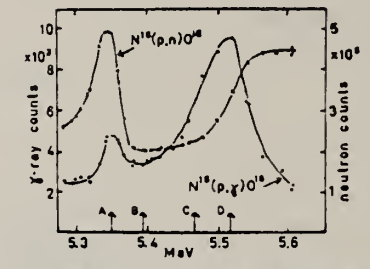

Fig. 5. The excitation functions near 5.5 MeV of $N^{15}(p,\gamma_0)O^{16}$ at 90° and $N^{15}(p,n)O^{15}$ at 0°. The two reactions were measured simultaneously.

TABLE 1
Analysis of electric dipole states of O^{16}

Experimental				Theoretical				
				Gillet [7])		Mikeska and Brenig [28])		
E_γ (MeV)	Γ (MeV)	$\int\sigma_{abs}$ (MeV · mb) [a])	% $\int_{12}^{26.5}\sigma_{abs}$	E_γ (MeV)	% sum rule	E_γ (MeV)	% Sum rule	Γ (MeV)
12.43 [b])	0.08	0.69	9.3	13.5	4	13.7	1	Sharp
13.09 [b])	0.11	17						
17.0	≈1	≈10						
17.13	0.044	0.8	7.7	18.1	1	17.5	1	0.5
17.29	0.090	4.0						
19.05	≈0.35							
19.56	≈0.40	95 (18.0 to	50	19.6	3	19.3	1	Sharp
21.0	≈0.80	23.75 MeV)		22.2	73	22.5	58	0.75
22.2	0.85							
23.0	≈0.60							
24.3	≈1	63 (23.75 to	33	25.2	20	25.6	39	1.0
25.2	≈0.5	26.5 MeV)						

[a]) Above 19 MeV, from the work of Burgov *et al.* [62]).
[b]) From Hebbard [34]).
The errors in the experimental cross-sections are of the order of 20 % while those in the % column are smaller.

N.W. Tanner and E.D. Earle
Phys. Rev. Letters 13, 410 (1964)

0	16	8

METHOD: Interpretation of data

REF. NO.: 64 Ta 4 | JOC

REACTION	RESULT	EXCITATION ENERGY	SOURCE TYPE	SOURCE RANGE	DETECTOR TYPE	DETECTOR RANGE	ANGLE
G,N	SPC	16-26	D	34	TØF		90

INTERPRETATION

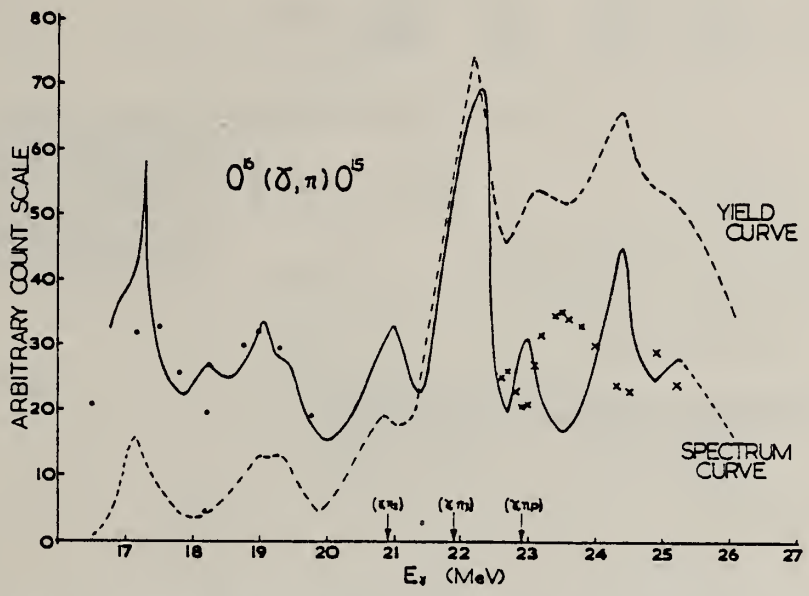

FIG. 1. Comparison of the neutron yield curve[4] of $O^{16}(\gamma,n)O^{15}$ with the neutron spectrum from bremsstrahlung irradiation.[1] The crosses show the difference between these two curves and indicate the yield of neutrons to excited states of O^{15}. The dots show the spectrum implied by the yield curve and the crosses, assuming neutron transitions only to the ground and 6.2-MeV states of O^{15}.

G. Tessler, W.E. Stephens
Phys. Rev. 135, B129-36 (1964)

0	16	8

METHOD: Tandem, $T^3(p,\gamma)$

REF. NO.: 64 Te 1 | NVB

REACTION	RESULT	EXCITATION ENERGY	SOURCE TYPE	SOURCE RANGE	DETECTOR TYPE	DETECTOR RANGE	ANGLE
G,MU-T	ABX	20-22	D	20-22	NAI-I		96

WATER TARGET

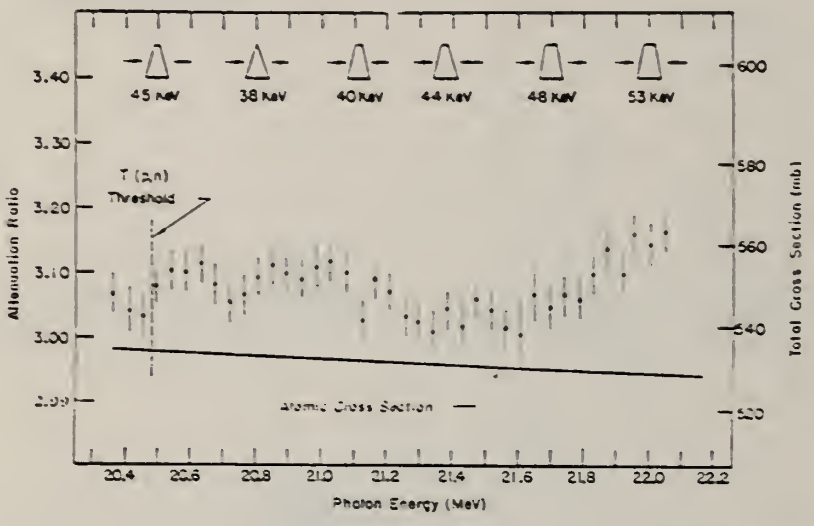

FIG. 5. Attenuation ratio for gamma rays in water as a function of photon energy. The total absorption cross section scale in millibarns is given also. The solid line is the calculated atomic cross section. The trapezoids illustrate the calculated resolution function.

TABLE IV. Structure observed in the nuclear absorption cross section curves.

Element	E_{peak} (MeV)	σ_{peak} (mb)	Half-width (MeV)	$\int_{peak}\sigma dE$ (MeV-mb)
Be^9	20.47	6.8	0.13	0.45
	20.73	10.1	0.15	0.9
O^{16}	20.62	21.5	0.19	3.9
	21.03 (20.56, 21.05)	23.5	~0.40	10.4
	>22			
F^{19}	20.09	21.9	0.16	3.5

M. Elaine Toms
Nucl. Phys. 54, 625-640 (1964)

[page 1 of 2]

0	16	8

METHOD

Betatron

REF. NO.

64 To 2 | JOC

REACTION	RESULT	EXCITATION ENERGY	SOURCE		DETECTOR		ANGLE
			TYPE	RANGE	TYPE	RANGE	
G,A	ABX	THR - 22	C	22	EMU-D		DST
G,4A	ABX	THR - 22	C	22	EMU-D		DST

48 events (γ,a) $\int_{\cdot}^{21.5} d\bar{E}_{\gamma} \sigma_{a} = 0.055 \pm .008$ MeV-mb

53 events $(\gamma,4a)$ $\int_{\cdot}^{21.5} d\bar{E}_{\gamma} \sigma_{4a} = 0.124 \pm 0.017$ MeV-mb

In (γ,a) E2/E1 = 0.3 for assumed ground state transitions.

E2/E1 = 0.2 for 7.7 MeV state

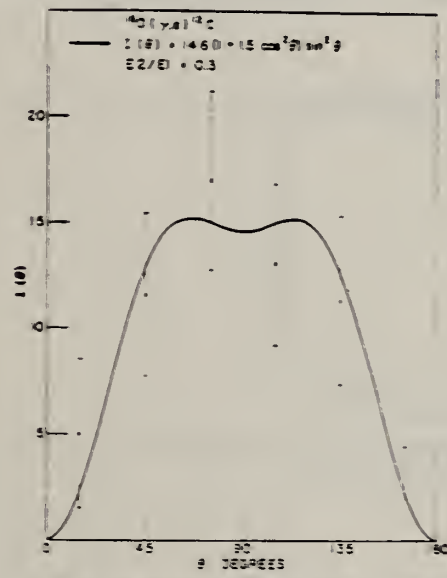

Fig. 4. The intensity distribution $I(\theta) = N(\theta)$ cosec θ in 30° intervals of θ, where θ is the angle between the alpha and the photon direction. The curve $I(\theta) = 14.6(1 + 1.5 \cos^2 \theta) \sin^2 \theta$ is based on the assumption that ^{12}C is left in its ground state. A ratio of the intensities of photon interactions E2/E1 = 0.3 is indicated from the fit of the curve.

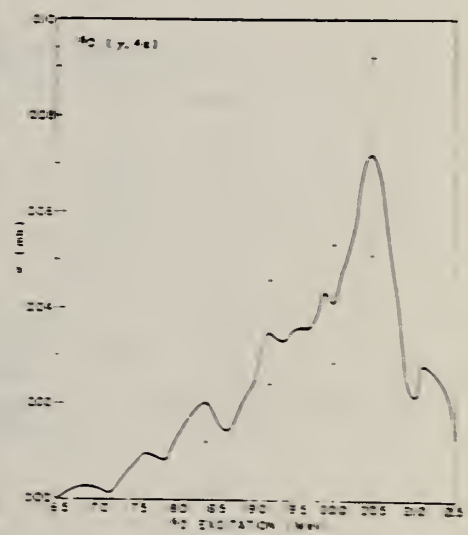

Fig. 5. The cross-section for the $^{16}O(\gamma, 4\alpha)$ reaction versus ^{16}O excitation energy.

0	16	8

METHOD

REF. NO. 64 To 2

REACTION	RESULT	EXCITATION ENERGY	SOURCE		DETECTOR		ANGLE
			TYPE	RANGE	TYPE	RANGE	

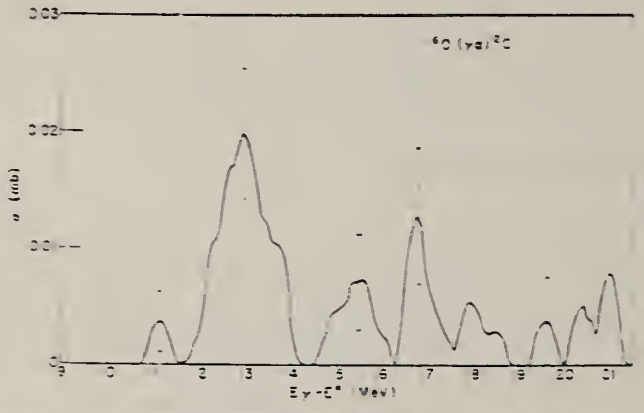

Fig. 3. The cross-section for the $^{16}O(\gamma, \alpha)^{12}C$ reaction versus $E_\gamma - E^*$ where E_γ is the photon energy if E^* equals zero and E^* can be either zero or 4.43 MeV, the ^{12}C excitation energy.

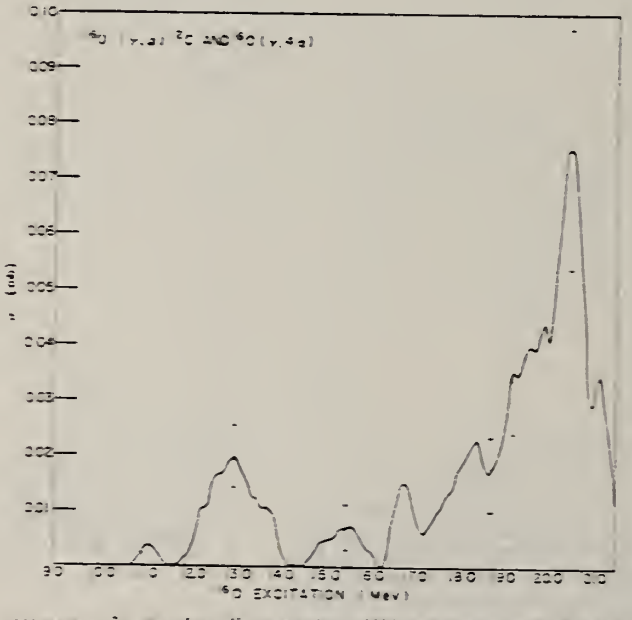

Fig. 12. The cross-section for the photodisintegration of ^{16}O yielding an alpha particle of four alpha particles. (Combination of figs. 3 and 5).

REF.

M. E. Toms
Proc. Paris Conference 1004 (1964)

ELEM. SYM.	A	Z
O	16	8

METHOD

REF. NO. 64 To 3 JDM

REACTION	RESULT	EXCITATION ENERGY	SOURCE		DETECTOR		ANGLE
			TYPE	RANGE	TYPE	RANGE	
G,A	ABX	9-21	C	22	EMU		DST
G,4A	ABX	9-21	C	22	EMU		DST

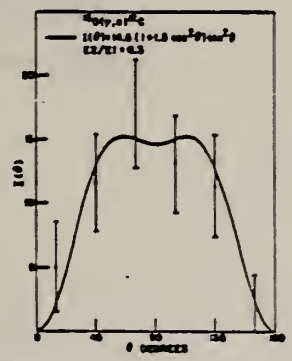

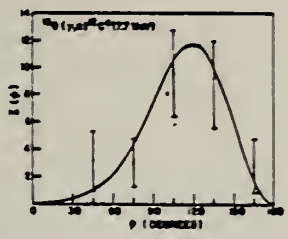

FIG. 1. — The intensity distribution $I(\theta) = N(\theta)$ cosec θ where θ is the angle between the alpha and the photon direction for single alphas from ^{16}O.

FIG. 2. — The intensity distribution $I(\phi) = N(\phi)$ cosec ϕ where ϕ is the angle between the first alpha and the photon direction leaving ^{12}C in the 7.7 MeV state.

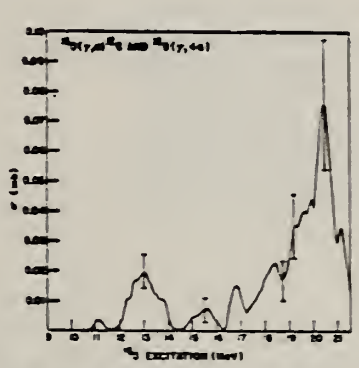

FIG. 3. — The cross-section for the photodisintegration of ^{16}O yielding an alpha particle or four alpha particles.

P.F. Yergin, R.H. Augustson, N.N. Kaushal, H.A. Medicus, W.R. Moyer, and E.J. Winhold
Phys. Rev. Letters 12, 733 (1964)

0	16	8

METHOD	REF. NO.	
Linac	64 Ye 1	JOC

REACTION	RESULT	EXCITATION ENERGY	SOURCE		DETECTOR		ANGLE
			TYPE	RANGE	TYPE	RANGE	
G,XN	SPC	THR - 35	C	35	TØF-D		90

BRANCHING RATIØS

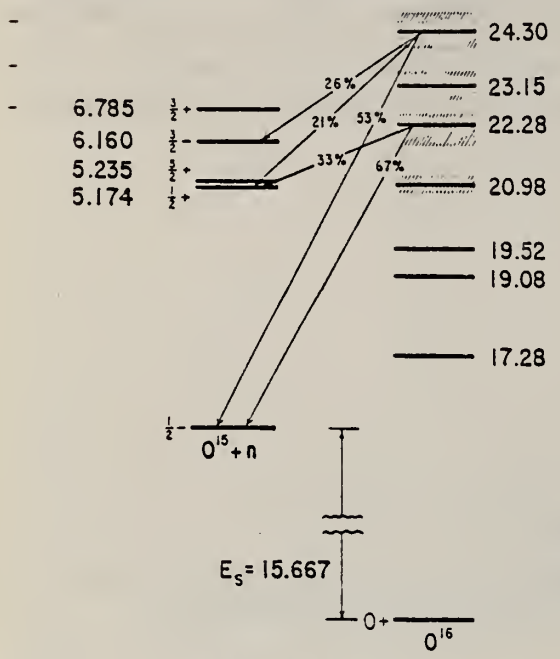

FIG. 1. Some energy levels of O^{16} and O^{15}. Only those levels of O^{16} which appear prominently in the photoneutron spectrum are shown. The energies are those measured in this experiment. All known levels of O^{15} up to the highest shown are included. The branching ratios for the neutron decays at 90° from the 22.2- and 24.3-MeV levels are those deduced from the measurements reported here. Ground-state decays only are observed for the other levels.

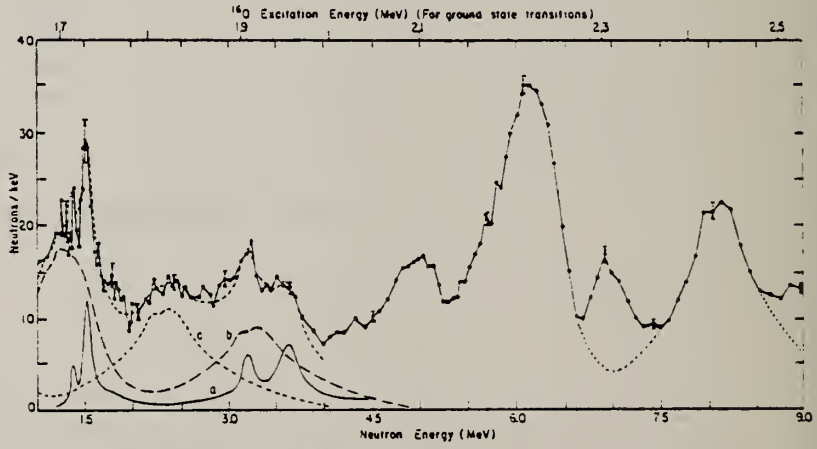

FIG. 2. Neutron spectrum from O^{16} photodisintegration by 35-MeV bremsstrahlung. The points connected by the solid lines, with typical error bars shown, are the experimental results corrected for the detector efficiency. From 1.0 to 1.2 MeV twelve channels of the time analyzer were averaged, from 1.2 to 4.9 MeV four channels, and above 4.9 MeV two channels. The upper dashed curve from 1.0 to 4.0 MeV is the composite fit to the data and is the sum of the lower three curves. (a) is derived from the cross-section curve of reference 14, (b) represents neutrons which leave O^{15} in the $\frac{1}{2}^-$ first excited state, and (c) represents neutrons which leave O^{15} in the $\frac{3}{2}^-$ third excited state. See the text for explanation of the dashed curve sections above 5 MeV. The scale at the top gives the excitation energy in O^{16} for the case of neutrons which leave O^{15} in its ground state. The ordinate is in arbitrary units, and represents the number of neutrons per unit energy interval.

H. Artus
Z. Naturforschg. 20, 320 (1965)

ELEM. SYM.		
0	16	8

METHOD

REF. NO.: 65 Ar 3 | JOC

REACTION	RESULT	EXCITATION ENERGY	SOURCE		DETECTOR		ANGLE
			TYPE	RANGE	TYPE	RANGE	
G,BE7	RLY	32-57	C	57	ACT-I		4PI

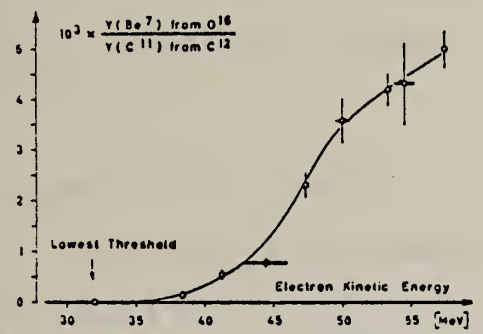

Fig. 1. Measured ratios of the yields $Y(Be^7)/Y(C^{11})$ as a function of electron kinetic energy E_m.

REF.

H. v. Buttlar and A. Goldmann
Z. Physik 187, 355 (1965)

ELEM. SYM.	A	Z
O	16	8

METHOD

Linac; Measured yield relative to $C^{12}(\gamma,n)C^{11}$

REF. NO. 65 Bu 1 JDM

REACTION	RESULT	EXCITATION ENERGY	SOURCE		DETECTOR		ANGLE
			TYPE	RANGE	TYPE	RANGE	
G,T	RLY	THR - 50	C	50	ACT-I		4PI

$Y[O(\gamma,t)] = Y_3$

$Y[C^{12}(\gamma,n)C^{11}] = Y_{11}$

$Y_3/Y_{11} = (2.0 \pm 0.2)10^{-2}$ $(E_{max}) = 50$ MeV.

The (γ,t) reaction below 50 MeV carries 0.4% of the bremsstrahlung-weighted cross section and less than 1% of the dipole sum for O^{18}.

REF. J. T. Caldwell, R. L. Bramblett, B. L. Berman, R. R. Harvey, and S. C. Fultz
Phys. Rev. Letters 15, 976 (1965)

ELEM. SYM.	A	Z
O	16	8

METHOD

REF. NO. 65 Ca 1 joc

REACTION	RESULT	EXCITATION ENERGY	SOURCE TYPE	SOURCE RANGE	DETECTOR TYPE	DETECTOR RANGE	ANGLE
G,XN	ABX	17- 28	D	17- 28	BF3-I		4PI

BRANCHING RATIOS 38+

$$\int_{21.5}^{26} \sigma_{g.s.}\, dE = 15.2 \pm 1.5 \text{ MeV-mb}$$

$$\int_{Thr}^{26} \sigma_{3/2^-}\, dE = 12.7 \pm 1.3 \text{ MeV-mb}$$

$$\frac{\int \sigma_{3/2^-}}{\int \sigma_{g.s.}} = 0.84 \pm 0.08$$

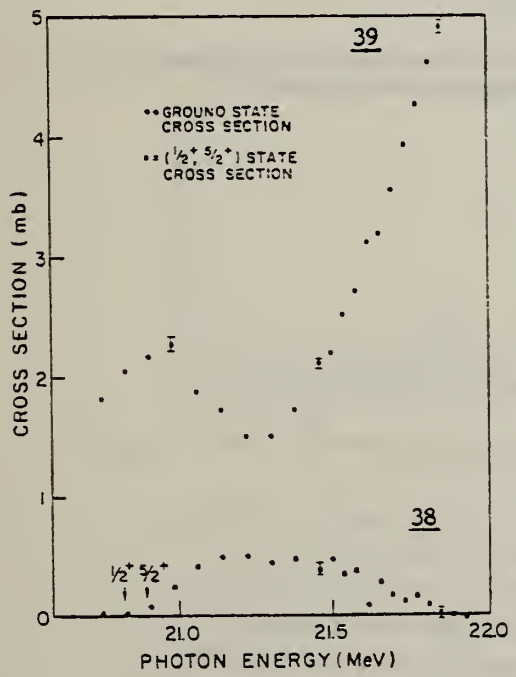

FIG. 2. Integrated-over-angle cross sections for $O^{16}(\gamma,n)$ in the region 21 to 22 MeV.

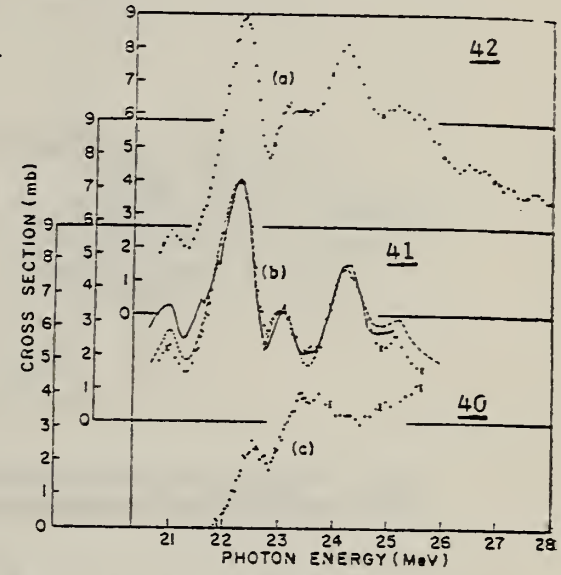

Fig. 3. (a) The total integrated-over-angle (γ,n) cross section, which is the sum of the ground-state and all excited-state cross sections. (b) Ground-state-only cross section. The solid-line curve is the neutron spectrum of Yergin et al.[1] and the dashed-line curve is the ground-state cross section of V. V. Verbinsky, J. C. Courtney, D. F. Herring, R. B. Walton, and R. E. Sund, Bull. Am. Phys. Soc. 9, 628 (1964); and to be published. (c) The 6.16-MeV ($\frac{3}{2}^-$) excited-state cross section.

REF.

J. T. Caldwell, R. L. Bramblett, B. L. Berman, R. R. Harvey, and S. C. Fultz
Phys. Rev. Letters 15, 976 (1965)

0	16	8

METHOD

REF. NO. 65 Ca 1 JOC

REACTION	RESULT	EXCITATION ENERGY	SOURCE		DETECTOR		ANGLE
			TYPE	RANGE	TYPE	RANGE	

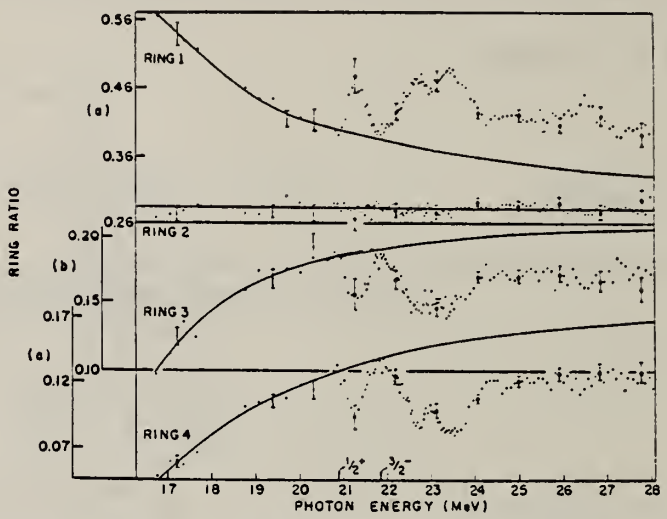

FIG. 1. Ring ratios obtained for the $O^{16}(\gamma,n)$ neutron spectrum as a function of excitation energy. (a) Scale for first and second ring ratios. (b) Scale for third ring ratio. (c) Scale for fourth ring ratio.

REF.

B.S. Dolbilkin, V.I. Korin, L.E. Lazareva, F.A. Nikolaev
JETP Letters 1, 148 (1965)

ELEM. SYM.	A	-
O	16	8

METHOD

REF. NO.

[Page 1 of 2] 65 Do 3 JOC

REACTION	RESULT	EXCITATION ENERGY	SOURCE		DETECTOR		ANGLE
			TYPE	RANGE	TYPE	RANGE	
G,MU-T	ABX	13-22	C		MGC-D		4PI

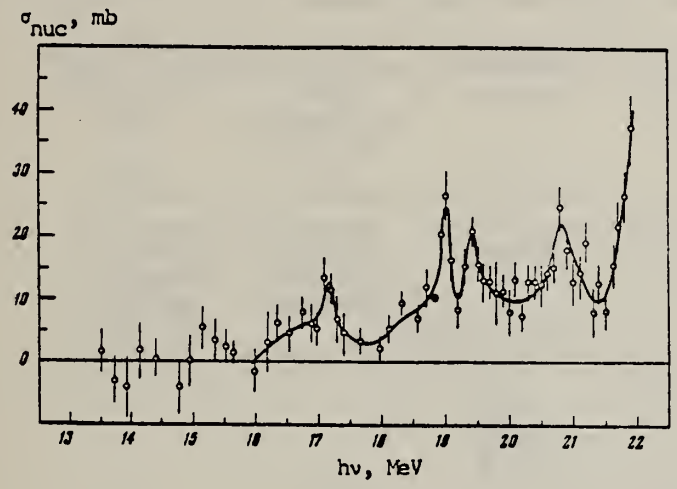

Fig. 1. Cross section for the absorption of γ quanta by O^{16} nuclei in the energy interval 13.5 - 22 MeV.

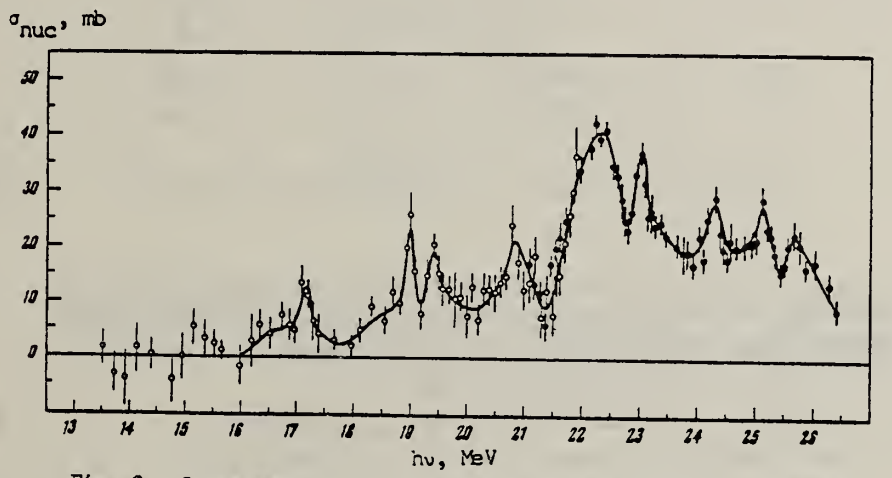

Fig. 2. Cross section for total nuclear absorption of γ quanta by O^{16} in the interval 13.5 - 27 MeV according to the present data (light circles) and [1] (filled circles). The energy scale for both curves has been corrected for the resolving power of the spectrometer. In the 21 - 22 MeV interval, where the data overlap, both curves coincide within the limits of errors.

B. S. Dolbilkin, V.I. Korin, L.E. Lazareva, F.A. Nikolaev
JETP Letters 1, 148 (1965)

0	16	8

METHOD

REF. NO. 65 Do 3

JOC

REACTION	RESULT	EXCITATION ENERGY	SOURCE TYPE	SOURCE RANGE	DETECTOR TYPE	DETECTOR RANGE	ANGLE

Energies of the O^{16} levels in the interval 16 - 21.5 MeV

Total cross section of nuclear absorption (present work)	Cross section of reaction (γ, n) [4]	Cross section of inverse reaction N^{15}(p, γ) [5]	Photoneutron spectrum [6]	Proton spectrum in the disintegrations (e, e'p) [7]	Total absorption cross section [8]
Absorption method, detector resolution ΔE ~ 100 keV	Measurements with annihilation γ-radiation of fast positrons ΔE ~ 500 keV	Measurements with tandem generator ΔE < 30 keV	Time-of-flight method, ΔE from ~ 5 to ~ 50 keV	Detection of protons with magnetic spectrometer ΔE ~ 150 keV	Measurements with monochromatic γ-rays T(p,γ) ΔE from 40 50 50 keV
	16.0	16.2			
		17.1	17.10		
17.2	17.1			17.3	
		17.3	17.25		
				18.1	
19.0	19.0	19.0	19.0	19.0	
19.4	19.3	19.6	19.4	19.6	
			20.1		20.6
20.9	20.8	21.0	20.9	20.6	21.0

[4] Bramblett, Caldwell, Harvey, and Fultz, Phys. Rev. 133, B869 (1964).

[5] Tanner, Thomas, and Earle, Nucl. Phys. 52, 45 (1964).

[6] F. W. K. Firk, Nucl. Phys. 52, 437 (1964).

[7] W. R. Dodge and W. C. Barber, Phys. Rev. 127, 1746 (1962).

[8] G. Tessler and W. E. Stephens, Phys. Rev. 135, B129 (1964).

J. Garvey, B. H. Patrick, J. G. Rutherglen and I. L. Smith
Nuclear Phys. 70, 241 (1965)

0	16	8

METHOD

REF. NO. 65 Ga 1 EGF

REACTION	RESULT	EXCITATION ENERGY	SOURCE		DETECTOR		ANGLE
			TYPE	RANGE	TYPE	RANGE	
G,NP	ABX	250	C	300	TEL-D	90-140	DST

77±17 MeV neutrons in coincidence with protons.
Neutrons detected in plastic scintillator.

For $\sigma = L \frac{NZ}{A} \sigma_d$ finds L = 10.3±2.6 for an r.m.s. radius = 4.45 fm.

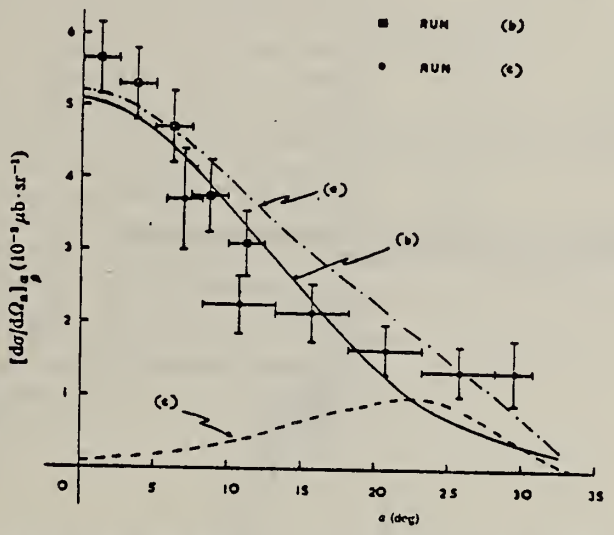

Fig. 8. The vertical angular distribution of protons at 65° in the laboratory detected in coincidence with neutrons of energy 76.5±17 MeV (FWHM) at 90° in the laboratory, from the photodisintegration of O^{16}. The protons are in the energy range 88.8 to 142.5 MeV. Curve (a) is a possible theoretical angular distribution evaluated using the $F(P)$ of eq. (5) as described in the text and corresponds to a r.m.s. nuclear radius of 3.32 fm.

REACTION	RESULT	EXCITATION ENERGY	SOURCE TYPE	SOURCE RANGE	DETECTOR TYPE	DETECTOR RANGE	ANGLE

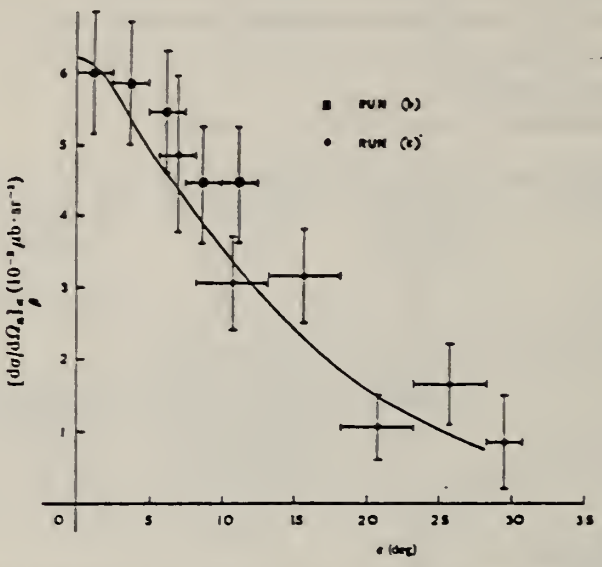

Fig. 12. The vertical angular distributions of protons of energy 88.8 to 108.5 MeV compared with the theoretical predictions using the $F(P)$ of fig. 10.

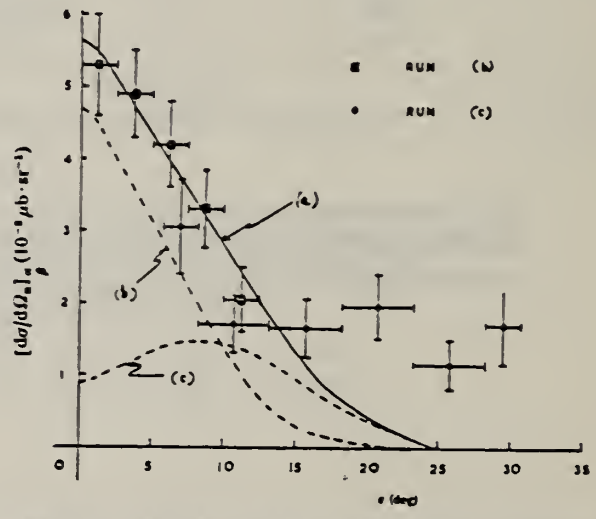

Fig. 9. The vertical angular distribution of coincident protons of energy 108.5 to 142. 5 MeV from the photodisintegration of O^{16}. Curve (a) is a possible theoretical angular distribution evaluated using the $F(P)$ of eq. (5) and corresponds to a r.m.s. nuclear radius of 5.55 fm.

REF. I.A. Grishaev, D. I. Sikora, V.A. Skoda-Ul'yanov, B.I. Shramenko
Atomnaya Energiya 18, 28 (1965)
Soviet Atomic Energy 18, 29 (1965)

ELEM. SYM.	A	Z
O	16	8

METHOD

REF. NO. 65 Gr 1 EGF

REACTION	RESULT	EXCITATION ENERGY	SOURCE		DETECTOR		ANGLE
			TYPE	RANGE	TYPE	RANGE	
G,N	ABX	THR-54	C	10-66	ACT-I		LPI

Measure yields from electrons bombarding thick targets. Cross section derived from shower theory.

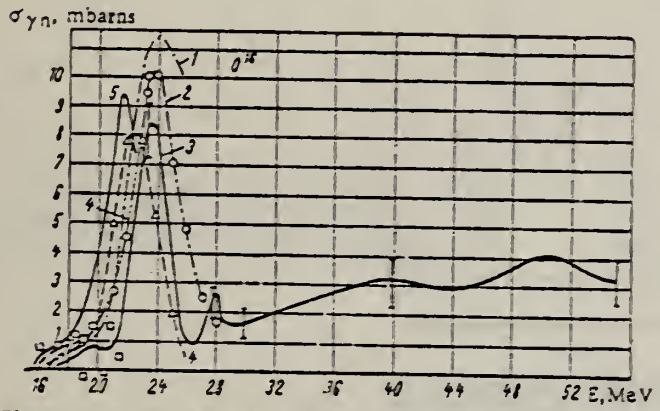

Fig. 4. Excitation function of the (γ,n) reaction for O^{16}: 1, 2, 4, 5) Curves obtained with thin specimens and the Schiff spectrum by using the photon-difference method, in [7, 8, 13, 14], respectively; 3) result of the present study.

E. Hayward and T. Stovall
Nuclear Phys. 69, 241 (1965)

0	16	8

METHOD

REF. NO. 65 Ha 1 EGF

REACTION	RESULT	EXCITATION ENERGY	SOURCE		DETECTOR		ANGLE
			TYPE	RANGE	TYPE	RANGE	
G,XN	ABX	THR - 30	C	6-30	BF3-I		4PI

572

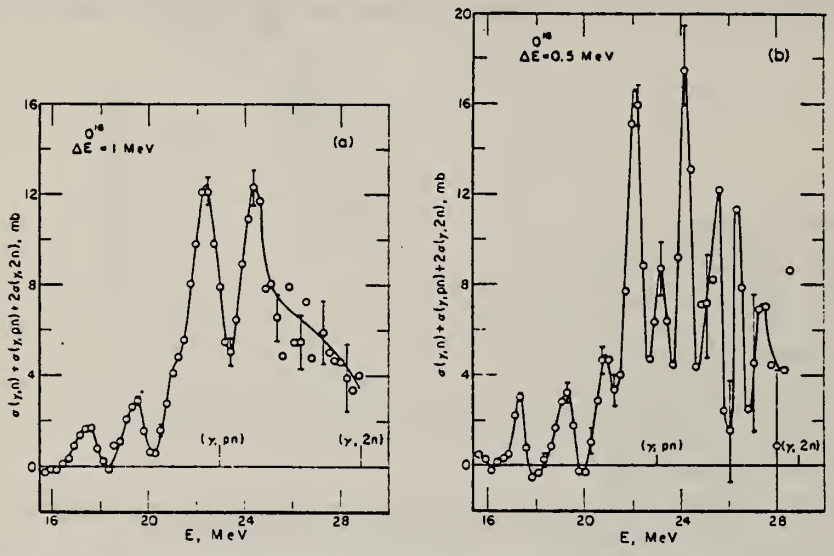

Fig. 2. The neutron production cross section for O^{16} where the analysis has been made using a 1 MeV grid (a) and a 0.5 MeV grid (b). Thresholds for the neutron producing cross sections are indicated by vertical lines at the bottom. The indicated errors are standard deviations based only on the number of counts.

TABLE 3

Neutron emission cross sections integrated to 29 MeV

Target	$\int \sigma dE$ (MeV · mb)	$\int \sigma dE/(60NZ/A)$	$\int^{30} \sigma dE/(60NZ/A)$ [a]
Li^6	36.1	0.40±0.03 [b]	0.42
Li^7	50.1	0.49±0.04	0.64
B^{10}	66.7	0.44±0.03	
B^{11}	68.6	0.42±0.03	0.47 [c]
O^{16}	61.9	0.26±0.02	0.30

[a]) Ref. [17]).
[b]) This value is for natural boron.
[c]) Estimated systematic errors.

REF.

J.M. Maison, M. Langevin et J.M. Loiseaux
Phys. Letters 19, 308 (1965)

CLEM. SYM.		
0	16	8

METHOD

REF. NO.	
65 Ma 1	egf

REACTION	RESULT	EXCITATION ENERGY	SOURCE		DETECTOR		ANGLE
			TYPE	RANGE	TYPE	RANGE	
G,NG	SPC	19- 30	C	21- 31	NAI-D	4- 8	140
G,PG	SPC	19- 30	C	21- 31	NAI-D	4- 8	140

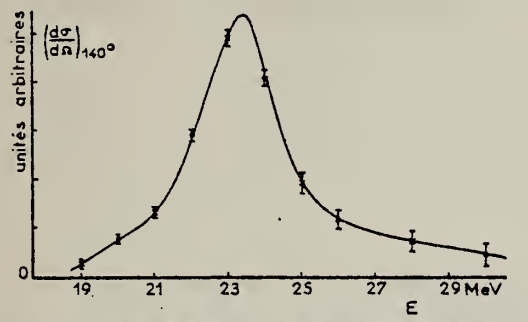

Fig. 1. Variation de la section efficace relative en fonction de l'énergie d'excitation pour l'émission de neutrons et protons vers les niveaux de parités négatives de ^{15}O (1.16 MeV) et ^{15}N (6.32 MeV). Les x et o correspondent à deux séries de mesures indépendantes.

Tableau 1
Rapports d'embranchements pour l'émission de neutrons et de protons vers les états de parité négative

E_{max} (MeV)	21	23	25	27	29	31
Niveaux 6.31 MeV (π^-)	68±6%	71±6%	70±6%	71±6%	73±6%	72.5±6%
Niveaux 5.3 MeV (π^+)	32±6%	29±6%	30±6%	29±6%	27±6%	27.5±6%

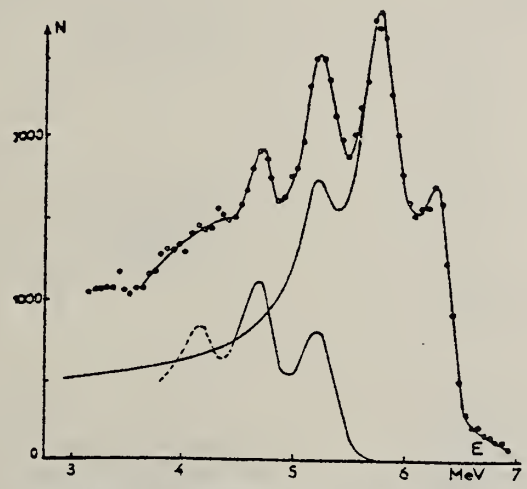

Fig. 1. Spectre expérimental pour un faisceau d'energie maximum de 27 MeV. Le fond dû aux neutrons a été deduit.

REF.

R. A. Meyer, W. B. Walters, J. P. Hummel
Phys. Rev. 138, B1421 (1965)

ELEM. SYM.	A	Z
O	16	8

METHOD

REF. NO. 65 Me 4 egf

REACTION	RESULT	EXCITATION ENERGY	SOURCE		DETECTOR		ANGLE
			TYPE	RANGE	TYPE	RANGE	
G,PI+	ABX	150-300	C	150-300	ACT-I		4PI

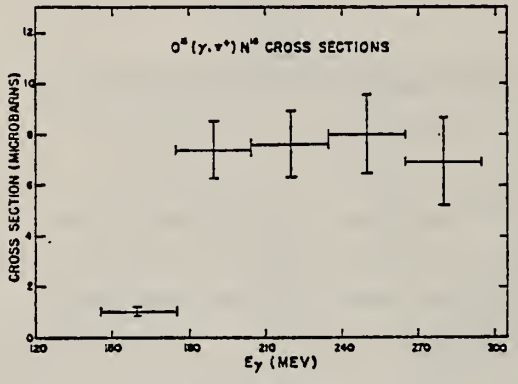

FIG. 3. Cross sections (in units of microbarns) for the $O^{16}(\gamma,\pi^+)N^{16}$ reaction.

REF.

R.C. Morrison, J.R. Stewart, and J.S. O'Connell
Phys. Rev. Letters 15, 367 (1965)

ELEM. SYM.	A	Z
O	16	8

METHOD

REF. NO. 65 Mo 1 JOC

REACTION	RESULT	EXCITATION ENERGY	SOURCE		DETECTOR		ANGLE
			TYPE	RANGE	TYPE	RANGE	
G,P	SPC	15-29	C	22,40	SCD-D		90

BRANCHING RATIOS

State	Branching Ratio 6.3/g.s.
22.3	.43 ± .1
23.	.58 ± .1
24.3	.43 ± .1

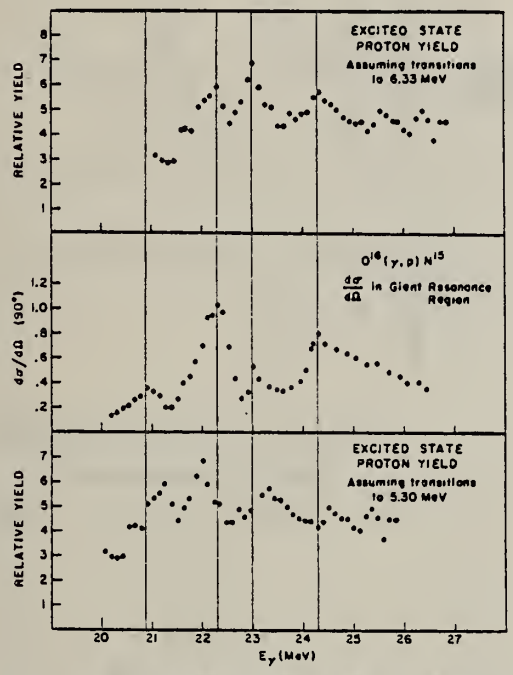

FIG. 1. A comparison between the proton spectrum from excited-state transitions and the giant-resonance ground-state cross section: In the upper portion of the figure, a gamma-energy scale has been assigned to the excited-state spectrum assuming all transitions are to 6.3 MeV. The lower portion shows the same spectrum assuming all transitions are to 5.3 MeV. The vertical lines are drawn through the cross-section peaks shown in the center portion of the figure.

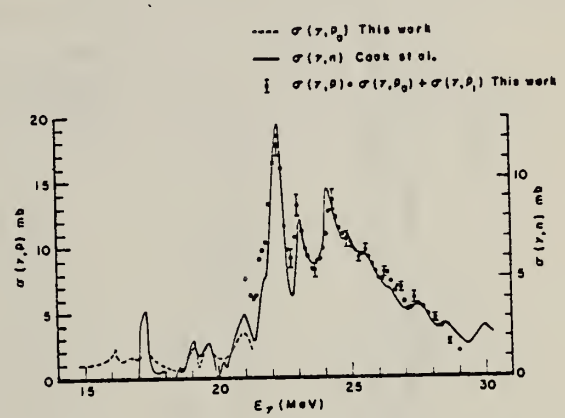

FIG. 2. A comparison between the (γ,p) cross section of this work, and the (γ,n) cross section of Cook et al. The proton-cross-section scale assumes an angular distribution of $1+\frac{3}{2}\sin^2\theta$.

REF.

Jan P. Roalsvig
Can. J. Phys. 43, 330 (1965)

ELEM. STM.	A	Z
0	16	8

METHOD

Emulsions in beam

[Page 1 of 2]

REF. NO. 65 Ro 1

JOC

REACTION	RESULT	EXCITATION ENERGY	SOURCE		DETECTOR		ANGLE
			TYPE	RANGE	TYPE	RANGE	
G,A	ABX	12 - 17	C	12-17	EMU-D		4PI
G,4A	ABX	12 - 17	C	12-17	EMU-D		4PI

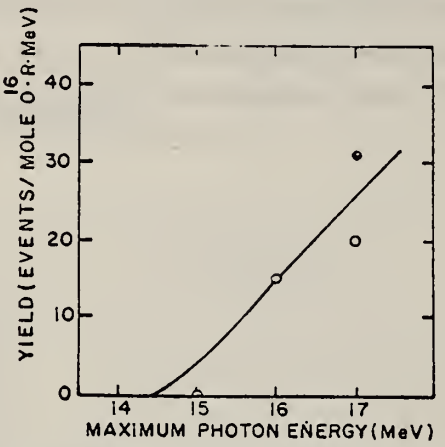

FIG. 3. The yield in events per mole ^{16}O per roentgen per MeV interval for the reaction $^{16}O(\gamma, 4\alpha)$, as a function of maximum photon energy. Open circles, present results; closed circle, from Greenberg *et al.* (1964). The solid curve was used to calculate the cross section in Fig. 4.

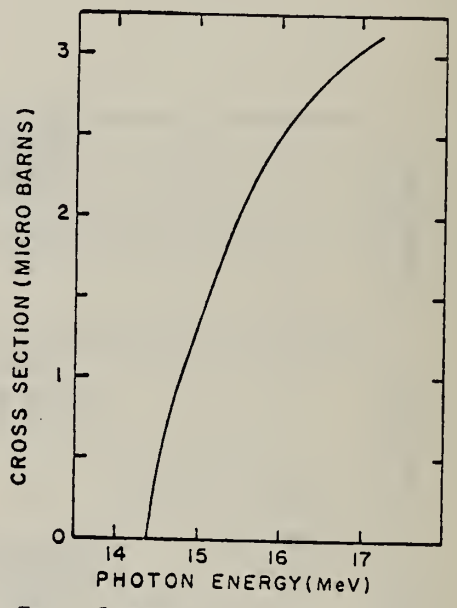

FIG. 4. Cross-section curve for the reaction $^{16}O(\gamma, 4\alpha)$.

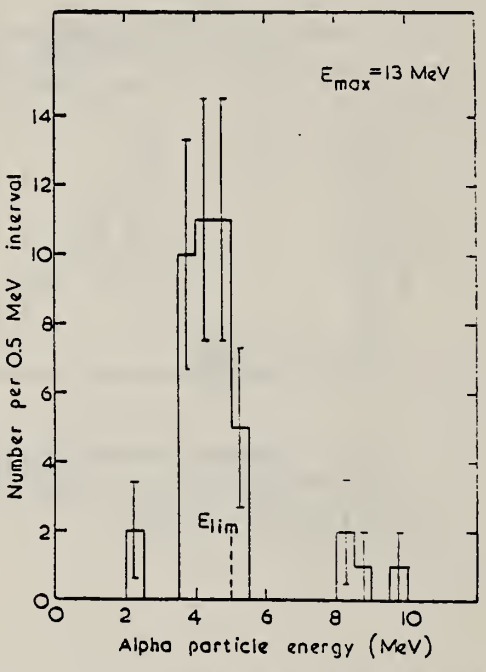

FIG. 5. Energy distribution of single alpha-particle tracks on plate B, exposed at 13-MeV maximum bremsstrahlung energy. The abscissa gives the apparent alpha-particle energy, as defined in the text. E_{lim} is the approximate maximum energy of an alpha particle from the reaction $^{16}O(\gamma, \alpha)^{12}C$, with ^{12}C in the ground state.

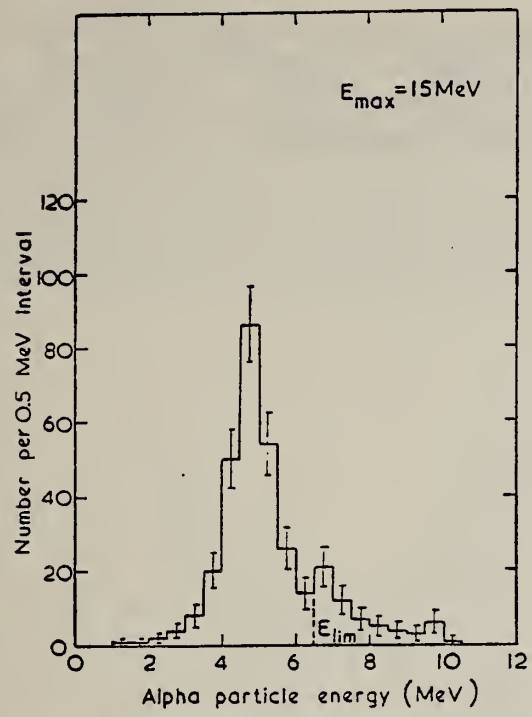

FIG. 7. Same as Fig. 5, but for plate D, exposed at 15 MeV.

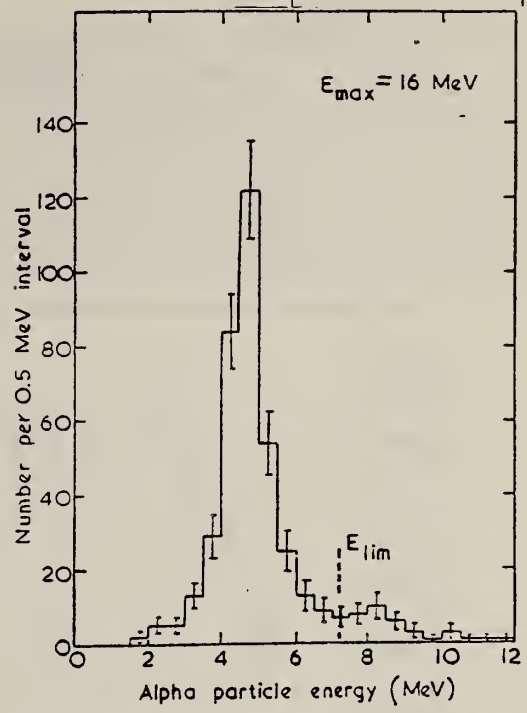

FIG. 8. Same as Fig. 5, but for plate E, exposed at 16 MeV.

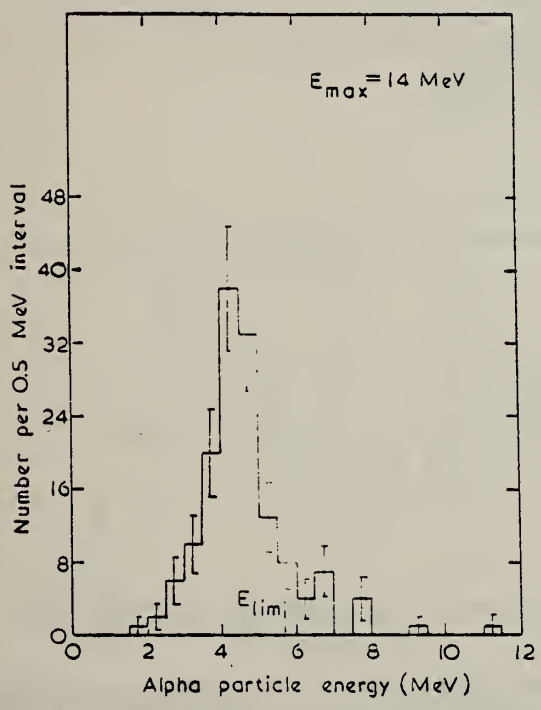

FIG. 6. Same as Fig. 5, but for plate C, exposed at 14 MeV.

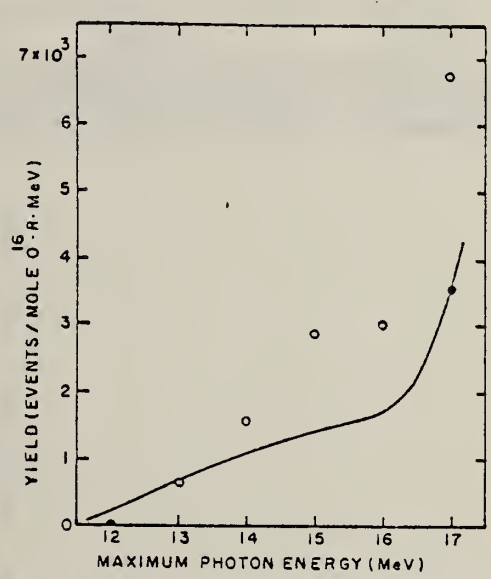

FIG. 9. The yield in events per mole ^{16}O per roentgen per MeV interval for the reactio $^{16}O(\gamma, \alpha)^{12}C$, as a function of maximum photon energy. Open circles, present results, assumin all single alpha-particle tracks to be due to the above reaction; closed circle, from Greenber *et al.* (1964). The solid curve is the yield curve as calculated from the cross-section curve Greenberg *et al.* (1964).

REF. J. P. Roalsvig
Can. J. Phys. 43, 1015 (1965)

ELEM. SYM.	A	Z
O	16	8

METHOD

REF. NO. 65 Ro 2 HMG

REACTION	RESULT	EXCITATION ENERGY	SOURCE		DETECTOR		ANGLE
			TYPE	RANGE	TYPE	RANGE	
G,A	RLY	17	C	17	EMU-D		DST

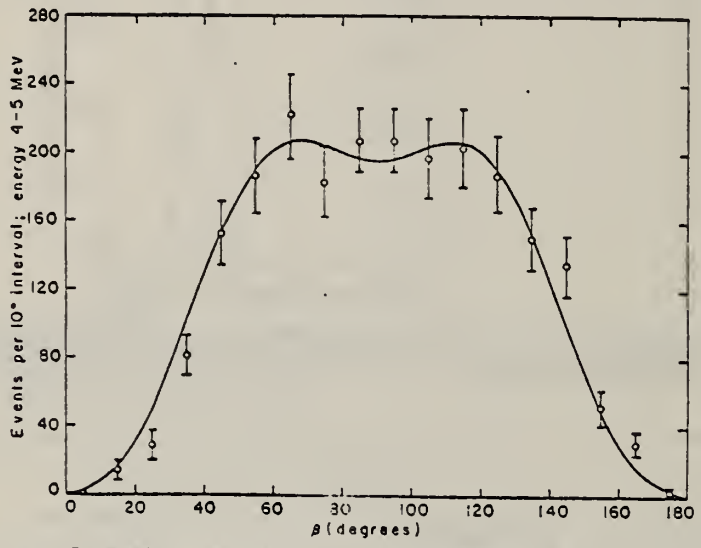

FIG. 1. Corrected number of alpha particles with energy between 4.0 and 5.0 MeV, per 10° interval as a function of β, the angle between the alpha particle and the photon direction. The curve is drawn for an admixture of 13% isotropic distribution and 87% E1 + E2, with an E2/E1 intensity ratio of 0.50, where both the initial and the final states have $J = 0^+$.

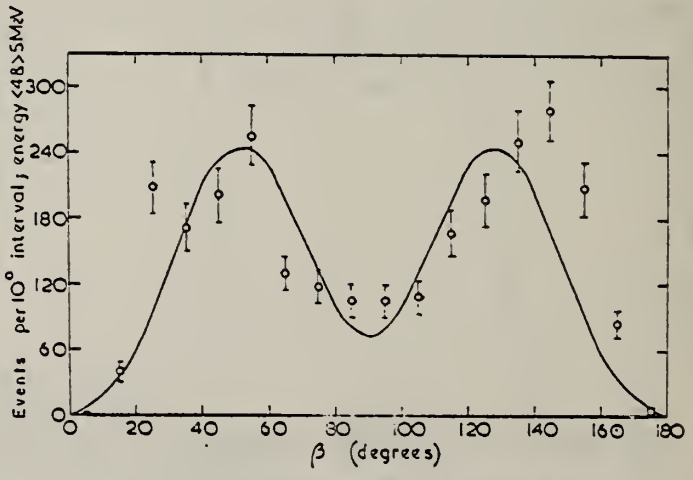

FIG. 2. Corrected number of alpha particles with energy <4.0 MeV or >5.0 MeV, per 10° interval as a function of β, the angle between the alpha particle and the photon direction. The curve is drawn for an admixture of 35% isotropic distribution and 65% pure E2, where both the initial and the final states have $J = 0^+$.

REF.

R.J.J. Stewart, P.H. Cannington and B.M. Spicer
Aust. J. Physics 18, 661 (1965)

ELEM. SYM.	A	Z
O	16	8

METHOD

Betatron

REF. NO.

65 St 2 JDM

REACTION	RESULT	EXCITATION ENERGY	SOURCE		DETECTOR		ANGLE
			TYPE	RANGE	TYPE	RANGE	
G,P_0	ABX	14 - 16	C	14 - 16	SCD-D	2 - 4	90

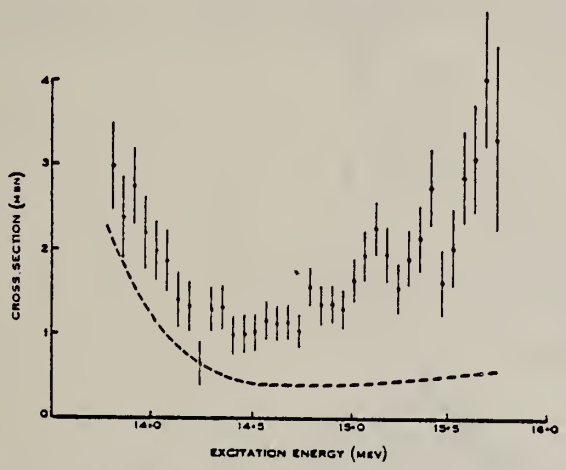

Fig. 2.—The cross section for the reaction $^{16}O(\gamma, p_0)^{15}N$, together with a cross section obtained from the inverse reaction using the principle of detailed balance.

REACTION	RESULT	EXCITATION ENERGY	SOURCE		DETECTOR		ANGLE
			TYPE	RANGE	TYPE	RANGE	
E,E/	ABX	10-30	D	43-69	MAG-D	35-70	180

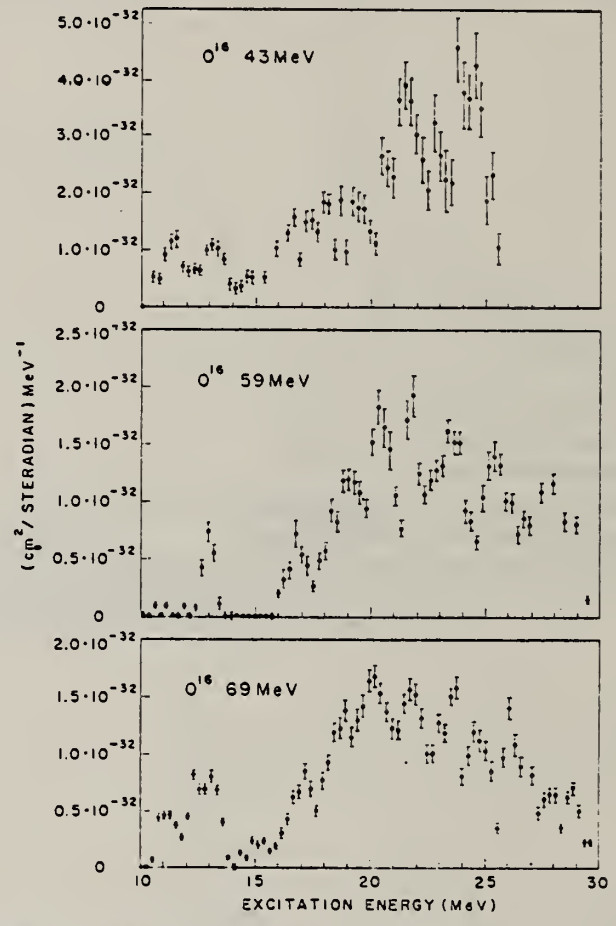

Fig. 2. Cross section for inelastic scattering of electrons at 180° with excitation of the ^{16}O nucleus, plotted as a function of excitation energy.

REF.

G. J. Vanpraet
Nuclear Phys. 74, 219 (1965)

0	16	8

REF. NO. 65 Va 4

[Page 2 of 2]

EGF

METHOD

REAC

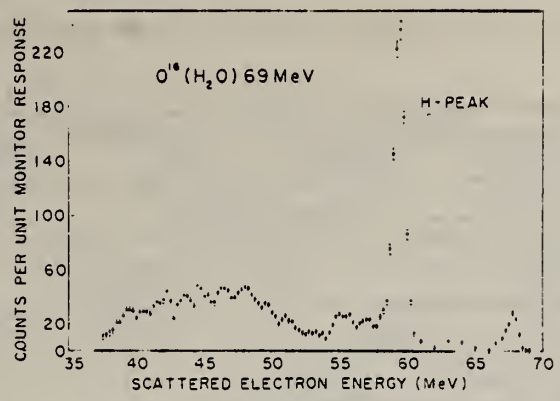

CE RANGE	DETECTOR TYPE	DETECTOR RANGE	ANGLE

Fig. 1. Energy distribution of 69 MeV electrons scattered inelastically through 180° from a water target.

TABLE 1

Cross sections and matrix elements of levels observed in the ^{16}O giant resonance region

Experimental levels (±0.25 MeV)		$d\sigma/d\Omega$ $\times 10^{33}$(cm²/sr)	$\lvert\langle J_f\rVert T(q)\rVert J_i\rangle\rvert^2$ $\times 10^2$
	19.2	1.8 ±0.27	0.56±0.85
	20.4	1.85±0.28	0.58±0.90
43 MeV	21.5	4.5 ±0.7	1.41±0.21
	22.8	2.6 ±0.4	0.82±0.13
	23.9		
	24.5	5.8 ±0.9	1.82±0.27
	19.2	1.5 ±0.18	0.88±0.12
	20.4	1.85±0.22	1.09±0.13
	22.0	2.12±0.25	1.25±0.15
59 MeV	22.8	1.0 ±0.12	0.59±0.07
	23.6	1.8 ±0.22	1.06±0.13
	25.5	1.9 ±0.23	1.12±0.13
	26.7	0.7 ±0.09	0.41±0.05
	19.0	1.6 ±0.16	1.29±0.13
	20.2	2.15±0.22	1.73±0.17
	22.0	2.27±0.23	1.83±0.18
69 MeV	23.0	0.68±0.07	0.55±0.06
	23.6	1.41±0.14	1.14±0.12
	24.5	1.18±0.12	0.95±0.10
	26.0	1.4 ±0.14	1.13±0.12

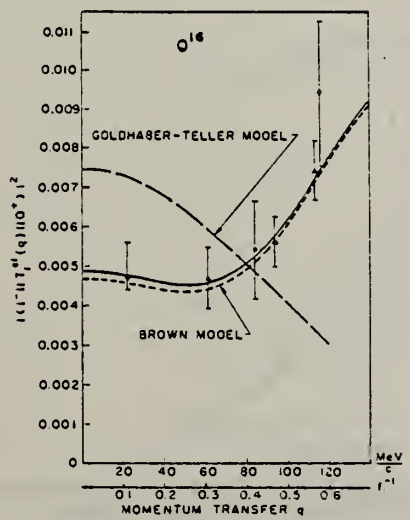

Fig. 3. Square of the form factor for the ^{16}O giant dipole resonance, plotted as a function of momentum transfer. The experimental point at 23 MeV is from photon work. The new experimental values from 180° electron scattering are represented by the triangles. The curves are calculated on the basis of different nuclear models refs. [6, 13]).

V. V. Verbinski and J. C. Courtney
Nuclear Phys. 73, 398 (1965)

0	16	8

METHOD

REF. NO. 65 Ve 1

[Page 1 of 2]

EGF

REACTION	RESULT	EXCITATION ENERGY	SOURCE		DETECTOR		ANGLE
			TYPE	RANGE	TYPE	RANGE	
G,N	SPC	THR-33	C	34	TØF-D	1-14	DST

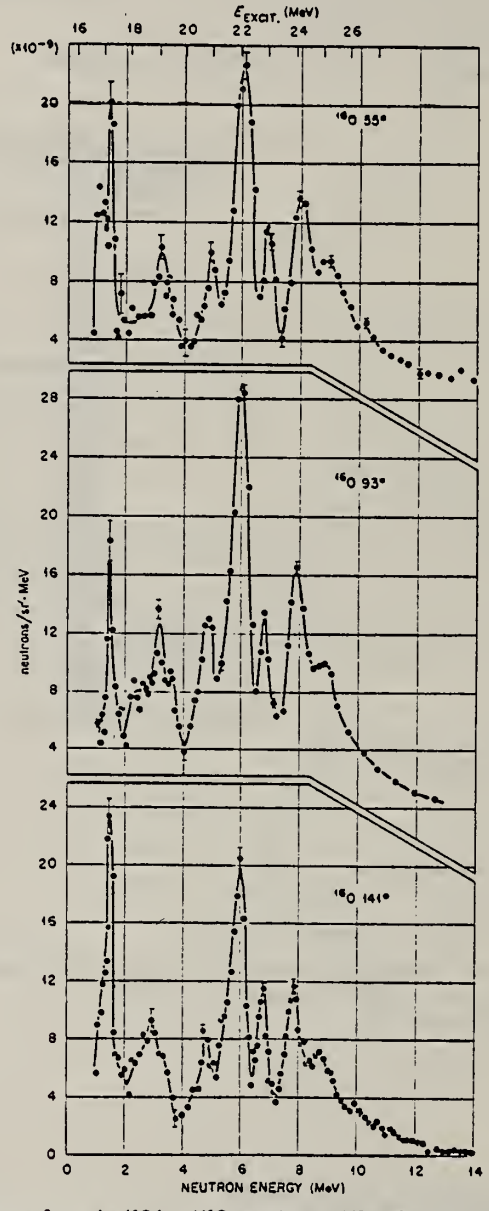

Fig. 4. Neutron spectra from the $^{16}O(\gamma, n)^{15}O$ reaction at 55°, 93° and 141° to a bremsstrahlung beam produced by 34 MeV electrons penetrating a 0.15 cm thick bismuth disk.

REACTION	RESULT	EXCITATION ENERGY	SOURCE TYPE	SOURCE RANGE	DETECTOR TYPE	DETECTOR RANGE	ANGLE

TABLE 1

Angular distributions for (γ, p) and (γ, n) reactions on ^{12}C and ^{16}O

Mode of excitation	Excited state spin and parity	l	Angular distribution	Relative intensity 55°	93°	141°
E1	1^-	0	isotropic	1.00	1.00	1.00
E1	1^-	2	$1+\frac{3}{4}\sin^2\theta$	0.81	1.00	0.64
E2,(E1) [a])	2^+, (1^-) [a])	1	$1-\frac{1}{4}\sin^2\theta$	1.32	1.00	1.63
E2	2^+	3	$1+2\sin^2\theta-\frac{3}{4}\sin^4\theta$	2.42	1.00	1.40

Target nucleus	Excitation energy (MeV)	Emitted particle	Ref.	Relative intensity 55°	93°	141°
^{12}C	22.35	p	Dodge and Barber [20])	0.81	1.00	0.45
^{12}C	>22	n	Allum *et al.* [21])	0.85	1.00	0.60
^{12}C	25.4	n	this paper	0.80	1.00	
^{16}O	22.3	p	Dodge and Barber [20])	0.86	1.00	0.46
^{16}O	22.1	n	this paper	0.81	1.00	0.64
^{16}O	24.2	p	Dodge and Barber [20])	0.97	1.00	0.45
^{16}O	24	n	this paper	0.89	1.00	0.68
^{16}O	23	n	this paper	0.81	1.00	0.64
^{16}O	20.8	n	this paper	0.73	1.00	0.63
^{16}O	18–20	n	this paper	0.77	1.00	0.73

[a]) This angular distribution is also possible for $l = 2$ neutrons or protons from ^{12}C (1^- states) to ^{11}C or ^{11}B ($\frac{3}{2}^-$ ground state).

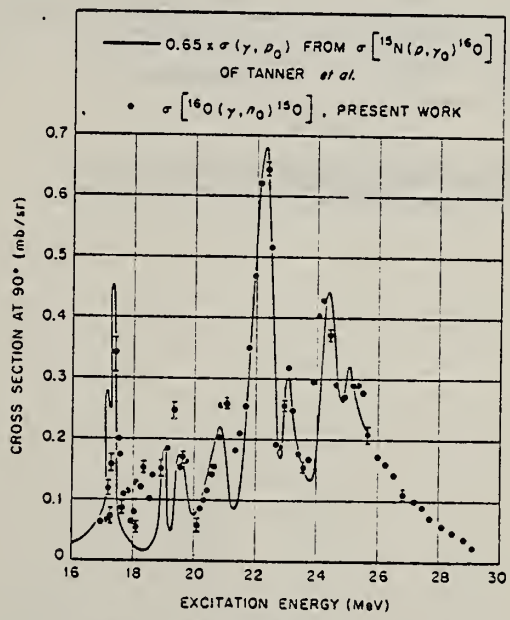

Fig. 5. The $^{16}O(\gamma, n_0)^{15}O$ cross section at 93° compared with 65 % of the $^{16}O(\gamma, p_0)^{15}N$ cross section at 90° derived from the $^{15}N(p, \gamma_0)^{16}O$ cross section of Tanner, Thomas and Earle [19]).

REF.

J.M. Wyckoff, B. Ziegler, H.W. Koch, and R. Uhlig
Phys. Rev. 137, B576-94 (1965)

ELEM. SYM.	A	Z
O	16	8

METHOD

Synchrotron; ion chamber monitor

REF. NO. 65 Wy 1 NVB

REACTION	RESULT	EXCITATION ENERGY	SOURCE TYPE	SOURCE RANGE	DETECTOR TYPE	DETECTOR RANGE	ANGLE
G,MU-T	ABX	10 - 35	C	90	SCI-D		4PI

50+

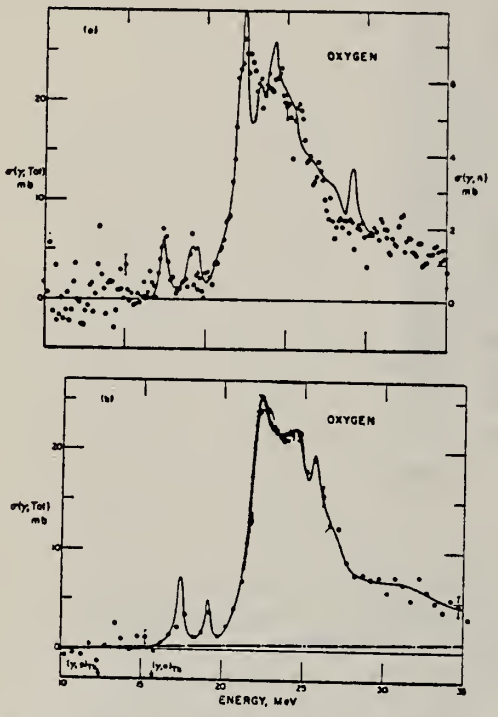

FIG. 8. Oxygen total photonuclear cross section. The Livermore photoneutron cross section represented by the solid line in (a) has been shifted up in energy by 250 keV.

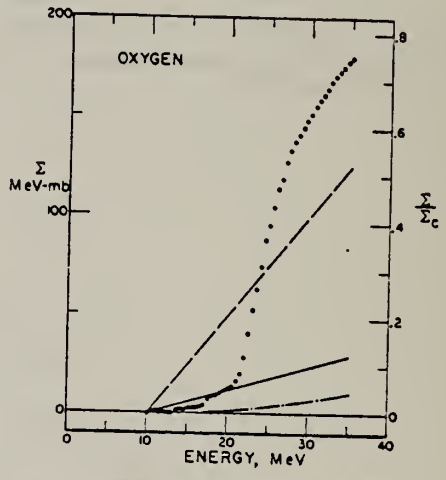

FIG. 10. Oxygen total photonuclear cross section integrated over energy.

REF.	ELEM. SYM.	A	Z
H. Artus Z. Physik 189, 355 (1966)	O	16	8

METHOD	REF. NO.	
60 MeV Linac	66 Ar 1	JDM

REACTION	RESULT	EXCITATION ENERGY	SOURCE		DETECTOR		ANGLE
			TYPE	RANGE	TYPE	RANGE	
G, BE7	ABX	30 - 57	C	30 - 57	ACT-I		4PI

$$\int_{Thr}^{o} \sigma dE = 0.7 \text{ MeV mb}$$

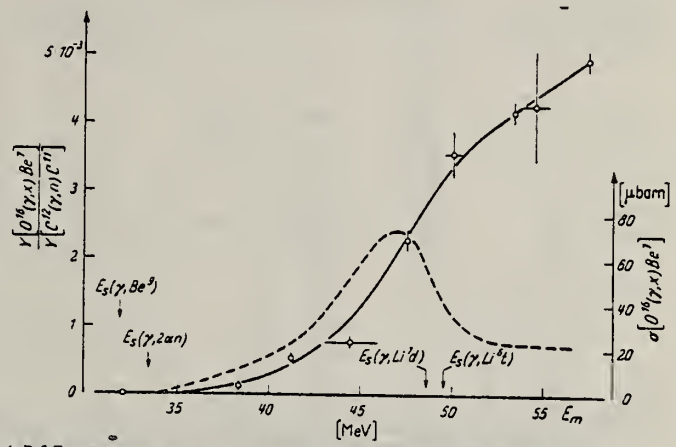

Fig. 4. Be^7-Erzeugung aus Sauerstoff. Alle Meßwerte sind mit einem zusätzlichen Eichfehler von ±10% behaftet. Die eingezeichnete Kurve für das Ausbeuteverhältnis entspricht dem gestrichelt angedeuteten Wirkungsquerschnitt. Die Schwellenenergien (E_s) für verschiedene Reaktionskanäle sind durch Pfeile gekennzeichnet

REF. H. Artus, P. Brix, H. G. Clerc, F. Eigenbrod, A. Goldmann, F. Gudden, E. Spamer, P. Strehl, M. Stroetzel, O. Titze, and K. J. Wetzel
Proc. Gatlinburg Conference, 314 (1966)

ELEM. SYM.	A	Z
O	16	8

METHOD

REF. NO. 66 Ar 2 hmg

REACTION	RESULT	EXCITATION ENERGY	SOURCE TYPE	SOURCE RANGE	DETECTOR TYPE	DETECTOR RANGE	ANGLE
E,E/	LFT	7,12	D	30-60	MAG-D		DST
		(6.92,11.52)					

7=6.92, 12=11.52 MEV

TABLE 1

Summary of Experimental Results[a]

Nuclide	E_x (MeV)	Type	Γ_γ^0(eV)	Γ_γ^0/Γ_w	R_w (F)
^{6}Li	2.18	E2	(3.9 ± 0.5) × 10^{-4}	14.4	3.77 ± 0.48
	3.56	M1	8.9 ± 0.4	9.4	2.96 ± 0.11
^{7}Li	11.28 ± 0.05	(M1) or	(1.3 ± 0.4)/g[b]	0.043/g	—
		(M2)	(0.026 ± 0.008) /g	2.6/g	—
^{9}Be	15.97 ± 0.03	M1	(3.7 ± 0.8) /g	0.043/g	—
^{11}B	4.46	E2 and	0.0173 ± 0.0021	8.2	3.44 ± 0.50
		M1	0.64 ± 0.08	0.34	2.60 ± 0.35
	5.04	M1	1.84 ± 0.14	0.69	2.60 ± 0.11
^{12}C	4.43	E2	0.0122 ± 0.0008	5.30	3.14 ± 0.30
^{16}O	6.92	E2	0.100 ± 0.015	3.28	3.82 ± 0.46
	11.52	E2	0.52 ± 0.13	1.31	—
^{24}Mg	9.85 ± 0.04	M1	7.95 ± 1.2	0.38	3.50 ± 0.49
	9.97 ± 0.03				
	10.35 ± 0.03	E2	0.24 ± 0.05	0.58	5.05 ± 0.50
	10.70 ± 0.03	M1	22.2 ± 2.4	0.86	3.60 ± 0.36
	10.93 ± 0.04	E2	0.26 ± 0.11	0.50	—
^{28}Si	4.97 ± 0.02	C0	(2.0 ± 0.5) × 10^{-5}[c]	—	6.90 ± 1.20
^{40}Ca	6.89 ± 0.05	E2	0.29 ± 0.04	2.85	4.60 ± 0.50

[a] The Born approximation has been used except for ^{16}O and ^{40}Ca.
[b] $g = (2I_f + 1)/(2I_i + 1)$.
[c] Γ_γ^2 equivalent to ME = (8.87 ± 1.00) F^2.

G. Baciu, D. Catana, C. Deberth and I. Raileanu
Rev. Roum. Phys. 11, 301 (1966)

0	16	8

METHOD

REF. NO. 66 Ba 5 egf

REACTION	RESULT	EXCITATION ENERGY	SOURCE		DETECTOR		ANGLE
			TYPE	RANGE	TYPE	RANGE	
G,N	ABX	15-25	C	15-25	ACT-I		4PI

296+

Table 2

[13] (γ, Tn)		[12] (γ, Tn)		[14] (p, γ)		Present work	
E	Γ	E	Γ	E	Γ	E	Γ (MeV)
		16.00				16.15	0.50
17.10				17.00	~1	17.15	0.35
17.25		17.10		17.13	0.044		
				17.29	0.090		
						18.00	0.43
19.00		19.00		19.05	~0.33	19.35	1.08
19.40		19.30		19.56	~0.40		
20.10							
20.90		20.80		21.00	~ 0.8	21.00	0.62
21.60		21.80					
22.10		22.10		22.20	0.85		
22.30						22.00	0.83
23.10		23.10		23.00	0.60	23.25	0.38
24.10		24.00				24.00	0.79
24.30				24.30	~1		

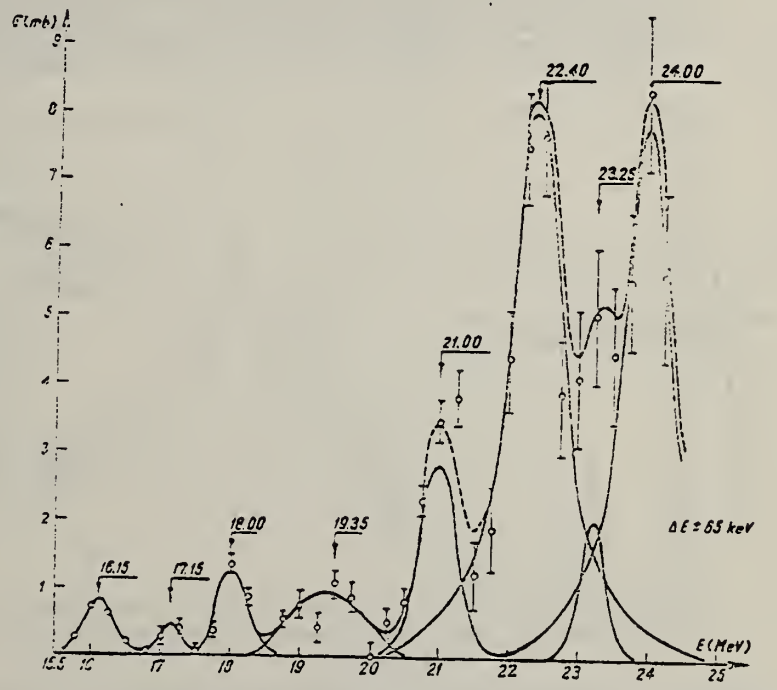

Fig. 2. — Absolute cross-section of the O^{16} (γ, n) O^{15} reaction.

REF.

B.C. Cook, J.E.E. Baglin, J.N. Bradford, and J.E. Griffin
Phys. Rev. 143, B712 (1966)

ELEM. SYM.	A	Z
O	16	8

METHOD

70 MeV synchrotron

REF. NO.

66 Co 1 JDM

REACTION	RESULT	EXCITATION ENERGY	SOURCE TYPE	SOURCE RANGE	DETECTOR TYPE	DETECTOR RANGE	ANGLE
G,N	ABX	THR - 65	C	THR - 70	ACT-I		4PI

113

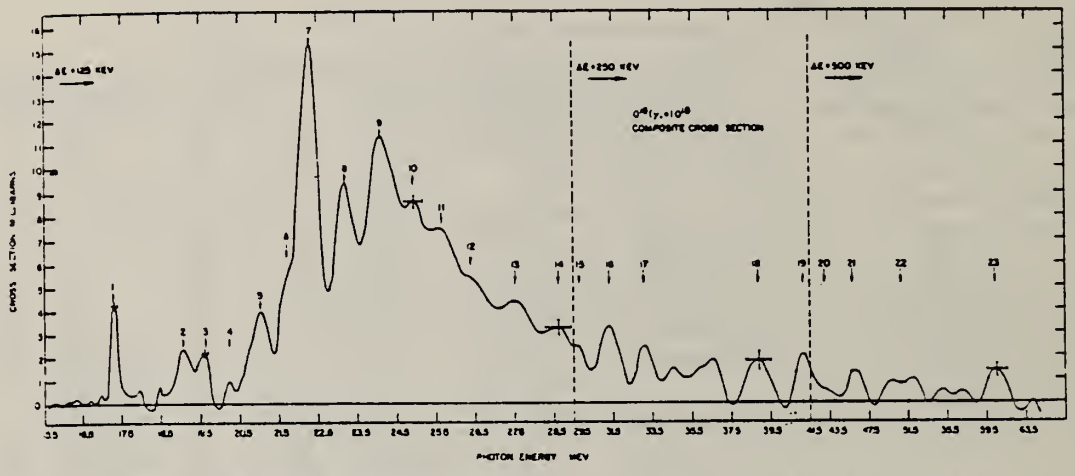

FIG. 3. The $O^{16}(\gamma,n)O^{15}$ cross section for energy to 65 MeV. This curve represents a fully converged least-structure solution for the yield function obtained using the average of six independent measurements. From 15.5 to 29.5 MeV data were taken in 125-keV intervals, from 29.5 to 41.5 MeV in 250-keV intervals, and above 41.5 MeV in 500-keV intervals. The vertical bars represent the standard deviation for the solution at representative energies. However, as adjacent cross-section points are strongly correlated, the interpretation of this bar as a random error is erroneous. The horizontal bar is the full width at half-maximum of the least-structure resolution function at representative energies. The numbered peaks occurred consistently in all cross sections derived from individual yield functions.

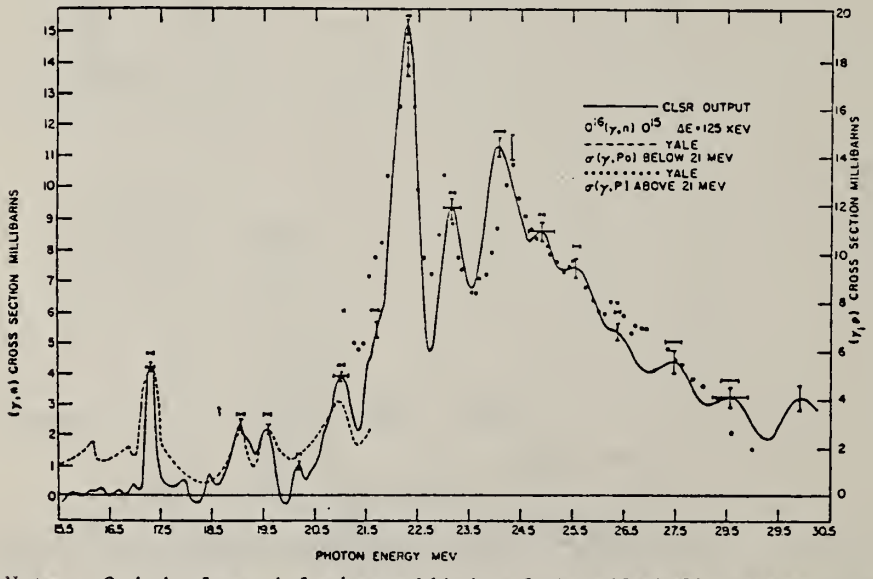

FIG. 6. A comparison between the (γ,p) and (γ,n) reaction in O^{16}. A recent measurement at Yale of the (γ,p) cross section obtained from the proton energy distribution is compared with results reported here. The scale on the left refers to the $O^{16}(\gamma,n)O^{15}$ cross section, while the scale on the right refers to the $O^{16}(\gamma,p)N^{16}$ cross section. The agreement between the cross sections for these differing processes is excellent.

Note: Original article has additional detailed figures and comparisons.

REF.

H. Crannell
Phys. Rev. 148, B1107 (1966)

ELEM. SYM.	A	Z
O	16	8

METHOD

Linac

REF. NO. 66 Cr 1 JDM

REACTION	RESULT	EXCITATION ENERGY	SOURCE		DETECTOR		ANGLE
			TYPE	RANGE	TYPE	RANGE	
E,E/	FMF	6.1	D	600-800	MAG-D	650-	32-60

q^2; 2.79 - 8.52 F^{-2}

RMS $\langle r^2 \rangle$ = 2.65 ± 0.04 F

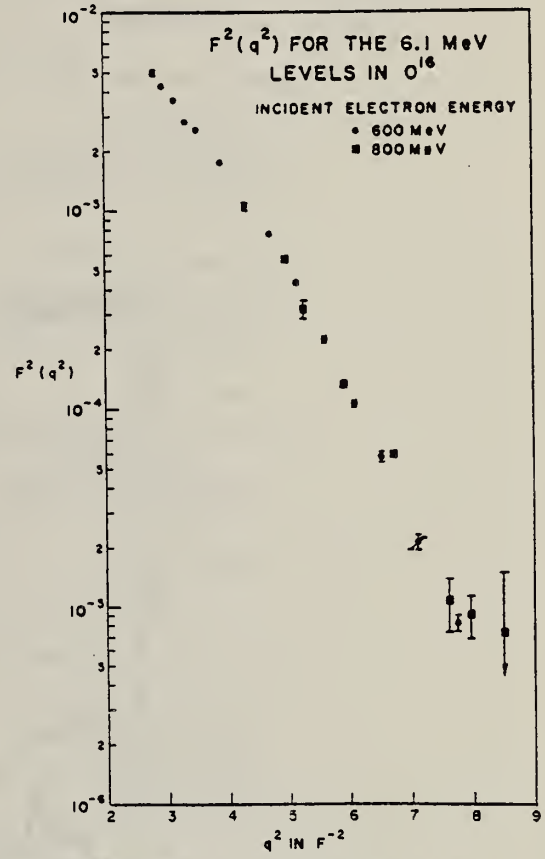

FIG. 9. $F^2(q^2)$ as a function of q^2 for the levels at approximately 6.1 MeV in O^{16}.

TABLE III. Elastic and inelastic cross sections for O^{16}.

E_0 (MeV)	θ (degrees)	Differential cross section in cm²/sr[a] Elastic scattering	Inelastic scattering 6.1-MeV levels
600	32.0	$(1.38\pm0.18)\times10^{-32}$	$(7.34\pm0.07)\times10^{-31}$
	33.0	$(2.98\pm0.13)\times10^{-32}$	$(5.46\pm0.05)\times10^{-31}$
	34.0	$(3.56\pm0.15)\times10^{-32}$	$(4.08\pm0.04)\times10^{-31}$
	35.0	$(3.76\pm0.12)\times10^{-32}$	$(2.86\pm0.03)\times10^{-31}$
	36.0	$(3.65\pm0.12)\times10^{-32}$	$(2.31\pm0.03)\times10^{-31}$
	38.0	$(3.06\pm0.10)\times10^{-32}$	$(1.27\pm0.02)\times10^{-31}$
	40.0	$(2.16\pm0.06)\times10^{-32}$	$(6.16\pm0.10)\times10^{-32}$
	42.0	$(1.28\pm0.04)\times10^{-32}$	$(3.67\pm0.06)\times10^{-32}$
	44.0	$(7.58\pm0.26)\times10^{-33}$	$(1.71\pm0.04)\times10^{-32}$
	46.0	$(3.59\pm0.12)\times10^{-33}$	$(7.33\pm0.19)\times10^{-33}$
	48.0	$(1.87\pm0.06)\times10^{-33}$	$(2.91\pm0.10)\times10^{-33}$
	50.0	$(8.23\pm0.38)\times10^{-34}$	$(1.32\pm0.07)\times10^{-33}$
	52.5	$(2.61\pm0.25)\times10^{-34}$	$(4.05\pm0.38)\times10^{-34}$
	52.5	$(2.48\pm0.15)\times10^{-34}$	$(4.04\pm0.24)\times10^{-34}$
	55.0	$(6.43\pm0.69)\times10^{-35}$	$(1.30\pm0.12)\times10^{-34}$
800	32.0	$(2.10\pm0.07)\times10^{-32}$	$(4.61\pm0.13)\times10^{-32}$
	33.0	$(1.11\pm0.02)\times10^{-32}$	$(2.29\pm0.24)\times10^{-32}$
	35.0	$(5.57\pm0.16)\times10^{-33}$	$(7.57\pm0.22)\times10^{-33}$
	37.5	$(1.60\pm0.06)\times10^{-33}$	$(2.56\pm0.10)\times10^{-33}$
	40.0	$(2.27\pm0.35)\times10^{-34}$	$(3.58\pm1.12)\times10^{-34}$
	41.0	$(1.08\pm0.09)\times10^{-34}$	$(2.76\pm0.72)\times10^{-34}$
	42.5	$(5.64\pm1.34)\times10^{-35}$	$(1.9\ ^{+1.9}_{-0.8})\times10^{-34}$

[a] All cross sections were measured with an angular acceptance in the horizontal plane ($\Delta\theta$) of 1.93°. Errors given are those due to counting statistics only.

REF. V.P. Denisov and L.A. Kul'chitskii
J. Nucl. Phys. (USSR) 2, 70 (1965)
Sov. J. Nucl. Phys. 2, 48 (1966)

ELEM. SYM.	A	Z
O	16	8

METHOD
Synchrotron

[Page 1 of 3]

REF. NO. 66 De 4 JDM

REACTION	RESULT	EXCITATION ENERGY	SOURCE		DETECTOR		ANGLE
			TYPE	RANGE	TYPE	RANGE	
G,P	ABI	THR - 44	C	21 - 44	TEL-D	3.4 - 12.4	90

$\int_{17}^{40} \sigma dE\gamma$ = 83 ± 8 mb-MeV

Paper gives comparison with other (γ,p) as well as (γ,n) data.

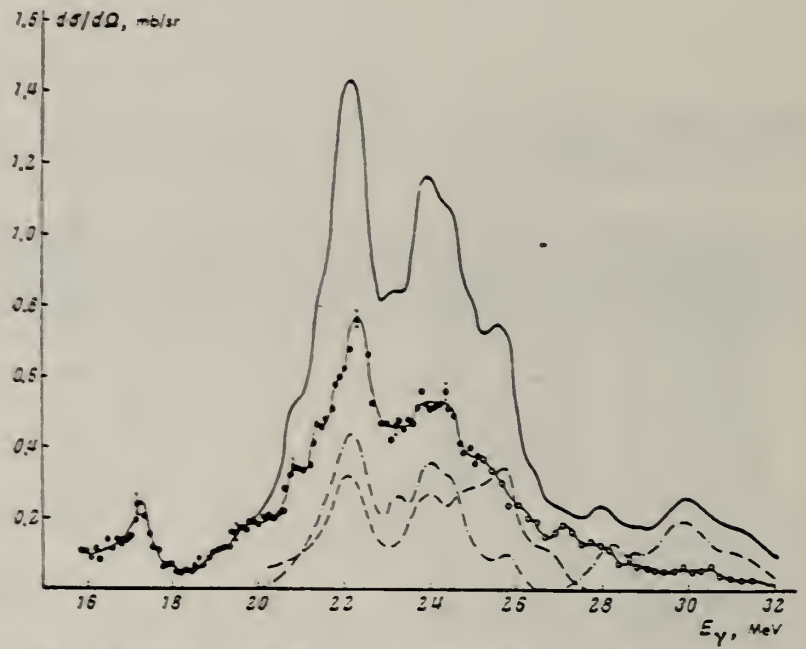

Fig. 3. Cross section $d\sigma/d\Omega$ for the reaction $O^{16}(\gamma,p)N^{15}$ for a proton emission angle of 90°. The curve with the experimental points is the cross section for the transition to the ground state of N^{15} (the hollow points are the data of Finckh and Hegel[11]). The dashed line is the cross section for the transition to the first and second excited states of N^{15}, and the dash-dot line for the transition to the third excited state. The upper curve is the total cross section.

REF. V.P. Denisov and L.A. Kul'chitskii
J. Nucl. Phys. (USSR) 2, 70 (1965)
Sov. J. Nucl. Phys. 2, 48 (1966)

ELEM. SYM.	A	Z
O	16	8

METHOD

REF. NO.	
66 De 4	JDM

REACTION	RESULT	EXCITATION ENERGY	SOURCE		DETECTOR		ANGLE
			TYPE	RANGE	TYPE	RANGE	

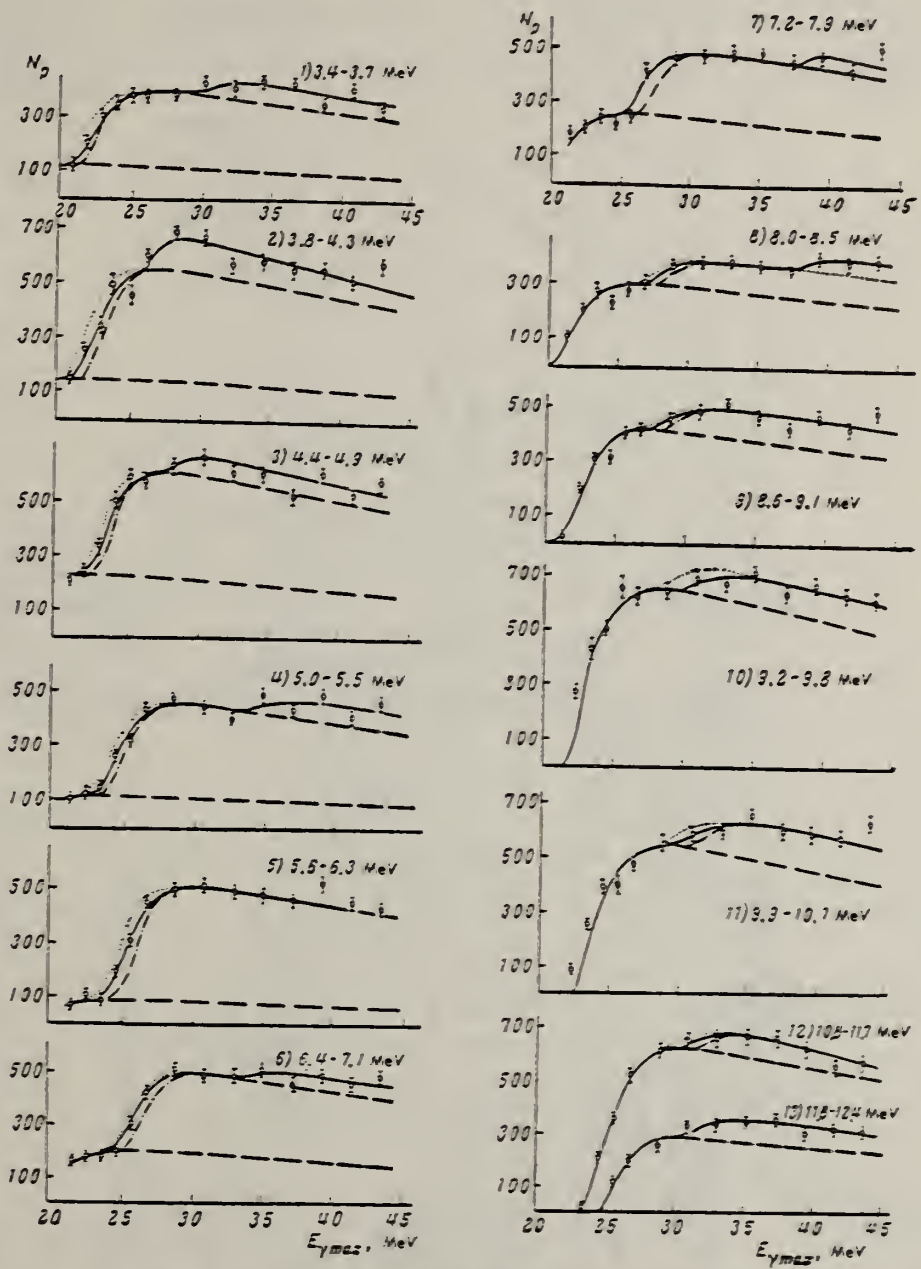

Fig. 2. Proton yield curves for individual sections of the spectra. N_p is the number of protons in a given section, per unit charge on the quantameter.

REF. V.P. Denisov and L.A. Kul'chitskii
J. Nucl. Phys. (USSR) 2, 70 (1965)
Sov. J. Nucl. Phys. 2, 48 (1966)

ELEM. SYM.	A	Z
O	16	8

METHOD

REF. NO. 66 De 4

JDM

REACTION	DETECTOR RANGE	DETECTOR ANGLE

Table I

Intensities $\int \sigma_1(E_\gamma)dE_\gamma$ and relative intensities I_{rel} of transitions to different states of the final nucleus N^{13} from excited states of O^{16} with energy E_{exc}

Ground state of N^{13}			First + second excited states (5.28, 5.30 MeV) of N^{13}			Third excited state (6.33 MeV) of N^{13}			Higher excited states of N^{13}				
E_{exc}, MeV	$\int \sigma_1(E_\gamma)\,dE_\gamma$, MeV·mb	I_{rel}, %	E_{exc}, MeV	$\int \sigma_1(E_\gamma)\,dE_\gamma$, MeV·mb	I_{rel}, %	E_{exc}, MeV	$\int \sigma_1(E_\gamma)\,dE_\gamma$, MeV·mb	I_{rel}, %	E_{exc}, MeV	$E_{exc}N^{13}$, MeV	$\int \sigma_1(E_\gamma)\,dE_\gamma$, MeV·mb	I_{rel}, %
21.9±0.2	8.3±0.8	45	22.0±0.3	4.65±0.90	25	22.2±0.3	5.45±1.10	30	—	—	—	—
22.4±0.2												
23.0±0.2	2.8±0.3	46	—	—	—	23.2±0.3	3.30±0.70	54	—	—	—	—
23.9±0.2	0.15±0.8	42	24.0±0.3	4.20±0.85	28	24.1±0.3	4.45±1.600	30	—	—	—	—
24.3±0.2												
25.2±0.2	2.9±0.30	46	24.9±0.3	3.40±0.70	54	—	—	—	—	—	—	—
25.9*	1.6	17	25.6±0.3	4.25±0.85	46	25.7±0.3	1.80±0.35	20	26.0±0.4	9.7	1.25±0.3	17
27.1*	2.6	72	26.6±0.3	0.95±0.20	28	—	—	—	—	—	—	—
28.0*	1.25	32	28.1±0.3	—	—	28.1±0.3	1.65±0.35	42	28.0±0.4	11.0	1.00±0.3	26
30.2*	1.25	21	30.0±0.3	1.10±0.20	18	29.8±0.3	1.35±0.30	22	30.0±0.4	7.3	1.40±0.4	23
									30.0±0.4	14.0	0.95±0.3	16
									~35	15	1.2	—
									~34	16	1.3	—
									~37	16	2.3	—

*The data are taken from the work of Fintelh and Gegel'tsa

REF.

F. W. K. Firk
Nuclear Instr. and Methods 43, 312 (1966)

EL EM. SYM.	A	Z
O	16	8

METHOD

$^{12}C(n,n)$ polarimeter

REF. NO. 66 Fi 1 JDM

REACTION	RESULT	EXCITATION ENERGY	SOURCE		DETECTOR		ANGLE
			TYPE	RANGE	TYPE	RANGE	
$G,N	NOX	THR-70	C	10-70	TOF-D	2-8	DST

No polarization effect seen.

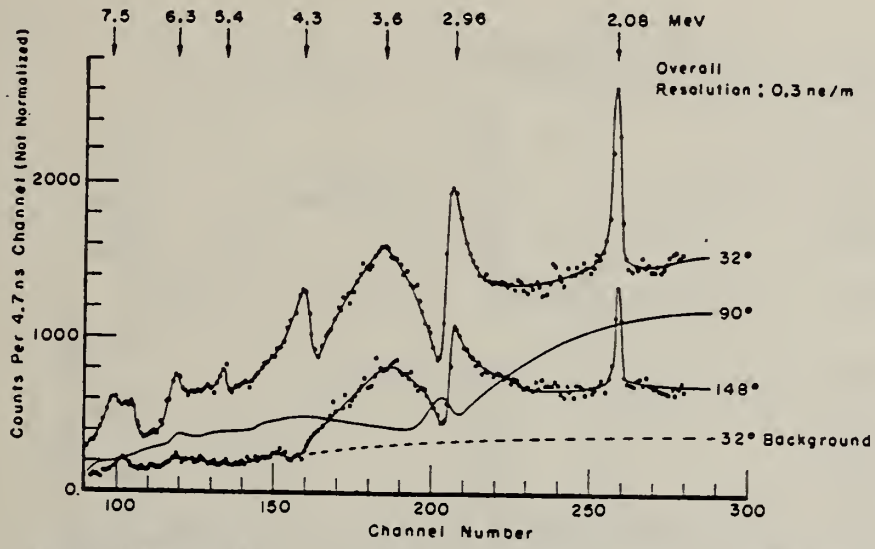

Fig. 5. Time-of-flight spectrum of neutrons from the reaction $^{12}C(n,n)^{12}C$ at 32°, 90° and 148°. Resolution 0.3 ns/m.

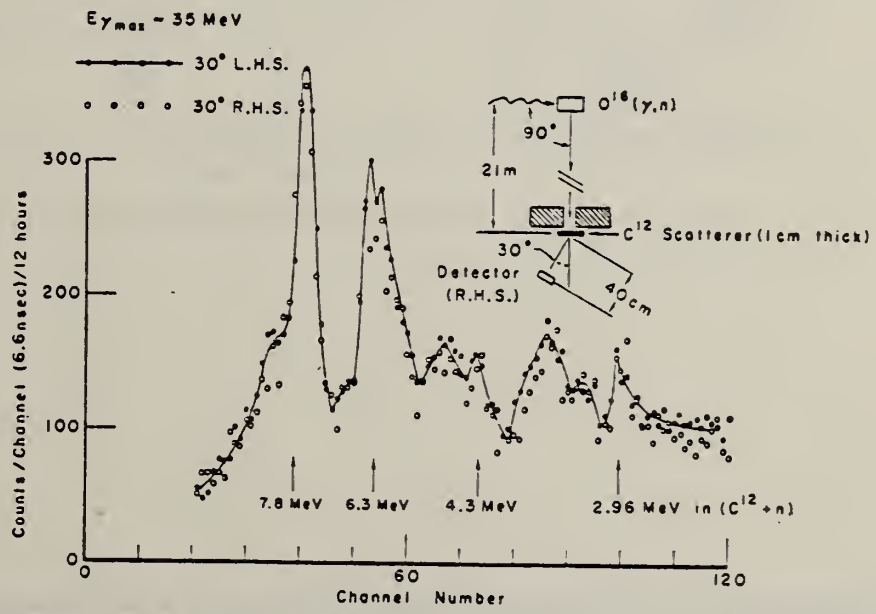

Fig. 6. Polarization studies, by 30° left-right scattering from ^{12}C, of photoneutrons from the $^{16}O(\gamma,n)^{15}O$ reaction.

REF. F. W. K. Firk
Proc. Gatlinburg Conference 352 (1966)

ELEM. SYM.	A	Z
O	16	8

METHOD

REF. NO. 66 Fi 2 hmg

REACTION	RESULT	EXCITATION ENERGY	SOURCE		DETECTOR		ANGLE
			TYPE	RANGE	TYPE	RANGE	
G,XN	SPC	THR-65	C	65	TOF-D	5-40	90

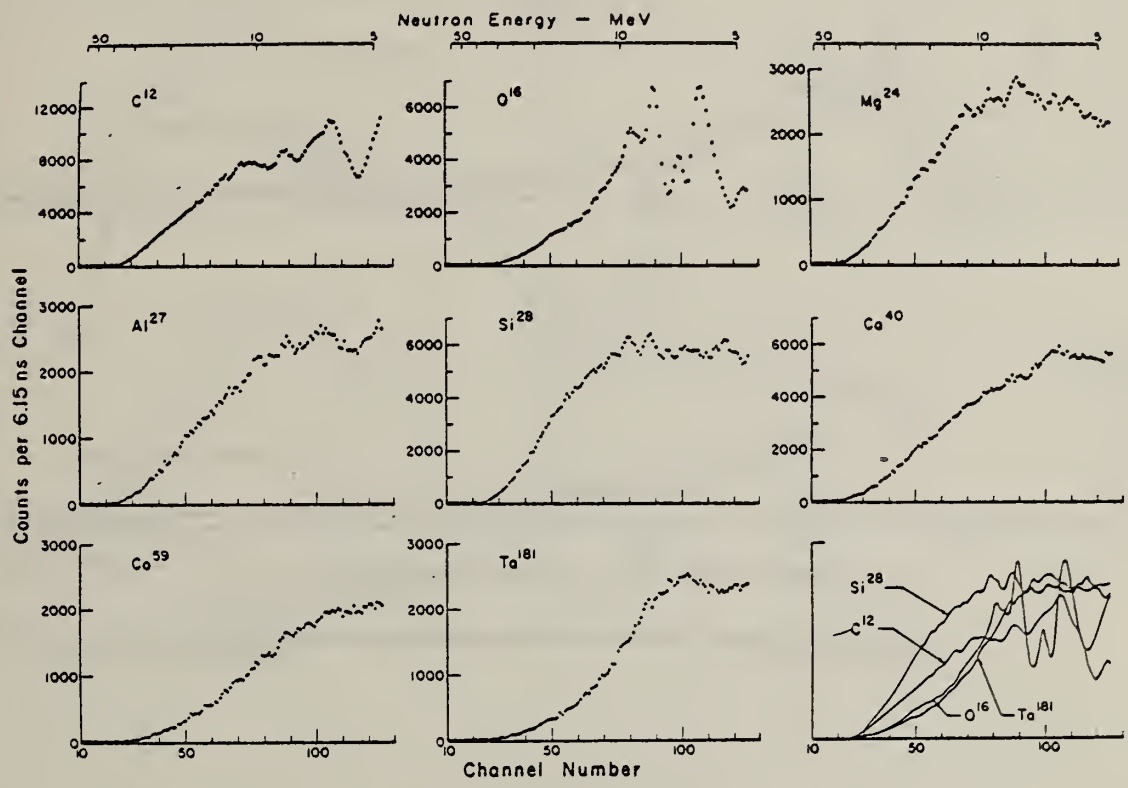

Fig. 1. Observed photoneutron time-of-flight spectra of C, O, Mg, Si, Ca, Co, V, and Ta.

[over]

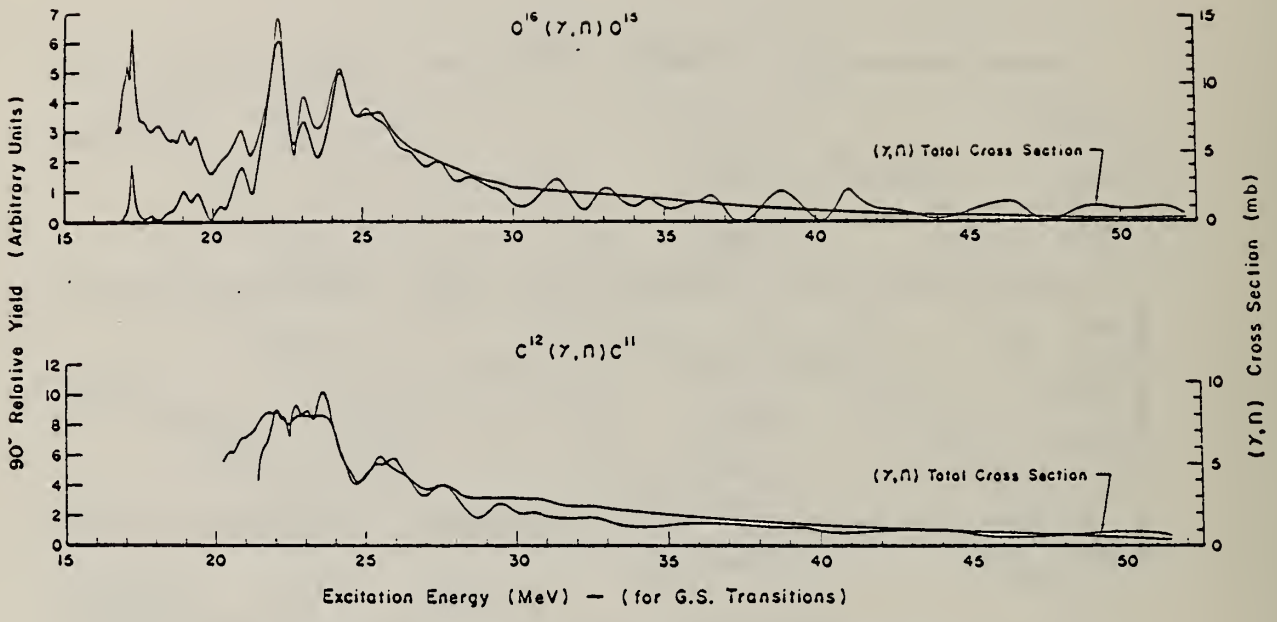

Fig. 2. The 90° relative yields of photoneutrons from ^{12}C and ^{16}O compared with the total (γ, n) yields.

REF. S. C. Fultz, R. L. Bramblett, B. L. Berman, J. T. Caldwell, and M. A. Kelly
Proc. Gatlinburg Conference 397 (1966)

ELEM. SYM.	A	Z
0	16	8

METHOD

REF. NO. 66 Fu 2 hmg

REACTION	RESULT	EXCITATION ENERGY	SOURCE		DETECTOR		ANGLE
			TYPE	RANGE	TYPE	RANGE	
G,NG/	RLY	20-26	D	20-26	BF3-I		4PI
G,PG/							

COINC

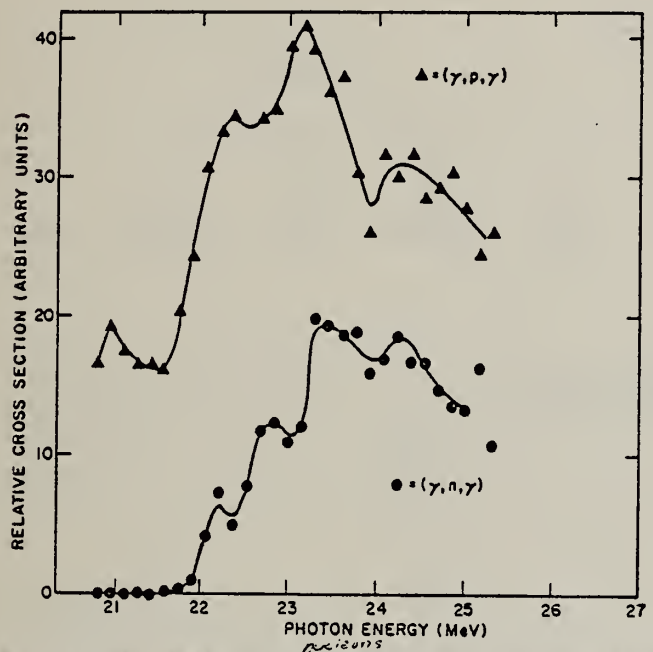

Fig. 2. Relative cross sections for neutrons emitted in transitions to excited states of ^{15}N (top curve) and ^{15}O (bottom curve).

REF.

A. Goldmann, P. Kneisel und H. v. Buttlar
Z. Physik, 192, 282 (1966)

ELEM. SYM.	A	Z
O	16	8

METHOD

REF. NO.	
66 Go 2	JDM

REACTION	RESULT	EXCITATION ENERGY	SOURCE		DETECTOR		ANGLE
			TYPE	RANGE	TYPE	RANGE	
G,T	ABX	THR-55	C	THR-55	ACT-I		4PI

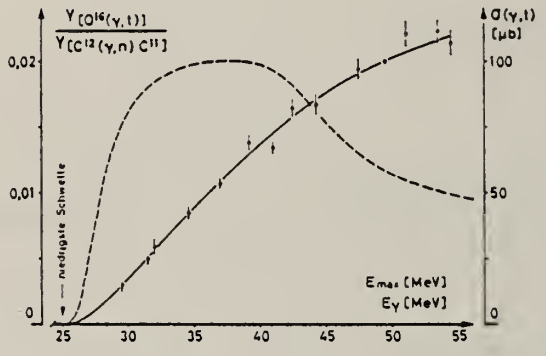

Fig. 1. Meßpunkte: Ausbeuteverhältnis $Y[O^{16}(\gamma, t)]/Y[C^{12}(\gamma, n)C^{11}]$ (linke Ordinatenskala). Die gestrichelt eingezeichnete Kurve für den Wirkungsquerschnitt (rechte Ordinatenskala) wurde aus der glatten Interpolationskurve durch die Meßpunkte berechnet

REF.	ELEM. SYM.	A	Z
J. Miller, C. Schuhl, G. Tamas, C. Tzara J. de Physique 27, 8 (1966)	O	16	8

METHOD	REF. NO.
	66 Mi 2 egf

REACTION	RESULT	EXCITATION ENERGY	SOURCE		DETECTOR		ANGLE
			TYPE	RANGE	TYPE	RANGE	
G,N	ABX	16-27	D	16-27	BF3-I		4PI

+71

TABLEAU V

σ_{int} à 26 MeV en MeV.mb

	^{16}O	^{40}Ca	^{12}C	Mg
γ, n	$41,5 \pm 4$	73 ± 7	$29,4 \pm 3$	58 ± 6

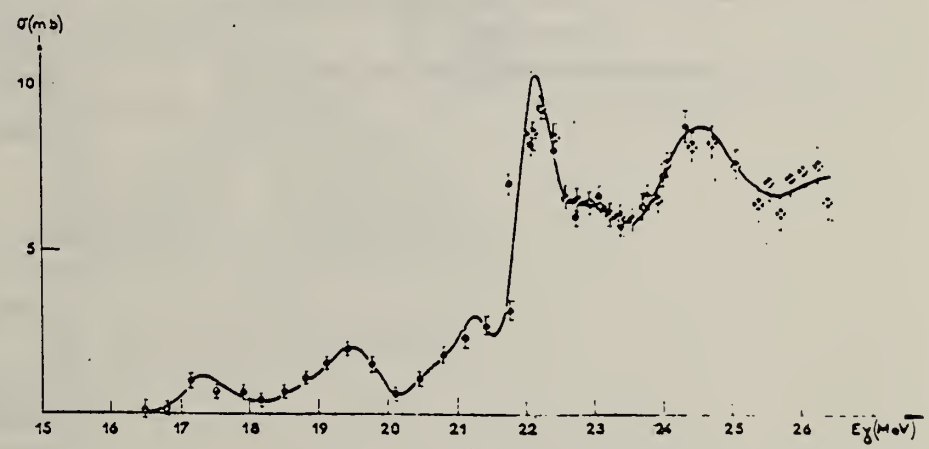

FIG. 1. — $\sigma(\gamma, n)$ dans ^{16}O. Points expérimentaux de mars 1962 (petits cercles noirs) et avril 1963 (grands cercles avec croix blanches).
La courbe tracée tient compte de la résolution finie de la raie de photons (400 keV).

REF.

R. O. Owens and J. E. E. Baglin
Phys. Rev. Letters 17, 1268 (1966)

EL EM. SYM.	A	Z
O	16	8

METHOD

Linac. NBS P2

REF. NO.	
66 Ow 1	JDM

REACTION	RESULT	EXCITATION ENERGY	SOURCE		DETECTOR		ANGLE
			TYPE	RANGE	TYPE	RANGE	
G,NG	RLY	THR-29	C	20-29	SCD-D	4-9	135
G,PG	RLY	THR-29	C	20-29	SCD-D	4-9	135

There is significant branching to (1/2+, 5/2+) states near 5 MeV.

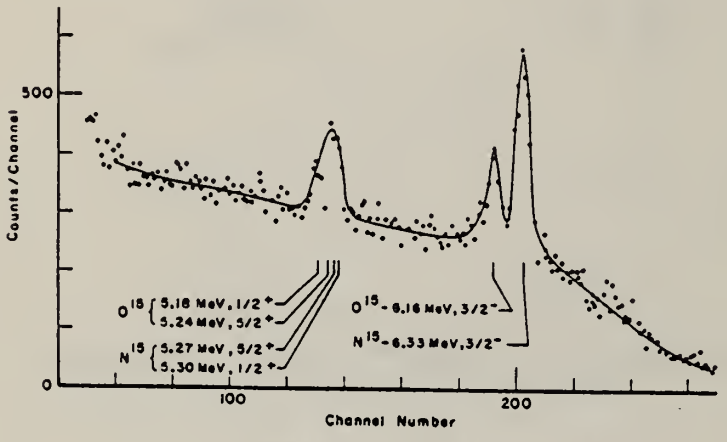

FIG. 1. Typical spectrum from germanium detector.

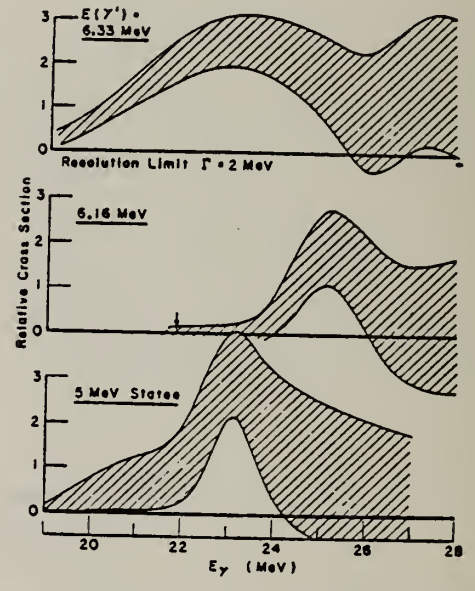

FIG. 2. Cross-section curves for $O^{16}(\gamma,p_3)$ (top), $O^{16}(\gamma,n_3)$ (center), and for the combined process $O^{16}(\gamma, p_{1,2})(\gamma,n_{1,2})$ (lower).

REF. R. O. Owens and J. E. E. Baglin
Proc. Gatlinburg Conference 337 (1966)

ELEM. SYM.	A	Z
O	16	8

METHOD

REF. NO. 66 Ow 2 hmg

REACTION	RESULT	EXCITATION ENERGY	SOURCE		DETECTOR		ANGLE
			TYPE	RANGE	TYPE	RANGE	
G,NG	RLX	THR-29	C	20-29	SCD-D		135
G,PG							

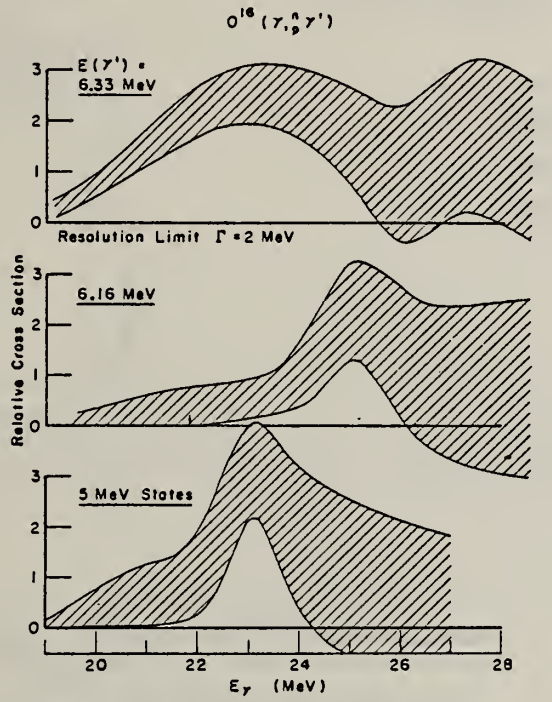

Fig. 2. Cross section curves for gamma peaks.

REF.

N. G. Puttaswamy and D. Kohler
Phys. Letters 20, 288 (1966)

EL.EM. SYM.	A	Z
O	16	8

METHOD

REF. NO.	
66 Pu 1	EGF

REACTION	RESULT	EXCITATION ENERGY	SOURCE		DETECTOR		ANGLE
			TYPE	RANGE	TYPE	RANGE	
HE3,G	RLX	23 - 26	D	1 - 4	NAI-D	15 - 26	90
				(1.0-3.5)			

Absolute cross section in terms of $^{13}C(^3He,\alpha\gamma)^{12}C(15.11MeV)$

$$\left.\frac{d\sigma}{d\Omega}\right|_{90^\circ}^{\gamma_0} = 0.7\ \mu b/sr \begin{pmatrix} +80\% \\ -50\% \end{pmatrix} \text{ at } 2.92 \text{ MeV}$$

Levels at 24.05±0.10 MeV
Γ = .45 MeV
25.12±0.05 MeV
Γ = .60 MeV

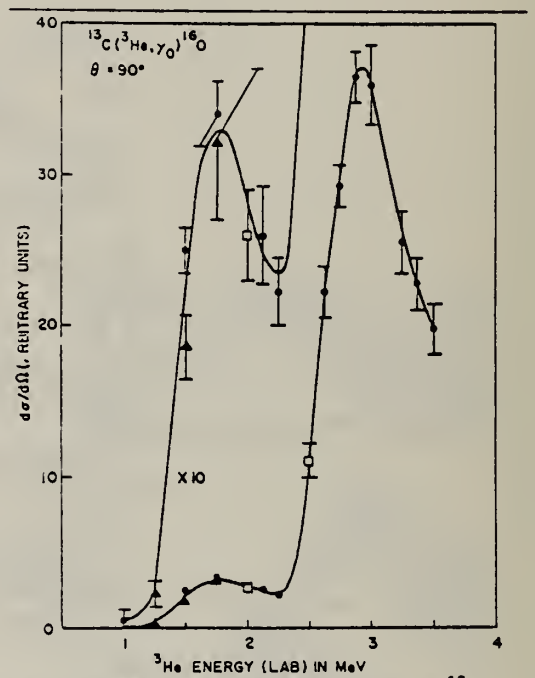

Fig. 2. Differential cross section at 90° for the ^{13}C $(^3He,\gamma_0)^{16}O$ reaction as a function of ^3He lab. energy. The data points for different target spot positions are shown by different symbols and were normalized to each other near 2.9 MeV ^3He energy. See text for further details.

REF.

M. Stroetzel and F. Gudden
Phys. Letters 22, 485 (1966)

ELEM. SYM.	A	Z
O	16	8

METHOD

REF. NO. 66 St 2 JDM

REACTION	RESULT	EXCITATION ENERGY	SOURCE TYPE	SOURCE RANGE	DETECTOR TYPE	DETECTOR RANGE	ANGLE
E,E/	FMF	5 - 14	D	60	MAG-D	46 - 60	117

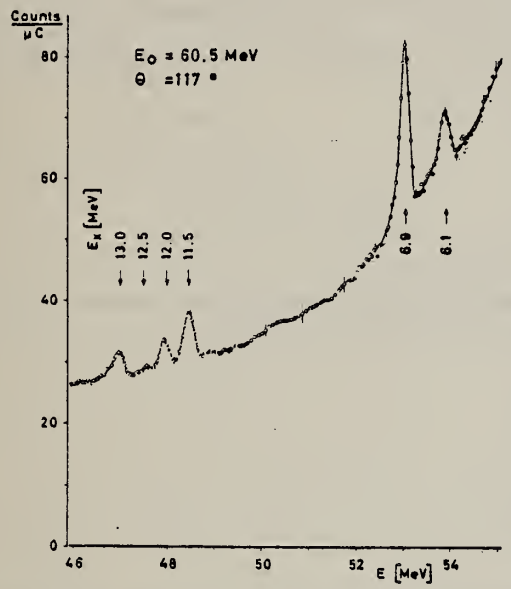

Fig. 1. Energy distribution of 60.5 MeV electrons scattered from 180 mg/cm^2 BeO through 117°.

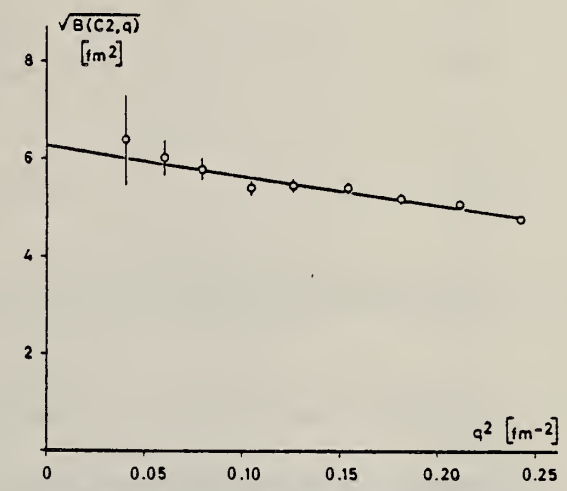

Fig. 2. Square root of the reduced transition probability of the 6.92 MeV (2^+) level in ^{16}O.

Table 1
Reduced transition probabilities $B(E2,\downarrow)$ which differ from the $B(E2,k)$ used in the text by the statistical factor $1/(2I+1) = \frac{1}{5}$, with
$B(E2,k) = 6.2\times10^6\,\Gamma^0(\text{eV})\,E_\chi^{-5}\,(\text{MeV})\ \text{fm}^4$.

	$B(E2,\downarrow) = \frac{1}{5}B(E2,k)$ fm^4		
Experiment	6.92 → g.s.	6.92 → 6.05	11.52 → g.s.
(γ,γ) [10]	$4.3\,^{+1.4}_{-0.9}$	40 *	
(γ,γ [11]	$5.2\,^{+2.3}_{-1.2}$	48 *	
(α,γ) [12]			5.5 ± 1.2
(α,γ) [13]			4.0 ± 0.6
(e,e') [5]			5.2 ± 0.6
this work	7.9 ± 1.2	73 *	3.1_5 ± 0.8
Theory [1]	5.3	103	3.3

* Values calculated with a branching ratio of 2.8×10^{-4} (average from [8] and [9]).

REF.

M. Suffert
Nucl. Phys. 75, 226 (1966)

ELEM. SYM.	A	Z
O	16	8

METHOD

6 MeV Van de Graaff

REF. NO. 66 Su 1 JDM

REACTION	RESULT	EXCITATION ENERGY	SOURCE TYPE	SOURCE RANGE	DETECTOR TYPE	DETECTOR RANGE	ANGLE
D,G	ABX	21- 25	D	1- 5	NAI-D	0 - 25	DST

79

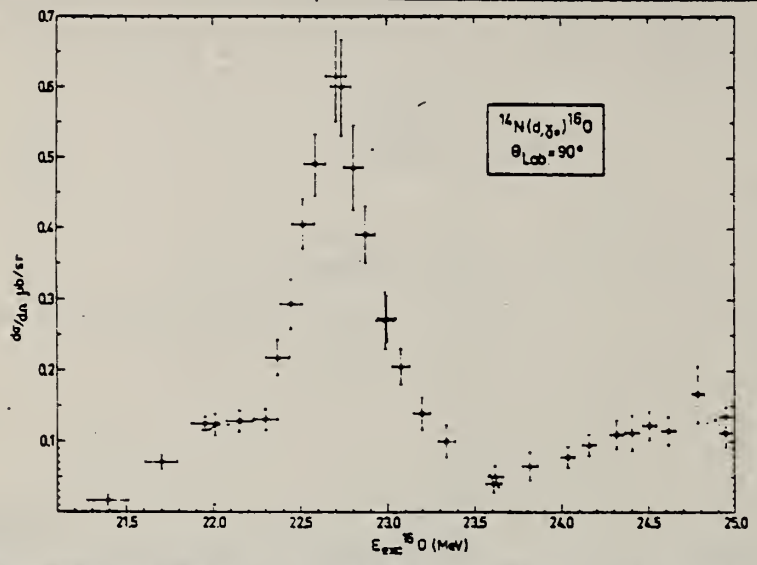

Fig. 9. Differential cross section at 90° of the $^{14}N(d, \gamma_0)^{16}O$ reaction as a function of excitation energy in ^{16}O at the centre of the gas target. The horizontal bars show the energy spread due to the target thickness. The indicated errors for the cross section do not contain a possible error of the absolute calibration (estimated maximum value ±30 %).

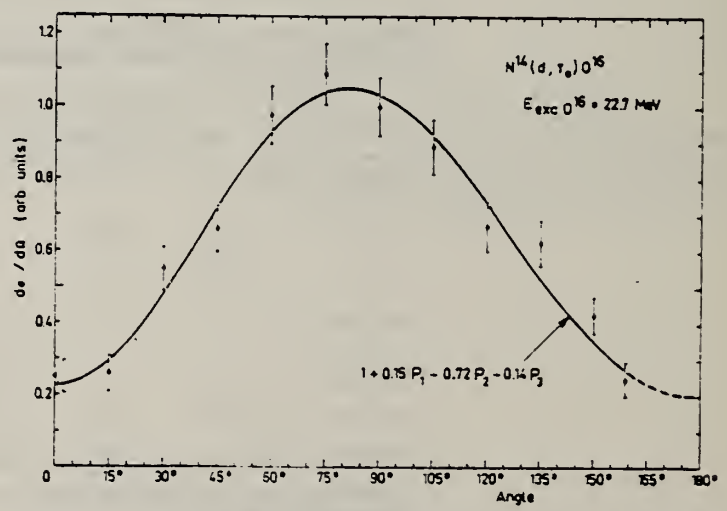

Fig. 10. Angular distribution of the $^{14}N(d, \gamma_0)^{16}O$ reaction at E_{ex} = 22.7 MeV. The curve is the Legendre polynomial fit.

REF.	ELEM. SYM.	A	Z
G. J. Vanpraet and W.C. Barber Nucl. Phys. 79, 550 (1966)	O	16	8

METHOD	REF. NO.	
Stanford Mk II Linac	66 Va 1	JDM

REACTION	RESULT	EXCITATION ENERGY	SOURCE		DETECTOR		ANGLE
			TYPE	RANGE	TYPE	RANGE	
E,E/	FMF	10 - 30	D	43 - 69	MAG-D	35 - 70	180

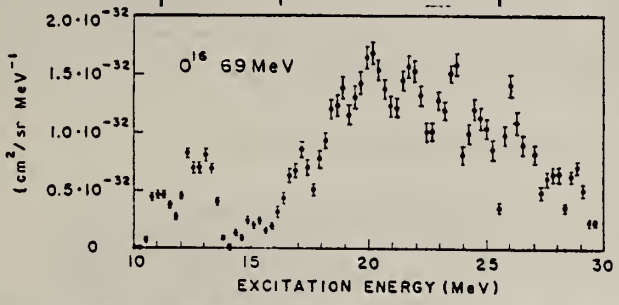

Fig. 3. Cross section for inelastic scattering of electrons at 180° with excitation of the ^{16}O nucleus, plotted as a function of excitation energy.

TABLE 1
Cross sections and matrix elements of levels excited in ^{16}O

Experimental levels (±0.25 MeV)		$(d\Omega/d\sigma) \times 10^{-8}$ (μb/sr)	$\lvert\langle J_f\rVert T(q)\rVert J_i\rangle\rvert^2 \times 10^4$
43 MeV	11.0	1.13±0.30	3.54±0.93
	12.0	0.30±0.08	0.94±0.25
	13.1	1.26±0.30	4.0 ±1.0
	17.1	0.67±0.50	2.10±1.57
59 MeV	11.0	0.05±0.02	0.3 ±0.12
	13.1	0.51±0.12	3.0 ±0.7
	17.1	0.61±0.13	3.6 ±0.8
69 MeV	11.0	0.40±0.06	3.2 ±0.48
	12.0	0.48±0.07	3.86±0.56
	13.1	0.84±0.21	6.75±1.70
	17.1	0.69±0.12	5.55±1.0

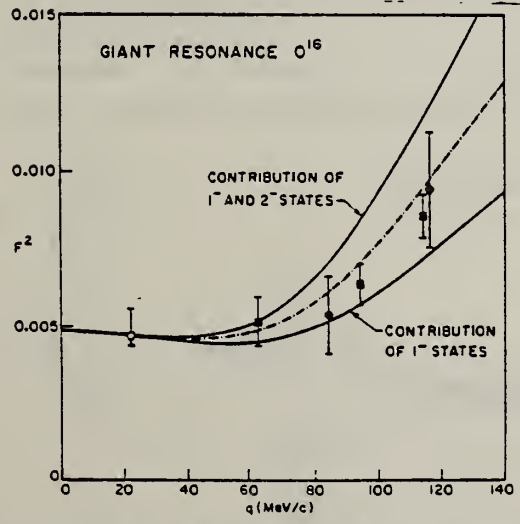

Fig. 7. Squared form factor for the giant resonance in ^{16}O. The lower line includes only 1^- states [12]), the upper line also includes the 2^- states [17]). The dash-dot line gives the result if only half of the 2^- states contribution is included. The open circle at $q = 22$ MeV/c represents the result of the photon experiments [4]). The black circles and the square are Stanford results as given respectively by refs. [3,13]).

REF.

Yu. M. Volkov, A.P. Komar and V.P. Chizhov
J. Nucl. Phys. (USSR) 3, 277 (1966)
Sov. J. Nucl. Phys. 3, 198 (1966)

ELEM. SYM.	A	Z
O	16	8

METHOD

REF. NO.	
66 Vo 1	JDM

REACTION	RESULT	EXCITATION ENERGY	SOURCE		DETECTOR		ANGLE
			TYPE	RANGE	TYPE	RANGE	
G,D	ABX	THR - 50	C	20 - 50	TEL-D	5 - 10	90

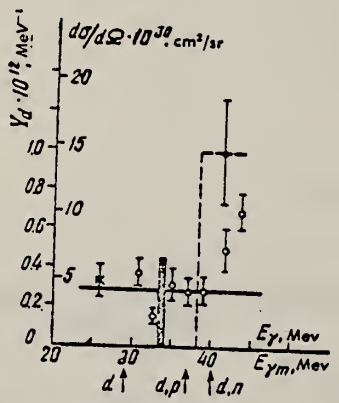

Fig. 3. Photodeuteron yield from O^{16} as a function of $E_{\gamma m}$ – hollow circles; differential cross section for the reaction $O^{16}(\gamma, d)N^{14}$ as a function of γ-ray energy E_γ–dashed line; the solid line denotes the background level. The heavy black bar is the result of the theoretical calculation of Madsen and Henley.[8] The arrows (d), (d, p), and (d, n) denote the locations of the energy thresholds of the reactions $O^{16}(\gamma, d)N^{14}$, $O^{16}(\gamma, dp)C^{13}$, and $O^{16}(\gamma, dn)N^{13}$ with emission of deuterons with energy $E_d = 7.5$ MeV.

REF. J. E. E. Baglin and M. N. Thompson
PICNS-67 Contributions, International Conference on Nuclear Structure, Tokyo, Japan 1967 (Institute for Nuclear Study, University of Tokyo, Tanashi-shi, Tokyo, Japan) 10.24, p. 388

ELEM. SYM.	A	Z
O	16	8

METHOD

REF. NO. 67 Ba 5 EGF

REACTION	RESULT	EXCITATION ENERGY	SOURCE		DETECTOR		ANGLE
			TYPE	RANGE	TYPE	RANGE	
G,NG	SPC	21-26	C	26	SCD-D	5-8	135
G,PG	SPC	17-26	C	26	SCD-D	5-8	135

G-SPECTRUM

Decay Modes of O^{16} Giant Resonance States

J. E. E. Baglin and M. N. Thompson*

Electron Accelerator Laboratory, Yale University
New Haven, Connecticut USA

A study has been made of the spectrum of γ-rays produced in the decay of excited levels of O^{15} and N^{15} which result from the $O^{16}(\gamma,n)$ and $O^{16}(\gamma,p)$ processes. Examination to find which residual configurations are produced by specific regions of the giant resonance can indicate the nature of the parent excited states in O^{16}.

The figure shows a spectrum obtained from a water target with a 6 cc Ge(Li) detector placed at 135° to an incident bremsstrahlung beam of maximum energy 26.5 MeV. Most of the O^{16} giant resonance can thus contribute to this spectrum. The spectral peaks shown are double-escape peaks which rise over the corresponding compton and bremsstrahlung components of their line profiles.

The 30 keV resolution used is sufficient to show comparable population of all four positive parity states at 5.18 MeV ($1/2^+$) 5.24 MeV ($5/2^+$)[O^{15}] and 5.27 MeV ($5/2^+$), 5.30 MeV ($1/2^+$)[N^{15}], as well as the two $(p_{3/2})^{-1}$, $3/2^-$ states at 6.18 MeV [O^{15}]and 6.33 MeV [N^{15}], and the $3/2^+$ state of O^{15} and 6.79 MeV. The 6 MeV peaks exhibit their expected Doppler broadening.

In other spectra, taken also with 26.5 MeV bremsstrahlung, evidence has appeared for a weak line whose likely origin is the positive parity state at 8.3 MeV.

In a previous measurement (1) it was established that some or all of the 5 MeV lines make up about 24% of the total excited-state cross section. It is now evident that both $1/2^+$ and $5/2^+$ states are produced in this process. Their production occurs strongly between 22 and 25 MeV and it implies an appreciable non-single-particle excitation in this part of the O^{16} giant resonance.

The $(p_{3/2})^{-1}$ 6 MeV states are populated readily by single-particle processes, and their dominance is to be expected. The suppression of the cross section for the 6.18 MeV (O^{15}) line at energies below 24 MeV, as reported in reference (1), remains to be explained.

References: (1) R. O. Owens, J. E. E. Baglin, Phys. Rev. Letters 17,1268(1966).

* Work supported by the United States Atomic Energy Commission.

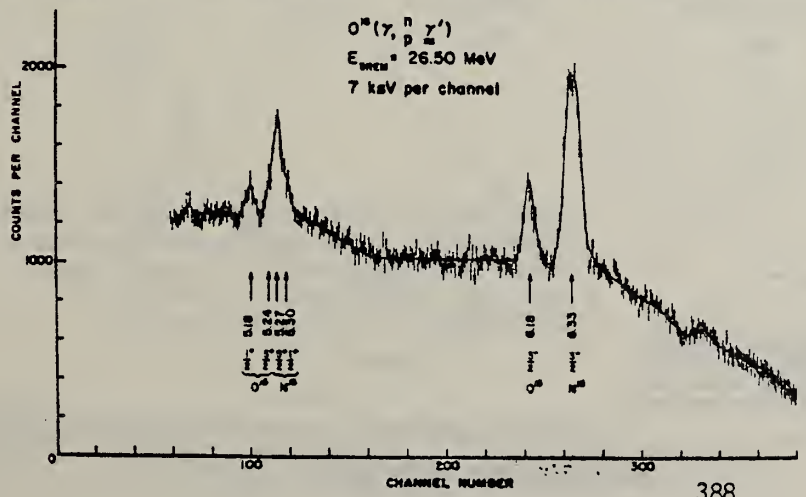

REF.

J. L. Black, W. J. O'Connell, S. S. Hanna, and G. L. Latshaw
Phys. Letters 25B, 405 (1967)

ELEM. SYM.	A	Z
O	16	8

METHOD

REF. NO.	
67 B1 1	EGF

REACTION	RESULT	EXCITATION ENERGY	SOURCE		DETECTOR		ANGLE
			TYPE	RANGE	TYPE	RANGE	
P,G	RLX	20-30	D	10-18	NAI-D	20-30	DST

78+

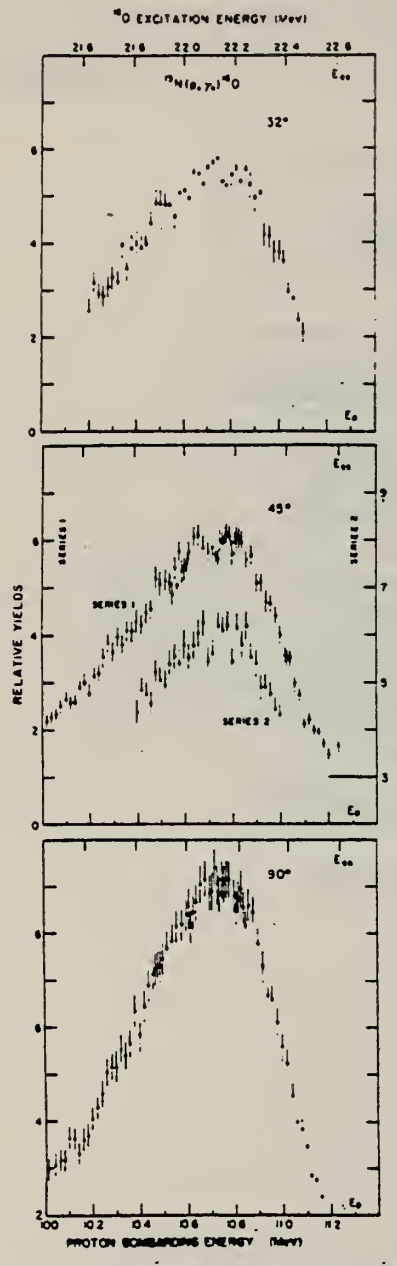

Fig. 1. Excitation functions for ^{15}N(p,γ_0)^{16}O from E_p = = 10.0 to 11.24 MeV, measured at 32°, 45° and 90°. In the calculation of the excitation energy scale allowance has been made for the energy loss in the entrance foil of the gas cell.

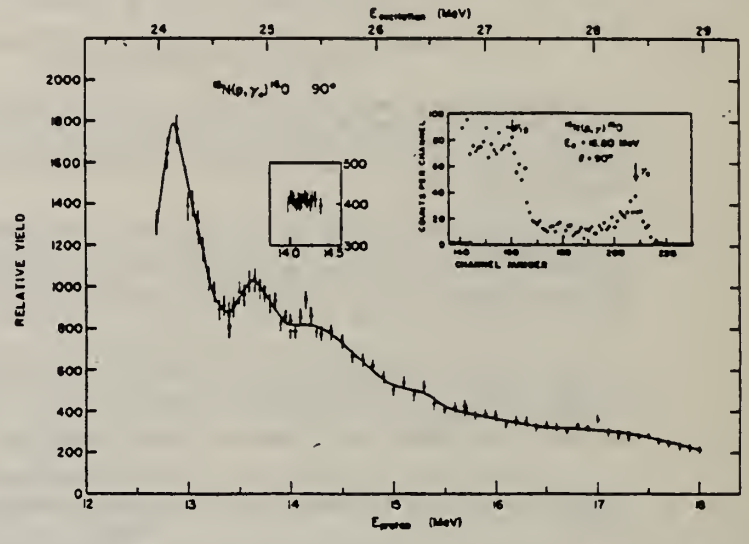

Fig. 2. Excitation function for ^{15}N(p,γ_0)^{16}O from E_p = 12.7 to 18.0 MeV measured at 90°. The inserts show a repeat run with 20 keV resolution and a typical gamma-ray spectrum.

Paper gives absolute cross section integrals obtained by normalizing relative yields to 64Ta2 (N.W. Tanner et al., Phys. Rev. Lett. 13, 410 (1964).

REF.
J.L. Black, F. Riess, P. Paul, W.J. O'Connell, G.A. Fisher, S. S. Hanna PICNS-67 Contributions, International Conference on Nuclear Structure, Tokyo, Japan 1967 (Institute for Nuclear Study, University of Tokyo, Tanashi-shi, Tokyo, Japan) 10,11, p. 375

METHOD

ELEM. SYM.	A	Z
0	16	8

REF. NO. 67 B1 2 EGF

REACTION	RESULT	EXCITATION ENERGY	SOURCE		DETECTOR		ANGLE
			TYPE	RANGE	TYPE	RANGE	
P,G	RLX	21-22	D	9-12	NAI-D	21-23	45

Giant Dipole Resonances in p-Shell Nuclei.*

J. L. Black, F. Riess, P. Paul,# W. J. O'Connell, G. A. Fisher, and S. S. Hanna

Department of Physics, Stanford University, Stanford, California, U.S.A.

The giant dipole resonances in p-shell nuclei have been studied by means of the (p,γ) capture reaction. The capture gamma rays are detected with good resolution with a 24 x 24 cm NaI detector encased in an anticoincidence plastic shield and employing pulse pile up suppression. The region of the giant resonance can be covered with good energy resolution with protons from an FN tandem accelerator up to proton energies of 18 MeV. Fine structure and gamma ray angular distributions for giant resonances observed in ^{8}Be, ^{14}N, and ^{16}O have been studied. For ^{8}Be and ^{14}N the giant resonances based on the first excited state can also be studied. The resonances observed in $^{7}Li(p,\gamma)^{8}Be$ are shown in Fig. 1. The γ_0 giant resonance shows little structure. The γ_1 resonance exhibits some structure at E_x = 22 MeV. The center of the γ_1 resonance lies about 2.5 MeV above the center of the γ_0 resonance. Thus, the excitation energy for both resonances is about the same, 21.5 MeV. The dipole strengths of the resonances are about equal i.e., the integrated yields are roughly proportional to $2J + 1$, where J is the spin of the final state. In ^{14}N the first excited state has T = 1, so that resonances based on a T = 1 level are observed. Previous measurements[1] on $^{15}N(p,\gamma_0)^{16}O$ have been extended to E_p = 17.5 MeV. Above E_x = 25.5 MeV, no pronounced structure was revealed. In addition, the main peak of the giant resonance at E_x = 22.2 MeV has been studied in detail with high resolution to search for possible fine structure. Results at θ = 45°, shown in Fig. 2, indicate the existence of structure in this peak. A measurement at θ = 90° displays similar structure. The results are compared with recent $^{16}O(\gamma,p)^{15}N$ data.[2]

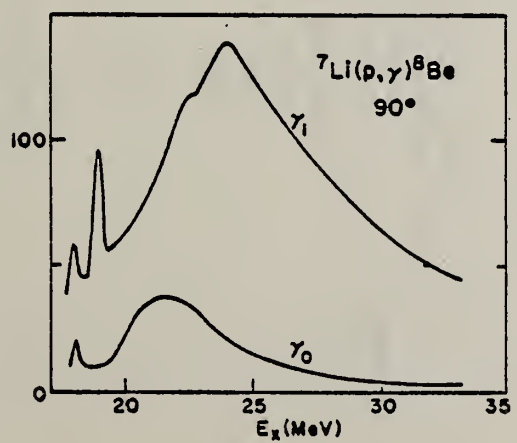

Fig. 1

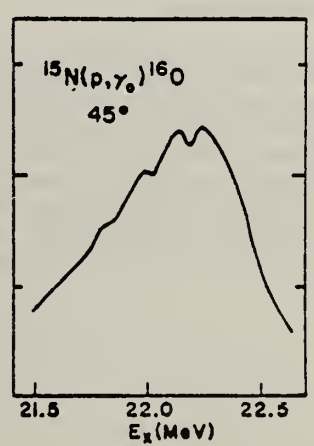

Fig. 2

* Supported in part by the National Science Foundation.
# Present address: State University of New York, Stony Brook, New York.
1 N. W. Tanner, G. C. Thomas, and E. D. Earle, Nucl. Phys. 52, 45 (1964).
2 J. Baglin, private communication.

REF. J. T. Caldwell, S. C. Fultz, R. L. Bramblett
Phys. Rev. Lett. 19, 447 (1967)

ELEM. SYM.	A	Z
O	16	8

METHOD

REF. NO. 67Ca3 egf

REACTION	RESULT	EXCITATION ENERGY	SOURCE		DETECTOR		ANGLE
			TYPE	RANGE	TYPE	RANGE	
G,NG	ABX	17-29	D	17-29	NAI	5-7	4PI
G,PG	ABX	20-29	D	17-29	NAI	5-7	4PI

(G,NG) 5.2, 6.2, 6.8 MEV STATES
(G,PG) 5.3, 6.3, 7.3 MEV STATES

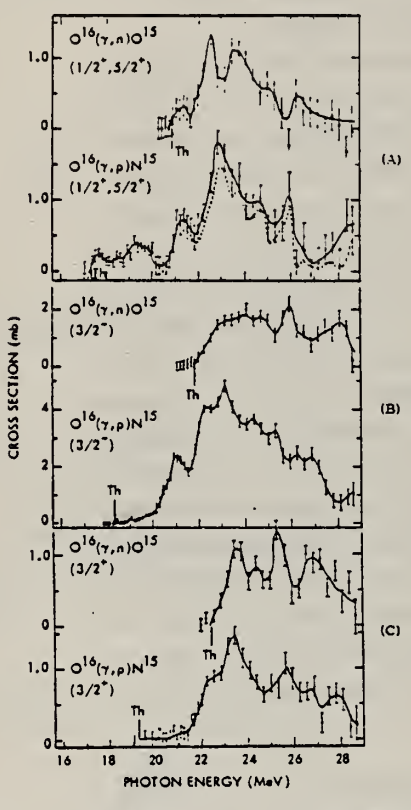

FIG. 2. $O^{18}(\gamma,\pi\gamma')$ and $(\gamma,p\gamma')$ mirror-level, final-state cross sections. (a) Top: $O^{15}(\frac{1}{2}^+,\frac{5}{2}^+$ unresolved) 5.2-MeV, final-state cross section. Bottom: $N^{15}(\frac{1}{2}^+,\frac{5}{2}^+$ unresolved) 5.3-MeV, final-state cross section. Dashed line shows effect of subtracting 9.22-MeV level cascades (Ref. 2). (b) Top: $O^{15}(\frac{3}{2}^-)$ 6.18-MeV, final-state cross section. Bottom: $N^{15}(\frac{3}{2}^-)$ 6.33-MeV, final-state cross section. (c) Top: $O^{15}(\frac{3}{2}^+)$ 6.79-MeV, final-state cross section. Bottom: $N^{15}(\frac{3}{2}^+)$ 7.30-MeV, final-state cross section.

Table I. Integrated cross sections for O^{16} photoreactions.

Reaction	Final state (MeV)	$\int_0^{28.7} \sigma d\mathcal{E}$ (MeV mb)	Fractional $\int_0^{28.7} \sigma d\mathcal{E}$
(γ,p)	ground state$(\frac{1}{2}^-)$	34.42[a]	0.286
	5.3$(\frac{1}{2}^+,\frac{5}{2}^+)$	4.94[b]	0.041
	6.33$(\frac{3}{2}^-)$	22.30	0.185
	7.30$(\frac{3}{2}^+)$	5.47	0.047
	9.1	2.03	0.017
	9.22	1.50	0.013
	9.9	2.36	0.020
	10.8	2.34[c]	0.020
(γ,n)	ground state$(\frac{1}{2}^-)$	26.67	0.223
	5.2$(\frac{1}{2}^+,\frac{5}{2}^+)$	3.49	0.029
	6.18$(\frac{3}{2}^-)$	9.43	0.079
	6.79$(\frac{3}{2}^+)$	4.50	0.038
(γ,α)	15.11$(1^+,T=1)$	0.23	0.002
		119.68	1.000

[a] From Refs. 6 to 8.
[b] The 9.22-MeV 100% cascade transition cross section has been subtracted from the observed 5.3-MeV yield cross section.
[c] The 10.6-MeV yields have been multiplied by $\Gamma_{tot}/\Gamma_{\gamma 0} = 3.0 \pm 0.5$ from Ref. 2.

REF. T. E. Drake, R. M. Hutcheon, V. W. Stobie, G. A. Beer, and H. S. Caplan
Phys. Rev. 163, 947 (1967)

ELEM. SYM.	A	Z
O	16	8

METHOD

REF. NO. 67 Dr 1 HMG

REACTION	RESULT	EXCITATION ENERGY	SOURCE		DETECTOR		ANGLE
			TYPE	RANGE	TYPE	RANGE	
E,E/	FMF	19	D	128	MAG-D		DST

J-PI

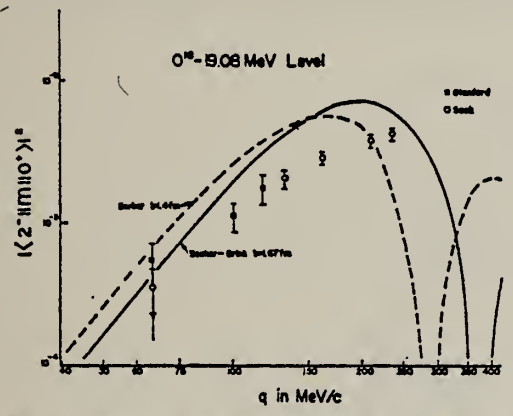

FIG. 2. The variation of the transition matrix element with momentum transfer. We use the formalism of deForest and Walecka [T. deForest and J. D. Walecka, Advan. Phys. 15, 1 (1966)], thus $|F_T(q)|^2 = (4\pi/Z^2)|\langle J^\pi||M||0^+\rangle|^2$.

REF. E. D. Earle and N. W. Tanner
Nucl. Phys. A95, 241 (1967)

ELEM. SYM.	A	Z
O	16	8

METHOD

REF. NO. 67 Ea 1 EGF

REACTION	RESULT	EXCITATION ENERGY	SOURCE TYPE	SOURCE RANGE	DETECTOR TYPE	DETECTOR RANGE	ANGLE
P,G	ABX	13-25	D	1-14	NAI-D		DST

1083

Detailed angular distribution plotted.

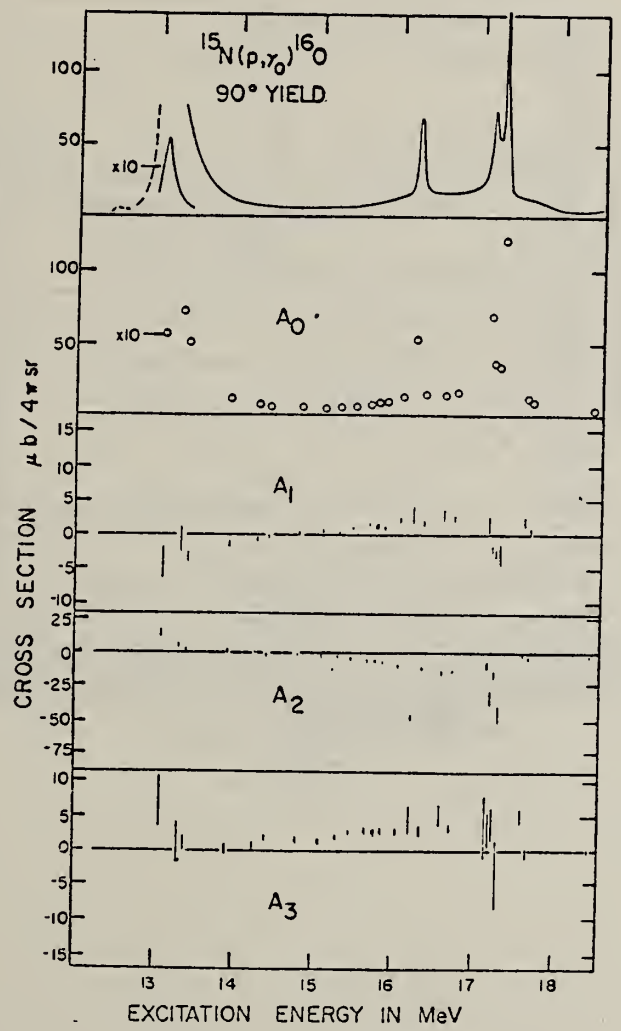

Fig. 6. The 90° excitation function for $^{15}N(p,\gamma_0)^{16}O$ (dashed portion is from ref. [9]) and the coefficients from the Legendre polynomial expansion $d\sigma/d\Omega = A_0 + A_1 P_1(\cos\theta) + A_2 P_2(\cos\theta) + A_3 P_3(\cos\theta)$.

[over]

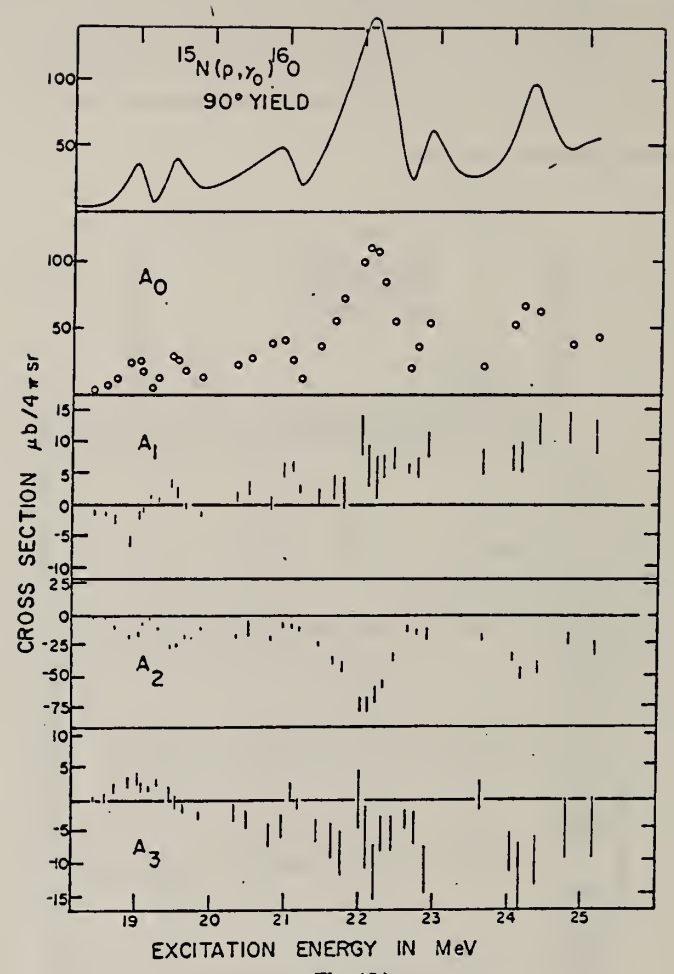
$^{15}N(p,\gamma_0)^{16}O$
90° YIELD
A_0
A_1
A_2
A_3
CROSS SECTION μb/4π sr
EXCITATION ENERGY IN MeV

Fig. 6(b).

REACTION	RESULT	EXCITATION ENERGY	SOURCE		DETECTOR		ANGLE
			TYPE	RANGE	TYPE	RANGE	

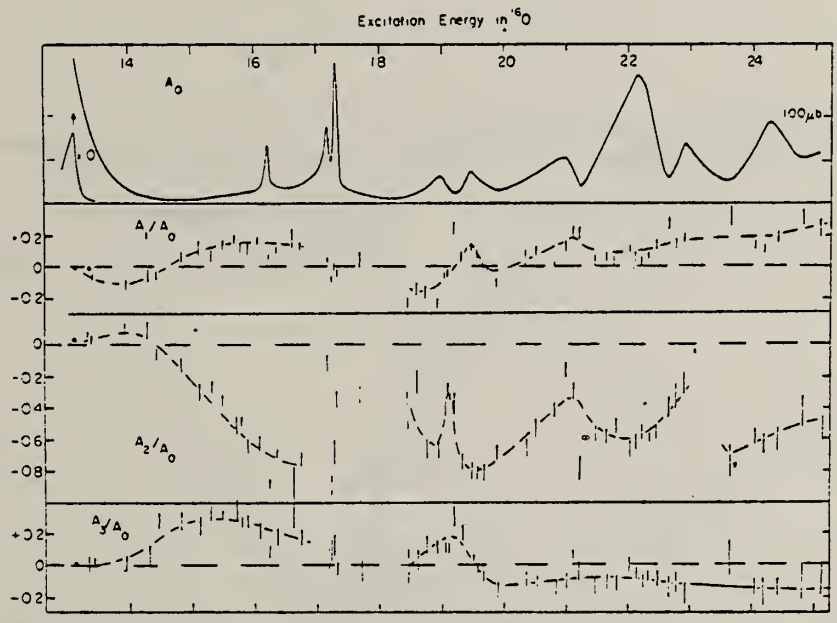

Fig. 7. The total cross section A_0 of $^{15}N(p, \gamma_0)^{16}O$ and the coefficients A_l/A_0 from the expansion $\Sigma_0^3 A_l P_l(\cos\theta)$. The vertical lines show the r.m.s. errors. Note that the angular distribution coefficients of fig. 6 are divided by A_0 and plotted in this figure. The dashed curves are drawn smoothly through the experimental points.

[over]

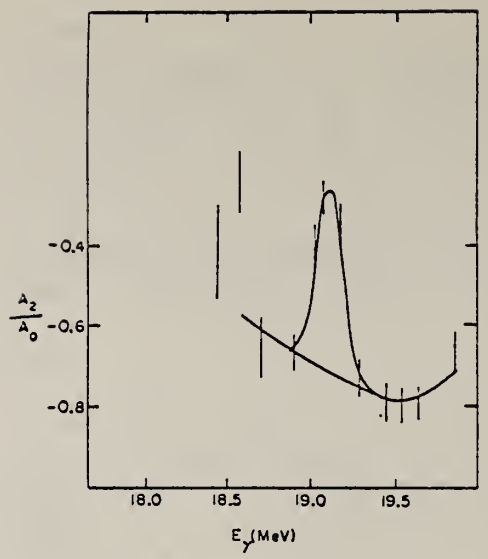

Fig. 9. Detail of the A_2/A_0 versus E_γ data in the region of 19 MeV. The peaked curve is consistent with the strong quadrupole state identified by Bishop and Isabelle [33]) at this energy.

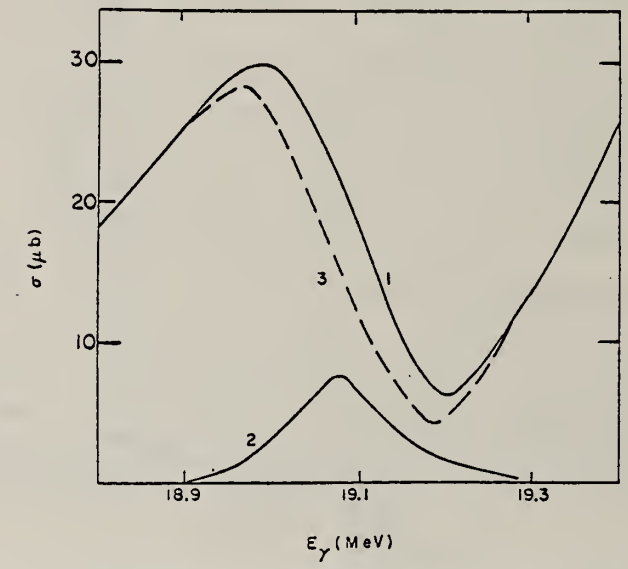

Fig. 10. Decomposition of the total cross section A_0 (curve 1) into the sharp quadrupole resonance at 19.08 MeV (curve 2) and the remaining dipole cross section (curve 3).

REF. S. Ferroni, V. Gracco, D. B. Isabelle, R. Malvano and M. Sanzone
Nucl. Phys. A98, 409 (1967)

ELEM. SYM.	A	Z
O	16	8

METHOD

REF. NO. 67 Fe 2 JOC

REACTION	RESULT	EXCITATION ENERGY	SOURCE		DETECTOR		ANGLE
			TYPE	RANGE	TYPE	RANGE	
G,XN	ABX	19-150	C	100-150	BF3-I		4PI

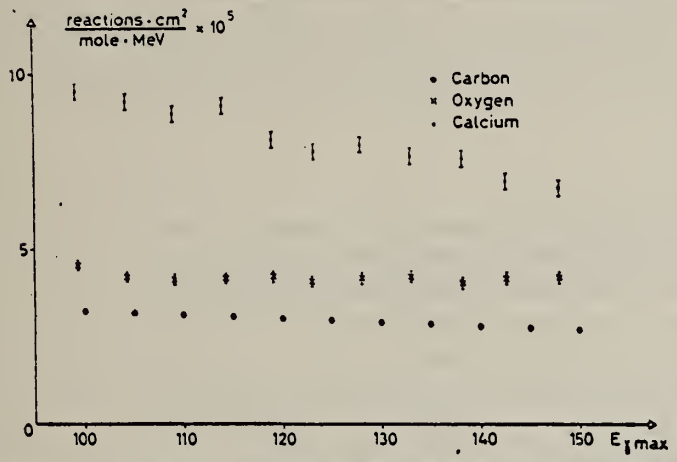

Fig. 3. Yields of the (γ, Tn) reaction for the three nuclei as a function of energy.

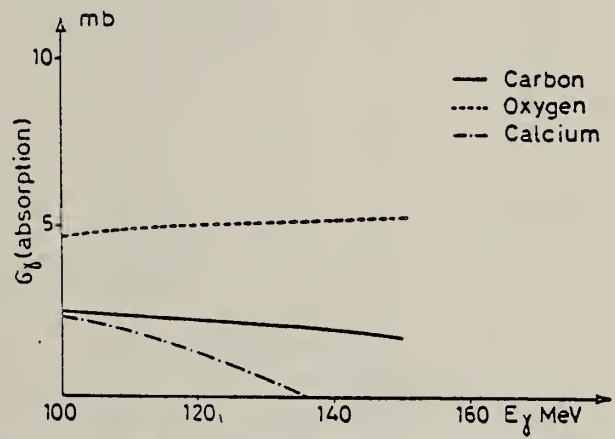

Fig. 6. The absorption cross sections for the three nuclei after all corrections have been applied.

TABLE 2

Values of the parameters for the best fit to the bremsstrahlung weighted cross sections

$$\int_{E_S}^{E_\gamma} \frac{\sigma(E)}{E}\,dE = (a_0 + a_1 E_\gamma)E_\gamma$$

	^{12}C	^{16}O	^{40}Ca
a_0 (10^{28})	7.03 $\pm$0.05	7.9 $\pm$0.5	24.6 $\pm$0.8
a_1 (10^{28})	$-$0.0173 $\pm$0.0004	$-$0.0072 $\pm$0.0036	$-$0.09 $\pm$0.006

REF.

H. M. Gerstenberg and E. G. Fuller
NBS Tech. Note 416, June 1967

ELEM. SYM.	A	Z
O	16	8

METHOD

REF. NO.	
67 Ge 2	HMG

REACTION	RESULT	EXCITATION ENERGY	SOURCE		DETECTOR		ANGLE
			TYPE	RANGE	TYPE	RANGE	
G,N	ABY	THR-27	C	22,27	BF3-I		4PI

Table 7. Comparison of neutron yields. Yields are given in units of (neutron cm^2/MeV nucleus)$\times 10^{-28}$. The estimated uncertainties in Y and Y_c are of the order of 6% and 10%, respectively.

Element	E_o	$Y(E_o)$	Y_c				Y_c/Y				Ref.
			UCRL	Saclay	Va.	NBS(Old)	UCRL Exp	Saclay Exp	Va. Exp	NBS(Old) Exp	
Pb	27	103	86				0.83				26,30
	22	111	92	116			0.83	1.05			
Au	27	89	97				1.09				24,30,
	22	92	98	88		115	1.07	0.96		1.25	38
Ta	27	81	82	77			1.01	0.95			27,30,
	22	85	79	80		113	0.93	0.94		1.33	38
Ho	27	67	75				1.12				27,31,
	22	69	77	82		103	1.12	1.19		1.49	39
Ag	27	36									
	22	34.8									
Cu	27	14.4	13.2				0.92				28,30
	22	12.6	11.5	12.4			0.91	0.98			
Co	27	12.7	12.1				0.95				29,34
	22	10.6	9.9		13.5		0.94		1.27		
Ca	27	1.69		1.13	1.01			0.67	0.60		32,35
P	27	2.35			1.76				0.75		36
Al	27	1.92	1.62		1.38		0.84		0.72		25,37
O^{16}	27	0.54	0.42	0.48	0.42		0.78	0.89			16,32, 37
C	27	0.50	0.35	0.33	0.46		0.70	0.66			25,32, 33

(OVER)

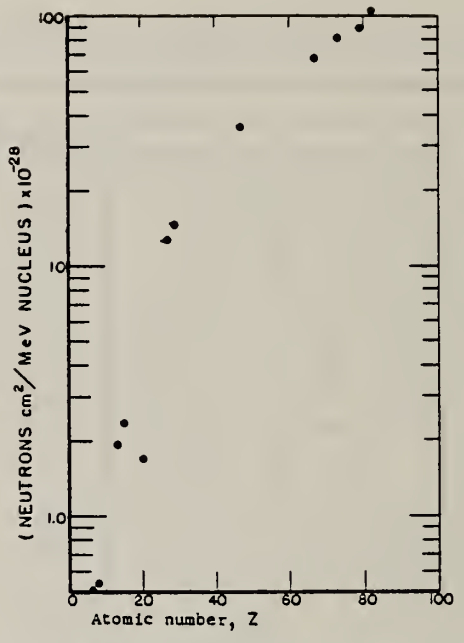

Fig. 31. Absolute neutron yield as a function of atomic number. The neutron yield from calcium (Z = 20) is particularly low in comparison with the other elements because its (γ,n) threshold is high compared to the mean energy of the giant resonance.

REF.

A. P. Komar, V. P. Denisov, and L. A. Kul'chitskii
Dokl. Akad. Nauk SSSR 169, 1307 (1966)
Soviet Phys. Doklady 11, 728 (1967)

ELEM. SYM.	A	-
0	16	8

METHOD

REF. NO.	
67 Ko 1	JDM

REACTION	RESULT	EXCITATION ENERGY	SOURCE		DETECTOR		ANGLE
			TYPE	RANGE	TYPE	RANGE	
G,P	ABX	THR-55	C	21-55	TEL-D	3-30	90

$$\int_{12.11}^{43} \sigma(\gamma,p_0)dE_\gamma = 47\pm6 \text{ MeV.mb}$$

$$\int_{21.0}^{38.5} \sigma(\gamma,p_{1,2})dE_\gamma = 7.5\pm2.0 \text{ MeV.mb}$$

$$\int_{22.0}^{37.5} \sigma(\gamma,p_3)dE_\gamma = 14.1\pm2.2 \text{ MeV.mb}$$

$$\int_{12.1}^{65} \sigma_p dE_\gamma = 152\pm22 \text{ MeV.mb}$$

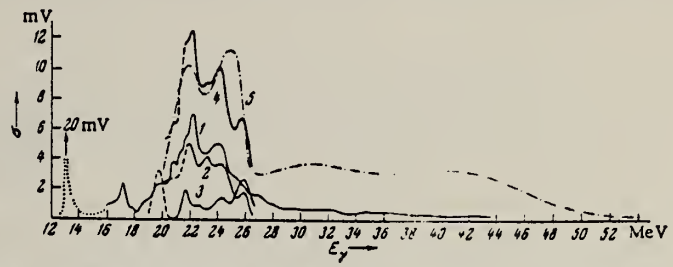

Fig. 1. Cross-section curves. 1) Curve for the cross section $\sigma(\gamma, p_0)$ (cross section for transition to the N^{15} ground state); 2) $\sigma(\gamma, p_3)$ (cross section for transition to the third excited state of N^{15}); 3) $\sigma(\gamma, p_{1,2})$ (cross section for transition to the first+second excited state of the N^{15} nucleus); 4) $\sigma(\gamma, p_0)+\sigma(\gamma, p_{1,2})+\sigma(\gamma, p_3)$; 5) σ_p (cross section for photoproduction of protons with an energy of 3.4 to 30.0 MeV). The dashed lines denote the parts of curves 2, 3, and 4 obtained from an analysis of data from [10-13] on on the basis of the results of our measurements. The dotted curve applies to the cross section $\sigma(\gamma, p_0)$ evaluated from data on the inverse reaction $N^{15}(p, \gamma_0)O^{16}$ [8, 9].

TABLE 1. Relative Intensities (in %) of Transitions to Various States of the N^{15} Nucleus from Excited States of O^{16} Having Energy E_i

E_i, MeV	Ground state of the N^{15} nucleus		First+second excited state of N^{15}		Third excited state of N^{15}	
	this paper	reference [16]	this paper	reference [16]	this paper	reference [16]
22.3	56±10	52±10	12±4	5±5	32±8	43±10
23.1	35±10	37±10	7±3	5±5	58±15	58±10
24.3	53±10	52±10	13±4	5±5	34±8	43±10

REF.

K. Krämer, H. v. Buttlar, A. Goldmann, and B. Huber
Z. Physik 207, 1 (1967)

ELEM. SYM.	A	Z
O	16	8

METHOD

REF. NO. 67 Kr 2 egf

REACTION	RESULT	EXCITATION ENERGY	SOURCE TYPE	SOURCE RANGE	DETECTOR TYPE	DETECTOR RANGE	ANGLE
G, N13	RLX	THR-55	C	30-55	ACT-I		4PI
G, C11	RLX	THR-55	C	30-55	ACT-I		4PI
G,T	RLX	THR-55	C	30-55	ACT-I		4PI

Tabular data given

Table 4. *Summary of integrated cross sections for various photoreactions in ^{12}C and ^{16}O*

Reaction	Threshold[23] MeV	$\int_0^{E_m} \sigma dE$ MeV·mb	at E_m MeV	Reference
$^{12}C(\gamma, n)^{11}C$	18	65.4	57	16
		77 ± 6	65	17
$^{12}C(\gamma, x)^{7}Be$	26.3+	6.0 ± 0.4	57	3
$^{12}C(\gamma, p\alpha)^{7}Li$	24.6	5.6 ± 0.4	55	6
$^{12}C(\gamma, pt)^{8}Be$	27.2	5.7	54	18*
$^{12}C(\gamma, t)$	27.4≠	5 ± 2	50	this work
$^{16}O(\gamma, n)^{15}O$	15.7	58	62	7
$^{16}O(\gamma, x)^{11}C$	25.9+	4.9 ± 0.9	65	5
		4.1 ± 0.4	55	this work
$^{16}O(\gamma, p\alpha)^{11}B$	23.1	4.8 ± 0.4	55	6
$^{16}O(\gamma, x)^{13}N$	25.0≠	1.2 ± 0.1	55	this work
$^{16}O(\gamma, t)$	25.0≠	2.1 ± 0.2	51	4

+ For $(\gamma, n\alpha)$-channel, which has lowest threshold.
≠ Lowest threshold.
* Calculated from Fig. 3 in ref. [18]; compare footnote on p. 8.

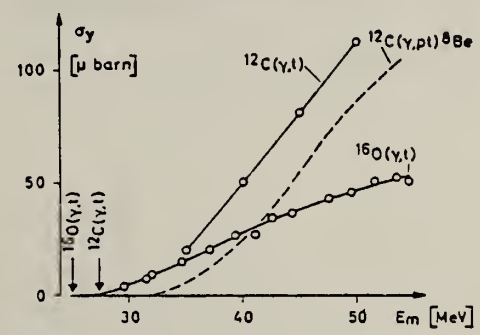

Fig. 3. Yields of phototritons from ^{12}C and ^{16}O. Error bars are of the same order of magnitude as the diameter of the circles. The lowest thresholds are indicated by arrows. Curves have been drawn arbitrarily through the data points. The dashed line shows σ_γ for the reaction $^{12}C(\gamma, pt)^{8}Be$ calculated from the cross section measured by MAIKOV[18]

[6]Maikov,V.N.: Soviet Phys.JETP 7, 973(1958).
[Zhur.Eksptl. i Teoret. Fiz.34, 1406 (1958)].

[over]

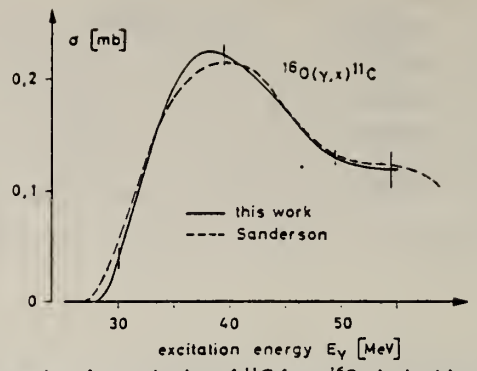

Fig. 4. Cross sections for production of ^{11}C from ^{16}O obtained by SANDERSON[5] and in this work. The error bars indicate the accuracy of unfolding the yield curve

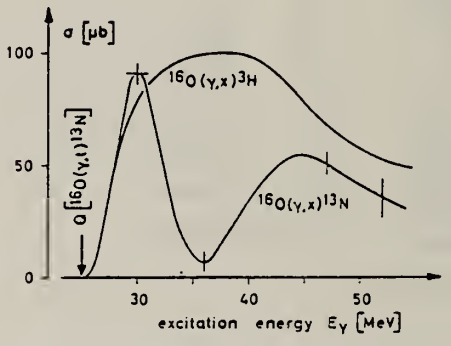

Fig. 5. Cross sections for production of ^{13}N and of tritons[4] from ^{16}O. The error bars indicate the accuracy of unfolding the yield curve

REF. J. M. Loiseaux, J. M. Maison, and M. Langevin
J. de Physique 28, 11 (1967)

ELEM. SYM.	A	Z
O	16	8

METHOD

REF. NO. 67 Lo 1 JOC

REACTION	RESULT	EXCITATION ENERGY	SOURCE TYPE	SOURCE RANGE	DETECTOR TYPE	DETECTOR RANGE	ANGLE
G,G/	ABX	18-32	C	34	NAI-D		DST

TABLEAU I

COEFFICIENT a DES DISTRIBUTIONS ANGULAIRES

$$W(\theta) = 1 + a\cos^2\theta$$

^{16}O	a(19-25 MeV)	$= 1 \pm 0,1$						
^{23}Na	a(15-18 MeV)	$= 0,1 \pm 0,1$	a(18,5-23 MeV)	$= 0,4 \pm 0,15$	a(25-30 MeV)	$= 0,85 \pm 0,2$		
^{24}Mg	a(16,5-20 MeV)	$= 0,3 \pm 0,1$	a(20-25 MeV)	$= 0,5 \pm 0,1$	a(25,5-32 MeV)	$= 0,5 \pm 0,1$		
^{28}Si	a(15-17,5 MeV)	$= 0,87 \pm 0,1$	a(18-23 MeV)	$= 0,7 \pm 0,1$	a(25,5-32 MeV)	$= 0,5 \pm 0,1$		
^{39}K	a(14,5-18,5 MeV)	$= 0,5 \pm 0,1$	a(19-24,5 MeV)	$= 1 \pm 0,1$	a(25-32 MeV)	$= 1 \pm 0,1$		

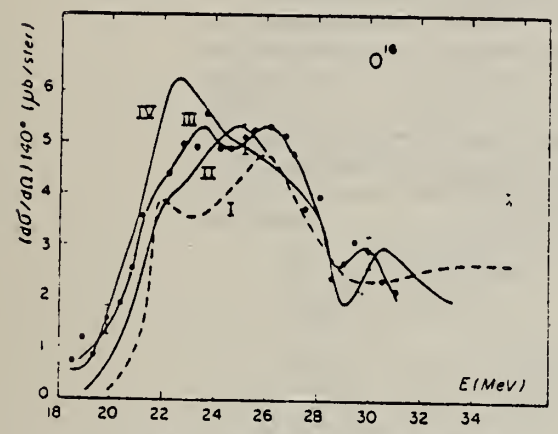

FIG. 1. — ^{16}O Sections efficaces différentielles de diffusion à 140° déterminées à $E_m = 27$ MeV (II), $E_m = 32$ MeV (III), $E_m = 34$ MeV (IV).

Courbe I : Section efficace prévue par la relation de dispersion.

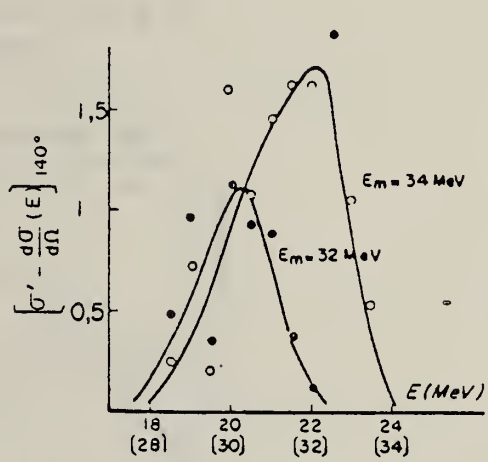

FIG. 2. — Contribution de la diffusion inélastique entre 18 et 24 MeV à $E_m = 32$ MeV et $E_m = 34$ MeV.

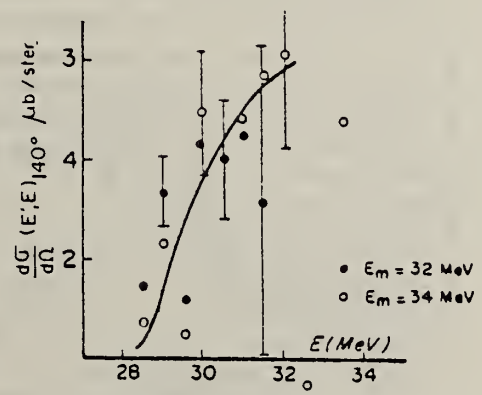

FIG. 3. — Section efficace de diffusion inélastique à 140°.

REF. M. Mishina, E. Tanaka, K. Kageyama, N. Mutsuro, A. Asami, Y. Kawarasaki and Y. Nakajima
J. Phys. Soc. Japan 23, 919 (1967)

ELEM. SYM.	A	Z
O	16	8

METHOD

REF. NO. 67 Mi 2 egf

REACTION	RESULT	EXCITATION ENERGY	SOURCE TYPE	SOURCE RANGE	DETECTOR TYPE	DETECTOR RANGE	ANGLE
G, XN	SPC	THR-20	C	23-27	TOF-D	2-12	100

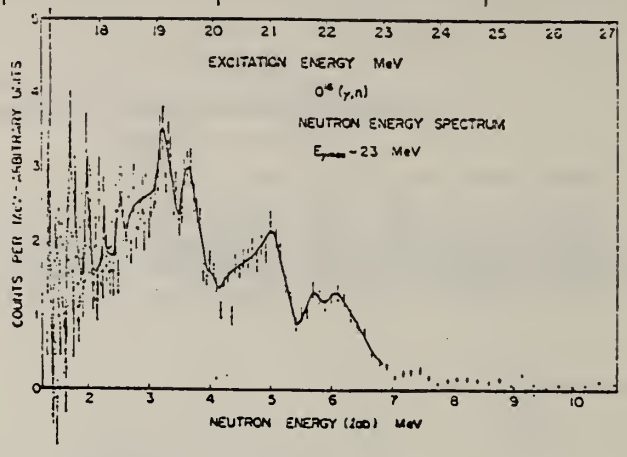

(a)

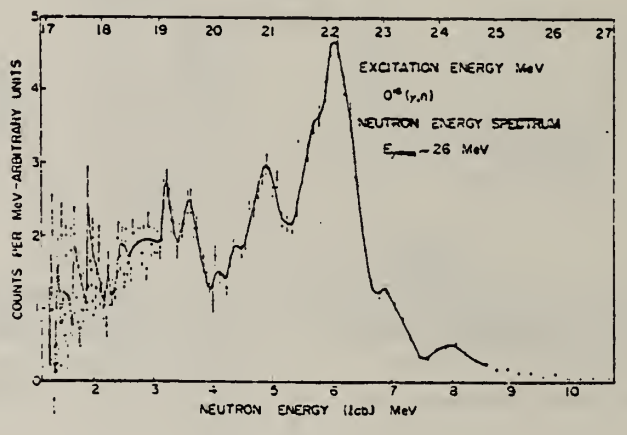

(b)

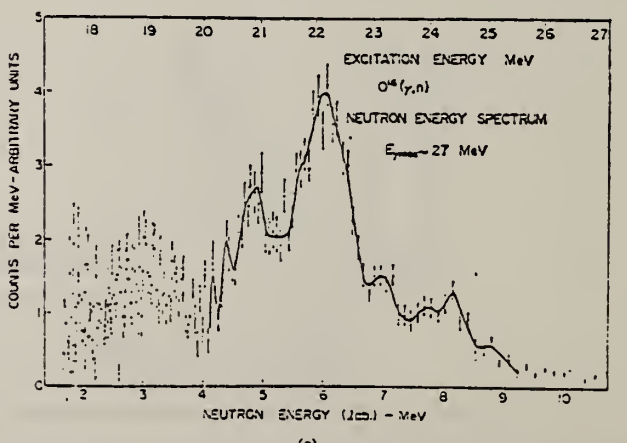

(c)

Fig. 6. Energy spectra of photoneutrons from O^{16} (γ, n) reaction deduced from the time spectrum in Fig. 5. Abscissa is scaled by both laboratory neutron energy and corresponding O^{16} excitation energy for the case of ground state transition.

K. M. Murray and J. C. Ritter
PICNS-67 Contributions, International Conference on Nuclear Structure, Tokyo, Japan 1967 (Institute for Nuclear Study, University of Tokyo, Tanashi-shi, Tokyo, Japan) 10.19, p. 383

ELEM. SYM.	A	Z
0	16	8

METHOD

REF. NO. 67 Mu 1 EGF

REACTION	RESULT	EXCITATION ENERGY	SOURCE		DETECTOR		ANGLE
			TYPE	RANGE	TYPE	RANGE	
G,PG	SPC	17-30	C	28,30	SCD-D	5-8	90
G,NG	SPC	21-30	C	28,30	SCD-D	5-8	90

G-SPECTRUM

γ,pγ and γ,nγ Reactions on ^{16}O

K. M. Murray and J. C. Ritter

U. S. Naval Research Laboratory

Washington, D. C. 20390

The absorption of electromagnetic photons in the energy range from approximately 10 MeV to 25 or 30 MeV is commonly referred to as the "photonuclear giant resonance". This absorption of energy generally results in particle emission and frequently the residual nucleus is left in an excited state. This excited state decays to its ground state thru the emission of one or more gamma rays. These deexcitation gamma rays from an ^{16}O target bombarded by bremsstrahlung from the US NRL Linac were observed using a large (30 cc) Li drifted Ge crystal.

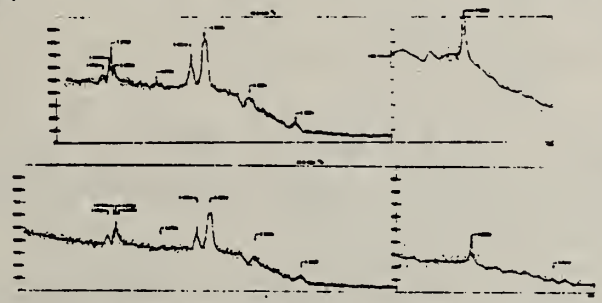

Fig. 1. A portion of the 4096 channel spectra for ^{16}O. The energies are in MeV. The letters indicate, d - double escape peak, s - single escape peak, and f - full energy peak.

Fig. 1 shows a portion of the spectra obtained with 28.0 and 30.0 MeV end-point-energy bremsstrahlung. Gamma rays from ^{15}N appear with energies of 3.924, 5.270, 5.299, 6.323, and 9.223 MeV while gamma rays from the corresponding isobaric analog levels in ^{15}O appear with energies of 5.188, 5.240, and 6.180 MeV. The lines are doppler broadened by recoil from particle emission. The two lines at 5.240 and 5.270 appear sharp because their life times are so long ($> 10^{-12}$sec.), that the recoil has been thermalized (thermalizing time $\sim 10^{-13}$ sec.). The level at 9.223 MeV has been seen in a recent run at 24.0 MeV. This indicates that it is probably coming from a level in ^{16}O at 22.5 MeV and this would imply a proton of approximately 1 MeV energy. Such a low energy proton would not produce very much recoil-doppler-broadening. This is consistent with the observed width of < 30 keV fwhm for this level.

The ^{15}O ground state decays thru a 124 sec. $^{+}\beta$ transition of ^{15}N. By observing this activity we measure the total number of ^{15}O ground states produced. Thereby the fractions of excited state transitions to ground state transitions can be calculated for the ^{15}O nucleus only.

REF.

M. Suffert and W. Feldman
Phys. Letters 24B, 579 (1967)

ELEM. SYM.	A	Z
O	16	8

METHOD

[Page 1 of 2]

REF. NO. 67 Su 1 JOC

REACTION	RESULT	EXCITATION ENERGY	SOURCE		DETECTOR		ANGLE
			TYPE	RANGE	TYPE	RANGE	
A,G	RLX	14-25	D	8-24	NAI-D		DST

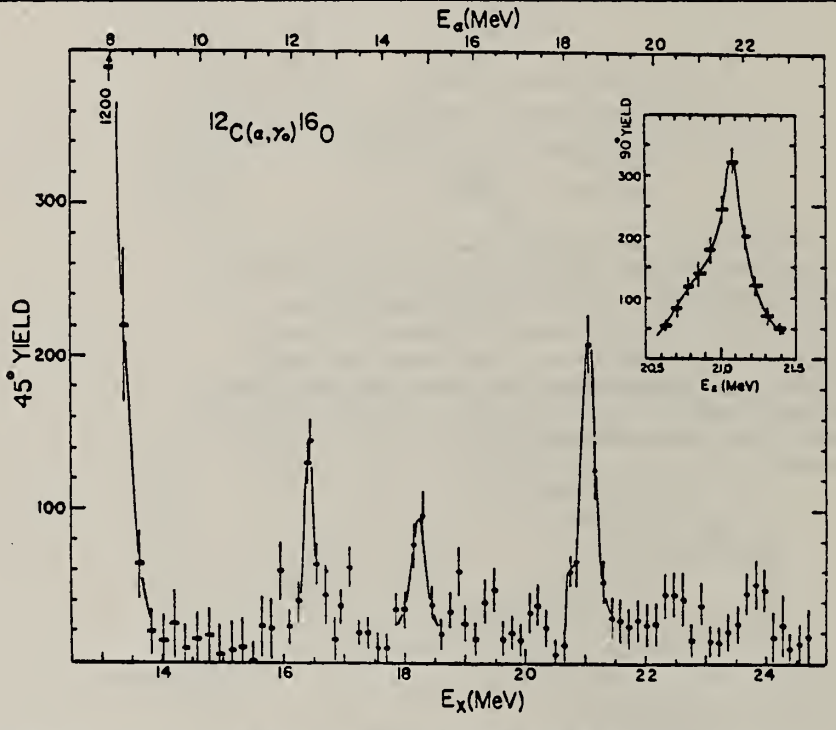

Fig. 1. Excitation function at 45° of the reaction $^{12}C(\alpha,\gamma_0)^{16}O$. The width of the data points indicates the target thickness. The yield in arbitrary units is corrected for the energy dependence of the detector efficiency.

Table 1
Resonance parameters

E_α (MeV)	E_x (MeV)	ΔE_α* (c.m.) (MeV)	Γ (c.m.) (MeV)	J^π	$\frac{\Gamma_\gamma \Gamma_\alpha}{\Gamma}$ (eV)
12.30	16.40	0.11	0.10 ± 0.10	2^+	0.2
14.70	18.20	0.09	0.39 ± 0.08	2^+	0.7
18.50	21.05	0.08	0.24 ± 0.08	1^-	6

* Target thickness.

REF.	ELEM. SYM.	A	Z
M. Suffert and W. Feldman Phys. Letters 24B, 579 (1967)	O	16	8

METHOD	REF. NO.	
[Page 2 of 2]	67 Su 1	JOC

REACTION	RESULT	EXCITATION ENERGY	SOURCE		DETECTOR		ANGLE
			TYPE	RANGE	TYPE	RANGE	

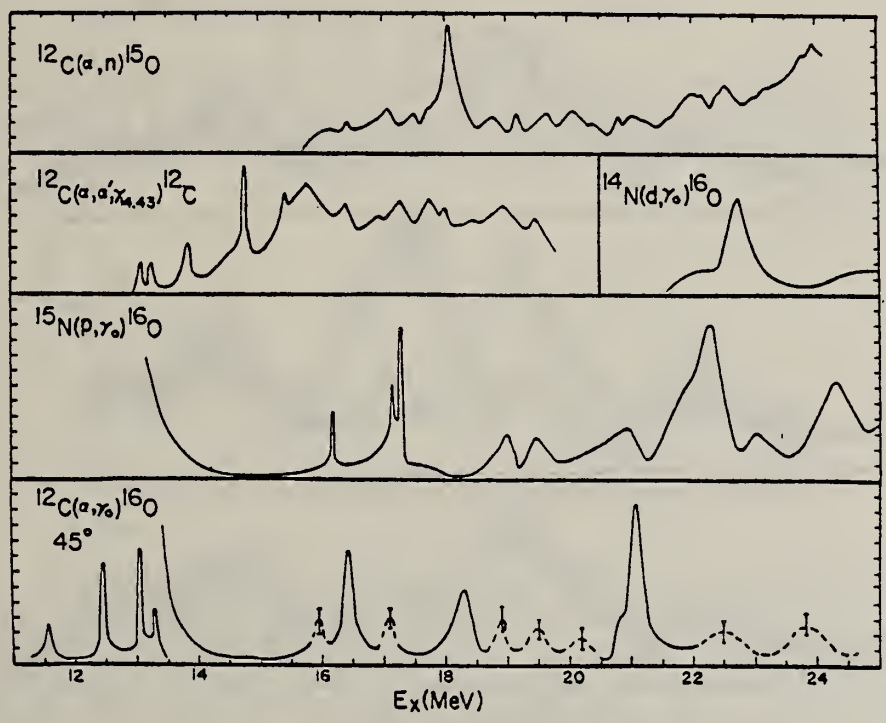

Fig. 2. Comparison of the results of this experiment with the results obtained in $^{15}N(p,\gamma_0)^{16}O$ [1], $^{12}C(\alpha,\gamma_0)^{16}O$ for $E_\alpha < 8.5$ [6], $^{14}N(d,\gamma_0)^{16}O$ [8], $^{12}C(\alpha,\alpha'\gamma_{4.43})^{12}C$ [13] and $^{12}C(\alpha,n)^{15}O$ [14].

REF.

M. N. Thompson and J. E. E. Baglin
Phys. Letters 25B, 256 (1967)

ELEM. SYM.	A	Z
O	16	8

METHOD

REF. NO. 67 Th 1

REACTION	RESULT	EXCITATION ENERGY	SOURCE		DETECTOR		ANGL
			TYPE	RANGE	TYPE	RANGE	
G,P	RLX	19-26	C	20-26	SCD-D	6-14	DST

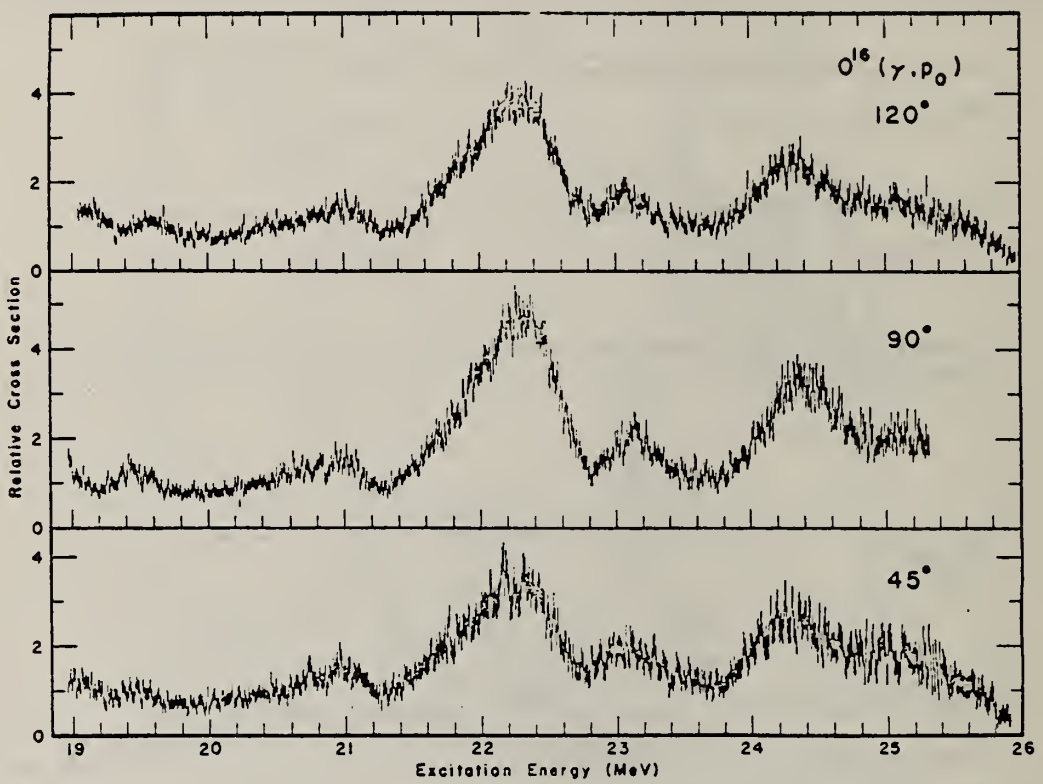

Fig. 1. Photoproton cross section of ^{16}O obtained at angles of 45°, 90° and 120° using 26 MeV bremsstrahlung.

REF.
M. N. Thompson and J. E. E. Baglin
PICNS-67 Contributions, International Conference on Nuclear Structure, Tokyo, Japan 1967 (Institute for Nuclear Study, University of Tokyo, Tanashi-shi, Tokyo, Japan) 10,22, p. 386

ELEM. SYM.	A	Z
O	16	8

METHOD

REF. NO. 67 Th 2 EGF

REACTION	RESULT	EXCITATION ENERGY	SOURCE		DETECTOR		ANGLE
			TYPE	RANGE	TYPE	RANGE	
G,P	RLX	20-25	C	26	SCD-D	7-12	135

Photoprotons from O^{16}

M. N. Thompson and J. E. E. Baglin*

Electron Accelerator Laboratory, Yale University
New Haven, Connecticut USA

Spectra of photoprotons emitted from O^{16} to the ground state of N^{15} have been observed at lab angles of 45°, 90°, 120° and 135° with an experimental resolution of 40 keV. The gaseous oxygen target was irradiated with 26 MeV bremsstrahlung and the protons were detected using cooled Si(Li) detectors.

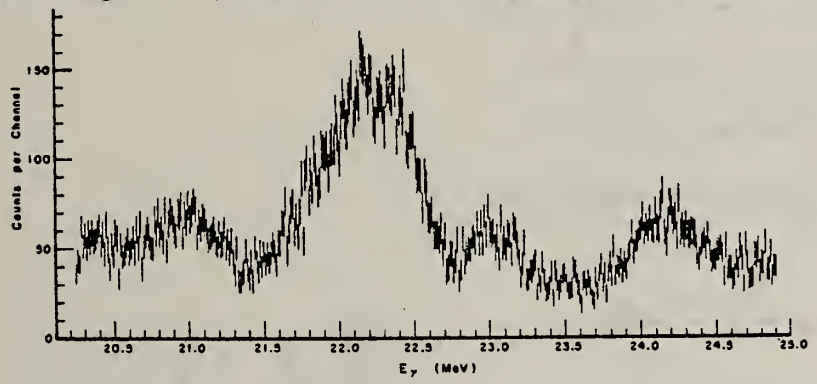

The figure shows an early 135° spectrum. Recent spectra at all four angles are statistically better and contain quantitative features similar to those shown. It is important to note that the former simplicity of the O^{16} ground state photoproton cross section is destroyed according to the above figure. Evidence from all the measured spectra suggests that the peaks previously considered to be the basic cross section entities, consist of narrower components. The "22 MeV peak" consists of at least three components (21.8, 22.1, 22.3 MeV) the "21MeV peak" has two (20.7, 21.0 MeV), as do both the "23 MeV peak" (23.0, 23.2 MeV), and the "24.5 MeV peak" (24.2, 25.1 MeV). In addition, much finer structure with a width of 50-70 keV is found over the whole energy region studied. Peaks of this nature appear repeatably in spectra at each angle, although with different relative intensities.

Although it is hoped to carry out a complete analysis of the angular distribution data, several observations can be made at this time. The two components of the "23 MeV peak" have different angular dependence. The one at 23.2 MeV is less strongly peaked at 90° than the 23.0 MeV component. Similarly for the peaks at 24.2 MeV and 25.1 MeV, the upper one is less dependent on angle than the other which is strongly peaked at 90°. It is also interesting to note that at 90° the valleys at 22.8 MeV and 23.5 MeV are of equal height as distinct from the situation shown here, indicating a cross section contribution at 23.5 MeV peaked at 90°.

The consistency of the fine (50 keV) structure at all angles implies that they are not statistical in nature. A paper by Duke et al. suggests that such fine structure may be accounted for by coupling between single particle and collective states of the O^{16} nucleus.

References: (1) C. B. Duke, F. B. Malik, Proceedings International Conference on Nuclear Physics, Gatlinburg Tennessee, September 12-17, 1966.

also C. B. Duke, F. B. Malik, F. W. K. Firk (submitted to Phys. Rev., 1967).

*Work supported by the United States Atomic Energy Commission

REF. P. M. Tutakin
J. Nucl. Phys. (USSR) 5, 1325 (1967)
Sov. J. Nucl. Phys. 5, 946 (1967)

ELEM. SYM.	A	Z
O	16	8

METHOD

REF. NO. 67 Tu 3 HMG

REACTION	RESULT	EXCITATION ENERGY	SOURCE		DETECTOR		ANGLE
			TYPE	RANGE	TYPE	RANGE	
G,P	SPC	THR-22	D	22	EMU-D		DST

Note: Observed angular distribution does not agree with Dodge and Barber or Allas et al.

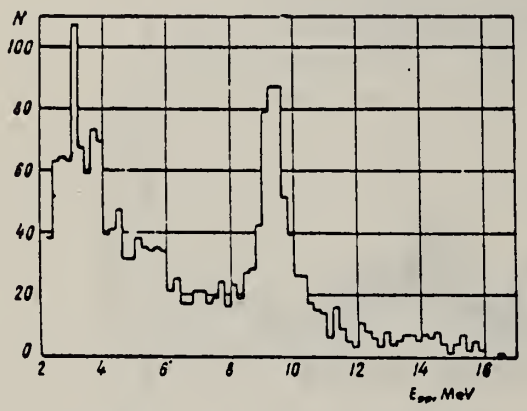

Fig. 1. Energy distribution of the photoprotons. The vertical axis represents the number of observed tracks N, and the horizontal axis the photoproton energy E_{pp}.

REF. V. P. Denisov, A. P. Komar and L. A. Kulchitsky
Nucl. Phys. A113, 289 (1968)

ELEM. SYM.	A	Z
O	16	8

METHOD

[Page 1 of 2]

REF. NO. 68 De 1 EGF

REACTION	RESULT	EXCITATION ENERGY	SOURCE		DETECTOR		ANGLE
			TYPE	RANGE	TYPE	RANGE	
G,P	ABX	16-55	C	21-55	TEL-D	4-30	90

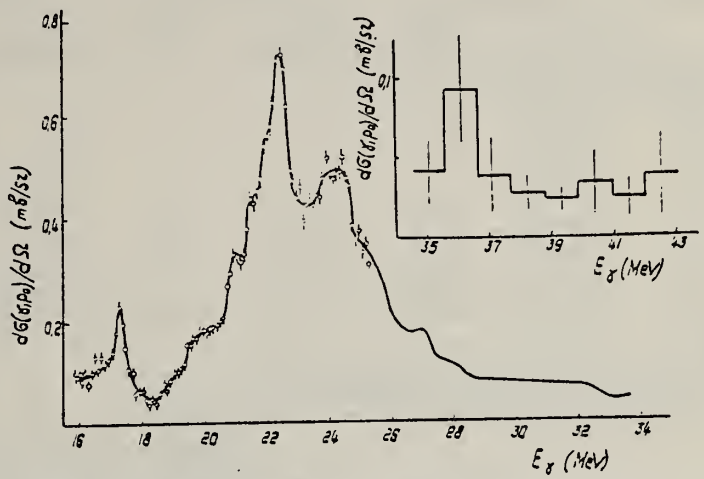

Fig. 2. Differential cross section of the reaction $^{16}O(\gamma, p_0)$ for protons emitted at 90° to the bremsstrahlung beam. In the interval E_γ = 26-34 MeV the cross section was obtained from the data of refs. [3,6]).

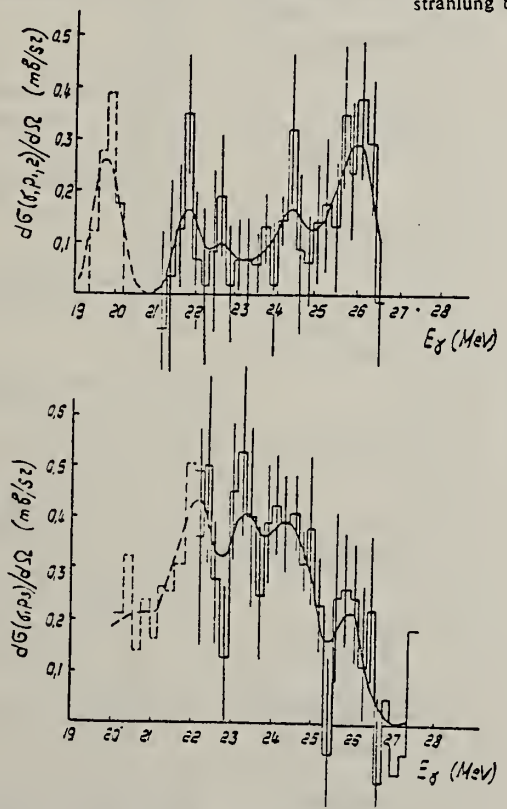

Fig. 3. Differential cross sections of the reactions $(\gamma, p_{1,2})$ and (γ, p_3) for protons emitted at 90° to the bremsstrahlung beam. The curves were obtained by smoothening out histograms by the method of Ferreira and Valoshek [18]). The dashed curve refers to cross sections obtained using other data (see sect. 3.2).

DETECTOR		ANGLE
TYPE	RANGE	

TABLE 4

Intensities of transitions to different states of ^{15}N

E_t (MeV)	Ground state		First + second excited states (5.28; 5.30 MeV)		Third excited state (6.33 MeV)	
	$(I_p)_{t,0}$ (MeV · mb)	$(W_p)_{t,0}$ (%)	$(I_p)_{t,1,2}$ (MeV · mb)	$(W_p)_{t,1,2}$ (%)	$(I_p)_{t,3}$ (MeV · mb)	$(W_p)_{t,3}$ (%)
17.13 } 17.29 }	2.0±0.2	100				
19.0	1.2±0.3	55			1 [a])	45
19.5	2.2±0.4	35	2.4 [b])	40	1.5 [a])	25
20.9	3.2±0.9	50			3.0 [b])	50
21.7 } 22.3 }	1.7±0.8 / 8.0±0.8	56± 8	2.2±0.9	12± 6	5.5±1.0	32± 8
23.1	2.7±0.8	35±12	0.5±0.3	7± 7	4.4±0.9	58±13
24.3	6.0±0.6	53± 9	1.5±0.6	13± 8	3.8±0.8	34± 9
25.0	2.7±1.0	80±17			0.7±0.5	20±17
25.6	1.2±0.4	20±17	3.3±0.7	52±12	1.8±0.8	28±12
26.3 } 27.4 }	2.5±0.6	100				

[a]) Obtained by extrapolating the cross section curve.
[b]) Obtained from analysis of the data of refs. [1,6,7,8,17–20]) (see sect. 3.2).

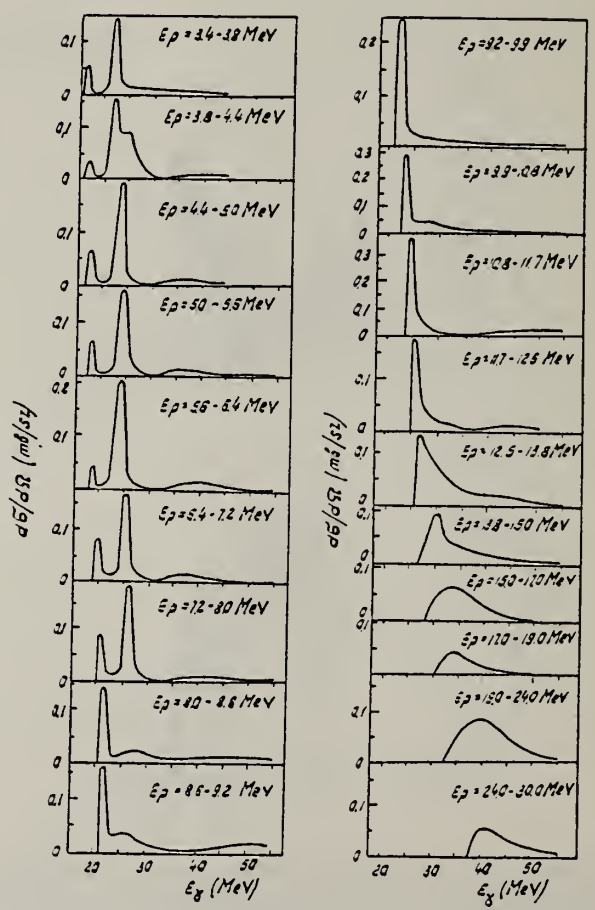

Fig. 4. Differential cross sections for the emission of protons at 90° to the bremsstrahlung beam for 19 different proton energy intervals.

REF. T. E. Drake, E. L. Tomusiak and H. S. Caplan
Nucl. Phys. A118, 138 (1968)

ELEM. SYM.	A	Z
O	16	8

METHOD

REF. NO. 68 Dr 1 egf

REACTION	RESULT	EXCITATION ENERGY	SOURCE		DETECTOR		ANGLE
			TYPE	RANGE	TYPE	RANGE	
E,E/	FMF	19,20	D	140	MAG-D		DST

19=19.1; 20=20.5

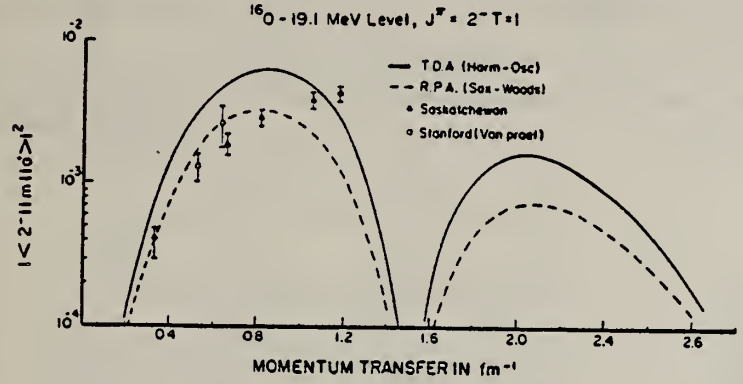

Fig. 5. The momentum-transfer dependence of the square of the matrix element for the 19.1 MeV level in ^{16}O. Theoretical curve I was obtained using the TDA with harmonic-oscillator single-particle wave functions, and curve II was obtained using the RPA with Saxon-Woods wave functions. The Boeker-Brink two-body residual interaction of appendix 1 was used for both curves, and in both curves the single-particle wave functions give the experimental rms radius of the ground-state charge distribution.

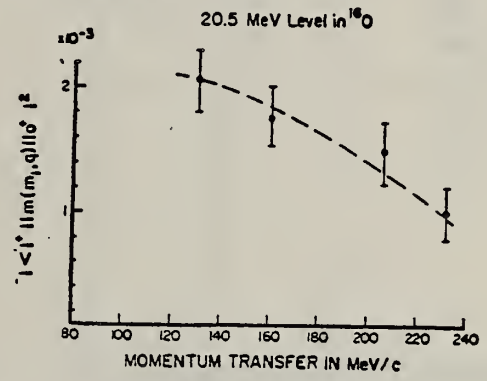

Fig. 9. The momentum-transfer dependence of the square of the transition matrix element for the 20.5 MeV level in ^{16}O.

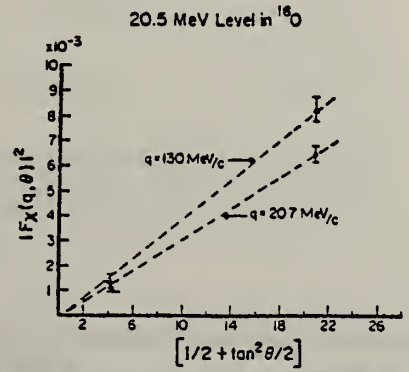

Fig. 10. The angular dependence of the total form factor $F_x(q,\theta)^2$ for the 20.5 MeV level in ^{16}O.

U.S. DEPARTMENT OF COMMERCE
NATIONAL BUREAU OF STANDARDS

REF. D. Evers, G. Flugge, J. Morgenstern, T. W. Retz-Schmid, H. Schmidt, J. W. Schmidt and S. J. Skorka
Phys. Letters 27B, 423 (1968)

ELEM. SYM.	A	Z
O	16	8

METHOD

REF. NO. 68 Ev 1 egf

REACTION	RESULT	EXCITATION ENERGY	SOURCE		DETECTOR		ANGLE
			TYPE	RANGE	TYPE	RANGE	
G,G	LFT	6-8	D	6-8	SCD-D	6-8	
		(6.92, 7.12)		(6.92, 7.12)			

LEVELS: 6.92;7.12

Source Doppler-broadened $^{19}F(p,\alpha\gamma)$ radiation.

Table 1
Radiative widths in ^{16}O.

Transition (MeV)	E2 6.92→0	E2 6.92→6.06	E1 7.12→0	E1 7.12→6.06
Γ_{exp}(meV)	80 ± 7	$(23 \pm 4) \times 10^{-3}$	47 ± 7	$<3.2 \times 10^{-4}$
$\|M\|^2$	2.6	25	3×10^{-4}	$<6.2 \times 10^{-7}$
Γ_{theor}(meV)	68	40×10^{-3}	20:100	-

REF. N. N. Kaushal, E. J. Winhold, P. F. Yergin, H. A. Medicus and R. H. Augustson
Phys. Rev. 175, 1330 (1968)

ELEM. SYM.	A	Z
O	16	8

METHOD

REF. NO. 68 Ka 1 HMG

REACTION	RESULT	EXCITATION ENERGY	SOURCE		DETECTOR		ANGLE
			TYPE	RANGE	TYPE	RANGE	
G,N	ABX	50-85	C	55,85	TOF-D	10-85	67
							(67.5)

NEUT ENGY SPEC

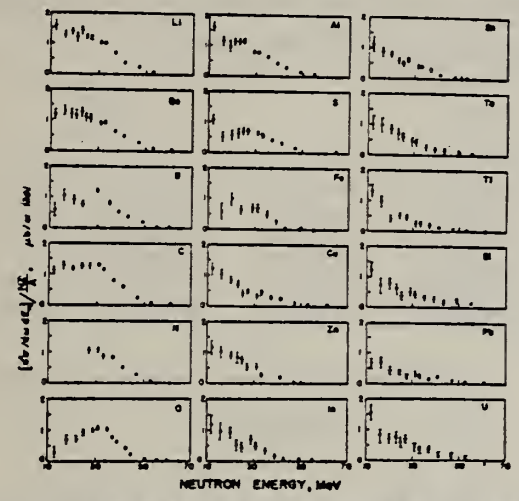

FIG. 6. Observed neutron spectra due to 55–85-MeV difference photon spectra. The effective cross sections have been divided by *NZ/A*.

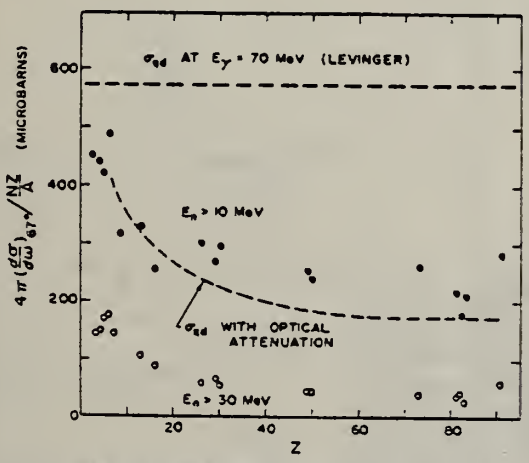

FIG. 7. Effective cross sections for production of fast neutrons with energies greater than 10 MeV (solid circles) and 30 MeV (open circles) by the 55–85-MeV photon difference spectrum. The dashed curves are modified quasideuteron model predictions as discussed in the text.

TABLE I. Comparison of present cross-section values in mb for production of high-energy photoneutrons by 55–85-MeV photons with measured cross sections $\sigma(\gamma,Tn)$, also in mb, for total photoneutron production. The present cross-section values are uncertain by 8 to 10% because of counting statistics and normalization errors; in addition all values depend on an absolute normalization in terms of the deuteron photodisintegration cross section, which is known to about 10% at these energies.

Target	$4\pi(d\sigma/d\omega)_{\pi^0}$ (E_n>10 MeV) [Present experiment]	$\sigma(\gamma,Tn)$ Jones and Terwilliger[a]	Costa *et al.*[b]	Other results
Li	0.75		1.0	
Be	1.0	2.7	2.3	2.3[c]
B	1.0		1.4	
C	1.5	1.3	1.4	2.4[d]
O	1.3		1.6	
Al	2.8	5.5	4.6	8[d]
S	2.1		4.4	6.5[d]
Fe	4.2	16	12	
Cu	4.3	20	19	
Zn	4.4		15	
In	7.4			
Sn	7.0			
Ta	10.7	95		
Tl	10.7			
Pb	8.3	100		
Bi	13			
U	16	65		

[a] Average cross sections between 55 and 85 MeV, as read from Figs. 4 and 5 of Ref. 4.
[b] $\int_{\pi^0}\sigma dE - \int_{\pi^+}\sigma dE/50$, as taken from Fig. 4 of Ref. 5 and Table I of Ref. 6.
[c] S. Costa, L. Pasqualini, G. Piragino, and L. Rosario, Nuovo Cimento 42, 306 (1966).
[d] G. Bishop, S. Costa, S. Ferroni, R. Malvano, and G. Ricco, Nuovo Cimento 42, 148 (1966).

R. A. Meyer, W. B. Walters, J. P. Hummel
Nucl. Phys. A122, 606 (1968)

ELEM. SYM.	A	Z
O	16	8

METHOD

REF. NO. 68 Me 4 egf

REACTION	RESULT	EXCITATION ENERGY	SOURCE		DETECTOR		ANGLE
			TYPE	RANGE	TYPE	RANGE	
G,2N	ABX	THR-300	C	20-300	ACT-I		4PI

TABLE 1

Summary of integrated cross sections $\int_0^{E_{max}} \sigma dE$(MeV · mb) for the reactions studied

Reaction/E_{max}(MeV)	65	105	145	215	295
$^{16}O(\gamma, 2n)^{14}O$	0.42 ±0.02	0.57 ±0.04	0.56 ±0.05	0.63 ±0.09	1.29 ±0.16
$^{19}F(\gamma, 2pn)^{16}N$	3.7 ±0.2	5.0 ±0.3	6.1 ±0.5	8.4 ±1.0	13.6 ±1.5
$^{27}Al(\gamma, 2pn)^{24}Na$	8.3 ±0.3	13.3 ±0.7	17.1 ±1.2	24.1 ±2.3	31.2 ±3.3 [a]
$^{51}V(\gamma, \alpha)^{47}Sc$	12.3 ±1.7	20.2 ±3.5	32.5 ±2.6	68.4 ±3.8	112 ±14
$^{51}V(\gamma, \alpha 3n)^{44}Sc$	0.7 ±0.2	6.0 ±0.9	12.2 ±1.3	34.1 ±4.1	91 ±11

[a] E_{max} = 275 MeV.

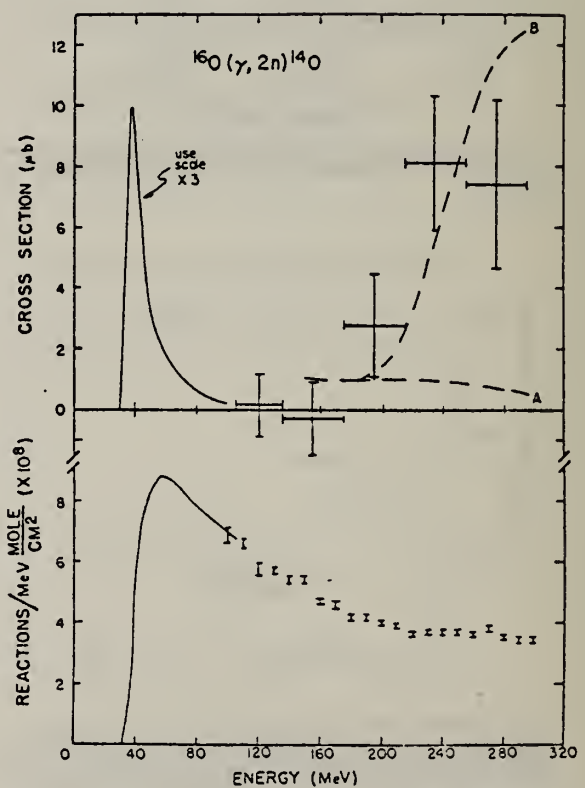

Fig. 1. Yields (lower graph) and cross sections (upper graph) for the $^{16}O(\gamma, 2n)^{14}O$ reaction. The solid lines represent the assumed yield and cross section behavior at the lower energies. They are based on displaced $^{32}S(\gamma, np)^{30}P$ cross sections (see text). The dashed lines show the cross sections expected for quasi-deuteron processes (curve A) and the sum of the cross sections expected for quasi-deuteron and pion emission processes (curve B).

REF.

R. J. J. Stewart
Aust. J. Phys. 21, 107 (1968)

EL.EM. SYM.	A	Z
O	16	8

METHOD

REF. NO. 68 St 1 egf

REACTION	RESULT	EXCITATION ENERGY	SOURCE		DETECTOR		ANGLE
			TYPE	RANGE	TYPE	RANGE	
G,P	SPC	20-26	C	26	SCD-D	8-13	DST

26=25.6 MEV

TABLE 1

EXPERIMENTAL ANGULAR DISTRIBUTION COEFFICIENTS FOR THE REACTION $^{16}O(\gamma, p_0)^{15}N$

In the form $W(\theta) = A\left(1 + \sum_{i=1}^{n} a_i P_i(\cos\theta)\right)$

E_γ (MeV)		a_1	a_2	a_3
21·00	(20·25–21·45)	0·04±0·07	−0·53±0·10	
21·75	(21·45–22·00)	0·06±0·08	−0·68±0·10	−0·21±0·15
22·30	(21·45–22·90)	0·00±0·02	−0·65±0·02	
23·10	(22·95–23·65)	0·12±0·02	−0·36±0·03	
23·75	(23·50–24·00)	0·14±0·06	−0·43±0·09	
24·30	(23·70–25·60)	0·10±0·08	−0·58±0·10	

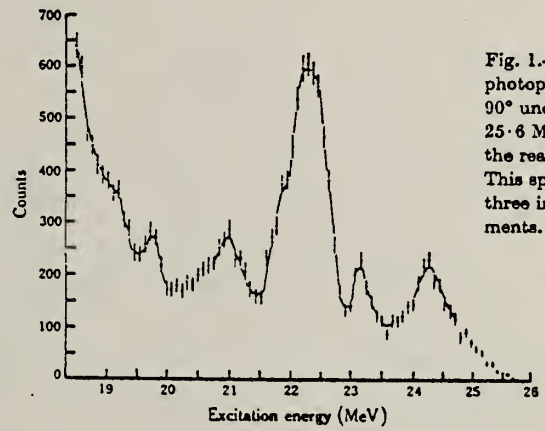

Fig. 1.—The spectrum of photoprotons from oxygen at 90° under bombardment by 25·6 MeV bremsstrahlung in the reaction $^{16}O(\gamma, p_0)^{15}N$. This spectrum is the sum of three independent measurements.

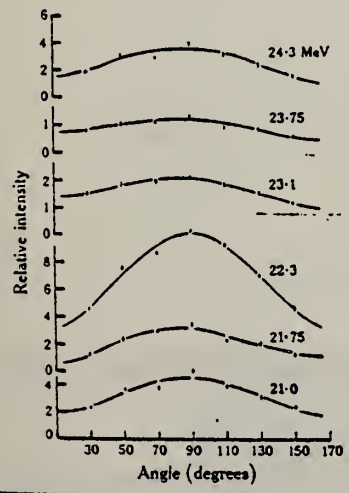

Fig. 2.—The measured photoproton angular distributions in the reaction $^{16}O(\gamma, p_0)^{15}N$ and the fits to them using the sum of Legendre polynomials with coefficients as given in Table 1. Note the changes in the vertical scale.

	Punched	Checked w/PO
IBM Card DATA	6/26/69	✓
IBM Card REFERENCE	"	✓

REF. Martin Stroetzel
Z. Phys. 214, 357 (1968)

ELEM. SYM.	A	Z
O	16	8

METHOD

REF. NO. 68 St 2 egf

REACTION	RESULT	EXCITATION ENERGY	SOURCE TYPE	SOURCE RANGE	DETECTOR TYPE	DETECTOR RANGE	ANGLE
E,E/	LFT	6- 14	D	33- 60	MAG-D		DST

Using electrons with up to 60 MeV energy, ten transitions in ^{16}O have been studied: two $E0$ (6.05 and 12.05 MeV), one $E1$ (13.10 MeV), four $E2$ (6.92, 9.85, 11.52 and 13.1 MeV), two $M2$ (12.53 and 12.96 MeV) and one $E3$ (6.13 MeV). The cross sections measured as a function of momentum transfer have been analyzed to yield transition probabilities to the ground state and transition radii. The results are compared with the theory of BROWN and GREEN, and with the particle-hole calculations of LEWIS and DEFOREST. For levels at 11.08 and 13.67 MeV, upper limits for the transition probabilities are given.

10 LEVELS 6.05-13.1 MEV

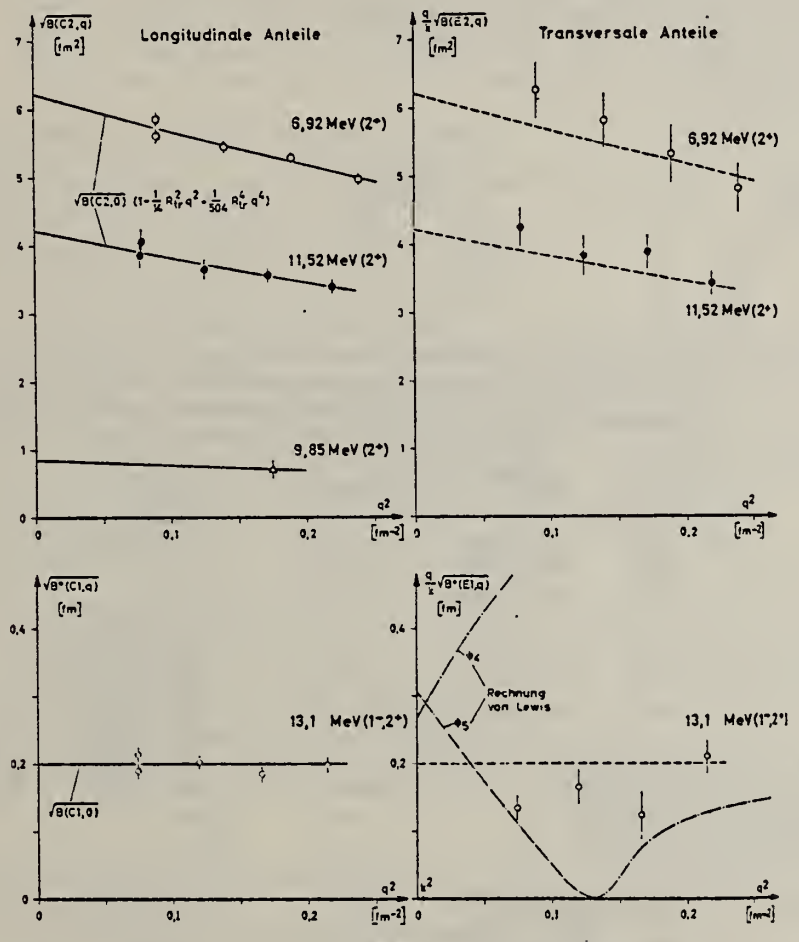

Fig. 2a

Fig. 2a und b. Longitudinale und transversale Übergangsmatrixelemente (nur statistische Fehler) aufgetragen über dem Quadrat der Impulsübertragung (BA-Auswertung). Eine Anpassung der angegebenen Funktionen an die Meßpunkte nach der Methode der kleinsten Fehlerquadrate liefert die durchgezogenen Kurven und die Parameter in Tabelle 2. Die gestrichelten Kurvenzüge für die transversal elektrischen Anteile wurden aus den zugehörigen longitudinalen Anteilen unter Annahme der Gültigkeit des Gleichheitszeichens in Formel (1) berechnet. Durch die gute Übereinstimmung mit den Meßpunkten wird diese Annahme für die hier betrachteten $E2$-Übergänge bewiesen. Die Ergebnisse von Teilchen-Loch-Rechnungen (strichpunktierte Kurven) werden im Text erläutert

(over)

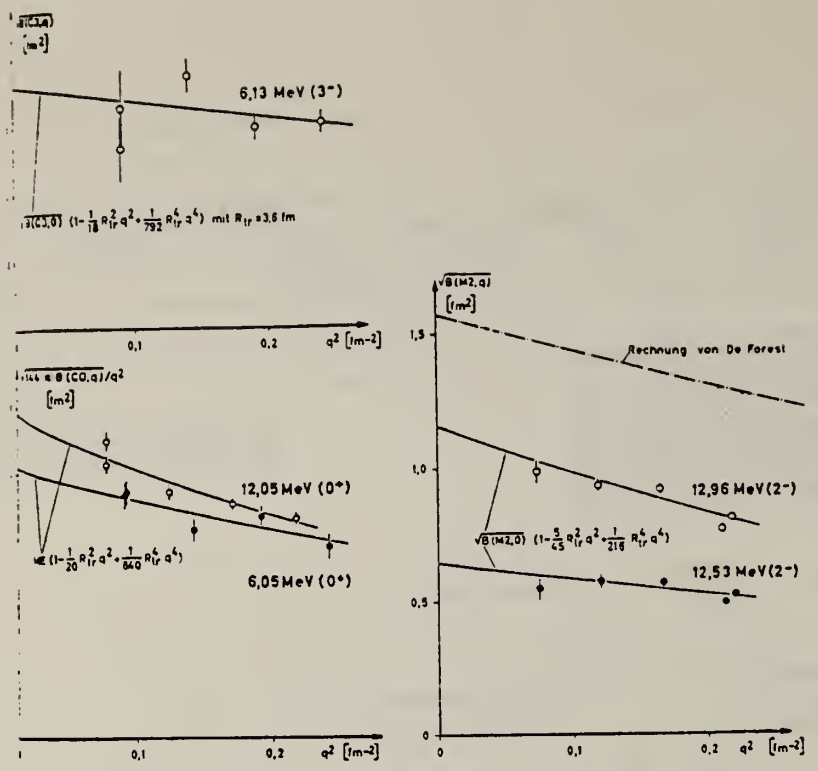

Fig. 2b

Tabelle 3. *Vergleich der gemessenen Grundzustandsübergangswahrscheinlichkeiten mit den Ergebnissen anderer Autoren.* Γ_γ^0 *wurde mit den Werten von Tabelle 2 berechnet* (Γ_γ^0 *proportional zu* $B(\lambda, q=k)$[22]). *Den* 0^+- *und* 2^+-*Zuständen liegt die DWBA-Auswertung zugrunde. Die Weißkopfabschätzung* Γ_W *erfolgte mit* $R_0 = 1{,}2\ fm \cdot A^{\frac{1}{3}}$

^{16}O-Niveau $I^\pi E_x$ [MeV]	Ergebnisse dieser Arbeit Γ_γ^0 [eV]	Γ_γ^0/Γ_W	Andere Autoren Γ_γ^0 [eV]
0^+ 6,05	3,66 ± 0,55[a]	–––	3,80 ± 0,19[a 7]
12,05	4,40 ± 0,44[a]	–––	–––
2^+ 6,92	0,093 ± 0,010[b]	3,02	0,055 ± 0,015[10]
			0,066 ± 0,022[11]
			0,080 ± 0,007[12]
9,85	0,010 ± 0,004	0,06	0,020 ± 0,010[13]
			0,0059 ± 0,0006[14]
11,52	0,55 ± 0,07[b]	1,40	0,90 ± 0,20[13]
			0,85 ± 0,10[18]
			0,66 ± 0,09[14]
13,1	≈0,13	≈0,17	0,6 ± 0,3[4]
1^- 13,10	31 ± 8	0,033	150[16]
			88[17]
			23 ± 4[15]
2^- 12,53	0,021 ± 0,006	0,7	0,15 ± 0,02[18]
12,96	0,078 ± 0,016	2,3	–––
3^- 6,13	$(2{,}3 \pm 1{,}1) \cdot 10^{-5}$	12	$(2{,}63 \pm 0{,}21) \cdot 10^{-5}$ [8]
? 11,08	$< 0{,}01 \cdot \Gamma_W(M1)$		
	$< 0{,}2 \cdot \Gamma_W(M2)$		
	$< 6 \cdot \Gamma_W(M3)$		$160 \cdot \Gamma_W(M3)$[19]
1^+ 13,67	$< 0{,}01 \cdot \Gamma_W(M1)$		$2{,}5 \cdot \Gamma_W(M3)$[18]

[a] Monopolmatrixelement ME in fm².

[b] Als Bestwerte für Γ_γ^0 soll für das 6,92 MeV-Niveau (0,085 ± 0,006) eV und für das 11,52 MeV-Niveau (0,59 ± 0,05) eV angegeben werden.

REF.

P. M. Tutakin
Yad. Fiz. 8, 661 (1968)
Sov. J. Nucl. Phys. 8, 383 (1969)

ELEM. SYM.	A	Z
O	16	8

METHOD

REF. NO.	
68 Tu 1	HMG

REACTION	RESULT	EXCITATION ENERGY	SOURCE		DETECTOR		ANGLE
			TYPE	RANGE	TYPE	RANGE	
G,P	SPC	21,22	D	21,22	EMU-D		DST
		(21.7, 22.2)					

21=21.71, 22=22.16

Nuclear emulsions placed in H_2O and monoenergetic γ rays from the reaction $T(p, \gamma)He^4$ have been used to measure the angular distributions of photoprotons from the reaction $O^{16}(\gamma, p)N^{15}$. The numbers of photoproton tracks observed at dip angles $\beta \leq 30°$ for emission-angle intervals θ = 0—15°, 15—30°, 30—45°, 45—60°, 60—75°, and 75—90° are respectively 305, 172, 89, 40, 25, and 33 (E_γ = 21.71 MeV) and 4, 18, 25, 33, 51, and 69 (E_γ = 22.16 MeV). The angular distributions obtained do not correspond to the angular distribution of γ rays for the inverse reaction $N^{15}(p, \gamma)O^{16}$ [$W_\gamma = 1 + 0.1P_1 - 0.6P_2$].[3]

We have studied the angular distribution of photoprotons from the reaction $O^{16}(\gamma, p)N^{15}$; nuclear emulsions and monoenergetic γ rays (E_γ = 22.16 MeV) were employed. As in our earlier work[1] the plates, in a cassette with H_2O, were placed in the plane of the incident protons and the γ rays emitted at 90°. The source of γ rays was the reaction $T(p, \gamma)He^4$. The track lengths were converted to photoproton energy by means of an experimentally determined range-energy relation: $\log E_{ph.pr.}(MeV) = -0.7147 + 0.5847 \log L(\mu)$.[2] The photoproton energy spectra obtained are shown in the figure. In the upper part are the results for E_γ = 22.16 MeV (E_p = 3.228 MeV, dip angle β_m = 30°), and in the lower part, the results for E_γ = 21.71 MeV (E_p = 2.622 MeV, β_m = 15°). The cross-hatched peaks correspond to photoprotons produced in the decay of O^{16*} to the ground state of N^{15}. The angular distributions of these photoprotons are shown by the solid curves in the upper corner of each part of the figure. The dashed curves are the angular distributions of γ rays from the inverse reaction $N^{15}(p, \gamma)O^{16}$ [3] ($F(\theta)$ is the yield of p or γ in relative units per unit solid angle).

It can be seen from the figure that the angular distributions differ strongly. For E_γ = 22.16 MeV the angular distribution is characterized by preferential emission of photoprotons at angles θ near 90°, and for E_γ = 21.71 MeV it has a sharply expressed directivity forward and backward.

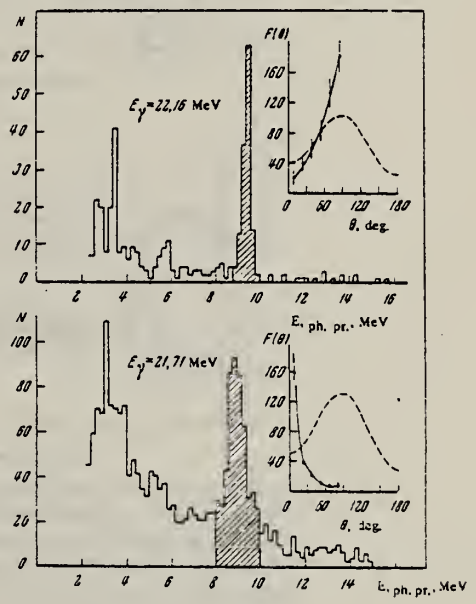

[1] P. M. Tutakin, Yad. Fiz. 5, 1325 (1967) [Sov. J. Nucl. Phys. 5, 946 (1967)].

[2] P. M. Tutakin, Progr. i tez. dokl. XVIII ezhegodn. soveshch. po yadern. spektrosk. i strukt. atomn. yadra (Program and Summary of Reports of the XVIII Annual Conference on Nuclear Spectroscopy and Nuclear Structure), Nauka, Leningrad, 1968, pp. 132, 230.

[3] N. W. Tanner, Nucl. Phys. 63, 383 (1965).

Translated by C. S. Robinson
94

REF. C. P. Wu, F. W. K. Firk, and T. W. Phillips
Phys. Rev. Letters 20, 1182 (1968)

ELEM. SYM.	A	Z
O	16	8

METHOD

REF. NO. 68 Wu 1 EGF

REACTION	RESULT	EXCITATION ENERGY	SOURCE		DETECTOR		ANGLE
			TYPE	RANGE	TYPE	RANGE	
G,N	ABX	THR-40	C	20-40	TOF-D	2-25	90

226

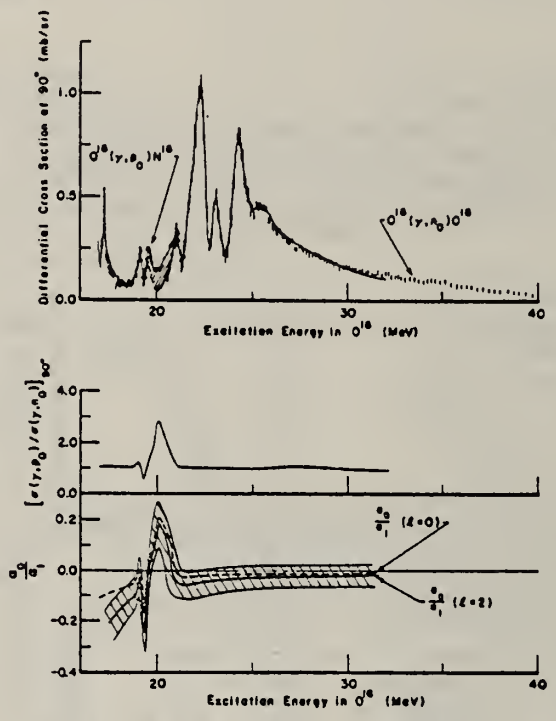

FIG. 2. The observed $O^{16}(\gamma, n_0)O^{15}$ differential cross section at 90° compared with the $O^{16}(\gamma, p_0)N^{15}$ data. The (γ, p_0) results are indicated by solid dots between 19 and 21 MeV and by a thin line elsewhere; Morrison's data (Ref. 15) are used between 17 and 22 MeV and between 25 and 32 MeV. In the region 22-25 MeV the (γ, p_0) data deduced from the $N^{15}(p, \gamma_0)O^{16}$ work of Tanner, Thomas, and Earle (Ref. 13) are used. The cross-hatched region indicates the error on a_0/a_1 due to statistics: The absolute $O^{16}(\gamma, n_0)O^{15}$ cross section has a systematic uncertainty of 10 % which is not included in the above diagrams.

J. E. E. Baglin and M. N. Thompson
Nucl. Phys. A138, 73 (1969)

ELEM. SYM.	A	Z
O	16	8

METHOD

REF. NO.	
69 Ba 2	egf

REACTION	RESULT	EXCITATION ENERGY	SOURCE		DETECTOR		ANGLE
			TYPE	RANGE	TYPE	RANGE	
G,P	ABX	20-30	C	26,31	SCD-D	8-18	DST

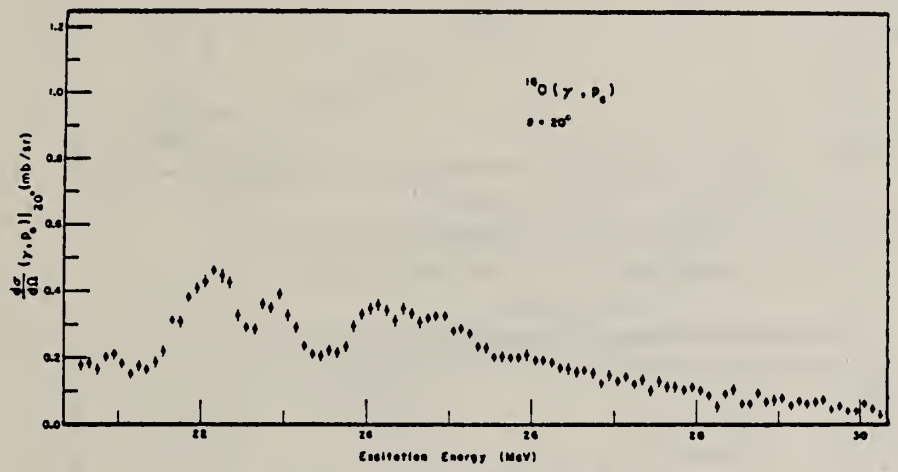

Fig. 2(a). $^{16}O(\gamma, p_0)$. Differential cross section at 20°.

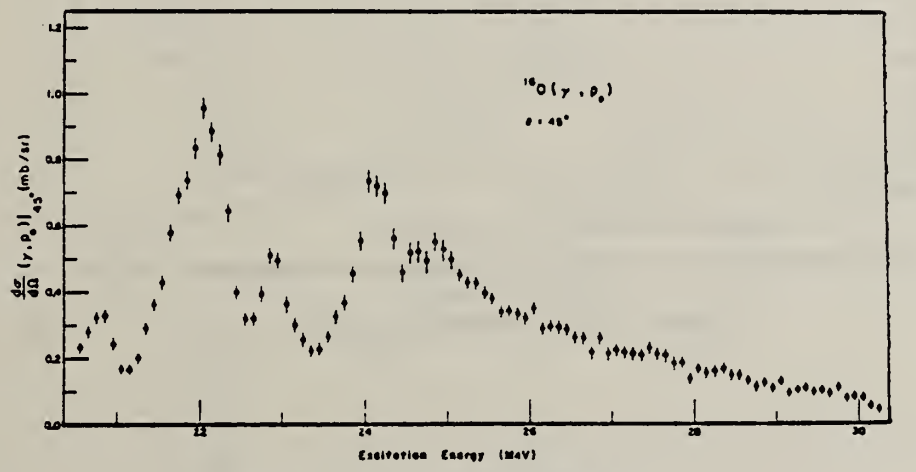

Fig. 2(b). $^{16}O(\gamma, p_0)$. Differential cross section at 45°.

[over]

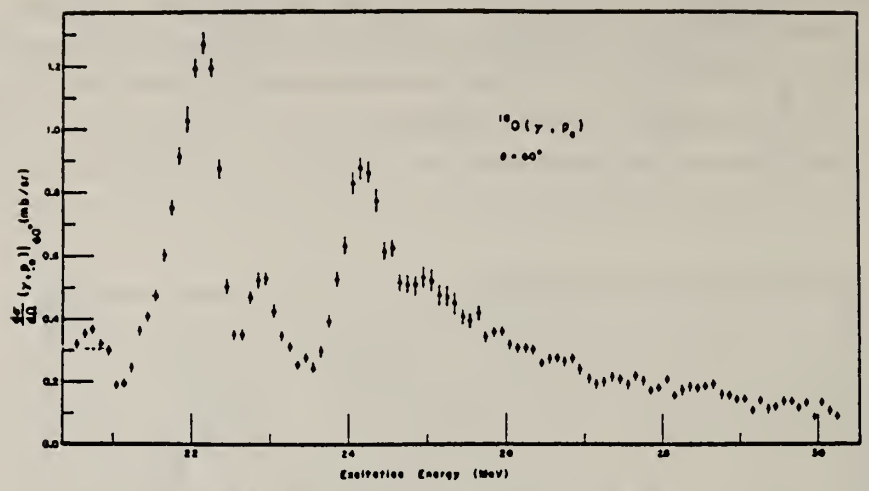

Fig. 2(c). $^{16}O(\gamma, p_0)$. Differential cross section at 60°.

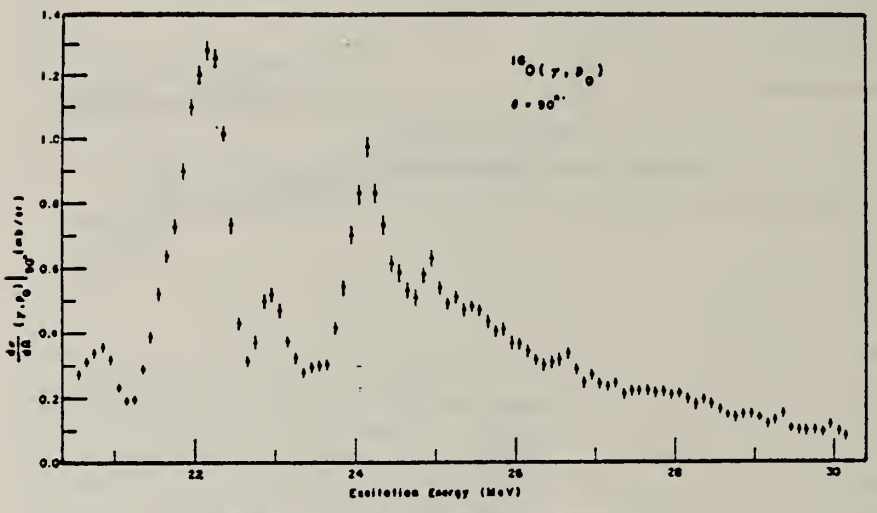

Fig. 2(d). $^{16}O(\gamma, p_0)$. Differential cross section at 90°.

REACTION	RESULT	EXCITATION ENERGY	SOURCE		DETECTOR		ANGLE
			TYPE	RANGE	TYPE	RANGE	

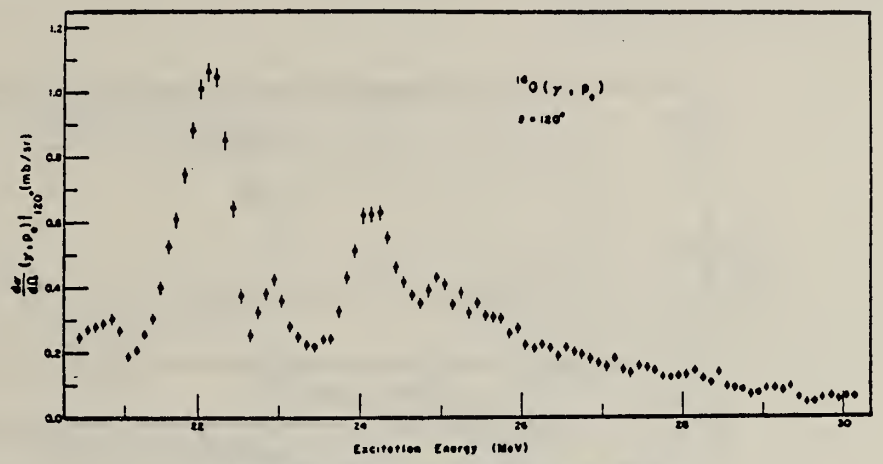

Fig. 2(e). $^{16}O(\gamma, p_0)$. Differential cross section at 120°.

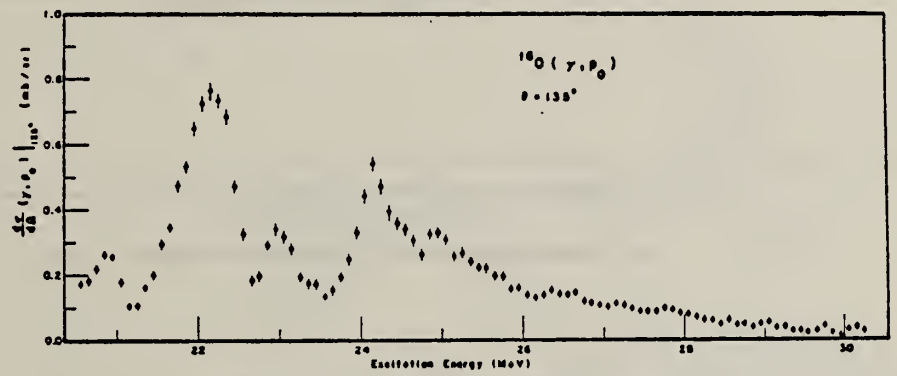

Fig. 2(f). $^{16}O(\gamma, p_0)$. Differential cross section at 135°.

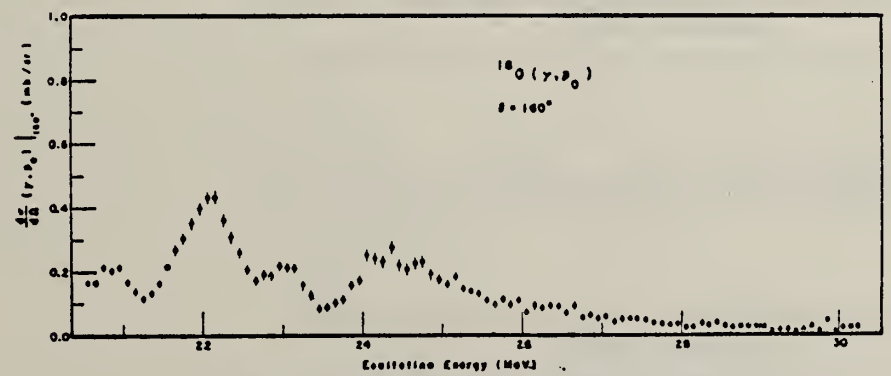

Fig. 2(g). $^{16}O(\gamma, p_0)$. Differential cross section at 160°.

[over]

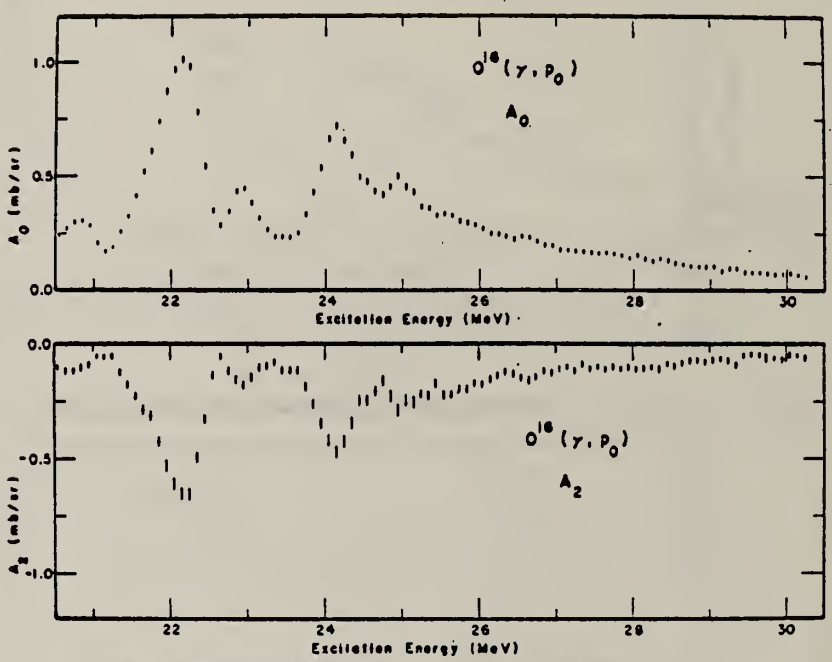

Fig. 3. Angular distribution for $^{16}O(\gamma, p_0)$. Legendre coefficients A_0 and A_2.

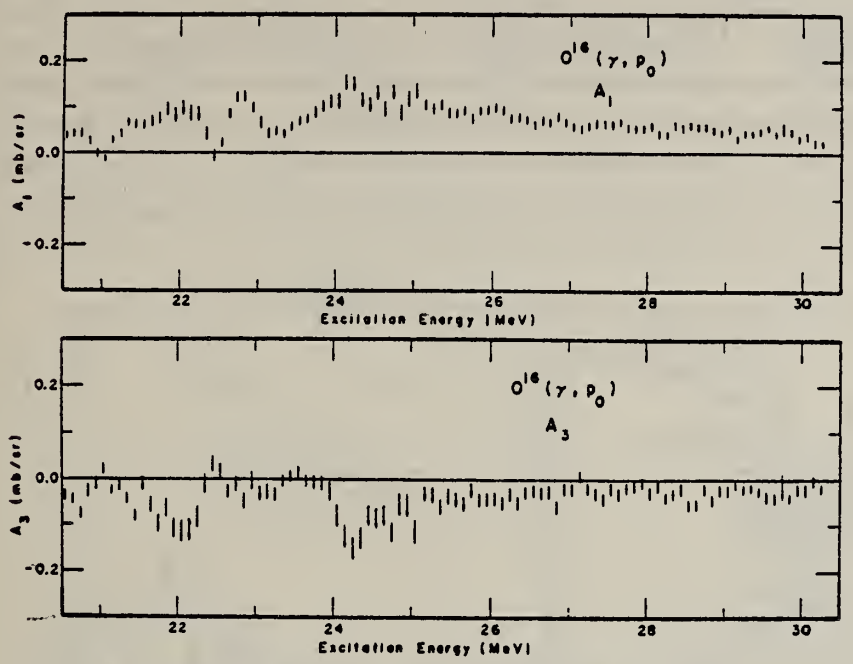

Fig. 4. Angular distribution for $^{16}O(\gamma, p_0)$. Legendre coefficients A_1 and A_3.

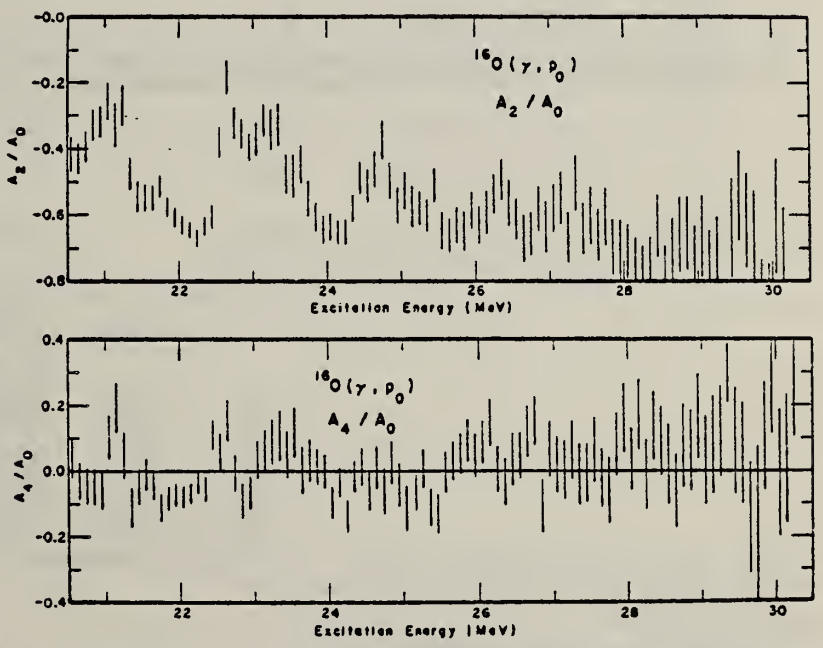

Fig. 5. Angular distribution for $^{16}O(\gamma, p_0)$. Legendre coefficients $a_2 = A_2/A_0$ and $a_4 = A_4/A_0$.

REF. N. Bezić, D. Brajnik, D. Jamnik and G. Kernel
Nucl. Phys. A128, 426 (1969)

ELEM. SYM.	A	Z
O	16	8

METHOD

REF. NO.	
69 Be 2	egf

REACTION	RESULT	EXCITATION ENERGY	SOURCE		DETECTOR		ANGLE
			TYPE	RANGE	TYPE	RANGE	
G,MU-T	ABX	10-30	C	35	MGC-D	10-30	4PI

109

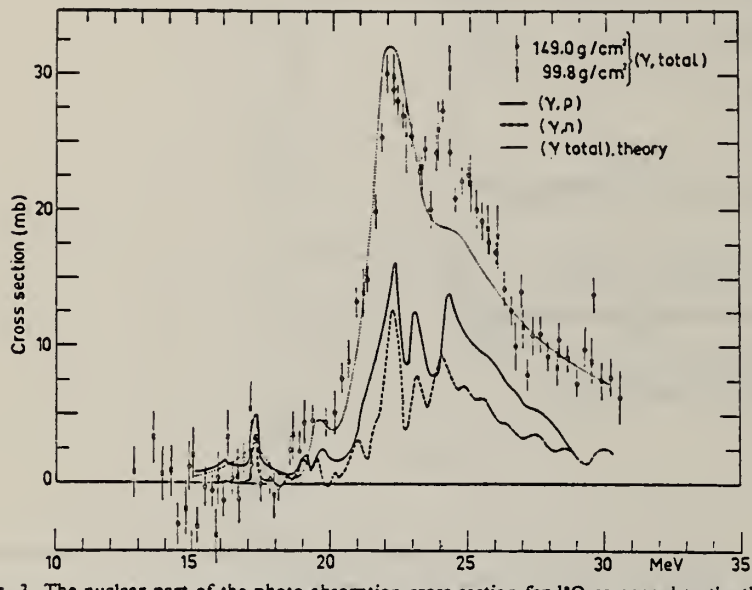

Fig. 3. The nuclear part of the photo-absorption cross section for ^{16}O compared to the theory [24]) and to the (γ, n) and (γ, p) cross sections [22, 23]). An estimated error of the zero line position is ±1.0 mb.

TABLE 1

Weighted energy-integrated total photonuclear cross sections

	σ_{int} (mb · MeV)	$\frac{\sigma_{int}}{60(NZ/A)}$ (mb · MeV)	σ_{-1} (mb)	$\frac{\sigma_{-1}}{0.30A^{\frac{1}{3}}\ \text{mb}}$	σ_{-2} (mb · MeV^{-1})	$\frac{\sigma_{-2}}{3.5\,A^{\frac{1}{3}}}$ (μb · MeV^{-1})
^{12}C	133±13	0.74±0.07	5.4±0.6	0.65±0.07	0.23±0.03	1.04±0.15
^{14}N	195±37	0.93±0.08	8.4±1.7	0.83±0.20	0.36±0.08	1.28±0.29
^{16}O	171±17	0.71±0.07	7.2±0.8	0.60±0.07	0.31±0.04	0.87±0.11
^{19}F	271±50	0.94±0.17	14.1±2.7	0.82±0.19	0.74±0.17	1.60±0.35
^{28}Si	360±30	0.86±0.07	17.5±1.7	0.68±0.07	0.83±0.10	0.93±0.11
^{40}Ca	580±60	0.96±0.10	29 ±3	0.71±0.08	1.5 ±0.2	0.92±0.12

The interval of integration is 10-30 MeV.

[22] B.C. Cook, J.E.E. Baglin, J.N. Bradford and J.E. Griffin, Phys. Rev. 143, (1966) 712.
[23] R.C. Morrison, J.R. Steward and J. S. O'Connell, Phys. Rev. Lett. 15, (1965) 367.
[24] B. Buck and A. D. Hill, Nucl. Phys. A95 (1967) 271.

G. W. Cole Jr., F. W. K. Firk and T. W. Phillips
Phys. Letters 30B, 91 (1969)

ELEM. SYM.	A	Z
0	16	8

METHOD

REF. NO. 69 Co 3 egf

REACTION	RESULT	EXCITATION ENERGY	SOURCE		DETECTOR		ANGLE
			TYPE	RANGE	TYPE	RANGE	
$ G,N	NOX	20-33	C	30,60	TOF-D	4-16	DST

N POLARIZATION

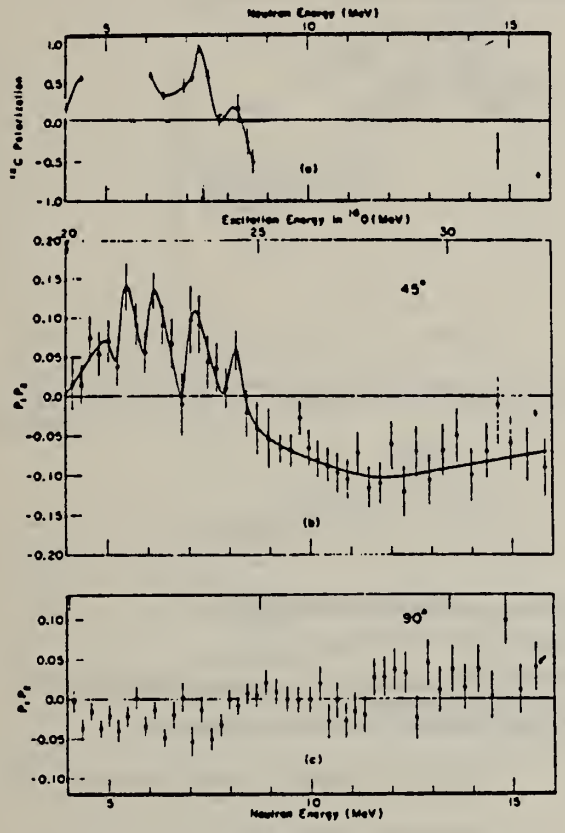

Fig. 2.
(a) Measurements of the analysing power of ^{12}C (P_2) for neutrons from 4 to 16 MeV, at a 50° scattering angle [8].
(b) P_1P_2, the product of the ^{16}O photoneutron polarization and the ^{12}C analysing power, for a reaction angle of 45°. The error bars reflect only the statistical uncertainty. (▲ indicates $E_{\gamma 0}$ = 30 MeV, ▼ indicates $E_{\gamma 0}$ = 60 MeV).
(c) P_1P_2 for a reaction angle of 90°, where for pure E1 transitions P_1 should be identically zero at all energies. ($E_{\gamma 0}$ = 60 MeV).

Table 1
Values of the polarization of photoneutrons from ^{16}O at 45°. The energies correspond to those at which the values of P_2 are known. Estimates of the ratio a_s/a_d are also listed.

Exc. Energy in ^{16}O (MeV)	P_1P_2	^{16}O Pol. at 45° P_1	$\frac{a_s}{a_d}$
22.17	0.133 ± 0.024	0.23 ± 0.05	$0.23^{+0.06}_{-0.04}$
22.51	0.092 ± 0.025	0.28 ± 0.10	$0.25^{+0.33}_{-0.06}$
23.06	0.020 ± 0.040	0.04 ± 0.08	~ 0.1
23.27	0.108 ± 0.037	0.19 ± 0.07	$0.20^{+0.05}_{-0.05}$
23.45	0.088 ± 0.036	0.09 ± 0.04	$0.08^{+0.05}_{-0.03}$
23.68	0.043 ± 0.035	0.08 ± 0.07	$0.07^{+0.05}_{-0.03}$
24.47	0.050 ± 0.025	0.29 ± 0.25	$0.26^{+2.9}_{-0.11}$
24.70	−0.021 ± 0.028	0.08 ± 0.14	~ 0.1
24.90	−0.037 ± 0.032	0.07 ± 0.09	$0.07^{+0.05}_{-0.04}$

[over]

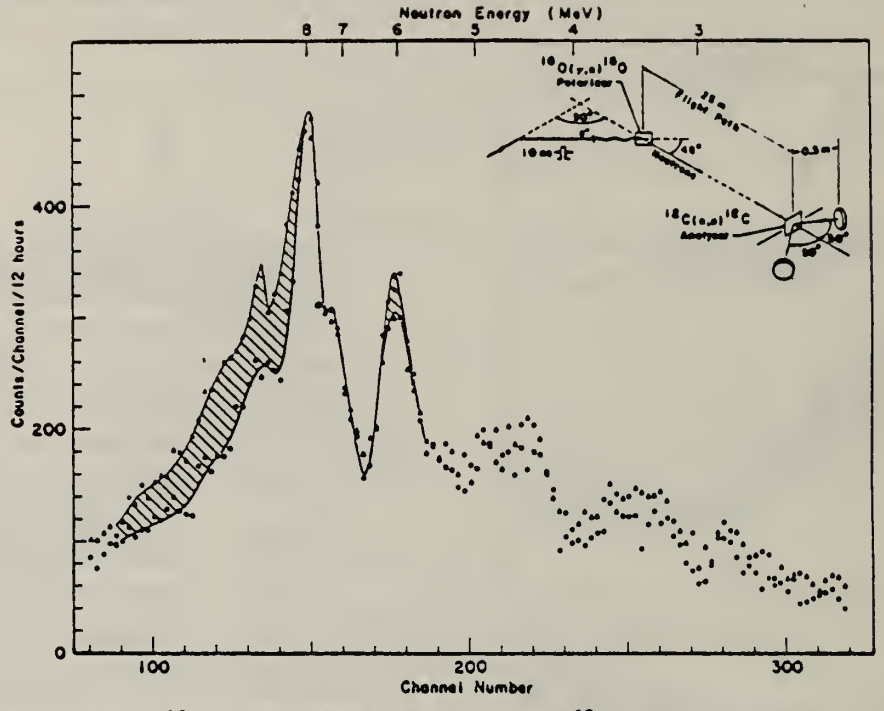

Fig. 1. Observed spectra of ^{16}O photoneutrons scattered ± 50° from the ^{12}C analyzer, for a reaction angle of 45° (▲ indicates left-hand side yield, + 50°). Measured background have been subtracted.
The inset shows the placement of the bremsstrahlung target, the oxygen target and the polarization analyser.

D. E. Frederick, R. J. J. Stewart, and R. C. Morrison
Phys. Rev. 186, 992 (1969)

ELEM. SYM.	A	Z
0	16	8

METHOD

REF. NO.	
69 Fr 1	hmg

REACTION	RESULT	EXCITATION ENERGY	SOURCE		DETECTOR		ANGLE
			TYPE	RANGE	TYPE	RANGE	
G,P	ABX	12-33	C	12-33	SCD-D		DST
		(12.1)		(12.1)			

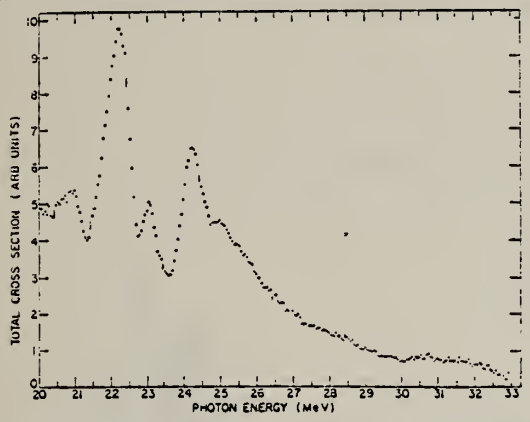

FIG. 3. The $O^{16}(\gamma, p_0)N^{15}$ total cross section obtained with bremsstrahlung of $E_\beta = 33.1$ MeV, assuming 100% ground-state transitions.

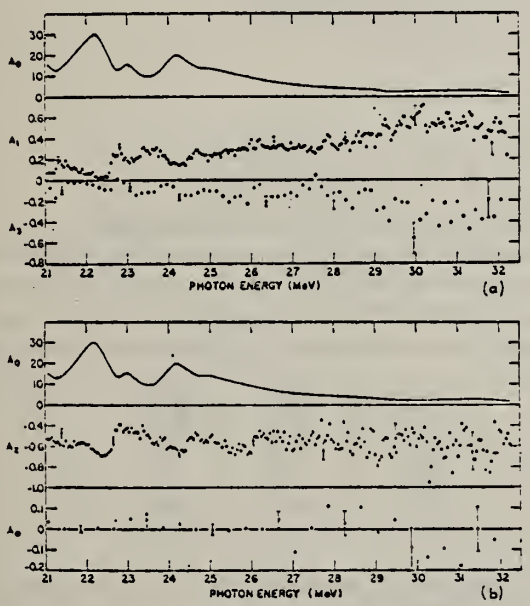

FIG. 4. (a) The angular distribution coefficients A_0, A_1, A_3. A_1 and A_3 are plotted at 50- and 150-keV intervals, respectively. (b) The angular distribution coefficients A_2 and A_4, with A_0 included for comparison. A_2 is plotted in 50-keV steps and A_4 at 400-keV intervals.

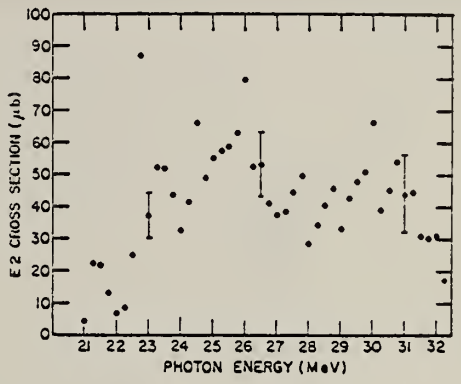

FIG. 6. The ground-state $E2$ cross section extracted from the data using Eq. (4). The errors shown reflect the statistical errors only of A_1 and A_3, with a 10% uncertainty assumed in Eq. (4) for $\sigma(E1)$.

$$\sigma(E2)/\sigma(E1) \approx (5.69A_1^2 + 6.65A_3^2 + 7.70A_1A_3)/22.9, \quad (4)$$

TABLE I. Comparison of resonances observed in O^{16} above 20 MeV (peak energies in MeV).

This work (γ, p)	Cook *et al.*[a] (γ, n)	Bramblett *et al.*[b] (γ, n)	Tanner *et al.*[c] (p, γ_0)	Morrison[d] (γ, p)
20.89	21.0	20.8	21.0	20.7
	21.7	21.8		21.7
22.20	22.26	22.1	22.2	22.3
23.03	23.15	23.1	23.0	23.0
24.23	24.1	24.0	24.3	24.3
24.99	24.9	25.0	25.2	25.0
(25.42)	25.55			25.5
26.37	26.38	26.2		26.3
	27.45	27.3		27.4
	28.55	28.9		
	29.6			
30.65 } 31.15 31.65	31.4			

[a] Reference 15.
[b] Reference 16.
[c] Reference 17.
[d] Reference 14.

[14] R. C. Morrison, Ph.D. thesis, Yale University, 1965 (unpublished).
[15] B. C. Cook, J. E. E. Baglin, J. N. Bradford, and J. E. Griffen, Phys. Rev. 143, 712 (1966).
[16] R. L. Bramblett, J. T. Caldwell, R. R. Harvey, and S. C. Fultz, Phys. Rev. 133, B869 (1964).
[17] N. W. Tanner, G. C. Thomas, and E. D. Earle, Nucl. Phys. 52, 45 (1964).

REF. V. G. Ivanchenko and B.S. Ratner
Izv. Akad. Nauk. Fiz. 34, 175 (1969)
Bull. Acad. Sci. USSR-Phys. 34, 159 (1970)

ELEM. SYM.	A	Z
O	16	8

METHOD

REF. NO. 69 Iv 1 hmg

REACTION	RESULT	EXCITATION ENERGY	SOURCE		DETECTOR		ANGLE
			TYPE	RANGE	TYPE	RANGE	
G,N	RLX	16-22	C	16-30	ACT-I		

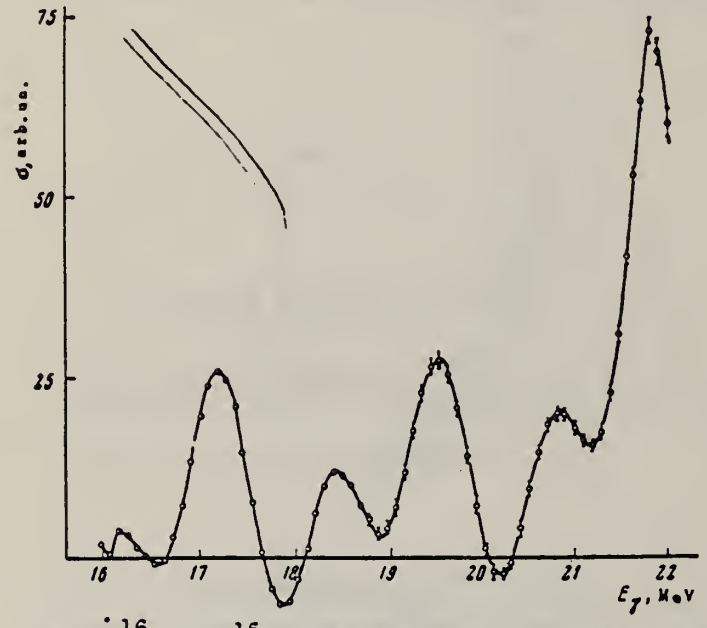

Fig.3. $^{16}O(\gamma,n)^{15}O$ cross section calculated from experimental data.

Resonances in the $^{16}O(\gamma,n)^{15}O$ Reaction

Our work		Ref. 3		Ref. 4	
E_{res}, MeV	σ, arb. un.	E_{res}, MeV	σ, arb. un.	E_{res}, MeV	σ, arb. un.
16,2	5,5	—	—	16,1	3,2
17,21	36	17,30	26,5	17,1	21,8
18,44	16	19,06	16,1	19,0	18
19,53	38	19,56	14,8	19,3	18
—	—	20,2	6,5	—	—
20,75	27	21,0	26	20,8	21,8
21,72	100	21,7	100	21,8	100

[3] B.S. Cook, J.E.E. Baglin, J.N. Bradford & J.E. Griffin, Phys. Rev. 143, 712 (1966).

[4] R.L. Bramblett, J.T. Caldwell, R.R. Harvey & S.C. Fultz, Ibid. 133B, 869 (1964).

REF.

N. K. Keller, J. K. P. Lee and D. B. McConnell
Can. J. Phys. 47, 611 (1969)

ELEM. SYM.	A	Z
O	16	8

METHOD

REF. NO.	
69 Ke 3	hmg

REACTION	RESULT	EXCITATION ENERGY	SOURCE		DETECTOR		ANGLE
			TYPE	RANGE	TYPE	RANGE	
G,P	SPC	16-26	C	26	SCD-D	4-14	90
		(26.5)		(26.5)			

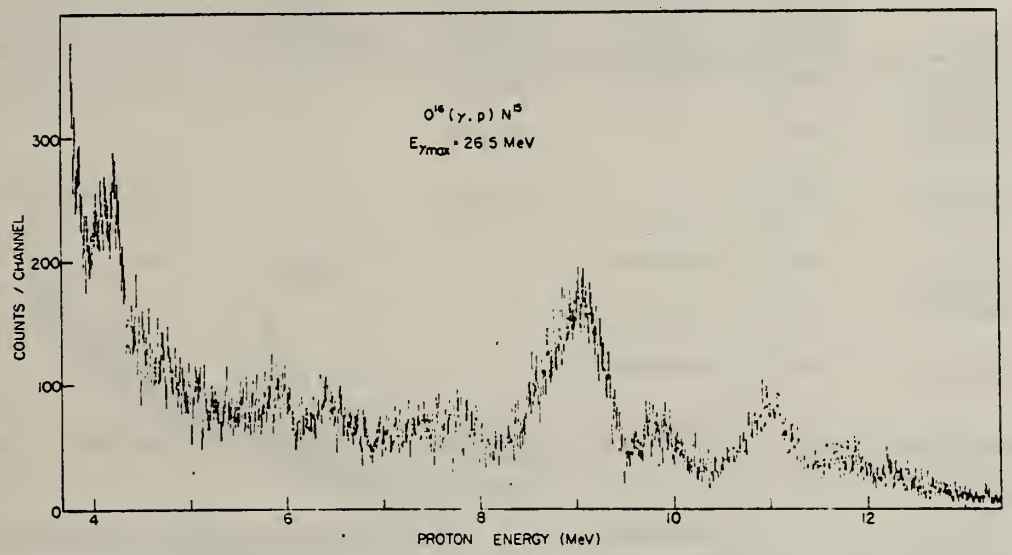

FIG. 4. Photoproton yield from $^{16}O(\gamma, p)^{15}N$ reaction at 90°. The proton energy is the true energy given by the detector, not corrected for losses in the target.

REF.

T. A. Khan, J. S. Hewitt, K. G. McNeill
Can. J. Phys. 47, 1037 (1969)

ELEM. SYM.	A	Z
O	16	8

METHOD

REF. NO.	
69 Kh 1	hmg

REACTION	RESULT	EXCITATION ENERGY	SOURCE		DETECTOR		ANGLE
			TYPE	RANGE	TYPE	RANGE	
G,N	ABX	16-33	C	22-33	TOF-D	1-14	98
						(.8)	

TABLE I

Measured values of the photon absorption cross section in ^{16}O at the 22.3 MeV peak for neutron (or proton) transitions to the ground state of ^{15}O (or ^{15}N)

Authors	Method	Resolution (keV)	Angle θ (deg)	Differential cross section $(d\sigma/d\Omega)_\theta$ (mb/sr)	Integral cross section $\int_{4\pi}(d\sigma/d\Omega)d\Omega$ (mb)
Present result*	$^{16}O(\gamma,n_0)$ TF† spectrum	100	98	1.00±0.05	—
Wu *et al.** (1968)	$^{16}O(\gamma,n_0)$ TF spectrum	100	90	1.05±0.05	—
Verbinski and Courtney (1965)	$^{16}O(\gamma,n_0)$ TF spectrum	100	93	0.69±0.01	—
Caldwell *et al.* (1965)	$^{16}O(\gamma,n_0)$ Yield from monochromatic gammas	200	4π-integrated	—	7.0±0.1
Geller and Muirhead (1963)	$^{16}O(\gamma,n)$ B‡ yield curves	140	4π-integrated	—	12.8±1.5
Earle and Tanner (1967)	$^{15}N(p,\gamma_0)$ + detailed balance	30	Many	1.0±0.25 (at 90°)	11.8±2.5
Morrison* (1966)	$^{16}O(\gamma,p)$ B‡	80	90	1.0±0.15	—
Cook *et al.* (1966)	$^{16}O(\gamma,n)$ B‡ yield curves		4π-integrated	—	19.5

*Obtained relative to the $^2H(\gamma,n)^1H$ cross section.
†Time-of-flight.
‡Bremsstrahlung.

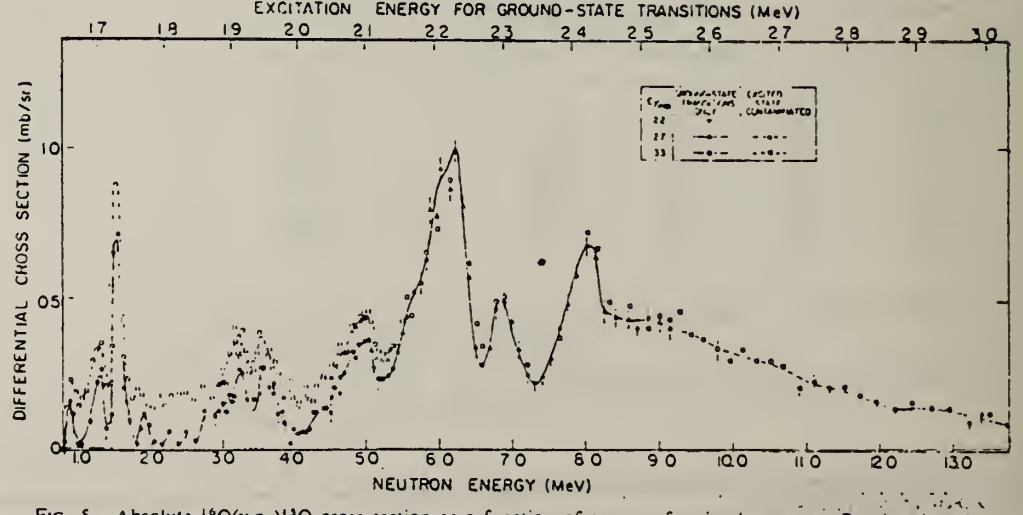

FIG. 5. Absolute $^{16}O(\gamma,n_0)^{15}O$ cross section as a function of energy of emitted neutrons. Results plotted were analyzed assuming all neutrons were due to neutron decays to the ground state of ^{15}O, but those indicated as solid symbols for each bremsstrahlung energy correspond definitely to ground-state transitions.

K. M. Murray and J. C. Ritter
Phys. Rev. 182, 1097 (1969)

ELEM. SYM.	A	Z
O	16	8

METHOD

REF. NO.	
69 Mu 1	HMG

REACTION	RESULT	EXCITATION ENERGY	SOURCE		DETECTOR		ANGLE
			TYPE	RANGE	TYPE	RANGE	
G,NG	SPC	16-30	C	21-30	SCD-D		90
G,PG	SPC	12-30	C	21-30	SCD-D		90

GAMMA SPECTRUM

γ rays resulting from the decay of excited states in O^{15} and N^{15} have been observed when these states were produced from (γ, n) and (γ, p) reactions on O^{16}. Bremsstrahlung from the Naval Research Laboratory's 60-MeV Electron Linac was used as a source of x rays to produce the photonuclear reactions leading to N^{15*} and O^{15*}. The 5-MeV positive-parity quadruplet resulting from the above-described reactions was resolved into its four separate components and the width of each component was observed. Limits on lifetimes for all of the observed transitions were determined from the Doppler broadening of these lines. The $\frac{1}{2}^+$ states at 5.240 MeV in O^{15} and at 5.270 MeV in N^{15} were observed to have lifetimes considerably greater than 10^{-13} sec. All other observed transitions showed lifetimes short compared to 10^{-13} sec. It was also observed that the branching ratio of the 9.223-MeV level in N^{15} to the $\frac{1}{2}^+$ state at 5.299 MeV could not be greater than ~50%.

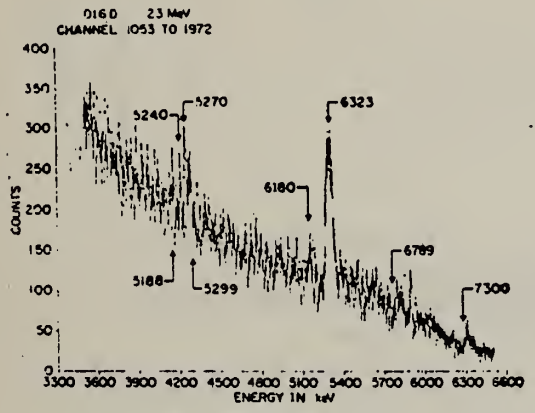

FIG. 7. See caption of Fig. 6.

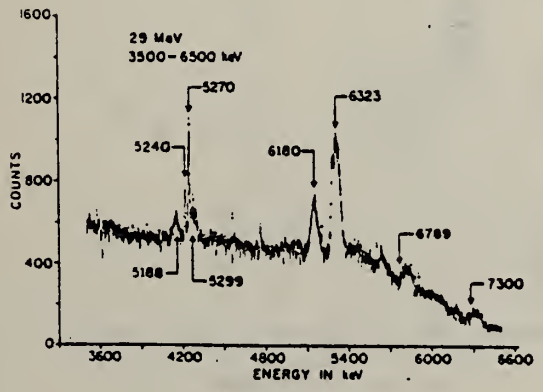

FIG. 10. See caption of Fig. 6.

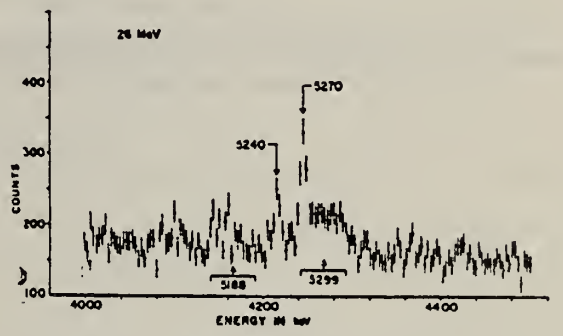

FIG. 12. Details in the region of the 5-MeV positive-parity group.

P. C. Nagle, E. J. Winhold, P. F. Yergin, P. Stoler and S. J. Mecca
Nucl. Phys. A127, 669 (1969)

ELEM SYM.	A	Z
O	16	8

METHOD

REF. NO. 69 Na 1 egf

REACTION	RESULT	EXCITATION ENERGY	SOURCE		DETECTOR		ANGLE
			TYPE	RANGE	TYPE	RANGE	
G,N	ABX	35-65	C	35-65	TOF-D	16-55	68

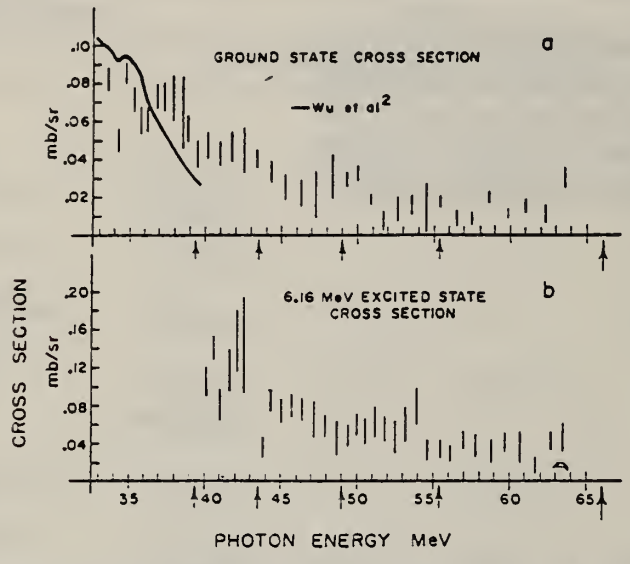

Fig. 2. The $^{16}O(\gamma, n)$ cross sections. a) 67.5° differential cross section to the ground state of ^{15}O (present work). The solid curve represents the 90° differential cross section obtained by Wu *et al.* [2]). b) Upper limit 67.5° differential cross section to the 6.16 MeV excited state of ^{15}O.

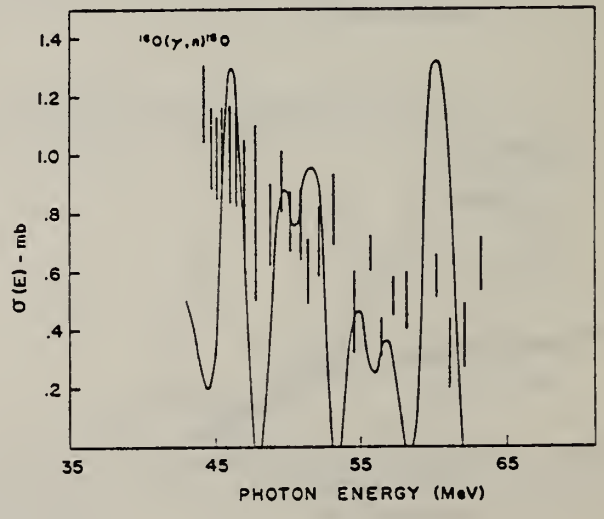

Fig. 3. The data bars are the sum of the $^{16}O(\gamma, n)$ differential cross sections leaving ^{15}O in the ground and 6.16 MeV excited states multiplied by a factor of 10. The solid curve is due to Cook *et al.* [1]).

REF.

T. Shintomi and M. Masuda
J. Phys. Soc. Japan 26, 607 (1969)

ELEM. SYM.	A	Z
O	16	8

METHOD

REF. NO. 69 Sh 3

[Page 1 of 2] hmg

REACTION	RESULT	EXCITATION ENERGY	SOURCE		DETECTOR		ANGLE
			TYPE	RANGE	TYPE	RANGE	
G,P	RLX	12-27	C	23,27	EMU-D	1-15	DST

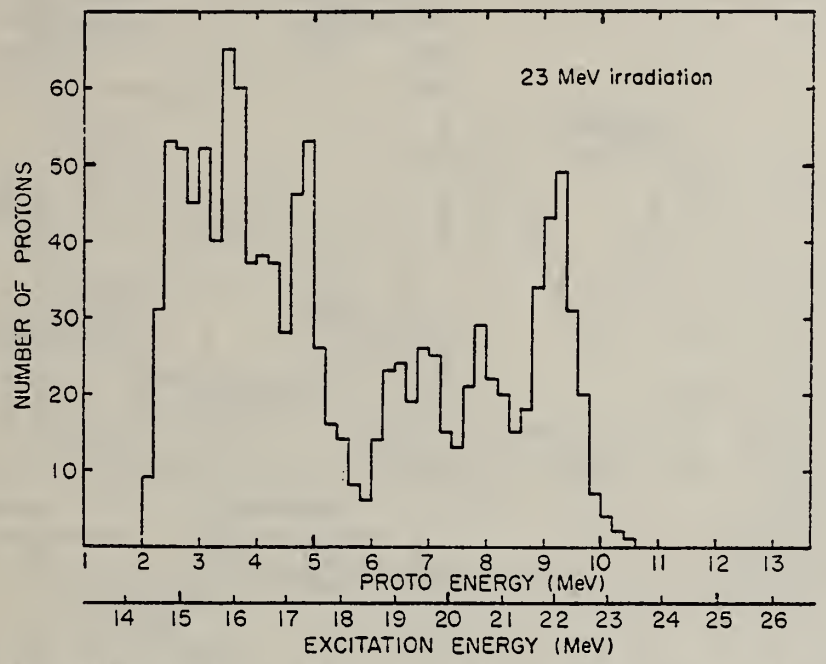

Fig. 2(a). Energy distribution of emitted protons from the $O^{16}(\gamma, p)$ reaction by the 23 MeV irradiation. Excitation energy is calculated assuming the ground state transitions from O^{16} to N^{15}.

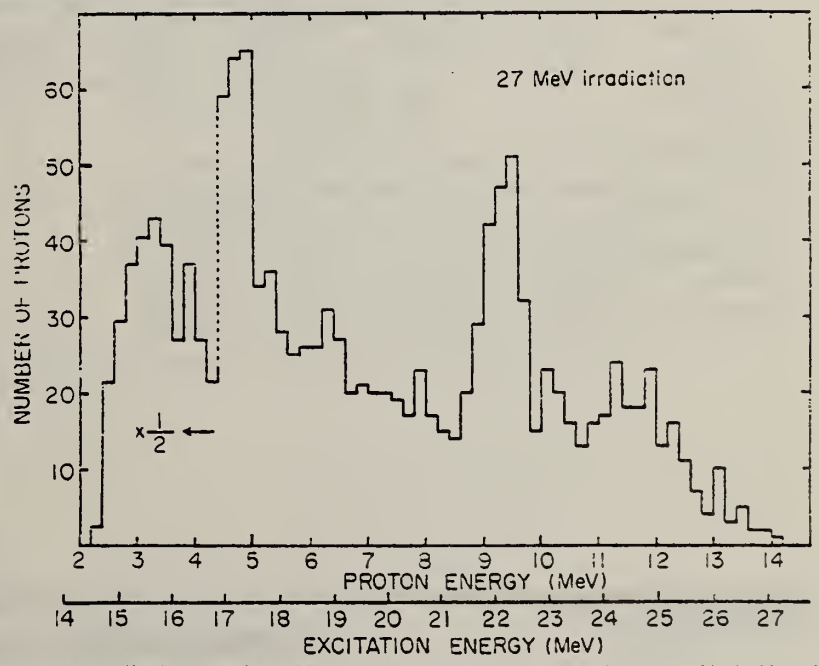

Fig. 2(b). Energy distribution of emitted protons from the $O^{16}(\gamma, p)$ reaction by the 27 MeV irradiation

REACTION	RESULT	EXCITATION ENERGY	SOURCE TYPE	SOURCE RANGE	DETECTOR TYPE	DETECTOR RANGE	ANGLE

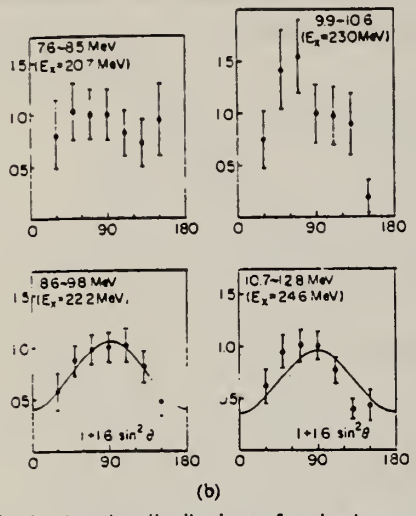

Fig. 4. Angular distributions of emitted protons for each peak appeared in Fig. 3(a); Fig. 4(a) and 4(b) show the angular distributions with the 23 MeV and the 27 MeV irradiations respectively.

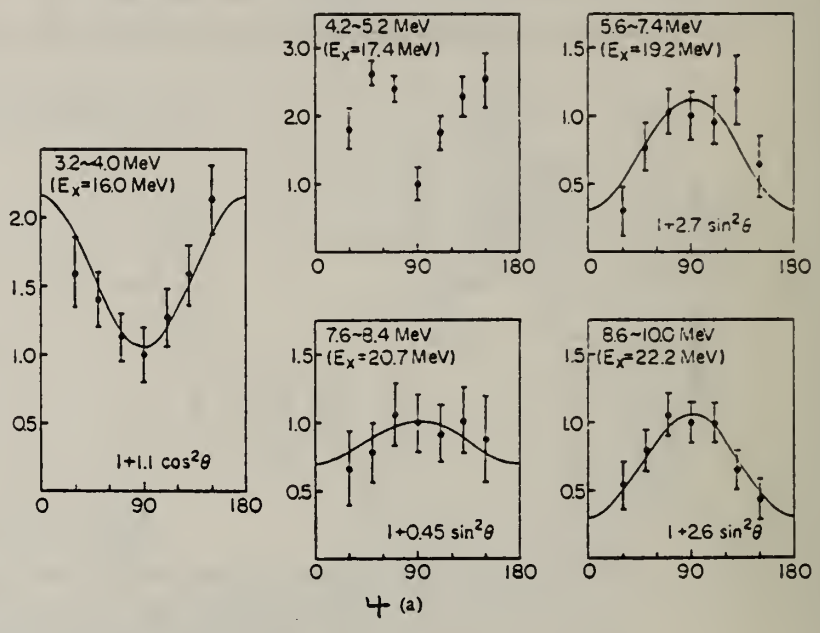

Table I. The branching ratios of the 22.2 MeV and the 24.6 MeV states.

The 22.2 MeV state	Present (γ, p)	Milone[5] (γ, p)	Morrison[18] (γ, p)	Yergin[18] (γ, n)	Caldwell[19] (γ, n)	theory[23] (γ, p)
the ground state	47%	85%	52%	67%	84%	58%
the doublet	2	10	<5	33	<1	0
the third excited state	51	5	43	0	16	42
The 24.6 MeV state						
the ground state	61	41	52	53		30
the doublet	8	12	<5	21		0
the third excited state	31	14	43	26		70

Table II. Fractional strength of the yield of the present experiment and the theory.

Energy (MeV)	present	Brown *et al*[23]
17.4	10%	1%
19.2	10	0
20.8	8	11
22.2	29	37
23.0	11	0
24.6	32	40

REF.

I. Sick, E. B. Hughes, T. W. Donnelly, J. D. Walecka and G. E. Walker
Phys. Rev. Letters 23, 1117 (1969)

ELEM. SYM.	A	Z
O	16	8

METHOD

REF. NO.: 69 Si 2 egf

REACTION	RESULT	EXCITATION ENERGY	SOURCE TYPE	SOURCE RANGE	DETECTOR TYPE	DETECTOR RANGE	ANGLE
E,E/	FMF	10-30	D	100-400	MAG-D	70-400	DST

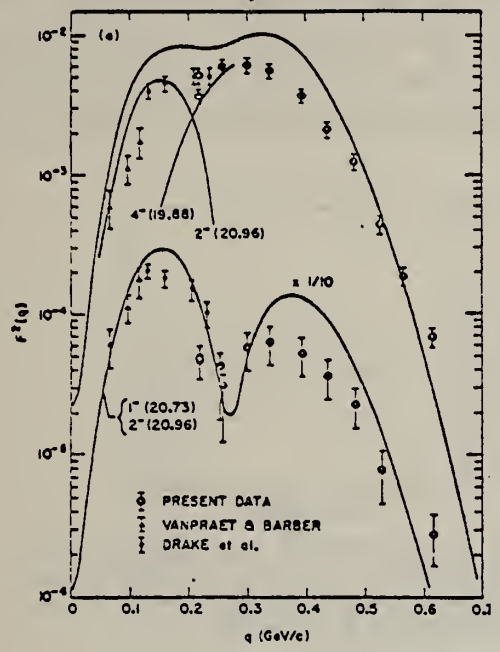

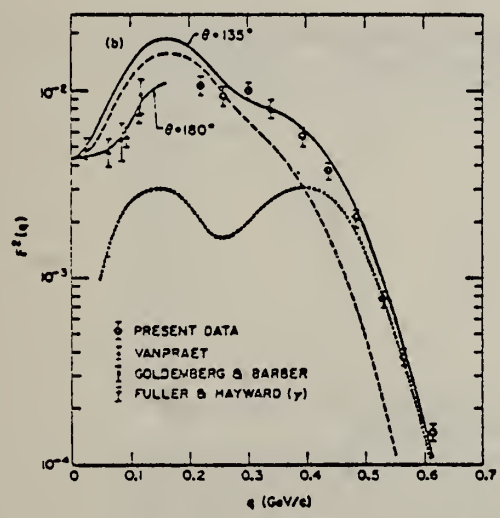

FIG. 3. Form factors as for Fig. 2. (a) 20-MeV region for $\theta = 135°$ (the longitudinal contributions are, in fact, small). Only the lower curve for the 1^- and 2^- states has been reduced in amplitude (by 1.4). The comparison there is for data at about 20.4 MeV. (b) Giant resonance region. The dotted curve is the quasielastic contribution and the dashed curve is the form factor for the discrete levels, both curves for $\theta = 135°$. The solid curves are the total. Data below 120 MeV/c are at $\theta = 180°$; the rest are at 135° except for the point at 219 MeV/c which, having $\theta = 145°$, lies relatively lower.

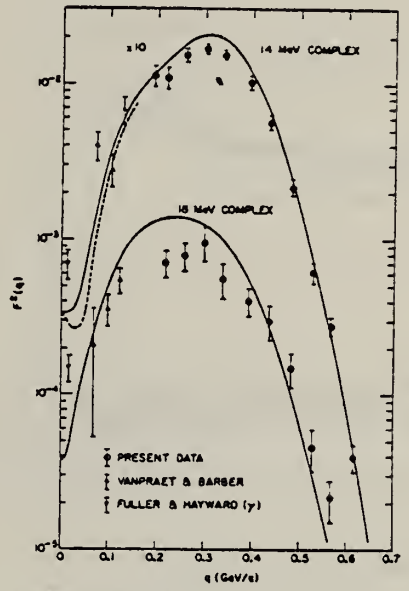

FIG. 2. Form factors

$$F^2(q) = \frac{d\sigma/d\Omega}{[4\pi\sigma_{Mott}(\frac{1}{2} + \tan^2\frac{1}{2}\theta)]}$$

for the 14- and 18-MeV complexes. The solid curves are for $\theta = 135°$, the scattering angle in the present experiment except at 191 and 219 MeV/c where $\theta = 145°$. The dashed curve is for $\theta = 180°$ to compare with the data below 120 MeV/c. Longitudinal contributions are relatively small for both complexes. The calculated curves for the 14-MeV complex have been reduced in amplitude by 1.7, the 18-MeV complex by 1.4.

U.S. DEPARTMENT OF COMMERCE
NATIONAL BUREAU OF STANDARDS

REF.

R. J. J.Stewart, R. C. Morrison, D. E. Frederick
Phys. Rev. Letters 23, 323 (1969)

ELEM. SYM.	A	Z
0	16	8

METHOD

REF. NO. 69 St 1 egf

REACTION	RESULT	EXCITATION ENERGY	SOURCE		DETECTOR		ANGLE
			TYPE	RANGE	TYPE	RANGE	
G,P	ABX	21-33	C	33	SCD-D	10-20	DST

194

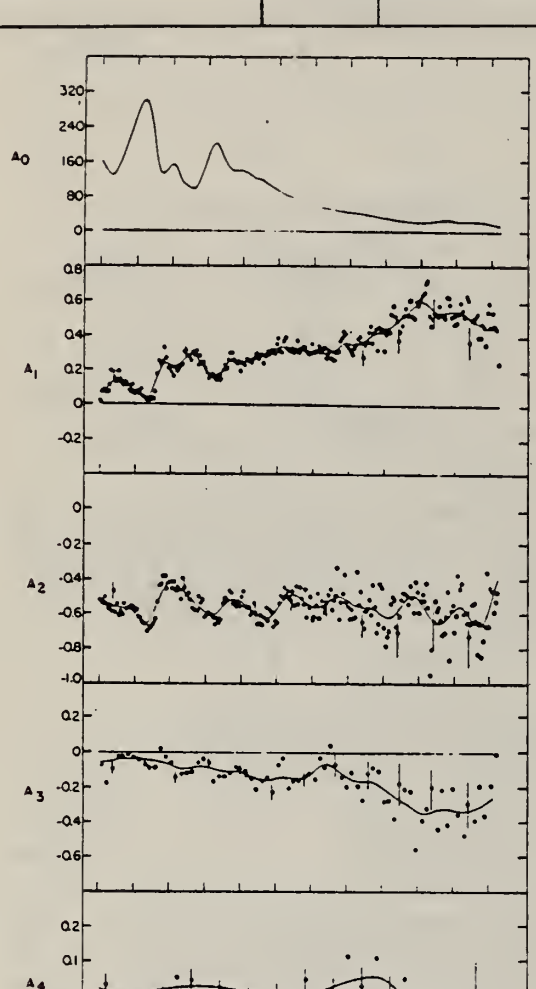

FIG. 1. The angular distribution coefficients A_1 through A_4. The total cross section (A_0) is also shown for comparison. Errors shown are statistical only. The solid lines are least-squares–smoothed fits to the data.

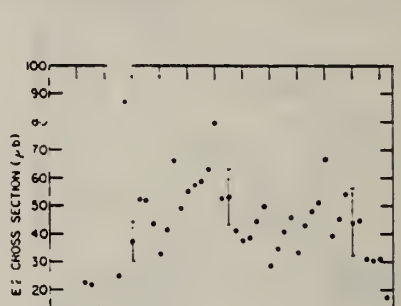

FIG. 2. The ground-state $E2$ cross section extracted from the data using Eq. (4). The errors shown reflect the statistical errors only of A_1 and A_3, with a 10% uncertainty assumed in Eq. (4) for $\sigma(E1)$.

Y. Torizuka, M. Oyamada, K. Nakahara, K. Sugiyama, Y. Kojima,
T. Terasawa, K. Itoh, A. Yamaguchi, M. Kimura
Phys. Rev. Letters 22, 544 (1969)

ELEM. SYM.	A	Z
0	16	8

METHOD

REF. NO.	
69 To 2	egf

REACTION	RESULT	EXCITATION ENERGY	SOURCE		DETECTOR		ANGLE
			TYPE	RANGE	TYPE	RANGE	
E,E/	FMF	7	D	183,250	MAG-D	150-250	DST

7=7.12 MEV

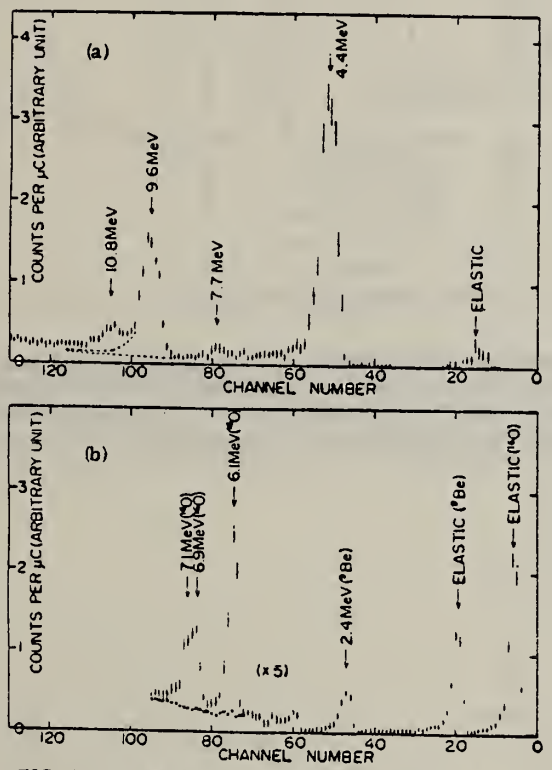

FIG. 1. Energy spectra of scattered electrons. (a) Carbon, $E_0 = 250$ MeV, $\theta = 85°$. The dashed lines are assumed to reproduce the 4.43-MeV peak shape for the 9.63-MeV peak. (b) Beryllium oxide, $E_0 = 183$ MeV, $\theta = 75°$. The crosses indicate the energy spectrum obtained for beryllium target. The 7-MeV peak was decomposed into two components by using shapes of other peaks.

[over]

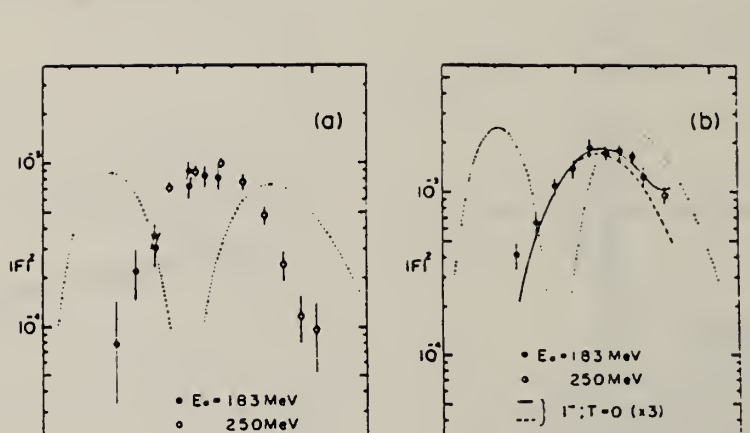

FIG. 2. Experimental and theoretical form factors squared. (a) The 10.8-MeV (1^-; $T = 0$) level of ^{12}C and (b) the 7.12-MeV (1^-; $T = 0$) level of ^{16}O. The dashed and solid curves in (b) are theoretical Coulomb and sum of Coulomb and transverse form factors for $E_0 = 183$ MeV, respectively, which have been calculated by Seaborn and Eisenberg (Ref. 2) in the 1p–1h model. They are multiplied by 3 in the figure. The dotted curves are $E1$ $\Delta T = 1$ form factors calculated using random-phase-approximation wave functions of Gillet and N. Vinh Mau [Nucl. Phys. 54, 321 (1964)].

REF. H. Ullrich and H. Krauth
Nucl. Phys. A123, 641 (1969)

ELEM. SYM.	A	Z
O	16	8

METHOD

REF. NO. 69 U1 1 egf

REACTION	RESULT	EXCITATION ENERGY	SOURCE		DETECTOR		ANGLE
			TYPE	RANGE	TYPE	RANGE	
G,PG	ABY	THR-32	C	32	SCD-D	5-11	120
G,NG	ABY	THR-32	C	32	SCD-D	5-11	120

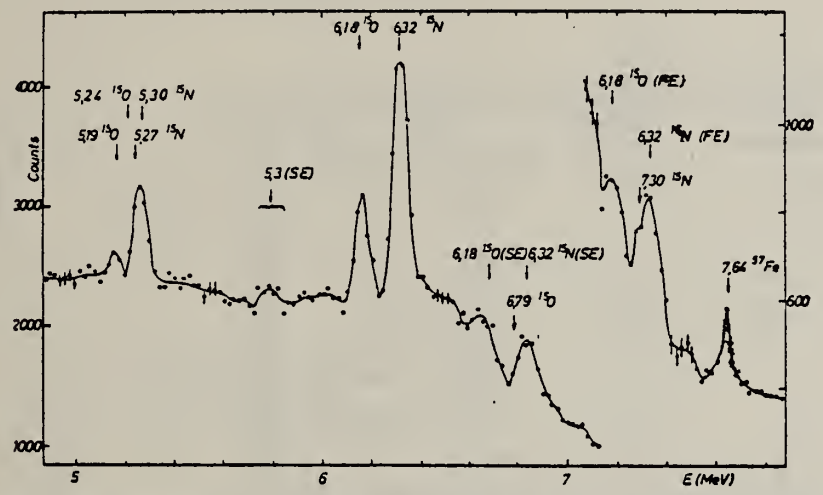

Flg. 1. Spectrum of γ-rays from the oxygen target in the 5-8 MeV range. The positions of some levels in the residual nuclei ^{16}N and ^{15}O, as well as that of the 7.64 MeV level in ^{57}Fe, are marked by arrows. The energy scale corresponds to double-escape peaks. Level positions corresponding to a single-escape peak and to full-energy peaks are labelled by (SE) and (FE), respectively.

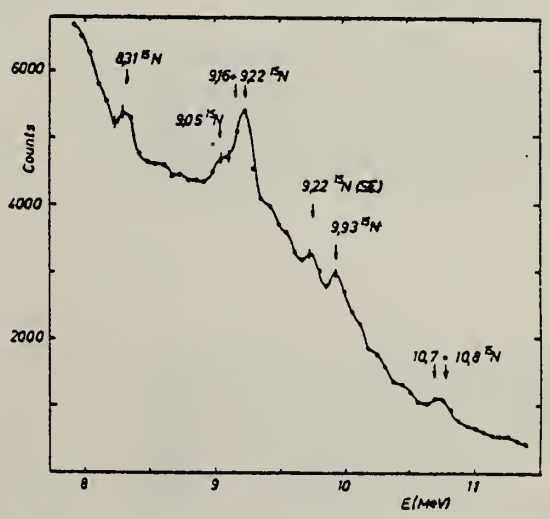

Fig. 2. Spectrum of de-excitation γ-rays from ^{16}N levels near particle threshold.

[over]

TABLE 1

Observed yields from the $^{16}O(\gamma, p\gamma')$ and $^{16}O(\gamma, n\gamma')$ reactions

Final state (MeV)	J^π	One-hole configuration	Parent state in ^{16}O(MeV)	Yield (10^4/mol · R)	Yield (MeV · mb)	Threshold (MeV)
^{15}O : 5.18	$\frac{1}{2}^+$			0.27	1.7	20.9
^{15}N : 5.30						17.4
^{15}O : 5.24	$\frac{3}{2}^+$	$(p_{\frac{1}{2}})^{-1}$	3^- 6.14	1.0 [a]	6 [a]	20.9
^{15}N : 5.28						17.4
^{15}O : 6.18	$\frac{1}{2}^-$	$(p_{\frac{1}{2}})^{-1}$	0^+ 0	1.3	8	21.9
^{15}N : 6.32				3.5 [b]	22 [b]	18.4
^{15}N : 8.31	$\frac{1}{2}^+$			0.05	0.3	20.4
^{15}N : 9.05	$\frac{1}{2}^+$			0.07 [c]	0.45 [c]	21.2
^{15}N : 9.22	$\frac{3}{2}^+$			0.5 [c, d]	3 [c, d]	21.3
^{15}N : 9.93	$\frac{1}{2}^+$			0.11 [c, e]	0.7 [c, e]	22.0
^{15}N : 10.7	$\frac{3}{2}^-$			0.3 [c]	1.9 [c]	22.8
^{15}N : 10.8	$\frac{3}{2}^-$					22.9

[a]) Cascade transitions from the 9.22 MeV level have been subtracted. Contributions from ^{16}O 6.86 MeV, 7.28 MeV, and ^{15}N 7.15 MeV, 7.56 MeV cascade transitions cannot be excluded.

[b]) Reference reaction. Value taken from refs. 1 and 6.

[c]) Error = 50 %.

[d]) Includes possible small contributions from the 9.16 MeV level in ^{15}N.

[e]) Assuming $\Gamma_{1_0}/\Gamma_{\gamma_0} = 3$ [ref. [3])].

REF. J. Ahrens, H. Borchert, K.-H. Czock, D. Mehlig and B. Ziegler
Phys. Letters 31B, 570 (1970)

ELEM. SYM.	A	Z
O	16	8

METHOD

REF. NO.	
70 Ah 1	egf

REACTION	RESULT	EXCITATION ENERGY	SOURCE		DETECTOR		ANGLE
			TYPE	RANGE	TYPE	RANGE	
G,G	ABX	15-80	C	108	NAI-D	5-75	135

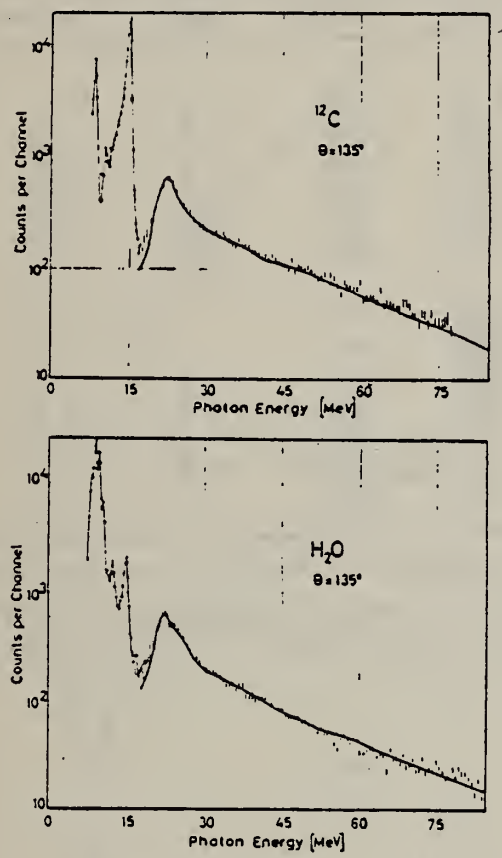

Fig. 1. Pulse height distribution for ^{12}C and ^{16}O. The simultaneously measured neutron background distribution is subtracted. The 15.11 MeV line in the oxygen distribution is the deexcitation of the 15.11 MeV level in ^{12}C, populated by ^{16}O(γ, α)^{12}C [7]. Lines below 10 MeV are γ-transitions in the daughter nuclei following (γ,n) or (γ,p) reactions. The heavy is calculated with the assumptions given in the text and with resonance parameters adjusted to give a good fit to the measured distribution.

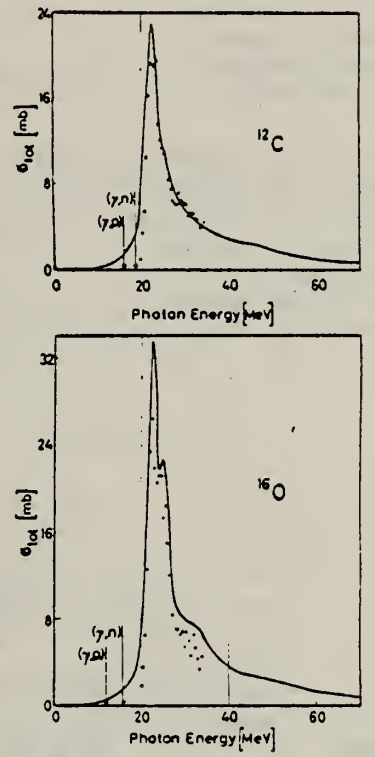

Fig. 2. The full line is the total absorption cross section σ_{tot} calculated from the imaginary part of the scattering amplitude. The points are taken from total absorption measurements [8]. Since particle threshold effects are not built into the scattering amplitude, agreement between the calculated and measured cross section cannot be expected in the threshold regions.

Table 1
Resonance energies (MeV) for the elements investigated.

Carbon	22.5±0.3	25.9±0.4	29.5±0.6	45 ±3
Oxygen	22.5±0.3	25.2±0.3	31.8±0.6	50 ±3
Magnesium	16.8±0.3	19.1±0.3	24.7±0.5	34 ±2
Silicon	17.8±0.3	19.3±0.3	21.2±0.4	28.5±1.0
Calcium	19.6±0.3	24.4±0.5	35 ±2	
Silver	15.3±0.3			

REF. A. R. Barnett and N. W. Tanner
Nucl. Phys. A152, 257 (1970)

ELEM. SYM.	A	Z
O	16	8

METHOD

REF. NO. 70 Ba 1 egf

REACTION	RESULT	EXCITATION ENERGY	SOURCE		DETECTOR		ANGLE
			TYPE	RANGE	TYPE	RANGE	
P,G	ABY	16-24	D	4-13	NAI-D	10-24	90
				(4.1-12.8)			

Data in Table 1 based on isotropic angular distribution and Breit-Wigner single level expression.

[1])N.W. Tanner, G.C. Thomas and E.D. Earle, Nucl. Phys. 52 (1964) 45.

[6])D.H. Wilkinson in Nuclear spectroscopy, part B, ed. F. Ajzenberg-Selove (Academic Press, New York 1966)

TABLE 1

$^{15}N(p,\gamma_0)^{16}O$ and $^{15}N(p,\gamma_1+\gamma_2)^{16}O$ resonances

E_{lab}(MeV)	Γ(keV)	E_x(MeV)	Γ_γ(eV)[a])	$M^2_{E1}\times10^3$
γ_0 resonances				
4.38±0.02	≦ 40	16.23	11 [b])	< 7
5.35±0.02	80	17.14	19	9
5.49±0.02	120	17.27	74	33
7.33±0.03	260	19.00	38	13
7.84±0.03	350	19.48	59	19
9.3 ±0.1	700	20.9	170	42
10.7 ±0.1	700	22.1	870	220
11.50±0.05	350	22.91	120	27
$\gamma_1+\gamma_2$ resonances				
(4.28±0.02)	(≦50)			
(4.38±0.02)	(≦50)			
(5.35±0.02)	(≦50)			
6.32±0.02	≦60	18.05	≦ 5	≦ 6
7.33±0.02	≦40	19.00	≦ 3	≦ 3
7.60±0.03	100	19.25	1.5	1.5
8.30±0.02	75	19.91	8	7
8.83±0.02	150	20.40	47	33
11.3 ±0.1	400	22.7	27	14

[a]) Since for this state there is a better estimate [1]) of $(2J+1)\Gamma_p/\Gamma = 3\times16/22 = 2.09$, we should adjust this value to 8 eV.

[b]) For γ_0 we assume $(2J+1)\Gamma_p/\Gamma = 1.5$; for $\gamma_1+\gamma_2$ we assume $(2J+1)\Gamma_p/\Gamma \approx 2.5$. The E1 Weisskopf unit is [6]) $\Gamma_{E1} = 0.43\,E_\gamma^3$ eV, transition strengths in terms of the M1 unit are given by ref. [6]), $M^2_K = 20\,M^2_{E1}$.

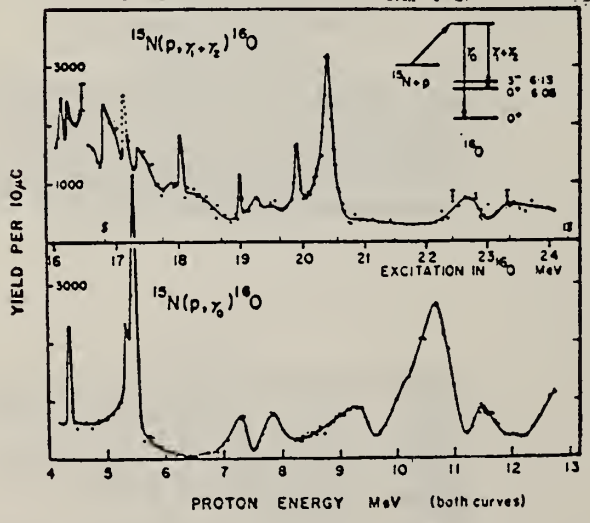

Fig. 2. Yield curves for the (p,γ_0) and $(p,\gamma_1+\gamma_2)$ reactions on ^{15}N taken simultaneously. The upper curve has the same proton energy scale as the lower curve; also indicated is the excitation energy in ^{16}O. The $^{15}N_2$ gas target thickness was ≈ 50 keV and below 9 MeV the yield was measured at < 50 keV intervals; above 9 MeV the intervals were 100 keV. The proton energy is that at the centre of the target and is accurate to ±10 keV. No correction has been made for the relative efficiency change with energy. Note the complete dissimilarity of the two yield curves.

J. C. Bergstrom, W. Bertozzi, S. Kowalski, X. K. Maruyama, J. W. Lightbody, Jr., S. P. Fivozinsky, and S. Penner
Phys. Rev. Letters 24, 152 (1970)

ELEM. SYM.	A	Z
O	16	8

METHOD

REF. NO. 70 Be 1 hmg

REACTION	RESULT	EXCITATION ENERGY	SOURCE TYPE	SOURCE RANGE	DETECTOR TYPE	DETECTOR RANGE	ANGLE
E,E/	FMF	6-8	D	51-105	MAG-D		DST
		(6.05-7.12)					(110,145)

6.05,6.13,6.91,7.12

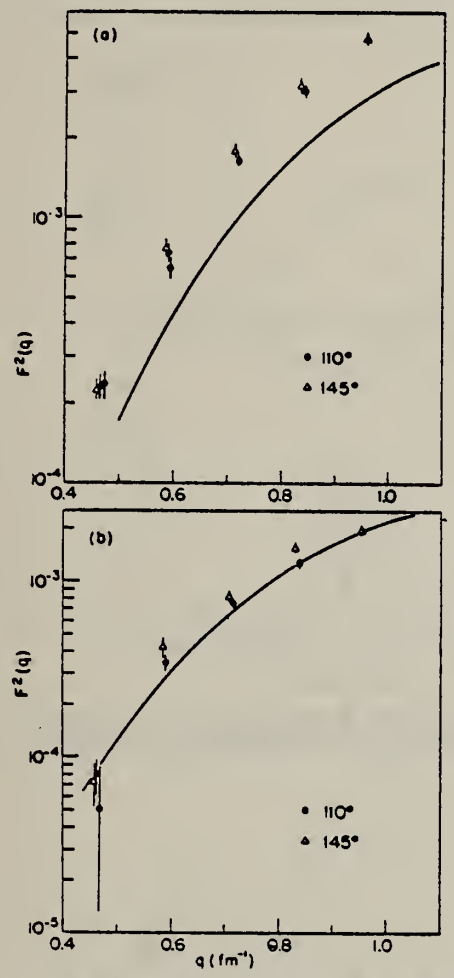

FIG. 2. (a) Form factor for the 3^- (6.131-MeV) state in O^{16}. The solid line is the form factor of Gillet and Melkanoff (Ref. 4). (b) Form factor for the 1^- (7.115-MeV) state. The solid line represents a simple shell-model form factor, multiplied by 3.6 (see text).

[4]V. Gillet and M. A. Melkanoff, Phys. Rev. 133, V1190 (1964).

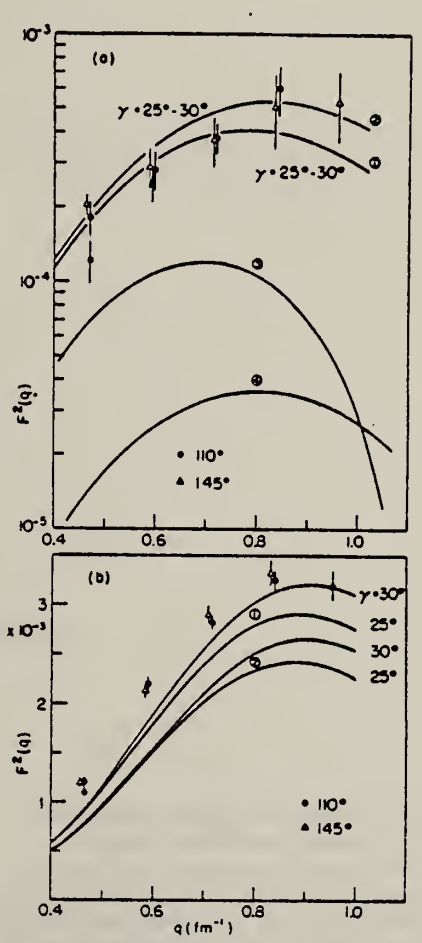

FIG. 3. (a) Form factor for the 0^+ (6.052-MeV) state. Curves 3 and 4 are the predictions of E. Boeker, Phys. Letters 24B, 616 (1967), using a deformed and spherical basis, respectively. Curves 1 and 2 are the predictions of the two-component model (see text) in which the 2^+ (6.916-MeV) ground-state radiative width was taken as 0.096 and 0.080 eV, respectively. (b) Form factor for the 2^+ (6.916-MeV) state. The solid curves are the predictions of the two-component model, as in (a).

REF. P. Filss, W. Collin, S. Guldbakke, K. Kayser, H. Reich, J.O. Trier, W. Witschel
Z. Physik 239, 461 (1970)

ELEM. SYM.	A	Z
O	16	8

METHOD

REF. NO. 70 Fi 1 egf

REACTION	RESULT	EXCITATION ENERGY	SOURCE		DETECTOR		ANGLE
			TYPE	RANGE	TYPE	RANGE	
G,N	ABX	16-34	C	15-120	ACT-I		4PI
G,2N	ABX	30-115	C	30-120	ACT-I		4PI

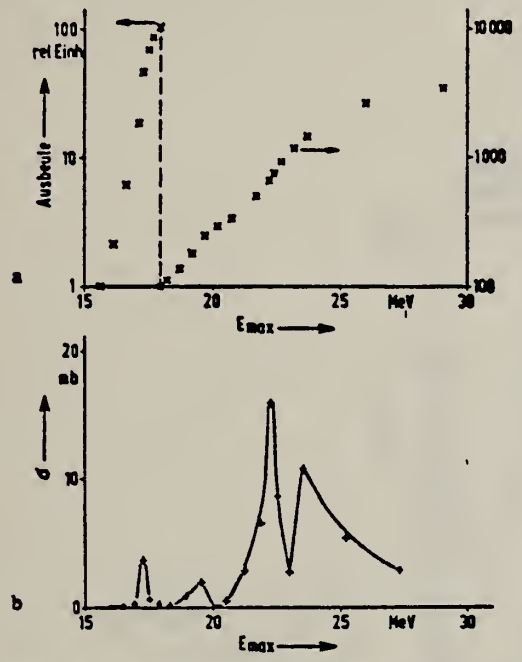

Fig. 1. a Verlauf der Ausbeutefunktion für die Reaktion $^{16}O(\gamma, n)^{15}O$. b Durch Entfaltung mit dem Schiffspektrum gewonnener Wirkungsquerschnitt

Photonuclear Reactions in Oxygen and their Use for the Control of Energy and Photon Spectrum at Electron Accelerators

The yields of the photonuclear reactions $^{16}O(\gamma, n)$ and $^{16}O(\gamma, 2n)$ are measured with a newly constructed device for fluid samples. The well known structures of the (γ, n) cross section are used for the energy calibration of our accelerator. Though the yield should be strongly dependent on small changes of the bremsspectrum no difference was found, using a thin or a thick target. The conclusion is, that also the thick target is in its effect a thin target under the accelerator conditions. The $(\gamma, 2n)$ cross section is measured for the first time between threshold and 120 MeV. It is unusually small compared to the (γ, n) cross section.

[over]

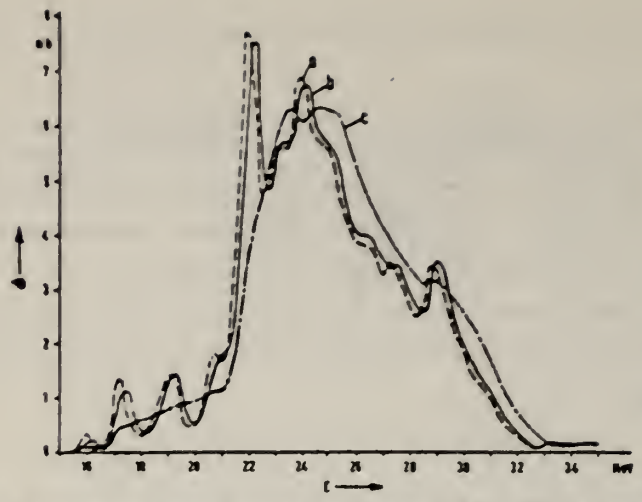

Fig. 2. Wirkungsquerschnitts-Spektrum der Reaktion $^{16}O(\gamma, n)^{15}O$. *a* Experimentelles Spektrum nach Bramblett u. a.[10]; *b* mit dem Schiffspektrum entfalteter Wirkungsquerschnitt aus einer Ausbeutekurve, die sich bei einer 0,3 MeV dicken Antikathode ergeben würde; *c* desgl., jedoch aus einer Ausbeutekurve, die sich bei einer 1,5 MeV dicken Antikathode ergeben würde

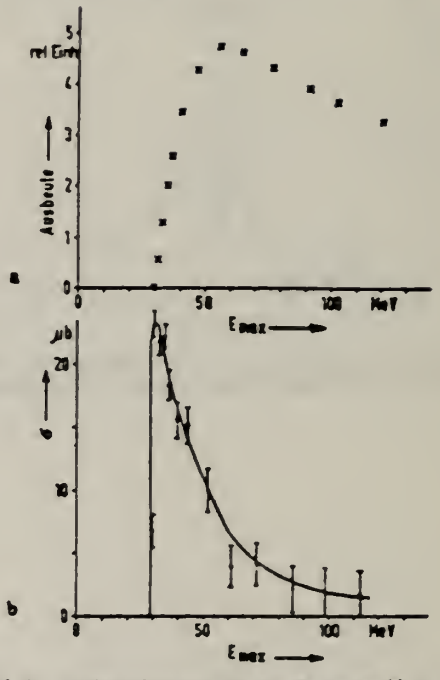

Fig. 3. a Verlauf der Ausbeutefunktion für die Reaktion $^{16}O(\gamma, 2n)^{14}O$. b Durch Entfaltung mit dem Schiffspektrum gewonnener Wirkungsquerschnitt

A. Goldmann and M. Stroetzel
Phys. Letters 31B, 287 (1970)

ELEM. SYM.	A	Z
0	16	8

METHOD

REF. NO.	
70 Go 1	egf

REACTION	RESULT	EXCITATION ENERGY	SOURCE		DETECTOR		ANGLE
			TYPE	RANGE	TYPE	RANGE	
E,E/	LFT	19,20	D	46,54	MAG-D	26-54	DST

Γ_γ(19.04) 1.5 ± 0.3 eV $J^\pi = 2^-$ 19.04, 20.36 MEV

Γ_γ(20.36) 2.9 ± 1.0 eV $= 2^-$

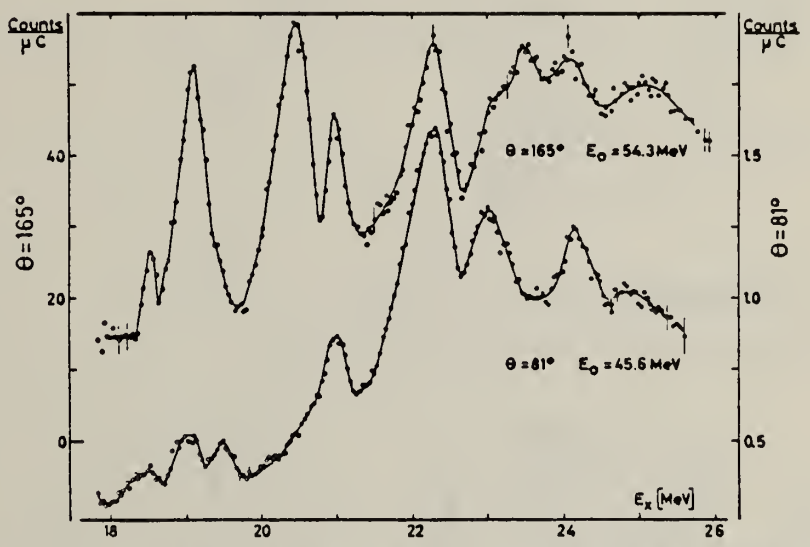

Fig. 1. Spectra of electrons scattered inelastically from ^{16}O at primary energy 45.6 MeV, scattering angle 81° (lower part) and 54.3 MeV, 165° (upper part), after subtraction of the elastic radiation tail; E_x = excitation energy. The energy resolution at 20 MeV is about 125 keV (lower spectrum) and 150 keV (upper spectrum).

REF. A. Goldmann and M. Stroetzel
Z. Physik 239, 235 (1970)

ELEM. SYM.	A	Z
O	16	8

METHOD

REF. NO. 70 Go 4 egf

REACTION	RESULT	EXCITATION ENERGY	SOURCE		DETECTOR		ANGLE
			TYPE	RANGE	TYPE	RANGE	
E,E/	FMF	21-26	D	43-58	MAG-D		DST

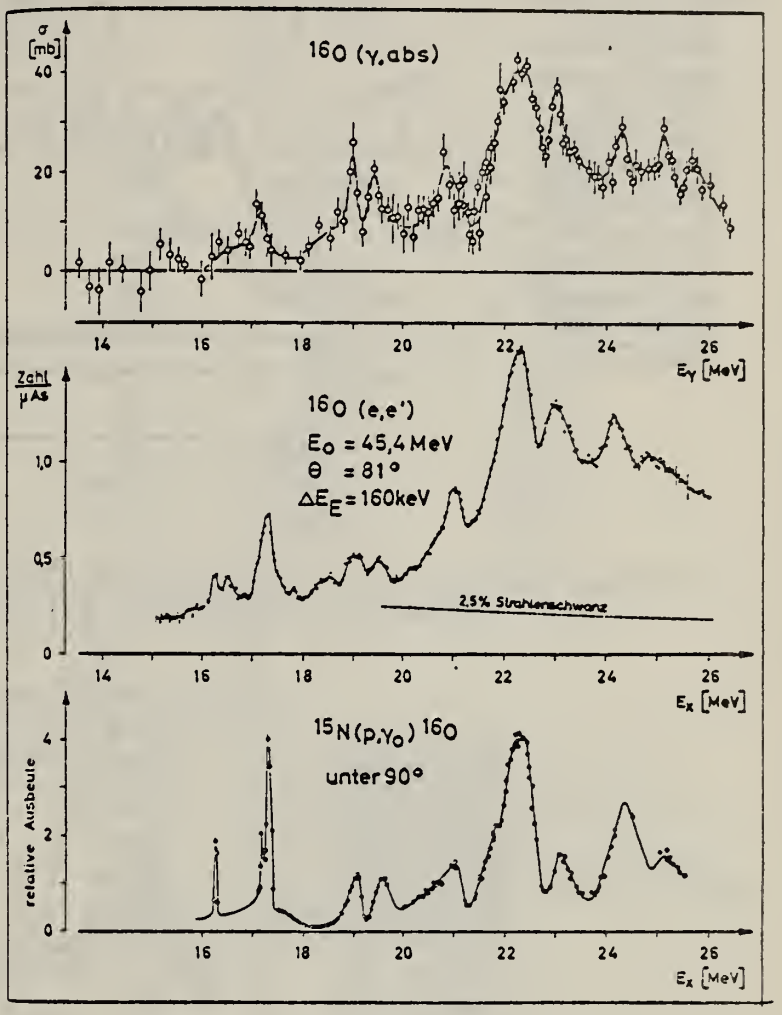

Fig. 2. Riesenresonanz von ^{16}O. Oben: Absorptionswirkungsquerschnitt nach Dolbilkin et al.[22]. Unten: (p, γ_0)-Spektrum nach Earle und Tanner[23]. Mitte: Spektrum unelastisch gestreuter Elektronen. Der berechnete Strahlenschwanz und die Untergrundbeiträge wurden subtrahiert. Die gestrichelte Linie gibt die Änderung der Nullinie bei einer willkürlichen Änderung des Strahlungsschwanzes um +2,5% an. E_x und E_γ sind Anregungs- bzw. Photonenenergien

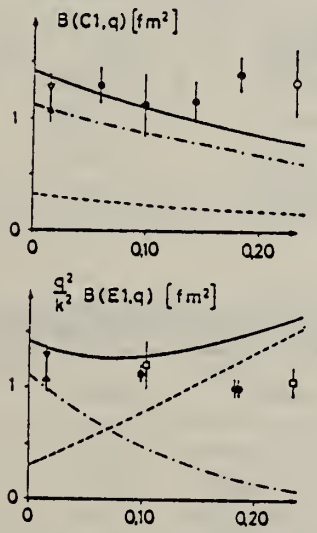

Fig. 5. Longitudinale und transversale reduzierte Übergangsmatrixelemente in Abhängigkeit vom Quadrat des Impulsübertrags für den Bereich der Riesenresonanz zwischen 21,4 und 26,0 MeV. Volle Kreise (•): diese Arbeit. Die anderen Werte wurden bestimmt aus [5] (o) und [6] (o), sowie [22] (•) und [31] (▲). Kurven: Rechnung nach [38–40] für zwei $1^-(T=1)$-Zustände bei $E_x = 23{,}26$ MeV (— · — · —), $E_x = 26{,}13$ MeV (- - - - - -) und Summe (———). Longitudinales Matrixelement mit Faktor 0,30 angepaßt, s. Text

(over)

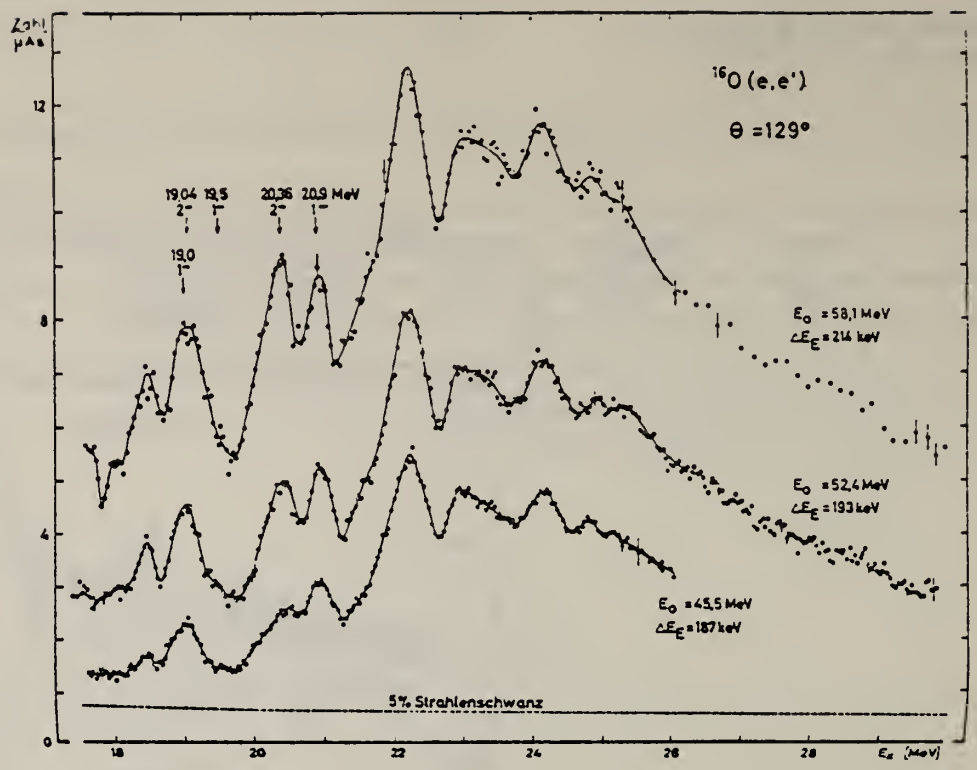

Fig. 3. Spektren der unter 129° gestreuten Elektronen im Bereich der ^{16}O-Riesenresonanz. Der berechnete Strahlungsschwanz und die Untergrundbeiträge wurden subtrahiert. Die gestrichelte Linie gibt die Änderung der Nullinie bei einer willkürlichen Änderung des Strahlungsschwanzes um +5% an. Alle Spektren sind auf gleiche elastische Fläche $A_E = 3{,}86 \cdot 10^3$ MeV/μAs normiert

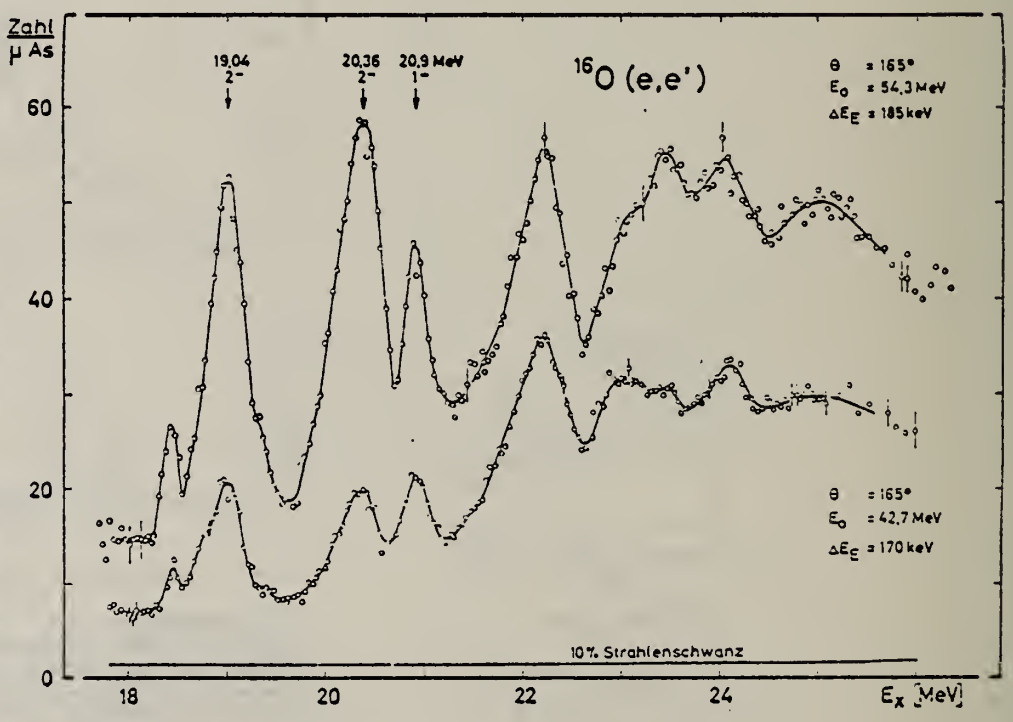

Fig. 4. Spektren der unter 165° gestreuten Elektronen. Der berechnete Strahlungsschwanz und die Untergrundbeiträge wurden subtrahiert. Die gestrichelte Linie gibt die Änderung der Nullinie bei einer willkürlichen Änderung des Strahlungsschwanzes um +10% an. Die Spektren sind auf gleiche elastische Fläche $A_E = 3{,}86 \cdot 10^3$ MeV/μAs normiert

REF. Y. S. Horowitz, D. B. McConnell, J. Ssengabi, N. Keller
Nucl. Phys. A151, 161 (1970)

ELEM. SYM.	A	Z
O	16	8

METHOD

REF. NO. 70 Ho 1 egf

REACTION	RESULT	EXCITATION ENERGY	SOURCE		DETECTOR		ANGLE
			TYPE	RANGE	TYPE	RANGE	
G,PG	RLY	17-27	C	27,36	SCD-D	2-9	DST
G,NG	RLY	21-27	C	27,36	SCD-D	2-9	DST

$$\frac{d\sigma}{d\Omega} = \sum a_i P_i(\cos\Theta)$$

TABLE 1
Relative intensities of γ-ray transitions observed at $E_\gamma = 36$ MeV

Nucleus	γ-ray transition (MeV)	Relative intensities (arbitrary units)
^{15}N	5.27–0	20 ±2.6
^{15}N	5.30–0	8.0±1.5
^{15}N	6.32–0	100 ±2.8
^{15}N, ^{15}O	7.30–0	[a]
	6.79–0	
^{15}N	8.31–0	2.0±0.4 [b]
^{15}N	9.06–0	1.9±0.5
^{15}N	9.22–0	3.6±0.5
^{15}N	3.92–0	13 ±2.4
^{15}O	5.19–0	8.0±1.2
^{15}O	5.24–0	9.9±1.4
^{15}O	6.18–0	39 ±1.3
^{15}O	6.86–0	7.8±2.7

[a]) The 7.30 MeV SE peak is impossible to resolve from the 6.79 MeV full-energy peak.
[b]) Assuming no contribution from the 7.30 MeV full-energy peak.

TABLE 2
Comparison of present measurement with the 90° cross-section data of Caldwell *et al.* [18])

Nucleus	Transition	$G\int_{th}^{27.0\ \mathrm{MeV}} \frac{d\phi(E_\gamma)}{dE_\gamma}\left.\frac{d\sigma}{d\Omega}\right\|_{90^\circ} dE_\gamma$	Present measurement
		no. of events	no. of events
^{15}N	6.323–0	1870±390	2640±550
^{15}N	5.270–0 [a]) 5.299–0	590±160	945±155
^{15}O	6.180–0	425± 90	385±105

[a]) These transitions were not resolved in the monochromatic photon experiment.

8) J.T. Caldwell, S.C. Fultz and R.L. Bramblett, Phys. Rev. Lett. 19 (1967) 447.
18) E.K. Warburton, J.W. Olness and D.E. Alburger, Phys. Rev. 140 (1965) B1202.

TABLE 3
Angular distributions and deduced total cross-sections of de-excitation γ-rays in ^{15}O and ^{15}N [a])

Nucleus	Transition	a_2/a_0	$\frac{2\pi\int_0^\pi \sigma(\theta)\sin\theta\, d\theta}{4\pi\bar{\sigma}_c(90^\circ)}$
^{15}N	5.299–g.s.($\frac{1}{2}^+ \to \frac{1}{2}^-$)	−0.19±0.19	1
^{15}N	5.270–g.s.($\frac{3}{2}^+ \to \frac{1}{2}^-$)	0.47±0.21	$1.27^{+0.27}_{-0.16}$
^{15}N	6.323–g.s.($\frac{3}{2}^- \to \frac{1}{2}^-$)	0.67±0.27	$1.52^{+0.32}_{-0.22}$
^{15}O	6.180–g.s.($\frac{3}{2}^- \to \frac{1}{2}^-$)	0.63±0.33	$1.58^{+0.50}_{-0.35}$

[a]) $\bar{\sigma}_c(90^\circ)$ is the cross section of Caldwell *et al.* [8]), averaged over the energy region as indicated in fig. 8.

[over]

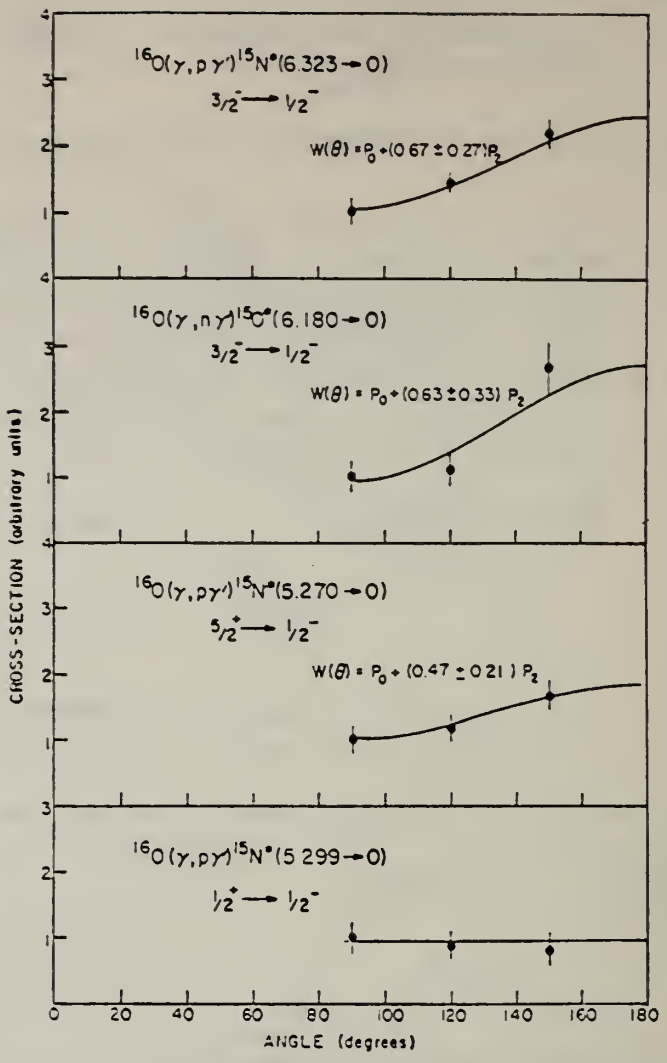

Fig. 7. Angular distributions for the $^{16}O(\gamma,_{p}{}^{n}\gamma')^{15}O^*,{}^{15}N^*$, reactions. The angular distribution for the 5.299 MeV ($\frac{1}{2}^+\rightarrow\frac{1}{2}^-$; ΔI 0) transition is isotropic and serves as an additional confirmation of the calibration procedures. The best fit to the angular distributions are indicated by the solid lines.

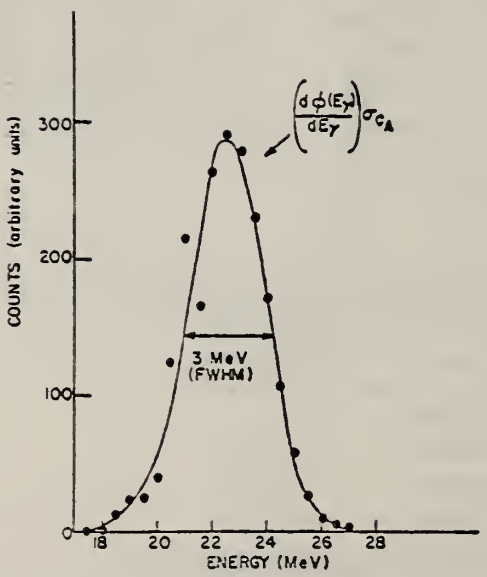

Fig. 8. 90° yield curve given by $(d\acute{o}(E_\gamma)/dE_\gamma)\sigma_{CA}$ (E_γ) illustrating the energy region of greatest applicability of the present angular distribution measurements. Here, σ_{CA} is the cross section from the data of Caldwell *et al.* [8]).

REF. B.S. Ishkhanov, I.M. Kapitonov, E.V. Lazutin, I.M. Piskarev, V.S. Sopov, V.G. Shevchenko
Yad. Fiz. 12, 892 (1970)
Sov. J. Nucl. Phys. 12, 484 (1971)

ELEM. SYM.	A	Z
O	16	8

METHOD

REF. NO. 70 Is 5 hmg

REACTION	RESULT	EXCITATION ENERGY	SOURCE TYPE	SOURCE RANGE	DETECTOR TYPE	DETECTOR RANGE	ANGLE
G,XN	ABX	16-25	C	16-25	BF3-I		4PI

341

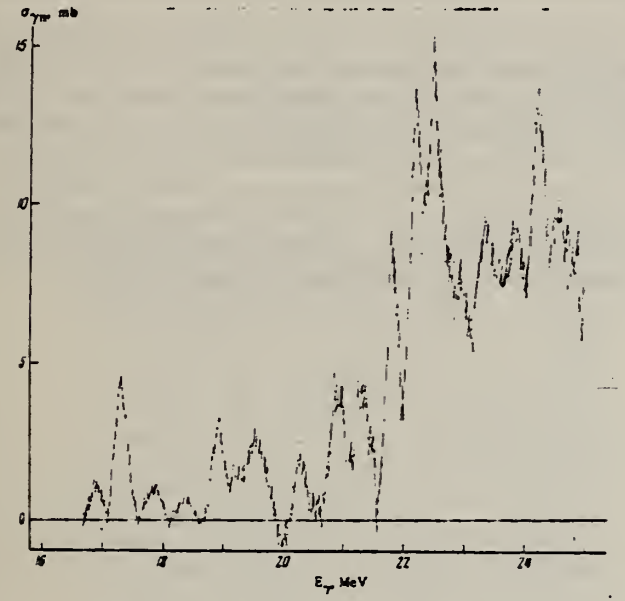

FIG. 1. Cross section of the reaction $O^{16}(\gamma, n)O^{15}$.

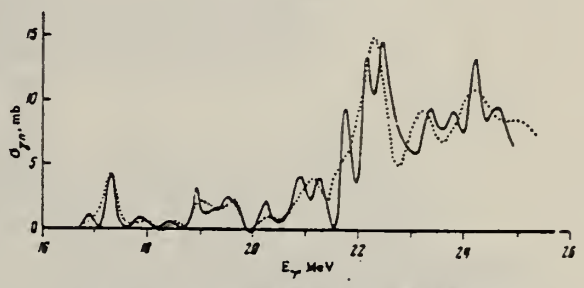

FIG. 2. Comparison of the cross sections of the reaction $O^{16}(\gamma, n)O^{15}$, obtained in the present work (solid curve) and in [2] (dotted).

[2] B.C. Cook, J.E.E. Baglin, J.N. Bradford, and J.E. Griffin, Phys. Rev. 143, 712 (66).

Table I. Energies of the maxima (in MeV) observed in different photo-nuclear reactions on the O^{16} nucleus in the region of the giant dipole resonance

$\sigma(\gamma, n)$ [1]	$\sigma(\gamma, n)$ [2]	Photoneutron spectrum [3]	$\sigma(\gamma, p)$ [2]	Photoproton spectrum [3]	$\sigma(\gamma, a)$ [2]	Total absorption cross section [4]	Present data: Position of resonances, MeV	Present data: Integral cross sections of resonances, MeV·mb	Present data: Relative contribution to the integral cross section of the (γ, n) reaction up to 25 MeV
		17.1			17.13		16.89	0.23	0.007
17.1	17.3	17.25	17.2	17.3	17.29	17.2	17.29	1.00	0.031
				18.1			17.85	0.25	0.008
							18.37	0.16	0.005
19.0	19.06	19.0		19.0	19.05	19.0	18.92	0.64	0.020
							19.25	0.40	0.012
19.3	19.56	19.4		19.6	19.56	19.4	19.52	0.91	0.028
	20.2	20.1					20.25	0.44	0.014
20.8	21.0	20.9	20.9	20.6	21.0	20.9	20.89	1.13	0.035
							21.27	1.32	0.041
21.8	21.7						21.75	2.01	0.065
22.1	22.26	22.3	22.4	22.3	22.2	22.3	22.17	3.57	0.111
							22.46	3.92	0.122
							22.90	2.24	0.070
23.1	23.15	23.1		23.1	23.0	23.1	23.33	3.36	0.105
							23.83	3.04	0.095
24.0	24.1	24.3	24.2	24.3	24.3	24.3	24.21	4.76	0.148
							24.56	2.56	0.083
25.0	24.9	25.0			25.2	25.2			
								32,12	

REF. R. J. Jaszczak, J. H. Gibbons, and R. L. Macklin
Phys. Rev. C2, 63 (1970)

ELEM. SYM.	A	Z
O	16	8

METHOD

REF. NO. 70 Ja 1 hmg

REACTION	RESULT	EXCITATION ENERGY	SOURCE TYPE	SOURCE RANGE	DETECTOR TYPE	DETECTOR RANGE	ANGLE
A,G	ABX	9-11	D	1-4 (1.86-3.11)	NAI-D		84

The $^{12}C(\alpha,\gamma)^{16}O$ capture cross section was measured for α-particle energies between 1.86 MeV ($\sigma = 1.1 \pm 0.4$ nb) and 3.11 MeV ($\sigma = 29 \pm 4$ nb) using a pulsed $^4He^+$ beam from the ORNL 6-MV Van de Graaff accelerator and a 23- by 30-cm NaI(Tl) crystal viewed by six matched, bialkali photomultiplier tubes. An upper limit was obtained for the capture cross section at $E_\alpha = 1.6$ MeV. The over-all time resolution (full width at half maximum) of the system for 8–10-MeV pulses due to γ rays is 2.7 nsec. Enriched (99.94%) ^{12}C targets ranging in thickness from 98 to 178 $\mu g/cm^2$ were used. Pulses resulting from fast neutrons [from the $^{13}C(\alpha,n)^{16}O$ reaction] interacting with the NaI(Tl) crystal were further separated from true γ pulses through the use of a new technique based on rise-time distribution differences of the respective neutron- and γ-ray-produced pulses. The face of the crystal (shielded with a 10.2 cm thickness of ^6LiH) was 12.2 cm from the target. The astrophysical significance of this reaction in the helium-burning sequence of stellar nucleosynthesis is also discussed.

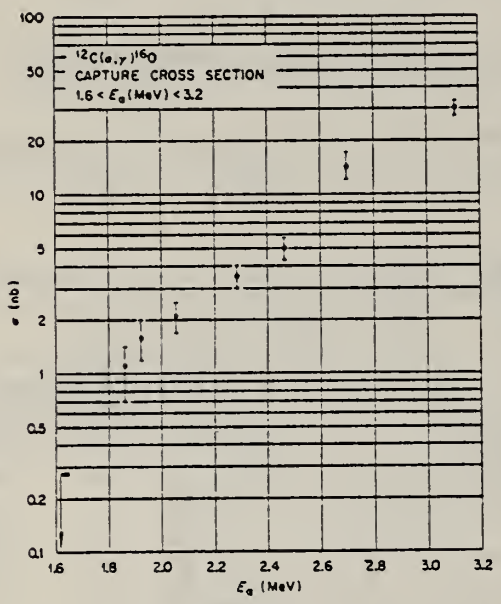

FIG. 9. The $^{12}C(\alpha,\gamma)^{16}O$ capture cross section measured in the present experiment. The errors include the effects due to target-thickness uncertainty, detector-efficiency uncertainty, current integration, statistics, and background subtraction. Refer to text for comparison of data with previous results.

REF. R. J. Jaszczak and R. L. Macklin
Phys. Rev. C2, 2452 (1970)

ELEM. SYM.	A	Z
O	16	8

METHOD

REF. NO. 70 Ja 2 hmg

REACTION	RESULT	EXCITATION ENERGY	SOURCE TYPE	SOURCE RANGE	DETECTOR TYPE	DETECTOR RANGE	ANGLE
A,G	ABX	8-11	D	1-5	NAI-D		
				(1.6 - 4.1)			

The possibility of 1^- states above the 9.58- and 7.12-MeV states in ^{16}O interfering with these lower states would strongly affect the $^{12}C(\alpha,\gamma)^{16}O$ capture cross sections near $E_\alpha = 3.2$ MeV and the inferred stellar-reaction rate. Cross sections below 3.2 MeV reported earlier have been extended to 4.1 MeV using similar techniques and overlap the previous measurement from ~2.9 to ~3.2 MeV.

In an earlier paper[1] the $^{12}C(\alpha,\gamma)^{16}O$ capture cross section below $E_\alpha = 3.2$ MeV was reported. A recent report[2] indicates that the rate of the $^{12}C(\alpha,\gamma)^{16}O$ reaction at stellar energies may be predicted with a precision that is limited only by the precision of the experimental data obtained at higher energies. This analysis is now in the stage of preparation for publication.[3] The cross section above the 3.2-MeV resonance is strongly affected through interferences with the tail from the region of the giant dipole resonance in ^{16}O.[4] Thus, further measurements of the $^{12}C(\alpha,\gamma)^{16}O$ capture cross sections were made at Oak Ridge National Laboratory (ORNL) for α-particle energies extending to 4.08 MeV using the terminally pulsed ^4He beam from the ORNL 5.5-MV Van de Graaff accelerator. The experimental methods (time-of-flight techniques, etc.) used have been described in detail earlier.[1] The results of these measurements are shown in Fig. 1. These values again consider only the ground-state transition γ ray and do not include any contribution from cascade γ rays, although ~7-MeV γ rays are observed in the pulse-height (time and energy) spectra. The α-particle energies reported are those at the center of the target. Data were taken such that resonances other than the tails of the 1^- levels did not contribute significantly to the γ-ray yield at the datum points shown. Particularly, the datum point at $E_\alpha = 3.39$ MeV was below the narrow resonance at $E_\alpha = 3.58$ MeV (the 2^+ 9.85-MeV state in ^{16}O with $\Gamma_{c.m.} = 0.75$ keV), while the datum point at 3.80 MeV was above this resonance. Furthermore, the angular distribution of the 2^+ ground-state radiation is a minimum at 90°.

The measurement at 4.08 MeV may contain a contribution to the yield from the resonance at $E_\alpha = 4.26$ MeV (the 4^+ level in ^{16}O at 10.36 MeV with $\Gamma_{c.m.} = 27$ keV), although the ground-state transition rate should be small compared with the rate of the 2^+ state.

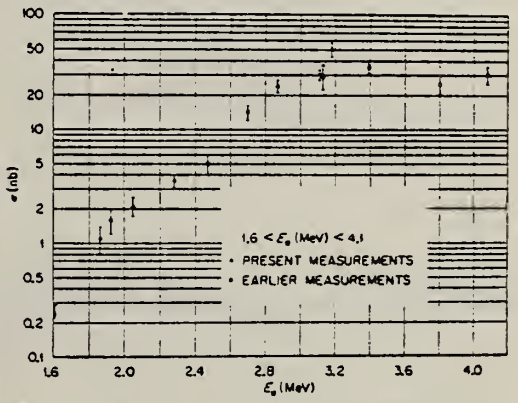

FIG. 1. The $^{12}C(\alpha,\gamma)^{16}O$ capture cross section below 4.1 MeV. This figure assumes a 1^- distribution of γ radiation and includes only the ground-state transition. The earlier data were taken from Ref. 1.

REF. J. W. Jury, J. S. Hewitt, and K. G. McNeill
Can. J. Phys. 48, 1635 (1970)

ELEM. SYM.	A	Z
O	16	8

METHOD

REF. NO. 70 Ju 1 egf

REACTION	RESULT	EXCITATION ENERGY	SOURCE TYPE	SOURCE RANGE	DETECTOR TYPE	DETECTOR RANGE	ANGLE
G,N	ABX	17-30	C	23-30	TOF-D		DST

1046

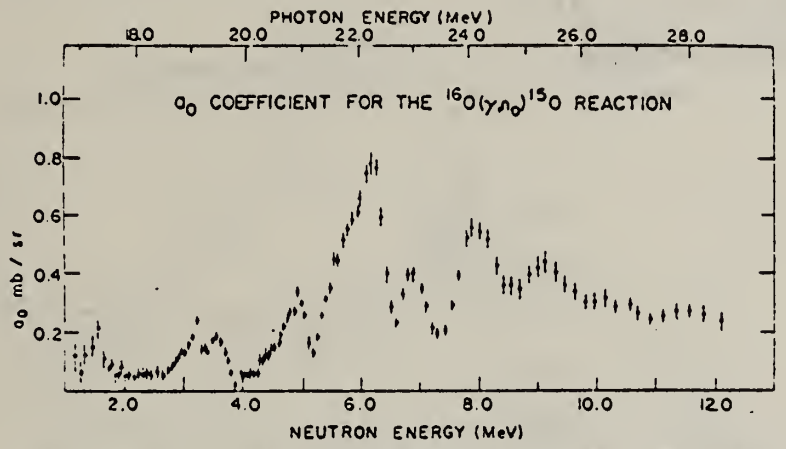

FIG. 6. The energy dependence of the a_0 Legendre coefficient for ground state photoneutron emission. The data are a combination of the results obtained with each of the 3 different bremsstrahlung end-point energies used. Energies given are in the center-of-mass system.

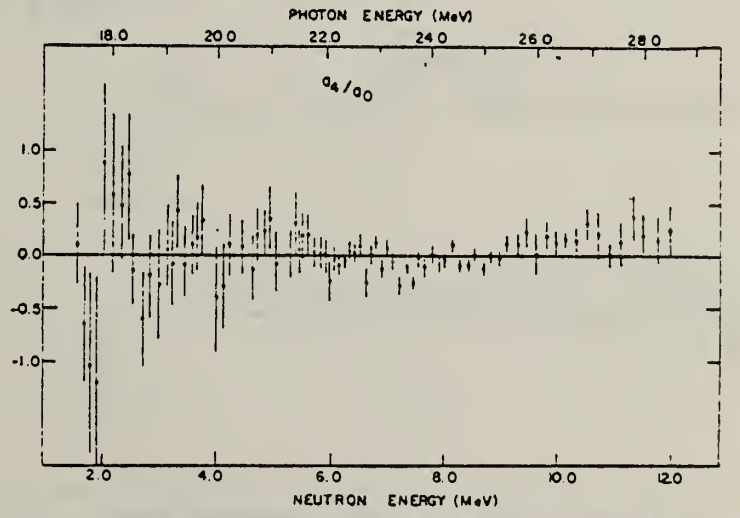

FIG. 8. The energy dependence of the normalized Legendre polynomial coefficient a_4/a_0. Energies are given i: the center-of-mass system.

[over]

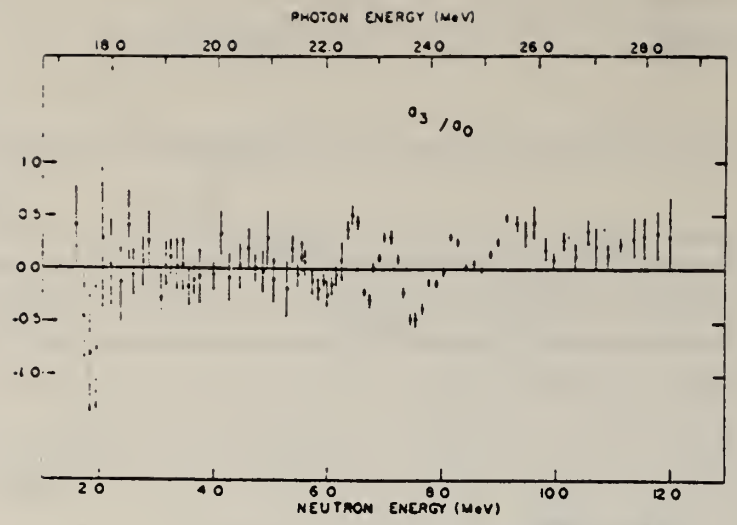

FIG. 9. The energy dependence of the normalized coefficient a_3/a_0.

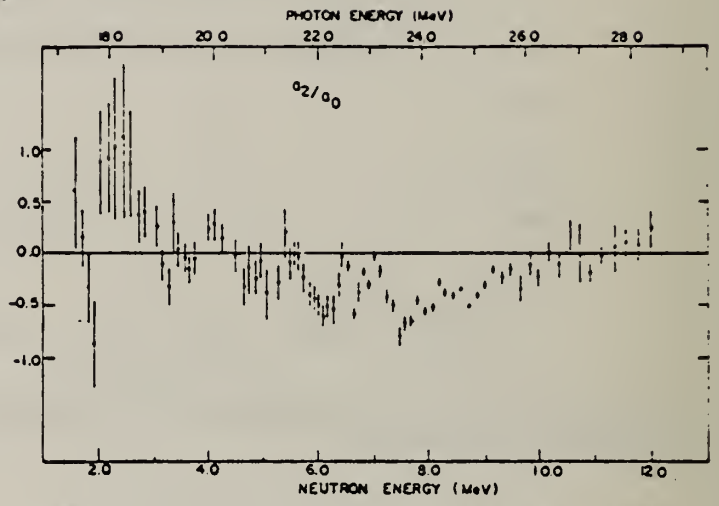

FIG. 10. The energy dependence of the normalized coefficient a_2/a_0.

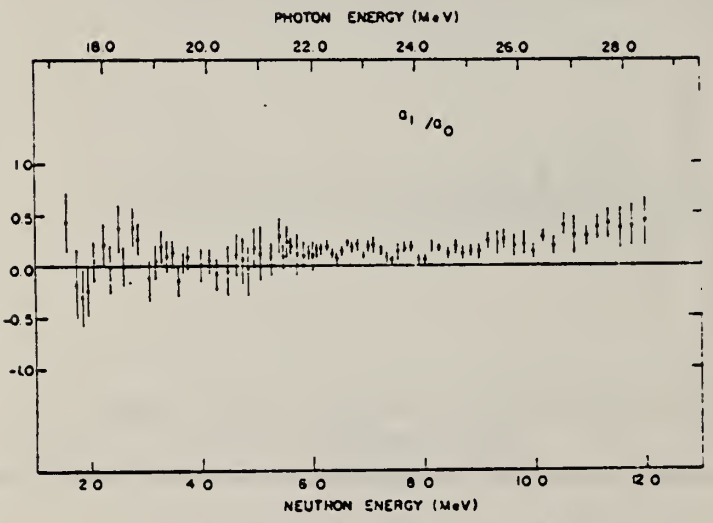

FIG. 12. The energy dependence of the normalized coefficient a_1/a_0.

J. C. Kim, R. P. Singhal, and H. S. Caplan
Can. J. Phys. 48, 83 (1970)

ELEM. SYM.	A	Z
O	16	8

METHOD

REF. NO.

 70 Ki 1 hmg

REACTION	RESULT	EXCITATION ENERGY	SOURCE		DETECTOR		ANGLE
			TYPE	RANGE	TYPE	RANGE	
E,E/	FMF	11-14	D	40-105	MAG-D		DST
		(11.5-13.25)					

FMF 11.5-13.1 MEV

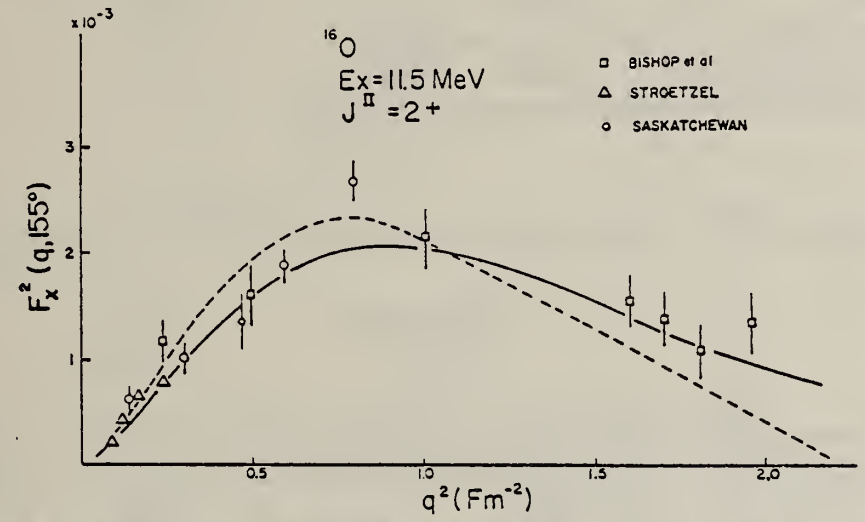

FIG. 2. Form factor F_x^2 of the 11.5 MeV (2^+) level. The dashed line is from a calculation of Seaborn and Eisenberg and has been arbitrarily multiplied by 25. The solid line is the generalized Helm model fit with charge radius and skin depth parameters $R = 1.084\ A^{1/3}$ fm, $g^2 = 0.88$ fm^2, respectively, and the magnetization radius and skin depth $\bar{R} = 1.15\ A^{1/3}$ fm, $\bar{g}^2 = 1.15$ fm^2, respectively, and level parameter $\beta = 0.45$, $\gamma = 0.62$.

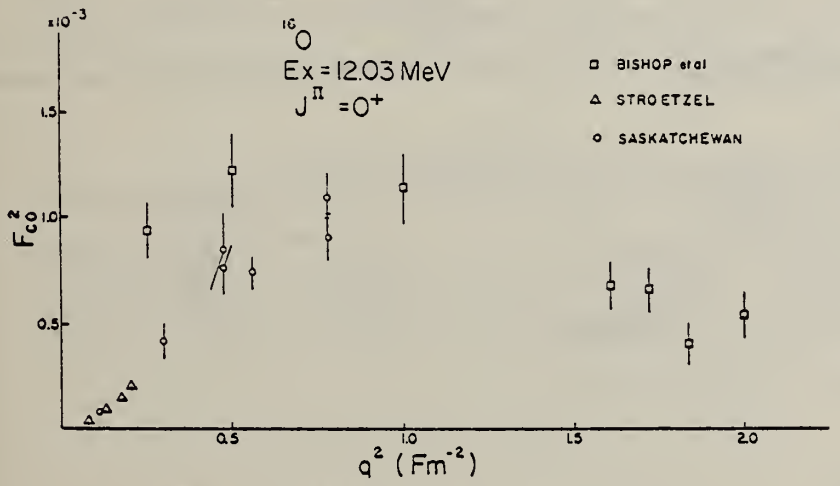

FIG. 3. Form factor F_{C0}^2 of the 12.03 MeV (0^+) level.

[over]

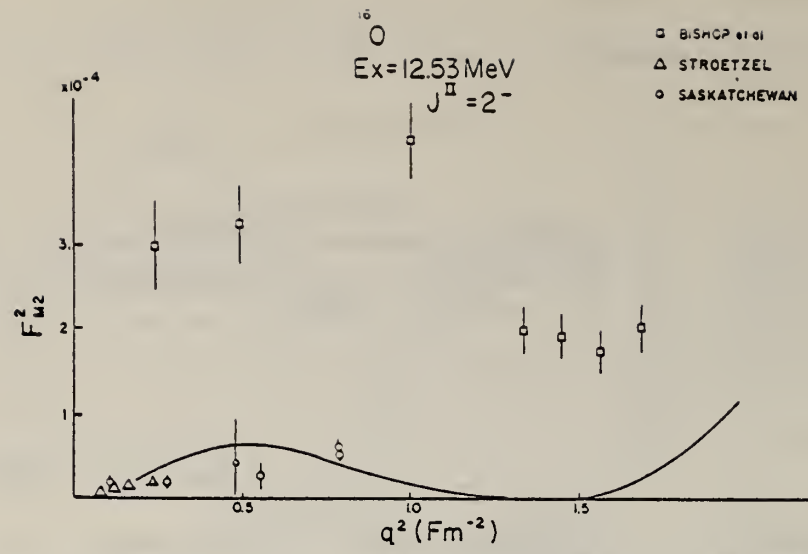

FIG. 4. Form factor $F_{M2}{}^2$ of the 12.53 MeV (2^-) level. The solid line is calculated from Gillet's wave function and has been arbitrarily multiplied by 10.

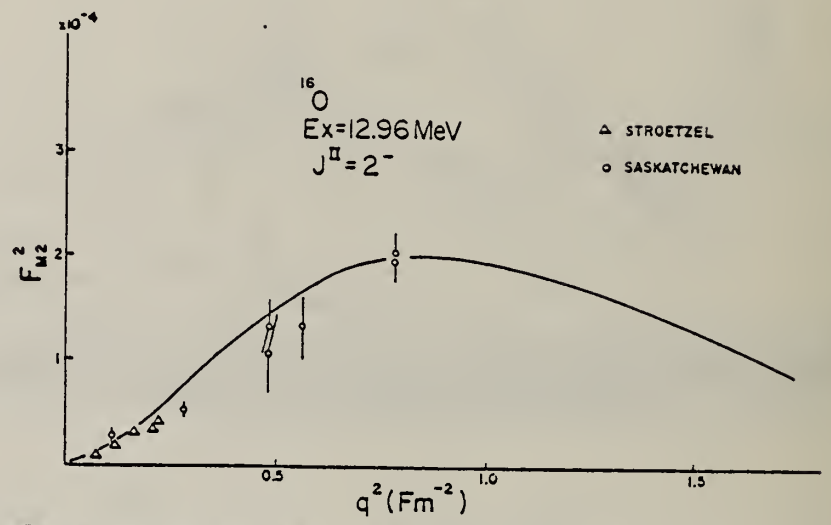

FIG. 5. Form factor $F_{M2}{}^2$ of the 12.96 MeV (2^-) level. The solid line is calculated from Gillet's wave function and has been arbitrarily divided by 3.

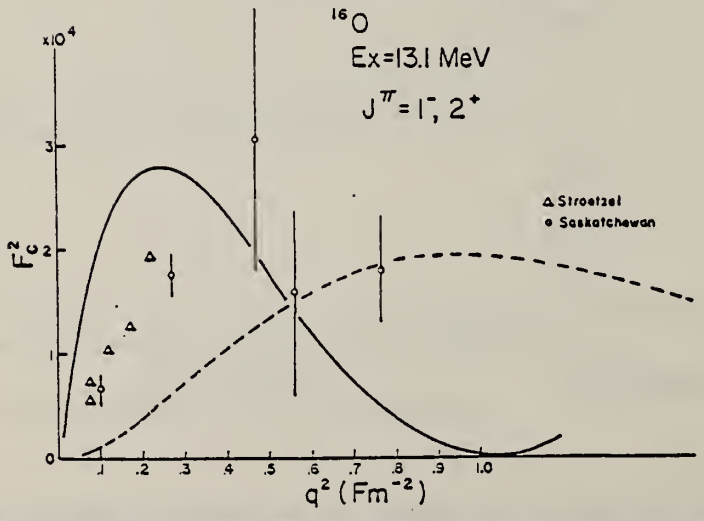

FIG. 6. Longitudinal form factors of the 13.1 MeV peak. The solid curve is calculated from Gillet's wave function (13.6 MeV, 1^-, $T=1$). The dashed curve which has been multiplied by 0.05 is calculated from the configuration $(1p_{3/2}, 1f_{7/2})2^+$, $T=0$ which contributes 88% of amplitude of the (13.7 MeV, 2^+, $T=0$) level predicted by Gillet.

TABLE III

Ground state radiative widths, transition radii, and reduced matrix elements for some states in ^{16}O

			Previous work			Present work		
T	J^π	E_x (MeV)	Γ_γ^0 (eV)	R_{tr} (fm)	$B(J, E_x)$ (fm^{2J})	Γ_γ^0 (eV)	R_{tr} (fm)	$B(J, E_x)$ (fm^{2J})
0	2^+	11.52	0.55 ±0.07[a] 0.85 ±0.1[b] 0.90 ±0.2[c] 0.66 ±0.09[d]	3.7±0.5	17.8±2.0 26.0±3	0.85 ± 0.09	4.4 ±0.05	25.67 ±2.83
	0^+	12.03		6.3±0.9	4.90±0.49		5.2 ±0.95	4.89 ±0.31
0	1^-	12.44	7 ±1[d]					
0	2^-	12.53	0.15 ±0.02[b] 0.021±0.006[e]	2.9±1.0	0.42±0.10	0.108± 0.0154	5.3	2.19 ±0.3
1	2^-	12.96	0.078±0.016[e]	3.6±0.5	1.34±0.27	0.071± 0.002	3.74±0.2	1.227±0.03
1	1^-	13.1 ±0.01	23 ±4[c] 88[f] 150[g]			48.5 ±12.8	3.68±2.50	0.057±0.015
			31 ±8[a]		0.04±0.01			
0	2^+	13.15±0.1	0.6 ±0.3[h] ~0.13[a]		~2	0.89		13.8
1	3^-	13.25±0.01						

[a]Stroetzel (1968). [b]Bishop *et al.* (1964). [c]Meads and Meldowie (1960). [d]Larson and Spear (1964). [e]Bethge and Strohbach (1965). [f]Hebbard (1960). [g]Schardt *et al.* (1952). [h]Mitchell and Ophel (1964).

TABLE IV

The summed form factors for the 12.9 MeV, 13.1 MeV, and 13.25 MeV levels

θ (°)	q^2 (fm^{-2})	ΣF_L^2 (Bishop) × 10^3	ΣF_L^2 (present) × 10^3	ΣF_L^2 (Willey) × 10^3
60	0.28		0.21±0.026	
60	0.457	1.10±0.13		0.43
60	0.57		0.43±0.05	
60	0.648	1.00±0.16		0.67
60	0.77		0.46±0.04	
80	1.01	2.92±0.27		
115	1.57	2.90±0.38		3.92
135	1.67	7.50±1.0		8.83
120	1.82	3.5 ±0.55		5.01
80	1.91	1.9 ±0.35		2.37

TABLE V

Transition matrix elements of 13.25 (3^-) and 12.70 (0^-)

13.25 (3^-)			12.70 (0^-)		
q^2 (fm^{-2})	$F_{coul}^2 \times 10^4$	$F_{elec}^2 \times 10^5$	θ (°)	$(F_L^2(q, \theta))_{average}$	Averaged over energies
0.57	1.61±0.24	0.19±0.029	125	0.8×10^{-4}	104 MeV, 90 MeV
0.76	0.60±0.40	3.3 ±2.2	155	1.0×10^{-4}	60 MeV, 95 MeV, 40 MeV

M. Stroetzel and A. Goldmann
Z. Physik 233, 245 (1970)

ELEM. SYM.	A	Z
O	16	8

METHOD

REF. NO. 70 St 1 egf

REACTION	RESULT	EXCITATION ENERGY	SOURCE		DETECTOR		ANGLE
			TYPE	RANGE	TYPE	RANGE	
E,E/	LFT	14-21	D	34-58	MAG-D	10-58	DST

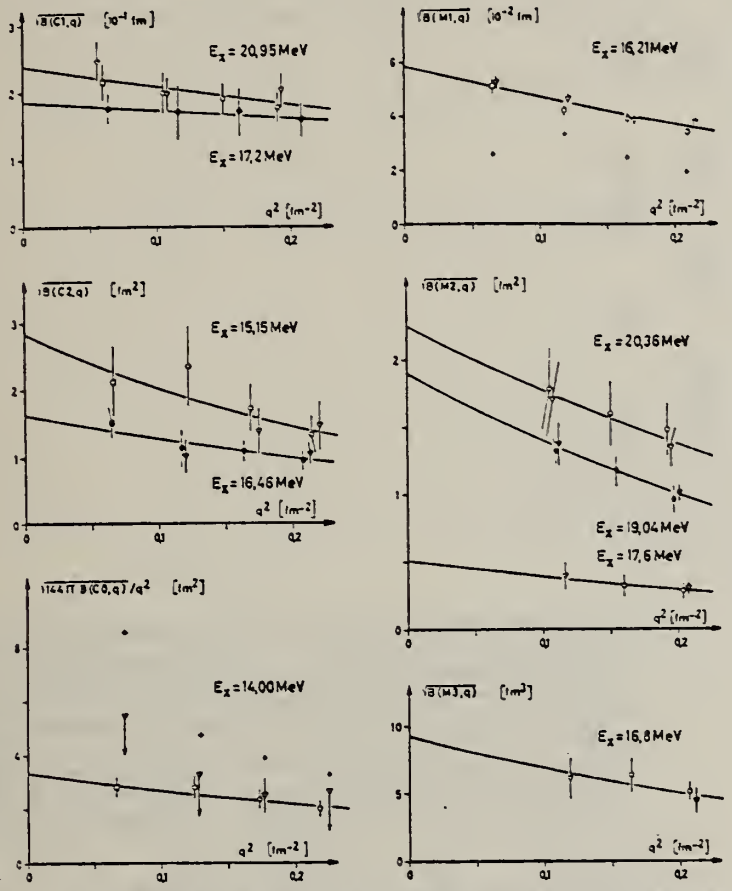

Fig. 3. Reduzierte Übergangsmatrixelemente (DWBA-Analyse) für 10 Niveaus des ^{16}O, aufgetragen über dem Quadrat der Impulsübertragung. Die Symbole der Punkte haben folgende Bedeutung: Messung bei 81° (□), 129° (○) bzw. 165° (▽); die Meßpunkte des 17,2 MeV-Niveaus (◇) wurden aus Winkelverteilungen bei konstantem Impulsübertrag gewonnen. Die Kreuze (+) geben theoretische Abschätzungen an und werden im Text erläutert. Die durchgezogenen Kurven stellen die beste Anpassung von Gl. (1) an die Meßpunkte dar. Aus ihnen folgen die in Tabelle 2 aufgeführten Ergebnisse für $B(X\lambda, 0)$ und R_{tr}

[over]

Tabelle 1. *Flächenverhältnisse $A_i/A_g \times 10^4$ für 13 durch ihre Anregungsenergie in MeV gekennzeichnete Niveaus in ^{16}O; in Klammern ist der Fehler in Prozent aufgeführt. Der nach[13] berechnete elastische Wirkungsquerschnitt $(d\sigma/d\Omega)_E$ hat die Dimension 10^{-30} cm²/sr*

Spektrum	1	2	3	4	5	6	7	8
θ [Grad]	164,9	164,9	164,9	164,9	129,0	129,0	129,0	80,9
E_0 [MeV]	54,30	48,90	42,73	34,09	58,09	52,45	45,53	45,64
$(d\sigma/d\Omega)_E$	0,953	1,387	2,140	4,122	13,53	19,50	30,18	438,7
14,00	≦3,7	1,74 (50)	≦1,4	≦0,7	1,91 (30)	1,43 (30)	0,91 (30)	0,20 (25)
15,15	6,9 (50)	3,7 (40)	—	—	1,83 (40)	1,72 (40)	1,49 (50)	0,23 (50)
16,21	18,0 (10)	12,8 (15)	11,3 (10)	7,0 (15)	1,17 (15)	1,07 (15)	0,76 (20)	0.12 (25)
16,46	4,1 (30)	—	1,4 (50)	—	0,93 (30)	0,68 (30)	0,36 (50)	0,13 (30)
16,8	6,4 (40)	—	1,5 (50)	—	0,65 (25)	0,40 (40)	—	—
17,2	23,3 (10)	20,0 (25)	18,5 (10)	13,7 (10)	3,88 (15)	3,18 (15)	2,44 (15)	0,68 (15)
17,6	7,1 (30)	—	2,7 (50)	—	0,49 (40)	0,34 (50)	—	—
18,5	6,86 (25)	—	2,46 (30)	—	3,95 (30)	2,29 (30)	0,92 (40)	0,23 (30)
19,0	—	—	—	—	—	—	—	0,25 (30)
19,04	77,8 (10)	—	31,8 (15)	—	5,55 (20)	4,39 (20)	2,39 (25)	—
19,5	—	—	—	—	—	—	—	0,22 (30)
20,36	129,7 (20)	—	45,3 (30)	—	12,43 (25)	7,76 (30)	4,04 (35)	—
20,95	28,9 (25)	—	18,5 (25)	23,4 (25)	4,06 (25)	3,38 (25)	2,62 (30)	0,82 (25)

Tabelle 2. *Endergebnisse für 13 Niveaus des ^{16}O: in Klammern sind die Fehler in Einheiten der letzten Stelle angegeben. Zur Bestimmung der totalen Breite wurde das „instrumentelle Auflösungsvermögen" mit Lorenzkurven verschiedener Breite Γ gefaltet, bis die experimentelle Halbwertsbreite der verschiedenen Resonanzen mit der Breite der Faltungskurve übereinstimmte. Die Form für das „instrumentelle Auflösungsvermögen" ist der elastischen Linie ähnlich, jedoch ist die Breite wegen der konstanten Dispersion des Spektrometers etwas kleiner. Die Übergongswahrscheinlichkeiten $B(X\lambda, 0)$ und Übergangsradien R_{tr} folgen aus der DWBA-Analyse der gemessenen Wirkungsquerschnitte. Die Weisskopfabschätzung Γ_w erfolgte nach[16a] mit $R = 1{,}2\,fm\,A^{\frac{1}{3}}$*

E_x [MeV]	I^π	Γ [keV]	$B(X\lambda, 0)$ [fm$^{2\lambda}$]	Γ_γ^0 [eV]	Γ_γ^0/Γ_w	R_{tr} [fm]
14,00 (5)	0^+	170 (50)	3,3 (7)[a]	—	—	6,5(16)
15,15(15)	2^+	500(200)	8,1 (41)	1,0 (5)	0,7	6,8(27)
16,21 (3)	1^+	—	0,0034 (5)	5,1 (8)	0,05	3,2 (3)
16,46 (7)	2^+	≦100	2,7 (9)	0,5 (2)	0,2	5,8(17)
16,80(10)	3^+?	≦100	86 (43)	0,0017 (9)	16	5,8(25)
17,20[b]	1^-	—	0,035 (7)	62 (12)	0,03	2,7 (7)
17,60(10)	2^-?	≦100	0,26 (13)	0,07 (4)	0,4	4,6(18)
18,50(10)	2?	50...400	—	—	—	—
19,00(10)	1^-	300(100)	0,017 (9)	41 (20)	0,014	mit 3,3[c]
19,04 (5)	2^-	400 (50)	3,6 (7)	1,5 (3)	6,2	4,9 (8)
19,50(10)	1^-	200 (70)	0,016 (8)	40 (20)	0,013	mit 3,3[c]
20,36 (7)	2^-	500(100)	5,1 (18)	2,9 (10)	8,6	4,4(11)
20,95 (5)	1^-	270 (70)	0,057 (14)	180 (50)	0,05	3,7 (9)

[a] *ME* in fm².
[b] Nicht aufgelöstes Doublett 17,14 ($1^\pm$?) und 17,30 (1^-) MeV.
[c] Für die Extrapolation ($q \to 0$) benutzt.

REF. U. Von Wimmersperg, G. Kernel, B. W. Allardyce, W. M. Mason and N. W. Tanner
Phys. Letters 33B, 291 (1970)

ELEM. SYM.	A	Z
O	16	8

METHOD

REF. NO. 70 Vo 1 egf

REACTION	RESULT	EXCITATION ENERGY	SOURCE		DETECTOR		ANGLE
			TYPE	RANGE	TYPE	RANGE	
G,A	NOX	13	D	13	ION-D		DST
		(13.1)					
A,G	NOX	13	D	8	NAI-D		DST
		(13.1)					

Check detailed balance on angular distribution.

13 = 13.1 MEV

$$W(\theta_{\alpha\gamma}) = A_o(P_o - P_4) + A_1(P_1 - P_3) + A_2(P_2 - P_4)$$

$A_1/A_o = +0.37 \pm 0.01$

$A_2/A_o = -0.93 \pm 0.02$ for (A,G) reaction

J. O. Adler, G. Andersson, B. Forkman, G. G. Jonsson, K. Lindgren
Nucl. Phys. A171, 560 (1971)

ELEM. SYM.	A	-
0	16	8

METHOD

REF. NO.: 71 Ad 1 | egf

REACTION	RESULT	EXCITATION ENERGY	SOURCE		DETECTOR		ANGLE
			TYPE	RANGE	TYPE	RANGE	
G,NG	ABY	22-800	C	100-800	SCD-D	6.2	135
G,PG	ABY	18-800	C	100-800	SCD-D	6.3	135

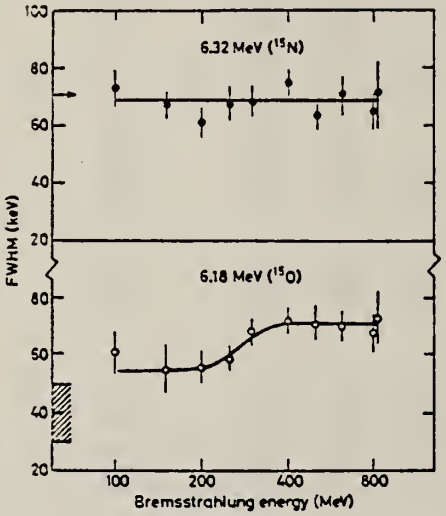

Fig. 7. The FWHM for the (γ, n) and (γ, p) peaks as functions of the maximum bremsstrahlung energy. The arrow and the dashed region indicates the value at 30 MeV (see fig. 8).

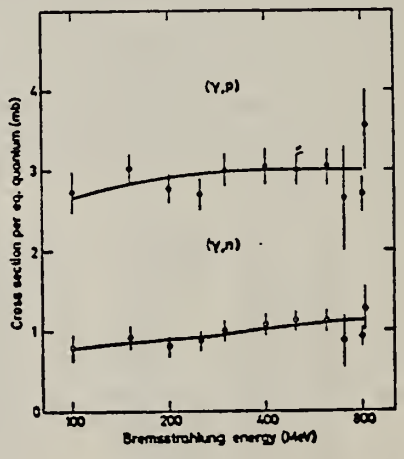

Fig. 9. The corrected (γ, p) and (γ, n) yields as functions of the maximum bremsstrahlung energy. The curves are least-squares fitted to the experimental points.

REF. J. Ahrens, H. Borchert, H.B. Eppler, H. Gimm, H. Gundrum, P. Riehn, G. Sita Ram, A. Zieger, and B. Ziegler
Elba-71, Tagungsbericht Elektronen Beschleuniger Arbeits Gruppen (Sept. 1971) Justus Liebig-Universitat Giessen.

ELEM. SYM.	A	Z
O	16	8

METHOD

REF. NO. 71 Ah 1 hmg

REACTION	RESULT	EXCITATION ENERGY	SOURCE		DETECTOR		ANGLE
			TYPE	RANGE	TYPE	RANGE	
G,MU-T	ABX	THR-150	C	10-150	MGC-D		4PI

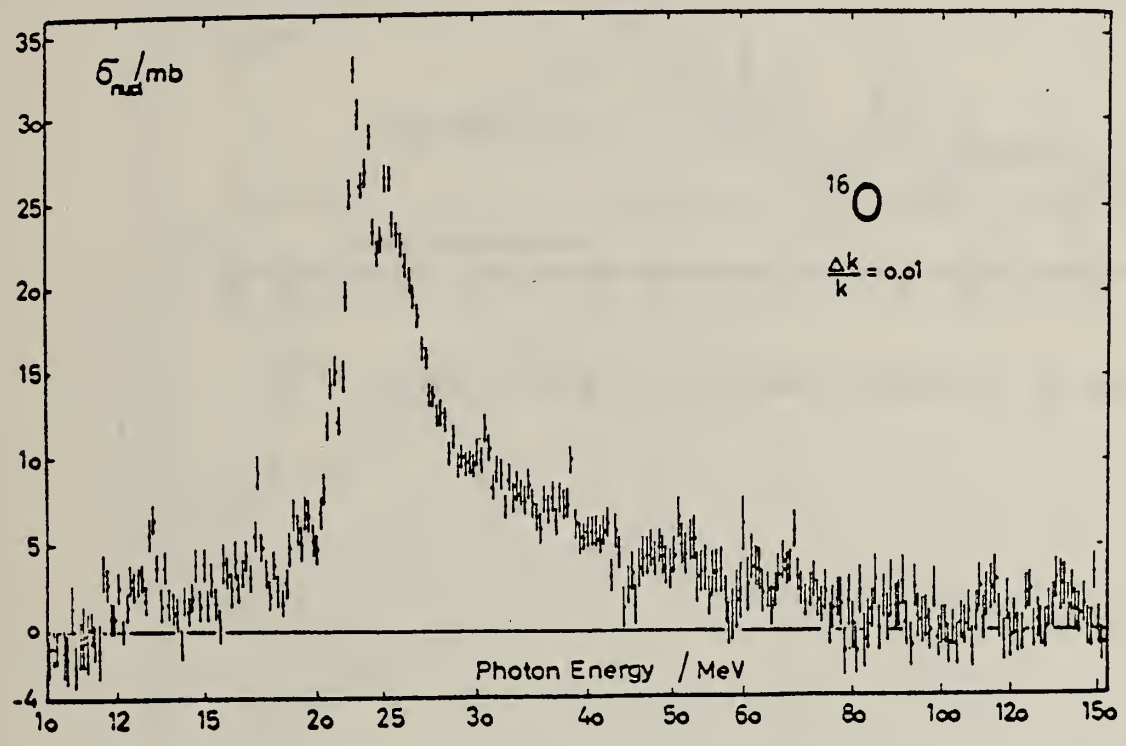

fig. 5

(over)

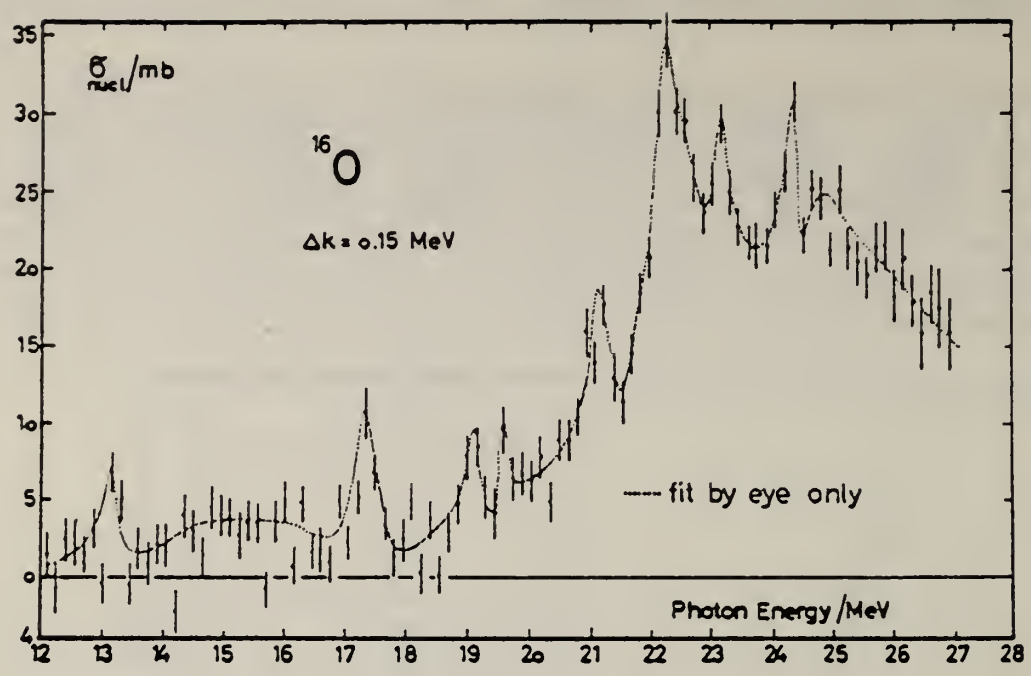

fig. 8: structures measured in the giant resonance of ^{16}O

REF.

B. Friberg, G. Andersson, and B. Forkman
Nucl. Phys. A171, 551 (1971)

ELEM. SYM.	A	Z
O	16	8

METHOD

REF. NO.	
71 Fr 1	egf

REACTION	RESULT	EXCITATION ENERGY	SOURCE		DETECTOR		ANGLE
			TYPE	RANGE	TYPE	RANGE	
G,N	ABY	16-800	C	100-800	ACT-I		4PI

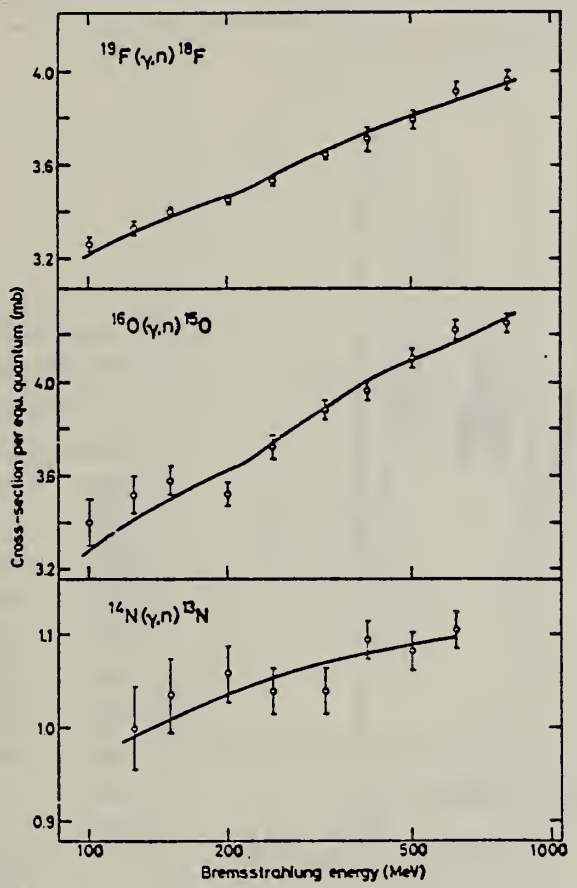

Fig. 1. Absolute yields for the (γ, n) reactions in ^{14}N, ^{16}O and ^{19}F. The solid lines are the least-squares fits of the yields from low-energy processes and photomeson yield.

REF. B.I. Goryachev, B.S. Ishkhanov, and V.G. Shevchenko
Proceedings of the Second Symposium on the Problems of Nuclear Physics, Novosibirsk, USSR, June 1970 (Kolybasov, V.M., Ed., Izdatel'stvo Nauka, Moscow 1971), pp. 362-78

ELEM. SYM.	A	Z
O	16	8

METHOD

REF. NO. 71 Go 3 egf

REACTION	RESULT	EXCITATION ENERGY	SOURCE		DETECTOR		ANGLE
			TYPE	RANGE	TYPE	RANGE	
G,XN	ABX	16- 25	C	16- 25	MOD-I		4PI

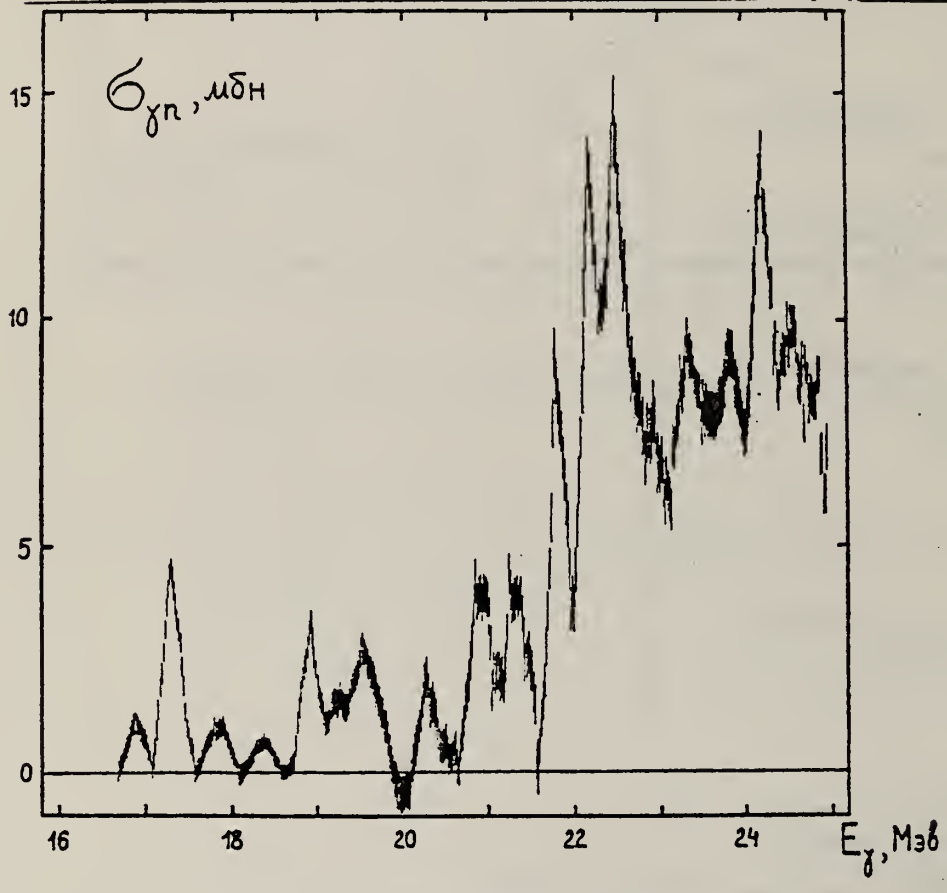

Фиг. 2. Сечение реакции $O^{16}(\gamma,n)$.

Таблица 1

Энергии резонансов (Мэв)

C^{12}	O^{16}	Ca^{40}
20,0	16,9	16,9
20,4	17,3	17,2
20,7	17,9	17,8
21,1	18,4	18,2
21,4	18,9	18,5
21,9	19,3	18,8
22,4	19,5	19,0
22,9	20,3	19,3
23,3	20,9	19,6
23,7	21,3	19,9
	21,8	20,4
	22,2	21,0
	22,5	21,2
	22,9	21,5
	23,3	22,0
	23,8	22,4
	24,2	22,6
	24,6	23,3
		24,2
		24,6
		25,5

REF. G. Kernel, W. M. Mason, U. Von Wimmersperg
Nucl. Phys. A167, 352 (1971)

ELEM. SYM.	A	Z
O	16	8

METHOD

REF. NO. 71 Ke 1 egf

REACTION	RESULT	EXCITATION ENERGY	SOURCE		DETECTOR		ANGLE
			TYPE	RANGE	TYPE	RANGE	
A,G	ABX	12-14	D	7-9	NAI-D		DST

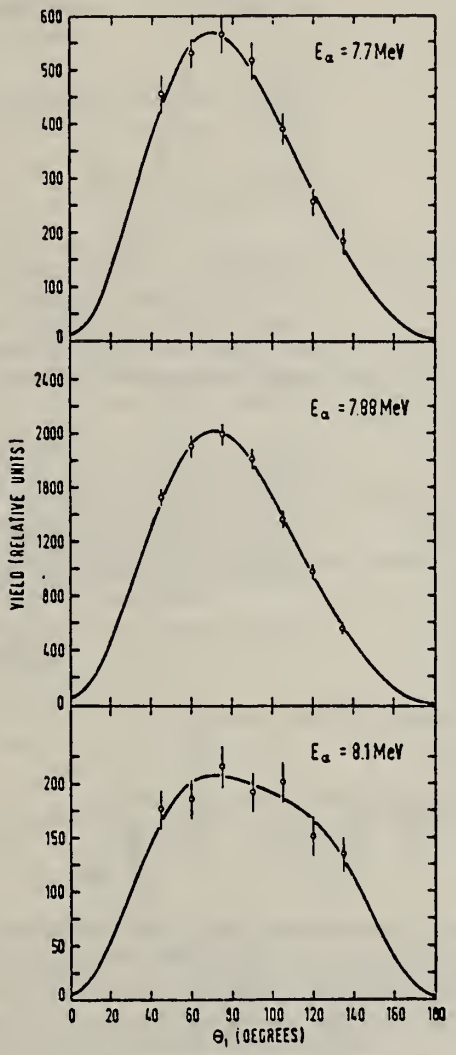

Fig. 7. Angular distributions measured with the small crystal. The curves result from the least-squares fit of the Legendre polynomial coefficients to the experimental values with the application of the conditions $A_0+A_2+A_4 = A_1+A_3 = 0$.

TABLE 2
Results

E_α (MeV)	Normalized yields			Legendre polynomial coefficients		
	$\theta = 45°$	$\theta = 90°$	$\theta = 135°$	A_0	A_1/A_0	A_2/A_0
7.60	265±15	341±21	122±11	240±10	0.303±0.045	−0.93±0.09
7.70	468± 8	528±16	165± 5	382± 7	0.411±0.016	−0.89±0.04
7.80	1096±30	1144±43	317±14	836±19	0.495±0.025	−0.88±0.05
7.88	1350±17	1637±24	529± 9	1158±11	0.366±0.010	−0.93±0.02
8.00	460±23	604±31	261±12	443±14	0.174±0.036	−0.86±0.07
8.10	180± 6	201± 7	120± 6	161± 4	0.172±0.032	−0.72±0.05

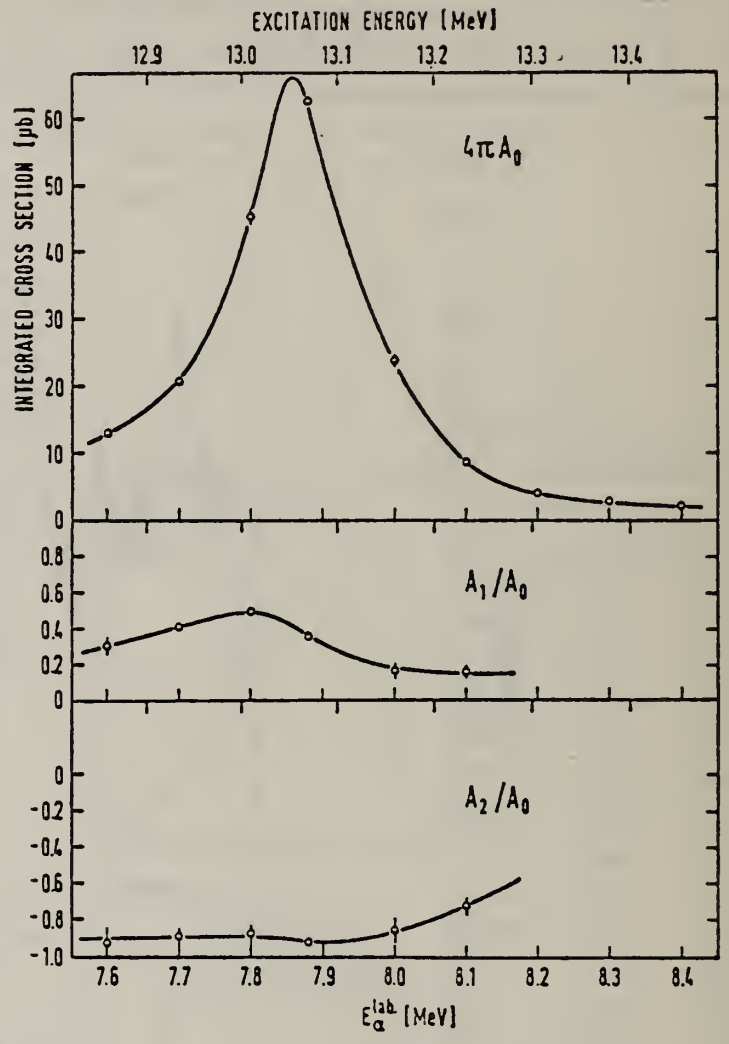

Fig. 8. Legendre polynomial coefficients. The upper diagram represents the integrated cross section. Values for A_1/A_0 and A_2/A_0 at energies higher than $E_\alpha = 8.1$ MeV are not shown due to large errors. The errors due to the normalization of A_0 values to each other are not given in the upper diagram; they amount to about 4%. Where the errors for A_1/A_0 and A_2/A_0 are not shown they are smaller than the radius of data circles. The upper scales for excitation energies were obtained using a Q-value of −7.161 MeV from ref. [7]).

[7] F. Ajzenberg-Selove and T. Lauritsen, Nucl. Phys. A114 (1968) 1.

REF.

Tatsuya Saito
Nippon Kagaku Zasshi 92, 164 (1971)

ELEM. SYM.	A	Z
O	16	8

METHOD

REF. NO. 71 Sa 1 egf

REACTION	RESULT	EXCITATION ENERGY	SOURCE		DETECTOR		ANGLE
			TYPE	RANGE	TYPE	RANGE	
G,N	ABY	15-68	C	10-68	ACT-I		4PI

Nippon Kagaku Zasshi, 92, 164~168(1971)

The Yields of Radioactivities Induced by (γ, n) Reactions with Bremsstrahlung up to 68 MeV

by Tatsuya SAITO

The (γ, n) yields of 12 target nuclides have been measured at 10, 13, 16, 30, 45 and 68 MeV bremsstrahlung by observing the induced activities.

The energy dependence of the yields has been investigated extensively in the same way as in the previous work at 20 MeV bremsstrahlung.

In the case of heavy nuclides, the yields rise greatly as a function of maximum bombarding energy up to 20 MeV, and rise gradually from 20 MeV up to 68 MeV. However, in the case of light nuclides, the yields rise greatly up to 30 MeV, because the neutron separation energies of light ones are larger than those of heavy ones, and the bremsstrahlung spectrum covers the giant resonance and so the yields rise gradually from 30 MeV up to 68 MeV.

The yields have approximately been estimated from the parameter of the giant resonance, that is the peak cross section and the half width, in order to compare with the experimental data. As a result, the experimental data of light nuclides and heavy ones are nearly in agreement with the estimated data of Nathans et al., Johns et al. and Montalbetti et al., but those of medium weight ones are relatively lower values.

Department of Chemistry, Faculty of Science, Tohoku University; Katahira-cho, Sendai-shi, Japan

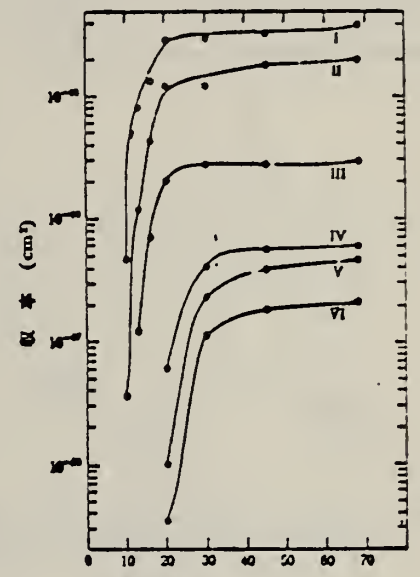

制動輻射最大エネルギー

I : $^{197}Au(\gamma,n)^{196}Au$, II : $^{127}I(\gamma,n)^{126}I$
III : $^{55}Mn(\gamma,n)^{54}Mn$, IV : $^{23}Na(\gamma,n)^{22}Na$
V : $^{16}O(\gamma,n)^{15}O$, VI : $^{12}C(\gamma,n)^{11}C$

図 3 (γ, n) 反応の収率

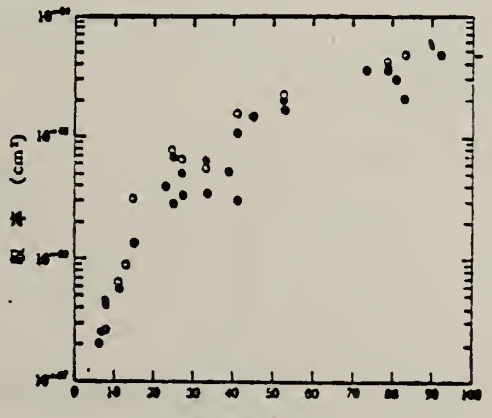

原子番号

●: 実験値, ⊕: Johns ら,
◑: Nathans ら, ○: Montalbetti ら

図 4 (γ, n) 反応の収率の比較

REF.

M. Suffert and A. Degre
J. de Physique 32, C5B-219 (1971)

ELEM. SYM.	A	Z
O	16	8

METHOD

REF. NO. 71 Su 1 egf

REACTION	RESULT	EXCITATION ENERGY	SOURCE TYPE	SOURCE RANGE	DETECTOR TYPE	DETECTOR RANGE	ANGLE
D,G	RLX	21- 26	D	1- 7	NAI-D		DST

851

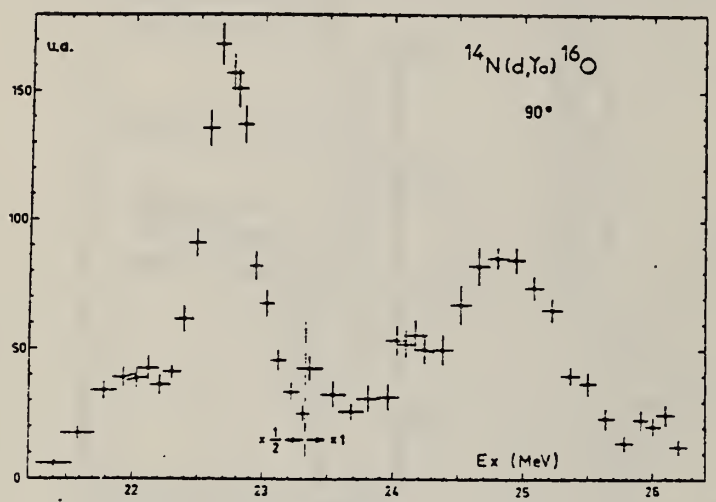

Fig. 2

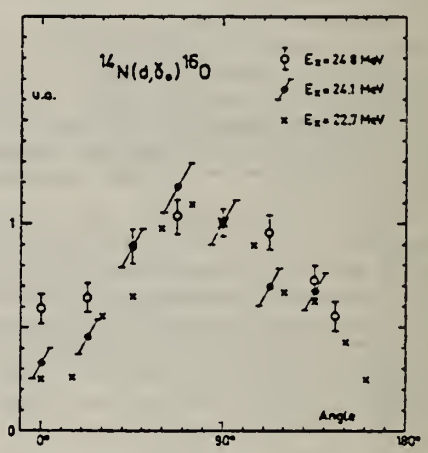

Fig. 3

REF. J. Ahrens, H. Borchert, H. B. Eppler, H. Gimm, H. Gundrum, P. Riehn, G. Sita Ram, A. Zieger, M. Kroning, B. Ziegler
Proc. International Conference on Nuclear Structure Studies Using Electron Scattering and Photoreaction, Sendai, Japan p. 213 (1972)

ELEM. SYM.	A	Z
O	16	8

METHOD

REF. NO.	
72 Ah 7	egf

REACTION	RESULT	EXCITATION ENERGY	SOURCE		DETECTOR		ANGLE
			TYPE	RANGE	TYPE	RANGE	
G,MUT	ABX	12-140	C	140	MGC-D		4PI

594

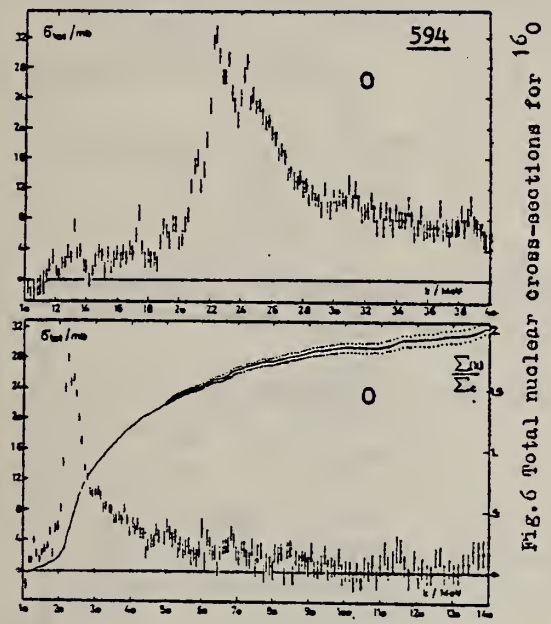

Fig.6 Total nuclear cross-sections for ^{16}O

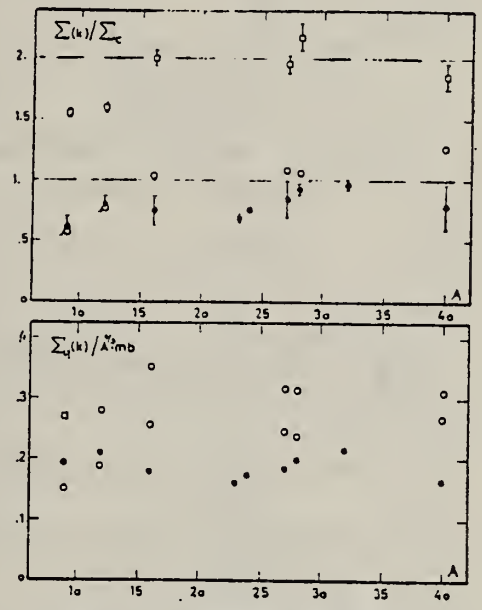

$\Sigma_c = 60 \frac{NZ}{A}$, $\Sigma(k) = \int_{10}^{k} \sigma(\tilde{k}) d\tilde{k}$, $\Sigma_1(k) = \int_{10}^{k} \sigma(\tilde{k}) \frac{d\tilde{k}}{\tilde{k}}$

• NBS k=35 MeV, o k=35 MeV, o k=140 MeV

Fig.11 Integrated cross-sections

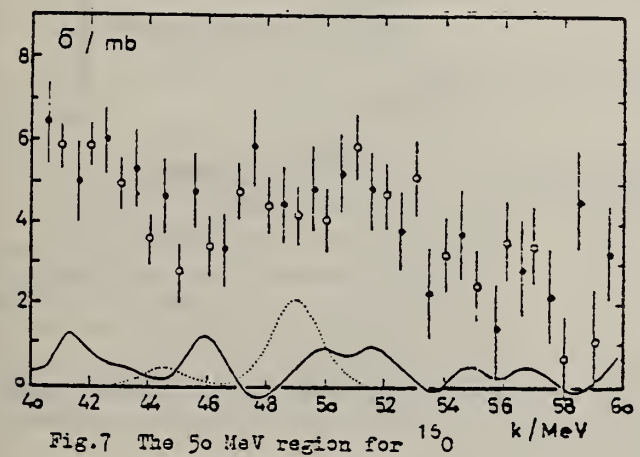

Fig.7 The 50 MeV region for ^{16}O

REF.

S.S. Hanna, H.F. Glavish, E.M. Diener, J.R. Calarco, C.C. Chang, R. Avida, and R.N. Boyd
Phys. Letters 40B, 631 (1972)

ELEM. SYM.	A	Z
O	16	8

METHOD

REF. NO.	
72 Ha 4	egf

REACTION	RESULT	EXCITATION ENERGY	SOURCE		DETECTOR		ANGLE
			TYPE	RANGE	TYPE	RANGE	
$ P,G	NOX	19- 26	D	7- 15	NAI-D		DST

$A(\theta) = P^{-1}(N_{up} - N_{dn})/(N_{up} + N_{dn})$

P = proton polarization

POLARIZED P

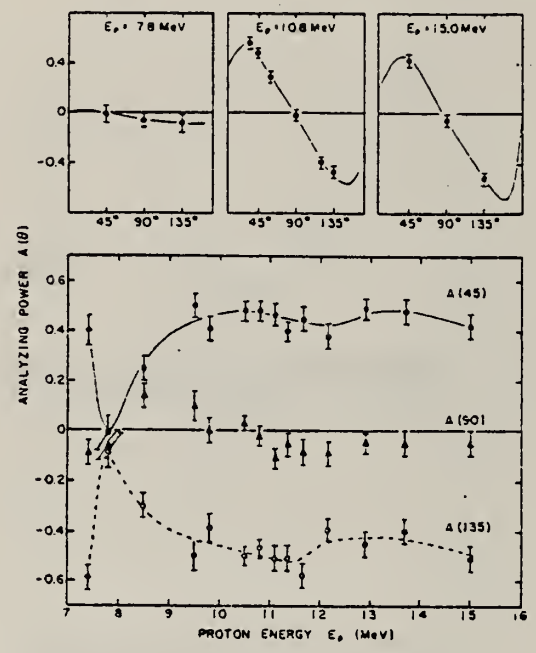

Fig.1. Measured analyzing powers for the reaction $^{15}N(\vec{p},\gamma_0)^{16}O$. Top: data plotted as a function of angle at three selected energies. Bottom: all the data at the angles 45°, 90°, and 135° presented as a function of energy.

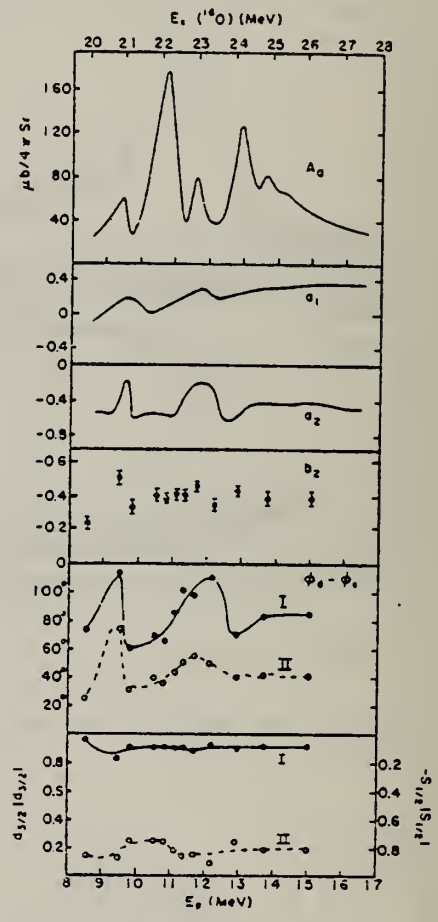

Fig.2. Summary of the existing information on the reaction $^{15}N(p,\gamma_0)^{16}O$. The curves for the total yield A_0 and the unpolarized angular distribution coefficients a_1 and a_2 are from ref.[2]. The values for b_2 were obtained from the data in fig.1 by use of eq.(2). The two solutions for $s_{1/2}|s_{1/2}|$ (right hand scale), $d_{3/2}|d_{3/2}|$, and $\phi_d - \phi_s$ were obtained by fitting the theoretical expressions (3), (4), and (5) to the experimental values of a_2 and b_2 at each energy.

[2] W. J. O'Connell, Ph.D. thesis, Stanford Univ. (1969) unpublished.

REF. Stanley S. Hanna
PICNS-72, p.453 Sendai

ELEM. SYM.	A	Z
0	16	8

METHOD

REF. NO. 72 Ha 9 hvm

REACTION	RESULT	EXCITATION ENERGY	SOURCE TYPE	SOURCE RANGE	DETECTOR TYPE	DETECTOR RANGE	ANGLE
$ P,G	NOX	19- 27	D	7- 15	NAI-D		DST

POLARIZED PROTONS

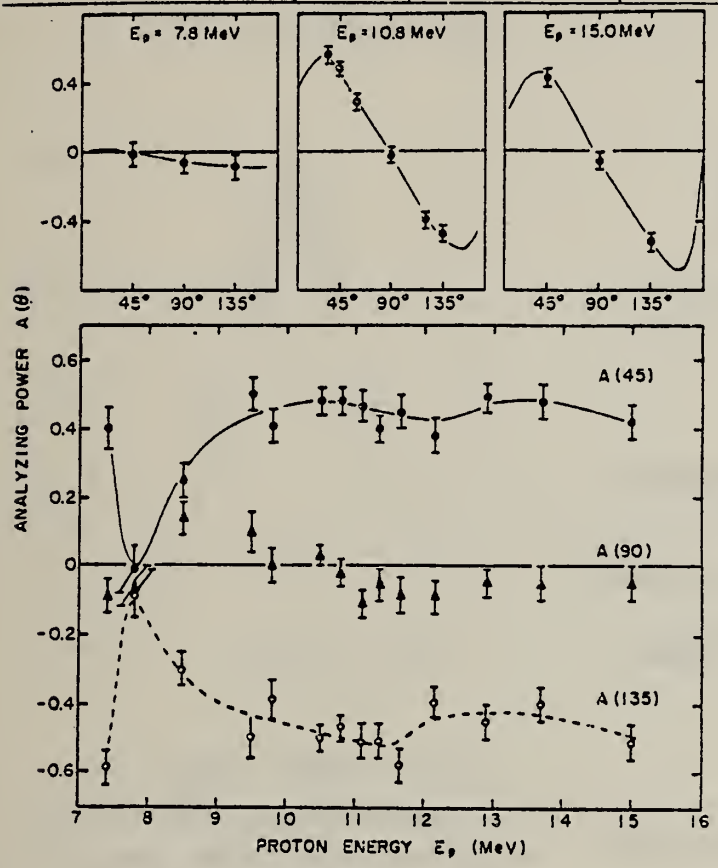

Fig. 3. Measured analyzing powers for $^{15}N(p,\gamma_0)^{16}O$. Top: data plotted vs. angle at three selected energies. Bottom: the data at 45°, 90°, and 135° plotted vs. energy.

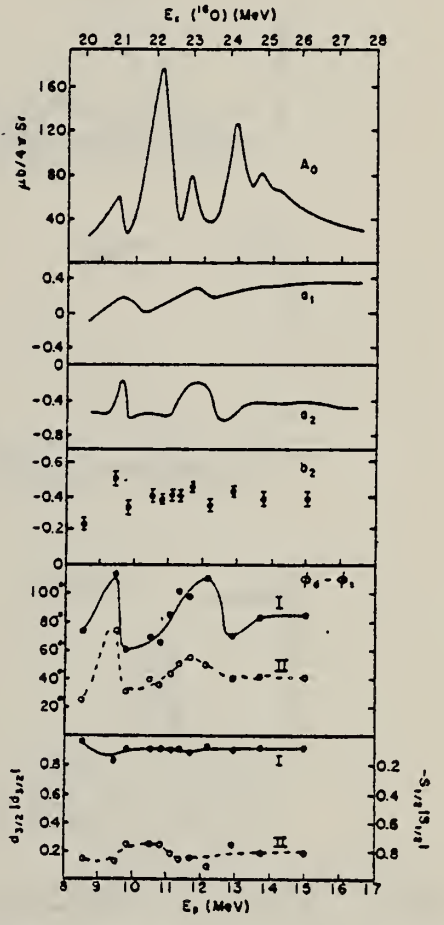

Fig. 1. Summary of the existing information on $^{15}N(p,\gamma_0)^{16}O$. The two solutions for the proton channel are indicated by I and II.

REF.

B.W. Thomas, D.M. Crawford and H. H. Thies
Nucl. Phys. A196, 89 (1972)

ELEM. SYM.	A	Z
O	16	8

METHOD

REF. NO.	
72 Th 2	egf

REACTION	RESULT	EXCITATION ENERGY	SOURCE		DETECTOR		ANGLE
			TYPE	RANGE	TYPE	RANGE	
G,XN	RLX	16-24	C	15-24	BF3-I		4PI

954

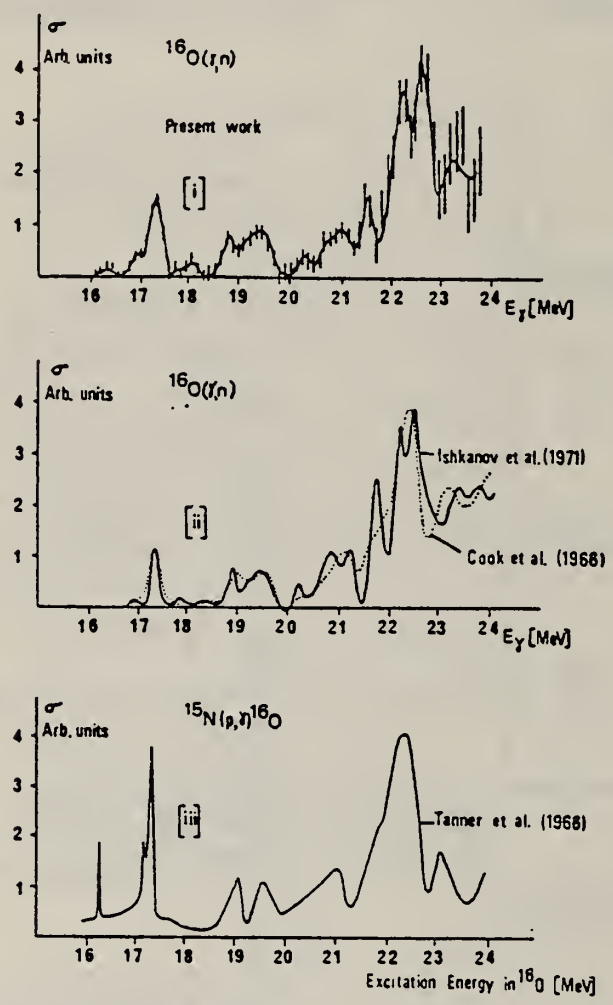

Fig. 5. (i) Cross section for $^{16}O(\gamma, n)$ (present work);, (ii) cross section for $^{16}O(\gamma, n)$ according to Cook *et al.* [14]) and Ishkhanov *et al.* [15]); (iii) cross section for $^{15}N(p, \gamma)$ according to Tanner *et al.*[16]).

[14] B. C. Cook et al., Phys. Rev. 143 (1966) 712.

[15] B. S. Ishkhanov et al., Sov. J. Nucl. Phys. 12 (1971) 484.

[16] N. W. Tanner et al., Nucl. Phys. 52 (1964) 45.

REF.

H. R. Weller, R. A. Blue and S. L. Blatt
Phys. Rev. C5, 648 (1972)

ELEM. SYM.	A	Z
O	16	8

METHOD

REF. NO. 72 We 1 hmg

REACTION	RESULT	EXCITATION ENERGY	SOURCE		DETECTOR		ANGLE
			TYPE	RANGE	TYPE	RANGE	
D,G	RLY	22-24	D	2-3	NAI-D		90
				(2.2-2.9)			

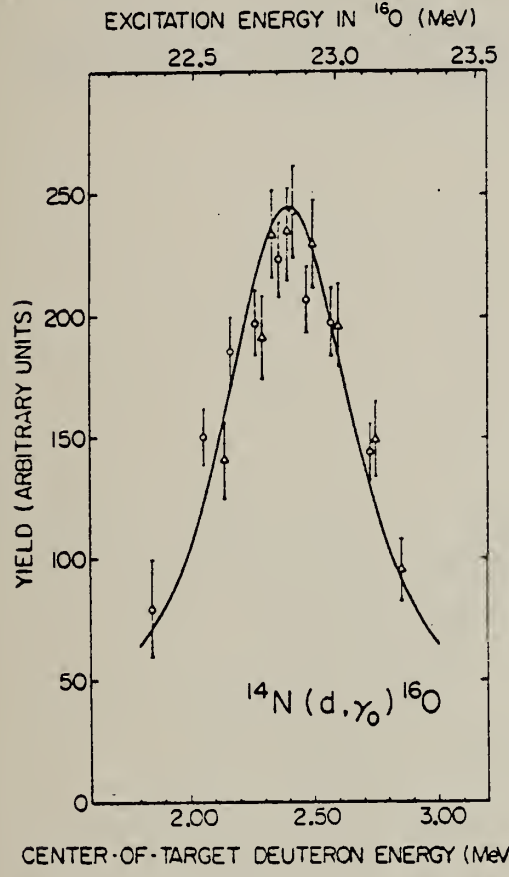

FIG. 2. Relative yield at 90° for the reaction $^{14}N(d,\gamma_0)^{16}O$. The triangles are data obtained with the tantalum nitride target, while the circles are data obtained with the nitrogen gas target. The deuteron energies have been corrected to correspond to center-of-target energies. The error bars represent the statistical uncertainties for the data points. The curve is a Breit-Wigner shape with $\Gamma(\text{lab}) = 700$ keV and $E_0 = 2.40$ MeV.

The 90° yield from the reaction $^{14}N(d,\gamma_0)^{16}O$ has been measured between 2.1 and 2.9 MeV to accurately determine the location of the strong resonance previously observed in this region. Two separate measurements were made. It is found that the resonance occurs at $E_d = 2.40 \pm 0.05$ MeV, moving it with respect to the dip $^{15}N(p,\gamma_0)^{16}O$ and $^{16}O(\gamma,n_0)^{15}O$. This result brings into question interpretations of the fine structure of the ^{16}O giant dipole resonance made on the basis of earlier experimental work.

REF. J. Ahrens, H.B. Eppler, H. Gimm, H. Gundrum, M. Kroning, P. Riehn, G. SitaRam, A. Zieger, and B. Ziegler
PICNS-73, Vol.I, p.23 Asilomar

ELEM. SYM.	A	Z
O	16	8

METHOD

REF. NO.	
73 Ah 4	hmg

REACTION	RESULT	EXCITATION ENERGY	SOURCE		DETECTOR		ANGLE
			TYPE	RANGE	TYPE	RANGE	
G,MU-T	ABX	10-140	C	140	MGC-D		4PI

Statistics may have been improved over those of 72Ah7.

See figure on other side.

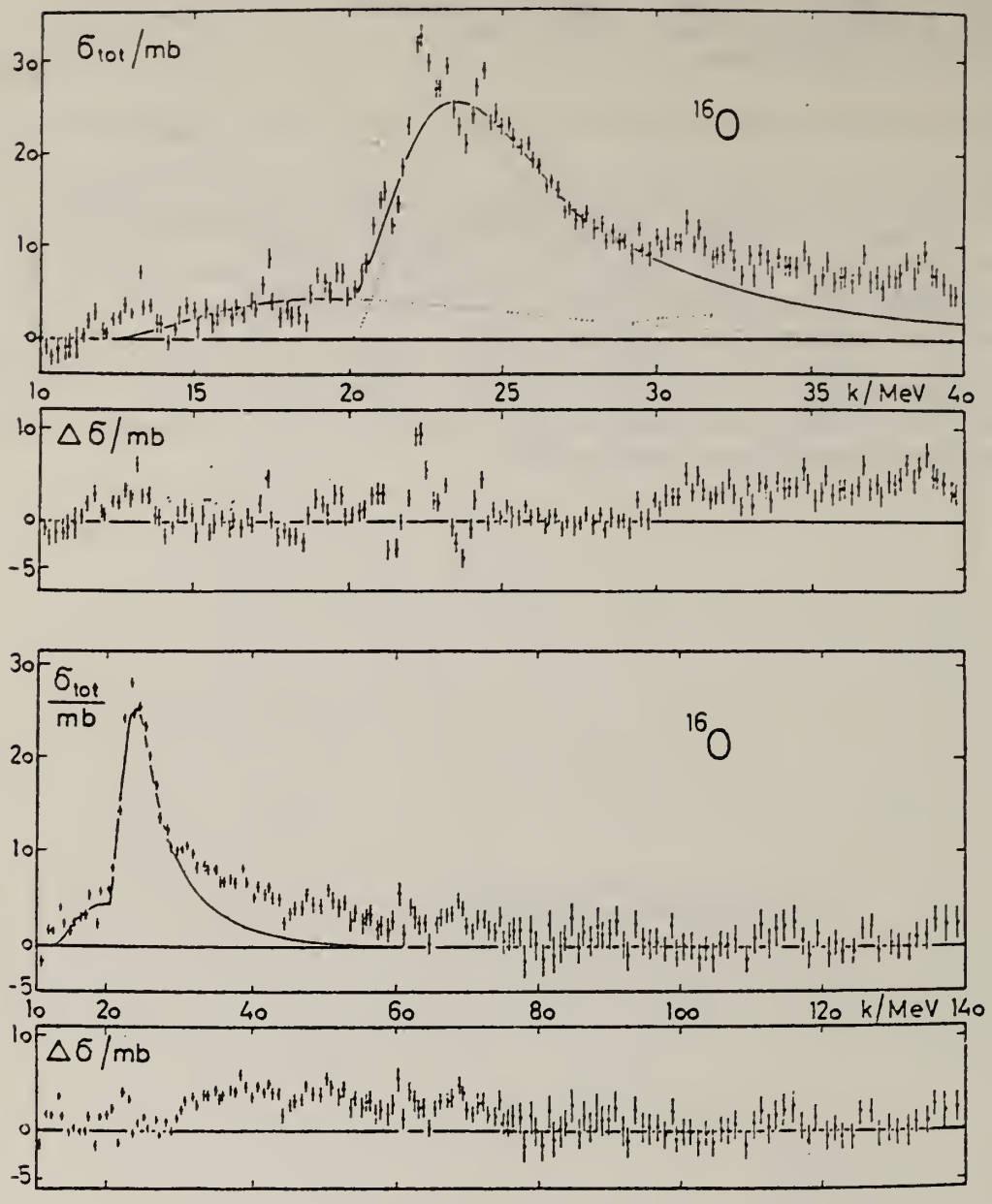

Fig. 5. Same as Fig. 2 for O.

REF. R. Bergere, H. Beil, P. Carlos, A. Lepretre, A. Veyssiere
PICNS-73, Vol.I, p.525 Asilomar

ELEM. SYM.	A	Z
O	16	8

METHOD

REF. NO. 73 Be 10 hmg

REACTION	RESULT	EXCITATION ENERGY	SOURCE		DETECTOR		ANGLE
			TYPE	RANGE	TYPE	RANGE	
G,N	ABX	16- 37	D	16- 37	BF3-I		4PI
G,PN	ABX	26- 37	D	26- 37	BF3-I		4PI
G,2N	ABX	28- 38	D	28- 38	BF3-I		4PI

857

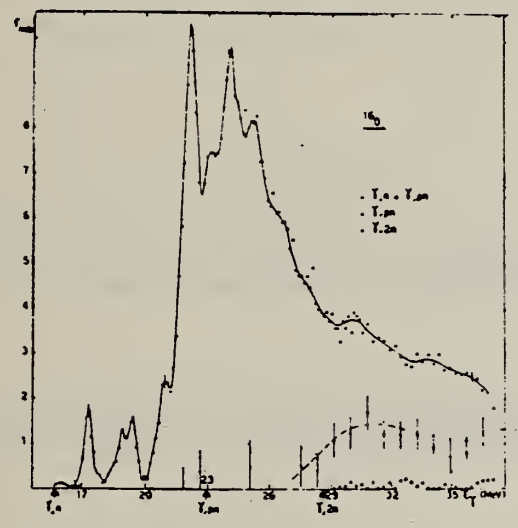

Fig. 9 Partial $\sigma(\gamma,n)$, $\sigma(\gamma,pn)$ and $\sigma(\gamma,2n)$ cross sections of ^{16}O.

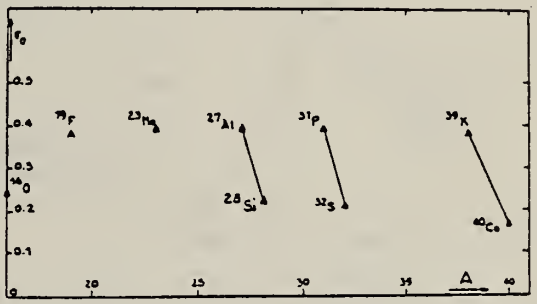

Fig. 13 Integrated photoneutron cross-sections for s-d shell nuclei.

REF.

J. C. Bergstrom and I. P. Auer
Nucl. Phys. A215, 232 (1973)

ELEM. SYM.	A	Z
O	16	8

METHOD

REF. NO.: 73 Be 16 egf

REACTION	RESULT	EXCITATION ENERGY	SOURCE		DETECTOR		ANGLE
			TYPE	RANGE	TYPE	RANGE	
E,E/	FMF	11, 12	D	101-126	MAG-D		DST

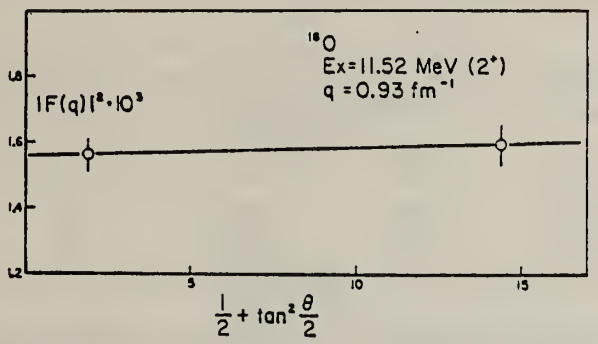

Fig. 2. Angular distribution of the total form factor of the 2$^+$ (11.52 MeV) level at $q \approx 0.93$ fm^{-1}. The small change in the form factor with angle indicates a negligible contribution of the transverse term in the angular range of the present experiment.

11=11.52, 12=12.05

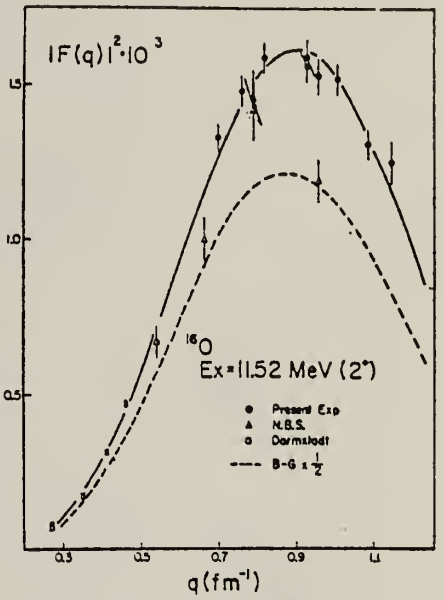

Fig. 3. Experimental form factor (squared) of the 2$^+$ (11.52 MeV) level of ^{16}O. The solid line represents a Helm model fit to the present results and the Darmstadt data. The broken line is the prediction (× $\frac{1}{2}$) of the Brown-Green model as evaluated by Erikson.

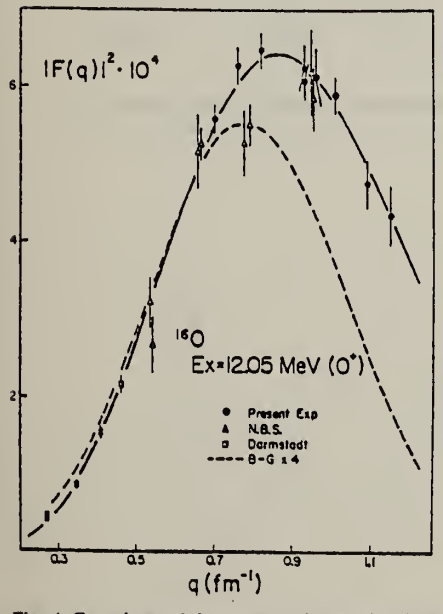

Fig. 4. Experimental form factor (squared) of the 0$^+$ (12.05 MeV) level of ^{16}O. The solid line represents a least-squares fit of the present results and the Darmstadt data to a function analogous to the Helm model but designed for monopole transitions (see text). The experimental points in this figure have not been corrected for Coulomb distortion. The broken line is the prediction (×4) of the Brown-Green model.

Fig. 5. Experimental strength function $f_3(q)$ of the 0$^+$ (12.05 MeV) state in ^{16}O as obtained from the present data and the Darmstadt results. Corrections have been applied for the distortion of the electron wave function by the Coulomb field of the nucleus. The data point at the left represents the "photon point" ($q = \omega$), based on the monopole matrix element = 4.03 fm^3. Also shown are least-squares fits to straight lines (one with zero slope).

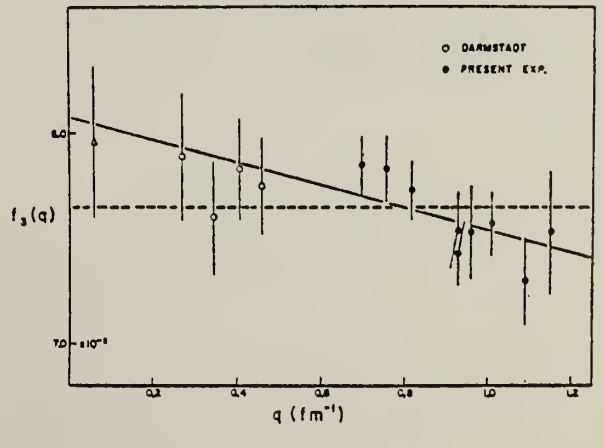

(over)

TABLE 1

Form factors for the 2^+ (11.52 MeV) and 0^+ (12.05 MeV) levels of ^{16}O as measured in the present experiment

E_i (MeV)	θ (deg.)	q (fm^{-1})	$\lvert F(q)\rvert^2 \times 10^4$	
			E_x (MeV)	
			11.52	12.05
125.9	70.0	0.70	13.3±0.4	5.6±0.2
100.8	105.0	0.76	14.8±0.5	6.3±0.2
125.8	85.0	0.82	15.9±0.5	6.5±0.2
125.8	100.0	0.93	15.6±0.5	6.1±0.2
101.4	150.0	0.93	15.9±0.6	6.3±0.3
118.3	115.0	0.96	15.3±0.6	6.1±0.4
125.7	113.0	1.01	15.2±0.5	5.9±0.2
125.7	129.8	1.09	13.1±0.5	4.8±0.3
125.8	145.0	1.15	12.5±0.7	4.3±0.4

TABLE 2

Summary of the radiative properties of the 2^+ (11.52 MeV) and 0^+ (12.05 MeV) levels of ^{16}O (ground-state transitions)

2^+ (11.52 MeV)			
$\Gamma_{\gamma 0}$ (eV)	R_{tr} (fm)	$B(E2: 2 \rightarrow 0)$ (fm)^4	Ref.
0.61±0.03	3.9±0.1	3.7±0.2	a, e)
0.59±0.07	3.8±0.5	3.6±0.4	c, d)
0.56±0.03	3.9±0.2	3.4±0.2	a)

0^+ (12.05 MeV)	
M_0 (fm^2)	Ref.
4.03±0.09	b, e)
4.44±0.10	a, e)
4.40±0.44	c, d)
4.08±0.12	a)

R_{tr} and M_0 represent the transition radius and monopole matrix element, respectively.

a) Present experiment, Born approximation.
b) Present experiment, corrected for Coulomb distortion.
c) Ref. [4]. d) Ref. [22]. e) Ref. [5].

[4] M. Stroetzel, Z. Phys. 214, 357 (1968).

[5] X. K. Maruyama, Ph. D. thesis, MIT (1970) unpublished.

[22] H. Theissen, Springer Tracts Mod. Phys. 65. 1 (1972).

REF.

J.C. Bergstrom, I.P. Auer, F.J. Kline, H.S. Caplan
Nucl. Phys. A213, 609 (1973)

ELEM. SYM.	A	Z
O	16	8

METHOD

REF. NO. 73 Be 17 egf

REACTION	RESULT	EXCITATION ENERGY	SOURCE TYPE	SOURCE RANGE	DETECTOR TYPE	DETECTOR RANGE	ANGLE
E,E/	FMF	9, 10	D	100-126	MAG-D		DST

9=9.85, 10=10.34

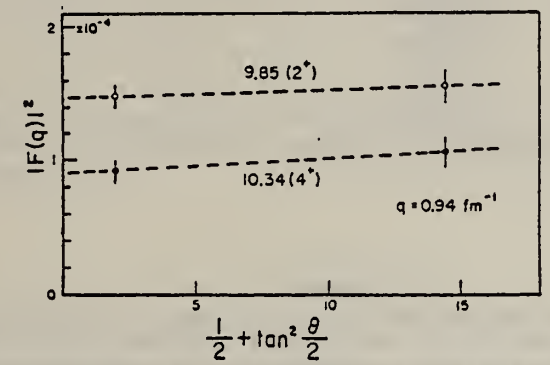

Fig. 3. Angular distribution of the total form factors of the 2⁺ (9.85 MeV) and 4⁺ (10.34 MeV) levels, at $q \approx 0.94$ fm^{-1}. The slopes of the dashed lines correspond to the transverse form factors, while the ordinate intercepts give the longitudinal form factors.

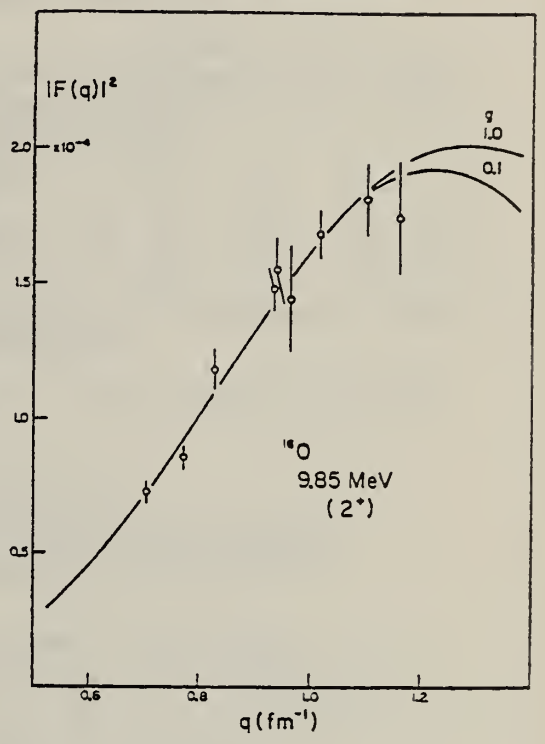

Fig. 4. Experimental form factor for the 2⁺ (9.85 MeV) level as measured in the present experiment. The solid line represents a least squares fit to the Helm model with $g = 0.1$ and 1.0 fm, as discussed in the text.

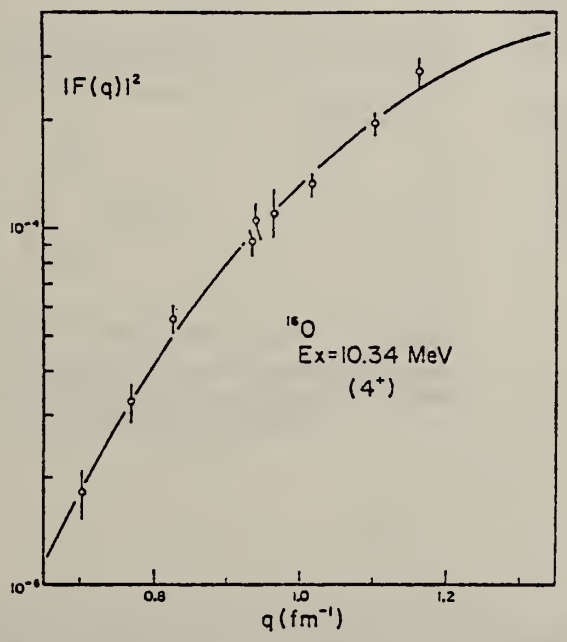

Fig. 5. Experimental form factor for the 4⁺ (10.34 MeV) level as measured in the present experiment. The solid line represents a Helm model fit.

(over)

TABLE 1

Form factors for levels in ^{16}O as measured in the present experiment

E_i (MeV)	θ (deg.)	q (fm^{-1})	$\lvert F(q)\rvert^2 \times 10^4$ E_x(MeV)	
			9.85	10.34
125.9	70.0	0.703	0.73±0.04	0.18±0.03
100.8	105.0	0.769	0.86±0.04	0.33±0.04
125.8	85.0	0.827	1.18±0.08	0.56±0.05
125.8	100.0	0.936	1.48±0.08	0.92±0.08
101.4	150.0	0.940	1.55±0.12	1.05±0.12
118.3	115.0	0.964	1.44±0.20	1.11±0.17
125.7	113.0	1.017	1.68±0.09	1.33±0.10
125.7	129.8	1.103	1.31±0.13	1.97±0.14
125.8	145.0	1.162	1.74±0.21	2.74±0.24

The momentum transfer q corresponds to 10.00 MeV excitation.

TABLE 2

Radiative widths $\Gamma'_{\gamma 0}$ for ground-state transitions and transition radii R_{tr} obtained from Helm model analysis of the 2^+ (6.92 MeV), 2^+ (9.85 MeV) and 4^+ (10.34 MeV) form factors of ^{16}O

E_x (MeV)	λ	$\Gamma_{\gamma 0}$ (meV)	R_{tr} (fm)
6.92	E2	130±9	4.3±0.2
9.85	E2	8.8±1.7	2.8±0.5
10.34	E4	$(5.6\pm2.0)\times10^{-3}$	4.3±0.8

REF. F. Brochard, P. Chevallier, D. Disdier, V. Rauch, and F. Scheibling
J. de Physique 34, 363 (1973)

ELEM. SYM.	A	Z
O	16	8

METHOD

REF. NO. 73 Br 23 egf

REACTION	RESULT	EXCITATION ENERGY	SOURCE TYPE	SOURCE RANGE	DETECTOR TYPE	DETECTOR RANGE	ANGLE
P,G	ABX	12- 13	D	0- 1	SCD-D		DST
A,G	ABX	12- 13	D	6- 8	SCD-D		DST

12.44, 13.09

Abstract. — Desexcitations of the 1⁻ levels situated at 12.44 and 13.09 MeV in ^{16}O have been studied and two new transitions were observed. A new determination of the parameters of the two 1⁻ levels was made.

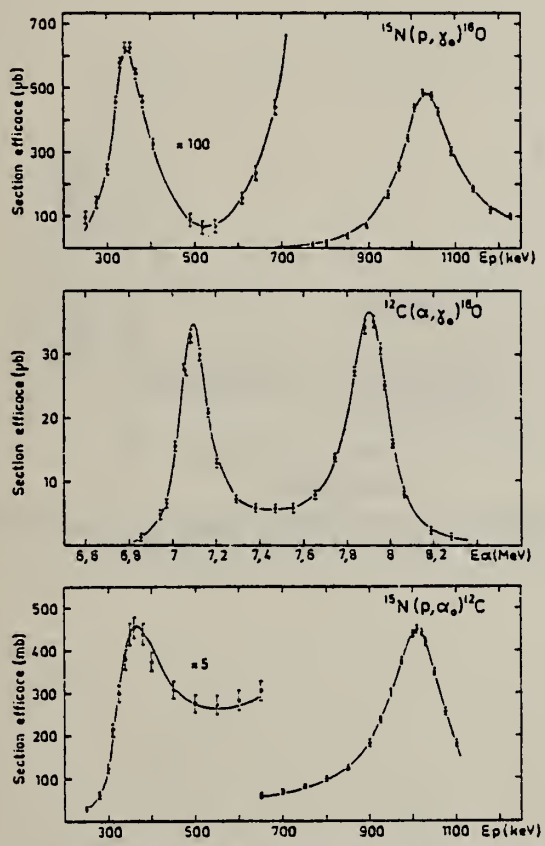

FIG. 3. — Comparaison des fonctions d'excitations théoriques obtenues à l'aide d'une formule à deux niveaux avec les valeurs expérimentales correspondantes.

TABLEAU III

Paramètres des niveaux situés à 12,44 *et* 13,09 MeV *déduits dans le formalisme de la matrice S en utilisant une formule à deux niveaux*

Niveaux (MeV)	Γ_p (keV)	Γ_{α_0} (keV)	Γ_{γ_0} (eV)	Γ (keV)	q_n (a)
12,44	1,25	95,3	9,5	96,5	0,988
13,09	95,5	39,5	44	135	1,2

(a) q_n représente le facteur défini par J. Humblet et L. Rosenfeld [15].

Nucl. Phys. 26 (1961) 529.

TABLEAU IV

Comparaison des largeurs réduites $\gamma^2_{\alpha_0}$, γ^2_p *et* Γ_{γ_0} *relatives aux niveaux* 12,44 *et* 13,09 *déterminées par D. F. Hebbard et lors de cette expérience (exprimées en* keV)

Niveaux (MeV)	D. F. Hebbard $\gamma^2_{\alpha_0}$	D. F. Hebbard γ^2_p	D. F. Hebbard Γ_{γ_0} (eV)	Nos résultats $\gamma^2_{\alpha_0}$	Nos résultats γ^2_p	Nos résultats Γ_{γ_0} (eV)
12,44	19,8	354	12,8	17,1	434	9.5
13,09	4,27	450	88	6,1	471	44

TABLEAU V

Largeurs partielles électromagnétiques des deux niveaux 1⁻ *situés à* 12,44 *et* 13,09 MeV *déterminées au cours de ce travail*

Transitions (MeV)	Γ (eV)
13,09 → 0	44 ± 8
12,44 → 0	9,5 ± 1,7
12,44 → 6,05	0,12 ± 0,06
13,09 → 7,12	1,35 ± 0,4

REF. V. di Napoli, F. Salvetti, M.L. Terranova, H.G. de Carvalho, and J.B. Martins
Phys. Rev. C8, 206 (1973)

ELEM. SYM.	A	Z
O	16	8

METHOD

REF. NO. 73 Di 4 hmg

REACTION	RESULT	EXCITATION ENERGY	SOURCE TYPE	SOURCE RANGE	DETECTOR TYPE	DETECTOR RANGE	ANGLE
G,SPL	ABY	THR-999	C	999	ACT-I		4PI

999 = 1 GEV

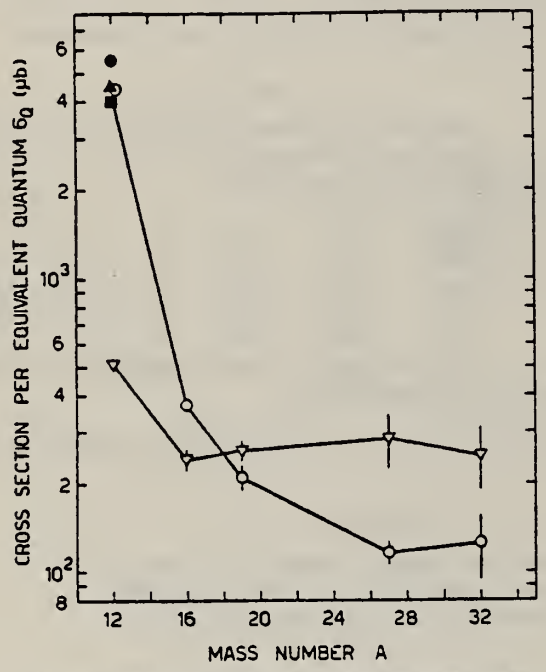

FIG. 3. Yields of ^{11}C and ^{7}Be versus the mass number of the target nucleus. Filled circle: ^{11}C, Ref. 16. Filled triangle: ^{11}C, Ref. 17. Filled square: ^{11}C, Ref. 8. Open circles: ^{11}C, present work. Reversed open triangles: ^{7}Be, present work.

[8] G. Anderson et al., Nucl. Phys. A197, 44 (1972).

[16] V. di Napoli et al., Nuovo Cimento 55B, 95 (1968).

[17] A. Masaike, J. Phys. Soc. Japan 19, 427 (1964).

REF. P. Dougan and W. Stiefler
Z. Physik 265, 1 (1973)

ELEM. SYM.	A	Z
O	16	8

METHOD

REF. NO. 73 Do 9 egf

REACTION	RESULT	EXCITATION ENERGY	SOURCE		DETECTOR		ANGLE
			TYPE	RANGE	TYPE	RANGE	
G,XP	ABY	92-400	C	400	TEL-D		DST

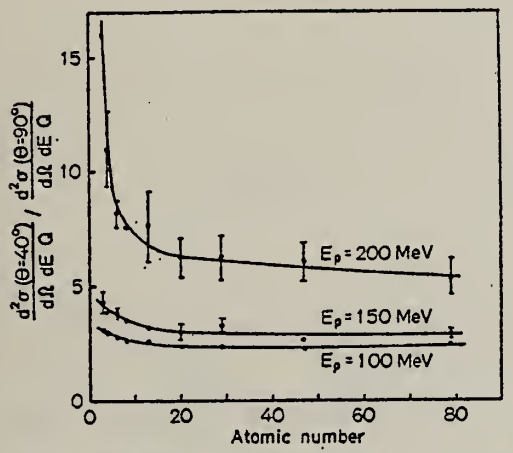

Fig. 6. The ratios of the experimental cross-sections at 40 and 90 degrees for selected proton energies as a function of atomic number

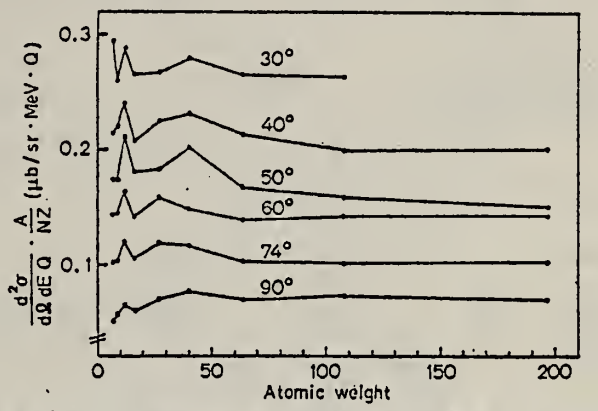

Fig. 8. Experimental cross-sections at various angles for $E_p = 150$ MeV divided by NZ/A plotted as a function of atomic weight

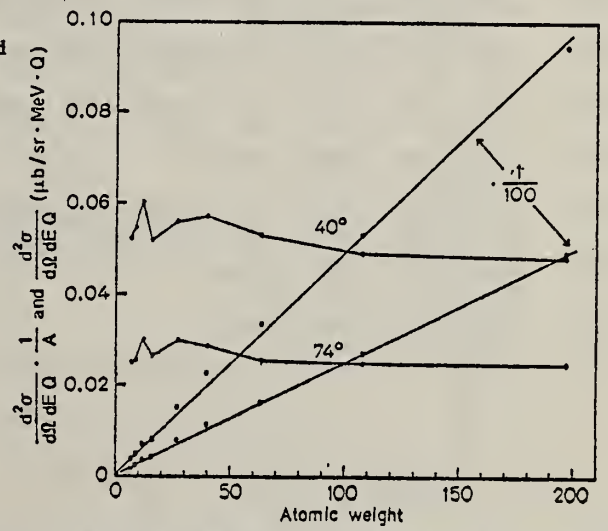

Fig. 9. In this figure, the straight lines show the experimental cross-sections at 40° and 74° for $E_p = 150$ MeV. The other curves are the same cross-sections divided by atomic weight

(over)

Table 5. Oxygen. Bremsstrahlung endpoint energy: 400 MeV. Differential cross-sections in microbarns/sterrad · MeV · eq. quantum. Quoted errors: statistical in percent

Energy	Angle							
	22	30	40	50	60	74	90	110
83.6	4.93 2.0	4.45 2.0	3.13 1.8	2.34 2.0	1.87 2.0	1.45 2.0	1.17 2.2	0.872 2.4
101.2	3.91 2.5	3.20 2.5	2.03 2.4	1.61 2.6	1.38 2.5	1.12 2.5	0.805 2.9	0.579 3.2
108.0	3.48 2.4		1.80 1.8		1.18 2.3	0.924 2.3	0.650 2.4	0.498 2.8
113.1		2.50 2.2	1.61 2.2	1.34 2.4				
118.0	2.77 2.9	2.05 3.1	1.49 2.7	1.15 3.0	1.02 2.9	0.770 3.0	0.576 3.4	0.345 4.1
130.4	2.22 3.1		1.15 2.4		0.821 2.9	0.604 3.0	0.384 3.3	0.257 4.0

Table 5 (continued)

Energy	Angle							
	22	30	40	50	60	74	90	110
134.9		1.41 3.0	1.12 2.8	0.925 3.0				
149.3			0.793 2.4					
151.4	1.30 4.2		0.782 2.9		0.537 3.7	0.410 3.7	0.219 4.5	0.129 5.8
155.6		0.945 3.7	0.754 3.4	0.743 3.6				
167.7			0.597 2.9					
174.5	0.803 2.9	0.682 2.5	0.621 2.6	0.477 2.7	0.377 2.9	0.247 3.5	0.125 4.9	
185.7			0.465 3.3					
191.3	0.577 3.6	0.529 3.0	0.442 3.2	0.363 3.2	0.258 3.7	0.148 4.7	0.0704 6.9	
207.8	0.403 4.3	0.369 3.5	0.333 3.6	0.233 4.0	0.169 4.5	0.0812 6.3	0.0319 10.2	
226.4	0.344 4.6	0.287 3.8	0.219 4.3	0.195 5.1	0.103 6.9	0.0429 10.1	0.0178 14.0	
242.6	0.244 5.8	0.190 5.6	0.135 5.7	0.128 6.6	0.0504 10.2	0.0195 15.6	0.00615 25.0	
254.0	0.187 4.3	0.148 5.4	0.0983 5.7	0.0579 8.1				
258.8	0.139 7.5	0.116 6.2	0.0744 7.5	0.0665 8.9	0.0268 13.9	0.00826 23.6	0.00259 37.8	
269.1	0.101 6.1	0.0862 7.4	0.0571 7.8	0.0250 12.7				
284.8	0.0653 7.4	0.0367 11.1	0.0286 10.8	0.0143 16.4				

REF. H. Hartmann, H. Hoffmann, B. Mecking, G. Noldeke
PICNS-73, Vol.II, p.967 (1973) Asilomar

ELEM. SYM.	A	Z
O	16	8

METHOD

REF. NO. 73 Ha 9 egf

REACTION	RESULT	EXCITATION ENERGY	SOURCE		DETECTOR		ANGLE
			TYPE	RANGE	TYPE	RANGE	
G,PN *	ABX	100-350	C	500	TEL-D		63
G,PD **							
G,PP ***							

Neutron angle 63°; proton angle varied 80°-90° to keep deuteron kinematics for PN. For PD kept angles fixed by free ^{3}He(γ,p)D kinematics.

* PN COINC
** PD COINC
*** PP COINC

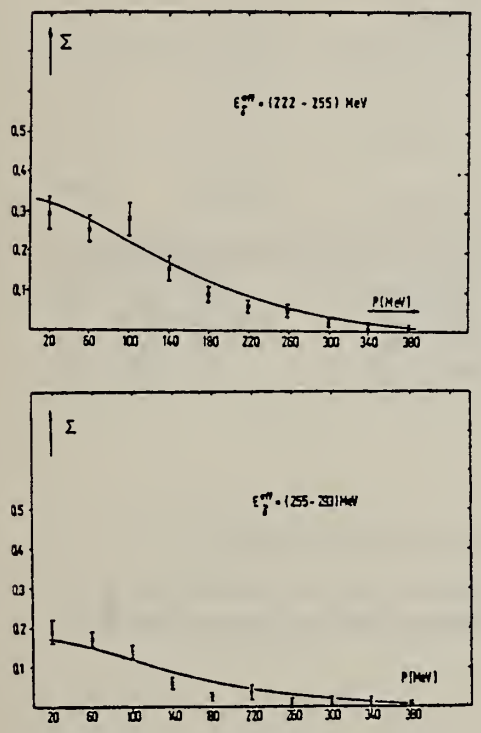

Fig. 9. Σ for the (γ,pd)-process

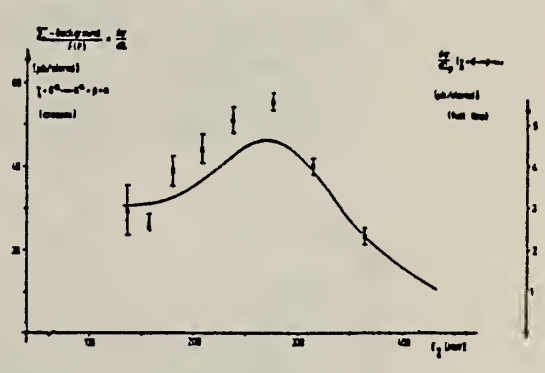

Fig. 8. Cross section for the (γ,pn)-process

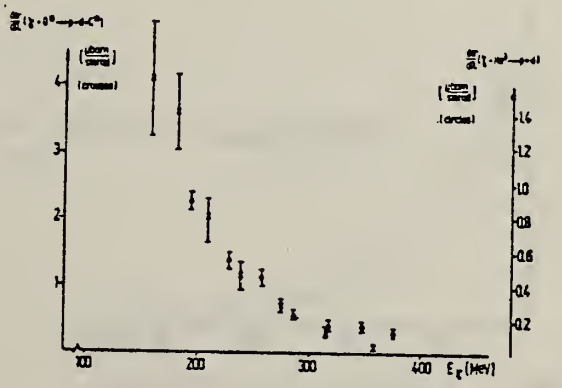

Fig.10. Cross section for the (γ,pd)-process

(over)

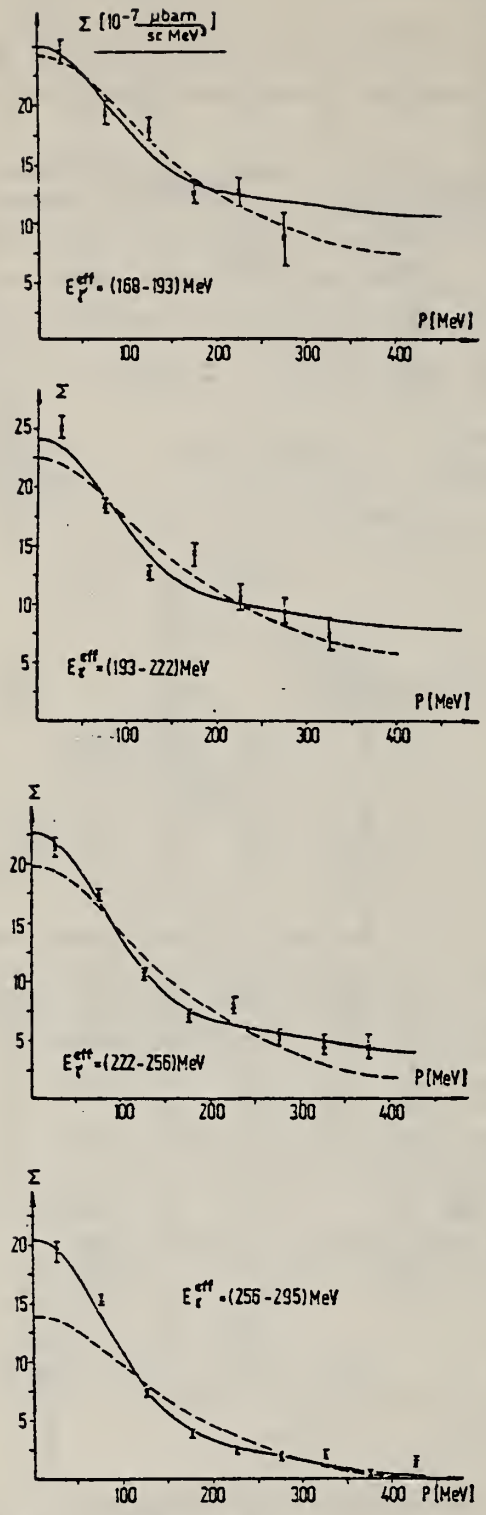

Fig. 7. Σ for the (γ,pn)-process

REF.

Stanley S. Hanna
PICNS-73, Vol. I, p.417 (1973) Asilomar

ELEM. SYM.	A	Z
O	16	8

METHOD

REF. NO.: 73 Ha 15 egf

REACTION	RESULT	EXCITATION ENERGY	SOURCE TYPE	SOURCE RANGE	DETECTOR TYPE	DETECTOR RANGE	ANGLE
P,G	ABX	22 (22.2)	D	11 (10.8)	NAI-D		90

Table IV. Summary of cross section measurements for (γ,p_o) and (γ,n_o) reactions on ^4He, ^{12}C, and ^{16}O. Underlined values are essentially the consensus of several values.

	E_x (MeV)	$\sigma(\gamma,p_o)$ in mb		$\sigma(\gamma,n_o)$ in mb	
		New[a]	Old	New	Old
^4He	26.0	1.95 ± 0.13	<u>1.84</u>[b]	<u>2.0</u>[c]	1.0[d]
^{12}C	22.5	12.2 ± 1.2	13.4[e], 8.0[f]	<u>6.0</u>[g]	6.0[h]
^{16}O	22.2	9.6 ± 1.5	8.8[i], 12.2[j]	~ 7.2[k]	9.1[h], 7.2[l]

a) Ref. 25
b) Refs. 30-32
c) Refs. 22-24
d) Ref. 33
e) Ref. 34
f) Ref. 35
g) Ref. 36,37
h) Ref. 38
i) Ref. 39
j) Ref. 40
k) Ref. 41
l) Ref. 42

See also 730c1 which gives $\sigma(\gamma,p_o)$ = 12.8 mb.

Note Stanford annual report to NSF dated August 1974 withdraws the cross section values quoted here for O-16.

(over)

[22] W. R. Dodge and J. J. Murphy, II, Phys. Rev. Letters 28, 839 (1972).

[23] J. D. Irish, R. G. Johnson, B. J. Thomas, B. L. Berman, K. G. McNeill, and J. W. Jury, contribution to this conference.

[24] D. V. Webb, C. K. Malcolm, Y. M. Smith, and D. M. Skopik, contribution to this conference.

[25] J. R. Calarco, G. A. Fisher, E. M. Diener, C. C. Chang, and S. S. Hanna, to be published.

[26] J. E. Brolley, Jr., T. M. Putman, and Louis Rosen, Phys. Rev. 107, 820 (1957).

[27] J. L. Detch, Jr., R. L. Hutson, N. Jarmie, and J. H. Jett, Phys. Rev. C4, 52 (1971).

[28] M. Suffert, W. Feldman, J. Mahieux, and S. S. Hanna, Nucl. Instr. and Meth. 63, 1 (1968).

[29] B. L. Berman, private communication.

[30] M. Suffert, private communication.

[31] J. E. Perry, Jr. and S. J. Bame, Jr., Phys. Rev. 99, 1368 (1955).

[32] W. E. Meyerhof, M. Suffert, and W. Feldman, Nucl. Phys. A148, 211 (1970); the cross sections in this paper are based on Ref. 31.

[33] B. L. Berman, S. C. Fultz, and M. A. Kelly, Phys. Rev. C4, 723 (1971); B. L. Berman, F. W. K. Firk, and C. P. Wu, Nucl. Phys. A179, 791 (1972).

[34] R. G. Allas, S. S. Hanna, L. Meyer-Schützmeister, and R. E. Segel, Nucl. Phys. 58, 122 (1964).

[35] C. Brassard, H. D. Shay, J. P. Coffin, W. Scholz, and D. A. Bromley, Phys. Rev. C6, 53 (1972).

[36] J. W. Jury, J. S. Hewitt, and K. G. McNeill, contribution to this conference.

[37] B. L. Berman et al., contribution to this conference.

[38] C. P. Wu, F. W. K. Firk, and T. W. Phillips, Phys. Rev. Letters 20, 1182 (1968).

[39] E. D. Earle and N. W. Tanner, Nucl. Phys. A95, 241 (1967).

[40] J. E. E. Baglin and M. N. Thompson, Nucl. Phys. A138, 73 (1969).

[41] D. B. C. B. Syme and G. I. Crawford, contribution to this conference.

[42] J. T. Caldwell, R. L. Bramblett, B. L. Berman, R. R. Harvey, and S. C. Fultz, Phys. Rev. Letters 15, 976 (1965).

REF. C. Hemmer, R. Stock, K. Wienhard, H. Wolf
PICNS-73, Vol.I, p.265 Asilomar

ELEM. SYM.	A	Z
O	16	8

METHOD

REF. NO. 73 He 10 hmg

REACTION	RESULT	EXCITATION ENERGY	SOURCE		DETECTOR		ANGLE
			TYPE	RANGE	TYPE	RANGE	
G,P	SPC	12- 30	C	30	TEL-D		90

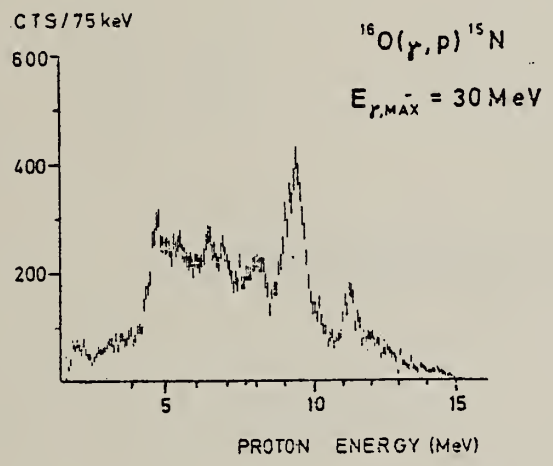

Fig. 2. Proton energy spectra from the reaction $^{16}O(\gamma,p)^{15}N$.
The data are corrected for the energy loss in the target.

REF. R. Nath, G.W. Cole, F.W.K. Firk, R.J. Holt, H.L. Schultz
PICNS-73, Vol.I, p.163 Asilomar

ELEM. SYM.	A	Z
0	16	8

METHOD

REF. NO. 73 Na 6 hmg

REACTION	RESULT	EXCITATION ENERGY	SOURCE		DETECTOR		ANGLE
			TYPE	RANGE	TYPE	RANGE	
$ G,N	NOX	15- 28	D	30, 64	TOF-D		DST

POLARIZED G.S. NEUTRONS

See other side for figure.

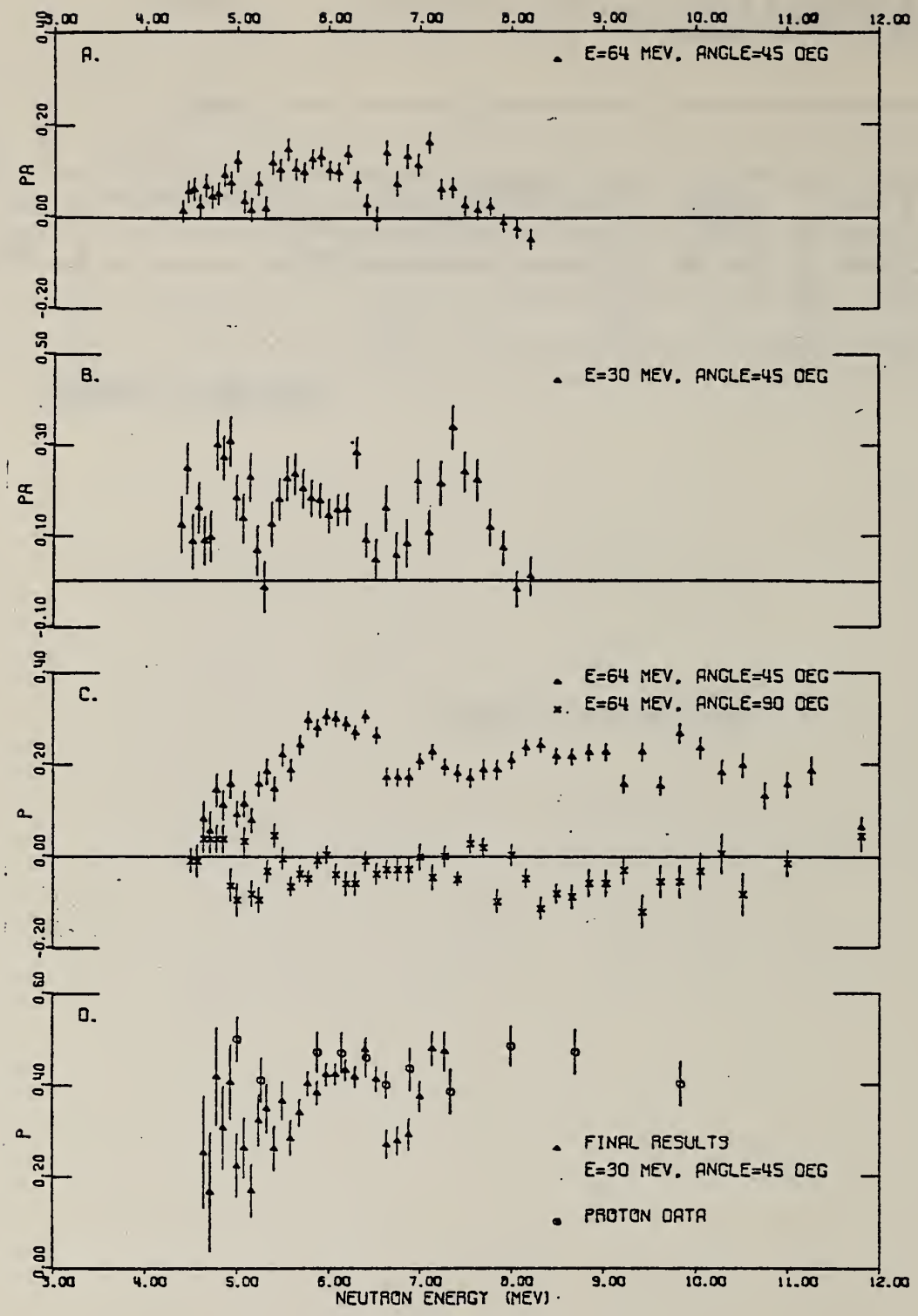
A.
E=64 MEV. ANGLE=45 DEG
PA
B.
E=30 MEV. ANGLE=45 DEG
PA
C.
E=64 MEV. ANGLE=45 DEG
E=64 MEV. ANGLE=90 DEG
P
D.
FINAL RESULTS
E=30 MEV. ANGLE=45 DEG
PROTON DATA
P
NEUTRON ENERGY (MEV)

FIG. 1

REF. W.J. O'Connell, G.L. Latshaw, J.L. Black, S.S. Hanna
PICNS-73, Vol.II, p.939 (1973) Asilomar

ELEM. SYM.	A	Z
O	16	8

METHOD

REF. NO. 73 O'C 1 egf

REACTION	RESULT	EXCITATION ENERGY	SOURCE		DETECTOR		ANGLE
			TYPE	RANGE	TYPE	RANGE	
P,G	ABX	20- 29	D	8- 18	NAI-D		DST

Table I Resonance Parameters Extracted from Fit

E_x(MeV)	Γ(MeV)	$\frac{(\Gamma_{p;\ell=0} + \Gamma_{p;\ell=2})\Gamma_\gamma}{\Gamma}$ (eV)
20.945 ± .002	0.317 ± .006	21.0 ± 4%
22.146 ± .005	0.725 ± .008	488.2 ± 4%
22.888 ± .013	0.320 ± .014	68.8 ± 7%
24.065 ± .030	0.591 ± .036	130. ± 10%
25.117 ± .065	3.15 ± .320	651. ± 18%

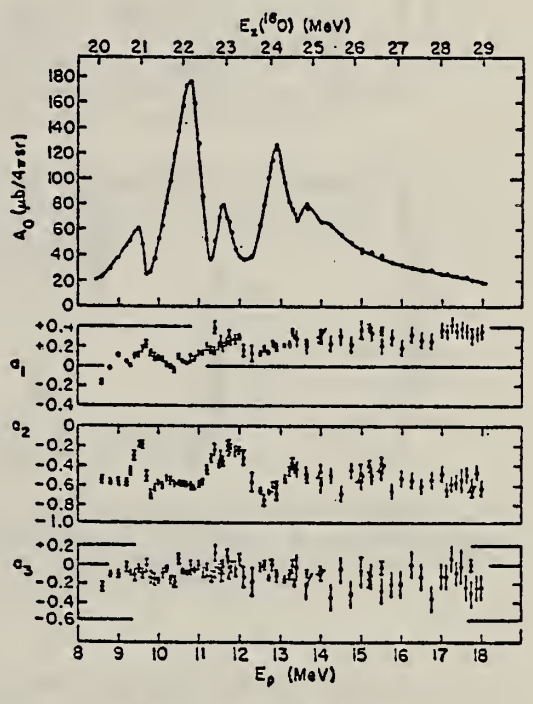

Fig.1 Legendre coefficients for $^{15}N(p,\gamma_0)$ angular distributions fitted up to ℓ=3. The curve is drawn to guide the eye.

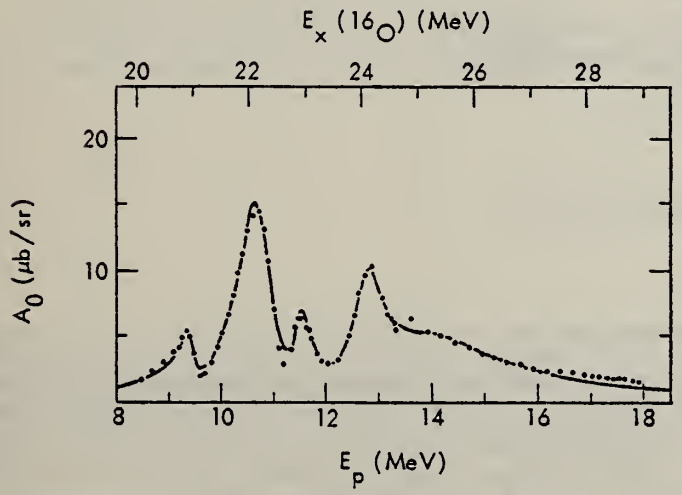

Fig.2 $^{15}N(p,\gamma_0)$ total cross section, fitted in the interval E_p = 8.8 - 16.25 MeV with a Breit-Wigner resonance formula with five $J^\pi = 1^-$ resonances

REF. S.H. Chew, J. Lowe, J.M. Nelson, and A.R. Barnett
Nucl. Phys. A229, 241 (1974)

EL EM. SYM.	A	Z
O	16	8

METHOD

REF. NO. 74 Ch 8 egf

REACTION	RESULT	EXCITATION ENERGY	SOURCE		DETECTOR		ANGLE
			TYPE	RANGE	TYPE	RANGE	
P,G	RLX	21- 30	D	9- 19	NAI-D		90

Cross section normalized to 730cl (W.J. O'Connell et al., PICNS-73, 939 (1973) Asilomar)

Data on $^{13}C(^3He,\gamma_{1+2})$ and $^{13}C(^3He,\gamma_{3+4})$ also given.

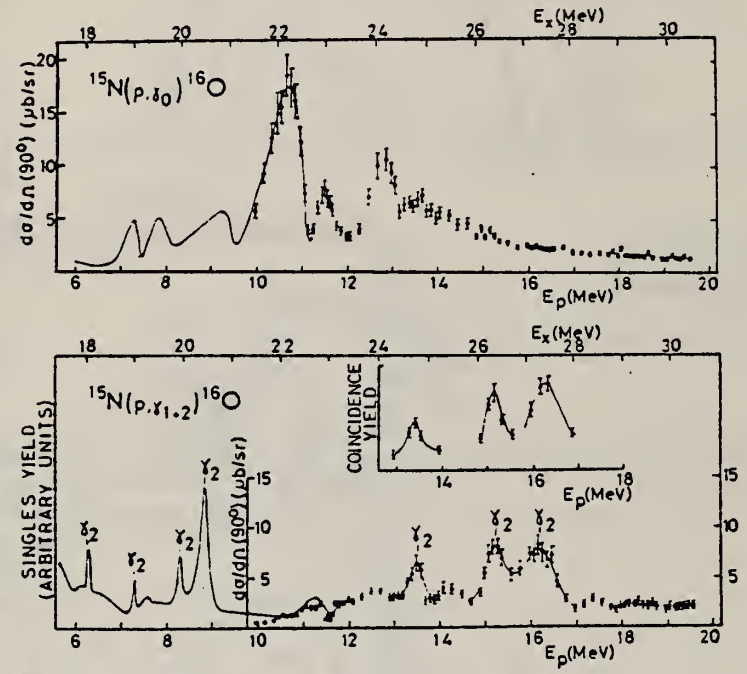

Fig. 3. Excitation functions from the present work for $^{15}N(p,\gamma_0)^{16}O$ and $^{15}N(p,\gamma_1+\gamma_2)^{16}O$ ($E_p > 10$ MeV). For $E_p < 12$ MeV, the yield curve from ref. [1]) is shown. The peaks denoted γ_2 have been found by coincidence measurements to decay through the 6.13 MeV, $J^\pi = 3^-$ state. The coincidence yield curve for $^{15}N(p,\gamma_2\gamma_{6.13})^{16}O$ is also shown.

1
A.R. Barnett and N.W. Tanner, Nucl. Phys. A152 (1970) 257

Abstract: Measurements are reported of the excitation function for $^{15}N(p,\gamma_1+\gamma_2)^{16}O$. Together with earlier data, the range $E_p = 6$–19.6 MeV is covered and is found to contain seven resonances. Coincidence measurements are described which, together with other data, establish that all seven decay to the $J^\pi = 3^-$ state at 6.13 MeV. One of these states is tentatively identified as the giant M2 state observed in inelastic electron scattering. Three higher states are attributed to the $(1p_{\frac{1}{2}}^{-1}\,1f_{\frac{7}{2}})$ excitation. The excitation function for $^{13}C(^3He,\gamma_1+\gamma_2)^{16}O$ is also given for $E_{^3He} = 4$–12 MeV. One resonance is found, which probably decays to the $J^\pi = 0^+$ state at 6.05 MeV, and, if so, is part of the deformed giant resonance in ^{16}O.

REF.

V. DiNapoli and M.L. Terranova
J. Inorg. Nucl. Chem. 36, 3633 (1974)

ELEM. SYM.	A	Z
O	16	8

METHOD

REF. NO. 74 Di 7 egf

REACTION	RESULT	EXCITATION ENERGY	SOURCE TYPE	SOURCE RANGE	DETECTOR TYPE	DETECTOR RANGE	ANGLE
G,C11	ABY	THR* 1	C	300* 1	ACT-I		4PI

1=1 GEV

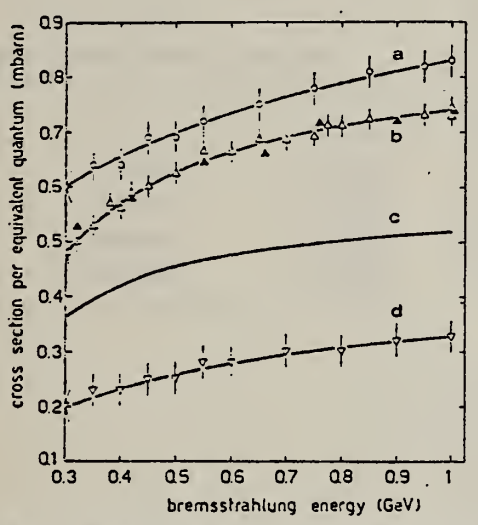

Fig. 1. Cross section per equivalent quantum σ_Q vs the bremsstrahlung maximum energy. Curve a is an eye-fit of the present work values (open circles) for the reaction ^{23}Na(γ, 2p 3n)^{18}F. Curve b is an eye-fit of the present work values (open triangles) and the values taken from Ref. [2] (filled triangles) for the reaction ^{27}Al(γ, 2p 3n)^{22}Na. Curve c is the best-fit of the present work values and values taken from Refs. [18, 20–22] for the reaction ^{12}C(γ, 2p 3n)^{7}Be; for the sake of simplicity, experimental points have not been reported. Curve d is an eye-fit of the present work values (reversed open triangles) for the reaction ^{16}O(γ, 2p 3n)^{11}C.

[2] V. di Napoli, A.M. Lacerenza, F. Salvetti, H.G. de Carvalho, and J.B. Martins, Nuovo Cimento Lettere 1, 835 (1971).

[18] V. di Napoli, D. Margadonna, F. Salvetti, H.G. de Carvalho, and J.B. Martins, Nucl.Inst. Meth. 93, 77 (1971).

[20] V. di Napoli, F. Dobici, O. Forina, F. Salvetti and H.G. de Carvalho, Lett. Nuovo Cimento 55B, 95 (1968).

[21] V. di Napoli, Nucl.Inst.Method 69, 155 (1969).

[22] V.I. Noga, Yu.N. Ranyuk, P.V. Sorokin, and V.A. Tkachenko, Ukr. J.Phys. 16, 1850 (1971) in Russian.

REF. P. Dyer and C.A. Barnes
Nucl. Phys. A233, 495 (1974)

ELEM. SYM.	A	Z
O	16	8

METHOD

REF. NO. 74 Dy 6 egf

REACTION	RESULT	EXCITATION ENERGY	SOURCE TYPE	SOURCE RANGE	DETECTOR TYPE	DETECTOR RANGE	ANGLE
A,G	ABX	8- 10	D	1- 3	NAI-D		DST

TABLE 1

$^{12}C(\alpha,\gamma)^{16}O$ angular distribution parameters

$E_{c.m.}$ (MeV)	$\lvert A_2\rvert/\lvert A_1\rvert$	$\cos\phi_{12}$
2.18	0.10 ± 0.10	$1.00^{+0.00}_{-0.55}$
2.42	0.14 ± 0.05	$0.80^{+0.20}_{-0.30}$
2.56	0.36 ± 0.06	$0.22^{+0.11}_{-0.12}$
2.83	0.58 ± 0.05	$0.09^{+0.12}_{-0.09}$

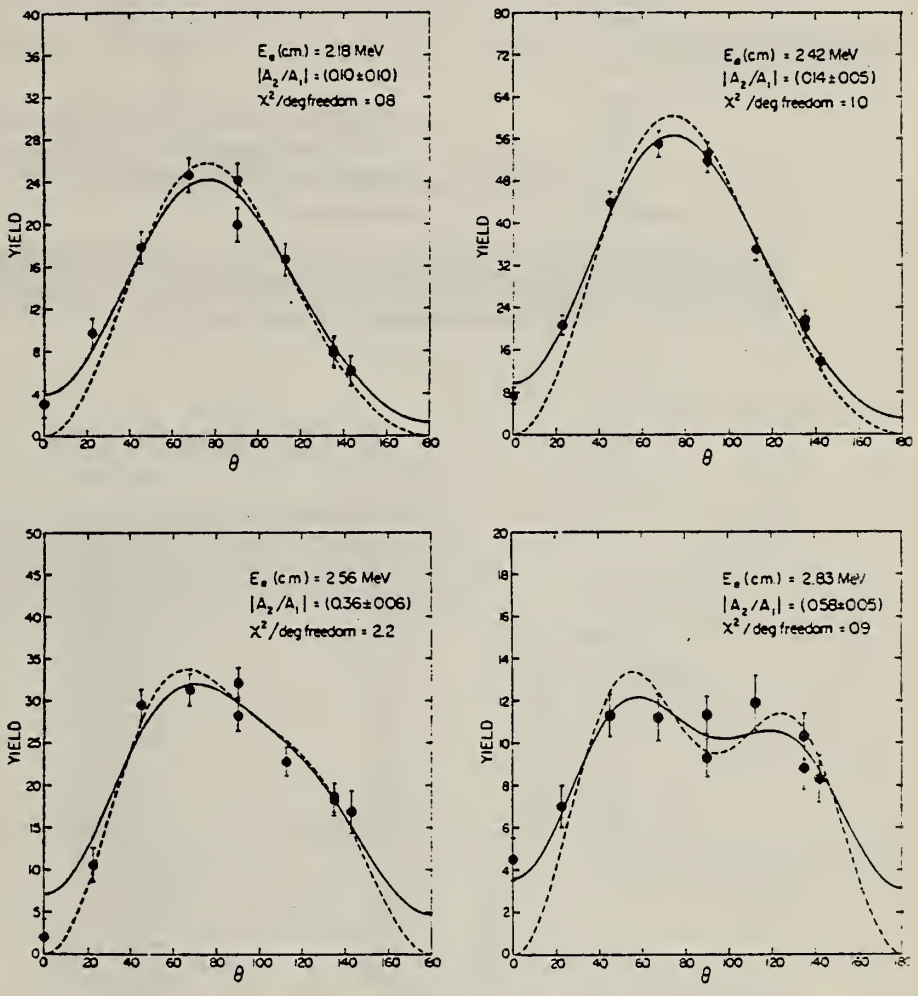

Fig. 6. $^{12}C(\alpha,\gamma)^{16}O$ angular distributions. The solid curves are fits to the data obtained by assuming interference between 1^- and 2^+ capture amplitudes, taking into account the finite size of the detectors. The dashed curves indicate the same angular distributions as they would be measured by a point detector. Yield is in arbitrary units.

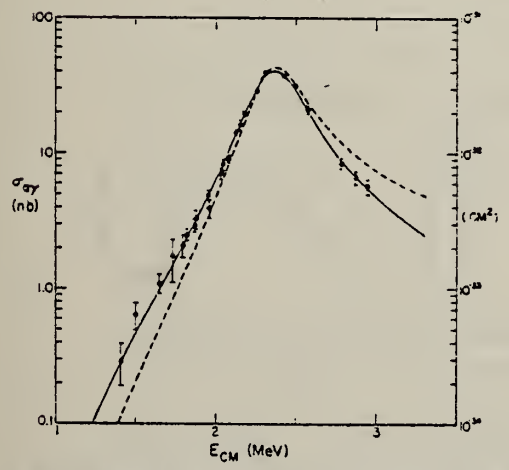

Fig. 8. Measured electric dipole contributions to the $^{12}C(\alpha,\gamma)^{16}O$ total cross sections and the "hybrid" R-matrix optical-model fits. The data are indicated by circles. The solid curve is the best fit to the data, with χ^2 per degree of freedom = 1.0. The dashed curve is a fit in which the reduced α-width of the bound 7.12 MeV state is constrained to zero, and the remaining parameter is free to vary; χ^2 per degree of freedom is 8.5. The theoretical curves for the three-level R-matrix fits are qualitatively similar.

(over)

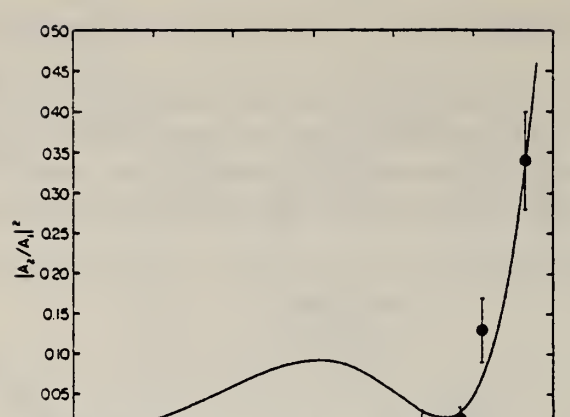

Fig. 7. Variation of the ratio $|A_2|^2/|A_1|^2$ with c.m. α-energy. The circles indicate the values derived from the angular distribution measurements. The solid curve shows the values calculated from the E2 direct capture formulation of Tombrello and Phillips [25], with θ_α^2(g.s., ^{16}O) = 0.04±0.01, and the three-level R-matrix fit to the E1 contributions.

TABLE 2

^{12}C(α, γ)^{16}O electric dipole cross sections

$E_{c.m.}$ (MeV)	σ_{E1} (nb)
1.41	0.29±0.10
1.50	0.64±0.14
1.64	1.09±0.17
1.73	1.71±0.60
1.79	2.09±0.40
1.81	2.49±0.25
1.87	2.93±0.31
1.87	3.25±0.50
1.95	4.92±0.40
1.96	3.90±0.60
2.03	7.04±0.60
2.04	8.34±0.65
2.08	9.10±0.60
2.11	14.17±0.70
2.15	16.13±1.30
2.18	19.50±0.81
2.26	28.91±1.01
2.32	39.53±1.31
2.42	37.06±1.61
2.49	31.23±1.22
2.56	20.98±1.33
2.78	8.41±0.73
2.86	6.66±0.70
2.94	5.69±0.75

[25] T.A. Tombrello and G.C. Phillips, Phys. Rev. 122 (1961) 224.

REF.

S.S. Hanna, H.F. Glavish, R. Avida, J.R. Calarco, E. Kuhlmann and R. LaCanna
Phys. Rev. Letters 32, 114 (1974)

CLASS.		
0	16	8

METHOD

REF. NO. 74 Ha 1 hmg

REACTION	RESULT	EXCITATION ENERGY	SOURCE		DETECTOR		ANGLE
			TYPE	RANGE	TYPE	RANGE	
$ P,G	ABX	20- 28	D	8- 16	NAI-D		DST

POLARIZED PROTONS

Measurements on the polarized-proton capture reaction $^{15}N(p,\gamma_0)^{16}O$ indicate a broad $E2$ resonance which lies above the giant $E1$ resonance of ^{16}O. The measurements show that the $E2$ radiation for the (γ,p_0) channel of ^{16}O exhausts approximately 30% of the quadrupole sum rule.

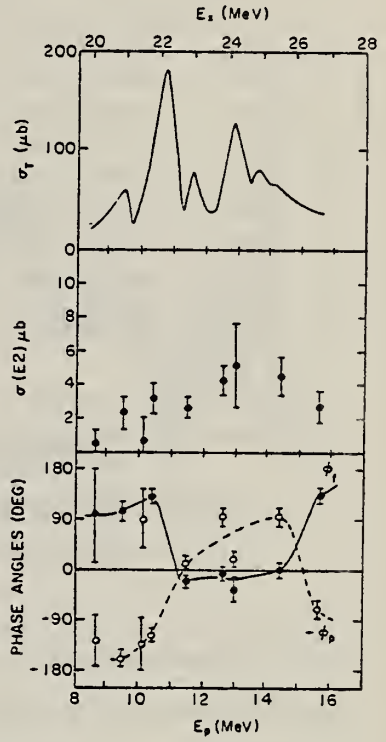

FIG. 2. Top: total cross section curve of $^{15}N(p,\gamma)^{16}O$ (Ref. 8). Middle: plot of total $E2$ cross sections derived from the analyses in Table I. Bottom: plot of the phases of the partial-wave amplitudes for proton capture leading to $E2$ radiation.

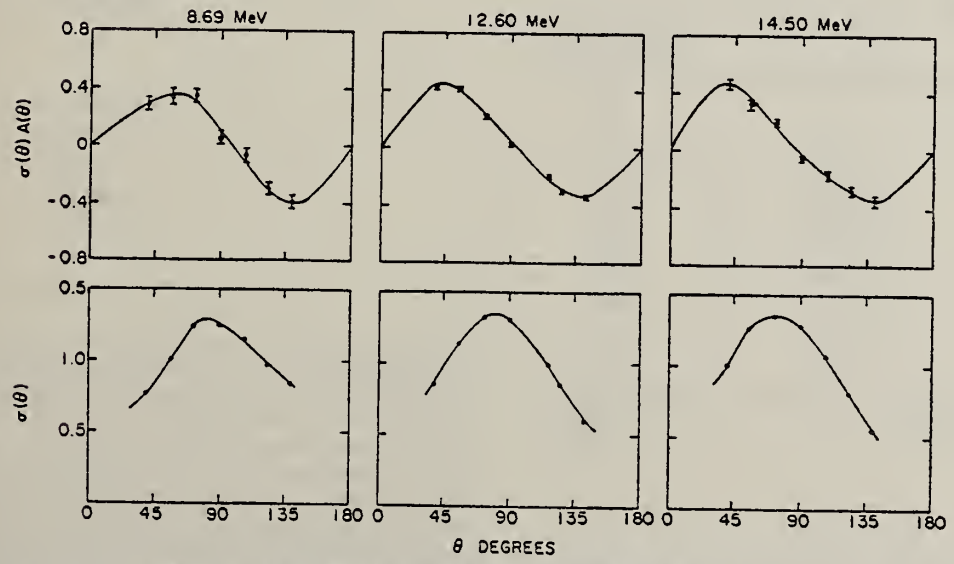

FIG. 1. Plots of $\sigma(\theta)$ and $\sigma(\theta)A(\theta)$ measured at three bombarding energies (listed at top) in the polarized-proton capture reaction $^{15}N(p,\gamma)^{16}O$. Where error bars are not shown the errors are of the same order as or smaller than the dot size. The analysis of these and all the data is given in Table I.

(over)

TABLE I. Unpolarized and polarized angular-distribution coefficients.

E_p	a_1	a_2	a_3	a_4
8.69	-0.051 ± 0.013	-0.528 ± 0.030	-0.205 ± 0.026	-0.022 ± 0.037
9.50	0.078 ± 0.029	-0.248 ± 0.048	0.129 ± 0.033	-0.053 ± 0.035
10.10	0.051 ± 0.014	-0.537 ± 0.022	-0.161 ± 0.021	-0.017 ± 0.026
10.40	0.019 ± 0.005	-0.566 ± 0.007	-0.073 ± 0.009	-0.040 ± 0.010
11.50	0.203 ± 0.066	-0.403 ± 0.011	-0.111 ± 0.011	-0.072 ± 0.015
12.60	0.158 ± 0.007	-0.640 ± 0.015	-0.156 ± 0.015	-0.022 ± 0.023
13.00	0.208 ± 0.016	-0.607 ± 0.017	-0.178 ± 0.034	-0.073 ± 0.025
14.50	0.301 ± 0.017	-0.603 ± 0.034	-0.142 ± 0.030	-0.022 ± 0.027
15.70	0.324 ± 0.029	-0.543 ± 0.079	-0.127 ± 0.043	-0.075 ± 0.074

E_p	b_1	b_2	b_3	b_4
8.69	0.066 ± 0.014	0.233 ± 0.009	-0.045 ± 0.009	-0.003 ± 0.009
9.50	0.064 ± 0.018	0.326 ± 0.008	0.000 ± 0.009	-0.010 ± 0.009
10.10	0.046 ± 0.010	0.267 ± 0.008	-0.010 ± 0.009	-0.002 ± 0.006
10.40	0.022 ± 0.006	0.301 ± 0.004	-0.015 ± 0.004	0.003 ± 0.003
11.50	-0.006 ± 0.008	0.297 ± 0.006	0.043 ± 0.005	-0.002 ± 0.005
12.60	0.061 ± 0.013	0.248 ± 0.007	0.011 ± 0.009	0.015 ± 0.006
13.00	0.064 ± 0.013	0.281 ± 0.008	0.037 ± 0.008	-0.004 ± 0.007
14.50	0.017 ± 0.020	0.246 ± 0.010	0.032 ± 0.017	0.027 ± 0.010
15.70	0.017 ± 0.018	0.244 ± 0.020	0.062 ± 0.020	0.030 ± 0.012

$$\sigma(\theta) = [\sigma_u(\theta) + \sigma_d(\theta)]/2 = A_0[1 + \sum_{k=1} a_k P_k(\cos\theta)], \quad (1)$$

$$\sigma(\theta)A(\theta) = [\sigma_u(\theta) - \sigma_d(\theta)]/2P = A_0 \sum_{k=1} b_k P_k^1(\theta), \quad (2)$$

[8] W.J. O'Connell, Ph. D. Thesis, Stanford University, 1969 (unpublished).

REF. A. Hotta, K. Itoh, and T. Saito
Phys. Rev. Lett. 33, 790 (1974)

ELEM. SYM.	A	Z
O	16	8

METHOD

REF. NO. 74 Ho 3 hmg

REACTION	RESULT	EXCITATION ENERGY	SOURCE TYPE	SOURCE RANGE	DETECTOR TYPE	DETECTOR RANGE	ANGLE
E,E/	FMF	9- 42	D	70-250	MAG-D		DST

LONG,TRANS FMF. B(E2)

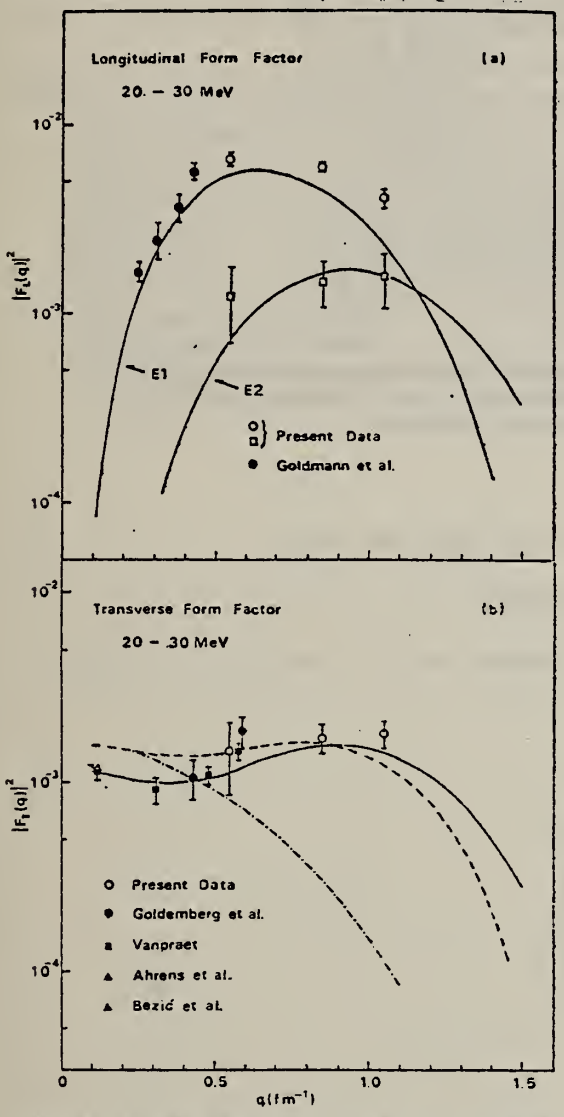

FIG. 3. (a) The longitudinal form factor for a range of 20–30 MeV as functions of q. The Darmstadt data are also plotted. The square shows the result of the subtraction of the $E1$ contribution from the experimental values. Also shown is the theoretical q dependence of the form factor for the $E1$ and $E2$ resonances. (b) The transverse form factor for the same range as for (a). The Stanford data and the photonuclear data are shown together with theoretical results calculated using the Goldhaber-Teller model (dash-dotted line), the generalized Goldhaber-Teller model (dashed line), and the particle-hole model (solid line).

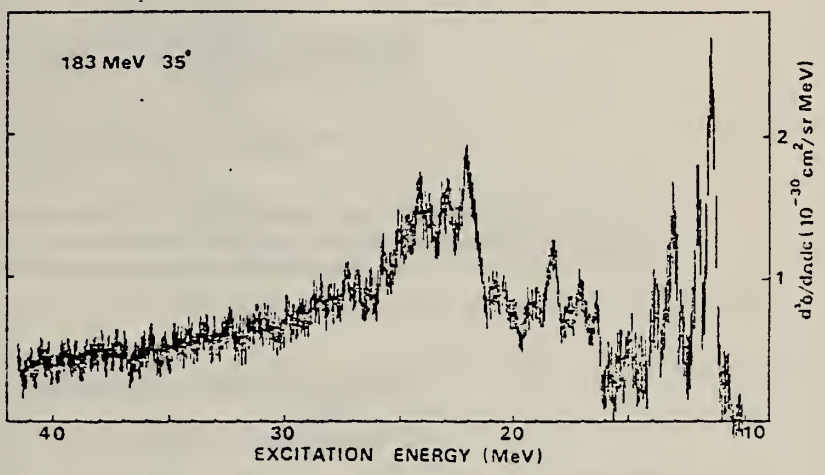

FIG. 1. Spectrum of electrons scattered from ^{16}O.

TABLE I. $B(E2)$, $B(E2)$ in Weisskopf units, and energy-weighted sum-rule (EWSR) limits.

E_x (MeV)	J^π	$B(E2)$	$B(E2)/B_W(E2)$		$E_xB(E2)$/EWSR
6.92	2^+	36 ± 4 [a]	3.0		0.11
9.85	2^+	0.67 ± 0.27 [a]	0.056		0.003
11.52	2^+	25.67 ± 2.83 [b]	2.1		0.13
13.15	2^+	13.8 [b]	1.2		0.08
15.15	2^+	8.1 ± 4.1 [c]	0.68		0.05
16.46	2^+	2.7 ± 0.9 [c]	0.22		0.02
18.5	2^+	5.1 ± 0.5	0.43		0.04
				SUM	0.43
20–30	2^+	20 ± 8	1.7		0.21

[a] Ref. 14. [b] Ref. 15. [c] Ref. 12.

(over)

U.S. DEPARTMENT OF COMMERCE
NATIONAL BUREAU OF STANDARDS

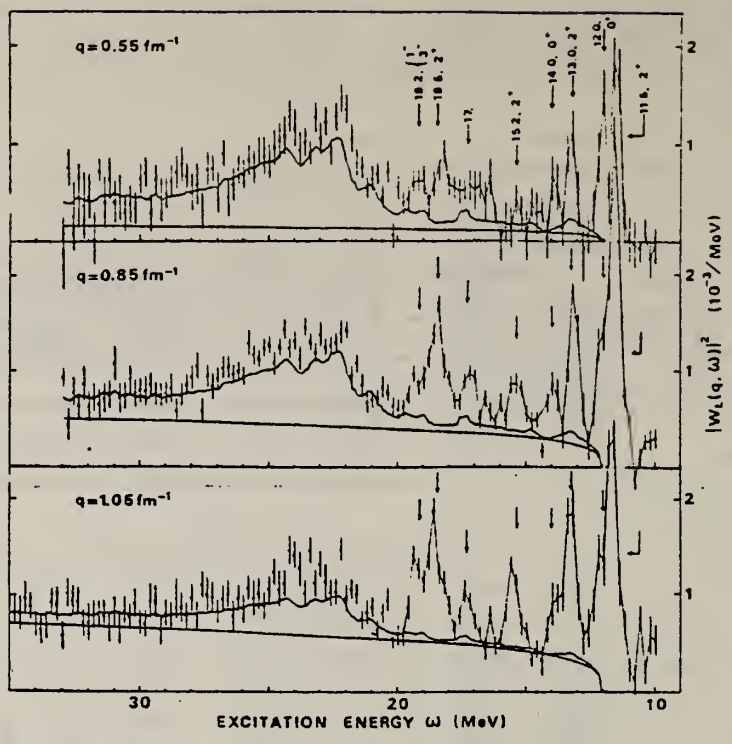

FIG. 2. The longitudinal form factors $|W_L(q,\omega)|^2$ for electroexcitation in ^{16}O from this experiment is shown as data points. The arrows show the positions of the form-factor peaks below $E_x = 20$ MeV. The middle and the lower solid curves show the total photoabsorption cross section and the continuum, respectively.

12
M. Stroetzel and A. Goldmann, Z. Phys. 233, 245 (1970).
14
M. Stroetzel, Z. Phys. 214, 357 (1968).
15
J.C. Kim, R.P. Singhal, and H.S. Caplan, Can. J. Phys. 48, 83 (1970).

REF.

C. Rolfs and W. S. Rodney
Nucl. Phys. A235, 450 (1974)

ELEM. SYM.	A	Z
O	16	8

METHOD

REF. NO.	
74 Ro 5	egf

REACTION	RESULT	EXCITATION ENERGY	SOURCE		DETECTOR		ANGLE
			TYPE	RANGE	TYPE	RANGE	
P,G	ABX	12- 15	D	0- 3	SCD-D		DST

Abstract: Excitation functions of the $^{15}N(p,\gamma)^{16}O$ proton capture reaction have been obtained at $\theta_\gamma = 45°$ and $E_p = 150$–2500 keV. Below $E_p = 400$ keV, the reaction is dominated by capture into the ground state of ^{16}O. The observed excitation function for the latter process can be explained if, in addition to the two well-known $J^\pi = 1^-$ resonances at $E_p = 338$ and 1028 keV, a direct radiative capture process (DC → 0) is included in the analysis. The direct capture component in the capture reaction is enhanced through interference effects on the tails of the two resonances. From the observed direct capture cross section, a single-particle spectroscopic factor of $C^2S(1p) = 1.8 \pm 0.4$ has been deduced for the ground state in ^{16}O. The extrapolated astrophysical S-factor of $S(0) = 64 \pm 6$ keV · b for the $^{15}N(p,\gamma_0)^{16}O$ reaction is a factor of 2.5 larger than previously reported. This result amplifies the role of the oxygen side cycle in the CNO hydrogen burning process.

The observed excitation function of the $^{15}N(p,\alpha_1\gamma_1)^{12}C$ reaction at $E_p = 150$–2500 keV shows that this reaction makes a negligible contribution to hydrogen burning at stellar energies [$S(0) \approx 0.1$ keV · b] compared to $^{15}N(p,\gamma_0)^{16}O$ and $^{15}N(p,\alpha_0)^{12}C$.

1053

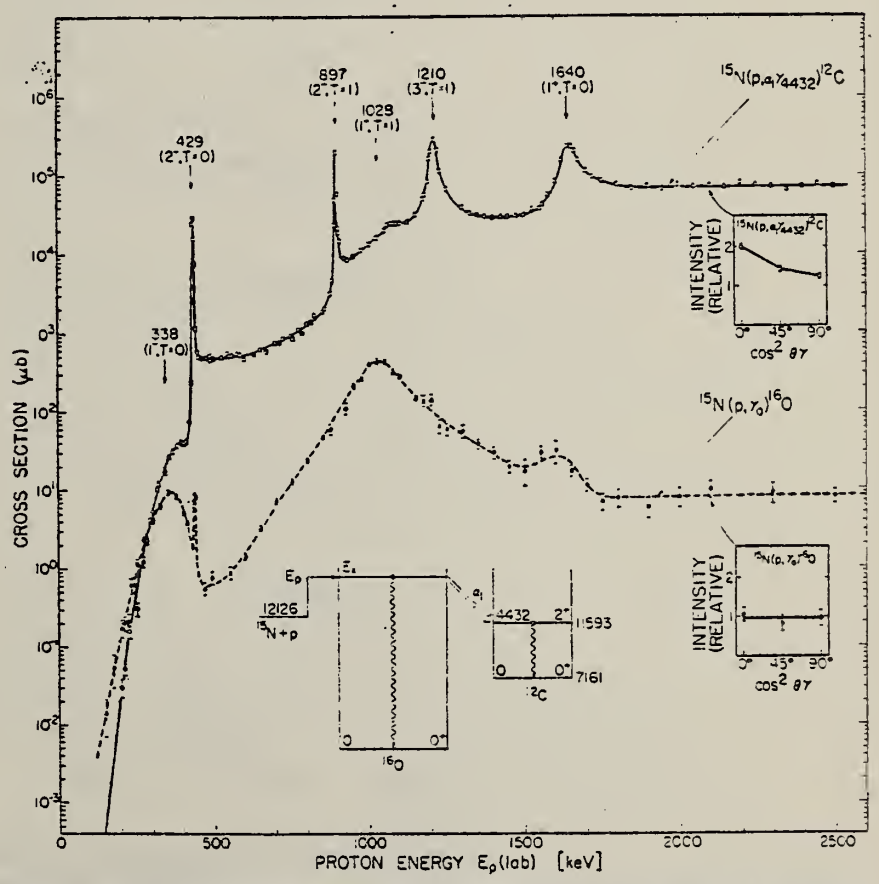

Fig. 2. Total cross sections for the $^{15}N(p,\alpha_1\gamma_1)^{12}C$ and $^{15}N(p,\gamma_0)^{16}O$ reactions are shown as a function of beam energy. The solid and dashed lines through the data points are placed to guide the eye. The insets show the γ-ray angular distributions observed at $E_p = 2.10$ MeV.

REF. H. Schier and B. Schoch
Nucl. Phys. A229, 93 (1974)

EL EM. SYM.	A	Z
O	16	8

METHOD

REF. NO. 74 Sc 8 egf

REACTION	RESULT	EXCITATION ENERGY	SOURCE TYPE	SOURCE RANGE	DETECTOR TYPE	DETECTOR RANGE	ANGLE
E,N	ABX	50-150	D	63-150	TOF-D		DST

PHOTON DIFF.

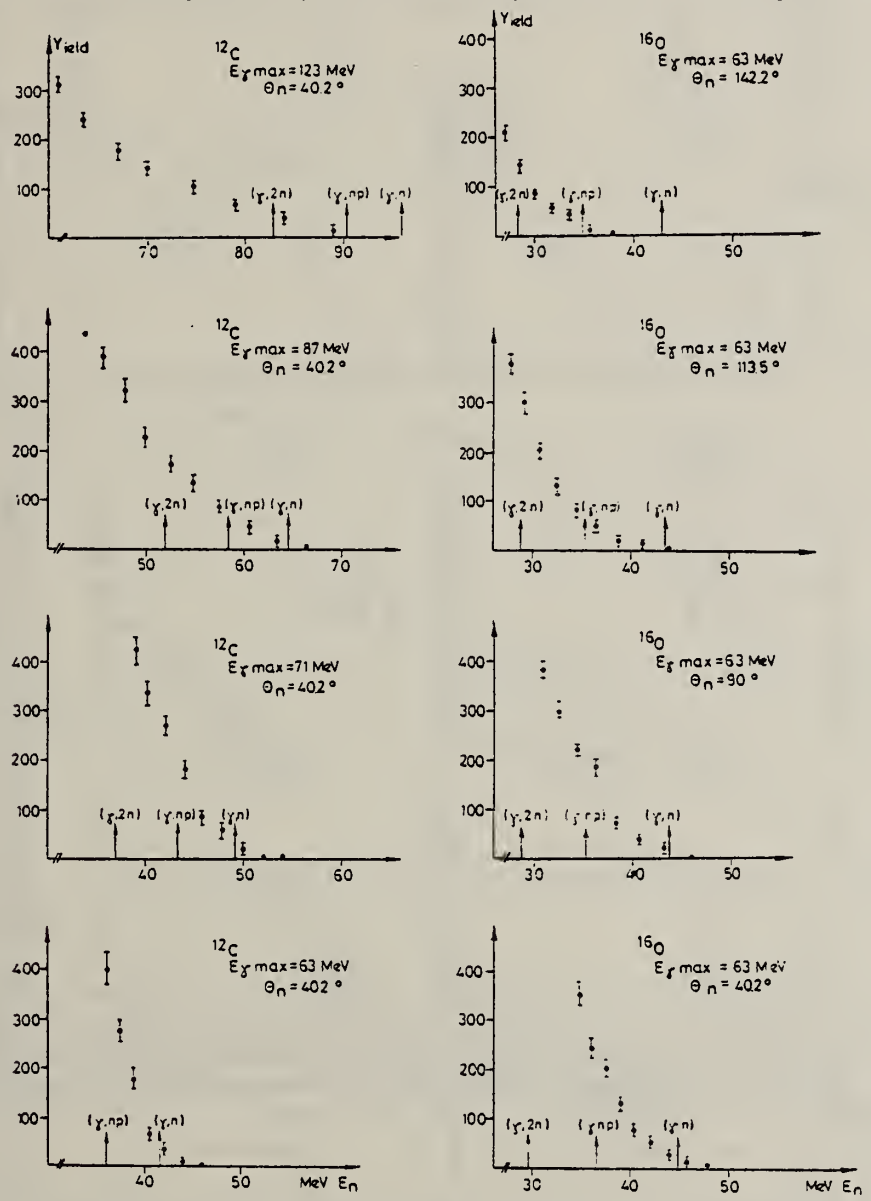

Fig. 4. Measured neutron yield. The data selected here qualitatively show the energy and angle dependence of the processes under investigation.

(over)

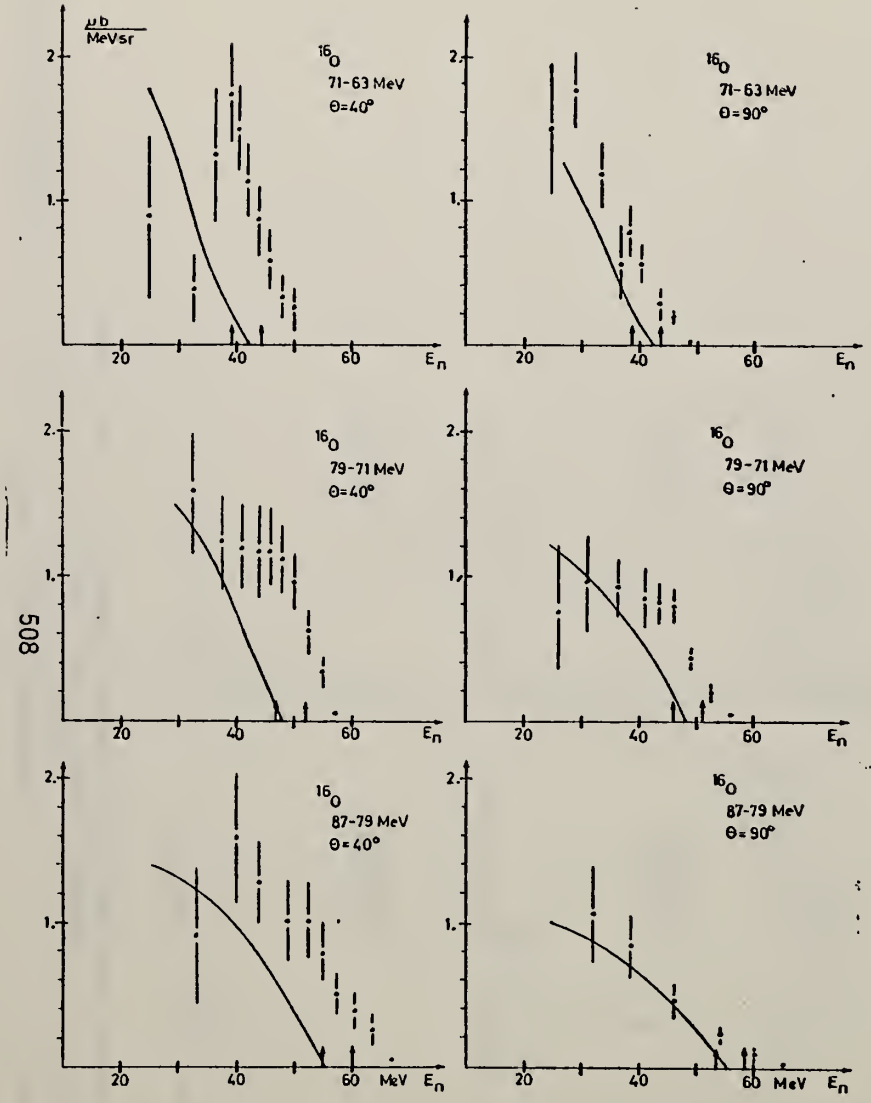

Fig. 7. Measured cross sections for the photoproduction of neutrons on ^{16}O by quasimonochromatic photons. The energy values given correspond to the photon end energies. The arrows mark the neutron energies E_n, calculated with formula (7) for the medium photon energy.

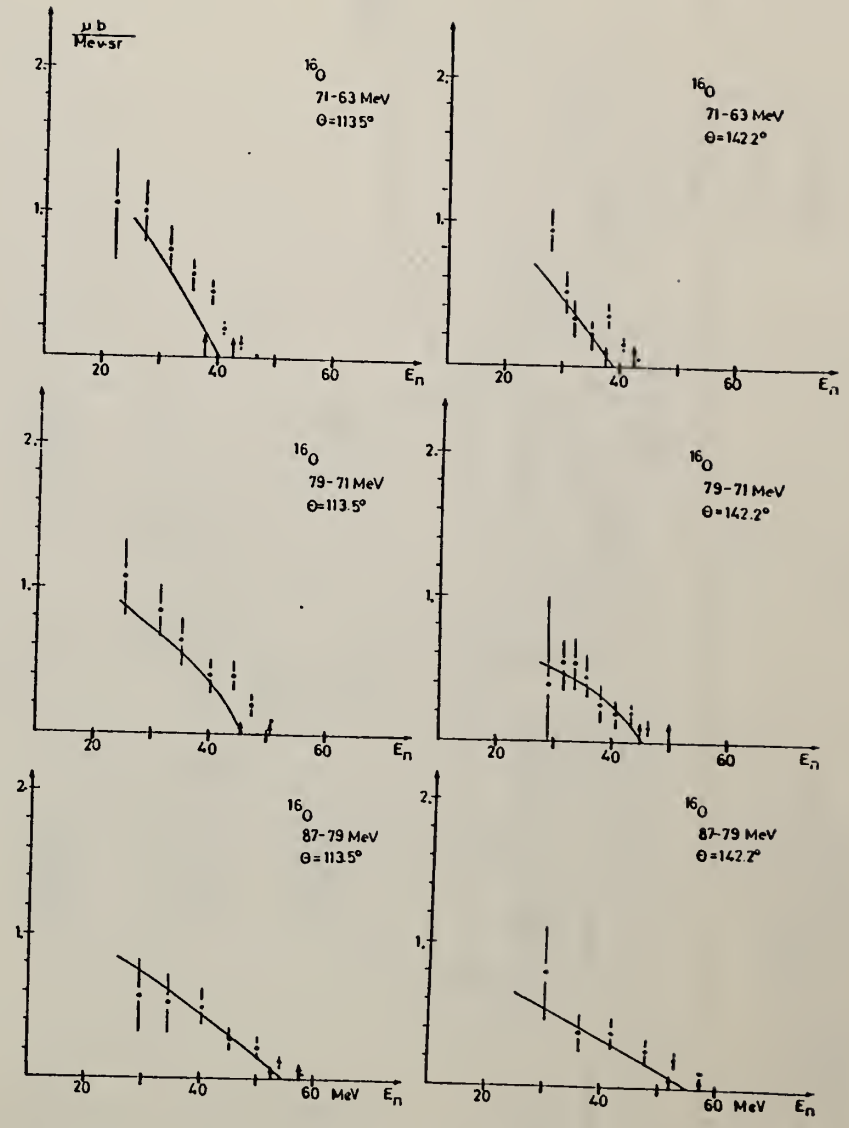

Fig. 8. Measured cross sections for the photoproduction of neutron on ^{16}O by quasimonochromatic photons. The energy values given correspond to the photon end energies. The arrows mark the neutron energies E_n, calculated with formula (7) for the medium photon energy.

REF. H. Schier and B. Schoch
Nucl. Phys. A229, 93 (1974)

ELEM. SYM.	A	Z
O	16	8

METHOD

REF. NO. 74 Sc 8 egf

REACTION	RESULT	EXCITATION ENERGY	SOURCE		DETECTOR		ANGLE
			TYPE	RANGE	TYPE	RANGE	

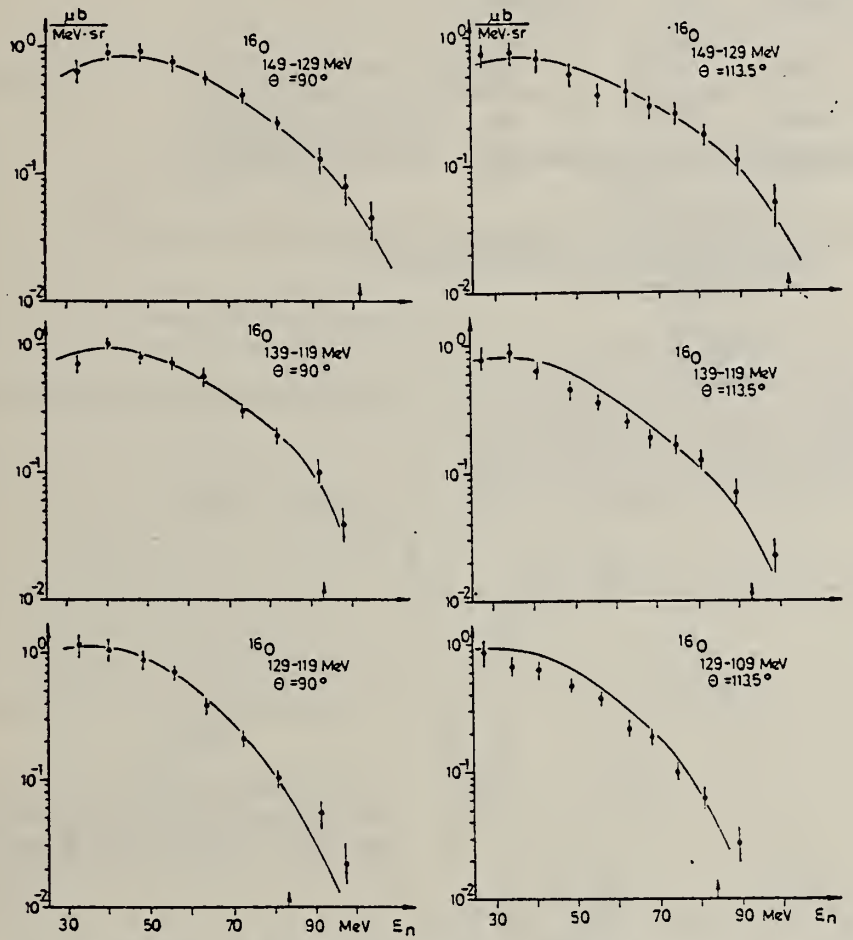

Fig. 14. Cross section for the photoproduction of neutrons by quasimonochromatic photons. The solid lines are calculations from the quasi-deuteron model for the $^{16}O(\gamma, np)^{15}O$ reaction. The neutron energy where the contribution of the $^{16}O(\gamma, n)^{15}O$ reaction is expected is marked by an arrow.

(over)

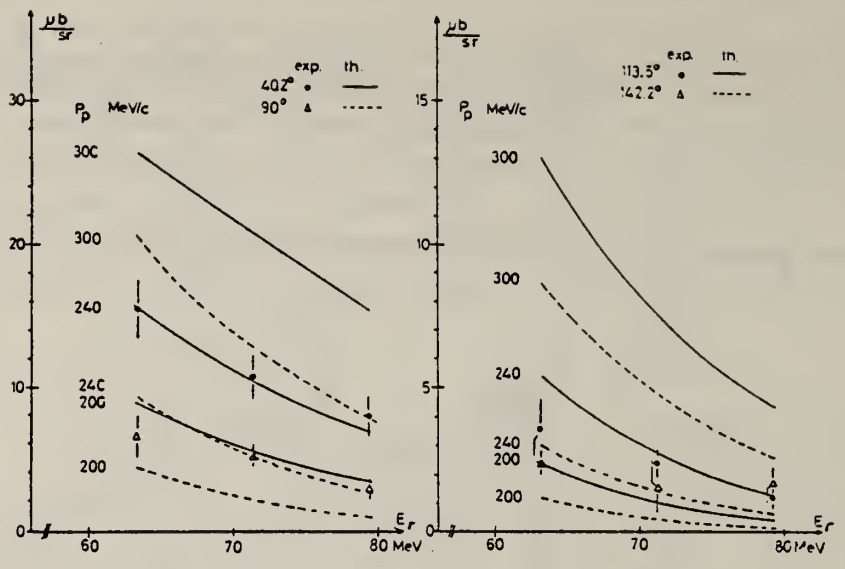

Fig. 11. Cross section for the direct $^{16}O(\gamma, n)^{15}O$ reaction. The lines are calculated using the modified quasi-deuteron model described in subsect. 3.5.

H.D. Shay, R.E. Peschel, J.M. Long, and D.A. Bromley
Phys. Rev. C9, 76 (1974)

0	16	8

METHOD

REF. NO. 74 Sh 3 hmg

REACTION	RESULT	EXCITATION ENERGY	SOURCE TYPE	SOURCE RANGE	DETECTOR TYPE	DETECTOR RANGE	ANGLE
He,G	ABX	28- 45	D	3- 16	NAI-D		DST

HE=HE3, 4 LEVELS
855

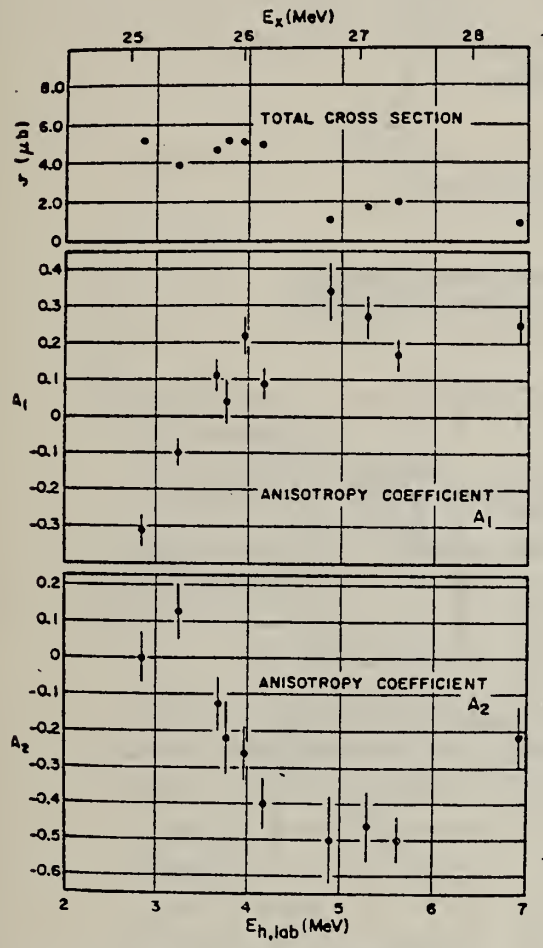

FIG. 25. Total cross section and anisotropy coefficients for the reaction $^{13}C(^3He,\gamma_0)^{16}O$. Shown are the results of fitting the $^{13}C(^3He,\gamma_0)^{16}O$ angular distributions with $d\sigma/d\Omega = (\sigma/4\pi)[1 + \sum_{i=1}^{2} A_i P_i(\cos\theta)]$. Errors are wholly statistical.

TABLE III. Average cross sections of radiative capture reactions in ^{16}O and their ratios.

Reaction	Energy range (MeV)	Average 90° differential cross section (μb/sr) γ_0 decay	γ_{1-4} decays
$^{15}N(p,\gamma)^{16}O$	20–29 [a]	3.45	...
	24.5–29 [a]	2.31	≥2.9 [b]
$^{13}C(^3He,\gamma)^{16}O$	23.6–35 [c]	0.105	0.95
	24.5–29	0.184	1.85

Ratios of cross sections averaged over the energy interval 24.5–29 MeV

$$R \equiv \frac{\sigma[^{13}C(^3He,\gamma_0)^{16}O]}{\sigma[^{15}N(p,\gamma_0)^{16}O]} = 1.12.5$$

$$R_{12} \equiv \frac{\sigma[^{15}N(p,\gamma_{1-4})^{16}O]}{\sigma[^{15}N(p,\gamma_0)^{16}O]} \geq 1.25$$

$$R_{22} \equiv \frac{\sigma[^{13}C(^3He,\gamma_{1-4})^{16}O]}{\sigma[^{13}C(^3He,\gamma_0)^{16}O]} = 10.0$$

[a] O'Connell (Ref. 11) normalized by factor of 1/1.6.
[b] O'Connell (Ref. 11) normalized by comparison with $^{15}N(p,\gamma_{1-2})^{16}O$ of Tanner and Barnett (Ref. 10).
[c] This work plus data of Puttaswany (Ref. 23) normalized to ours in region of overlap (1/1.6).

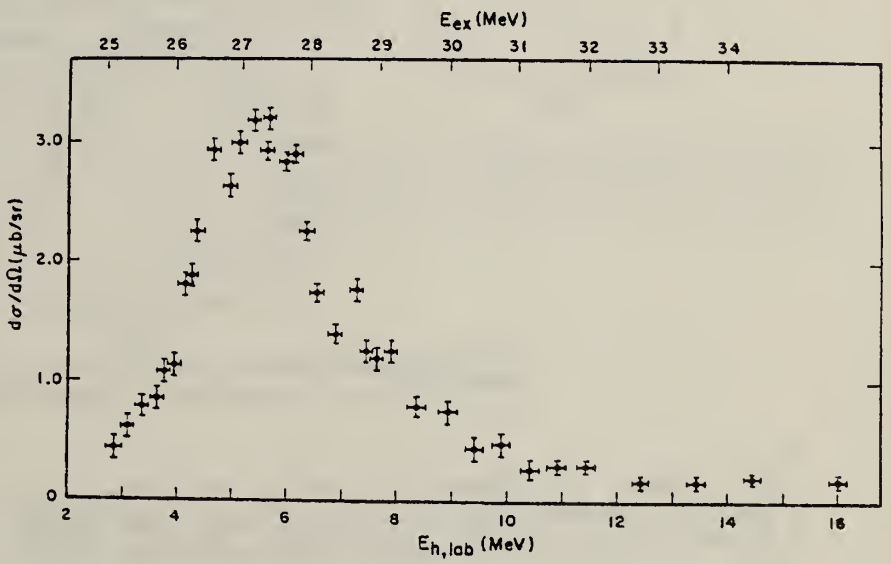

FIG. 14. 90° differential cross section for the reactions $^{13}C(^3He,\gamma_{1-4})^{16}O$. The cross sections of the four unresolved transitions are summed. Error bars represent statistical errors only. Horizontal bars signify the target thicknesses.

(over)

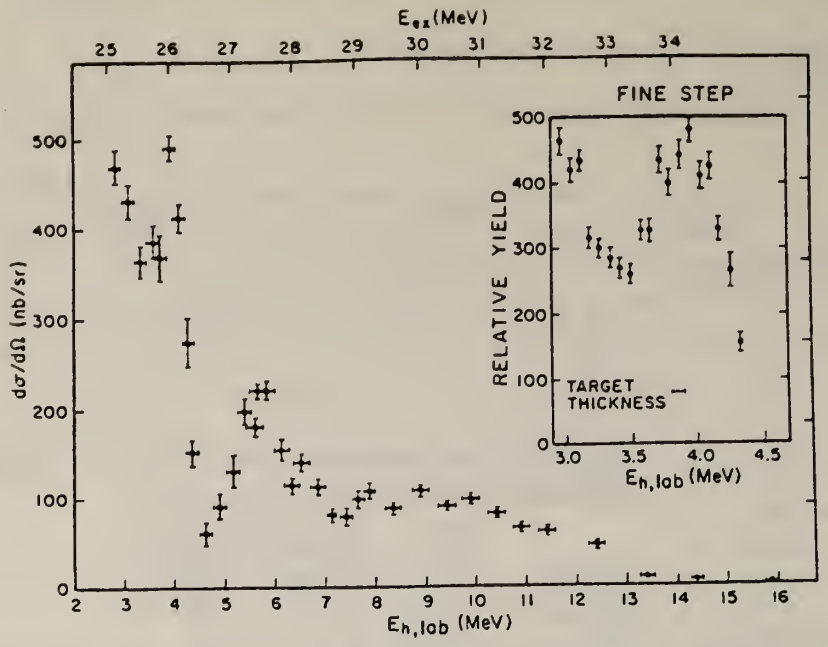

FIG. 13. 90° differential cross sections for the reaction $^{13}C(^3He,\gamma_0)^{16}O$. Errors assigned to the cross sections are wholly statistical. Horizontal bars represent the target thicknesses. The inset depicts a fine-step excitation function across the region of greatest structure, $3.0 < E_h < 4.5$ MeV; its ordinate is in relative units.

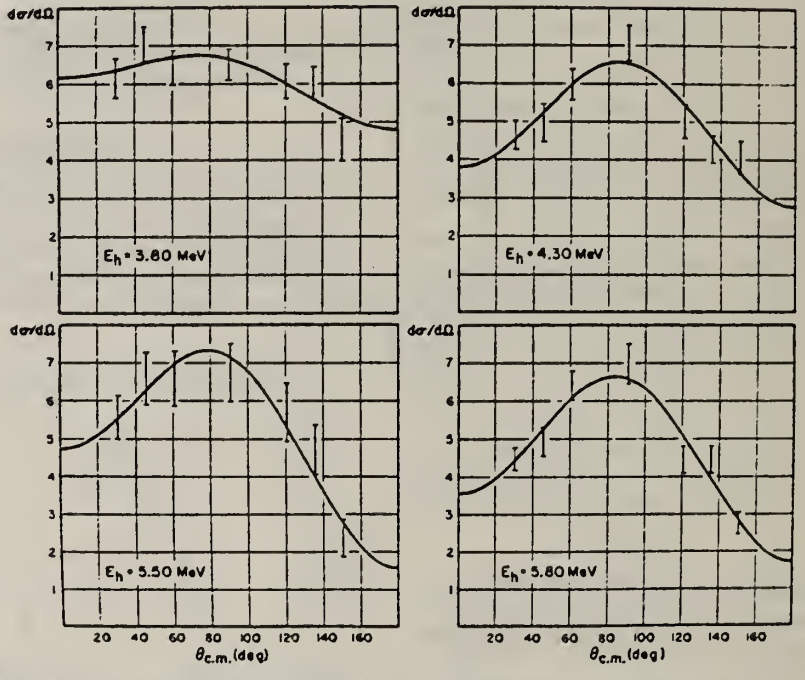

FIG. 19. Angular distributions of the reaction $^{13}C(^3He,\gamma_0)^{16}O$. Data are shown as bars, the height of which represents the statistical errors. The solid lines are Legendre polynomial fits, $d\sigma/d\Omega = \sum_{n=0}^{4} A_n P_n(\cos\theta_{c.m.})$. Units are arbitrary.

10
N.W. Tanner, G.C. Thomas, E.D. Earle, Nucl. Phys. 52, 29,451 (1964); A.R. Barnett and N.W. Tanner, Nucl. Phys. A152, 257 (1970); E.D. Earle and N.W. Tanner, Nucl. Phys. A95, 241 (1967).
11
W.J. O'Connell, Ph.D. thesis, Stanford University, 1969 (unpub.)
23
N.G. Puttaswamy, Ph.D. thesis, Stanford University, 1966 (unpub.); N.G. Puttaswamy and D. Kohler, Phys. Lett. 20, 288 (1966).

REF.
K.A. Snover, E.G. Adelberger, and D.R. Brown
Phys. Rev. Letters 32, 1061 (1974)

ELEM. SYM.	A	Z
O	16	8

METHOD

REF. NO.: 74 Sn 9 hmg

REACTION	RESULT	EXCITATION ENERGY	SOURCE		DETECTOR		ANGLE
			TYPE	RANGE	TYPE	RANGE	
A,G	ABX	12- 28	D	7- 28	NAI-D		DST

1075
1076
1077
1078
1080
1081

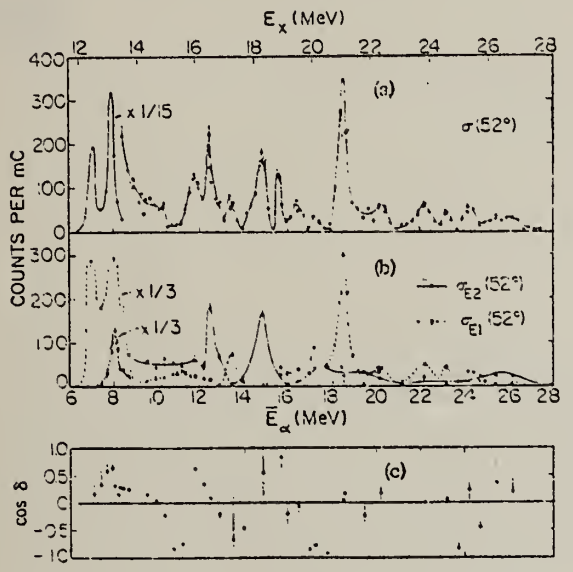

FIG. 1. (a) Measured cross section at 52° for $^{12}C(\alpha, \gamma_1)^{16}O$; (b) excitation curves for $\sigma_{E1}(52°)$, $\sigma_{E2}(52°)$; (c) cosδ. The absolute normalization (in μb/sr) is given by $\sigma(52°) = [4.10 - 0.22\,E_x\ (\text{MeV})] \times 10^{-4} \times \text{counts/mC}$.

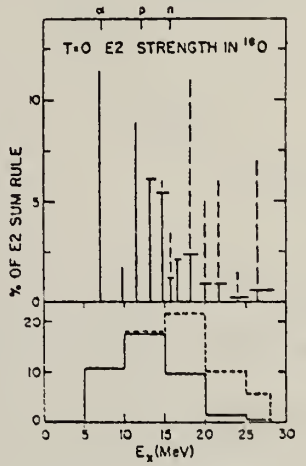

FIG. 2. Top, measured $E2$ strength (solid bars) and estimated strength (dashed bars). Bottom, measured and estimated $E2$ strength summed over 5-MeV intervals.

REF.

A. Veyssiere, H. Beil, R. Bergere, P. Carlos, A. Lepretre, and A. De Miniac
Nucl. Phys. A227, 513 (1974)

ELEM. SYM.	A	Z
O	16	8

METHOD

REF. NO.	
74 Ve 1	egf

REACTION	RESULT	EXCITATION ENERGY	SOURCE		DETECTOR		ANGLE
			TYPE	RANGE	TYPE	RANGE	
* G,N	ABX	15- 37	D	15- 37	BF3-I		4PI
** G,ZN	ABX	29- 37	D	29- 37	BF3-I		4PI
*** G,NP	ABX	23- 37	D	23- 37	BF3-I		4PI

* 879+
** 877 +
*** 878

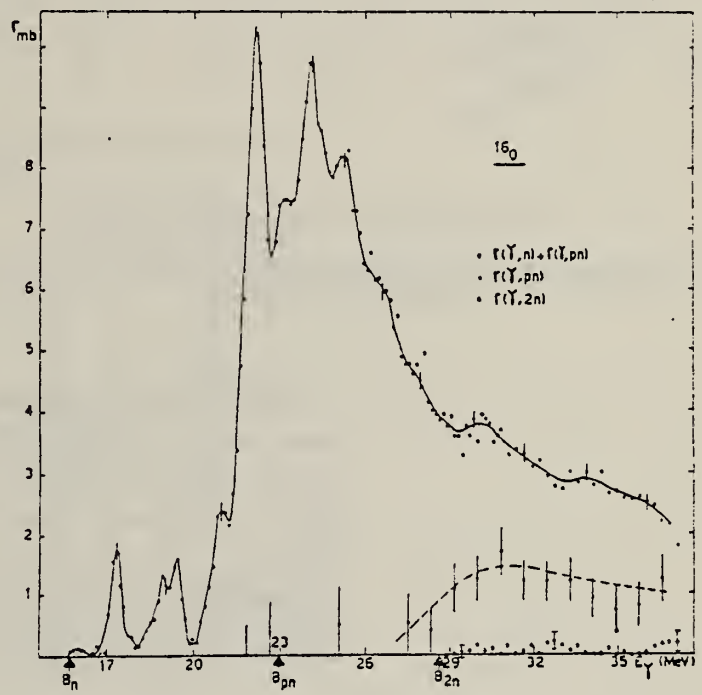

Fig. 1. Partial photonuclear cross sections $[\sigma(\gamma, n)+\sigma(\gamma, pn)]$, $\sigma(\gamma, pn)$ and $\sigma(\gamma, 2n)$ of ^{16}O obtained by means of neutron and β^+ measurements, as explained in the text.

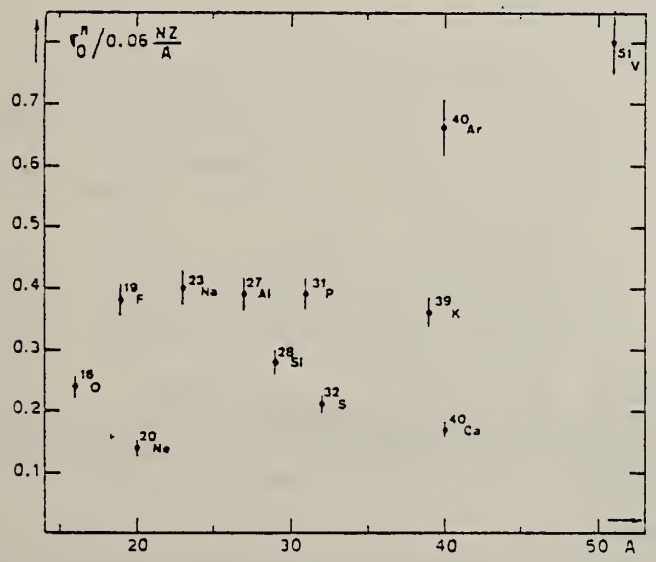

Fig. 22. Ratio of experimental integrated photoneutron cross section σ_0^n over the Thomas, Reiche and Kuhn sum rule $[0.06\ NZ/A]$. Numerical values and upper integration limits E_M are taken from table 3. Also $\Delta\sigma_0^n = \pm 7\%$ for all nuclei.

(over)

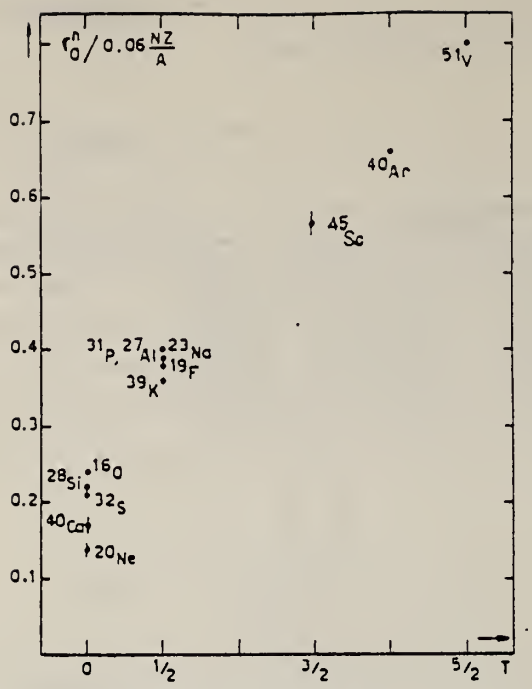

Fig. 24. The $[\sigma_0^n/(0.06\,NZ/A)]$ ratio as a function of isospin T. Possible overall errors of ±7%, are to be applied to all nuclei shown.

TABLE 3

Experimental integrated photoneutron cross sections $\sigma_0^n = \int_0^{E_M} \sigma_{Tn}(E)dE$ compared with the classical sum rule [0.06 NZ/A] of Thomas, Reich and Kuhn

	$T=0$					$T=\frac{1}{2}$					$T=\frac{3}{2}$	$T=2$	$T=\frac{5}{2}$
Nucleus	^{16}O	^{20}Ne	^{28}Si	^{32}S	^{40}Ca	^{19}F	^{23}Na	^{27}Al	^{31}P	^{39}K	^{45}Sc	^{40}Ar	^{51}V
σ_0^n (MeV · mb)	58 ±4	42 ±3	94 ±7	98 ±7	100 ±7	108 ±7	137 ±9	158 ±10	182 ±12	210 ±14	383 ±25	393 ±28	602 ±42
$\sigma_0^n/(0.06NZ/A)$	0.24	0.14	0.22	0.21	0.17	0.38	0.40	0.39	0.39	0.36	0.57	0.66	0.8
E_M (MeV)	30	26.7	30	30	29.5	29	30	30	29	30	28.1	26.7	28

REF.		ELEM. SYM.	A	Z
	J. Ahrens, H. Borchert, K.H. Czock, H.B. Eppler, H. Gimm, H. Gundrum, M. Kroning, P. Riehn, G. Sita Ram, A. Zieger, and B. Ziegler Nucl. Phys. A251, 479 (1975)	O	16	8

METHOD	REF. NO.	
	75 Ah 3	egf

REACTION	RESULT	EXCITATION ENERGY	SOURCE		DETECTOR		ANGLE
			TYPE	RANGE	TYPE	RANGE	
G,MU-T	ABX	10-160	C	140-275	MGC-D		4PI

924+

TABLE 2

The moments of the experimental nuclear cross section distributions integrated from 10 MeV to the energy E, and their statistical errors

	E (MeV)	$\sum_{-2}$ (mb/MeV)	±(%)	$\sum_{-1}$ (mb)	±(%)	$\sum_{0}$ (mb·MeV)	±(%)	$\sum_{+1}$ (b·MeV²)	±(%)	$\sum_{-2}$ (b·MeV³)	±(%)
Li	100	0.196	1.1	4.64	1.0	143	1.7	5.82	3.1	305	5
	140	0.197	1.1	4.79	1.0	161	1.9	8.03	3.4	577	5
	210	0.198	1.1	5.03	1.0	206	2.0	16.60	3.7	2220	5
Be	100	0.192	2.5	5.19	1.5	173	2.0	7.11	3.4	362	5
	140	0.194	2.5	5.33	1.5	189	2.1	9.09	3.6	600	6
	210	0.195	2.5	5.58	1.5	236	2.1	17.80	3.5	2240	5
C	100	0.313	1.7	8.81	1.1	291	1.6	12.00	2.9	630	4
	140	0.316	1.7	9.18	1.2	334	2.2	17.10	5	1250	7
O	100	0.580	1.6	14.50	1.3	432	2.0	16.00	4	748	8
	140	0.585	1.6	15.10	1.3	508	2.5	25.20	5	1880	8
Al	100	1.10	1.8	25.70	1.5	739	2.6	27.9	5	1400	8
	140	1.11	1.8	26.3	1.7	807	3.9	36.4	9	2450	16
Ca	100	2.22	1.2	45.5	1.5	1120	3.6	34.9	9	1430	18
	140	2.23	1.2	46.8	1.7	1290	4.6	56.6	11	3710	19

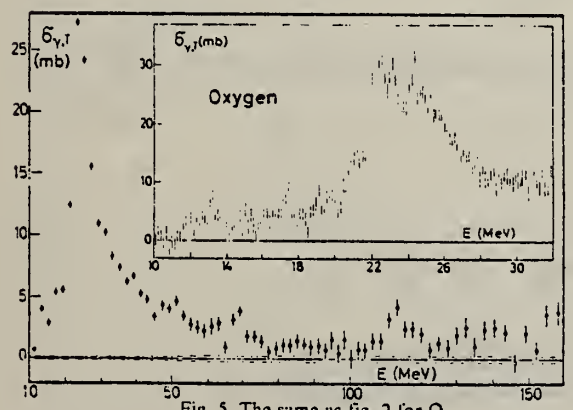

Fig. 5. The same as fig. 2 for O.

Fig. 2. Total photonuclear cross section for natural Li. The error bars indicate one standard deviation of counting statistics from the main spectrometer. The dashed lines along the abscissa indicate the uncertainty due to counting statistics in the normalizing spectrometer. Oscillations of the base line within this area are possible, the period of these oscillations, however, must not be smaller than 10% in photon energy. The dashed and dotted lines through the cross section values have been drawn to guide the eye.

REF. R. G. Johnson, J. D. Irish, and K. G. McNeill
Can. J. Phys. 53, 1434 (1975)

ELEM. SYM.	A	Z
O	16	8

METHOD

REF. NO. 75 Jo 2 hmg

REACTION	RESULT	EXCITATION ENERGY	SOURCE		DETECTOR		ANGLE
			TYPE	RANGE	TYPE	RANGE	
G,N	ABX	16- 28	C	22- 31	TOF-D		98

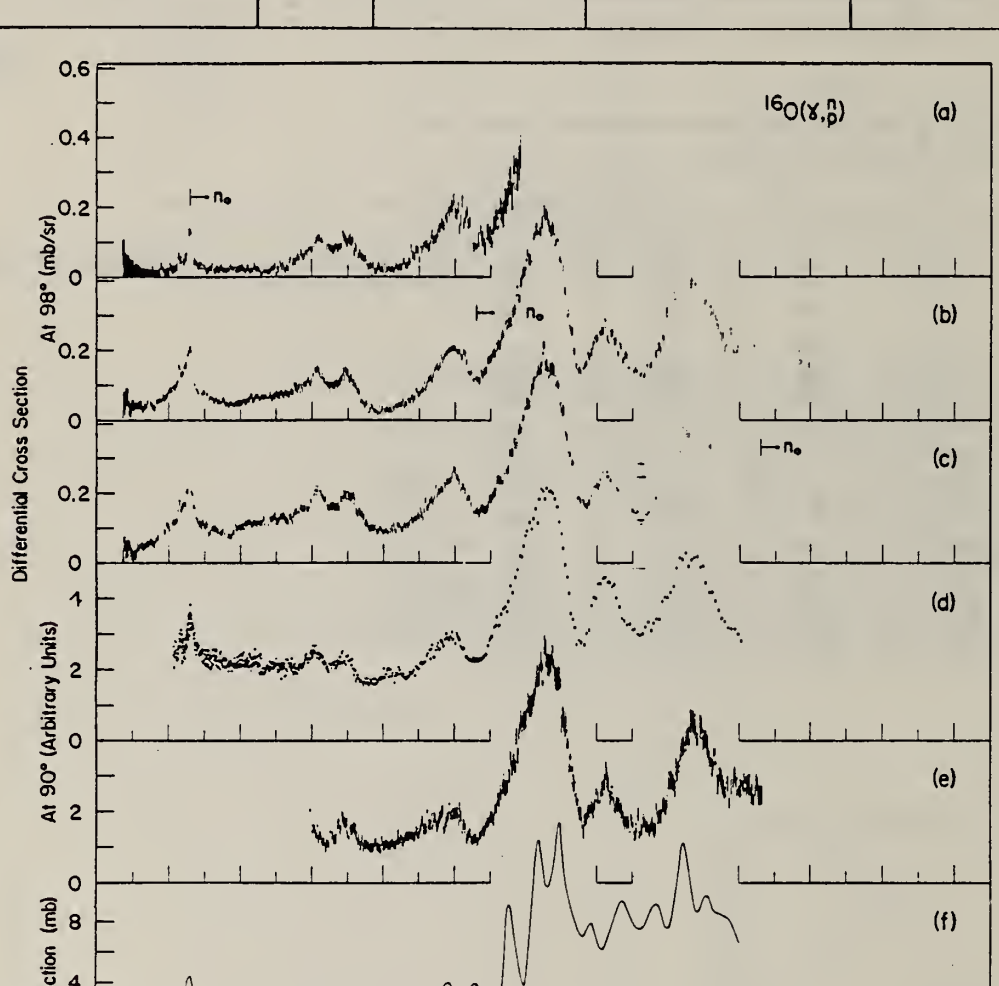

FIG. 1. Results of the present measurement of $d\sigma/d\Omega$ (98°) for the $^{16}O(\gamma,n)^{15}O$ reaction at bremsstrahlung endpoint energies of (*a*) 22.5 MeV, (*b*) 26.5 MeV, and (*c*) 30.5 MeV compared to (*d*) $d\sigma/d\Omega$ (90°) for $^{16}O(\gamma,n)^{15}O$ (Firk 1964); (*e*) $d\sigma/d\Omega$ (90°) for $^{16}O(\gamma,p)^{15}N$ (Thompson and Baglin 1967), and (*f*) $^{16}O(\gamma,n)^{15}O$ total cross section (Ishkhanov *et al.* 1971*b*).

REF. U. Kneissl, E. A. Koop, G. Kuhl, K. H. Leister, A. Weller
Nucl. Instrum. Methods 127, 1 (1975)

ELEM. SYM.	A	Z
O	16	8

METHOD

REF. NO. 75 Kn 8 egf

REACTION	RESULT	EXCITATION ENERGY	SOURCE TYPE	SOURCE RANGE	DETECTOR TYPE	DETECTOR RANGE	ANGLE
G,XN	ABX	17- 37	D	17- 37	MOD-I		4PI

1039

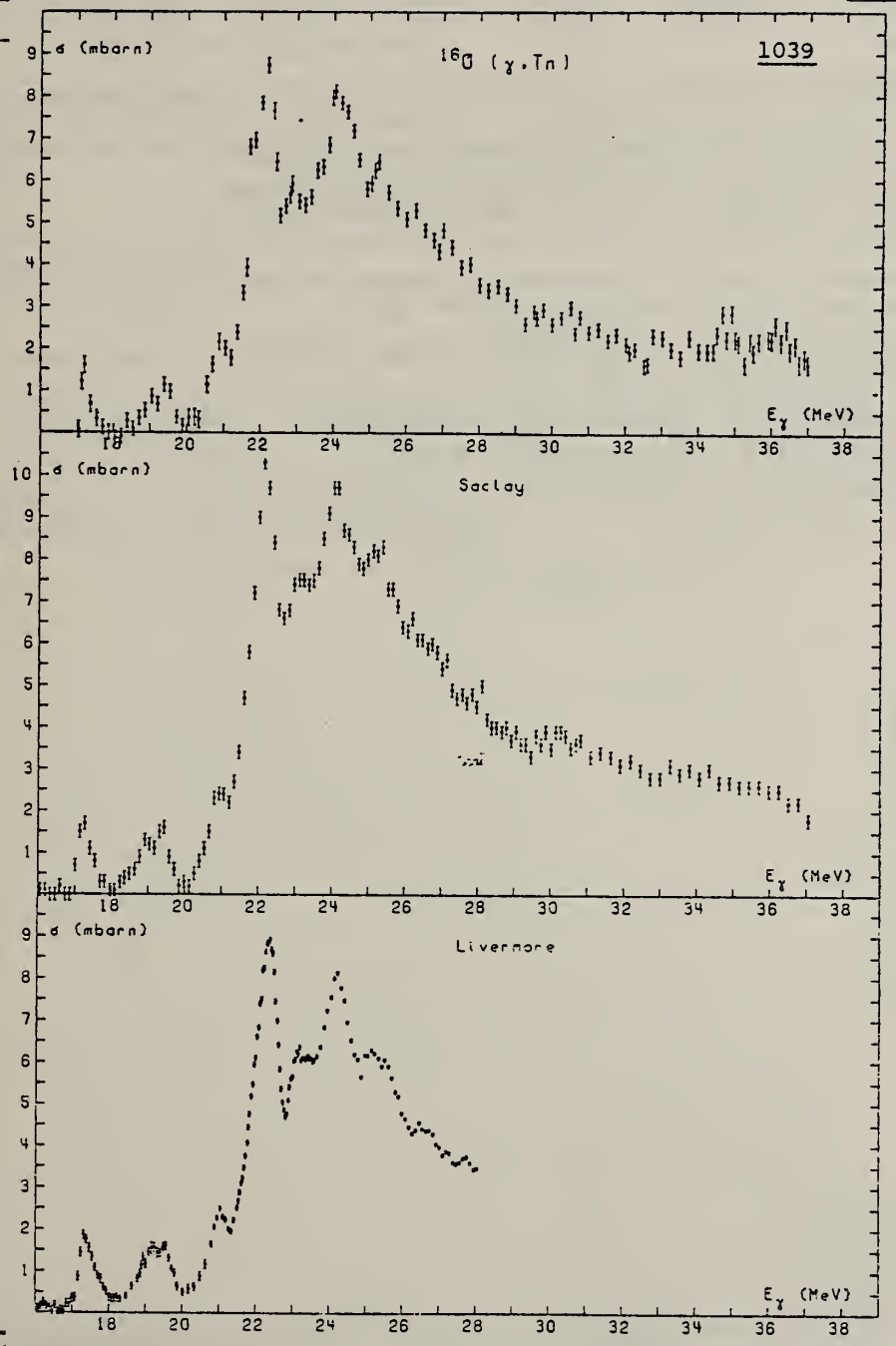

Fig. 6. $\sigma(\gamma,\mathrm{Tn})$ for ^{16}O, our results together with those from Saclay[34]) and Livermore[43]).

(over)

TABLE 2

Experimental energies of the strongest peaks in the ^{16}O giant resonance.

Ref.	Stanford[28])	Gießen[41])	Livermore[42])	Livermore[43])	Saclay[34])	This exp.
Exp.	(p,γ_0)	(γ,p)	(γ,n)	(γ,n)	(γ,n)	(γ,n)
Energies (MeV)	20.945±0.002	20.86±0.05	20.8	21.02	20.9	20.9 ±0.1
	22.146±0.005	22.16±0.05	22.1	22.34	22.2	22.2 ±0.1
	22.888±0.013	22.88±0.05	23.1	?	?	22.9 ±0.1
	24.065±0.030	24.04±0.05	24.0	24.22	24.1	24.05±0.1
	25.117±0.065	-	25.0	25.15	25.2	25.2 ±0.1

[28] W.J. O'Connel, G.W. Latshaw, J.L. Black and S.S. Hanna, Proc. of the Intern. Conf. on Photonuclear reactions and applications (Asilomar, 1973) (ed. by B.L. Berman) vol.II, p.939.

[34] A. Veyssiere, H. Beil, R. Bergere, P. Carlos, A. Lepretre and A. de Miniac, Nucl. Phys. A227 (1974) 513.

[41] K. Wienhard (Giessen), priv. communication; K. Bangert, Diploma Thesis (Giessen, 1974).

[42] J.T. Caldwell, R.R. Harvey, R.L. Bramblett and S.C. Fultz, Phys. Letters 6 (1963) 213.

[43] R.L. Bramblett, J.T. Caldwell, R.R. Harvey and S.C. Fultz, Phys. Rev. 133B (1964) 869.

REF. H. Miska, H. D. Graf, A. Richter, R. Schneider, D. Schull, E. Spamer, H. Theissen, O. Titze, Th. Walcher
Phys. Lett. 58B, 155 (1975)

ELEM. SYM.	A	Z
O	16	8

METHOD

REF. NO. 75 Mi 2 egf

REACTION	RESULT	EXCITATION ENERGY	SOURCE TYPE	SOURCE RANGE	DETECTOR TYPE	DETECTOR RANGE	ANGLE
E,E/	LFT	6- 7	D	38- 60	MAG-D		DST

6.05,6.13,6.92,7.12 MEV

Inelastic electron scattering with high energy resolution (FWHM = 30 keV) has been used to study the states at 6.05(0^+), 6.13(3^-) and 6.92(2^+) MeV excitation energy in ^{16}O for momentum transfers q = 0.22 – 0.49 fm^{-1}. The experiment yields a new determination of reduced transition probabilities and radiative widths for ground-state transitions.

Table 1
Reduced transition probability, transition radius and ground-state radiation width from $^{16}O(e, e')$. For comparison the results from lifetime measurements are quoted.

I^π	E_x (MeV)	$B(C\lambda, k; 0^+ \to I^\pi)$ (fm$^{2\lambda}$)	R_{tr} (fm)	Γ_γ^0(eV) present work	Γ_γ^0(eV) from lifetimes
0^+	6.05	3.55 ± 0.21 a)	5.4 ± 0.4	(8.5 ± 0.5) × 10^{-3} a)	(8.7 ± 0.8) × 10^{-3} [15]
3^-	6.13	1490 ± 70	4.22 ± 0.17	(2.60 ± 0.13) × 10^{-5}	(2.63 ± 0.21) × 10^{-5} [16]
2^+	6.92	39.3 ± 1.6	4.06 ± 0.16	(1.00 ± 0.04) × 10^{-1}	(1.10 ± 0.05) × 10^{-1} [13]
1^-	7.12	(3.6 ± 1.8) × 10^{-4}		(4.6 ± 2.3) × 10^{-2}	(6.2 ± 0.5) × 10^{-2} [13]

a) Matrixelement and radiation width calculated after ref. [20].

20 R.H. Dalitz, Proc. Roy. Soc. A206, 521 (1951).

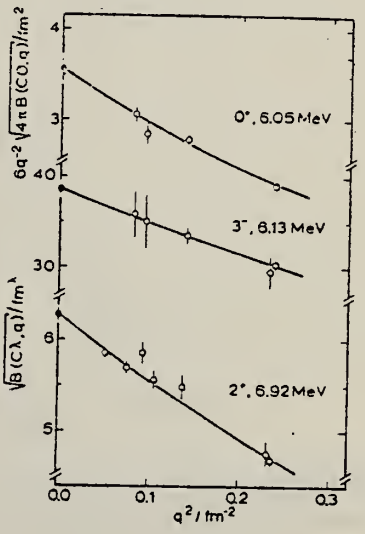

Fig. 2. Square root of the reduced transition probability as a function of the square of the momentum transfer. Open circles represent the experimental points with statistical errors and the full circle is the result of the extrapolation to the photon point. Note the difference in the ordinate scale and the suppressed zero.

REF.

H. Miska, H. D. Graf, A. Richter, D. Schull, E. Spamer, and O. Titze

Phys. Lett. 59B, 441 (1975)

ELEM. SYM.	A	Z
O	16	8

METHOD

REF. NO. 75 Mi 7 egf

REACTION	RESULT	EXCITATION ENERGY	SOURCE		DETECTOR		ANGLE
			TYPE	RANGE	TYPE	RANGE	
E,E/	FMF	7	D	38- 60	MAG-D		DST

7=7.12

The isospin-forbidden electroexcitation of the 1^-, $T = 0$ state at 7.12 MeV in ^{16}O has been studied for momentum transfers $q = 0.22 - 0.49$ fm^{-1}. The form factor at these momentum transfers is determined by the sum of the isospin $T = 0$ part and a $T = 1$ contribution. A single particle-hole harmonic oscillator shell model calculation reproduces the q-dependence of the measured form factor which shows that the isovector contribution interferes destructively with the isoscalar part and has a strength of about 2% of the $T = 0$ amplitude.

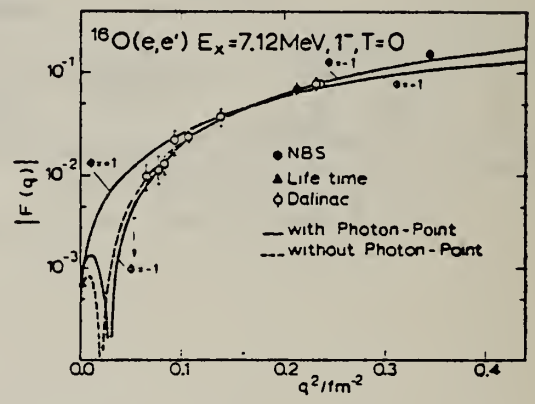

Fig. 2. Form factor $F(q)$ as a function of q^2. In addition to the present measurements at the DALINAC, data from NBS (see ref. [7] and $F(q)$ at the photon point from the lifetime of ref. [2] are also shown. The full line is a fit of the harmonic oscillator model [eq. (1)] to the present data and the photon point; for the dashed line the photon point is not included.

[2] C.P. Swann, Nucl. Phys. A150 (1970) 300.

[7] J.C. Bergstrom et al., Phys. Rev. Lett. 24 (1970) 152.

REF.

H. Schier and B. Schoch
Nuovo Cimento Lett. 12, 334 (1975)

ELEM. SYM.	A	Z
O	16	8

METHOD

REF. NO. 75 Sc 7 egf

REACTION	RESULT	EXCITATION ENERGY	SOURCE		DETECTOR		ANGLE
			TYPE	RANGE	TYPE	RANGE	
G,N	ABX	62- 66	D	62- 66	TOF-D		DST

62.7-65.7 MEV

TABLE I. – *Measured cross-sections obtained from Fig.* 1-5. The photon energy corresponds to the maximum value of the difference spectrum.

Nucleus	Photon energy (MeV)	Excitation energy (MeV)	$d\sigma/d\Omega$ (40.2°) (μb/sr)	$d\sigma/d\Omega$ (90°) (μb/sr)
^{16}O	63.0	ground state	5.0 ± 0.75	
		$0 \div 6.18$	20.7 ± 3.1	
^{12}C	62.75	ground state	11.1 ± 0.8	7.8 ± 0.36
		$0 \div 4.79$	22.5 ± 1.1	17.1 ± 0.56
^{9}Be	61.25	ground state	0.8 ± 0.13	0.85 ± 0.1
		$0 \div (\gamma, np)$ threshold	3.4 ± 0.3	4.1 ± 0.22

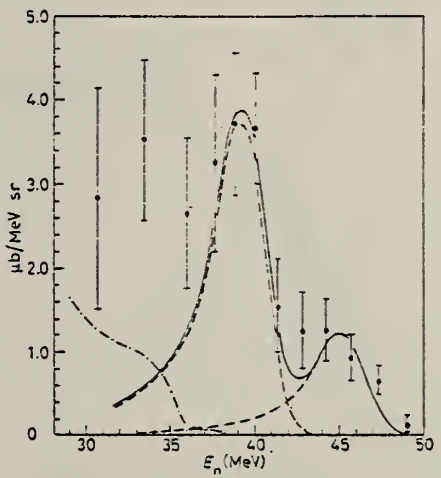

Fig. 1. – Cross-section for the photoproduction of neutrons in ^{16}O by quasi-monochromatic photons. The dashed lines show the photon spectrum fitted to the ground state and the 6.18 MeV level in ^{16}O, and the solid line gives the sum of both levels. A calculation for the (γ, np) reaction based on a quasi-deuteron model is indicated by the dashed-dotted line. (65.7 ÷ 62.7) MeV, $\vartheta_n = 40.2°$.

REF. D. M. Skopik, Y. M. Shin, and J. J. Murphy, II
Can. J. Phys. 53, 1398 (1975)

ELEM. SYM.	A	Z
O	16	8

METHOD

REF. NO. 75 Sk 10 hmg

REACTION	RESULT	EXCITATION ENERGY	SOURCE		DETECTOR		ANGLE
			TYPE	RANGE	TYPE	RANGE	
E,A	ABX	17- 26	D	UKN	MAG-D		DST

GND STATE SIGMA

The electrodisintegration cross sections, $^{16}O(e,\alpha_0)^{12}C,e'$ and $^{20}Ne(e.\alpha_0)^{16}O,e'$, have been measured and, by using virtual photon analysis, a comparison with photodisintegration experiments has been made. Satisfactory agreement with earlier $^{12}C(\alpha,\gamma_0)^{16}O$ experiments was found and the $^{20}Ne(\gamma,\alpha_0)^{16}O$ reaction reveals several pronounced resonances.

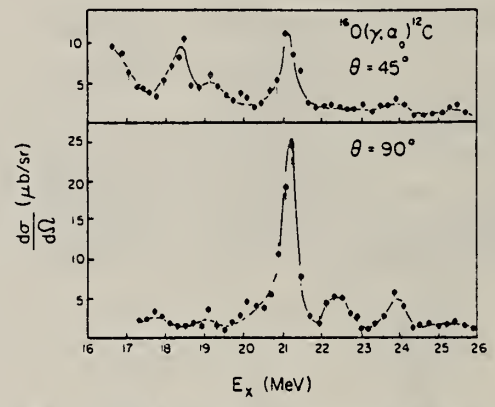

FIG. 1. Comparison of the $^{16}O(\gamma,\alpha_0)$ cross sections at θ = 45° and 90°. The solid line is only meant to guide the eye.

REF. D. J. S. Findlay and R. O. Owens
Phys. Rev. Lett. 37, 674 (1976)

ELEM. SYM.	A	Z
O	16	8

METHOD

REF. NO. 76 Fi 4 hmg

REACTION	RESULT	EXCITATION ENERGY	SOURCE		DETECTOR		ANGLE
			TYPE	RANGE	TYPE	RANGE	
G,P	NOX	60-100	D	40-105	UKN		DST

The momentum distribution of $p_{1/2}$ shell nucleons in ^{16}O is deduced from measurements of the angular distribution of the $^{16}O(\gamma,p_0)$ reaction cross section between $E_\gamma = 40$ and 105 MeV. The results are found to deviate from the Elton-Swift distribution.

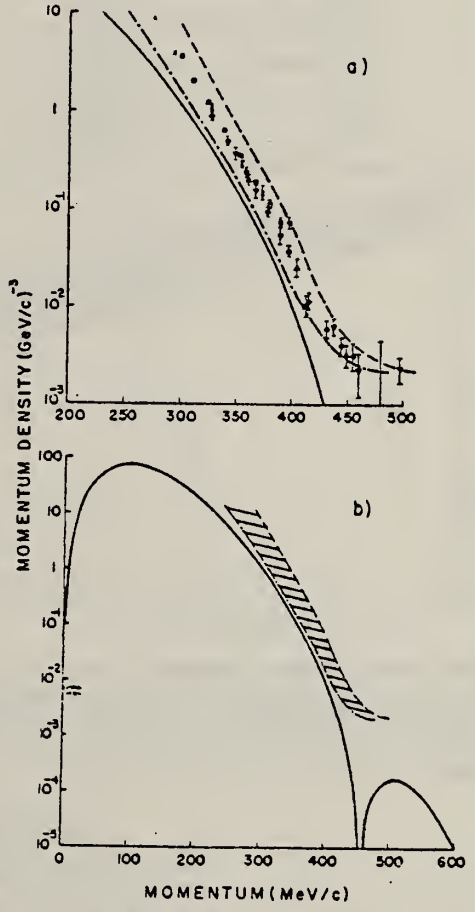

FIG. 1. The experimental $1p_{1/2}$ momentum distribution for ^{16}O ($E_\gamma = 60$ MeV, ■; 80 MeV, ◆; 95 MeV, ▲; 100 MeV, ▼; 40, 50, 70, 90, 105 MeV, 45°, X). The distributions for $V_0 = 18$ and 36 MeV are shown as -·-·- and ———, respectively. The Elton-Swift momentum distribution is shown as ———.

REF.

J.B. Martins, O.A.P. Tavares, M.L. Terranova, and V.Di Napoli
Lett. Nuovo Cimento 15, 364 (1976)

ELEM. SYM.	A	Z
0	16	8

METHOD

REF. NO. 76 Ma 10 egf

REACTION	RESULT	EXCITATION ENERGY	SOURCE TYPE	SOURCE RANGE	DETECTOR TYPE	DETECTOR RANGE	ANGLE
G,N13	ABY	THR-999	C	300-999	ACT-I		4PI

999=1 GEV

TABLE II. – *Cross-sections per equivalent quantum* σ_Q *for the reaction* $^{16}O(\gamma, p2n)^{13}N$.

Bremsstrahlung energy (GeV)	σ_Q (μb)	Bremsstrahlung energy (GeV)	σ_Q (μb)
0.30	122±10	0.60	135±10
0.35	125±10	0.70	145±10
0.40	132±10	0.80	143±10
0.45	132±10	0.85	147±10
0.50	132±10	0.95	153±10
0.55	143±10	1.00	151±10

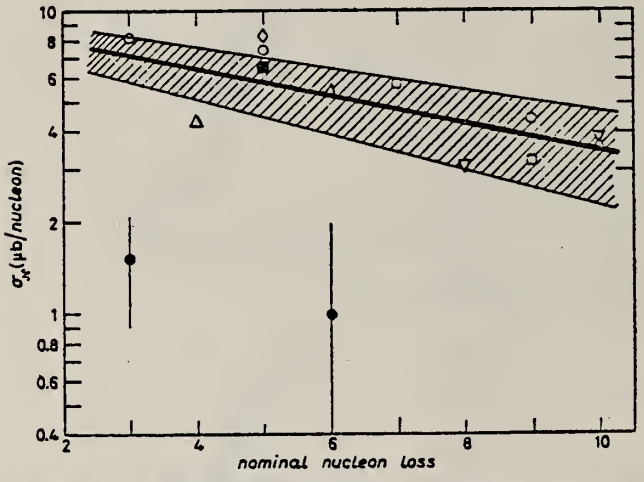

Fig. 1. – Values of mean absolute cross-section *per* nucleon σ_N as a function of the nominal nucleon loss (semi-logarithmic plot). Open circles: ^{27}Al target, ref. ([3,12,16]); open triangles: ^{28}Si target, ref. ([2]); open rhomb: ^{23}Na target, ref. ([2]); open reversed triangles: ^{32}S target, ref. ([2]); open squares: ^{31}P target, ref. ([2]); filled square: ^{16}O target, ref. ([2]). The straight line is a least-squares fit of all the experimental points. The shaded area represents the standard deviation. Filled circles with error bars: present-work results for ^{16}O and ^{19}F targets.

[2] V. Di Napoli and M.L. Terranova: Journal Inorg. Nucl. Chem., 36, 3633 (1974)

[3] V. Di Napoli, G. Rosa, F. Salvetti, M.L. Terranova, H.G. De Carvalho, J.B. Martins and O.A.P. Tavares: Journal. Inorg. Nucl. Chem., 37, 1101 (1975)

[12] V. Di Napoli, A.M. Lacerenza, F. Salvetti, S.M. Terenzi, H.G. De Carvalho and J.B. Martins: Joural Inorg. Nucl. Chem. 35, 1419 (1973)

[16] V. Di Napoli, A.M. Lacerenza, F. Salvetti, H.G. De Carvalho and J.B. Martins: Lett. Nuovo Cimento, 1, 835 (1971)

REF.

T. R. Ophel, A. D. Frawley, P. B. Treacy, K. H. Bray
Nucl. Phys. A273, 397 (1976)

ELEM. SYM.	A	Z
O	16	8

METHOD

REF. NO.: 76 Op 1 | egf

REACTION	RESULT	EXCITATION ENERGY	SOURCE		DETECTOR		ANGLE
			TYPE	RANGE	TYPE	RANGE	
A,G	ABX	13- 16	D	6- 9	NAI-D		90

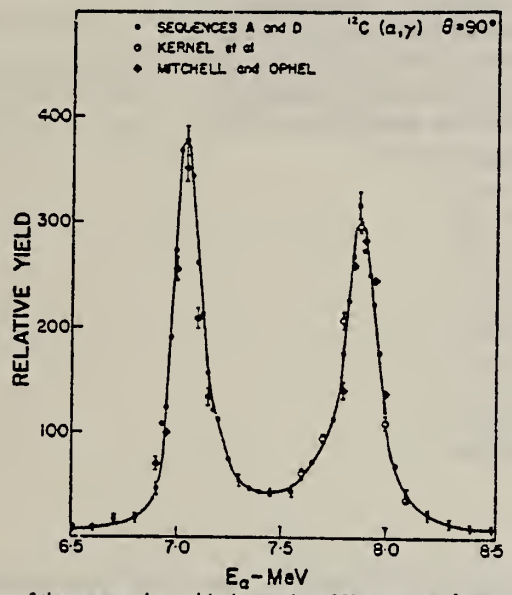

Fig. 4. Comparison of the present data with the results of Kernel *et al.* [3]) and Mitchell and Ophel [21]). The relative normalizations are discussed in the text.

TABLE 3

Summary of the relative peak cross sections of the 1^- resonance [$A_0(7.05)/A_0(7.88)$]

Measurement	Cross-section ratio
Present work, target I	1.20±0.04
Present work, target II	1.22±0.05
Larson and Spear [a])	1.12±0.04
Mitchell and Ophel [b])	1.17±0.04
Brochard *et al.* [c])	0.96

[a]) Ref. [1]). [b]) Ref. [21]). [c]) Ref. [3]).

TABLE 4

Summary of resonance energy measurements

Measurement	Lower resonance	Upper resonance
Larson and Spear [a])	7.05±0.02	7.88 ±0.03
Mitchell and Ophel [b])	7.04±0.02	7.90 ±0.02
Kernel *et al.* [c])		7.864±0.013
Brochard *et al.* [d])	≈ 7.10	≈ 7.90
Present work	7.04±0.01	7.880±0.015

[a]) Ref. [1]). [b]) Ref. [2]). [c]) Ref. [3]). [d]) Ref. [6]).

(over)

3.5. THE $^{12}C(\alpha, \gamma_0)$ ABSOLUTE CROSS SECTION AND TOTAL CROSS SECTION

It was not possible to obtain a measurement of the absolute cross section from the above data because of the emphasis placed on cosmic ray rejection to minimize background at off-resonance energies. It is difficult to determine accurately how many of the total interactions within the detector by the γ-rays of interest are rejected due to detection of escape radiation by the surrounding anticoincidence annulus.

Accordingly, a 12.6 cm × 10.2 cm NaI detector, was used to determine the cross section independently at 90°. The detector was surrounded by lead shielding 10 cm thick, except for the front face which was 27 cm from the target. The cross section obtained at 7.05 MeV was 2.1 ± 0.5 μb/sr and, at 7.90 MeV, 1.7 ± 0.5 μb/sr. Both measurements have been corrected for angular distribution effects. The stated errors arise mainly from the uncertainty in the target thickness and in the extrapolation of the spectrometer response to low energy in order to determine the total number of γ-ray interactions. The result at 7.90 MeV corresponds to a total cross section of 22 ± 7 μb, confirming the results of Larson and Spear and Brochard *et al.* It is tempting to speculate that the use of a singly ionized helium beam by Kernel *et al.* led to incorrect interpretation of the integrated charge by a factor of two.

[1] J. D. Larson et al., Nucl. Phys. 56 (1964) 497.

[2] I. V. Mitchell et al., Nucl. Phys. 58 (1964) 529.

[3] G. Kernel et al., Nucl. Phys. A167 (1971) 352.

[6] F. Brochard et al., J. de Phys. 34 (1973) 363.

[21] I. V. Mitchell et al., unpublished.

REF. B.H. Patrick, E.M. Bowey, E.G. Muirhead
J. Phys. G: Nucl. Phys. 2, 751 (1976)

ELEM. SYM.	A	Z
O	16	8

METHOD

REF. NO. 76 Pa 1 egf

REACTION	RESULT	EXCITATION ENERGY	SOURCE		DETECTOR		ANGLE
			TYPE	RANGE	TYPE	RANGE	
G,PG	ABI	17- 29	C	29	SCD-D		112
G,NG	ABI	21- 29	C	29	SCD-D		112

Absolute yields based on normalization to $^{59}Co(\gamma,n)$ cross section of Fultz (62Ful). If newer $^{59}Co(\gamma,1n)$ data from Alvarez (73Al7) is used, yields should be increased by a factor of 1.41.

Abstract. The photodisintegration of ^{15}N through excited states of the residual nuclei has been studied by measuring the yields of de-excitation γ rays in a Ge(Li) detector. Cross sections for all observed transitions were deduced from measurements with bremsstrahlung end-point energies ranging from 15 to 35 MeV and account for an integrated cross section of 44 MeV mb. Bound states in ^{14}N and ^{14}C with a dominant $(1p_{1/2})^{-1}$ or $(1p_{3/2})^{-1}$ configuration are found to be strongly populated. On the whole the results do not agree well with the meagre existing experimental information or with published theoretical calculations, with the possible exception of those of Zhusupov and Eramzhyan. The nature of the states in the ^{15}N giant resonance is discussed. The $^{15}N(\gamma,t)^{12}C^*$ (4·44 MeV) reaction was also observed and its integrated cross section is ~5% of the expected value of the E1 sum rule. Integrated cross sections for $^{16}O(\gamma,p_0\gamma_1)$ transitions measured at the same time are given. Resonance fluorescence is observed from the ^{15}N 10·07 MeV level, for which $\Gamma_{\gamma_0} = 4{\cdot}2 \pm 1{\cdot}5$ eV is deduced.

Table 2. A comparison of cross sections for neutron and proton emission from ^{16}O to specific final states, integrated up to 29 MeV, as measured in the present experiment with errors of ~ ±30%, with those of Caldwell *et al* (1967).

Reaction	Final state (MeV)	$\int_0^{29\,MeV} \sigma\,dE$ (MeV mb) Present expt	Caldwell *et al*
$^{16}O(\gamma,p)^{15}N$	GS	—	(34·4)
	5·3	4·3	4·9
	6·3	23·6	22·3
	7·2	2·0	5·5
	7·3	2·2	
	9·1	—	(2·0)
	9·2	0·4	1·5
	9·9	—	(2·4)
	10·8	—	(2·3)
	Total	32·5	34·2
$^{16}O(\gamma,n)^{15}O$	GS	—	(26·7)
	5·18	2·1	3·5
	5·24	4·4	
	6·2	12·2	9·4
	6·8	—	(4·5)
	Total	18·9	12·9

(over)

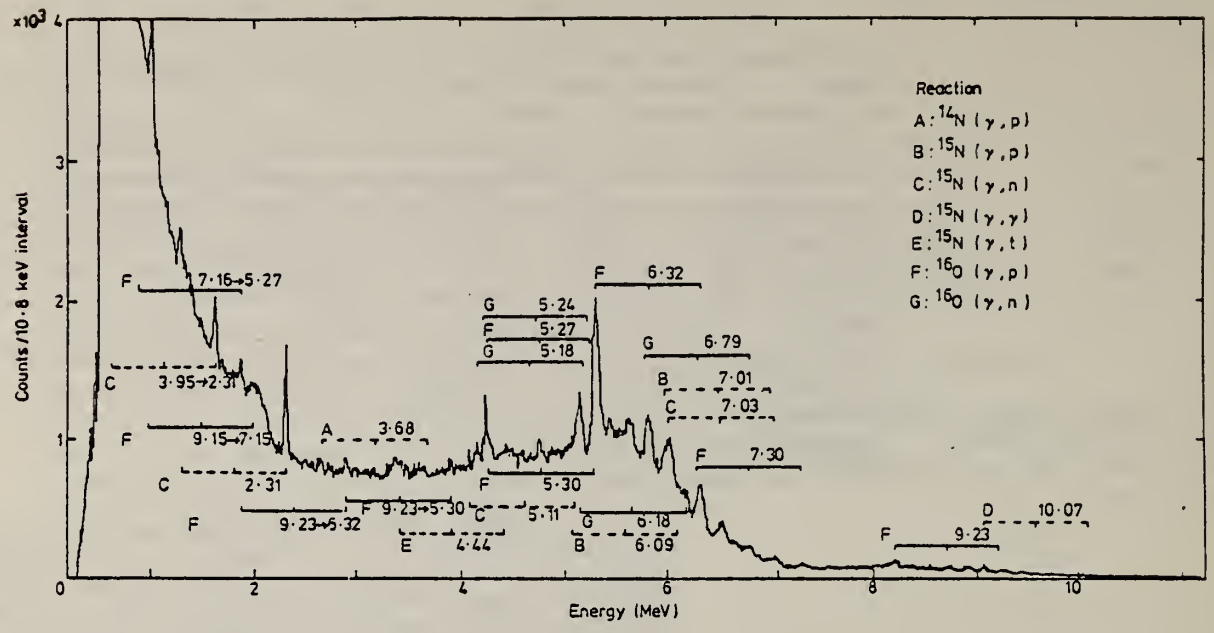

Figure 1. The γ ray spectrum, measured in the Ge(Li) detector, from the $^{15}NH_4{}^{15}NO_3$ target irradiated with bremsstrahlung end-point energy 31 MeV. The positions of the peaks for various transitions, and the reactions producing them, are marked.

REF. F. Borowski, Ch. Schmitt, G. G. Simon, V. Walther, D. Drechsel, W. Haxton, R. Rosenfelder
Phys. Rev. Lett. 38, 742 (1977)

ELEM. SYM.	A	Z
O	16	8

METHOD

REF. NO. 77 Bo 12 hmg

REACTION	RESULT	EXCITATION ENERGY	SOURCE		DETECTOR		ANGLE
			TYPE	RANGE	TYPE	RANGE	
E,P+	RLX	150-280	D	280	MAG-D	-	DST
E,P-	ABX	150-280	D	280	MAG-D		DST

SIG PI-/SIG PI+

Double-differential cross sections for the electroproduction of pions of both charges have been measured. We compare the data obtained for production near threshold from ^{12}C and ^{16}O with theoretical treatments employing both shell-model and sum-rule nuclear descriptions with full inclusion of the final-state interaction.

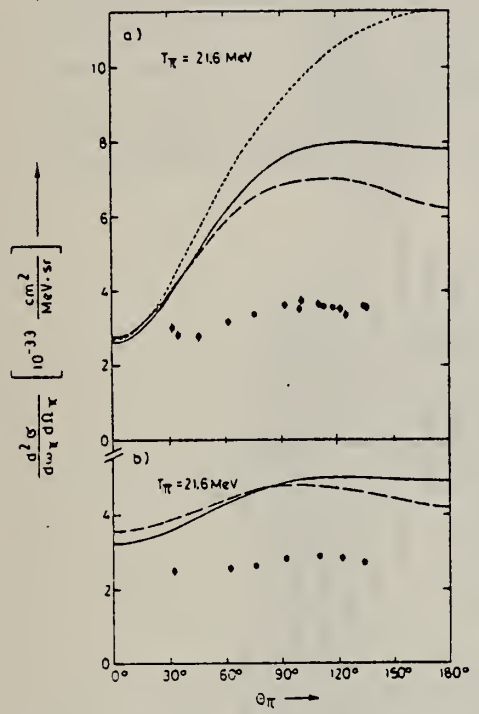

FIG. 1. Double-differential cross sections for production of negative pions by 280-MeV electrons from (a) ^{16}O and (b) ^{12}C as a function of the pion angle. The shell-model results (solid line) are compared with the predictions of the sum-rule results when evaluated with (dashed line) and without (dotted line) the effective two-body Skyrme II (Ref. 14) interaction.

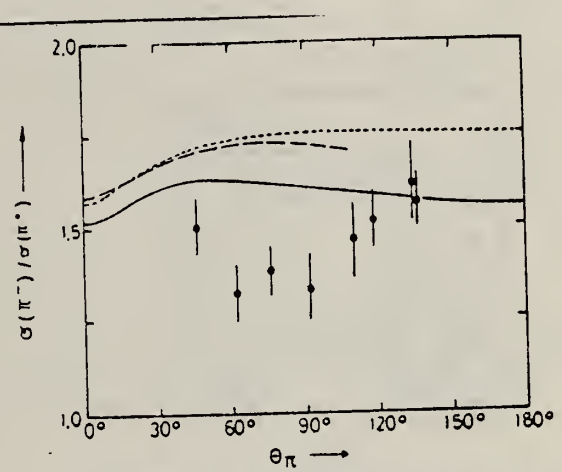

FIG. 3. Same in Fig. 2, but for production of 30.25-MeV pions from ^{16}O. The theoretical curves are as in Fig. 1. The sum-rule calculation with the Skyrme II interaction breaks down for angles above 110°, as discussed in Ref. 15.

[14] M. Beiner, H. Flocard, N. van Giai and P. Quentin, Nucl. Phys. A283, 29 (1975)

[15] The discrepancy between theory and experiment also shows up in weak and electromagnetic excitations of giant dipole states. This is probably due to complicated many-particle-many-hole states and can be taken into account by an overall reduction factor, at least at low momentum transfer. [See, e.g., T.W. Donnelly and J.D. Walecka, Annu. Rev. Nucl. Sci. 25, 329 (1975)]. Note, however, that in our calculations we have to include states well above the giant resonances, particularly in backward direction.

REF. J.R. Calarco, S.W. Wissink, M. Sasao, K. Wienhard, and S.S. Hanna
Phys. Rev. Lett. 39, 925 (1977)

ELEM. SYM.	A	Z
O	16	8

METHOD

REF. NO. 77 Ca 2 hmg

REACTION	RESULT	EXCITATION ENERGY	SOURCE		DETECTOR		ANGLE
			TYPE	RANGE	TYPE	RANGE	
$ (P,G)	ABX	20-24	D	8-13	NAI-D		DST

Sharp fluctuations in the coefficients describing the angular distribution and analyzing power in the reaction $^{15}N(p_{pol},\gamma_0)^{16}O$ are observed near $E_\gamma = 21$ MeV. These correspond to structure in the total cross section. All these structures can be fitted by introducing a narrow secondary doorway state interfering with the primary giant dipole resonance of ^{16}O.

Pol P, Doorway States

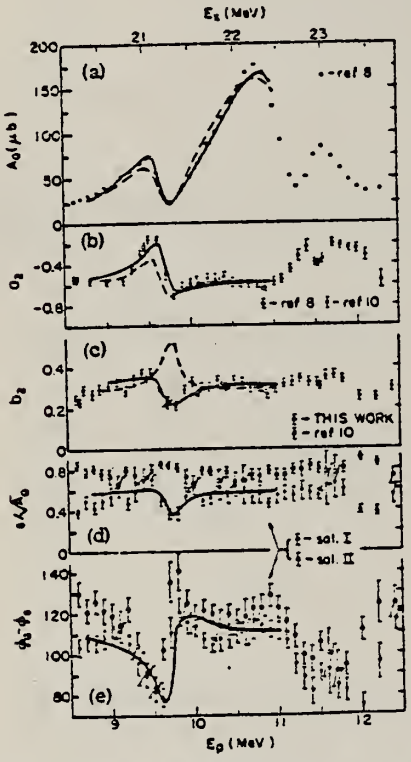

FIG. 1. (a) The cross section from Ref. 8 along with the fits from Ref. 9 (dashed curve) and the present work (solid curve); (b) the coefficient a_2 from Refs. 8 and 10 (which agree quite well) along with the fits corresponding to those in (a); (c) the observed b_2 from the present work and Ref. 10 along with the prediction of Ref. 9 (dashed line) and our fit (solid curve); (d) the normalized s-wave amplitude and fit; and (e) the relative phase $\phi_d - \phi_s$ and fit. All solid lines correspond to the same fit and represent the best χ^2.

TABLE I. The best-fit values of the resonance parameters.

Doorway[a]		E_i (MeV)	Γ_i (MeV)	$g_i^d g_0^\gamma$ (keV)	$g_i^s g_0^\gamma$ (keV)	φ_s (deg)	φ_d (deg)
	A	21.26[a]	0.1[a]	7.6 ± 0.4	1.2 ± 0.4	52 ± 14	163 ± 2
		(21.3–21.22)	(0.0–0.2)	(10.8–3.5)	[4.3–(–3.2)]	(44–75)	(158–162)
	B	22.15[b]	1.6 ± 0.6	37.6 ± 0.5	27.5 ± 0.7	0[c]	109 ± 1
				(36.8–39.6)	(26.8–28.9)		(111–107)

[a]The energy and width of resonance A, which do not include the shift and damping, respectively, were fixed and stepped; equally good χ^2 were obtained for Γ_A ranging from 0.0 to 0.2 MeV. The corresponding value of V is from 0.54 to 0.39 MeV. Corresponding excursions of the best-fit parameters are shown in parentheses.
[b]The energy of resonance B was fixed to the value in Ref. 9.
[c]φ_s for resonance B was arbitrarily chosen to be zero.

[9]W. J. O'Connell, Ph.D. thesis, Stanford University, 1969 (unpublished); W. J. O'Connell, G. L. Latshaw, J. L. Black, and S. S. Hanna, in *Proceedings of the International Conference on Photonuclear Reactions and Applications, Pacific Grove, California, 1973*, edited by B. L. Berman (Lawrence Livermore Laboratory, Livermore, Calif., 1973), Vol. 2, p. 939.
[9]N. M. Kabachnik and V. N. Razuvaev, Phys. Lett. 61B, 420 (1976).
[10]S. S. Hanna, H. F. Glavish, R. Avida, J. R. Calarco, E. Kuhlmann, and R. LaCanna, Phys. Rev. Lett. 32, 114 (1974).

REF. S. H. Chew, J. Lowe, J. M. Nelson and A. R. Barnett
Nucl. Phys. A286, 451 (1977)

ELEM. SYM.	A	Z
O	16	8

METHOD

REF. NO. 77 Ch 4 egf

REACTION	RESULT	EXCITATION ENERGY	SOURCE		DETECTOR		ANGLE
			TYPE	RANGE	TYPE	RANGE	
P,G	ABX	18- 33	D	6- 22	NAI-D		DST

Abstract: Previous data on excitation functions for $^{15}N(p, \gamma_1+\gamma_2)^{16}O$ have been extended to cover the energy range E_p = 6–22 MeV (E_x = 18–33 MeV). In addition, angular distribution measurements have been made throughout this range, and γ-γ angular correlation measurements made over the region of a resonance at E_p = 8.86 MeV. From the data, and from comparison with other work, spin assignments are made for resonances as follows: E_x = 18.02 MeV, J = 3; E_x = 18.98 MeV, J = 2, 4; E_x = 19.90 MeV, J = 3; E_x = 20.43 MeV, $J^\pi = 2^-$; E_x = 24.77 MeV, $J^\pi = 2^+, 4^+$; E_x = 26.42 MeV, $J^\pi = 2^+, 4^+$ and E_x = 27.36 MeV, $J^\pi = 2^-, 4^-$. Radiative widths are also deduced. The region E_x = 23–32 MeV is identified as a giant dipole resonance on the 6.13 MeV, $J^\pi = 3^-$, T = 0 state of ^{16}O from angular distribution measurements. The nature of this giant resonance is discussed and it is compared with the ground-state giant dipole resonance; it is shown that the main part of the excited-state giant resonance can be accounted for by broad states with $J^\pi = 2^+$ and 4^+ with configuration $(1p_{1/2}^{-1}(2p, 1f))$ in this region.

TABLE I

Level parameters for resonances in $^{15}N(p, \gamma_2)^{16}O$

E_p (MeV)	E_x (MeV)	$\Gamma_{c.m.}$ (keV)	A_0 (μb/sr)	Γ_{p_0}/Γ	J^π	T	Γ_{γ_2} (eV)
6.29±0.02	18.02±0.02	≤ 40	5.0±1.7	0.38	3	0, 1	4± 2
7.31±0.02	18.98±0.02	≤ 40	2.2±0.7	1	2 4	0, 1	≤ 2 ≤ 1
8.29±0.02	19.90±0.02	75± 30	4.9±2.1	≤ 0.45 ≥ 0.22	3	0, 1	≥ 12 ≤ 23
8.86±0.03	20.43±0.03	190± 40	6.7±2.2	0.45	2^-	1	120± 45
13.49±0.06	24.77±0.06	340± 55	7.1±2.4	0.25	2^+ 4^+	1	230± 90 130± 50
15.25±0.08	26.42±0.08	530± 80	9.4±3.1	0.23	2^+ 4^+	1	740±240 410±140
16.25±0.10	27.36±0.10	825±115	8.7±2.9	0.25	2^+ 4^+	1	1070±380 590±210

over

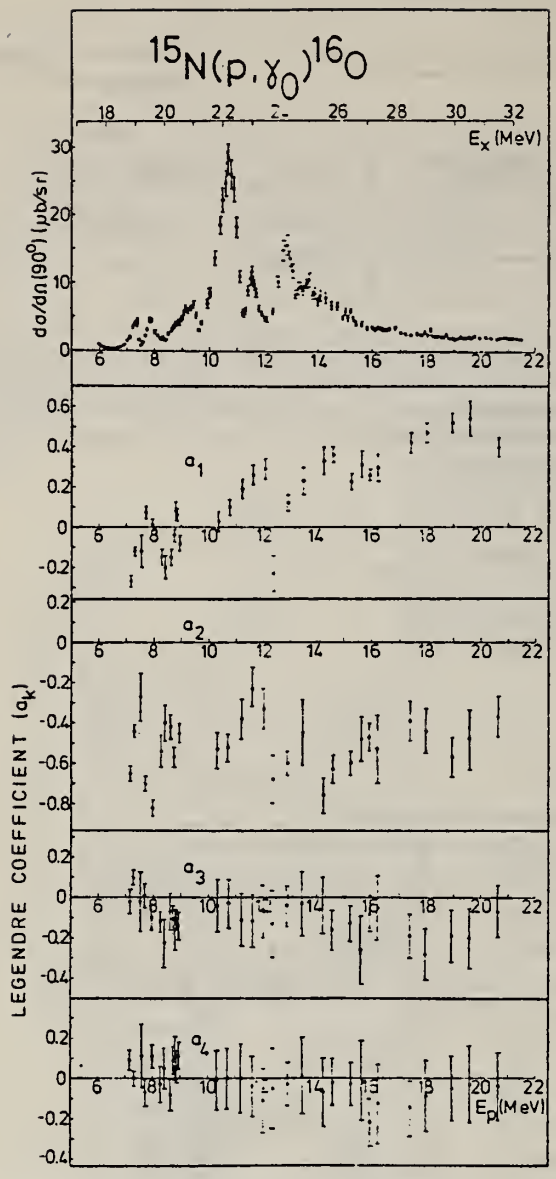

Fig. 2. The 90° excitation function and Legendre coefficients for $^{15}N(p,\gamma_0)^{16}O$.

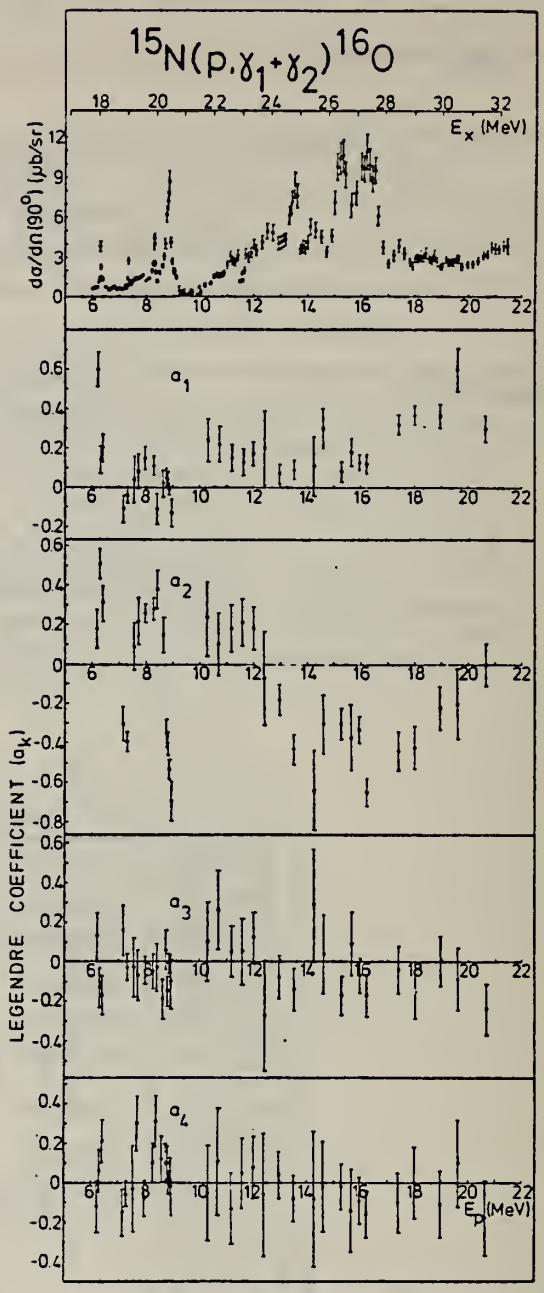

Fig. 3. The 90° excitation function and Legendre coefficients for $^{15}N(p,\gamma_1+\gamma_2)^{16}O$.

REF.

D.J.S. Findlay and R.O. Owens
Nucl. Phys. A279, 385 (1977)

ELEM SYM	A	Z
O	16	8

METHOD

REF. NO.	
77 Fi 3	egf

REACTION	RESULT	EXCITATION ENERGY	SOURCE		DETECTOR		ANGLE
			TYPE	RANGE	TYPE	RANGE	
G,P	ABX	40 - 105	C	40-105	MAG-D		DST

TABLE 1

The $^{16}O(\gamma, p_0)^{15}N$ reaction cross sections

E_γ^{Lab} (MeV)	θ_{Lab} (deg)	$\left(\frac{d\sigma}{d\Omega}\right)_{Lab}$ (μb/sr)	σ_{tot} (μb)
40	45.0	44.1 ±1.3	
50	45.0	21.2 ±0.7	
60			65.8 ±2.0
	30.1	11.04 ±0.63	
	45.0	12.30 ±0.69	
	60.1	10.92 ±0.73	
	75.0	6.94 ±0.47	
	90.0	4.12 ±0.23	
	105.2	2.00 ±0.15	
	120.0	0.953 ±0.076	
	135.1	0.405 ±0.040	
	149.9	0.200 ±0.025	
70	45.0	6.97 ±0.45	
80			13.95±0.74
	30.2	3.07 ±0.29	
	45.0	3.34 ±0.33	
	60.0	2.38 ±0.25	
	75.0	1.16 ±0.14	
	90.1	0.478 ±0.061	
	105.1	0.135 ±0.027	
	120.0	0.0554±0.0106	
	135.1	0.0249±0.0059	
	150.0	0.0096±0.0029	
90	45.0	2.04 ±0.14	
95	45.0	1.45 ±0.18	
	75.0	0.331 ±0.062	
	105.0	0.0401±0.0096	
100			4.36±0.59
	30.0	1.39 ±0.20	
	45.0	1.14 ±0.18	
	60.0	0.589 ±0.114	
	75.0	0.140 ±0.033	
	90.0	0.0883±0.0175	
	105.0	0.0288±0.0138	
	120.0	≤ 0.0451	
	135.1	0.0154±0.0042	
105	45.0	1.12 ±0.17	

(over)

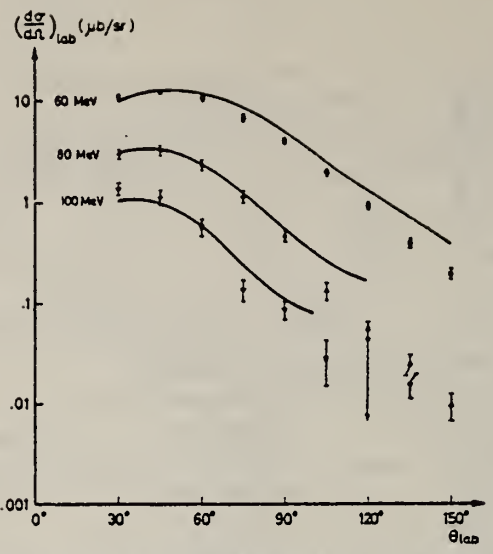

Fig. 2. Angular distributions of the $^{16}O(\gamma, p_0)$ reaction at $E_\gamma^{lab} = 60, 80$ and 100 MeV. The calculations of Hebach *et al.* (see text) are also shown. (These theoretical curves have been computed from Hebach's results at neighbouring energies.)

B. Johnsson, M. Nilsson and K. Lindgren
Nucl. Phys. A278, 365 (1977)

ELEV. ENR.	A	Z
0	16	8

METHOD

REF. NO.
77 Jo 3

egf

REACTION	RESULT	EXCITATION ENERGY	SOURCE		DETECTOR		ANGLE
			TYPE	RANGE	TYPE	RANGE	
G,2N	ABX	100 - 600	C	100-800	ACT-I		4PI

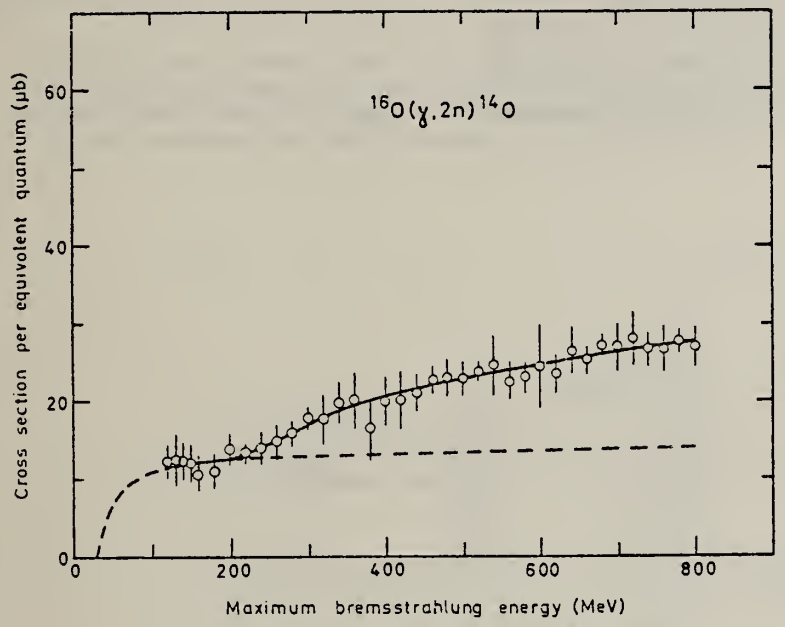

Fig. 2. The same as fig. 1 but for the reaction $^{16}O(\gamma, 2n)^{14}O$.

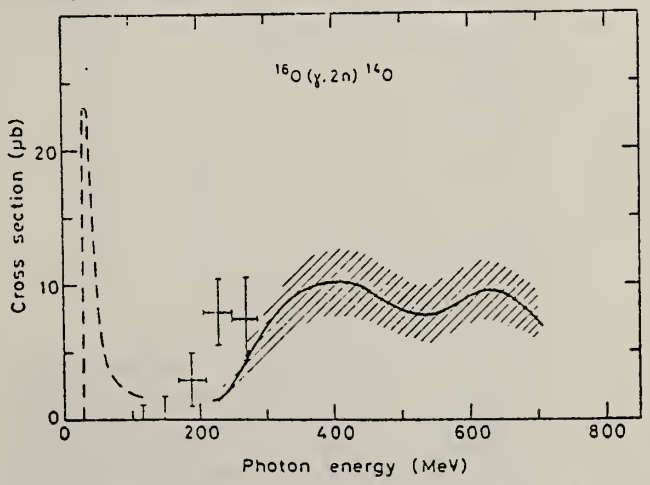

Fig. 4. The same as fig. 3 but for the reaction $^{16}O(\gamma, 2n)^{14}O$. The dashed curve and crosses show results from ref. [8]) and ref. [12]) respectively.

[8] K. Kayser, W. Collin, P. Fliss, S. Guldbakke, G. Nolte, H. Reich, J.O. Trier and W. Witschel, Z. Phys. 239, 447 (1970)

[12] K.A. Meyer, W.B. Walters and J.P. Hummel, Nucl. Phys. A122, 606 (1968)

REF. H. Lancman, A. P. M. Van 'T Westende and H. D. Graber
Nucl. Phys. A291, 293 (1977)

ELEM. SYM.	A	Z
0	16	8

METHOD

REF. NO. 77 La 3 egf

REACTION	RESULT	EXCITATION ENERGY	SOURCE		DETECTOR		ANGLE
			TYPE	RANGE	TYPE	RANGE	
G,G	G.G	7	D	7	SCD-D		DST

Abstract: The strengths of the isospin forbidden E1 ground-state transitions from the 1^-, 6.95 MeV state of ^{40}Ca and the 1^-, 7.12 MeV state of ^{16}O were determined in a γ-ray resonance scattering experiment; the partial widths are $\Gamma_0 = 0.41 \pm 0.03$ eV and 0.06 ± 0.01 eV, respectively. The results are in good agreement with previous determinations, confirming the unusually large strengths of these E1 transitions. In addition, the widths of the 2^+, 6.91 MeV state of ^{40}Ca and the 2^+, 6.92 MeV state of ^{16}O were measured as $\Gamma_0 = 0.13 \pm 0.06$ eV and 0.094 ± 0.010 eV, respectively.

7.12,6.92 MeV

TABLE 2
Widths of ^{16}O states

E_x (MeV)	J^π	Γ_0 (meV)		
		this work	ref. [9])	theory
6.92	2^+	94 ± 10	110 ± 6	
7.12	1^-	60 ± 10	55 ± 5	45 [4])

[4]) Ref. [4]).

[4]D.H. Glockner and R.D. Lawson, Phys. Lett. 56B, 301 (1975)

REF. J. L. Matthews, W. Bertozzi, M. J. Leitch, C. A. Peridier, B. L. Roberts, C. P. Sargent, W. Turchinetz, D. J. S. Findlay, R. O. Owens
Phys. Rev. Lett. 38, 8 (1977)

ELEM. SYM.	A	Z
O	16	8

METHOD

REF. NO. 77 Ma 1 hmg

REACTION	RESULT	EXCITATION ENERGY	SOURCE		DETECTOR		ANGLE
			TYPE	RANGE	TYPE	RANGE	
G,P	ABX	95-280	C	110-300	MAG-D		DST

GROUND STATE PROTONS

The $^{16}O(\gamma,p_0)$ cross section has been measured for a series of photon energies between 100 and 300 MeV at proton angles of 45°, 90°, and 135°. Above 250 MeV, the results exceed simple shell-model predictions by several orders of magnitude. The data are compared with a calculation which involves Δ excitation in an intermediate state.

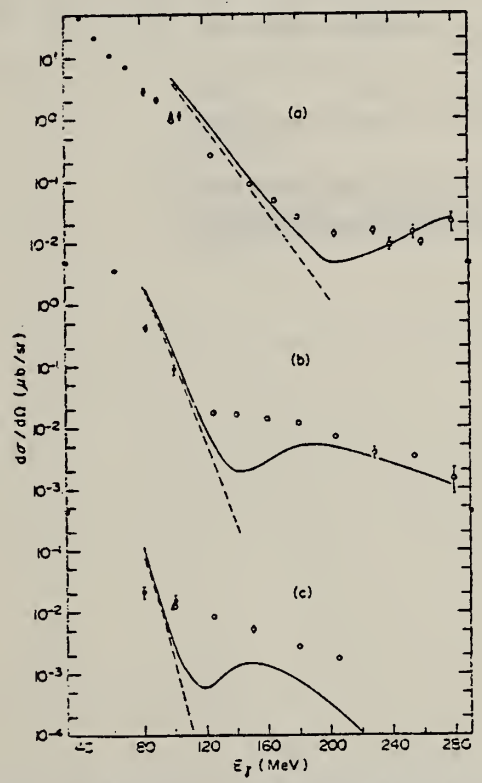

FIG. 1. Differential cross section in the laboratory system for the reaction $^{16}O(\gamma,p_0)^{15}N$ as a function of photon energy at proton angles (a) 45°, (b) 90°, and (c) 135°. Solid circles are used for the data of Ref. 2, open circles for the present results. Only statistical errors are shown. The curves represent the theoretical predictions of Ref. 5, as discussed in the text: dashed curve, single-step process only; solid curve, one-step plus two-step process (see Fig. 2).

[2] D.J.S. Findlay, R.O. Owens, to be published.

[5] G.D. Nixon et al., Bull. Am. Phys. Soc. 21, 67 (1976), and to be published.

REF. S. V. Dementii, V. I. Ogurtsov, N. G. Afanas'ev
Yad. Fiz. 28, 865 (1978)
Sov. J. Nucl. Phys. 28, 443 (1978)

ELEM. SYM.	A	Z
O	16	8

METHOD

REF. NO. 78De11

hg

REACTION	RESULT	EXCITATION ENERGY	SOURCE		DETECTOR		ANGLE
			TYPE	RANGE	TYPE	RANGE	
E,E/	ABX	50-200	D	1*2	MAG-D		DST
				(799-1178)			

Measurements were made of quasielastic scattering of electrons in the (e, e') reaction by the nuclei ^{9}Be, ^{12}C, ^{14}N, ^{16}O, and ^{27}Al. An experimental estimate is obtained of the effective mass of an intranuclear nucleon. At excitation energies up to 80 MeV, a ratio $M^*/M = 0.6$ is obtained, corresponding to a linear potential $V(E) = V_0 + 0.4E$ and in good agreement with the data on proton scattering by nuclei [C. M. and F. G. Perey, Atomic Data and Nuclear Tables 13, 294 (1974)]. At excitation energies above 120 MeV the nucleon effective mass turned out to be close to that of the free nucleon, $M^*/M = 0.9$.

*GEV, QUASIELASTIC

PACS numbers: 25.30.Cg, 27.20. + n, 27.30. + t

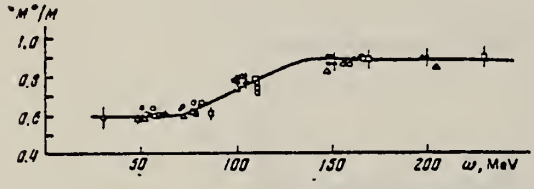

FIG. 4. Reduction coefficient M^*/M as a function of energy transfer: ●—^{9}Be, ▲—^{12}C, ○—^{14}N, △—^{16}O, □—^{27}Al. The curve has been drawn through the experimental points by hand.

REF. V. Di Napoli, J. B. Martins, G. Rosa, F. Salvetti, O. A. P. Tavares, M. L. Terranova and H. G. De Carvalho
J. Inorg. Nucl. Chem. 40, 1619 (1978)

ELEM. SYM.	A	Z
O	16	8

METHOD

REF. NO. 78 Di 10 | hg

REACTION	RESULT	EXCITATION ENERGY	SOURCE TYPE	SOURCE RANGE	DETECTOR TYPE	DETECTOR RANGE	ANGLE
G,C11	ABY	26(26.78)-999	C	300-999	ACT-I		4PI

Abstract—Mean cross sections for the photoproduction of ^{7}Be and ^{11}C from ^{19}F, ^{27}Al, ^{28}Si and ^{32}S targets, ^{7}Be from ^{10,11}B, and ^{11}C from ^{14}N and ^{16}O targets have been measured using bremsstrahlung beams in the energy range 0.3–1.0 GeV. The results have been compared with previous measurements and an excellent agreement has been found. In most cases, the values obtained turned out to be much larger than those expected from a simple spallation mechanism. A fragmentation and/or a fission-like process has been suggested in explaining the mechanism of such reactions.

999=1 GEV

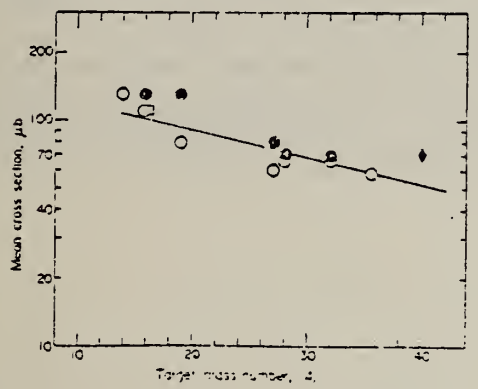

Fig. 1. Mean cross sections per photon, $\bar{\sigma}_\gamma$, of ^{11}C photoproduction vs the target mass number A_t. Experimental data are taken from: ●, Ref. [9]; □, Ref. [13]; ◆, Ref. [2]; ○, present work. The straight line is a least squares fit of the experimental points.

Table 1. Cross sections per equivalent quantum of ^{11}C photoproduction

E_0 (GeV)	Cross Section, σ_Q (μb) ^{14}N	^{16}O	^{19}F	^{27}Al	^{28}Si	^{32}S	^{35,37}Cl
0.30	520±30	200±20	110±20	28±10	35±10	45±10	30±10
0.32	520±30	210±20	120±20	30±10	42±10	50±10	30±10
0.35	530±30	230±20	125±20	38±10	45±10	60±10	40±10
0.40	530±30	230±20	130±20	42±10	52±10	65±10	50±10
0.48	550±30	255±20	150±20	60±10	70±10	80±10	60±10
0.55	570±30	260±20	160±20	60±10	78±10	85±10	50±10
0.65	600±30	290±20	180±20	70±10	85±10	98±10	75±10
0.75	620±30	300±20	180±20	79±10	95±10	110±10	85±10
0.90	650±30	320±20	190±20	90±10	110±10	120±10	95±10
1.00	680±30	330±20	210±20	100±10	115±10	125±10	100±10

Table 3. Comparison between experimentally determined and calculated cross sections of ^{7}Be and ^{11}C photoproduction and indication of the dominant reaction channels

Target Nucleus	Product Nucleus	Nominal Nucleon Loss, ΔA	$\Delta A/A_t$ (x10^{-2})	$\bar{\sigma}_{exp}$ (*) (μb)	$\bar{\sigma}_{CDMO}$ (**) (μb)	$\bar{\sigma}_{exp}/\bar{\sigma}_{CDMO}$	Apparent Threshold (Exp.) E_{th} (MeV)	Possible Mechanism of Production
^{10,11}B	^{7}Be	(3)	(30);36	67	28	2	≤ 50	Spallation
^{12}C	^{7}Be	5	42	110	20	5	≤ 50	Spallation
^{14}N	^{7}Be	7	50	108	12	9	≤ 50	Fission Spallation
^{14}N	^{11}C	3	21	130	60	2	≤ 50	Spallation
^{16}O	^{7}Be	9	56	107	8	13	50<E_{th}<200	Fission Fragmentation
^{16}O	^{11}C	5	31	117	33	3	≤ 50	Spallation
^{19}F	^{7}Be	12	63	106	5	21	50<E_{th}<200	Fission Fragmentation
^{19}F	^{11}C	8	42	105	16	7	50<E_{th}<200	Fission Fragmentation Spallation
^{27}Al	^{7}Be	20	74	142	2	71	> 200	Fragmentation
^{27}Al	^{11}C	16	59	70	5	14	50<E_{th}<200	Fission Fragmentation
^{28}Si	^{7}Be	21	75	56	2	28	> 200	Fragmentation
^{28}Si	^{11}C	17	61	68	4	17	50<E_{th}<200	Fission Fragmentation
^{32}S	^{7}Be	25	78	114	2	57	> 200	Fragmentation
^{32}S	^{11}C	21	66	68	3	23	50<E_{th}<200	Fission Fragmentation
^{35,37}Cl	^{11}C	24;(26)	69;(70)	59	3	20	50<E_{th}<200	Fission Fragmentation
^{40}Ca	^{7}Be	33	83	70	1	70	> 200	Fragmentation
^{40}Ca	^{11}C	29	73	70	2	35	> 200	Fragmentation

(*) Mean values of the different measurements (see Figs. 1 and 2).

(**) Calculated values according to Ref. [3].

REF. R.J. Holt, H.E. Jackson, R.M. Laszewski, J.E. Monahan, and J.R. Specht
Phys. Rev. C 18, 1962 (1978)

ELEM. SYM.	A	Z
0	16	8

METHOD

REF. NO. 78 Ho 2 hg

REACTION	RESULT	EXCITATION ENERGY	SOURCE TYPE	SOURCE RANGE	DETECTOR TYPE	DETECTOR RANGE	ANGLE
G,NO	ABX	4- 7	C	9	TOF-D		DST
		(4.3-7)		(8.5)			

The angular distribution for the $^{17}O(\gamma,n_0)^{16}O$ reaction was observed throughout the excitation energy region 4.3–7 MeV and at angles of 90° and 135°. The ground-state radiation widths for resonances in this energy region were extracted from the data. The value of the radiation width for the $d_{5/2} \rightarrow d_{3/2}$ spin-flip transition at 5.08 MeV was found to be approximately 1/3 of the value expected for a pure single-particle transition. The implications that this result has for the nuclear structure of ^{17}O is discussed. The effects of potential radiative capture were observed directly in a photoneutron reaction for the first time. At the location of the 5.38-MeV, 3/2⁻ resonance in ^{17}O, an anomalous symmetric dip was observed in the cross section at both reaction angles. The data were interpreted in terms of a general R-matrix reaction theory which includes the effects of internal, channel, and potential radiative capture in a self-consistent manner. The neutron channel was defined by incorporating an R-matrix analysis of the $^{16}O(n,n)^{16}O$ reaction into the present interpretation. The anomalous minimum at 5.38 MeV was found to be due to a unique feature of channel capture. The R-matrix prediction for the total cross section was extrapolated into the keV region and the significance that this cross section has for stellar nucleosynthesis is discussed.

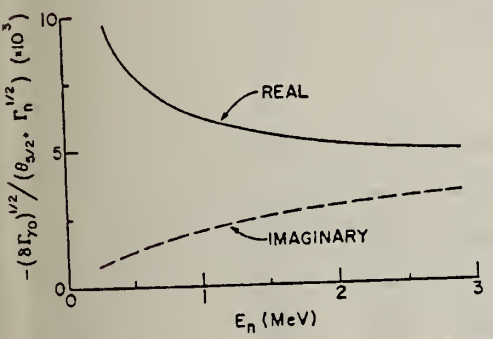

FIG. 3. Real and imaginary components of the $E1$ radiative channel capture for $p_{3/2}$ neutrons. In the MeV region the imaginary part is not negligible in comparison with the real component.

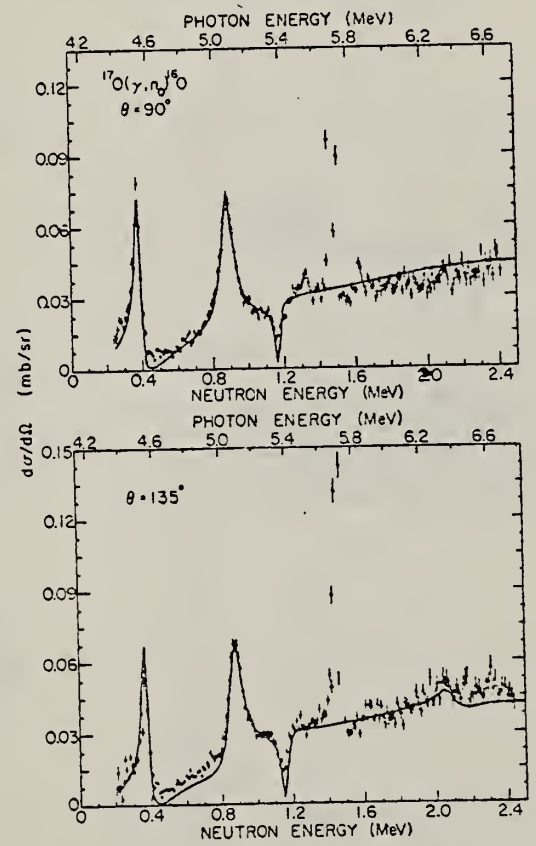

FIG. 4. R-matrix interpretation of the differential cross section for the $^{17}O(\gamma,n_0)^{16}O$ reaction. The points represent the observations while the curves represent the results of a "hard-sphere" external capture model.

over

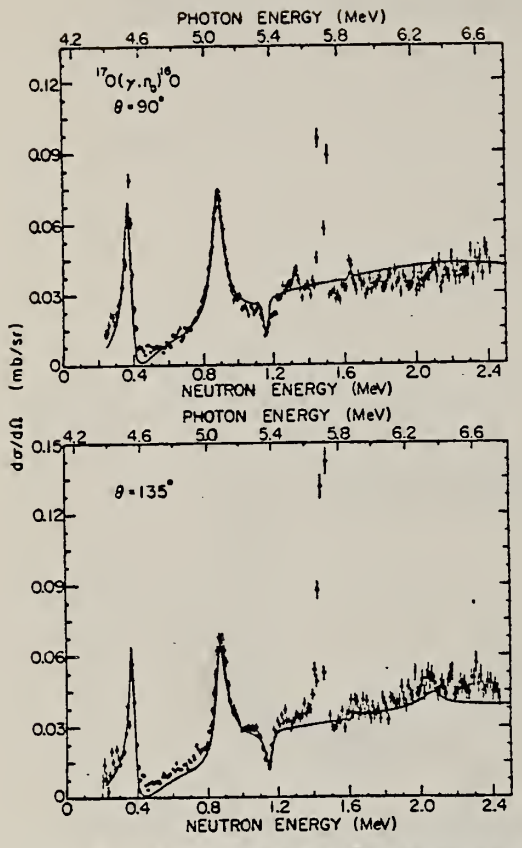

FIG. 5. Final R-matrix analysis of the observations of the $^{17}O(\gamma,n_0)^{16}O$ reaction. The parameters used in this analysis, Tables III and IV, also describe the $^{16}O(n,n)^{16}O$ reaction. The interference minimum at 5.38 MeV is not as deep as that given by the simple hard-sphere model.

TABLE II. R-matrix parameters which were used in the present analysis for the $^{16}O(n,n)^{16}O$ reaction. [Note that the $p_{1/2}$ parameters are not necessary for the (γ,n) channel.]

l_J	$E_{\lambda lJ}$ (MeV)	$\gamma_{\lambda lJ}{}^2$ (MeV)	R_{0lJ}	b_{lJ}
$s_{1/2}$	−3.272	0.46	0	0
	2.35	0.056		
$p_{3/2}$	0.392	0.165	0.54	−0.405
	1.305	0.033		
	3.445	0.214		
$d_{3/2}$	0.69	0.816	0.06	−1.194
	1.834	0.014		
	3.300	0.187		
	4.160	0.012		
$d_{5/2}$	−4.143	0.80	0	−0.787

TABLE III. R-matrix parameters for the $^{17}O(\gamma,n_0)^{16}O$ reaction for $\theta_{5/2^+} = -0.59$, $R_c = 4.93$ fm.

$M\mathcal{L}$	J^π	E_γ (MeV)	Γ_n (MeV)	$\Gamma_{\gamma\gamma}{}^{1/2}$ $(\text{eV})^{1/2}$
$E1$	$\frac{3}{2}^-$	4.549	0.043	0.49
		5.378	0.038	0.65
		7.532	0.442	0.71
$M1$	$\frac{3}{2}^+$	5.077	0.094	−0.69
		7.213	0.255	1.44
$E2$	$\frac{1}{2}^+$	6.354	0.130	−0.22

TABLE IV. Deduced ground-state radiation widths for levels in ^{17}O.

$M\mathcal{L}$	J^π	E_γ (MeV)	$\Gamma_{\gamma 0}$ (eV)	$g_J\Gamma_{\gamma 0}\Gamma_n/\Gamma$ (eV)
$E1$	$\frac{3}{2}^-$	4.549	0.42	0.14
		5.378	0.06	0.02
	$\frac{7}{2}^-$	5.690	0.4[a]	0.27[a]
$M1$	$\frac{3}{2}^+$	5.077	1.0	0.33
$E2$	$\frac{1}{2}^+$	6.354	<0.07	<0.012
$E1,M1$	$\frac{3}{2},\frac{5}{2},\frac{7}{2}$	5.729		1.5[a]

[a] Value was deduced from area analysis.

REF. W.J. O'Connell and S.S. Hanna
Phys. Rev. C 17, 892 (1978)

[page 1 of 4]

ELEM. SYM.	A	Z
O	16	8

comment: Final Publication of Data Given in 730cl

REF. NO. 78 Oc 1 hg

REACTION	RESULT	EXCITATION ENERGY	SOURCE TYPE	SOURCE RANGE	DETECTOR TYPE	DETECTOR RANGE	ANGLE
$ (P,GO)	ABX	20- 29	D	8- 18	NAI-D		DST
				(8.6-18)			

The giant electric dipole resonance based on the ground state (0^+) of ^{16}O has been studied with the reaction $^{15}N(p,\gamma_0)^{16}O$ from E_p=8.6 to 18.0 MeV (E_γ=20.2 to 29.0 MeV). The $E1$ strength in (γ,p_0) is concentrated between E_γ=20 and 29 MeV where it exhausts about 15% of the $E1$ sum rule. Major peaks are displayed at 22.2 and 25.0 MeV and secondary structure at 21.0, 22.9, and in the 24 MeV region. The angular distributions indicate predominantly dipole radiation and are fairly constant over the entire range, except in the region of the secondary peaks where the coefficient of $P_2(\cos\theta)$ displays striking interference effects. This behavior supports the suggestion that these structures are due to interference between more complex states and the simple particle-hole configurations of the $E1$ resonance. The value of the coefficient of $P_2(\cos\theta)$ can be used to restrict greatly the allowed configurations of the p_0 channel—the solution is predominantly either $d_{3/2}$ wave or $s_{1/2}$ wave. The presence of terms in $P_1(\cos\theta)$ and $P_3(\cos\theta)$ indicates significant $E2$ strength which increases above the $E1$ resonance. Data are also presented on the reactions $^{15}N(p,\gamma_1-\gamma_4)^{16}O$ and $^{15}N(p,\alpha\gamma_{15.1})^{12}C$.

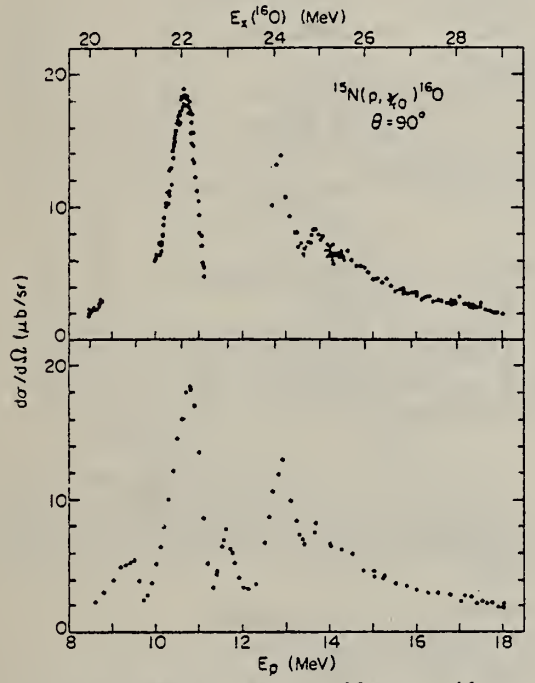

FIG. 2. The 90° yield of $^{15}N(p,\gamma_0)^{16}O$. Top: Measurements taken over selected areas to search for intermediate and fine structure. Bottom: Yields extracted from the angular distribution measurements. The proton energy scale here and in subsequent figures is corrected for the energy loss in the entrance foil of the cell.

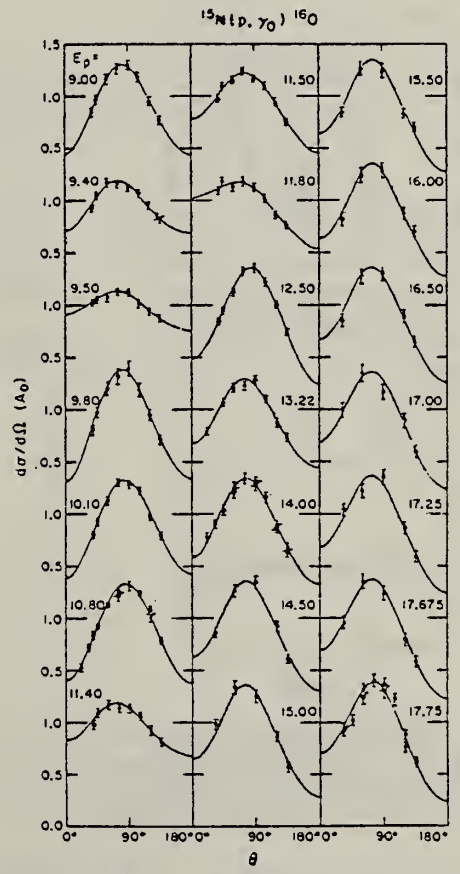

FIG. 3. Selected angular distribution measurements from $^{15}N(p,\gamma_0)^{16}O$, plotted in units of A_0.

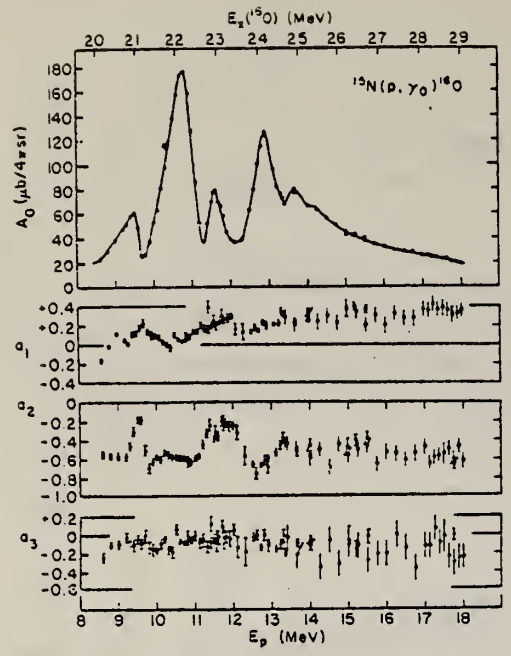

FIG. 4. Plot of A_0, a_1, a_2, and a_3 obtained from Legendre polynomial fits (k = 3) to the measured angular distributions of $^{15}N(p,\gamma_0)^{16}O$.

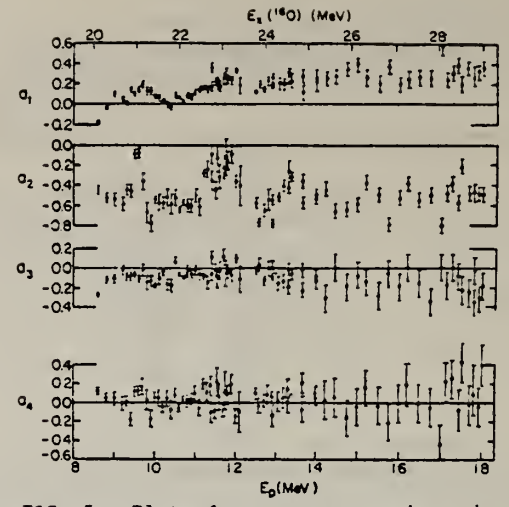

FIG. 5. Plot of a_1, a_2, a_3, and a_4 obtained from Legendre polynomial fits (k = 4) to the measured angular distributions of $^{15}N(p,\gamma_0)^{16}O$.

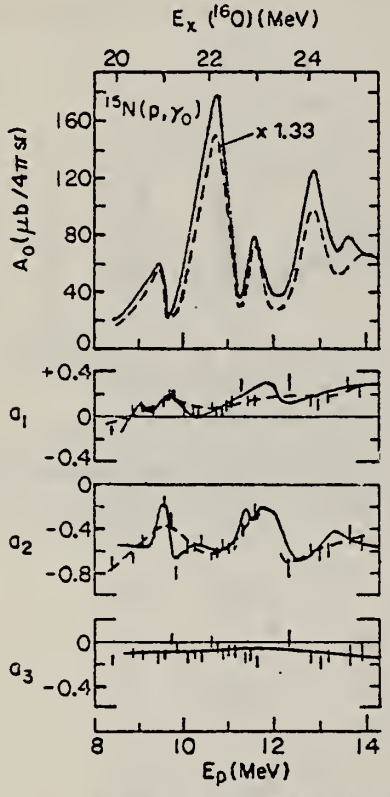

FIG. 6. The results of this experiment on $^{15}N(p,\gamma_0)^{16}O$ (solid curves) compared with those of Earle and Tanner[24] (data points and dashed curves). To facilitate comparison the A_0 curve of Ref. 24 has been multiplied by 1.33.

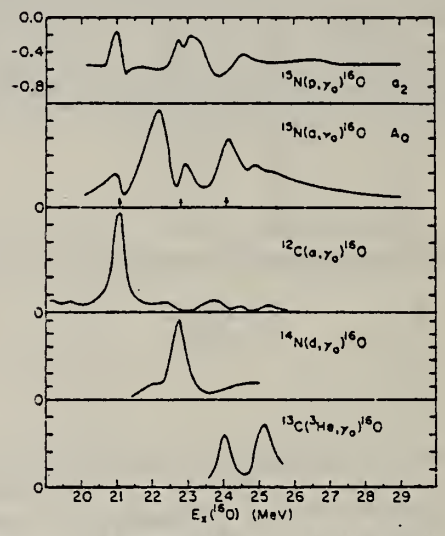

FIG. 10. Structures in the reactions $^{12}C(\alpha,\gamma_0)^{16}O$ (Refs. 27,28), $^{14}N(d,\gamma_0)^{16}O$ (Ref. 30), and $^{13}C(^3He,\gamma_0)^{16}O$ (Ref. 29) compared with the structures in A_0 and a_2 of the present experiment.

24 E.D. Earle and N.W. Tanner, Nucl. Phys. A95, 241 (1967).

27 M. Suffert and W. Feldman, Phys. Lett. 24B, 579 (1967)

28 K.A. Snover, E.G. Adelberger, and D.R. Brown, Phys. Rev. Lett. 32, 1061 (1974)

29 N.G. Puttaswamy and D. Kohler, Phys. Lett. 20, 288 (1966)

30 M. Suffert, Nucl. Phys. 75, 226 (1965)

ELEM. SYM.	A	Z
O	16	8

METHOD

REF. NO. 78 Oc 1 hg

REACTION	RESULT	EXCITATION ENERGY	SOURCE		DETECTOR		ANGLE
			TYPE	RANGE	TYPE	RANGE	

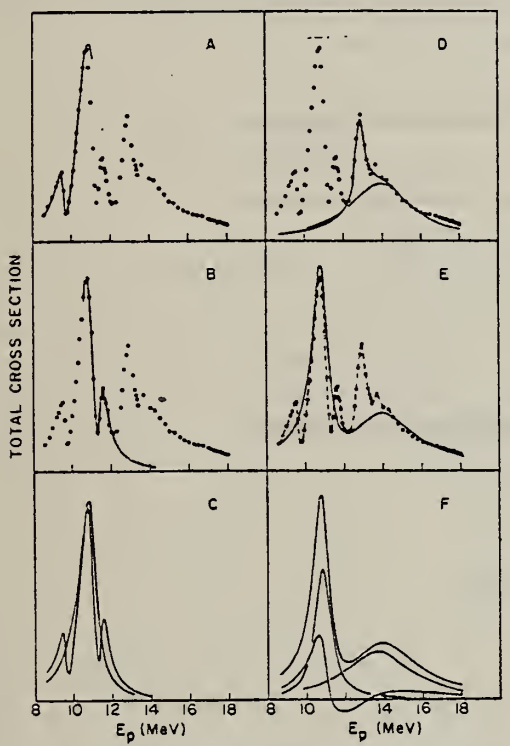

FIG. 11. Decomposition of the GDR of $^{15}N(p,\gamma_0)^{16}O$ into two main peaks and three narrower, secondary peaks. The various stages of the decomposition are explained in the text.

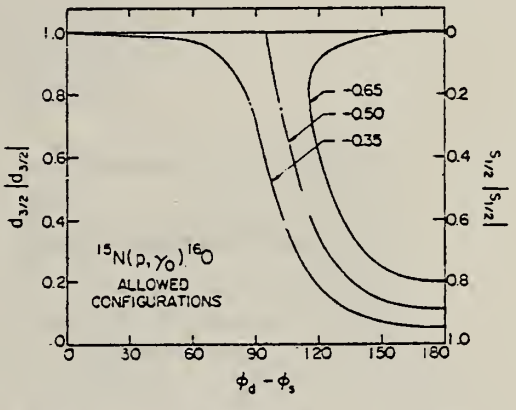

FIG. 12. Configurations in $^{15}N(p,\gamma_0)^{16}O$ allowed by the angular distributions a_2 = -0.35, -0.50, and -0.65. The curves define the relationship between the intensity $d_{3/2}|d_{3/2}|$ and the phase difference $\phi_d - \phi_s$.

TABLE I. Comparison of total cross-section measurements on the peak of the GDR (E_x = 22.15 MeV) in $^{16}O(\gamma,p_0)^{15}N$ and $^{16}O(\gamma,n_2)^{15}O$.

Reaction	σ^a (mb)	Reference
$^{15}N(p,\gamma_0)^{16}O$	12.9	Present work
$^{15}N(p,\gamma_0)^{16}O$	8.0	24
$^{16}O(\gamma,p_0)^{15}N$	10.7	23
$^{16}O(\gamma,p_0)^{15}N$	12.6	22
$^{16}O(\gamma,n_0)^{15}O$	5.6[b]	20
$^{16}O(\gamma,n_2)^{15}O$	7.2	19
$^{16}O(\gamma,n_\sigma)^{15}O$	9.3[b]	18
$^{16}O(\gamma,n_0)^{15}O$	10.1	21
$^{16}O(\gamma,n_0)^{15}O$	7.2	40

[a] It is not possible to give errors for these measurements on a consistent basis. Our own estimate is that the errors lie in the range ± 20-30%.

[b] Obtained from a 90° differential measurement, using the angular distribution measured later in (γ,n_0), see Fig. 9.

over

TABLE II. Parameters of the five states used to fit the structure in the GDR of ^{16}O.

E_x (MeV)	Γ (MeV)	$\Gamma_p\Gamma_\gamma/\Gamma$ (eV)
20.95 ± 0.01	0.32 ± 0.01	21 ± 1
22.15 ± 0.01	0.73 ± 0.01	488 ± 20
22.89 ± 0.01	0.32 ± 0.01	69 ± 5
24.07 ± 0.03	0.59 ± 0.04	130 ± 13
25.12 ± 0.06	3.15 ± 0.32	651 ± 117

TABLE III. Configurations of the dipole states in ^{16}O from Ref. 3.[a]

E_x MeV	$p^{-1}_{1/2}s_{1/2}$	$p^{-1}_{1/2}d_{3/2}$	$p^{-1}_{3/2}s_{1/2}$	$p^{-1}_{3/2}d_{5/2}$	$p^{-1}_{3/2}d_{3/2}$	Strength %
13.7	1.00	-0.02	-0.06	-0.02	0.02	1
17.6	0.01	0.90	-0.09	-0.38	-0.21	1
20.0	0.06	-0.02	0.96	-0.24	-0.08	1
22.2	0.04	0.35	0.20	0.90	-0.20	68
25.0	-0.01	0.27	0.10	0.09	0.95	29

[a] A zero-range force with a Soper mixture is used.

3
G.E. Brown, L. Castillejo, and J.A. Evans, Nucl. Phys. 22, 1 (1961)

REF. J.D. Steck
Phys. Rev. C 17, 1034 (1978)

ELEM. SYM.	A	Z
O	16	8

METHOD

REF. NO. 78 St 5 hg

REACTION	RESULT	EXCITATION ENERGY	SOURCE TYPE	SOURCE RANGE	DETECTOR TYPE	DETECTOR RANGE	ANGLE
A,GO	ABX	11	D	8	NAI-D		DST
		(11.26)		(8.16)			

Six ^{20}Ne levels have been investigated in detail via the $^{16}O + \alpha$ channel between $6.9 \lesssim E_\alpha \lesssim 10.2$ MeV. Level parameters for states at $E_x(^{20}Ne) = 10.264 \pm 0.008$, 11.077 ± 0.008, 11.259 ± 0.008, 11.552 ± 0.008, 12.237 ± 0.008, and 12.390 ± 0.008 MeV have been extracted from γ decay properties and phase shift analysis of the elastic scattering. With the exception of the 11.552 and 12.39 MeV states, these levels display primarily $T = 1$ characteristics. In addition to some previously reported $T = 0$ states, several other weak γ decaying resonances were observed at 11.97 ± 0.04, 12.05 ± 0.04, and 12.49 ± 0.02 MeV but were not studied in detail. Charge dependent matrix elements (4–120 keV) for isospin mixing of $T = 1$ states with nearby $T = 0$ states were estimated from the measured level parameters.

LIFETIME

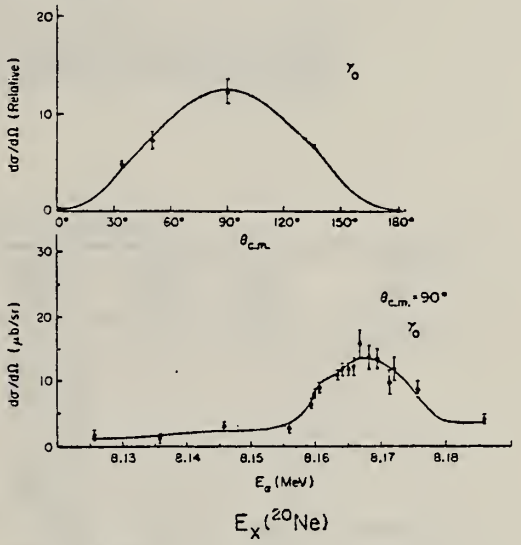

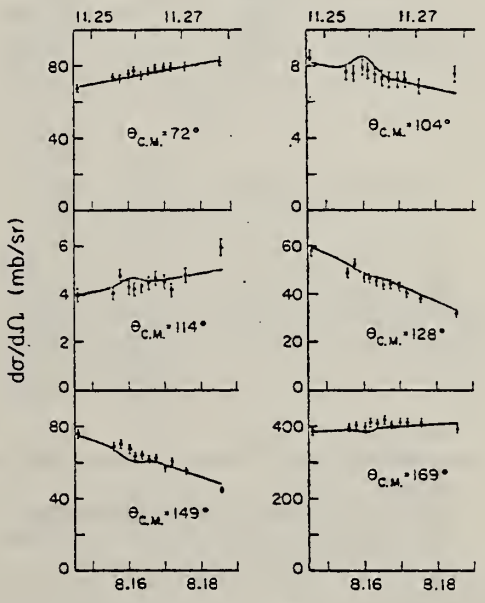

FIG. 4. The $E_\alpha = 8.16$ MeV resonance ($E_x = 11.26$ MeV). Same format as Fig. 2. The angular distribution fit is typical of a $1^- \rightarrow 0^+$, $E1$ transition. The γ_0 excitation function fit has a CL of 0.9. The ES fit includes the contributions from a 300 eV, $L = 1$ resonance.

over

TABLE I. Measured angular distribution coefficients.

E_α	Final state J^π; E_x (MeV)	CL[a]	a_2/a_0	a_4/a_0	b_2/b_0[b]	b_4/b_0[b]
6.92	2^+; 1.63	0.6	0.33±0.09	•••	0.38±0.10	•••
		0.2	0.33±0.09	0.03±0.13	0.38±0.10	0.04±0.15 ($\delta=-0.1\pm0.2$)[c]
7.93	4^+; 4.25	0.6	0.26±0.10	•••	0.29±0.11	•••
		0.5	0.25±0.10	−0.10±0.2	0.28±0.11	−0.12±0.20 ($\delta=-0.27\pm0.30$)[c]
8.16	0^+; 0	0.5	−0.99±0.10	•••	−1.08±0.10	•••
8.53	2^+; 1.63	0.2	•••	•••	•••	•••
		0.25	−0.1 ±0.20	•••	−0.11±0.3	•••
9.38	2^+; 1.63	0.35	0.39±0.11	•••	0.43±0.12	•••
		0.4	0.34±0.12	0.30±0.20	0.40±0.13	0.35±0.25 ($\delta=-0.1\pm0.07$)[c]
9.57	2^+; 1.63	0.4	•••	•••	•••	•••
		0.5	−0.12±0.30	•••	−0.13±0.30	•••
		0.2	−0.11±0.30	0.10±0.40	−0.12±0.30	0.10±0.4
9.70	2^+; 1.63	0.5	•••	•••	•••	•••
		0.5	0.2 ±0.20	•••	0.2 ±0.2	•••

[a] CL denotes angular distribution fit confidence level (0.1 to 0.9 acceptable).
[b] Coefficients corrected for angular acceptance and edge effect.
[c] $\delta = \langle E2\rangle/\langle M1\rangle$.

TABLE II. Radiative capture resonance parameters.

E_α (MeV)	E_x (MeV)	$\Gamma^\Gamma_{c.m.}$ (keV)	Final state (J^π; E_x)	$\omega\gamma_{c.m.}$ (eV)	Branching ratio	$\Gamma^\gamma_{c.m.}$[a] (eV)	$\lvert M\rvert^2$ (W.u.)	[b]
6.918±0.01[c]	10.264	≤1	0^+; 0		≤0.1			
			2^+; 1.63	19.2 ±1.9	1.0	3.85±0.39	0.28	($M1$)
			2^-; 4.97		≤0.2			
			3^-; 5.62		≤0.2			
7.932±0.01	11.077	≤3	0^+; 0		≤0.01			
			2^+; 1.63		≤0.02			
			4^+; 4.25	30.4 ±3	1.0	3.4 ±0.3	0.50	($M1$)
8.131±0.01	11.26	≤3	0^+; 0	0.58±0.05	1.0	0.19±0.02	2.8×10^{-6}	($E1$)
			2^+; 1.63		0.4±0.1			
8.53 ±0.01	11.55	≤5	0^+; 0		≤0.4			
			2^+; 1.63	0.41±0.05	1.0	0.08±0.01 ($J=2$)	3.9×10^{-3} [0.31	($M1$) ($E2$)]
			4^+; 4.25		0.5±0.4			
			2^-; 4.97		≤0.3			
9.384±0.01	12.237		0^+; 0		0.45±0.10			
		18±5	2^+; 1.63	5.8 ±0.5	1.0	1.2 ±0.1	0.046	($M1$)
			4^+; 4.25		≤0.3			
			2^-; 4.97		≤0.3			
9.57 ±0.01	12.39		0^+; 0		0.01			
		27±5	2^+; 1.63		0.4±0.1			
			4^+; 4.25	1.94±0.15	1.0	0.28±0.02	1.1×10^{-3}	($E1$)
		40±10	$\alpha_2\gamma_{6.13}$	1.96±0.1[d] $\times10^3$	2.2±0.3 $\times10^3$			
9.70 ±0.03	12.49	≤10	2^+; 1.63	0.17±0.05	1.0			

[a] Assume $\Gamma_\alpha \ll \Gamma_\gamma$.
[b] Multipolarity based on most likely transition.
[c] The energy uncertainty reflects the maximum of the relative uncertainty and the absolute uncertainty (0.01).
[d] $\omega\gamma = (2J+1)\,\Gamma_\alpha\Gamma_{\alpha_2}/\Gamma$.

REF. E.C. Booth, B. Chasan, F.L. Milder, B.L. Roberts, J. Comuzzi
Phys. Rev. C20, 1603 (1979)

ELEM. SYM.	A	Z
O	16	8

METHOD

REF. NO. 79 Bo 2 hg

REACTION	RESULT	EXCITATION ENERGY	SOURCE		DETECTOR		ANGLE
			TYPE	RANGE	TYPE	RANGE	
G,PI+	ABX	150-170	C	150-170	ACT-I		90

The total cross sections relative to photoproduction off the proton have been measured for the reactions $^{16}O(\gamma,\pi^+)^{16}N$ and $^{9}Be(\gamma,\pi^-)^{9}Li$ over the energy region from the production threshold up to 12 MeV over threshold. A distorted wave impulse approximation calculation has been performed for the $^{16}O(\gamma,\pi^+)^{16}N$ reaction and is seen to be $\simeq$30% higher than the observed cross section from threshold to 10 MeV. The $^{9}Be(\gamma,\pi^-)^{9}Li$ reaction represents the first (γ,π^-) measurement near threshold in which the cross section is not dominated by the $\vec{\sigma}\cdot\vec{\epsilon}$ term in the production Hamiltonian.

[NUCLEAR REACTIONS $^{16}O(\gamma,\pi^+)^{16}N$, $^{9}Be(\gamma,\pi^-)^{9}Li$, bremsstrahlung end point energies to 175 MeV, measured $\sigma(E)$; calculated $\sigma(E)$, DWIA.]

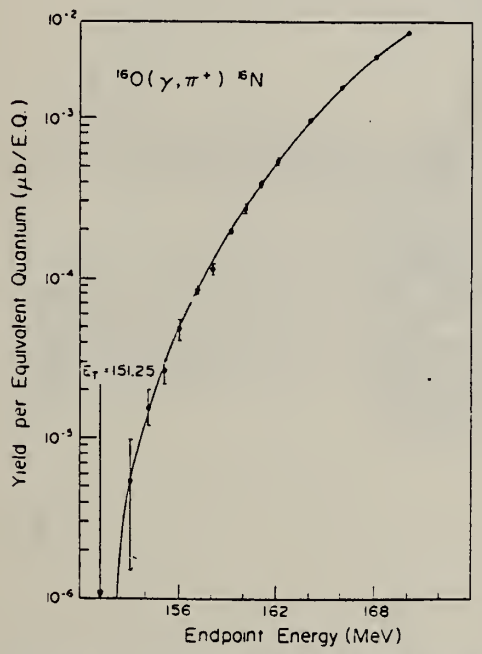

FIG. 1. The $^{16}O(\gamma,\pi^+)^{16}N$ yield per equivalent quantum. The solid curve is the result of a fit as described in the text.

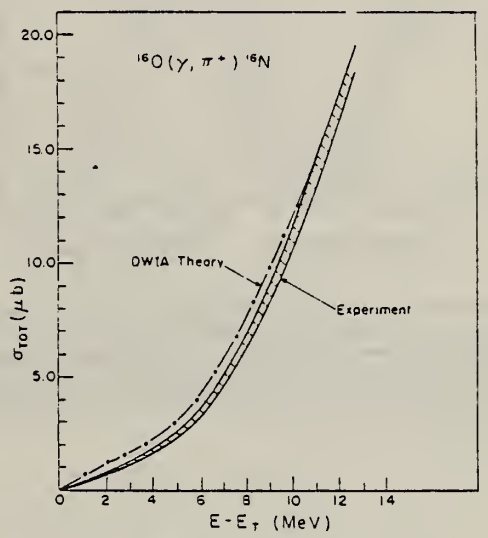

FIG. 3. The measured and calculated total cross sections for $^{16}O(\gamma,\pi^+)^{16}N$. E_T is the pion threshold energy and E is the bremsstrahlung end point energy. The shaded region represents the statistical uncertainty on the cross section. The systematic error is an additional 5%.

REF. V.N. Eponeshnikov, Yu.F. Krechetov
JETP Lett. 29, 401 (1979)

ELEM. SYM.	A	Z
0	16	8

METHOD

REF. NO. 79 Ep 2 hg

REACTION	RESULT	EXCITATION ENERGY	SOURCE		DETECTOR		ANGLE
			TYPE	RANGE	TYPE	RANGE	
G,PIOP	ABY	60-130	C	450	CKV-D		DST

*MOM,MEV/C, COIN

The cross sections of reaction $(\gamma,\pi^{+}p)$ on Li^{6} C^{12} nuclei were measured in the 0–600 MeV/c range of momentum transfer to the residual nucleus. For large values of momenta, cross section values disagree with calculations carried out within the framework of a shell model and a model of quasi-free meson photoproduction on nuclei.

PACS numbers: 25.20. + y

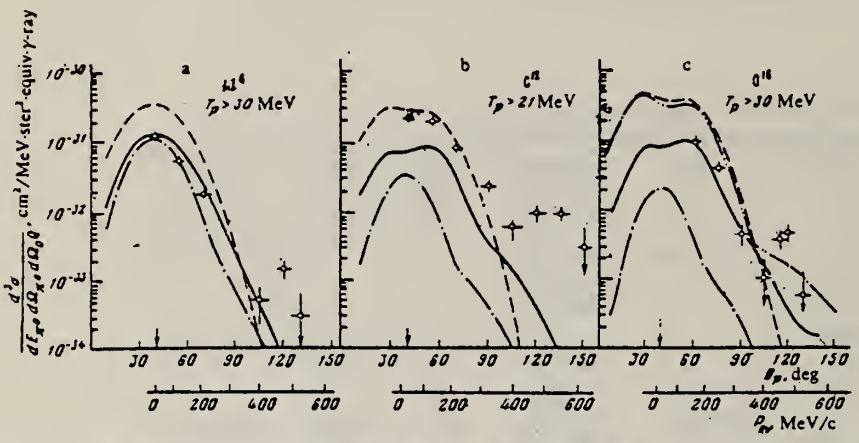

FIG. 1. Dependence of reaction cross section on the proton angle of emission: O—experiment, with total measurement errors; — —calculations using plane waves; —— final state interactions taken into account; ————effect of S-shell shown separately; ————calculations with momentum distribution from Ref. 3 with allowance for correlation by the Jastrow model. Oscillator parameters $\alpha_1 = \alpha_2 = 115$ MeV/sec for Li^6 nucleus,[12] 120 MeV/sec for C^{12} and 113 MeV/sec for O^{16}.[13] Arrow indicates angle of proton emission in the case of reaction $\gamma + p \rightarrow \pi^0 + p$.

REF. T.W. Phillips, R.G. Johnson
Phys. Rev. C20, 1689 (1979)

ELEM. SYM.	A	Z
O	16	8

METHOD

REF. NO. 79 Ph 2

REACTION	RESULT	EXCITATION ENERGY	SOURCE		DETECTOR		ANGLE
			TYPE	RANGE	TYPE	RANGE	
G,NØ	ABX	25-45	C	30-45	TOF-D		DST

The cross section and angular distribution for the reaction $^{16}O(\gamma,n_0)^{15}O$ have been measured over an excitation energy range of 25–45 MeV. Neutron time-of-flight spectra were recorded at six angles (22.5°, 45°, 67.5°, 90°, 112.5°, and 135°) and at four bremsstrahlung end-point energies (30, 35, 40, and 45 MeV). Differential cross sections deduced from these spectra were fitted by a fourth-order Legendre-polynomial expansion. The cross section obtained from this expansion decreases smoothly from 3.95 mb at 25.5 MeV to 0.22 mb at 43.8 MeV. The appearance in this analysis of large first-, third-, and especially fourth-order coefficients, is strong evidence for significant $E2$ cross section. An $E2$ cross section extracted from the data exhausts approximately 68% of the isovector $E2$ energy-weighted sum rule. The present data are compared to previous related measurements and excellent agreement is seen. In comparisons with theoretical studies on ^{16}O, there is good general agreement but relatively poor detailed agreement.

[NUCLEAR REACTIONS $^{16}O(\gamma,n_0)^{15}O$, $E_x = 25–45$ MeV; measured $\sigma(E_x,\theta)$; deduced $E2$ strength.]

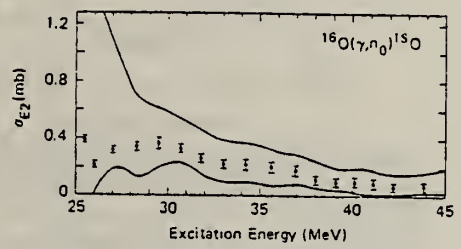

FIG. 6. Electric-quadrupole cross section vs excitation energy for the $^{16}O(\gamma,n_0)^{15}O$ reaction. The solid lines are upper and lower limits on this cross section based on the present data alone. The data points were obtained by including information from polarization measurements (see text).

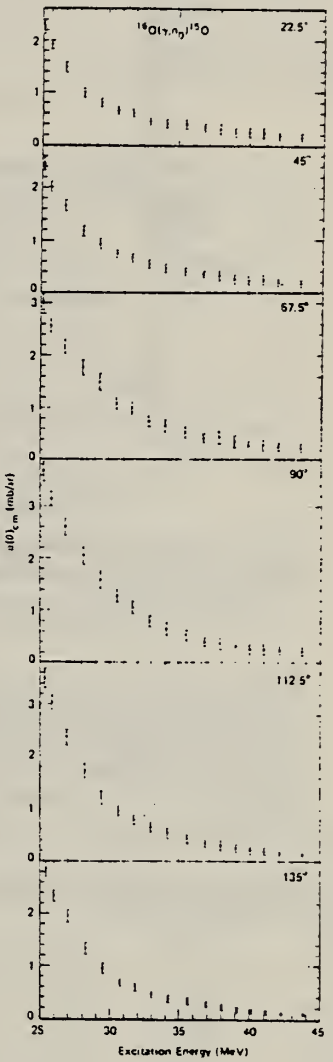

FIG. 4. Center-of-mass differential cross sections vs excitation energy for the $^{16}O(\gamma,n_0)^{15}O$ reaction. (The angles labeling these cross sections are the laboratory angles.)

(over)

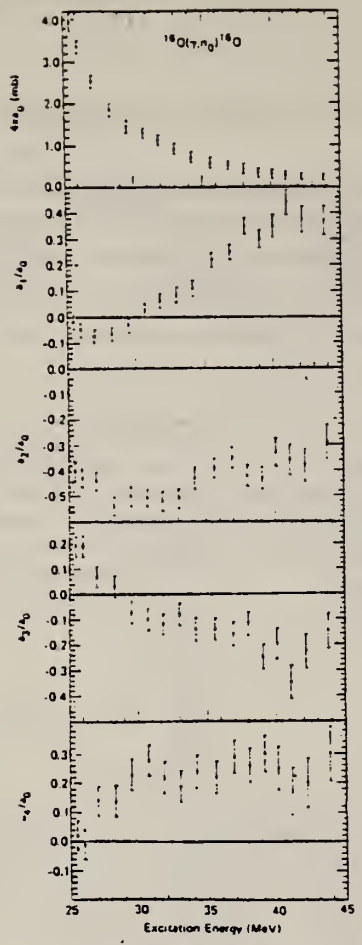

FIG. 5. Cross section ($4\pi a_0$) and relative angular-distribution coefficients (a_i/a_0) vs e :citation energy for the $^{16}O(\gamma,n_0)^{15}O$ reaction.

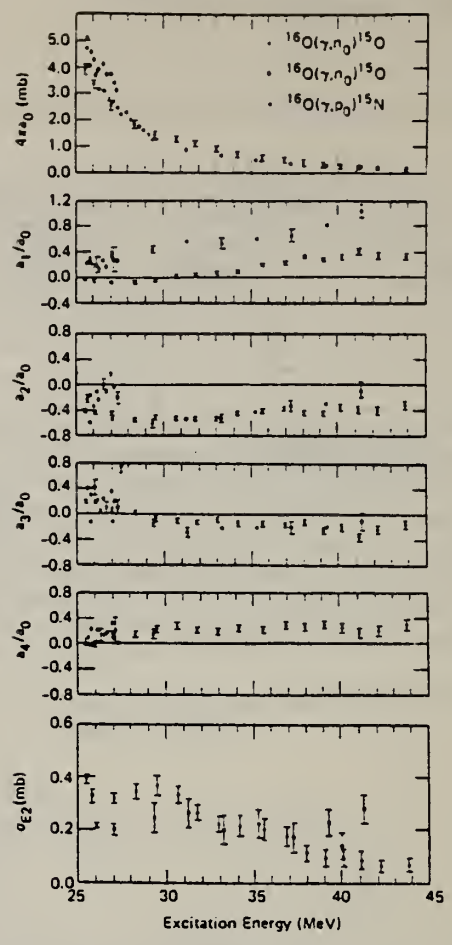

FIG. 7. Comparison of the present results (solid circles) for the $^{16}O(\gamma,n_0)^{15}O$ reaction with the results of Ref. 26 (open diamonds) for the same reaction and with the results of Refs. 8 and 9 (open squares) for the $^{16}O(\gamma,p_0)^{15}N$ reaction [obtained from $^{15}N(p,\gamma_0)^{16}O$ data by detailed balance].

[8]P. Paul, J. W. Noe, K. A. Snover, M. Suffert, E. K. Warburton, and H. M. Kuan, in *International Symposium on Highly Excited States in Nuclei, Julich, 1975*, edited by A. Faessler, C. Mayer-Boricke, and P. Turek, Proceedings, Vol. 1, p. 2.
[9]W. J. O'Connell and S. S. Hanna, Phys. Rev. C 17, 892 (1978).

[26]J. W. Jury, J. S. Hewitt, and K. G. McNeill, Can. J. Phys. 48, 1635 (1970).

REF. K.A. Snover, P.G. Ikossi, and T.A. Trainor
Phys. Rev. L 43, 117

ELEM. SYM.	A	Z
O	16	8

METHOD

REF. NO. 79 Sn 1 egf

REACTION	RESULT	EXCITATION ENERGY	SOURCE TYPE	SOURCE RANGE	DETECTOR TYPE	DETECTOR RANGE	ANGLE
$ P,GO	ABX	16-21	D	4-9	NAI-D		DST

We demonstrate that polarized-proton radiative capture may be used to unambiguously identify concentrations of magnetic dipole strength. Three $M1$ resonances are observed in the doubly magic ^{16}O nucleus between $E_x = 16$ and 20 MeV, with a relatively large total γ_0-transition strength $B(M1)\uparrow \geq 0.24\mu_0^2$.

POLARIZED PROTONS

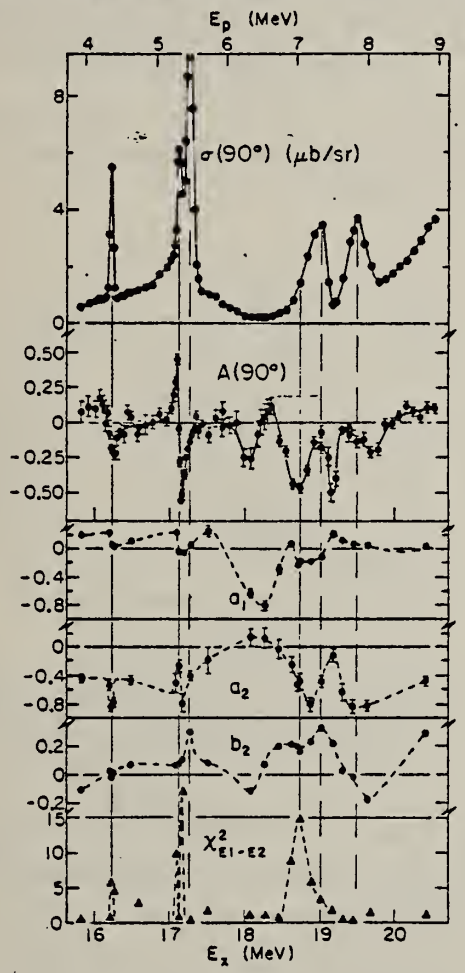

FIG. 1. Excitation curves for $^{15}N(p_{pol},\gamma_0)^{16}O$. From top to bottom: $\sigma(90°)$, $A(90°)$, and the a_1, a_2, and b_2 coefficients (third- and fourth-order coefficients not shown); reduced χ^2 for the angular distribution fits assuming only $E1$ and $E2$ radiation. The curves are to guide the eye. The vertical solid and dashed lines indicate $M1$ and $E1$ resonances, respectively.

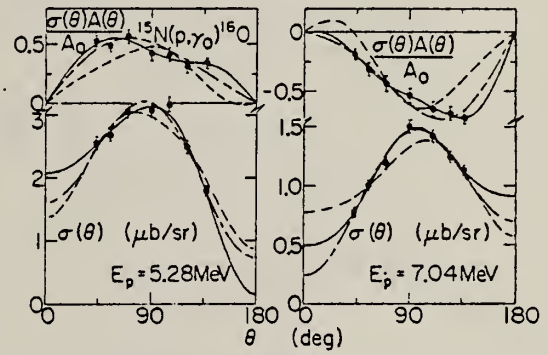

FIG. 2. Representative angular distributions which require $M1$ radiation. Solid curve, $E1+E2+M1$; dashed curve, $E1+E2$; long-short dashed curve, $E1+M1$ calculated fits.

TABLE I. 1^+ states in ^{16}O. Results are from the present work, except where noted.

E_x (MeV)	$\Gamma_{c.m.}$ (keV)	$\Gamma_p\Gamma_{\gamma_0}/\Gamma$ (eV)	Γ_p/Γ	Γ_{γ_0} (eV)	$B(M1)\uparrow$ (μ_0^2)
16.22[a]	18±3[a]	2.65±0.22	0.73[a]	3.6	0.073
				(5.1±0.8)[b]	(0.103±0.016)[b]
17.14[a]	36±5[a]	3.75±0.50	0.58[a]	6.5	0.110
18.8	~250	≥ 1.8 ±0.3	≤ 0.5	≥ 3.6	≥ 0.047
Total					≥ 0.24[c]

[a] Ref. 5.
[b] Ref. 4.
[c] Based on the average of the present work and Ref. 4 for the 16.22-MeV state.

REF. E. Ventura, J.R. Calarco, C.C. Chang, E.M. Diener, D.G. Mavis, S.S. Hanna, G.A. Fisher
Phys. Rev. C19, 1705 (1979)

ELEM. SYM.	A	Z
O	16	8

METHOD

REF. NO. 79 Ve 2 hg

REACTION	RESULT	EXCITATION ENERGY	SOURCE		DETECTOR		ANGLE
			TYPE	RANGE	TYPE	RANGE	
HE,G	ABX	25-30	D	3-9	NAI-D		DST

The capture reaction $^{13}C(^3He,\gamma)^{16}O$ has been studied over an excitation energy range of 25 to 30 MeV in ^{16}O. The 90° differential yield curve for the ground state transition shows resonances at E_x = 25.1, 26.0 and 27.3 MeV. The measured angular distributions are consistent with a spin and parity assignment of $J^\pi = 1-$ to these states. The relation between this structure and that observed in the $^{15}N(p,\gamma_0)^{16}O$ reaction is discussed. The 90° differential yield curves for the doublet transitions $\gamma_1 + \gamma_2$ and $\gamma_3 + \gamma_4$ were also measured. The former shows resonances at E_x = 26.0, 26.6, 27.2, 27.7, and 28.6 MeV, while the latter shows a broad resonance centered at $E_x \simeq 27.5$ MeV with mild structure. Both curves suggest the existence of giant resonance strength built on the excited states of ^{16}O.

HE=HE3

[NUCLEAR REACTIONS $^{13}C(^3He,\gamma)^{16}O$, $E_{^3He}$ = 3.0-8.5 MeV, measured $\sigma(E_{^3He},E_\gamma,\theta)$. ^{16}O deduced resonances and structure in giant resonance region. Enriched ^{13}C target.]

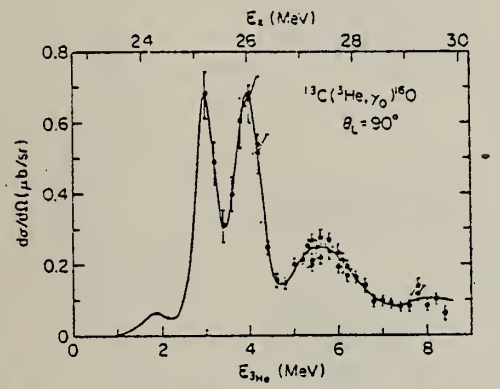

FIG. 2. Excitation function of the differential cross section for $^{13}C(^3He,\gamma_0)^{16}O$ at θ_{lab} = 90°. The data up to $E(^3He)$ = 3.0 MeV are taken from Ref. 5 and normalized to the present work at $E(^3He)$ = 3.0 MeV.

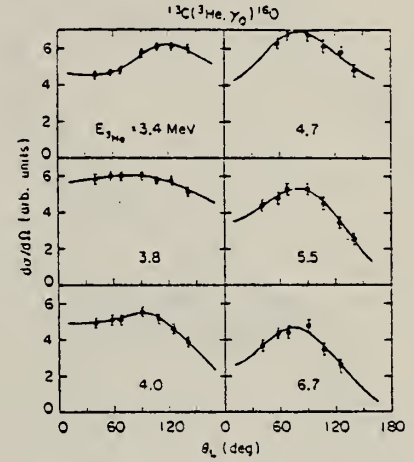

FIG. 3. Angular distributions for the $^{13}C(^3He,\gamma_0)^{16}O$ reaction. The curves are least squares fits of Eq. (1) with k = 1 → 3.

TABLE I. Angular distributions in $^{13}C(^3He,\gamma_0)^{16}O$ as determined from the data of Fig. 3 and a measurement at 2.9 MeV.

$E_{^3He}$ (MeV)	E_x (MeV)	W(θ) a_1	a_2	a_3
2.9	25.1	≃0	≃0	≃0
3.4	25.5	-0.16 ± 0.03	-0.08 ± 0.04	0.12 ± 0.05
3.8	25.9	0.06 ± 0.02	-0.09 ± 0.02	0.01 ± 0.03
4.0	26.0	0.15 ± 0.03	-0.24 ± 0.04	0.10 ± 0.05
4.7	26.6	0.05 ± 0.07	-0.27 ± 0.08	-0.06 ± 0.09
5.5	27.3	0.30 ± 0.04	-0.49 ± 0.06	0.02 ± 0.08
6.7	28.1	0.37 ± 0.13	-0.56 ± 0.14	-0.08 ± 0.15

$$W(\theta) = A_0\left[1 + \sum_1^3 a_K P_K(\cos\theta)\right]. \quad (1)$$

(over)

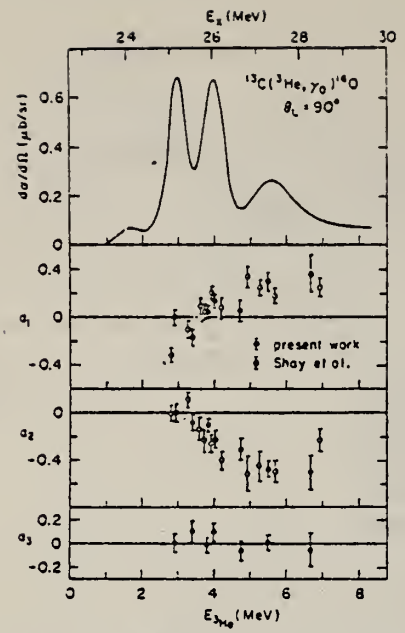

FIG. 4. Top: excitation function for the reaction $^{13}C(^3He,\gamma_0)^{16}O$ at $\theta_{lab} = 90°$. Bottom: the angular distribution coefficients a_k plotted against energy.

REF. P.E. Bosted, K.I. Blomqvist, A.M. Bernstein, S.A. Dytman, R.A. Miskimen
Phys. Rev. Lett. 45, 1544 (1980)

ELEM. SYM.	A	Z
O	16	8

METHOD

REF. NO. 80 Bo 2

hg

REACTION	RESULT	EXCITATION ENERGY	SOURCE		DETECTOR		ANGLE
			TYPE	RANGE	TYPE	RANGE	
G,PI+	ABX	150-360	C	220-360	CKV-I		DST

Differential cross sections for $^{10}B(\gamma,\pi^+)^{10}Be$ to the ground and first excited states of ^{10}Be separately and $^{16}O(\gamma,\pi^+)^{16}N$ to the sum of the four lowest-lying states in ^{16}N have been measured at laboratory angles of 45° and 90° for pions with kinetic energies from 80 and 210 MeV. The results, which are the first to discrete nuclear final states in the $\Delta(1236)$ region, are in qualitative agreement with several distorted-wave impulse-approximation calculations.

PACS numbers: 25.20.+y

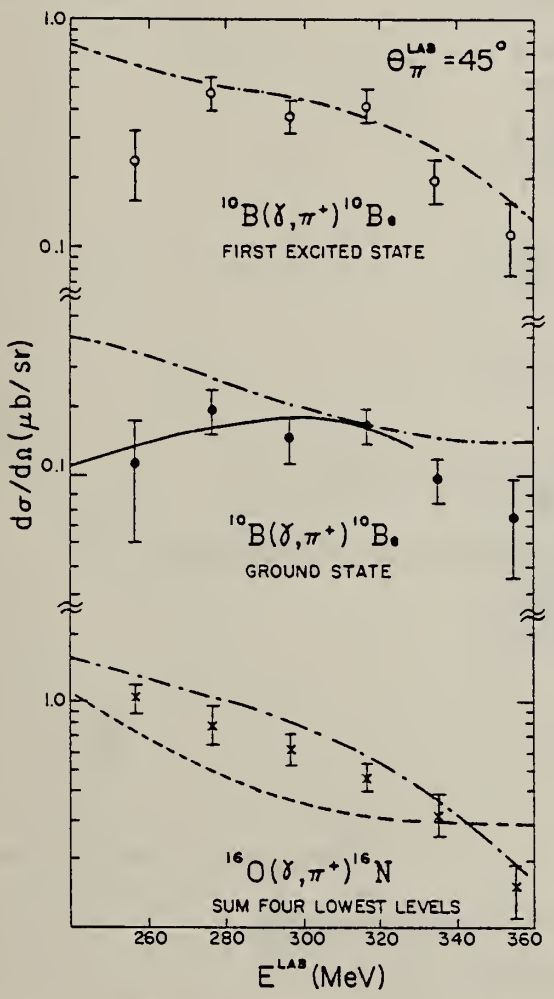

FIG. 3. Same as for Fig. 2, but at a pion laboratory angle of 45°.

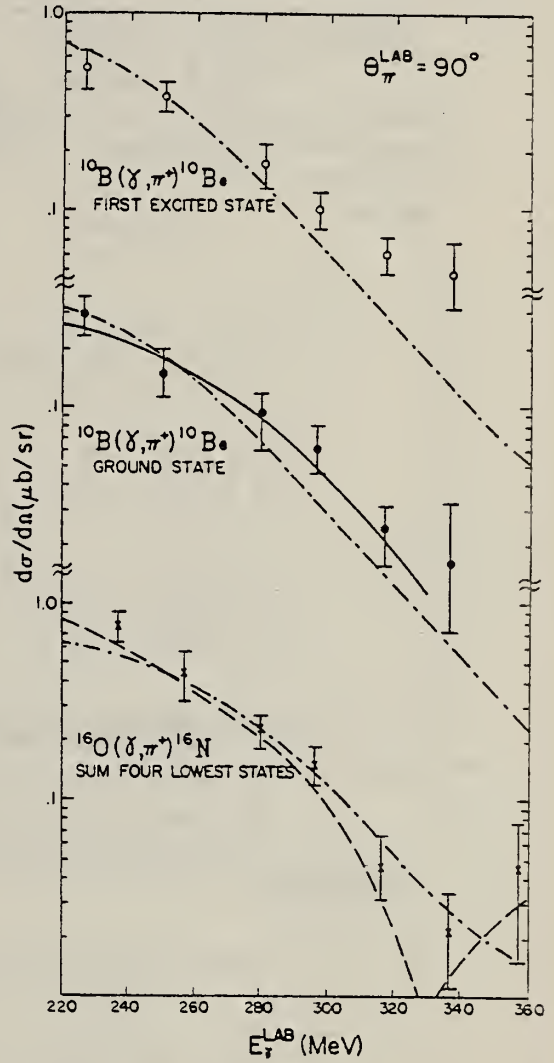

FIG. 2. Differential cross sections for $^{16}O(\gamma,\pi^+)^{10}Be$ at 90°. The solid circles represent the contributions from the ground state of ^{10}Be, the open circles are for the first excited state of ^{10}Be, and the crosses are for the sum of the four lowest-lying levels in ^{16}N. The solid line is the calculation of Singham and Tabakin (Ref. 8), the dashed line that of Devanathan *et al.* (Ref. 9), and the dot-dashed lines are from Nagl and Uberall (Ref. 10). Pion energies can approximately be found by subtracting 140 MeV from the photon energies.

REF. H. Göringer, B. Schoch
Phys. Lett. 97B, 41 (1980)

ELEM. SYM.	A	Z
O	16	8

METHOD

REF. NO. 80 Go 7 hg

REACTION	RESULT	EXCITATION ENERGY	SOURCE TYPE	SOURCE RANGE	DETECTOR TYPE	DETECTOR RANGE	ANGLE
G,NO	ABX	60 - 160	C	60 - 160	TOF - D		DST

$\Delta E_n/E_n$ = 3% @ E_n = 40 MeV
= 6% @ E_n = 140 MeV

BREMS. TIP

Differential (γ, n_0) cross sections on ^{12}C and ^{16}O have been measured for photon energies 60 MeV $\leq E_\gamma \leq$ 160 MeV. These results combined with the corresponding (γ, p_0) cross sections support an absorption mechanism of the photon by neutron–proton pairs.

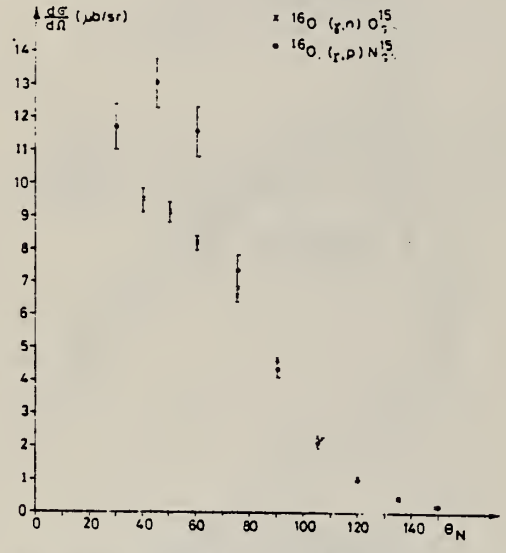

Fig. 2. Angular distribution at E_γ = 60 MeV. Proton data: ref. [11].

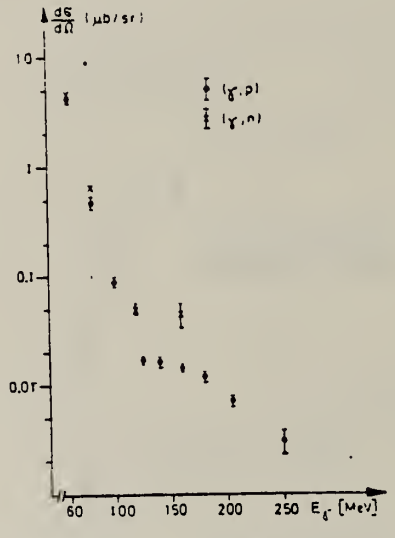

Fig. 3. Differential cross sections for θ_N = 90° and ^{16}O. Proton data: refs. [11,12].

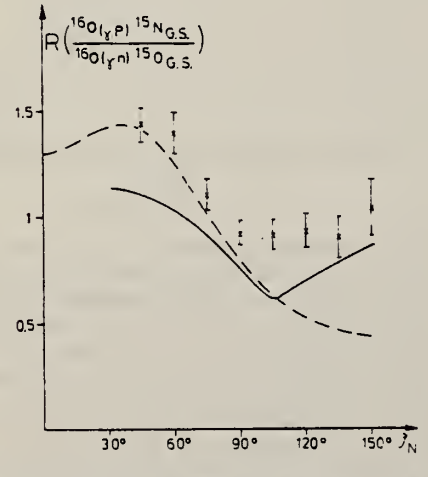

Fig. 4. Ratios $(\gamma, p_0)/(\gamma, n_0)$ for E_γ = 60 MeV and ^{16}O. Calculations from ref. [6] (full line) and ref. [8] (broken line).

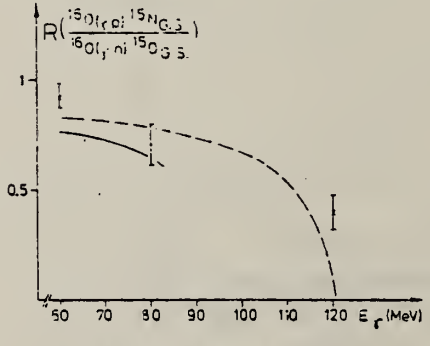

Fig. 6. As fig. 4 for θ_N = 90°.

[11] D.J.S. Findlay and R.O. Owens, Nucl. Phys. A279 (1977) 385.
[12] M.J. Leitch, Ph.D. Thesis, MIT 1979.

U.S. DEPARTMENT OF COMMERCE
NATIONAL BUREAU OF STANDARDS

REF. B.S. Ishkhanov, V.I. Mokeev, E.S. Omarov, I.M. Piskarev, V.M. Sorvin
Sov. J. Nucl. Phys. 31, 730 (1980)
Yad. Fiz. 31, 1407 (1980)

ELEM. SYM.	A	Z
O	16	8

METHOD

REF. NO. 80 Is 4 hg

REACTION	RESULT	EXCITATION ENERGY	SOURCE		DETECTOR		ANGLE
			TYPE	RANGE	TYPE	RANGE	
G,G	ABX	15-32	C	32	NAI-D		90

Cross sections have been measured for elastic scattering of photons by the nuclei ^{12}C and ^{16}O in the region of the giant resonance. The energy resolution achieved in the experiment is comensurate with the energy resolution in the total photoabsorption cross section. It is shown that study of the cross sections for total absorption and elastic scattering of photons permits spectroscopic information to be obtained on the high-lying states of nuclei.

PACS numbers: 25.20. + y

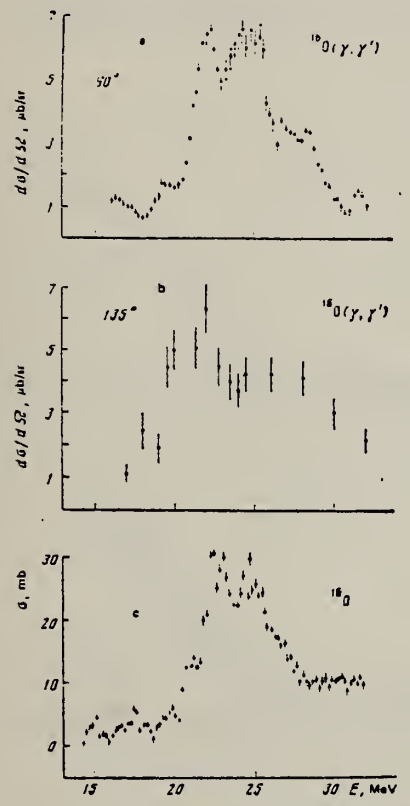

FIG. 2. The same as in Fig. 1 but for ^{16}O.

TABLE II.

Energy of levels, MeV: Ref. 10, total absorption	Energy of levels, MeV: Present work	J^π, T	σ_{tot}, mb (Ref. 10)	σ_{el}, mb, present work	$\sigma^2_{tot}/\sigma_{el}$, b	$\sum A^2$, b
			^{12}C			
18.4	18.3±0.2	3⁻, 1 *	2	4±2	1±0.6	23.2
20.5	20.5±0.2	3⁺, 1 *	2	6±3	0.7±0.4	17.3
22–24	22–24	1⁻, 1*	25	50±5	12.6±4	13.7
26.2	26.5±0.4	–	3.5	5±2	2.5±1	10.3
27.5	–	–	1.5	–	–	–
29.5	29.5±0.3	–	–	3±1	1.3±0.5	8.3
			^{16}O			
17.1	–	1⁻, 1 **	3	–	–	–
19.5	19.5±0.2	1⁻, 1 **	3	10±3	0.9±0.4	19.1
21	–	1⁻, 1 **	6	–	–	–
22.3	22.3±0.2	1⁻, 1 **	30	85±10	10.7±4	14.4
24–25	24–25	1⁻, 1 ***	30	85±10	10.7±4	12.1
27.2	27.3±0.2	2⁺, 1 **	3	10±3	0.9±0.5	10.3
–	28.5±0.2	–	–	–	–	–
–	31.5±0.2	–	–	–	–	–

***Data of the present work and also of Refs. 16 and 17 on the position of the maximum of the giant dipole resonance.

FIG. 1. Cross section for elastic scattering of photons by ^{12}C obtained in the present work (a) and in Ref. 9 (b); cross section for total absorption of protons by ^{12}C from Ref. 10 (c).

[9]A. S. Penfold and E. L. Garwin, Phys. Rev. 116, 120 (1959).
[10]J. Ahrens *et al.*, Nucl. Phys. A251, 479 (1975).

REF. B. Schoch, H. Göringer, P. Jennewein, F. Klein, G. Lührs, F. Zettl
Phys. Rev. C22, 2630 (1980)

ELEM. SYM.	A	Z
O	16	8

METHOD

REF. NO. 80 Sc 8 hg

REACTION	RESULT	EXCITATION ENERGY	SOURCE		DETECTOR		ANGLE
			TYPE	RANGE	TYPE	RANGE	
E,PØ	ABX	80	D	80	MAG-D		DST

Via the reaction $^{16}O(e,p_0)^{15}N$ cross sections for the transition $^{16}O(\gamma,p_0)^{15}N$ have been extracted at angles $\theta_e = 5°-40°$. Whereas a modified quasideuteron model fails to describe the data, a calculation of Gari and Hebach with the inclusion of spin currents comes close to the results.

VIRT PHOTON ANALYSIS

[NUCLEAR REACTIONS $^{16}O(e,p_0)^{15}N$, $E_e = 80$ MeV, measured $\sigma_e(E_e,\vartheta)$, deduced $\sigma_\gamma(E_\gamma,\vartheta)$; BeO target.]

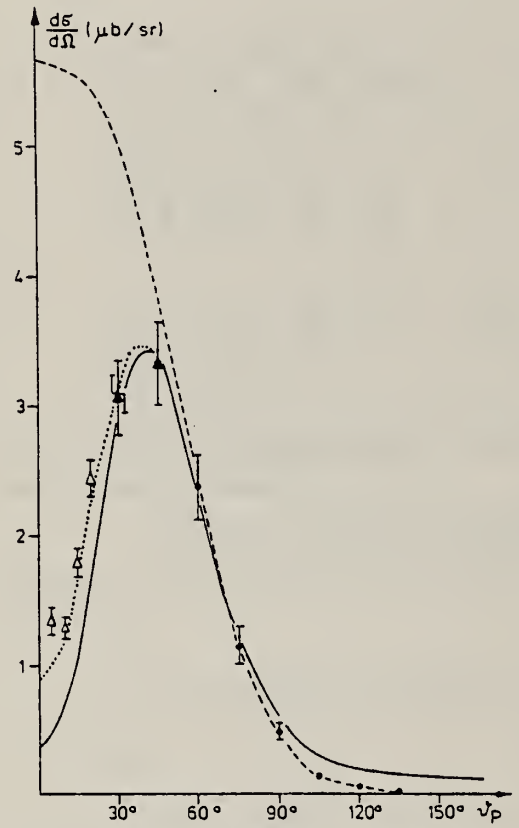

FIG. 4. Extracted cross sections (triangles) and the data from Glasgow (full circles). The calculations of Gari and Hebach without (full line) and with (dotted line) spin current contributions, and modified quasideuteron model (broken line).

REF. P. Stoler, E.J. Winhold, F. O'Brien, P.F. Yergin, D. Rowley, K. Min, J. LeRose, A.M. Bernstein, K.I. Blomqvist, G. Franklin, N. Paras, M. Pauli
Phys. Rev. C22, 911 (1980)

ELEM. SYM.	A	Z
O	16	8

METHOD

REF. NO. 80 St 3 hg

REACTION	RESULT	EXCITATION ENERGY	SOURCE		DETECTOR		ANGLE
			TYPE	RANGE	TYPE	RANGE	
E,PI+	RLY	177-180	C	180	MAG-D		90
G,PI+	RLY	177-180	C	180	MAG-D		90

TEST VIRTUAL PHOTONS

The virtual photon spectrum shape and intensity within several MeV of the kinematic limit was measured for $^{9}Be(e,\pi^{+})^{9}Li,e'$ and $^{16}O(e,\pi^{+})^{16}N,e'$ ($T_{\pi}=28$ MeV, $\theta_{\pi}=90°$). The intensity over this interval is 1.25 ± 0.10 times plane-wave virtual photon theory predictions; the shape agrees with theory within errors. Measurements on the proton 30 to 55 MeV below the end point agree with the intensity predictions of virtual photon theory within the errors ($\pm 8\%$).

[NUCLEAR REACTIONS $^{16}O(e,\pi^{+})$, $E=180.4$ MeV; $^{9}Be(e,\pi^{+})$, $E=184.8$ MeV; measured $\sigma(E_{\gamma},90°_{lab})$ relative to (γ,π^{+}), near $E_{\gamma}=28$ MeV. $^{1}H(e,\pi^{+})$, $E=230$ MeV; measured $\sigma(E_{\gamma},90°_{lab})$ relative to (γ,π^{+}), near $E_{\gamma}=18$, 30 MeV. Compared to PWBA virtual photon theory.]

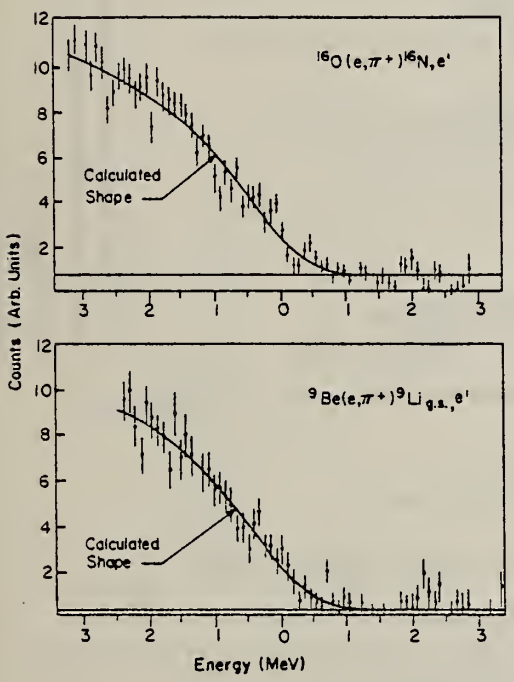

FIG. 1. Number of pions as a function of virtual photon energy. The zero on the abscissa corresponds to the virtual photon spectrum end point, 179.9 MeV for ^{16}O and 184.3 MeV for ^{9}Be. The solid curves were obtained as described in the text and normalized to the experimental data.

TABLE I. Results for R/V, the real-to-virtual ratio as defined in the text. The quantity E_0 is the incident electron total energy, T_{π} the pion kinetic energy, k the virtual photon energy, and ΔT_{π} the averaging interval over pion energy in the experiment (corresponding to the range of k). Note that k is close to the end point for ^{16}O and ^{9}Be but 30 to 55 MeV below for ^{1}H.

	$^{16}O(e,\pi^{+})$	$^{9}Be(e,\pi^{+})$	$^{1}H(e,\pi^{+})$	
E_0(MeV)	180.4	184.8	230	230
T_{π}(MeV)	28	28	18	30
k(MeV)	176.8–179.9	182.2–184.3	174.7–181.7	188.3–199.4
ΔT_{π}(MeV)	3.0	2.0	4.9	7.6
$(R/V)_{expt}$	78 ± 9	72 ± 8	71 ± 6	80 ± 6
$(R/V)_{theor}$	91	96	70	77
$(R/V)_{theor}/(R/V)_{expt}$	1.17 ± 0.14	1.33 ± 0.15	0.99 ± 0.08	0.96 ± 0.08

REF. J. Arends, J. Eyink, A. Hegerath, K.G. Hilger, B. Mecking, G. Noldeke, H. Rost
Phys. Lett. 98B, 423 (1981)

ELEM. SYM.	A	Z
O	16	8

METHOD

REF. NO. 81 Ar 1

REACTION	RESULT	EXCITATION ENERGY	SOURCE		DETECTOR		ANGL
			TYPE	RANGE	TYPE	RANGE	
G,MU-T	ABX	215-386	D	215-386	TOF-D		4PI

DATA ALSO IN 81AR3

Double differential cross sections for the photo-emission of protons and charged pion production were investigated for a number of target nuclei (He, Be, C, O, Al, Ti, Cu, Sn, Pb) in the photon energy range k = (215–386) MeV. On the basis of these experimental results the total hadronic cross section was determined.

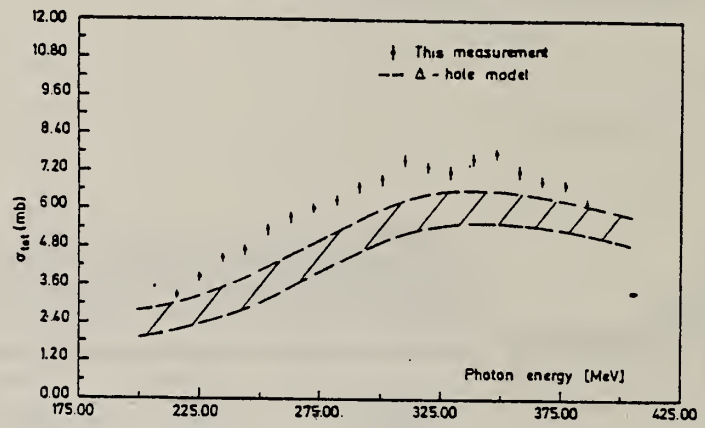

Fig. 6. Total hadronic cross section for ^{16}O (statistical errors only). Data are compared to a calculation in the Δ-hole formalism [11].

The total hadronic cross sections for all measured elements can be parametrized in the form

$\sigma(k,A) = \sigma_0(k) \cdot A^x$,

A being the atomic number, with a constant exponent $x = 1.1$. The photon energy dependence of σ_0 is shown in fig. 7. Compared to the mean cross section for a free nucleon (the solid line in fig. 7) the excitation of the Δ-resonance is suppressed. Such a suppression is expected in the Δ-hole model [11].

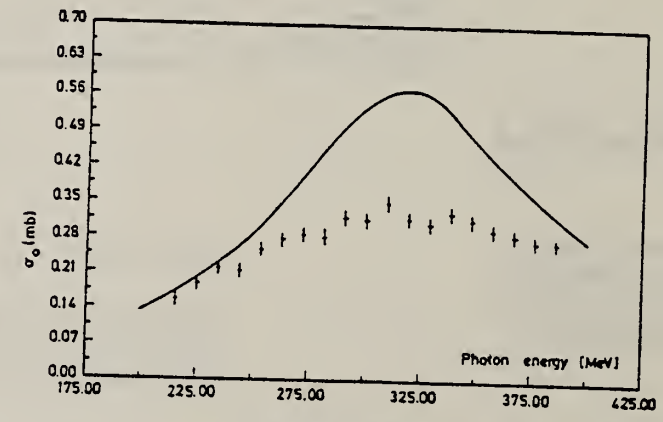

Fig. 7. Parameter σ_0 as a function of photon energy (data points) compared to the mean cross section for a free nucleon (solid line).

REF. J. Arends, J. Eyink, A. Hegerath, K.G. Hilger, B. Mecking, G. Nöldeke, H. Rost
Nucl. Phys. A358, 367c (1981)

ELEM. SYM.	A	Z
0	16	8

METHOD

REF. NO. 81 Ar 3 | hg

REACTION	RESULT	EXCITATION ENERGY	SOURCE TYPE	SOURCE RANGE	DETECTOR TYPE	DETECTOR RANGE	ANGLE
G,MU-T	ABX	215-386	D	215-386	TOF-D		4PI

Abstract: Double differential cross sections for the photoemission of protons and charged pion photoproduction were investigated for a number of target nuclei (He, Be, C, O, Al, Ti, Cu, Sn, Pb) using the tagged bremsstrahlung beam at the Bonn 500 MeV-Synchrotron in the photon range k = (215-386)MeV. On the basis of these experimental results the total hadronic cross section was determined.

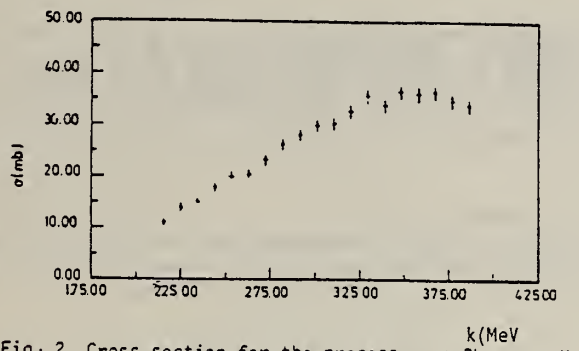

Fig. 2. Cross section for the process: $\gamma + Pb \rightarrow p + X$. The proton threshold is 58 MeV.

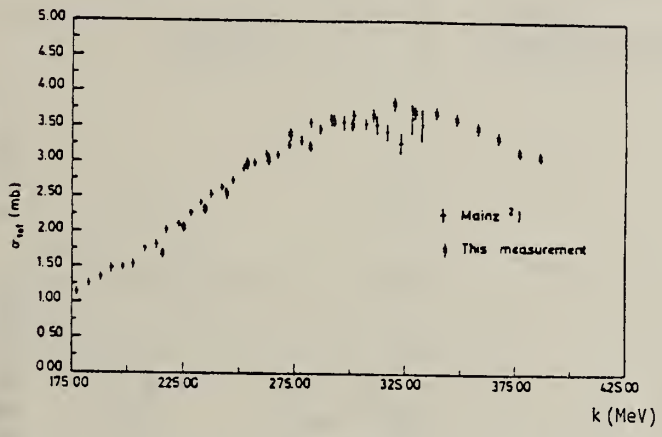

Fig. 3. Total hadronic cross section for Be. The data are compared to the cross section taken from ref.[2]).

The photon energy dependence of the total cross sections for heavier nuclei are similar to the Be results. The complete data set can be parametrized in the form

$$\sigma(k,A) = \sigma_0(k) \cdot A^x.$$

The exponent is constant x = 1.1. The photon energy dependence of σ_0 is shown in fig. 4. Compared to the mean cross section for a free nucleon, the excitation of the Δ-resonance is suppressed.

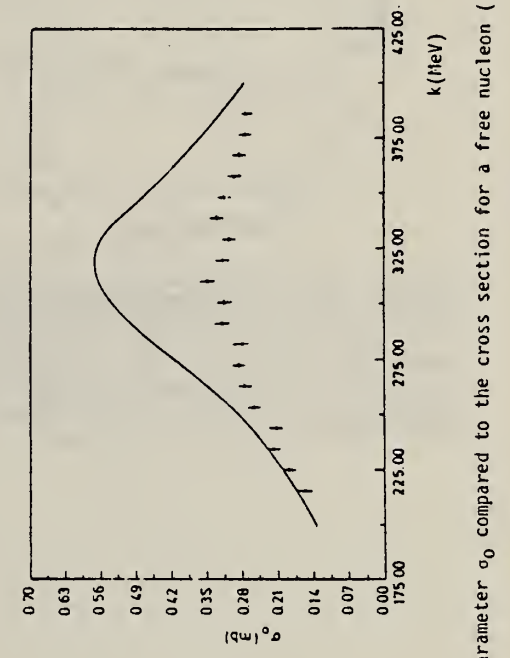

Fig. 4. Parameter σ_0 compared to the cross section for a free nucleon (full line).

REF. K. Wienhard, C. Bläsing, K. Ackermann, K. Bangert, U.E.P. Berg, K. Kobras, W. Naatz, D. Rück, R.K.M. Schneider, R. Stock
Z. Phy. A302, 185 (1981)

ELEM. SYM.	A	Z
O	16	8

METHOD

REF. NO. 81 Wi 1 hg

REACTION	RESULT	EXCITATION ENERGY	SOURCE		DETECTOR		ANGLE
			TYPE	RANGE	TYPE	RANGE	
$ G,G	NOX	7	C	UKN	SCD-D		90

POL INCOMING PHOTONS

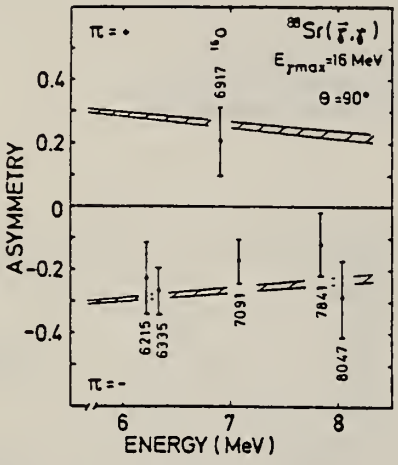

Fig. 1. Observed asymmetries for five ground state dipole transitions in ^{88}Sr and for the 2^+ transition at 6917 keV in ^{16}O. The energies for the ^{88}Sr states were taken from /2/. The hatched band represents the expected asymmetry for states with positive parity (upper part) and negative parity (lower part)

Abstract. The unknown parities of five strong dipole states between 6 and 8 MeV in ^{88}Sr are shown to be negative.

REF. K. Wienhard, R.K.M. Schneider, K. Ackermann, K. Bangert, U.E.P. Berg, P. Stock
Phys. Rev. C24, 1363 (1981)

ELEM. SYM.	A	Z
O	16	8

METHOD

REF. NO. 81 Wi 2 hg

REACTION	RESULT	EXCITATION ENERGY	SOURCE		DETECTOR		ANGLE
			TYPE	RANGE	TYPE	RANGE	
G,P	SPC	15 - 25	C	22, 30	SCD-D		DST

Angular distribution coefficient a_2 for the $^{16}O(\gamma,p_3)$ reaction is $-0.14\ ^{+0.19}_{-0.23}$

POLARIZED PHOTONS

The $^{16}O(\gamma,p_0)$ reaction has been studied with linearly polarized bremsstrahlung photons in and below the giant $E1$ resonance. The parity of the absorbed radiation was determined from the observed azimuthal asymmetry of the emitted protons. Combined with unpolarized measurements the polarized results determine the proton decay amplitudes of the $M1$ resonance at $E_x = 16.2$ MeV in ^{16}O. The shape of the unpolarized $^{16}O(\gamma,p_3)$ angular distribution in the giant $E1$ resonance was derived from the measured analyzing power.

[NUCLEAR REACTIONS $^{16}O(\gamma,p)$, $E = 15-25$ MeV; measured analyzing power $\theta = 90°$ linearly polarized bremsstrahlung; ^{16}O dipole levels deduced π; 16.2 MeV 1^+ resonance deduced p_0 decay amplitudes; ^{16}O GEDR deduced p_3 angular distribution.]

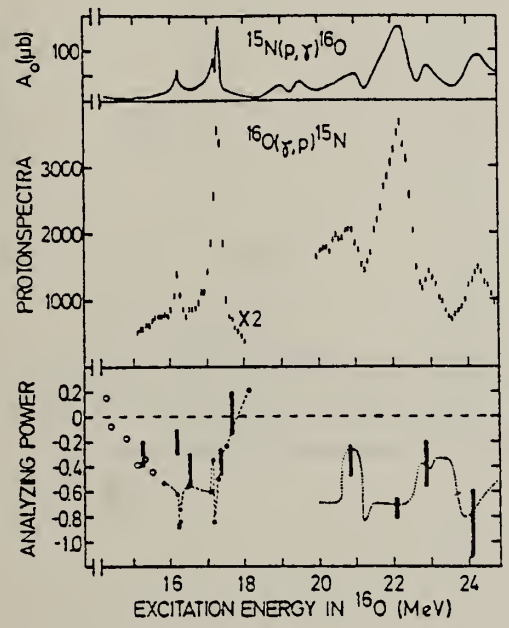

FIG. 2. The upper part shows the total $^{15}N(p,\gamma)^{16}O$ cross section from Ref. 8. The middle part gives the original proton energy spectra from this measurement. In the lower part the measured analyzing power at 90° is presented as error bars together with calculated values taking a_2 coefficients from the literature and assuming only $E1$ excitation.

[8]E. D. Earle and N. W. Tanner, Nucl. Phys. A95, 241 (1967).
[9]K. A. Snover, P. G. Ikossi, and T. A. Trainor, Phys. Rev. Lett. 43, 117 (1979).

REF. M. Bernheim, A. Bussière, J. Mougey, D. Royer, D. Tarnowski, S. Turck-Chieze, S. Frullani, S. Boffi, C. Giusti, F.D. Pacati, G.P. Capitani, E. De Sanctis, G.J. Wagner
Nucl. Phys. A375, 381 (1982)

ELEM. SYM.	A	Z
O	16	8

METHOD

REF. NO. 82 Be 3 egf

REACTION	RESULT	EXCITATION ENERGY	SOURCE		DETECTOR		ANGLE
			TYPE	RANGE	TYPE	RANGE	
E,E/P	NOX	444	D	500	MAG-D		DST

Abstract: The measurement of recoiling nucleus momentum distributions in (e,e'p) reactions has been performed for p-hole states in ^{12}C and ^{16}O under extended kinematical conditions. The analysis of the experimental data has been performed without requiring the usual factorization of the cross section. The sensitivity of the data and of the analysis for deducing bound and scattering proton states is discussed.

DLTQ MEV/C

E NUCLEAR REACTIONS ^{12}C, $^{16}O(e,e'p)$, $E = 500$ MeV; measured σ (missing energy, recoil momentum); deduced proton–hole spectral functions. Unfactorized DWIA analysis.

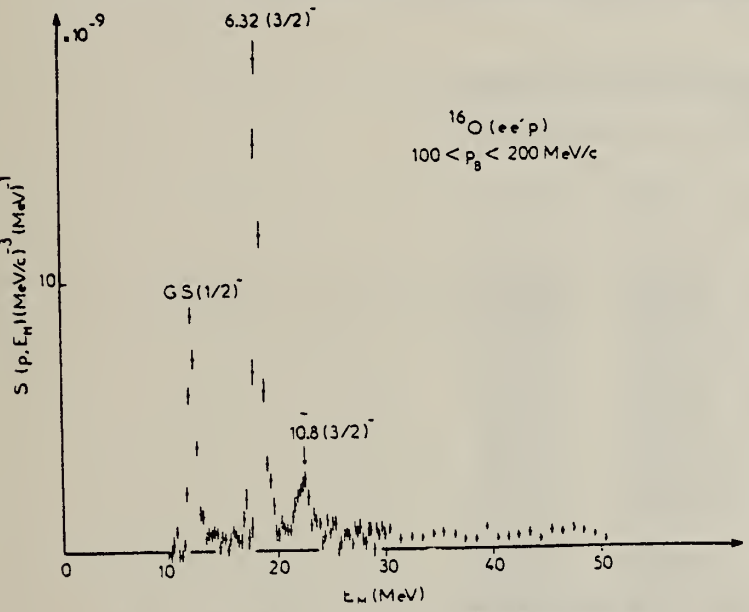

Fig. 6. Missing energy distribution of the ^{16}O spectral function.

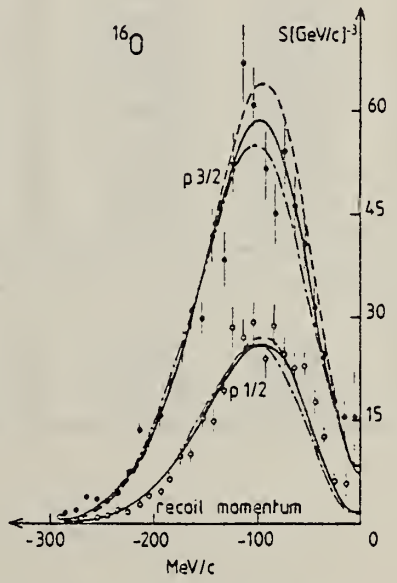

Fig. 7. Momentum distributions of proton $\frac{3}{2}$ and $\frac{1}{2}$ hole states in ^{16}O. Theoretical distributions are computed using the same optical potential (JA) and different bound-state wave functions: —— (ES), – – – (NE), – . – (GO).

(OVER)

TABLE 9

Experimental values of the momentum distribution (with corrections for radiative effects) for $^{16}O(e, e'p)^{15}N$

$p_B<0$ (MeV/c)	$S(p)\pm\Delta S(p)(GeV/c)^{-3}$		$p_B<0$ (MeV/c)	$S(p)\pm\Delta S(p)(GeV/c)^{-3}$	
	$1p_{1/2}$	$1p_{3/2}$		$1p_{1/2}$	$1p_{3/2}$
5		15.5±7.0	155	15.3±1.5	29.9±2.5
15	5.8±1.9	15.4±2.7	165	10.1±1.2	30.8±2.7
25	6.2±1.4	17.8±2.3	175	9.9±1.4	26.1±2.5
35	12.7±1.6	24.6±2.8	185	6.5±1.1	20.7±1.6
45	17.8±1.9	31.5±3.2	195	4.7±0.8	15.6±1.6
55	23.1±2.3	40.8±3.9	205	4.1±0.6	12.3±1.3
65	22.7±2.3	46.3±4.2	215	2.7±0.8	13.6±1.5
75	24.8±2.6	54.1±4.8	225	2.0±0.8	7.6±1.2
85	28.9±3.1	45.2±4.7	235	1.8±0.7	4.5±1.0
95	24.0±3.0	51.6±6.1	245	1.1±0.5	3.2±0.7
105	29.3±3.1	60.7±5.8	255	0.9±0.5	3.5±0.7
115	27.2±2.7	67.0±5.8	265		3.7±0.7
				0.78±0.34	
125	28.5±3.1	52.1±4.9	275		1.9±0.6
135	19.4±2.2	38.6±3.9	285		1.5±0.6
				0.82±0.52	
145	15.0±1.8	41.9±3.9	295		0.06±0.6

TABLE 10

Experimental values of the momentum distribution (without corrections for radiative effects) for $^{16}O(e, e'p)^{15}N$

p_B (MeV/c)	$1p_{1/2}$ $(GeV/c)^{-3}$	$1p_{3/2}$	p_B	$1p_{1/2}$	$1p_{3/2}$
(a) $p_B<0$					
5			155	11.6±1.1	23.1±2.0
15	4.2±1.3	12.5±1.8	165	8.5±0.9	22.9±1.9
25	5.1±1.0	15.5±1.7	175	8.2±1.0	19.2±1.7
35	9.9±1.2	17.8±1.9	185	5.4±0.8	15.9±1.7
45	13.7±1.4	23.3±2.2	195	3.6±0.6	11.9±1.2
55	18.4±1.7	29.3±2.7	205	3.3±0.5	9.2±0.9
65	18.6±1.8	32.8±2.9	215	2.4±0.6	10.2±1.0
75	20.1±1.9	37.9±3.3	225	1.6±0.5	5.5±0.8
85	22.5±2.2	35.3±3.3	235	0.95±0.5	3.8±0.6
95	19.2±2.2	38.6±4.2	245	1.1±0.4	2.5±0.5
105	22.3±2.2	44.7±4.1	255	0.64±0.34	2.8±0.4
115	20.9±2.0	47.4±4.0	265	0.71±0.34	2.7±0.4
125	21.7±2.2	40.2±4.3	275		1.8±0.4
135	14.4±1.5	29.9±2.8	285	0.38±0.35	1.14±0.4
145	11.5±1.3	31.5±2.8	295	0.69±0.36	0.23±0.46
(b) $p_B>0$					
25		15.1±2.8	65		
35	9.8±1.5	16.2±1.8	75	23.8±2.9	27.6±4.7
45	11.0±1.30	19.8±2.1	85	26.9±3.0	32.8±3.1
55	17.3±1.9	24.2±2.9	95	17.3±3.8	31.9±4.6

REF. B.L. Berman, R. Bergère, P. Carlos
Phys. Rev. C26, 304 (1982)

ELEM. SYM.	A	Z
O	16	8

METHOD

REF. NO. 82 Be 5 egf

REACTION	RESULT	EXCITATION ENERGY	SOURCE		DETECTOR		ANGLE
			TYPE	RANGE	TYPE	RANGE	
G,MU-T	ABX	15-133	D	15,133	BF3-I		4PI

DATA ANALYSIS

A large discrepancy is found between the value for the integrated total photonuclear cross section for ^{16}O determined from the sum of the partial cross sections and that obtained from a total photon absorption measurement.

[NUCLEAR REACTIONS $^{16}O(\gamma, \text{tot}:E_\gamma)$, $(\gamma, \text{partial}: E_\gamma)$: integrated cross sections; sum rule; meson-exchange factor K, A dependence.]

REF. P. Carlos, H. Beil, R. Bergere, B.L. Berman, A. Lepretre, A. Veyssiere
Nucl. Phys. A378, 317 (1982)

ELEM. SYM.	A	Z
O	16	8

METHOD

REF. NO. 82 Ca 1 egf

REACTION	RESULT	EXCITATION ENERGY	SOURCE		DETECTOR		ANGLE
			TYPE	RANGE	TYPE	RANGE	
G,SN	ABX	24-133	D	24-133	MOD	I	4PI
G,1N	ABX	24-89	D	24-89	MOD	I	4PI
G,2N	ABX	24-89	D	24-89	MOD	I	4PI

Abstract: The inclusive partial photoneutron cross section $\sigma(\gamma, 1n\ldots)$ and $\sigma(\gamma, 2n\ldots)$ and the total photoneutron cross section $\sigma^{(1)}(E_\gamma) = \sum_{i=1}\sigma(\gamma, in\ldots)$ for ^{16}O have been measured with monoenergetic photons in the energy region above the giant resonance and below the meson thresholds. Comparison with other data shows the dominance of the (γ, pn) process in this energy region and thus underscores the importance of the mechanism of photon absorption by a correlated proton-neutron pair in the nucleus; thus, satisfactory agreement of modern versions of the quasideuteron theory with the data has been obtained. The measured integrated total photoneutron cross section up to 140 MeV is 0.67 ± 0.07 TRK sum-rule units.

E NUCLEAR REACTIONS $^{16}O(\gamma, xn)$, $E = 24$–133 MeV; integrated σ for $x = 1, 2$, moments; deduced interaction mechanisms. Monoenergetic beam.

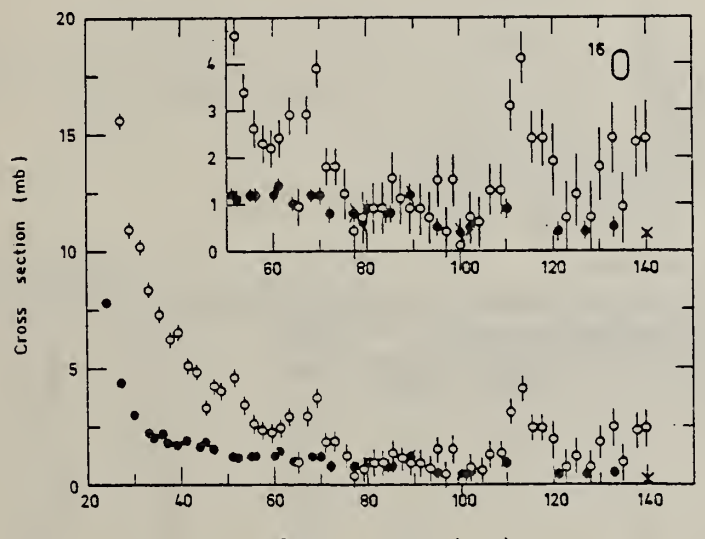

Fig. 7. Comparison of the present results for $\sigma^{(1)}(E_\gamma)$ (solid data points) with the $\sigma(\gamma, \text{tot}: E_\gamma)$ data from Mainz [43] (open data points) and the $\sigma(\gamma, pn)$ datum at $E_\gamma = 140$ MeV from Bonn [44] (cross; converted to a total cross section by multiplication by 4π).

(OVER)

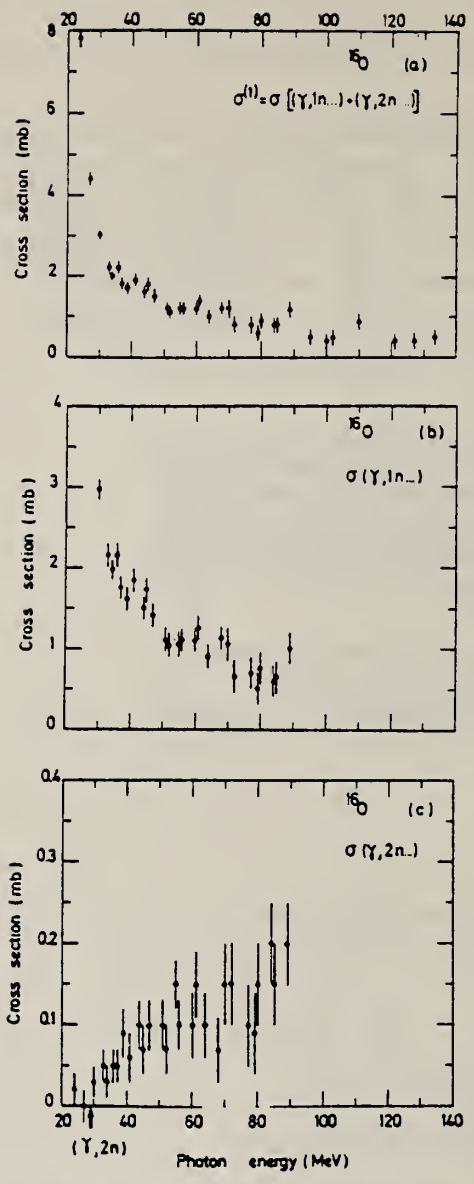

Fig. 3. Photoneutron cross sections for ^{16}O measured in the present experiment: (a) total photoneutron cross section $\sigma^{(1)}(E_\gamma)$; (b) single-photoneutron inclusive cross section $\sigma(\gamma, 1n\ldots)$ [the two lowest-energy points are shown in part (a)]; (c) double-photoneutron inclusive cross section $\sigma(\gamma, 2n\ldots)$. The error flags include the contributions of the major systematic as well as the statistical uncertainties (see text).

REF. H. Göringer, B. Schoch, G. Lührs
Nucl. Phys. A384, 414 (1982)

ELEM. SYM.	A	Z
O	16	8

METHOD

REF. NO. 82 Go 2 egf

REACTION	RESULT	EXCITATION ENERGY	SOURCE TYPE	SOURCE RANGE	DETECTOR TYPE	DETECTOR RANGE	ANGLE
G,NØ	ABX	6-160	C	62-163	TOF-D		DST

Abstract: A new TOF facility has been built for measurements of differential (γ, n) cross sections to discrete final states of light nuclei in the photon energy range between giant resonance and pion threshold. The observed neutron angle θ_n can continuously be varied between 0° and 150°, and additionally measurements at 175° and 180° are possible. Differential cross sections for the reaction $^{16}O(\gamma, n_0)^{15}O$ are presented for $E_\gamma = 60$ MeV ($40° \leq \theta_n \leq 149°$) and for $\theta_n = 90°$ (60 MeV $\leq E_\gamma \leq$ 160 MeV). The results, combined with the corresponding (γ, p_0) cross sections, indicate an absorption mechanism of high energy photons by neutron–proton pairs.

E NUCLEAR REACTION $^{16}O(\gamma, n_0)$, $E = 60$–160 MeV, $\theta_n = 40°$–149°, measured $\sigma(E_\gamma, \theta_n)$. Targets D_2O and H_2O.

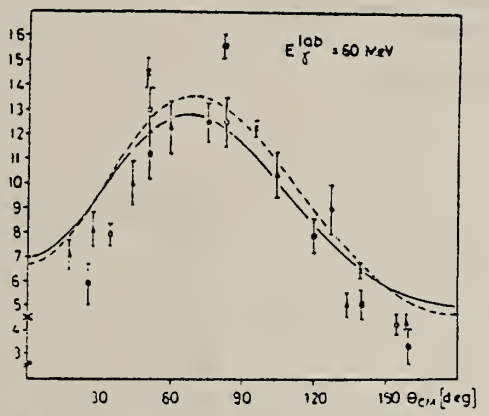

Fig. 3. Differential cross sections for the photodisintegration of the deuteron as a function of proton angle [c.m. system, μb/sr, taken from ref. [32])]. 0° point: ref. [40]).

32) H. Arenhövel and W. Fabian, Lecture notes in physics, vol. 86 (Springer, Berlin 1978) p. 84; H. Arenhövel, private communication (1979)

76 Hu 4 40) R.J. Hughes, A. Zieger, H. Wäffler and B. Ziegler, Nucl. Phys. A267 (1976) 329

TABLE 5

The measured differential cross sections for the reaction $^{16}O(\gamma, n_0)^{15}O$ and the errors involved

E_γ (MeV)	θ_n (°)	$d\sigma/d\Omega_n$ (μb/sr)	Stat errors (%)	Systematical errors (%) background	normaliz	β	sum
60	40	9.47	±3.9	±4.5	±4	<±1	±9.5
	50	9.11	3.3	3.5	4	<1	8.5
	60	8.21	2.6	3	4	<1	8
	75	6.62	2.7	2	4	<1	7
	90	4.68	1.5	1.5	4	<1	6.5
	105	2.30	2.7	2	4	2.5	8.5
	120	1.08	3.1	3	4	4	11
	135	0.45	4.2	5	4	5	14
	149	0.194	4.3	7	7	5	19
80	90	0.65	3.2	2	5	<1	8
120		0.049	12	8	10	5	23
160		0.046	25	23	30	2	55

(OVER)

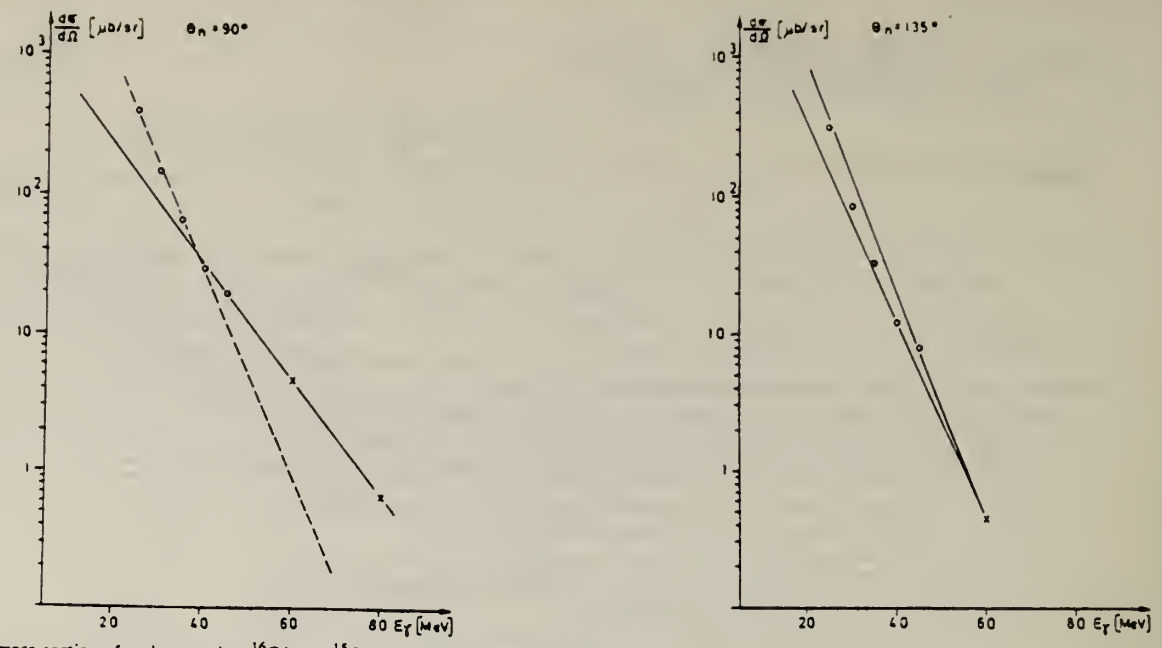

Fig. 16. Differential cross sections for the reaction $^{16}O(\gamma, n_0)^{15}O$ as a function of photon energy. (a) $\theta_n = 90°$, (b) $\theta_n = 40°$, (c) $\theta_n = 135°$. × this experiment, • Livermore [37]).

37) T.W. Phillips and R.G. Johnson, Phys. Rev. C20 (1979) 1689

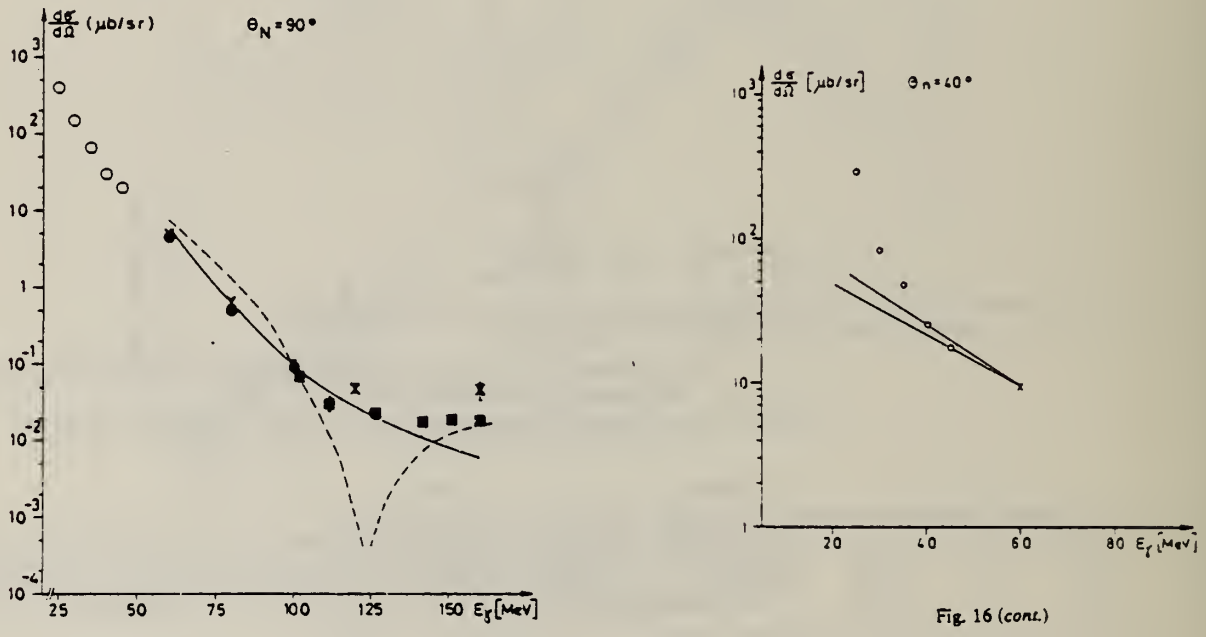

Fig. 16 (*cont.*)

Fig. 21. Differential cross sections for the reactions $^{16}O(\gamma, n_0)^{15}O$ and $^{16}O(\gamma, p_0)^{15}N$ as a function of photon energy for $\theta = 90°$: (γ, n_0): × this paper; ◦ ref. [37]); full line, ref. [23]); dot-dashed line, ref. [22]); (γ, p_0): • ref. [6]); ■ ref. [8]).

77 Fi 3

6) D.J.S. Findlay and R.O. Owens, Nucl. Phys. A279 (1977) 385

8) M.J. Leitch, Ph.D. thesis, MIT (1979)

22) B. Schoch, Phys. Rev. Lett. 41 (1978) 80, Habilitationsschrift, Universität Mainz, KPH/11/80, 1980;
B. Schoch and H. Göringer, to be published

23) M. Gari and H. Hebach, Phys. Reports 72 (1981) 1

0
A=17

0
A=17

0
A=17

A.K. Berzin, A.L. Gryaznov, R.P. Meshcheryakov, A.A. Startsev, and Yu.V. Khimenkov
Yad. Geofiz. Geokhim. 9, 113 (1971)

0	17	8

METHOD

REF. NO. 71 Be 5 egf

REACTION	RESULT	EXCITATION ENERGY	SOURCE TYPE	SOURCE RANGE	DETECTOR TYPE	DETECTOR RANGE	ANGLE
G,N	ABX	4- 9	C	4- 9	BF3-I		4PI

16885 MEASUREMENT OF THE OUTFLOW OF PHOTONEUTRONS AND CALCULATION OF THE CROSS SECTION OF THE $^{17}O(\gamma,n)^{16}O$ REACTION AT LOW ENERGIES. Berzin, A. K.; Gryaznov, A. L.; Meshcheryakov, R. P.; Startsev, A. A.; Khimenkov, Yu. V. Tr., Vses. Nauch.-Issled. Inst. Yadern. Geofiz. Geokhim.; No. 9, 113-115(1971). (In Russian).

Yields from the reaction $^{17}O(\gamma,n)^{16}O$ were measured from 4 to 8.5 MeV, and the cross section for the reaction was calculated. It exceeded 0.3 mb at the highest energy. Errors in the determination of photoneutron yield were estimated to be 10 to 15%. Application of these data and the photoneutron method to the estimation of the water-to-oil contact position in oil wells was explored. (2 figures) (RWR)

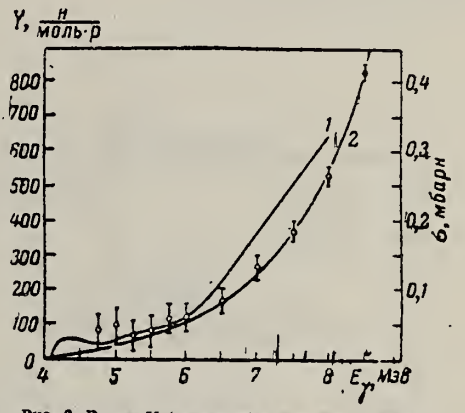

Рис. 2. Выход Y (кривая 2) и сечение σ (кривая 1) реакции O^{17} (γ, n) O^{16}.
Измеренные значения выхода обозначены точками с указанием ошибок.

REF.	I. Linck, L. Kraus and S.L. Blatt PICNS-73, Vol.II, p.931 (1973) Asilomar)	ELEM. SYM.	A	Z
		O	17	8
METHOD		REF. NO.		
		73 Li 2		egf

REACTION	RESULT	EXCITATION ENERGY	SOURCE		DETECTOR		ANGLE
			TYPE	RANGE	TYPE	RANGE	
T,G	ABX	19- 22	D	15- 35	NAI-D		DST

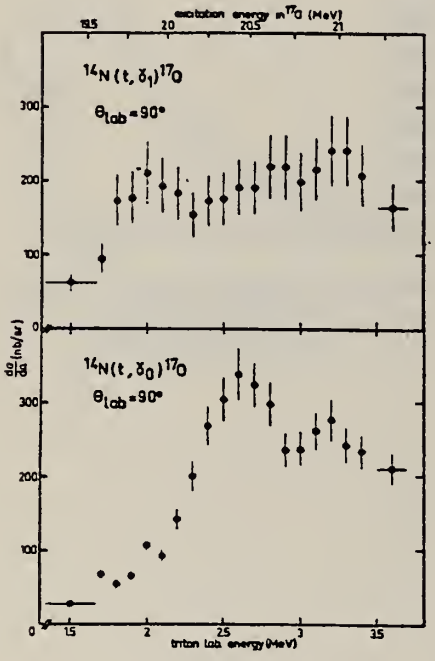

Fig. 2. γ_0 and γ_1 excitation curves. The excitation energies in ^{17}O are given at the target center, but the incident triton energies have not been corrected.

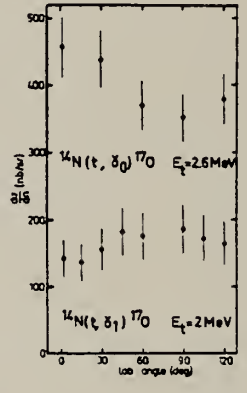

Fig. 3. Angular distributions for the two lowest resonances.

REF. J. C. Kim, R. Yen, I. P. Auer, H. S. Caplan
Phys. Lett. 57B, 341 (1975)

ELEM. SYM.	A	Z
O	17	8

METHOD

REF. NO. 75 Ki 11 egf

REACTION	RESULT	EXCITATION ENERGY	SOURCE		DETECTOR		ANGLE
			TYPE	RANGE	TYPE	RANGE	
E,E/	LFT	3- 8	D	84-122	MAG-D		DST

12 LEVELS 3.05-7.75

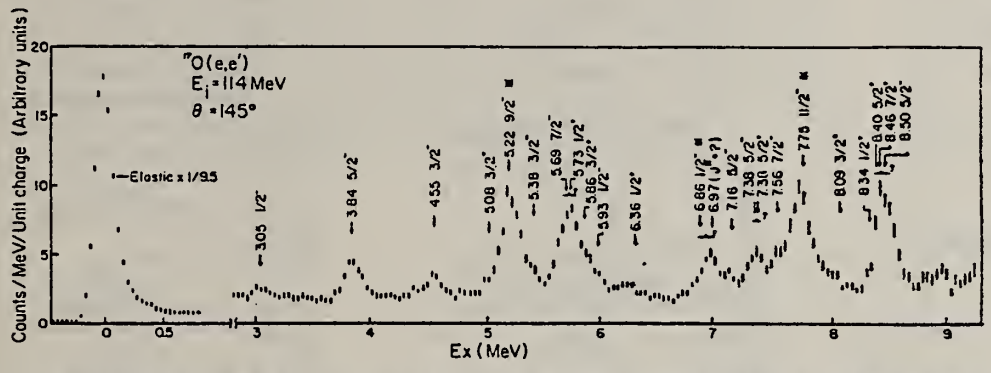

Fig. 1. The raw spectrum of 114 MeV electrons scattered by ^{17}O at an angle of 145°. The elastic peak has been multiplied by a factor of 2/19. The level identifications are due to ref. [6]. Levels with tentative spin assignments are marked with asterisks. Daggers and brackets denote multiple peaks where no attempt was made to determine individual contributions.

[6] F. Ajzenberg-Selove, Nucl. Phys. A166, 1 (1971).

Table 1
B(E3)† values for ^{17}O determined by the present experiment in units of e^2fm^6.

E_x (MeV)	J^π						
	$\frac{1}{2}^-$	$\frac{3}{2}^-$	$\frac{5}{2}^-$	$\frac{7}{2}^-$	$\frac{9}{2}^-$	$\frac{11}{2}^-$	Total
3.05	31 ± 6						
3.84			153 ± 6				
4.55		98 ± 8					
5.22*					360 ± 11		
5.37		45 ± 12					
5.69†				270 ± 32			
5.93	17 ± 10						
6.86*†	(147 ± 34)						
7.16			22 ± 25				
7.38†			47 ± 38				
7.56†				109 ± 26			
7.75*						369 ± 15	
8.5†			(negligible)				
Subtotal (Exp)	195 ± 36	143 ± 15	222 ± 44	379 ± 41	360 ± 11	369 ± 15	1670 ± 70
$\frac{2J+1}{.42}$ B(E3, (3⁻)^{16}O†	75 ± 3	150 ± 6	224 ± 9	299 ± 12	374 ± 14	449 ± 17	1570 ± 60

* Spin assignments tentative.
† q-dependence of form factors was used to separate C3 contribution.

REF. C. C. Chang, E. M. Diener, E. Ventura
Nucl. Phys. A258, 91 (1976)

ELEM. SYM.	A	Z
O	17	8

METHOD

REF. NO. 76 Ch 2 egf

REACTION	RESULT	EXCITATION ENERGY	SOURCE		DETECTOR		ANGLE
			TYPE	RANGE	TYPE	RANGE	
HE,G	ABX	22- 25	D	3- 8	NAI-D		DST

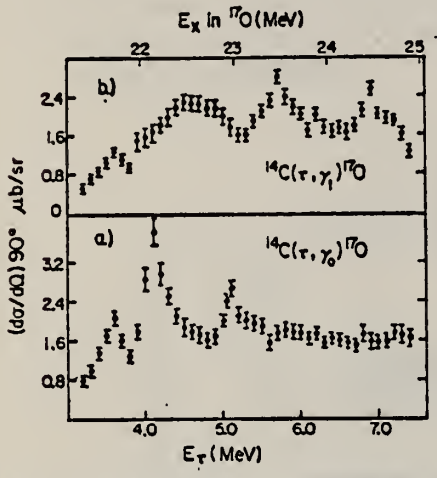

Fig. 2. Absolute differential cross sections as a function of E_τ for $^{14}C(\tau,\gamma_0)^{17}O$ and $^{14}C(\tau,\gamma_1)^{17}O$ at 90° (lab).

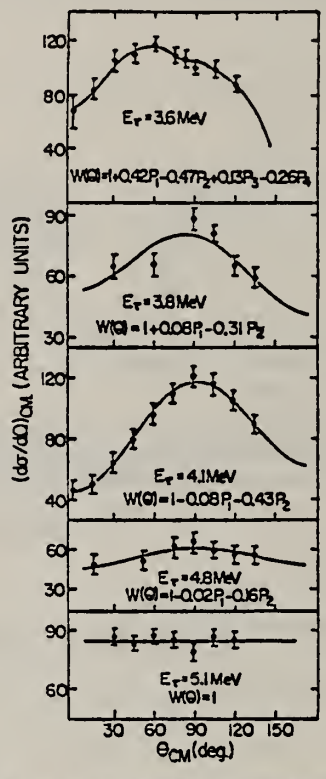

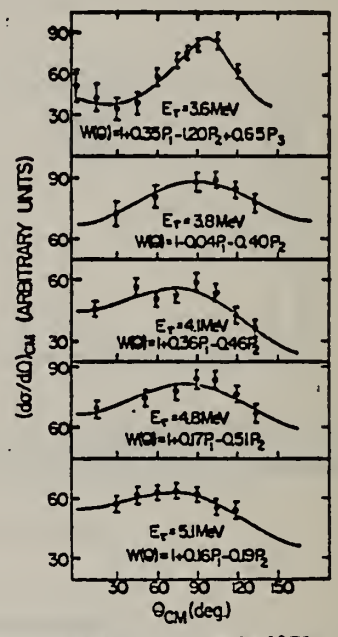

Fig. 4. Angular distributions for $^{14}C(\tau,\gamma_1)^{17}O$. The curves are the least-square fits to the expansion $W(\theta) = A_0[1 + \Sigma_{i=1}^{n} a_i P_i(\cos\theta)]$.

Fig. 3. Angular distributions for $^{14}C(\tau,\gamma_0)^{17}O$. The curves are the least-square fits to the expansion $W(\theta) = A_0[1 + \Sigma_{i=1}^{n} a_i P_i(\cos\theta)]$.

TABLE 1

$^{14}C(\tau,\gamma_0)^{17}O$ angular distribution as determined from fig. 3

E_τ (MeV)	E_x (MeV)	$W(\theta)$
3.6	21.7	$P_0+(0.42\pm0.17)P_1-(0.47\pm0.21)P_2+(0.13\pm0.18)P_3-(0.26\pm0.11)P_4$
3.8	21.9	$P_0+(0.08\pm0.05)P_1-(0.31\pm0.08)P_2$
4.1	22.1	$P_0-(0.08\pm0.03)P_1-(0.43\pm0.04)P_2$
4.8	22.7	$P_0-(0.02\pm0.05)P_1-(0.16\pm0.06)P_2$
5.1	23.0	P_0

REF. B. E. Norum, J. C. Bergstrom and H. S. Caplan
Nucl. Phys. A289, 275 (1977)

ELEM. SYM.	A	Z
O	17	8

METHOD

REF. NO. _77 No. 1 egf

REACTION	RESULT	EXCITATION ENERGY	SOURCE		DETECTOR		ANGLE
			TYPE	RANGE	TYPE	RANGE	
E,E/	FMF	10- 30	D	65-168	MAG-D		75

Abstract: The giant resonance region of ^{17}O has been investigated by means of inelastic electron scattering in a momentum transfer range 0.34–0.98 fm^{-1}. The data reveal a broad dipole resonance centred at 22–23 MeV excitation, with strength extending down to 10–12 MeV. A smaller resonance found between 17.5 and 19.6 MeV excitation has a form factor consistent with a C2 transition. Levels at 16.5 and 17.1 MeV excitation are also reported for the first time. Fine structure is observed between 11 and 15 MeV which correlates well with the positions of previously known levels. A particle-hole model with the Kuo-Brown residual interaction gives a satisfactory description of the strength distribution and q-dependence of the giant dipole resonance, although a scale factor of 1.85 is required to achieve agreement in magnitude.

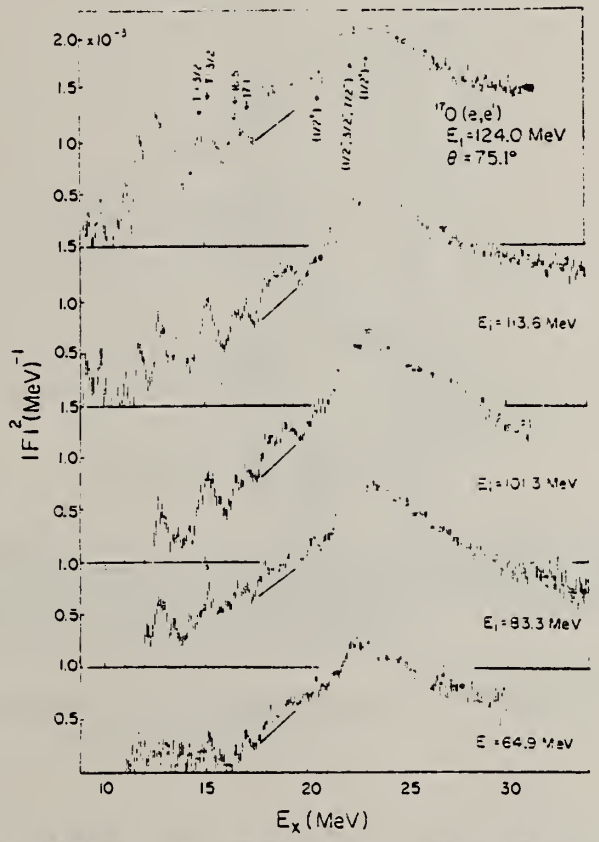

Fig. 3. Electron scattering spectra from ^{17}O in the giant resonance region, presented as differential form factors. The radiation and background tails have been removed. The straight lines approximately delineate the 17.5–19.6 MeV structure.

over

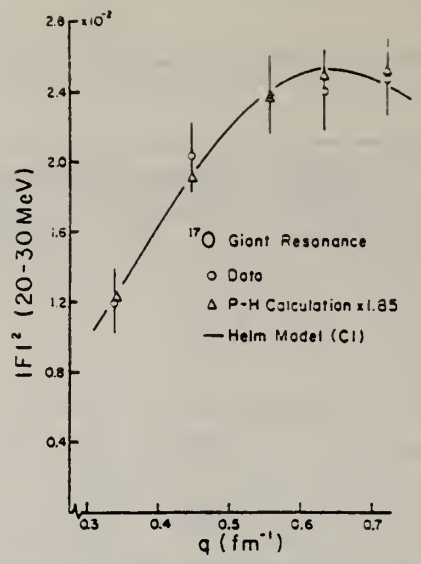

Fig. 4. The total form factor in the 20–30 MeV region of ^{17}O. The triangles represent the particle-hole calculations, scaled upward by 1.85, based on the Kuo-Brown matrix elements. The solid line is a Helm model fit assuming a C1 transition.

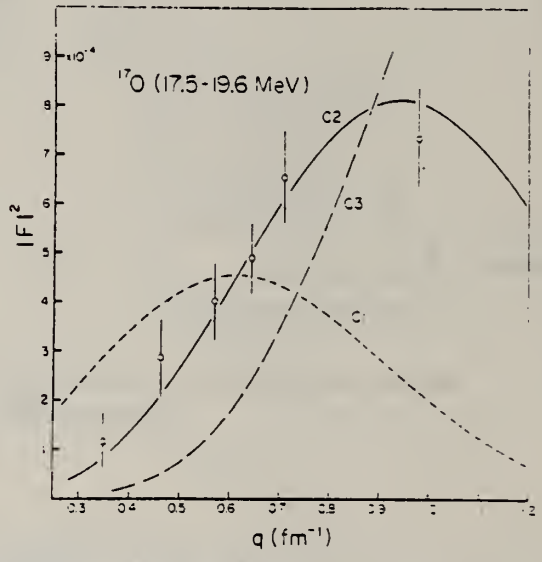

Fig. 5. The total form factor for the 17.5–19.6 MeV region of ^{17}O. The Helm model fits are based on R and q determined from the C1 fit in fig. 4.

REF. J.C. Kim, R.S. Hicks, R. Yen, I.P. Auer, H.S. Caplan and J.C. Bergstrom
Nucl. Phys. A297, 301 (1978)

ELEM. SYM.	A	Z
0	17	8

METHOD

REF. NO. 78 Ki 3 rs

REACTION	RESULT	EXCITATION ENERGY	SOURCE		DETECTOR		ANGLE
			TYPE	RANGE	TYPE	RANGE	
E,E/	LFT	1- 9	D	63-125	MAG-D		DST

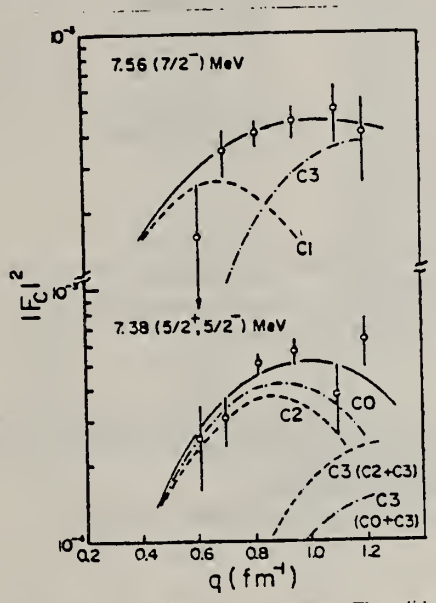

Fig. 4. Form factors of the 7.56 ($\frac{7}{2}^-$) and 7.38 ($\frac{1}{2}^+$, $\frac{5}{2}^-$) MeV peaks. The solid curves show the fitted form factors, each of which is taken as the sum of two contributions, C1 + C3 for the 7.56 MeV state, and C0 + C3 or C2 + C3 for the 7.38 MeV doublet. The shapes of the separated form factor components were predetermined as described in the text; only their magnitudes were varied in the fitting procedure.

over

TABLE 2

The ^{17}O reduced transition probabilities and ground-state radiative widths

E_x (MeV)	J^π	Cλ	$B(C\lambda\uparrow)$ ($e^2 \cdot fm^{2\lambda}$)	$\Gamma_{\gamma 0}(C\lambda)$ (eV)	Mλ	$B(M\lambda\uparrow)$ ($e^2 \cdot fm^{2\lambda}$)	$\Gamma_{\gamma 0}(M\lambda)$ (eV)
0.871	$\frac{1}{2}^+$	C2	2.10 ± 0.01 [a]				
3.055	$\frac{1}{2}^-$	C3	31 ± 6	$(8.7 \pm 1.7) \times 10^{-8}$			
3.841	$\frac{3}{2}^-$	C3	153 ± 6	$(7.1 \pm 0.3) \times 10^{-7}$	M2	$(5 \pm 2) \times 10^{-2}$	$(4.6 \pm 1.8) \times 10^{-3}$
4.554	$\frac{3}{2}^-$	C3	98 ± 8	$(2.2 \pm 0.2) \times 10^{-6}$	M2	$(5.4 \pm 2.1) \times 10^{-2}$	$(1.8 \pm 0.7) \times 10^{-2}$
5.083	$\frac{1}{2}^+$	C2	2.5 ± 0.7	$(1.0 \pm 0.3) \times 10^{-2}$			
5.217	$(\frac{3}{2}^-)$	C3	360 ± 11	$(8.5 \pm 0.3) \times 10^{-6}$	M2	$< 4 \times 10^{-2}$	$< 1 \times 10^{-2}$
5.377	$\frac{3}{2}^-$	C3	45 ± 12	$(3.3 \pm 0.9) \times 10^{-6}$	M2	$(6 \pm 3) \times 10^{-2}$	$(4.5 \pm 2.2) \times 10^{-2}$
5.696	$\frac{7}{2}^-$	C3	270 ± 32	$(1.5 \pm 0.2) \times 10^{-5}$	M2	0.3 ± 0.2	0.15 ± 0.10
5.935	$\frac{1}{2}^-$	C3	17 ± 10	$(5.0 \pm 2.9) \times 10^{-6}$			
6.356	$\frac{1}{2}^+$	C2	2.1 ± 1.3	$(5.3 \pm 3.3) \times 10^{-2}$			
6.859	$(\frac{1}{2}^-)$	C3	147 ± 34	$(1.2 \pm 0.3) \times 10^{-4}$			
6.970	$(\frac{1}{2}^+)$	C2	1.9 ± 1.0	$(2.5 \pm 1.3) \times 10^{-2}$			
7.378	$\frac{1}{2}^+$	C0	5.5 ± 1.0 [b]				
		or C2	3.6 ± 1.0	$(6.3 \pm 1.8) \times 10^{-2}$			
7.379	$\frac{1}{2}^-$	C3	47 ± 38	$(2.1 \pm 1.7) \times 10^{-5}$			
7.569	$\frac{7}{2}^-$	C1	$(7.8 \pm 2.0) \times 10^{-2}$	26 ± 7			
		C3	109 ± 26	$(4.3 \pm 1.0) \times 10^{-5}$			
7.751	$(\frac{11}{2}^-)$	C3	369 ± 15	$(1.16 \pm 0.05) \times 10^{-4}$			
8.347	$\frac{1}{2}^+$	C0	7.6 ± 1.4 [b]				
8.402	$\frac{3}{2}^+$	or C2	8.3 ± 2.6				
8.467	$\frac{7}{2}^+$						
8.502	$\frac{1}{2}^-$						

The bracketed levels were unresolved and have been analyzed as a group. Bracketed spins are tentative and were used to evaluate the radiative widths.

[a]) Deduced from the lifetime measurement [6]).

[b]) For C0 transitions the monopole matrix element is tabulated.

[6] F. Ajzenberg-Selove, Nucl. Phys. A166 (1971) 1

REF. R.G. Johnson, B.L. Berman, K.G. McNeill, J.G. Woodworth, J.W. Jury
Phys. Rev. C20, 27 (1979)

ELEM. SYM.	A	Z
O	17	8

METHOD

REF. NO. 79 Jo 2 hg

REACTION	RESULT	EXCITATION ENERGY	SOURCE		DETECTOR		ANGLE
			TYPE	RANGE	TYPE	RANGE	
G,NO	ABX	5-33	C	13-34	TOF-D		98

J-PI, LFT, ENRICHED 017

Photoneutron spectra from ^{17}O have been obtained at bremsstrahlung end-point energies of 13.7, 16, 22, 28, and 34 MeV using the neutron time-of-flight technique. The angle between the incident photon beam and the 49.2-m flight path was 98°. From the measured spectra the differential cross section for the $^{17}O(\gamma,n_0)^{16}O$ reaction between 5 and 33 MeV was obtained. The considerable structure in the cross section is compared with the known spectrum of levels for this nucleus compiled from previous studies using various reactions. In the region below 19 MeV, 18 resonances correspond to levels previously identified. In addition at least 12 other resonances which have not been seen previously have been observed. In the giant-dipole resonance region (above 19 MeV) the present results delineate the $T = 1/2$ strength. The measurement is compared to the $^{16}O(p,\gamma_0 + \gamma_1)^{17}F$ reaction with the expected similarities observed. The measurement also is compared to 1p,2p-1h shell-model calculations.

[NUCLEAR REACTIONS $^{17}O(\gamma,n_0)^{16}O$, $E_x = 5.0-33.0$ MeV; measured photoneutron time-of-flight spectra; deduced $(d\sigma/d\Omega)$ $(E_x, 98°)$, resonant structure; $T=\frac{1}{2}$ strength of the GDR.]

TABLE II. Detailed analysis of some ^{17}O negative-parity levels below 9.5-MeV excitation energy.

J^π	Ref. 18 Excitation energy E_x (MeV)	Ref. 18 Neutron width Γ_n (keV)	Ref. 18 Alpha width Γ_α (keV)	Ref. 19 $B(E3\uparrow)$ (e^2fm^6)	This measurement Excitation energy E_x (MeV)	This measurement Gamma width $\Gamma_{\gamma 0}$ (eV)
$\frac{1}{2}^-$	5.377	41.5			5.43	0.7 ± 0.4
$\frac{5}{2}^-$	5.696	3.4		270 ± 32	5.71	1.1 ± 0.4
$\frac{5}{2}^-$	7.380	1.1	0.003	47 ± 38	7.37	0.8 ± 0.4
$\frac{7}{2}^-$	7.685	18	0.01		7.66	1.5 ± 0.5
$\frac{1}{2}^-$	8.197	48	4.0		8.24	1.4 ± 0.5
$\frac{5}{2}^-$	8.505	3.4	1.9	(negligible)	8.48	6.6 ± 1.8
$\frac{1}{2}^-$	8.689	42	1.8		8.69	1.2 ± 0.6
$\frac{7}{2}^-$	8.969	23	2.3		8.98	4.1 ± 0.8

(over)

in ^{15}O.

Resonance number [a]	Excitation energy E_x (MeV)	Integrated strength A (MeV μb/sr)	Levels compiled in Ref. 15 E_x (MeV ± keV)	J^π	Γ_{cm} (keV)
1	5.14	6.7 ± 2.9	5.086 ± 2	$\frac{1}{2}^+$	95 ± 5
(2) [b]	5.27				
3	5.43	4.9 ± 2.6	5.380 ± 2	$\frac{1}{2}^-$	28 ± 7
(4)	5.57	3.5 ± 2.2			
5	5.71	15.0 ± 4.8	5.698 ± 2	$\frac{3}{2}^-$	3.4 ± 3
((6)) [b]	5.96		5.870 ± 2	$\frac{1}{2}^+$	6.6 ± 0.7
			5.940 ± 4	$\frac{1}{2}^-$	32 ± 3
(7)	6.30	5.5 ± 2.8			
8	6.61	21.3 ± 9.2			
9	6.97	10.0 ± 3.3	6.973 ± 2		<1
((10)) [b]	7.21		7.202 ±10	$\frac{1}{2}^+$	280 ±30
11	7.37	5.3 ± 1.9	7.3831 ± 1.5	$\frac{5}{2}^+$	0.6 ± 0.2
			7.3860 ± 1.5	$\frac{5}{2}^-$	0.9 ± 0.3
12	7.66	11.6 ± 3.8	7.690 ± 4	$\frac{3}{2}^-$	18 ± 2
(13)	7.80	4.2 ± 2.0			
(14)	7.91	3.1 ± 1.5			
15	8.24	4.0 ± 1.5	8.200 ± 7	$\frac{1}{2}^-$	60
16	8.48	14.1 ± 3.8	8.474 ± 3	$\frac{7}{2}^+$	7 ± 3
			8.508 ± 3	$\frac{5}{2}^-$	5 ± 3
(17)	8.69	3.2 ± 1.5	8.700 ± 5	$\frac{1}{2}^-$	50 ± 3
(18)	8.80	3.6 ± 1.8			
19	8.98	21.1 ± 4.2	8.972 ± 4	$\frac{3}{2}^-$	21 ± 3
			9.148 ± 4	$\frac{1}{2}^-$	4 ± 3
((20))	9.13		9.15 ±20	$\frac{3}{2}^-$	
21	9.28	7.0 ± 2.5			
(22)	9.55	3.4 ± 1.4			
23	9.72	13.1 ± 3.1	9.720 ± 5	$\frac{7}{2}^+$	16 ± 1
(24)	10.25	13.1 ± 3.6	10.178 ± 5	$\frac{7}{2}^-$	40
			10.337 ±15	$\frac{5}{2}, \frac{7}{2}^-$	150
25	10.53	17.4 ± 2.9	10.563 ±10	$\frac{7}{2}^-$	47 ±15
(26)	11.02	20.6 ± 4.5	11.03 ± 4		
27	11.39	39.9 ± 6.2			
28	11.89	13.9 ± 3.2			
29	12.53	10.5 ± 3.2			
30	12.83	13.1 ± 4.9	12.81 ±25		
31	13.06	18.2 ± 6.0	13.077 ±15		16 ± 4
32	13.30	31.9 ± 8.1			
33	13.68	46 ±14	13.672		400
34	14.65	125 ±30	14.621		340
35	15.56	32.6 ± 8.3	15.5		broad
(36)	15.95	10.8 ± 4.5			
37	17.00	53 ±13	17.09 ±50 [c]		
((38))	17.67				
39	18.25	42 ±10			
40	19.0	14.5 ± 4.3			
41	19.7	78 ±15			
42	21.2	368 ±79			
43	21.7	27 ±14	21.7 ±100	$\frac{5}{2}^+$	750
44	25.7	171 ±47			
45	26.9	91 ±28			

[a] Parentheses in this column are used to indicate that the evidence for a resonance is not compelling. Double parentheses are used when the evidence is even weaker.
[b] Possibly results from an excited-state transition(s).
[c] From Ref. 20.

EL EM. SYM.	A	Z
0	17	8

METHOD

REF. NO.	
79 Jo 2	hg

RANGE	ANGLE

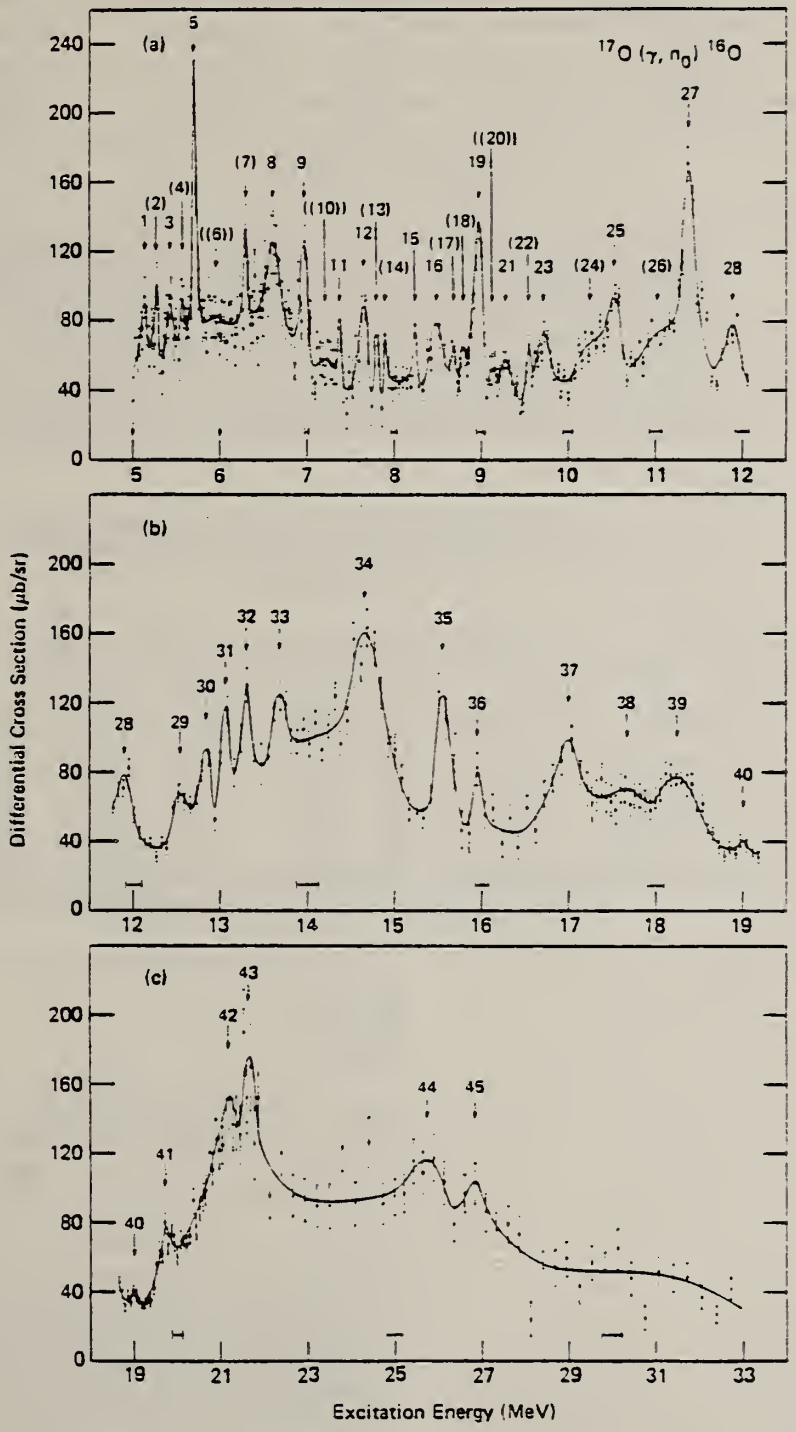

FIG. 1. The $^{17}O(\gamma,n_0)^{16}O$ differential cross section at 98°. The solid line is drawn to guide the eye. Numbered arrows indicate possible resonances. Horizontal bars represent the energy resolution of the measurement. (a) Threshold to 12 MeV. (b) 12 to 19 MeV. (c) 19 to 33 MeV (note that the energy scale has been doubled for this part).

REF. J.W. Jury, B.L. Berman, D.D. Faul, P. Meyer, J.G. Woodworth
Phys. Rev. C21, 5Q3 (1980)

ELEM. SYM.	A	Z
O	17	8

METHOD

REF. NO. 80 Ju 4 hg

REACTION	RESULT	EXCITATION ENERGY	SOURCE		DETECTOR		ANGLE
			TYPE	RANGE	TYPE	RANGE	
G,1N	ABX	8-40	D	8-40	BF3-I		4PI
G,2N	ABX	20-40	D	10-40	BF3-I		4PI
		(19.7-39.7)					

Photoneutron cross sections involving the emission of one and two neutrons from ^{17}O have been measured over the energy interval 8.5 to 39.7 MeV using monoenergetic photons from positron in-flight annihilation. The 6-MeV wide giant dipole resonance is observed to be centered at 23 MeV and a pygmy resonance is seen at about 13 MeV. Such structure as is apparent in the cross sections is not as pronounced as for the cases of ^{16}O and ^{18}O. Comparison of the total photoneutron cross section with recent ground-state data indicates that much of the pygmy resonance decays to the ground or first excited state of ^{16}O, but that the giant dipole resonance decays mainly to highly excited states in the daughter. Excellent agreement is observed between the present results and a recent two-particle, one-hole shell-model calculation of the isospin-split giant dipole resonance states for this nucleus. New photoneutron cross-section results for ^{16}O up to 39.7 MeV are reported as well.

[NUCLEAR REACTIONS $^{17}O(\gamma,n)$, E_γ=8.5–39.7 MeV and $^{16}O(\gamma,n)$, E_γ=15.9–39.7 MeV; measured 4π neutron yield for monenergetic photons; $\sigma(E_\gamma,1n)$, $\sigma(E_\gamma,2n)$, integrated cross sections, isospin splitting of the giant resonance for ^{17}O.]

TABLE I. Integrated cross sections and their moments.

Nucleus	reaction	E_{thresh} (MeV) [a]	$E\gamma_{max}$ (MeV)	σ_{int} (MeV mb)	σ_{-1} (mb)	σ_{-2} (mb MeV^{-1})	Reference
^{17}O	$(\gamma,1n)$	4.14	39.7	111	4.94	0.256	This work
	$(\gamma,2n)$	19.81	39.7	9	0.31	0.010	This work
^{16}O	$(\gamma,1n)$	15.66	39.7	63	2.4	0.10	This work
	$(\gamma,1n)$	15.66	37.0	63	2.4	0.09	Ref. 11
	$(\gamma,1n)$	15.66	37.1	79	3.0	0.12	Ref. 12

[a] From A. H. Wapstra and K. Bos, At. Data Nucl. Data Tables 19, 215 (1977).

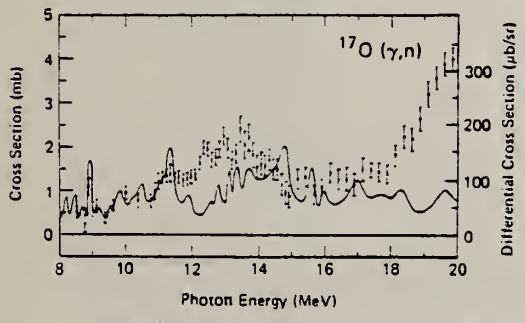

FIG. 5. The present results for the $^{17}O(\gamma,n)$ cross section at low energies (data points) are compared with the ground-state differential cross section of Ref. 2 (solid line). The vertical scale has been chosen to reflect a factor of 4π between the two cross-section scales. Below 10.2 MeV (the threshold for photoneutron emission to the first excited state of ^{16}O), the two results should be identical except for (a) angular-distribution effects in the differential measurement and (b) resolution differences.

(over)

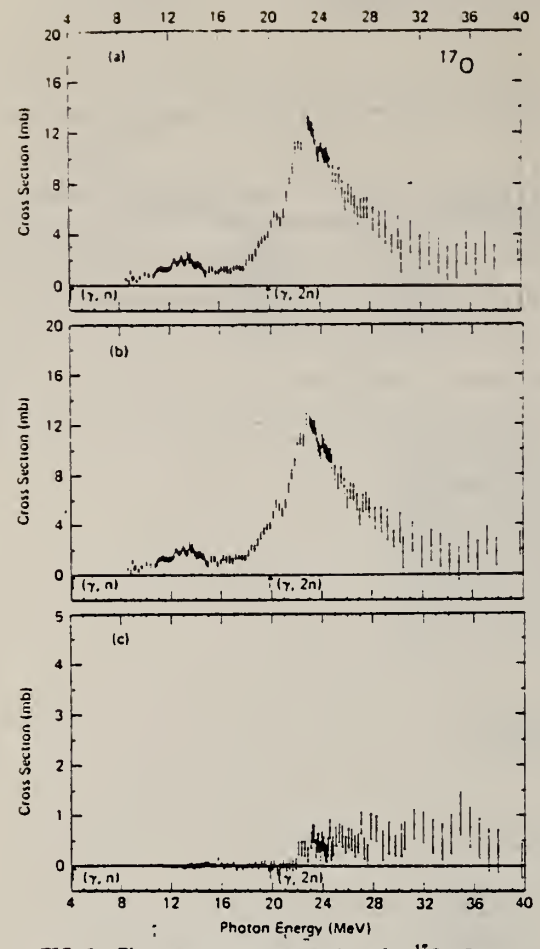

FIG. 3. Photoneutron cross sections for ^{17}O: Part (a) shows the total photoneutron cross section $\sigma(\gamma, n_{tot}) = \sigma[(\gamma, n) + (\gamma, pn) + (\gamma, \alpha n) + (\gamma, 2n)]$; part (b) shows the single photoneutron cross section $\sigma(\gamma, 1n) = \sigma[(\gamma, n) + (\gamma, pn) + (\gamma, \alpha n)]$; part (c) shows $\sigma(\gamma, 2n)$. The plotted error bars indicate the statistical uncertainties. The threshold energies are indicated by arrows in this and other plots.

REF. I. Linck, L. Kraus, S.L. Blatt
Phys. Rev. C21, 791 (1980)

ELEM. SYM.	A	Z
O	17	8

METHOD

REF. NO. 80 Li 2 hg

REACTION	RESULT	EXCITATION ENERGY	SOURCE		DETECTOR		ANGLE
			TYPE	RANGE	TYPE	RANGE	
T,G	ABX	19-22	0-3		NAI-D		DST
		(19.3-21.3)	(.8-3.3)				

J-PI, LFT

Cross sections for the radiative capture of tritons by ^{14}N have been measured in the incident energy range 0.8 to 3.3 MeV and found to be of order 200–300 nb/sr. The 90° excitation functions exhibit resonant structures for the transitions to the $5/2^+$ ground state of ^{17}O and the $1/2^+$ (0.87-MeV) first excited state. Multilevel S-matrix fits of both excitation functions and angular distributions, on the assumption that dipole transitions dominate, permit J^π assignments for the observed resonances to be limited to a very few possibilities; the best fit results, which are also most consistent with other relevant arguments, give the most likely assignments $3/2^-$, $5/2^-$, $1/2^+$, and $3/2^-$ for states at 19.76, 20.39, 20.58, and 21.05 MeV, respectively, although the parities cannot be individually ascertained. The lower limit for the radiative widths Γ_γ ranges from 1 to 6 eV. An additional level also appears to be present at ~19.3 MeV.

[NUCLEAR REACTION $^{14}N(t,\gamma)^{17}O$, $E=0.8-3.3$ MeV; measured $\sigma(\theta,E)$, ^{17}O deduced levels, J^π, Γ, $\Gamma_t \cdot \Gamma_{\gamma_0}$, $\Gamma_t \cdot \Gamma_{\gamma_1}$. Natural nitrogen target.]

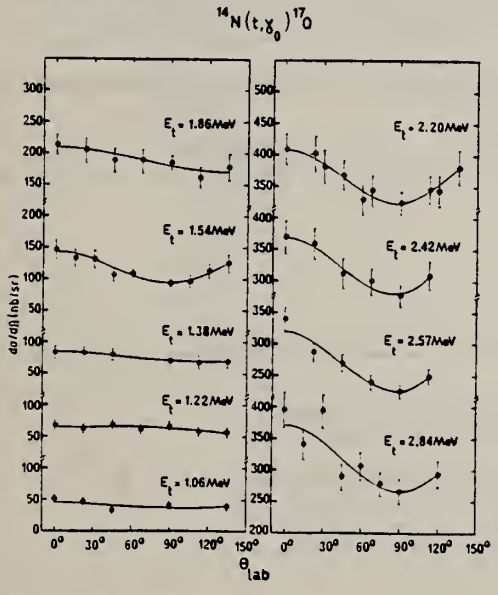

FIG. 3. Experimental angular distributions of t-capture γ rays to the ^{17}O ground state. The incident energies are given at the gas target center as in Fig. 2. The solid curves are least squares fits to Legendre polynomials up to order 2. The resulting coefficients are shown in Fig. 5.

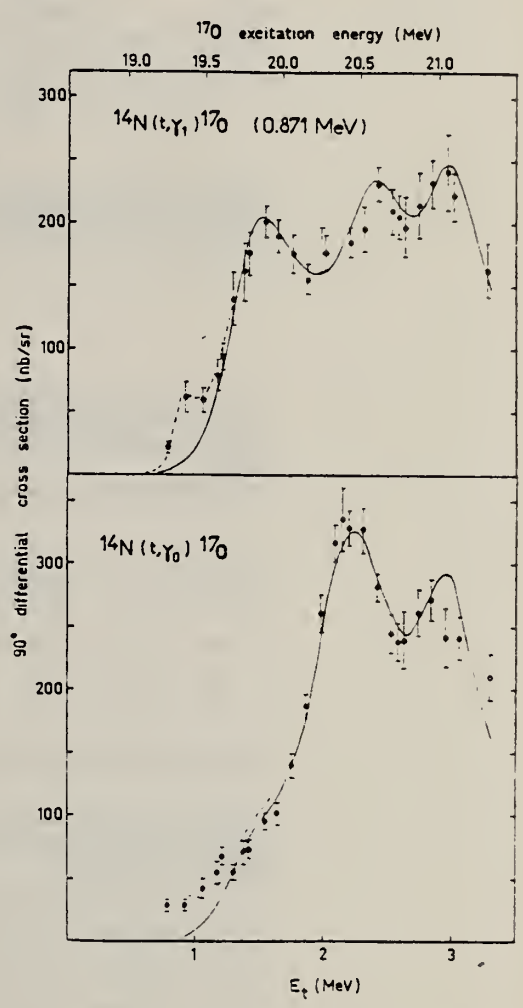

FIG. 2. Excitation functions at 90° for t-capture γ rays to the ^{17}O ground state and first excited state. The bombarding energies have been corrected for energy losses in the entrance Ni foil and target gas. The curves correspond to the "best" fit, as described in the text.

(OVER)

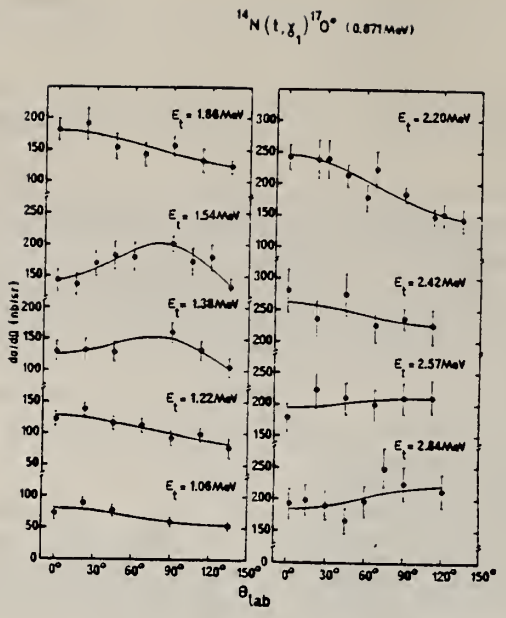

FIG. 4. Experimental angular distributions of t-capture γ rays to the ^{17}O first excited state. Also see comments of Fig. 3; the resulting Legendre coefficients are shown in Fig. 6.

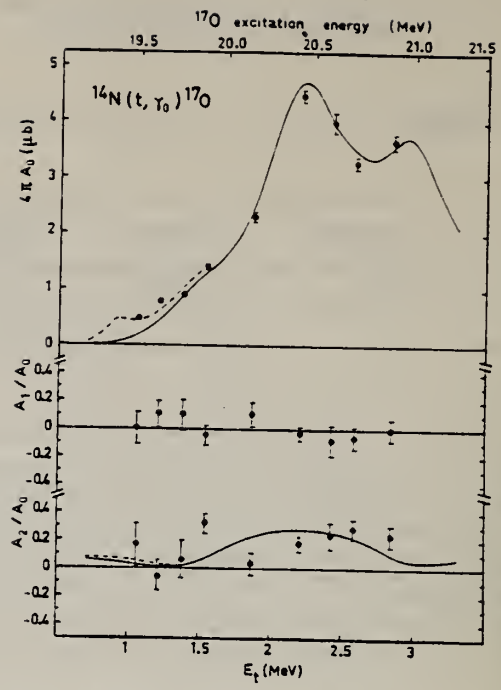

FIG. 5. Legendre polynomial fit coefficients of the γ_0 angular distributions. The curves correspond to the fit obtained with the sequence $(\frac{1}{2}^-, \frac{5}{2}^-, \frac{3}{2}^-)$ and the parameters of Table I. The dashed curve corresponds to the inclusion of a $\frac{3}{2}^-$ state at low energy.

TABLE I. Best fit resonance parameters resulting from the three-level fit of the 90° excitation functions and coefficients of the Legendre polynomial fit to the angular distributions, in the reactions $^{14}N(t,\gamma_0)^{17}O$ and $^{14}N(t,\gamma_1)^{17}O^*$. The corresponding calculated curve is drawn on Figs. 2, 5, and 6. The possibility of other spin sequences is discussed in the text.

					Transition γ_0		Transition γ_1	
E_η (MeV)	J^π	l, s	$\mathcal{L}$	Γ (MeV)	X_{cn} (10^{-4} MeV$^{-1/2}$ – $b^{1/4}$)	ξ_{cn} rad	X_{cn} (10^{-4} MeV$^{-1/2}$ – $b^{1/4}$)	ξ_{cn} rad
1.14	$\frac{3}{2}^-$	1, $\frac{1}{2}$	$E1$	0.55	0.172	0.53	0.280	1.31
1.77	$\frac{5}{2}^-$	1, $\frac{3}{2}$	$E1$	0.66	0.197	0.56		
1.96	$\frac{1}{2}^+$	0, $\frac{1}{2}$	$M1$	0.57			0.158	3.42
2.43	$\frac{3}{2}^-$	1, $\frac{1}{2}$	$E1$	0.47	0.131	−1.32	0.148	−0.51

TABLE II. ^{17}O level data deduced from the study of $^{14}N(t,\gamma)^{17}O$. Errors in this table correspond to uncertainties given by the fitting procedure, including the different possible J^π assignments indicated.

					Lower limit	
J^π	E_{exc} (MeV)	Γ (MeV)	$\Gamma_t\Gamma_{\gamma_0}$ (keV)^2	$\Gamma_t\Gamma_{\gamma_1}$ (keV)^2	Γ_{γ_0} (eV)	Γ_{γ_1} (eV)
$\frac{3}{2}^\mp$	19.76 ± 0.06	0.55 ± 0.05	0.54 ± 0.1	1.25 ± 0.15	1.0	2.3
$\frac{5}{2}^\mp$ $\frac{7}{2}^-$	20.39 ± 0.05	0.66 ± 0.07	2.9 ± 0.3		4.3	
$\frac{1}{2}^\pm$	20.58 ± 0.05	0.57 ± 0.08		2.9 ± 0.5		5.1
$\frac{3}{2}^\mp$	21.05 ± 0.05	0.47 ± 0.06	2.7 ± 0.4	3.0 ± 0.4	5.8	6.5

0
A=18

0
A=18

Ref. D. Reagan
Phys. Rev. 100, 113 (1955)

Elem. Sym.	A	Z
O	18	8

Method N^{17} detector

Ref. No. 55 Re 1 EGF

Reaction	E or ΔE	E_o	Γ	$\int \sigma dE$	Jπ	Notes
(γ,p)		25		67 MeV-mb		Yield seemed to follow 25 MeV isochromat or electron energy was varied from 50 to 400 MeV.

Ref. F. Lacoste, G.R. Bishop
Nuclear Phys. 26, 511 (1961)

Elem. Sym.	A	Z
O	18	8

Method: Electron elastic scattering and inelastic scattering

Ref. No: 61 La 1 JOC

Reaction	E or ΔE	E_o	Γ	$\int \sigma dE$	Jπ	Notes
$O^{18}(e,e)$	150					
$O^{18}(e,e')$	7	2.0 5.0 5.5			2^+ E2	$\tau = (3.3 \pm 1.5)10^{-12}$ sec.

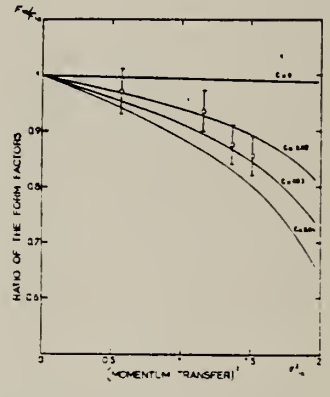

Fig. 7. Experimental ratios of the O^{18} and O^{16} elastic form factors versus x_0 (defined in sect. 3). The curves labelled $\varepsilon = 0$, $\varepsilon = 0.02$, $\varepsilon = 0.03$ and $\varepsilon = 0.04$ give the shell model predictions assuming a parabolic well potential with $x_{0n}(O^{18}) = 1 - \varepsilon x_{0n}(O^{16})$.
For $\varepsilon = 0$ the predicted ratio is different from unity because the masses of the two nuclei are different and therefore the recoil corrections are not identical.

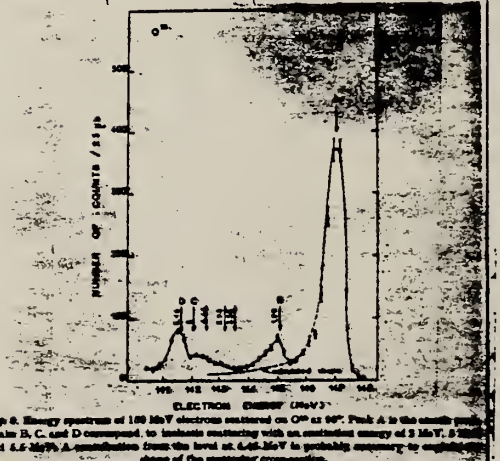

Fig. 8. Energy spectrum of 150 MeV electrons scattered on O^{16} at 90°. Peak A is the elastic peak. Peaks B, C and D correspond, to inelastic scattering with an excitation energy of 3 MeV, 6 MeV and 6.6 MeV. A contribution from the level at 6.46 MeV is probably responsible for asymmetric shape of the scattering cross-section.

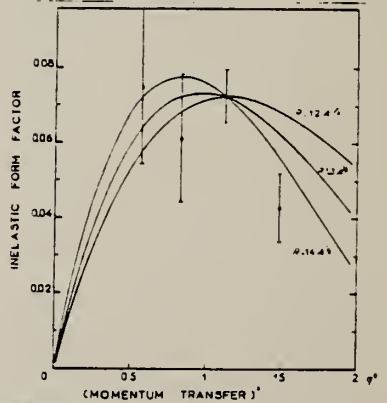

Fig. 10. Inelastic form factor F_1 corresponding to the first excited state of O^{16}. The solid curves are the values of $r_s\,(qR)\,Cl$, normalized at our best experimental point, with $R = r_0 A^{\frac{1}{3}}$ ($r_0 = 1.2$, $r_0 = 1.3$ and $r_0 = 1.4$).

H. Fuchs
Z. Physik 171, 416 (1963)

0	18	8

METHOD: Betatron; neutron spectrum; cross section; Stilhene scintillator; ion chamber

REF. NO.: 63 Fu 2 | NVB

REACTION	RESULT	EXCITATION ENERGY	SOURCE		DETECTOR		ANGLE
			TYPE	RANGE	TYPE	RANGE	
G,XN	SPC	11-31	C	31	SCI-D	3-20	90
				(30.5)		(2.5 - 20)	

$\frac{d\sigma}{d\Omega}$ (90°) ≤ 0.32 mb/str

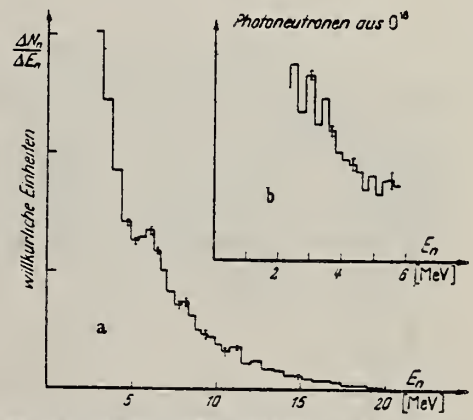

Fig. 1 a u. b. Energieverteilung der Photoneutronen aus O^{16} unter 90° bei $E_\gamma = 30{,}5$ MeV. a von 2,5 bis 20 MeV, b von 2,5 bis 6 MeV in feinerer Kanaleinteilung

REF.
R. Kosiek, K. Schlüpmann, H. W. Siebert und R. Wendling
Z. Physik 179, 9 (1964)

ELEM. 3 A. | 0 | 18 | 8

METHOD
Betatron; proton spectrum, yield; CsI scintillator; ion chamber monitor

REF. NO. 64 Ko 2 | NVB

REACTION	RESULT	EXCITATION ENERGY	SOURCE TYPE	SOURCE RANGE	DETECTOR TYPE	DETECTOR RANGE	ANGLE
G,P	SPC	18-32	C 32		SCI-D	2 - 14	90

Tabelle 1. *Überblick über die Messungen*

Bei der Berechnung des integrierten Wirkungsquerschnittes wurde isotrope Winkelverteilung angenommen.

E_{min}: untere Abschneidegrenze bei der Bestimmung der Protonenausbeute.

Target	Isotop	Anreicherungsgrad des seltenen Isotops %	Druck des Targetgases mm Hg	$\left(\frac{dY}{d\Omega}\right)_{90°}$ $\frac{\mu b}{\text{MeV} \cdot \text{ster}}$	registrierte integrale Protonenzahl	E_{min} MeV	$\int_{E_0}^{} \sigma dE_\gamma$ MeV mb
Methan CH_4	C^{13}	55,2	700	2,5 ± 15%	8327	3,5	37 ± 20%
Knallgas H_2+O_2	O^{18}	90	a) 1560 b) 750	— 4,6 ± 15%	9560 7376	3,5 2,5	— 33 ± 20%

SEPARATED ISOTOPES

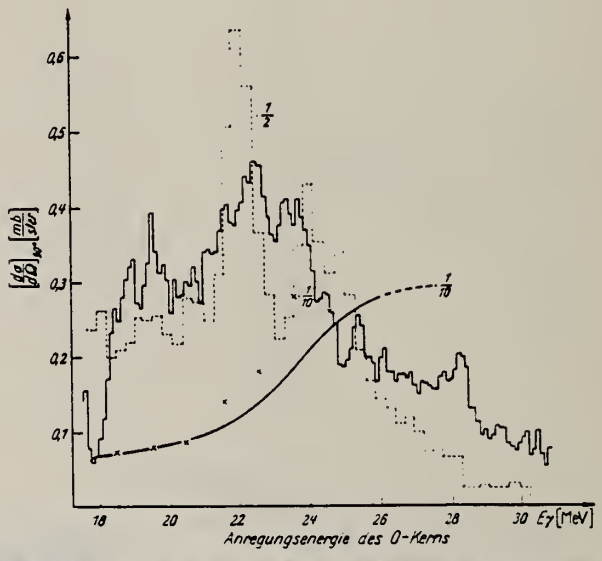

Fig. 6. Differentieller Wirkungsquerschnitt für Photoprotonenemission aus O^{18}. a) Unter 90° zum γ-Strahl unter der Annahme, daß nur Grundzustandsübergänge vorliegen, diese Arbeit (Histogramm ———). b) Nach STEPHENS et al.[5] (×) (siehe c). c) Nach MONTALBETTI und KATZ[6] (Kurve). Die unter b) und c) eingetragenen Werte wurden gewonnen, indem die Resultate der genannten Autoren mit $1/10 \cdot 1/4\pi$ multipliziert wurden.
Differentieller Wirkungsquerschnitt für Photoprotonenemission aus O^{16} nach (I), mit dem Faktor $\frac{1}{4}$ multipliziert (Histogramm – – –)

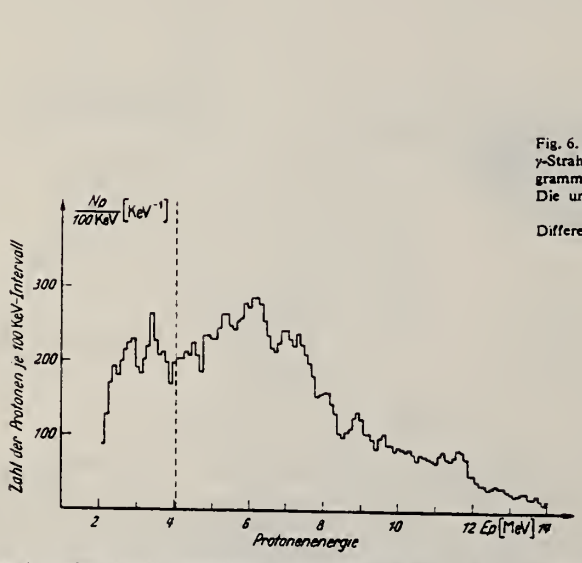

Fig. 4. Energieverteilung der Photoprotonen aus O^{18}. Das Histogramm wurde aus dem der Fig. 2 gewonnen, indem der Anteil der Protonenemission aus O^{16} abgezogen wurde. Für Protonenenergie oberhalb der gestrichelten Senkrechten wurden zusätzlich die Ergebnisse einer weiteren Messung verwandt. Nähere Erläuterungen im Text

Said F. Mughabghab, W. E. Stephens
Phys. Rev. 133, B660-62 (1964)

0	18	8

METHOD: Betatron

REF. NO.: 64 Mu 1 NVB

REACTION	RESULT	EXCITATION ENERGY	SOURCE TYPE	SOURCE RANGE	DETECTOR TYPE	DETECTOR RANGE	ANGLE
G,N	SPC	10-20	C	20	EMU-D	1-10	DST

Target enriched to 90% O^{18}.

J-PI, 2189 TRACKS

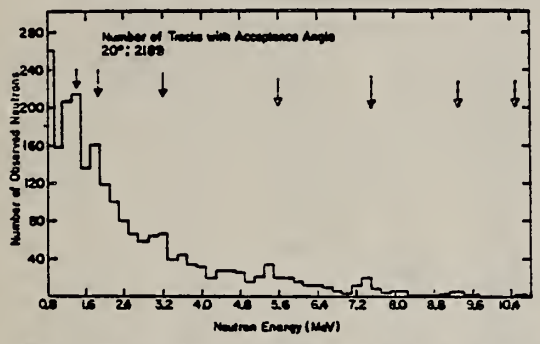

FIG. 1. Number of neutrons deduced from proton recoils plotted as a function of neutron energy in MeV. Solid arrows indicate neutron group while dashed arrows indicate further possible structure.

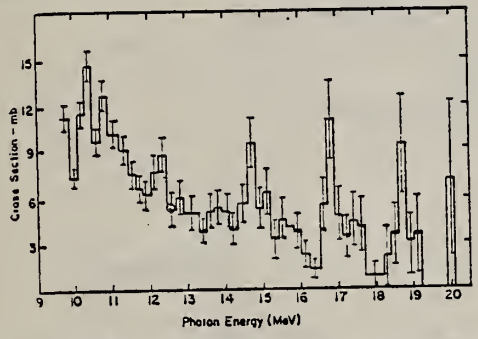

FIG. 2. Cross section versus photon energy for the photoneutrons from oxygen-18 calculated from Fig. 1 using the neutron-proton scattering cross section, the Schiff bremsstrahlung spectrum, experimental details and the assumption of transitions to the first excited state of oxygen-17. The vertical bars show statistical errors only.

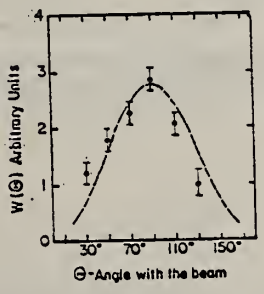

FIG. 3. Angular distribution of the neutron group at 1.3-MeV neutron energy.

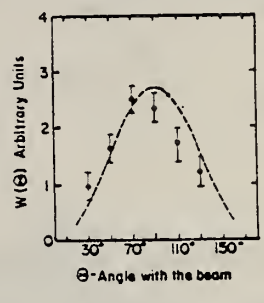

FIG. 4. Angular distribution of the neutron group at 3.1 MeV.

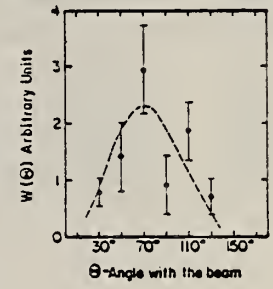

FIG. 5. Angular distribution of the 7.4-MeV neutron group.

TABLE II. Summary of results.

Neutron energy	O^{18} Excitation energy	Spin and parity	Excited-state configuration	Integrated cross section
1.3	10.3 MeV	1^-	$2S_{1/2}$, $2P_{3/2}$	7±2 MeV-mb
3.1	12.2 MeV	1^-	$2S_{1/2}$, $2P_{1/2}$	4.6±2 MeV-mb

REF.

G. J. Vanpraet
Phys. Letters 17, 120 (1965)

CLASS		
0	.18	8

METHOD	REF. NO.	
Mark II, Linac	65 Va 2	EGF

REACTION	RESULT	EXCITATION ENERGY	SOURCE		DETECTOR		ANGLE
			TYPE	RANGE	TYPE	RANGE	
E,E/	ABX	2-27	D	69	MAG	35-70	180

Enriched target (97.55%) 0.160 g/cm^2

Absolute σ based on E,P elastic scattering

Finds $\int_{19.5}^{27} \sigma dE$ for $^{18}O/16_0 = 0.80 \pm 0.08$

Table 1
Levels observed in ^{18}O by inelastic scattering at 180° of 69 MeV incident electrons.

Levels (MeV) (± 0.2 MeV)	Cross section $\times 10^{32}$ (cm^2/sr)	Levels (MeV)	Cross section $\times 10^{32}$ (cm^2/sr)
2.0	0.13 ± 0.03	16.6	1.50 ± 0.17
4.45	0.20 ± 0.03	18.4	1.86 ± 0.20
5.6	0.14 ± 0.02	20.2	1.85 ± 0.20
10.9	0.34 ± 0.05	21.9	1.75 ± 0.20
12.6	0.54 ± 0.05	23.7	1.38 ± 0.20
14.0	0.32 ± 0.07	25.2	1.40 ± 0.21
15.1	0.45 ± 0.17	26.9	0.92 ± 0.13

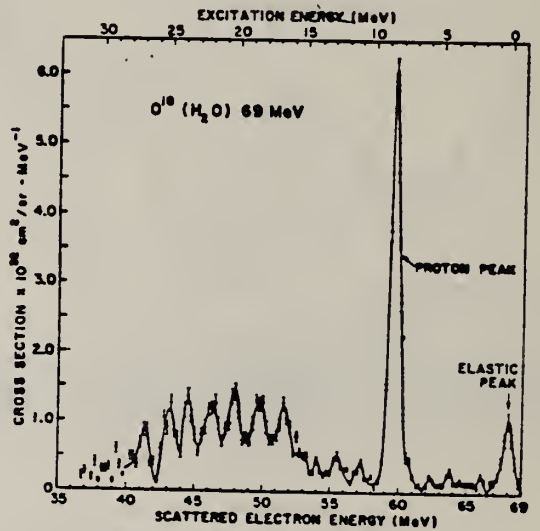

Fig. 1. Energy spectrum of 69 MeV electrons scattered at 180° from an $^{18}O(H_2O)$ target. Top scale gives the excitation energy (MeV).

W. Hofmann, R. Kosiek, G. Kraft and R. Mundhenke
Z. Physik 225, 303 (1969)

0	18	8

METHOD

REF. NO. 69 Ho 1 | egf

REACTION	RESULT	EXCITATION ENERGY	SOURCE TYPE	SOURCE RANGE	DETECTOR TYPE	DETECTOR RANGE	ANGLE
G,XP	ABY	THR- 33	C	24-33	SCI-D	3-14	90

Tabelle 1. *Daten zu den einzelnen Reaktionen. Die Werte für den integrierten Wirkungsquerschnitt wurden unter der Annahme ausschließlicher Grundzustandsübergänge berechnet. Für ^{23}Na und ^{39}K als Ausnahme s. Text*

Target	Anreicherungsgrad %	(γ,p)-Schwelle MeV	Druck oder Dicke	Endenergie MeV	Zahl gemess. Protonen	Ausbeute µb/MeV sr	$\int_{32,5}^{\sigma(E)dE}$ MeVmb	Figur
^{18}O	99	16,0	230 Torr	32,5	36074	58 ± 7	38 ± 6	1, 2
^{20}Ne	90,9	12,8	450 Torr	28,0	3175	7,4 ± 1	—	—
			610 Torr	32,5	6293	14,9 ± 2	61 ± 11	5, 6
^{22}Ne	99,9	15,3	240 Torr	24,0	1960	2,3 ± 0,4	—	4, 5
				28,0	4790	3,6 ± 0,6	—	4, 5
				32,5	5210	6,7 ± 0,9	45 ± 8	4, 5
^{23}Na	100	8,8	65µ	24,0	14182	6,3 ± 1,0	—	7
			60µ	32,5	11152	12,8 ± 2,0	117 ± 30	7
^{36}Ar	99	8,5	250 Torr	32,5	45173	57 ± 6	270 ± 40	8, 10
^{40}Ar	99,6	12,5	230 Torr	32,5	29559	14,2 ± 15	104 ± 15	9, 11
^{39}K	93,1	6,4	80µ	24,0	24230	17,4 ± 2,8	—	12
			90µ	32,5	24941	41,9 ± 6,7	405 ± 100	12
^{84}Kr	99	10,7	170 Torr	32,5	35515	12,7 ± 2,0	80 ± 20	14
Kr	natürl.	10	170 Torr	32,5	13570	12,5 ± 2,0	75 ± 20	13
Xe	natürl.	9	150 Torr	32,5	7553	7,6 ± 0,9	40 ± 7	15

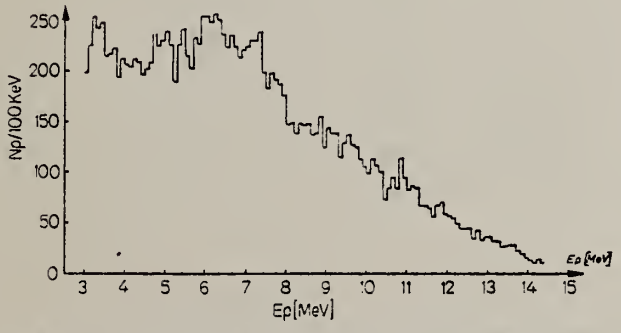

Fig. 1. Energieverteilung der Photoprotonen aus ^{18}O. $E_0 = 32,5$ MeV

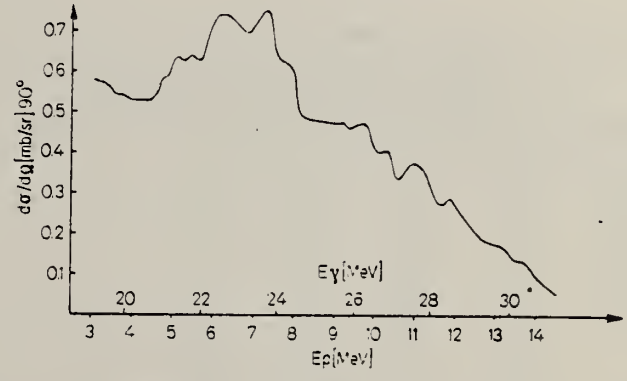

Fig. 2. Der (γ, p)-Wirkungsquerschnitt für ^{18}O

REF.

J. L. Groh, R. P. Singhal, H. S. Caplan, B. S. Dolbilkin
Can. J. Phys. 49, 2743 (1971)

ELEM. SYM.	A	Z
0	18	8

METHOD

REF. NO.: 71 Gr 1 hmg

REACTION	RESULT	EXCITATION ENERGY	SOURCE TYPE	SOURCE RANGE	DETECTOR TYPE	DETECTOR RANGE	ANGLE
E,E/	FMF	2-6	D	92,106	MAG-D		DST

7 LEVELS, B(EL)

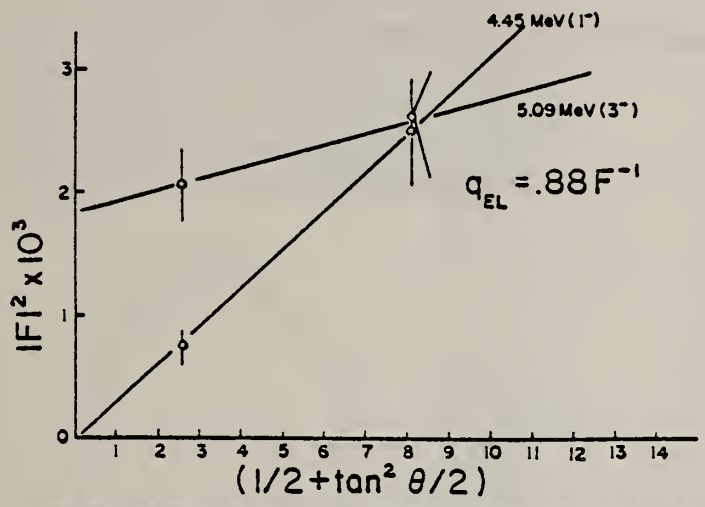

FIG. 4. Angular separation of the longitudinal and transverse form factors for the negative parity levels in ^{18}O.

TABLE 1. Parameters of experimental runs performed and experimental results

E_0 (MeV)	q elastic (fm^{-1})	θ (deg)	Square of experimental form factor × 10^4 for each excitation $\lvert F(q,\theta)\rvert^2$ (bracketed numbers are percentage error in $\lvert F\rvert^2$) 1.98(2_1^+)	3.63(0_2^+)	3.92(2_2^+)	4.45(1_1^-)	5.09(3_1^-)	5.25(2_3^+)	5.33(0_3^+)
92.5	0.57	75	18.9 (9.5)	3.9 (26.7)	6.25 (10.2)	1.9 (42.7)	2.28 (16.2)	12.6 (18.4)	1.3 (46.0)
92.5	0.66	90	—	3.7 (30.9)	8.92 (10.1)	5.8 (19.7)	7.07 (17.6)	13.9 (19.2)	2.2 (48)
92.5	0.77	110	28.1 (7.1)	5.2 (30.3)	12.6 (10.1)	8.5 (19.7)	19.6 (15.0)	17.6 (18.4)	4.3 (45.6)
92.5	0.88	140	35.2 (7.1)	6.3 (28.9)	18.8 (12.0)	25.2 (17.4)	25.8 (16.3)	15.8 (21.7)	9.4 (44)
105.9	0.88	110	38.0 (7.8)	3.8 (27.6)	8.53 (10.2)	7.6 (15.7)	20.7 (13.5)	16.1 (17.9)	<5
105.9	0.95	125	38.5 (7.2)	3.0 (35.2)	5.82 (15.8)	10.9 (18.7)	28.4 (13.5)	20.4 (18.2)	<5

(over)

TABLE 2. Comparison of experiment with model calculations for ^{18}O. Single particle (Weisskopf) estimates for the transition probabilities are $B(E2\downarrow) = 4.7\ e^2\ fm^4$, $B(E3\downarrow) = 44.2\ e^2\ fm^6$

Level parameters		Helm model parameters (fitted to experiment)		Transition probabilities to the ground state $B(EJ)(e^2\ fm^{2J})$ or $\lvert ME\rvert^2(e^2\ fm^4)$				
Energy (MeV)	J_n^π	β_J	γ_J	Helm model	Liquid drop	Shell model	Deformed state	Other experiments
1.98	2_1^+	0.524	Longitudinal	9.0[a]	9.0[a]	9.0[a]	9.0[a]	9.0 ± 2[a] 8.2 ± 0.8[b]
3.63	0_2^+	0.0578	Longitudinal	6.9	1.4	0	12.4	—
3.92	2_2^+	Model does not give a satisfactory fit to the data		(1.7)	0.12	(4–6) × 10^{-4}	1.16	0.97 ± 0.6[b]
4.45	1_1^-	Transverse	1.51	—	—	—	—	—
5.09	3_1^-	0.739	0.167	160	90	—	—	—
5.25	2_3^+	0.382	Longitudinal	4.8	—	—	3.96	—
5.33	0_3^+	0.0592	Longitudinal	(7.2)	—	—	0.3	—

[a]Model parameters were adjusted to reproduce the experimental value of Litherland *et al.* (1963).
[b]Allen and Lawson (1971).

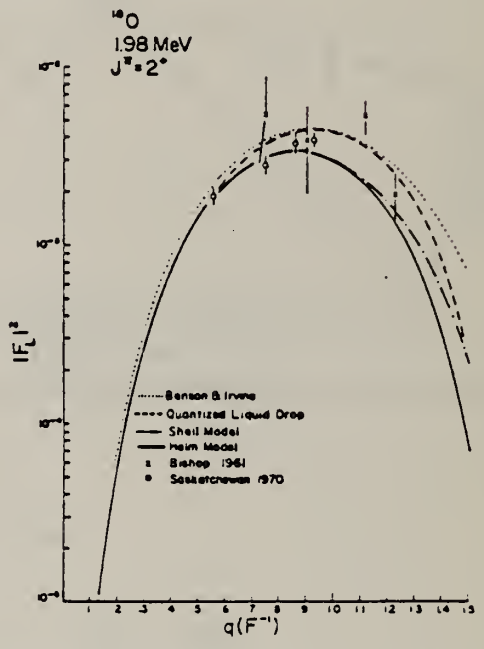

FIG. 5. Longitudinal form factor for the 1.98 MeV, 2^+ level in ^{18}O. The model curves are fitted to reproduce the transition probability to the ground state. An effective charge $e_n = 0.5$ is required for the deformed state model (Benson and Irvine 1966) and $e_n = 0.65$ for the shell model (Kanestroem and Koren 1969). In the notation of Walecka (1962) the liquid drop strength parameter is $(b_2c_2)^{1/2} = 7.33$. Harmonic oscillator wave functions have been assumed with an oscillator parameter $b = 1.869$ fm (Singhal *et al.* 1970) except for Benson and Irvine who use a value $b = 1.77$ fm.

REF.

M.M. Dorosh, N.P. Mazyukevich, V.A. Shkoda-Ul'yanov
Ukr. Fiz. Zh. 17, 847 (1972)

0	18	8

METHOD

REF. NO. 72 Do 13 egf

REACTION	RESULT	EXCITATION ENERGY	SOURCE		DETECTOR		ANGLE
			TYPE	RANGE	TYPE	RANGE	
G,P	ABX	16- 25	C	16- 24	*-I		4PI

21064 CROSS SECTION OF THE (γ,p) REACTION WITH THE ^{18}O NUCLEUS. Dorosh, M. M.; Mazyukevich, N. P.; Shkoda-Ul'yanov, V. A. (Uzhgorod State Univ., USSR). Ukr. Fiz. Zh. (Russ. Ed.); 17: No. 5, 847-9(May 1972). (In Russian).

The cross section of the reaction $^{18}O(\gamma,p)^{17}N$ was investigated as a possible basis for a novel analytical method for geology, metallurgy, and the chemical industry. The delayed neutron yield from O was measured by a betatron using two independent methods (thin and thick targets) within the limits from threshold (16.4 MeV) to 24.5 MeV. Averaged values for the maximum observed cross section (12 mb at 23.0 MeV), which is considerably smaller than the cross section published by other workers, are given. (KSW)

* DELAYED NEUTS

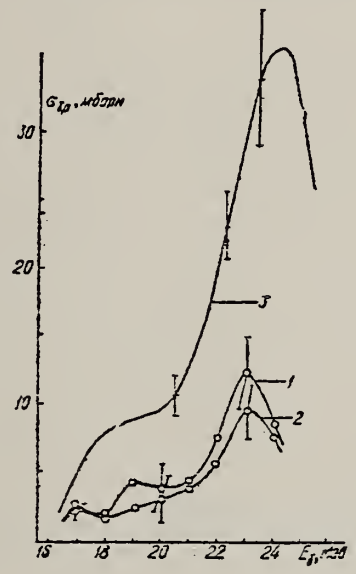

Сечение реакции $O^{18}(\gamma, p)$, рассчитанное по выходу запаздывающих нейтронов: *1* — тонкая мишень расчет по методу Пенфольда—Лейсса; *2* — толста мишень, расчет по методу работы [13]; *3* — сечение полученное в [6], показаны статистические ошибки

M. Hass, Z. Shkedi, D.F.H. Start, Y. Wolfson, and Y.S. Horowitz
Nucl. Phys. A220, 217 (1974)

0	18	8

METHOD

REF. NO. 74 Ha 2 egf

REACTION	RESULT	EXCITATION ENERGY	SOURCE TYPE	SOURCE RANGE	DETECTOR TYPE	DETECTOR RANGE	ANGLE
G,G	LFT	6	D	6	SCD-D		UKN
		(6.20)		(6.20)			

SELF-ABSORPTION

Abstract: The width of the 6.20 MeV, $J^\pi = 1^-$ state of ^{18}O has been measured using a resonance fluorescence self-absorption technique. For a ground state branching ratio, $\Gamma_0/\Gamma = 0.88$, one finds $\Gamma_0 = 180 \pm 30$ meV. The energy of this state was determined to be 6202.7 ± 0.8 keV.

E NUCLEAR REACTIONS $^{18}O(\gamma,\gamma')$, $E = 6.20$ MeV, measured self-absorption ratio, $\sigma(E_\gamma)$. ^{18}O deduced level, Γ. Resonance fluorescence.

REF. J.D. Allan, J.W. Jury, R.G. Johnson, K.G. McNeill, J.G. Woodworth, and Y.S. Horowitz
Can. J. Phys. 53, 786 (1975)

ELEM. SYM.	A	Z
O	18	8

METHOD

REF. NO. 75 Al 4 hmg

REACTION	RESULT	EXCITATION ENERGY	SOURCE TYPE	SOURCE RANGE	DETECTOR TYPE	DETECTOR RANGE	ANGLE
G,N	ABX	10- 18	C	11- 18	TOF-D		98

GROUND-STATE SIGMA

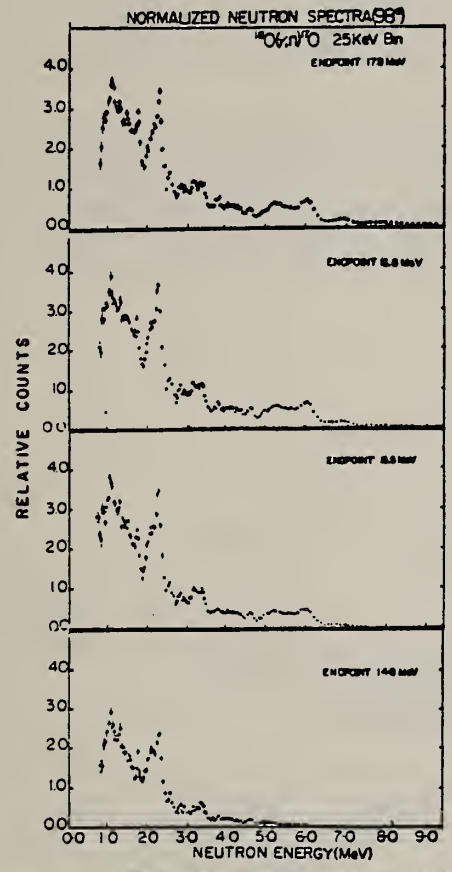

FIG. 5. Normalized neutron spectra between 17.8 and 14.8 MeV for $^{18}O(\gamma, n)^{17}O$.

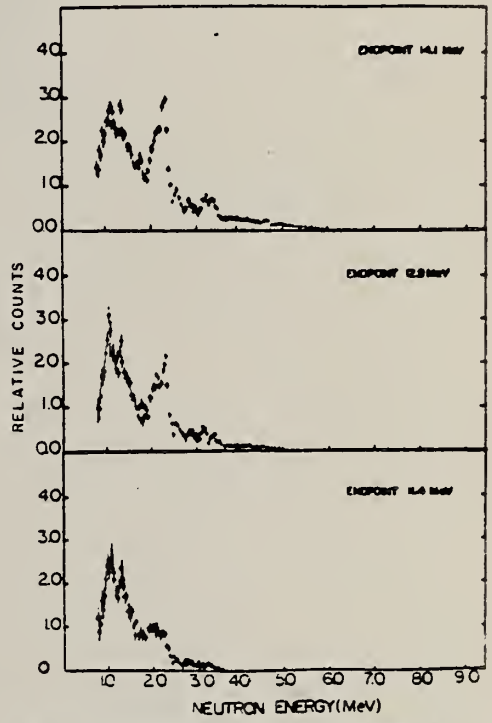

FIG. 6. Normalized neutron spectra between 14.1 and 11.4 MeV for $^{18}O(\gamma, n)^{17}O$.

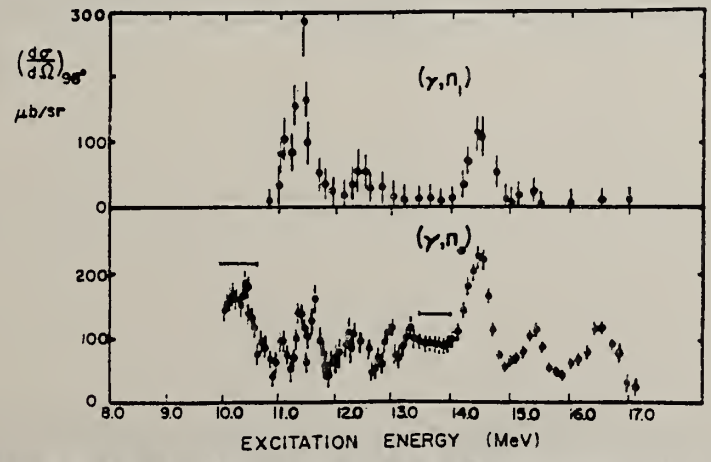

FIG. 7. Differential ground state and first excited state cross sections for $^{18}O(\gamma, n)^{17}O$ at 98°. The horizontal bars indicate regions of uncertainty due to significant transitions to the first excited state. The error bars are statistical only.

excited state ($J^\pi = 1/2^+$). It can be seen that there is a significant ground state contribution to the cross section in contrast to the small contribution previously reported (Mughabghab and Stephens 1964).

REF. K. Bangert, U.E.P. Berg, K. Wienhard and H. Wolf
Z. Physik A278, 295 (1976)

ELEM. SYM.	A	Z
O	18	8

METHOD

REF. NO. 76 Ba 10 .egf

REACTION	RESULT	EXCITATION ENERGY	SOURCE		DETECTOR		ANGLE
			TYPE	RANGE	TYPE	RANGE	
G,NG	ABY	9-28	C	23,28	SCD-D		125
G,2NG	ABY	18-28		23,28			
G,PG	ABY	17-28		23,28			
G,AG	ABY	12-28		23,28			

The decay of the ^{18}O GDR to excited residual nuclear states has been examined by measuring spectra of prompt deexcitation γ-rays. The target was irradiated by bremsstrahlung with endpoint energies of 23.5 and 28 MeV. "Bremsstrahlung-weighted" integrated cross sections are given for the population of the residual nuclear states in ^{17}O, ^{17}N, ^{16}O and ^{14}C. Proton decay to excited states in ^{17}N is remarkably weak. It seems that $1p_{3/2}$ excitations play only a minor role in the ^{18}O GDR.

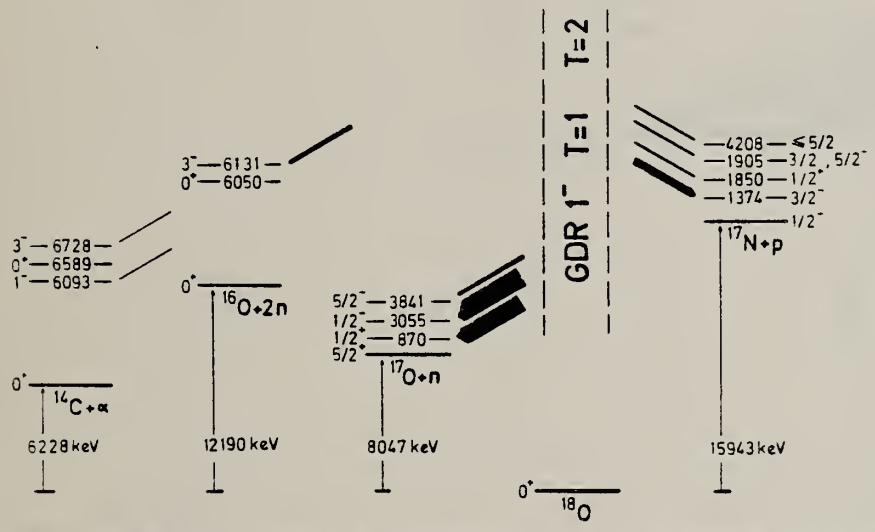

Fig. 1. Population of excited residual nuclear states measured with 28 MeV bremsstrahlung endpoint energy. The thickness of the arrows pointing to the states is proportional to the population strength. (Note that only the ground and first excited state of each nucleus are drawn in correct scale)

(over)

Table 1. Results of the $^{18}O(\gamma, x\gamma)$ experiment, giving "bremsstrahlung-weighted" integrated cross sections in MeV · mb for the population of excited residual nuclear states. The bremsstrahlung spectra have been normalized at 10.7 MeV

	Bremsstrahlung endpoint energy (MeV)	
	23.5	28
^{17}N states[a]		
g.s. $1/2^-$	9.34[b]	17.37[b]
1,374 keV $3/2^-$	0.31	2.01
1,846 keV $1/2^+$	0.28	0.88
1,905 keV $(3/2, 5/2)^-$	0.16	0.86
4,208 keV $\leqq 5/2$	0.31	0.88
Sum of observed (γ, p) excited state cross sections	1.06	4.63
^{17}O states		
870 keV $1/2^+$	6.01	6.71
3,055 keV $1/2^-$	5.18	8.69
3,841 keV $5/2^-$	0.77[c]	1.17[c]
Sum of observed (γ, n) excited state cross sections	11.96	16.57
^{16}O states		
6,131 keV 3^-	0.18	1.07
^{14}C states		
6,093 keV 3^-	0.35	0.48
6,728 keV 1^-	0.31	0.38
Sum of observed (γ, α) excited state cross sections	0.66	0.86

[a] Spin assignments from Reference 4
[b] Calculated from the data of Reference 7
[c] This value contains admixtures from the decay of the ^{13}C 3,854 keV state

REF. B.L. Berman, D.D. Faul, R.A. Alvarez, P. Meyer
Phys. Rev. Lett. 36, 1441 (1976)

ELEM. SYM.	A	Z
O	18	8

METHOD

REF. NO. 76 Be 4 hmg

REACTION	RESULT	EXCITATION ENERGY	SOURCE		DETECTOR		ANGLE
			TYPE	RANGE	TYPE	RANGE	
G,P	ABX	16- 31	D	16- 31	ACT-I		4PI

DELAYED N FROM N17

The $^{18}O(\gamma,p)^{17}N$ cross section has been measured with monoenergetic photons from threshold to 30 MeV. The results show striking similarities and differences with the $^{16}O(\gamma,p)^{15}N$ cross section.

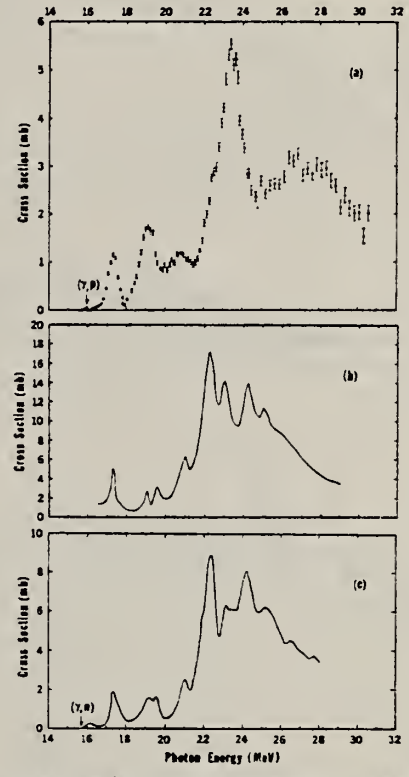

FIG. 1. (a) The $^{18}O(\gamma,p)^{17}N$ cross section measured in the present experiment compared with (b) the $^{16}O(\gamma,p)^{15}N$ and (c) the $^{16}O(\gamma,n)^{15}O$ cross sections taken from the literature (see text). Threshold energies (from Ref. 2) are indicated by the arrows. Solid lines are used to represent the ^{16}O cross sections because they have been synthesized from several experimental results; in any case, the relative precision of these results is good enough so that no important structure has been created or obscured by this procedure.

[2] A.H. Wapstra and N.B. Gove, Nucl. Data Tables 9, 303 (1971).

REF. U. Kneissl, K. H. Leister, H. O. Neidel, A. Weller
Nucl. Phys. A272, 125 (1976)

ELEM. SYM.	A	Z
O	18	8

METHOD

REF. NO. 76 Kn 4 egf

REACTION	RESULT	EXCITATION ENERGY	SOURCE TYPE	SOURCE RANGE	DETECTOR TYPE	DETECTOR RANGE	ANGLE
G,1N	ABX	8- 33	D	8- 33	MOD-I		4PI
G,2N	ABX	11- 33	D	11- 33	MOD-I		4PI

1054+

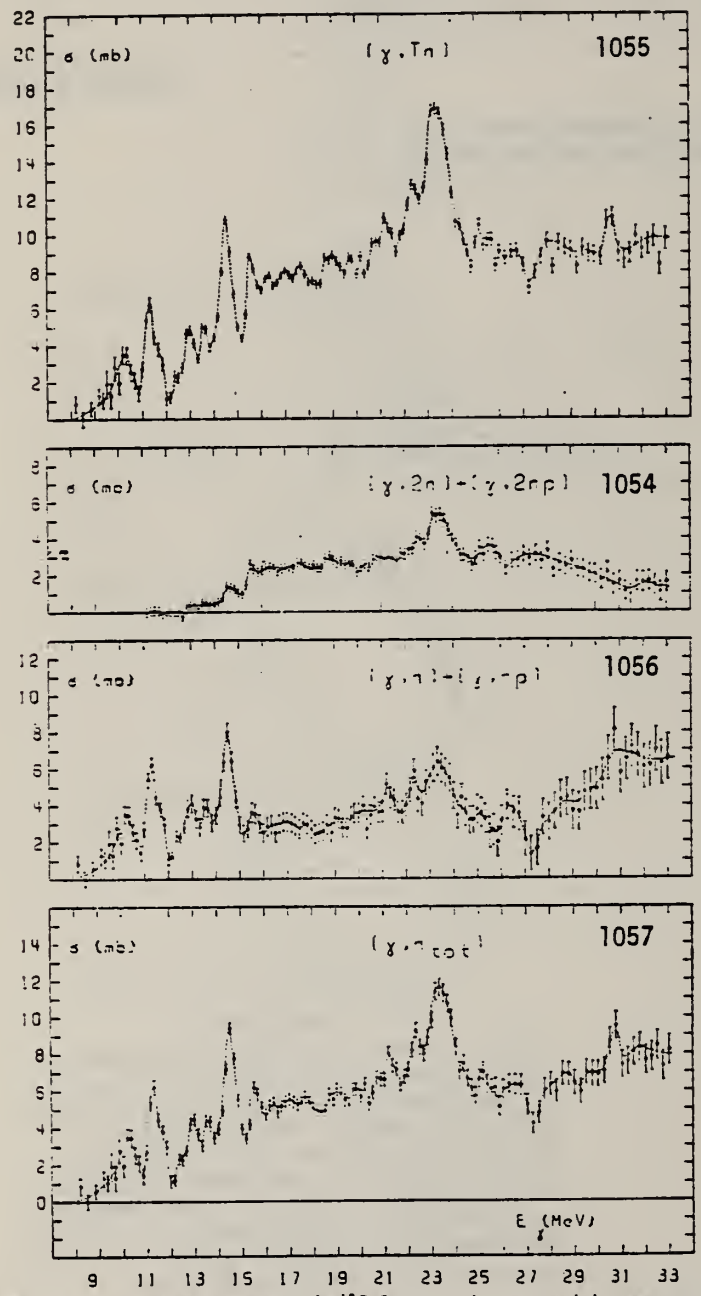

Fig. 1. Measured photoneutron cross sections for ^{18}O, from top to bottom: total photoneutron production cross section $\sigma(\gamma, Tn) = \sigma(\gamma, n)+\sigma(\gamma, pn)+2\sigma(\gamma, 2n)+2\sigma(\gamma, 2np)$; double neutron cross section $\sigma(\gamma, 2n)+\sigma(\gamma, 2np)$; single neutron cross section $\sigma(\gamma, n)+\sigma(\gamma, pn)$; total photoneutron cross section $\sigma(\gamma, n_{tot}) = \sigma(\gamma, n)+\sigma(\gamma, pn)+\sigma(\gamma, 2n)+\sigma(\gamma, 2np)$. The lines are drawn merely to guide the eye.

Abstract: Absolute (γ, xn) cross sections for ^{18}O were measured up to 33 MeV, using a quasimonoenergetic photon beam from positron annihilation in flight. The cross sections show pronounced structure in particular at energies below the main giant dipole resonance. The (γ, 2n) cross section is large in the whole energy region. The integrated total photoneutron cross section amounts to 0.53 in units of the classical dipole sum. No pronounced isospin splitting could be observed in the photoneutron decay channel.

U.S. DEPARTMENT OF COMMERCE
NATIONAL BUREAU OF STANDARDS

REF. J.G. Woodworth, K.G. McNeill, J.W. Jury, R.A. Alvarez, B.L. Berman, D.D. Faul, P. Meyer
Phys. Rev. C19, 1667 (1979)

ELEM. SYM.	A	Z
O	18	8

METHOD

REF. NO.	
79 Wo 1	egf

REACTION	RESULT	EXCITATION ENERGY	SOURCE		DETECTOR		ANGLE
			TYPE	RANGE	TYPE	RANGE	
G,P	ABX	16-42	D	8-42	BF3-I		4PI
G,1N	ABX	8-42	D	8-42			
G,2N	ABX	13-42	D	8-42			

All the major photonuclear cross sections for ^{18}O, including $\sigma(\gamma,p)$, $\sigma[(\gamma,n)+(\gamma,np)]$, and $\sigma(\gamma,2n)$, were measured as a function of photon energy from threshold to 42 MeV. The photon energy resolution was between 200 and 300 keV. The source of radiation was the monoenergetic photon beam obtained from the annihilation in flight of fast positrons. The partial photoneutron cross sections were determined by neutron multiplicity counting, and the average neutron energies for both single- and double-photoneutron events were determined simultaneously with the cross-section data by the ring-ratio technique. The photoproton cross section was determined by counting the delayed neutrons from the β-decay of the residual ^{17}N nuclei. Integrated cross sections were extracted from the data and compared with sum-rule predictions. Resonances in the pygmy-resonance region exhibit substantial decay branching to negative-parity states in ^{17}O. Significant differences in the branching of resonances in the giant-resonance region to the various partial cross sections, together with the photoneutron-energy data, allow isospin assignments to be made for all the resonances, with the consequent delineation of the isospin strength distribution for ^{18}O. Evidence was found for two weak but broad resonances above the giant-resonance region. Finally, comparison with the corresponding cross sections for ^{16}O shows considerable differences between the two nuclei.

(G,P) COUNTED DELAYED NEUT

[NUCLEAR REACTIONS $^{18}O(\gamma,n)$, E_γ=8.0–41.8 MeV; measured 4π prompt, delayed neutron yield for monoenergetic photons; $\sigma(E_\gamma,1n)$, $\sigma(E_\gamma,2n)$, $\sigma(E_\gamma,p)$, integrated cross sections; detailed distribution of isospin strength; comparison with ^{16}O.]

TABLE III. Energies (in MeV) of resonances observed in ^{18}O.

Present work			Ref. 13			Ref. 14	
(γ,tot)	(γ,n)	$(\gamma,2n)$	(γ,p)	(γ,n_0)	(γ,n_1)	(γ,n)	$(\gamma,2n)$
9.1	9.1			10.2			
10.3	10.3			10.4		10.3	
				11.1			
11.4	11.4			11.4	11.5	11.3	
				11.7			
				12.4	(12.6)		
13.1	13.1	13.2		13.1		13.0	
				(13.4)			
13.8	13.8	13.9				13.6	
14.7	14.7	14.8		14.7	14.6	14.5	14.5
15.8	15.7	15.8		15.6		15.6	15.6
				16.7			
17.3	17.1		17.5			(17.0)	
19.4		(19.1)	19.4			19.0	
						19.7	18.8
21.1		21.1	21.0			21.2	21.2
22.6	(22.6)	22.7	22.7			22.3	22.5
23.7	23.7	23.5	23.7			23.4	23.5
							25.6
27	27		27–28				
30	30						
36							

TABLE IV. Integrated cross sections for ^{18}O (integrated up to 41.8 MeV).

Reaction	σ_{int} (MeV mb)	σ_{int} (sum-rule units)	σ_{-1} (mb)	σ_{-2} (mb MeV^{-1})
$^{18}O(\gamma,p)$	44.4	0.17	1.66	0.064
$^{18}O(\gamma,n)$	121.5	0.46	5.93	0.342
$^{18}O(\gamma,2n)$	76.7	0.29	3.14	0.141
$^{18}O(\gamma,n_1)$	198.3	0.74	9.08	0.483
$^{18}O(\gamma,tot)$	242.6	0.91	10.73	0.547

TABLE V. Comparison of the integrated cross sections for ^{16}O and ^{18}O (integrated up to 29.0 MeV). The lower limit of integration for the photoneutron cross sections for ^{16}O is 16.5 MeV.)

	(γ,p)	(γ,n)	$(\gamma,2n)$	(γ,n_1)	(γ,tot)
^{16}O:					
σ_{int} (MeV mb)	83.6	41.8	0	41.8	125.5
σ_{-1} (mb)	3.61	1.87	0	1.87	5.52
^{18}O:					
σ_{int} (MeV mb)	28.3	55.5	41.1	96.6	124.9
σ_{-1} (mb)	1.18	2.39	1.85	4.21	5.42

(over)

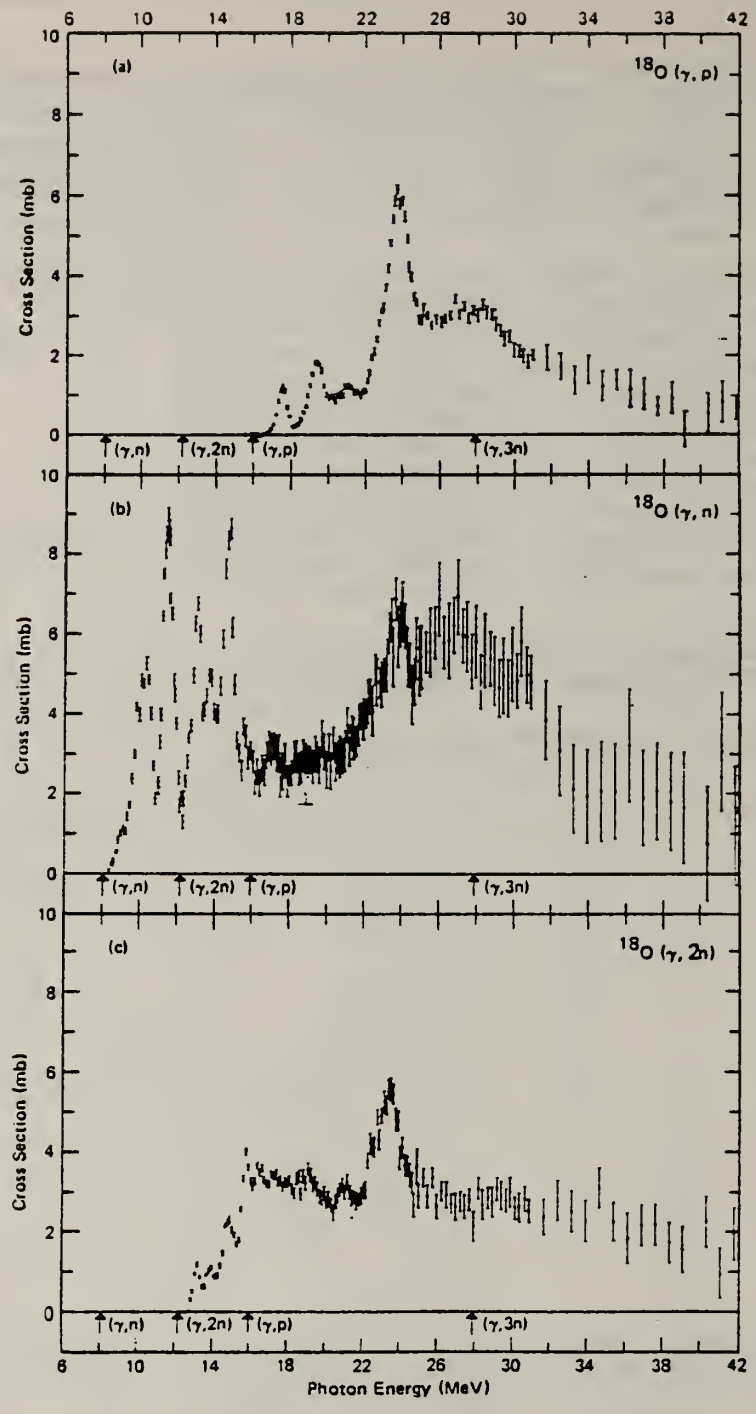

FIG. 3. Photonuclear cross section for ^{18}O: (a) $\sigma(\gamma,p)$; (b) $\sigma(\gamma,1n)=\sigma((\gamma,n)+(\gamma,np))$; (c) $\partial(\gamma,2n)$; (d) $\sigma(\gamma,n_s)$ $=\sigma((\gamma,1n+(\gamma,2n))$; and (e) $\sigma(\gamma,\text{tot})=\sigma((\gamma,p)+(\gamma,n_s))$.

ELEM. SYM.	A	Z
O	18	8

METHOD

REF. NO.	
79 Wo 1	egf

REACTION	RESULT	EXCITATION ENERGY	SOURCE		DETECTOR		ANGLE
			TYPE	RANGE	TYPE	RANGE	

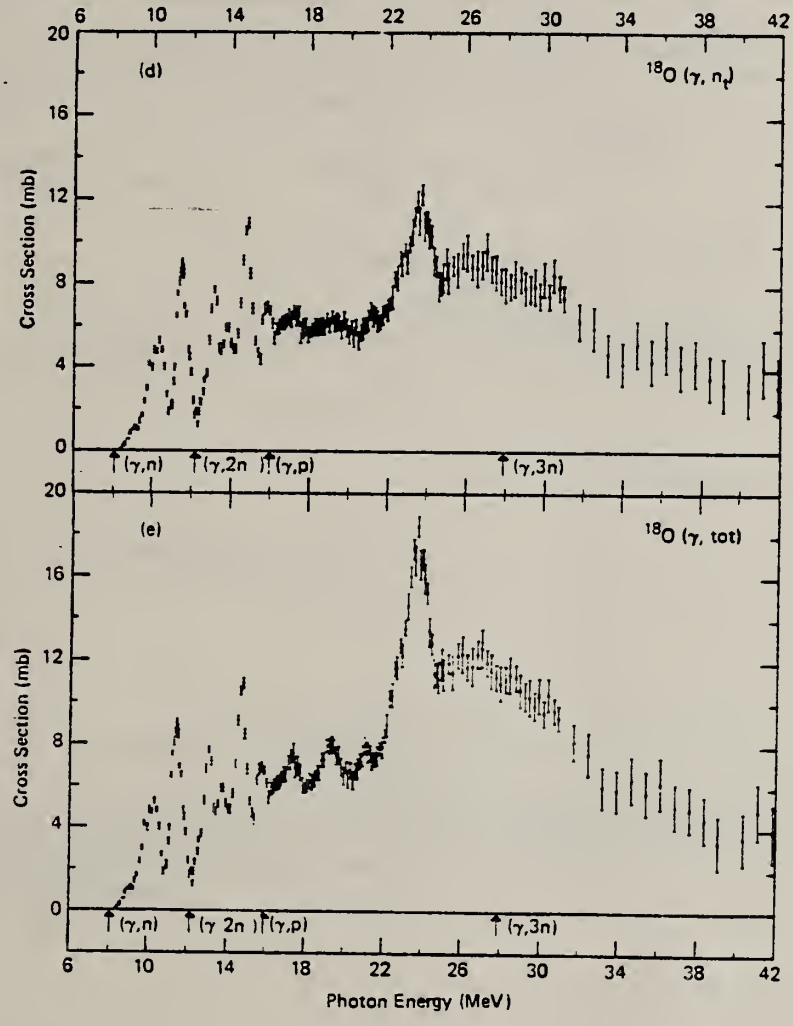

FIG. 3. (*Continued*)

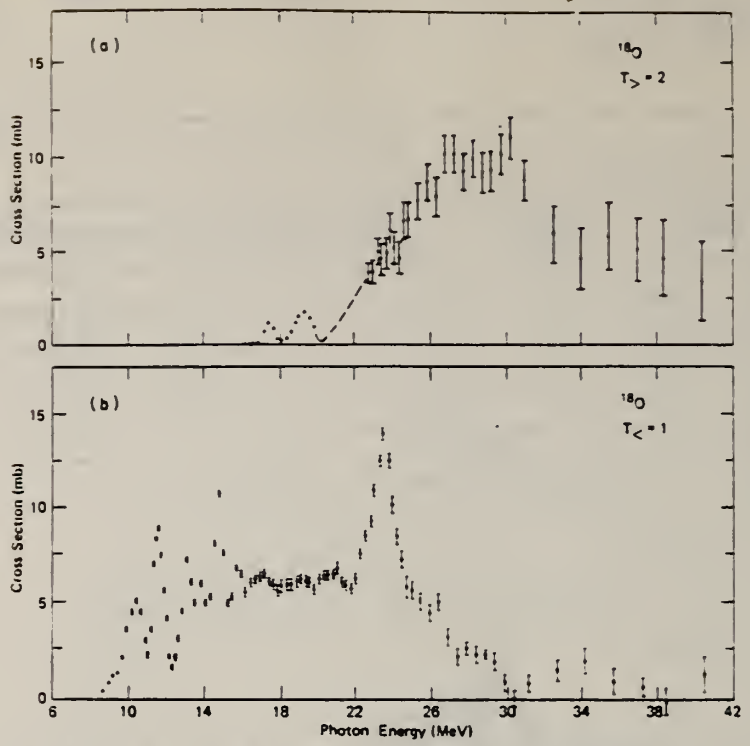

FIG. 9. Isospin components of the ^{18}O photoabsorption cross section, derived as described in the text: (a) $\sigma_>$, the $T_> = 2$ cross section; and (b) $\sigma_<$, the $T_< = 1$ cross section. The data points have been average in pairs for purposes of this of this analysis. The dashed line represents estimated values.

REF. E.J. Ansaldo
Phys. Rev. C22, 915 (1980)

ELEM. SYM.	A	Z
O	18	8

METHOD

REF. NO. 80 An 5 hg

REACTION	RESULT	EXCITATION ENERGY	SOURCE		DETECTOR		ANGLE
			TYPE	RANGE	TYPE	RANGE	
E,E/	FMF	10-47	D	80-166	MAG-D		DST

The giant resonance region of ^{18}O has been investigated by means of inelastic electron scattering at three values of the momentum transfer. The main features of the giant dipole resonance correlate well with photonuclear reaction data. In addition, considerable contribution from quadrupole excitations is apparent in the excitation energy range from 10 to 23 MeV, with some additional strength from 30 to 45 MeV.

[NUCLEAR REACTIONS $^{18}O(e,e')$, $E=80.0-165.7$ MeV, $\theta=67.0-132.0°$—enriched gas target. Measured $\sigma(E',\theta)$. Deduced differential form factors.]

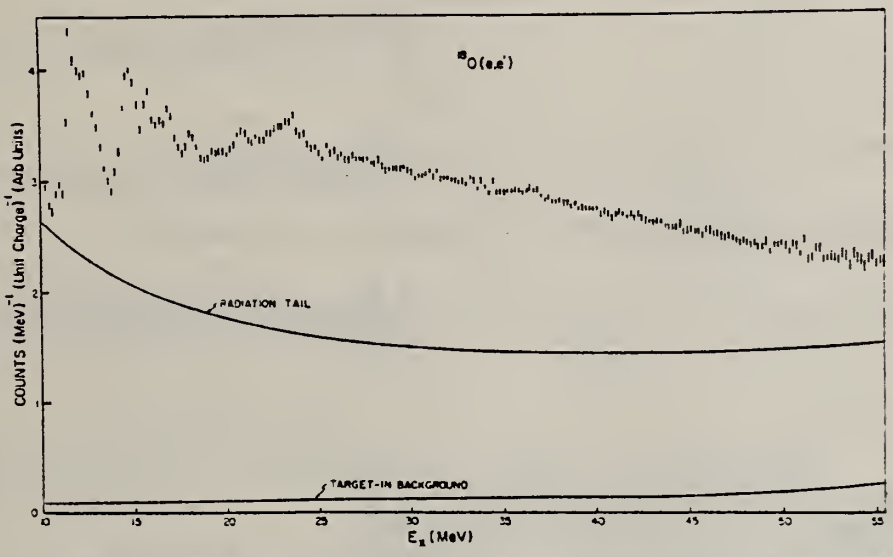

FIG. 1. Inelastic electron scattering spectrum at 165.7 MeV, 67°, showing the contributions due to the elastic peak radiation tail and background due to the target. The target-in background shown was obtained by fitting a smooth curve through the data obtained with an empty target and scaling that curve by a factor 1.12 that takes into account multiple scattering events in the target gas.

(OVER)

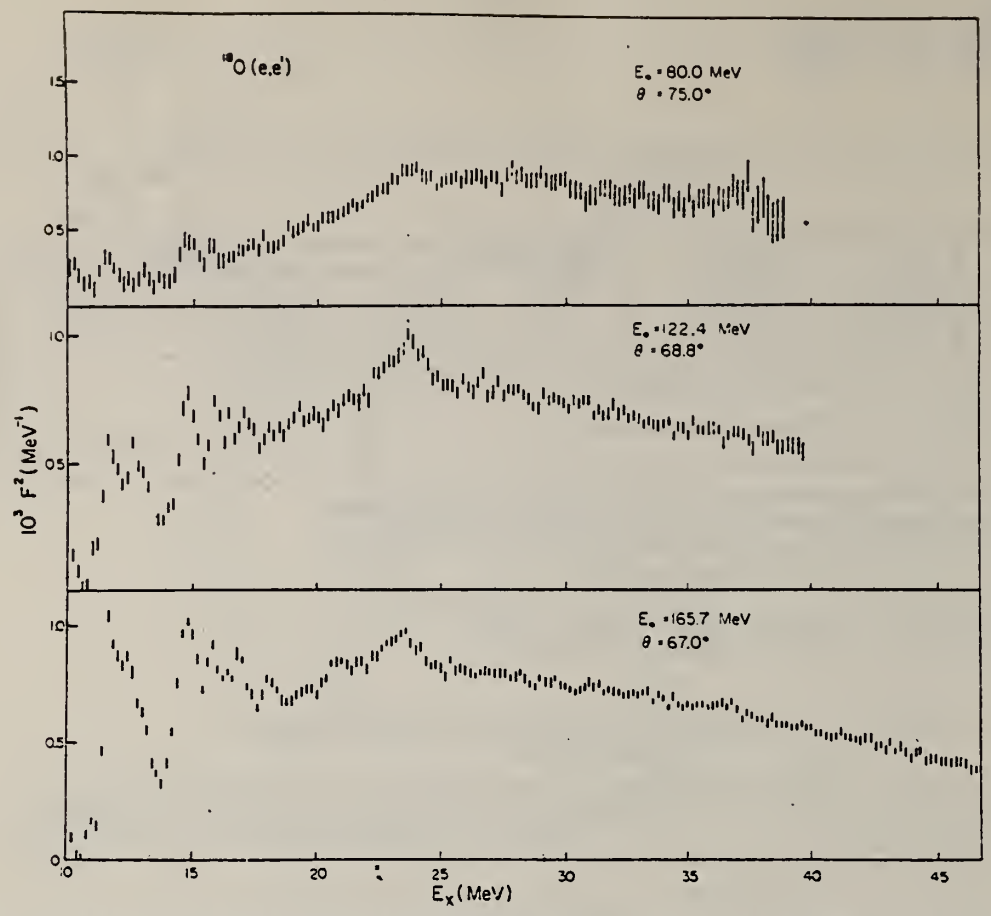

FIG. 2. Differential form factors at forward angles (energy bin width = 200 keV). The three spectra correspond to q(23 MeV) = 0.43, 0.63, and 0.86 fm^{-1}, top to bottom, respectively.

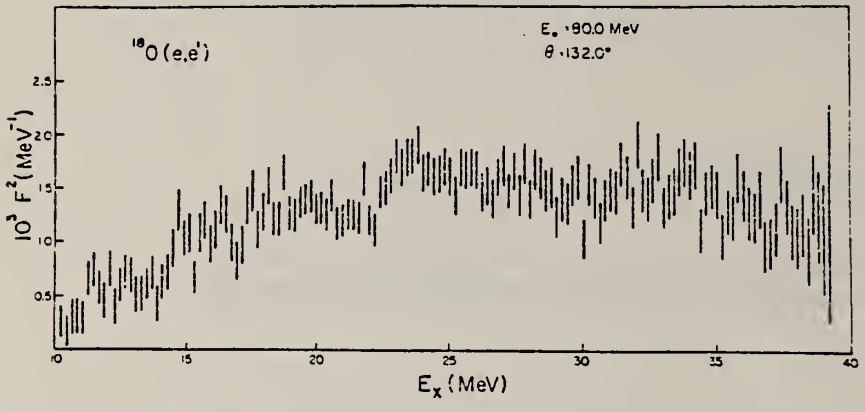

FIG. 3. Differential form factor at 132° corresponding to a momentum transfer q (23 MeV) = 0.64 fm^{-1}.

REF. E.J. Ansaldo, C. Rangacharyulu, D. Bender, U. Krämer, A. Richter, E. Spamer, W. Knüpfer

Phys. Lett. 95B, 31 (1980)

EL.EM. SYM.	A	Z
O	18	8

METHOD

REF. NO. 80 An 6 hg

REACTION	RESULT	EXCITATION ENERGY	SOURCE TYPE	SOURCE RANGE	DETECTOR TYPE	DETECTOR RANGE	ANGLE
E,E/	SPG	13-27	D	25-59	MAG-D		DST

In a high-resolution $^{18}O(e, e')$ experiment sharp states at $E_X = 16.38 \pm 0.01$ MeV ($J^\pi = 2^-$, ground state analogue of ^{18}N) and at $E_X = 18.86 \pm 0.01$ MeV ($J^\pi = 1^+$) and clustering of strength (possibly with $J^\pi = 1^-, 2^-$) at $E_X \approx 23.7$ MeV have been observed and compared to theoretical predictions. The transition strengths for the narrow states are $B(M2) \uparrow = 58 \pm 8\ \mu_K^2$ fm^2 and $B(M1) \uparrow = 0.28 \pm 0.04\ \mu_K^2$, respectively. These results agree qualitatively with the results from the analogous $^{18}O(\pi^-, \gamma)\,^{18}N$ reaction.

J-PI, BEL, 16.4, 18.9

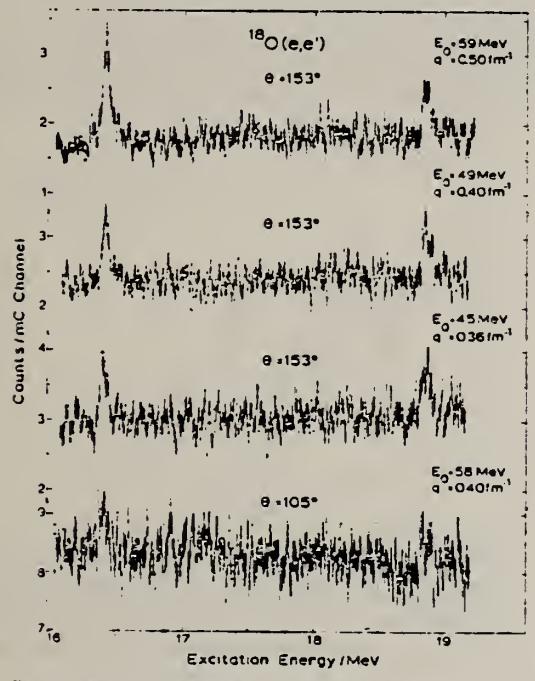

Fig. 1. Spectra of inelastically scattered electrons at three different momentum transfers. Notice the suppressed zero of the scales on both axes.

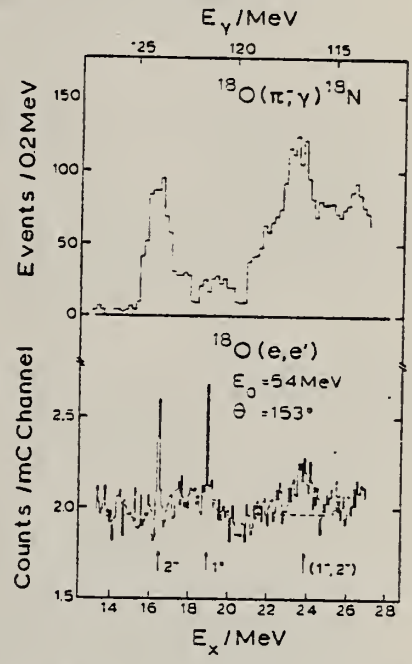

Fig. 2. A comparison of the photon spectrum from the (π^-, γ) experiment (top, adapted from ref. [1]) with the inelastic (e, e') spectrum at 54.3 MeV (153°) (bottom). The area above the dashed line has been used in the cross section estimates discussed in the text.

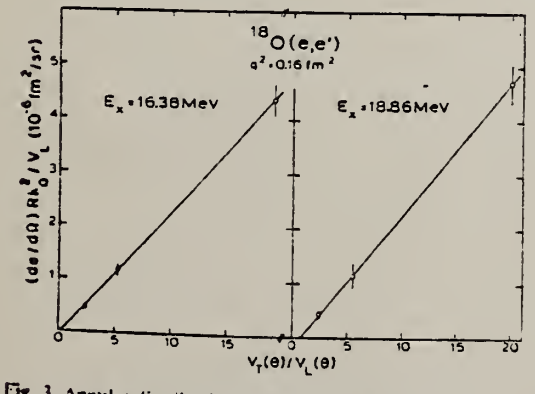

Fig. 3. Angular distributions at constant $q = 0.4$ fm^{-1} showing that both narrow peaks observed in this work are purely transverse. For procedural details and notation see main text and ref. [9].

REF. R.E. Pywell, M.N. Thompson, B.L. Berman
Nucl. Inst. Meth. 178, 149 (1980)

ELEM. SYM.	A	Z
O	18	8

METHOD

REF. NO. 80 Py 4 hg

REACTION	RESULT	EXCITATION ENERGY	SOURCE		DETECTOR		ANGLE
			TYPE	RANGE	TYPE	RANGE	
G,XN	ABX	8-28	C	8-29	BF3-I		4PI
G,P	ABX	16-28	C	8-29	ACT-I		4PI

The $^{18}O[(\gamma, n) + 2(\gamma, 2n)]$ and $^{18}O(\gamma, p)$ cross sections have been measured using the bremsstrahlung yield-curve technique. Unfolding of the yield curves to obtain the cross sections is carried out using the Variable-Bin-Penfold–Leiss technique. The results obtained agree very well with the results obtained using monoenergetic photons. The accuracy of the bremsstrahlung yield-curve technique and the resolution obtainable with this technique are thereby established.

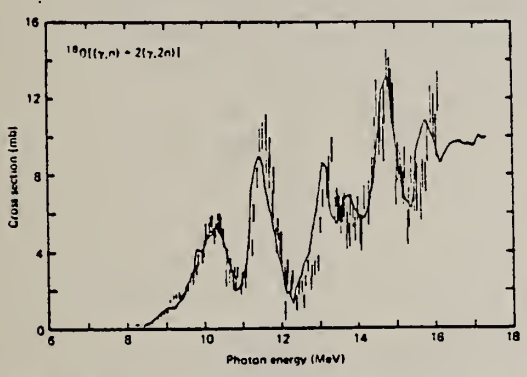

Fig. 3. The $^{18}O[(\gamma, n) + 2(\gamma, 2n)]$ cross section derived from the ^{18}O "fine-resolution" prompt-neutron yield curve, by analysis using the VBPL method using a smoothing factor $f = 1.75$. The solid line is drawn between the data points for the same cross section measured at Livermore.

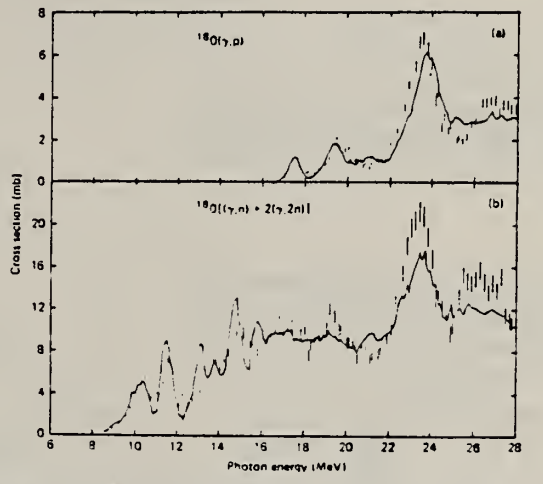

Fig. 4. (a) $^{18}O(\gamma, p)$ and (b) $^{18}O[(\gamma, n) + 2(\gamma, 2n)]$ cross sections derived from the "coarse-resolution" yield curves using the VBPL analysis method with the smoothing factor $f = 1.75$. The solid lines are drawn between the data points for the same cross sections measured at Livermore.

(OVER)

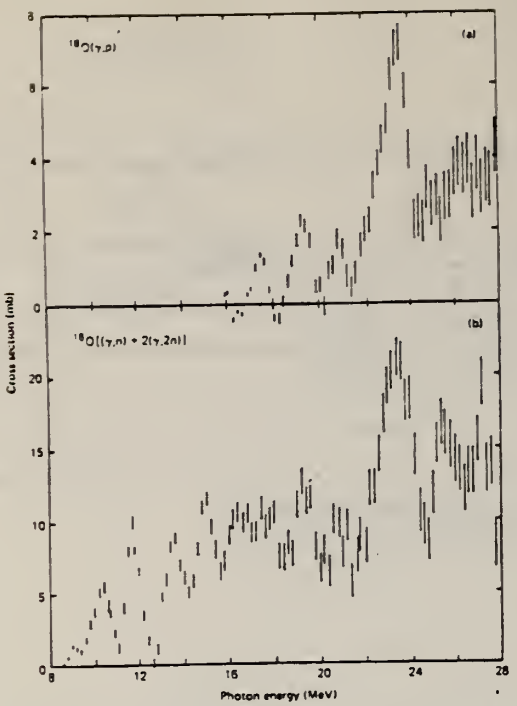

Fig. 5. (a) $^{18}O(\gamma, p)$ and (b) $^{18}O[(\gamma, n) + 2(\gamma, 2n)]$ cross sections derived from the "coarse-resolution" yield curves using analysis bin widths which varied smoothly with energy, and which follow the Thies-criterion optimum bin width as closely as possible.

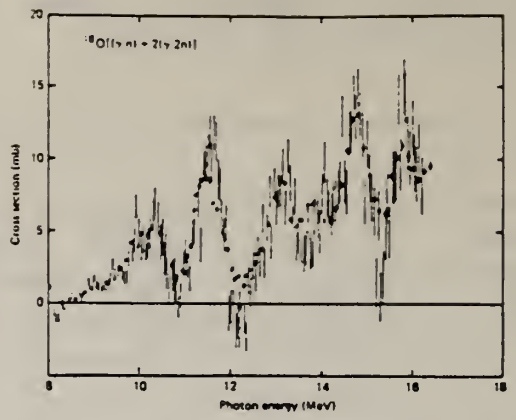

Fig. 6. The error bars show the $^{18}O[(\gamma, n) + 2(\gamma, 2n)]$ cross section obtained by analysis bin widths following the Thies criterion. The solid dots with error bars show the same cross section measured at Livermore.

Table 1
Parameters of resonances observed in the ^{18}O photonuclear cross sections measured at Melbourne and Livermore. Where an unambiguous assignment of cross section or width is not possible the figures have been omitted

Livermore			Melbourne			
Energy (MeV)	Peak cross section (mb)	Width (MeV)	Energy (MeV)	Peak cross section (mb)	Width (MeV)	
$^{18}O[(\gamma, n) + 2\sigma(\gamma, 2n)]$ reaction						
9.1	1.1	0.6	9.1	1.4	0.4	
			9.6	2.4	0.3	
			10.0	5.0	0.3	
10.3	5.3	0.9	10.4	6.5	0.4	
			11.3			
11.5	9.0	0.7	11.6	11.5	0.6	b
13.1	8.6	0.7	13.2	8.5	0.6	
13.8	6.9	0.6	14.0	8.5	0.6	
14.8	13.1	0.8	14.8	14.0	0.6	
15.8	10.9	0.7	15.8	13.0	0.7	
			16.5	10.5	–	
17.2	10.1	–	17.6	10.5	–	
19.1	10.0	–	19.3	12.0	0.6	c
21.1	9.7	–	21.1	–	–	
23.7	17.7	~2.5 [a]	23.6	21.0	1.8	
$^{18}O(\gamma, p)$ reaction						
17.5	1.2	0.6	17.5	1.2	0.7	
19.4	1.8	0.9	19.4	2.2	0.9	d
21.0	1.2	–	21.0	1.6	0.9	
23.7	6.1	1.6	23.7	6.8	1.7	

a) This may include additional structures. b) From fig. 6. c) From fig. 5(b). d) From fig. 5(a).

REF. K. Bangert, U.E.P. Berg, G. Junghans, R. Stock, K. Wienhard
Nucl. Phys. A376, 15 (1982)

ELEM. SYM.	A	Z
O	18	8

METHOD

REF. NO. 82 Ba 7 egf

REACTION	RESULT	EXCITATION ENERGY	SOURCE TYPE	SOURCE RANGE	DETECTOR TYPE	DETECTOR RANGE	ANGLE
G,P	SPC	19-32	C	24,32	TEL-D		DST
G,D	SPC	23-29	C	24,32	TEL-D		DST

Abstract: Emission of charged photoparticles from the ^{18}O giant E1 resonance region was investigated at the University of Giessen electron linac at bremsstrahlung endpoint energies of 24 and 32 MeV. Spectra of protons, deuterons, tritons and α-particles were measured at six angles. Proton decay shows strong transitions to excited states in ^{17}N. Deuterons and tritons have a nearly isotropic angular distribution. The $^{18}O(\gamma, t_0)^{15}N$ and the $^{18}O(\gamma, \alpha_0)^{14}C$ cross sections are determined in the giant E1 resonance region. E1 and E2 $^{18}O(\gamma, \alpha_0)^{14}C$ cross sections are derived from the angular distribution measurement.

E NUCLEAR REACTIONS $^{18}O(\gamma, p)$, (γ, d), (γ, t), (γ, α), $E_x < 32$ MeV, measured particle spectra, deduced $\sigma_{\gamma,t_0}(E_\gamma; \theta)$, $\sigma_{\gamma,\alpha_0}(E_\gamma; \theta)$. Enriched target.

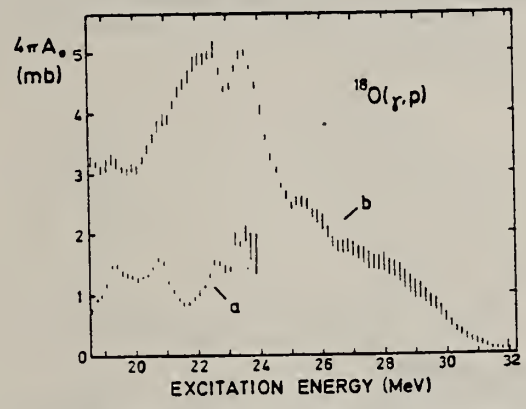

Fig. 1. Total (γ, p) cross section determined under the assumption of transitions to the ground state of ^{17}N (a) for the measurement with 24 MeV endpoint energy and (b) for the measurement with 32 MeV endpoint energy. The energy scale is valid only for transitions to the ground state of ^{17}N.

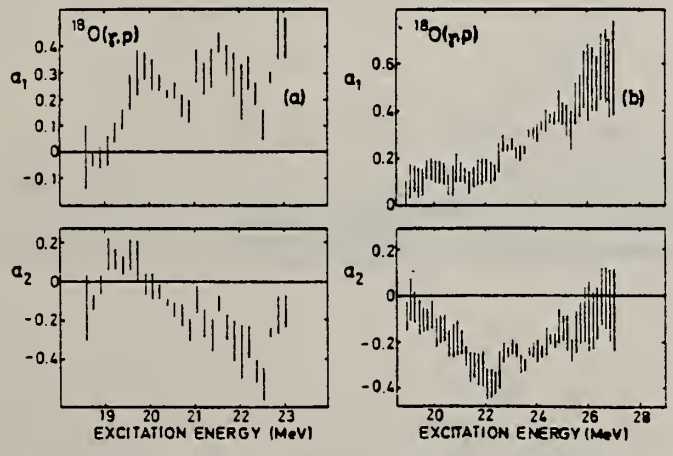

Fig. 2. The $a_1 = A_1/A_0$ and $a_2 = A_2/A_0$ coefficients for the angular distribution of protons derived from the measurement with (a) 24 MeV and (b) 32 MeV bremsstrahlung endpoint energy.

(OVER)

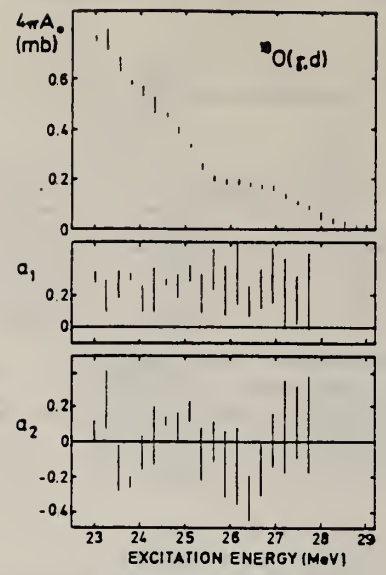

Fig. 3. Total (γ, d) cross section and angular distribution coefficients a_1 and a_2 calculated under the assumption of transitions to the ground state of ^{16}N from the measurement with 32 MeV endpoint energy.

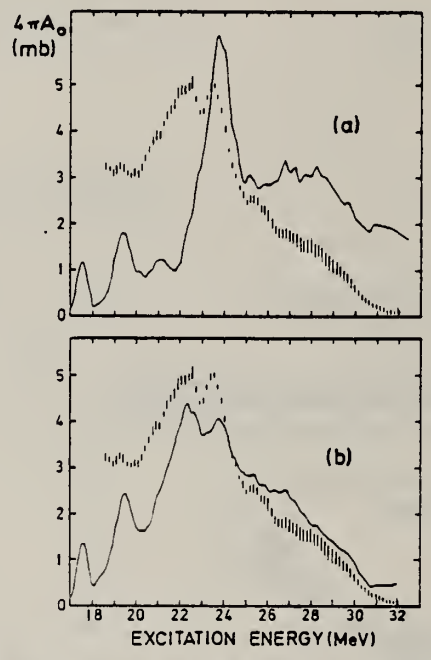

Fig. 7. Total (γ, p) cross section determined under the assumption of ground-state transitions from the 32 MeV measurement (error bars). The solid curve in part (a) shows the total ^{18}O(γ, p) cross section as given in ref. [2]). The solid curve in part (b) was calculated from ref. [2]) as explained in the text.

REF. K. Bangert, U.E.P. Berg, G. Junghans, R. Stock, K. Wienhard
Nucl. Phys. A376, 15 (1982)

ELEM. SYM.	A	Z
0	18	8

METHOD

REF. NO. 82 Ba 7 egf

REACTION	RESULT	EXCITATION ENERGY	SOURCE		DETECTOR		ANGLE
			TYPE	RANGE	TYPE	RANGE	
G,T	SPC	21-26	C	24,32	TEL-D		DST
G,A	SPC	19-27	C	24,32	TEL-D		DST

Abstract: Emission of charged photoparticles from the ^{18}O giant E1 resonance region was investigated at the University of Giessen electron linac at bremsstrahlung endpoint energies of 24 and 32 MeV. Spectra of protons, deuterons, tritons and α-particles were measured at six angles. Proton decay shows strong transitions to excited states in ^{17}N. Deuterons and tritons have a nearly isotropic angular distribution. The $^{18}O(\gamma, t_0)^{15}N$ and the $^{18}O(\gamma, \alpha_0)^{14}C$ cross sections are determined in the giant E1 resonance region. E1 and E2 $^{18}O(\gamma, \alpha_0)^{14}C$ cross sections are derived from the angular distribution measurement.

E NUCLEAR REACTIONS $^{18}O(\gamma, p)$, (γ, d), (γ, t), (γ, α), $E_x < 32$ MeV, measured particle spectra, deduced $\sigma_{\gamma,t_0}(E_\gamma; \theta)$, $\sigma_{\gamma,\alpha_0}(E_\gamma; \theta)$. Enriched target.

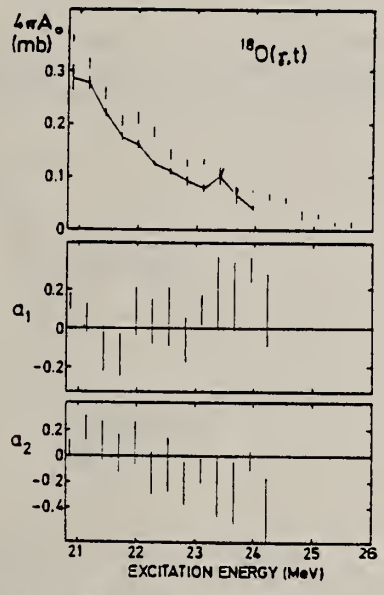

Fig. 4. Total (γ, t) cross section and angular distribution coefficients a_1 and a_2. The solid line connects the $^{18}O(\gamma, t_0)^{15}N$ cross-section data derived from the 24 MeV measurement. The other data points are from the 32 MeV measurement evaluated under the assumption of transitions to the ground state of ^{15}N. The angular distribution coefficients were derived from the 32 MeV measurement.

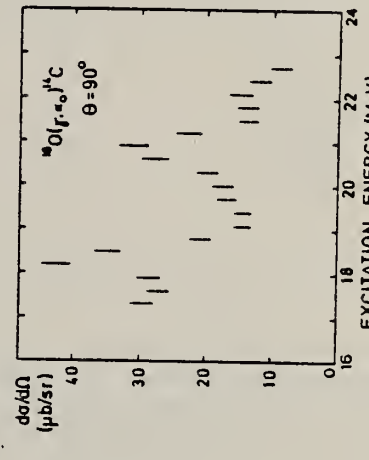

Fig. 5. Differential cross section for the $^{18}O(\gamma, \alpha_0)^{14}C$ reaction at $\theta = 90°$ from the measurement with 24 MeV endpoint energy.

(OVER)

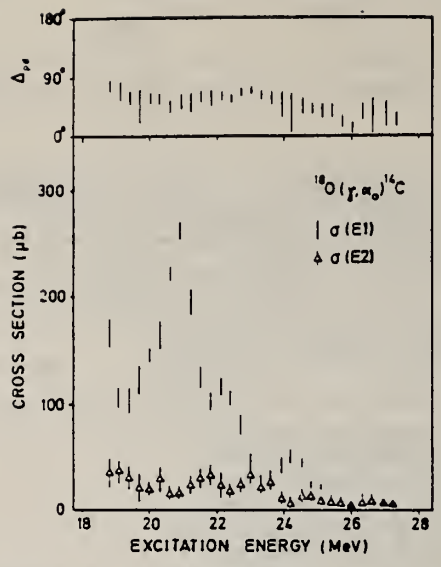

Fig. 6. E1 and E2 cross sections and their phase difference for the $^{18}O(\gamma, \alpha_0)^{14}C$ reaction. The error bars were derived from the statistical uncertainties of the data.

REF. B.E. Norum, M.V. Hynes, H. Miska, W. Bertozzi, J. Kelly, S. Kowalski, F.N. Rad, C.P. Sargent, T. Sasanuma, W. Turchinetz, B.L. Berman
Phys. Rev. C25, 1778 (1982)

ELEM. SYM.	A	Z
O	18	8

METHOD

REF. NO. 82 No 1 egf

REACTION	RESULT	EXCITATION ENERGY	SOURCE TYPE	SOURCE RANGE	DETECTOR TYPE	DETECTOR RANGE	ANGLE
E,E/	FMF	2-8	D	1*3	MAG-D		DST

Inelastic electron scattering from the low-lying even-parity states of ^{18}O has been performed. The measurements span a range in momentum transfer from 0.6 to 2.7 fm^{-1}. Form factors have been determined for the two lowest 0^+ excitations, the three lowest 2^+ excitations, and the three lowest 4^+ excitations. Transition densities for the 2^+ and 4^+ excitations have been obtained from a Fourier-Bessel analysis of these data. Comparisons were made with the predictions of various theoretical calculations and the agreement was found generally to be poor. A coexistence model was used to decompose the measured form factors into their single-particle and collective components, which in turn were compared with their counterparts in ^{16}O and ^{17}O. The results indicate that this model provides a useful framework within which to understand the structure of the oxygen isotopes. Transition densities also were obtained within the context of this model.

[NUCLEAR REACTIONS $^{18}O(e,e')$ low-lying even-parity excited states; measured form factors at 90° and 160°, $0.6 \leq q \leq 2.7$ fm^{-1}; comparison to shell and coexistence models; transition densities extracted.]

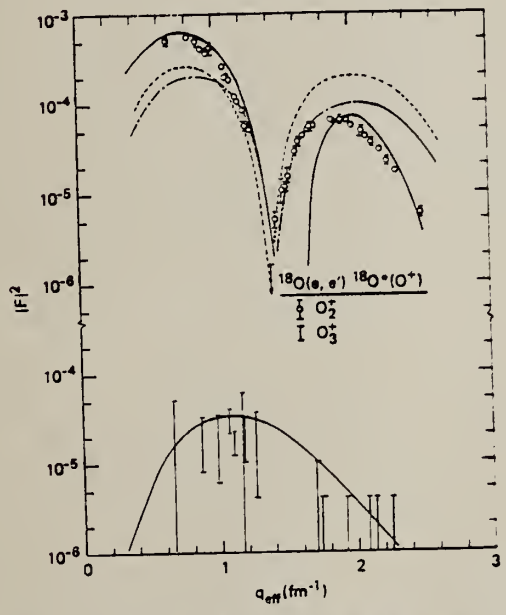

FIG. 4. Form factors for the lowest two 0^+ excitations in ^{18}O, measured at 90° (data points). The solid and dashed curves are from Refs. 33 and 34, respectively. The dotted-dashed curve was computed from wave functions given in Ref. 10.

0.6*2.7 FM-1 8 STATES

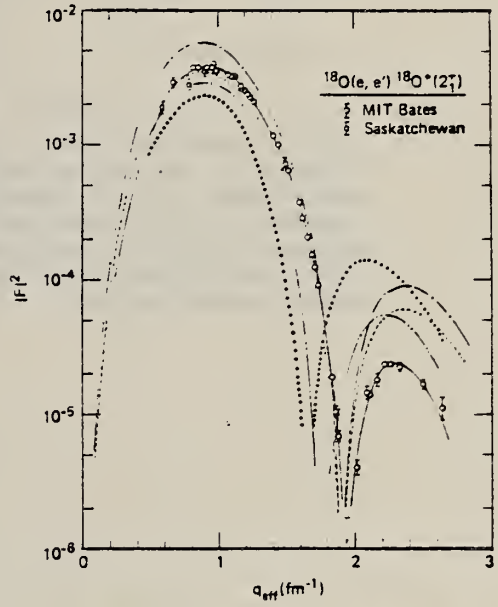

FIG. 5. Measured form factors for the lowest 2^+ excitation in ^{18}O. The circles represent our measurements made at 90°; the squares are taken from Ref. 17. The solid curve shows the result of an FBA fit to the data. The dashed (dashed-dotted) curve was computed using wave functions from Ref. 14 and $e_{pol}=0.33e$ ($e_{pol}=0.50e$). The dashed-dotted-dotted curve is taken from Ref. 34, while the dotted curve was computed using wave functions from Ref. 10.

TABLE II. Reduced transition probabilities.

State	$B(EL;\ 0_1^+ \rightarrow L^+)$ (e^2fm^{2L})
2_1^+ (1.982 MeV)	44.8±1.3
2_2^+ (3.919 MeV)	22.2±1.0
2_3^+ (5.250 MeV)	28.3±1.5
4_1^+ (3.553 MeV)	(9.04±0.90)×10^2
4_2^+ (7.114 MeV)	(1.31±0.06)×10^4

(OVER)

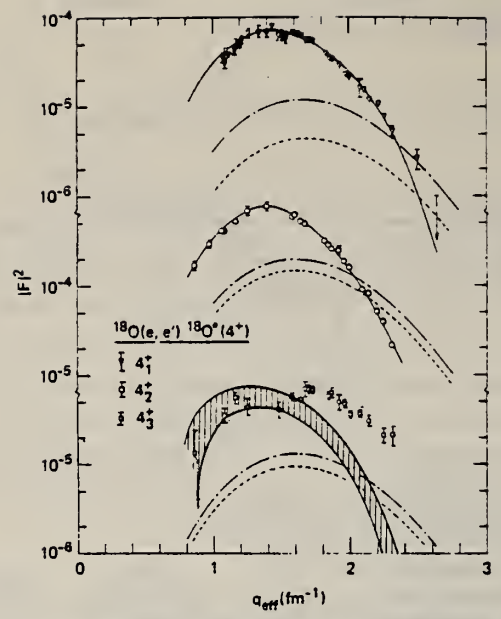

FIG. 8. Measured form factors for the lowest three 4^+ states in ^{18}O. The data points represent our measurements made at 90°. See caption for Fig. 5 for descriptions of curves. The shaded band represents the form factor for the third 4^+ state computed [within the context of the LSF (Ref. 11) model] from those measured for the lowest two 4^+ states.

DEFINITIONS OF ABBREVIATIONS AND SYMBOLS

Note: In this list definitions are given for various photoneutron reactions in which the following symbols are used: N, NL, nN, SN and XN. Corresponding definitions apply for reactions involving other nuclear particles where the symbols N (neutron) is replaced by, e.g. P, D, T, HE, A etc. Where unknown reactions result in the production of a specific radionuclide, the chemical symbol and mass number is listed as the reaction product, e.g. a G,NA22 reaction in ^{59}Co.

A	alpha particle
ANAL	analysis
ABI	absolute integrated cross-section data
ABX	absolute cross-section data
ABY	absolute yield data. Often means cross-section per equivalent quantum is listed.
ACT	measurement of induced radioactivity of the target
ASM	asymmetric, asymmetry
AVG	average
BBL	bubble chamber
BEL B(EL)	reduced electric radiative transition probability
BF3	BF_3 neutron counter with moderator e.g., Halpern detector, long counter
BML	reduced magnetic radiative transition probability, B(ML)
BREAKS	levels located by "breaks" in the yield curve
BRKUP	breakup
BRMS	bremsstrahlung
BTW	between
C	continuous. Used to describe a photon source or a detector response function. Contrast with D = discrete.
CCH	cloud chamber
CF	compared with
CHRGD	charged
CMPT	Compton
COIN COINC	coincidence, coincide
COH	coherent
CK	Cerenkov
D	deuteron or discrete. When discrete, it is used to describe a photon source or a detector response function. Contrast with C = continuous.
DLTE	energy loss
DLTQ	momentum transfer
DST	distribution
DT BAL	detailed balance
E	electron
E/	inelastically scattered electron
E+	positron
EDST	energy distribution or spectrum
E/N	used only to indicate a coincidence experiment as in (E,E/N).

	N stands for any outgoing particle measured in coincidence with an inelastically scattered electron. Distinguish from eg., (E,N) which is used to represent an electron induced reaction when only the outgoing particle N is detected.
EMU	emulsions (photographic plates)
EXCIT	excited
F	fission
FMF	form factor
FM-1	inverse femtometers
FRAG	fragment
G	photon
G/	inelastically scattered photon
G-WIDTH	gamma-ray transition width
HAD	hadrons, hadron production
HE He3	^{3}He particle
INT	interaction, integral, intensity
INC	includes
ION	ionization chamber
ISOB	isobaric
ISM	isomer
J	multiplicity of particle defined by following symbol e.g. (G,PJN) with remark J = 2,3,5,7
JPI J-PI	spin and parity of a nuclear state
K	second multiplicity index, e.g. (G,JPKN) with both J & K positive integers greater than 1
KE	kinetic energy
L	may be an integer or zero that always follows a reaction product symbol. This is used to indicate transitions to specific states in the residual nuclide. When the letter is used as in (G,NL) the cross section given is that for the sum of transitions to two or more specific final states.
LFT	excited state lifetime
LIM	limit
LV,LVS	level, levels
LQD	liquid
MAG	magnetic spectrometer
MEAS	measurement(s)
MGC	magnetic Compton spectrometer
MGP	magnetic pair spectrometer
MOD	moderated neutron detector not employing a BF_3 counter, e.g. rhodium foil, Szilard-Chalmers reaction, ^{3}He, ^{6}Li reactions, GD loaded liquid scintillator, etc.
MSP	mass spectrometer
MULT	multiple, multipole, multiplicity
MU-T	used only in combination with G to indicate a total photon absorption cross section measurement, i.e. (G,MU-T)
N	neutron (see also XN and SN). The notation (G,N) is used to indicate a reaction in which only a single neutron is emitted, i.e. the reaction that can, in many cases, be measured by observing the radioactive decay of the residual nuclide.

nN	where n is any integer. (G,nN) indicates the sum over all reaction cross sections in which n neutrons are emitted.
NAI	NaI(Tl) spectrometer
NEUT	neutron(s)
NOX	no cross-section data
P	proton (see also XP)
PART	particle(s)
PHOT	photon(s)
PI	pion, usually written as PI+, PI-, PIO to indicate charge
POL	polarized or polarization
Q-SQUAR	momentum transfer squared (q^2)
RCL	recoil
REL	relative
RLI	relative integrated cross-section data
RLX	relative cross-section data
RSP	reaction spectrometer
RLY	relative yield data
SCTD	scattered
SCD	semiconductor (solid state) detector
SCI	scintillator detector other than NaI, e.g., CsI, KI, organic (liquid or solid), stilbene, He
SEP	separation
SEP ISOTP	separated isotope used
SIG	SIGMA (cross section)
SN	sum of neutron producing reactions, $\sigma(\gamma,SN)=\sigma(\gamma,N) + \sigma(\gamma,NP) + \sigma(\gamma,2N) + \sigma(\gamma,3N)$ + etc.
SPC	photon or particle energy spectrum
SPK	spark chamber
SPL	spallation
STAT	statistical
SYM	symetric, symmetry
T	triton
TEL	counter telescope
THR	threshold for reaction or threshold detector, e.g., $^{29}Si(n,p)^{29}Al$.
TOF	time-of-flight detector
TRK	tracks of particles or fragments observed in solid materials (glass, mylar, etc.)
TRNS	transition
UKN UNK	unknown
VIB	vibrational
VIR PHOT	virtual photon(s)
XN	all neutrons, total neutron yield, $\sigma(\gamma,XN) = \sigma(\gamma,N) + 2\sigma(\gamma,2N) + 3\sigma(\gamma,3N) + \sigma(\gamma,NP)$ + etc.
XP	all protons, total proton yield $\sigma(\gamma,XP) = \sigma(\gamma,P) + \sigma(\gamma,NP) + 2\sigma(\gamma,2P)$ + etc.
XX XXX	reaction products defined in REMARKS
YLD	yield

4PI	a 4π geometry was used or a method like radioactivity or a total absorption measurement		products was determined. The polarized particle is indicated in REMARKS.
999	energy defined in REMARKS	* or @	symbols used to indicate that the units associated with the numerals on one or both sides of the symbol in a specific column are not MeV. The units are defined in REMARKS.
$	indicates the measurement involved beams or targets that were either polarized or aligned, or that the polarization of the reaction		

NBS-114A (REV. 2-8C)

U.S. DEPT. OF COMM. BIBLIOGRAPHIC DATA SHEET (See instructions)	1. PUBLICATION OR REPORT NO.	2. Performing Organ. Report No.	3. Publication Date

4. TITLE AND SUBTITLE

Photonuclear Data-Abstract Sheets
1955-1982

5. AUTHOR(S)

E.G. Fuller and Henry Gerstenberg

6. PERFORMING ORGANIZATION (If joint or other than NBS, see instructions)

NATIONAL BUREAU OF STANDARDS
DEPARTMENT OF COMMERCE
WASHINGTON, D.C. 20234

7. Contract/Grant No.

8. Type of Report & Period Covered

9. SPONSORING ORGANIZATION NAME AND COMPLETE ADDRESS (Street, City, State, ZIP)

10. SUPPLEMENTARY NOTES

☐ Document describes a computer program; SF-185, FIPS Software Summary, is attached.

11. ABSTRACT (A 200-word or less factual summary of most significant information. If document includes a significant bibliography or literature survey, mention it here)

These abstract sheets cover most classes of experimental photonuclear data leading to information of the electromagnetic matrix element between the ground and excited states of a given nucleus. This fifteen volume work contains nearly 7200 abstract sheets and covers 89 chemical elements from hydrogen through americium. It represents a twenty-seven year history of the study of electromagnetic interactions. The sheets are ordered by target element, target isotope, and by an assigned bibliographic reference code. Information is given on the type of measurement, excitation energies studied, source type and energies, detector type, and angular ranges covered in the measurement. For a given reference, the relevant figures and tables are mounted on a separate sheet for each nuclide studied.

12. KEY WORDS (Six to twelve entries; alphabetical order; capitalize only proper names; and separate key words by semicolons)

data-abstract sheets, elements, experimental, isotopes, nuclear physics, photonuclear reactions

13. AVAILABILITY

☐ Unlimited

☒ For Official Distribution. Do Not Release to NTIS

☐ Order From Superintendent of Documents, U.S. Government Printing Office, Washington, D.C. 20402.

☐ Order From National Technical Information Service (NTIS), Springfield, VA. 22161

14. NO. OF PRINTED PAGES

@ 635

15. Price

USCOMM-DC 6043-P80


AMERICAN BINDERY, EAST
1993